

Antimicrobial peptides and their druggability, bio-safety, stability, and resistance

Edited by

Jianhua Wang, Octavio Luiz Franco, Rustam Aminov, Cesar de la Fuente-Nunez and Guangshun Wang

Published in

Frontiers in Microbiology



FRONTIERS EBOOK COPYRIGHT STATEMENT

The copyright in the text of individual articles in this ebook is the property of their respective authors or their respective institutions or funders. The copyright in graphics and images within each article may be subject to copyright of other parties. In both cases this is subject to a license granted to Frontiers.

The compilation of articles constituting this ebook is the property of Frontiers.

Each article within this ebook, and the ebook itself, are published under the most recent version of the Creative Commons CC-BY licence. The version current at the date of publication of this ebook is CC-BY 4.0. If the CC-BY licence is updated, the licence granted by Frontiers is automatically updated to the new version.

When exercising any right under the CC-BY licence, Frontiers must be attributed as the original publisher of the article or ebook, as applicable.

Authors have the responsibility of ensuring that any graphics or other materials which are the property of others may be included in the CC-BY licence, but this should be checked before relying on the CC-BY licence to reproduce those materials. Any copyright notices relating to those materials must be complied with.

Copyright and source acknowledgement notices may not be removed and must be displayed in any copy, derivative work or partial copy which includes the elements in question.

All copyright, and all rights therein, are protected by national and international copyright laws. The above represents a summary only. For further information please read Frontiers' Conditions for Website Use and Copyright Statement, and the applicable CC-BY licence.

ISSN 1664-8714
ISBN 978-2-8325-4981-0
DOI 10.3389/978-2-8325-4981-0

About Frontiers

Frontiers is more than just an open access publisher of scholarly articles: it is a pioneering approach to the world of academia, radically improving the way scholarly research is managed. The grand vision of Frontiers is a world where all people have an equal opportunity to seek, share and generate knowledge. Frontiers provides immediate and permanent online open access to all its publications, but this alone is not enough to realize our grand goals.

Frontiers journal series

The Frontiers journal series is a multi-tier and interdisciplinary set of open-access, online journals, promising a paradigm shift from the current review, selection and dissemination processes in academic publishing. All Frontiers journals are driven by researchers for researchers; therefore, they constitute a service to the scholarly community. At the same time, the *Frontiers journal series* operates on a revolutionary invention, the tiered publishing system, initially addressing specific communities of scholars, and gradually climbing up to broader public understanding, thus serving the interests of the lay society, too.

Dedication to quality

Each Frontiers article is a landmark of the highest quality, thanks to genuinely collaborative interactions between authors and review editors, who include some of the world's best academicians. Research must be certified by peers before entering a stream of knowledge that may eventually reach the public - and shape society; therefore, Frontiers only applies the most rigorous and unbiased reviews. Frontiers revolutionizes research publishing by freely delivering the most outstanding research, evaluated with no bias from both the academic and social point of view. By applying the most advanced information technologies, Frontiers is catapulting scholarly publishing into a new generation.

What are Frontiers Research Topics?

Frontiers Research Topics are very popular trademarks of the *Frontiers journals series*: they are collections of at least ten articles, all centered on a particular subject. With their unique mix of varied contributions from Original Research to Review Articles, Frontiers Research Topics unify the most influential researchers, the latest key findings and historical advances in a hot research area.

Find out more on how to host your own Frontiers Research Topic or contribute to one as an author by contacting the Frontiers editorial office: frontiersin.org/about/contact

Antimicrobial peptides and their druggability, bio-safety, stability, and resistance

Topic editors

Jianhua Wang — Chinese Academy of Agricultural Sciences (CAAS), China
Octavio Luiz Franco — Catholic University of Brasilia (UCB), Brazil
Rustam Aminov — University of Aberdeen, United Kingdom
Cesar de la Fuente-Nunez — University of Pennsylvania, United States
Guangshun Wang — University of Nebraska Medical Center, United States

Citation

Wang, J., Franco, O. L., Aminov, R., de la Fuente-Nunez, C., Wang, G., eds. (2024). *Antimicrobial peptides and their druggability, bio-safety, stability, and resistance*. Lausanne: Frontiers Media SA. doi: 10.3389/978-2-8325-4981-0

Table of contents

- 06 **Editorial: Antimicrobial peptides and their druggability, bio-safety, stability, and resistance**
Xuanxuan Ma, Rustam Aminov, Octavio Luiz Franco, Cesar de la Fuente-Nunez, Guangshun Wang and Jianhua Wang
- 14 **Cecropin D-derived synthetic peptides in the fight against *Candida albicans* cell filamentation and biofilm formation**
Ibeth Guevara-Lora, Grazyna Bras, Magdalena Juszczak, Justyna Karkowska-Kuleta, Andrzej Gorecki, Marcela Manrique-Moreno, Jakub Dymek, Elzbieta Pyza, Andrzej Kozik and Maria Rapala-Kozik
- 35 **Prediction and bioactivity of small-molecule antimicrobial peptides from *Protaetia brevitarsis* Lewis larvae**
Qian Fu, Dengtian Cao, Jing Sun, Xinbo Liu, Haitao Li, Changlong Shu and Rongmei Liu
- 48 **Detection of antimicrobial producing *Staphylococcus* from migratory birds: Potential role in nasotracheal microbiota modulation**
Rosa Fernández-Fernández, Idris Nasir Abdullahi, Carmen González-Azcona, Adriana Ulloa, Agustí Martínez, Sara García-Vela, Ursula Höfle, Myriam Zarazaga, Carmen Lozano and Carmen Torres
- 59 **Antibiotic synergist OM19r reverses aminoglycoside resistance in multidrug-resistant *Escherichia coli***
Qi Cui, Han-Dong Yu, Qi-Jun Xu, Yue Liu, Yu-Ting Wang, Peng-Hui Li, Ling-Cong Kong, Hai-Peng Zhang, Xiu-Yun Jiang, Anna Maria Giuliadori, Attilio Fabbretti, Cheng-Guang He and Hong-Xia Ma
- 76 **Enzymatic synthesis of new antimicrobial peptides for food purposes**
Mauricio Adaro, Ángel Gabriel Salinas Ibáñez, Anabella Lucia Origone, Diego Vallés, Fanny Guzmán, Alba Vega and Sonia Barberis
- 87 **Cathelicidin-derived antiviral peptide inhibits herpes simplex virus 1 infection**
Xiaomin Guo, Yanxing An, Wanmin Tan, Ling Ma, Mingyang Wang, Juyan Li, Binghong Li, Wei Hou and Li Wu
- 97 **High expression of antimicrobial peptides cathelicidin-BF in *Pichia pastoris* and verification of its activity**
Xufeng Dong, Hu Shan, Shubai Wang, Zhengjun Jiang, Shaojuan Wang and Zhihua Qin
- 107 **Characterization and expression of fungal defensin in *Escherichia coli* and its antifungal mechanism by RNA-seq analysis**
Yu-Pei Chen, Yingying Li, Fangfang Chen, Hongtan Wu and Shudi Zhang

- 122 **Novel leaderless bacteriocin geobacillin 6 from thermophilic bacterium *Parageobacillus thermoglucosidasius***
Ana Koniuchovaitė, Akvilė Petkevičiūtė, Emilija Bernotaitė, Alisa Gricajeva, Audrius Gegeckas, Lilija Kalėdienė and Arnoldas Kaunietis
- 134 **Anti-*Pseudomonas aeruginosa* activity of natural antimicrobial peptides when used alone or in combination with antibiotics**
Xueqi Chen, Shan Su, Yan Yan, Limei Yin and Lihong Liu
- 153 **Antimicrobial peptide temporin derivatives inhibit biofilm formation and virulence factor expression of *Streptococcus mutans***
Shangjun Jiang, Yanmei Zha, Ting Zhao, Xiao Jin, Ruiying Zhu, Shuangshuang Wei, Rong Wang, Yanting Song, Lushuang Li, Junchen Lyu, Wenting Hu, Daqi Zhang, Manchuriga Wang and Yingxia Zhang
- 167 **Structure modification of an antibiotic: by engineering the fusaricidin bio-synthetase A in *Paenibacillus polymyxa***
Yunlong Li and Sanfeng Chen
- 177 **Recent advances on cyclodepsipeptides: biologically active compounds for drug research**
Si-Xuan Liu, Si-Yi Ou-Yang, Yong-Fu Lu, Chun-Lin Guo, Si-Yang Dai, Chang Li, Tian-Yi Yu and Yue-Hu Pei
- 191 **Antimicrobial activity, membrane interaction and structural features of short arginine-rich antimicrobial peptides**
Bruna Agrillo, Alessandra Porritiello, Lorena Gratio, Marco Balestrieri, Yolande Therese Proroga, Andrea Mancusi, Loredana Cozzi, Teresa Vicenza, Principia Dardano, Bruno Miranda, Pablo V. Escribá, Marta Gogliettino and Gianna Palmieri
- 206 **Antimicrobial peptide 2K4L disrupts the membrane of multidrug-resistant *Acinetobacter baumannii* and protects mice against sepsis**
Fangyu Ji, Guoxu Tian, Dejing Shang and Fengquan Jiang
- 224 **Ceragenins exhibit bactericidal properties that are independent of the ionic strength in the environment mimicking cystic fibrosis sputum**
Karol Skłodowski, Łukasz Suprewicz, Sylwia Joanna Chmielewska-Deptuła, Szczepan Kaliniak, Sławomir Okła, Magdalena Zakrzewska, Łukasz Minarowski, Robert Mróz, Tamara Daniluk, Paul B. Savage, Krzysztof Fiedoruk and Robert Bucki

- 238 **Dual antibacterial mechanism of [K4K15]CZS-1 against *Salmonella* Typhimurium: a membrane active and intracellular-targeting antimicrobial peptide**
Sebastián Bermúdez-Puga, Meriellen Dias, Taciana Freire de Oliveira, Carlos Miguel Nóbrega Mendonça, Sonia Regina Yokomizo de Almeida, Enrique Eduardo Rozas, Claudio Augusto Oller do Nascimento, Maria Anita Mendes, Pamela Oliveira De Souza de Azevedo, José R. Almeida, Carolina Proaño-Bolaños and Ricardo Pinheiro de Souza Oliveira
- 252 **Plectasin: from evolution to truncation, expression, and better druggability**
Xuan Li, Ya Hao, Na Yang, Ruoyu Mao, Da Teng and Jianhua Wang
- 265 **Evaluation of proline-rich antimicrobial peptides as potential lead structures for novel antimycotics against *Cryptococcus neoformans***
Alexandra Brakel, Thomas Grochow, Stefanie Fritsche, Daniel Knappe, Andor Krizsan, Simone A. Fietz, Gottfried Alber, Ralf Hoffmann and Uwe Müller
- 279 **Anticancer activities of natural antimicrobial peptides from animals**
Baozhen Qu, Jiangshui Yuan, Xueli Liu, Shicui Zhang, Xuezhen Ma and Linlin Lu
- 296 **Mechanistic and biophysical characterization of polymyxin resistance response regulator PmrA in *Acinetobacter baumannii***
Zhenlin Ouyang, Wenbo He, Min Jiao, Qinyue Yu, Yucheng Guo, Moath Refat, Qian Qin, Jiaxin Zhang, Qindong Shi, Fang Zheng and Yurong Wen
- 308 **PAM-1: an antimicrobial peptide with promise against ceftazidime-avibactam resistant *Escherichia coli* infection**
Yijia Han, Yi Zhang, Xiaodong Zhang, Zeyu Huang, Jingchun Kong, Xiuxiu Wang, Lijiang Chen, Yue Wang, Jianming Cao, Tieli Zhou and Mo Shen



OPEN ACCESS

EDITED AND REVIEWED BY
Shangshang Qin,
Zhengzhou University, China

*CORRESPONDENCE

Jianhua Wang
✉ wangjianhua@caas.cn;
✉ wangjianhua.peking@qq.com
Rustam Aminov
✉ rustam.aminov@gmail.com
Octavio Luiz Franco
✉ ocfranco@gmail.com
Cesar de la Fuente-Nunez
✉ cfuente@upenn.edu
Guangshun Wang
✉ gwang@unmc.edu

RECEIVED 30 April 2024

ACCEPTED 14 May 2024

PUBLISHED 23 May 2024

CITATION

Ma X, Aminov R, Franco OL, de la
Fuente-Nunez C, Wang G and Wang J (2024)
Editorial: Antimicrobial peptides and their
druggability, bio-safety, stability, and
resistance. *Front. Microbiol.* 15:1425952.
doi: 10.3389/fmicb.2024.1425952

COPYRIGHT

© 2024 Ma, Aminov, Franco, de la
Fuente-Nunez, Wang and Wang. This is an
open-access article distributed under the
terms of the [Creative Commons Attribution
License \(CC BY\)](#). The use, distribution or
reproduction in other forums is permitted,
provided the original author(s) and the
copyright owner(s) are credited and that the
original publication in this journal is cited, in
accordance with accepted academic practice.
No use, distribution or reproduction is
permitted which does not comply with these
terms.

Editorial: Antimicrobial peptides and their druggability, bio-safety, stability, and resistance

Xuanxuan Ma^{1,2,3}, Rustam Aminov^{4*}, Octavio Luiz Franco^{5,6*},
Cesar de la Fuente-Nunez^{7,8,9,10*}, Guangshun Wang^{11*} and
Jianhua Wang^{1,2,3*}

¹Innovative Team of Antimicrobial Peptides and Alternatives to Antibiotics, Feed Research Institute, Chinese Academy of Agricultural Sciences, Beijing, China, ²Gene Engineering Laboratory, Feed Research Institute, Chinese Academy of Agricultural Sciences, Beijing, China, ³Key Laboratory of Feed Biotechnology, Ministry of Agriculture and Rural Affairs, Beijing, China, ⁴The School of Medicine, Medical Sciences and Nutrition, University of Aberdeen, Aberdeen, United Kingdom, ⁵S-Inova Biotech, Universidade Católica Dom Bosco, Campo Grande, MS, Brazil, ⁶Centro de Análises Proteômicas e Bioquímicas Programa de Pós-Graduação em Ciências Genômicas e Biotecnologia, Universidade Católica de Brasília, Brasília, DF, Brazil, ⁷Machine Biology Group, Departments of Psychiatry and Microbiology, Perelman School of Medicine, Institute for Biomedical Informatics, Institute for Translational Medicine and Therapeutics, University of Pennsylvania, Philadelphia, PA, United States, ⁸Departments of Bioengineering and Chemical and Biomolecular Engineering, School of Engineering and Applied Science, University of Pennsylvania, Philadelphia, PA, United States, ⁹Department of Chemistry, School of Arts and Sciences, University of Pennsylvania, Philadelphia, PA, United States, ¹⁰Penn Institute for Computational Science, University of Pennsylvania, Philadelphia, PA, United States, ¹¹Department of Pathology, Microbiology, and Immunology, University of Nebraska Medical Center, Omaha, NE, United States

KEYWORDS

antimicrobial peptide (AMPs), druggability, bio-safety, stability, resistance

Editorial on the Research Topic

[Antimicrobial peptides and their druggability, bio-safety, stability, and resistance](#)

1 Introduction

The excessive and often indiscriminate use of antibiotics in many areas of human activities has caused a widespread antibiotic resistance, which poses a major threat to the public health worldwide (Carratalá et al., 2020; Murray et al., 2022; Bessa et al., 2023; De la Fuente-Núñez et al., 2023). Even more worrying is the dearth of new antimicrobial drugs (Durand et al., 2019; Li S. et al., 2021). Under these circumstances, the development of new antimicrobial drugs is essential (Tacconelli et al., 2018; Hamad et al., 2019). Antimicrobial peptides (AMPs) have attracted attention for their potent antibacterial activities and unique antibacterial mechanisms, which are efficient against many bacterial pathogens, including those that are multidrug-resistant (MDR) (Boaro et al., 2023; Maasch et al., 2023; Wong et al., 2023; Xuan et al., 2023). However, the entry of AMPs into clinical practice has encountered many challenges, including peptide stability, bioavailability, and toxicity, all of which limit their clinical applicability (Durand et al., 2019; Sarkar et al., 2021). Therefore, rational design, advanced drug formulations and tailored routes of administration and delivery systems are crucial for the development of AMPs as viable therapeutic options. The third volume of the

Research Topic on AMPs targeted the above issues to bring AMPs closer to clinical practice.

2 Challenges in the clinical translation of AMPs

2.1 Low bioavailability *in vivo*

Despite the intrinsic properties of AMPs that make them highly attractive for a potential use, relatively few of them have been successfully translated into the clinical use or as food preservatives (Mishra et al., 2017; Costa et al., 2019; Adaro et al.; Koniuchovaitė et al.). One of the key constraints is the mismatch between their *in vivo* and *in vitro* activities. Particularly frustrating is the fact that highly anticipated peptides such as pexiganan, iseganan, neuprex and omiganan have failed in phase III clinical trials due to low *in vivo* efficacy (<http://dramp.cpu-bioinform.org/>). Many factors may contribute to the low bioavailability *in vivo*. However, poor stability of these molecules in complex microenvironments has been identified as the most significant factor (Jiang et al., 2021; Fu et al.; Guevara-Lora et al.; Skłodowski et al.).

2.2 Toxicity

One of the important prerequisites for clinical use is the drug safety, and this is the second major obstacle on the way of AMPs toward clinical translation (Payne et al., 2015). Toxicity of AMPs includes cytotoxicity and systemic toxicity (Li et al., 2017). Cytotoxicity is usually an inherent property of membrane-active AMPs, the cationic and hydrophobic components of which can directly interact with the membrane of host cells (Agrillo et al.). This interaction is exhibited in a concentration-dependent toxicity. Typical examples are melittin, CZS-1 and alamethicin, which exhibit potent cytotoxicity, including hemolysis (Askari et al., 2021; Farid et al., 2023; Bermúdez-Puga et al.; Brakel et al.). Considering the potential cytotoxic mechanisms of AMPs relative to their successful application, it can be generally concluded that narrow-spectrum peptides are relatively safer for clinical translation due to their lower cytotoxicity and the lack of off-target effects against the beneficial microbiota (Xu et al., 2020; Zong et al., 2020). Conversely, broad-spectrum AMPs tend to display the increased cytotoxicity toward the host and adverse effects on the microbiota, thereby limiting their potential for clinical use (Hao et al., 2023). Systemic toxicity may result from off-target effects, accumulation of drug in kidneys, undesirable immune responses or chronic inflammation (e.g., atopic dermatitis or hidradenitis suppurativa) due to the increased drug concentrations (Takahashi et al., 2018). Therefore, preclinical safety evaluation of AMPs should not be limited to basic hemolysis and cytotoxicity but also requires the evaluation of systemic toxicity. In fact, the antimicrobial and immunomodulatory properties and toxicity of AMPs are often compounded. Thus, a careful attention has to be paid to the delicate balance of antimicrobial properties, immunomodulation, and toxicity.

2.3 Pharmacokinetic assays

Although several papers in this Research Topic have discussed the pharmacokinetic (PK) properties of AMPs, it has to be emphasized here that PK is still a bottleneck for AMP translation. It is known that the physicochemical properties of AMPs are quite different from the traditional small-molecule chemical drugs. Hence, the PK of traditional small-molecule drugs should be further modified, improved and optimized for AMPs so that the quantitative PK methodology can be successfully applied for this class of antimicrobials (Wang et al., 2012). Therefore, the development of suitable quantification methods for PK of AMPs, which are different from small-molecule chemical drugs, is the 3rd key challenge for their entry into clinical applications (Ewles and Goodwin, 2011; Mercer and O'Neil, 2013). Usually, linear cationic AMPs are rapidly metabolized *in vivo* and degraded into smaller fragments or amino acids and absorbed as nutrients. This process interferes with the determination of the main four PK parameters such as absorption, distribution, metabolism, and excretion. Although the safety of AMP degradation products, especially amino acids, *in vivo* is not of a major concern from the nutrient metabolism point of view, it is difficult to determine the concentration of these products with the use of regular analytical tools. Therefore, there is an urgent need for updating PK principles so that they suit to AMPs, especially protocols for their clinical evaluation (Giguère et al., 2017). In brief, we believe that the use of the latest material analysis methods for exploratory pharmacokinetic detection combined with the calculation of PK parameters based on non-compartmental model is an important prerequisite for AMPs to resolve the bottleneck of drug development and transition to clinical practice (Zheng et al., 2022, 2024).

2.4 Resistance

The likelihood of resistance development toward AMPs is generally much lower than that against conventional antibiotics. Numerous parameters influence resistance development, including the dose used, period of application, temperature, exposure/contact with inhibitory substances, and others. Metabolic pathways and genes within bacterial cells can be replaced or compensated over time, as has been shown for defensins derived from plants and polymyxin from microbes (Ouyang et al.); On the contrary, molecules that have multiple targets in bacteria are less likely to select for bacterial resistance. AMPs with the low probability of resistance development include melittin, bombesin, venoms and cecropins (Chen et al., 2022a). Additional attention has to be paid to AMP-induced cross-resistance. Chen et al. (2022b) found that *Staphylococcus aureus* acquired limited resistance to PIS-3, with a concomitant resistance toward polymyxin B, vancomycin, and tetracycline, but with no resistance development toward PIS-1. Thus, it is important to gain a better understanding of pharmacology, evolutionary effects and potential resistance acquisition during the development and application of AMPs, the above steps have been largely ignored in the past with traditional antibiotics (Lazzaro et al., 2020).

3 R&D directions of AMPs

3.1 AMP stabilization technology

The molecular stability of AMPs is another important parameter to take into account. The stability of these agents needs to be sufficient to exert their function, ideally without causing off-target effects. At the same time, when assessing peptide stability, it is necessary to focus on the route of administration as this may substantially affect stability.

3.1.1 Chemical modification

Strategies for the improvement of stability of AMPs include two complementary approaches. The first is chemical modification(s) to improve the stability and bioavailability and reduce toxicity. Currently effective chemical modifications include the following:

1. Replacement of L-amino acids in natural sequences with proteinogenic amino acids (unnatural α -amino acids, unnatural β -amino acids, unnatural γ -amino acids, and D-amino acids) (De la Fuente-Núñez et al., 2015; Zhang et al., 2016; Sandín et al., 2021; He et al., 2023). For example, Li T. et al. (2021) used D-amino acids (Val and Pro) to replace the natural L-amino acids in N6 to improve the stability of the antibacterial N6NH2 against protease.
2. Cyclisation is an effective strategy to improve the metabolic stability of AMPs. This notion is supported by the fact that some of the successfully marketed AMPs are cyclic such as bacitracin A, daptomycin, polymyxins B1 and B2 (Falanga et al., 2017; Mishra et al., 2017; Costa et al., 2019; Liu et al.).
3. PEG modification is one of the effective methods to improve the biocompatibility and bioavailability of peptides. The success of this approach was proven in a number of studies, involving AMPs such as OM19r-8, N6NH₂ and SAMP-A₄, the stability of which was substantially improved by PEG modification (Lau and Dunn, 2018; Manteghi et al., 2020; Li R. et al., 2021; Li et al., 2022).
4. N-/C-terminal modification (C-terminal amidation, N-terminal acylation or methylation modification) is the most straightforward methods to improve the AMP stability (Teixeira et al., 2010; Li D. et al., 2021). Although these AMP modification methods have been supported by several corresponding studies, they are not universal and each peptide may require a set of their own design strategies depending on the peptide scaffold and the desired activity (Torres et al., 2018, 2019; Silva et al., 2020; Cesaro et al., 2022).

3.1.2 Delivery systems

In addition to chemical modifications, improvements in pharmacokinetics and pharmacodynamics of AMPs can be achieved via the use of nanotechnology, which may increase the stability of AMPs and thus facilitate their clinical translation (Carratalá et al., 2020; Cesaro et al., 2023; Xuan et al., 2023). Currently, various types of carriers are employed in AMP delivery studies (Li et al., 2023):

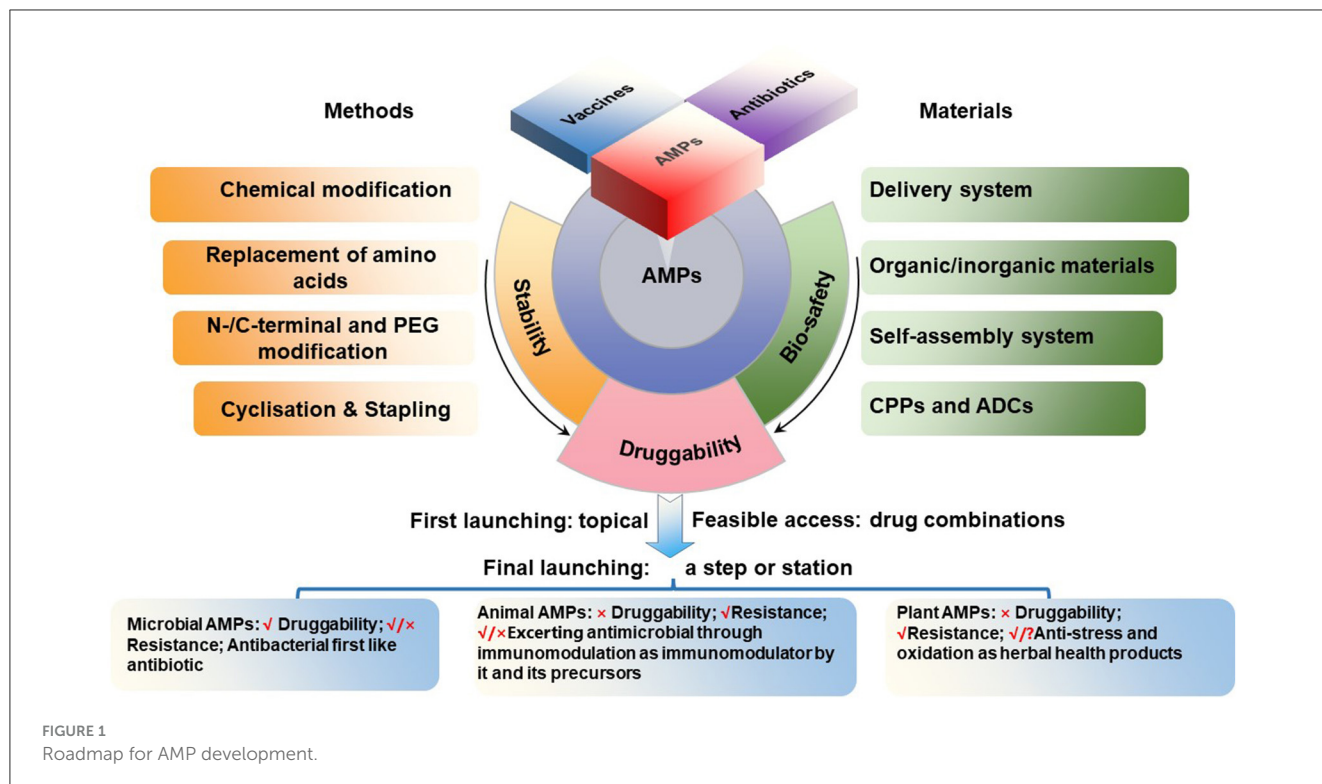
1. These can be inorganic materials such as mesoporous silica, metal nanoparticles, carbon nanotubes, and others. Izquierdo-Barba et al. (2009), for instance, demonstrated that incorporation of antimicrobial peptide LL-37 into mesoporous silica significantly increased its half-life, with the maximum release rate of LL-37 achieved after 200 h.
2. Organic polymers such as chitosan, polylactide-glycolide (PLGA), liposomes and others can also serve as efficient delivery systems for AMPs. For example, d'Angelo et al. (2015) demonstrated that chitosan and PLGA-coated colistin could be continuously released in biofilms, thereby eradicating biofilms formed by *Pseudomonas aeruginosa*. In another study, Ma et al. (2024) successfully increased the trypsin tolerance of AMP NZ2114 by 4.24-fold using PLGA encapsulation.
3. Another approach to improve the pharmacokinetics and pharmacodynamics of AMPs is the use of peptide self-assembly properties. As comprehensively overviewed by Habibi et al. (2016) and Zou et al. (2020), a variety of peptides can self-assemble into nanoparticles, nanofibers or nanogels according to their hydrophobicity, length, and structures to achieve precisely controlled release rates. Self-assembly of peptides can also overcome the problem of low encapsulation efficiency and release rates of traditional coating strategies. This approach, therefore, has attracted a great interest for potential applications in drug delivery, functional materials, and regenerative medicine. Recently, an increasing number of studies have supported the view that self-assembly of AMPs can effectively increase their stability, prolong the half-life and improve biosafety, thus contributing to better pharmacokinetic and pharmacodynamic properties of AMPs (Chen et al., 2019; Tram et al., 2022).

3.2 AMP application strategy

After exploration toward clinical translation for over 50 years, there is a huge number of publications and patents with innovative results on AMPs, but also there is still room for improvement, and it is expected that the original intentions could be realized as soon as possible (Zasloff, 2015; Czaplewski et al., 2016; Arciola et al., 2018).

3.2.1 Topical applications

Among the 11 commercially available AMPs, daptomycin, dalbavancin, telavancin and oritavancin were initially approved for the treatment of skin infections, bacitracin and polymyxin B—for conjunctivitis and keratitis, and tyrothricin—for acute pharyngitis. Besides, the majority of AMP drugs currently in clinical trials are intended for topical use (<http://dramp.cpu-bioinform.org/>). The emphasis of pharmaceutical companies on topical AMP drugs is logical and economically feasible because topical administration does not require the level of pharmacokinetic and pharmacodynamic characterization required for the internal use. An increasing number of studies have shown that AMPs play a crucial role in promoting wound infection clearance and recovery (Gao et al., 2023) and in managing local inflammation in pyoderma, conjunctivitis, mastitis, and biofilms (Yang et al., 2022; Zhang et al.,



2024; Fernández-Fernández et al.; Ji et al.; Jiang et al.). Thus the topical use of AMPs asserts their promising prospects as a viable treatment option.

3.2.2 Drug combinations

Antibiotic combinations became important therapeutic tools to deal with multidrug-resistant or mixed infections. Other advantages include synergetic effects between antibiotics that allow the decrease of antibiotic concentration(s), especially of toxic ones, and also a lower probability of resistance development. In this regard, combination of AMPs with traditional antibiotics is also a valuable approach (Reffuveille et al., 2014; Mishra et al., 2017; Mhlongo et al., 2023; Chen X. et al.). AMPs, antibiotics and vaccines could complement each other to maintain the health of the organism (Hao et al., 2022; Yang et al., 2023), these combination therapies can improve both the efficacy of treatment and reduce the dose of each drug, thereby reducing excessive toxicity and side effects, while maintaining a reasonable balance between the therapeutic efficiency and drug resistance development (Zakaryan et al., 2021). For example, the combination of AMP OM19r with gentamicin increased the antibacterial activity of the latter against MDR *Escherichia coli* B2 by 64-fold (Cui et al.). Thus, AMPs can increase the permeability of the cytoplasmic membrane, which facilitates the entry of antibiotics into bacterial cells (Duong et al., 2021). The combination of cecropin D-derived peptide and caspofungin showed the synergistic effects against *Candida albicans* (Guevara-Lora et al.). The study of Alencar-Silva et al. (2023) demonstrated the decreased cytotoxicity of Synoeca MP through its combination with IDR-1018. The combination also enhanced cell proliferation and migration and

accelerated wound re-epithelialization, which opens the possibility for the development of new strategies in treatment of skin injuries (Alencar-Silva et al., 2023).

Presently the Antimicrobial Peptide Database (APD) (<https://aps.unmc.edu>) contains the information about 4231 peptides, from which 3223 are natural AMPs. The use of the majority of them is limited to topical and combination applications, including the early or preventive treatments. Thus, there are decreasing numbers of cases, where treatments involving AMPs include emergency treatments at ICUs or treatment of serious infections in modern husbandry.

3.3 Reduction of AMPs production costs

Two main AMPs production routes include chemical synthesis and recombinant expression. Chemical synthesis can be executed via solid and liquid phase synthesis methods or their combination. The representative examples of peptide-based drug production at multi-ton scale are HIV fusion inhibitory peptide T-20 (Fuzeon, Roche), semaglutide and insulin (Walsh, 2005; Thayer, 2011; Aggarwal et al., 2021). With technological advances, more and more AMPs including those longer than 30 amino acids, with complex structures and modification processes, will be industrialized utilizing chemical synthesis or transgenic expressions at acceptable costs. Multiple studies have been published recently along this line. For example, optimisation of culture conditions of recombinant *Pichia pastoris* and induction process of cathelicidin BF expression allowed to reach the product concentration of 0.5 g/L after 240 h (Dong et al.). Li and Chen engineered synthetase to create a synthetic pathway for the production of a novel fusaricidin and

constructed the recombinant M6 yielding a 55 mg/L of fusaricidin LI-F07a. In addition, the codon use optimisation in heterologous expression of AFP in *E. coli* allowed to reach its production at 780 µg/ml (Chen Y.-P. et al.). Different strategies have been used to optimize AMPs production and develop large-scale facilities, some of which were successfully accomplished. For example, after nearly two decades of efforts, Wang's team has successfully established a 20 and 30 cubic meter-scale production system for high-yield preparation of plectasin analogs with an affordable cost comparable to traditional antibiotics, a milestone for the translation of AMPs (Zhang et al., 2014; Yang et al., 2022; Hao et al., 2023; Jin et al., 2023; Li et al.).

4 Conclusions

Based on their antimicrobial activities and immunomodulatory properties, AMPs can be used for disease prevention and treatment. However, the development of AMPs as a viable therapeutic option faces challenges such as cytotoxicity, stability, and bioavailability. As discussed below, the strategies for the development of different AMP classes may require their own specific challenges to be addressed.

1. The category of microbial AMPs is very broad, covering natural AMPs from four kingdoms of life (bacteria, archaea, protists, and fungi) as annotated in APD (Wang et al., 2016; Santos-Júnior et al., 2023; Wang, 2023; <https://aps.unmc.edu>). Most of them share natural druggability properties similar to traditional microbial antibiotics. Microbial AMPs are made either ribosomally or non-ribosomally. Ribosomally synthesized peptides are exemplified by nisin, plectasin and its derivatives, while non-ribosomally synthesized peptides are represented by vancomycin, polymyxins and daptomycin, all currently in medical use. Thus, these AMPs can be easily developed by following the path of modern antibiotic pharmaceutical industry, including genetic modification, recombinant expression and chemical synthesis. These AMPs are expected to have a wide range of therapeutic uses. A potential drug resistance emergence, however, should be carefully monitored during the drug development process as well as during the use. At same time, need to keep in mind the similarity and differences in their dual transmembrane entry mechanisms and targets/paths, which should be separately addressed in animals and pathogens (Figure 1).
2. After the recent refinement, the category of animal AMPs in the APD include 2515 representatives from both invertebrates and vertebrates. These include melittin, bombesin, venoms, and cecropins with weak druggability, because their strong antimicrobial activity is accompanied by high toxicity and interference with immunological and metabolic processes. Their development, therefore, has been more difficult and complicated. There are possibilities that these peptides or their derivatives could be developed as antiviral (Guo et al.) or anti-cancer (Qu et al.) drugs. Nevertheless, some animal AMPs such as small and cyclic θ -defensins possess a great development potential as antibacterial agents (Schaal et al., 2021), as demonstrated for cathelicidin-derived PAM-1 against ceftazidime-avibactam (CZA)-resistant *E. coli*. (Han et al.). Additional mechanistic studies are necessary for better understanding whether the impact of AMPs *in vivo* is a consequence of immunological or other metabolic regulation or brake to the bona fide antimicrobial activity (Figure 1).
3. After the recent refinement, the category of plant AMPs in the APD includes 258 plant peptides with known antimicrobial activities. Compared to the first two categories, the number of AMPs in this category is relatively less and include peptide compounds such as plant defensins (for instance, Rs-AFP1), thionins (for instance, Tu-AMP 1), soybean peptides and other peptide products that can be developed into products with antimicrobial and other activities (Shwaiki et al., 2021; Sharma et al., 2022). Many traditional herbal medicines in China and other countries have been used for millennia as anti-infective agents. In the modern medicine, however, the active antimicrobial compounds have to be purified, characterized, and thus their mechanism(s) of action must be elucidated and revealed. In this regard, traditional herbal medicines represent a valuable source of potentially useful AMPs, which can be explored further for our benefit (Figure 1).

The current structure-and-function and spatiotemporal relationship of AMPs is the product of long-term evolution of these molecules, with the selection of molecules that provided the best protection of host organisms against the invasion of other organisms, mainly microorganisms. The use of these molecules by humans in medicine or in other applications not necessarily coincides exactly with the functions that have been selected during the previous natural evolutionary process. For example, AMPs are continuously produced by living organisms and act *in situ*, while humans need them in various acceptable pharmaceutical formulations, with the concomitant problem of stability or bioavailability. Thus, our task in this Research Topic was to provide a framework for future development of AMPs for the use in medicine and other applications (Figure 1). We hope this Research Topic of 22 papers contributed to this goal (Supplementary Table S1).

Author contributions

XM: Visualization, Writing – original draft, Data curation, Formal analysis, Investigation, Validation. RA: Conceptualization, Methodology, Resources, Supervision, Writing – review & editing, Investigation, Formal analysis. OF: Supervision, Writing – review & editing. CF-N: Conceptualization, Funding acquisition, Supervision, Writing – review & editing. GW: Conceptualization, Funding acquisition, Software, Supervision, Writing – review & editing. JW: Conceptualization, Funding acquisition, Methodology, Resources, Supervision, Writing – original draft, Writing – review & editing.

Funding

The author(s) declare financial support was received for the research, authorship, and/or publication of this article. JW: the National Natural Science Foundation of China (Grant No.

31872393, 2018–2022), National Key R&D Plan - High Expression of Thiopeptides and their Analogs (2022YFC2105000-03, 2022–2026), the National Key Research and Development Program of China (Grant No. 2023YFD1800805 and 2023YFD1301102), the National Agricultural Science and Technology Innovation Program (ASTIP) of Chinese Academy of Agricultural Sciences (CAAS-ASTIP-2017-FRI-02, 2013), and its key projects of Alternatives to Antibiotics for Animal (Grant No. CAAS-ZDRW202111, 2021–2023) and Feed (Grant No. CAASZDXT2018008, 2018–2020) Usages. OF was supported by CAPEs, CNPq, FAPDE, and FUNDECT. CF-N holds a Presidential Professorship at the University of Pennsylvania, is a recipient of the Langer Prize by the AIChE Foundation, and acknowledges funding from the IADR Innovation in Oral Care Award, the Procter & Gamble Company, United Therapeutics, a BBRF Young Investigator Grant, the Nemirovsky Prize, Penn Health-Tech Accelerator Award, the Dean's Innovation Fund from the Perelman School of Medicine at the University of Pennsylvania, the National Institute of General Medical Sciences of the National Institutes of Health under award number R35GM138201, and the Defense Threat Reduction Agency (DTRA; HDTRA1-22-10031, HDTRA1-21-1-0014, and HDTRA1-23-1-0001). GW was supported by funds from National Institute of General Medical Sciences (R01GM138552) and National Institute of Allergy and Infectious Diseases (R56AI175209), the National Institutes of Health, USA as well as Chair, Department of Pathology, Microbiology, and Immunology of the University of Nebraska Medical Center (Omaha, Nebraska, USA) for the cost of maintenance of the Antimicrobial Peptide Database (<https://aps.unmc.edu>).

Acknowledgments

We would like to sincerely thank a total of 192 authors of 23 papers and over 80 peer editors and reviewers for their valuable professional contributions into this Research Topic *Antimicrobial*

peptides and their druggability, bio-safety, stability, and resistance, along with the staff of Frontiers in Microbiology, and also team supports of five Topic editors JW, RA, OF, CF-N, and GW.

Conflict of interest

OF was employed by S-Inova Biotech.

The remaining authors declare that the research was conducted in the absence of any commercial or financial relationships that could be construed as a potential conflict of interest.

The author(s) declared that they were an editorial board member of Frontiers, at the time of submission. This had no impact on the peer review process and the final decision.

Publisher's note

All claims expressed in this article are solely those of the authors and do not necessarily represent those of their affiliated organizations, or those of the publisher, the editors and the reviewers. Any product that may be evaluated in this article, or claim that may be made by its manufacturer, is not guaranteed or endorsed by the publisher.

Author disclaimer

This manuscript documents the opinions of the authors/editors and does not represent the funding agencies.

Supplementary material

The Supplementary Material for this article can be found online at: <https://www.frontiersin.org/articles/10.3389/fmicb.2024.1425952/full#supplementary-material>

References

- Aggarwal, R., Vaduganathan, M., Chiu, N., and Bhatt, D. L. (2021). Potential implications of the FDA approval of semaglutide for overweight and obese adults in the United States. *Prog. Cardiovasc. Dis.* 68, 97–98. doi: 10.1016/j.pcad.2021.09.007
- Alencar-Silva, T., Diaz-Martín, R. D., Zonari, A., Foyt, D., Guiang, M., Pogue, R., et al. (2023). The combination of Synoeca-MP antimicrobial peptide with IDR-1018 stimulates proliferation, migration, and the expression of pro-regenerative genes in both human skin cell cultures and 3D skin equivalents. *Biomolecules* 13:804. doi: 10.3390/biom13050804
- Arciola, C. R., Campoccia, D., and Montanaro, L. (2018). Implant infections: adhesion, biofilm formation and immune evasion. *Nat. Rev. Microbiol.* 16, 397–409. doi: 10.1038/s41579-018-0019-y
- Askari, P., Namaei, M. H., Ghazvini, K., and Hosseini, M. (2021). *In vitro* and *in vivo* toxicity and antibacterial efficacy of melittin against clinical extensively drug-resistant bacteria. *BMC Pharmacol. Toxicol.* 22:42. doi: 10.1186/s40360-021-00503-z
- Bessa, L. J., Shaaban, M., and Aminov, R. (2023). Editorial: Insights in antimicrobials, resistance chemotherapy: 2022. *Front. Microbiol.* 14:1310156. doi: 10.3389/fmicb.2023.1310156
- Boaro, A., Ageitos, L., Torres, M. T., Blasco, E. B., Oztekin, S., and de la Fuente-Nunez, C. (2023). Structure-function-guided design of synthetic peptides with anti-infective activity derived from wasp venom. *Cell Rep. Phys. Sci.* 4:101459. doi: 10.1016/j.xcrp.2023.101459
- Carratalá, J. V., Serna, N., Villaverde, A., Vázquez, E., and Ferrer-Miralles, N. (2020). Nanostructured antimicrobial peptides: the last push towards clinics. *Biotechnol. Adv.* 44:107603. doi: 10.1016/j.biotechadv.2020.107603
- Cesaro, A., Lin, S., Pardi, N., and de la Fuente-Nunez, C. (2023). Advanced delivery systems for peptide antibiotics. *Adv. Drug Deliv. Rev.* 196:114733. doi: 10.1016/j.addr.2023.114733
- Cesaro, A., Torres, M. T., and de la Fuente-Nunez, C. (2022). Methods for the design and characterization of peptide antibiotics. *Meth. Enzymol.* 663, 303–326. doi: 10.1016/bs.mie.2021.11.003
- Chen, W., Yang, S., Li, S., Lang, J. C., Mao, C., Kroll, P., et al. (2019). Self-assembled peptide nanofibers display natural antimicrobial peptides to selectively kill bacteria without compromising cytocompatibility. *ACS Appl. Mater. Interfaces* 11, 28681–28689. doi: 10.1021/acsami.9b09583
- Chen, X., Han, J., Cai, X., and Wang, S. (2022a). Antimicrobial peptides: sustainable application informed by evolutionary constraints. *Biotechnol. Adv.* 60:108012. doi: 10.1016/j.biotechadv.2022.108012
- Chen, X., Han, J., and Wang, S. (2022b). Integrated evolutionary analysis reveals the resistance risk to antimicrobial peptides in *Staphylococcus aureus*. *Food Control* 138:108966. doi: 10.1016/j.foodcont.2022.108966

- Costa, F., Teixeira, C., Gomes, P., and Martins, M. C. L. (2019). Clinical application of AMPs. *Adv. Exp. Med. Biol.* 1117, 281–298. doi: 10.1007/978-981-13-3588-4_15
- Czaplewski, L., Bax, R., Clokic, M., Dawson, M., Fairhead, H., Fischetti, V. A., et al. (2016). Alternatives to antibiotics—a pipeline portfolio review. *Lancet Infect. Dis.* 16, 239–251. doi: 10.1016/S1473-3099(15)00466-1
- d'Angelo, I., Casciaro, B., Miro, A., Quaglia, F., Mangoni, M. L., and Ungaro, F. (2015). Overcoming barriers in *Pseudomonas aeruginosa* lung infections: engineered nanoparticles for local delivery of a cationic antimicrobial peptide. *Colloids Surf. B Biointerfaces* 135, 717–725. doi: 10.1016/j.colsurf.2015.08.027
- De la Fuente-Núñez, C., Cesaro, A., and Hancock, R. E. W. (2023). Antibiotic failure: beyond antimicrobial resistance. *Drug Resist. Updat.* 71:101012. doi: 10.1016/j.drug.2023.101012
- De la Fuente-Núñez, C., Refuville, F., Mansour, S. C., Reckseidler-Zenteno, S. L., Hernández, D., Brackman, G., et al. (2015). D-enantiomeric peptides that eradicate wild-type and multidrug-resistant biofilms and protect against lethal *Pseudomonas aeruginosa* infections. *Chem. Biol.* 22, 196–205. doi: 10.1016/j.chembiol.2015.01.002
- Duong, L., Gross, S. P., and Siryaporn, A. (2021). Developing antimicrobial synergy with AMPs. *Front. Med. Technol.* 3, 640981. doi: 10.3389/fmedt.2021.640981
- Durand, G. A., Raoult, D., and Dubourg, G. (2019). Antibiotic discovery: history, methods and perspectives. *Int. J. Antimicrob. Agents.* 53, 371–382. doi: 10.1016/j.ijantimicag.2018.11.010
- Ewles, M., and Goodwin, L. (2011). Bioanalytical approaches to analyzing peptides and proteins by LC–MS/MS. *Bioanalysis* 3, 1379–1397. doi: 10.4155/bio.11.112
- Falanga, A., Nigro, E., De Biasi, M. G., Daniele, A., Morelli, G., Galdiero, S., et al. (2017). Cyclic peptides as novel therapeutic microbicides: engineering of human defensin mimetics. *Molecules* 22:1217. doi: 10.3390/molecules22071217
- Farid, A., Mohamed, D., Mostafa, D., Tarek, R., Sherif, V., and Safwat, G. (2023). Novel grape seed extract nanoparticles attenuate amikacin-induced nephrotoxicity in rats. *AMB Express* 13:129. doi: 10.1186/s13568-023-01639-3
- Gao, F., Ahmed, A., Cong, H., Yu, B., and Shen, Y. (2023). Effective strategies for developing potent, broad-spectrum antibacterial and wound healing promotion from short-chain antimicrobial peptides. *ACS Appl. Mater. Interfaces* 15:32136–32147. doi: 10.1021/acsami.3c03069
- Giguère, S., Burton, A. J., Berghaus, L. J., and Haspel, A. D. (2017). Comparative pharmacokinetics of minocycline in foals and adult horses. *J. Vet. Pharmacol. Ther.* 40, 335–341. doi: 10.1111/jvp.12366
- Habibi, N., Kamaly, N., Memic, A., and Shafiee, H. (2016). Self-assembled peptide-based nanostructures: smart nanomaterials toward targeted drug delivery. *Nano Today* 11, 41–60. doi: 10.1016/j.nantod.2016.02.004
- Hamad, M., Al-Marzooq, F., Orive, G., and Al-Tel, T. H. (2019). Superbugs but no drugs: steps in averting a post-antibiotic era. *Drug Discov. Today* 24, 2225–2228. doi: 10.1016/j.drudis.2019.08.004
- Hao, Y., Teng, D., Mao, R., Yang, N., and Wang, J. (2023). Site mutation improves the expression and antimicrobial properties of fungal defense. *Antibiotics* 12:1283. doi: 10.3390/antibiotics12081283
- Hao, Y., Wang, J., de la Fuente-Núñez, C., and Franco, O. L. (2022). Editorial: antimicrobial peptides: molecular design, structure-function relationship, and biosynthesis optimization. *Front. Microbiol.* 13:888540. doi: 10.3389/fmicb.2022.888540
- He, S., Yang, Z., Li, X., Wu, H., Zhang, L., Shan, A., et al. (2023). Boosting stability and therapeutic potential of proteolysis-resistant antimicrobial peptides by end-tagging β -naphthylalanine. *Acta. Biomater.* 164, 175–194. doi: 10.1016/j.actbio.2023.04.030
- Izquierdo-Barba, I., Vallet-Regí, M., Kupferschmidt, N., Terasaki, O., Schmidtchen, A., and Malmsten, M. (2009). Incorporation of antimicrobial compounds in mesoporous silica film monolith. *Biomaterials* 30, 5729–5736. doi: 10.1016/j.biomaterials.2009.07.003
- Jiang, Y., Chen, Y., Song, Z., Tan, Z., and Cheng, J. (2021). Recent advances in design of antimicrobial peptides and polypeptides toward clinical translation. *Adv. Drug Deliv. Rev.* 170, 261–280. doi: 10.1016/j.addr.2020.12.016
- Jin, Y., Yang, N., Teng, D., Hao, Y., Mao, R., and Wang, J. (2023). Molecular modification of Kex2 P1' site enhances expression and druggability of fungal defensin. *Antibiotics* 12, 786. doi: 10.3390/antibiotics12040786
- Lau, J. L., and Dunn, M. K. (2018). Therapeutic peptides: historical perspectives, current development trends, and future directions. *Bioorg. Med. Chem.* 26, 2700–2707. doi: 10.1016/j.bmc.2017.06.052
- Lazzaro, B. P., Zasloff, M., and Rolff, J. (2020). Antimicrobial peptides: application informed by evolution. *Science* 368:eaau5480. doi: 10.1126/science.aau5480
- Li, D., Yang, Y., Li, R., Huang, L., Wang, Z., Deng, Q., et al. (2021). N-terminal acetylation of antimicrobial peptide L163 improves its stability against protease degradation. *J. Pept. Sci.* 27:e3337. doi: 10.1002/psc.3337
- Li, G., Lai, Z., and Shan, A. (2023). Advances of antimicrobial peptide-based biomaterials for the treatment of bacterial infections. *Adv Sci (Weinh)* 10:e2206602. doi: 10.1002/adv.202206602
- Li, J., Koh, J.-J., Liu, S., Lakshminarayanan, R., Verma, C. S., and Beuerman, R. W. (2017). Membrane active antimicrobial peptides: translating mechanistic insights to design. *Front. Neurosci.* 14:73. doi: 10.3389/fnins.2017.00073
- Li, R., He, S., Yin, K., Zhang, B., Yi, Y., Zhang, M., et al. (2021). Effects of N-terminal modifications on the stability of antimicrobial peptide SAMP-A4 analogues against protease degradation. *J. Pept. Sci.* 27:e3352. doi: 10.1002/psc.3352
- Li, S., Wang, Y., Xue, Z., Jia, Y., Li, R., He, C., et al. (2021). The structure-mechanism relationship and mode of actions of antimicrobial peptides: a review. *Trends Food Sci. Tech.* 109, 103–115. doi: 10.1016/j.tifs.2021.01.005
- Li, T., Wang, Z., Han, H., Teng, D., Mao, R., Hao, Y., et al. (2021). Potent intracellular antibacterial activity of a marine peptide-N6NH₂ and its D-enantiomer against multidrug-resistant *Aeromonas veronii*. *Appl. Microbiol. Biotechnol.* 105, 2351–2361. doi: 10.1007/s00253-021-11176-3
- Li, T., Yang, N., Teng, D., Mao, R., Hao, Y., Wang, X., et al. (2022). C-terminal mini-PEGylation of a marine peptide N6 had potent antibacterial and anti-inflammatory properties against *Escherichia coli* and *Salmonella* strains *in vitro* and *in vivo*. *BMC. Microbiol.* 22:128. doi: 10.1186/s12866-022-02534-w
- Ma, X., Yang, N., Mao, R., Hao, Y., Teng, D., Huang, Y., et al. (2024). Polylactic glycolic acid-mediated delivery of plectasin derivative NZ2114 in *Staphylococcus epidermidis* biofilms. *Antibiotics (Basel)* 13:228. doi: 10.3390/antibiotics130
- Maasch, J. R. M. A., Torres, M. D. T., Melo, M. C. R., and de la Fuente-Núñez, C. (2023). Molecular de-extinction of ancient antimicrobial peptides enabled by machine learning. *Cell Host Microbe* 31, 1260–1274.e6. doi: 10.1016/j.chom.2023.07.001
- Manteghi, R., Pallagi, E., Olajos, G., and Csóka, I. (2020). Pegylation and formulation strategy of anti-microbial peptide (AMP) according to the quality by design approach. *Eur. J. Pharm. Sci.* 144:105197. doi: 10.1016/j.ejps.2019.105197
- Mercer, D. K., and O'Neil, D. A. (2013). Peptides as the next generation of anti-infectives. *Future Med. Chem.* 5, 315–337. doi: 10.4155/fmc.12.213
- Mhlongo, J. T., Waddad, A. Y., Albericio, F., and De La Torre, B. G. (2023). Antimicrobial peptide synergies for fighting infectious diseases. *Adv. Sci. (Weinh)* 10:e2300472. doi: 10.1002/adv.202300472
- Mishra, B., Reiling, S., Zarena, D., and Wang, G. (2017). Host defense antimicrobial peptides as antibiotics: design and application strategies. *Curr. Opin. Chem. Biol.* 38, 87–96. doi: 10.1016/j.cbpa.2017.03.014
- Murray, C. J. L., Ikuta, K. S., Sharara, F., Swetschinski, L., Robles Aguilar, G., Gray, A., et al. (2022). Global burden of bacterial antimicrobial resistance in 2019: a systematic analysis. *Lancet* 399, 629–655. doi: 10.1016/S0140-6736(21)02724-0
- Payne, D. J., Miller, L. F., Findlay, D., Anderson, J., and Marks, L. (2015). Time for a change: addressing R&D and commercialization challenges for antibacterials. *Philos. Trans. R. Soc. Lond. B. Biol. Sci.* 370:20140086. doi: 10.1098/rstb.2014.0086
- Reffuveille, F., de la Fuente-Núñez, C., Mansour, S., and Hancock, R. E. (2014). A broad-spectrum antibiofilm peptide enhances antibiotic action against bacterial biofilms. *Antimicrob. Agents. Chemother.* 58, 5363–5371. doi: 10.1128/AAC.03163-14
- Sandín, D., Valle, J., Chaves-Arquero, B., Prats-Ejarque, G., Larrosa, M. N., González-López, J. J., et al. (2021). Rationally modified antimicrobial peptides from the N-Terminal domain of human RNase 3 show exceptional serum stability. *J. Med. Chem.* 64, 11472–11482. doi: 10.1021/acs.jmedchem.1c00795
- Santos-Júnior, C. D., Der Torossian Torres, M., Duan, Y., Del Rio, Á. R., Schmidt, T. S. B., Chong, H., et al. (2023). Computational exploration of the global microbiome for antibiotic discovery. *bioRxiv [Preprint]*. doi: 10.1101/2023.08.31.555663
- Sarkar, T., Chetia, M., and Chatterjee, S. (2021). Antimicrobial peptides and proteins: from nature's reservoir to the laboratory and beyond. *Front. Chem.* 18:691532. doi: 10.3389/fchem.2021.691532
- Schaal, J. B., Eriguchi, Y., Tran, D. Q., Tran, P. A., Hawes, C., Cabebe, A. E., et al. (2021). A host-directed macrocyclic peptide therapeutic for MDR gram negative bacterial infections. *Sci. Rep.* 11:23447. doi: 10.1038/s41598-021-02619-y
- Sharma, P., Kaur, J., Sharma, G., and Kashyap, P. (2022). Plant derived antimicrobial peptides: mechanism of target, isolation techniques, sources and pharmaceutical applications. *J. Food Biochem.* 46:e14348. doi: 10.1111/jfbc.14348
- Shwaiki, L. N., Lynch, K. M., and Arendt, E. K. (2021). Future of antimicrobial peptides derived from plants in food application – a focus on synthetic peptides. *Trends Food Sci. Tech.* 112, 312–324. doi: 10.1016/j.tifs.2021.04.010
- Silva, O. N., Torres, M. D. T., Cao, J., Alves, E. S. F., Rodrigues, L. V., Resende, J. M., et al. (2020). Repurposing a peptide toxin from wasp venom into anti-infectives with dual antimicrobial and immunomodulatory properties. *Proc. Natl. Acad. Sci. USA* 117, 26936–26945. doi: 10.1073/pnas.2012379117
- Tacconelli, E., Carrara, E., Savoldi, A., Harbarth, S., Mendelson, M., Monnet, D. L., et al. (2018). Discovery, research, and development of new antibiotics: the WHO priority list of antibiotic-resistant bacteria and tuberculosis. *Lancet Infect. Dis.* 18, 318–327. doi: 10.1016/S1473-3099(17)30753-3
- Takahashi, T., Kulkarni, N. N., Lee, E. Y., Zhang, L.-J., Wong, G. C. L., and Gallo, R. L. (2018). Cathelicidin promotes inflammation by enabling binding of self-RNA to cell surface scavenger receptors. *Sci. Rep.* 8:4032. doi: 10.1038/s41598-018-22409-3

- Teixeira, V., Feio, M. J., Rivas, L., De La Torre, B. G., Andreu, D., Coutinho, A., et al. (2010). Influence of lysine N(ε)-trimethylation and lipid composition on the membrane activity of the cecropin A-melittin hybrid peptide CA(1-7)M(2-9). *J. Phys. Chem. B* 114, 16198–16208. doi: 10.1021/jp106915c
- Thayer, A. M. (2011). Making peptides at large scale. *Chem. Eng. News* 89, 9–12. doi: 10.1021/cen-v089n022.p021
- Torres, M. D. T., Pedron, C. N., Higashikuni, Y., Kramer, R. M., Cardoso, M. H., Oshiro, K. G. N., et al. (2018). Structure-function-guided exploration of the antimicrobial peptide polybia-CP identifies activity determinants and generates synthetic therapeutic candidates. *Commun. Biol.* 1:221. doi: 10.1038/s42003-018-0224-2
- Torres, M. D. T., Sothiselvam, S., Lu, T. K., and de la Fuente-Nunez, C. (2019). Peptide design principles for antimicrobial applications. *J. Mol. Biol.* 431, 3547–3567. doi: 10.1016/j.jmb.2021.12.015
- Tram, N. D. T., Xu, J., Mukherjee, D., Obanel, A. E., Mayandi, V., Selvarajan, V., et al. (2022). Bacteria-responsive self-assembly of antimicrobial peptide nanonets for trap-and-kill of antibiotic-resistant strains. *Adv. Funct. Mater.* 33:2210858. doi: 10.1002/adfm.202210858
- Walsh, G. (2005). Therapeutic insulins and their large-scale manufacture. *Appl. Microbiol. Biotechnol.* 67, 151–159. doi: 10.1007/s00253-004-1809-x
- Wang, G. (2023). The antimicrobial peptide database is 20 years old: recent developments and future directions. *Protein Sci.* 32:e4778. doi: 10.1002/pro.4778
- Wang, G., Li, X., and Wang, Z. (2016). APD3: the antimicrobial peptide database as a tool for research and education. *Nucleic Acids Res.* 44, D1087–D1093. doi: 10.1093/nar/gkv1278
- Wang, H., Wu, H., Ciofu, O., Song, Z., and Høiby, N. (2012). *In vivo* pharmacokinetics/pharmacodynamics of colistin and imipenem in *Pseudomonas aeruginosa* biofilm infection. *Antimicrob. Agents Chemother.* 56, 2683–2690. doi: 10.1128/AAC.06486-11
- Wong, F., de la Fuente-Nunez, C., and Collins, J. J. (2023). Leveraging artificial intelligence in the fight against infectious diseases. *Science* 381, 164–170. doi: 10.1126/science.adh1114
- Xu, L., Shao, C., Li, G., Shan, A., Chou, S., Wang, J., et al. (2020). Conversion of broad-spectrum antimicrobial peptides into species-specific antimicrobials capable of precisely targeting pathogenic bacteria. *Sci. Rep.* 10:944. doi: 10.1038/s41598-020-58014-6
- Xuan, J., Feng, W., Wang, J., Wang, R., Zhang, B., Bo, L., et al. (2023). Antimicrobial peptides for combating drug-resistant bacterial infections. *Drug Resist. Updat.* 68:100954. doi: 10.1016/j.drug.2023.100954
- Yang, N., Aminov, R., Franco, O. L., de la Fuente-Nunez, C., and Wang, J. (2023). Editorial: community series in antimicrobial peptides: molecular design, structure function relationship and biosynthesis optimization. *Front. Microbiol.* 14:1125426. doi: 10.3389/fmicb.2023.1125426
- Yang, N., Zhang, Q., Mao, R., Hao, Y., Ma, X., Teng, D., et al. (2022). Effect of NZ2114 against *Streptococcus dysgalactiae* biofilms and its application in murine mastitis model. *Front. Microbiol.* 13:1010148. doi: 10.3389/fmicb.2022.1010148
- Zakaryan, H., Chilingaryan, G., Arabyan, E., Serobian, A., and Wang, G. (2021). Natural antimicrobial peptides as a source of new antiviral agents. *J. Gen. Virol.* 102:001661. doi: 10.1099/jgv.0.001661
- Zasloff, M. (2015). “Antimicrobial peptides: do they have a future as therapeutics?” in *Antimicrobial Peptides. Birkhäuser Advances in Infectious Diseases*, eds. J. Harder, and J. M. Schröder (Cham: Springer).
- Zhang, S., Yang, N., Mao, R., Hao, Y., Teng, D., and Wang, J. (2024). *In vitro/vivo* mechanisms of antibacterial peptide NZ2114 against *Staphylococcus pseudintermedius* and its biofilms. *Antibiotics (Basel)* 13:341. doi: 10.3390/antibiotics13040341
- Zhang, T., Wang, Z., Hancock, R. E., de la Fuente-Núñez, C., and Haapasalo, M. (2016). Treatment of oral biofilms by a D-Enantiomeric peptide. *PLoS ONE* 11:e0166997. doi: 10.1371/journal.pone.0166997
- Zhang, Y., Teng, D., Mao, R., Wang, X., Xi, D., Hu, X., et al. (2014). High expression of a plectasin-derived peptide NZ2114 in *Pichia pastoris* and its pharmacodynamics, postantibiotic and synergy against *Staphylococcus aureus*. *Appl. Microbiol. Biotechnol.* 98, 681–694. doi: 10.1007/s00253-013-4881-2
- Zheng, X., Yang, N., Mao, R., Hao, Y., Teng, D., and Wang, J. (2022). Pharmacokinetics and pharmacodynamics of fungal defensin NZX against *Staphylococcus aureus*-induced mouse peritonitis model. *Front. Microbiol.* 13:865774. doi: 10.3389/fmicb.2022.865774
- Zheng, X., Yang, N., Mao, R., Hao, Y., Teng, D., and Wang, J. (2024). Pharmacokinetics and pharmacodynamics of antibacterial peptide NZX in *Staphylococcus aureus* mastitis mouse model. *Appl. Microbiol. Biotechnol.* 13:260. doi: 10.1007/s00253-024-13101-w
- Zong, X., Fu, J., Xu, B., Wang, Y., and Jin, M. (2020). Interplay between gut microbiota and antimicrobial peptides. *Anim. Nutr.* 6, 389–396. doi: 10.1016/j.aninu.2020.09.002
- Zou, P., Chen, W. T., Sun, T., Gao, Y., Li, L. L., and Wang, H. (2020). Recent advances: peptides and self-assembled peptide-nanosystems for antimicrobial therapy and diagnosis. *Biomater. Sci.* 8, 4975–4996. doi: 10.1039/D0BM00789G



OPEN ACCESS

EDITED BY

Yue Qu,
The Alfred Hospital,
Australia

REVIEWED BY

Jianhua Wang,
Chinese Academy of Agricultural Sciences
(CAAS), China
Lisa Lombardi,
University College Dublin,
Ireland

*CORRESPONDENCE

Maria Rapala-Kozik
✉ maria.rapala-kozik@uj.edu.pl

[†]These authors share first authorship

SPECIALTY SECTION

This article was submitted to
Antimicrobials, Resistance and
Chemotherapy,
a section of the journal
Frontiers in Microbiology

RECEIVED 20 September 2022

ACCEPTED 28 December 2022

PUBLISHED 13 January 2023

CITATION

Guevara-Lora I, Bras G, Juszczak M,
Karkowska-Kuleta J, Gorecki A,
Manrique-Moreno M, Dymek J, Pyza E,
Kozik A and Rapala-Kozik M (2023)
Cecropin D-derived synthetic peptides in
the fight against *Candida albicans* cell
filamentation and biofilm formation.
Front. Microbiol. 13:1045984.
doi: 10.3389/fmicb.2022.1045984

COPYRIGHT

© 2023 Guevara-Lora, Bras, Juszczak,
Karkowska-Kuleta, Gorecki,
Manrique-Moreno, Dymek, Pyza, Kozik and
Rapala-Kozik. This is an open-access article
distributed under the terms of the [Creative
Commons Attribution License \(CC BY\)](#). The
use, distribution or reproduction in other
forums is permitted, provided the original
author(s) and the copyright owner(s) are
credited and that the original publication in
this journal is cited, in accordance with
accepted academic practice. No use,
distribution or reproduction is permitted
which does not comply with these terms.

Cecropin D-derived synthetic peptides in the fight against *Candida albicans* cell filamentation and biofilm formation

Ibeth Guevara-Lora^{1†}, Grazyna Bras^{2†}, Magdalena Juszczak²,
Justyna Karkowska-Kuleta², Andrzej Gorecki³,
Marcela Manrique-Moreno⁴, Jakub Dymek⁵, Elzbieta Pyza⁵,
Andrzej Kozik¹ and Maria Rapala-Kozik^{2*}

¹Department of Analytical Biochemistry, Faculty of Biochemistry, Biophysics and Biotechnology, Jagiellonian University, Krakow, Poland, ²Department of Comparative Biochemistry and Bioanalytics, Faculty of Biochemistry, Biophysics and Biotechnology, Jagiellonian University, Krakow, Poland, ³Department of Physical Biochemistry, Faculty of Biochemistry, Biophysics and Biotechnology, Jagiellonian University, Krakow, Poland, ⁴Chemistry Institute, Faculty of Exact and Natural Sciences, University of Antioquia, Medellin, Colombia, ⁵Department of Cell Biology and Imaging, Institute of Zoology and Biomedical Research, Jagiellonian University, Krakow, Poland

The recent progressive increase in the incidence of invasive fungal infections, especially in immunocompromised patients, makes the search for new therapies crucial in the face of the growing drug resistance of prevalent nosocomial yeast strains. The latest research focuses on the active compounds of natural origin, inhibiting fungal growth, and preventing the formation of fungal biofilms. Antimicrobial peptides are currently the subject of numerous studies concerning effective antifungal therapy. In the present study, the antifungal properties of two synthetic peptides ($\Delta M3$, $\Delta M4$) derived from an insect antimicrobial peptide – cecropin D – were investigated. The fungicidal activity of both compounds was demonstrated against the yeast forms of *Candida albicans*, *Candida tropicalis*, and *Candida parapsilosis*, reaching a MFC_{99.9} in the micromolar range, while *Candida glabrata* showed greater resistance to these peptides. The scanning electron microscopy revealed a destabilization of the yeast cell walls upon treatment with both peptides; however, their effectiveness was strongly modified by the presence of salt or plasma in the yeast environment. The transition of *C. albicans* cells from yeast to filamentous form, as well as the formation of biofilms, was effectively reduced by $\Delta M4$. Mature biofilm viability was inhibited by a higher concentration of this peptide and was accompanied by increased ROS production, activation of the *GPX3* and *SOD5* genes, and finally, increased membrane permeability. Furthermore, both peptides showed a synergistic effect with caspofungin in inhibiting the metabolic activity of *C. albicans* cells, and an additive effect was also observed for the mixtures of peptides with amphotericin B. The results indicate the possible potential of the tested peptides in the prevention and treatment of candidiasis.

KEYWORDS

antimicrobial peptides, cecropin, *Candida*, candidiasis, biofilm

1. Introduction

The development of infections caused by *Candida* species consistently represents a serious threat, especially in individuals with different immunodeficiencies. Candidiasis are generally treated with drugs such as azoles, polyenes, pyrimidine analogs, and echinocandins (Lee et al., 2021). However, when applied to *Candida* clinical isolates, the effectiveness of these drugs decreases significantly. The constant emergence of fungal strains resistant to classical treatment has prompted the search for new drugs for *Candida* infections, particularly among products of natural origin, including those from plants, insects, algae, etc. (Aldholmi et al., 2019; Guevara-Lora et al., 2020). These active substances include also antimicrobial peptides (AMPs), many of which have also shown antifungal activity (Bondaryk et al., 2017; Huan et al., 2020). A group of peptides that currently attracts particular attention for their potential role in the fight against candidiasis is cecropins (Brady et al., 2019). These peptides, identified currently in various insects, were originally isolated from the hemolymph of the *Hyalophora cecropia* moth (Boman et al., 1991) and are actually classified into several subfamilies – cecropins A, B, C, D, E and cecropin-like peptides (Romoli et al., 2017; Peng et al., 2019). These α -helical AMPs generally possess a strongly basic N-terminal region linked to a more hydrophobic C-terminal region through a segment rich in proline and glycine residues and their antimicrobial properties are attributed to their specific chemical structure (Boman et al., 1991; Sato and Feix, 2006). The presence of aromatic residues such as tryptophan and phenylalanine in the amphipathic N-terminal helix was shown to be essential for peptide-pathogen interactions, with subsequent permeabilization of the inner membrane of Gram-negative bacteria (Lee et al., 2015). The hydrophobic C-terminal region synergistically enhances this effect through the interaction with hydrophobic cell membrane. Although cecropins and cecropin-like peptides are more efficient in fighting Gram-negative microorganisms, the antimicrobial effects have also been shown for a broad range of Gram-positive bacteria (for a review, see Brady et al., 2019). Their activity against yeasts and other fungi was also proven, but the effects observed were not satisfactory. Most of the peptides demonstrating anticandidal activity belonged to the cecropin A or B subfamilies and required high concentration doses for effective action. Nevertheless, it was also shown that the use of analogs of these peptides could improve their antifungal properties (De Lucca et al., 2000; Ji et al., 2014), as certain modifications of the peptides, including the substitution of selected amino acid residues with tryptophan or D-amino acids, resulted in improved fungicidal activity due to the increased resistance to microbial proteolysis.

Promising antimicrobial properties were also previously reported for the cecropin D-like peptide (UniProtKB accession number: P85210) from the greater wax moth *Galleria mellonella* (Cytrynska et al., 2007). Modification of particular residues resulting in an increase of peptide charge and basic residues on the polar face of the molecule compared to a neutral wild-type peptide, enhanced the antibacterial activity of peptides derived from the cecropin D-like natural sequence. One such type of derivative was the synthetic cationic peptide Δ M2 with 39 amino acid residues and a charge of +9, which acts most effectively against Gram-negative bacteria (Oñate-Garzón et al., 2017). The necessity to continue the search for derivatives with enhanced antimicrobial properties, extended also to other bacterial and fungal pathogens, has led to further modifications. In this study, the anticandidal potential of two synthetic peptides specified as Δ M3 (NFFKRIRIRAGKRIRKAIISA) and Δ M4 (NFFKRIRRAWKRIWKWIYSA), composed of 20 amino acids and derived from the N-terminal fragments of Δ M2, was analyzed. The Δ M3 peptide has a charge of +8 at physiological pH and was previously demonstrated to possess a high antimicrobial activity against *Staphylococcus aureus* and low hemolytic activity in human erythrocytes (Manrique-Moreno et al., 2021). The Δ M4 peptide with additional substitution of selected amino acids by three tryptophan and one tyrosine residues and a charge of +7 at physiological pH, presented anticancer properties against human melanoma cells (Santa-González et al., 2020). The helical-wheel projection of Δ M3 and Δ M4 and the predicted α -helical structure of the peptides generated with I-TASSER V5.1 software were presented in previous reports (Santa-González et al., 2020; Manrique-Moreno et al., 2021).

The main aim of this study was first to evaluate the fungicidal activity of Δ M3 and Δ M4 peptides against *Candida* species determining the minimal fungicidal concentration (MFC). Subsequently, the effects of different concentrations of peptides on *Candida albicans* hyphae, biofilm formation, and mature biofilm eradication were investigated. The mechanism of action of peptides was verified by examining the permeabilization of fungal cell membranes, pore formation, and occurrence of oxidative stress and apoptosis. Finally, a potential synergism of the tested peptides with conventional antifungal drugs was analyzed.

2. Materials and methods

2.1. Peptides

Peptides Δ M3 (NFFKRIRIRAGKRIRKAIISA) and Δ M4 (NFFKRIRRAWKRIWKWIYSA), both synthesized by the

solid-phase method, were purchased from GenScript (Piscataway, NJ, United States). Purity of the peptides was verified by analytical high performance liquid chromatography (HPLC) and MALDI-TOF mass spectrometry and was determined as >95% for both peptides.

2.2. Circular dichroism

Peptides at concentration of 1 mg/ml, diluted in 10 mM HEPES pH 7.0 or PBS, without or with 2,2,2-trifluoroethanol (TFE, Sigma-Aldrich, St Louis, MO, United States) at concentrations in the range of 5–25% (commonly used to stabilize secondary structure of polypeptides), and diluted in 10 mM HEPES pH 7.0 with 30 mM SDS (BioShop Canada Inc., Burlington, Canada) (to mimic anionic environment) were prepared. Peptides diluted in 10 mM HEPES pH 7.0 with NaCl at concentrations in the range of 50–200 mM were used to analyze the effect of salt ions on the peptide secondary structure. Circular dichroism (CD) measurements were conducted using a J-715 spectropolarimeter (Jasco, Tokyo, Japan) equipped with an F25 temperature control unit (Julabo, Seelbach, Germany) in quartz cuvettes of 0.01 cm path-length (Hellma, Jena, Germany) at 30°C. The spectra were recorded in the range of 195–250 nm with 1 nm data pitch, 20 nm/min scanning speed, 4 s integrating time, and 2 nm bandwidth and averaged over five acquisitions. All spectra were corrected for the effect from the buffer and all measurements were converted to molar residual ellipticity units. Secondary structure content was determined using JSE program (Jasco) using CD spectra of α -chymotrypsin A, hemoglobin, lysozyme, myoglobin and ribonuclease A as protein references.

2.3. Yeast strains and culture conditions

Candida albicans strain 3147 (ATCC® 10231™), *Candida tropicalis* strain T1 (ATCC® MYA-3404™), *Candida parapsilosis* strain CDC 317 (ATCC® MYA-4646™) and *Candida glabrata* strain CBS138 (ATCC® 2001™) were purchased from the American Type Culture Collection (ATCC) (Manassas, VA, United States). Yeast cells (5×10^5 /ml at the start) were routinely cultured in YPD medium (1% yeast extract, 2% soybean peptone and 2% glucose) (Sigma-Aldrich) for 18 h at 30°C with shaking (170 rpm) using an orbital rotary shaker MaxQ 6000 (ThermoFisher Scientific, Waltham, MA, United States). Before each experiment, fungal cells were washed three times with the appropriate buffer – phosphate buffered saline pH 7.4 (PBS; Biowest, Nuaille, France) or 10 mM HEPES pH 7.0 with 5 mM glucose (HEPES/glucose) – and optical density at 600 nm (OD) was measured to estimate the number of cells. To determine the number of colony forming units (CFUs) per ml after treatment with peptide, fungal cells were cultured on solid YPD medium containing 1.5% agar for 24 h at 30°C. Due to the complex

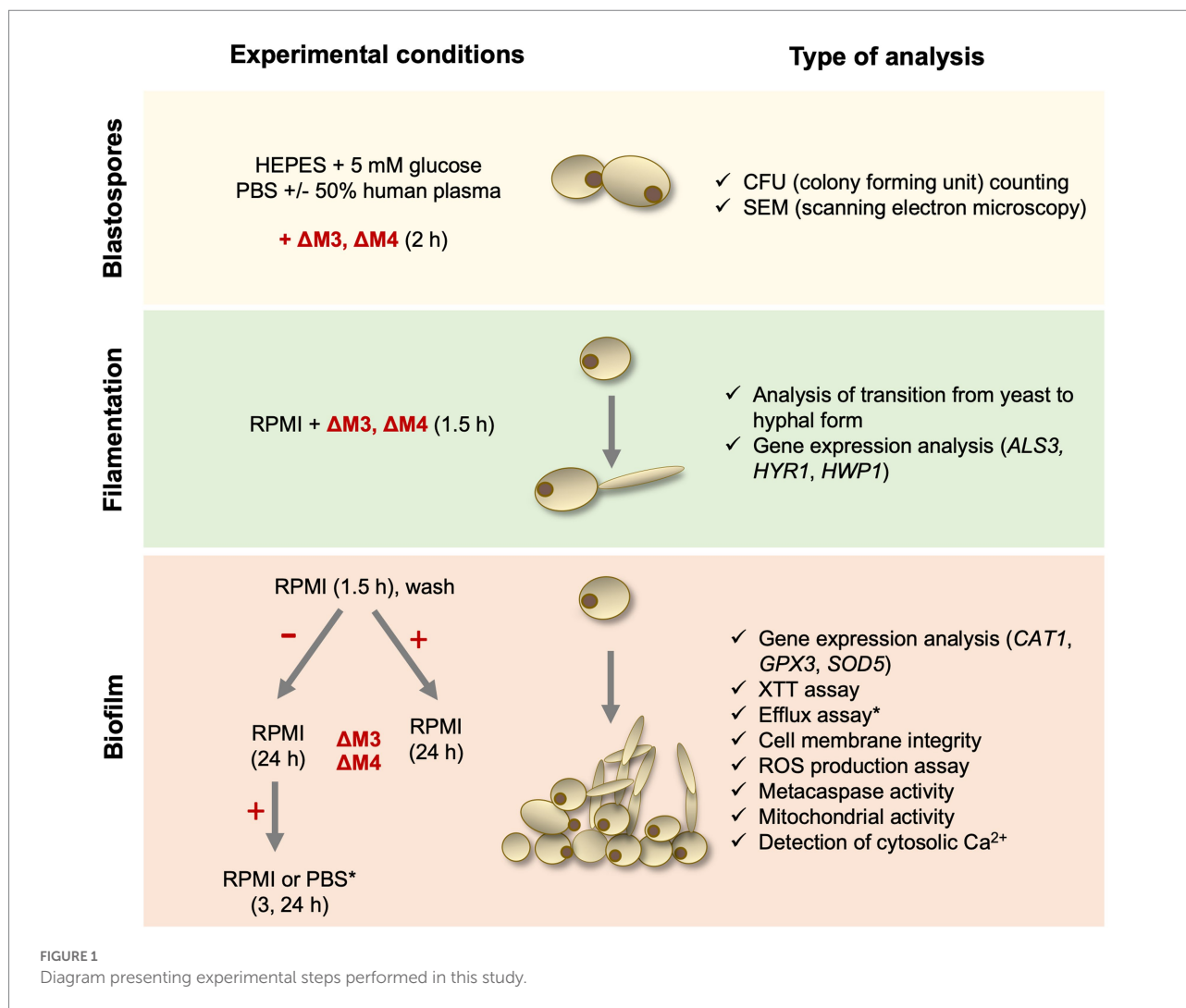
experimental setup of this study, a diagram showing the consecutive steps of the experiments is presented (Figure 1).

2.4. Fungicidal activity against *Candida* yeast cells

The analysis of fungicidal activity of Δ M3 and Δ M4 peptides was performed as previously described (Bochenska et al., 2016; van Dijck et al., 2018) with minor modifications. Briefly, 1×10^5 yeast cells of *C. albicans* were incubated in 100 μ l of Δ M3 or Δ M4 solution at concentrations in the range of 0.4–100 μ M in 10 mM HEPES pH 7.0, 10 mM HEPES pH 7.0 with 5 mM glucose, PBS or PBS with 50% of human plasma for 2 h at 30°C with shaking (110 rpm) in Eppendorf tubes. Additionally, cells from each strain were incubated in the buffer without peptides under the same conditions. After incubation, 10 μ l of the cell suspensions undiluted and diluted (10 and 100-fold) with PBS or sterile water were plated to the YPD agar dishes for determination of CFUs. Similar experiments with yeast cells of *C. parapsilosis*, *C. tropicalis* or *C. glabrata* were performed in 10 mM HEPES pH 7.0 with 5 mM glucose with peptides in the same range of concentrations. The experiments were performed independently at least three times in triplicates. The minimal fungicidal concentrations – MFC₉₀ and MFC_{99.9} that cause mortality of 90 or 99.9% of fungi, respectively, were determined.

2.5. Analysis of cell surface morphology of *Candida albicans* yeast cells by scanning electron microscopy (SEM)

Candida albicans yeast cells (1×10^6 /ml) obtained after 16 h of growth in YPD medium were incubated for 2 h at 30°C in a solution of peptides Δ M3 (1.6 μ M) and Δ M4 (3.1 μ M) in HEPES/glucose. Cells incubated under the same conditions, but without peptides, served as an untreated control. The preparation of the cells for observation with scanning electron microscopy (SEM) was performed similarly to that described by Staniszevska et al. (2013) with minor modifications. Briefly, *C. albicans* cells were fixed overnight at 4°C in 2.5% glutaraldehyde (Sigma-Aldrich) on round coverslips (\varnothing 13 mm, Bionovo, Legnica, Poland) precoated with 0.001% poly-L-lysine (Sigma-Aldrich), and then washed five times with 0.1 M phosphate buffer, pH 7.2. The further steps included incubation of specimens in 2% osmium tetroxide (Sigma-Aldrich) for 2 h at room temperature and dehydration in a series of ethanol solutions (Lineal Chemicals, Poland), starting from 10 min twice in 50 and 70%, followed by 5 min twice in 95% and 1 min twice in 100% ethanol solution. The samples were then dehydrated with acetone (Merck, Darmstadt, Germany) twice for 30 s, dried by the critical point method in liquid CO₂ using an E300 critical point dryer (Quorum Technologies, East Sussex, United Kingdom) and coated with gold in a vacuum evaporator JEOL JFC-1100E (JEOL Ltd., Tokyo, Japan). Visualization was



performed at an accelerating voltage of 20kV with the Hitachi S-4700 scanning electron microscope (Hitachi, Tokyo, Japan) in the Laboratory of Scanning Electron Microscopy and Microanalysis, Institute of Geological Sciences, Jagiellonian University, Krakow, Poland.

2.6. Microscopic analysis of *Candida albicans* transition from yeast to hyphal form

Candida albicans yeast cells (1×10^5 per well) were suspended in 100 μ l of RPMI 1640 medium (Biowest) containing peptides at concentrations in the range of 3.1–50 μ M and 0.8–6.2 μ M for Δ M3 and Δ M4, respectively, and placed in triplicates into the wells of 96-well black/clear flat bottom polystyrene high binding microplate (Corning Inc., Corning, NY, United States). Fungal cells were also suspended in medium without peptide as a control of the correct morphological transition. The incubation was carried out at 37°C in an atmosphere of 5% CO₂ and 95% humidity

for 90 min without shaking. Subsequently, fungal cells were stained with Calcofluor White (Sigma-Aldrich) at a final concentration of 1 μ g/ml and Sytox Orange (ThermoFisher Scientific, Waltham, MA, United States) at a final concentration of 1 μ M for 10 min in the dark. *C. albicans* cells were visualized using an Olympus IX73 microscope (Olympus, Tokyo, Japan) equipped with a Hamamatsu Orca Spark camera (Hamamatsu, Hamamatsu City, Japan) and a UPLXAPO60XO lens (Olympus), and the images were analyzed using Olympus CellSens Dimension 3.1 software. To determine the length of the hyphae, three images were taken in each well (40 \times magnification) and for each image the length of the hyphae was measured for 20 cells.

2.7. Gene expression analysis

The expression of genes characteristic for the filamentous form of *C. albicans* – encoding agglutinin-like protein 3 (*ALS3*), hyphally regulated cell wall protein 1 (*HYR1*) and hyphal wall protein 1 (*HWP1*) was analyzed after the isolation of total RNA

from cells prepared as follows. Yeast cells (2×10^7) were seeded in plates ($\varnothing 10$ cm) with 10 ml of RPMI medium in the presence of $\Delta M3$ (at concentrations of 12.5 μM and 25 μM), $\Delta M4$ (at concentrations of 1.2 μM and 2.1 μM) and without peptide. Two plates were prepared for each sample. After 90 min of incubation at 37°C in an atmosphere of 5% CO₂ and 95% humidity, cells were harvested, washed with PBS and frozen in liquid nitrogen. The expression of genes associated with the generation of oxidative stress (encoding catalase – *CAT1*, glutathione peroxidase – *GPX3*, superoxide dismutase 5 – *SOD5*) was analyzed in mature biofilms. Briefly, yeast cells (5×10^7) were seeded in plates ($\varnothing 10$ cm) with 10 ml of RPMI medium and incubated for 24 h at 37°C in an atmosphere of 5% CO₂ and 95% humidity. Subsequently, the medium was changed to a fresh medium supplemented with 50 μM $\Delta M3$, 6.2 μM $\Delta M4$ or without peptide and the biofilms were incubated for 3 h at 37°C. Two plates were prepared for each sample. The concentration chosen for the analysis of gene expression resulted from the need to perform experiments on living cells in order to obtain undegraded mRNA. Cells were prepared for RNA isolation as described below.

Total RNA from cells was isolated with Tri Reagent (Merck Millipore, Burlington, MA, United States) according to a standard procedure preceded by cell homogenization in the Precellys® Evolution tissue homogenizer (Bertin Technologies SAS, Montigny-le Bretonneux, France). cDNA was synthesized with the M-MLV Reverse Transcriptase kit (Promega, Madison, WI, United States) according to the manufacturer's instructions. The expression of the selected genes was quantified with the QuantStudio™ 3 Real-Time PCR System (ThermoFisher Scientific). cDNA amplification was performed at an annealing temperature of 58°C using Kappa SYBR Green Master Mix (Merck Millipore) with specific primers (Table 1). Some primers were projected and verified with Primer3, OligoAnalyzer, and BLAST software. Relative gene expression was determined using the $2^{-\Delta\Delta Ct}$ method normalized to the expression of the *ACT1* housekeeping gene.

2.8. Formation of biofilms

Candida albicans biofilms were formed generally in 96-well black/clear flat bottom polystyrene high binding microplate

(Corning Inc.) after seeding the cells (1×10^5) in 100 μl of RPMI 1640, followed by incubation for 90 min at 37°C in an atmosphere of 5% CO₂ and 95% humidity, without shaking to allow cell adhesion. Then non-adherent cells were removed by gentle washing with 200 μl of PBS and 100 μl of fresh RPMI 1640 were added to sessile *C. albicans* cells for further incubation under the same conditions for 24 h to allow formation of the biofilm.

2.9. Antibiofilm assay

To determine the impact of peptides on the formation of biofilm, adherent cells, gently washed as described above, were incubated with peptides at a concentration range of 0.4–100 μM in 100 μl of RPMI medium for 24 h at 37°C in an atmosphere of 5% CO₂ and 95% humidity. After this time biofilms were washed, and the biofilm metabolic activity was assessed. To examine the effect of peptides on the eradication of the 24-h developed biofilm, a method previously described (Roschetto et al., 2018) was used. The 24-h biofilms (prepared as described above) were washed twice with 200 μl of PBS and then further incubated for 24 h at 37°C in an atmosphere of 5% CO₂ and 95% humidity, with 100 μl of RPMI 1640 medium (control) or with $\Delta M3$ or $\Delta M4$ at a concentration ranging from 1.6 μM to 100 μM in the same medium. After incubation, the biofilms were washed twice with 200 μl of PBS and the metabolic activity of *C. albicans* was measured using the XTT reduction test. All experiments were carried out in triplicate.

2.10. Analysis the metabolic activity of *Candida albicans* cells

To determine the viability of *C. albicans*, the 2,3-bis(2-methoxy-4-nitro-5-sulfo-phenyl)-2H-tetrazolium-5-carboxanilide (XTT) (ThermoFisher Scientific) reduction assay is used as a routine tool for quantitative measurement of fungal metabolic activity, growth and response to antifungal treatment (van Dijk et al., 2018). The tests were performed as described (Kulig et al., 2022) with some modifications. Briefly, 100 μl of RPMI 1640 medium without phenol red (Biowest) and 50 μl of XTT solution

TABLE 1 The list of primers used for quantification of genes for: *ACT1* – actin; *ALS3* – agglutinin-like protein 3; *CAT1* – catalase; *GPX3* – glutathione peroxidase; *HYR1* – hyphally regulated cell wall protein 1; *HWP1* – hyphal wall protein 1; *SOD5* – superoxide dismutase 5.

Gene	Primer forward 5'→3'	Primer reverse 5'→3'	Reference
<i>ACT1</i>	GATTTTGTCTGAACGTGGTTAACAG	GGAGTTGAAAGTGGTTGGTCAATAC	Wolak et al. (2015)
<i>ALS3</i>	TGCTGGTGGTTATTGGCAAC	GTCGCGGTTAGGATCGAATG	Bartnicka et al. (2019)
<i>CAT1</i>	TGGTGGTGAATTAGGTTCTGC	GTGAGTTTCTGGGTTTCTCTT	Wolak et al. (2015)
<i>GPX3</i>	TTCACCTCCACAATACAAAGGT	TTCATTAGTTCACGGTTCTTG	This work
<i>HYR1</i>	TTGTTTGCGTCATCAAGACTTTG	GTCTTCATCAGCAGTAACACAACCA	Tsang et al. (2012)
<i>HWP1</i>	TCAACTGCTCAACTTATTGCT	GCTTCCTCTGTTTCACCTTG	Bartnicka et al. (2019)
<i>SOD5</i>	ATCTTACATTGGCGGTTTAT	GACCATTTACTACTGCTCTCTCA	This work

(1 mg/ml; Invitrogen, Waltham, MA, United States), freshly activated with phenazine methosulfate (5 µg/ml; Sigma-Aldrich) in the same medium, were added to *C. albicans* cells. After 40 min of incubation at 37°C in the dark, 100 µl of supernatants were transferred to the wells of a new 96-well microplate (Sarstedt, Nümbrecht, Germany). The absorbance of the formazan product was measured spectrophotometrically at 450 nm using a Synergy H1 microplate reader (BioTek Instruments, Winooski, VT, United States).

2.11. Analysis of the cell membrane integrity in the mature biofilm

To determine the impact of peptides on the integrity of *C. albicans* membranes in the mature biofilm, two types of permeabilization assays were performed. In one of them, 24-h biofilms were washed with 200 µl of PBS and then incubated with peptides diluted in RPMI at concentrations in the range of 12.5 µM to 100 µM (Δ M3) and 3.1 µM to 12.5 µM (Δ M4) for 24 h at 37°C in an atmosphere of 5% CO₂ and 95% humidity. After incubation, the biofilms were stained with Sytox™ Orange Nucleic Acid Stain (Invitrogen) at a final concentration of 1 µM in the dark for 5 min and visualized using an Olympus IX73 microscope. All images were taken and presented using the same parameters (exposure time, spectrum range), which enabled comparison of the fluorescence of the dye between different preparations. The photographs were taken in the form of the Z-stacks and subjected to the process of 3D deconvolution.

The second type of experiment was performed as described previously by [Do Nascimento Dias et al. \(2020\)](#). The 24-h biofilms were washed three times with 200 µl of PBS and then incubated in 100 µl of PBS for 2 h at 37°C. After this time, 100 µl solution of Rhodamine 6G (Sigma-Aldrich) in PBS (final dye concentration – 10 µM) was added to the wells and the biofilms were incubated for additional 30 min under the same conditions. To remove non-internalized dye, the wells were washed four times with PBS. Then 100 µl of peptide solutions were added to biofilms at concentrations in the range of 1.6 µM to 100 µM in PBS and incubated for 24 h at 37°C in an atmosphere of 5% CO₂ and 95% humidity. The untreated biofilms served as controls. After incubation, the supernatants were transferred to the new black microplate and the fluorescence intensity was measured using a Synergy H1 microplate reader with excitation at 550 nm and emission at 580 nm.

2.12. Metacaspase activity

Metacaspase activity was determined using the fluorescent method described previously ([Shirazi and Kontoyiannis, 2015](#)) with minor modifications. Briefly, the 24-h biofilm of *C. albicans* was formed in 96 well glass-like microplate (Cellvis, Sunnyvale, CA, United States) and incubated for 24 h at 37°C with Δ M3 or

Δ M4 at concentrations in the range of 3.1–12.5 µM or 12.5–100 µM, respectively, diluted in 100 µl of RPMI 1640. After incubation, the biofilms were washed three times with 200 µl of PBS and stained with CaspACE™ FITC-VAD-FMK *In Situ* Marker (Promega, Madison, WI, United States) at a final concentration of 10 µM for 1 h at room temperature in the dark. The biofilms were washed four times with PBS and the activity of metacaspase was analyzed using the Olympus IX73 microscope.

2.13. ROS production assay

The generation of intracellular reactive oxygen species (ROS) by *C. albicans* was determined using a method based on the measurement of the fluorescence of oxidized dihydrorhodamine 123 (DHR 123). The 24-h biofilms of *C. albicans*, formed as described above, were washed with PBS and then incubated with 100 µl of RPMI 1640 medium (untreated control), or solutions of Δ M3 (50 µM), Δ M4 (6.2 µM), or amphotericin B (2.7 µM; positive control) (Biowest) prepared in RPMI 1640 medium. For the analysis of ROS production, the concentration of peptides corresponding to the apoptotic effect observed with the activity of metacaspases was selected. The incubation was carried out for 3 h at 37°C. Biofilms were then washed with PBS and incubated with non-fluorescent DHR 123 (Invitrogen) at a final concentration of 10 µM for 30 min at 37°C. The fluorescence of oxidized DHR 123 (rhodamine 123) was measured with excitation at 488 nm and emission at 525 nm using a Synergy H1 microplate reader.

2.14. Determination of mitochondrial activity

The 24-h biofilms of *C. albicans* were incubated with 100 µl of Δ M3 (50 µM) or Δ M4 (6.2 µM) and amphotericin B (2.7 µM; positive control) solutions in RPMI 1640 medium for 3 h at 37°C. After that time, biofilms were washed with 200 µl of PBS and incubated for 30 min at 37°C with MitoTracker Green TM dye (Invitrogen) at final concentration of 500 nM, used to detect the change in total mitochondrial mass, and MitoTracker Orange (500 nM), used to detect the change in mitochondrial activity. Mitochondria were imaged in the FITC and TRIC channel, using the Olympus IX73 microscope.

2.15. Detection of cytosolic Ca²⁺

Accumulation of cytosolic Ca²⁺ was measured with the Fura-2 Calcium Flux Assay Kit (Abcam, Cambridge, Great Britain). The 24-h biofilms of *C. albicans* were incubated for 3 h with 100 µl of Δ M3 (25 µM and 50 µM) or Δ M4 (6.2 µM and 12.5 µM) and H₂O₂ (10 mM; positive control) solutions prepared in RPMI 1640. The concentration of peptides was chosen close to those for which the effect of apoptosis was obtained in

experiments analyzing the activity of metacaspases. After incubation, biofilms were washed with Hanks Balanced Salt Solution (Biowest) with Pluronic® F127 Plus (Abcam). Then 100 µl of Fura-2 AM solution was added to the biofilms and incubated for 1 h at room temperature. The fluorescence was then measured using a Synergy H1 microplate reader with excitation at 340 nm and emission at 510 nm.

2.16. Actions of $\Delta M3$ and $\Delta M4$ peptides mixed with conventional antifungal drugs

The following concentrations of peptides and antifungal drugs were used for the assay: $\Delta M3$ 0.4–50 µM, $\Delta M4$ 0.4–3.1 µM, amphotericin B 0.2–1.6 µM, fluconazole 0.2–1.6 µM and caspofungin 0.003–0.2 µM (the latter two from Sigma-Aldrich). The combinatory effects of each peptide and each conventional antimycotic drug were tested by the previously described checkerboard method (Guo et al., 2008; Do Nascimento Dias et al., 2020) with minor modification. *C. albicans* cells (3×10^2) were suspended in 100 µl of RPMI 1640 medium, containing peptide, drug, or their combination, in wells of Falcon® 96-well clear flat bottom TC-treated culture microplate (Corning). Fungal cells only in RPMI 1640 medium without peptides and drugs served as a control. Incubation was carried out for 24 h at 37°C in an atmosphere of 5% CO₂ and 95% humidity without shaking. After this time, cell viability was measured using an XTT reduction assay. The analysis was performed in biological triplicate. For each combination, Fractional Inhibitory Concentration Index (FICI) was determined using the following formula:

$$FICI = FICa + FICb$$

Where FICa is the ratio of IC₅₀ value for the compound a in combination to the IC₅₀ value of the agent a alone; FICb is the ratio of IC₅₀ value for compound b in combination to the IC₅₀ value of the agent b alone.

The FICI ≤ 0.5 was interpreted as a synergistic effect, $0.5 < FICI \leq 1.0$ as additive, $1.0 < FICI \leq 2.0$ as indifferent and $FICI > 2.0$ as antagonism.

2.17. The effect of $\Delta M3$ and $\Delta M4$ on human dermal fibroblasts

The toxicity of the peptides was analyzed on primary human dermal fibroblasts (HDF) obtained from Cell Applications Inc. (San Diego, CA, United States). Cells (1×10^5), seeded in a microplate, were treated with peptides with a concentration in the range of 1.6–100 µM for 24 h in culture HDF basal medium (Cell Applications Inc.). After this time, cell viability was assessed with the Alamar blue test (ThermoFisher Scientific). Briefly, after medium removal, 100 µl of Alamar blue reagent were added and after 1 h of incubation the fluorescence was measured with

excitation at 560 nm and emission at 590 nm with Synergy H1 microplate reader.

2.18. Statistical analysis

Statistical analysis was performed with the GraphPad Prism 8 software (GraphPad Software, San Diego, CA, United States). To evaluate the significance between groups, the t-test or one-way ANOVA with Dunnett's multiple comparison *post hoc* test was performed. The results were considered statistically significant at value of $p < 0.05$: * $p \leq 0.05$, ** $p < 0.01$, *** $p < 0.005$, **** $p < 0.0001$ or not statistically significant (ns) for $p > 0.05$.

3. Results

3.1. Synthetic peptides $\Delta M3$ and $\Delta M4$ possess fungicidal activity

The interaction between antimicrobial peptides and the pathogen cell wall plays an important role in their fungicidal activity. The achieved effect depends, among others, on environmental factors such as pH, the presence of salt or the presence of substances that can change the hydrophobicity of the peptide (Kandasamy and Larson, 2006). To test the influence of the environment on the fungicidal activity of two cationic peptides, $\Delta M3$ and $\Delta M4$, the viability of *C. albicans* cells was analyzed in the presence of some commonly used media: HEPES buffer supplemented with 5 mM glucose (HEPES/glucose) and PBS without or with 50% human plasma. The peptides showed different activity against *Candida* cells depending on the conditions used (Figure 2). The $\Delta M4$ peptide, which is more hydrophobic, was active in the presence of PBS or HEPES/glucose, while the $\Delta M3$ peptide was active only in the HEPES/glucose. Both peptides, $\Delta M3$ and $\Delta M4$ incubated in HEPES/glucose had a strong fungicidal effect against *C. albicans* after 2 h of incubation at concentrations of 1.6 µM and 3.1 µM, respectively. Peptide $\Delta M4$ in PBS caused a weaker effect compared to that in HEPES/glucose.

To clarify the observed effect of both peptides on fungal cell viability, peptide structural studies were performed using circular dichroism measurements (Figure 3; Supplementary Figure S1). In this analysis, we used TFE (2,2,2-trifluoroethanol) as a cosolvent that promotes the stability of the peptide helical structure (Maisetta et al., 2008; Górecki et al., 2015). Nonetheless, upon contact with the fungal cell surface, hydrophobic interactions may also be primary forces driving the formation of the secondary peptide structure. As demonstrated in Figure 3, $\Delta M3$ peptide in buffer solution, containing TFA at increasing concentrations, was less susceptible to adopt a helical structure compared to $\Delta M4$, even in the presence of SDS, popularly used in such tests. The pH changes of the buffers used (pH 7.0 versus pH 7.4) did not exert a significant effect on the peptide helical structure. However, the structural preferences of both peptides differ significantly in the presence of salt, which is

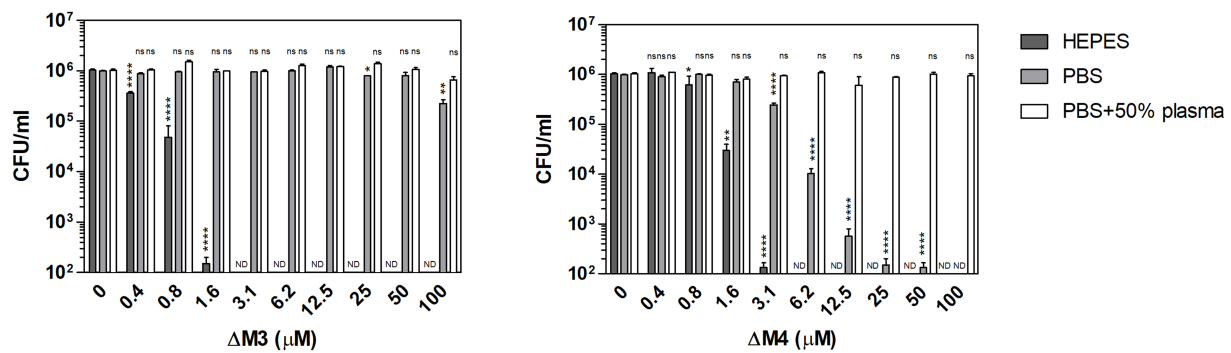


FIGURE 2

Fungicidal activity of $\Delta M3$ and $\Delta M4$ against *C. albicans* under various conditions. *C. albicans* yeast cells ($10^5/100\mu\text{l}$) were incubated with $\Delta M3$ and $\Delta M4$ at concentrations in a range of 0.4–100 μM for 2h in 10mM HEPES, PBS, or PBS with 50% human plasma. The cell suspensions were plated on solid YPD medium. After 24h of cultivation at 30°C, the number of CFUs was determined. The experiment was performed in triplicate. Graphs present mean values \pm SD from representative results ($n=4$). For statistical analysis one-way ANOVA with Dunnett's multiple comparisons *post hoc* test was used (* $p<0.05$, ** $p<0.005$, *** $p<0.0001$, ns>0.05 vs. untreated cells). A value of 10^2 CFU/ml on the y-axis was the limit of quantification. Values that were below this limit were marked ND.

particularly relevant for experiments conducted in PBS and in RPMI 1640 medium. The presence of salt in a concentration-dependent manner enhanced the helicity of $\Delta M4$ but had no effect on structural properties of $\Delta M3$. These observations may explain the results obtained for the peptide treatment of fungal cells and their killing effects. Furthermore, supplementation with human plasma resulted in a loss of activity of both peptides, as no significant changes in fungal viability were observed within the range of peptide concentrations tested. Such reduction in the antibacterial activity of the peptides was often observed due to their nonspecific binding to the plasma proteinous components (Sovadinová et al., 2021).

Since the investigated peptides showed the best fungicidal properties against *C. albicans* in HEPES/glucose, the antifungal activity of these compounds against different *Candida* species was tested under the same conditions. Both peptides showed high efficiency against *C. tropicalis* and *C. parapsilosis*, reaching values of minimal fungicidal concentrations (MFCs) in the same range as those determined for *C. albicans* (Table 2). The values of MFC₉₀ and MFC_{99.9} were of 0.8 μM and 1.6 μM , respectively, for $\Delta M3$, and of 1.6 μM and 3.1 μM , respectively, for $\Delta M4$. *C. glabrata* showed higher resistance to these peptides. For the $\Delta M3$ peptide, the value of MFC_{99.9} was not determined within a range of peptide concentration used, while for $\Delta M4$, which presented greater antifungal activity, MFC_{99.9} was estimated to be 50 μM . Nevertheless, these observations indicate that both peptides under these conditions may be potential antifungal agents against yeast-like forms of *Candida* species, especially *C. albicans*, *C. parapsilosis* and *C. tropicalis*.

The identified effects of $\Delta M3$ and $\Delta M4$ on *C. albicans* cell viability were also confirmed by SEM analysis of their cell surface structure. The yeast cells showed altered cell surface morphology after incubation with peptides (Figure 4). The untreated cells had a smooth surface and normal shape, whereas treatment with peptides at fungicidal concentration in HEPES/glucose buffer

resulted in damage of the cell surface with leakage of intracellular content, marked with arrows on the figures. Similar observations were shown in a recent work, in which *C. albicans* cells were treated with the cecropin 4-derived peptide C18 (Sun et al., 2022). The cells treated with $\Delta M4$ showed also a rough surface. These quite distinct changes in the cell surface under the influence of both tested peptides may indicate their differential interaction with the cell wall of *C. albicans*.

3.2. The $\Delta M4$ peptide affects the morphological transition of *Candida albicans*

Candida albicans is characterized by morphological diversity that allows it to adapt to various environmental conditions to survive, and the transition from yeast to hyphae is essential for host cell colonization by *C. albicans* (Karkowska-Kuleta et al., 2009; Jacobsen et al., 2012). In this study, the effect of both peptides on inhibition of yeast to hyphae transition was investigated using *C. albicans* cells cultured in RPMI 1640 medium that activates filamentation (Figure 5A). The increasing concentration of $\Delta M3$ peptide caused a progressive decrease in cell filamentation. The average length of cell hyphae at peptide concentrations that do not affect cell permeability – 12.5 μM and 25 μM – was approximately 30 and 50% shorter, respectively, compared to that observed in untreated cells (Figure 5B). Incubation of cells with higher concentrations of this peptide (50 μM) led to an increased influx of Sytox Orange dye, indicating permeabilization of the cells. In turn, $\Delta M4$ peptide already at 2.1 μM concentration inhibited the *C. albicans* hypha formation, reducing their length by approximately 30%. However, for concentrations of 3.1 μM and 6.2 μM , $\Delta M4$ completely blocked filamentation, probably killing the cells, as

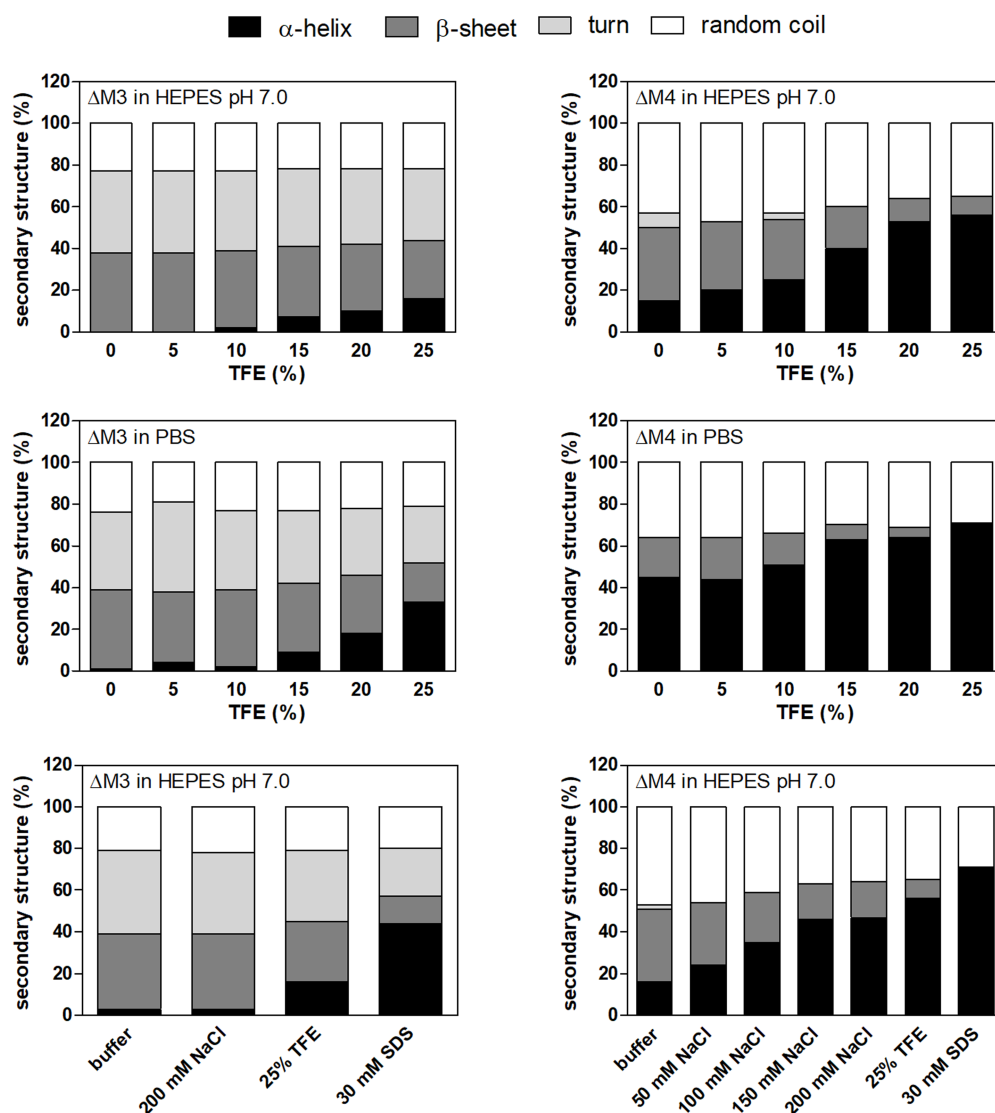


FIGURE 3

The secondary structure of peptides in different solutions analyzed by circular dichroism (CD) measurements. $\Delta M3$ and $\Delta M4$ peptides (both at a concentration of 1mg/ml) were prepared in 10mM HEPES pH 7.0 or PBS. Trifluoroethanol (TFE) at a final concentration in a range of 5–25% was used to enhance secondary structure stability. To check the effect of NaCl on the secondary structure of the peptides, samples were prepared in 10mM HEPES pH 7.0 with NaCl (50–200mM). Buffer supplemented with 30mM SDS was used to mimic microbial membrane. CD spectra of peptides were measured in the range of 195–250nm and averaged over five acquisitions. Secondary structure content was determined using JSSE program (Jasco) using CD spectra of α -chymotrypsin A, hemoglobin, lysozyme, myoglobin and ribonuclease A proteins as a reference.

demonstrated by cell permeability test performed with Sytox Orange staining (Figure 5A). The observations of the effect of peptides on fungal morphology were also confirmed by the analysis of the expression of genes associated with hypha formation. Cell treatment with $\Delta M3$ (12.5 μM and 25 μM) significantly decreased the expression of genes encoding the main fungal adhesins: *ALS3*, *HYR1* and *HWP1* compared to untreated cells (Figure 5C), which corroborated the assumption that $\Delta M3$ contributes to the inhibition of hypha formation. However, for fungal cell treatment with $\Delta M4$, only minor

changes in expression of these genes were observed, suggesting that $\Delta M4$ is less effective in inhibiting hypha formation by *C. albicans* cells.

3.3. Effect of $\Delta M3$ and $\Delta M4$ peptides on *Candida albicans* biofilm

The ability to form filaments by *Candida* spp. is not only required for increased virulence but also plays an important role

in biofilm formation (Gulati and Nobile, 2016). The potential of the peptides to inhibit biofilm formation was tested after 24 h of incubation at a wide range of peptide concentrations (Figure 6A). The metabolic activity of cells in the biofilms was determined by the XTT reduction assay and compared to biofilm cells not treated with peptides. As expected, the $\Delta M4$ peptide showed a better

TABLE 2 Minimal fungicidal concentrations (MFC₉₀ and MFC_{99.9}) of $\Delta M3$ and $\Delta M4$ against yeast cells of *Candida* species.

Yeast	$\Delta M3$		$\Delta M4$	
	MFC ₉₀ (μM)	MFC _{99.9} (μM)	MFC ₉₀ (μM)	MFC _{99.9} (μM)
<i>C. albicans</i> strain 3147	0.8	1.6	1.6	3.1
<i>C. tropicalis</i> strain T1	0.8	1.6	1.6	3.1
<i>C. parapsilosis</i> strain CDC 317	0.8	1.6	1.6	3.1
<i>C. glabrata</i> strain CBS138	1.6	ND	1.6	50

MFC₉₀ and MFC_{99.9} were determined against 10^5 planktonic cells of *C. albicans*, *C. tropicalis*, *C. parapsilosis* and *C. glabrata* incubated for 2 h at 30°C with peptides in the concentration range of 0.4–100 μM , diluted in 10 mM HEPES pH 7.0 with 5 mM glucose, using the CFU assay. The experiment was carried out three times independently. All strains were obtained from ATCC. MFC₉₀ and MFC_{99.9} – minimal concentration of peptide that causes mortality of 90 and 99.9% fungal cells, respectively, ND – not detected in the range 0.4–100 μM peptide (over the detection limit).

ability to completely inhibit biofilm formation already at a concentration of 12.5 μM , while $\Delta M3$ was less effective, achieving a similar effect only at a concentration of 100 μM .

Biofilm elimination is an important target in candidiasis, as the formation of this structure is strongly associated with its increased drug resistance (Tsui et al., 2016). The ability of $\Delta M3$ and $\Delta M4$ peptides to eradicate the *C. albicans* biofilm was revealed with the XTT reduction assay. The mature biofilm was more susceptible to $\Delta M4$ than to $\Delta M3$ (Figure 6B). As estimated after 24 h of biofilm incubation in the presence of $\Delta M4$, the metabolism of cells was completely abolished at a concentration higher than 50 μM , while $\Delta M3$ was unable to achieve this effect at this concentration. At a concentration of 100 μM , $\Delta M3$ reduced cell metabolic activity only by 60%.

To confirm the effect of the peptides on *C. albicans* biofilm, cell membrane permeabilization was tested with two different assays. In the Rhodamine G6 efflux assay modified according to Do Nascimento Dias et al. (2020), at the beginning cells were loaded with dye, and after washing and incubation with peptides in glucose-free PBS, the efflux of dye was assessed in the supernatant (Figure 6C). The biofilm was affected by both peptides in a dose-dependent manner, although $\Delta M4$ concentrations above 12.5 μM caused a strongly increased membrane permeabilization, while for $\Delta M3$ it was observed at concentrations above 50 μM . The membrane permeability was also studied using Sytox Orange dye, which stain nucleic acids in

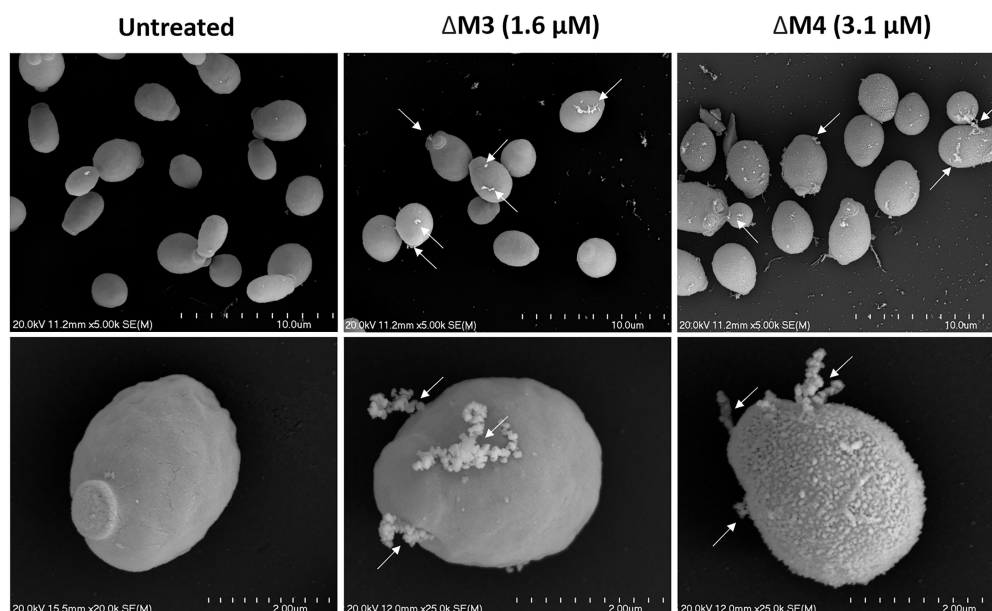


FIGURE 4

Scanning electron microscopy of the *C. albicans* cell surface after treatment with $\Delta M3$ and $\Delta M4$. *C. albicans* yeast cells ($10^5/100\mu l$) were incubated with $\Delta M3$ (1.6 μM) or $\Delta M4$ (3.1 μM) in 10 mM HEPES pH 7.0 with 5 mM glucose for 2 h at 30°C, then fixed overnight with glutaraldehyde, dehydrated, coated with gold and examined with a scanning electron microscope HITACHI S-4700. Cells incubated in buffer without peptides served as an untreated control. Arrows indicate surface damage that leads to intracellular material leakage.

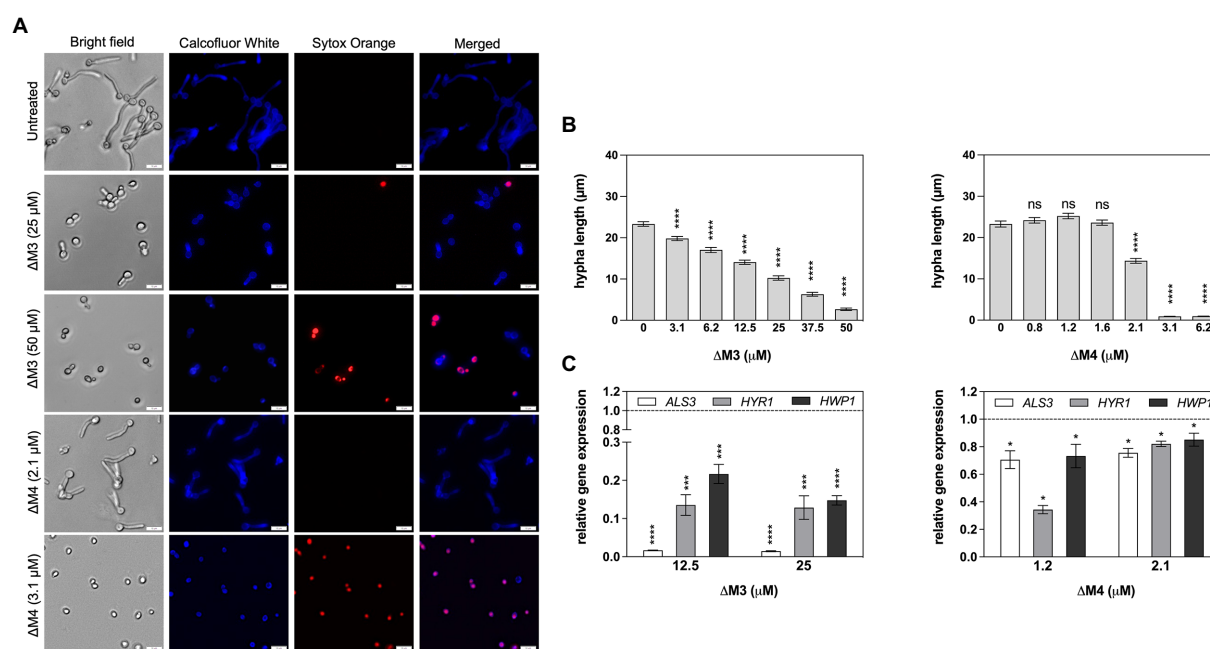


FIGURE 5 Impact of $\Delta M3$ and $\Delta M4$ on the transition of *C. albicans* from yeast to filamentous form. **(A)** *C. albicans* ($10^5/100\mu\text{l}$) were incubated in RPMI 1640 medium with peptides at concentrations in the range of 3.1–50 μM ($\Delta M3$) or 0.8–6.2 μM ($\Delta M4$) for 90min at 37°C. The fungi were stained with Calcofluor White (1 $\mu\text{g/ml}$) or Sytox Orange (1 μM) and visualized using Olympus IX73 microscope. **(B)** The length of the hyphae ($n=20$) was measured using Olympus CellSens programming. For statistical analysis one-way ANOVA with Dunnett's multiple comparisons *post hoc* test was used (**** $p<0.001$). **(C)** The mRNA expression of *ALS3*, *HYR1* and *HWP1* was determined after contact of *C. albicans* cells ($2 \times 10^6/\text{ml}$) with $\Delta M3$ (12.5 μM and 25 μM) and with $\Delta M4$ (1 μM and 2 μM) for 90min at 37°C. Bars represent the mean value \pm SD from at least three independent experiments. A paired Student's *t* test was used for statistical analysis. * $p<0.05$, *** $p<0.005$ and **** $p<0.0001$ vs. untreated cells (dashed line).

cells with altered membranes. The dye load was increased with rising peptide concentration, showing a significant change in cell permeability treated with 6.2 μM $\Delta M4$ and 50 μM $\Delta M3$. Representative images from microscopic analysis showed cell dye load for peptides at these concentrations (Figure 6D). These results correlated with that of the Rhodamine G6 test confirming the influence of peptides on the membrane alteration of *C. albicans* cells forming biofilms; however, $\Delta M4$ was more effective at lower concentrations.

3.4. $\Delta M3$ and $\Delta M4$ peptides induce oxidative stress and pro-apoptotic responses in *Candida albicans* biofilm

Mechanisms of antifungal activity of peptides are diverse and include not only cell wall disturbances, but also more sophisticated processes associated with the induction of oxidative stress that can lead to cell apoptosis (Vriens et al., 2014; Seyyedjavadi et al., 2020). To determine a possible mechanism of *C. albicans* biofilm destruction, the activity of yeast metacaspases was examined in biofilm treated with $\Delta M3$ and $\Delta M4$ at different concentrations of peptides. The metacaspase activity was detected with CaspACE™ FITC-VAD-FMK *In Situ* Marker, an FITC-marked inhibitor of caspases, which irreversible binds to the enzyme, emitting fluorescence *in situ*. Representative images of microscopic analysis

of treated biofilms are shown in Figure 7A. The minimum concentration of peptides, which triggers metacaspase activity in yeast cells and hyphae, was 6.2 μM and 50 μM for $\Delta M4$ and $\Delta M3$, respectively. Pro-apoptotic processes often result in loss of ROS concentration balance in cells and lead to oxidative stress. Here, the effect of $\Delta M3$ and $\Delta M4$ peptides on the induction of oxidative stress was investigated in the biofilm of *C. albicans*. For the analysis of ROS production with dihydrorhodamine 123 (DHR 123), the concentration of the peptide that showed pro-apoptotic activity was selected. Increased amount of intracellular ROS oxidizes non-fluorescent DHR to cationic rhodamine, which exhibits green fluorescence. Both peptides, $\Delta M3$ (50 μM) and $\Delta M4$ (6.2 μM) increased ROS production by approximately 38% compared to the untreated fungal biofilm (Figure 7B). At the same time, the expression of selected genes encoding antioxidant enzymes was tested at the peptide concentration inducing proapoptotic responses. The $\Delta M3$ induced higher gene expression of *GPX3* and *SOD5* showing a 2-fold and 80-fold increase in mRNA level, respectively. The biofilm stimulation with $\Delta M4$ peptide caused an increase in *GPX3* and *SOD5* mRNA level by 3.3- and 12.2-fold, respectively (Figure 7C). Additionally, a slight decrease in *CAT1* expression was observed when mature biofilms were treated with both peptides.

To further characterize the action of the peptides on cell mitochondria, their functionality and dynamics were evaluated. Active mitochondria showing normal membrane potential were

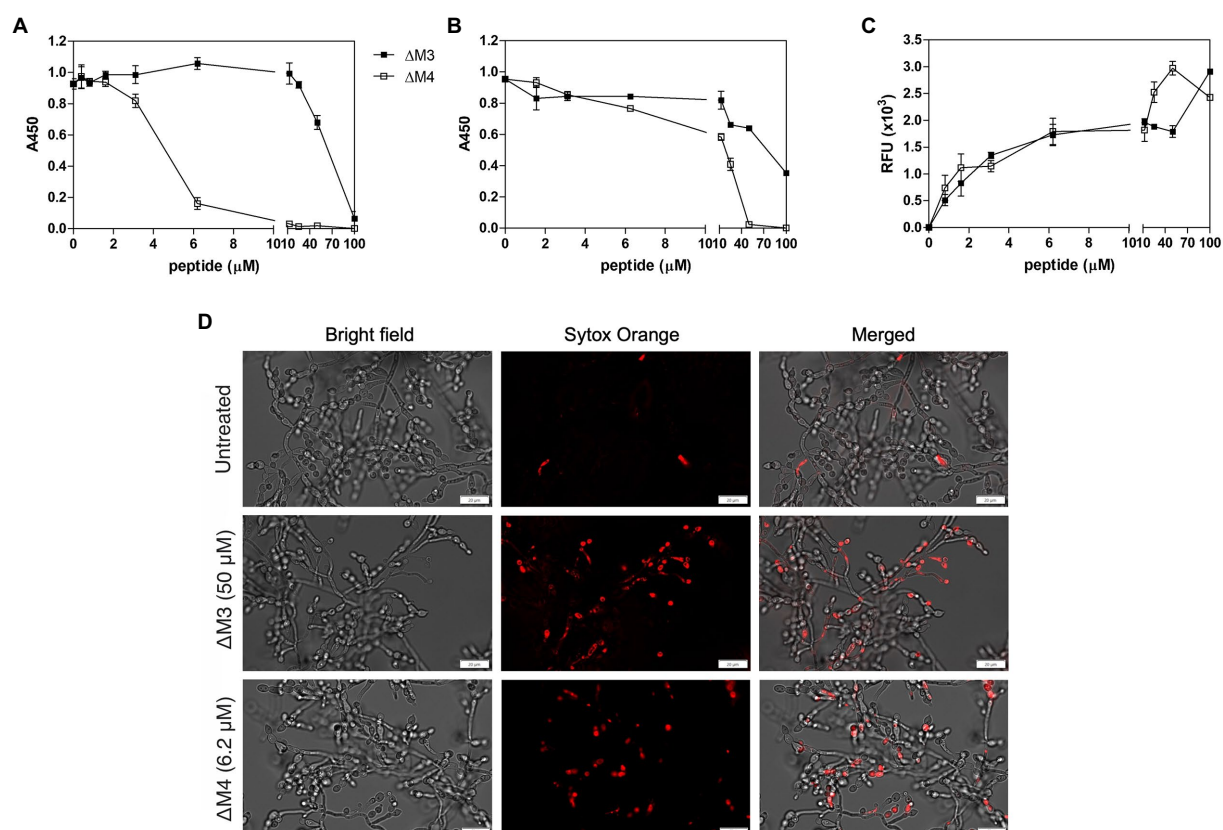


FIGURE 6

Effect of ΔM3 and ΔM4 on *C. albicans* biofilm. (A) The effect of peptides on biofilm formation was performed with *C. albicans* cells ($1 \times 10^5/100\mu\text{l}$) incubated in RPMI 1640 medium with peptides at concentrations in a range of $0.4\text{--}100\mu\text{M}$ for 24h at 37°C in a microplate wells, after removing unbound cells. The metabolic activity of the biofilm cells was determined using an XTT reduction assay with absorbance measurements at 450nm (A450). The untreated biofilm served as a control. The mean value \pm SD from at least three independent experiments was presented. (B) Changes in metabolic activity of *C. albicans* biofilm-forming cells were evaluated using an XTT reduction assay after 24-h biofilm treatment with peptides at concentrations in a range of $0.8\text{--}100\mu\text{M}$ for 24h at 37°C . (C) Membrane permeability in mature biofilm cells was determined using an adaptation of the Rhodamine G6 efflux assay. The leakage of the fluorescence dye, previously internalized by *C. albicans* cells from mature biofilm, was measured in the supernatants after 24h of contact of the biofilm with peptides at concentration range of $0.8\text{--}100\mu\text{M}$ at 37°C . The results of three independent experiments are presented as means \pm SD. RFU – relative fluorescence units. (D) Representative images of the membrane permeabilization study with Sytox Orange dye. The mature *C. albicans* biofilms, untreated or treated with ΔM3 ($50\mu\text{M}$) or ΔM4 ($6.2\mu\text{M}$) for 24h at 37°C , were incubated with $1\mu\text{M}$ dye for 5min in the dark. The biofilms were analyzed using the Olympus IX73 microscope.

visualized with MitoTracker Orange, while the entire mitochondrial pool was determined by MitoTracker Green staining (Figure 8A). Representative photographs show a partial loss of mitochondrial activity after incubation with peptides and amphotericin B, as a decrease in MitoTracker Orange fluorescence was noted. In addition, the distribution of active mitochondria was altered in treated cells. Since mitochondrial function depends on intracellular Ca^{2+} concentration, the cytosolic concentration of these ions in peptide-treated *C. albicans* biofilm was also investigated. Intracellular Ca^{2+} mobilization in live cells was determined with a ratiometric calcium assay, in which the fluorescent indicator Fura-2 changes spectral properties when calcium ions are bound. Higher peptide concentrations ($50\mu\text{M}$ ΔM3 and $12.5\mu\text{M}$ ΔM4) resulted in increased cytosolic Ca^{2+} concentration, while no effect was observed at lower peptide concentrations. The ΔM4 peptide more effectively stimulated cells to Ca^{2+} production (by

approximately 100% compared to untreated cells), while ΔM3 showed an increase in Ca^{2+} concentration of approximately 70% (Figure 8B). In a positive control, cells were treated with 10mM H_2O_2 and demonstrated an increase in Ca^{2+} concentration of up to 50%. These findings indicate that, at least in part, the antifungal activity of the peptides might be related to their pro-apoptotic properties.

3.5. The antifungal activity of ΔM3 and ΔM4 peptides was enhanced in combination with conventional antifungal drugs

Increased drug resistance of *Candida* spp. to conventional antifungal compounds, together with their toxicity, limits the effectiveness of candidiasis treatment (Tsui et al., 2016). In the

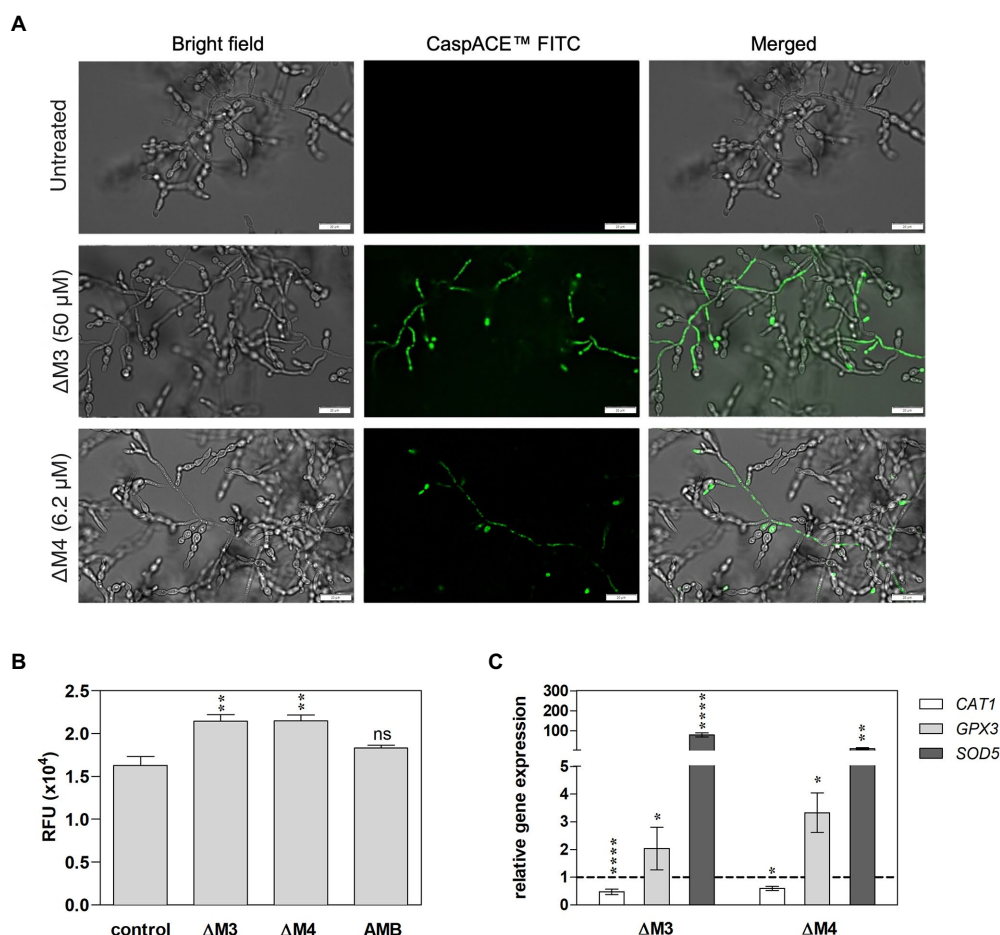


FIGURE 7

Apoptotic response and oxidative stress induced by $\Delta M3$ and $\Delta M4$ in *C. albicans* mature biofilm. (A) *C. albicans* cells (10^5 /ml) were seeded in a 96-well plate and biofilms were grown for 24h, then peptides were added to the cells in the concentration range of 12.5–100 μM ($\Delta M3$) or 3.1–12.5 μM ($\Delta M4$). The biofilm was grown in the presence of peptides for a further 24h. The CaspACE™ FITC-VAD-FMK *In Situ* Marker kit was used to assess metacaspase activation. The marker (10 μM) was added to the biofilms and incubation was carried out for 1h at 37°C. Biofilms were imaged with an Olympus IX73 microscope and representative images for $\Delta M3$ (50 μM) and $\Delta M4$ (6.2 μM) are presented. (B) Intracellular ROS production in mature biofilm by peptides was evaluated with DHR test. The 24-h *C. albicans* biofilms were treated with $\Delta M3$ (50 μM), $\Delta M4$ (6.2 μM) and amphotericin B (2.7 μM) for 3h at 37°C, washed with PBS and then incubated with DHR 123 (10 μM) for 30min. The untreated *C. albicans* biofilm served as a control. The fluorescence of oxidized DHR 123 was measured using the BioTek Synergy H1 microplate reader. The graphs present values as mean \pm SD ($n=3$), RFU- relative fluorescence units. Statistical analysis was performed with one-way ANOVA with Dunnett's multiple comparisons *post-hoc* test. ** $p<0.01$ (C) Analysis of *CAT1*, *GPX1*, and *SOD5* gene expression was performed in mature biofilm cells treated with $\Delta M3$ (50 μM) or $\Delta M4$ (6.2 μM) for 3h at 37°C. The bars represent the mean values \pm SD from at least 3 experiments. A paired Student's t-test was used for statistical analysis. * $p<0.05$, ** $p<0.01$, **** $p<0.0001$ vs. untreated cells (dashed line).

fight against fungal infections, additional substances are often introduced in combination with conventional drugs to enhance the effect of treatment and to use lower concentrations of these, often toxic, drugs. This study investigated the effect of combined treatment of *C. albicans* with $\Delta M3$ and $\Delta M4$ peptides and conventional drugs, according to the modified checkerboard microdilution method in which *C. albicans* cells were seeded into microplate wells in RPMI with or without peptides, drugs or their combination over a wide range of two-fold serial dilutions of both agents, and then incubated for 24h. To determine the inhibitory concentrations (IC) the XTT metabolic activity assay was used. The capacity for drug/peptide interaction with *C. albicans* was measured by calculating the

fractional inhibitory concentration index (FICI), which was defined in the Materials and Methods section. A FICI value of less than or equal to 0.5 indicates that there is a drug and peptide synergism; a value between 0.5 and 1.0 indicates an additive effect of both substances, while a value between 1.0 and 2.0 indicates that the combination of the two substances is indifferent to cell effects. The FICI values calculated for the combination of $\Delta M3$ and $\Delta M4$ with amphotericin B, caspofungin, or fluconazole are presented in Table 3. Synergy against *C. albicans* was observed between caspofungin and each peptide. The FICI achieved a value of 0.062 and 0.370 for $\Delta M3$ and $\Delta M4$, respectively. In the case of the caspofungin/ $\Delta M3$ combination, the minimal inhibitory concentration that inhibits

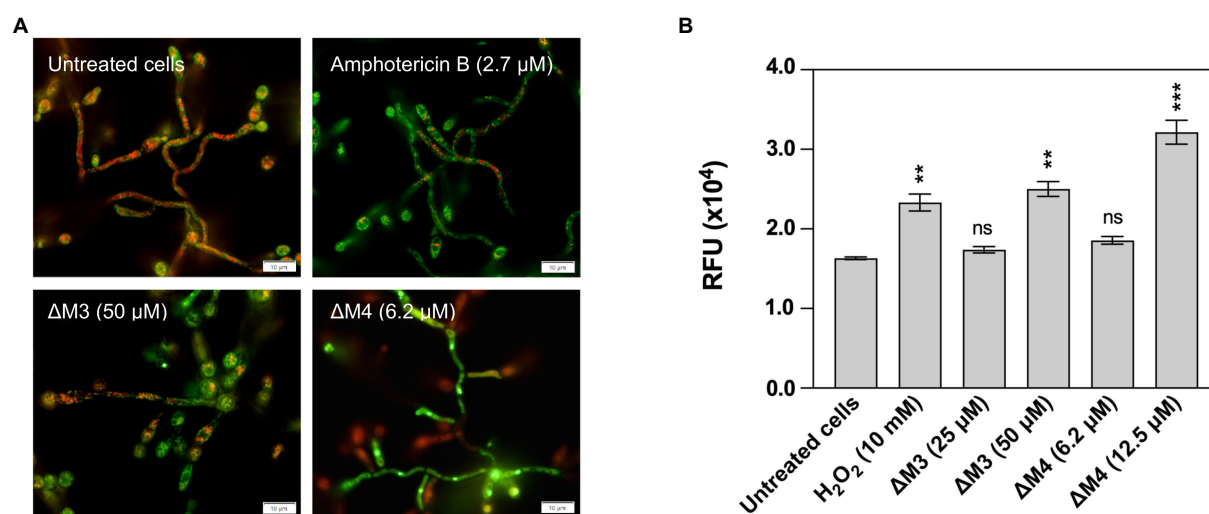


FIGURE 8
Induction of mitochondria activation and increased intracellular Ca²⁺ concentration by ΔM3 and ΔM4. **(A)** The changes in mitochondrial activity after treatment with peptides were detected in 24-h biofilms of *C. albicans*. Cells were incubated with 50 μM ΔM3, 6.2 μM ΔM4 or 2.7 μM amphotericin B for 3 h. Changes in mitochondrial activity and the entire mitochondrial pool was determined with 0.5 μM Mitotracker Orange and 0.5 μM Mitotracker Green, respectively. Representative images of microscope analysis performed with the Olympus IX73 microscope for each sample are presented. **(B)** To detect intracellular Ca²⁺, 24-h biofilms of *C. albicans* were incubated with ΔM3 (25 μM and 50 μM), ΔM4 (6.2 μM and 12.5 μM) or H₂O₂ (10 mM, positive control) for 3 h. Next the Fura-2 Calcium Flux Assay Kit was performed according to the manufacturer's instructions. The bars represent the values of mean ± SD (*n* = 3). RFU – relative fluorescence unit. Statistical analysis was performed with one-way ANOVA with Dunnett's multiple comparisons *post-hoc* test. ***p* < 0.01, ****p* < 0.005.

TABLE 3 Combined antifungal activity of ΔM3 and ΔM4 with conventional antifungals.

Compound a	Compound b	FICa	FICb	FICI	Action
Amphotericin B	ΔM3	0.5 (0.8 μM)	0.008 (0.4 μM)	0.508	Additive
	ΔM4	0.5 (0.8 μM)	0.125 (0.4 μM)	0.625	Additive
Caspofungin	ΔM3	0.03 (0.003 μM)	0.032 (1.6 μM)	0.062	Synergism
	ΔM4	0.12 (0.012 μM)	0.25 (0.8 μM)	0.37	Synergism
Fluconazole	ΔM3	0.25 (0.2 μM)	1.0 (50 μM)	1.25	Indifferent
	ΔM4	0.25 (0.2 μM)	1.0 (3.1 μM)	1.25	Indifferent

The combinatory effect of peptides and antifungal drugs was determined using the modified checkerboard assay. *C. albicans* cells (3×10^3 /ml) were treated with ΔM3, ΔM4, amphotericin B, caspofungin, fluconazole alone or with mixtures in a wide concentration range for 24 h at 37°C in RPMI 1640 medium. The minimal concentration that inhibits the metabolic activity of fungi by 90% (IC₉₀) for each compound and each combination of compounds was determined using the XTT reduction assay in at least three biological replicates. IC₉₀ determined for self-acting peptides and drugs: 50 μM for ΔM3, 3.1 μM for ΔM4, 1.6 μM for amphotericin B, 0.8 μM for fluconazole, and 0.1 μM for caspofungin. The IC₉₀ values for the compounds acting in the combination are given in brackets. FICI values: FICI ≤ 0.5 = synergism, 0.5 < FICI ≤ 1.0 = additive, 1.0 < FICI ≤ 2.0 = indifferent, FICI > 2.0 = antagonism.

fungal metabolism by 90% was 0.003 μM and 1.6 μM for caspofungin and peptide, respectively. IC₉₀ values for the caspofungin/ΔM4 combination were 0.012 μM and 0.8 μM for caspofungin and peptide, respectively. Due to the fact that the IC₉₀ for these substances is 0.1 μM for caspofungin and 50 μM or 3.1 μM for ΔM3 and ΔM4, respectively (Table 2), it can be concluded that the treatment of cells with this drug in combination with the peptide strongly lowered the IC₉₀. An additive effect was observed for the combination of peptides with amphotericin B, showing FICI values of 0.508 and 0.625 for ΔM3 and ΔM4, respectively. As with the caspofungin/peptide combination, in this case, the IC₉₀ for the drug combination is reduced compared to the effect achieved by

administering these substances alone, reaching values of 0.8 μM for amphotericin B and 0.4 μM for peptides. In turn, the effect of combining peptides with fluconazole turned out to be indifferent. The calculated FICI values were equal to 1.25 for both peptides. In fact, the IC₉₀ values for the peptides were the same as the values obtained when the peptides were used alone. However, IC₉₀ for fluconazole was four-fold lower when administered in combination with each peptide than when administered alone. Inhibition curves for each drug/peptide combination are presented in Supplementary Figure S2. They indicate that both peptides are useful for reducing the dose of conventional drugs such as caspofungin and amphotericin B in inhibiting the growth of *C. albicans*.

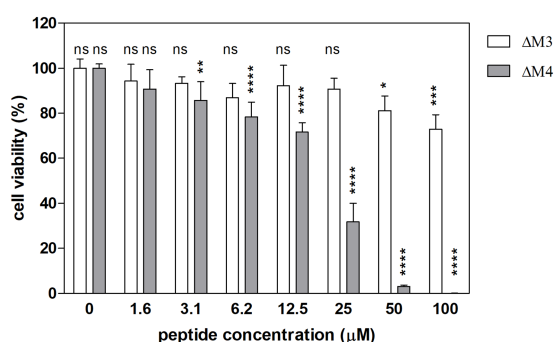


FIGURE 9

Viability of human dermal fibroblasts (HDF) after treatment with ΔM3 and ΔM4 peptides. The cytotoxicity of the peptides was assessed with Alamar blue test in primary HDF. Cells, seeded on microplate (1×10^5), were treated with peptides at different concentrations for 24h in culture HDF basal medium. After medium removal, 100μl of Alamar blue reagent were added. Fluorescence was measured at $\lambda_{ex}=560\text{nm}$, $\lambda_{em}=590\text{nm}$ with Synergy H1 microplate reader after 1h of incubation. The cell viability is presented as the percentage of the untreated cells, the number of which was assumed as 100%. The samples were performed in triplicate. The bars present the mean \pm SD ($n=3$). Statistical analysis was performed with two-way ANOVA with Tukey's multiple comparison test. Selected statistical significances were presented vs. untreated cells. * $p < 0.05$, ** $p < 0.01$, *** $p < 0.005$, **** $p < 0.001$.

3.6. The viability of human dermal fibroblasts varies depending on the peptide used

The cytotoxicity of the tested peptides was determined in primary human dermal fibroblasts (HDF) with the Alamar blue assay. Living cells convert the resazurin indicator to highly fluorescent resorufin. The effects of the two peptides on fibroblast viability differed (Figure 9). ΔM3 peptide caused only a slight decrease in cell viability, achieving the major effect at the concentration of 100 μM (by 24%). Differently, the second peptide, ΔM4 was more aggressive toward fibroblasts, causing a 25% decrease in cell viability at the concentration of 12.5 μM. Higher concentrations of this peptide resulted in a strong reduction in cell viability, leading to a complete cell killing at 100 μM.

4. Discussion

The incidence of fungal infections and their mortality rates have increased significantly in recent years, particularly for candidiasis which are most common (Pfaller et al., 2020). *C. albicans* still remains the predominant etiological agent of candidiasis; however, non-*albicans* *Candida* species, including *C. parapsilosis*, *C. tropicalis*, and *C. glabrata*, are emerging as major opportunistic fungal pathogens, causing increased rate of hospital-acquired infections, with high risk for immunosuppressed patients undergoing surgical procedures or anticancer therapy (Pfaller et al., 2019). These pathogens also often present a reduced

susceptibility to commonly used antifungal drugs, due to the increase in frequency of multidrug resistant strains or the formation of biofilms that protect them from conventional therapies (Mayer et al., 2013). Therefore, successful treatment of *Candida* infections that are often associated with biofilm formation requires novel and more effective antifungal strategies. The selection of efficient antimicrobial peptides possesses some advantages over conventional antifungal agents, the effectivity of which can be reduced by their toxicity toward human host cells. Cecropins have recently become an important source of AMPs, which, thanks to their specific structure and interactions with the lipid membranes of various cells, present antimicrobial and anticancer effects (Hollmann et al., 2018). It has been found that AMPs may use two or more mechanisms to penetrate membranes that depend on the polar and non-polar distribution of amino acids; however, other characteristics such as net charge, amphipathicity, hydrophobicity, percentage of α -helix structure may be important for interaction with the cell wall (Madani et al., 2011). Recent reports have demonstrated the effect of cecropin-derived amphipathic positive peptides on antifungal activity against *C. albicans* (Peng et al., 2022; Sun et al., 2022). These studies, however, focused on the antifungal activity of peptides that differ in amino acid sequence, charge, and hydrophobicity from the peptides tested in this study.

To test antifungal activity on different forms of *Candida* cells, we chose two cecropin D-derived cationic peptides, ΔM3 and ΔM4, which are both rich in Lys and Arg residues, while ΔM4 peptide was additionally enriched with three Trp residues and one Tyr residue, thus presenting more hydrophobic properties compared to ΔM3. Differences in amino acid composition resulted in different predisposition of peptides to the formation of α -helical structures in the presence of agents, simulating contact with the microbial cell membrane, as determined by the CD study. Furthermore, the presence of salt in the environment can promote this property with respect to the peptide ΔM4, while such effect was not observed for ΔM3. These structural properties turn directly into the effectiveness of these peptides in contact with yeast cells, especially those that occur in the form of blastospores. In fact, we observed different patterns of the fungal cell surface damage for both investigated peptides by SEM. In accordance with our results, similar observations were reported, showing that incorporation of hydrophobic amino acid residues in AMPs resulted in reduced MIC₉₀ values (Pandit et al., 2020; Ramamourthy et al., 2020). Furthermore, the presence of hydrophobic residues in the transmembrane fragment of antimicrobial peptides was believed to lead to the formation of ion channels within the cell membrane (Buda De Cesare et al., 2020). The amino acid composition also influenced the differences in fungicidal activity of the peptides studied, depending on the presence of ions in the environment. The ΔM3 peptide, which has a charge of +8, appeared to be more susceptible to the salt effect, regardless of the ability to form helical structures, since no activity against *C. albicans* was observed after treatment of fungal cells with a peptide dissolved in PBS, compared to the strong activity detected when HEPES buffer was used. Such a negative impact of salt on the

fungicidal activity of short cationic peptides against *C. albicans* has previously been demonstrated (Do Nascimento Dias et al., 2020; Ghosh et al., 2021). It may be the result of compensation for the peptide charge or of affecting the local peptide structure by electrostatic interactions of ions with amino acid functional groups (Baldauf et al., 2013). Contrary, $\Delta M4$ was able to kill *C. albicans* even in PBS but with a lower efficiency compared to the results obtained in HEPES buffer. Such differences can be explained by different mechanisms and/or kinetics of both peptide action, where membrane compromising activity is accompanied by more complex and diverse mechanisms including DNA damage, inhibition of protein synthesis or metabolic pathway, induction of apoptosis, and oxidative stress (Nguyen et al., 2011; Wang et al., 2015; Li et al., 2016). For example, in the case of the application of the tryptophan-rich PuroA peptide, its rapid translocation inside *C. albicans* cells and its binding to intercellular targets was proposed as a mechanism of yeast inactivation, before subsequent perturbation of the cell membrane (Shagaghi et al., 2017). Another component of the incubation solution that radically inhibited the antifungal activity of the tested peptides was human plasma. Similar observations have also been reported for several AMPs, including LL-37. One study pointed to the possibility of forming complexes between peptides and plasma proteins such as albumin/ $\alpha 1$ -antitrypsin complex or apolipoprotein AI, resulting in the inactivation of AMPs (Tang et al., 2021).

Preliminary studies on other *Candida* species have been performed, indicating that the susceptibility of *C. albicans*, *C. tropicalis*, and *C. parapsilosis* cells to both peptides was comparable, while *C. glabrata* cells were killed at higher concentrations of peptides. This was expected as *C. glabrata* is known to present a low susceptibility to azoles (Arendrup et al., 2013) and a significant resistance to amphotericin B (Pappas et al., 2016), which was proposed to be associated with the presence of fungal cell wall transporters and their increased activity in the export of antifungal agents (Cavalheiro et al., 2021). Limited susceptibility of *C. glabrata* to AMPs was also observed in the treatment with histatin 5, magainin 2, cathelicidins, and defensins (Helmerhorst et al., 2005; Del Gaudio et al., 2013).

In the presented study, the observed influence of peptides on fungal cell adhesion and filamentation was also significant, as the regulation of these processes may prevent biofilm formation and fungal cell resistance to treatment. A noticeable inhibition of fungal cell filamentation was observed at a concentration of the peptides lower than fungicidal, and it was manifested by the formation of shorter hyphae and decreased expression of genes encoding proteins characteristic for the filamentous form of *C. albicans* cells (Hwp1, Hyr1, and Als3). A recent study demonstrated a similar effect on *C. albicans* by the cecropin-derived peptide C18 (Sun et al., 2022). It should be noted that the arresting of fungal cells in the form of blastospores may facilitate their elimination, even at lower peptide concentration. Such a strategy has been proposed for many antimicrobial peptides (Ogasawara et al., 2007; Akerey et al., 2009; Theberge et al., 2013; Do Nascimento Dias et al., 2020). The development of hyphae by *C. albicans* cells is a hallmark of the

initial steps in biofilm formation (Tsui et al., 2016). Then the consequence of the observed inhibition of hypha production by the peptides was the disruption of biofilm development, which was identified at the same peptide concentration range.

The diagnosis of a yeast infection and the necessity for its treatment often come at the stage of a biofilm formed. Therefore, we also tested the efficacy of both peptides against a mature biofilm, with a developed matrix, which hinders the penetration of various antifungal drugs, forcing an increase in the dose of the drug, which in turn could be toxic to the cells of the treated host (Taff et al., 2013; Cavalheiro and Teixeira, 2018). For $\Delta M4$ peptide, as in the case of many other AMPs (Kodedová and Sychrová, 2017; Do Nascimento Dias et al., 2020), we observed a noticeable decrease in the metabolic activity of mature biofilms at a peptide concentration approximately 15-fold or 8-fold higher compared to its effectiveness against yeast-like or biofilm-initiating cells. However, these concentrations of $\Delta M4$ were close to its cytotoxic properties toward host cells, where HDF viability decreased gradually with increasing $\Delta M4$ concentration, and was eliminated at the $\Delta M4$ concentration of 100 μM . In turn, the $\Delta M3$ peptide showed a lower toxicity in relation to HDF cells; at a concentration of 100 μM fibroblast viability was decreased only by 25%. However, at this concentration, the peptide lost the ability to eradicate the mature biofilm. Regardless of the effect of the peptides on host cells, it can be concluded that at least in the case of $\Delta M4$, all morphological forms of *C. albicans* can be destroyed. The second peptide, $\Delta M3$, worked better on blastospores and, at high concentrations, can significantly reduce pre-formed and mature biofilms.

Although the effects of AMPs on microorganisms are mainly attributed to their interaction with the cell membrane, other mechanisms have also been identified, including inhibition of cell wall biosynthesis or interaction with DNA (Buda De Cesare et al., 2020). However, certain peptides, such as salivary histatin 5 (Helmerhorst et al., 2001) or the venom wasp protonection (Wang et al., 2015) involved also ROS production in their antifungal mechanism and induced oxidative stress in yeasts through uncontrolled accumulation of intracellular ROS, which led to cell apoptosis or necrosis (Kim et al., 2020; Seyedjavadi et al., 2020; Zhang et al., 2021). For $\Delta M3$ and $\Delta M4$ peptides, increased cell permeability was also accompanied by increased ROS production within the *C. albicans* biofilm, suggesting a more complex antifungal mechanism of peptide action. However, *C. albicans* possesses adaptive responses that allow ROS detoxification, including activation of superoxide dismutase, catalase, and other enzymes involved in the production of ROS scavengers (Jamieson et al., 1996; Dantas et al., 2015). Activation of these reactions was also observed after treatment of the *C. albicans* biofilm with $\Delta M4$ peptide, where increased expression of the *GPX3* and *SOD5* genes was detected. However, the expression of *CAT1* was reduced, suggesting that ROS detoxification upon $\Delta M4$ treatment may not be completed. The explanation for such a result was indicated by Kaloriti et al. (2014), who showed that simultaneous exposure of *C. albicans* cells to oxidative and cationic stress may be more effective in yeast killing than oxidative stress alone (Kaloriti et al., 2014). These authors also

demonstrated that cationic ions can inhibit catalase, leading to ROS accumulation and inhibition of the Cap1 signaling molecule, which is critical for the response to oxidative stress of *C. albicans* cells.

Mitochondria are considered the main source of ROS, but uncontrolled ROS production also makes mitochondria a target, influencing mitochondrial membrane functionality. As a result, changes in membrane potential, increased mitochondrial permeability, and finally mitochondrial apoptosis are observed (Choi and Lee, 2015). In this study, mitochondrial functionality was investigated with fluorescence dyes, which identify active mitochondria with normal membrane potential versus the total number of mitochondria in *C. albicans* cells that form a biofilm, treated with both peptides. In each case, a significant loss of active mitochondria was observed, confirming that peptides contribute to biofilm disruption. These organelles develop different repair mechanisms, including mitochondrial fission-fusion processes, which are important for their proper functioning (Youle and van der Bliek, 2012). A previous study showed that *C. albicans* can lose its virulence due to the loss of the ability of mitochondria to fuse (Liang et al., 2018). It is possible that biofilm treatment with the peptides can induce such processes, but to confirm this observation, more research is needed.

The fact that the tested peptides increased ROS production and disrupted mitochondrial functionality was confirmed by the detection of increased cytosolic Ca^{2+} concentration after peptide treatment of *C. albicans* cells. On the other hand, the accumulation of Ca^{2+} violates its homeostasis and inhibits mitochondrial respiration, leading to its dysfunction (Rossi et al., 2019). Several studies have demonstrated that high cytosolic Ca^{2+} concentration causes an increased influx of these ions into mitochondria, resulting in increased permeability and depolarization of the mitochondrial membrane, and enhanced ROS production by *C. albicans* (Lee and Lee, 2018; Niu et al., 2020; Kwun et al., 2021). Furthermore, it has been shown that deregulated calcium ion homeostasis can induce *C. albicans* apoptosis (Kwun et al., 2021). Our study demonstrated increased metacaspase activity in the *C. albicans* biofilm treated with both peptides, which confirms the development of apoptotic processes in the treated biofilm. Previously, the apoptotic effects of various peptides have been demonstrated for *Candida* yeast cells (Lee and Lee, 2014; Li et al., 2019; Chen and Lan, 2020; Kim et al., 2020). In summary, taking into account increased ROS production and Ca^{2+} concentration, enhanced mitochondrial dysfunction, and increased metacaspase activity, we can propose a partial pro-apoptotic mechanism in the fungicidal activity of the studied peptides.

Strategies to reduce peptide toxicity include peptide further modification or encapsulation (van Gent et al., 2021). Combining them with conventional antifungal drugs is also a good approach, especially because the use of drug combinations can not only improve the efficiency of both antifungal agents, often with lowering their active concentration range and reducing their cytotoxic effect, but also can decrease the development of the resistance. Therefore, we evaluated the effects of each of the peptides along with amphotericin B, caspofungin and fluconazole that resulted in three

different types of effects. In the first type of interaction, synergism was observed only for the combination of peptides with caspofungin, especially strong in the case of ΔM3 , for which a 30-fold reduction in IC_{50} was identified (Table 3). Similar observations have been reported for the combination of caspofungin with many other AMPs (Vriens et al., 2015; Kovács et al., 2019; Shen et al., 2021). Caspofungin inhibits β -1,3-glucan synthase, located in the cell membrane of *Candida* cells, responsible for an essential component of the fungal cell wall. The reduced content of glucan in the fungal cell wall may facilitate its better penetration by the peptide. The second type of action, additivity, was determined for the combination of the peptides with amphotericin B. For both peptides, a two-fold reduction in IC_{50} was observed in cooperation with amphotericin B. However, it was found that the concentration of peptides needed to inhibit the formation of *C. albicans* biofilms to 10% was 125- and 8-fold lower for amphotericin B combination with ΔM3 and ΔM4 , respectively, compared to peptides acting alone. Although the interaction between these compounds has not been classified as synergistic, it is relatively strong and after the verification by different types of tests or *in vivo* studies (Vitale et al., 2005) it might change character, as it was observed previously in the case of caspofungin/amphotericin B combination used against *C. parapsilosis* (Barchiesi et al., 2007). When peptides were combined with fluconazole, no changes in antifungal properties were observed. Although the determined FICI of 1.25 suggests in both cases an independent effect, where both peptides clearly negatively affect the antifungal activity of fluconazole, as it was detected even at the lowest peptide concentration tested (0.4 μM). However, the negative effect of fluconazole on the antifungal activity of both peptides was not detected (Supplementary Figure S2). Trapping fluconazole by peptides and consequently the drug's failure to reach its target site without affecting its own antimicrobial activity is one of the possible reasons for the observation of such a phenomenon. It is also possible that the peptides, like some other AMPs (Ma et al., 2020), may increase the expression of Erg11, an essential enzyme in the ergosterol biosynthesis pathway, which is inhibited by fluconazole. Moreover, it is also not excluded that the peptides can increase expression and/or activity of *C. albicans* efflux pumps and thus increase the fungus resistance to fluconazole but it needs further research.

In conclusion, cecropin D-derived synthetic cationic peptides presented strong antifungal activity against *Candida* cells, regardless of the morphological form of the fungi. A scheme that demonstrates the most relevant results is presented in Figure 10. As expected, yeast cells of *C. albicans* were more susceptible to the action of peptides compared to the fungal biofilm. The mode of action of peptides is most likely complex, involving both destabilization of the cell wall and additional intracellular mechanisms such as increased oxidative stress, which contributes to cell death by apoptosis. Moreover, the synergism of tested peptides with caspofungin was demonstrated. That offers an opportunity for a new approach to combating *Candida* infections by constraining their virulence and dealing with drug resistance.



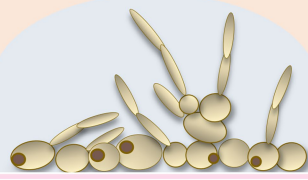
$\Delta M3$		$\Delta M4$
<ul style="list-style-type: none"> ✓ Active only in HEPES (+glucose) ✓ $MFC_{90} = 0.8 \mu M$ $MFC_{99.9} = 1.6 \mu M$ ✓ Affects the structure of cell wall 	Blastospores 	<ul style="list-style-type: none"> ✓ Active in PBS and HEPES (+glucose) ✓ $MFC_{90} = 1.6 \mu M$ $MFC_{99.9} = 3.1 \mu M$ ✓ Affects the structure of cell wall
<ul style="list-style-type: none"> ✓ Inhibits hyphal formation ($\geq 3.1 \mu M$) ✓ Decreases mRNA expression of <i>ALS3</i>, <i>HYR1</i> and <i>HWP1</i> genes 	Filamentation 	<ul style="list-style-type: none"> ✓ Inhibits hyphal formation ($\geq 2.1 \mu M$) ✓ Decreases mRNA expression of <i>ALS3</i>, <i>HYR1</i> and <i>HWP1</i> genes
<ul style="list-style-type: none"> ✓ Inhibits biofilm formation ($\geq 50 \mu M$) but less effective than $\Delta M4$ ✓ Membrane permeabilization ($\geq 50 \mu M$) ✓ Activates metacaspases ($\geq 50 \mu M$) ✓ Activates ROS generation and Ca^{2+} accumulation ✓ Increases <i>GPX3</i> and <i>SOD5</i> mRNA level 	Biofilm 	<ul style="list-style-type: none"> ✓ Inhibits biofilm formation ($\geq 6.2 \mu M$) more effective than $\Delta M3$ ✓ Membrane permeabilization ($\geq 6.2 \mu M$) ✓ Activates metacaspases ($\geq 6.2 \mu M$) ✓ Activates ROS generation and Ca^{2+} accumulation ✓ Increases <i>GPX3</i> and <i>SOD5</i> mRNA level

FIGURE 10
Diagram presenting a summary of the results.

Data availability statement

The original contributions presented in the study are included in the article/Supplementary material, further inquiries can be directed to the corresponding author.

Author contributions

IG-L: methodology, investigation, formal analysis, conceptualization, writing-original draft, and writing-review and editing. GB: methodology, investigation, formal analysis, funding acquisition, writing-original draft, and writing-review and editing. MJ and AG: methodology, investigation, and formal analysis. JK-K: investigation and writing-review and editing. MM-M and EP: resources and writing-review and editing. JD: methodology and investigation. AK: writing-review and editing and funding acquisition. MR-K: conceptualization, supervision, funding acquisition, writing-original draft, and writing-review and editing. All authors contributed to the article and approved the submitted version.

Funding

This work was supported by the National Science Centre of Poland (grant no. 2019/33/B/NZ6/02284 awarded to MR-K) and

the Jagiellonian University in Krakow and the Statutory Funds of the Faculty of Biochemistry, Biophysics and Biotechnology (project No. N19/MNS/000035 awarded to GB).

Conflict of interest

The authors declare that the research was conducted in the absence of any commercial or financial relationships that could be construed as a potential conflict of interest.

Publisher's note

All claims expressed in this article are solely those of the authors and do not necessarily represent those of their affiliated organizations, or those of the publisher, the editors and the reviewers. Any product that may be evaluated in this article, or claim that may be made by its manufacturer, is not guaranteed or endorsed by the publisher.

Supplementary material

The Supplementary material for this article can be found online at: <https://www.frontiersin.org/articles/10.3389/fmicb.2022.1045984/full#supplementary-material>

References

- Akerey, B., Le-Lay, C., Fliss, I., Subirade, M., and Rouabhi, M. (2009). In vitro efficacy of nisin Z against *Candida albicans* adhesion and transition following contact with normal human gingival cells. *J. Appl. Microbiol.* 107, 1298–1307. doi: 10.1111/j.1365-2672.2009.04312.x
- Aldholmi, M., Marchand, P., Ourliac-Garnier, I., Le Pape, P., and Ganesan, A. (2019). A decade of antifungal leads from natural products: 2010–2019. *Pharmaceuticals* 12:182. doi: 10.3390/ph12040182
- Arendrup, M. C., Dzajic, E., Jensen, R. H., Johansen, H. K., Kjaeldgaard, P., Knudsen, J. D., et al. (2013). Epidemiological changes with potential implication for antifungal prescription recommendations for fungaemia: data from a nationwide fungaemia surveillance programme. *Clin. Microbiol. Infect.* 19, E343–E353. doi: 10.1111/1469-0691.12212
- Baldauf, C., Pagel, K., Warnke, S., von Helden, G., Kokschi, B., Blum, V., et al. (2013). How cations change peptide structure. *Chemistry* 19, 11224–11234. doi: 10.1002/chem.201204554
- Barchiesi, F., Spreghini, E., Tomassetti, S., Giannini, D., and Scalise, G. (2007). Caspofungin in combination with amphotericin B against *Candida parapsilosis*. *Antimicrob. Agents Chemother.* 51, 941–945. doi: 10.1128/AAC.00880-06
- Bartnicka, D., Karkowska-Kuleta, J., Zawrotniak, M., Satała, D., Michalik, K., Zielinska, J., et al. (2019). Adhesive protein-mediated cross-talk between *Candida albicans* and *Porphyromonas gingivalis* in dual species biofilm protects the anaerobic bacterium in unfavorable oxic environment. *Sci. Rep.* 9:4376. doi: 10.1038/s41598-019-40771-8
- Bochenska, O., Rapala-Kozik, M., Wolak, N., Aoki, W., Ueda, M., and Kozik, A. (2016). The action of ten secreted aspartic proteases of pathogenic yeast *Candida albicans* on major human salivary antimicrobial peptide, histatin 5. *Acta Biochim. Pol.* 63, 403–410. doi: 10.18388/abp.2016_1318
- Boman, H. G., Faye, I., Gudmundsson, G. H., Lee, J. Y., and Lidholm, D. A. (1991). Cell-free immunity in *Cecropia*. A model system for antibacterial proteins. *Eur. J. Biochem.* 201, 23–31. doi: 10.1111/j.1432-1033.1991.tb16252.x
- Bondaryk, M., Stanisewska, M., Zielińska, P., and Urbańczyk-Lipkowska, Z. (2017). Natural antimicrobial peptides as inspiration for design of a new generation antifungal compounds. *J. Fungi Basel* 3:46. doi: 10.3390/jof3030046
- Brady, D., Grapputo, A., Romoli, O., and Sandrelli, F. (2019). Insect cecropins, antimicrobial peptides with potential therapeutic applications. *Int. J. Mol. Sci.* 20:5862. doi: 10.3390/ijms20235862
- Buda De Cesare, G., Cristy, S. A., Garsin, D. A., and Lorenz, M. C. (2020). Antimicrobial peptides: a new frontier in antifungal therapy. *mBio* 11, e02123–e02120. doi: 10.1128/mBio.02123-20
- Cavalheiro, M., Romão, D., Santos, R., Mil-Homens, D., Pais, P., Costa, et al. (2021). Role of CgTpo4 in polyamine and antimicrobial peptide resistance: determining virulence in *Candida glabrata*. *Int. J. Mol. Sci.* 22:1376. doi: 10.3390/ijms22031376
- Cavalheiro, M., and Teixeira, M. C. (2018). *Candida* biofilms: threats, challenges, and promising strategies. *Front. Med. (Lausanne)*. 5:28. doi: 10.3389/fmed.2018.00028
- Chen, R. C., and Lan, C. Y. (2020). Human antimicrobial peptide Hepcidin 25-induced apoptosis in *Candida albicans*. *Microorganisms*. 8:585. doi: 10.3390/microorganisms8040585
- Choi, H., and Lee, D. G. (2015). Lycopene induces apoptosis in *Candida albicans* through reactive oxygen species production and mitochondrial dysfunction. *Biochimie* 115, 108–115. doi: 10.1016/j.biochi.2015.05.009
- Cytrynska, M., Mak, P., Zdybicka-Barabas, A., Suder, P., and Jakubowicz, T. (2007). Purification and characterization of eight peptides from *Galleria mellonella* immune hemolymph. *Peptides* 28, 533–546. doi: 10.1016/j.peptides.2006.11.010
- Dantas, A., Day, A., Ike, M., Kos, I., Achan, B., and Quinn, J. (2015). Oxidative stress responses in the human fungal pathogen. *Candida albicans*. *Biomolecules*. 5, 142–165. doi: 10.3390/biom5010142
- De Lucca, A. J., Bland, J. M., Vigo, C. B., Jacks, T. J., Peter, J., and Walsh, T. J. (2000). D-ecropin B: proteolytic resistance, lethality for pathogenic fungi and binding properties. *Med. Mycol.* 38, 301–308. doi: 10.1080/mmy.38.4.301.308
- Del Gaudio, G., Lombardi, L., Maisetta, G., Esin, S., Batoni, G., Sanguinetti, M., et al. (2013). Antifungal activity of the noncytotoxic human peptide Hepcidin 20 against fluconazole-resistant *Candida glabrata* in human vaginal fluid. *Antimicrob. Agents Chemother.* 57, 4314–4321. doi: 10.1128/AAC.00904-13
- Do Nascimento Dias, J., De Souza Silva, C., De Araújo, A. R., Souza, J., De Holanda Veloso Júnior, P. H., Cabral, W. F., et al. (2020). Mechanisms of action of antimicrobial peptides ToAP2 and NDBP-5.7 against *Candida albicans* planktonic and biofilm cells. *Sci. Rep.* 10:10327. doi: 10.1038/s41598-020-67041-2
- Ghosh, S., Pandit, G., Deb Nath, S., Chatterjee, S., and Satpati, P. (2021). Effect of monovalent salt concentration and peptide secondary structure in peptide-micelle binding. *RSC Adv.* 11, 36836–36849. doi: 10.1039/d1ra06772a
- Górecki, A., Bonarek, P., Górka, A. K., Figiel, M., Wilamowski, M., and Dziedzicka-Wasylewska, M. (2015). Intrinsic disorder of human Yin Yang 1 protein. *Proteins* 83, 1284–1296. doi: 10.1002/prot.24822
- Guevara-Lora, I., Bras, G., Karkowska-Kuleta, J., González-González, M., Ceballos, K., Sidlo, W., et al. (2020). Plant-derived substances in the fight against infections caused by *Candida* species. *Int. J. Mol. Sci.* 21:6131. doi: 10.3390/ijms21176131
- Gulati, M., and Nobile, C. J. (2016). *Candida albicans* biofilms: development, regulation, and molecular mechanisms. *Microbes Infect.* 18, 310–321. doi: 10.1016/j.micinf.2016.01.002
- Guo, Q., Sun, S., Yu, J., Li, Y., and Cao, L. (2008). Synergistic activity of azoles with amiodarone against clinically resistant *Candida albicans* tested by checkerboard and time-kill methods. *J. Med. Microbiol.* 57, 457–462. doi: 10.1099/jmm.0.047651-0
- Helmerhorst, E. J., Troxler, R. F., and Oppenheim, F. G. (2001). The human salivary peptide histatin 5 exerts its antifungal activity through the formation of reactive oxygen species. *PNAS* 98, 14637–14642. doi: 10.1073/pnas.141366998
- Helmerhorst, E. J., Venuleo, C., Beri, A., and Oppenheim, F. G. (2005). *Candida glabrata* is unusual with respect to its resistance to cationic antifungal proteins. *Yeast* 22, 705–714. doi: 10.1002/yea.1241
- Hollmann, A., Martinez, M., Maturana, P., Semorile, L. C., and Maffia, P. C. (2018). Antimicrobial peptides: interaction with model and biological membranes and synergism with chemical antibiotics. *Front. Chem.* 6:204. doi: 10.3389/fchem.2018.00204
- Huan, Y., Kong, Q., Mou, H., and Yi, H. (2020). Antimicrobial peptides: classification, design, application and research progress in multiple fields. *Front. Microbiol.* 11:582779. doi: 10.3389/fmicb.2020.582779
- Jacobsen, I. D., Wilson, D., Wächter, B., Brunke, S., Naglik, J. R., and Hube, B. (2012). *Candida albicans* dimorphism as a therapeutic target. *Expert Rev. Anti-Infect. Ther.* 10, 85–93. doi: 10.1586/eri.11.152
- Jamieson, D. J., Stephen, D. W., and Terrière, E. C. (1996). Analysis of the adaptive oxidative stress response of *Candida albicans*. *FEMS Microbiol. Lett.* 138, 83–88. doi: 10.1111/j.1574-6968.1996.tb08139.x
- Ji, S., Li, W., Zhang, L., Zhang, Y., and Cao, B. (2014). Cecropin A-melittin mutant with improved proteolytic stability and enhanced antimicrobial activity against bacteria and fungi associated with gastroenteritis in vitro. *Biochem. Biophys. Res. Commun.* 451, 650–655. doi: 10.1016/j.bbrc.2014.08.044
- Kaloriti, D., Jacobsen, M., Yin, Z., Patterson, M., Tillmann, A., Smith, D. A., et al. (2014). Mechanisms underlying the exquisite sensitivity of *Candida albicans* to combinatorial cationic and oxidative stress that enhances the potent fungicidal activity of phagocytes. *MBio* 5, e01334–e01314. doi: 10.1128/mBio.01334-14
- Kandasamy, S. K., and Larson, R. G. (2006). Effect of salt on the interactions of antimicrobial peptides with zwitterionic lipid bilayers. *Biochim. Biophys. Acta* 1758, 1274–1284. doi: 10.1016/j.bbame.2006.02.030
- Karkowska-Kuleta, J., Rapala-Kozik, M., and Kozik, A. (2009). Fungi pathogenic to humans: molecular bases of virulence of *Candida albicans*, *Cryptococcus neoformans* and *Aspergillus fumigatus*. *Acta Biochim. Pol.* 56, 211–224. doi: 10.18388/abp.2009_2452
- Kim, S., Hwang, J. S., and Lee, D. G. (2020). Lactoferricin B like peptide triggers mitochondrial disruption-mediated apoptosis by inhibiting respiration under nitric oxide accumulation in *Candida albicans*. *IUBMB Life* 72, 1515–1527. doi: 10.1002/iub.2284
- Kodedová, M., and Sychrová, H. (2017). Synthetic antimicrobial peptides of the halictines family disturb the membrane integrity of *Candida* cells. *Biochim. Biophys. Acta Biomembr.* 1859, 1851–1858. doi: 10.1016/j.bbame.2017.06.005
- Kovács, R., Nagy, F., Tóth, Z., Bozó, A., Balázs, B., and Majoros, L. (2019). Synergistic effect of nikkomycin Z with caspofungin and micafungin against *Candida albicans* and *Candida parapsilosis* biofilms. *Lett. Appl. Microbiol.* 69, 271–278. doi: 10.1111/lam.13204
- Kulig, K., Karnas, E., Woznicka, O., Kuleta, P., Zuba-Surma, E., Pyza, E., et al. (2022). Insight into the properties and immunoregulatory effect of extracellular vesicles produced by *Candida glabrata*, *Candida parapsilosis*, and *Candida tropicalis* biofilms. *Front. Cell. Infect. Microbiol.* 12:879237. doi: 10.3389/fcimb.2022.879237
- Kwon, M. S., Lee, H. J., and Lee, D. G. (2021). β -Amyrin-induced apoptosis in *Candida albicans* triggered by calcium. *Fungal Biol.* 125, 630–636. doi: 10.1016/j.funbio.2021.03.006
- Lee, E., Kim, J. K., Jeon, D., Jeong, K. W., Shin, A., and Kim, Y. (2015). Functional roles of aromatic residues and helices of papiliocin in its antimicrobial and anti-inflammatory activities. *Sci. Rep.* 5:12048. doi: 10.1038/srep12048
- Lee, J., and Lee, D. G. (2014). Melittin triggers apoptosis in *Candida albicans* through the reactive oxygen species-mediated mitochondria/caspase-dependent pathway. *FEMS Microbiol. Lett.* 355, 36–42. doi: 10.1111/1574-6968.12450

- Lee, W., and Lee, D. G. (2018). Reactive oxygen species modulate itraconazole-induced apoptosis via mitochondrial disruption in *Candida albicans*. *Free Rad. Res.* 52, 39–50. doi: 10.1080/10715762.2017.1407412
- Lee, Y., Puumala, E., Robbins, N., and Cowen, L. E. (2021). Antifungal drug resistance: molecular mechanisms in *Candida albicans* and beyond. *Chem. Rev.* 121, 3390–3411. doi: 10.1021/acs.chemrev.0c00199
- Li, R., Chen, C., Zhang, B., Jing, H., Wang, Z., Wu, C., et al. (2019). The chromogranin A-derived antifungal peptide CGA-N9 induces apoptosis in *Candida tropicalis*. *Biochem. J.* 476, 3069–3080. doi: 10.1042/BCJ20190483
- Li, L., Sun, J., Xia, S., Tian, X., Cheserek, M. J., and Le, G. (2016). Mechanism of antifungal activity of antimicrobial peptide APP, a cell-penetrating peptide derivative, against *Candida albicans*: intracellular DNA binding and cell cycle arrest. *Appl. Microbiol. Biotechnol.* 100, 3245–3253. doi: 10.1007/s00253-015-7265-y
- Liang, C., Zhang, B., Cui, L., Li, J., Yu, Q., and Li, M. (2018). Mgm1 is required for maintenance of mitochondrial function and virulence in *Candida albicans*. *Fungal Genet. Biol.* 120, 42–52. doi: 10.1016/j.fgb.2018.09.006
- Ma, H., Zhao, X., Yang, L., Su, P., Fu, P., Peng, J., et al. (2020). Antimicrobial peptide AMP-17 affects *Candida albicans* by disrupting its Cell Wall and cell membrane integrity. *Infect. Drug Resist.* 13, 2509–2520. doi: 10.2147/IDR.S250278
- Madani, F., Lindberg, S., Langel, U., Futaki, S., and Gräslund, A. (2011). Mechanisms of cellular uptake of cell-penetrating peptides. *J. Biophys.* 2011:414729. doi: 10.1155/2011/414729
- Maisetta, G., Di Luca, M., Esin, S., Florio, W., Brancatisano, F. L., Bottai, D., et al. (2008). Evaluation of the inhibitory effects of human serum components on bactericidal activity of human beta defensin 3. *Peptides* 29, 1–6. doi: 10.1016/j.peptides.2007.10.013
- Manrique-Moreno, M., Suwalsky, M., Patiño-González, E., Fandiño-Devia, E., Jemioła-Rzemińska, M., and Strzalka, K. (2021). Interaction of the antimicrobial peptide ΔM3 with the *Staphylococcus aureus* membrane and molecular models. *Biochim. Biophys. Acta Biomembr.* 1863:183498. doi: 10.1016/j.bbamem.2020.183498
- Mayer, F. L., Wilson, D., and Hube, B. (2013). *Candida albicans* pathogenicity mechanisms. *Virulence* 4, 119–128. doi: 10.4161/viru.22913
- Nguyen, L. T., Haney, E. F., and Vogel, H. J. (2011). The expanding scope of antimicrobial peptide structures and their modes of action. *Trends Biotechnol.* 29, 464–472. doi: 10.1016/j.tibtech.2011.05.001
- Niu, C., Wang, C., Yang, Y., Chen, R., Zhang, J., Chen, H., et al. (2020). Carvacrol induces *Candida albicans* apoptosis associated with Ca²⁺/Calcein pathway. *Front. Cell. Infect. Microbiol.* 10:192. doi: 10.3389/fcimb.2020.00192
- Ogasawara, A., Komaki, N., Akai, H., Hori, K., Watanabe, H., Watanabe, T., et al. (2007). Hyphal formation of *Candida albicans* is inhibited by salivary mucin. *Biol. Pharm. Bull.* 30, 284–286. doi: 10.1248/bpb.30.284
- Oñate-Garzón, J., Manrique-Moreno, M., Trier, S., Leidy, C., Torres, R., and Patiño, E. (2017). Antimicrobial activity and interactions of cationic peptides derived from *Galleria mellonella* cecropin D-like peptide with model membranes. *J. Antimicrob. Chem.* 70, 238–245. doi: 10.1038/ja.2016.134
- Pandit, G., Biswas, K., Ghosh, S., Debnath, S., Bidkar, A. P., Satpati, P., et al. (2020). Rationally designed antimicrobial peptides: insight into the mechanism of eleven residue peptides against microbial infections. *Biochim. Biophys. Acta Biomembr.* 1862:183177. doi: 10.1016/j.bbamem.2020.183177
- Pappas, P. G., Kauffman, C. A., Andes, D. R., Clancy, C. J., Marr, K. A., Ostrosky-Zeichner, L., et al. (2016). Clinical practice guideline for the Management of Candidiasis: 2016 update by the Infectious Diseases Society of America. *Clin. Infect. Dis.* 62, e1–e50. doi: 10.1093/cid/civ933
- Peng, C., Liu, Y., Shui, L., Zhao, Z., Mao, X., and Liu, Z. (2022). Mechanisms of action of the antimicrobial peptide Cecropin in the killing of *Candida albicans*. *Life (Basel)* 12:1581. doi: 10.3390/life12101581
- Peng, J., Wu, Z., Liu, W., Long, H., Zhu, G., Guo, G., et al. (2019). Antimicrobial functional divergence of the cecropin antibacterial peptide gene family in *Musca domestica*. *Parasit. Vectors* 12:537. doi: 10.1186/s13071-019-3793-0
- Pfaller, M. A., Carvalhaes, C. G., Smith, C. J., Diekema, D. J., and Castanheira, M. (2020). Bacterial and fungal pathogens isolated from patients with bloodstream infection: frequency of occurrence and antimicrobial susceptibility patterns from the SENTRY antimicrobial surveillance program (2012–2017). *Diagn. Microbiol. Infect. Dis.* 97:115016. doi: 10.1016/j.diagmicrobio.2020.115016
- Pfaller, M. A., Diekema, D. J., Turnidge, J. D., Castanheira, M., and Jones, R. N. (2019). Twenty years of the SENTRY antifungal surveillance program: results for *Candida* species from 1997–2016. *Open Forum Infect. Dis.* 6, S79–S94. doi: 10.1093/ofid/ofy358
- Ramamourthy, G., Park, J., Seo, C., Vogel, H. J., and Park, Y. (2020). Antifungal and Antibiofilm activities and the mechanism of action of repeating lysine-tryptophan peptides against *Candida albicans*. *Microorganisms* 8:758. doi: 10.3390/microorganisms8050758
- Romoli, O., Saviane, A., Bozzato, A., D'Antona, P., Tettamanti, G., Squartini, A., et al. (2017). Differential sensitivity to infections and antimicrobial peptide-mediated immune response in four silkworm strains with different geographical origin. *Sci. Rep.* 7:1048. doi: 10.1038/s41598-017-01162-z
- Rosetto, E., Contursi, P., Vollaro, A., Fusco, S., Notomista, E., and Catania, M. R. (2018). Antifungal and anti-biofilm activity of the first cryptic antimicrobial peptide from an archaeal protein against *Candida* spp. clinical isolates. *Sci. Rep.* 8:17570. doi: 10.1038/s41598-018-35530-0
- Rossi, A., Pizzo, P., and Filadi, R. (2019). Calcium, mitochondria and cell metabolism: a functional triangle in bioenergetics. *Biochim. Biophys. Acta, Mol. Cell Res.* 1866, 1068–1078. doi: 10.1016/j.bbamcr.2018.10.016
- Santa-González, G. A., Patiño-González, E., and Manrique-Moreno, M. (2020). Synthetic peptide ΔM4-induced cell death associated with cytoplasmic membrane disruption, mitochondrial dysfunction and cell cycle arrest in human melanoma cells. *Molecules* 25:5684. doi: 10.3390/molecules25235684
- Sato, H., and Feix, J. B. (2006). Peptide-membrane interactions and mechanisms of membrane destruction by amphipathic alpha-helical antimicrobial peptides. *Biochim. Biophys. Acta* 1758, 1245–1256. doi: 10.1016/j.bbamem.2006.02.021
- Seyedjavadi, S. S., Khani, S., Eslamifard, A., Ajdary, S., Goudarzi, M., Halabian, R., et al. (2020). The antifungal peptide MCh-AMP1 derived from *Matricaria chamomilla* inhibits *Candida albicans* growth via inducing ROS generation and altering fungal cell membrane permeability. *Front. Microbiol.* 10:3150. doi: 10.3389/fmicb.2019.03150
- Shagaghi, N., Bhavne, M., Palombo, E. A., and Clayton, A. H. (2017). Revealing the sequence of interactions of PuroA peptide with *Candida albicans* cells by live-cell imaging. *Sci. Rep.* 7:43542. doi: 10.1038/srep43542
- Shen, J., Lu, R., Cai, Q., Fan, L., Yan, W., Zhu, Z., et al. (2021). Mangiferin enhances the antifungal activities of caspofungin by destroying polyamine accumulation. *Virulence* 12, 217–230. doi: 10.1080/21505594.2020.1870079
- Shirazi, F., and Kontoyiannis, D. P. (2015). Micafungin triggers caspase-dependent apoptosis in *Candida albicans* and *Candida parapsilosis* biofilms, including caspofungin non-susceptible isolates. *Virulence* 6, 385–394. doi: 10.1080/21505594.2015.1027479
- Sovadinová, I., Kuroda, K., and Palermo, E. F. (2021). Unexpected enhancement of antimicrobial polymer activity against *Staphylococcus aureus* in the presence of fetal bovine serum. *Molecules* 26:4512. doi: 10.3390/molecules26154512
- Staniszewska, M., Bondaryk, M., Swoboda-Kopec, E., Siennicka, K., Sygitowicz, G., and Kurzatowski, W. (2013). *Candida albicans* morphologies revealed by scanning electron microscopy analysis. *Braz. J. Microbiol.* 44, 813–821. doi: 10.1590/S1517-83822013005000056
- Sun, C. Q., Peng, J., Yang, L. B., Jiao, Z. L., Zhou, L. X., Tao, R. Y., et al. (2022). A Cecropin-4 derived peptide C18 inhibits *Candida albicans* by disturbing mitochondrial function. *Front. Microbiol.* 13:872322. doi: 10.3389/fmicb.2022.872322
- Taff, H. T., Mitchell, K. F., Edward, J. A., and Andes, D. R. (2013). Mechanisms of *Candida* biofilm drug resistance. *Future Microbiol.* 8, 1325–1337. doi: 10.2217/fmb.13.101
- Tang, W. H., Wang, C. F., and Liao, Y. D. (2021). Fetal bovine serum albumin inhibits antimicrobial peptide activity and binds drug only in complex with α1-antitrypsin. *Sci. Rep.* 11:1267. doi: 10.1038/s41598-020-80540-6
- Theberge, S., Semail, A., Alamri, A., Leung, K. P., and Rouabhi, M. (2013). *C. albicans* growth, transition, biofilm formation, and gene expression modulation by antimicrobial decapeptide KSL-W. *BMC Microbiol.* 13:246. doi: 10.1186/1471-2180-13-246
- Tsang, P. W., Bandara, H. M., and Fong, W. P. (2012). Purpurin suppresses *Candida albicans* biofilm formation and hyphal development. *PLoS One* 7:e50866. doi: 10.1371/journal.pone.0050866
- Tsui, C., Kong, E. F., and Jabra-Rizk, M. A. (2016). Pathogenesis of *Candida albicans* biofilm. *Pathog. Dis.* 74:ftw018. doi: 10.1093/femspd/ftw018
- Van Dijk, P., Sjollem, J., Cammue, B. P., Lagrou, K., Berman, J., d'Enfert, C., et al. (2018). Methodologies for *in vitro* and *in vivo* evaluation of efficacy of antifungal and antibiofilm agents and surface coatings against fungal biofilms. *Microb. Cell.* 5, 300–326. doi: 10.15698/mic2018.07.638
- van Gent, M. E., Ali, M., Nibbering, P. H., and Klodzińska, S. N. (2021). Current advances in lipid and polymeric antimicrobial peptide delivery systems and coatings for the prevention and treatment of bacterial infections. *Pharmaceutics* 13:1840. doi: 10.3390/pharmaceutics13111840
- Vitale, R. G., Afeltra, J., and Dannaoui, E. (2005). Antifungal combinations. *Methods Mol. Med.* 118, 143–152. doi: 10.1385/1-59259-943-5:143
- Vriens, K., Cammue, B. P., and Thevissen, K. (2014). Antifungal plant defensins: mechanisms of action and production. *Molecules* 19, 12280–12303. doi: 10.3390/molecules190812280
- Vriens, K., Cools, T. L., Harvey, P. J., Craik, D. J., Spincemille, P., Cassiman, D., et al. (2015). Synergistic activity of the plant Defensin HsAFP1 and Caspofungin against *Candida albicans* biofilms and planktonic cultures. *PLoS One* 10:e0132701. doi: 10.1371/journal.pone.0132701

Wang, K., Dang, W., Xie, J., Zhu, R., Sun, M., Jia, F., et al. (2015). Antimicrobial peptide protonectin disturbs the membrane integrity and induces ROS production in yeast cells. *Biochim. Biophys. Acta* 1848, 2365–2373. doi: 10.1016/j.bbame.2015.07.008

Wolak, N., Tomasi, M., Kozik, A., and Rapala-Kozik, M. (2015). Characterization of thiamine uptake and utilization in *Candida* spp. subjected to oxidative stress. *Acta Biochim. Pol.* 62, 445–455. doi: 10.18388/abp.2015_1044

Youle, R. J., and van der Bliek, A. M. (2012). Mitochondrial fission, fusion, and stress. *Science* 337, 1062–1065. doi: 10.1126/science.1219855

Zhang, M., Lu, J., Duan, X., Chen, J., Jin, X., Lin, Z., et al. (2021). Rimonabant potentiates the antifungal activity of amphotericin B by increasing cellular oxidative stress and cell membrane permeability. *FEMS Yeast Res.* 21:foab016. doi: 10.1093/femsyr/foab016



OPEN ACCESS

EDITED BY

Jianhua Wang,
Key Laboratory for Feed Biotechnology,
Feed Research Institute (CAAS),
China

REVIEWED BY

Piyush Baidara,
University of Missouri,
United States
Wilma Van Rensburg,
Stellenbosch University,
South Africa

*CORRESPONDENCE

Changlong Shu
✉ shuchanglong@caas.cn
Rongmei Liu
✉ liurongmei@neau.edu.cn

[†]These authors have contributed equally to this work

SPECIALTY SECTION

This article was submitted to
Antimicrobials,
Resistance and Chemotherapy,
a section of the journal
Frontiers in Microbiology

RECEIVED 15 December 2022

ACCEPTED 02 March 2023

PUBLISHED 16 March 2023

CITATION

Fu Q, Cao D, Sun J, Liu X, Li H, Shu C and
Liu R (2023) Prediction and bioactivity of small-
molecule antimicrobial peptides from *Protaetia*
brevitarsis Lewis larvae.
Front. Microbiol. 14:1124672.
doi: 10.3389/fmicb.2023.1124672

COPYRIGHT

© 2023 Fu, Cao, Sun, Liu, Li, Shu and Liu. This
is an open-access article distributed under the
terms of the [Creative Commons Attribution
License \(CC BY\)](https://creativecommons.org/licenses/by/4.0/). The use, distribution or
reproduction in other forums is permitted,
provided the original author(s) and the
copyright owner(s) are credited and that the
original publication in this journal is cited, in
accordance with accepted academic practice.
No use, distribution or reproduction is
permitted which does not comply with these
terms.

Prediction and bioactivity of small-molecule antimicrobial peptides from *Protaetia brevitarsis* Lewis larvae

Qian Fu^{††}, Dengtian Cao^{††}, Jing Sun¹, Xinbo Liu¹, Haitao Li¹,
Changlong Shu^{2*} and Rongmei Liu^{1*}

¹College of Life Sciences, Northeast Agricultural University, Harbin, China, ²State Key Laboratory for Biology of Plant Diseases and Insect Pests, Institute of Plant Protection, Chinese Academy of Agricultural Sciences, Beijing, China

Antimicrobial peptides (AMPs) are widely recognized as promising natural antimicrobial agents. Insects, as the group of animals with the largest population, have great potential as a source of AMPs. Thus, it is worthwhile to investigate potential novel AMPs from *Protaetia brevitarsis* Lewis larvae, which is a saprophagous pest prevalent in China. In this study, comparing the whole-genome sequence of *Protaetia brevitarsis* Lewis larvae with the Antimicrobial Peptide Database (APD3) led to the identification of nine peptide templates that were potentially AMPs. Next, based on the peptide templates, 16 truncated sequences were predicted to the AMPs by bioinformatics software and then underwent structural and physicochemical property analysis. Thereafter, candidate small-molecule AMPs were artificially synthesized and their minimal inhibitory concentration (MIC) values were assessed. A candidate peptide, designated FD10, exhibited strong antimicrobial activity against both bacteria and fungi comprising *Escherichia coli* (MIC: 8 µg/mL), *Pseudomonas aeruginosa* (MIC: 8 µg/mL), *Bacillus thuringiensis* (MIC: 8 µg/mL), *Staphylococcus aureus* (MIC: 16 µg/mL), and *Candida albicans* (MIC: 16 µg/mL). Additionally, two other candidate peptides, designated FD12 and FD15, exhibited antimicrobial activity against both *E. coli* (MIC: both 32 µg/mL) and *S. aureus* (MIC: both 16 µg/mL). Moreover, FD10, FD12, and FD15 killed almost all *E. coli* and *S. aureus* cells within 1h, and the hemolytic effect of FD10 (0.31%) and FD12 (0.40%) was lower than that of ampicillin (0.52%). These findings indicate that FD12, FD15, and especially FD10 are promising AMPs for therapeutic application. This study promoted the development of antibacterial drugs and provided a theoretical basis for promoting the practical application of antimicrobial peptides in the *Protaetia brevitarsis* Lewis larvae.

KEYWORDS

Protaetia brevitarsis Lewis larvae, AMPs, small molecule design, antimicrobial activity, APD3, truncated sequence

1. Introduction

As one of the greatest inventions of the last century, antibiotics are widely used in the treatment of infectious diseases (Durand et al., 2019). However, antibiotic resistance has become a key concern, largely due to the natural selection of resistant bacteria in response to irrational use of antibiotics (Frieri et al., 2017). The World Health Organization has been concerned about

the problems of antibiotic resistance. These issues have been identified as highly serious challenges to public health and sustainable health care (Manniello et al., 2021). Therefore, there is an urgent need to find ways to tackle antibiotic resistance.

Antimicrobial peptides (AMPs) are a potential alternative to antibiotics due to their broad-spectrum antimicrobial activities and low drug resistance (Zhang et al., 2019), and they exhibit broad biomedical application prospects on account of their anticancer, antiviral, antiparasitic, and immunomodulatory effects (Shi et al., 2021). According to the site of action, AMPs are divided into two categories: membrane and non-membrane disruption AMPs. The former increases the permeability of phospholipid bilayers and leads to cell death. The latter may interact with intracellular macromolecules and eventually kill cells (Thakur et al., 2022). Regardless of the mechanism of action, AMPs must proceed through four steps: (1) attract, i.e., AMPs are attracted to the surface of microbes by electrostatic interaction; (2) enrichment, i.e., AMPs replace cations on the cell membrane and cause outer membrane lysis; (3) combination, i.e., AMPs interact with the lipid membrane; and (4) AMP insertion and membrane permeation followed by the AMPs killing cells in a variety of ways (Yeasmin et al., 2021). At present, five models explaining membrane permeabilization are widely accepted: carpet model (Dean et al., 2010), barrel stave model (Ferreira Cespedes et al., 2012), aggregate channel model (Wu et al., 1999), toroidal model (Bozelli et al., 2012), and detergent-like model (Bechinger and Lohner, 2006). To date, the sources of AMPs are extremely broad (Di Somma et al., 2020). The Antimicrobial Peptide Database (APD) shows that most AMPs are derived from animals, while only a few are from plants and bacteria. Therefore, insects, as the group of animals with the largest population, have great potential as a source of AMPs (Sahoo et al., 2021).

Insect AMPs are small cationic molecules with various biological activities, and they are an essential component of the insect innate immune system (Wu et al., 2018). According to their structure and function, insect AMPs can be classified into four categories: comprising α -helical (cecropin and moricin), cysteine-rich (defensin and drosomycin), proline-rich (apidaecin and lebecin), and glycine-rich (attacin and glover) peptides (Yi et al., 2014). Cecropins are made up of two α -helical structures, and they exhibit antimicrobial activity against both Gram-positive and Gram-negative bacteria (Peng et al., 2019). Insect defensins are composed of α -helix and β -pleated structures, and they mainly exhibit antimicrobial activity against Gram-positive bacteria (Koehbach, 2017). Proline-rich peptides consist of 15–34 amino acids, and they exhibit antimicrobial activity against both Gram-positive and Gram-negative bacteria (Rayaprolu et al., 2010; Rao et al., 2012; Armas et al., 2021). Glycine-rich peptides mainly exhibit antimicrobial activity against Gram-negative bacteria (Mrinal and Nagaraju, 2008; Moreno-Habel et al., 2012). Currently, there are more than 300 insect AMPs listed in the APD, including from Coleoptera (Manniello et al., 2021; Xia et al., 2021), Diptera (Aittomaki et al., 2017; Gong et al., 2022), Hemiptera (Nishide et al., 2022), and Lepidoptera (Chowdhury et al., 2020).

Protaetia brevitarsis Lewis (Coleoptera: Scarabaeidae) is an important agricultural pest distributed in most areas of China. Its larvae are saprophytic, which means that they are exposed to many different pathogenic microorganisms in the living environment (Wang et al., 2019), so their immune system secretes AMPs. In 2003, three AMPs from *P. brevitarsis* Lewis, designated protaetins 1, 2, and 3, were

purified and characterized; protaetin 2 was shown to have activity against Gram-positive and Gram-negative bacteria (Yoon et al., 2003). In 2007, Yoo et al. (2007) extracted fatty acids with anticancer activity from *P. brevitarsis* Lewis. In addition, Kang et al. (2012) demonstrated that a *P. brevitarsis* Lewis larval extract exhibits potent hepatoprotective effects. Later, Lee et al. (2014) found that *P. brevitarsis* Lewis larval extracts exhibit hepatoprotective and antineoplastic properties. However, despite the many studies on the control of *P. brevitarsis* Lewis, there are few studies on its medicinal value, though it has important research value as a kind of medicinal insect.

In our laboratory, *P. brevitarsis* Lewis was subjected to whole-genome sequencing (unpublished data). By comparing the whole-genome sequence with the APD, it was found that some *P. brevitarsis* Lewis gene sequences corresponded to AMP sequences. To obtain highly active small-molecular-weight AMPs, truncation, amino acid substitutions, and N-terminal acetylation were used to modify the AMP sequences. Thereafter, their antimicrobial activity, hemolytic effects, cytotoxicity, and stability were studied *in vitro*. This study could provide ideas for the design of small-molecule AMPs and contribute to solutions for the issue of antibiotic resistance. To increased awareness of this study, it was illustrated with the strategic diagram (Figure 1).

2. Materials and methods

2.1. Microbial strains and cell lines

The bacterial strains *Staphylococcus aureus* (*S. aureus*) CMCC(B) 26003 and *Pseudomonas aeruginosa* (*P. aeruginosa*) CMCC(B)10104, and the fungal strain *Candida albicans* (*C. albicans*) CMCC(F) 98001, were purchased from Beijing Kezhan Biotechnology Co., Ltd. 2019, China. The bacterial strains *Bacillus thuringiensis* and *Escherichia coli* were obtained from our laboratory. Mouse RAW 264.7 macrophages were purchased from Shanghai Yaji Biotechnology Co., Ltd. 2022, China.

2.2. Reagents

Mueller–Hinton broth (MHB), Mueller–Hinton agar (MHA), nutrient agar (NA), and Sabouraud dextrose agar (SDA) were obtained from BEIJING AOBXING BIO-TECH Co., Ltd. 2019, China. Trypsin was obtained from Nanjing Beyotime Biotechnology Co., Ltd., 2021. 3-(4,5-dimethylthiazol-2-yl)-2,5-diphenyltetrazolium bromide (MTT) was purchased from Sigma-Aldrich, 2021 (China).

2.3. Preparation of microbial suspensions

Staphylococcus aureus CMCC(B) 26003, *B. thuringiensis*, *E. coli*, and *P. aeruginosa* CMCC(B)10104 were cultured in NA medium and *C. albicans* CMCC(F) 98001 was cultured in SDA medium. They were incubated in a constant-temperature (bacteria: 37°C; fungi: 28°C) incubator for 16–20 h. Thereafter, single colonies were picked and incubated in 50 mL MHB at 160 rpm/min at the optimal growth temperature (bacteria: 37°C; fungi: 28°C). Microbial suspensions of 1×10^6 CFU/mL were then prepared (Chen et al., 2016).

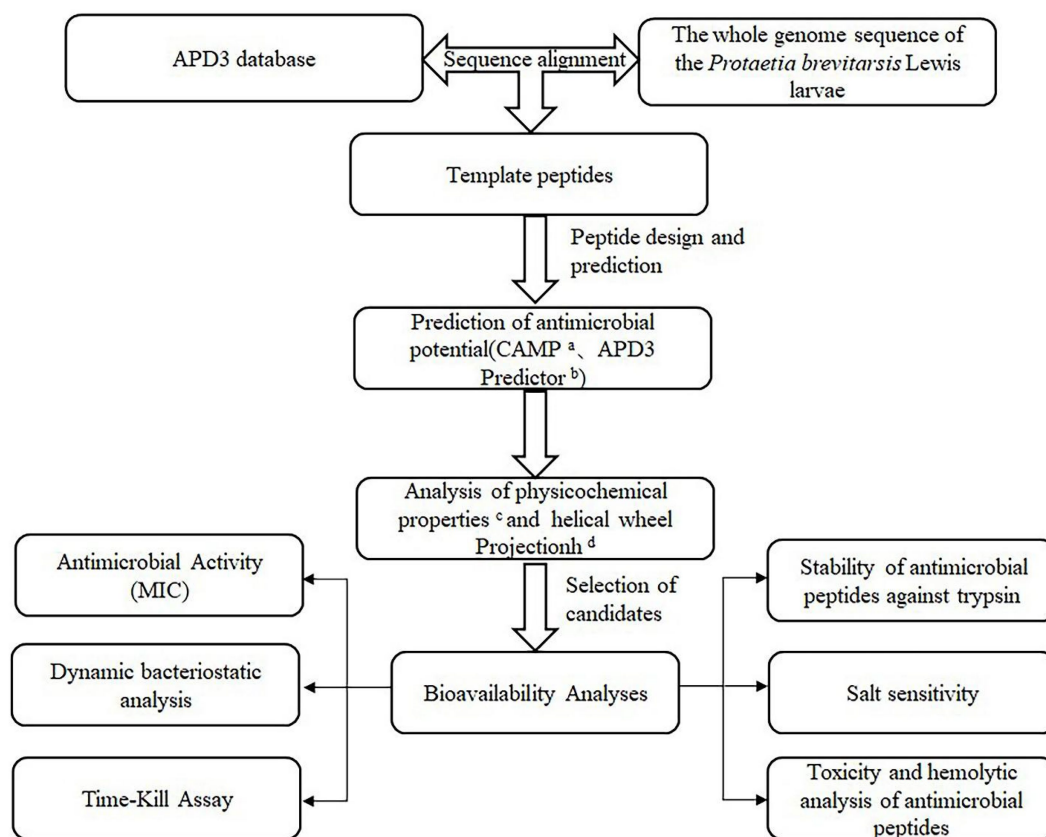


FIGURE 1

Strategic diagram of the methodology used to select potential antibacterial peptides in the *P. brevitarsis* Lewis. ^aCAMP (<http://www.camp.bicnirrh.res.in/>). ^bAPD3 Predictor (http://aps.unmc.edu/AP/prediction/prediction_main.php). ^cExPASy-ProtParam (<http://web.expasy.org/protparam/>). ^dHeliquist (<https://heliquist.ipmc.cnrs.fr/>).

2.4. Screening for template peptides

The whole-genome sequence of *Protaetia brevitarsis* Lewis larvae (GenBank accession number: CM014285.1) was compared to the AMP sequences in APD3.¹ Aligned sequences were used as template peptide sequences (Houyvet et al., 2018).

2.5. Predicted AMPs

The template peptide was used to screen out the truncated sequences, and then the antimicrobial region within the predicted peptide was screened using the random forest classifier calculation method in CAMP² to predict the possibility of becoming AMPs. Thereafter, the obtained truncated candidate peptides were inputted into Antimicrobial Peptide Predictor³ in APD3 for prediction of the probability of being the truncated sequence of an AMP. The physicochemical properties of the peptides were analyzed by using the ExPASy website software ProtParam⁴ in order to select peptides with

a high electrostatic charge, high hydrophobic amino acid ratio, high stability, CAMP prediction of high probability of being an AMP, and APD3 prediction of high probability of being the truncated sequence of an AMP (Yang et al., 2018).

In addition, depending on the structure–function relationships relevant to each AMP, the peptide was selectively modified by amino acid substitution or N-terminal acetylation. For example, negatively charged amino acid residues could be replaced with positively charged amino acid residues (ANWDKVir changed to ANWKKVir) and -NH₂ could be added to the end of the peptide (STLHLVRLRL-NH₂; STLHLVRLRL) to preserve its functional activity (Chen et al., 2016; Yang et al., 2018). The 16 designed peptides were sent to Beijing Coolaber Technology Ltd. (2020). for chemical synthesis.

2.6. Preliminary screening of 16 candidate peptides for antimicrobial activity by agar punch method

100 μL of 1 × 10⁶ CFU/mL microbial suspension (*E. coli*, *P. aeruginosa* CMCC(B)10104, *B. thuringiensis*, *S. aureus* CMCC(B) 26003, or *C. albicans* CMCC(F) 98001) was evenly applied to dishes containing 20 mL NA (bacteria) or SDA (fungi). After the microbial solution solidified, six holes per dish were punched with a sterile pipette tip of 6 mm in diameter, with each hole spaced >20 mm apart

1 <http://aps.unmc.edu/AP/>

2 <http://www.camp.bicnirrh.res.in/>

3 http://aps.unmc.edu/AP/prediction/prediction_main.php

4 <http://web.expasy.org/protparam/>

and > 10 mm apart from the edge of the dish. The holes were marked with (+), (−), and (1–16), representing the positive control (ampicillin), negative control (deionized water), and treatment groups (16 candidate peptides dissolved in sterile water), respectively. Next, 55 µL of 1 mg/mL control/treatment was added to each hole and incubated in a constant-temperature (bacteria: 37°C; fungi: 28°C) incubator for 16–18 h (Chen et al., 2016; Gong et al., 2022), with three replicates for each treatment group. The diameter of the inhibition circle was measured using ImageJ software (National Institutes of Health, United States) in order to preliminarily determine whether the candidate peptides had inhibitory activity.

2.7. Minimal inhibitory concentration (MIC) of five candidate peptides

The MIC values of five candidate peptides (FD4, FD10, FD12, FD14, and FD15), which were selected based on physicochemical properties and antimicrobial effects (determined by the agar punch method), were evaluated using a micro-broth dilution method (Zhou and Zhou, 2018). Serial two-fold dilutions of the candidate peptides were prepared in 96-well plates containing the same microbial inoculum (*E. coli*, *P. aeruginosa* CMCC(B)10104, *B. thuringiensis*, *S. aureus* CMCC(B) 26003, or *C. albicans* CMCC(F) 98001). The plates were incubated (bacteria: 37°C; fungi: 28°C) for 16–18 h. Ampicillin was used as the positive control. The MIC was defined as the lowest peptide concentration where no visible growth occurred (Diao et al., 2014). The experiment was conducted in triplicate.

2.8. Predicted helical wheel projection diagrams of six AMPs

Six AMPs (FD10, FD12, FD13, FD14, FD15, and FD16), selected based on antimicrobial activity and the peptide modifications, were processed by Heliquest⁵ (Gautier et al., 2008) in order to generate helical wheel projection diagrams.

2.9. Dynamic antimicrobial analysis of three AMPs

During the antimicrobial activity screening it was found that the five antimicrobial AMPs (FD4, FD10, FD12, FD14, and FD15) had inhibitory effects against *E. coli* and *S. aureus* CMCC(B) 26003. Therefore, the follow-up experiments involved these two bacteria, along with the three AMPs with the best antimicrobial effects (FD10, FD12, and FD15). The dynamic antimicrobial effects were analyzed by measuring the effects of the AMPs on bacterial growth over 10 h. First, 100 µL microbial solution (1.0×10^6 CFU/mL) was added to the wells of a 96-well culture plate, and then 100 µL AMP (at 1× and 1/4× MIC) was added and the mixtures were cultured at 37°C (Mishra et al., 2013; Memariani et al., 2016). 100 µL MHB with 100 µL microbial solution was used as the control group. The optical density

at 600 nm (OD_{600}) was measured every hour for 10 h using a microplate reader (Hou et al., 2007). The experiment was conducted in triplicate.

2.10. Time–kill assay of three AMPs

The kill-time curve assay method was used to investigate the bactericidal effects of the essential oil according to the technique described by Joray et al. (2011). A time–kill assay was used to examine the rate at which three AMPs (FD10, FD12, and FD15) killed two microbes (*S. aureus* CMCC(B) 26003 and *E. coli*) *in vitro* over time, based on the number of viable bacteria left at various time points after AMP exposure. Briefly, AMP at 2× MIC was added to MHB containing 10^6 CFU/mL *S. aureus* CMCC(B) 26003 or *E. coli* and the mixture was then incubated at 37°C and 100 rpm. At various time points, a sample was taken, serially diluted, and plated on MHA for colony counting (Flamm et al., 2019).

2.11. Enzyme stability assay of three AMPs

AMP at 2× MIC was incubated with the same volume of 1 mg/mL trypsin solution at 37°C for 1 h, followed by a 5 min 95°C exposure to inactivate the trypsin. Thereafter, 100 µL of the resulting solution was added to 96-well plates, followed by 100 µL microbial suspension (1×10^6 CFU/mL). Sterile water with 1×10^6 CFU/mL microbial suspension was used as the blank control. After culturing at 37°C for 16–18 h, colony counting was conducted (Tresnak and Hackel, 2020). The experiment was conducted in triplicate.

2.12. Salt sensitivity assays of three AMPs

E. coli and *S. aureus* CMCC(B) 26003 (1×10^6 CFU/mL) were incubated in MHB with various final physiological concentrations of serum salts (150 mM NaCl, 4.5 mM KCl, 1 mM MgCl₂, and 4 mM FeCl₃). 50 µL of these *E. coli* or *S. aureus* CMCC(B) 26003 suspensions and 50 µL of AMP (serially diluted two-fold to a final concentration of 256 µg/mL) were added to a 96-well plate and incubated at 37°C for 16–18 h (Chou et al., 2016). The MIC values were then determined. The experiment was conducted in triplicate.

2.13. Hemolysis and cytotoxicity assays of three AMPs

The hemolytic activity of AMPs on mammalian erythrocytes was determined by optical absorption (Lee et al., 2011). Briefly, fresh mouse erythrocytes were collected, washed, and resuspended in phosphate-buffered saline PBS at a concentration of 8% (v/v). Thereafter, 100 µL of this solution was added to a 96-well plate containing an equal volume of AMP (1–256 µg/mL) and incubated at 37°C for 1 h. The positive control was 100 µL 1% Triton X-100 and 100 µL 8% erythrocytes, and the negative control was 100 µL phosphate-buffered saline PBS and 100 µL 8% erythrocytes. Next, each mixture was centrifuged at 1,200 g for 15 min, and 100 µL of the supernatant was transferred to a clean 96-well plate to measure the light absorption value at 576 nm with a microplate reader. The percent

⁵ <https://heliquest.ipmc.cnrs.fr/>

TABLE 1 Amino acid sequences of candidate peptides.

Peptide	Sequence	Peptide	Sequence
FD1	VACAKRVVR	FD9	SLARAGKVR
FD2	LARTLKRLGM	FD10	VFRLKKWIQKVI
FD3	IRAWVAWRNR	FD11	FPVGRVHRL
FD4	IVHLLTKMTK	FD12	KIYVLLRRQA
FD5	AFQRTIRKFL	FD13	ANWDKVR
FD6	KLLVPRCR	FD14	ANWKKVR
FD7	RIGRLVTRAAF	FD15	STLHLVLRRL-NH ₂
FD8	LVTRAAFHGKKV	FD16	STLHLVLRRL

hemolysis was calculated using the following formula: *Percent hemolysis* = $[(A - A_0)/(A_+ - A_0)] \times 100\%$, where A , A_+ , and A_0 represent the absorbance of the peptide sample and positive and negative controls, respectively (Li et al., 2020).

The cytotoxicity of AMPs toward mouse RAW 264.7 macrophages was determined by MTT assays (Meng and Kumar, 2007). Cells were added into 96-well microtiter plates (2.5×10^4 cells/well) and incubated for 24 h. After another 24 h incubation with Amp and FD10, FD12, FD15 (1 to 256 $\mu\text{g/mL}$), MTT solution was added and incubated for 4 h. Followed the removing of the MTT, dimethyl sulfoxide (DMSO) (150 μL /well) was added and the absorbance was measured at 570 nm. Untreated cells were used as a control. The cell survival rate was calculated using the following formula: *survival rate* (%) = $(\text{Abs}_{570 \text{ nm}} \text{ of treated sample} / \text{Abs}_{570 \text{ nm}} \text{ of control}) \times 100\%$ (Wang et al., 2018). The cytotoxicity detection was repeated in triplicate.

2.14. Statistical analysis

All data are presented as mean \pm standard deviation (SD), with “ n ” represents the number of samples. One-way analysis or two-way analysis of variance (ANOVA) in SPSS software was used to analyze significant differences between groups. $p < 0.05$ indicated that the differences were statistically significant. GraphPad Prism 8.0 (GraphPad Software, United States) was used for statistical computing and plotting.

3. Results

3.1. Template peptides and secondary structure prediction

After comparing the *Protaetia brevitaris* Lewis genomic sequence to known AMP sequences in a database, nine aligned sequences were identified and used as template peptides (AP02030, AP02257, AP02096, AP00489, AP01575, AP02128, AP01540, AP02012, and AP00208) (Supplementary Figure S1).

PHYRE²⁶ was used to predict the secondary structure of the nine template peptides to clearly and intuitively observe their structures,

and to help to predict their functions. They all have typical secondary structures, i.e., α -helical structures (green spirals) and β -pleated structures (blue arrows) (other lines are random coil regions) (Supplementary Figure S2). The figure, which indicates the confidence of predictions (decreasing from red to purple), shows that the α -helical region prediction confidence is high (mostly in red). AMPs mainly depend on their α -helical structures, while the β -pleated structures were treated as auxiliary structures in terms of the subsequent related design work.

3.2. Screening for candidate peptides

Based on the nine template peptides, key truncated sequences were identified (Supplementary Tables S1–S9), and 16 candidate peptides, designated FD1–16, were designed (Table 1). FD13(ANWDKVR) contains a negatively charged amino acid residue, which was detrimental to the interaction of the antimicrobial peptide with bacterial membranes, so it could be considered to be replaced with Lys, which becomes FD14 (ANWKKVR), thereby increasing the net charge from +1 to +3 without changing the hydrophobic amino acid ratio. The polypeptide sequence of FD16 (STLHLVLRRL) was the C-terminal sequence of the template peptide, and the control peptide FD15 (STLHLVLRRL-NH₂) could be set up, and -NH₂ could be added to the FD16 terminal in order to preserve the integrity of functional activity.

3.3. Physicochemical properties of candidate peptides

The physicochemical properties of the 16 candidate peptides were clearly and concisely compared (Table 2). The net charge of each candidate peptide was 2–4, which was favorable for interacting with the negatively charged bacterial membrane. The high ratio of hydrophobic residues indicated easy insertion into the membrane interior to destroy the bacterial cells. The small molecular weight lowered chemical synthesis costs. The instability index was not high except for FD1, FD15, and FD16, which showed that most of the candidate peptides were relatively stable.

3.4. Antimicrobial activity of candidate peptides based on agar punch method

The antimicrobial effects of the 16 candidate peptides against five microbes (*E. coli*, *P. aeruginosa* CMCC(B)10104, *B. thuringiensis*, *S. aureus* CMCC(B) 26003, and *C. albicans* CMCC(F) 98001) were compared to the effects of ampicillin (positive control) and sterile water (negative control). The candidate peptides differed in their inhibitory action against the five microbes, based on the size of the inhibition circles formed (Supplementary Figure S3).

Five peptides (FD4, FD10, FD12, FD14, and FD15) generated inhibition circles, with the growth of the five microbes being prevented in these zones (the remaining candidate peptides did not form inhibition circles). FD4 was effective against *E. coli* and *S. aureus* CMCC(B) 26003, with inhibition circle diameters of 10.12 and 9.47 mm, respectively (Table 3). However, they were much smaller

6 <http://www.sbg.bio.ic.ac.uk/phyre2/html/>

TABLE 2 Comparison of physicochemical properties of candidate peptides.

Peptide	MW (Da) ^a	Net charge	pI	Hydrophobic	HRR ^b (%)	α -spiral proportion (%)	II ^c	LI ^d
FD1	1,001.26	+3	10.86	0.644	66	100	43.93	118.89
FD2	1,158.47	+3	12.01	0.110	50	80	33.11	127.00
FD3	1,327.56	+3	12.30	−0.650	60	60	12.85	88.00
FD4	1,183.52	+2	10.00	0.580	55	100	30.23	146.00
FD5	1,279.55	+3	12.01	−0.140	50	90	9.00	88.00
FD6	984.27	+3	10.86	−0.025	55	100	12.79	133.75
FD7	1,259.52	+3	12.30	0.391	54	100	1.37	115.45
FD8	1,326.61	+3	11.17	0.167	50	67	−20.70	97.50
FD9	957.142	+3	12.01	−0.278	44	100	−9.98	97.78
FD10	1,557.99	+4	11.26	0.283	58	100	−4.98	145.83
FD11	1,193.46	+2	12.00	0.460	50	80	39.03	136.00
FD12	1,259.56	+3	11.00	0.040	50	100	46.31	156.00
FD13	1,001.15	+1	8.79	−0.725	50	75	−25.44	97.50
FD14	1,014.24	+3	11.17	−0.775	50	75	−14.82	97.50
FD15	1,458.73	+2	12.00	−0.083	50	80	51.55	154.17
FD16	1,207.48	+2	12.00	0.570	50	80	47.52	185.00

^aMolecular weight; ^bHydrophobic residue ratio; ^cInstability index; ^dLiposolubility index.

than those of ampicillin (29.37 and 19.98 mm), indicating a lower antimicrobial effect. FD10 was more effective (larger inhibition circle diameter) than ampicillin against *P. aeruginosa* CMCC(B)10104, *B. thuringiensis*, and *S. aureus* CMCC(B) 26003, and it was the only candidate peptide with activity against fungi (*C. albicans* CMCC(F) 98001), indicating excellent inhibitory effects. FD12 was comparable to ampicillin against *B. thuringiensis* and *S. aureus* CMCC(B) 26003, indicating antimicrobial activity against Gram-positive bacteria. FD14 and FD15 were both much less effective than ampicillin.

3.5. Further antimicrobial activity of candidate peptides

Based on the physicochemical properties and antimicrobial effects of the candidate peptides determined using the agar punch method, five (FD4, FD10, FD12, FD14, and FD15) were selected for further antimicrobial activity analysis. FD10 had an antimicrobial effect on all five microbes at a low MIC; the MIC against Gram-negative bacteria *E. coli* and *P. aeruginosa* CMCC(B)10104 was as low as 8 µg/mL, while those against Gram-positive *B. thuringiensis* and *S. aureus* CMCC(B) 26003 were 8 and 16 µg/mL, respectively, and that against *C. albicans* CMCC(F) 98001 was 16 µg/mL. FD12 and FD15 also had antimicrobial activity against *S. aureus* CMCC(B) 26003 with a MIC of 16 µg/mL each and against *E. coli* with a MIC of 32 µg/mL each (Table 4).

3.6. Helical wheel projection diagrams

Heliquet was used to calculate the helix properties of six AMPs (FD10, FD12, FD13, FD14, FD15, and FD16). Supplementary Figure S4 shows the helical wheel projection diagrams of the AMPs. In this

conformation, they did not have different physicochemical properties from those predicted by ExPASy-ProtParam. Both FD10 and FD12 (especially FD10) had a high proportion of electrostatically charged and hydrophobic amino acids, which are favorable for adsorption to the bacterial cell membrane and insertion into the membrane, causing bacterial death. Despite FD14 having a positively charged Lys in place of the negatively charged Asp in FD13, neither FD13 nor FD14 were antimicrobial, with both having a low hydrophilic index. The C-terminal acetylation modification gave FD15 antimicrobial activity. Helical wheel projection diagrams could not be constructed for FD13 and FD14 because the sequences were considered excessively short (only eight amino acid residues).

3.7. Dynamic antimicrobial analysis

In the dynamic antimicrobial analysis, the OD₆₀₀ of the microbial solutions were essentially unchanged until 1 h, indicating slow microbe proliferation (Figure 2). At 1× MIC, for both AMPs and ampicillin, *E. coli* and *S. aureus* CMCC(B) 26003 growth was almost inhibited at 10 h (relative to the control [MHB with microbial solution]).

Ampicillin at 1/4× MIC led to slow *E. coli* growth after 1 h and increased growth after 2 h, while the AMPs at 1/4× MIC led to *E. coli* growth only after 3–4 h, and after 4 h, *E. coli* continued to grow. FD10 had a significantly higher inhibitory effect against *E. coli* than the other AMPs (Figure 2A). Similarly, ampicillin at 1/4× MIC led to *S. aureus* CMCC(B) 26003 growth at around 2 h, while AMPs at 1/4× MIC led to slow growth after 3 h (Figure 2B), and after 4 h, the number of *S. aureus* CMCC(B) 26003 began to increase more rapidly.

This indicates that, compared to ampicillin, the AMPs exhibited good microbial inhibition and broad antimicrobial activity even at concentrations below the MIC.

TABLE 3 Diameter of the inhibition zone of 16 peptides.

Peptide	Inhibition circle diameter (mm)				
	<i>E. coli</i>	<i>P. aeruginosa</i> CMCC(B)10104	<i>B. thuringiensis</i>	<i>S. aureus</i> CMCC(B) 26003	<i>C. albicans</i> CMCC(F) 98001
FD1	0	0	0	0	0
FD2	0	0	0	0	0
FD3	0	0	0	0	0
FD4	10.12 ± 0.26	0	0	9.47 ± 0.11	0
+	29.37 ± 0.31	14.48 ± 0.29	15.97 ± 0.49	19.98 ± 0.42	19.69 ± 0.53
–	0	0	0	0	0
FD5	0	0	0	0	0
FD6	0	0	0	0	0
FD7	0	0	0	0	0
FD8	0	0	0	0	0
+	27.03 ± 0.47	15.10 ± 0.43	17.95 ± 0.36	14.35 ± 0.49	16.16 ± 0.51
–	0	0	0	0	0
FD9	0	0	0	0	0
FD10	21.52 ± 0.32	20.71 ± 0.26	17.19 ± 0.21	14.93 ± 0.54	13.52 ± 0.30
FD11	0	0	0	0	0
FD12	14.10 ± 0.28	0	13.46 ± 0.36	14.71 ± 0.61	0
+	27.84 ± 0.30	16.52 ± 0.55	13.99 ± 0.61	15.58 ± 0.58	17.74 ± 0.47
–	0	0	0	0	0
FD13	0	0	0	0	0
FD14	10.24 ± 0.23	9.50 ± 0.10	8.09 ± 0.12	10.11 ± 0.41	0
FD15	11.18 ± 0.38	0	9.15 ± 0.44	10.02 ± 0.22	0
FD16	0	0	0	0	0
+	30.50 ± 0.21	16.99 ± 0.39	17.47 ± 0.19	16.02 ± 0.34	17.80 ± 0.25
–	0	0	0	0	0

+Is the positive control (Ampicillin). –Is the negative control (sterile water).

TABLE 4 MIC of AMPs.

Species and strains		MIC (μg/mL)				
		FD4	FD10	FD12	FD14	FD15
Gram-negative bacteria	<i>E. coli</i>	-	8	32	256	32
	<i>P. aeruginosa</i> CMCC(B)10104	-	8	-	256	-
Gram-positive bacteria	<i>B. thuringiensis</i>	-	8	128	256	128
	<i>S. aureus</i> CMCC(B) 26003	256	16	16	-	16
Fungi	<i>C. albicans</i> CMCC(F) 98001	-	16	-	-	-

–Indicated that the MIC was greater than 256 μg/mL.

3.8. Time–kill assay

All three tested AMPs (FD10, FD12, and FD15) were bactericidal immediately after *E. coli* was exposed to them, with FD10 having the steepest curve and the fastest decline at any given time point, indicating that it was the most effective at killing *E. coli*, followed by FD12 and then FD15 (Figure 3A). The bactericidal effect of the three AMPs on both bacteria (*E. coli* and *S. aureus* CMCC(B) 26003) was most rapid before 0.5 h, with a large reduction in the number of

colonies, and the rate of bactericidal action gradually decreased with time until the curves plateaued. Similarly, all three AMPs were bactericidal immediately after *S. aureus* CMCC(B) 26003 was exposed to them, with FD10 and FD12 causing a more rapid decline in *S. aureus* CMCC(B) 26003 than FD15, indicating that they were better than FD15 at killing *S. aureus* CMCC(B) 26003 (Figure 3B). By 10 h, the inhibitory effect of all three AMPs on *S. aureus* CMCC(B) 26003 decreased and the number of colonies began to increase, but the bacteria grew more slowly in the FD10 group.

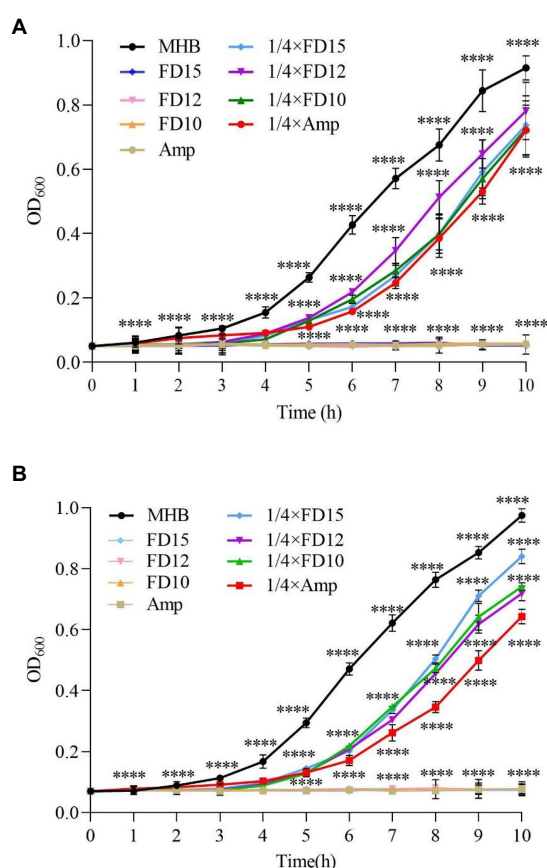


FIGURE 2

Dynamic antimicrobial analysis of the effects of antimicrobial peptides (AMPs) FD10, FD12, and FD15 against (A) *E. coli* ($n=3$) and (B) *S. aureus* CMCC(B) 26003 ($n=3$). Cells were treated with 1x and 1/4x MIC FD10, FD12, or FD15, with MHB and ampicillin (Amp) as the positive control. The statistical significance of differences was determined using the two-way ANOVA for (A) and (B). (*) indicates the significance between Amp, FD10, FD12, FD15 and MHB, **** $p<0.0001$.

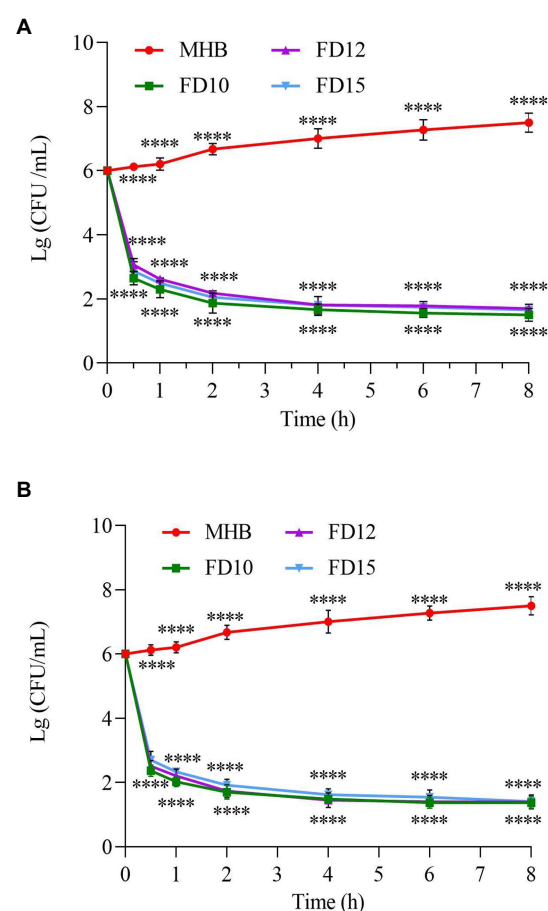


FIGURE 3

Time-kill curve of (A) *E. coli* ($n=3$) and (B) *S. aureus* CMCC(B) 26003 ($n=3$). Cells were treated with 2x MIC of FD10, FD12, or FD15, with MHB as the control. **** $p<0.0001$ based on two-way ANOVA.

3.9. Stability of AMPs against trypsin

After being treated with trypsin for 1 h, the antimicrobial activity of the three AMPs was greatly reduced. The antimicrobial activity was less than half of the original activity, with >60% of the bacteria surviving (Figure 4). This shows that the three AMPs were easily decomposed by trypsin and exhibited reduced activity.

3.10. Salt sensitivity

The salt sensitivity of antimicrobial agents is generally tested by the addition of physiological concentrations of various salts (Table 5). The antimicrobial activities of the three AMPs (FD10, FD12, and FD15) against *E. coli* and *S. aureus* CMCC(B) 26003 were minimally affected, or even promoted, by the presence of certain monovalent (K^+) and trivalent (Fe^{3+}) cations, while they were slightly decreased in the presence of Na^+ or Mg^{2+} . Among FD10, FD12, and FD15, FD10 was the most stable in the presence of salt; when certain salt ions were present, it maintained or increased its antimicrobial activity.

3.11. Hemolytic effects and cytotoxicity of AMPs

The percentage of mouse erythrocyte hemolysis after FD10 and FD12 treatment (at 256 μ g/mL) were 0.31 and 0.40%, respectively, which were lower than that of ampicillin (0.52%), while the rate after FD15 treatment was 0.55%, which was higher than that of ampicillin (Figure 5A). The survival rates of mouse RAW 264.7 macrophages after FD10, FD12, and FD15 treatment (at 256 μ g/mL) were 75.37, 67.56, and 60.50%, respectively, which were lower than that of ampicillin (84.90%) (Figure 5B). The results showed that the hemolytic effects and cytotoxicity of FD10 and FD12 were lower than those of ampicillin, while the hemolytic effect of FD15 was higher than that of ampicillin.

4. Discussion

With the overuse of traditional antibiotics for animal and human health, a large number of super-resistant bacteria have emerged, which seriously threatens animal and human health and the development of industries such as the aquaculture industry. Therefore, the exploration

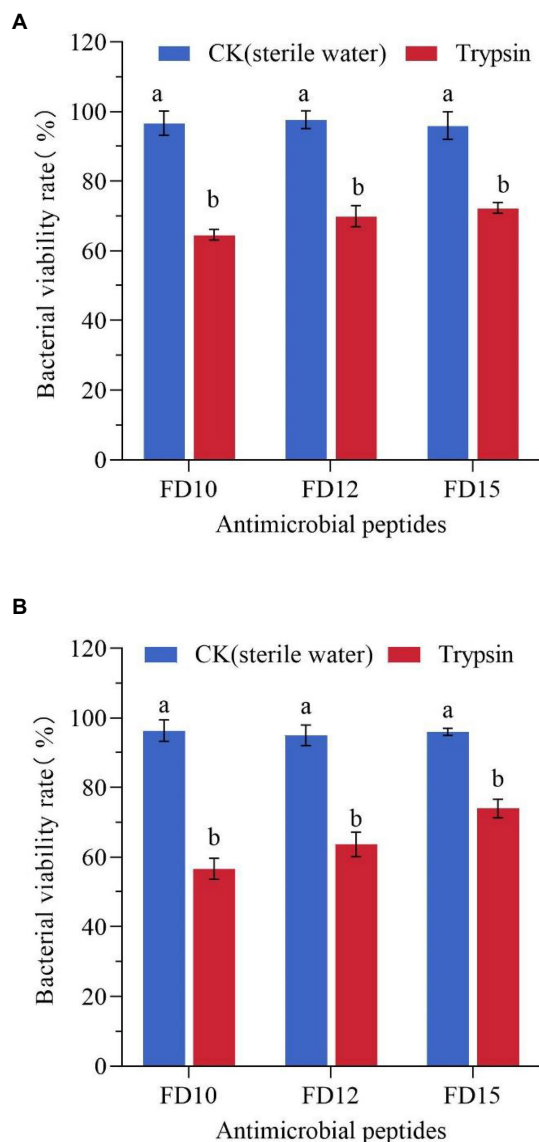


FIGURE 4
Changes in the antimicrobial activity of AMPs against (A) *E. coli* ($n=3$) and (B) *S. aureus* CMCC(B) 26003 ($n=3$) after trypsin treatment. *E. coli* or *S. aureus* CMCC(B) 26003 were treated with 2x MIC FD10, FD12, or FD15 and the same volume of 1mg/mL trypsin or sterile water (control). Different lowercase letters (a, b) indicate a significant difference ($p < 0.05$) based on one-way ANOVA.

and development of new antimicrobial drugs have become a hot research area. Due to the broad-spectrum antimicrobial properties of AMPs and their unique antimicrobial mechanisms, it is difficult for bacteria to become resistant to AMPs, and AMPs are one of the most potent agents to replace antibiotics. At present, there are many studies on insect AMPs, but few studies on the AMPs of *P. brevitarsis* Lewis larvae.

In this study, nine natural AMP sequences were used as templates to design small-molecule AMPs with strong antimicrobial activity and low cytotoxicity. Traditionally, the secondary structures of AMPs mainly include α -helix, β -pleated, random coil, and loop structures. The antimicrobial activity of AMPs is associated with their structures (Hilpert et al., 2006). Therefore, the template peptide sequences with

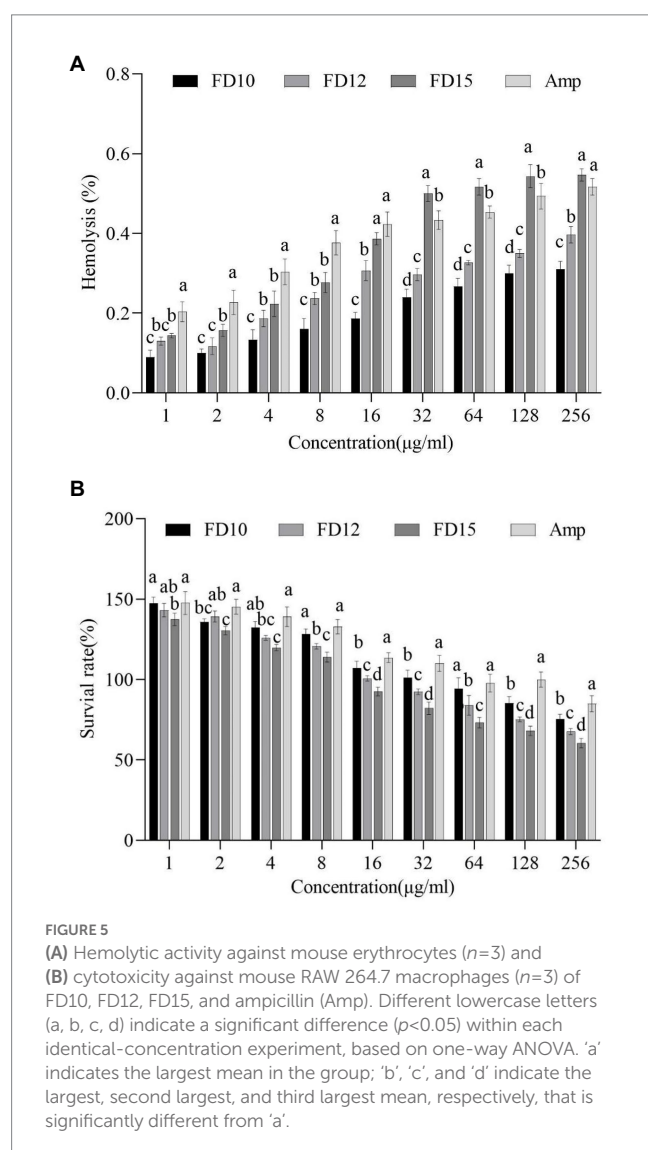
secondary structures were retained. In addition, while most natural AMPs are long, truncated peptides have been shown to retain antimicrobial activity (Wang et al., 2022). By generating various heterogeneous peptides by truncating AMP sequences at the N- or C-terminus of the peptide chain, researchers have demonstrated experimentally that retaining only 10 amino acid residues at the N-terminus of AMPs still results in bacteriostatic and neutrophilic activity (Kwon et al., 2014). In the current study, we designed truncated peptides using the natural AMPs as templates along with bioinformatics software. However, N- and C-terminal amino acids were not removed, replaced, or added. FD15 (STLHLVLRRLR-NH₂) had an obvious antimicrobial effect but FD16 (STLHLVLRRLR) had no effect without -NH₂. Although C-terminal acetylation is not a requirement for antimicrobial activity, it can increase the charge of peptides and enhance their interaction with microbial membranes. In contrast, adding amino acid residues or truncating sequences at the N-terminus makes it more difficult for the AMP to insert into the membrane, which reduces the AMP's activity (Cerovsky et al., 2011). C-terminal acetylation provides additional hydrogen bonds to the α -helix and there has been reported to be a significant correlation between this and biological activity (Rangel et al., 2011; Dos Santos Cabrera et al., 2019). Moreover, cationic AMPs can bind to the bacterial cell membrane, which is negatively charged. When the net charge of the truncated peptide is low (<2), Arg or Lys (with a higher isoelectric point) can be used to replace Glu and Asp to increase the net charge of AMPs (Arias et al., 2018). Due to containing a negatively charged amino acid residue, FD13 (ANWDKQVIR) could not readily interact with bacterial membranes. Based on FD13, FD14 (ANWKKVIR) was designed by replacing Asp with Lys. However, neither had antimicrobial activity, potentially due to their weak hydrophilicity. On the other hand, when the hydrophobicity of the AMPs is low ($<40\%$), hydrophobic amino acid residues can be added. The helical wheel projection diagrams predicted the hydrophobic distance of individual peptides. The hydrophobic moments (μH) of peptides can be utilized to represent their amphiphilic nature (Zhao and London, 2006). Peptide-membrane interactions are strongly affected by using the amphiphilic structure of peptides. The amphiphilic property of peptides permits amino acids to create hydrophobic moments on the facets of the helix (Tan et al., 2022).

An important factor for identifying candidate AMPs is the MIC. In general, the MIC should be $<16\mu\text{g/mL}$ to preliminarily qualify (Barreto-Santamaria et al., 2019). In this study, FD10 (VFRLKKWIQKVI) was shown to have antimicrobial activity against both bacteria and a fungus at low MIC values of 8– $16\mu\text{g/mL}$. More importantly, FD10 had stronger antimicrobial effects than ampicillin in some respects, indicating excellent antimicrobial function. Additionally, FD12 and FD15 had antimicrobial activity against *S. aureus* CMCC(B) 26003, which is resistant to antibiotics (Chambers and DeLeo, 2009). Moreover, although most natural AMPs cannot be widely used because of their high cytotoxicity and hemolytic effects (Kubicek-Sutherland et al., 2017), FD10, FD12, and FD15 are promising antimicrobial agents because of their strong activity and low cytotoxicity and hemolytic effects. The inactivity of other AMPs may be related to their structural stability or hydrophilicity (Diao et al., 2014; Li et al., 2019). The dynamic antimicrobial analysis showed that the AMPs could completely kill bacteria and act rapidly at 1x MIC, and the microbes would also be affected at 1/4x MIC, indicating that FD10, FD12, and FD15 had rapid and extensive antimicrobial

TABLE 5 MIC of peptides in the presence of physiological salts.

Peptide	Control (mM) ^a	NaCl (mM) ^a	KCl (mM) ^a	MgCl ₂ (mM) ^a	FeCl ₃ (mM) ^a
Gram-negative bacteria <i>E. coli</i>					
FD10	8	16	4	16	4
FD12	32	64	16	64	32
FD15	32	64	64	64	16
Gram-positive bacteria <i>S. aureus</i> CMCC(B) 26003					
FD10	16	32	8	32	16
FD12	16	32	8	32	32
FD15	16	64	32	64	32

^aThe final concentrations of NaCl, KCl, MgCl₂, and FeCl₃ were 150 mM, 4.5 mM, 1 mM, and 4 mM, respectively, and the control MIC values were determined in the absence of these physiological salts.



activity. According to the time–kill curves, FD10, FD12, and FD15 had obvious antimicrobial effects, with highly rapidly killing *E. coli* and *S. aureus* CMCC(B) 26003 before 0.5 h in the colony numbers. The best antimicrobial activity was observed for FD10. The designed peptides exert a similar rapid antimicrobial activity as what has been

observed for naturally produced antimicrobial peptides. This rapid activity has been linked to the lower resistance development potential against AMPs (Lazzaro et al., 2020; Gan et al., 2021; Sarkar et al., 2021; Vanzolini et al., 2022).

However, the application of AMPs is limited due to the high cost of synthesis and the difficulties regarding extraction and purification. At present, two methods are widely used: the genetic engineering method and the chemical synthesis method (Wang et al., 2022). The former involves obtaining AMPs by constructing an expression system. However, there are several problems: AMPs cannot be easily detected because of their small molecular weight; their isolation and purification are complicated; and the spatial structure may not be consistent with the designed peptides. Therefore, the chemical synthesis method is widely used to synthesize AMPs because the isolation and purification procedures are simple, and the resulting AMPs are highly pure (Chen et al., 2022). Moreover, the antimicrobial mechanism of the AMPs in this study is still not clear. Further work should focus on the impacts of AMPs on the cell membrane and probing the potential intracellular targets. The mechanisms could be explored by observing the structural changes of cell membranes using transmission and scanning electron microscopy.

Furthermore, some studies have shown that AMPs are not stable (Lai et al., 2022). Thus, salt stability and enzyme stability experiments were carried out and the results showed that FD10 had the best stability and was more stable than FD12 and FD15. In addition, it was previously shown that AMPs can be coupled with functional polymers to form AMP–polymer conjugates and the antimicrobial effect increased 10-fold compared to the original AMP, with a largely unchanged hemolysis index (Liu et al., 2006). This should be researched further in future. Moreover, a peptide variant designed to be cationic exhibited stronger antimicrobial activity than before the modification (Li et al., 2020). Based on these findings, more novel AMPs with strong antimicrobial activity are expected to be developed.

There are several limitations in this study. First, only mouse cells were used to verify the cytotoxicity and hemolytic effects of AMPs. As the AMPs were developed to use to improve human health by enriching the types of AMPs available, erythrocytes from humans or other species could be selected to verify the cytotoxicity and hemolytic effects of the AMPs (Houyvet et al., 2018; Chowdhury et al., 2020). Second, only ampicillin was used as the positive control, which made our experimental results conservative. There are many classifications of antibiotics, such as peptides (vancomycin), β -lactams (ampicillin),

and quinolones (norfloxacin), and as the antimicrobials in this study were polypeptides, the selected control group antibiotics are preferably peptide antibiotics (Yang et al., 2018), which should be explored in future studies. Our study preliminarily verified the physiological activity of the screened AMPs, in follow-up experiments, we should study the mechanism of action of the AMPs.

In summary, 16 small-molecule potential AMPs were designed in this study. Among them, FD10 had the best antimicrobial activity, especially regarding antifungal activity. FD12 and FD15 also exhibited activity against *S. aureus*. Some of the small-molecule AMPs delayed the growth of microorganisms better than ampicillin. Time–kill assays showed that FD10, FD12, and FD15 act rapidly and can inhibit the growth of *E. coli* and *S. aureus* CMCC(B) 26003 in a short time. The findings indicate that FD10 in particular may be a novel promising antimicrobial agent. This study provides a basis for the design of small-molecule AMPs and enriches AMP resources.

Data availability statement

The original contributions presented in the study are included in the article/Supplementary material, further inquiries can be directed to the corresponding authors.

Ethics statement

The experiments were approved by the Institutional Animal Care and Use Committee of the Northeast Agricultural University (SRM-11) in 2022 (China).

Author contributions

QF, DC, RL, and CS contributed to the conception and design of the study. QF and JS organized the database. QF performed the statistical analysis and wrote the first draft of the manuscript. DC and XL wrote sections of the manuscript. DC, RL, and HL reviewed and edited the manuscript. QF and DC contributed equally to this work.

References

- Aittomaki, S., Valanne, S., Lehtinen, T., Matikainen, S., Nyman, T. A., Ramet, M., et al. (2017). Proprotein convertase Furin1 expression in the drosophila fat body is essential for a normal antimicrobial peptide response and bacterial host defense. *FASEB J.* 31, 4770–4782. doi: 10.1096/fj.201700296R
- Arias, M., Piga, K. B., Hyndman, M. E., and Vogel, H. J. (2018). Improving the activity of Trp-rich antimicrobial peptides by Arg/Lys substitutions and changing the length of cationic residues. *Biomol. Ther.* 8:20019. doi: 10.3390/biom8020019
- Armas, F., Di Stasi, A., Mardirossian, M., Romani, A. A., Benincasa, M., and Scocchi, M. (2021). Effects of lipidation on a proline-rich antibacterial peptide. *Int. J. Mol. Sci.* 22:959. doi: 10.3390/ijms22157959
- Barreto-Santamaria, A., Patarroyo, M. E., and Curtidor, H. (2019). Designing and optimizing new antimicrobial peptides: all targets are not the same. *Crit. Rev. Clin. Lab. Sci.* 56, 351–373. doi: 10.1080/10408363.2019.1631249
- Bechinger, B., and Lohner, K. (2006). Detergent-like actions of linear amphipathic cationic antimicrobial peptides. *Biochim. Biophys. Acta* 1758, 1529–1539. doi: 10.1016/j.bbamem.2006.07.001
- Bozelli, J. C. Jr., Sasahara, E. T., Pinto, M. R., Nakaie, C. R., and Schreier, S. (2012). Effect of head group and curvature on binding of the antimicrobial peptide tritrpticin

All authors contributed to the manuscript revision and read and approved the submitted version of the manuscript.

Funding

This research was funded by Heilongjiang Provincial National Science Foundation (LH2020C007), China from 2020-07-01 to 2023-07-01.

Acknowledgments

Special acknowledgment is given to all those involved in this research for their guidance and material support during the laboratory work. We thank the open fund of the State Key Laboratory of Biology for Plant Diseases and Insect Pests for their support.

Conflict of interest

The authors declare that the research was conducted in the absence of any commercial or financial relationships that could be construed as a potential conflict of interest.

Publisher's note

All claims expressed in this article are solely those of the authors and do not necessarily represent those of their affiliated organizations, or those of the publisher, the editors and the reviewers. Any product that may be evaluated in this article, or claim that may be made by its manufacturer, is not guaranteed or endorsed by the publisher.

Supplementary material

The Supplementary material for this article can be found online at: <https://www.frontiersin.org/articles/10.3389/fmicb.2023.1124672/full#supplementary-material>

to lipid membranes. *Chem. Phys. Lipids* 165, 365–373. doi: 10.1016/j.chemphyslip.2011.12.005

Cerovsky, V., Slaninova, J., Fucik, V., Monincova, L., Bednarova, L., Malon, P., et al. (2011). Lucifensin, a novel insect defensin of medicinal maggots: synthesis and structural study. *Chembiochem* 12, 1352–1361. doi: 10.1002/cbic.201100066

Chambers, H. F., and Deleo, F. R. (2009). Waves of resistance: *Staphylococcus aureus* in the antibiotic era. *Nat. Rev. Microbiol.* 7, 629–641. doi: 10.1038/nrmicro2200

Chen, C. H., Bepler, T., Pepper, K., Fu, D., and Lu, T. K. (2022). Synthetic molecular evolution of antimicrobial peptides. *Curr. Opin. Biotechnol.* 75:102718. doi: 10.1016/j.copbio.2022.102718

Chen, M., Wang, T., Lin, X., Hu, H., Luo, Z., and Wu, J. (2016). Study on *Canidia albicans* activity of *Musca domestica* antifungal derivatives peptide -1C (MAF -1C). *Biotechnology* 26, 64–69.

Chou, S., Shao, C., Wang, J., Shan, A., Xu, L., Dong, N., et al. (2016). Short, multiple-stranded beta-hairpin peptides have antimicrobial potency with high selectivity and salt resistance. *Acta Biomater.* 30, 78–93. doi: 10.1016/j.actbio.2015.11.002

Chowdhury, T., Mandal, S. M., Kumari, R., and Ghosh, A. K. (2020). Purification and characterization of a novel antimicrobial peptide (QAK) from the hemolymph of

- Antheraea mylitta. *Biochem. Biophys. Res. Commun.* 527, 411–417. doi: 10.1016/j.bbrc.2020.04.050
- Dean, R. E., Obrien, L. M., Thwaite, J. E., Fox, M. A., Atkins, H., and Ulaeto, D. O. (2010). A carpet-based mechanism for direct antimicrobial peptide activity against vaccinia virus membranes. *Peptides* 31, 1966–1972. doi: 10.1016/j.peptides.2010.07.028
- Di Somma, A., Moretta, A., Cane, C., Cirillo, A., and Duilio, A. (2020). Antimicrobial and antibiofilm peptides. *Biomol. Ther.* 10:652. doi: 10.3390/biom10040652
- Diao, W.-R., Hu, Q.-P., Zhang, H., and Xu, J.-G. (2014). Chemical composition, antibacterial activity and mechanism of action of essential oil from seeds of fennel (*Foeniculum vulgare* mill.). *Food Control* 35, 109–116. doi: 10.1016/j.foodcont.2013.06.056
- Dos Santos Cabrera, M. P., Rangel, M., Ruggiero Neto, J., and Konno, K. (2019). Chemical and biological characteristics of antimicrobial alpha-helical peptides found in solitary wasp venoms and their interactions with model membranes. *Toxins (Basel)* 11:559. doi: 10.3390/toxins11100559
- Durand, G. A., Raoult, D., and Dubourg, G. (2019). Antibiotic discovery: history, methods and perspectives. *Int. J. Antimicrob. Agents* 53, 371–382. doi: 10.1016/j.ijantimicag.2018.11.010
- Ferreira Cespedes, G., Nicolas Lorenzon, E., Festozo Vicente, E., Jose Soares Mendes-Giannini, M., Fontes, W., De Souza Castro, M., et al. (2012). Mechanism of action and relationship between structure and biological activity of Ctx-ha: a new ceratotoxin-like peptide from *Hypsiboas albopunctatus*. *Protein Pept. Lett.* 19, 596–603. doi: 10.2174/092986612800494011
- Flamm, R. K., Rhomberg, P. R., Lindley, J. M., Sweeney, K., Ellis-Grosse, E. J., and Shortridge, D. (2019). Evaluation of the bactericidal activity of Fosfomycin in combination with selected antimicrobial comparison agents tested against gram-negative bacterial strains by using time-kill curves. *Antimicrob. Agents Chemother.* 63:18. doi: 10.1128/AAC.02549-18
- Frieri, M., Kumar, K., and Boutin, A. (2017). Antibiotic resistance. *J. Infect. Public Health* 10, 369–378. doi: 10.1016/j.jiph.2016.08.007
- Gan, B. H., Gaynord, J., Rowe, S. M., Deingruber, T., and Spring, D. R. (2021). The multifaceted nature of antimicrobial peptides: current synthetic chemistry approaches and future directions. *Chem. Soc. Rev.* 50, 7820–7880. doi: 10.1039/D0CS00729C
- Gautier, R., Douguet, D., Antonny, B., and Drin, G. (2008). HELIQUEST: a web server to screen sequences with specific alpha-helical properties. *Bioinformatics* 24, 2101–2102. doi: 10.1093/bioinformatics/btn392
- Gong, T., Du, J., Li, S. W., Huang, H., and Qi, X. L. (2022). Identification and functional analysis of a Defensin CcDef2 from *Coridius chinensis*. *Int. J. Mol. Sci.* 23:2789. doi: 10.3390/ijms23052789
- Hilpert, K., Elliott, M. R., Volkmer-Engert, R., Henklein, P., Donini, O., Zhou, Q., et al. (2006). Sequence requirements and an optimization strategy for short antimicrobial peptides. *Chem. Biol.* 13, 1101–1107. doi: 10.1016/j.chembiol.2006.08.014
- Hou, L., Shi, Y., Zhai, P., and Le, G. (2007). Inhibition of foodborne pathogens from the larvae of the by Hf-1, a novel antibacterial peptide housefly (*Musca domestica*) in medium and orange juice. *Food Control* 18, 1350–1357. doi: 10.1016/j.foodcont.2006.03.007
- Houyvet, B., Zanuttini, B., Corre, E., Le Corguille, G., Henry, J., and Zatylny-Gaudin, C. (2018). Design of antimicrobial peptides from a cuttlefish database. *Amino Acids* 50, 1573–1582. doi: 10.1007/s00726-018-2633-4
- Joray, M. B., Del Rollan, M. R., Ruiz, G. M., Palacios, S. M., and Carpinella, M. C. (2011). Antibacterial activity of extracts from plants of Central Argentina— isolation of an active principle from *Achyrocline satureioides*. *Planta Med.* 77, 95–100. doi: 10.1055/s-0030-1250133
- Kang, M., Kang, C., Lee, H., Kim, E., Kim, J., Kwon, O., et al. (2012). Effects of fermented aloe vera mixed diet on larval growth of *Protaetia brevitarsis seoulensis* (Kolbe) (coleoptera:Cetoniidae) and protective effects of its extract against CCl4-induced hepatotoxicity in Sprague-Dawley rats. *Entomol. Res.* 42, 111–121. doi: 10.1111/j.1748-5967.2012.00444.x
- Koebach, J. (2017). Structure-activity relationships of insect Defensins. *Front. Chem.* 5:45. doi: 10.3389/fchem.2017.00045
- Kubicek-Sutherland, J. Z., Lofton, H., Vestergaard, M., Hjort, K., Ingmer, H., and Andersson, D. I. (2017). Antimicrobial peptide exposure selects for *Staphylococcus aureus* resistance to human defence peptides. *J. Antimicrob. Chemother.* 72, 115–127. doi: 10.1093/jac/dkw381
- Kwon, Y. S., Raston, N. H. A., and Gu, M. B. (2014). An ultra-sensitive colorimetric detection of tetracyclines using the shortest aptamer with highly enhanced affinity. *Chem. Commun.* 50, 40–42. doi: 10.1039/C3CC47108J
- Lai, Z., Yuan, X., Chen, H., Zhu, Y., Dong, N., and Shan, A. (2022). Strategies employed in the design of antimicrobial peptides with enhanced proteolytic stability. *Biotechnol. Adv.* 59:107962. doi: 10.1016/j.biotechadv.2022.107962
- Lazzaro, B. P., Zasloff, M., and Rolff, J. (2020). Antimicrobial peptides: application informed by evolution. *Science* 368:5480. doi: 10.1126/science.aau5480
- Lee, J.-E., Jo, D.-E., Lee, A.-J., Park, H.-K., Youn, K., Yun, E.-Y., et al. (2014). Hepatoprotective and antineoplastic properties of *Protaetia brevitarsis* larvae. *Entomol. Res.* 44, 244–253. doi: 10.1111/1748-5967.12075
- Lee, E., Kim, J.-K., Shin, S., Jeong, K.-W., Lee, J., Lee, D. G., et al. (2011). Enantiomeric 9-mer peptide analogs of protaetiamycin with bacterial cell selectivities and anti-inflammatory activities. *J. Pept. Sci.* 17, 675–682. doi: 10.1002/psc.1387
- Li, T., Liu, Q., Wang, D., and Li, J. (2019). Characterization and antimicrobial mechanism of CF-14, a new antimicrobial peptide from the epidermal mucus of catfish. *Fish Shellfish Immunol.* 92, 881–888. doi: 10.1016/j.fsi.2019.07.015
- Li, B., Yang, N., Wang, X., Hao, Y., Mao, R., Li, Z., et al. (2020). An enhanced variant designed from DLP4 cationic peptide against *Staphylococcus aureus* CVCC 546. *Front. Microbiol.* 11:1057. doi: 10.3389/fmicb.2020.01057
- Liu, Z., Deshazer, H., Rice, A. J., Chen, K., Zhou, C., and Kallenbach, N. R. (2006). Multivalent antimicrobial peptides from a reactive polymer scaffold. *J. Med. Chem.* 49, 3436–3439. doi: 10.1021/jm0601452
- Manniello, M. D., Moretta, A., Salvia, R., Scieuzo, C., Lucchetti, D., Vogel, H., et al. (2021). Insect antimicrobial peptides: potential weapons to counteract the antibiotic resistance. *Cell. Mol. Life Sci.* 78, 4259–4282. doi: 10.1007/s00018-021-03784-z
- Memariani, H., Shahbazzadeh, D., Sabatier, J. M., Memariani, M., Karbalaieimahi, A., and Bagheri, K. P. (2016). Mechanism of action and in vitro activity of short hybrid antimicrobial peptide PV3 against *Pseudomonas aeruginosa*. *Biochem. Biophys. Res. Commun.* 479, 103–108. doi: 10.1016/j.bbrc.2016.09.045
- Meng, H., and Kumar, K. (2007). Antimicrobial activity and protease stability of peptides containing fluorinated amino acids. *J. Am. Chem. Soc.* 129, 15615–15622. doi: 10.1021/ja075373f
- Mishra, B., Leishangthem, G. D., Gill, K., Singh, A. K., Das, S., Singh, K., et al. (2013). A novel antimicrobial peptide derived from modified N-terminal domain of bovine lactoferrin: design, synthesis, activity against multidrug-resistant bacteria and *Candida*. *Biochim. Biophys. Acta* 1828, 677–686. doi: 10.1016/j.bbamem.2012.09.021
- Moreno-Habel, D. A., Biglang-Awa, I. M., Dulce, A., Luu, D. D., Garcia, P., Weers, P. M., et al. (2012). Inactivation of the budded virus of *Autographa californica* *M. nucleopolyhedrovirus* by gloverin. *J. Invertebr. Pathol.* 110, 92–101. doi: 10.1016/j.jip.2012.02.007
- Mrinal, N., and Nagaraju, J. (2008). Intron loss is associated with gain of function in the evolution of the gloverin family of antibacterial genes in *Bombyx mori*. *J. Biol. Chem.* 283, 23376–23387. doi: 10.1074/jbc.M801080200
- Nishide, Y., Nagamine, K., Kageyama, D., Moriyama, M., Futahashi, R., and Fukatsu, T. (2022). A new antimicrobial peptide, Pentatomycin, from the stinkbug *Plautia stali*. *Sci. Rep.* 12:16503. doi: 10.1038/s41598-022-20427-w
- Peng, J., Wu, Z., Liu, W., Long, H., Zhu, G., Guo, G., et al. (2019). Antimicrobial functional divergence of the cecropin antibacterial peptide gene family in *Musca domestica*. *Parasit. Vectors* 12:537. doi: 10.1186/s13071-019-3793-0
- Rangel, M., Cabrera, M. P., Kazuma, K., Ando, K., Wang, X., Kato, M., et al. (2011). Chemical and biological characterization of four new linear cationic alpha-helical peptides from the venoms of two solitary eumenine wasps. *Toxicon* 57, 1081–1092. doi: 10.1016/j.toxicon.2011.04.014
- Rao, X.-J., Xu, X.-X., and Yu, X.-Q. (2012). Functional analysis of two lebecin-related proteins from *Manduca sexta*. *Insect Biochem. Mol. Biol.* 42, 231–239. doi: 10.1016/j.ibmb.2011.12.005
- Rayaprolu, S., Wang, Y., Kanost, M. R., Hartson, S., and Jiang, H. (2010). Functional analysis of four processing products from multiple precursors encoded by a lebecin-related gene from *Manduca sexta*. *Dev. Comp. Immunol.* 34, 638–647. doi: 10.1016/j.dci.2010.01.008
- Sahoo, A., Swain, S. S., Behera, A., Sahoo, G., Mahapatra, P. K., and Panda, S. K. (2021). Antimicrobial peptides derived from insects offer a novel therapeutic option to combat biofilm: a review. *Front. Microbiol.* 12:661195. doi: 10.3389/fmicb.2021.661195
- Sarkar, T., Chetia, M., and Chatterjee, S. (2021). Antimicrobial peptides and proteins: from Nature's reservoir to the laboratory and beyond. *Front. Chem.* 9:691532. doi: 10.3389/fchem.2021.691532
- Shi, S., Shen, T., Liu, Y., Chen, L., Wang, C., and Liao, C. (2021). Porcine myeloid antimicrobial peptides: a review of the activity and latest advances. *Front. Vet. Sci.* 8:664139. doi: 10.3389/fvets.2021.664139
- Tan, H., Wang, J., Song, Y., Liu, S., Lu, Z., Luo, H., et al. (2022). Antibacterial potential analysis of novel alpha-helix peptides in the Chinese wolf spider *Lycosa sinensis*. *Pharmaceutics* 14:540. doi: 10.3390/pharmaceutics14112540
- Thakur, A., Sharma, A., Alajangi, H. K., Jaiswal, P. K., Lim, Y.-B., Singh, G., et al. (2022). In pursuit of next-generation therapeutics: antimicrobial peptides against superbugs, their sources, mechanism of action, nanotechnology-based delivery, and clinical applications. *Int. J. Biol. Macromol.* 218, 135–156. doi: 10.1016/j.ijbiomac.2022.07.103
- Tresnak, D. T., and Hackel, B. J. (2020). Mining and statistical modeling of natural and variant class IIa Bacteriocins elucidate activity and selectivity profiles across species. *Appl. Environ. Microbiol.* 86:20. doi: 10.1128/AEM.01646-20
- Vanzolini, T., Bruschi, M., Rinaldi, A. C., Magnani, M., and Fraternali, A. (2022). Multitalented synthetic antimicrobial peptides and their antibacterial, antifungal and antiviral mechanisms. *Int. J. Mol. Sci.* 23:545. doi: 10.3390/ijms23010545

- Wang, X., Hong, X., Chen, F., and Wang, K. J. (2022). A truncated peptide Spigillicin177-189 derived from mud crab *Scylla paramamosain* exerting multiple antibacterial activities. *Front. Cell. Infect. Microbiol.* 12:928220. doi: 10.3389/fcimb.2022.928220
- Wang, K., Li, P., Gao, Y., Liu, C., Wang, Q., Yin, J., et al. (2019). De novo genome assembly of the white-spotted flower chafer (*Protaetia brevitarsis*). *Gigascience* 8:19. doi: 10.1093/gigascience/giz019
- Wang, X., Wang, X., Teng, D., Mao, R., Hao, Y., Yang, N., et al. (2018). Increased intracellular activity of MP1102 and NZ2114 against *Staphylococcus aureus* in vitro and in vivo. *Sci. Rep.* 8:4204. doi: 10.1038/s41598-018-22245-5
- Wu, M., Maier, E., Benz, R., and Hancock, R. E. (1999). Mechanism of interaction of different classes of cationic antimicrobial peptides with planar bilayers and with the cytoplasmic membrane of *Escherichia coli*. *Biochemistry* 38, 7235–7242. doi: 10.1021/bi9826299
- Wu, Q., Patocka, J., and Kuca, K. (2018). Insect antimicrobial peptides, a mini review. *Toxins (Basel)* 10:461. doi: 10.3390/toxins10110461
- Xia, J., Ge, C., and Yao, H. (2021). Antimicrobial peptides from black soldier Fly (*Hermetia illucens*) as potential antimicrobial factors representing an alternative to antibiotics in livestock farming. *Animals (Basel)* 11:937. doi: 10.3390/ani11071937
- Yang, S., Huang, H., Wang, F., Aweya, J. J., Zheng, Z., and Zhang, Y. (2018). Prediction and characterization of a novel hemocyanin-derived antimicrobial peptide from shrimp *Litopenaeus vannamei*. *Amino Acids* 50, 995–1005. doi: 10.1007/s00726-018-2575-x
- Yeasmin, R., Brewer, A., Fine, L. R., and Zhang, L. (2021). Molecular dynamics simulations of human Beta-Defensin type 3 crossing different lipid bilayers. *ACS Omega* 6, 13926–13939. doi: 10.1021/acsomega.1c01803
- Yi, H. Y., Chowdhury, M., Huang, Y. D., and Yu, X. Q. (2014). Insect antimicrobial peptides and their applications. *Appl. Microbiol. Biotechnol.* 98, 5807–5822. doi: 10.1007/s00253-014-5792-6
- Yoo, Y.-C., Shin, B.-H., Hong, J.-H., Lee, J., Chee, H.-Y., Song, K.-S., et al. (2007). Isolation of fatty acids with anticancer activity from *Protaetia brevitarsis* larva. *Arch. Pharm. Res.* 30, 361–365. doi: 10.1007/BF02977619
- Yoon, H. S., Lee, C. S., Lee, S. Y., Choi, C. S., Lee, I. H., Yeo, S. M., et al. (2003). Purification and cDNA cloning of inducible antibacterial peptides from *Protaetia brevitarsis* (Coleoptera). *Arch. Insect Biochem. Physiol.* 52, 92–103. doi: 10.1002/arch.10072
- Zhang, Q., Ma, P., Xie, J., Zhang, S., Xiao, X., Qiao, Z., et al. (2019). Host defense peptide mimicking poly-beta-peptides with fast, potent and broad spectrum antibacterial activities. *Biomater. Sci.* 7, 2144–2151. doi: 10.1039/C9BM00248K
- Zhao, G., and London, E. (2006). An amino acid "transmembrane tendency" scale that approaches the theoretical limit to accuracy for prediction of transmembrane helices: relationship to biological hydrophobicity. *Protein Sci.* 15, 1987–2001. doi: 10.1110/ps.062286306
- Zhou, X., and Zhou, C. (2018). Design, synthesis and applications of antimicrobial peptides and antimicrobial peptide-mimetic copolymers. *Progress Chem.* 30, 913–920. doi: 10.7536/PC171125



OPEN ACCESS

EDITED BY

Rustam Aminov,
University of Aberdeen, United Kingdom

REVIEWED BY

Katarzyna Garbacz,
Medical University of Gdańsk, Poland
Süleyman Yıldırım,
İstanbul Medipol University, Türkiye

*CORRESPONDENCE

Carmen Torres
✉ carmen.torres@unirioja.es

SPECIALTY SECTION

This article was submitted to
Frontiers in Microbiology Antimicrobials,
Resistance and Chemotherapy,
a section of the journal
Frontiers in Microbiology

RECEIVED 15 January 2023

ACCEPTED 06 March 2023

PUBLISHED 11 April 2023

CITATION

Fernández-Fernández R, Abdullahi IN,
González-Azcona C, Ulloa A, Martínez A,
García-Vela S, Höfle U, Zarazaga M, Lozano C
and Torres C (2023) Detection of antimicrobial
producing *Staphylococcus* from migratory
birds: Potential role in nasotracheal
microbiota modulation.
Front. Microbiol. 14:1144975.
doi: 10.3389/fmicb.2023.1144975

COPYRIGHT

© 2023 Fernández-Fernández, Abdullahi,
González-Azcona, Ulloa, Martínez, García-Vela,
Höfle, Zarazaga, Lozano and Torres. This is an
open-access article distributed under the terms
of the [Creative Commons Attribution License
\(CC BY\)](https://creativecommons.org/licenses/by/4.0/). The use, distribution or reproduction
in other forums is permitted, provided the
original author(s) and the copyright owner(s)
are credited and that the original publication in
this journal is cited, in accordance with
accepted academic practice. No use,
distribution or reproduction is permitted which
does not comply with these terms.

Detection of antimicrobial producing *Staphylococcus* from migratory birds: Potential role in nasotracheal microbiota modulation

Rosa Fernández-Fernández¹, Idris Nasir Abdullahi¹,
Carmen González-Azcona¹, Adriana Ulloa¹, Agustí Martínez¹,
Sara García-Vela^{1,2}, Ursula Höfle³, Myriam Zarazaga¹,
Carmen Lozano¹ and Carmen Torres^{1*}

¹Area of Biochemistry and Molecular Biology, One Health-UR Research Group, University of La Rioja, Logroño, Spain, ²Department of Food Science, University of Laval, Québec City, QC, Canada, ³SaBio (Health and Biotechnology) Research Group, Game and Wildlife Research Institute, Spanish National Research Council/University of Castilla–La Mancha, Ciudad Real, Spain

A collection of 259 staphylococci of 13 different species [212 coagulase-negative (CoNS) and 47 coagulase-positive (CoPS)] recovered from nasotracheal samples of 87 healthy nestling white storks was tested by the *spot-on-lawn* method for antimicrobial-activity (AA) against 14 indicator bacteria. Moreover, extracts of AP isolates were obtained [cell-free-supernatants (CFS) both crude and concentrated and butanol extracts] and tested against the 14 indicator bacteria. The microbiota modulation capacity of AP isolates was tested considering: (a) intra-sample AA, against all Gram-positive bacteria recovered in the same stork nasotracheal sample; (b) inter-sample AA against a selection of representative Gram-positive bacteria of the nasotracheal microbiota of all the storks (30 isolates of 29 different species and nine genera). In addition, enzymatic susceptibility test was carried out in selected AP isolates and bacteriocin encoding genes was studied by PCR/sequencing. In this respect, nine isolates (3.5%; seven CoNS and two CoPS) showed AA against at least one indicator bacteria and were considered antimicrobial-producing (AP) isolates. The AP isolates showed AA only for Gram-positive bacteria. Three of these AP isolates (*S. hominis* X3764, *S. sciuri* X4000, and *S. chromogenes* X4620) revealed AA on all extract conditions; other four AP isolates only showed activity in extracts after concentration; the remaining two AP isolates did not show AA in any of extract conditions. As for the microbiota modulation evaluation, three of the nine AP-isolates revealed intra-sample AA. It is to highlight the potent inter-sample AA of the X3764 isolate inhibiting 73% of the 29 representative Gram-positive species of the nasotracheal stork microbiota population. On the other hand, enzymatic analysis carried out in the two highest AP isolates (X3764 and X4000) verified

the proteinaceous nature of the antimicrobial compound and PCR analysis revealed the presence of lantibiotic-like encoding genes in the nine AP isolates. In conclusion, these results show that nasotracheal staphylococci of healthy storks, and especially CoNS, produce antimicrobial substances that could be important in the modulations of their nasal microbiota.

KEYWORDS

staphylococci, coagulase-negative staphylococci, bacteriocins, antimicrobial activities, storks, nasal microbiota

1. Introduction

Bacteria thrive in complex niches establishing inter-species and intra-environment relationships, including the ability to acquire and transfer several adaptation mechanisms (Krismer et al., 2017; Heilbronner et al., 2021). The nasal cavity is directly connected to the external media and in close contact with a wide diversity of microorganisms that can be acquired through inhalation (Biswas et al., 2015). Moreover, the microenvironment of the nasal cavity varies depending on the anatomical location.

The anterior nares (nostrils) are the most difficult area for the survival of microbes due to their acidic environment with high salinity (Geurkink, 1983). Therefore, microbes that live in the nasal cavity are subjected to a variety of stress conditions and they must counteract to survive and persist (Krismer et al., 2014). In this respect, species competition in the nasal cavity can be mediated by direct or indirect mechanisms such as the acquisition of nutrients, the production of antimicrobial substances and the activation of specific host defense mechanisms (Krismer et al., 2017).

Human nasal microbiota is mainly composed of *Staphylococcus*, *Cutibacterium*, *Corynebacterium*, and *Moraxella* (Zhou et al., 2014), and bacteria from other genera are less frequently found (Liu et al., 2015). Focusing on the *Staphylococcus* genus, human nasal isolates have been frequently described as producers of antimicrobial substances against bacterial competitors. For instance, *S. epidermidis* or *S. lugdunensis*, among others favorably ousted *S. aureus* (Janek et al., 2016; Zipperer et al., 2016). However, there could be limitations in the detection and/or production of antimicrobial activity due to some producing isolates require specific environmental stress conditions commonly present in the human nose, such as hydrogen peroxide release and iron limitation (Janek et al., 2016).

The nasal microbiota of animals has also been analysed revealing composition differences. For example, companion and farm animals or rodents have higher abundances of Proteobacteria as compared to humans (Weese et al., 2014; Chaves-Moreno et al., 2015; Misic et al., 2015), and some *S. aureus* lineages, including livestock-associated MRSA, are increasingly found in the noses of livestock (Bal et al., 2016). However, staphylococci and especially coagulase-negative staphylococci (CoNS) from wildlife remain largely understudied. In this respect, some studies carried out in Spain and Portugal revealed that wild animals (birds and mammals) are frequently colonized by CoNS and *S. sciuri* being one of the predominant species among this group of microorganisms (Sousa et al., 2016; Mama et al., 2019; Ruiz-Ripa et al., 2020).

Birds have been postulated as sentinels, reservoirs, and potential disseminators of antimicrobial resistance due to their interaction with the human interface, diverse ecological niches, and capacity to travel for long distances (Bonnedaahl and Järhult, 2014). Consequently, the nasotracheal bacterial communities of white storks have recently been studied by our research group (Abdullahi et al., 2023). Moreover, storks can also be a source of antimicrobial substances thanks to the adaptation strategies of the isolates present in their bacterial communities. Here, the present study aims to detect and partially characterize the production profile of antimicrobial substances in *Staphylococcus* isolates from nasotracheal samples of nestling white storks obtained from a previous study (Abdullahi et al., 2023), and to evaluate their capacity as modulators of the nasotracheal microbiota of these animals.

2. Materials and methods

2.1. Staphylococcal isolates used for the detection of antimicrobial activity (AA)

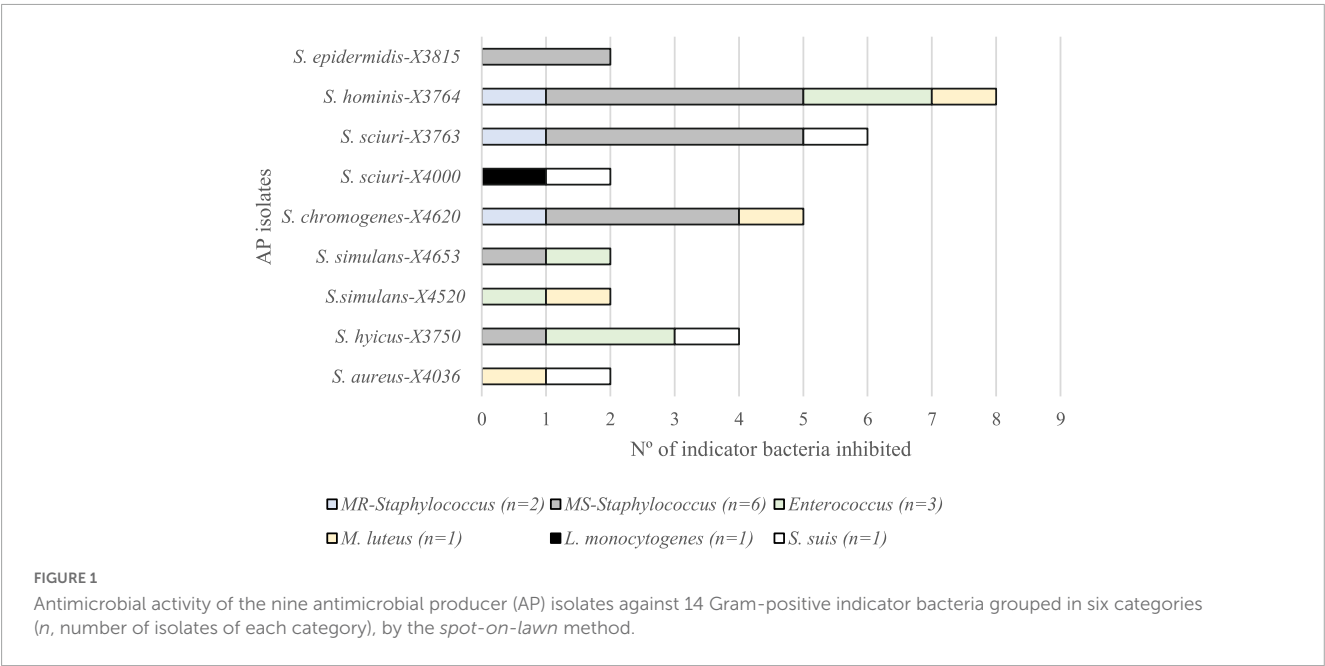
A total of 259 Staphylococcal isolates of stork origin were included in this study and they were tested for the production of antimicrobial activity (AA). These isolates were of 13 different species (number of isolates): *S. aureus* (46), *S. sciuri* (138), *S. epidermidis* (16), *S. lentus* (14), *S. chromogenes* (11), *S. xylosus* (8), *S. hominis* (7), *S. simulans* (7), *S. saprophyticus* (6), *S. haemolyticus* (3), *S. hyicus* (1), *S. capitis* (1), and *S. arlettae* (1).

These 259 Staphylococcal isolates were obtained from 136 samples (84 tracheal and 52 nasal) of 87 nestling white storks in a previous study (Abdullahi et al., 2023). The animals included belonged to four different colonies of storks located in South-central Spain. For bacterial isolation, the nasal or tracheal samples were pre-enriched in brain heart infusion broth supplemented with 6.5% NaCl and after overnight incubation, four culture media were used for bacteria recovery [blood agar, mannitol salt agar, oxacillin screening agar base supplemented with oxacillin (ORSAB medium), and CHROMagar™ LIN]. Finally, up to 12 different colonies were randomly selected per sample and identified by matrix-assisted laser desorption/ionization time-of-flight mass spectrometry (MALDI-TOF-MS; Bruker Daltonics, Bremen, Germany). Thus, 259 distinct staphylococci were included

TABLE 1 Staphylococcal isolates evaluated^a for antimicrobial activity by the *spot-on-lawn* method against 14 indicator bacteria and antimicrobial-producing (AP) isolates detected.

Species	N° of isolates ^a	Origin (n° of isolates)		AP isolates	
		Nasal	Tracheal	N° of AP isolates	Stork sample ID code (origin) ^b
<i>S. aureus</i>	46	22	24	1	436 (T)
<i>S. hyicus</i>	1	0	1	1	538 (T)
<i>S. sciuri</i>	138	54	84	2	507 (T), 433 (T)
<i>S. epidermidis</i>	16	3	13	1	506 (T)
<i>S. lentus</i>	14	5	9	0	–
<i>S. chromogenes</i>	11	7	4	1	481 (N)
<i>S. xylosus</i>	8	6	2	0	–
<i>S. hominis</i>	7	0	7	1	507 (T)
<i>S. saprophyticus</i>	6	1	5	0	–
<i>S. simulans</i>	7	6	1	2	480 (N), 481 (N)
<i>S. haemolyticus</i>	3	0	3	0	–
<i>S. capitis</i>	1	0	1	0	–
<i>S. arlettae</i>	1	1	0	0	–
Total	259	105	154	9	–

^aIsolates were obtained from a previous study (Abdullahi et al., 2023).
^bT, tracheal; N, nasal.

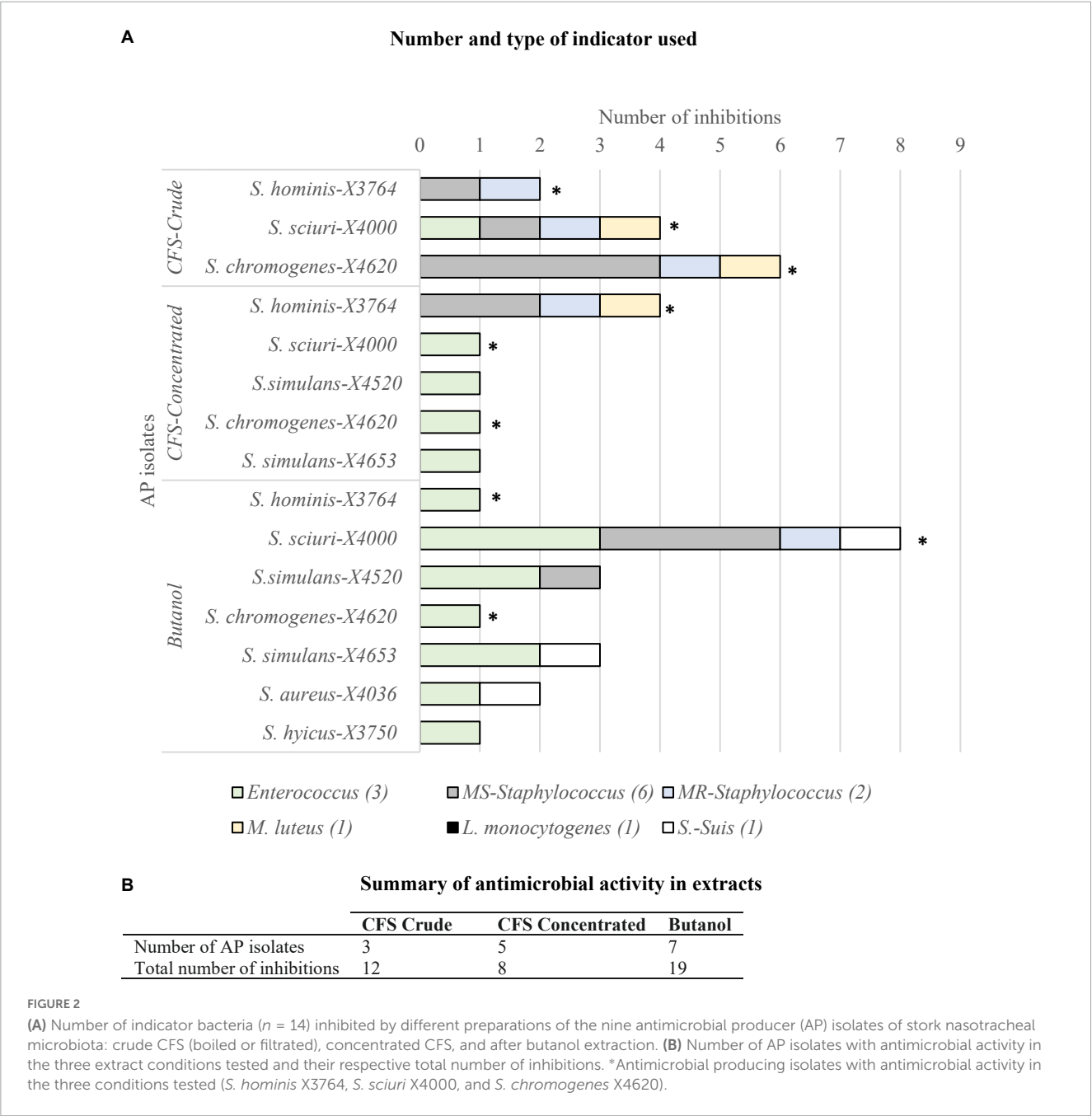


in the present study (one isolate of each *Staphylococcal* species per animal), which corresponded to 2–5 staphylococci/animal.

2.2. Isolates used as indicator bacteria in the screening for detection of antimicrobial-producing (AP) staphylococci

Fourteen Gram-positive (G+) isolates of different genera and species were used as indicator bacteria to evaluate the AA of

the collection of 259 *Staphylococcal* isolates of storks. The list of these 14 indicator bacteria is shown in [Supplementary Table 1](#) and includes relevant pathogenic, zoonotic, and multidrug-resistant (MDR) bacteria methicillin-resistant *S. aureus* (MRSA) (C1570), methicillin-susceptible *S. aureus* (MSSA) (ATCC29213), methicillin-resistant *Staphylococcus pseudintermedius* (MRSP) (C2381), methicillin-susceptible *S. pseudintermedius* (MSSP) (C3468), *Staphylococcus lugdunensis* (C10107), *S. epidermidis* (C2663), *S. sciuri* (C9780), *Staphylococcus delphini* (C9459), *Enterococcus cecorum* (X3809), *Enterococcus faecalis* (ATCC29212), *Enterococcus faecium* (C2321), *Micrococcus luteus* (CECT241),



Listeria monocytogenes (CECT4032), and *Streptococcus suis* (X2060). Two additional Gram-negative (G⁻) indicator bacteria were tested in the AP staphylococci detected: *Escherichia coli* (ATCC25922) and *P. aeruginosa* (PAO1).

2.3. Detection of antimicrobial activity (AA)

Four methods were used to determine antimicrobial activity:

1. *Spot-on-lawn* method: Indicator isolates were resuspended in Brain Heart Infusion broth (BHI; Condalab, Madrid, Spain)
2. Crude cell-free supernatant (CFS): Antimicrobial-producing isolates were grown in 10 mL of BHI medium for 24 h

up to 0.5 MacFarland and 10 μ L of the cultures were added to five-milliliter aliquots of Tryptic Soy Broth supplemented with 0.3% yeast extract (TSB; Condalab, Madrid, Spain) and 0.7% agar tempered at 45°C. Then, the mixture was seeded onto plates containing Tryptic Soy agar plus 0.3% yeast extract (TSA; Condalab, Madrid, Spain), and the putative antimicrobial-producing (AP) isolates were spotted on the surface and plates were incubated overnight at 37°C. When *Streptococcus suis* was the indicator bacteria, Columbia agar with 5% sheep blood (bioMérieux SA, France) was used instead of TSA. Growth inhibition was detected by a clearing zone with no bacterial growth around the AP isolate.

at 37°C, centrifuged (4,500 rpm, 10 min) and sterilized by boiling or filtration through a low-protein binding 0.45 µm Millipore filter.

3. Concentrated CFS: The resulting crude CFS was concentrated by speed vacuum and resuspended in dimethyl sulfoxide (DMSO).
4. Butanol extraction: 1-butanol was added to a fresh overnight BHI broth culture at a ratio of 1:2 and shaken for 1 h at 37°C. After phases differentiation, samples were centrifuged at 4,500 rpm for 15 min. The organic phase was tested for antimicrobial activity.

For methods 2–4, 50 µL of the *Staphylococcal* extracts were filled on wells done on TSA agar plates previously inoculated with the indicator bacteria, and the plates were incubated for 24 h at 37°C. The AA was assessed by the analysis of the inhibition zones around the wells. Positive (a previously described AP-isolate) and negative (BHI medium, DMSO, butanol) controls under all conditions were included in the assays.

2.4. Analysis of microbiota modulation

In the *Staphylococcal* isolates that showed antimicrobial activity by the *spot-on-lawn* method (AP isolates), their antimicrobial activity was also analysed against G⁺ bacteria obtained from the storks' samples (used in this case as indicator bacteria), using the same procedure. Two different approaches were used:

1. Intra-sample activity. The activity of the AP isolates against all the G⁺ bacteria recovered in the same stork nasotracheal sample of the selected AP isolate was analyzed.
2. Inter-sample activity. From the whole collection of bacteria obtained from the nasotracheal samples of the 87 storks included in this study (Abdullahi et al., 2023), one isolate of each G⁺ species was selected (avoiding the selection as representants of the isolates recovered in the same samples in which AP bacteria were detected). Following these criteria, a collection of 30 isolates of 29 different G⁺ species and nine genera was used as indicator bacteria (representative of the inter-sample community) (Supplementary Table 2).

2.5. Characterization of the antimicrobial compounds in AP staphylococci

1. Susceptibility to proteolytic enzymes. The following enzymes were assayed (treatment conditions): trypsin (pH = 7.6; 25°C), α-chymotrypsin (pH = 7.8; 25°C), proteinase-K (pH = 7.5; 37°C), papain (pH = 6.2; 25°C) and protease (pH = 7.5; 37°C) (Sigma). Boiled CFS of two selected AP isolates (*S. sciuri* X4000 and *S. hominis* X3764) were prepared as described above. After adjusting to optimal pH, aliquots were independently incubated for 1 h with 1 g/L of each enzyme. After treatment, the enzymes were inactivated by boiling and antimicrobial activity was assayed (Navarro et al., 2000).

Hemoglobin was used as negative control in all assays under all conditions.

2. Bacteriocin gene detection. The presence of 22 bacteriocin structural genes was tested by PCR and sequencing in all the AP-isolates detected in this study (*aurA*, *aucA*, *epiA*, *sacaA/sacbA*, *gdmA*, *bacSp222*, *nsj*, *hyiA*, *hycS*, *bacCH91*, *bsaA2*, *acIA*, *ale-1*, *lss*, *nukA*, *nkqA*, *eciA*, *pepA*, *elxA*, *elkA*, *ecdA*, *orf4*), as well as three bacteriocin gene families described elsewhere (BS, GEST, and NUK) (Fernández-Fernández et al., 2022).

2.6. Antibiotic resistance phenotype of AP isolates

The susceptibility to 13 antibiotics was evaluated in the AP isolates by the disk diffusion method and they were interpreted using the European Committee on Antimicrobial Susceptibility Testing criteria (EUCAST, 2022). The antibiotics tested were as follows: penicillin, ceftiofur, oxacillin, erythromycin, clindamycin, gentamicin, tobramycin, tetracycline, ciprofloxacin, chloramphenicol, linezolid, trimethoprim–sulfamethoxazole, and mupirocin.

3. Results

3.1. Antimicrobial activity of the collection of staphylococci isolates of storks against Gram-positive bacteria

Antimicrobial activity was detected by the *spot-on-lawn* method in 9 of the 259 staphylococci (3.5%) of stork origin tested, and they were considered as AP-isolates: *S. aureus* X4036, *S. hyicus* X3750, *S. sciuri* X3763 and X4000, *S. epidermidis* X3815, *S. chromogenes* X4620, *S. hominis* X3764, and *S. simulans* X4520 and X4653 (Table 1). These AP isolates were obtained from seven different storks and revealed AA against at least one of the 14 G⁺ indicator bacteria tested. Figure 1 represents the number of G⁺ bacteria inhibited by each of the nine AP-bacteria, grouping the indicators in six categories: methicillin-resistant and -susceptible (MR and MS, respectively) *Staphylococcus*, *Enterococcus*, *M. luteus*, *L. monocytogenes*, and *S. suis*. Nevertheless, the AP staphylococci did not show AA against the two G[−] isolates tested (*E. coli* and *P. aeruginosa*). For this reason, all the next steps were performed only with G⁺ indicator bacteria.

In this respect, the isolate with broader AA was *S. hominis* X3764, that inhibited all but one G⁺ indicator (*L. monocytogenes*). The most susceptible indicator category was MS-staphylococci (inhibited by six AP-isolates, 66.7%), followed by enterococci, *M. luteus* and *S. suis* (44.4%) and MR-staphylococci (33.3%). Interestingly, one out of the nine AP-isolates (*S. sciuri* X4000) revealed AA against *L. monocytogenes*. Moreover, most of the AP-isolates showed AA against more than one G⁺ indicator category tested. However, *S. epidermidis* X3815 isolate revealed a narrow inhibition profile, inhibiting only the MS-staphylococci indicators (Figure 1).

TABLE 2 Activity of the antimicrobial-producing (AP) isolates against Gram-positive (G⁺) bacteria cohabiting in the same stork (intra-activity) or representative of the nasotracheal microbiota of the storks (inter-activity).

Stork sample/origin	AP-isolate	Intra-activity ^a	Inter-activity ^b
538/Tracheal	X3750- <i>S. hyicus</i>	<i>S. sciuri</i> , <i>S. lentus</i> , <i>S. saprophyticus</i>	<i>S. aureus</i> , <i>E. durans</i> , <i>E. hirae</i> , <i>M. caseolyticus</i> , <i>M. luteus</i> , <i>Glutamicibacter</i> sp., <i>C. falsenii</i> , <i>C. aurimucosum</i> , <i>Corynebacterium</i> sp.
507/Tracheal	X3763- <i>S. sciuri</i>	<i>E. faecalis</i> , <i>S. sciuri</i>	None
507/Tracheal	X3764- <i>S. hominis</i>	<i>S. sciuri</i> , <i>E. faecalis</i>	<i>S. sciuri</i> , <i>S. aureus</i> , <i>S. chromogenes</i> , <i>S. epidermidis</i> , <i>S. xylosum</i> , <i>S. lentus</i> , <i>S. saprophyticus</i> , <i>S. hyicus</i> , <i>S. arlettae</i> , <i>S. capitis</i> , <i>E. faecium</i> , <i>E. gallinarum</i> , <i>E. durans</i> , <i>E. hirae</i> , <i>M. caseolyticus</i> , <i>L. garvieae</i> , <i>M. luteus</i> , <i>V. lutrae</i> , <i>Glutamicibacter</i> sp., <i>Corynebacterium</i> sp., <i>C. falsenii</i> , <i>C. aurimucosum</i>
506/Tracheal	X3815- <i>S. epidermidis</i>	<i>Corynebacterium</i> sp., <i>E. faecium</i> .	<i>S. aureus</i> , <i>S. capitis</i>
433/Tracheal	X4000- <i>S. sciuri</i>	<i>E. faecalis</i> , <i>S. sciuri</i>	<i>E. durans</i> , <i>Glutamicibacter</i> sp.
436/Tracheal	X4036- <i>S. aureus</i>	<i>S. sciuri</i> , <i>E. hirae</i> , <i>S. aureus</i> , <i>S. sciuri</i>	None
480/Nasal	X4520- <i>S. simulans</i>	<i>M. caseolyticus</i> , <i>S. xylosum</i> , <i>S. sciuri</i>	<i>M. caseolyticus</i> , <i>E. durans</i> , <i>Glutamicibacter</i> sp., <i>C. falsenii</i> , <i>Corynebacterium</i> sp., <i>C. aurimucosum</i>
481/Nasal	X4620- <i>S. chromogenes</i>	<i>M. caseolyticus</i> , <i>S. chromogenes</i>	<i>S. lentus</i> , <i>S. simulans</i>
481/Nasal	X4653- <i>S. simulans</i>	<i>M. caseolyticus</i> , <i>S. chromogenes</i>	<i>E. durans</i> , <i>M. caseolyticus</i> , <i>Glutamicibacter</i> sp., <i>C. falsenii</i> , <i>Corynebacterium</i> sp., <i>C. aurimucosum</i>

^aFor intra-activity, the G⁺ species cohabitant with AP-isolate in the same stork sample, that showed inhibition activity, are marked in bold.

^bFor inter-activity, 30 isolates of 29 different G⁺ species representative of the G⁺ nasotracheal diversity of storks were tested as indicator bacteria (see Table 3 and Supplementary Table 2).

Regarding extracts obtained in different conditions, only three AP-isolates (*S. hominis* X3764, *S. sciuri* X4000, and *S. chromogenes* X4620) revealed inhibitory capacity in all the conditions tested: crude CFS (filtered or boiled), CFS concentrated and butanol extraction. Moreover, other four isolates showed AA in the concentrated extracts: 55.6% revealed bioactivity in the concentrated CFS and this percentage increased to 77.8% after butanol treatment. Two additional isolates considered as AP by the spot-on-lawn method (*S. epidermidis* X3815 and *S. sciuri* X3763) were negative for all the extracts conditions against all the 14 G⁺ indicators tested (Figure 2).

Going deeper into the AA of the extracts obtained under different conditions, Figure 2 also represents the G⁺ indicator bacteria category inhibited in each of the extract conditions. This shows that extracts of all conditions tested (CFS crude and concentrated and butanol) inhibited MS-*Staphylococcus*, MR-*Staphylococcus*, and *Enterococcus* while none of them was active against *L. monocytogenes*. Interestingly, only the crude or concentrated CFS of some AP isolates showed AA against *M. luteus*, and *S. suis* was inhibited exclusively after butanol extraction of some AP isolates. Moreover, the three types of extracts were active against at least three indicator categories and as expected, concentrated CFS and butanol extracts showed a higher diversity of AP isolates and indicators.

3.2. Microbiota modulation

To analyse the ability for managing bacterial communities, the intra-sample AA of the nine AP isolates were firstly studied against the previously isolated G⁺ bacteria of the same sample as the producer isolate (Table 2). Only three of the AP-isolates (*S. hominis* X3764, *S. simulans* X4520, and *S. chromogenes* X4620) inhibited one of the G⁺ bacteria isolated in their respective samples (one *S. sciuri*

and four *M. caseolyticus* isolates). Focusing on *S. hominis* X3764, it revealed AA against one of the two *S. isolates* recovered in the same stork tracheal sample. However, *S. hominis* X3764 did not show antimicrobial activity against co-habitant *E. faecalis* isolates. In the same way, the AP isolates *S. simulans* X4520 and *S. chromogenes* X4620 inhibited the *M. caseolyticus* isolates co-habitant in the same nasotracheal sample when used as indicator bacteria (Table 2).

In addition, the inter-sample AA of the nine AP isolates was tested against a collection of 30 G⁺ bacteria of 29 different species and nine genera representative of the G⁺ bacterial diversity of the stork nasotracheal microbiota (Table 3). The high AA of *S. hominis* X3764, inhibiting 73% of the isolates selected as a representative G⁺ microbial stork community is noteworthy. On the other hand, six AP isolates revealed AA against 7–33% of the G⁺ indicators tested. However, *S. sciuri* X3763 and *S. aureus* X4036 isolates lacked inhibitory capacity against any of those indicator bacteria (Table 3). Focusing on the AA of these AP-isolates, *Glutamicibacter* sp., (66.7%), *M. caseolyticus*, and *E. durans* (55.6%, respectively) were the most susceptible indicator bacteria inhibited by of AP-isolates (Table 3).

However, considering each AP-isolate independently, the isolates of some species as *S. hominis*, *S. haemolyticus*, *S. pasteurii*, *E. faecalis*, *E. canis*, and *S. gallolyticus* were completely resistant to the antimicrobial activity of all the AP-isolates tested. Moreover, it is to note that some of those species (*E. faecalis*) were isolated in the same sample as the AP strains X3764 and X4000 (Table 3).

3.3. Characterization of the antimicrobial compound

It is of interest the detection of two AP-isolates (*S. hominis* X3764 and *S. sciuri* X4000) with the widest AA profile and

TABLE 3 Antimicrobial activity of the nine antimicrobial-producing (AP) isolates against a representative Gram-positive stork microbial community (30 isolates of 29 species used as indicator bacteria).

Species of indicator bacteria	Isolate ID code	Antimicrobial producing isolates									N° of AP isolates that inhibited the indicator bacteria (%)
		<i>S. hyicus</i> X3750	<i>S. sciuri</i> X3763	<i>S. hominis</i> X3764	<i>S. epidermidis</i> X3815	<i>S. sciuri</i> X4000	<i>S. aureus</i> X4036	<i>S. simulans</i> X4520	<i>S. chromogenes</i> X4620	<i>S. simulans</i> X4653	
<i>S. sciuri</i>	X4121	–	–	+	–	–	–	–	–	–	1 (11%)
<i>S. aureus</i>	X4013	+	–	+	+	–	–	–	–	–	3 (33%)
<i>S. aureus</i>	X4409	+	–	–	–	–	–	–	–	–	1 (11%)
<i>S. chromogenes</i>	X4697	–	–	+	–	–	–	–	–	–	1 (11%)
<i>S. epidermidis</i>	X4146	–	–	+	–	–	–	–	–	–	1 (11%)
<i>S. xylosus</i>	X4413	–	–	+	–	–	–	–	–	–	1 (11%)
<i>S. lentus</i>	X4149	–	–	+	–	–	–	–	+	–	2 (22%)
<i>S. simulans</i>	X4525	–	–	–	–	–	–	–	+	–	1 (11%)
<i>S. hominis</i>	X3726	–	–	–	–	–	–	–	–	–	0
<i>S. saprophyticus</i>	X4145	–	–	+	–	–	–	–	–	–	1 (11%)
<i>S. hyicus</i>	X3750	–	–	+	–	–	–	–	–	–	1 (11%)
<i>S. haemolyticus</i>	X3784	–	–	–	–	–	–	–	–	–	0
<i>S. arlettae</i>	X4721	–	–	+	–	–	–	–	–	–	1 (11%)
<i>S. capitis</i>	X3968	–	–	+	+	–	–	–	–	–	2 (22%)
<i>S. pasteurii</i>	X4093	–	–	–	–	–	–	–	–	–	0
<i>E. faecalis</i>	X4126	–	–	–	–	–	–	–	–	–	0
<i>E. faecium</i>	X4688	–	–	+	–	–	–	–	–	–	1 (11%)
<i>E. gallinarum</i>	X4634	–	–	+	–	–	–	–	–	–	1 (11%)
<i>E. durans</i>	X4532	+	–	+	–	+	–	+	–	+	5 (56%)
<i>E. canis</i>	X3928	–	–	–	–	–	–	–	–	–	0
<i>E. hirae</i>	X4037	+	–	+	–	–	–	–	–	–	2 (22%)
<i>M. caseolyticus</i>	X4488	+	–	+	–	–	–	+	+	+	5 (56%)
<i>Lactococcus garvieae</i>	X4417	–	–	+	–	–	–	–	–	–	1 (11%)
<i>Streptococcus gallolyticus</i>	X4698	–	–	–	–	–	–	–	–	–	0
<i>M. luteus</i>	X4481	+	–	+	–	–	–	–	+	–	3 (33%)
<i>Vagococcus lutrae</i>	X4122	–	–	+	–	–	–	–	–	–	1 (11%)
<i>Glutamicibacter</i> sp.	X4102	+	–	+	–	+	–	+	+	+	6 (67%)
<i>C. falsenii</i>	X4270	+	–	+	–	–	–	+	–	+	4 (44%)
<i>Corynebacterium</i> sp.	X4486	+	–	+	–	–	–	+	–	+	4 (44%)
<i>C. aurimucosum</i>	X4660	+	–	+	–	–	–	+	–	+	4 (44%)
n=30 (%)*		10 (33%)	0	22 (73%)	2 (7%)	2 (7%)	0	6 (20%)	5 (17%)	6 (20%)	–

*Number of indicator bacteria (%) inhibited by each antimicrobial-producing (AP) isolate. Color: in dark green are marked the AP isolate with the strongest inhibition capacity against the major number of indicators and the indicator isolate that was inhibited by a higher number of AP isolates. In soft gray is shaded all the positive interactions of the AP isolates against the indicators.

TABLE 4 Characteristics of the nine antimicrobial producer isolates of the nasotracheal microbiota of storks.

Isolate	Stork sample ID code (origin) ^a	AMR phenotype ^b	Bacteriocin genes
<i>S. aureus</i> X4036	436 (T)	Susceptible	Lantibiotic-like
<i>S. hyicus</i> X3750	538 (T)	Susceptible	Lantibiotic-like
<i>S. sciuri</i> X3763	507 (T)	PEN	Lantibiotic-like
<i>S. sciuri</i> X4000	433 (T)	PEN, CIP	Lantibiotic-like
<i>S. epidermidis</i> X3815	506 (T)	ERY	Lantibiotic-like
<i>S. chromogenes</i> X4620	481 (N)	Susceptible	Lantibiotic-like
<i>S. hominis</i> X3764	507 (T)	PEN, FOX, ERY	Lantibiotic-like
<i>S. simulans</i> X4520	480 (N)	PEN	Lantibiotic-like
<i>S. simulans</i> X4653	481 (N)	Susceptible	Lantibiotic-like

^aT, tracheal; N, nasal.

^bAntibiotics tested were the following ones: PEN, penicillin; FOX, cefoxitin; ERY, erythromycin; CIP, ciprofloxacin; oxacillin, clindamycin, tetracycline, gentamicin, tobramycin, linezolid, chloramphenicol, trimethoprim-sulfamethoxazole, and mupirocin; AMR: antimicrobial resistance.

strong inhibitory capacity in their respective extracts obtained in all conditions tested: crude (boiled and filtered), concentrated CFS and butanol extraction. These isolates were selected, and the susceptibility of their extracts to the enzymatic activity of trypsin, α -chymotrypsin, proteinase-K, papain, and protease was tested to verify the peptidic nature of the antimicrobial substances of AP isolates. The absence of AA against MRSA and MRSP indicators in the CFS of AP isolates after enzymatic treatment allowed to confirm the peptide nature of the antimicrobial substance present on these isolates.

Moreover, the presence of 22 bacteriocin structural genes were analysed by PCR and sequencing in the nine AP isolates. Genes encoding lantibiotic-like antimicrobial peptides were detected in all the nine AP isolates (Table 4).

3.4. Antibiotic resistance profile of the AP isolates

Antibiotic susceptibility testing was performed with the collection of nine AP isolates. In this sense, 44.4% of the AP isolates showed susceptibility to the antimicrobial agents tested and the remaining isolates presented low resistance rates, highlighting the absence of MDR isolates. In this respect, 44.4% of the isolates showed resistance to penicillin, 22.2% to erythromycin and only 11.1% revealed resistance to cefoxitin or ciprofloxacin (Table 4).

4. Discussion

Antimicrobial resistance is a dynamic and multifaceted One-Health problem involving humans, animals, and the environment (Prestinaci et al., 2015). In this respect, the urgency to find new alternatives to antibiotics has induced the scientific community to focus on the antimicrobial substances produced by bacteria isolated from natural sources among which bacteriocins are of particular interest.

However, studies reporting the frequency of antimicrobial activity in bacteria of wildlife and livestock animals are limited (Poeta et al., 2007; Almeida et al., 2011), and those focused on

Staphylococcus are even scarcer (Fernández-Fernández et al., 2022), and storks have never been studied in this respect. The current work represents to the best of our knowledge, the largest study of antimicrobial activity, as well as the presence of bacteriocin structural genes in nasotracheal *Staphylococcus* isolates recovered from healthy wild storks.

Considering the inhibitory capacity of a collection of 259 *Staphylococcal* isolates recovered from nasotracheal samples of healthy storks in this study, nine of the isolates (3.5%) revealed antimicrobial activity against at least one of the 14 G⁺ indicators tested including methicillin-resistant and susceptible *Staphylococcus*, *Enterococcus*, and *L. monocytogenes*, among others. The AP isolates did not show antimicrobial activity against Gram-negative bacteria, such as *E. coli* and *P. aeruginosa*. Recent studies have detected *Staphylococcus* with antimicrobial activity among staphylococci of wild mammals and birds (excluding storks) (Fernández-Fernández et al., 2022), human nares (Janek et al., 2016), and those recovered from food (Van der Veken et al., 2020).

Among the *Staphylococcus* genus, several bacteriocins have been isolated from commensal CoNS species. Many of them display inhibitory activity against *S. aureus*, a CoPS widely considered an important pathogen of both humans and animals and implicated in a wide range of infections (Laux et al., 2019; Newstead et al., 2020).

To better characterize the inhibitory effect of the identified AP isolates, the antimicrobial activity of CFS was studied. However, bacteriocin production is costly and it is often regulated depending on cell density and environmental factors (Heilbronner et al., 2021), so we decided to extract the antimicrobial compounds from the inner cell. Thus, three of the nine AP isolates showed inhibition capacity in all the extract conditions tested (CFS crude or concentrated as well as butanol extract). However, when concentrating the extracts, most of the AP-isolates revealed bioactivity mainly against *Enterococcus* indicator bacteria. Nevertheless, two AP isolates (detected by the *spot-on-lawn* method) were negative for all the extract conditions and against all the indicators tested.

Regarding genetics, the nine AP isolates detected were positive for a lantibiotic-like structural gene although we can not discard that other structural bacteriocin genes, not tested in this study or not already described, could be responsible for the antimicrobial activity. A high variety of lantibiotics have been reported on

Staphylococcus isolates such as epidermin, epilancins, and various nukacins, among others, showing antimicrobial activity exclusively against G^+ bacteria (Laux et al., 2019).

According to microbiota composition, each community reflects specific niche conditions, and associations among species and concrete locations have been described (Wei et al., 2022). On the other hand, it is widely accepted that antibacterial molecules that inhibit major microbial competitors have a particularly important role in shaping the microbiome (Krismer et al., 2017; Lewis and Pamer, 2017; García-Bayona and Comstock, 2018).

Based on bacteriocin effects on the microbial community, the present study demonstrates the strong inhibitory capacity of the recovered AP-isolates. Especially, *S. hominis* X3764 could act as a microbiota modulator due to its high inter-sample AA against 73% of the G^+ representative stork community and the intra-sample activity, inhibiting the *S. sciuri* isolate recovered from stork 507. In this respect, potent antimicrobial activity has been previously reported in nasal staphylococci of human origin (80%) against bacteria of the nasal ecosystem (Janek et al., 2016).

As for the nasal microbiome, *S. aureus* is also regarded as a human commensal that colonizes asymptotically about 30% of human nares (Laux et al., 2019). However, nasal carriage of *S. aureus* predisposes to invasive infection (Zipperer et al., 2016). For example, it has been described that nasal *S. lugdunensis* can prevent *S. aureus* colonization by producing an unusual antimicrobial compound termed lugdunin (Zipperer et al., 2016). Moreover, *S. epidermidis* has been reported as an *S. aureus* inhibitor although there is no clear correlation between the absence of *S. aureus* with the presence of *S. epidermidis* (Bierbaum and Sahl, 2009; Iwase et al., 2010; Yan et al., 2013).

On the other hand, recent studies with antimicrobial-producing isolates indicate that a specific bacteriocin may not affect all microbiome members equally and may only affect those with closer physical proximity. Therefore, bacteriocin-producing isolates have an important role in niche competition and colonization conferring to the producer an ecological superiority against other microbiome constituents without natural bioactive compounds that allows maintaining of stable communities and can lead to the redistribution of microbiome members into sub-niches (Heilbronner et al., 2021).

Although migratory and resident wild birds are not implicated directly in the development of antimicrobial resistance, they are considered important reservoirs and vectors of zoonotic and antimicrobial-resistant bacteria (Gómez et al., 2016; Wang et al., 2017; Abdullahi et al., 2021). In combating the global antimicrobial resistance problem, they could be considered due to their potential ability to carry *Staphylococcus* spp. which produce effective antimicrobial compounds of relevance in biomedical and food production sciences. Fortunately, half of the AP isolates were susceptible to all antibiotics tested and none of them was MDR.

5. Conclusion

Exploring the mechanisms of how bacteriocins affect microbiota dynamics requires an improved understanding of the functions of these diverse molecules. Many studies have been carried out to elucidate the exclusion mechanisms of *S. aureus* from

the human nose. However, more studies should be undertaken to clarify which antimicrobial substances are produced by nasal commensals among other strategies used in their competition with nasal microbiota for nutrients and adhesion sites.

In this respect, the two highly AP isolates identified in this study (*S. hominis* X3764 and *S. sciuri* X4000) could be excellent candidates for further studies as an alternative to the alarming situation of antibiotic resistance. This highlights the relevant role of the nasotracheal microbiota of storks as a model for the control of bacterial communities by bacteriocin-producing isolates and their transmission to humans, other animals, and the environment.

Moreover, the evaluation of bacteriocins production by staphylococci from wild animal can contribute to their potential application on other hosts and ecosystems.

Data availability statement

The original data presented in this study are included in the article/Supplementary material, further inquiries can be directed to the corresponding author.

Ethics statement

The sampling procedures performed in the previous study in which the staphylococci isolates were obtained (Abdullahi et al., 2023, in press), and were approved by the ethical committee for animal experimentation of the University of Castilla-La Mancha and authorized by the regional government of Castilla-La Mancha (permit no. VS/MLCE/avp_21_198); moreover, all applicable international, national, and/or institutional guidelines for the care and ethical use of animals, specifically directive 2010/63/EU and Spanish laws 9/2003 and 32/2007, and RD 178/2004 and RD 1201/2005 were followed.

Author contributions

CT, CL, and RF-F designed the study, made the first analysis of the data, and prepared the draft of the manuscript. RF-F, UH, INA, AU, and CG-A performed sampling, recovery of isolates, and experimental work. RF-F, SG-V, and AM participated in the graphical design of data and some methodological issues. CT and CL supervised the study. All authors read and agreed to the published version of the manuscript.

Funding

This work was supported by MCIN/AEI/10.13039/501100011033 of Spain (project PID2019-106158RB-I00). RF-F had a predoctoral contract FPU from the Ministerio de Ciencia, Innovación y Universidades of Spain (FPU18/05438). INA received funding from the European Union's H2020 Research and Innovation Programme under the Marie Skłodowska-Curie grant agreement No. 801586. SG-V had a predoctoral fellowship financed by IDRC.

Conflict of interest

The authors declare that the research was conducted in the absence of any commercial or financial relationships that could be construed as a potential conflict of interest.

Publisher's note

All claims expressed in this article are solely those of the authors and do not necessarily represent those of their affiliated

organizations, or those of the publisher, the editors and the reviewers. Any product that may be evaluated in this article, or claim that may be made by its manufacturer, is not guaranteed or endorsed by the publisher.

Supplementary material

The Supplementary Material for this article can be found online at: <https://www.frontiersin.org/articles/10.3389/fmicb.2023.1144975/full#supplementary-material>

References

- Abdullahi, I. N., Fernández-Fernández, R., Juárez-Fernández, G., Martínez-Álvarez, S., Eguizábal, P., Zarazaga, M., et al. (2021). Wild animals are reservoirs and sentinels of *Staphylococcus aureus* and MRSA clones: A problem with "One Health" concern. *Antibiotics* 10:1556. doi: 10.3390/antibiotics10121556
- Abdullahi, I. N., Juárez-Fernández, G., Hofle, U., Cardona-Cabrera, T., Minguez, D., Pineda-Pampliega, J., et al. (2023). Nasotracheal microbiota of nestlings of parent white storks with different foraging habits in Spain. *Ecohealth*. doi: 10.1007/s10393-023-01626-x
- Almeida, T., Brandão, A., Muñoz-Atienza, E., Gonçalves, A., Torres, C., Igrejas, G., et al. (2011). Identification of bacteriocin genes in enterococci isolated from game animals and saltwater fish. *J. Food Prot.* 74, 1252–1260. doi: 10.4315/0362-028X.JFP-11-016
- Bal, A. M., Coombs, G. W., Holden, M. T. G., Lindsay, J. A., Nimmo, G. R., Tattavin, P., et al. (2016). Genomic insights into the emergence and spread of international clones of healthcare-, community- and livestock-associated methicillin-resistant *Staphylococcus aureus*: Blurring of the traditional definitions. *J. Glob. Antimicrob. Resist.* 6, 95–101. doi: 10.1016/j.jgar.2016.04.004
- Bierbaum, G., and Sahl, H.-G. (2009). Lantibiotics: Mode of action, biosynthesis and bioengineering. *Curr. Pharm. Biotechnol.* 10, 2–18. doi: 10.2174/138920109787048616
- Biswas, K., Hoggard, M., Jain, R., Taylor, M. W., and Douglas, R. G. (2015). The nasal microbiota in health and disease: Variation within and between subjects. *Front. Microbiol.* 9:134. doi: 10.3389/fmicb.2015.00134
- Bonnedahl, J., and Järhult, J. D. (2014). Antibiotic resistance in wild birds. *Upsala J. Med. Sci.* 119, 113–116. doi: 10.3109/03009734.2014.905663
- Chaves-Moreno, D., Plumeier, I., Kahl, S., Krismer, B., Peschel, A., Oxley, A. P. A., et al. (2015). The microbial community structure of the cotton rat nose: Community structure of the cotton rat nose. *Environ. Microbiol. Rep.* 7, 929–935. doi: 10.1111/1758-2229.12334
- EUCAST (2022). *The European committee on antimicrobial susceptibility testing. Breakpoint tables for interpretation of MICs and Zone Diameters. Version 12.0*. Available online at: <http://www.eucast.org> (accessed December 27, 2022)
- Fernández-Fernández, R., Lozano, C., Eguizábal, P., Ruiz-Ripa, L., Martínez-Álvarez, S., Abdullahi, I. N., et al. (2022). Bacteriocin-like inhibitory substances in staphylococci of different origins and species with activity against relevant pathogens. *Front. Microbiol.* 13:870510. doi: 10.3389/fmicb.2022.870510
- García-Bayona, L., and Comstock, L. E. (2018). Bacterial antagonism in host-associated microbial communities. *Science* 361, eaat2456. doi: 10.1126/science.aat2456
- Geurkink, N. (1983). Nasal anatomy, physiology, and function. *J. Allergy Clin. Immunol.* 72, 123–128. doi: 10.1016/0091-6749(83)90518-3
- Gómez, P., Lozano, C., Camacho, M. C., Lima-Barbero, J. F., Hernández, J. M., Zarazaga, M., et al. (2016). Detection of MRSA ST3061-t843-mecC and ST398-t011-mecA in white stork nestlings exposed to human residues. *J. Antimicrob. Chemother.* 71, 53–57. doi: 10.1093/jac/dkv314
- Heilbronner, S., Krismer, B., Brötzel-Oesterheld, H., and Peschel, A. (2021). The microbiome-shaping roles of bacteriocins. *Nat. Rev. Microbiol.* 19, 726–739. doi: 10.1038/s41579-021-00569-w
- Iwase, T., Uehara, Y., Shinji, H., Tajima, A., Seo, H., Takada, K., et al. (2010). *Staphylococcus epidermidis* Esp inhibits *Staphylococcus aureus* biofilm formation and nasal colonization. *Nature* 465, 346–349. doi: 10.1038/nature09074
- Janek, D., Zipperer, A., Kulik, A., Krismer, B., and Peschel, A. (2016). High frequency and diversity of antimicrobial activities produced by nasal *Staphylococcus* strains against bacterial competitors. *PLoS Pathog.* 12:e1005812. doi: 10.1371/journal.ppat.1005812
- Krismer, B., Liebeke, M., Janek, D., Nega, M., Rautenberg, M., Hornig, G., et al. (2014). Nutrient limitation governs *Staphylococcus aureus* metabolism and niche adaptation in the human nose. *PLoS Pathog.* 10:e1003862. doi: 10.1371/journal.ppat.1003862
- Krismer, B., Weidenmaier, C., Zipperer, A., and Peschel, A. (2017). The commensal lifestyle of *Staphylococcus aureus* and its interactions with the nasal microbiota. *Nat. Rev. Microbiol.* 15, 675–687. doi: 10.1038/nrmicro.2017.104
- Laux, C., Peschel, A., and Krismer, B. (2019). *Staphylococcus aureus* colonization of the human nose and interaction with other microbiome members. *Microbiol. Spectr.* 7. doi: 10.1128/microbiolspec.GPP3-0029-2018
- Lewis, B. B., and Pamer, E. G. (2017). Microbiota-based therapies for clostridium difficile and antibiotic-resistant enteric infections. *Annu. Rev. Microbiol.* 71, 157–178. doi: 10.1146/annurev-micro-090816-093549
- Liu, C. M., Price, L. B., Hungate, B. A., Abraham, A. G., Larsen, L. A., Christensen, K., et al. (2015). *Staphylococcus aureus* and the ecology of the nasal microbiome. *Sci. Adv.* 1:e1400216. doi: 10.1126/sciadv.1400216
- Mama, O. M., Ruiz-Ripa, L., Lozano, C., González-Barrio, D., Ruiz-Fons, J. F., and Torres, C. (2019). High diversity of coagulase negative staphylococci species in wild boars, with low antimicrobial resistance rates but detection of relevant resistance genes. *Comp. Immunol. Microbiol. Infect. Dis.* 64, 125–129. doi: 10.1016/j.cimid.2019.03.006
- Misic, A. M., Davis, M. F., Tyldsley, A. S., Hodgkinson, B. P., Tolomeo, P., Hu, B., et al. (2015). The shared microbiota of humans and companion animals as evaluated from *Staphylococcus* carriage sites. *Microbiome* 3:2. doi: 10.1186/s40168-014-0052-7
- Navarro, L., Zarazaga, M., Sáenz, J., Ruiz-Larrea, F., and Torres, C. (2000). Bacteriocin production by lactic acid bacteria isolated from Rioja red wines. *J. Appl. Microbiol.* 88, 44–51. doi: 10.1046/j.1365-2672.2000.00865.x
- Newstead, L., Varjonen, K., Nuttall, T., and Paterson, G. (2020). Staphylococcal-produced bacteriocins and antimicrobial peptides: Their potential as alternative treatments for *Staphylococcus aureus* infections. *Antibiotics* 9:40. doi: 10.3390/antibiotics9020040
- Poeta, P., Costa, D., Rojo-Bezares, B., Zarazaga, M., Klibi, N., Rodrigues, J., et al. (2007). Detection of antimicrobial activities and bacteriocin structural genes in faecal enterococci of wild animals. *Microbiol. Res.* 162, 257–263. doi: 10.1016/j.micres.2006.06.003
- Prestinaci, F., Pezzotti, P., and Pantosti, A. (2015). Antimicrobial resistance: A global multifaceted phenomenon. *Pathog. Glob. Health* 109, 309–318. doi: 10.1179/2047773215Y.0000000030
- Ruiz-Ripa, L., Gómez, P., Alonso, C. A., Camacho, M. C., Ramiro, Y., de la Puente, J., et al. (2020). Frequency and characterization of antimicrobial resistance and virulence genes of coagulase-negative staphylococci from wild birds in Spain. Detection of *tst*-Carrying *S. sciuri* Isolates. *Microorganisms* 8:1317. doi: 10.3390/microorganisms8091317
- Sousa, M., Silva, N., Igrejas, G., Sargo, R., Benito, D., Gómez, P., et al. (2016). Genetic diversity and antibiotic resistance among coagulase-negative staphylococci recovered from birds of prey in Portugal. *Microb. Drug Resist.* 22, 727–730. doi: 10.1089/mdr.2015.0266
- Van der Veken, D., Benhachemi, R., Charmpi, C., Ockerman, L., Poortmans, M., Van Reckem, E., et al. (2020). Exploring the ambiguous status of coagulase-negative staphylococci in the biosafety of fermented meats: The case of antibacterial activity versus biogenic amine formation. *Microorganisms* 8:167. doi: 10.3390/microorganisms8020167

- Wang, J., Ma, Z.-B., Zeng, Z.-L., Yang, X.-W., Huang, Y., and Liu, J.-H. (2017). The role of wildlife (wild birds) in the global transmission of antimicrobial resistance genes. *Zool. Res.* 38, 55–80. doi: 10.24272/j.issn.2095-8137.2017.003
- Weese, J., Slifierz, M., Jalali, M., and Friendship, R. (2014). Evaluation of the nasal microbiota in slaughter-age pigs and the impact on nasal methicillin-resistant *Staphylococcus aureus* (MRSA) carriage. *BMC Vet. Res.* 10:69. doi: 10.1186/1746-6148-10-69
- Wei, Q., Li, Z., Gu, Z., Liu, X., Krutmann, J., Wang, J., et al. (2022). Shotgun metagenomic sequencing reveals skin microbial variability from different facial sites. *Front. Microbiol.* 13:933189. doi: 10.3389/fmicb.2022.933189
- Yan, M., Pamp, S. J., Fukuyama, J., Hwang, P. H., Cho, D.-Y., Holmes, S., et al. (2013). Nasal microenvironments and interspecific interactions influence nasal microbiota complexity and *S. aureus* carriage. *Cell Host Microbe* 14, 631–640. doi: 10.1016/j.chom.2013.11.005
- Zhou, Y., Mihindukulasuriya, K. A., Gao, H., La Rosa, P. S., Wylie, K. M., Martin, J. C., et al. (2014). Exploration of bacterial community classes in major human habitats. *Genome Biol.* 15:R66. doi: 10.1186/gb-2014-15-5-r66
- Zipperer, A., Konnerth, M. C., Laux, C., Berscheid, A., Janek, D., Weidenmaier, C., et al. (2016). Human commensals producing a novel antibiotic impair pathogen colonization. *Nature* 535, 511–516. doi: 10.1038/nature18634



OPEN ACCESS

EDITED BY

Rustam Aminov,
University of Aberdeen, United Kingdom

REVIEWED BY

Paola Sperandio,
University of Milan, Italy
Vigyasa Singh,
University of Arizona, United States

*CORRESPONDENCE

Hong-Xia Ma
✉ hongxia0731001@163.com
Cheng-Guang He
✉ hechengguang@163.com

[†]These authors have contributed equally to this work and share first authorship

SPECIALTY SECTION

This article was submitted to
Antimicrobials,
Resistance and Chemotherapy,
a section of the journal
Frontiers in Microbiology

RECEIVED 15 January 2023

ACCEPTED 24 March 2023

PUBLISHED 18 April 2023

CITATION

Cui Q, Yu H-D, Xu Q-J, Liu Y, Wang Y-T, Li P-H,
Kong L-C, Zhang H-P, Jiang X-Y, Giuliadori AM,
Fabbretti A, He C-G and Ma H-X (2023)
Antibiotic synergist OM19r reverses
aminoglycoside resistance in multidrug-
resistant *Escherichia coli*.
Front. Microbiol. 14:1144946.
doi: 10.3389/fmicb.2023.1144946

COPYRIGHT

© 2023 Cui, Yu, Xu, Liu, Wang, Li, Kong, Zhang,
Jiang, Giuliadori, Fabbretti, He and Ma. This is
an open-access article distributed under the
terms of the [Creative Commons Attribution
License \(CC BY\)](https://creativecommons.org/licenses/by/4.0/). The use, distribution or
reproduction in other forums is permitted,
provided the original author(s) and the
copyright owner(s) are credited and that the
original publication in this journal is cited, in
accordance with accepted academic practice.
No use, distribution or reproduction is
permitted which does not comply with these
terms.

Antibiotic synergist OM19r reverses aminoglycoside resistance in multidrug-resistant *Escherichia coli*

Qi Cui^{1†}, Han-Dong Yu^{1†}, Qi-Jun Xu², Yue Liu², Yu-Ting Wang²,
Peng-Hui Li¹, Ling-Cong Kong¹, Hai-Peng Zhang²,
Xiu-Yun Jiang¹, Anna Maria Giuliadori³, Attilio Fabbretti³,
Cheng-Guang He^{2*} and Hong-Xia Ma^{1,2*}

¹College of Animal Science and Technology, Jilin Agricultural University, Changchun, China,

²Engineering Research Center of the Chinese Ministry of Education for Bioreactor and Pharmaceutical Development, College of Life Sciences, Jilin Agricultural University, Changchun, China, ³School of Biosciences and Veterinary Medicine, University of Camerino, Camerino, Italy

Introduction: The continued emergence and spread of multidrug-resistant (MDR) bacterial pathogens require a new strategy to improve the efficacy of existing antibiotics. Proline-rich antimicrobial peptides (PrAMPs) could also be used as antibacterial synergists due to their unique mechanism of action.

Methods: Utilizing a series of experiments on membrane permeability, *In vitro* protein synthesis, *In vitro* transcription and mRNA translation, to further elucidate the synergistic mechanism of OM19r combined with gentamicin.

Results: A proline-rich antimicrobial peptide OM19r was identified in this study and its efficacy against *Escherichia coli* B2 (*E. coli* B2) was evaluated on multiple aspects. OM19r increased antibacterial activity of gentamicin against multidrug-resistance *E. coli* B2 by 64 folds, when used in combination with aminoglycoside antibiotics. Mechanistically, OM19r induced change of inner membrane permeability and inhibited translational elongation of protein synthesis by entering to *E. coli* B2 via intimal transporter SbmA. OM19r also facilitated the accumulation of intracellular reactive oxygen species (ROS). In animal models, OM19r significantly improved the efficacy of gentamicin against *E. coli* B2.

Discussion: Our study reveals that OM19r combined with GEN had a strong synergistic inhibitory effect against multi-drug resistant *E. coli* B2. OM19r and GEN inhibited translation elongation and initiation, respectively, and ultimately affected the normal protein synthesis of bacteria. These findings provide a potential therapeutic option against multidrug-resistant *E. coli*.

KEYWORDS

multidrug-resistant bacteria, SbmA, transcription, antimicrobial peptide, PrAMPs

1. Introduction

The emergence of multi-drug resistant (MDR) bacterial pathogens is a major threat to global public health (Aslam et al., 2018). At present, due to the extensive use of antibiotics, the family *Enterobacteriaceae* associated with animals have developed multidrug resistance (Van Boeckel et al., 2019). *Escherichia coli* (*E. coli*) is one of the most common pathogens of this family leading to infections in animals and humans with pathogenicity of 10–15% and mortality of 3.8–72%. Usually, aminoglycosides have been used for therapy against *E. coli* infections; however, recent studies have shown that a large number of *E. coli* strains are resistant to aminoglycosides. The resistance rate of

aminoglycosides resistant genes and its related phenotypes in *E. coli* from lactating dairy cows have been reported for about 20% in the US (Jeamsripong et al., 2021). Likewise, aminoglycosides resistant bacterial strains of *Enterobacteriaceae* family isolated from different sources in Ireland have also been reported. The bacteria develop different frequencies of aminoglycosides resistance based on their habitat and geographical distribution. The highly exposed areas to antibiotics receives the highest frequency of resistance (Hooban et al., 2022). With the continuous evolution of pathogenic bacteria under the pressure of antimicrobial drugs, the existing antimicrobial drugs are no longer effective in the clinical treatment of bacterial infections; therefore, alternatives to traditional antibiotics are required on priority basis.

Using antibiotic synergists is a promising strategy as it could extend the half-life of existing antibiotics, alleviate the current shortage of effective antibiotics, and reduce the lengthy drug development time and thereby the economic risk. Currently, novel β -lactam antibacterial synergists (Si et al., 2020; Durand-Reville et al., 2021), tetracycline antibacterial synergists (Zheng et al., 2017; Liu Y. et al., 2020), polymyxin antibacterial synergists (Stokes et al., 2017; Song et al., 2021) and macrolides antibacterial synergists (Sturge et al., 2019) have been identified. Furthermore, bee venom enhances the bacteriostatic effect of gentamicin (GEN) and vancomycin (VAN) against methicillin-resistant *Staphylococcus aureus* (MRSA) (Peng et al., 2021). In addition, thiosemicarbazide combined with gentamicin (GEN) prevent Gram-positive bacterial infection by inhibiting DNA gyrase activity by approximately 50% (Wang et al., 2019). However, data on antimicrobial peptides as synergists to restore gentamicin (GEN) sensitivity of Gram-negative bacteria, especially drug-resistant *E. coli*, are limited.

Cationic antimicrobial peptides (AMPs) have also been used as synergists to enhance the antibacterial activity of antibiotics owing to their unique membrane-breaking mechanism (Randhawa et al., 2016; Si et al., 2020; Song et al., 2020; Bai et al., 2021; Zhu et al., 2021). Certain proline-rich antimicrobial peptides (PrAMPs) can directly cross the bacterial cell membrane and exert their antibacterial effects (Roy et al., 2015; Böttger et al., 2016). However, there have been no studies on the use of PrAMPs as adjuvants to improve the antibacterial effect of existing antibiotics. Proline-rich antimicrobial peptide OM19r (VDKPPYLPRPRPIRrPGGr-NH₂) is a sequence-derived peptide from the existing AMP sequences. The new peptide OM19r of this study was designed by substitution of D-type amino acid at positions 15 and 19 of OM19R (Cui et al., 2021), while OM19R (VDKPPYLPRPRPIRrPGGr-NH₂) was a hybrid obtained from Oncocin and MDAP-2 fragments (Liu L. et al., 2020). OM19r shown the effective restoration the gentamicin (GEN) sensitivity of multidrug resistant *E. coli*. The effect of OM19r combined with gentamicin (GEN) on the cell membrane and DNA of *E. coli* B2 (mcr-1) was determined via a series of fluorescence permeability and DNA binding assays. Meanwhile, an *in vitro* transcription-translation system (TX-TL) was constructed to investigate the effects of OM19r against multidrug resistant *E. coli* B2. Our findings suggest the potential use of OM19r as an aminoglycosides antibacterial synergist to improve the antibacterial activity of aminoglycosides.

2. Materials and methods

2.1. Bacterial strains and cell culture

Mueller-Hinton (MH) broth and Mueller-Hinton (MH) agar culture medium were purchased from Haibo Biotechnology Co.,

Ltd. (Qingdao, China) and the antibiotics were purchased from the Institute of China Food and Drug Administration. The bacterial strains were obtained from the Key Laboratory of New Veterinary Drug Research and Development of Jilin Province. The *E. coli* ATCC25922 strain served a quality control. Multidrug resistant *E. coli* B2 (mcr-1) strain was provided by the China Agricultural University while *E. coli* ATCC25922 (Δ SbmA) strain was provided by the Key Laboratory of Animal Production, Product Quality and Security, Ministry of Education. HeLa Cells and mouse macrophage cells (RAW264.7) were cultured in Dulbecco's Modified Eagle Medium (Gibco) supplemented with 1% (w:v) penicillin-streptomycin and 10% (w:v) heat-inactivated FBS (Sigma-Aldrich) at 37°C in a 5% CO₂ atmospheric environment.

2.2. Experimental animals

BALB/c mice (4 weeks old, weighing 20–22 g) were obtained from the laboratory of Jilin Agricultural University Changchun, China. All the animals were housed in an environment with a temperature of 22 ± 1°C, a relative humidity of 50 ± 1%, and a light/dark cycle of 12/12 h. The laboratory animal usage license (SYXK-2018-0023) was issued by the Laboratory Animal Center of Jilin Agricultural University Changchun, China. All animal studies (including the mice euthanasia procedure) were performed in compliance with the regulations and guidelines of Institutional Animal Care of Jilin Agricultural University Changchun, China.

2.3. Antimicrobial activity

The minimum inhibitory concentration (MIC) of antimicrobials was determined by the broth microdilution method (Miao et al., 2020; Zhong et al., 2021). Briefly, the strains to be tested were inoculated into 5 ml of MH broth medium and cultured to logarithmic growth phase (OD₆₀₀ = 0.5), and diluted with fresh MH broth to obtain 1 × 10⁶ CFU/ml. The diluted bacterial solution (100 µl) was added to 96-well plates containing different concentrations of antibiotics or different concentrations of antimicrobial peptides. The final concentrations of OM19r strain were 1–128 µg/ml (0.45–57.5 µM). A 100 µl bacterial solution + 100 µl MH broth medium served as positive control while 200 µl MH broth medium was kept as negative control. The 96-well plate was incubated at 37°C for 18–20 h, and the MICs were measured at 600 nm. The experiment was conducted in triplicate.

2.4. Checkerboard assays

The synergistic antibacterial activity was measured by the checkerboard method (Zhong et al., 2019). Briefly, a 50 µl of diluted OM19r (0–8 µg/ml) and 50 µl of diluted antibiotics (0–512 µg/ml) were put into a 96-well plate, then added a 100 µl of the diluted bacterial solution (1 × 10⁶ CFU/ml) and incubated at 37°C for 16–18 h, and measured the FIC at 600 nm. The experiment was performed in triplicate. The FIC index was calculated as: FIC = MIC (group A combined)/MIC (group A used alone) + MIC (group B combined)/MIC (group B used alone). Where the following were considered as, FIC ≤ 0.5 for synergistic effect, 0.5 < FIC ≤ 1 for

additive effect, $1 < \text{FIC} \leq 4$ for no effect, and $\text{FIC} > 4$ for antagonistic effect.

2.5. Bacterial growth curve and time-kill curve analysis

Growth curves were measured according to the previously described method at OD₆₀₀ nm wavelength at 37°C for 24 h at every 1 h interval (Song et al., 2020). Briefly, different concentrations of OM19r (2 µg/ml), GEN (32 µg/ml), or OM19r combined with GEN (2 + 32 µg/ml) were added to 96-well microplates with an equal amounts of bacterial dilutions (1×10^6 CFU/ml). The time-kill curve was drawn with time as the abscissa and the Log value of the number of colonies as the ordinate (Falciani et al., 2020). Different concentrations of OM19r (8 µg/ml), GEN (128 µg/ml), OM19r combined with GEN (4 + 2 µg/ml) or OM19r combined with GEN (4 + 4 µg/ml) were diluted to contain indicator bacteria (OD = 0.5) in a 1.5 ml centrifuge tube. PBS was kept as a negative control group. After every half an hour, a 100 µl of the diluted bacterial solution was taken out and spread on MH agar medium, and counted after culturing at 37°C for 16–18 h. The procedures were conducted triplicate.

2.6. Hemolytic activity

The fresh sheep blood (1–2 ml) was collected at 4°C and centrifuged at $1238 \times g$ for 10 min according to a previously described method (Zhong et al., 2020). The collected red blood cells were washed three times with PBS (10 mM, PH = 7.4), and then resuspended in a 9 ml PBS with approximate cell concentration of 10^9 cells/mL. Erythrocyte suspension (100 µl) was successively added to 96-well plates that were added with antimicrobial peptides (ranging from 1 µg/mL to 64 µg/mL) and PBS. After incubation at 37°C for 2 h, the samples were centrifuged at $8800 \times g$ for 10 min. The supernatants (180 µl) were transferred to a new 96-well plate, and the absorbance was measured at 570 nm. The absorbance of PBS (100 µl) treated-erythrocyte supernatants (100 µl) served as negative control while the absorbance of 0.1% Triton X-100 (100 µl) treated-erythrocyte supernatants (100 µl) as positive control. Hemolysis was calculated using the following formula:

$$\text{Hemolysis (\%)} = [(A_{420, \text{peptide}} - A_{420, \text{PBS}}) / (A_{420, 0.2\% \text{ Triton X-100}} - A_{420, \text{PBS}})] \times 100.$$

2.7. Cytotoxicity assays

The cytotoxicity of OM19r was determined using 3-(4,5-dimethylthiazol-2-yl)-2,5 diphenyltetrazolium bromide (MTT, United Kingdom) dye reduction test according to a previously described method (Mwangi et al., 2019). Briefly, mouse mononuclear macrophage RAW264.7 and HeLa cells (2.0×10^4 cells/well) were added into 96-well plates at 37°C overnight. Then OM19r was added to the cell cultures to reach a final concentration of 1–64 µg/ml and cultured under a 5% CO₂ atmospheric environment at 37°C for 24 h. After incubation with MTT (50 µl, 0.5 mg/ml) at 37°C for 2 h, the cell cultures without supernatants were collected by centrifuging at $413 \times g$ for 5 min. Subsequently, a 150 µl of dimethyl sulfoxide

(DMSO) was added to dissolve the formazan crystals that were created during experimnt. Absorbance (490 nm) was measured using a microplate reader. Cytotoxicity was calculated using the following formula:

$$\text{Cytotoxicity (\%)} = 100 - [(A_{570 \text{ of peptide treated cells}} / A_{570 \text{ of control}}) \times 100].$$

2.8. Membrane permeability assays

The outer membrane changes were measured using 1-N-phenylanthranilic acid (NPN) dye (Ma et al., 2020). NPN is a hydrophobic fluorescent agent normally used for emission of weak fluorescence in aqueous solution but it emits strong fluorescence upon entering to a hydrophobic medium. We added a 10 µl of 1 mM NPN solution to each 990 µl of bacterial suspension (1×10^6 CFU/ml) and incubated it at room temperature for 30 min in the dark environment. The groups were as follow: experimental group (Fbos) holding a 100 µl of NPN-containing bacterial suspension + 100 µl of antimicrobial peptide mixture, control group (F0) holding a 100 µl of NPN bacterial suspension + 100 µl of PBS and control group (F100) holding a 100 µl of NPN-containing bacterial suspension + 100 µl of polymyxin B. Fluorescence intensity was detected after every 10 min for 150 min. The mixture was placed in a 96-well dark plate, the excitation wavelength and emission wavelength was adjusted to 350 nm and 420 nm, respectively, and the fluorescence intensity was detected. Each experiment was set up with 3 replicates. Absorption was measured as,

$$\text{NPN absorption rate} = (\text{Fbos} - \text{F0}) / (\text{F100} - \text{F0}) \times 100\%.$$

The membrane changes were measured using propidium iodide (PI) dye (Mattiuzzo et al., 2010; Mwangi et al., 2019; Ma et al., 2020). Propidium iodide (PI) is a popular red-fluorescent nuclear and chromosome counterstain. Since propidium iodide is not permeant to live cells, it is commonly used to detect dead cells in a population. PI binds to DNA by intercalating between the bases with little or no sequence preference. The bacterial suspension was adjusted to 1×10^6 CFU/ml by the same method mentioned above. First PI dye was added to the bacterial suspension to reach a final concentration of 10 µM. Then PI-containing suspension was mixed at 1:1 with the antimicrobial peptide mixture in a total volume of 200 µl and added to a 96-well dark plate. The excitation wavelength and emission wavelength was set to 535 nm and 615 nm, respectively. Fluorescence intensity was detected after every 10 min for 150 min.

2.9. Proton motive force assays

The PMF consists of a pH gradient (ΔpH) and a potential gradient ($\Delta\phi$), which together constitute an electrochemical gradient (Corbalan et al., 2013). Membrane depolarization was measured using 3,3'-dipropylthiadicarbocyanine iodide DiSC3(5) fluorescent dye (Xu et al., 2020). DiSC3(5) was added to the bacterial suspension (1×10^6 CFU/ml) to a final concentration of 0.5 µM, and then the bacterial suspension containing DiSC3(5) was mixed at 1:1 with different concentrations of peptide mixture in a total volume of 200 µl. It was placed on a 96-well light-shielding plate, and the excitation wavelength and emission wavelength was set at 670 nm and 622 nm, respectively. Polymyxin B and PBS served as the positive and negative control, respectively. Membrane depolarization was measured by using BCECF-AM fluorescent dye (Ding et al., 2020). BCECF-AM was added to the bacterial

suspension (1×10^6 CFU/ml) to a final concentration of $20 \mu\text{M}$, then mixed with the different concentrations of peptide mixture at 1:1 to a total volume of $200 \mu\text{l}$, and then added to a 96-well plate protected in dark environment. The excitation wavelength and emission wavelength was set to 522 nm and 488 nm, respectively. The positive control was glucose, and the negative control was PBS, and each group had three replicates.

2.10. Efflux pump assays

Fluorescent probe Ethidium bromide (EtBr) was used to detect the effect of drug on non-specific bacterial pumping system and to monitor EtBr efflux from the cell. The bacterial solution was re-suspended in PBS buffer until $\text{OD}_{600} = 0.5$, then a $2 \mu\text{g/ml}$ EtBr was added, mixed evenly, and incubated in the dark for 30 min. The suspensions containing EtBr in the two experiments were then mixed at 1:1 with antimicrobial peptides to make a total volume of $200 \mu\text{l}$. It was placed on a 96-well dark plate, and the excitation wavelength and emission wavelength was set at 600 nm and 530 nm, respectively. The fluorescence intensity was detected after every 10 min for 150 min. The positive control was the efflux pump inhibitor CCCP, and the negative control was PBS, and each group had three replicates (Wang et al., 2015).

2.11. Real-time PCR

The qPCR was performed according to a previously described method (Bustin et al., 2009). The bacterial suspension was adjusted to 1×10^6 CFU/ml by the same method as stated. RNA was extracted using RNAiso Plus and the values at 260 nm/280 nm were measured on spectrophotometer. The primers used were SbmA primers (SbmA-F: GAACCTCGAGCTGATCTTCG; SbmA-R: CTGAGCTCCGATTCGAAGG) and internal reference gene primers (rsmC-F: GAAATTCTGGGCGAATACA; rsmC-R: CTTTCACCTCGGAAAAGACG). The reaction system was $10 \mu\text{l}$ of SYBR Green I Master ($2\times$), $8 \mu\text{l}$ of ddH_2O , $1 \mu\text{l}$ of cDNA upstream and downstream primers, and $0.5 \mu\text{l}$ of upstream and downstream primers. Reaction program was as follow: pre-denaturation at 95°C for 5 min, denaturation at 95°C for 10 s, annealing at 60°C for 15 s, extension at 72°C for 20 s and a total of 40 cycles. Each experiment was repeated three times. And the fold change of gene expression was calculated by the $2^{-\Delta\Delta\text{Ct}}$ method.

2.12. Recombinant expression of SbmA

The pET28a-SbmA-6His recombinant expression vector was constructed and transformed to *E. coli* BL21 competent cell for the overexpression SbmA-6His protein. The SbmA protein was purified using Ni-NTA 6FF column. [The process was as follows: Lysed *E. coli* cell with Buffer A (20 mM Tris-HCl pH 7.4, 5% glycerol, 500 mM NaCl. That 6 mM β -Mercaptoethanol, 0.1 mM Benzamidine and 0.1 mM PMSF added immediately before use). Non-affinity protein was washed off by Buffer A added 20 mM imidazole. The target protein was finally eluted by Buffer A added 200 mM imidazole.] The effect of SbmA on the bacteriostatic

activity of OM19r against *E. coli* was determined by *in vitro* competitive inhibition assay. The secondary structure of OM19r was constructed by <https://zhanggroup.org/I-TASSER/>. The structure of SbmA protein was constructed by using the online server Swiss-Model.¹

2.13. Molecular docking

The HDock online software was used for molecular docking. The resulting conformations were set to 100 and the scoring function was used to select the conformation with the negative energy. The docking results were visualized by using pymol software.

2.14. Confocal laser scanning microscopy

Confocal laser scanning microscopy (CLSM) was performed according to the previously described method (Si et al., 2020). *E. coli* B2 precipitates in logarithmic growth phase (OD_{600} value 0.5) were collected at $2000 \times g$ for 5 min and washed three times with sterile PBS. C-terminal FITC-labeled antimicrobial peptides were added to a final concentration of $0.5 \times \text{MIC}$ and $1 \times \text{MIC}$, and incubated at 37°C for 30 min. The site of FITC-labeled antimicrobial peptide OM19r entering *E. coli* B2 was observed by confocal laser scanning microscope (FV1000).

2.15. Transmission electron microscopy

The intracellular changes in *E. coli* B2 cells induced by OM19r were determined by transmission electron microscope (TEM) according to a previously described method (Türkez et al., 2019). The *E. coli* B2 treated with OM19r and Melittin ($0.5 \times \text{MIC}$, $1 \times \text{MIC}$) were streaked on slides and washed with PBS 3 times, fixed with 2.5% glutaraldehyde for 12 h and 1% osmium for 4 h, then gradient elution was performed with different concentrations (30, 50, 70, 90 and 100%) of acetone, embedded in epoxy resin polymer. Finally, the sections were coated and stained with 2% bisoxyl acetate and lead citrate, and the bacterial samples were observed by using E-1010 TEM (HITACHI JEOL, Tokyo, Japan).

2.16. Measurement of total reactive oxygen species

The accumulation of intracellular ROS was measured using DCFH-DA fluorescent dye (Maisuria et al., 2015). DCFH-DA was added to bacterial suspension (1×10^6 CFU/ml) with a final concentration of $10 \mu\text{M}$ and incubated at 37°C for 30 min. Then centrifuged at $1000 \times g$ for 10 min, resuspended in PBS, and removed the fluorescent probe that did not enter the cells. The

¹ <https://swissmodel.expasy.org/>

bacterial suspension containing DCFH-DA was mixed at 1:1 with the different concentrations of peptide mixture in a total volume of 200 μ L and added to a 96-well dark plate. The fluorescence emission was measured by excitation and emission wavelength of 535 nm and of 485 nm, respectively. Hydrogen peroxide and PBS served as positive and negative control, respectively and three replicates were set for each group.

2.17. DNA binding assay

The genome of *E. coli* B2 was extracted using genome extraction kit according to manufacturer's instructions (Shanghai Shangon Biotech Co., LTD., China), and the concentration was adjusted to 100 ng/ μ L. A 20 μ L of peptides and antibiotics with different concentrations were combined with the genome were set in the reaction system. LR_{PG} was used as positive control (Jia et al., 2020). After incubation at 37°C for 1 h, a 2 μ L 10 \times loading buffer was added and the effect of OM19r on DNA migration was analyzed by 1% agarose electrophoresis.

2.18. In vitro protein synthesis

In vitro protein synthesis was performed according to a previously described method (Garamella et al., 2016). myTXTL[®] Sigma 70 Master Mix Kit (Daicel Arbor Biosciences, United States) was used to determine the effect of GEN combined with OM19r on protein synthesis *in vitro*. The concentration of OM19r was 0.5 μ g/ml and GEN was 0.05, 0.25, 0.5, 1, 2, 5 and 50 μ g/ml.

2.19. In vitro transcription

In vitro transcription assays were performed according to a previously described method (Marras et al., 2004). Molecular beacons were purchased from ComateBio, which sequence was: 5'-6-FAM-CCGCGCATCTCGGTTGATTCTTTTCCTCGGGC GCGG-Dabcyl-3'. The 5' end was linked to a fluorescent dye (6-FAM), while the 3'-end was coupled to a quencher molecule (Dabcyl). The region which base-pairs with the target rRNA was indicated under the black solid line. Both sides of the end contained repeated GC bases, which were considered the stem of the Molecular beacon, made it quench normally. After mating with the target rRNA sequence, the fluorescence was emitted. OM19r was competitively bound to the target sequence, the molecular beacon configuration did not change and the fluorescence was quenched. The Components of experimental group were as follow: 5 \times Buffer (80 μ L), NTPs (8 μ L), DNA template (4 μ L), RNA polymerase (50 μ L), RNA inhibitor (1 μ L), different concentrations of OM19r (18 μ L) and H₂O replenishment to 200 μ L. The Components of negative control group were as follow: 5 \times Buffer(80 μ L), NTPs (8 μ L), RNA inhibitor (1 μ L), different concentrations of OM19r (18 μ L) and H₂O and H₂O replenishment to 200 μ L. The Components of positive control group were as follow: 5 \times Buffer(80 μ L), NTPs (8 μ L), 23SrRNA (2 μ L), RNA polymerase (50 μ L), RNA inhibitor (1 μ L), different concentrations of OM19r (18 μ L) and H₂O and H₂O replenishment to 200 μ L. Each

group was incubated at 37°C for 20 min. Subsequently, 100% ethanol and 3 M NaAc(pH-5.2) were added, followed by an ice bath for 30 min, and the precipitate was removed by centrifugation at 13523 \times g for 10 min at 4°C. After addition of 80% ethanol, the precipitate was removed by centrifugation at 13523 \times g for 10 min at 4°C. After vacuum drying for 30 min, a 2 μ L molecular beacon was added. Subsequently, a 100 μ L of Tris-HCL (pH = 8.8) was added to each well, followed by incubation at 95°C for 2 min and 45°C for 10 min. It was transferred to a 96-well dark plate, and the excitation and emission wavelength was 485 nm and 520 nm, respectively.

2.20. mRNA translation

E. coli S30 extract translation system(Brandi et al., 2007): The reaction mixture to test standard mRNA translation in bacterial extracts contains, in 30 μ L of 10 mM Tris-HCl (pH 7.7): 7 mM Mg acetate, 100 mM NH₄Cl, 2 mM DTT, 2 mM ATP, 0.4 mM GTP, 10 mM PEP, 0.025 mg/ml PK, 0.12 mM 10-formyl-terahydrofolate, 3 μ g/ μ L tRNA (*Escherichia coli* BL21), an amino acid mixture containing 0.2 mM of all amino acids (with the exception of phenylalanine); 9 μ M [³H] phenylalanine and 36 μ M non-radioactive phenylalanine, an optimized amount of the S30 cell extract (generally 2–6 μ L/reaction mixture) and 1–3 μ M mRNA (pre-heated 5 min at 65°C). After 30–60 min incubation at 37°C, 20 μ L aliquots from each reaction mixture are spotted on 3 mm paper disks which are dropped into 10% ice-cold TCA and processed according to the hot TCA procedure (Mans and Novelli, 1961).

Poly(U) hybrid translation system (Kaminishi et al., 2015): Translation was carried out in Poly(U) hybrid translation system. A 30 μ L of buffer containing 3 mM phosphoenolpyruvate (PEP), 0.05 μ g/ml pyruvate kinase (PK), 1 mM GTP, 0.15 μ g/ μ L poly(U), 10 μ M [³H]-Phe-tRNA and 0.2 μ M of *Escherichia coli* 30S and 50S were added to the mix after a 5 min incubation at room temperature in the presence of increasing concentrations of OM19r. After 30 min at 37°C the level of poly(U) translation was quantified from the amount of acid-insoluble [³H] Phe-tRNA incorporated.

2.21. Animal infection model

Mouse peritonitis model: The sample size was selected according to the preliminary infection test (n = 8 per group). Some 6-week-old female mice were intraperitoneally injected with 0.5 ml of *E. coli* B2 (3 \times 10⁸ CFU/ml) to establish a mouse peritonitis model. Then after 1 h, different doses of OM19r (8 mg/kg), GEN (8 mg/kg) and OM19r combined with GEN (4 + 2 mg/kg) were injected intraperitoneally. The blank control mice were injected with the same dose of normal saline. Survival of mice treated and colony counts in each organ were recorded over 7 days.

G. mellonella infection model: *G. mellonella* larvae were randomly divided into 6 groups (n = 8 per group) and infected with 10 μ L of *E. coli* B2 (2 \times 10⁶ CFU/ml) in the right hind ventral foot. Then after 1 h, different doses of OM19r (8 mg/kg), GEN (8 mg/kg) and OM19r combined with GEN (4 + 2 mg/kg) were injected intraperitoneally. The blank control mice were injected with the

same dose of normal saline. Survival in response to treatment was recorded over 5 days.

2.22. Data analysis

All the experimental data were processed by SPSS software using an unpaired two-tailed Student's *t*-test. Quantitative data were expressed as mean \pm standard deviation, *p*-values was considered statistically significant as * *p* < 0.05, ** *p* < 0.01, *** *p* < 0.001, and ns represented non-significant.

3. Results

3.1. Antimicrobial activity and checkerboard assays

A total of Seven AMPs with good antibacterial activity *E. coli* were synthesized from the existing AMP sequences and evaluated for their efficacy on multiple aspects. OM19r in combination with gentamicin revealed the lowest FIC (FIC = 0.156; [Supplementary Table S2](#)) among seven experimental antibacterial peptides. Therefore, a proline-rich antimicrobial peptide OM19r was derived and synthesized ([Supplementary Figure S1](#); [Supplementary Table S3](#)). The results of OM19r combined with other antibiotics acting on different sites showed that when combined with gentamicin, the synergistic antibacterial activity was the strongest, and it could restore the sensitivity of multi-drug resistant *E. coli* to gentamicin ([Supplementary Table S4](#)). The MIC of OM19r against some Gram-negative bacteria was 1–8 μ g/ml ([Table 1](#)).

The antibacterial effect of OM19r combined with GEN against drug-resistant bacteria including *E. coli* B2, *S. typhimurium* 1A, *A. baumannii* JS1, *S. dysenteriae* A3, and *K. pneumoniae* JP20 ([Supplementary Table S5](#)), was determined using the microbroth dilution method and checkerboard assay. The results showed that OM19r combined with GEN had a synergistic antibacterial effect (FIC \leq 0.5) against some Gram-negative bacteria ([Figures 1A–F](#)). When OM19r was used at a sub-minimum inhibitory concentration (2 μ g/ml), the MIC of GEN against resistant *E. coli* B2 decreased from 64 to 1 μ g/ml. The FIC of OM19r combined with kanamycin, streptomycin, tobramycin and spectinomycin against drug-resistant *E. coli* B2 was \leq 0.5. These results indicate that OM19r combined with aminoglycoside produced synergistic antibacterial effect against drug-resistant *E. coli* B2 ([Supplementary Table S6](#)).

3.2. Growth curves and time-kill curves of bacteria

Growth curve analysis showed that OM19r combined with GEN (2 + 32 μ g/ml) inhibited the growth of *E. coli* B2, indicating no antagonistic effect between OM19r combined with GEN against *E. coli* B2 ([Figure 2A](#)). The time-kill curve of OM19r combined with GEN (4 + 4 μ g/ml) showed that *E. coli* B2 could be eliminated within

TABLE 1 Minimum inhibitory concentrations (MICs) of OM19r against different bacteria.

Bacterial Species	OM19r (μ g/mL)
Gram-negative	
<i>E. coli</i> ATCC25922	1
<i>E. coli</i> ATCC25922 (Δ SbmA)	>128
<i>E. coli</i> k88	2
<i>S. enterica</i> ATCC 14028	2
<i>S. typhimurium</i> CMCC50115	2
<i>S. flexneri</i> ATCC12022	2
<i>S. dysenteriae</i> CMCC51252	2
<i>K. pneumoniae</i> CMCC46117	4
Gram-negative (Clinical isolate strains)	
<i>E. coli</i> SN5	1
<i>E. coli</i> SN3	2
<i>E. coli</i> Q12	4
<i>E. coli</i> Q14	4
<i>E. coli</i> Q45	4
<i>E. coli</i> W23	4
<i>E. coli</i> QY	4
<i>E. coli</i> B2(mcr-1)	4
<i>S. typhimurium</i> 1A	4
<i>A. baumannii</i> JS1	8
<i>S. dysenteriae</i> A3	4
<i>S. flexneri</i> RH	8
<i>K. pneumoniae</i> JP20	4
Gram-positive	
<i>S. aureus</i> ATCC25923	>512
<i>S. aureus</i> (MRSA)	>512
<i>S. faecalis</i> ATCC29212	>512
<i>B. subtilis</i> ATCC63501	>512

3 h in a dose dependent manner ([Figure 2B](#)). The combined antibacterial activity of OM19r and GEN against 60 other clinical isolates of *E. coli* was also determined. The result showed that OM19r at a low dose (2 μ g/ml) combined with GEN (1 μ g/ml) inhibited growth of 36 *E. coli* strains (60%) ([Figure 2C](#)), while OM19r at a high dose (4 μ g/ml) combined with GEN (0.5 μ g/ml) inhibited growth of 54 *E. coli* strains (90%) ([Figure 2C](#)).

3.3. Hemolytic and cytotoxicity assays

The hemolysis rate of sheep red blood cells was <5% following treatment with different concentrations of antimicrobial peptide OM19r combined with GEN ([Figure 3A](#)). Alternatively, cytotoxicity assays showed that the survival rate of mouse macrophages (RAW264.7) and human cervical cancer cells (HeLa) exceeded 90% after treatment with different concentrations of OM19r combined with GEN ([Figures 3B,C](#)).

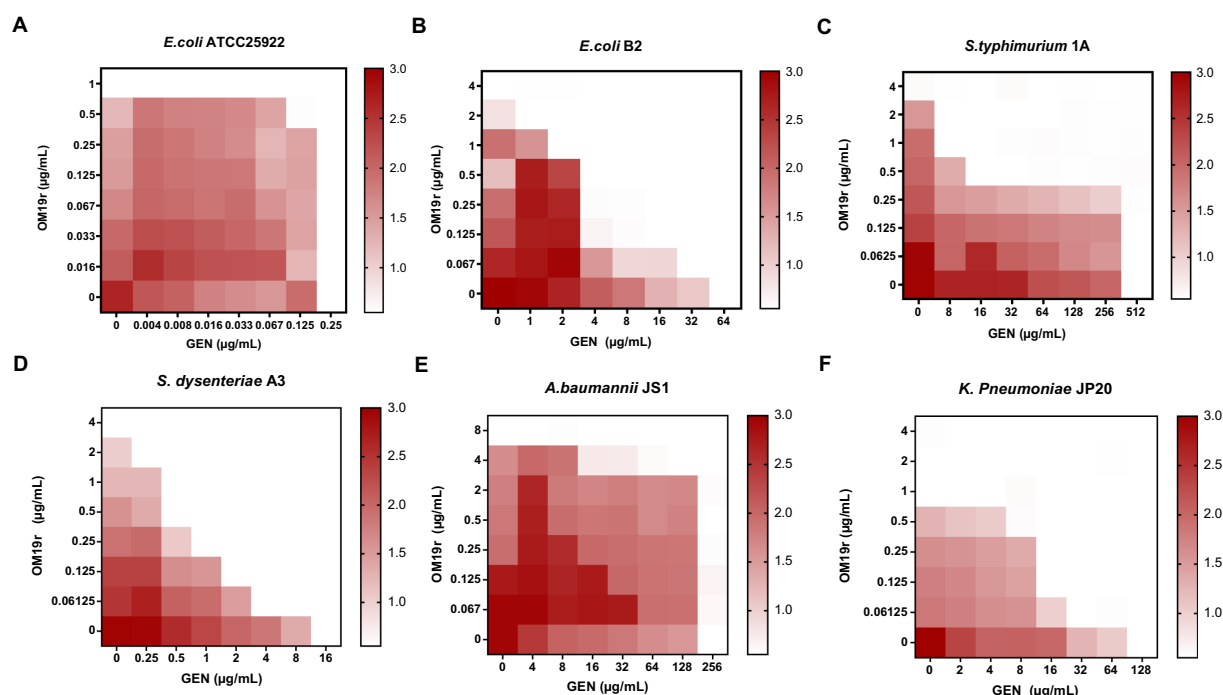


FIGURE 1

OM19r enhances the antibacterial activity of GEN against some Gram-negative bacteria. (A–F) Checkerboard test results of OM19r combined with GEN against *E. coli* ATCC25922, *E. coli* B2, *S. typhimurium* 1A, *A. baumannii* JS1, *S. dysenteriae* A3, and *K. pneumoniae* JP20. The X-axis represents gentamicin 0-MIC concentration, and the Y-axis represents OM19r 0-MIC concentration.

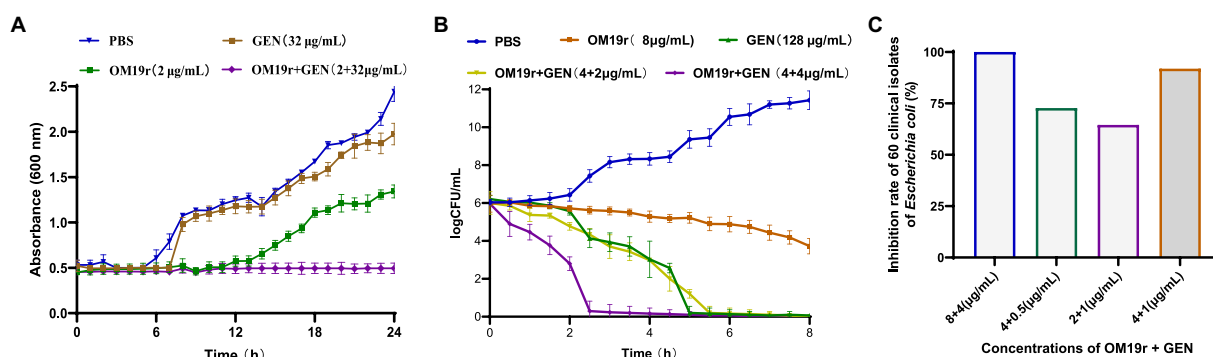


FIGURE 2

Antibacterial effect of OM19r combined with GEN against *E. coli*. (A) 24h growth curves of OM19r (2 µg/ml) combined with GEN (32 µg/ml) against *E. coli* B2. (B) 8h Time-kill curves of OM19r (8 µg/ml), GEN (128 µg/ml) and OM19r combined with GEN (4+2 µg/ml and 4+4 µg/ml) against *E. coli* B2. (C) Synergistic antibacterial activity of OM19r combined with GEN against 60 clinically isolated *E. coli*. Graphs show means from at least three biological replicates, and error bars indicate standard deviations.

3.4. Membrane permeability

The results of outer membrane permeability assays showed that OM19r combined with GEN had no effect on the outer membrane permeability of *E. coli* B2 (Figure 4A; Supplementary Figure S2). Meanwhile, inner membrane permeability assays showed that OM19r combined with GEN (2+1 µg/ml) increased the inner membrane permeability of *E. coli* B2. There was no significant difference in membrane permeability between OM19r combined with GEN (2+1 µg/ml) group and OM19r (4 µg/ml) group

(Figures 4B,C). These results indicate that OM19r affected the inner membrane integrity of *E. coli* B2, while GEN had no effect on the cell membrane.

3.5. Proton motive force assays

PMF assays results showed no significant differences in $\Delta\phi$ and ΔpH of *E. coli* B2 in OM19r combined with GEN group compared with the negative control group (Supplementary Figures S3A,B).

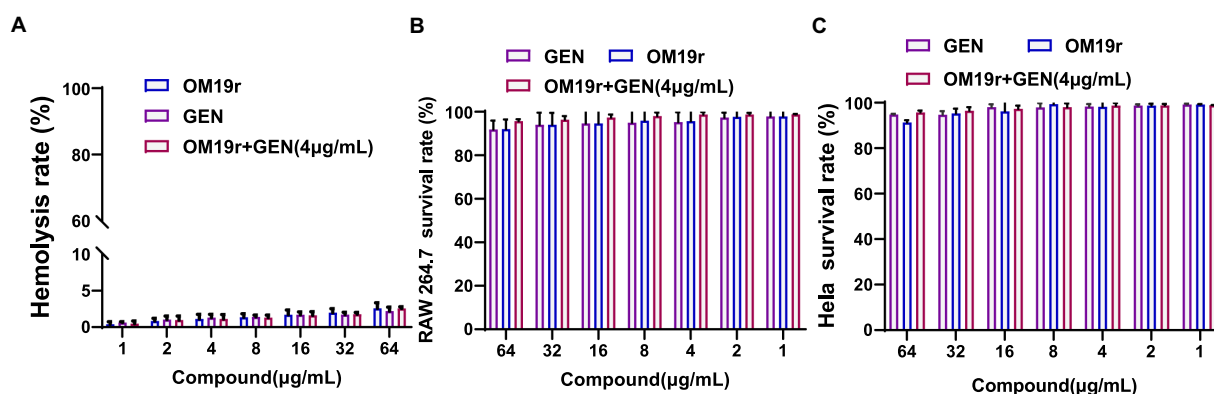


FIGURE 3

Safety evaluation of OM19r combined with GEN at cell level. (A), Hemolysis of sheep red blood cells treated with OM19r combined with GEN. (B) Cytotoxicity of RAW264.7 cells treated with OM19r, GEN and OM19r combined with GEN. (C) Cytotoxicity of HeLa cells treated with OM19r, GEN and OM19r combined with GEN. Graphs show mean of three biological replicates, *p*-values were determined using an unpaired two-tailed Student's *t*-test.

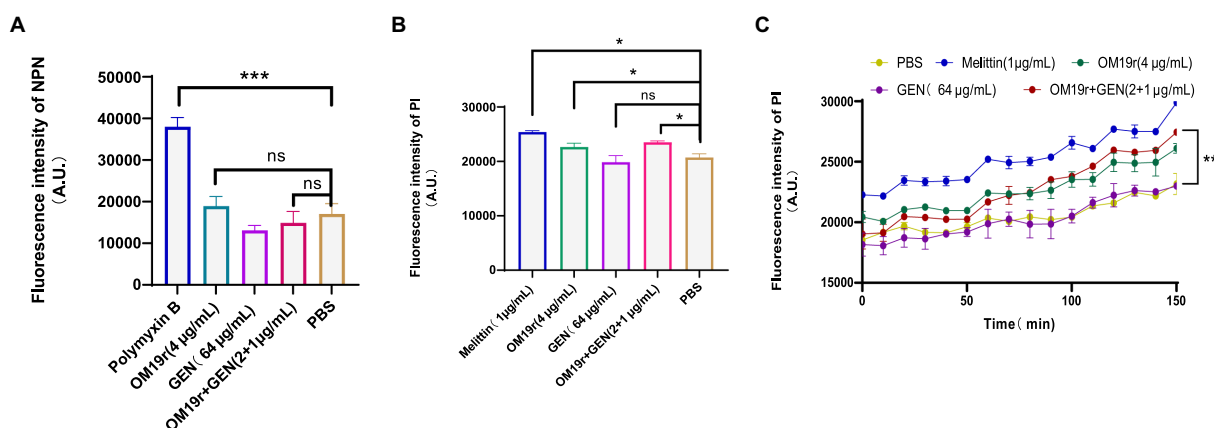


FIGURE 4

Effect of OM19r combined with GEN on membrane permeability of *E. coli* B2. (A) Outer membrane permeability of *E. coli* B2 was measured by NPN probe at 30min. (B), Inner membrane permeability of *E. coli* B2 was measured by PI probe at 30min. (C) Inner membrane permeability of *E. coli* B2 was measured by PI probe, fluorescence intensity was detected after every 10min for 150min. Graphs show mean of three biological replicates, *p*-values were determined using an unpaired two-tailed Student's *t*-test.

3.6. Efflux pump assays

The fluorescent probe EtBr was used to detect the effects of drugs on the non-specific bacterial pumping system. OM19r combined with GEN did not inhibit the bacterial efflux pump (Supplementary Figures S4A,B).

3.7. Real-time PCR and *in vitro* expression of SbmA

SbmA is a member of the peptide uptake permease family (PUP) and involved in transporting antimicrobial peptides (Armas et al., 2021). The results of qPCR revealed that OM19r combined with GEN upregulated ($p < 0.05$) the mRNA expression level of SbmA in *E. coli* B2 significantly (Figure 5A). But there was no significant difference in SbmA expression between OM19r combined with GEN (2 + 1 μg/ml) group and OM19r (4 μg/ml) group and indicated that SbmA plays a vital role in the entry OM19r to *E. coli* B2. Therefore, SbmA protein

(48 kDa) was expressed and purified using *E. coli* expression system, Ni²⁺ column and SDS-PAGE (Figure 5B). The effect of SbmA on the antibacterial activity of OM19r was determined *in vitro*. The results showed that the MIC of OM19r against *E. coli* B2 was increased as SbmA protein concentration increased (Figure 5C). In addition, SbmA protein also affected the synergistic antibacterial effect of OM19r combined with GEN against *E. coli* B2 (Figure 5D). The SbmA gene deletion in *E. coli* ATCC25922 resulted in the loss of the bacteriostatic activity of OM19r (MIC > 128 μg/ml) (Figure 5E). Molecular docking showed that OM19r had a good binding affinity with SbmA (binding energy was −262.92 kcal/mol), the binding sites of OM19r and SbmA transporter were ILE-47, ILE-217 and TYR-241 (Figure 5F).

3.8. Confocal laser scanning microscopy

FITC-OM19r in the 0.5 × MIC treatment group displayed a small amount of green fluorescence in the cytoplasm of *E. coli* B2 after 30 min., On the other hand, FITC-OM19r in the 1 × MIC treatment group

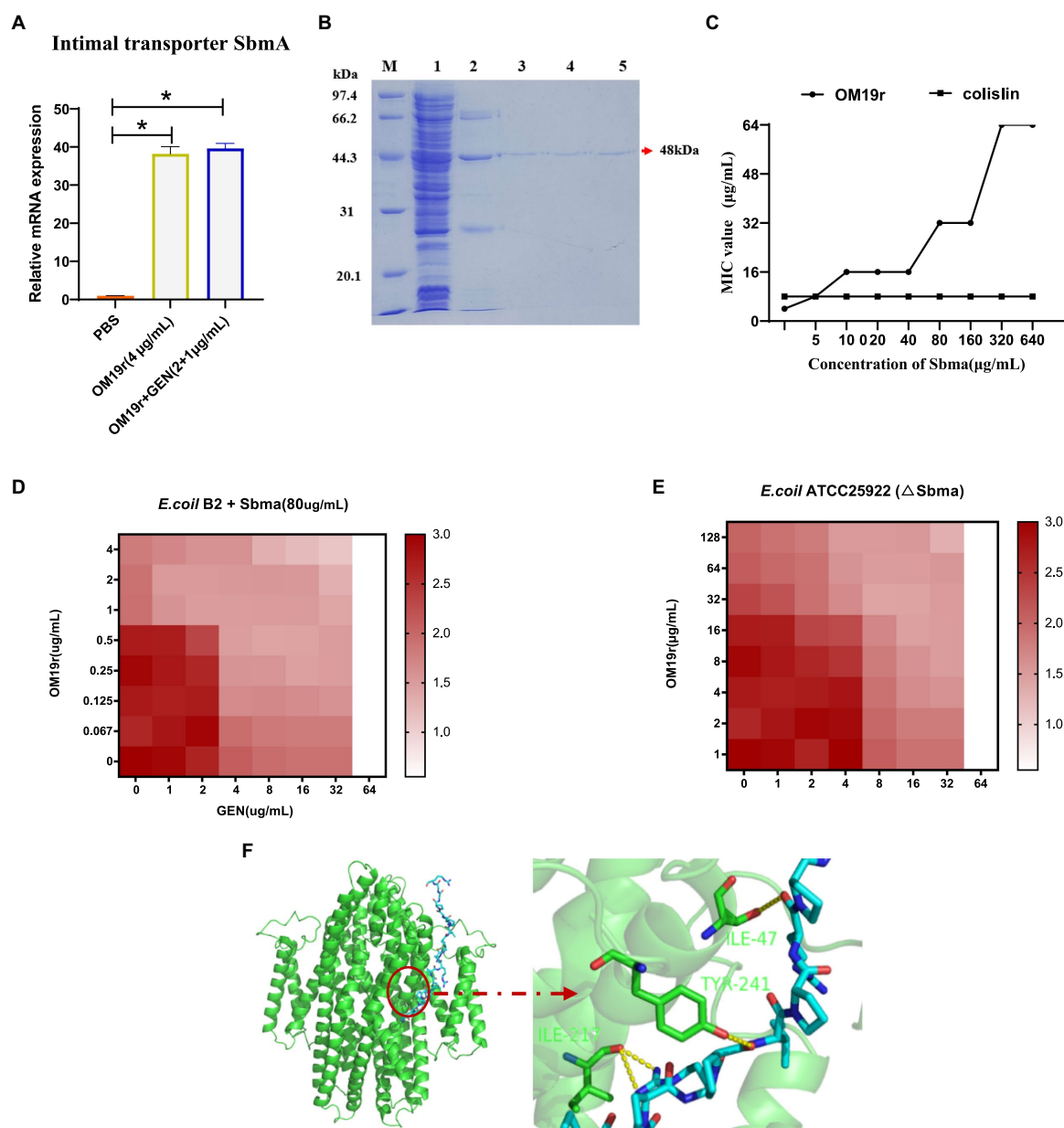


FIGURE 5

OM19r transported to cytoplasm by the SbmA protein on bacterial inner membrane. (A) The mRNA expression of SbmA gene increased after OM19r and OM19r combined with GEN against *E. coli* B2. (B) SDS-PAGE results of SbmA protein. M: Premixed Protein Marker(low), 1: flow through 2: 50mM imidazole wash, 3: 100mM imidazole wash, 4: 300mM imidazole first wash, 5: 300mM imidazole second wash. (C) Effect of SbmA on the antibacterial activity of OM19r and colistin against *E. coli* B2 was determined by adding SbmA protein *in vitro*. (D) Effect of SbmA on the FIC of OM19r combined with GEN against *E. coli* B2 was determined by adding SbmA protein *in vitro*. (E) FIC of OM19r combined with GEN against *E. coli* ATCC25922 (ΔSbmA) was determined *in vitro*. (F) Molecular docking results of both OM19r and SbmA protein binding.

showed a large amount of green fluorescence in the cytoplasm of *E. coli* B2 (Figures 6A–C). Indicating the binding ability of the antimicrobial peptide OM19r to the cell membrane or accumulation in the cytoplasm.

3.9. Transmission electron microscopy

The TEM results showed that the cell membrane of *E. coli* B2 was smooth, while the cell contents were full prior to OM19r treatment (Figures 7A,D). The membrane of *E. coli* B2 cells treated with Melittin was not clear and the contents were separated (Figures 7B,C). After one hour of OM19r treatment with Melittin at 0.5 × MIC, some

contents were leaked and the edge of *E. coli* B2 membrane (Figure 7E). While *E. coli* B2 treated for one hour with OM19r at 1 × MIC shown a complete leakage of the contents (Figure 7F). This suggests that OM19r entered bacteria and exerted its antibacterial effect.

3.10. Measurement of total reactive oxygen species

DCFH-DA fluorescent probe was used to determine the intracellular ROS accumulation in *E. coli* B2 following OM19r combined with GEN treatment. The intracellular ROS

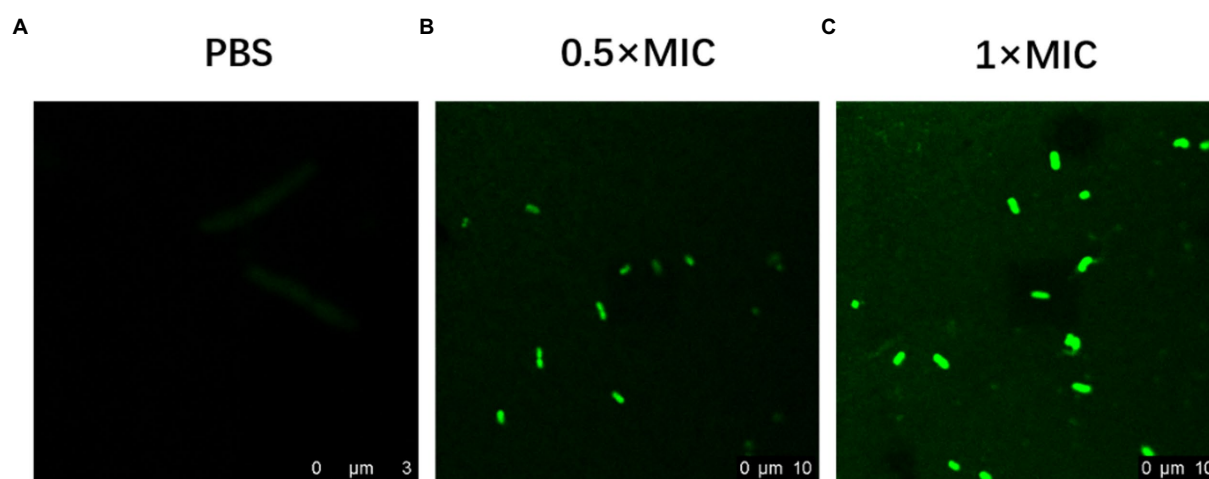


FIGURE 6
Confocal laser scanning micrograph of *E. coli* B2 treated with OM19r and FITC-OM19r. (A–C) Images obtained by fluorescence microscope.

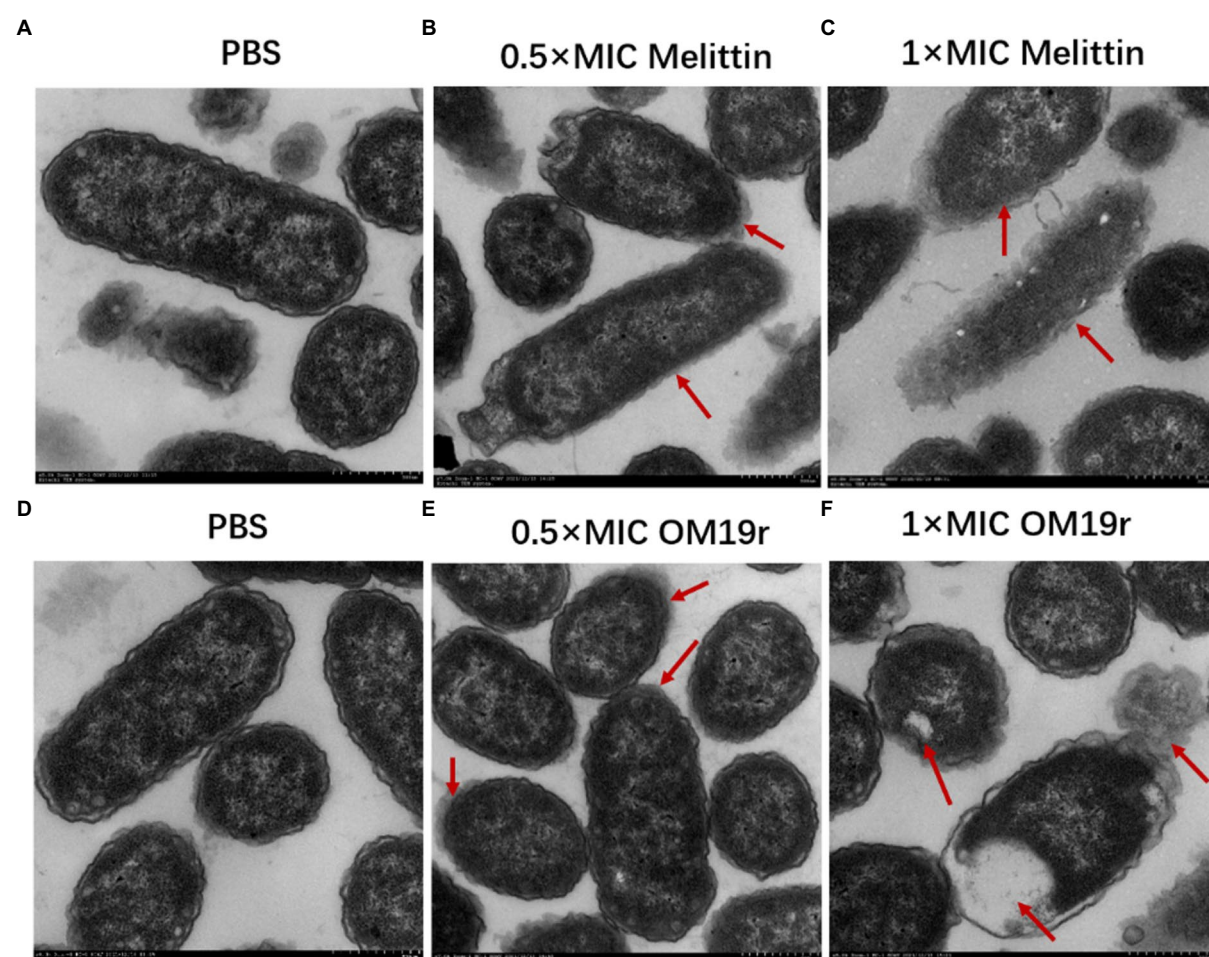


FIGURE 7
Transmission electron microscopy results of *E. coli* B2 treated with OM19r. (A) Transmission electron microscopic images of *E. coli* B2. (B) Transmission electron microscopic images of *E. coli* B2 treated with Melittin (0.5×MIC) for 1h. (C) Transmission electron microscopic images of *E. coli* B2 treated with Melittin (1×MIC) for 1h. (D) Transmission electron microscopic images of *E. coli* B2. E, Transmission electron microscopic images of *E. coli* B2 treated with OM19r (0.5×MIC) for 1h. D, Transmission electron microscopic images of *E. coli* B2 treated with OM19r (1×MIC) for 1h. Red arrows in B, C, and E points to the cell membrane; The red arrow in F points to intracellular vacuolization.

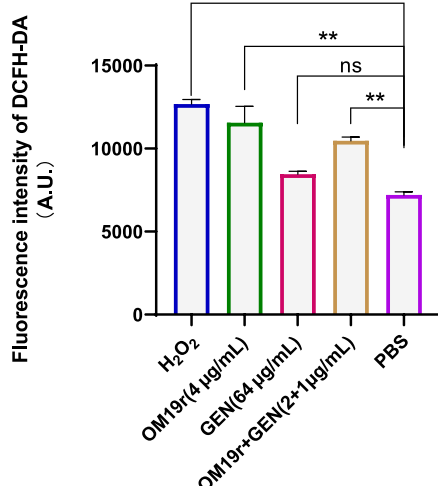


FIGURE 8
ROS accumulation in *E. coli* B2 cells determined by DCFH-DA fluorescent probe. Graphs show mean of three biological replicates, p-values were determined using an unpaired two-tailed Student's *t*-test.

accumulation of *E. coli* B2 was significantly increased ($p < 0.01$) in OM19r and OM19r combined with GEN treated groups compared with the control group (Figure 8). This suggests that OM19r treatment accumulated intracellular ROS, but gentamicin alone had no effect.

3.11. DNA binding assay

OM19r ($\geq 128 \mu\text{g/ml}$) bound to *E. coli* B2 genomic DNA (Figures 9A–B), and OM19r ($\geq 64 \mu\text{g/ml}$) attached to the plasmid DNA (Figures 9C,D). However, OM19r combined with GEN ($8 + 4 \mu\text{g/ml}$) had no binding effect on *E. coli* B2 genomic DNA and plasmid DNA. These results indicated that the bacterial genomic DNA was not the target for OM19r combined with GEN.

3.12. *In vitro* protein synthesis

EGFP green fluorescence was observed under UV light after the reaction of GEN and OM19r with the mixture at 29°C for 16 h. The results showed that the fluorescence intensity of EGFP decreased with

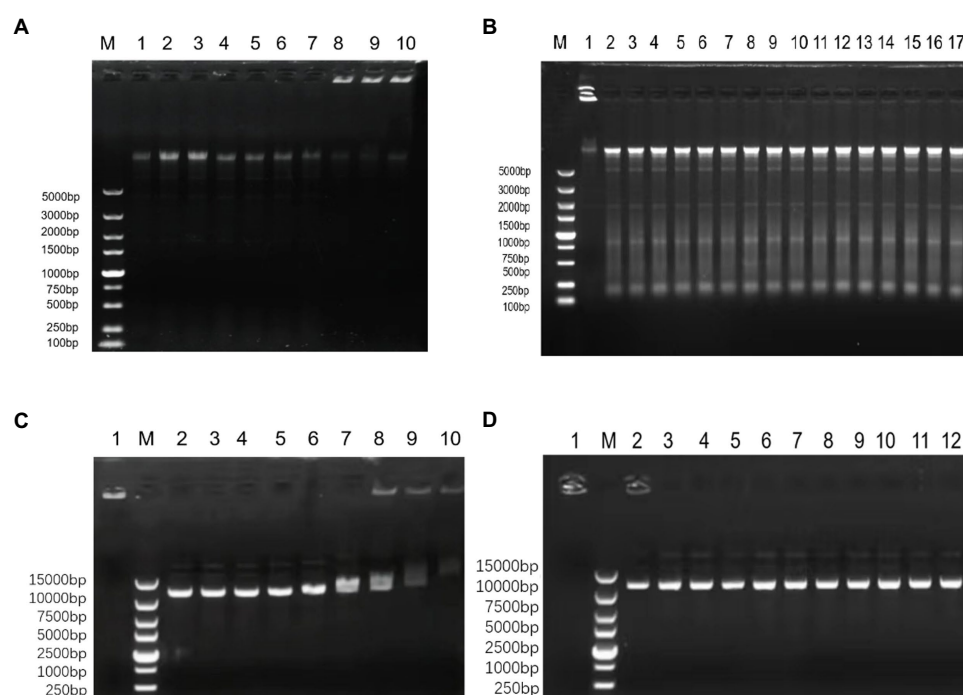


FIGURE 9
The effect of OM19r combined with GEN on the DNA of *E. coli* determined by DNA binding assay. (A) The effect of different concentrations of OM19r on the genomic DNA of *E. coli* B2, M: DL5000Marker; 1: *E. coli* B2 genome; 2: OM19r ($2 \mu\text{g/ml}$); 3: OM19r ($4 \mu\text{g/ml}$); 4: OM19r ($8 \mu\text{g/ml}$); 5: OM19r ($16 \mu\text{g/ml}$); 6: OM19r ($32 \mu\text{g/ml}$); 7: OM19r ($64 \mu\text{g/ml}$); 8: OM19r ($128 \mu\text{g/ml}$); 9: OM19r ($256 \mu\text{g/ml}$); 10: Positive control. (B) Effects of different concentrations of GEN and OM19r combined with GEN on the genomic DNA of *E. coli* B2. M: DL5000Marker; 1: Positive control 2: GEN ($512 \mu\text{g/ml}$); 3: GEN ($256 \mu\text{g/ml}$); 4: GEN ($128 \mu\text{g/ml}$); 5: GEN ($64 \mu\text{g/ml}$); 6: GEN ($32 \mu\text{g/ml}$); 7: GEN ($16 \mu\text{g/ml}$); 8: GEN ($8 \mu\text{g/ml}$); 9: GEN ($4 \mu\text{g/ml}$); 10: GEN ($2 \mu\text{g/ml}$); 11: GEN ($1 \mu\text{g/ml}$); 12: OM19r combined with GEN ($2 + 1 \mu\text{g/ml}$); 13: OM19r combined with GEN ($2 + 2 \mu\text{g/ml}$); 14: OM19r combined with GEN ($4 + 2 \mu\text{g/ml}$); 15: OM19r combined with GEN ($4 + 4 \mu\text{g/ml}$); 16: OM19r combined with GEN ($8 + 4 \mu\text{g/ml}$); 17: *E. coli* B2 genome. (C) The effects of different concentrations of OM19r on plasmid, 1: Positive control; M: 15000 DNA Marker; 2: plasmid; 3: OM19r ($2 \mu\text{g/ml}$); 4: OM19r ($4 \mu\text{g/ml}$); 5: OM19r ($8 \mu\text{g/ml}$); 6: OM19r ($16 \mu\text{g/ml}$); 7: OM19r ($32 \mu\text{g/ml}$); 8: OM19r ($64 \mu\text{g/ml}$); 9: OM19r ($128 \mu\text{g/ml}$); 10: OM19r ($256 \mu\text{g/ml}$); (D) Effects of different concentrations of GEN and OM19r combined with GEN on plasmid. 1: Positive control; M: 15000 DNA Marker; 2: GEN ($512 \mu\text{g/ml}$); 3: GEN ($256 \mu\text{g/ml}$); 4: GEN ($128 \mu\text{g/ml}$); 5: GEN ($64 \mu\text{g/ml}$); 6: GEN ($32 \mu\text{g/ml}$); 7: OM19r combined with GEN ($2 + 1 \mu\text{g/ml}$); 8: OM19r combined with GEN ($2 + 2 \mu\text{g/ml}$); 9: OM19r combined with GEN ($4 + 2 \mu\text{g/ml}$); 10: OM19r combined with GEN ($4 + 4 \mu\text{g/ml}$); 11: OM19r combined with GEN ($8 + 4 \mu\text{g/ml}$); 12: plasmid.

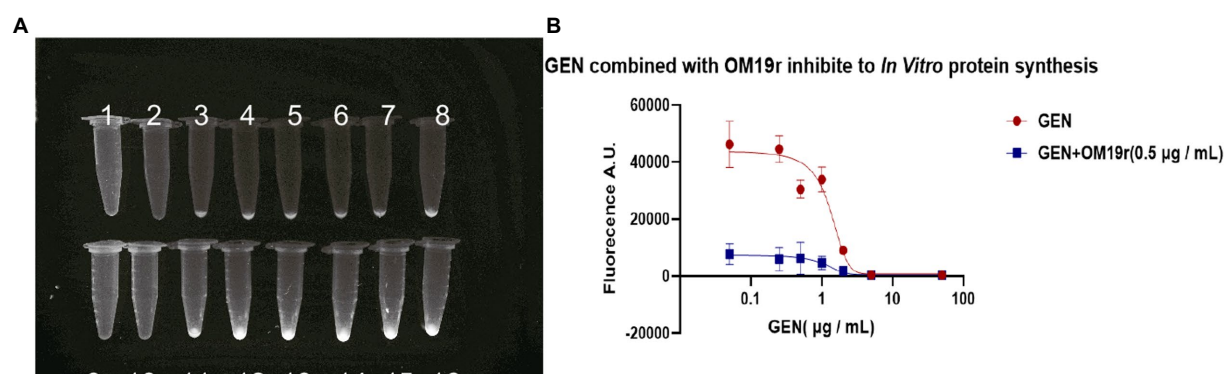


FIGURE 10

The effect of OM19r combined with GEN on *in vitro* protein synthesis. (A) EGFP green fluorescence observed under UV light by different concentrations of GEN and OM19r(0.5μg/ml) combined with GEN for 16h. 1: OM19r combined with GEN (50μg/ml), 2: OM19r combined with GEN (5μg/ml), 3: OM19r combined with GEN (2μg/ml), 4: OM19r combined with GEN (1μg/ml), 5: OM19r combined with GEN (0.5μg/ml), 6: OM19r combined with GEN (0.25μg/ml), 7: OM19r combined with GEN(0.05μg/ml), 8: OM19r (0.5μg/ml), 9: GEN (50μg/ml), 10: GEN (5μg/ml), 11: GEN (2μg/ml), 12: GEN (1μg/ml), 13: GEN (0.5μg/ml), 14: GEN (0.25μg/ml), 15: GEN (0.05μg/ml), 16: negative control. (B) The fluorescence value of EGFP induced by the GEN and OM19r (0.5μg/ml). Graphs show mean of three biological replicates.

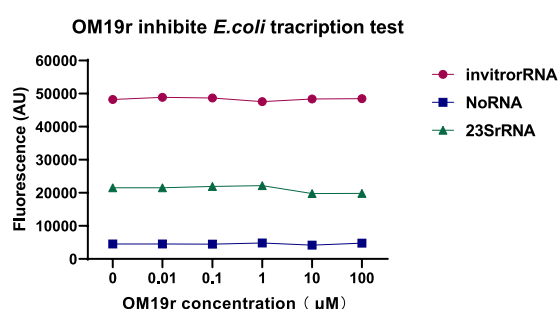


FIGURE 11

The effect of OM19r on the transcription process of *E. coli* determined by constructing the transcription system *in vitro*. Graphs show mean of three biological replicates.

the increase in GEN concentration (Figure 10A). These results suggested that GEN can inhibit EGFP expression *in vitro*. However, when OM19r (0.5μg/ml) was added to each group, the fluorescence value of EGFP decreased significantly more than that GEN alone (Figure 10B). The above results indicated that OM19r alone could affect the synthesis of EGFP fluorescent protein.

3.13. *In vitro* transcription

The effect of OM19r on bacterial transcription was detected *in vitro*. The molecular beacon fluorescence signal of *E. coli* transcribed *in vitro* remained unchanged following treatment with OM19r, suggesting that OM19r had no effect on the transcription of *E. coli in vitro* (Figure 11).

3.14. mRNA translation

The dose–response curves for OM19r showed the inhibition of mRNA translation and Poly (U) formation overlap (Figure 12A),

suggesting that inactivation of peptidyl transferase center (PTC) was caused by OM19r blocking mRNA translation. OM19r appeared to be an inhibitor of PTC activity, effectively blocking PTC specifically from producing the “first peptide bond” and mRNA translation. This may explain why the dose–response curves for inhibition of mRNA translation and Poly (U) formation were essentially overlapped. The molecular docking revealed that OM19r and GEN bind to ribosomes at different sites. The binding energy of OM19r to the ribosome was -115.33 kcal/mol (Supplementary Table S7). OM19r was predicted to bind to the ribosome's A-5, A-14, A-64, A-66, A-67 and U-50 sites (Figure 12B). The binding energy of GEN to the ribosome was -140.8 kcal/mol (Supplementary Table S7). GEN was predicted to bind to the ribosome's C-56, A-57, and G-19 sites (Figure 12C), proposing that OM19r entered the bacteria *via* SbmA and influenced the translation elongation process and ROS accumulation (Figure 12D).

3.15. Animal infection model

OM19r restored susceptibility of drug-resistant strains to GEN, which was assessed in animal models infected with *E. coli* B2 (Figure 13). In mouse model of peritonitis, 80% of mice survived within 7 days of treatment with OM19r combined with GEN (4 + 2 mg/kg), significantly higher ($p < 0.01$) than the GEN (8 mg/kg) treated group (Figure 13A). The bacterial load test results showed that OM19r combined with GEN (4 + 2 mg/kg) significantly reduced the bacterial content in mice. The bacterial content in the liver, spleen, lung, and kidney was reduced by five-, four-, four-, and five-fold, respectively (Figures 13B–F). In *Galleria mellonella* (*G. mellonella*) larval model, 80% of *G. mellonella* survived within 7 days of treatment with OM19r combined with GEN (4 + 2 mg/kg), significantly higher ($p < 0.01$) than the GEN (8 mg/kg, 25% survival) treated group (Figure 13G). These findings suggested that LRGG is an antibiotic potentiator to enhance the antibacterial activity of GEN against *E. coli* B2 *in vivo*.

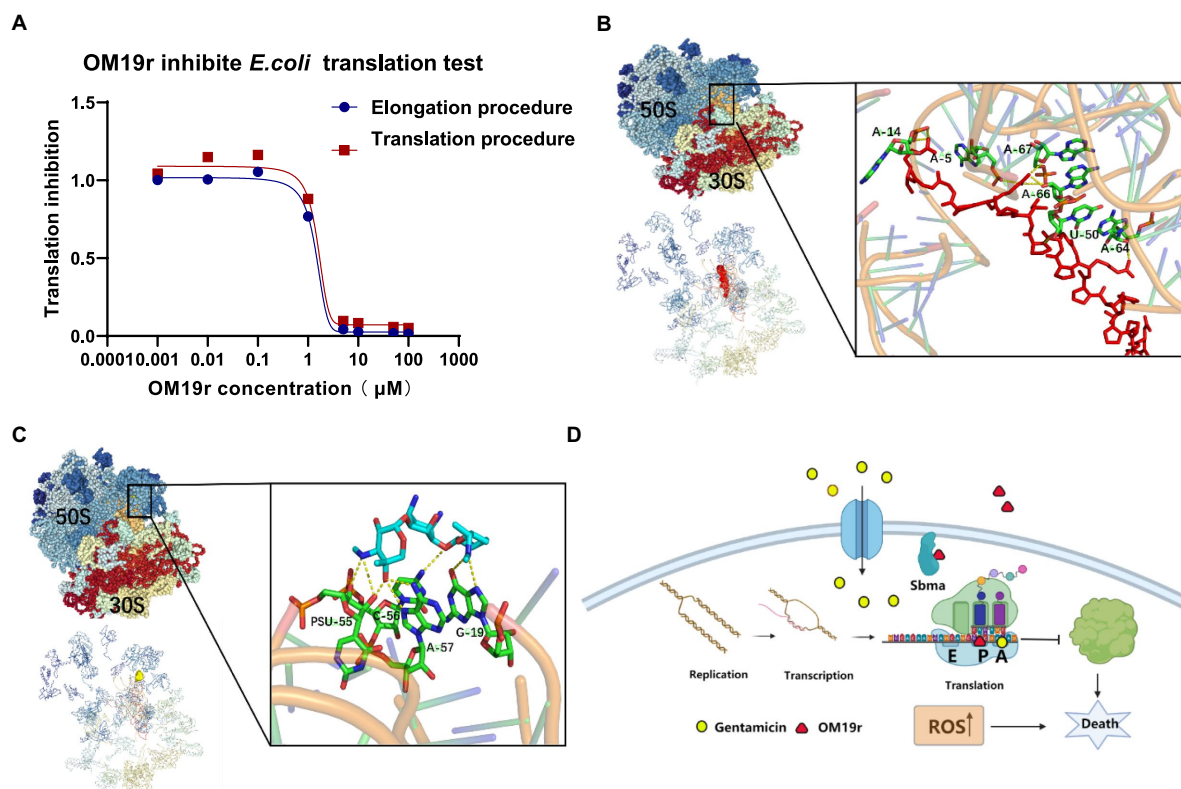


FIGURE 12

Translation elongation process of OM19r-targeted mRNA. (A) Dose–response of OM19r inhibition mRNA translation (red) and fMet-Phe dipeptide formation (blue) *in vitro*. (B) Molecular docking results of OM19r and ribosome. (C) Molecular docking results of GEN and ribosome. (D) Schematic diagram of synergistic antibacterial action mechanism of OM19r combined with GEN.

4. Discussion

Antibacterial synergists when used in combination with antibiotics could restore the sensitivity of drug-resistant pathogens up to some extent and prolong the effective life of antibiotics by reducing the resistance. Although there have been reports that AMPs used as synergists can enhance the antibacterial activity of antibiotics (Randhawa et al., 2016; Zhong et al., 2020), studies on antimicrobial peptides combined with gentamicin to reverse drug resistance in *E. coli* are lacking. Most AMPs contain cationic and amphiphilic molecules, which may be drawn to negatively charged cell membranes and damage the lipid bilayer (Shai, 2002). Therefore, AMPs usually exhibit low selectivity and broad-spectrum antibacterial activity against pathogenic bacteria (Matsuzaki, 2009). However, the antibacterial targets of some proline-rich antimicrobial peptides (PrAMPs) are often located inside the bacterial cells and do not cause obvious membrane damage (Nicolas, 2009; Scocchi et al., 2011, 2016; Graf et al., 2017). An antimicrobial peptide OM19r containing both proline and arginine was derived from the available peptide sequences in our laboratory. Compared with the broad-spectrum antimicrobial peptides, OM19r had a narrow antibacterial spectrum and antibacterial activity only against some Gram-negative bacteria. Meanwhile, OM19r had no combined

antibacterial effect with other antibiotics at different action sites (FIC > 0.5), and OM19r reduced the MIC of GEN against multidrug-resistant *E. coli* B2 from 64 to 1 $\mu\text{g}/\text{ml}$. Some disadvantages of AMPs, such as hemolysis, cytotoxicity, and instability reported by other scientists hinder their clinical application (Kumar et al., 2017). In this study, the cytotoxicity and hemolytic activity of OM19r was measured *in vitro*. The results of safety assessment experiments at the cellular level indicated that OM19r had no hemolytic activity and cytotoxicity at OM19r $\leq 64 \mu\text{g}/\text{ml}$. The results of animal infection model showed that OM19r restored GEN sensitivity of *E. coli* B2 *in vivo*. In conclusion, OM19r acted as a potential aminoglycoside antibiotic synergist.

The antibacterial mechanism of antimicrobial peptides involves membranous and non-membranous targeting. The antibacterial mechanism of OM19r on bacterial cell membranes was investigated *via* membrane permeability assay. The inner membrane permeability assays results showed that OM19r increased the inner membrane permeability of *E. coli* B2. Sbma as a member of the peptide uptake permease family (PUP) was located in some Gram-negative bacteria and played an important role in antibiotic transport (Paulsen et al., 2016). In previous studies, Oncocin was shown to enter the cell by the Sbma transporter. OM19r is an antimicrobial peptide heterozygous by Oncocin with the MDAP-2 fragment (Liu L. et al., 2020). So, the

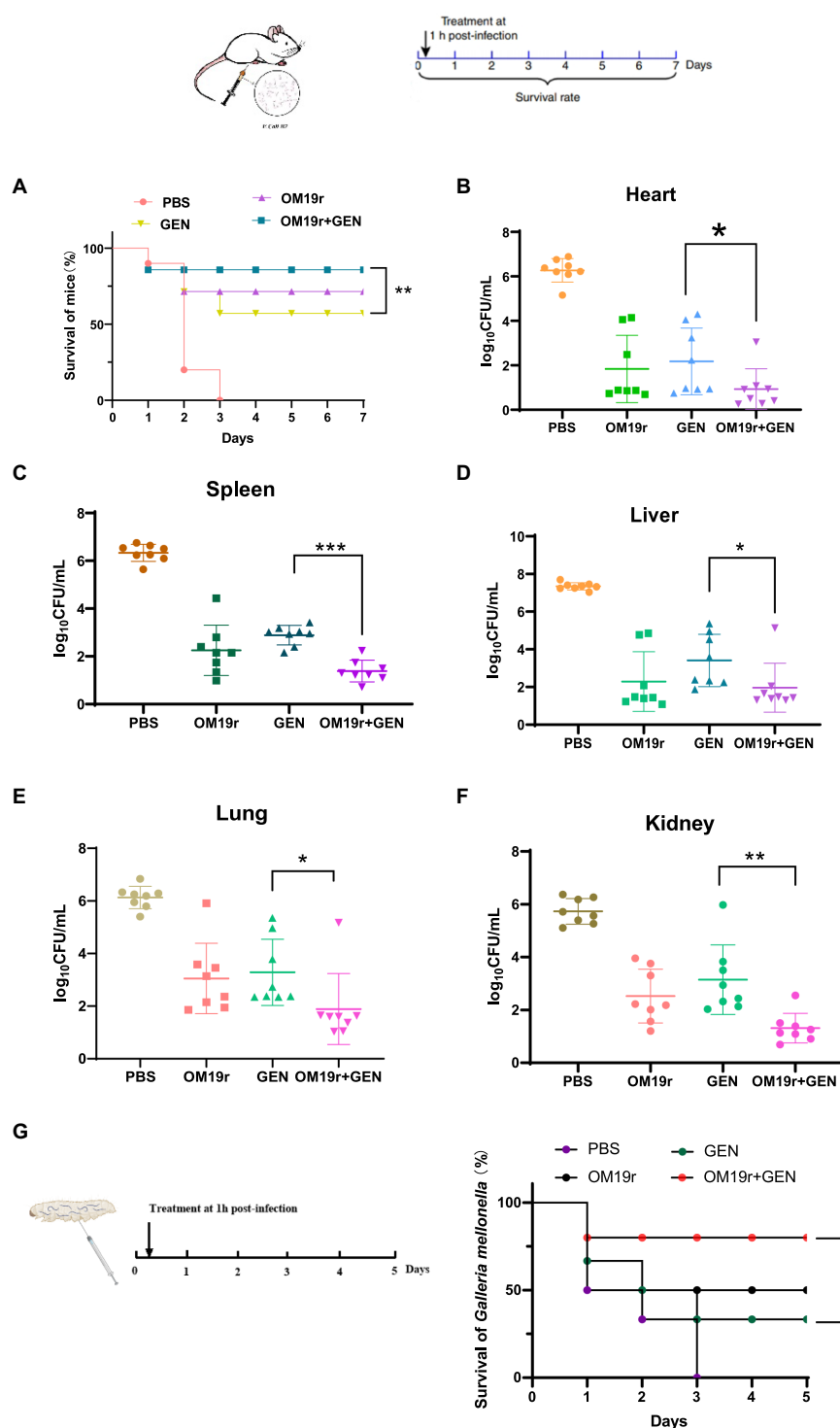


FIGURE 13

OM19r rescues GEN activity in two animal models of infection. (A) Survival curve of mice infected with non-lethal dose of *E. coli* B2 (3×10^8 cfu/ml) for 7 days. *p*-values determined using a two-sided log[rank] (Mantel-Cox) test. (B–F) Bacterial load in all organs (heart, spleen, liver, lung and kidney) of mice measured after OM19r combined with GEN treatment. G, Survival curve of *G. mellonella* larvae infected with a non-lethal dose of *E. coli* B2 (1×10^5 cfu/ml) for 5 days. *p*-values determined using a two-sided log[rank] (Mantel-Cox) test.

effect of OM19r on the bacterial inner membrane transporter SbmA protein was further determined by qPCR assays, SmbA protein was added *in vitro* and gene deletion strains were

constructed. The qPCR results showed that mRNAs expression of SbmA was up-regulated following treatment with OM19r or OM19r combined with GEN. And the MIC of OM19r against

E. coli B2 increased by adding purified SbmA protein *in vitro*. Meanwhile, SbmA gene deletion in *E. coli* ATCC25922 resulted in the loss of the bacteriostatic activity of OM19r. It was further demonstrated that OM19r could enter the bacteria through membrane transporter SbmA. Molecular docking results showed that OM19r could bound to the ILE-47, ILE-217 and TYR-241 sites of SbmA. Finally, the CLSM and TEM results showed that OM19r entered *E. coli* B2 resulted in the release of the bacterial contents. In summary, OM19r was transported into *E. coli* B2 via SbmA to exert the bacteriostatic mechanism.

For non-membrane targeted antimicrobial peptides, current research on the mechanism has mainly focused on the effect of antimicrobial peptides on bacterial DNA (Bai et al., 2021) and protein levels (Roy et al., 2015). Therefore, the antibacterial mechanism of OM19r combined with GEN was studied in this study using DNA binding assay and cell-free expression assay. DNA binding test showed that OM19r could bind to *E. coli* genome at 128 µg/ml and *E. coli* plasmid at 64 µg/ml. GEN can bind to *E. coli* plasmid at concentration of 512 µg/ml. This indicate that high concentrations of OM19r and GEN (higher than the MIC) have binding effect on DNA. Therefore, OM19r combined with GEN mainly exerted antibacterial effects *via* mechanisms other than bacterial DNA. The effects of GEN and OM19r combined with GEN on protein synthesis were measured by fluorescence intensity of EGFP protein. GEN alone or OM19r combined with GEN affected the EGFP protein expression *in vitro*. Moreover, OM19r combined with GEN had a greater effect on the expression of EGFP protein than GEN alone. GEN influences the initial phase of bacterial translation, leading to mRNA misreading, and might explain the effect of GEN on EGFP protein expression *in vitro*. In summary, these results suggest that OM19r had no effect on DNA, but can affect protein synthesis.

Transcription and translation are important stages of protein synthesis in cells (Marras et al., 2004). The stage at which a drug acts on bacterial transcription and translation can be measured by constructing transcriptional translation systems *in vitro* (Marras et al., 2004; Brandi et al., 2007). Therefore, a transcription and translation systems were established to determine the specific inhibitory mechanism of OM19r on protein synthesis *in vitro*. Firstly, we proved by *in vitro* transcription experiments that the peptide has no effect on the transcription process. Secondly, since the *in vitro* protein synthesis could be inhibited by OM19r, but having no effect on RNA synthesis. Therefore, we focused on the protein translation process *in vitro*. A series of experiments was conducted and the results showed that OM19r had inhibition activity on the translation elongation process. Finally, molecular docking results further demonstrated that OM19r and GEN binds to different sites in the ribosome, with OM19r inhibiting the extension phase of protein translation and GEN inhibiting the initiation phase of translation.

Meanwhile, ROS has been reported to play a key role in bacterial resistance and the bactericidal activity of antibiotics (Van Acker and Coenye, 2017; Hong et al., 2019). Non-lethal concentrations of antibiotics cause ROS produced by bacteria, which can promote the SOS-DNA damage repair system, activate the stress protection mechanism, and form drug-resistant bacteria. Conversely, ROS produced by bacteria with lethal concentration of antibiotics can

further accelerate the death of pathogens (Kohanski et al., 2010). The OM19r combined with GEN caused ROS accumulation in *E. coli* B2. In conclusion, OM19r can enter the cell through the intimal transporter SbmA, causing ROS accumulation in bacteria and inhibiting the translation extension stage of the protein, and ultimately causing death of the pathogen.

5. Conclusion

This study showed that OM19r combined with GEN had a strong synergistic inhibitory effect (FIC = 0.156) against multi-drug resistant *E. coli* B2. The combined inhibitory mechanism of OM19r and GEN shown that OM19r entered bacterial cells through SbmA transporter on cell membranes, thus causing intracellular ROS accumulation. Simultaneously, OM19r and GEN inhibited translation elongation and initiation, respectively, and ultimately affected the normal protein synthesis of bacteria. Two animal models shown that OM19r can also restore the sensitivity of multidrug-resistant *E. coli* B2 to GEN in animals. These findings offer a potential treatment option for the infections caused globally by multidrug-resistant *E. coli*.

Data availability statement

The original contributions presented in the study are included in the article/Supplementary material, further inquiries can be directed to the corresponding authors.

Ethics statement

The animal study was reviewed and approved by Jilin Agricultural University guidelines.

Author contributions

H-XM, L-CK, and C-GH conceived and designed research. Q-JX, H-DY, YL, AG, AF, and X-YJ conducted experiments. H-PZ and P-HL contributed new reagents or analytical tools. Q-JX analyzed data. QC wrote the manuscript. All authors read and approved the manuscript.

Funding

This study was funded by National Natural Science Foundation of China (31872519) and Jilin Scientific and Technological Development Program (20210202033NC, 20220508049RC, YDZJ202203CGZH050, 20230402037GH).

Acknowledgments

We are grateful to China Agricultural University for multi-drug resistant *E. coli* B2.

Conflict of interest

The authors declare that the research was conducted in the absence of any commercial or financial relationships that could be construed as a potential conflict of interest.

Publisher's note

All claims expressed in this article are solely those of the authors and do not necessarily represent those of their affiliated

organizations, or those of the publisher, the editors and the reviewers. Any product that may be evaluated in this article, or claim that may be made by its manufacturer, is not guaranteed or endorsed by the publisher.

Supplementary material

The Supplementary material for this article can be found online at: <https://www.frontiersin.org/articles/10.3389/fmicb.2023.1144946/full#supplementary-material>

References

- Armas, F., di Stasi, A., Mardirossian, M., Romani, A. A., Benincasa, M., and Scocchi, M. (2021). Effects of Lipidation on a proline-rich antibacterial peptide. *Int. J. Mol. Sci.* 22:7959. doi: 10.3390/ijms22157959
- Aslam, B., Wang, W., Arshad, M. I., Khurshid, M., Muzammil, S., Rasool, M. H., et al. (2018). Antibiotic resistance: a rundown of a global crisis. *Infect. Drug Resist.* 11, 1645–1658. doi: 10.2147/IDR.S173867
- Bai, S., Wang, J., Yang, K., Zhou, C., Xu, Y., Song, J., et al. (2021). A polymeric approach toward resistance-resistant antimicrobial agent with dual-selective mechanisms of action. *Sci. Adv.* 7:eabc9917. doi: 10.1126/sciadv.abc9917
- Böttger, R., Knappe, D., and Hoffmann, R. (2016). Readily adaptable release kinetics of prodrugs using protease-dependent reversible PEGylation. *J. Control. Release* 230, 88–94. doi: 10.1016/j.jconrel.2016.04.010
- Brandi, L., Fabbretti, A., Milon, P., Carotti, M., Pon, C. L., and Gualerzi, C. O. (2007). Methods for identifying compounds that specifically target. *Methods Enzymol.* 431, 229–267. doi: 10.1016/S0076-6879(07)31012-4
- Bustin, S. A., Benes, V., Garson, J. A., Hellemans, J., Huggett, J., Kubista, M., et al. (2009). The MIQE guidelines: minimum information for publication of quantitative real-time PCR experiments. *Clin. Chem.* 55, 611–622. doi: 10.1373/clinchem.2008.112797
- Corbalan, N., Runti, G., Adler, C., Covacevich, S., Ford, R. C., Lamba, D., et al. (2013). Functional and structural study of the dimeric inner membrane protein SbmA. *J. Bacteriol.* 195, 5352–5361. doi: 10.1128/JB.00824-13
- Cui, Q., Qi-Jun, X., Lei, L., Li-Li, G., Xiu-Yun, J., Muhammad, I., et al. (2021). Preparation, characterization and pharmacokinetic study of N-terminal PEGylated D-form antimicrobial peptide OM19r-8. *J. Pharm. Sci.* 110, 1111–1119. doi: 10.1016/j.xphs.2020.10.048
- Ding, X., Yang, C., Moreira, W., Yuan, P., Periaswamy, B., Sessions, P. F., et al. (2020). A macromolecule reversing antibiotic resistance phenotype and repurposing drugs as potent antibiotics. *Adv. Sci.* 7:2001374. doi: 10.1002/adv.202001374
- Durand-Reville, T. F., Miller, A. A., O'Donnell, J. P., Wu, X., Sylvester, M. A., Guler, S., et al. (2021). Rational design of a new antibiotic class for drug-resistant infections. *Nature* 597, 698–702. doi: 10.1038/s41586-021-03899-0
- Falciani, C., Zevolini, F., Brunetti, J., Riolo, G., Gracia, R., Marradi, M., et al. (2020). Antimicrobial peptide-loaded nanoparticles as inhalation therapy for *Pseudomonas aeruginosa* infections. *Int. J. Nanomedicine* 15, 1117–1128. doi: 10.2147/IJN.S218966
- Garamella, J., Marshall, R., Rustad, M., and Noireaux, V. (2016). The all E. coli TX-TL toolbox 2.0: a platform for cell-free synthetic biology. *ACS Synth. Biol.* 5, 344–355. doi: 10.1021/acssynbio.5b00296
- Graf, M., Mardirossian, M., Nguyen, F., Seefeldt, A. C., Guichard, G., Scocchi, M., et al. (2017). Proline-rich antimicrobial peptides targeting protein synthesis. *Nat. Prod. Rep.* 34, 702–711. doi: 10.1039/c7np00020k
- Hong, Y., Zeng, J., Wang, X., Drlica, K., and Zhao, X. (2019). Post-stress bacterial cell death mediated by reactive oxygen species. *Proc. Natl. Acad. Sci. U. S. A.* 116, 10064–10071. doi: 10.1073/pnas.1901730116
- Hooban, B., Fitzhenry, K., O'Connor, L., Miliotis, G., Joyce, A., Chueiri, A., et al. (2022). A longitudinal survey of antibiotic-resistant Enterobacterales in the Irish environment, 2019–2020. *Sci. Total Environ.* 828:154488. doi: 10.1016/j.scitotenv.2022.154488
- Jamsripong, S., Li, X., Aly, S. S., Su, Z., Pereira, R. V., and Atwill, E. R. (2021). Antibiotic resistance genes and associated phenotypes in *Escherichia coli* and *Enterococcus* from cattle at different production stages on a dairy farm in Central California. *Antibiotics (Basel)* 10:1042. doi: 10.3390/antibiotics10091042
- Jia, B. Y., Wang, Y. M., Zhang, Y., Wang, Z., Wang, X., Muhammad, I., et al. (2020). High cell selectivity and bactericidal mechanism of symmetric peptides centered on d-pro-Gly pairs. *Int. J. Mol. Sci.* 21:1140. doi: 10.3390/ijms21031140
- Kaminishi, T., Schedlbauer, A., Fabbretti, A., Brandi, L., Ochoa-Lizarralde, B., He, C. G., et al. (2015). Crystallographic characterization of the ribosomal binding site and molecular mechanism of action of Hygromycin a. *Nucleic Acids Res.* 43, 10015–10025. doi: 10.1093/nar/gkv975
- Kohanski, M., DePristo, M. A., and Collins, J. J. (2010). Sublethal antibiotic treatment leads to multidrug resistance via radical-induced mutagenesis. *Mol. Cell* 37, 311–320. doi: 10.1016/j.molcel.2010.01.003
- Kumar, A., Mahajan, M., Awasthi, B., Tandon, A., Harioudh, M. K., Shree, S., et al. (2017). Piscidin-1-analogs with double L- and D-lysine residues exhibited different conformations in lipopolysaccharide but comparable anti-endotoxin activities. *Sci. Rep.* 7:39925. doi: 10.1038/srep39925
- Liu, Y., Jia, Y., Yang, K., Li, R., Xiao, X., Zhu, K., et al. (2020). Metformin restores Tetracyclines susceptibility against multidrug resistant bacteria. *Adv. Sci. (Weinh)* 7:1902227. doi: 10.1002/adv.201902227
- Liu, L., Liu, J., Cui, Q., Jia, B. Y., and Ma, H. X. (2020). Design and characterization of a novel hybrid antimicrobial peptide om19r based on onocin and mdap-2. *Int. J. Pept. Res. Ther.* 26, 1839–1846. doi: 10.1007/s10989-019-09984-3
- Ma, L., Xie, X., Liu, H., Huang, Y., Wu, H., Jiang, M., et al. (2020). Potent antibacterial activity of MSI-1 derived from the magainin 2 peptide against drug-resistant bacteria. *Theranostics* 10, 1373–1390. doi: 10.7150/thno.39157
- Mans, R. J., and Novelli, G. D. (1961). Measurement of the incorporation of radioactive amino acids into protein by a filter-paper disk method. *Archives of Biochemistry and Biophysics* 94, 48–53. doi: 10.1016/0003-9861(61)90009-1
- Maisuria, V. B., Hosseini, Z., and Tufenkji, N. (2015). Polyphenolic extract from maple syrup potentiates antibiotic susceptibility and reduces biofilm formation of pathogenic bacteria. *Appl. Environ. Microbiol.* 81, 3782–3792. doi: 10.1128/AEM.00239-15
- Marras, S. A., Gold, B., Kramer, F. R., Smith, I., and Tyagi, S. (2004). Real-time measurement of *in vitro* transcription. *Nucleic Acids Res.* 32:e72. doi: 10.1093/nar/gnh068
- Matsuzaki, K. (2009). Control of cell selectivity of antimicrobial peptides. *Biochim. Biophys. Acta* 1788, 1687–1692. doi: 10.1016/j.bbame.2008.09.013
- Mattiuzzo, M., Bandiera, A., Gennaro, R., Benincasa, M., Pacor, S., Antcheva, N., et al. (2010). Role of the *Escherichia coli* SbmA in the antimicrobial activity of proline-rich peptides. *Mol. Microbiol.* 66, 151–163. doi: 10.1111/j.1365-2958.2007.05903.x
- Miao, X., Zhou, T., Zhang, J., Xu, J., Guo, X., Hu, H., et al. (2020). Enhanced cell selectivity of hybrid peptides with potential antimicrobial activity and immunomodulatory effect. *Biochim. Biophys. Acta Gen. Subj.* 1864:129532. doi: 10.1016/j.bbagen.2020.129532
- Mwangi, J., Yin, Y., Wang, G., Yang, M., Li, Y., Zhang, Z., et al. (2019). The antimicrobial peptide ZY4 combats multidrug-resistant *Pseudomonas aeruginosa* and *Acinetobacter baumannii* infection. *Proc. Natl. Acad. Sci. U. S. A.* 116, 26516–26522. doi: 10.1073/pnas.1909585117
- Nicolas, P. (2009). Multifunctional host defense peptides: intracellular-targeting antimicrobial peptides. *FEBS J.* 276, 6483–6496. doi: 10.1111/j.1742-4658.2009.07359.x
- Paulsen, V. S., Mardirossian, M., Blencke, H. M., Benincasa, M., Runti, G., Nepa, M., et al. (2016). Inner membrane proteins YgdD and SbmA are required for the complete susceptibility of *E. coli* to the proline-rich antimicrobial peptide arasin 1(1-25). *Microbiology* 162, 601–609. doi: 10.1099/mic.0.000249
- Peng, T., Huiyang, F., and Xi, M. (2021). Design, optimization, and nanotechnology of antimicrobial peptides: from exploration to applications. *Nano Today* 39:101229. doi: 10.1016/j.nantod.2021.101229
- Randhawa, H. K., Gautam, A., Sharma, M., Bhatia, R., Varshney, G. C., Raghava, G. P., et al. (2016). Cell-penetrating peptide and antibiotic combination therapy: a potential

alternative to combat drug resistance in methicillin-resistant *Staphylococcus aureus*. *Appl. Microbiol. Biotechnol.* 100, 4073–4083. doi: 10.1007/s00253-016-7329-7

Roy, R. N., Lomakin, I. B., Gagnon, M. G., and Steitz, T. A. (2015). The mechanism of inhibition of protein synthesis by the proline-rich peptide oncocin. *Nat. Struct. Mol. Biol.* 22, 466–469. doi: 10.1038/nsmb.3031

Scocchi, M., Mardirossian, M., Runti, G., and Benincasa, M. (2016). Non-membrane Permeabilizing modes of action of antimicrobial peptides on bacteria. *Curr. Top. Med. Chem.* 16, 76–88. doi: 10.2174/1568026615666150703121009

Scocchi, M., Tossi, A., and Gennaro, R. (2011). Proline-rich antimicrobial peptides: converging to a non-lytic mechanism of action. *Cell. Mol. Life Sci.* 68, 2317–2330. doi: 10.1007/s00018-011-0721-7

Shai, Y. (2002). Mode of action of membrane active antimicrobial peptides. *Biopolymers* 66, 236–248. doi: 10.1002/bip.10260

Si, Z., Lim, H. W., Tay, M. Y. F., Du, Y., Ruan, L., Qiu, H., et al. (2020). A glycosylated cationic block poly(β -peptide) reverses intrinsic antibiotic resistance in all ESKAPE gram-negative bacteria. *Angew. Chem. Int. Ed. Engl.* 59, 6819–6826. doi: 10.1002/anie.201914304

Song, M., Liu, Y., Huang, X., Ding, S., Wang, Y., Shen, J., et al. (2020). A broad-spectrum antibiotic adjuvant reverses multidrug-resistant gram-negative pathogens. *Nat. Microbiol.* 5, 1040–1050. doi: 10.1038/s41564-020-0723-z

Song, M., Liu, Y., Li, T., Liu, X., Hao, Z., Ding, S., et al. (2021). Plant natural flavonoids against multidrug resistant pathogens. *Adv. Sci.* 8:e2100749:2100749. doi: 10.1002/adv.202100749

Stokes, J. M., MacNair, C. R., Ilyas, B., French, S., Côté, J. P., Bouwman, C., et al. (2017). Pentamidine sensitizes gram-negative pathogens to antibiotics and overcomes acquired colistin resistance. *Nat. Microbiol.* 2:17028. doi: 10.1038/nmicrobiol.2017.28

Sturge, C. R., Felder-Scott, C. F., Pifer, R., Pybus, C., Jain, R., Geller, B. L., et al. (2019). AcrAB-TolC inhibition by peptide-conjugated Phosphorodiamidate Morpholino oligomers restores antibiotic activity in vitro and in vivo. *ACS Infect. Dis.* 5, 1446–1455. doi: 10.1021/acsinfecdis.9b00123

Türkez, H., Enes, A. M., Erdal, S., Fatime, G., Metin, A., and Abdulgani, T. (2019). Microarray assisted toxicological investigations of boron carbide nanoparticles on human primary alveolar epithelial cells. *Chem. Biol. Interact.* 300, 131–137. doi: 10.1016/j.cbi.2019.01.021

Van Acker, H., and Coenye, T. (2017). The role of reactive oxygen species in antibiotic-mediated killing of bacteria. *Trends Microbiol.* 25, 456–466. doi: 10.1016/j.tim.2016.12.008

Van Boeckel, T. P., Pires, J., Silvester, R., Zhao, C., Song, J., Criscuolo, N. G., et al. (2019). Global trends in antimicrobial resistance in animals in low- and middle-income countries. *Science* 365:eaaw1944:365. doi: 10.1126/science.aaw1944

Wang, J., Chou, S., Xu, L., Zhu, X., Dong, N., Shan, A., et al. (2015). High specific selectivity and membrane-active mechanism of the synthetic centrosymmetric α -helical peptides with Gly-Gly pairs. *Sci. Rep.* 5:15963. doi: 10.1038/srep15963

Wang, J., Dou, X., Song, J., Lyu, Y., Zhu, X., Xu, L., et al. (2019). Antimicrobial peptides: promising alternatives in the post feeding antibiotic era. *Med. Res. Rev.* 39, 831–859. doi: 10.1002/med.21542

Xu, L., Shao, C., Li, G., Shan, A., Chou, S., Wang, J., et al. (2020). Conversion of broad-Spectrum antimicrobial peptides into species-specific antimicrobials capable of precisely targeting pathogenic bacteria. *Sci. Rep.* 10:944. doi: 10.1038/s41598-020-58014-6

Zheng, Z., Tharmalingam, N., Liu, Q., Jayamani, E., Kim, W., Fuchs, B. B., et al. (2017). Synergistic efficacy of *Aedes aegypti* antimicrobial peptide Cecropin A2 and tetracycline against *Pseudomonas aeruginosa*. *Antimicrob. Agents Chemother.* 61, e00686–e00617. doi: 10.1128/AAC.00686-17

Zhong, C., Gou, S., Liu, T., Zhu, Y., Zhu, N., Liu, H., et al. (2019). Study on the effects of different dimerization positions on biological activity of partial d-amino acid substitution analogues of Anoplin. *Microb. Pathog.* 139:103871. doi: 10.1016/j.micpath.2019.103871

Zhong, C., Zhang, F., Zhu, N., Zhu, Y., Yao, J., Gou, S., et al. (2021). Ultra-short lipopeptides against gram-positive bacteria while alleviating antimicrobial resistance. *Eur. J. Med. Chem.* 212:113138. doi: 10.1016/j.ejmech.2020.113138

Zhong, C., Zhu, N., Zhu, Y., Liu, T., Gou, S., Xie, J., et al. (2020). Antimicrobial peptides conjugated with fatty acids on the side chain of D-amino acid promises antimicrobial potency against multidrug-resistant bacteria. *Eur. J. Pharm. Sci.* 141:105123. doi: 10.1016/j.ejps.2019.105123

Zhu, N., Zhong, C., Liu, T., Zhu, Y., Gou, S., Bao, H., et al. (2021). Newly designed antimicrobial peptides with potent bioactivity and enhanced cell selectivity prevent and reverse rifampin resistance in gram-negative bacteria. *Eur. J. Pharm. Sci.* 158:105665. doi: 10.1016/j.ejps.2020.105665



OPEN ACCESS

EDITED BY

Santi M. Mandal,
Indian Institute of Technology Kharagpur,
India

REVIEWED BY

Jianhua Wang,
Chinese Academy of Agricultural Sciences
(CAAS), China
Michał Obuchowski,
Medical University of Gdansk, Poland
Hemraj S. Nandanwar,
Institute of Microbial Technology (CSIR), India

*CORRESPONDENCE

Sonia Barberis
✉ soniaebbarberis@gmail.com

RECEIVED 28 January 2023

ACCEPTED 28 April 2023

PUBLISHED 16 May 2023

CITATION

Adaro M, Ibáñez ÁGS, Origone AL, Vallés D,
Guzmán F, Vega A and Barberis S (2023)
Enzymatic synthesis of new antimicrobial
peptides for food purposes.
Front. Microbiol. 14:1153135.
doi: 10.3389/fmicb.2023.1153135

COPYRIGHT

© 2023 Adaro, Ibáñez, Origone, Vallés,
Guzmán, Vega and Barberis. This is an open-
access article distributed under the terms of
the [Creative Commons Attribution License
\(CC BY\)](https://creativecommons.org/licenses/by/4.0/). The use, distribution or reproduction
in other forums is permitted, provided the
original author(s) and the copyright owner(s)
are credited and that the original publication in
this journal is cited, in accordance with
accepted academic practice. No use,
distribution or reproduction is permitted which
does not comply with these terms.

Enzymatic synthesis of new antimicrobial peptides for food purposes

Mauricio Adaro^{1,2}, Ángel Gabriel Salinas Ibáñez^{2,3}, Anabella Lucia Origone^{1,2}, Diego Vallés⁴, Fanny Guzmán⁵, Alba Vega³ and Sonia Barberis^{1,2*}

¹Laboratorio de Bromatología, Facultad de Química, Bioquímica y Farmacia, Universidad Nacional de San Luis, San Luis, Argentina, ²Instituto de Física Aplicada (INFAP) – CCT – San Luis – CONICET, Piso, San Luis, Argentina, ³Laboratorio de Microbiología e Inmunología, Facultad de Química, Bioquímica y Farmacia, Universidad Nacional de San Luis, San Luis, Argentina, ⁴Laboratorio de Biocatalizadores y sus Aplicaciones, Instituto de Química Biológica, Facultad de Ciencias, Universidad de la República (UdelaR), Montevideo, Uruguay, ⁵Laboratorio de Péptidos, Núcleo de Biotecnología Curauma, Pontificia Universidad Católica de Valparaíso, Curauma, Valparaíso, Chile

Growing consumer awareness of the potential negative health effects of synthetic antibiotics has prompted the search for more natural preservatives that can improve the safety and quality of food. In this study we report the enzymatic synthesis of N- α -[Carbobenzyloxy]-Ile-Gln (Z-IQ) which is the precursor of Ile-Gln (IQ), a new antibacterial dipeptide, using an aqueous–organic biphasic system formed by 50% (v/v) ethyl acetate in 0.1M Tris – HCl buffer pH 8. A partially purified proteolytic extract from the fruits of *Solanum granuloso leprosum*, named granulosa, proved to be a robust biocatalyst for the synthesis of Z-IQ, eliciting 71 \pm 0.10% maximal peptide yield in the above described conditions. After cleaving and purifying IQ dipeptide, antimicrobial activity was assayed against *Staphylococcus aureus* ATCC 25923, *Staphylococcus hominis* A17771, and *Staphylococcus aureus* C00195, and MIC values between 118 \pm 0.01 μ g/mL and 133.7 \pm 0.05 μ g/mL were obtained. In addition, IQ showed MIC of 82.4 \pm 0.01 μ g/mL and 85.0 \pm 0.00 μ g/mL against *Escherichia coli* ATCC 25922 and *Escherichia coli* A17683, respectively. IQ did not show inhibitory activity against single-drug resistance (SDR) strains, such as *Klebsiella oxytoca* A19438 (SDR) and *Pseudomonas aeruginosa* C00213 (SDR), and against multidrug-resistant *Enterococcus faecalis* I00125 (MDR). IQ also caused growth inhibition of *Helicobacter pylori* NCTC 11638 and three wild-type *H. pylori* strains, which are sensitive to AML, MTZ, LEV and CLA (*H. pylori* 659), resistant to LEV (*H. pylori* 661 SDR), and resistant to MTZ (*H. pylori* 662 SDR). Finally, this study contributes with a new dipeptide (IQ) that can be used as an antimicrobial agent for food preservation or as a safe ingredient of functional foods.

KEYWORDS

antibacterial peptide, enzymatic synthesis of peptides, Ile-Gln (IQ), novel peptide against sensitive and SDR Gram positive and Gram negative strains, food preservation

Introduction

The International Network of Food Safety Authorities (INFOSAN), the World Health Organization (WHO) and the Food and Agriculture Organization of the United Nations (FAO), estimate that 600 million people in the world (almost 1 out of 10) suffer from diseases from eating contaminated food and 420,000 die each year. Children under 5 years of age make up 40% of foodborne illness, with 125,000 deaths each year (CDC – Centers for Disease Control and Prevention, 2018). In the food industry, the control of pathogenic bacteria is achieved through

different preservation methods (thermal treatment, salting, acidification, drying) and the addition of synthetic antibiotics in those foods that are authorized by the food regulations of each country (Sabillón et al., 2016).

Synthetic antibiotics are chemical compounds that are added to food, packaging, food contact surfaces, or food processing environments to inhibit microbial growth or kill microorganisms. The main functions of antimicrobials in food are: (1) control natural spoilage processes (food preservation) and (2) prevent/control the growth of food spoilage microorganisms and/or pathogens (food safety) (Davidson et al., 2014). However, the use of synthetic antibiotics can cause undesirable effects in the consumer; the development of bacterial resistance to antibiotics being a true global public health emergency (Hashempour-Baltork et al., 2019).

Growing consumer awareness of the potential negative health impact of synthetic antibiotics has prompted the search for alternative, more natural preservatives that can improve food safety and quality.

According to WHO, *Helicobacter pylori* is 1 of the 16 microorganisms causing the greatest threats to human health with a high impact on public health (World Health Organization, 2022).

The most frequent *H. pylori* pathologies are related to chronic gastritis and gastric ulcer, affecting more than half the world's population. In addition, infection with *H. pylori* is the strongest recognized risk factor for gastric adenocarcinoma and lymphoma (Dang and Graham, 2017). *H. pylori* infections are usually treated with at least two different antibiotics at once, such as clarithromycin (CLA), metronidazole (MTZ), levofloxacin (LEV) and amoxicillin (AML) (Marcus et al., 2016). Treatment also include other medications, such as proton pump inhibitor and bismuth subsalicylate. However, the success of those treatments is decreasing due to bacterial resistance to antibiotics (Malfertheiner et al., 2017; Ozturk et al., 2017).

There is a little history of the use of antimicrobial peptides (AMPs) against *H. pylori* (Xiong et al., 2017; Guzman et al., 2018), but it was reported that stomach cells express AMP during infection and could play a role in the immune response (Gopal et al., 2014). This suggests that the use of AMPs in functional foods could be an effective strategy for the prevention of *H. pylori* infection.

The IQ-motif occurs in a wide range of eukaryotic proteins and peptides, and some of them were associated with antimicrobial activity (McLean et al., 2013). The literature reports that 3IQ1 and 3IQ2 have displayed MIC values toward *E. coli* and *S. aureus* which are similar to or better than those seen with the antimicrobial peptide cathelicidin (LL-37; McLean et al., 2013; Neshani et al., 2018; Kang et al., 2019). Instead, other IQ-motif peptides such as 2IQ4 and the anionic peptide 2IQ1 displayed no bioactivity (McLean et al., 2013). To the best of our knowledge, there are no literature reports on the enzymatic synthesis of IQ dipeptide and its potential antimicrobial activity.

Peptidase-catalyzed synthesis of peptide bonds has shown several advantages over other methodologies used to produce peptides (Wall et al., 1997; Barberis et al., 2008; Wakasa et al., 2011; Agyei and Danquah, 2012; Ortíz-Martínez et al., 2014; Fosgerau and Hoffmann, 2015; Hartsough et al., 2015; Limón et al., 2015). Enzymes are exquisitely selective catalysts, capable of choosing a single substrate from a large number of similar compounds and reacting with high specificity under mild conditions. In addition, enzymatic processes are usually cheaper and more sustainable than chemical processes (Barberis et al., 2018). However, only some plant proteases have been used in peptide synthesis processes (Origone et al., 2018, 2020; Adaro et al., 2021).

Vallés et al. (2004) reported the isolation, partial purification, and characterization of a proteolytic extract obtained by grinding the ripe fruits of *Solanum granuloso leprosum* (Solanaceae), a South American native plant. The crude extract had maximum activity in the pH range from 5.2 to 7.6 and temperatures between 50°C and 55°C. It showed a remarkable stability at pH 7.6 and freezing temperature (−18°C). The main purified fraction (granulosain I) displayed optimal proteolytic activity in the pH range from 7 to 8.6 and high stability at ≤4°C. The crude enzyme extract and the purified fraction were tested against several protease inhibitors, and the results showed that they belong to the cysteine protease type (Vallés et al., 2004).

In industrial processes, minimum enzyme purity criteria are often applied for economic reasons (Abreu and de Figueiredo, 2019). Consequently, a partially purified extract was used as biocatalyst in this study.

Synthesis of peptides will not proceed efficiently in aqueous medium where the hydrolytic potential of the enzyme prevails. The design of reaction media is a major challenge for peptide synthesis, since proteases, different from lipases, are not structurally conditioned to act in such environments (Illanes et al., 2009; Origone et al., 2020).

The aim of this work was to study the ability of soluble granulosain (the partially purified proteolytic extract from the fruits of *Solanum granuloso leprosum*) as a biocatalyst for the synthesis of N- α -[Carbobenzyloxy]-Ile-Gln (Z-IQ), which is a precursor of IQ, a novel dipeptide potentially useful as antibacterial agent for food applications. Synthesis was carried out under kinetic and thermodynamic control; in 50% (v/v) ethyl acetate in 0.1 M Tris – HCl buffer pH 8. The results were compared with the amine-terminal IQ analogous peptide obtained by chemical synthesis.

Materials and methods

Reagents

(N- α -[(benzyloxy)carbonyl]-amino acid-p-nitrophenyl ester hydrochloride (≥ 98.0%), N- α -[(benzyloxy)carbonyl]-L-Ile (Z-Ile-OH) (≥ 98.0%), N- α -benzoyl-DL-arginine-p-nitroanilide (BAPNA, ≥ 96.0%), monobasic sodium orthophosphate anhydrous (≥ 99.0%), Tris-HCl (Tris(hydroxymethyl) aminomethane hydrochloride, ≥ 99.0%), 4-nitrophenol (≥ 99.0%), 4-nitroaniline (≥ 99.0%), 2-mercaptoethanol (≥ 99.0%), trifluoroacetic acid for HPLC (≥ 99.0%), and bovine serum albumin by agarose gel electrophoresis (BSA, ≥ 99.0%) were bought from Sigma-Aldrich (St. Louis, MO, United States).

L-cysteine hydrochloride monohydrate (≥ 98%), NaOH (≥ 98.0%), phosphate buffer solution (Certipur®, pH 7.00, at 20°C), bicarbonate buffer solution pH 10 (100 mM sodium carbonate and 100 mM sodium bicarbonate), sulfuric acid (98%) and NaOH (≥ 98.0%), were bought from Merck KGaA (Darmstadt, Germany). Acetonitrile, acetone, 1,2-dichloroethane, isopropyl ether, n-hexane, toluene, 2-chlorotoluene, 1-heptanol, phenyl acetone and ethyl acetate, piperidine, dichloromethane (DCM), N,N-dimethylformamide (DMF) (gradient grade for liquid chromatography LiChrosolv®), methanol (gradient grade for liquid chromatography LiChrosolv®), formic acid (98–100% for HPLC LiChropur™) and 0.5 nm molecular sieve beads, were also purchased from Merck KGaA (Darmstadt,

Germany). Ethylenedinitrilotetraacetic acid (EDTA, disodium salt, dehydrate, molecular biology grade) was purchased from Calbiochem (San Diego, CA, USA).

Preparation of partially purified enzymatic extract

Solanum granuloso leprosum (Solanaceae), popularly known as fumo bravo, is a pioneer species of the Missionary Forest in Argentina, but it also inhabits Brazil and Uruguay (Burkart, 1979). The orange globular fruits of *Solanum granuloso-leprosum* were harvested in an experimental plantation of Montevideo, Uruguay.

The partially purified proteolytic extract from the fruits of *Solanum granuloso leprosum*, was obtained according to Vallés et al. (2004) and it was lyophilized for later use as biocatalyst. The ripe fruits were ground together with abrasives and centrifuged at 6,654g for 30 min at 4°C (Vallés et al., 2004). The supernatant was filtered through gauze and the filtrate was called crude extract. A portion (8 mL) of the crude extract was mixed with an equal volume of cold ethanol (−20°C) under gentle stirring, left to settle for 10 min at −20°C, and then centrifuged at 16,000g for 20 min at 4°C (Scopes, 1994). The precipitate was suspended in 8 mL of 0.2 M phosphate buffer pH 7.0. This partially purified extract containing the soluble proteases, collectively named *granulosain*, was frozen at −20°C for further studies.

Protein content and enzyme activity assays

Protein concentration in the enzyme extracts was determined by the Bradford protein assay, using BSA as standard (Bradford, 1976). The proteolytic activity of *granulosain* was determined as the initial rate of hydrolysis against N-α-benzoyl-DL-arginine-p-nitroanilide (BAPNA) as substrate. The reaction mixture was prepared by mixing 0.5 mL of partially purified *granulosain* (2.47 mg protein/mL) with 0.5 mL of 5 mM BAPNA containing 20 mM cysteine in 0.1 M Tris–HCl buffer pH 8. After 5 min of incubation at 37°C and 200 rpm, the absorbance of the p-nitroaniline released was measured at 410 nm. Enzymatic units of activity (IU) were obtained by performing a standard curve of p-nitroaniline in 0.1 M Tris–HCl buffer pH 8. An international unit of enzyme activity (IU) is the amount of enzyme that catalyzes the conversion of 1 μmol of substrate per min, under defined operating conditions. A control without substrate under similar conditions was carried out.

Stability assay method

Stability of soluble *granulosain* was evaluated at 40°C under nonreactive conditions in 0.1 M Tris–HCl buffer solution pH 8, and in 30, 50 and 70% (v/v) of immiscible organic solvents in 0.1 M Tris–HCl buffer solution pH 8. Immiscible organic solvents were selected from an optimized statistical design of 72 organic solvents based on the principal components analysis, which allowed to cluster the organic solvents according to their physicochemical properties (Barberis et al., 2006).

The residual proteolytic activity of *granulosain* after 8 h was determined, which was previously evaluated as the end process time

for catalyst replenishment. These results allowed to select the most promising liquid – liquid aqueous – organic media for the peptide synthesis reaction.

Amino acid preference assay

The amino acid preference assay of *granulosain* was performed against 12 N-α-[Carbobenzyloxy]-amino-p-nitrophenyl esters as substrates, according to the protocol described by Priolo et al. (2001). The enzyme activity unit (Ucbz) was established as the amount of enzyme that cleaves 1.0 μmol of p-nitrophenol per min under the reaction conditions. The most preferred substrate was selected as an acyl donor for peptide synthesis.

Enzymatic synthesis of Z-IQ peptide

Based on the *granulosain* preferences for synthetic amino acid derivatives, N-α-[(benzyloxy)carbonyl]-L-Isoleucine-p-nitrophenyl ester (Z-Ile-ONp) and L-Glutamine (Gln-OH) were selected as acyl donor and nucleophile, respectively.

The reaction of synthesis under kinetic control (Guzmán et al., 2007) was carried out at 40°C in a system formed by 50% (v/v) of ethyl acetate in 0.1 M Tris–HCl buffer solution pH 8, containing soluble *granulosain* (2.47 mg/mL, 32.49 ± 0.186 IU/mg), 20 mM 2-mercaptoethanol, 0.392 mM of both Z-Ile-ONp and triethyl ammonium (TEA), and 3.180 mM of Gln-OH. In addition, the synthesis reaction under thermodynamic control (Guzmán et al., 2007) was also carried out, using 0.392 mM N-α-[(benzyloxy)carbonyl]-L-Isoleucine (Z-Ile-OH) as acyl donor (instead of Z-Ile-ONp) under the same reaction conditions.

The synthesis was carried out in a GFL Shaking Incubator Orbital Motion (Model 3,031, Germany) at 200 rpm and several aliquots (1 mL) were withdrawn during 24 h. The reaction was stopped with 0.2 mL of 0.1% (v/v) trifluoroacetic acid (TFA). A control group consisting of the enzyme alone, each individual substrate and all the reagents together but without the enzyme was also carried out.

Substrate, product and byproducts were analyzed by RP-HPLC and identified by mass spectrometry (MS). The cleavage of the Z group to deprotect the α-amino-group was performed using the protocol described by Isidro-Llobet et al. (2009).

The product yield (η) and the degree of conversion (αs) of acyl donor substrate into product were evaluated by equations (1, 2) (Origone et al., 2018).

$$\alpha_s = \frac{[S_o] - [S_t]}{[S_o]} 100 \quad (1)$$

$$\eta = \frac{[P]}{[S_o]} 100 \quad (2)$$

Where: [P] is the molar concentration of the product after a certain period of time, [S_o] is the initial molar concentration of the acyl donor, [S_t] is the molar concentration of the acyl donor after a certain period of time.

Chemical synthesis of amine-terminal IQ peptide

For the solid-phase chemical synthesis of the amine-terminal IQ peptide, 0.2 g of 2-chloro-trityl resin (1.6 mmol/g, 100–200 mesh) and 0.1 g of rink amide AM resin (0.59 mmol/g, 100–200 mesh) were used. Resin loading was calculated according to Wanka et al. (2007). The chemical synthesis protocol used in this work was described in previous publications of our research team (Origone et al., 2018). The coupling reaction was validated with the Kaiser test (Sarin et al., 1981). A solution consisting of TFA, H₂O, and triisopropylsilane (95:2.5:2.5) (v/v) was used to deprotect the amino acid side chains and cleave the peptide from the resin, during 90 min at 200 rpm and at room temperature.

The amine-terminal IQ peptide was precipitated with cooled ethyl ether at –70°C, purified in a C₁₈ cartridge (Merck) and lyophilized. Then, its purity and molecular mass was determined by RP-HPLC (Jasco, AS-2055, PW de Meern, Nederland), Electrospray ionization-mass spectrometry (ESI-MS) (LC-MS 2020, Shimadzu, Montevideo, Uruguay) and MALDI-TOF Microflex (Bruker Daltonics, Bremen, Germany).

Analytical assays of peptide synthesis reactions

RP-HPLC

In order to study the reaction kinetics of the enzymatic synthesis of Z-IQ in the liquid - liquid aqueous - organic media which was previously selected, the reaction progress was followed by RP-HPLC (Thermo Electron North America LLC, Palm Beach, FL, United States) using a C₁₈ column, 4.60 mm × 250 mm, particle size: 5 μm (Hypersil BSD, Base Silica Deactivated, USA) and UV Detector at λ: 254 nm and 25°C. The injection volume was 20 μL, the flow rate of the mobile phase (50% (v/v) acetonitrile in 0.1 M Tris-HCl buffer pH 3) was 0.8 mL/min.

Enzymatically and chemically synthesized peptides (Z-IQ and IQ) were purified by means of a C₁₈ cartridge (Merck) (> 95% purity) and dried in a concentrating device (Thermo Scientific Savant™ SPD131DDA SpeedVac, Madrid, España).

The purified Z-IQ and IQ peptides were analyzed by HPLC (Jasco, AS-2055, PW de Meern, Nederland) with a Photo Diode Array Detector, using a C₁₈ column (100 × 4.6 mm, 3.5 μm) (XBridge™ BEH, Waters). Injection volume was 20 μL and mobile phase flowrate was 1 mL/min. The mobile phase consisted of a solution A (2.5% TFA in Mili Q water) and a 30–100% gradient of solution B (2.5% TFA in acetonitrile), during 20 min.

Mass spectrometry

Two micro gram of each peptide were analyzed in an electrospray ionization-mass spectrometry (ESI-MS) (LC-MS 2020, Shimadzu, Montevideo, Uruguay) under positive ion mode during 20 min at 350°C and 4.5 kV. Data were evaluated with a LabSolutions software (version 5.42, Shimadzu).

MALDI-TOF

One micro liter of each peptide (1 μg/μL) and 1 μL of the CHCA matrix (10 μg/μL α-cyano-4-hydroxycinnamic acid in a solution

consisting in 0.1% methanoic acid and 50% acetonitrile) were placed in a micro scout plate. Samples were air dried and analyzed on a MALDI-TOF Microflex (Bruker Daltonics, Bremen, Germany). The equipment operated under reflection detection in positive ion mode and was calibrated with an external standard (700–1800 Da). Spectra were recorded using flexControl software (version 3.0, Bruker Daltonics GmbH).

Bacterial strains

S. aureus ATCC 25923, *E. coli* ATCC 25922, *H. pylori* NCTC 11638 and nine wild-type strains were used in this study. Six Gram positive and Gram negative wild-type strains were isolated from patients in the Microbiology Laboratory of the Regional Polyclinic of San Luis, Argentina. *H. pylori* NCTC 11638 was kindly provided by Dra. Teresa Alarcón Cavero, Microbiology Service of Hospital Universitario de la Princesa, Madrid, Spain. Three wild-type *H. pylori* strains were isolated in our laboratories from biopsy samples of the gastric antrum of patients from San Luis (Argentina). The patients who attended at the healthcare center fulfilled the informed consent form prior to sample collection. *H. pylori* isolates were identified by microscopy, urease, catalase, and oxidase tests. All strains were stored at –80°C in trypticase soy broth (TSB, Britania) with 20% glycerol (Biopack, Buenos Aires, Argentina). Antimicrobial susceptibility was tested according to the Clinical and Laboratory Standards Institute (Clinical and Laboratory Standards Institute (CLSI), 2015).

Determination of antibacterial activity

The antibacterial activity of IQ-OH and IQ-NH₂ against 12 Gram positive and Gram negative bacteria was determined using a kinetic-turbidimetric method (Talia et al., 2009, 2011, 2012). The strains were inoculated in 30 mL of a Müller-Hinton broth and incubated at 37°C for 20 h under gentle agitation. *H. pylori* strains were incubated in Müller Hinton broth supplemented with 5% fetal bovine serum and incubated at 37°C for 48 h under microaerophilic conditions.

The microbial growth kinetic assays were performed in 25 mL titration flasks with Müller-Hinton broth inoculated with a 200 μL of log-phase culture and increasing peptide concentrations. Titration flasks were placed in a GFL Shaking Incubator Orbital Motion (Model 3,031, Burgwedel, Germany) at 37°C, under stirring at 180 rpm. A control without peptide was carried out. Aliquots were removed every 30 min for 6 h and the transmittance (T) was read at λ: 720 nm. The transmittance (T) was related to Nt (Colony Forming Units (CFU)/mL) according to the following equations:

$$\ln Nt (\text{Gram positive}) = 27.4 - 10.3 \times T \quad (3)$$

$$\ln Nt (\text{Gram negative}) = 27.1 - 8.56 \times T \quad (4)$$

Specific microbial growth rates were determined from ln Nt versus time plots.

The minimum inhibitory concentration (MIC) was obtained graphically, from the curve of the specific microbial growth rate versus

the peptide concentration ($\mu\text{g/mL}$). MIC is established as the lowest concentration of a substance that inhibits the microbial growth after incubation in its presence (Andrews, 2001). The MIC of Nisin (a natural food preservative) and several synthetic antibiotics, frequently used in human and animal medicine, and often found in food, were used as control (Jensen et al., 2020; IDEXX Laboratories Inc©, 2022). Besides, AMX was used as a positive control in assay with *H. pylori* strains.

Statistical analysis

Residual proteolytic activity, degree of conversion (α s) of acyl donor substrate into product, and peptide yield (η) were obtained from three independent trials which were done by duplicate, and data were reported as mean \pm SD. The linear range of proteolytic activity reaction was previously determined for each assay. IBM® SPSS® Statistics V22.0 software was used for statistical analysis.

Results

Granulosain stability

Plant extracts, such as that from the fruits of *Solanum granulosum leprosum*, contain many water-soluble components, including pigments, phenolic compounds, and carbohydrates. These components usually interfere with the expression of enzymatic activity and therefore it is necessary to purify the proteins.

The use of organic solvents, such as acetone, allows to obtain a solid protein concentrate which can be dissolved in an appropriate buffer solution. This partially purified enzyme extract is jointly called granulosain and retained high enzyme activity (>90%; Vallés et al., 2008).

The residual proteolytic activity of granulosain (2.47 mg/mL, 32.49 ± 0.186 IU/mg) after 8 h in liquid – liquid aqueous organic systems formed by 30, 50, and 70% (v/v) of different immiscible organic solvents in 0.1 M Tris–HCl buffer pH 8 at 40°C, is shown in Table 1.

Granulosain exhibited similar or slightly lower residual proteolytic activity in several biphasic media, such as 50% (v/v) ethyl acetate, 1,2-dichloroethane, 2-chlorotoluene and n-hexane, than in 0.1 M Tris–HCl buffer pH 8. Those values ranged from 73 to 99% of the residual proteolytic activity obtained in buffer under the same conditions. Particularly, in 30% (v/v), 50% (v/v), and 70% (v/v) ethyl acetate in 0.1 M Tris–HCl buffer pH 8 at 40°C the following residual proteolytic activity values (IU/mg) were obtained: 19.63 ± 0.210 , 31.98 ± 0.209 , and 0.148 ± 0.134 , respectively. In other biphasic media (toluene, 1-heptanol, isopropyl ether and phenyl acetone) granulosain showed little or no proteolytic activity. In addition, in all liquid–liquid biphasic media, when the organic solvent concentration was increased to 70% (v/v) the residual proteolytic activity of granulosain decreased sharply or was null under the studied conditions.

Some factors that contribute to the loss of enzymatic activity in organic media, such as the partitioning of immiscible organic solvents in the aqueous phase and the increase of the interfacial area, has been reported in the literature (Illanes et al., 2013; Kumar et al., 2016).

TABLE 1 Residual proteolytic activity of granulosain after 8 h in liquid–liquid biphasic media formed by different percentages of organic solvent in 0.1 M Tris HCl buffer pH 8, at 40°C.

Organic solvent	Residual proteolytic activity (IU/mg)		
	30%	50%	70%
Toluene	3.00 ± 0.00	4.13 ± 0.173	6.14 ± 0.161
1-Heptanol	0.33 ± 0.175	0.49 ± 0.141	0.00 ± 0.000
1,2-Dichloroethane	11.93 ± 0.205	29.05 ± 0.185	3.89 ± 0.210
Isopropyl ether	0.33 ± 0.144	0.41 ± 0.112	0.00 ± 0.000
n-Hexane	14.90 ± 0.186	23.71 ± 0.109	7.29 ± 0.124
2-Chlorotoluene	12.90 ± 0.06	27.21 ± 0.214	7.02 ± 0.227
Phenyl acetone	0.33 ± 0.175	0.41 ± 0.042	0.00 ± 0.000
Ethyl acetate	19.63 ± 0.210	31.98 ± 0.209	0.148 ± 0.134

Residual proteolytic activity of granulosain in 0.1 M Tris–HCl buffer pH 8 at 40°C was 32.49 ± 0.186 (IU/mg).

Several cysteine proteases from South American plants of the family Asclepiadaceae, such as araujiain from the latex of fruits of *Araujia hortorum* Fourn., funastrain from the latex of stems of *Funastrum clausum* (Jacq.) Schlechter, and asclepain from *Asclepias curassavica* L.; expressed higher enzymatic activity in biphasic media than in buffer solution (Barberis et al., 2006; Quiroga et al., 2006, 2007; Origone et al., 2018). However, enzymes from the same family may show different behavior toward organic solvents. Cysteine proteases are hydrolase enzymes that share a common catalytic mechanism involving a nucleophilic cysteine thiol in a catalytic triad or diad. Organic solvents can act not only around the active site of the enzyme but also on the surface of the protein, modifying their interactions and leading to structural and functional changes in the protein. Such changes sometimes lead to more active enzyme structures or may cause loss of enzyme activity.

Ethyl acetate in 0.1 M Tris–HCl buffer pH 8 at 50% (v/v) was selected as the reaction medium for the synthesis of the Z-IQ peptide based on the high proteolytic activity and stability of granulosain, as also due to the adequate solubility of the substrates and their partition coefficients to the aqueous phase where the enzyme is dissolved.

Granulosain preferences for synthetic amino acids

Figure 1 shows the preferences of granulosain for N- α -[Carbobenzyloxy]-amino acid-p-nitrophenyl esters in 50% (v/v) ethyl acetate in 0.1 M Tris–HCl buffer pH 8, at 40°C. Granulosain in 50% (v/v) ethyl acetate in 0.1 M Tris–HCl buffer pH 8 showed high preferences for Ile, Val and Tyr derivatives.

In the enzymatic synthesis of peptides, amino acids acting as acyl donor and nucleophile are recognized by the S subsite and S' region of the enzyme, respectively. The specificity of the enzyme for the acyl donor defines the rate of the reaction, while the specific binding of the nucleophile to the S' subsite of the protease is necessary to achieve high yields (Schechter and Berger, 1967).

The high preference of granulosain for Z-I-ONp suggests that it would be a good acyl donor substrate and Gln OH was selected as nucleophile for the peptide synthesis reaction.

Enzymatic synthesis of carboxyl-terminal Z-IQ peptide

The concentration of the acyl donor was established after determining the Z-I-ONp solubility in the organic phase of the reaction medium (50% (v/v) ethyl acetate in 0.1 M Tris-HCl buffer pH 8) at 40°C and 200 rpm, which was 0.318 mM; the partition coefficient of Z-I-ONp between the phases (P: 4.30), and the kinetic parameters of granulosain I (0.6158 mM; Vallés et al., 2008).

The partition coefficient of Z-I-ONp in the selected reaction medium was several times higher than in other biphasic media. Consequently, 50% (v/v) ethyl acetate in 0.1 M Tris-HCl buffer pH 8 at 40°C not only allowed to express high activity and stability to granulosain but also allowed a high concentration of acyl donor to be available in the aqueous phase where the enzyme is dissolved.

Figure 2 shows the separation of reactants and products by RP-HPLC from a representative sample of the enzymatic synthesis of Z-IQ under kinetic control, after 1 h of reaction. According to

Figure 2, at a retention time (t_R) of 6.5 min a peak of the main product (III) was observed in the organic phase. After 30 min, the main product was hydrolyzed to Z-I-OH (II) and partitioned to the aqueous phase. The Z-IQ peptide could be separated easily from the byproduct by stopping the agitation at the end of the reaction.

Table 2 shows the Z-IQ product yields (η) and the conversion percentage of acyl donor substrate into product (α s) for the enzymatic synthesis under kinetic control of Z-IQ peptide, using 50% (v/v) ethyl acetate in 0.1 M Tris-HCl buffer pH 8 as reaction medium and granulosain as biocatalysts, at 40°C and 200 rpm.

The synthesis of Z-IQ under kinetically controlled conditions, and with one of the substrates in excess, allowed to increase the selective conversion toward a single product until 71% after 15 min, remaining unconverted 12.7% of the limiting substrate remaining unconverted. These results revealed the high specificity and catalytic capacity of granulosain.

Peptide synthesis reactions under kinetic control in aqueous-organic media proceed via an acyl-enzyme intermediate, which reacts with the N-terminal nucleophile and becomes the C-terminal segment of the peptide product. However, the nucleophile competes with water for cleaving that intermediate and to form either a peptide or a hydrolyzed substrate. In fact, the hydrolysis of the acyl donor substrate decreased the product yield in the synthesis reaction of Z-IQ. When the thermodynamic equilibrium conditions prevailed the reaction did not proceed.

The reaction product was separated from the organic phase, purified by means of a C_{18} column, dried with a concentrator equipment (Thermo Scientific Savant™ SPD 131 DDA Speed Vac) and analyzed by electrospray ionization mass spectrometry (LCMS-2020, Shimadzu).

Figure 3 shows the chromatogram obtained by (a) RP-HPLC and (b) mass spectrum of the carboxy terminal peptide N- α -CBZ-Ile-Gln-OH (Z-IQ). The mass spectrum of the main product of the enzymatic synthesis reaction (III, t_R : 6.5 min) showed ion mass (m/z): 393, corresponding to the peptide Z-IQ.

Chemical synthesis of amine-terminal IQ peptide

The IQ peptide was chemically synthesized using N α -Fmoc strategy, as it was previously described. The purity was higher than 95% and the molecular mass was confirmed by MALDI-TOF mass spectrometry (Figure 4).

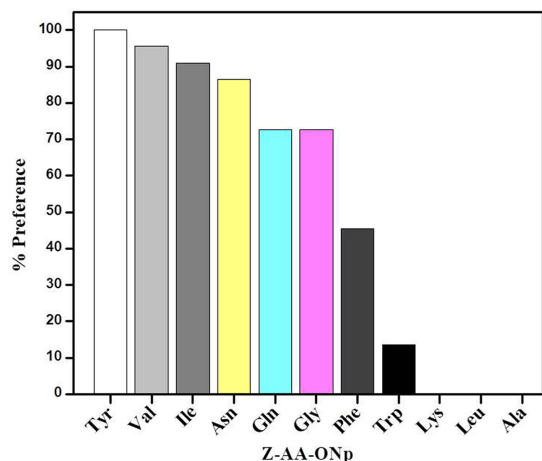


FIGURE 1
Preferences of granulosain for N- α -[Carbobenzyloxy]-amino acid-p-nitrophenyl esters (Z-AA-ONp) in 50% (v/v) ethyl acetate in 0.1M Tris-HCl buffer pH 8, at 40°C.

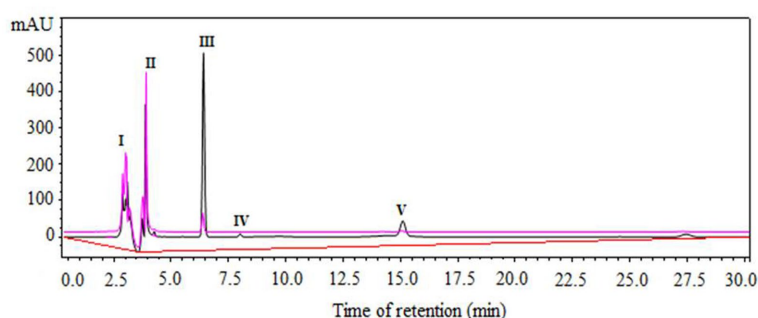


FIGURE 2
Component separation by RP-HPLC of a representative sample from N- α -CBZ-Ile-Gln-OH (Z-IQ) enzymatic synthesis under kinetic control, using granulosain (2.47mg/mL, 32.49 \pm 0.186IU/mg) as soluble biocatalysts in 50% (v/v) ethyl acetate in 0.1M Tris-HCl buffer pH 8, after 1h of reaction at 40°C and 200rpm. I: granulosain (t_R : 2.7–3.2min); II: N- α -CBZ-Ile-OH (Z-I-OH) (t_R : 4min); III: N- α -CBZ-Ile-Gln-OH (Z-IQ) (t_R : 6.5min); IV: 4-Nitrophenol (ONp) (t_R : 8.0min); V: N- α -CBZ-Ile-ONp (Z-I-ONp) (t_R : 15.2min). Aqueous phase: pink line. Organic phase: black line.

Antibacterial activity of Ile-Gln (IQ)

Antibacterial activity of Ile-Gln (IQ) was tested through three independent trials, in duplicate, against Gram positive and Gram negative strains in batch culture with Müller-Hinton broth at 37°C under agitation at 180 rpm, using increasing concentrations of IQ (0–500 µg/mL).

Table 3 shows the minimum inhibitory concentrations (MIC) values of IQ against three reference strains: *S. aureus* ATCC 25923, *E. coli* ATCC 25922, and *H. pylori* NCTC 11638, and six Gram positive and Gram negative type-wild strains isolated in the

TABLE 2 Product yield (η) and conversion percentage of acyl donor substrate (α s) in the kinetically controlled synthesis of Z-IQ in 50% (v/v) ethyl acetate in 0.1M Tris-HCl buffer pH 8, using granulosain as biocatalysts, at 40°C and 200rpm.

Time (min)	Z-IQ (mM)	Z-I-OH (mM)	α s (%)	η (%)
0	0.000 ± 0.00	0.000 ± 0.00	0.0	0.0
1	0.027 ± 0.01	0.009 ± 0.00	9.0	6.9
5	0.248 ± 0.03	0.027 ± 0.01	70.1	63.3
15	0.278 ± 0.00	0.063 ± 0.01	87.3	71.0
30	0.252 ± 0.02	0.131 ± 0.01	97.7	64.3
60	0.239 ± 0.01	0.153 ± 0.00	100	61.0
180	0.175 ± 0.00	0.217 ± 0.00	100	44.6

Microbiology Laboratory of the Regional Polyclinic of San Luis, Argentina, and three wild-type *H. pylori* strains isolated in our laboratories from biopsy samples of the gastric antrum of patients from San Luis, Argentina.

The new dipeptide (IQ) caused growth inhibition of Gram-positive bacteria, such as *S. aureus* ATCC 25923, *S. hominis* A17771 and *S. aureus* C00195, between 118 ± 0.01 µg/mL and 133.7 ± 0.05 µg/mL; but did not inhibit the growth of the multidrug resistant *E. faecalis* I00125 (MDR). In addition, IQ showed MIC of 82.4 ± 0.01 µg/mL and 85.0 ± 0.00 µg/mL against *E. coli* ATCC 25922 and *E. coli* A17683, respectively, but did not show inhibitory activity against simple resistant strains, such as *Klebsiella oxytoca* A19438 (SDR) and *Pseudomonas aeruginosa* C00213 (SDR).

IQ also inhibited the microbial growth of *H. pylori* NCTC 11638 and three wild-type *H. pylori* strains isolated from antral-gastric biopsies of patients from San Luis, Argentina. MIC values of 250 ± 0.01 µg/mL and 500 ± 0.01 µg/mL were obtained for *H. pylori* NCTC 11638 and the other *H. pylori* strains, respectively. MIC of synthetic antibiotics frequently used in human and animal medicine; and often found in food, were used as control (IDEXX Laboratories Inc®, 2022).

Figure 5 shows the kinetics of growth in batch culture of (A) *S. aureus* C00195, using Müller-Hinton broth and increasing concentration of IQ (0 to 118 µg/mL) at 37°C and 180 rpm, (B) *H. pylori* NCTC 11638, using Müller-Hinton broth supplemented with 5% fetal bovine serum, and increasing concentration of IQ (0 to 250 µg/mL), at 37°C under microaerophilic conditions. Control (without IQ).

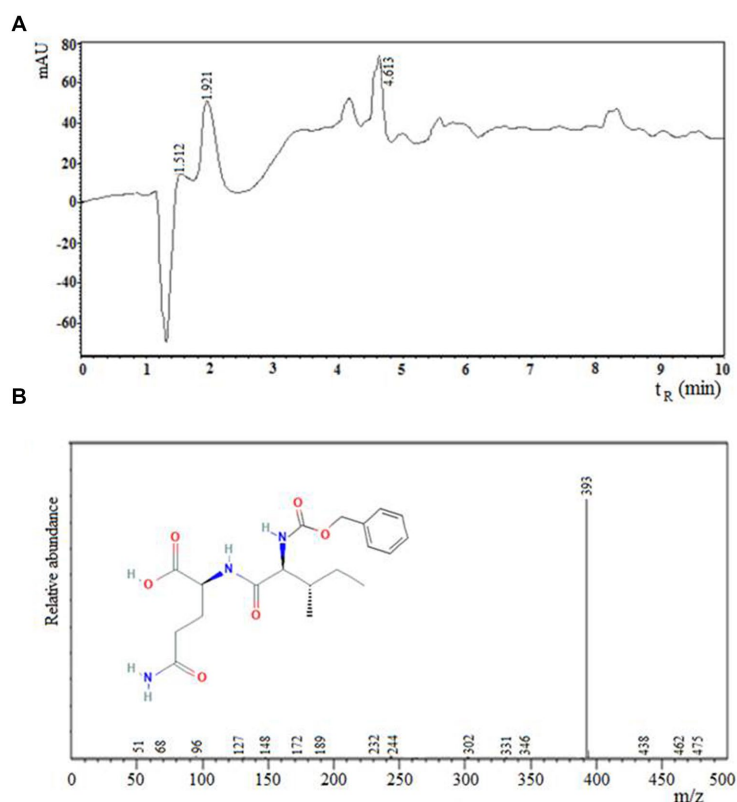


FIGURE 3

Chromatogram obtained by (A) RP-HPLC and (B) mass spectrum of the carboxyl terminal peptide N-α-CBZ-Ile-Gln-OH (Z-IQ). The mass spectrum of the main product of the enzymatic synthesis reaction (III, t_R : 6.5min) showed ion mass (m/z): 393, corresponding to the peptide Z-IQ.

Figure 6 shows the kinetics of growth in batch culture of *E. coli* ATCC 25922, using Müller-Hinton broth and increasing concentration of (A) IQ (0 to 164.8 µg/mL), (B) Z-IQ (0 to 164.8 µg/mL), at 37°C and 180 rpm.

As shown in Figure 6, benzyloxycarbonyl group (Z) did not significantly modify the bacterial growth inhibitory activity of the IQ dipeptide. In contrast, the carboxyl terminus of the IQ dipeptide was essential for antibacterial activity. In fact, the amine-terminal dipeptide IQ-NH₂ had no antibacterial activity against the strains studied.

Those results suggest that the new dipeptide (IQ-OH) can be used as an antimicrobial agent against sensitive Gram positive and Gram negative bacteria, for food preservation or as an ingredient of functional foods.

It is important to highlight that the IQ-OH sequence has not yet been reported in bioactive peptide databases (Dziuba et al., 1999;

Shtatland et al., 2007; Liu et al., 2008; Thomas et al., 2010; Wang et al., 2017), and according to our results, it is a promising antimicrobial agent.

Discussion

Synthetic antibiotics are known to be more effective than natural antimicrobial agents, such as AMPs. However, AMPs do not produce resistance and are safe at higher concentrations (Adaro et al., 2021). Besides, as food preservatives, it is expected that small peptides (such as IQ) can be rapidly hydrolyzed in the digestive system.

Peptide therapies are currently targeted at the treatment of cancer (goserelin, bortezomib, leuporelin), cardiovascular (bivalir, eptifibatide) and central nervous system (glatiramer) diseases,

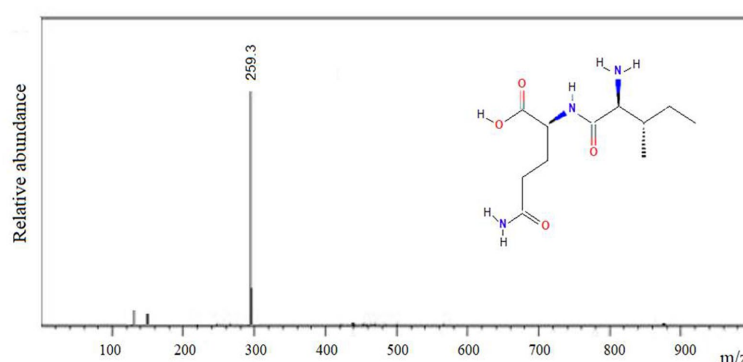


FIGURE 4
Mass spectrum of the amine-terminal IQ peptide, m/z: 259.3.

TABLE 3 Minimum inhibitory concentrations (MIC) values of Ile-Gln-OH dipeptide against Gram positive and Gram negative strains.

Microorganism		MIC				
	Ile-Gln-OH (µg/ mL)	1	2	3	4	5
			(µg/mL)			
Gram positive bacteria						
<i>Staphylococcus aureus</i> ATCC 25923	133.7 ± 0.05	8–16	6.4–12.8	0.4	2–4	8–32
<i>Staphylococcus aureus</i> C00195	118.0 ± 0.01					
<i>Staphylococcus hominis</i> A17771	125.0 ± 0.05					
<i>Enterococcus faecalis</i> I00125 (MDR)	–					
Gram negative bacteria						
<i>Escherichia coli</i> ATCC 25922	82.4 ± 0.01	8–32	--	0.4	8–32	4–16
<i>Escherichia coli</i> A17683	85.0 ± 0.00					
<i>Klebsiella oxytoca</i> A19438 (SDR)	–					
<i>Pseudomonas aeruginosa</i> C00213 (SDR)	–					
<i>Helicobacter pylori</i> NCTC 11638 ¹	250 ± 0.01					
<i>Helicobacter pylori</i> 659 ¹	500 ± 0.01					
<i>Helicobacter pylori</i> 661 (SDR) ²	500 ± 0.01					
<i>Helicobacter pylori</i> 662 (SDR) ³	500 ± 0.01					

The MIC of Nisin (a natural food preservative) and several synthetic antibiotics often found in food, were used as control: 1. Ampicillin, 2. Nisin, 3. Erythromycin, 4. Chloramphenicol, 5. Gentamicin. ¹Sensitive to AML, MTZ, LEV, and CLA. Pathology: Chronic gastritis.

²Resistant to LEV. Pathology: Gastric ulcer.

³Resistant to MTZ. Pathology: Chronic gastritis.

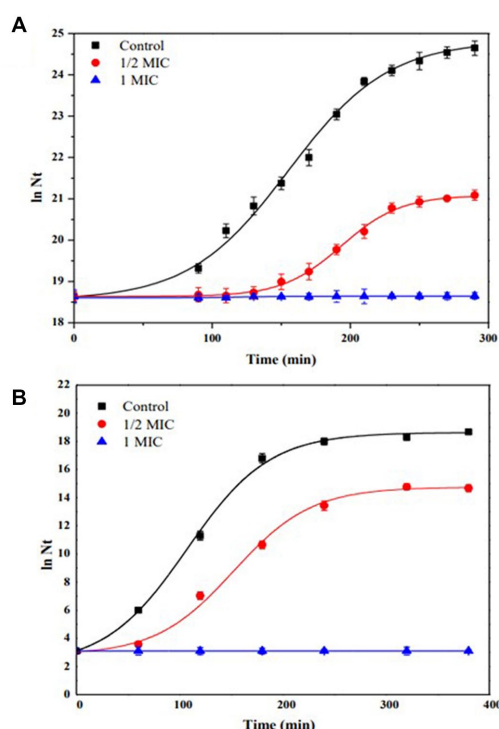


FIGURE 5

Growth kinetics in batch culture of (A) *Staphylococcus aureus* C00195, using Müller-Hinton broth and increasing concentration of IQ (0 to 118 µg/mL) at 37°C and 180rpm. (B) *Helicobacter pylori* NCTC 11638, using Müller-Hinton broth supplemented with 5% fetal bovine serum, and increasing concentration of IQ (0 to 250 µg/mL), at 37°C under microaerophilic conditions. Control (without IQ).

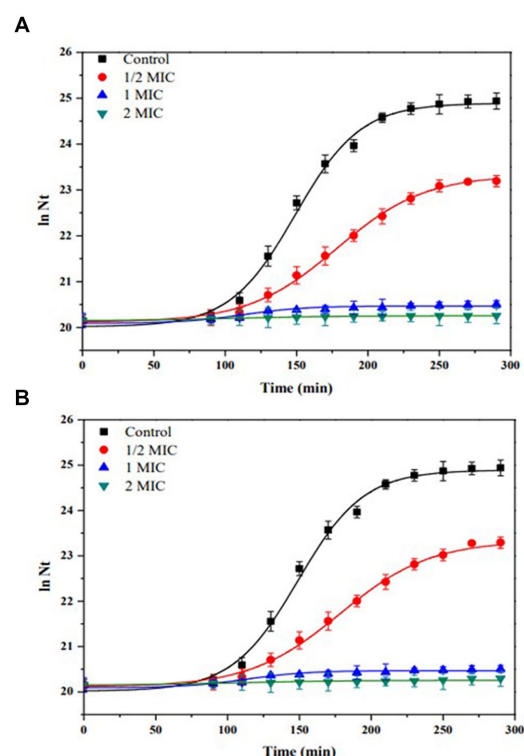


FIGURE 6

Growth kinetics in batch culture of *Escherichia coli* ATCC 25922, using Müller-Hinton broth and increasing concentration of (A) IQ (0 to 164.8 µg/mL). (B) Z- IQ (0 to 164.8 µg/mL), at 37°C and 180rpm. Control (without IQ).

infections (telaprevir, boceprevir), metabolic disorders (liraglutide, exenatide), hematological (icatibant, ecallantide) and gastrointestinal (teduglutide, linaclotide) diseases, among others (Yu and Rao, 2014; Fosgerau and Hoffmann, 2015; Zhang et al., 2016).

In contrast to the widespread development of therapeutic peptides, the commercial production of bioactive peptides with specific properties for food use (nutraceuticals, functional foods, and preservatives) is rare, although it is an area of intense research. Nisin (of bacterial origin) and lysozyme (of animal origin), designated E234 and E1105 in the JECFA list of food additives, are so far the only peptides approved for marketing by the WHO (World Health Organization, 2010).

Soluble granulosain catalyzed the Z-IQ dipeptide synthesis under kinetic-control with high yield ($71 \pm 0.10\%$) using an aqueous-organic biphasic system formed by 50% (v/v) ethyl acetate and 0.1 M Tris – HCl buffer pH 8. Nowadays, the molecular effect of organic solvents on the activity, operational stability, flexibility and secondary structure of granulosain, using different aqueous-organic biphasic media, are being evaluated.

This paper reports a novel carboxyl-terminal antibacterial peptide (Ile-Gln-OH) that significantly decreased ($p \leq 0.05$) the specific growth rates of several Gram positive and Gram negative sensitive strains, at low concentrations. Particularly, MIC values from 118 ± 0.01 µg/mL to 133.7 ± 0.05 µg/mL for several *S. aureus* strains and from 82.4 ± 0.01 µg/mL to 85.0 ± 0.00 µg/mL for *E. coli* strains were obtained. These MIC values were several time lower than others

reported in the literature for *S. aureus* and *E. coli* strains, using novel dipeptides (Soares et al., 2023).

IQ also inhibited the microbial growth of *H. pylori* NCTC 11638 at $\geq 250 \pm 0.01$ µg/mL and three wild-type *H. pylori* strains at $\geq 500 \pm 0.01$ µg/mL. It is important to note that, among these last three strains, one is sensitive to AML, MTZ, LEV and CLA (*H. pylori* 659), another is resistant to LEV (*H. pylori* 661), and the third is resistant to MTZ (*H. pylori* 662).

Finally, this study contributes with a new dipeptide (IQ) that can be used as an antimicrobial agent for food preservation or as a safe ingredient of functional foods.

Further studies will be conducted to elucidate the mechanism of action of IQ against those bacterial strains.

Data availability statement

The original contributions presented in the study are included in the article/Supplementary material, further inquiries can be directed to the corresponding author.

Ethics statement

Ethical review and approval was not required for this study in the Universidad Nacional de San Luis, San Luis, Argentina, because the samples were collected during routine care and the patients fulfilled

the written informed consent form at Healthcare Centers of San Luis, Province of San Luis, Argentina, prior to sample collection. The isolated strains were later donated to the Faculty of Chemical, Biochemical and Pharmacy of the Universidad Nacional de San Luis.

Author contributions

SB designed the experiments, did the data analyzing, and manuscript writing. MA did the experimental assays, data collection, and analysis. AI, AV, and AO collaborated in the antimicrobial activity experiments. DV collaborated in the preparation of partially purified enzymatic extracts. FG collaborated in the chemical synthesis and analysis of the IQ-NH₂ peptide. All authors contributed to the article and approved the submitted version.

Funding

This research was funded by the National University of San Luis, San Luis, Argentina (Grant number 2–0718, 2018–2022). MA and AI are Postdoctoral Fellows at CONICET, Argentina. SB is Researcher Career Member at CONICET, Argentina.

Acknowledgments

The authors would like to thank the Microbiology Laboratory of the Regional Polyclinic of San Luis, Argentina, for the kind gift of six

clinical strains isolated from patients of San Luis (Argentina). The authors also thank to Teresa Alarcon Cavero (Hospital Universitario de la Princesa, Madrid, Spain) for the donation of *H. pylori* NCTC 11638, used as a reference strain in this study, and Patricia Gomez and Patricia Vallejos for the donation of gastric biopsy specimens.

Conflict of interest

The authors declare that the research was conducted in the absence of any commercial or financial relationships that could be construed as a potential conflict of interest.

Publisher's note

All claims expressed in this article are solely those of the authors and do not necessarily represent those of their affiliated organizations, or those of the publisher, the editors and the reviewers. Any product that may be evaluated in this article, or claim that may be made by its manufacturer, is not guaranteed or endorsed by the publisher.

Supplementary material

The Supplementary material for this article can be found online at: <https://www.frontiersin.org/articles/10.3389/fmicb.2023.1153135/full#supplementary-material>

References

- Abreu, D. C. A., and de Figueiredo, K. C. (2019). Separation processes. Bromelain separation and purification processes from pineapple extract. *Braz. J. Chem. Eng.* 36, 1029–1039. On line version. doi: 10.1590/0104-6632.20190362s20180417
- Adaro, M., Bersi, G., Talia, J. M., Bernal, C., Guzmán, F., Vallés, D., et al. (2021). Biosynthesis of a novel antibacterial dipeptide, using proteases from south American native fruits, useful as a food preservative. *Front. Nutr.* 8, 1–15. doi: 10.3389/fnut.2021.685330
- Aguei, D., and Danquah, K. (2012). Industrial-scale manufacturing of pharmaceutical-grade bioactive peptides. *Biotechnol. Adv.* 29, 272–277. doi: 10.1016/j.biotechadv.2011.01.001
- Andrews, J. M. (2001). Determination of minimum inhibitory concentration. *J. Antimicrob. Chemother.* 48, 5–16. doi: 10.1093/jac/48.suppl_1.5
- Barberis, S., Adaro, M., Origone, A., Bersi, G., Guzmán, F., and Illanes, A. (2018). in *Peptide synthesis using proteases as catalyst*. eds. M. G. Guevara and G. Daleo (Switzerland: Springer Nature Switzerland AG), 69–106.
- Barberis, S., Guzmán, F., Illanes, A., and López-Santín, J. (2008) in *Study cases of enzymatic processes*. ed. A. Illanes (Netherlands. UK: Springer), 253–273.
- Barberis, S., Quiroga, E., Morcelle, S., Priolo, N., and Luco, J. M. (2006). Study of phytoteases stability in aqueous-organic biphasic systems using linear free energy relationships. *J. Mol. Catal. B Enzym.* 38, 95–103. doi: 10.1016/j.molcatb.2005.11.011
- Bradford, M. M. (1976). A rapid and sensitive method for the quantitation of microgram quantities of protein utilizing the principles of protein-dye binding. *Anal. Biochem.* 72, 248–254. doi: 10.1006/abio.1976.9999
- Burkart, A. (1979). *Dicotiledóneas metacámideas*. (Buenos Aires: Colección científica del I.N.T.A.).
- CDC – Centers for Disease Control and Prevention (2018). Estimates of foodborne illness in the United States. Available at: <https://www.cdc.gov/foodborneburden/index.html> (Accessed April 20, 2023).
- Clinical and Laboratory Standards Institute (CLSI) (2015). *Methods for antimicrobial susceptibility testing of anaerobic Bacteria. Approved Standard-Eighth Edition*. CLSI document M11-A8: Wayne, PA: Clinical and Laboratory Standard Institute, 1–39.
- Dang, B. N., and Graham, D. Y. (2017). *Helicobacter pylori* infection and antibiotic resistance: a WHO high priority? *Nat. Rev. Gastroenterol. Hepatol.* 14, 383–384. doi: 10.1038/nrgastro.2017.57
- Davidson, P. M., Bozkurt Cekmer, H., Monu, E., and Techathuvanan, C. (2014). “The use of natural antimicrobials in food: an overview,” in *Handbook of natural antimicrobials for food safety and quality*. ed. T. M. Taylor (Cambridge: Woodhead Publishing/Elsevier), 1–26.
- Dziuba, J., Minkiewicz, P., Nalecz, D., and Iwaniak, A. (1999). Database of biologically active peptides. *Nahrung* 43, 190–195. doi: 10.1002/(SICI)15213803(19990601)43:3<190::AID-FOOD190>3.0.CO;2-A
- Fosgerau, K., and Hoffmann, T. (2015). Peptide therapeutics: current status and future directions. *Review. Drug Discov. Today* 20, 122–128. doi: 10.1016/j.drudis.2014.10.003
- Gopal, R., Jeong, E., Seo, C. H., and Park, Y. (2014). Role of antimicrobial peptides expressed by host cells upon infection by *Helicobacter pylori*. *Protein Pept. Lett.* 21, 1057–1064. doi: 10.2174/0929866521666140708092032
- Guzmán, F., Barberis, S., and Illanes, F. (2007). Peptide synthesis: chemical or enzymatic review article. *Electron. J. Biotechnol.* 10:0. doi: 10.2225/vol10-issue2-fulltext-13
- Guzman, J., Téné, N., Touchard, A., Castillo, D., Belkhelfa, H., Haddioui-Hbabi, L., et al. (2018). M. Anti-*Helicobacter pylori* properties of the ant-venom peptide bicarinalin. *Toxins* 10, 21–31. doi: 10.3390/toxins10010021
- Hartsough, E. M., Shah, P., Larsen, A. C., and Chaput, J. C. (2015). Comparative analysis of eukaryotic cell - free expression systems. *BioTechniques* 59, 149–151. doi: 10.2144/000114327
- Hashempour-Baltork, F., Hosseini, H., Shojaei-Aliabadi, S., Torbati, M., Alizadeh, A. M., and Alizadeh, M. (2019). Drug resistance and the prevention strategies in food borne bacteria: an update review. *Adv. Pharm. Bull.* 9, 335–347. doi: 10.15171/apb.2019.041
- IDEXX Laboratories Inc© (2022). Microbiological guide to interpret the minimum inhibitory concentration (MIC) Available at: https://www.idexx.com/media/filer_public/9a/96/ (Accessed April 20, 2023).
- Illanes, A., Cauerhff, A., Wilson, L., and Castro, G. R. (2013). Recent trends in biocatalysis engineering. *Bioresour. Technol.* 115, 48–57. doi: 10.1016/j.biortech.2011.12.050
- Illanes, A., Guzmán, F., and Barberis, S. (2009). in *Proteases as powerful catalysts for organic synthesis*. ed. A. B. Hughes, vol. 2 (Weinheim, Alemania: Wiley-VCH), 341–377.

- Isidro-Llobet, A., Álvarez, M., and Albericio, F. (2009). Amino acid-protecting groups. *Chem. Rev.* 109, 2455–2504. doi: 10.1021/cr800323s
- Jensen, C., Li, H., Vestergaard, M., Dalsgaard, A., Frees, D., and Leisner, J. J. (2020). Nisin damages the septal membrane and triggers DNA condensation in methicillin-resistant *Staphylococcus aureus*. *Front. Microbiol.* 11:1007. doi: 10.3389/fmicb.2020.01007
- Kang, J., Dietz, M. J., and Li, B. (2019). Antimicrobial peptide LL-37 is bactericidal against *Staphylococcus aureus* biofilms. *PLoS One* 14:e0216676. doi: 10.1371/journal.pone.0216676
- Kumar, A., Dhar, K., Kanwar, S. S., and Arora, P. K. (2016). Lipase catalysis in organic solvents: advantages and applications. *Biol. Proced. Online* 18, 1–11. doi: 10.1186/s12575-016-0033-2
- Limón, R., Peñas, E., Torino, M., Martínez-Villaluenga, C., Dueñas, M., and Frias, J. (2015). Fermentation enhances the content of bioactive compounds in kidney bean extracts. *Food Chem.* 172, 343–352. doi: 10.1016/j.foodchem.2014.09.084
- Liu, F., Baggerman, G., Schoofs, L., and Wets, G. (2008). The construction of a bioactive peptide database in metazoan. *J. Proteome Res.* 7, 4119–4131. doi: 10.1021/pr800037n
- Malfertheiner, P., Megraud, F., O'Morain, C. A., Gisbert, J. P., Kuipers, E. J., Axon, A. T., et al. (2017). Management of *Helicobacter pylori* infection—the Maastricht V/Florence consensus report. *Gut* 66, 6–30. doi: 10.1136/gutjnl-2016-312288
- Marcus, E. A., Sachs, G., and Scott, D. R. (2016). Eradication of *Helicobacter pylori* infection. *Curr. Gastroenterol. Rep.* 18, 33–15. doi: 10.1007/s11894-016-0509-x
- McLean, D. T., Lundy, F. T., and Timson, D. J. (2013). IQ-motif peptides as novel antimicrobial agents. *Biochimie* 95, 875–880. doi: 10.1016/j.biochi.2012.12.004
- Neshani, A., Zare, H., Eidgahi, M. R. A., Kakhki, R. K., Safdari, H., Khaledi, A., et al. (2018). LL-37: review of antimicrobial profile against sensitive and antibiotic-resistant human bacterial pathogens. *Gene Rep.* 17:100519. doi: 10.1016/j.genrep.2019.100519
- Origone, A., Barberis, S., Illanes, A., Guzmán, F., Camí, G., Liggieri, C., et al. (2020). Improvement of enzymatic performance of *Asclepias curassavica* L. proteases by immobilization. Application to the synthesis of an antihypertensive peptide. *Process Biochem.* 95, 36–46. doi: 10.1016/j.procbio.2020.05.013
- Origone, A., Bersi, G., Illanes, A., Sturniolo, H., Liggieri, C., Guzmán, F., et al. (2018). Enzymatic and chemical synthesis of new anticoagulant peptides. *Biotechnol. Prog.* 34, 1093–1101. doi: 10.1002/btpr.2658
- Ortiz-Martínez, M., Winkler, R., and García-Lara, S. (2014). Preventive and therapeutic potential of peptides from cereals against cancer. *J. Proteome* 111, 165–183. doi: 10.1016/j.jprot.2014.03.044
- Ozturk, O., Doganay, L., Colak, Y., Yilmaz Enc, F., Ulasoglu, C., Ozdil, K., et al. (2017). Therapeutic success with bismuth-containing sequential and quadruple regimens in *Helicobacter pylori* eradication. *Arab J. Gastroenterol.* 18, 62–67. doi: 10.1016/j.ajg.2017.05.002
- Priolo, N., Arribé, M. C., Caffini, N., Barberis, S., Nieto Vázquez, R., and Luco, J. M. (2001). Isolation and purification of cysteine peptidases from the latex of *Araujia hortorum* fruits. Study of their esterase activities using partial least-squares (PLS) modeling. *J. Mol. Catal. B Enzym.* 15, 177–189. doi: 10.1016/S1381-1177(01)00022-4
- Quiroga, E., Camí, G., Marchese, J., and Barberis, S. (2007). Organic solvents effect on the secondary structure of araujiain hI, in different media. *Biochem. Eng. J.* 35, 198–202. doi: 10.1016/j.bej.2007.01.014
- Quiroga, E., Priolo, N., Marchese, J., and Barberis, S. (2006). Behaviour of araujiain, a new cysteine phytoprotease, in organic media with low water content. *Electron. J. Biotechnol.* 9, 18–25. doi: 10.2225/vol9-issue1-fulltext-6
- Sabillón, L., Stratton, J., Rose, D. J., Flores, R. A., and Bianchini, A. (2016). Reduction in microbial load of wheat by tempering with organic acid and saline solutions. *Cereal Chem.* 93, 638–646. doi: 10.1016/j.jfoodmicro.2019.108381
- Sarin, V. K., Kent, S. B., Tam, J. P., and Merrifield, R. B. (1981). Quantitative monitoring of solid-phase peptide synthesis by the ninhydrin reaction. *Anal. Biochem.* 117, 147–157. doi: 10.1016/0003-2697(81)90704-1
- Schechter, I., and Berger, A. (1967). On the size of the active site in proteases. I. *Papain. Biochem. Biophys. Res. Commun.* 27, 157–162. doi: 10.1016/0003-2697(81)90704-1
- Scopes, R. K. (1994). *Separation by precipitation*. (New York: Springer-Verlag) 85–91.
- Shtatland, T., Guettler, D., Kossodo, M., Pivovarov, M., and Weissleder, R. (2007). PepBank a database of peptides based on sequence text mining and public peptide data sources. *BMC Bioinform.* 8, 1–10. doi: 10.1186/1471-2105-8-280
- Soares, I., Rodrigues, I., da Costa, P. M., and Gales, L. (2023). Antibacterial and antibiofilm properties of self-assembled dipeptide nanotubes. *Int. J. Mol. Sci.* 24:328. doi: 10.3390/ijms24010328
- Talia, J. M., Debattista, N. B., and Pappano, N. B. (2009). *Staphylococcus aureus* strains susceptibility against oxacillin–2,4-dihydroxychalcone combinations. *Folia Microbiol.* 54, 516–520. doi: 10.1007/s12223-009-0074-x
- Talia, J. M., Debattista, N., and Pappano, N. (2011). New antimicrobial combinations: substituted chalcones-oxacillin against methicillin resistant *Staphylococcus aureus*. *Braz. J. Microbiol.* 42, 470–475. doi: 10.1590/S1517-83822011000200010
- Talia, J. M., Tonn, C. E., Debattista, N. B., and Pappano, N. B. (2012). Antibacterial efficacy of dihydroxylated chalcones in binary and ternary combinations with nalidixic acid and nalidixic acid–rutin against *Escherichia coli* ATCC 25922. *Indian J. Microbiol.* 52, 638–641. doi: 10.1007/s12088-012-0302-y
- Thomas, S., Karnik, S., Shankar Barai, R., Jayaraman, V. K., and Idicula-Thomas, S. (2010). CAMP: a useful resource for research on antimicrobial peptides. *Nucleic Acids Res.* 38, D774–D780. doi: 10.1093/nar/gkp1021
- Vallés, D., Bruno, M., López, L. M. I., Caffini, N. O., and Cantera, A. M. (2008). Granulosain I, a cysteine protease isolated from ripe fruits of *Solanum granuloso-leprosum* (Solanaceae). *Protein J.* 27, 267–275. doi: 10.1007/s10930-008-9133-4
- Vallés, D., Furtado, S., Villadóniga, C., and Cantera, A. M. B. (2004). Characterisation, stabilisation and possible biotechnological applications of new proteolytic enzymes from *Solanum granuloso-leprosum*. *Int. J. Biotechnol.* 6, 346–360. doi: 10.1504/IJBT.2004.005517
- Wakasa, Y., Tamakoshi, C., Ohno, T., Hirose, S., Goto, T., Nagaoka, S., et al. (2011). The hypocholesterolemic activity of transgenic rice seed accumulating lactostatin, a bioactive peptide derived from bovine milk β -lactoglobulin. *J. Agric. Food Chem.* 59, 3845–3850. doi: 10.1021/jf200044j
- Wall, R. J., Kerr, D. E., and Bondioli, K. R. (1997). Transgenic dairy cattle: genetic engineering on a large scale. *J. Dairy Sci.* 80, 2213–2224. doi: 10.3168/jds.S0022-0302(97)76170-8
- Wang, G., Li, X., and Wang, X. L. Z. (2017). APD3: the antimicrobial peptide database as a tool for research and education. *Nucleic Acids Res.* 44, D1087–D1093. doi: 10.1093/nar/gkv1278
- Wanka, L., Cabrele, C., Vanejews, M., and Schreiner, P. R. (2007). γ -Aminoadamantane carboxylic acids through direct C–H bond amidations. *Eur. J. Org. Chem.* 2007, 1474–1490. doi: 10.1002/ejoc.200600975
- World Health Organization. (2010). *JECFA*. Geneva: World Health Organization.
- World Health Organization. (2022). Report signals increasing resistance to antibiotics in bacterial infections in humans and need for better data. Available at: <https://www.who.int/news/item/09-12-2022-report-signals-increasing-resistance-to-antibiotics-in-bacterial-infections-in-humans-and-need-for-better-data> (accessed December 9, 2022).
- Xiong, M., Bao, Y., Xu, X., Wang, H., Han, Z., Wang, Z., et al. (2017). Selective killing of *Helicobacter pylori* with pH-responsive helix–coil conformation transitional antimicrobial polypeptides. *Proc. Natl. Acad. Sci. U. S. A.* 114, 12675–12680. doi: 10.1073/pnas.1710408114
- Yu, S. W. B., and Rao, S. S. C. (2014). Advances in the management of constipation-predominant irritable bowel syndrome: the role of linacotide. *Ther. Adv. Gastroenterol.* 7, 193–205. doi: 10.1177/1756283X14537882
- Zhang, L., Hapon, M. B., Goyeneche, A. A., Srinivasan, R., Gamarrá-Luques, C. D., Callegar, E. A., et al. (2016). Mifepristone increases mRNA translation rate, triggers the unfolded protein response, increases autophagic flux, and kills ovarian cancer cells in combination with proteasome or lysosome inhibitors. *Mol. Oncol.* 10, 1099–1117. doi: 10.1016/j.molonc.2016.05.001



OPEN ACCESS

EDITED BY

Guangshun Wang,
University of Nebraska Medical Center,
United States

REVIEWED BY

Theresa Li-Yun Chang,
Rutgers, The State University of New Jersey,
United States
Gill Diamond,
University of Louisville, United States

*CORRESPONDENCE

Li Wu
✉ wuli211@163.com

[†]These authors have contributed equally to this work

RECEIVED 06 April 2023

ACCEPTED 16 May 2023

PUBLISHED 05 June 2023

CITATION

Guo X, An Y, Tan W, Ma L, Wang M, Li J, Li B, Hou W and Wu L (2023) Cathelicidin-derived antiviral peptide inhibits herpes simplex virus 1 infection. *Front. Microbiol.* 14:1201505. doi: 10.3389/fmicb.2023.1201505

COPYRIGHT

© 2023 Guo, An, Tan, Ma, Wang, Li, Li, Hou and Wu. This is an open-access article distributed under the terms of the [Creative Commons Attribution License \(CC BY\)](#). The use, distribution or reproduction in other forums is permitted, provided the original author(s) and the copyright owner(s) are credited and that the original publication in this journal is cited, in accordance with accepted academic practice. No use, distribution or reproduction is permitted which does not comply with these terms.

Cathelicidin-derived antiviral peptide inhibits herpes simplex virus 1 infection

Xiaomin Guo^{1†}, Yanxing An^{1†}, Wanmin Tan², Ling Ma²,
Mingyang Wang², Juyan Li², Binghong Li², Wei Hou¹ and Li Wu^{2*}

¹College of Veterinary Medicine, Shanxi Agricultural University, Jinzhong, China, ²Department of Medical Imaging, First Affiliated Hospital of Kunming Medical University, Kunming, China

Herpes simplex virus 1 (HSV-1) is a widely distributed virus. HSV-1 is a growing public health concern due to the emergence of drug-resistant strains and the current lack of a clinically specific drug for treatment. In recent years, increasing attention has been paid to the development of peptide antivirals. Natural host-defense peptides which have uniquely evolved to protect the host have been reported to have antiviral properties. Cathelicidins are a family of multi-functional antimicrobial peptides found in almost all vertebrate species and play a vital role in the immune system. In this study, we demonstrated the anti-HSV-1 effect of an antiviral peptide named WL-1 derived from human cathelicidin. We found that WL-1 inhibited HSV-1 infection in epithelial and neuronal cells. Furthermore, the administration of WL-1 improved the survival rate and reduced viral load and inflammation during HSV-1 infection via ocular scarification. Moreover, facial nerve dysfunction, involving the abnormal blink reflex, nose position, and vibrissae movement, and pathological injury were prevented when HSV-1 ear inoculation-infected mice were treated with WL-1. Together, our findings demonstrate that WL-1 may be a potential novel antiviral agent against HSV-1 infection-induced facial palsy.

KEYWORDS

cathelicidins, antiviral peptide, HSV-1, facial palsy, WL-1

1. Introduction

Herpes simplex virus 1 (HSV-1), a member of the family Herpesviridae, subfamily Alphaherpesvirinae, is an enveloped virus with a double-stranded (ds) DNA genome consisting of a non-spherical capsid, cortex, and capsule (Whitley and Roizman, 2001; Rechenchoski et al., 2017). HSV-1 is a ubiquitous but important human pathogen. Recent epidemiologic studies estimate that over half of the world's population is infected with HSV-1, making it a global health concern (James et al., 2020; Imafuku, 2023). HSV-1 initially prefers to infect the genital and oral mucosa. Painful blisters or ulcers at the site of infection are caused by contagious and long-lasting infections. The virus can then migrate to the sensory ganglia and enter the latent stage, preventing clearance by the immune system (McQuillan et al., 2018). In brief, HSV-1 infection begins with primary infection in the periphery, followed by lifelong latency in the peripheral nervous system, which can cause various clinical signs and symptoms, such as skin lesions, acute retinal necrosis, genital sores, and other pathologies (Khalesi et al., 2023). Furthermore, HSV-1 can cause fatal systemic infections or encephalitis, problems typically most associated with immune naive or immunocompromised patients (Imafuku, 2023). HSV-1 has been reported to be the most common cause of infectious blindness and fatal encephalitis worldwide. It can also cause

Bell's palsy when it infects the facial nerve, an acute spontaneous facial paralysis that accounts for 50–70% of all peripheral facial paralysis (Imafuku, 2023; Khalesi et al., 2023). Reactivation of latent HSV-1 infection in the geniculate ganglion is considered a major cause of Bell's palsy. Approximately 30% of patients with Bell's palsy are still at risk for continued facial paralysis and pain, while most people can recover fully on their own (Zhang et al., 2023). The majority of treatment drugs for HSV-1 are acyclovir, a nucleoside analog, and its derivatives, as these compounds are activated by the viral thymidine kinase (TK) and inhibit the viral polymerase, resulting in preventing the production of infectious virions (Aribi Al-Zoobae et al., 2020; Stoyanova et al., 2023). The latent stage and the development of resistance are limitations to the use of these drugs. However, ACV can be responsible for renal cytotoxicity with acute renal failure requiring dialysis (Neto et al., 2007). Additionally, the drug-resistant HSV-1 strains, especially acyclovir-resistant strains, which are related to mutations of the viral TK or DNA polymerase genes, have been the major challenges facing HSV-1 treatment (Gu et al., 2014). Consequently, new cure strategies are needed, and to do so, it is necessary to develop new effective anti-HSV-1 drugs.

Antimicrobial peptides have received increasing attention from the scientific community over the last 20 years due to the worldwide increase in antibiotic resistance among microorganisms. At present, more than 3,200 natural antimicrobial peptides have been reported in the antimicrobial peptide database (<https://aps.unmc.edu>). Antimicrobial peptides (AMPs) are molecules present in the innate immune system of almost all living organisms, invertebrates, and vertebrates and have been identified as potential agents with therapeutic potential as they exhibit marked antibacterial, antiviral, antiparasitic, and antifungal properties (Zasloff, 2002; Barashkova and Rogozhin, 2020; Memariani et al., 2020; De Angelis et al., 2021). Cathelicidin is a member of the AMPs family, which is a part of the immune system and can be produced by a variety of eukaryotic organisms (Chessa et al., 2020). They are well-conserved during genome evolution and have similar modes of action (Zhang et al., 2023). Cathelicidins have revealed potent antimicrobial activity against bacteria and viruses, which has gradually become an interesting and promising research topic (Cebrián et al., 2023). Cathelicidins are characterized by two functional domains, namely the conserved cathelin-like proregion and the N-terminal active domain region (Kościuczuk et al., 2012). Several studies have demonstrated that cathelicidins exhibit potent anti-endotoxin properties *in vitro* and *in vivo*, both by binding bacterial LPS and by intervening in TLR signaling mechanisms (Rosenfeld et al., 2006). Their antiviral mechanisms include the inhibition of viral entry, intracellular viral replication, and assembly and induction of the immune response. For instance, CRAMP, a cathelicidin identified in mouse, can affect the survival and replication of the influenza A virus (IAV) in host cells by directly disrupting the IAV envelope (Gallo et al., 1997). PG-1, an antimicrobial peptide of the cathelicidins family, has been reported to inhibit viral infection by blocking the adsorption of porcine reproductive and respiratory syndrome virus (PRRSV) on embryonic kidney cells of African green monkey (Guo et al., 2015). In addition, they show a lower tendency to induce resistance than conventional bacterial antibiotics (Mehmood Khan et al., 2023). As a consequence, they are a new generation of antiviral biomolecules with very low

toxicity to human host cells and play a role in the treatment of a variety of diseases and symptoms, which can be considered an appropriate choice for the treatment of resistant pathogens in the future (Chen et al., 2013; AlMukdad et al., 2023; Baidara et al., 2023).

LL-37, a peptide derived from the human cathelicidin, has been shown to resist HSV-1 infection (Lee et al., 2014; Roy et al., 2019), whereas LL-37 is limited in its therapeutic use due to its length of 37 residues, resulting in high chemical synthesis costs. Herein, we designed a 16-amino acid peptide, WL-1, which is based on human cathelicidin LL-37 and its fragments (Li et al., 2006; He et al., 2018). Moreover, we displayed the antiviral activity of WL-1 against HSV-1 infection. Furthermore, the administration of WL-1 ameliorated the pathological symptoms of inflammation and facial paralysis induced by HSV-1 infection. In summary, this study shows that WL-1 may be a potent agent candidate against HSV-1 infection.

2. Materials and methods

2.1. Mice

C57 female mice (8-week-old, weighing 17–19 g) were purchased from SPF (Beijing, China) Biotechnology Co., Ltd. Mice were group-housed at room temperature and a 12-h light/dark cycle, with free access to water and standard animal food. The animal care and experimental protocol were approved by the Animal Care Committee of Shanxi Agricultural University, approval number: SXAU-EAW-2022M.RX.00906001.

2.2. Cells, viruses, and peptides

U251 cells and Vero cells were obtained from the Kunming Cell Bank, Kunming Institute of Zoology, Chinese Academy of Sciences. All cells were cultured in a DMEM medium (Gibco, Waltham, MA, USA) supplemented with 10% fetal bovine serum (FBS), 100 U/mL of penicillin, and 100 µg/ml of streptomycin in 5% CO₂ at 37°C. HSV-1 was stored at –80°C in our laboratory. The peptide WL-1 (GWKRIKQRIKDKLRNL) was designed based on human cathelicidin LL-37 and the existing derived GF-17 (He et al., 2018). Three residues were redesigned (F2W, V6K, and F12K), and one residue was removed (V17) in combination with C-terminal amidation (-NH₂) compared to GF-17. It was synthesized by GL Biochem (Shanghai) Ltd. (Shanghai, China). The peptide was analyzed by reversed-phase high-performance liquid chromatography (RP-HPLC) and mass spectrometry. The purity of WL-1 was over 98%.

2.3. Cytotoxicity assay

The cytotoxicity of WL-1 was tested on U251 and Vero cells. The cells were seeded in a 96-well plate with 2×10^5 cells/ml for 12 h, and a certain amount of WL-1 was added (the final concentration increased gradually in the range of 0–250 µM). After incubation for 24 h, cell viability was evaluated by conventional 3-(4,5-dimethyl-2-thiazolyl)-2, 5-diphenyl-2H-tetrazolium bromide

(MTT) reduction assays. In detail, 20 μ l of MTT (5 mg/mL) was added to each well. The MTT solution was then removed, and 200 μ l dimethyl sulfoxide (DMSO) was added to solubilize the MTT-formazan crystals in living cells. The absorbance at 570 nm of the resulting solution was measured.

2.4. Plaque-forming assays

HSV-1 (MOI = 0.1) was first co-cultured with different concentrations of WL-1 (0, 2, 10, and 50 μ M) or acyclovir (50 μ M) for 2 h and then diluted to infect Vero cells. The maintenance medium containing 1% methylcellulose was used to replace the cell culture medium. After 3 days of incubation, 10% formalin was used to fix the cells, and 1% crystal violet was subsequently used to stain the cells. Finally, the plaque-forming units were counted.

2.5. Cell infection

Vero and U251 cells were seeded in a 12-well plate with 5×10^5 cells/well for 12 h and then infected with HSV-1 at 0.1 MOI combined with WL-1 (0, 2, 10, 50 μ M) or acyclovir (50 μ M) administration for 24 h. Cells were then lysed in a TRIzol reagent (TIANGEN, Beijing, China), and the total RNA was extracted under the manufacturer's instructions. The relative expression levels of HSV-1 (HSV-1, UL27, UL52, and UL54) were detected by RT-qPCR using GAPDH as a reference gene.

2.6. Quantitative real-time PCR (RT-qPCR)

For the RT-qPCR analysis, total RNA was isolated from cells, and cDNA was reverse-transcribed by using M-MLV reverse transcriptase (Promega, Madison, WI, USA). RT-qPCR was performed on the StepOnePlus Real-Time PCR Systems (Thermo, Waltham, MA, USA). The primers used are shown in Table 1 (Liu et al., 2023). Primer was designed to target the ICP0 gene of HSV-1 to represent virus replication.

2.7. Mice infection

For ocular scarification infection reported in other studies (Li et al., 2016), mice were divided into four groups: HSV-1 only as the model group, HSV-1 and WL-1 (5 mg/kg) as the experimental group, HSV-1 and acyclovir (5 mg/kg) as the positive control group, and PBS as the negative control group. The infection dose of HSV-1 was 4×10^4 plaque forming units (PFU). WL-1 was treated via tail vein injection after 1 h of HSV-1 infection. Mice were weighed and monitored daily over time. The survival rate of mice was observed by day 20. Mice were euthanized on day 5 after infection, and brains were harvested to determine the viral burden by plaque assay. In addition, enzyme-linked immunosorbent assay (ELISA) was used to detect the content of inflammatory factors in serum and brain.

Moreover, HSV-1 infection via ear inoculation was used to induce facial paralysis (Takahashi et al., 2001). Following anesthesia

with an intraperitoneal injection of sodium pentobarbital (50 mg/kg), the posterior surface of the left auricle was scratched 20 times with a 27-gauge needle, and then, 25 μ l of virus solution (1.0×10^6 PFU) was placed on the scratched area. The negative control group was injected with normal saline, and the positive control group and the experimental group were injected with HSV-1. Then, the experimental group was treated with WL-1 (5 mg/kg) via tail vein injection after 1 h of HSV-1 infection. Next, blink reflex, vibrissae movements, and nose tip position were carefully observed every 12 h so as to evaluate the facial paralysis. The blink reflex was performed by blowing air into the eye at a distance of 2 cm away from the eye by the use of a 5 ml syringe without a needle, and the movement and closure condition of the eyelid were observed. The time of vibrissa movement of the inoculated side in 30 s was counted, compared with that of the contralateral side. Meanwhile, the nose tip position was recorded. After 72 h, tissue from the facial nerve and its connection to the brain was cut and observed. We also performed an inflammatory score.

2.8. ELISA

The brains of infected mice as described above were excised and then homogenized in 0.9% NaCl with a glass homogenizer. The supernatant was collected after centrifugation at 2,000 g for 15 min. The serum was obtained by centrifugation of blood at 3,000 rpm for 10 min. The concentration of TNF- α and IL-6 in the supernatant and serum harvested above was measured by using enzyme-linked immunosorbent assay kits (Dakewe, Beijing, China) according to the manufacturer's instructions.

2.9. Statistical analysis

Data are given as mean \pm SEM. Statistical analysis was performed using a two-tailed Student's *t*-test and log-rank test. A *p*-value of < 0.05 was considered to be statistically significant.

3. Results

3.1. Cytotoxicity of WL-1

To distinguish antiviral activity from cellular toxicity, the cytotoxicity of WL-1 was tested on various HSV-1 host cells, including neuronal cell (U251) and epithelial cell (Vero; Figure 1). Cells were treated with different concentrations of WL-1 (0, 0.4, 2, 10, 50, and 250 μ M) for 24 h, and the cell viability was analyzed by MTT assays. We found that the cell viability was reduced by no more than 10% by 50 μ M WL-1 in all cell lines, which suggested that WL-1 did not exert toxic effects on cells up to 50 μ M concentration. Therefore, a concentration of WL-1 below 50 μ M was used for the subsequent research.

TABLE 1 Sequences of primers used for RT-qPCR.

Gene	Forward (5'-3')	Reverse (5'-3')
HSV-1 (ICP0)	CCCACTATCAGGTACACCAGC	CTGCGCTGCGACACCTTTT
UL27	GCCTTCTTCGCCTTTCGC	CGCTCGTGCCCTTCTTCTT
UL52	AGGCCATCAAGGACATCTGC	AATACGGCGCTCCACGTAAA
UL54	TGGCGGACATTAAGGACATTG	TGGCCGTCAACTCGCAGA
GAPDH	CACCATCTTCCAGGAGCGAG	AGAGGGGGCAGAGATGATGA

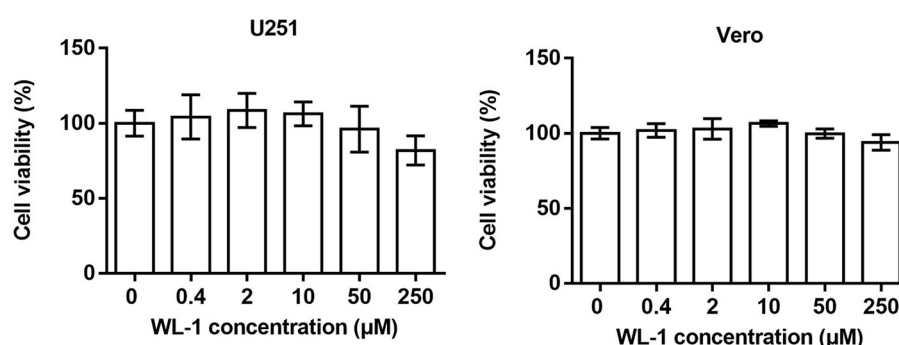


FIGURE 1

Cytotoxicity of WL-1. U251 and Vero cells were treated with increasing concentrations of WL-1 (0, 0.4, 2, 10, 50, and 250 μM), and then, cell viability was detected after 24 h culture by using MTT assays. Data represent three independent experiments and are presented as mean ± SEM.

3.2. WL-1 inhibits HSV-1 infection *in vitro*

To determine whether WL-1 has direct anti-HSV-1 activity, HSV-1 was incubated with different concentrations of WL-1, and plaque assay was performed on Vero cells. As shown in Figure 2A, the viral plaque number was significantly decreased by WL-1 in a dose-dependent manner. Only half of the infectious particles were present in the cells treated with WL-1 at 10 μM concentration with a 50% antiviral activity at this dose, which suggested that WL-1 reduces the viable viral load. In order to further assess the antiviral activity of WL-1, epithelial cells Vero were infected with HSV-1 at 0.1 MOI for 24 h in the presence or absence of WL-1. Acyclovir, a major clinical drug used in the treatment of HSV-1 infection, was chosen as a positive control (Gurgel Assis et al., 2021). Notably, administration of WL-1 decreased the intracellular load of HSV-1 in Vero cells (Figure 2B). To confirm these results, we also examined the antiviral effects of WL-1 on neuronal U251 cells, an HSV-1-sensitive cell line. Similarly, WL-1 significantly inhibited the replication of HSV-1. In addition, RT-qPCR analysis showed that WL-1 markedly reduced the expression of viral late gene UL27, early gene UL52, and immediate early gene UL54. In addition, the effect of HSV-1 inhibition became stronger with increasing WL-1 concentration (Figure 2C). The antiviral activity of WL-1 was equivalent to or even better than that of acyclovir at an equal concentration on all experiment cells. Taken together, these results indicate the strong antiviral effect of WL-1 against HSV-1 infection, which depends on the dose of WL-1 within a certain concentration range.

3.3. WL-1 suppresses HSV-1 infectivity in mice

To define the role of WL-1 against HSV-1 infection *in vivo*, wild-type mice were infected with 4×10^4 PFU of HSV-1 to each eye (via ocular scarification) with or without WL-1 administration, and survival was monitored over time. Mortality of normal infected mice occurred at 3 days postinfection, while infected mice with WL-1 administration began to die at 4 days postinfection. In addition, the survival rate of HSV-1-infected mice in the presence of WL-1 was ~90% by day 20, which was markedly higher than that of mice without WL-1 administration (Figure 3A). To investigate whether the attenuated pathogenesis noted above was due to a decreased burden of HSV-1 in the mouse with WL-1 administration, we analyzed viral loads of HSV-1 in the brain after 2 days of infection. Plaque assay revealed that a lower level of virus titer was observed in the brain of HSV-1-infected mice following the administration of WL-1 than those mice in the absence of WL-1 (Figure 3A). Moreover, we detected the content of inflammatory cytokines in the peripheral blood and brain, which is a hallmark of the immune response to pathogenic infection. Strikingly, the production of inflammatory cytokines IL-6 and TNF-α in mice induced by HSV-1 infection was substantially reduced in the presence of WL-1 or acyclovir in the peripheral blood (Figure 3B). In line with these findings, the production of IL-6 and TNF-α in the brain was significantly decreased by the administration of WL-1 or acyclovir during infection with HSV-1 (Figure 3C). Overall, HSV-1 infection in the presence of WL-1 administration resulted in increased survival and decreased replication and inflammation in

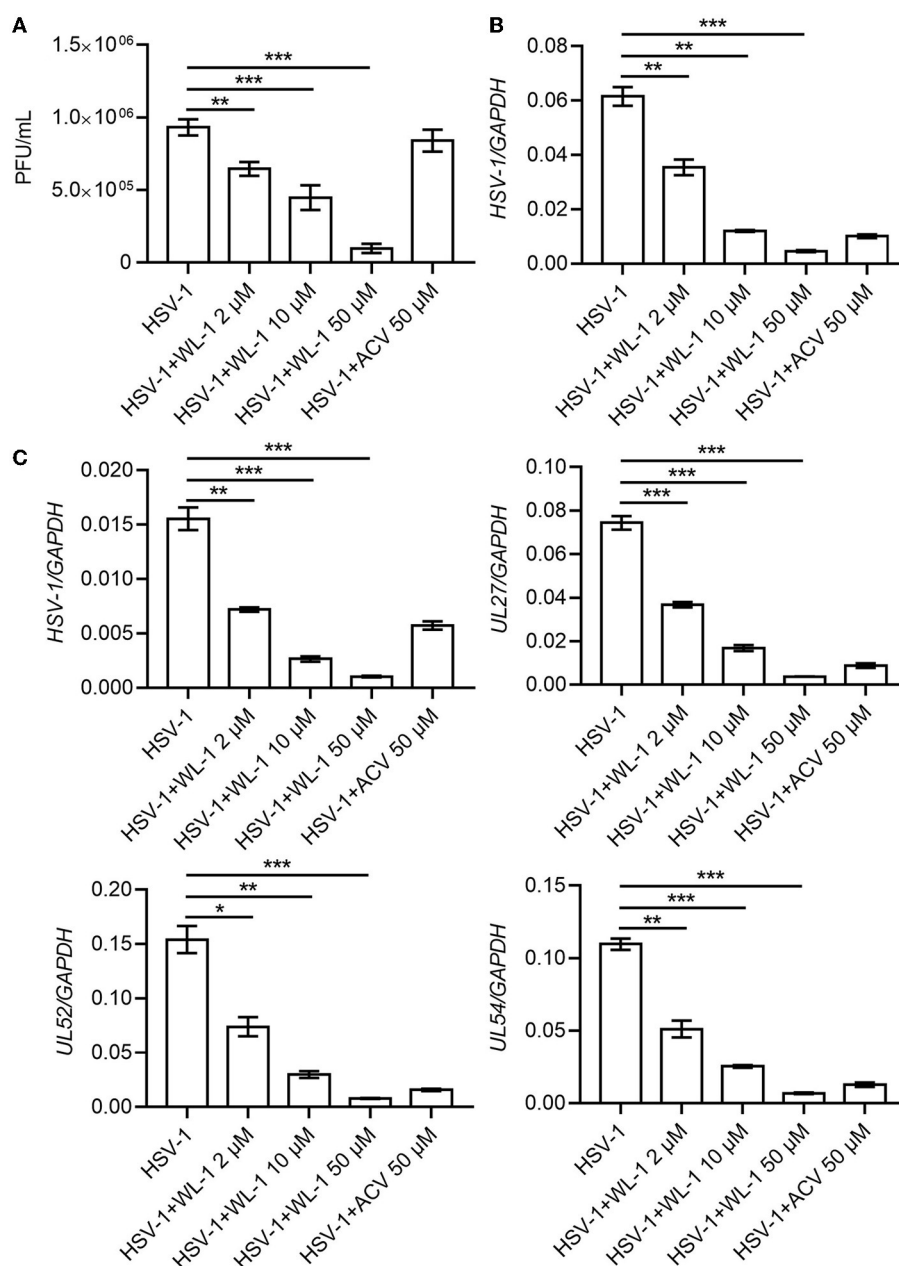


FIGURE 2

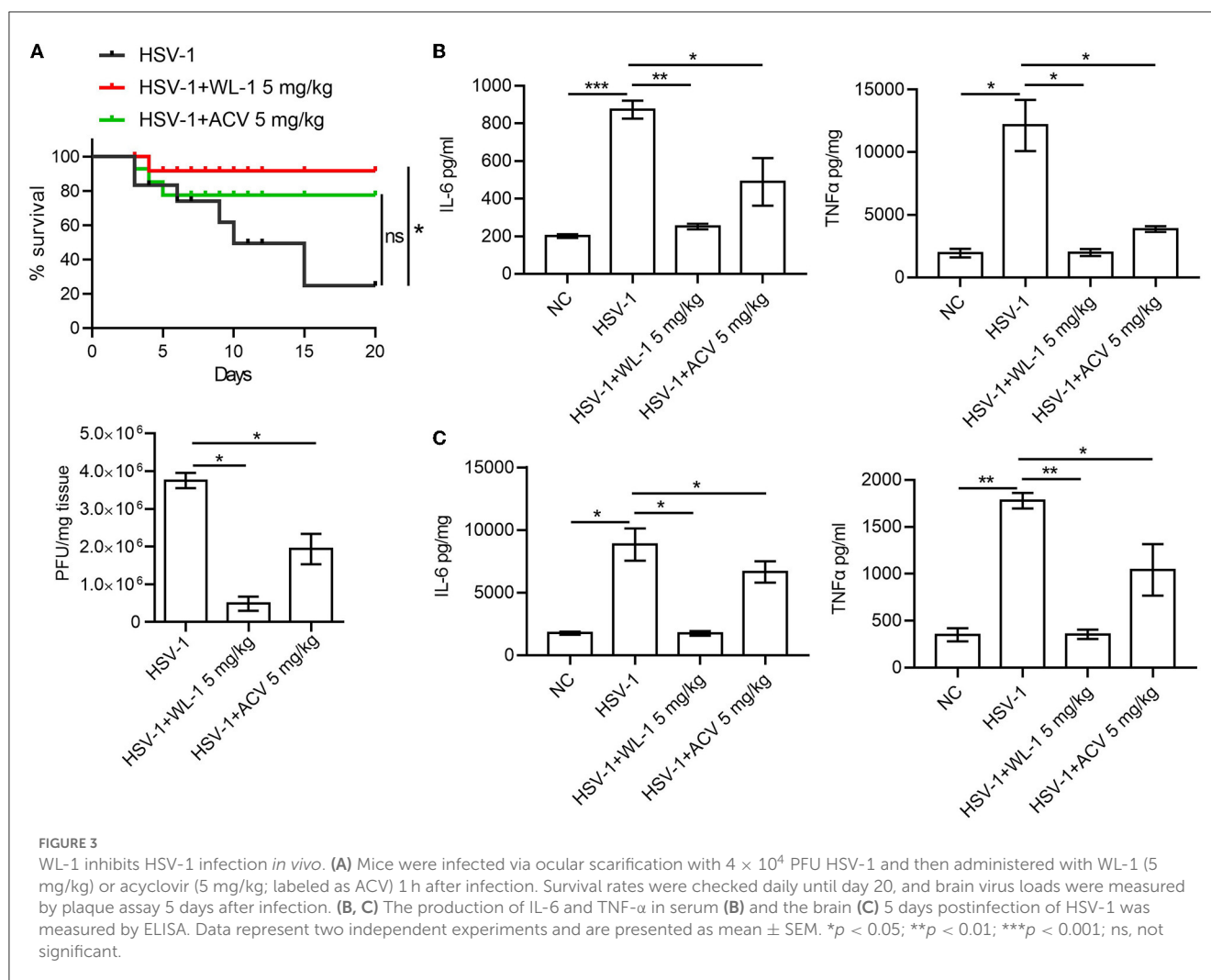
WL-1 inhibits HSV-1 in cells. (A) The HSV-1 (MOI = 0.1) virus was co-cultured with different concentrations of WL-1 or acyclovir (labeled as ACV) for 2 h, and then, plaque-forming units were detected. (B) Vero cells were infected with HSV-1 (MOI = 0.1) with different concentrations of WL-1 or ACV for 24 h, and the viral gene was analyzed by RT-qPCR. (C) U251 cells were infected with HSV-1 (MOI = 0.1) with different concentrations of WL-1 (0, 2, 10, and 50 μM) or acyclovir (labeled as ACV) for 24 h, and the viral genes were analyzed by RT-qPCR. Data represent three independent experiments and are presented as mean ± SEM. * $p < 0.05$; ** $p < 0.01$; *** $p < 0.001$.

the host, suggesting that the WL-1 has the ability to suppress HSV-1 infection.

3.4. WL-1 prevents facial palsy induced by HSV-1

Published studies report that HSV-1 can infect the host in various manners to cause different symptoms (Honda et al., 2002;

Kastrukoff et al., 2012; Lee et al., 2015; Caliento et al., 2018). An animal disease model of HSV-1 infection has been developed to study Bell's palsy caused by HSV-1 reactivation. To examine whether the protective role of WL-1 on HSV-1 was specific to the infection method and whether WL-1 also had an effect on facial palsy, HSV-1 was infected via ear inoculation known to induce facial palsy with the administration of WL-1 and facial nerve function indicators were evaluated up to day 3. As reported, HSV-1 infection resulted in a series of facial nerve dysfunctions, including



loss of blink reflex, unnatural nose position, and weakness of vibrissae movement. There was no significant difference in the time to onset of abnormal blink reflex between the WL-1 administration and the control group. Instead, the ratio of the normal blink reflex in WL-1 treated mice was significantly higher than that in untreated mice. The nose tip position and vibrissae movement of HSV-1 alone infected mice were abnormal from the 36th h postinfection, but almost all the WL-1 treated mice were normal throughout the infection period. In addition, the administration of WL-1 also markedly increased the percentage of mice with normal nose position and vibrissae movement 3 days after HSV-1 infection (Figure 4A). Histopathologic examination of the facial nerve displayed that mouse treated with WL-1 had a lower HSV-1-induced inflammation score, indicating that WL-1 reduced facial nerve injury (Figure 4B). Taken together, our results indicated that WL-1 can resist viral infection and thereby prevent the occurrence of facial paralysis.

4. Discussion

HSV-1 causes a wide range of infections from mild to life-threatening in the human population. There are effective

treatments for HSV-1 infections, which are limited due to HSV-1 latency and the development of resistance to current therapeutics. It is urgent to develop new specific agents against HSV-1 infection due to the universality of HSV-1 infection and the limitations of existing clinical drugs (Sadowski et al., 2021). Antimicrobial peptides (AMPs) are widely distributed in many species and represent highly effective natural defenses that are central weapons for the host to resist infection (Nizet, 2006; Mookherjee and Hancock, 2007; Rossi et al., 2012). They have different mechanisms of action from traditional antibiotics, showing potent and broad-spectrum antibacterial, antifungal, and antiviral activities and are not easy to induce drug resistance (Neto et al., 2007; Aribi Al-Zoobaee et al., 2020). The cathelicidin family is one of the most important AMPs in the host immune defense system. So far, some of the cathelicidin-related drugs are undergoing clinical trials, indicating that cathelicidins have great potential to be developed as new antimicrobial drugs as alternatives to traditional antibiotics and medicines (Steintraesser et al., 2011; Wang et al., 2019; Mookherjee et al., 2020; Díez-Aguilar et al., 2021; Bhattacharjya et al., 2022; Talapko et al., 2022). It has been reported that cathelicidins possess many important activities such as broad-spectrum and high antibacterial activity, anti-inflammation, and tissue damage

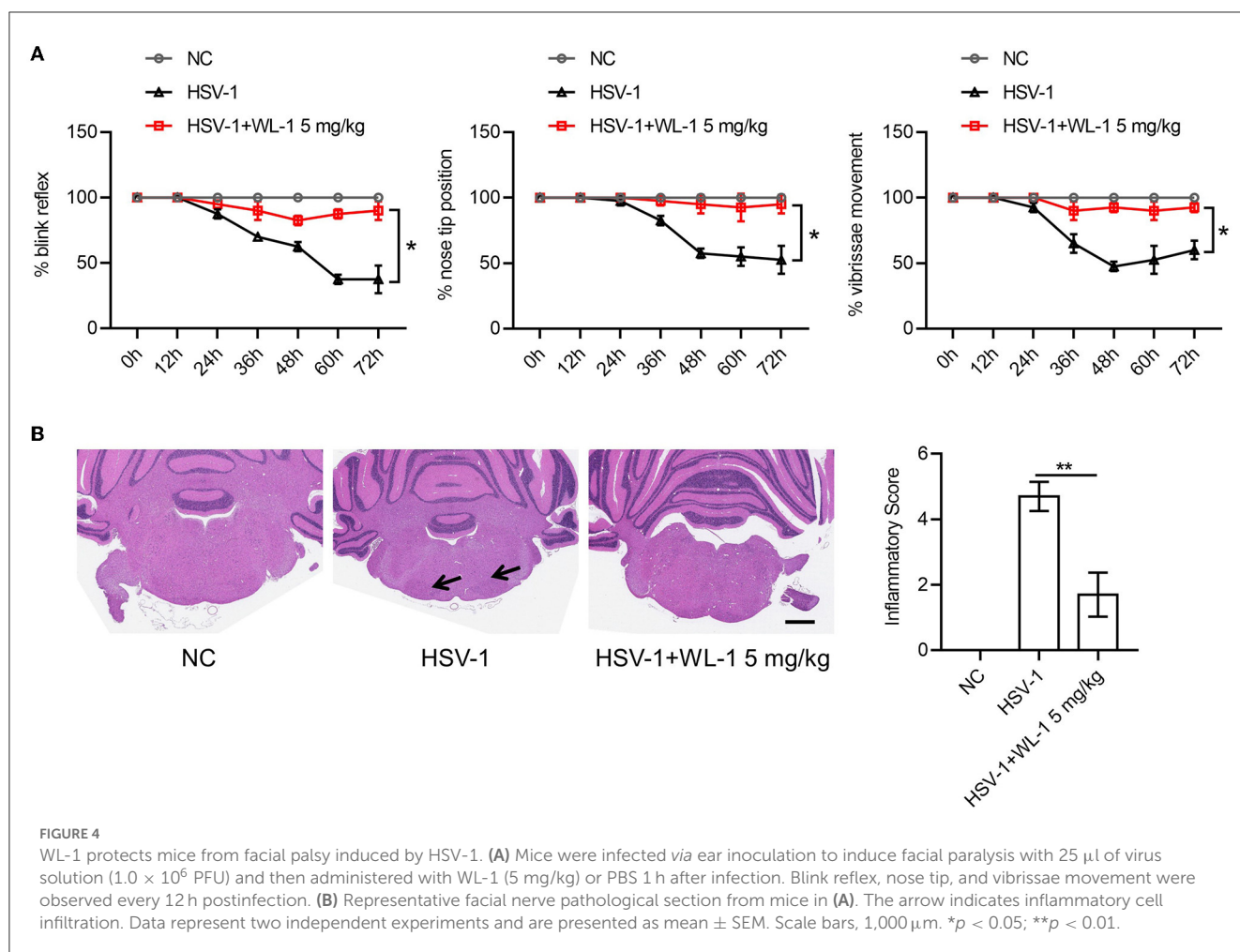


FIGURE 4

WL-1 protects mice from facial palsy induced by HSV-1. (A) Mice were infected *via* ear inoculation to induce facial paralysis with 25 μ l of virus solution (1.0×10^6 PFU) and then administered with WL-1 (5 mg/kg) or PBS 1 h after infection. Blink reflex, nose tip, and vibrissae movement were observed every 12 h postinfection. (B) Representative facial nerve pathological section from mice in (A). The arrow indicates inflammatory cell infiltration. Data represent two independent experiments and are presented as mean \pm SEM. Scale bars, 1,000 μ m. * p < 0.05; ** p < 0.01.

inhibition (Auvynet and Rosenstein, 2009; Nijnik and Hancock, 2009; Wueth and Hancock, 2011; Choi et al., 2012; Kahlenberg and Kaplan, 2013). In fact, a few cathelicidins have been found to have inhibitory effects on various viral infections, including hepatitis C virus, vaccinia virus, and human immunodeficiency virus 1. In this study, we revealed that WL-1, an antiviral peptide derived from cathelicidins with low toxicity, inhibits the HSV-1 infection *in vitro* and *in vivo*, adding antiviral activity to the broad-spectrum function of cathelicidins. Specifically, WL-1 can not only restrain viral replication but also prevent the pathological symptoms induced by HSV-1 infection. In addition, the anti-HSV-1 effect of WL-1 is superior to acyclovir, the most clinically used nucleoside analog against HSV-1 infection, at the same concentration. Our data have demonstrated that WL-1 may have great potential to be optimized as an anti-HSV-1 compound. Furthermore, it remains to be evaluated whether WL-1 has similar effects on other HSV-1 strains and DNA viruses.

Viral infection can be resisted in many ways by antimicrobial peptides, drugs, and other small-molecule inhibitors. For example, the antimicrobial peptide CATH-2 has been reported to modulate the inflammatory response by regulating the secretion of inflammatory cytokines and activation of the NLRP3 inflammasome, resulting in protection against IAV infection

(Coorens et al., 2017; Peng et al., 2022). A defense peptide called An1a restricts dengue and Zika virus infection by inhibiting the viral NS2B-NS3 protease (Ji et al., 2019). Acyclovir inhibits the enzymatic activity of HSV thymidine kinase (TK), thereby interrupting viral DNA replication (Vashishtha and Kuchta, 2016; Sadowski et al., 2021). Moreover, Artemisia argyi leaf extract AEE destroys the membrane integrity of HSV-1 viral particles, resulting in impaired viral attachment and penetration (Liu et al., 2023). These results reveal various molecular mechanisms of host-defense peptides against viral infections, including direct viral killing, regulation of viral infection, and participation in host immune regulation against viral infections. We found that WL-1 treatment could reduce viral titer. So that we speculated that WL-1 may have the same anti-HSV-1 infection mechanism as LL-37, which has been described to damage the viral membrane envelope or inhibit HSV-1 adsorption to cells (Howell et al., 2004; Lee et al., 2014). Likewise, the administration of WL-1 obviously reduced the virus load and viral gene expression as well as the inflammatory factors production in cells and mice, which reminds us that WL-1 perhaps participates in the regulation of the viral replication cycle and inflammatory response caused by viral infection. In brief, the mechanism of WL-1 resistance against HSV-1 infection is more complicated and requires further research to discuss.

Today, multiple treatments and drugs have no significant effect on Bell's palsy, the most common form of peripheral facial palsy (Gronseth and Paduga, 2012; Zandian et al., 2014; Newadkar et al., 2016; Zhang et al., 2019). Antivirals and steroids were the most commonly prescribed medications in the early days of Bell's palsy (Jalali et al., 2021). There was no benefit from antiviral therapy alone compared with placebo (Gallo et al., 1997). When researchers compared the effect of steroids with placebo, they found that the reduction in the proportion of patients who did not fully recover at 6 months was small and not statistically significant (Gu et al., 2014). Combined oral steroids and antivirals were associated with a lower rate of incomplete recovery when compared with oral steroids alone (Gallo et al., 1997). Another study showed that patients treated with steroids combined with acyclovir had a higher overall recovery rate than those treated with steroids alone, but the difference was not statistically significant (Yeo et al., 2008). Because acyclovir's bioavailability is relatively low (15–30%), new drugs are being investigated (Newadkar et al., 2016). Surprisingly, we found that WL-1 can not only reduce the viral load of HSV-1 but also prevent the occurrence of facial palsy induced by infection, indicating that WL-1 can be used as a potential drug for treating Bell's palsy. Certainly, further studies are needed to evaluate the effect of WL-1 on Bell's palsy using other models.

5. Conclusion

In summary, the designed peptide WL-1 showed high antiviral abilities against HSV-1 infection and prevented the facial palsy occurrence induced by HSV-1 in mice. Therefore, it may be an excellent candidate or template for the development of a therapeutic agent to treat clinical infection of HSV-1. Much more effort should be made to understand the antiviral mechanism of WL-1.

Data availability statement

The raw data supporting the conclusions of this article will be made available by the authors, without undue reservation.

References

- AlMukdad, S., Harfouche, M., Farooqui, U. S., Aldos, L., and Abu-Raddad, L. J. (2023). Epidemiology of herpes simplex virus type 1 and genital herpes in Australia and New Zealand: Systematic review, meta-analyses, and meta-regressions. *Epidemiol. Infect.* 2023, 1–23. doi: 10.1017/S0950268823000183
- Aribi Al-Zoobae, F. W., Yee Shen, L., Veettil, S. K., Gopinath, D., Maharajan, M. K., and Menon, R. K. (2020). Antiviral agents for the prevention and treatment of herpes simplex virus type-1 infection in clinical oncology: A network meta-analysis. *Int. J. Environ. Res. Public Health* 17, 238891. doi: 10.3390/ijerph17238891
- Auvynet, C., and Rosenstein, Y. (2009). Multifunctional host defense peptides: Antimicrobial peptides, the small yet big players in innate and adaptive immunity. *FEBS J.* 276, 6497–6508. doi: 10.1111/j.1742-4658.2009.07360.x
- Baindara, P., Ganguli, S., Chakraborty, R., and Mandal, S. M. (2023). Preventing respiratory viral diseases with antimicrobial peptide master regulators in the lung airway habitat. *Clin. Pract.* 13, 125–147. doi: 10.3390/clinpract13010012
- Barashkova, A. S., and Rogozhin, E. A. (2020). Isolation of antimicrobial peptides from different plant sources: Does a general extraction method exist? *Plant Methods* 16, 143. doi: 10.1186/s13007-020-00687-1
- Bhattacharjya, S., Mohid, S. A., and Bhunia, A. (2022). Atomic-resolution structures and mode of action of clinically relevant antimicrobial peptides. *Int. J. Mol. Sci.* 23, 94558. doi: 10.3390/ijms23094558
- Caliento, R., Sarmento, D. J. d. S., Silva, É. M. a. P., Tozetto-Mendoza, T. R., Tobouti, P. L., Benini, V., et al. (2018). Oral shedding of HSV-1 and EBV and oral manifestations in paediatric chronic kidney disease patients and renal transplant recipients. *Acta Odontol. Scand.* 76, 539–544. doi: 10.1080/00016357.2018.1437218
- Cebrián, R., Lucas, R., Fernández-Cantos, M. V., Slot, K., Peñalver, P., Martínez-García, M., et al. (2023). Synthesis and antimicrobial activity of aminoalkyl resveratrol derivatives inspired by cationic peptides. *J. Enzyme Inhibit. Med. Chem.* 38, 267–281. doi: 10.1080/14756366.2022.2146685
- Chen, D., Zhang, D., Xu, L., Han, Y., and Wang, H. (2013). The alterations of matrix metalloproteinase-9 in mouse brainstem during herpes simplex virus type 1-induced facial palsy. *J. Mol. Neurosci.* 51, 703–709. doi: 10.1007/s12031-013-0051-3
- Chessa, C., Bodet, C., Jousselin, C., Wehbe, M., Leveque, N., and Garcia, M. (2020). Antiviral and immunomodulatory properties of antimicrobial peptides produced by human keratinocytes. *Front. Microbiol.* 11, 1155. doi: 10.3389/fmicb.2020.01155

Ethics statement

The animal study was reviewed and approved by the Animal Care Committee of Shanxi Agricultural University, approval number: SXAU-EAW-2022M.RX.00906001.

Author contributions

LW and XG: conceptualization and funding acquisition. XG: methodology and writing—original draft preparation. XG, YA, WT, LM, MW, JL, BL, and WH: investigation. LW: resources and writing—review and editing. All authors have read and agreed to the published version of the manuscript.

Funding

This research was funded by the National Natural Science Foundation of China (grant number: 82102409) and the Science and Technology Plan Project, Yunnan Provincial Health Commission (grant number: 202105AD160039).

Conflict of interest

The authors declare that the research was conducted in the absence of any commercial or financial relationships that could be construed as a potential conflict of interest.

Publisher's note

All claims expressed in this article are solely those of the authors and do not necessarily represent those of their affiliated organizations, or those of the publisher, the editors and the reviewers. Any product that may be evaluated in this article, or claim that may be made by its manufacturer, is not guaranteed or endorsed by the publisher.

- Choi, K.-Y., Chow, L. N. Y., and Mookherjee, N. (2012). Cationic host defence peptides: Multifaceted role in immune modulation and inflammation. *J. Innate Immunity* 4, 361–370. doi: 10.1159/000336630
- Coorens, M., Schneider, V. A. F., de Groot, A. M., van Dijk, A., Meijerink, M., Wells, J. M., et al. (2017). Cathelicidins inhibit *Escherichia coli*-induced TLR2 and TLR4 activation in a viability-dependent manner. *J. Immunol.* 199, 1418–1428. doi: 10.4049/jimmunol.1602164
- De Angelis, M., Casciaro, B., Genovese, A., Brancaccio, D., Marcocci, M. E., Novellino, E., et al. (2021). Temporin G, an amphibian antimicrobial peptide against influenza and parainfluenza respiratory viruses: Insights into biological activity and mechanism of action. *FASEB J.* 35, e21358. doi: 10.1096/fj.202001885RR
- Diez-Aguilar, M., Hernández-García, M., Morosini, M.-I., Fluit, A., Tunney, M. M., Huertas, N., et al. (2021). Murepavadin antimicrobial activity against and resistance development in cystic fibrosis *Pseudomonas aeruginosa* isolates. *J. Antimicrob. Chemother.* 76, 984–992. doi: 10.1093/jac/ckaa529
- Gallo, R. L., Kim, K. J., Bernfield, M., Kozak, C. A., Zanetti, M., Merluzzi, L., et al. (1997). Identification of CRAMP, a cathelin-related antimicrobial peptide expressed in the embryonic and adult mouse. *J. Biol. Chem.* 272, 13088–13093. doi: 10.1074/jbc.272.20.13088
- Gronseth, G. S., and Paduga, R. (2012). Evidence-based guideline update: steroids and antivirals for Bell palsy: Report of the Guideline Development Subcommittee of the American Academy of Neurology. *Neurology* 79, 2209–2213. doi: 10.1212/WNL.0b013e318275978c
- Gu, L., Han, Y., Liu, W., Mao, Y., Li, J., and Wang, H. (2014). The expression of IL-2 and IL-4 in CD4(+) T cells from mouse lymph nodes and spleen during HSV-1-induced facial palsy. *Inflamm. Res.* 63, 117–125. doi: 10.1007/s00011-013-0680-6
- Guo, C., Cong, P., He, Z., Mo, D., Zhang, W., Chen, Y., et al. (2015). Inhibitory activity and molecular mechanism of protegrin-1 against porcine reproductive and respiratory syndrome virus *in vitro*. *Antiviral Therapy* 20, 573–582. doi: 10.3851/IMP2918
- Gurgel Assis, M. S., Fernandes Pedrosa, T. C., de Moraes, F. S., Caldeira, T. G., Pereira, G. R., de Souza, J., et al. (2021). Novel insights to enhance therapeutics with acyclovir in the management of herpes simplex encephalitis. *J. Pharmaceut. Sci.* 110, 1557–1571. doi: 10.1016/j.xphs.2021.01.003
- He, M., Zhang, H., Li, Y., Wang, G., Tang, B., Zhao, J., et al. (2018). Cathelicidin-derived antimicrobial peptides inhibit Zika virus through direct inactivation and interferon pathway. *Front. Immunol.* 9, 722. doi: 10.3389/fimmu.2018.00722
- Honda, N., Hato, N., Takahashi, H., Wakisaka, H., Kasaki, H., Murakami, S., et al. (2002). Pathophysiology of facial nerve paralysis induced by herpes simplex virus type 1 infection. *Ann. Otol. Rhinol. Laryngol.* 111, 616–622. doi: 10.1177/000348940211100709
- Howell, M. D., Jones, J. F., Kisich, K. O., Streib, J. E., Gallo, R. L., and Leung, D. Y. M. (2004). Selective killing of vaccinia virus by LL-37: Implications for eczema vaccinatum. *J. Immunol.* 172, 1763–1767. doi: 10.4049/jimmunol.172.3.1763
- Imafuku, S. (2023). Recent advance in management of herpes simplex in Japan. *J. Dermatol.* 50, 299–304. doi: 10.1111/1346-8138.16734
- Jalali, M. M., Soleimani, R., Soltanipour, S., and Jalali, S. M. (2021). Pharmacological treatments of Bell's Palsy in adults: A systematic review and network meta-analysis. *Laryngoscope* 131, 1615–1625. doi: 10.1002/lary.29368
- James, C., Harfouche, M., Welton, N. J., Turner, K. M., Abu-Raddad, L. J., Gottlieb, S. L., et al. (2020). Herpes simplex virus: Global infection prevalence and incidence estimates, 2016. *Bullet. World Health Org.* 98, 315–329. doi: 10.2471/BLT.19.237149
- Ji, M., Zhu, T., Xing, M., Luan, N., Mwangi, J., Yan, X., et al. (2019). An antiviral peptide from *Alopecosa nagpae* spider targets NS2B-NS3 protease of flaviviruses. *Toxins* 11, 100584. doi: 10.3390/toxins11100584
- Kahlenberg, J. M., and Kaplan, M. J. (2013). Little peptide, big effects: The role of LL-37 in inflammation and autoimmune disease. *J. Immunol.* 191, 4895–4901. doi: 10.4049/jimmunol.1302005
- Kastrukoff, L. F., Lau, A. S., and Thomas, E. E. (2012). The effect of mouse strain on herpes simplex virus type 1 (HSV-1) infection of the central nervous system (CNS). *Herpesviridae* 3, 4. doi: 10.1186/2042-4280-3-4
- Khalesi, Z., Tamrchi, V., Razizadeh, M. H., Letafati, A., Moradi, P., Habibi, A., et al. (2023). Association between human herpesviruses and multiple sclerosis: A systematic review and meta-analysis. *Microb. Pathog.* 2023, 106031. doi: 10.1016/j.micpath.2023.106031
- Kościczyk, E. M., Lisowski, P., Jarczak, J., Strzalkowska, N., Józwiak, A., Horbańczyk, J., et al. (2012). Cathelicidins: Family of antimicrobial peptides. A review. *Mol. Biol. Rep.* 39, 10957–10970. doi: 10.1007/s11033-012-1997-x
- Lee, C.-J., Buznyk, O., Kuffova, L., Rajendran, V., Forrester, J. V., Phopase, J., et al. (2014). Cathelicidin LL-37 and HSV-1 corneal infection: Peptide versus gene therapy. *Transl. Vis. Sci. Technol.* 3, 4. doi: 10.1167/tvst.3.3.4
- Lee, S., Ives, A. M., and Bertke, A. S. (2015). Herpes simplex virus 1 reactivates from autonomic ciliary ganglia independently from sensory trigeminal ganglia to cause recurrent ocular disease. *J. Virol.* 89, 8383–8391. doi: 10.1128/JVI.00468-15
- Li, L., Li, Z., Li, X., Wang, E., Lang, F., Xia, Y., et al. (2016). Reactivation of HSV-1 following explant of tree shrew brain. *J. Neurovirol.* 22, 293–306. doi: 10.1007/s13365-015-0393-4
- Li, X., Li, Y., Han, H., Miller, D. W., and Wang, G. (2006). Solution structures of human LL-37 fragments and NMR-based identification of a minimal membrane-targeting antimicrobial and anticancer region. *J. Am. Chem. Soc.* 128, 5776–5785. doi: 10.1021/ja0584875
- Liu, P., Zhong, L., Xiao, J., Hu, Y., Liu, T., Ren, Z., et al. (2023). Ethanol extract from *Artemisia argy* leaves inhibits HSV-1 infection by destroying the viral envelope. *Virol. J.* 20, 8. doi: 10.1186/s12985-023-01969-5
- McQuillan, G., Kruszon-Moran, D., Flagg, E. W., and Paulose-Ram, R. (2018). Prevalence of herpes simplex virus type 1 and type 2 in persons aged 14–49: United States, 2015–2016. *NCHS Data Brief* 304, 1–8. Available online at: <https://www.cdc.gov/nchs/products/databriefs/db304.htm>
- Mehmood Khan, F., Manohar, P., Singh Gondil, V., Mehra, N., Kayode Oyejobi, G., Odiwuor, N., et al. (2023). The applications of animal models in phage therapy: An update. *Hum. Vac. Immunotherapeut.* 19, 2175519. doi: 10.1080/21645515.2023.2175519
- Memariani, H., Memariani, M., Moravvej, H., and Shahidi-Dadras, M. (2020). Melittin: A venom-derived peptide with promising anti-viral properties. *Eur. J. Clin. Microbiol. Infect. Dis.* 39, 5–17. doi: 10.1007/s10096-019-03674-0
- Mookherjee, N., Anderson, M. A., Haagsman, H. P., and Davidson, D. J. (2020). Antimicrobial host defence peptides: Functions and clinical potential. *Nat. Rev. Drug Disc.* 19, 311–332. doi: 10.1038/s41573-019-0058-8
- Mookherjee, N., and Hancock, R. E. W. (2007). Cationic host defence peptides: Innate immune regulatory peptides as a novel approach for treating infections. *Cell. Mol. Life Sci.* 64, 922–933. doi: 10.1007/s00018-007-6475-6
- Neto, R., Oliveira, G., and Pestana, M. (2007). Antiviral drug-induced nephrotoxicity. *Acta Med. Port* 20, 59–63. doi: 10.1053/j.ajkd.2005.02.010
- Newadkar, U. R., Chaudhari, L., and Khalekar, Y. K. (2016). Facial palsy, a disorder belonging to influential neurological dynasty: Review of literature. *N. Am. J. Med. Sci.* 8, 263–267. doi: 10.4103/1947-2714.187130
- Nijnik, A., and Hancock, R. E. W. (2009). The roles of cathelicidin LL-37 in immune defences and novel clinical applications. *Curr. Opin. Hematol.* 16, 41–47. doi: 10.1097/MOH.0b013e32831ac517
- Nizet, V. (2006). Antimicrobial peptide resistance mechanisms of human bacterial pathogens. *Curr. Iss. Mol. Biol.* 8, 11–26. doi: 10.21775/cimb.008.011
- Peng, L., Lu, Y., Tian, H., Jia, K., Tao, Q., Li, G., et al. (2022). Chicken cathelicidin-2 promotes IL-1 β secretion via the NLRP3 inflammasome pathway and serine proteases activity in LPS-primed murine neutrophils. *Dev. Comparat. Immunol.* 131, 104377. doi: 10.1016/j.dci.2022.104377
- Rechenchoski, D. Z., Faccin-Galhardi, L. C., Linhares, R. E. C., and Nozawa, C. (2017). Herpesvirus: An underestimated virus. *Folia Microbiol.* 62, 151–156. doi: 10.1007/s12223-016-0482-7
- Rosenfeld, Y., Papo, N., and Shai, Y. (2006). Endotoxin (lipopolysaccharide) neutralization by innate immunity host-defense peptides. Peptide properties and plausible modes of action. *J. Biol. Chem.* 281, 1636–1643. doi: 10.1074/jbc.M504327200
- Rossi, D. C., Muñoz, J. E., Carvalho, D. D., Belmonte, R., Faintuch, B., Borelli, P., et al. (2012). Therapeutic use of a cationic antimicrobial peptide from the spider *Acanthoscurria gomesiana* in the control of experimental candidiasis. *BMC Microbiol.* 12, 28. doi: 10.1186/1471-2180-12-28
- Roy, M., Lebeau, L., Chessa, C., Damour, A., Ladram, A., Oury, B., et al. (2019). Comparison of anti-viral activity of frog skin anti-microbial peptides temporin-sha and [K³]SHA to LL-37 and temporin-Tb against herpes simplex virus type 1. *Viruses* 11, 77. doi: 10.3390/v11010077
- Sadowski, L. A., Upadhyay, R., Greeley, Z. W., and Margulies, B. J. (2021). Current drugs to treat infections with herpes simplex viruses-1 and-2. *Viruses* 13, 71228. doi: 10.3390/v13071228
- Steintraesser, L., Kraneburg, U., Jacobsen, F., and Al-Benna, S. (2011). Host defense peptides and their antimicrobial-immunomodulatory duality. *Immunobiology* 216, 322–333. doi: 10.1016/j.imbio.2010.07.003
- Stoyanova, A., Popatanasov, A., Rashev, V., Tancheva, L., Quideau, S., and Galabov, A. S. (2023). Effect of castalagin against HSV-1 infection in newborn mice. *Nat. Prod. Res.* 2023, 1–6. doi: 10.1080/14786419.2023.2173191
- Takahashi, H., Hitsuimoto, Y., Honda, N., Hato, N., Mizobuchi, M., Murakami, S., et al. (2001). Mouse model of Bell's palsy induced by reactivation of herpes simplex virus type 1. *J. Neuropathol. Exp. Neurol.* 60, 621–627. doi: 10.1093/jnen/60.6.621
- Talapko, J., Meštrović, T., Juzbašić, M., Tomas, M., Erić, S., Horvat Aleksijević, L., et al. (2022). Antimicrobial peptides-mechanisms of action, antimicrobial effects and clinical applications. *Antibiotics* 11, 101417. doi: 10.3390/antibiotics11101417
- Vashishtha, A. K., and Kuchta, R. D. (2016). Effects of acyclovir, foscarnet, and ribonucleotides on herpes simplex virus-1 DNA polymerase: Mechanistic insights and a novel mechanism for preventing stable incorporation of ribonucleotides into DNA. *Biochemistry* 55, 1168–1177. doi: 10.1021/acs.biochem.6b00065

- Wang, J., Dou, X., Song, J., Lyu, Y., Zhu, X., Xu, L., et al. (2019). Antimicrobial peptides: Promising alternatives in the post feeding antibiotic era. *Med. Res. Rev.* 39, 831–859. doi: 10.1002/med.21542
- Whitley, R. J., and Roizman, B. (2001). Herpes simplex virus infections. *Lancet* 357, 1513–1518. doi: 10.1016/S0140-6736(00)04638-9
- Wuerth, K., and Hancock, R. E. W. (2011). New insights into cathelicidin modulation of adaptive immunity. *Eur. J. Immunol.* 41, 2817–2819. doi: 10.1002/eji.201142055
- Yeo, S. G., Lee, Y. C., Park, D. C., and Cha, C. I. (2008). Acyclovir plus steroid vs. steroid alone in the treatment of Bell's palsy. *Am. J. Otolaryngol.* 29, 163–166. doi: 10.1016/j.amjoto.2007.05.001
- Zandian, A., Osiro, S., Hudson, R., Ali, I. M., Matusz, P., Tubbs, S. R., et al. (2014). The neurologist's dilemma: A comprehensive clinical review of Bell's palsy, with emphasis on current management trends. *Med. Sci. Monitor* 20, 83–90. doi: 10.12659/MSM.889876
- Zasloff, M. (2002). Antimicrobial peptides of multicellular organisms. *Nature* 415, 389–395. doi: 10.1038/415389a
- Zhang, H., Du, H., Qian, M., Wang, Y., Zhou, S., Chen, J., et al. (2019). A study of affecting the recovery of Chinese patients with Bell palsy. *Medicine* 98, e14244. doi: 10.1097/MD.00000000000014244
- Zhang, L., Zhang, L., Li, F., Liu, W., Tai, Z., Yang, J., et al. (2023). When herpes simplex virus encephalitis meets antiviral innate immunity. *Front. Immunol.* 14, 1118236. doi: 10.3389/fimmu.2023.1118236



OPEN ACCESS

EDITED BY

Jack Wong,
Caritas Institute of Higher Education,
Hong Kong SAR, China

REVIEWED BY

Niu Mingfu,
Henan University of Science and Technology,
China
Jai K Kaushik,
National Dairy Research Institute (ICAR), India

*CORRESPONDENCE

Zhihua Qin
✉ qq_1126@163.com

RECEIVED 29 January 2023

ACCEPTED 19 May 2023

PUBLISHED 09 June 2023

CITATION

Dong X, Shan H, Wang S, Jiang Z,
Wang S and Qin Z (2023) High expression of
antimicrobial peptides cathelicidin-BF in *Pichia*
pastoris and verification of its activity.
Front. Microbiol. 14:1153365.
doi: 10.3389/fmicb.2023.1153365

COPYRIGHT

© 2023 Dong, Shan, Wang, Jiang, Wang and
Qin. This is an open-access article distributed
under the terms of the [Creative Commons
Attribution License \(CC BY\)](#). The use,
distribution or reproduction in other forums is
permitted, provided the original author(s) and
the copyright owner(s) are credited and that
the original publication in this journal is cited,
in accordance with accepted academic
practice. No use, distribution or reproduction is
permitted which does not comply with these
terms.

High expression of antimicrobial peptides cathelicidin-BF in *Pichia pastoris* and verification of its activity

Xufeng Dong¹, Hu Shan¹, Shubai Wang², Zhengjun Jiang³,
Shaojuan Wang³ and Zhihua Qin^{1*}

¹College of Veterinary Medicine, Qingdao Agricultural University, Qingdao, Shandong, China, ²College of Animal Science and Technology, Qingdao Agricultural University, Qingdao, Shandong, China, ³Shandong Hwatson Biochem Co. Ltd, Weifang, Shandong, China

Antibacterial peptides are endogenous polypeptides produced by multicellular organisms to protect the host against pathogenic microbes, they show broad spectrum antimicrobial activities against various microorganisms and possess low propensity for developing resistance. The purpose of this study is to develop recombinant antibacterial peptide cathelicidin-BF by genetic engineering and protein engineering technology, and study its antibacterial activity *in vitro* and *in vivo*, so as to provide reference for the production and application of recombinant antibacterial peptide cathelicidin-BF. In this study, on account of *Pichia pastoris* eukaryotic expression system, we expressed and prepared antibacterial peptide cathelicidin-BF. Then, the minimum inhibitory concentration of antibacterial peptide cathelicidin-BF and the comparison with the antibacterial activity of antibiotics were determined through the antibacterial experiment *in vitro*. Chickens as infection model were used to verify the antibacterial peptide activity *in vivo*. The results show that the bacteriostatic ability of antibacterial peptide cathelicidin-BF is similar to that of antibiotics in certain concentration, and can reach the treatment level of antibiotics. Although the mode of administration of antibacterial peptide is still limited, this study can provide reference for the future research of antibacterial peptide.

KEYWORDS

antimicrobial peptides, eukaryotic expression, bacteriostatic effect, *in vitro* activity, *in vivo* activity

1. Introduction

The prevention and treatment of bacterial diseases has long relied on traditional antibiotics such as penicillin. However, the range of bacterial pathogens that have developed antibiotic resistance is huge and new antibiotics are urgently needed. One alternative is the use of antimicrobial peptides that are derived from immune response products produced in response to invasion by bacteria and associated microbial factors (Hancock and Diamond, 2000; Hancock, 2001; Cunliffe and Mahida, 2004; Reddy et al., 2004; Hancock and Sahl, 2006; Takahashi et al., 2010; Wang, 2015). These peptides are an important part of animal immune defense systems and have the advantages of broad-spectrum antibacterial action and lack of bacterial resistance (Epand and Vogel, 1999; Scott et al., 2000; Lai and Gallo, 2009; Nguyen et al., 2011; Pasupuleti et al., 2011; Kang et al., 2019). Antimicrobial peptides have been used as feed additives to prevent and treat digestive tract inflammation such as diarrhea in livestock and aquatic organisms. These

compounds have been shown to reduce or completely replace antibiotics for livestock rearing and reduce the incidence of disease. However, the use of antimicrobial peptides as clinical drugs has not been reported although they have demonstrated potent antibacterial activities *in situ* in mammalian hosts (Skerlavaj et al., 1996; Bulet, 1999; Hancock and Chapple, 1999; Hancock, 2000, 2001; Hunter et al., 2005).

Theoretically, antimicrobial peptides are ideal candidates for new antibiotics but their use has been hampered by a lack of experimental data of their action in animals. These data include stability, effectiveness and safety using *in vivo* models and this has limited their application. For example, polyphemusin I isolated from horseshoe crab has robust antibacterial activity *in vitro* but was not effective *in vivo* (Turner et al., 1998). Interestingly, sequence modification of the peptide enhanced its *in vivo* effectiveness but decreased its *in vitro* activity (Zhang et al., 2000). The primary factor that limits *in vivo* effectiveness of peptides may be their degradation by host proteases. Therefore, modifications such as liposome embedding, the use of precursors, the use of carrier proteins or sequence modification are key components of improving their effectiveness.

According to different classification standards, there are many ways to classify antimicrobial peptides, but it is generally believed that it is more meaningful to classify antimicrobial peptides according to their structural characteristics. Therefore, antimicrobial peptides are mainly divided into α - and β -Helix Collapse two types (Liu et al., 2015). Although antimicrobial peptides have potential in drug development, they still have some undesirable characteristics in clinical application. Natural peptides in gastrointestinal tract and other body fluids are usually unstable, resulting in low bioavailability of antimicrobial peptides in organisms (Cunliffe and Mahida, 2004; Tan et al., 2021).

cathelicidin-BF is a new antibacterial peptide isolated from *Bungarus multicinctus*, which is amphiphilic α -Helical conformation (Costa et al., 2019). cathelicidin-BF has broad-spectrum antibacterial activity, especially against gram-negative bacteria. It can be used as a good drug to treat acne vulgaris (Wang et al., 2008). Up to now, the research on cathelicidin-BF has mainly focused on the antibacterial effect, and cathelicidin-BF has rarely been reported on the immune regulation and epithelial barrier protection. Some re-searchers speculate that exogenous Cathelicidin-BF may affect the development and healing of UC mucosal injury and inflammation (Wang et al., 2011). In addition, cathelicidin-BF shows low cytotoxicity and high stability to mammalian cells (Zhang et al., 2015).

In this study, we expressed the antimicrobial peptide cathelicidin-BF with the help of *Pichia pastoris* that were secreted into the culture medium and processed for use as a therapeutic drug. We examined *in vivo* antibacterial activity in chickens infected with a highly pathogenic *Escherichia coli* strain. Our data will provide a useful reference for further research into the use of antimicrobial peptides as clinical antibiotic reagents.

2. Results

2.1. Antimicrobial peptide gene splicing and *Pichia pastoris* expression

PCR amplification yielded a fragment of 310bp that was consistent with the expected size of the cathelicidin-BF gene

fragment. The cathelicidin-BF gene fragment was cloned into the *Pichia pastoris* expression vector and expressed in *Pichia pastoris*. Positive colonies were identified by *EcoR* I digestion and the insert identities were verified by DNA sequencing. The constructed expression plasmid pICZ α -A-cathelicidin-BF was correctly inserted downstream of the Kex 2 cleavage site of the vector. Due to the insertion of the target fragment between the pPICZ α -A poly-clonal sites, the original enzyme digestion site in the pPICZ α -A multicloning site was destroyed so the plasmid could be identified by *EcoR* I digestion. Following *EcoR* I digestion, the electrophoresis patterns indicated the correct construct was cloned and was verified using sequence analysis. We induced expression of the cathelicidin-BF peptide using the methanol-regulated AOX promoter and examined culture supernatants for the presence of the peptide. The peptide migrating at 17kDa was present only in the supernatant from the induced *Pichia pastoris* but not in parental cells or cells containing the empty vector or when methanol was excluded from the culture medium. Through repeated testing, we have found the optimal induction conditions for antibacterial peptides cathelicidin-BF. In BMGY medium, recombinant *Pichia pastoris* cells were inoculated with 1% volume. Then, at 200 rpm, pH = 5.5, and 22°C, methanol was added to the culture medium twice every 24 h, adding 1% of the total volume each time, with a phosphate concentration of 100 mM/L, and a ammonium sulfate concentration of 0.5%. After 240 h of induction, the expression of antibacterial peptides reached 0.5 g/L. We collected a large number of antimicrobial peptides cathelicidin-BF, concentrated the antimicrobial peptides by vacuum freeze-drying, and the treated antimicrobial peptides were stored in a low-temperature refrigerator. Because the antibacterial peptide cathelicidin-BF we prepared was a compound peptide expressed in series, we need to treat the compound peptide to turn the compound antibacterial peptide into a single active peptide. Under the action of acetic acid, the treatment results of composite antimicrobial peptides are as shown in the Figure 1F. The results were in line with our expectations. (Figure 1).

2.2. Minimal inhibitory concentration determination of antimicrobial peptide cathelicidin-BF

The MIC determination results of antibacterial peptide cathelicidin-BF are as Table 1.

2.3. Determination of median lethal dose of test bacteria

The determination results of the median lethal dose of the test bacteria are as Tables 2, 3. The result is calculated according to the following formula:

$$\log LD_{50} = X_k - i(\sum p - 0.5),$$

Xk in the formula represents the maximum logarithmic dose, i represents the difference between two adjacent logarithmic measurements, p represents the mortality of each dose group.

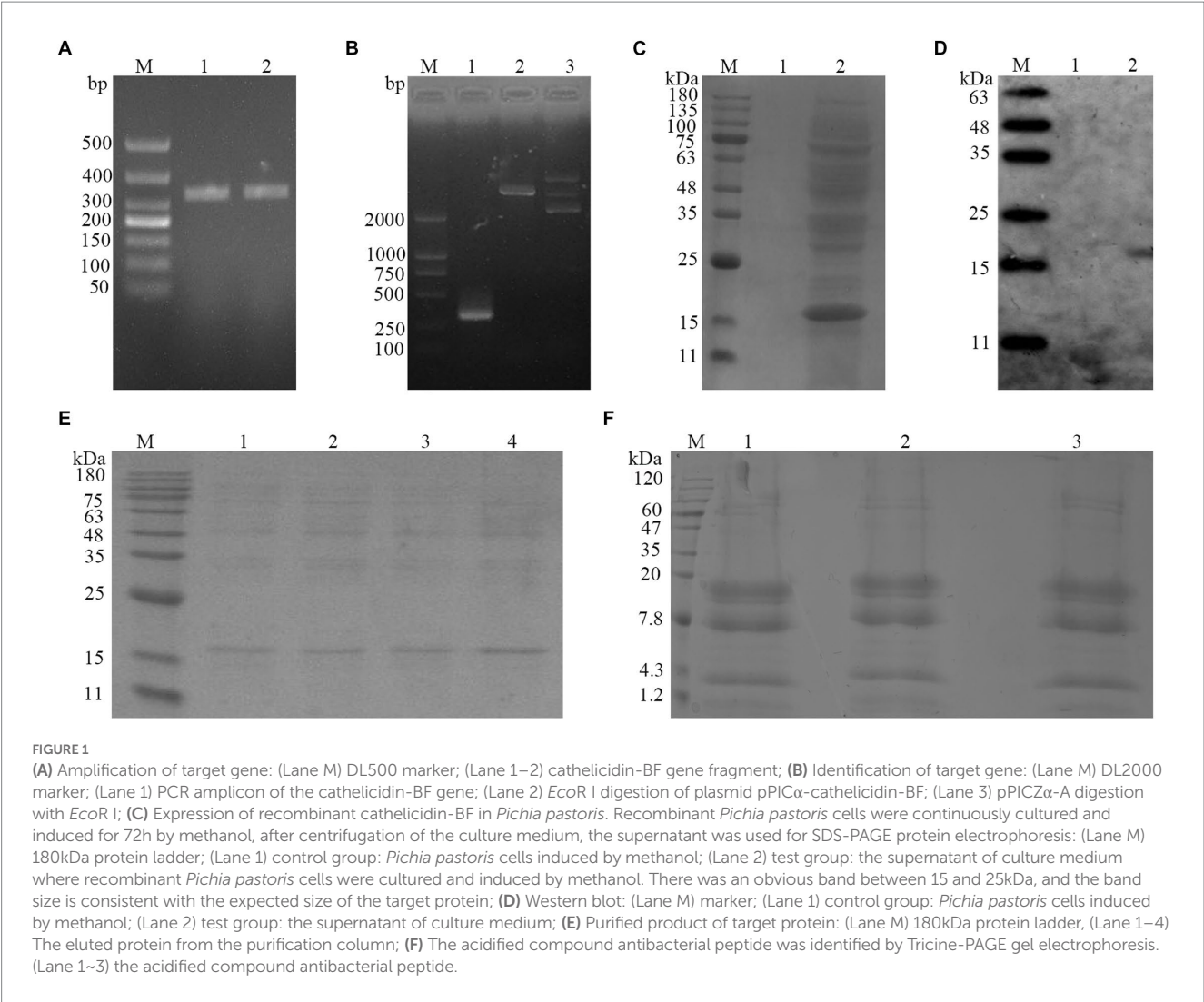


TABLE 1 Minimal inhibitory concentration of antibacterial peptide cathelicidin-BF.

Tested strain	Antibacterial peptide cathelicidin-BF ($\mu\text{g/mL}$)
<i>Escherichia coli</i> (ATCC 25922)	27
<i>Escherichia coli</i> (E058)	29
<i>Escherichia coli</i> (Drug resistant bacteria)	29
<i>Staphylococcus aureus</i> (ATCC 29213)	30
<i>Staphylococcus aureus</i> (Drug resistant bacteria)	32

In the chicken infection model, the dose used to inoculate the tested bacteria was twice the median lethal dose.

2.4. *In vitro* bacteriostatic test

The secreted peptides were examined for its effects on bacterial growth *in vitro* using agar plate cultures (Figures 2, 3). Meanwhile, synthetic peptides were used to compare with secreted peptides (Figure 4).

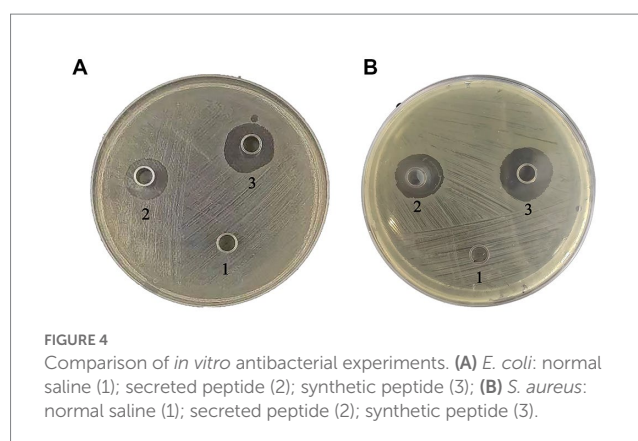
TABLE 2 Determination of median lethal dose of *Escherichia coli* to chicks.

Bacterial concentration (CFU/mL)	Number of samples	Number of deaths
1.00×10^7	6	6
3.33×10^7	6	6
1.11×10^6	6	5
3.70×10^5	6	4
1.23×10^5	6	2
4.11×10^4	6	1
1.37×10^4 CFU/mL	6	0
LD ₅₀	2.12×10^4 CFU/mL	

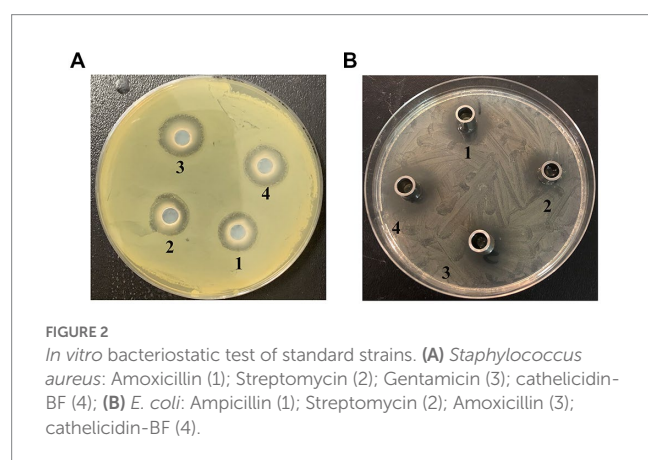
The test results show that: according to the numerical order marked in the Figure 2A, the bacteriostatic circle of 10 μL (25 $\mu\text{g/mL}$) antibiotic solution were 24.6 mm, 26.9 mm, 27.5 mm. The bacteriostatic circle of 10 μL (30 $\mu\text{g/mL}$) antimicrobial peptide cathelicidin-BF solution was 26.8 mm. According to the numerical order marked in the Figure 2B, the bacteriostatic circle of 10 μL (25 $\mu\text{g/mL}$) antibiotic solution were 29.6 mm, 30.6 mm, 34 mm. The

TABLE 3 Determination of median lethal dose of *Staphylococcus aureus* to chicks.

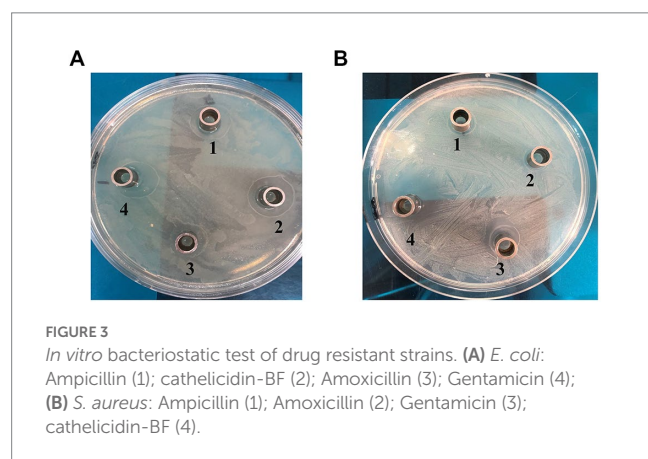
Bacterial concentration (CFU/mL)	Number of samples	Number of deaths
1.00×10^7	6	6
3.33×10^7	6	6
1.11×10^6	6	4
3.70×10^5	6	4
1.23×10^5	6	3
4.11×10^4	6	1
1.37×10^4 CFU/mL	6	0
LD ₅₀	2.27×10^5 CFU/mL	

**FIGURE 4**

Comparison of *in vitro* antibacterial experiments. (A) *E. coli*: normal saline (1); secreted peptide (2); synthetic peptide (3); (B) *S. aureus*: normal saline (1); secreted peptide (2); synthetic peptide (3).

**FIGURE 2**

In vitro bacteriostatic test of standard strains. (A) *Staphylococcus aureus*: Amoxicillin (1); Streptomycin (2); Gentamicin (3); cathelicidin-BF (4); (B) *E. coli*: Ampicillin (1); Streptomycin (2); Amoxicillin (3); cathelicidin-BF (4).

**FIGURE 3**

In vitro bacteriostatic test of drug resistant strains. (A) *E. coli*: Ampicillin (1); cathelicidin-BF (2); Amoxicillin (3); Gentamicin (4); (B) *S. aureus*: Ampicillin (1); Amoxicillin (2); Gentamicin (3); cathelicidin-BF (4).

bacteriostatic circle of 10 μ L (28 μ g/mL) Antimicrobial peptide cathelicidin-BF solution was 30.9 mm.

The test results show that: the antibacterial effect of antimicrobial peptides was the same as that of Amoxicillin, and was better than that of Ampicillin and streptomycin, but not as good as that of Gentamicin.

The test results show that: according to the numerical order marked in the Figure 3A, the bacteriostatic circle of 10 μ L (25 μ g/mL) antibiotic solution were 16.5 mm, 17.3 mm, 30.5 mm. The bacteriostatic circle of 10 μ L (29 μ g/mL) antimicrobial peptide

cathelicidin-BF solution was 31.2 mm. It can be seen from the bacteriostatic circle that the bacteriostatic effect of the antimicrobial peptide test group was significantly better than that of the antibiotic group, and there was little difference between the inhibitory effect of the antimicrobial peptide on drug-resistant bacteria and the standard strain at the same dose, which indicates that the antimicrobial peptide may have better resistance to bacterial drug resistance.

In Figure 3B, the bacteriostatic circle of 10 μ L (25 μ g/mL) antibiotic solution were 9.5, 10.2, and 20.5 mm. The bacteriostatic circle of 10 μ L (32 μ g/mL) antimicrobial peptide cathelicidin-BF solution was 27.5 mm. In addition, the bacteriostatic effect of Ampicillin and Gentamicin decreased sharply in the drug-resistant strain test, which indicates that the problem of bacterial drug resistance of Ampicillin and Gentamicin may be more prominent in actual production.

In Figure 4A, the bacteriostatic circle of 10 μ L (30 μ g/mL) synthetic peptides solution were 30 mm, the bacteriostatic circle of 10 μ L (30 μ g/mL) secreted peptides solution were 27 mm.

In Figure 4B, the bacteriostatic circle of 10 μ L (30 μ g/mL) synthetic peptides solution were 31.2 mm, the bacteriostatic circle of 10 μ L (30 μ g/mL) secreted peptides solution were 27.8 mm.

2.5. *In vivo* bacteriostatic test

These peptides inhibited the growth of both Gram-positive and Gram-negative bacteria so we therefore examined whether this activity translated into *in vivo* activity. Our challenge bacterial strain for the chicken infection model was the pathogenic *S. aureus* and *E. coli* (Figures 5–7).

The results show that: administration of peptides reduced the severity of clinical symptoms and these animals gradually recovered compared with the infected control group.

3. Discussion

The rapid rise in the numbers of antibiotic resistant bacteria is also a concern of global food safety. Many antibiotics are no longer effective and this is a major concern for both animal and human health. Many countries have already adopted strict regulations for the use of

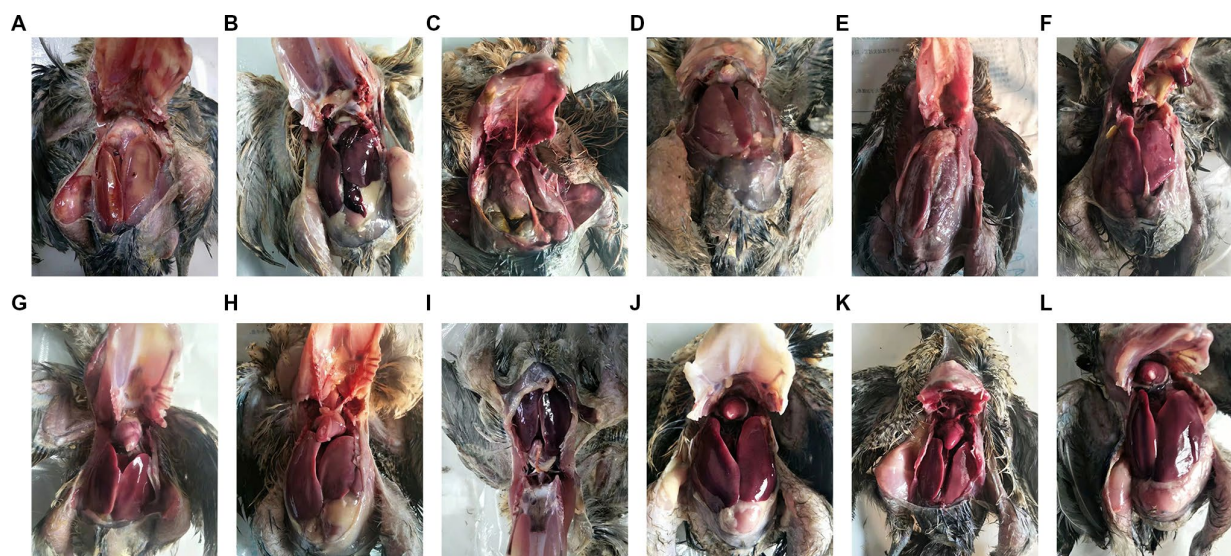


FIGURE 5

Animal Experiment. (A–C) Diagram of internal organs of chicken after death of *S. aureus* inoculation: the feathers of the chicken's chest and abdomen fell off, and the skin presented purplish black swelling. After autopsy, the chickens were found to have significant subcutaneous congestion, accompanied by a large amount of gelatinous pink or yellowish red edema fluid. The major signs included hepatomegaly, splenomegaly, and ascites, with pericardial effusion. The liver and spleen were purplish red; (D–F) Diagram of chicken viscera after *E. coli* inoculation: The test chickens developed fibrinous pericarditis, with thickening of the pericardium, accompanied by pericardial effusion. The liver was significantly swollen with fibrous exudates on its surface. The spleen was congested and swollen, bile extravasation in some chickens, intestinal mucosa hyperemia or a little patchy hyperemia. (G–I) Diagram of internal organs of experimental chickens in the treatment group: Compared to the untreated infected group, the chickens in the antibacterial peptide treatment group had normal viscera color and no significant pathological changes. (J–L) Visceral organ diagram of control group: The color of each organ was normal without obvious lesions.

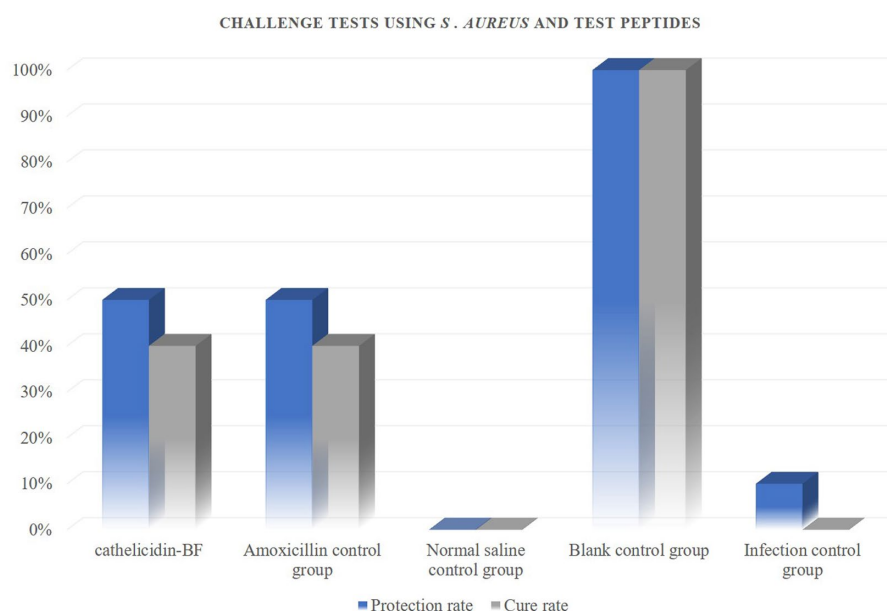
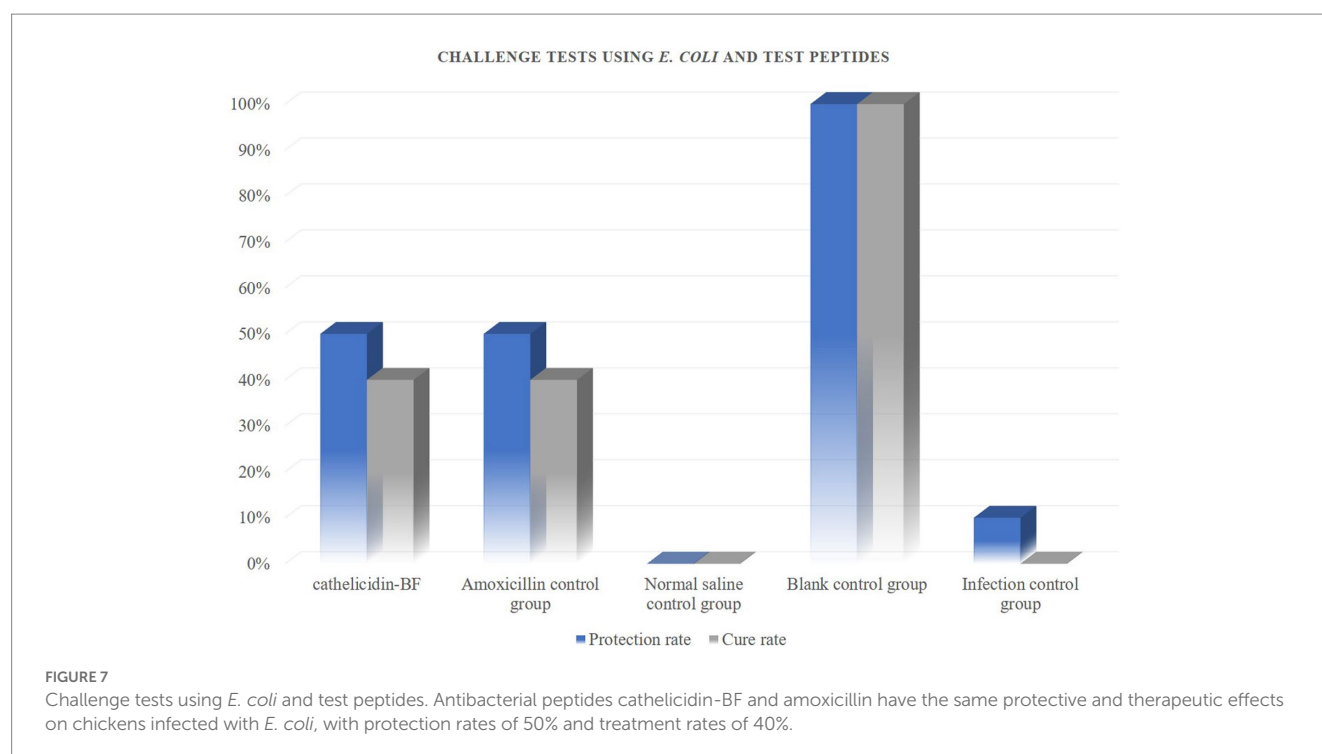


FIGURE 6

Challenge tests using *S. aureus* and test peptides. Antibacterial peptides cathelicidin-BF and amoxicillin have the same protective and therapeutic effects on chickens infected with *S. aureus*, with protection rates of 50% and treatment rates of 40%.

antibiotics and the use of antibiotics as growth promoters in animals will certainly be globally banned. The animal feed industry is still using 20 types of antibiotics shared by human and livestock or as special additives for livestock and poultry. The entry of China into the

World Trade Organization will seriously affect its global competitiveness in the international market if antibiotics are used as growth promoters. Therefore, the development of non-toxic, pollution-free, safe and efficient new antibacterial agents to replace



antibiotics as feed additives has become a worldwide proposition. The research and development of antibacterial peptide biological agents can yield highly effective and safe new antimicrobials.

Other scholars used the *Bacillus subtilis* expression system and SUMO technology to isolate and purify the antibacterial cathelicidin-BF from the venom of the golden ring snake. The chimeric genes His-SUMO-cathelicidin-BF and His-SUMO proteolytic enzyme 1 were ligated to the vector pHT43 and expressed in *Bacillus subtilis* WB 800 N (He et al., 2015). This is the first report on the production of endotoxin free antibacterial peptide cathelicidin-BF by recombinant DNA technology, and also the first report on the production of highly active purified SUMO Protease 1 from *Bacillus subtilis*.

At present, there are few reports on *Pichia pastoris* expression of the antifungal peptide cathelicidin-BF. In this experiment, we selected the *Pichia pastoris* preferred codon to optimize the target gene. With the help of *Pichia pastoris* expression system, we obtained the antibacterial peptide cathelicidin-BF by methanol induction. After the fusion peptide was secreted into the culture medium, the target protein was purified by affinity chromatography (Luan et al., 2014; Karbalaee et al., 2020).

One of the innovations of this study is to optimize the conditions for the induction and culture of recombinant *Pichia pastoris*. Compared to typical induction conditions which is used to induce expression in recombinant *Pichia pastoris* (28 ~ 30°C, 220 ~ 250 rpm, pH = 6.0; Weidner et al., 2010; De Brabander et al., 2023; Turner et al., 2023), through repeated testing, we have found the optimal induction conditions for antibacterial peptides cathelicidin-BF. In BMGY medium, recombinant *Pichia pastoris* cells were inoculated with 1% volume. Then, at 200 rpm, pH = 5.5, and 22°C, methanol was added to the culture medium twice every 24 h, adding 1% of the total volume each time, with a phosphate concentration of 100 mM/L, and a ammonium sulfate concentration of 0.5%. After 240 h of induction, the expression of antibacterial peptides reached 0.5 g/L.

In vitro experiments, we compared the activity of synthetic peptides and secreted peptides, and the results were gratifying. Although secreted peptides were lower in purity than synthetic peptides, the difference in activity between the two was not significant under the same dose. However, the cost of synthesizing peptides is much higher than that of secreted peptides, this brings infinite possibilities for the application of secreted peptides in production.

In vivo experiments, it must be admitted that the number of sample animals may be one of the factors that restrict the test results. Increasing the number of test animals may be able to more accurately demonstrate the difference in the efficacy of antimicrobial peptides cathelicidin-BF and amoxicillin. In addition, although there were no significant differences in the activity status of chickens treated with the two drugs, after treatment with antimicrobial peptides, there were still residual infection symptoms on the organs of chickens. In the follow-up study, we will optimize the delivery method of antimicrobial peptides, hoping to achieve that antimicrobial peptide therapy can completely replace antibiotics.

Regarding the mode of action of antimicrobial peptides on test chickens, oral administration was one of the options, but due to the effect of the digestive enzyme and intestinal fluids in chickens, the effect was not ideal. Finally, intraperitoneal injection was selected as the drug delivery method. Some researchers had used nanomaterials to coat antimicrobial peptides, a smart epigallocatechin-3-gallate (EGCG)-loaded silk fibroin-based nanoparticle (NP) with the surface functionalization of antimicrobial peptides was constructed (Liu et al., 2022). This has brought us new ideas, and we have conducted new exploration based on it. In addition, compared to the method of prokaryotic expression (*E. coli*) (Tajbakhsh et al., 2018), the antibacterial peptide expressed by recombinant *Pichia pastoris* has a better antibacterial effect *in vitro*, which may be due to the modification of the peptide by the eukaryotic expression system.

The decomposition of intestinal fluid limits the therapeutic effect of antimicrobial peptides in animal intestinal infections. The

application of antimicrobial peptides in animal intestinal therapy is currently relatively limited, and more attention has been focused on feed additives. Xie et al. (2020) explored effects of antibacterial peptide combinations on growth performance, intestinal health, and immune function of broiler chickens. In general, the two combinations of ABPs added in broiler's basal diets can promote broiler growth and improve feed conversion rate instead of antibiotics. But in this study, antimicrobial peptides were added to the feed along with other additives, the intestinal fluid also had an impact on the decomposition of antimicrobial peptides and cannot be avoided. In another study, Xu et al. (2023) made an evaluation of the efficacy of the antimicrobial peptide HJH-3 in chickens infected with *Salmonella Pullorum*. The research results confirmed the role of antimicrobial peptides in the treatment of chicken intestinal bacterial infections. Similarly, the therapeutic effect of antimicrobial peptides was reduced by intestinal fluid. Regarding the use of AMPs, the choice of administration mode plays a very important role in the prevention and treatment of corresponding diseases (Knappe et al., 2019; Lee et al., 2019; Yu et al., 2020). At present, the combination therapy of nanomaterials and antimicrobial peptides may be full of vitality.

4. Materials and methods

4.1. Strains and plasmids

Pichia pastoris X-33 (His-Mut+) and pPICZ α -A were purchased from Invitrogen (Carlsbad, CA, United States). *S. aureus* (ATCC 29213) and *E. coli* (ATCC 25922, E058) were from the clinical examination center of the Ministry of health of China. The clinical resistant strains of *E. coli* (drug resistance spectrum: AMP-STR-FLO-DOX-AMO-NEO) and *S. aureus* came from our laboratory (drug resistance spectrum: AMP-CIP-STR-ERY-FOX-GEN-TET). Synthetic peptides from Bankpeptide Biological Technology Co. Ltd. of China (purity \geq 98%).

4.2. Reagents

Xho I, *Xba* I, *Sac* I and *Eco* R I endonucleases, T4 DNA ligase, *rTaq* and *exTaq* enzymes were purchased from Takara (Japan). A DNA gel recovery kit was obtained from Shanghai Huashun Bioengineering (Shanghai, China). Zeocin and expression vector pPICZ α A and pierce micro BCA protein detection kit were purchased from Invitrogen. D-glucose, D-sorbitol, peptone, yeast extract and biotin were purchased from BBI (Kent, United Kingdom). Trichloroacetic acid, methanol, acetone and other reagents were of analytical grade and purchased from Shanghai Reagent No. 2 factory (Shanghai, China). Other reagents were of analytical grade.

4.3. Test drug and application method

According to the experimental method in this paper, the antibacterial peptides of cathelicidin-BF expressed by *Pichia pastoris* eukaryotic expression system were prepared. In agar diffusion test, amoxicillin was used as the control group to evaluate the antibacterial effect of antibacterial peptide cathelicidin-BF.

4.4. Culture media

Luria Bertani (LB), yeast extract, peptone and dextrose (YPD) medium and *Pichia pastoris* growth medium (BMGY) were used for bacterial and yeast cultivation as previously described (Pasupuleti et al., 2011). *Pichia pastoris* induction medium for plasmid-based expression utilized BMMY where glycerol was replaced with 0.5% methanol in BMGY.

4.5. Experimental animals

Sanhuang broiler chickens were purchased from Nanjing Sany Breeding factory and kept in isolation for 21 days prior to the start of the experiments. The normal growth and development of chicks was regarded as clinical health.

4.6. Antimicrobial peptide gene design and expression

The amino acid sequence of antibacterial peptide cathelicidin-BF was queried by NCBI as follows:

KFFRKLKKS VKKRAKEFFKKPRVIGVSIPE.

Because antimicrobial peptides are toxic in cells, in order to avoid cytotoxicity, we designed linker to connect the expression gene of antibacterial peptide, antibacterial peptides would be expressed in tandem. When the expressed antimicrobial peptides are collected, we add acetic acid to dissolve linker. Finally, we get an active antibacterial peptide. Three cathelicidin-BF were connected in series through linker (GTGDP).

The gene fragment was synthesized by Sangon Biotech (Shanghai, China) after modification. The synthesized target gene was used as a template for PCR amplification.

The PCR amplicons were digested with *Xho* I and *Xba* I and cloned into the *Pichia pastoris* expression vector pPICZ α -A and introduced into *Pichia pastoris* competent cell by transformation using standard molecular biology methods. Colonies that grew on zeocin plates were purified and correct plasmids were identified using *Eco* R I digestion and PCR amplification using primers 5'AOX and 3'AOX. The insert identity was verified by DNA sequence analysis (Shanghai Boya, Shanghai, China). The plasmid pPICZ α -cathelicidin-BF was linearized and introduced into *Pichia pastoris* by electroporation using the standard recommendations of the manufacturer (Invitrogen). Integration of the plasmid into the *Pichia pastoris* was determined using genomic DNA isolated using the liquid nitrogen freeze-thaw method. In addition, pPICZ α -A empty carrier was tangentially transformed by enzyme and also entered into *Pichia pastoris* X-33 by means of electrotransformation, which was used as the control of follow-up work. The PCR cycling conditions were: 94°C 1 min and 30 cycles of 94°C 1 min, 56°C 1 min and 72°C 1 min and a final extension at 72°C for 10 min. Amplicons were analyzed using 1% agarose gel electrophoresis.

Positive recombinants were inoculated into YPD containing 100 μ g/mL zeocin and cultured overnight at 30°C at 250 rpm and transferred to 100 mL BMGY medium with zeocin and incubated again until the OD₆₀₀ nm reached 3~6. The cultures were centrifuged and the pellets were weighed and then suspended in 500 mL BMMY for induction and expression at different temperatures (20, 22, 24, 26,

28, and 30°C), speed (160, 180, 200, and 220 rpm) and times (12, 24, 36, 48, and 72 h). The culture supernatants were collected by centrifugation at 6,000 rpm for 10 min and WB test was used to verify the successful expression of antimicrobial peptides. Finally, we determined the anti-bacterial activity of the supernatant samples.

4.7. Antimicrobial peptide cathelicidin-BF sample treatment

Because the antibacterial peptide prepared was a complex protein in series, it has to be cleaved. Our method is acetic acid acidification. The 20% acetic acid solution was prepared and used for dissolving the sample (precipitation: 20% acetic acid = 1:4). The peptide dissolution conditions were 65°C and 2~4 h. The NaHCO₃ solution was prepared and filtered for sterilization. The cracked samples were neutralized by NaHCO₃ solution to pH 7.2 and centrifuged at 12,000 rpm at 4°C for 5 min. Because acidification treatment cannot completely cleave the antimicrobial peptide, passes through Pierce™ Protein Concentrators PES (3,000 MWCO, Thermo Fisher Scientific Inc.), in order to ensure the availability of antibacterial peptide cathelicidin-BF. The processed peptides were concentrated and stored in the refrigerator at -20°C for standby.

4.8. Minimal inhibitory concentration determination of antimicrobial peptide cathelicidin-BF

Minimal inhibitory concentrations (MICs) were measured by standard microdilution method. The bacterial strains were incubated in nutrient broth at a concentration of 10⁶ CFU/mL containing appropriate aliquots of the peptides. MIC was defined as the lowest concentration of the peptides inhibiting visible growth after overnight incubation at 37°C. Each test was performed 3 times. The antibacterial peptide cathelicidin-BF diluted 2-fold dilution was added to the sterile 96 well plate, and 10 µL was added to each well from the first to the eleventh wells. The 12th hole was not added as the growth control. We added 100 µL of test bacterial suspension diluted by LB broth at 1:1,000 to each well, the 96 well culture plate was placed in a 37°C constant temperature incubator. We observed and recorded it every 2 h. At this time, the final concentration of antimicrobial peptides was 128, 64, 32, 16, 8, 4, 2, 1, 0.5, 0.25, and 0.125 µg/mL. Finally, the lowest concentration of antimicrobial peptides that completely inhibit bacterial growth in 96 well plates was identified as MIC.

4.9. *In vitro* bacteriostatic test

Antibacterial activity of the peptides was determined by a standard top agar assay. In brief, the bacterial strains used in this study were grown overnight in nutrient broth and inoculated into 10 mL of molten 1.0% nutrient agar at a final concentration of 10⁶ CFU/mL, followed by overlaying on a 90 mm Petri dish containing solidified 2% nutrient agar. After the top agar had solidified, 5-mm-diameter holes were punched out from each plate, and 10 µL of the peptide samples was added to the wells. The Petri dishes were incubated at 37°C. The peptide samples with antibacterial activity would form a clear zone around the holes. Meanwhile, synthetic peptides were used to compare

with secreted peptides, synthetic and secreted peptides were added to the agar well (10 µL, 30 µg/mL).

4.10. Determination of median lethal dose of test bacteria

A single colony of pathogenic *S. aureus* and *E. coli* were cultured in LB at 37°C for 18 h and used to inoculate the chickens as previously described. We isolated bacteria from dead chickens and inoculated them into LB plate medium, selected single colonies with good growth and inoculated them in LB liquid medium, prepared the test bacterial solution, and measured their growth turbidity by plate counting method. We configured the cultured test bacteria into bacterial solutions of different concentrations, and the concentrations were set as 1.00 × 10⁷ CFU/mL, 3.33 × 10⁷ CFU/mL, 1.11 × 10⁶ CFU/mL, 3.70 × 10⁵ CFU/mL, 1.23 × 10⁵ CFU/mL, 4.11 × 10⁴ CFU/mL, 1.37 × 10⁴ CFU/mL and 100 µL different concentrations of bacterial suspension were injected into the tested chickens through intraperitoneal injection, and the same amount of normal saline was used as the control group. The experimental chickens were randomly divided into two groups corresponding to *E. coli* and *S. aureus*. The concentration of each tested bacterial solution was verified with 6 chickens. During the experiment, the experimental chickens were raised in the most suitable environment for 7 days, and the growth and death were observed and recorded. The experimental chickens were dissected and observed after the experiment.

4.11. *In vivo* bacteriostatic test

Chickens (160) of the same weights were randomly divided into 2 parts, corresponding to two bacterial infection models of *S. aureus* and *E. coli*. The chickens were inoculated intraperitoneally with the tested bacteria, and the inoculation dose was twice the half lethal dose of the tested bacteria. Each part had five groups, with 10 chickens in each group, and received the following treatment (Table 4).

Experimental animals were observed before and after bacterial inoculations and physiological indexes such as mental state, feeding, drinking, feces and respiration were monitored. Chickens that succumbed to bacterial infections were examined for pathological changes. The livers, spleens and mesenteric lymph nodes of these animals were isolated and homogenates were diluted with normal saline and cultured on LB plates for CFU counting. Animals that were challenged with bacterial cultures developed typical symptoms. These animals then received antimicrobial peptides daily for 5 days as outlined in Table 4. The animals were observed for clinical changes and animals that succumbed were subjected to pathological examinations and bacterial isolation as per above.

5. Conclusion

The results indicated that the cathelicidin-BF peptide produced in *Pichia pastoris* had a good therapeutic effect for chickens challenged with a pathogenic strain of *S. aureus* and *E. coli*. In particular, the peptide cathelicidin-BF had the best therapeutic effect that was equivalent to Amoxicillin treatment. The current study provides a

TABLE 4 Overview of experimental groups used for animal testing.

Group	Processing method	Administration route
cathelicidin-BF	Infection, inoculated intraperitoneally antimicrobial peptides	Inoculated intraperitoneally, 300 µg/d
Normal saline control group	Infection, inoculated intraperitoneally normal saline	Inoculated intraperitoneally, 1.5 mL/d
Amoxicillin control group	Infection, inoculated intraperitoneally amoxicillin	Inoculated intraperitoneally, 300 µg/d
Blank control group	Infection, No administration	
Infection control group	No infection, No administration	

reference method for the prevention and treatment of *S. aureus* and *E. coli* disease.

All financial, commercial or other relationships that might be perceived by the academic community as representing a potential conflict of interest must be disclosed. If no such relationship exists, authors will be asked to confirm the following statement.

Data availability statement

The original contributions presented in the study are included in the article/supplementary material, further inquiries can be directed to the corresponding author.

Ethics statement

The animal study was reviewed and approved by Ethics Committee of Qingdao Agricultural University. Written informed consent was obtained from the owners for the participation of their animals in this study.

Author contributions

XD: methodology and writing—original draft. HS: project administration. SBW: technical support. ZJ and SJW: investigation. ZQ: supervision and review and editing. All authors contributed to the article and approved the submitted version.

References

Bulet, P. (1999). Drosophila antimicrobial peptides [J]. *Med. Sci.* 15, 23–29. doi: 10.4267/10608/1192

Costa, F., Teixeira, C., Gomes, P., and Martins, M. C. L. (2019). “Clinical application of antimicrobial peptides” in *Antimicrobial Peptides: Basics for Clinical Application*. ed. K. Matsuzaki (Singapore: Springer Singapore), 281–298.

Cunliffe, R. N., and Mahida, Y. R. (2004). Expression and regulation of antimicrobial peptides in the gastrointestinal tract [J]. *Leukoc Biol* 75, 49–58. doi: 10.1189/jlb.0503249

De Brabander, P., Uitterhaegen, E. D., De Winter, T., and Soetaert, W. (2023). Challenges and progress towards industrial recombinant protein production in yeasts: a review. *Biotechnol. Adv.* 64:108121. doi: 10.1016/j.biotechadv.2023.108121

Epand, R. M., and Vogel, H. J. (1999). Diversity of antimicrobial peptides and their mechanisms of action [J]. *Biochim. Biophys. Acta* 1462, 11–28. doi: 10.1016/S0005-2736(99)00198-4

Hancock, R. E. (2000). Cationic Antimicrobial Peptides: Towards clinical applications. *Expert Opin Invest Dis* 9:172329, 1723–1729. doi: 10.1517/13543784.9.8.1723

Hancock, R. E. (2001). Cationic peptides: effectors in innate immunity and novel antimicrobials [J]. *Lancet Infect. Dis.* 1, 156–164. doi: 10.1016/S1473-3099(01)00092-5

Funding

This research was supported by the Research and industrial development of new veterinary APIs and preparations, a major scientific and technological innovation project in Shandong Province (Major scientific and technological innovation projects in Shandong Province 2019JZZY020601); and the Study on the Mechanism of Immune Regulation of *Echinacea purpurea polysaccharides* on Macrophages of the Head Kidney of Turbot (General program of Shandong Natural Science Foundation, ZR2021MC173).

Conflict of interest

ZJ and SJW are employed by Shandong Hwatson Biochem Co. Ltd.

The remaining authors declare that the research was conducted in the absence of any commercial or financial relationships that could be construed as a potential conflict of interest.

Publisher’s note

All claims expressed in this article are solely those of the authors and do not necessarily represent those of their affiliated organizations, or those of the publisher, the editors and the reviewers. Any product that may be evaluated in this article, or claim that may be made by its manufacturer, is not guaranteed or endorsed by the publisher.

Hancock, R. E., and Chapple, D. D. (1999). Peptide antibiotics. *Antimic. Agents Chemother.* 43, 1317–1323. doi: 10.1128/AAC.43.6.1317

Hancock, R. E., and Diamond, G. (2000). The role of cationic antimicrobial peptides in innate host defences [J]. *Trends Microbiol.* 8, 402–410. doi: 10.1016/S0966-842X(00)01823-0

Hancock, R. E., and Sahl, H. G. (2006). Antimicrobial and host-defense peptides as new anti-infective therapeutic strategies. *Nat. Biotechnol.* 24, 1551–1557. doi: 10.1038/nbt1267

He, Q., Fu, A. Y., and Li, T. J. (2015). Expression and one-step purification of the antimicrobial peptide cathelicidin-BF using the intein system in *Bacillus subtilis*. *J. Ind. Microbiol. Biotechnol.* 42, 647–653. doi: 10.1007/s10295-014-1582-5

Hunter, H. N., Demcoe, A. R., Jenssen, H., Gutteberg, T. J., and Vogel, H. J. (2005). Human lactoferricin is partially folded in aqueous solution and is better stabilized in a membrane mimetic solvent [J]. *Antimicrob. Agents Chemother.* 49, 3387–3395. doi: 10.1128/AAC.49.8.3387-3395.2005

Kang, X., Dong, F., Shi, C., Liu, S., Sun, J., Chen, J., et al. (2019). DR antimicrobial peptides 2.0, an updated data repository of antimicrobial peptides. *Sci. Data.* 6:148. doi: 10.1038/s41597-019-0154-y

- Karbalaei, M., Rezaee, S. A., and Farsiani, H. (2020). *Pichia pastoris*: a highly successful expression system for optimal synthesis of heterologous proteins. *J. Cell. Physiol.* 235, 5867–5881. doi: 10.1002/jcp.29583
- Knappe, D., Schmidt, R., Adermann, K., and Hoffmann, R. (2019). Continuous subcutaneous delivery of proline-rich antimicrobial peptide api137 provides superior efficacy to intravenous administration in a mouse infection model. *Front. Microbiol.* 10:2283. doi: 10.3389/fmicb.2019.02283
- Lai, Y., and Gallo, R. L. (2009). AMPed up immunity: how antimicrobial peptides have multiple roles in immune defense [J]. *Trends Immunol.* 30, 131–141. doi: 10.1016/j.it.2008.12.003
- Lee, B. C., Hung, C. W., Lin, C. Y., Shih, C. H., and Tsai, H. J. (2019). Oral administration of transgenic biosafe microorganism containing antimicrobial peptide enhances the survival of tilapia fry infected bacterial pathogen. *Fish Shellfish Immunol.* 95, 606–616. doi: 10.1016/j.fsi.2019.10.052
- Liu, S., Cao, Y., Ma, L., Sun, J., Ramos-Mucci, L., Ma, Y., et al. (2022). Oral antimicrobial peptide-EGCG nanomedicines for synergistic treatment of ulcerative colitis. *J. Control. Release* 347, 544–560. doi: 10.1016/j.jconrel.2022.05.025
- Liu, R., Zhao, B., Zhang, Y., Gu, J., Yu, M., Song, H., et al. (2015). High-level expression, purification, and enzymatic characterization of truncated human plasminogen (Lys531-Asn791) in the methylotrophic yeast *Pichia pastoris*. *BMC Biotechnol.* 15:50. doi: 10.1186/s12896-015-0179-z
- Luan, C., Zhang, H. W., Song, D. G., Xie, Y. G., Feng, J., and Wang, Y. Z. (2014). Expressing antimicrobial peptide cathelicidin-BF in *Bacillus subtilis* using SUMO technology. *Appl. Microbiol. Biotechnol.* 98, 3651–3658. doi: 10.1007/s00253-013-5246-6
- Nguyen, L. T., Haney, E. F., and Vogel, H. J. (2011). The expanding scope of antimicrobial peptide structures and their modes of action[J]. *Trends Biotechnol.* 29, 464–472. doi: 10.1016/j.tibtech.2011.05.001
- Pasupuleti, M., Schmidtchen, A., and Malmsten, M. (2011). Antimicrobial peptides: key components of the innate immune system [J]. *Crit. Rev. Biotechnol.* 32, 143–171. doi: 10.3109/07388551.2011.594423
- Reddy, K. V., Yedery, R. D., and Aranha, C. (2004). Antimicrobial peptides: premises and promises [J]. *Int. J. Antimicrob. Agents* 24, 536–547. doi: 10.1016/j.ijantimicag.2004.09.005
- Scott, M. G., Rosenberger, C. M., Gold, M. R., Finlay, B. B., and Hancock, R. E. W. (2000). An α -helical cationic antimicrobial peptide selectively modulates macrophage response to LPS and directly alters macrophage gene expression [J]. *J. Immunol.* 165, 3358–3365. doi: 10.4049/jimmunol.165.6.3358
- Skerlavaj, B., Gennaro, R., Bagella, L., Merluzzi, L., Risso, A., and Zanetti, M. (1996). Biological characterization of two novel cathelicidin derived peptides and identification of structural requirements for their antimicrobial and cell lytic activities. *J. Biol. Chem.* 271, 28375–28381. doi: 10.1074/jbc.271.45.28375
- Tajbakhsh, M., Akhavan, M. M., Fallah, F., and Karimi, A. (2018). A recombinant Snake cathelicidin derivative peptide: antibiofilm properties and expression in *Escherichia coli*. *Biomol. Ther.* 8:118. doi: 10.3390/biom8040118
- Takahashi, D., Shukla, S. K., Prakash, O., and Zhang, G. (2010). Structural determinants of host defense peptides for antimicrobial activity and target cell selectivity[J]. *Biochimie* 92, 1236–1241. doi: 10.1016/j.biochi.2010.02.023
- Tan, P., Fu, H., and Ma, X. (2021). Design, optimization, and nanotechnology of antimicrobial peptides: from exploration to applications [J]. *Nano Today* 39:101229. doi: 10.1016/j.nantod.2021.101229
- Turner, J., Cho, Y., Dinh, N. N., Waring, A. J., and Lehrer, R. I. (1998). Activities of LL-37, a cathelin-associated antimicrobial peptide of human neutrophils [J]. *ASM journals on CD* 42, 2206–2214. doi: 10.1128/AAC.42.9.2206
- Turner, A., Lanser, D., and Gelli, A. (2023). Optimized expression and isolation of recombinant active secreted proteases using *Pichia pastoris*. *Bio-protocol* 13:e4628. doi: 10.21769/BioProtoc.4628
- Wang, G. (2015). Improved methods for classification, prediction, and design of antimicrobial peptides [J]. *Methods Mol. Biol.* 1268, 43–66. doi: 10.1007/978-1-4939-2285-7_3
- Wang, Y., Hong, J., Liu, X., Yang, H., Liu, R., Wu, J., et al. (2008). Snake cathelicidin from *Bungarus fasciatus* is a potent peptide antibiotics. *PLoS One* 3:e3217. doi: 10.1371/journal.pone.0003217
- Wang, Y., Zhang, Z., Chen, L., Guang, H., Li, Z., Yang, H., et al. (2011). Cathelicidin-BF, a snake cathelicidin-derived antimicrobial peptide, could be an excellent therapeutic agent for acne vulgaris. *PLoS One* 6:e22120. doi: 10.1371/journal.pone.0022120
- Weidner, M., Taupp, M., and Hallam, S. J. (2010). Expression of recombinant proteins in the methylotrophic yeast *Pichia pastoris*. *J. Vis. Exp.* 25:1862.
- Xie, Z., Zhao, Q., Wang, H., Wen, L., Li, W., Zhang, X., et al. (2020). Effects of antibacterial peptide combinations on growth performance, intestinal health, and immune function of broiler chickens. *Poult. Sci.* 99, 6481–6492. doi: 10.1016/j.psj.2020.08.068
- Xu, Y., Wang, Q., Dong, M., Song, H., Hang, B., Sun, Y., et al. (2023). Evaluation of the efficacy of the antimicrobial peptide HJH-3 in chickens infected with *Salmonella pullorum*. *Front. Microbiol.* 14:1102789. doi: 10.3389/fmicb.2023.1102789
- Yu, H., Wang, Y., Zeng, X., Cai, S., Wang, G., Liu, L., et al. (2020). Therapeutic administration of the recombinant antimicrobial peptide microcin J25 effectively enhances host defenses against gut inflammation and epithelial barrier injury induced by enterotoxigenic *Escherichia coli* infection. *FASEB J.* 34, 1018–1037. doi: 10.1096/fj.201901717R
- Zhang, L., Scott, M. G., Yan, H., Mayer, L. D., and Hancock, R. E. W. (2000). Interaction of polyphemusin I and structural analogs with bacterial membranes, lipopolysaccharide and lipid monolayers [J]. *Biochemistry* 39, 14504–14514. doi: 10.1021/bi0011173
- Zhang, H., Xia, X., Han, F., Jiang, Q., Rong, Y., Song, D., et al. (2015). Cathelicidin-BF, a novel antimicrobial peptide from *Bungarus fasciatus*, attenuates disease in a dextran sulfate sodium model of colitis [J]. *Mol. Pharm.* 12, 1648–1661. doi: 10.1021/acs.molpharmaceut.5b00069



OPEN ACCESS

EDITED BY

Octavio Luiz Franco,
Catholic University of Brasilia (UCB), Brazil

REVIEWED BY

Stawomir Milewski,
Gdansk University of Technology, Poland
Kamila Oliveira,
Catholic University of Brasilia (UCB), Brazil

*CORRESPONDENCE

Yu-Pei Chen

✉ 201600080006@xmmmc.edu.cn

RECEIVED 23 February 2023

ACCEPTED 22 May 2023

PUBLISHED 14 June 2023

CITATION

Chen Y-P, Li Y, Chen F, Wu H and Zhang S
(2023) Characterization and expression of
fungal defensin in *Escherichia coli* and its
antifungal mechanism by RNA-seq analysis.
Front. Microbiol. 14:1172257.
doi: 10.3389/fmicb.2023.1172257

COPYRIGHT

© 2023 Chen, Li, Chen, Wu and Zhang. This is
an open-access article distributed under the
terms of the [Creative Commons Attribution
License \(CC BY\)](#). The use, distribution or
reproduction in other forums is permitted,
provided the original author(s) and the
copyright owner(s) are credited and that the
original publication in this journal is cited, in
accordance with accepted academic practice.
No use, distribution or reproduction is
permitted which does not comply with these
terms.

Characterization and expression of fungal defensin in *Escherichia coli* and its antifungal mechanism by RNA-seq analysis

Yu-Pei Chen^{1,2,3*}, Yingying Li^{2,4}, Fangfang Chen^{1,2}, Hongtan Wu^{1,2}
and Shudi Zhang^{1,2}

¹Department of Public Health and Medical Technology, Xiamen Medical College, Xiamen, Fujian, China,

²Engineering Research Center of Natural Cosmeceuticals College of Fujian Province, Xiamen Medical College, Xiamen, Fujian, China, ³School of Public Health, Fujian Medical University, Fuzhou, Fujian, China, ⁴Department of Medical Technology, Xiamen Medical College, Xiamen, Fujian, China

Introduction: Invasive fungal infections (IFIs) are fatally threatening to critical patients. The fungal defensin as an antifungal protein can widely inhibit fungi.

Methods: In this study, eight antifungal genes from different filamentous fungi were optimized by synonymous codon bias and heterologously expressed in *Escherichia coli*.

Results and discussion: Only the antifungal protein (AFP) from *Aspergillus giganteus* was produced, whereas the AFP from its mutation of the chitin-binding domain could not be expressed, thereby suggesting the importance of the motif for protein folding. In addition, the recombinant AFP (rAFP, 100 µg/mL) pre-heated at 50°C for 1 h effectively inhibited *Paecilomyces variotii* CICC40716 of IFIs by 55%, and no cell cytotoxicity was observed in RAW264.7 cells. After being pre-heated at 50°C for 8 h, the fluorescence emission intensity of the rAFP decreased and shifted from 343 nm to 335 nm. Moreover, the helix and β-turn of the rAFP gradually decreased with the pre-heated treatment temperature of 50°C via circular dichroism spectroscopy. Propidium iodide staining revealed that the rAFP could cause damage to the cell membrane. Moreover, the corresponding differentially expressed genes (DEGs) for downregulation such as amino sugar and nucleotide sugar metabolism, as well as mitogen-activated protein kinase (MAPK) signaling pathway involved in the cell wall integrity were found via the RNA-seq of rAFP treatment. By contrast, the upregulated DEGs were enriched in response to the oxidative stress of Biological Process by the Gene Ontology (GO) database. The encoding proteins of laccase, multicopper oxidase, and nitroreductase that contributed to reactive oxygen species (ROS) scavenging could be recognized. These results suggested that the rAFP may affect the integrity of the cell wall and cell membrane, and promote the increase in ROS, thereby resulting in fungal death. Consequently, drug development could be based on the inhibitory effect of the rAFP on IFIs.

KEYWORDS

invasive fungal infections, fungal defensin, antifungal protein, *Paecilomyces variotii*, RNA-seq

1. Introduction

Invasive fungal infections (IFIs) have been increasing because of weak human immunity caused by diseases and the increase in antifungal resistance (Sanguinetti et al., 2019). Thus, they can affect various organs and cause infections such as meningitis, sinusitis, pneumonia, osteomyelitis, and enteritis. IFIs are caused by the filamentous fungus *Aspergillus* and yeast

Candida. However, with the aid and development of diagnostic technology, non-*Aspergillus* hyaline molds such as *Paecilomyces* spp., *Penicillium* spp., *Fusarium* spp., *Trichoderma* spp., and *Scedosporium* spp. were identified (Jacobs et al., 2020). In general, *Paecilomyces variotii* is distributed in air, soil, water, foods, and decaying plants. Recently, various cases of IFIs caused by *P. variotii* have been successively reported, such as pulmonary mycetoma, cutaneous mycetoma, intravascular infection, and pneumonia (Paixão Marques et al., 2019; Lazarus et al., 2020; Asif et al., 2021; Criado et al., 2021). Fluconazole is commonly used in patients with hematological malignancies, and it can effectively reduce the incidence of IFIs. However, fluconazole cannot protect an individual against *Aspergillus* and non-*Aspergillus* infections (Lionakis et al., 2018). In contrast, voriconazole with an extended spectrum inhibits *Aspergillus* and non-*Aspergillus* fungi (Ben-Ami, 2023). Thus, it has been applied in the clinical treatment of *P. variotii* infection (Sprute et al., 2021). Five patients were successfully cured out of the six cases of *P. variotii* infection.

Defensins derived from fungi have antifungal characteristics and can be found in different molds such as AnAFP, AcAFP, and AFP of *Aspergillus*; PgAFP, PAF, PAFB, and NAF of *Penicillium*; NFAP of *Neosartorya*; FgPAP of *Fusarium*; and MAFPI of *Monascus* (Tu et al., 2016; Patino et al., 2018; Varadi et al., 2018). The structure of fungal defensin has been explored based on the protein database (PDB) as AFP of *Aspergillus giganteus*, PAFB of *Penicillium chrysogenum*, and NFAP of *Neosartorya fischeri* (Campos-Olivas et al., 1995; Fizil et al., 2015; Huber et al., 2018). Typical fungal defensins contain antiparallel β -sheets with a β -barrel topology and disulfide bonds formed by 6–8 cysteines which may help maintain stability. Moreover, the signal secretion sequences and cutting site of mature protein were observed in the fungal defensins. In addition to being able to resist fungi, the defensin of PAF from *P. chrysogenum* is involved in its apoptotic and autophagic processes (Kovacs et al., 2014). A similar result was also consistent with the AnAFP from *Aspergillus niger* via transcriptome meta-analysis (Paege et al., 2016).

Generally, the antifungal mechanism of defensins is the interaction between the positively charged residues and the negatively charged residues of the plasma membrane, thereby resulting in temporary pores in the cell membrane. This phenomenon can be demonstrated by molecular dynamic simulations and nuclear magnetic resonance (NMR) spectroscopy analyses (Utesch et al., 2018). The γ -core motif of the structurally conserved AFP is involved in protein–membrane interactions, and it indirectly destroys the membranes' integrity through a multi-step process. The defensin enters the fungus, causing an intracellular disturbance, increasing reactive oxygen species (ROS), and leading to fungal death (Oshiro et al., 2019). In addition, the AFP of *A. giganteus* can inhibit chitin synthesis in sensitive fungi (Hagen et al., 2007). Furthermore, a well-conserved bacterial type 3 chitin-binding domain was found in the AFP of *A. giganteus*. The cell wall was further interfered with, and polar growth was retarded. However, the antifungal mechanism of defensin remains unclear.

In the present study, eight antifungal genes derived from different fungi using their optimal codon were heterologously expressed in *Escherichia coli* to produce and characterize fungal defensins. However, only the AFP from *A. giganteus* (CAA43181) was produced. The chitin-binding domain of the AFP was further

explored by point mutation assay to verify its importance. *P. variotii* CICC40716 was used for pathogen antagonistic assay. Antifungal capacity, cell cytotoxicity, and thermostability of recombinant AFP were carried out by the Oxford plate assay, propidium iodide (PI) staining, the 3-(4,5-cimethylthiazol-2-yl)-2,5-diphenyl tetrazolium bromide (MTT) assay, fluorescence assay, and circular dichroism spectroscopy. Finally, to examine the difference in gene expression in *P. variotii* CICC40716 with and without the recombinant AFP treatment, an RNA-seq analysis was carried out.

2. Materials and methods

2.1. Antifungal gene design

The OptimumGene software (GenScript Biotech Corp., Nanjing, China) was used to design eight antifungal genes from *Fusarium poae* (CAR79017), *N. fischeri* (CAQ42994), *A. giganteus* (CAA43181), *Fusarium asiaticum* (CAR79023), *Aspergillus clavatus* (ABR10398), *Colletotrichum gloeosporioides* (ELA33717), *P. chrysogenum* (DOEXD3), and *Fusarium boothii* (CAR79010) for codon optimization analysis (Supplementary Table 1). The optimal sequences were synthesized and introduced into pET-23a(+) within the *Sall/XhoI* sites by GeneDireX Inc. (Las Vegas, NV, United States) for the expression of plasmids to be obtained.

2.2. Expression of antifungal protein in *E. coli*

For the confirmation of the expression of antifungal proteins, these plasmids were transformed into *E. coli* C43(DE3) to confirm. A single colony of transformants was obtained from a Luria–Bertani (LB) agar plate with 100 μ g/ml of ampicillin. The transformant was incubated overnight in an LB broth and then transferred into a fresh LB broth at 37°C until OD₆₀₀ reached 0.4–0.5. The culture was incubated with and without IPTG (0.5 mM) at 25°C overnight. Afterward, the cells disrupted by a JY92-IIN sonicator (Ningbo Scientz Biotechnology, Ningbo, China) were harvested and suspended in a native buffer (50 mM NaH₂PO₄, pH 8.0, and 0.5 M NaCl). Subsequently, the supernatant was verified by sodium dodecyl sulfate-polyacrylamide gel electrophoresis (SDS-PAGE) and Coomassie blue staining. Furthermore, a Western blot analysis was carried out as described by Sambrook and Russell (2001). A primary antibody against His-tag at a dilution of 1:1,000 (BBI Life Sciences, Shanghai, China) and horseradish peroxidase-conjugated antibody to mouse immunoglobulin G (1:5,000 dilution; West Grove, PA, United States) were utilized. Finally, proteins were identified and performed using a SuperSignal West Pico Kit (Thermo Fisher Scientific Pierce, IL, United States).

2.3. Purification of antifungal protein

The antifungal protein was purified by a Ni-NTA purification system (Invitrogen, Carlsbad, CA, United States) and dissolved in a native buffer. The dissolved protein was dialyzed against the 1 \times native buffer, and the buffer was replaced four times for 2

days, followed by $0.1 \times$ native buffer for 1 day to remove the imidazole from the native elution buffer (Ni-NTA purification system). The dialysis protein was concentrated by lyophilization for antifungal analysis. The purified antifungal protein from *A. giganteus* (CAA43181) was designated as the rAFP.

2.4. Point mutation of antifungal protein

The point mutation of the chitin-binding domain was designed to verify the chitin-binding domain of recombinant AFP from *A. giganteus* (CAA43181) as follows: RYKAQ: AGGTACAAAGCGCAG (K15R); KNKAQ: AAGAACAAGCGCAG (Y16N); KYRAQ: AAGTACAGAGCGCAG (K17R); KYKVQ: AAGTACAAAGTGCAG (A18V); KYKAT: AAGTACAAAGCGACG (Q19T). The AFP genes with different chitin-binding domains were synthesized and introduced into pET-23a(+) within the *SalI/XhoI* sites by Azenta Life Sciences (Suzhou, Jiangsu, China) to obtain the expression plasmids. These plasmids were expressed in *E. coli* C43(DE3) and confirmed by the SDS-PAGE and Western blot analysis.

2.5. Antifungal assay of the rAFP

The Oxford plate assay was used to determine the antagonistic dosage of anti-fungi. The *P. variotii* CICC40716 was cultivated in Petri dishes containing potato dextrose agar. The Oxford plates with different concentrations of the rAFP from 0 to 200 μ g were set on the plate with *P. variotii* CICC40716 for 30°C cultivation. The clear zone of fungal inhibition was observed after 24 h of culture. In addition, the *P. variotii* CICC40716 spores obtained from the PDA plate were introduced into the PDB medium with OD₆₀₀ of ~ 0.1 – 0.2 about 3×10^6 spores/mL to 8×10^6 spores/mL. Then, 1 ml of broth with spores was added to a 24-well plate. Different concentrations of the rAFP (0, 12.5, 25, 50, and 100 μ g/mL) pre-treated from 30 to 80°C for 1 h were prepared to determine the antifungal rate by an enzyme-linked immunosorbent assay (ELISA) reader (Molecular Devices, Sunnyvale, CA, United States) at 600 nm. Furthermore, 100 μ g/mL of rAFP was incubated at 50°C for 1–8 h to explore the thermostability of the rAFP. The rAFP of thermal treatment was immediately chilled and used for antifungal rate assay in a 24-well plate.

2.6. Effect of the rAFP on cell viability

The cell viability of the RAW264.7 cell was determined by the MTT method to verify the cytotoxicity of the rAFP. The RAW264.7 cells were placed into a 96-well plate for 24 h and incubated at 5% CO₂ and 37°C. The rAFP proteins with the final concentrations of 0, 12.5, 25, 50, and 100 μ g/mL were added to the RAW264.7 cells for 24 h of reaction. The supernatant was removed, and cells were washed with PBS buffer. The fresh medium with 20 μ l of MTT (0.5%) was added to the cells for 4 h of reaction and 5% CO₂ incubation at 37°C. Finally, the medium was discarded, and

150 μ l of DMSO was utilized to dissolve the crystal product. The absorbance of OD₅₁₀ was measured using an ELISA reader (Molecular Devices).

2.7. Fluorescence assay of the rAFP

The rAFP of thermal treatment with a final concentration of 100 μ g/mL was utilized for fluorescence assay by an ELISA reader (Molecular Devices). The wavelength range of 300–500 nm with excitation at 280 nm was performed. The slit width of 4.66 nm was set in both excitation and emission.

2.8. Protein secondary structure assay of the rAFP

The secondary structure of 100 μ g/mL of rAFP with thermal treatment was analyzed over the wavelength of 180–260 nm by circular dichroism spectroscopy (Applied Photophysics, UK). The bandwidth and time-per-point were set to 1.0 nm and 0.5 s, respectively. The wavelength was recorded and treated by subtracting the baseline, and the CDNN software was utilized to evaluate the secondary structure content of the protein.

2.9. PI staining of fungi

The *P. variotii* CICC40716 spores were prepared with an OD₆₀₀ of 0.1–0.2 and mixed with the rAFP (0, 50, and 100 μ g/mL) at 30°C for 24 h of incubation. The hyphae were harvested and washed with a PBS buffer three times. The hyphae were suspended in a PBS buffer, and 20 μ l of PI (100 μ g/mL) was added for 5 min of reaction in the dark. The fluorescence image was obtained with a fluorescence microscope (Olympus BX43F-R, Tokyo, Japan).

2.10. RNA-seq analysis of *P. variotii* CICC40716

The *P. variotii* CICC40716 spores were introduced into fresh potato dextrose broth with an OD₆₀₀ of 0.1–0.2 in the presence and absence of the rAFP (50 μ g/mL). The *P. variotii* CICC40716 broth was cultured at 30°C for 24 h. *P. variotii* CICC40716 was harvested by Biomarker Technologies (Beijing, China) for RNA extraction, cDNA synthesis, library construction, cDNA sequencing, and *de novo* analysis. cDNA sequencing was carried out by an Illumina NovaSeq 6000 (Illumina, San Diego, CA). The sequencing reads were assembled and aligned by Trinity (Grabherr et al., 2011) and bowtie2 (Langmead et al., 2009). The unigenes were subjected to DIAMOND (Buchfink et al., 2015) for NR (Deng et al., 2006), Swiss-Prot (Apweiler et al., 2004), COG (Tatusov et al., 2000), and KEGG (Koonin et al., 2004) analyses. The InterProScan (Jones et al., 2014) was performed to obtain the result of GO Orthology (Ashburner et al., 2000). The differentially expressed genes (DEGs) were compared using DESeq2 (Love et al., 2014). A false discovery rate of <0.01 and a

fold change of >2 were used as the criteria. These RNA-seq data were deposited at DDBJ/ENA/GenBank under the accession no. of BioProject PRJNA924260, and SRA, SRR23091293, SRR23092107, SRR23095547, SRR23095642, SRR23095643, and SRR23095641.

2.11. Quantitation of gene expression by real-time RT-PCR

RNA was obtained according to the experimental condition of the RNA-seq analysis to confirm the result of RNA-seq. The HiFi-MMLV cDNA kit with oligo (dT) and random hexamers (Beijing ComWin Biotech, China) was utilized for the synthesis of first-strand cDNA at 42°C for 1 h of reaction. The cDNA was mixed with the UltraSYBR Mixture (Beijing ComWin Biotech) in a final volume of 12.5 μ l for real-time PCR using the Roche LightCycler[®] 480 System (Roche Group, Switzerland). The thermal cycling parameters included initial heating at 95°C for 10 min, denaturing at 95°C for 10 s, annealing at 58°C for 30 s, and extension at 72°C for 32 s, with an amplification of 40 cycles. The primer set of 18S rRNA as the internal control was 18SrRNA-F: CGATGG AAGTTTGAGGCAAT and 18SrRNA-R: CACGACGGAGTTTCA CAAGA. The primer sets of *P. variotii* CICC40716 genes were C24077-F: GCGTCGTCGCAATGTACTTC, C24077-R: CCAGAC CACGACTGTCAAGT; C24160-F: CCACCAGCAGTTATCAAG GG, C24160-R: GCCAGAACTATGACAGGCAC; C24458-F: TC CCTGGGTCTGCTCAACAA, C24458-R: GTCATCAACTCAGG ACGACC; C21938-F: AGGCTTCAACAAGCTCTCCG, C21938-R: CTCGCTGCCATGTTCGGAAT; C20865-F: GGGGAAGGGGG TCGTTTAAA, C20865-R: CCTAACCCGGACAGTCCTTT; C225 77-F: GCCAAGGAGAGGTGACAATG, C22577-R: GGAGCTTAT TCGAAGCTGGC; C13492-F: CTTTTCAGGGTCTCTGGTACG, C 13492-R: GCTGCTCATTACTCGTCCTC; and C13322-F: TCTTC GAGGTCGTCTGGCAA, C13322-R: GAGTACAGGTATGCAGC TGG.

3. Results

3.1. Expression and purification of antifungal protein

OptimumGene for heterologous expression of *E. coli* was used to optimize the codons of eight antifungal genes from *F. poae* (CAR79017), *N. fischeri* (CAQ42994), *A. giganteus* (CAA43181), *F. asiaticum* (CAR79023), *A. clavatus* (ABR10398), *C. gloeosporioides* (ELA33717), *P. chrysogenum* (DOEXD3), and *F. boothii* (CAR79010). The optimal antifungal sequences were synthesized and cloned into pET-23a(+) by the restriction sites of *Sall* and *XhoI*, with C-terminal His-tag triggered by the T7 promoter. The expression plasmids were introduced into *E. coli* C43(DE3). The band with an approximate molecular mass of 9.2 kDa derived from *A. giganteus* (CAA43181) could be observed on the SDS-PAGE after gene expression with IPTG induction in *E. coli* C43 (DE3) (Figure 1). The recombinant AFP fused with His-tag was verified through a Western blot analysis. The recombinant AFP was purified using a nickel

column, and a major band on SDS-PAGE was observed (Supplementary Figure 1). After purification, the yield of the recombinant AFP was ~ 780 μ g/L of culture. The purified recombinant AFP, namely, rAFP, was further used for follow-up analyses of antifungal activity, cell viability, thermostability, and RNA-seq.

3.2. Chitin-binding domain assay of the antifungal protein

Herein, the CKYKAQ sequence of the AFP from *A. giganteus*, which was similar to a conserved motif of AKWWTQ in the bacterial type 3 chitin-binding domain, was observed (Hagen et al., 2007). The point mutation of the antifungal protein was performed via sequence synthesis, which was introduced into the expression vector pET-23a(+) of *E. coli* to confirm the role of the chitin-binding domain in antifungal activity. Each point mutation of KYKAQ was replaced based on its related amino acid characteristics such as RNRVT. Five expression plasmids containing K15R, Y16N, K17R, A18V, and Q19T were cloned and expressed in *E. coli*. However, no protein was expressed at each point mutation based on the SDS-PAGE gel and Western blot analysis (Figure 2).

3.3. Antifungal ability of the rAFP on *P. variotii* CICC40716

Oxford plate assay and antifungal rate assay were conducted to verify the antifungal activity of purified rAFP against *P. variotii* CICC40716. The Oxford plate assay revealed an antifungal clear zone by adding 50 μ g of rAFP (Figure 3). As the concentration of rAFP increased, the clear zone was discernible. In addition, different doses of rAFP were pre-heated from 3 to 80°C for 1 h, which were utilized for the antifungal rate assay in 1 ml of broth of a 24-well plate. The result showed that a 79.3% inhibition rate of *P. variotii* CICC40716 was attained after 100 μ g/ml of rAFP pretreatment at 30°C for 1 h (Figure 4). Even if the rAFP was as low as 12.5 μ g/ml, the fungal inhibition rate remained at 57.3%. As the temperature increased, the antifungal rate declined. The fungal inhibition rate was lower than 20% after 100 μ g/ml of rAFP was pretreated at 70°C for 1 h. In contrast, the rAFP pre-heated at 50°C from 1 to 8 h was used to measure its fungal inhibition rate to detect the thermostability of antifungal protein. After 7 h of thermal pretreatment, the antifungal rate of 100 μ g/ml rAFP reduced to half of that after 1 h. However, no fungal inhibition was observed when the rAFP was lower than 25 μ g/ml after 8 h of thermal pretreatment.

3.4. Cell viability under the rAFP treatment

The RAW264.7 cell was utilized to detect the effect of rAFP on cell viability to identify the potential of rAFP

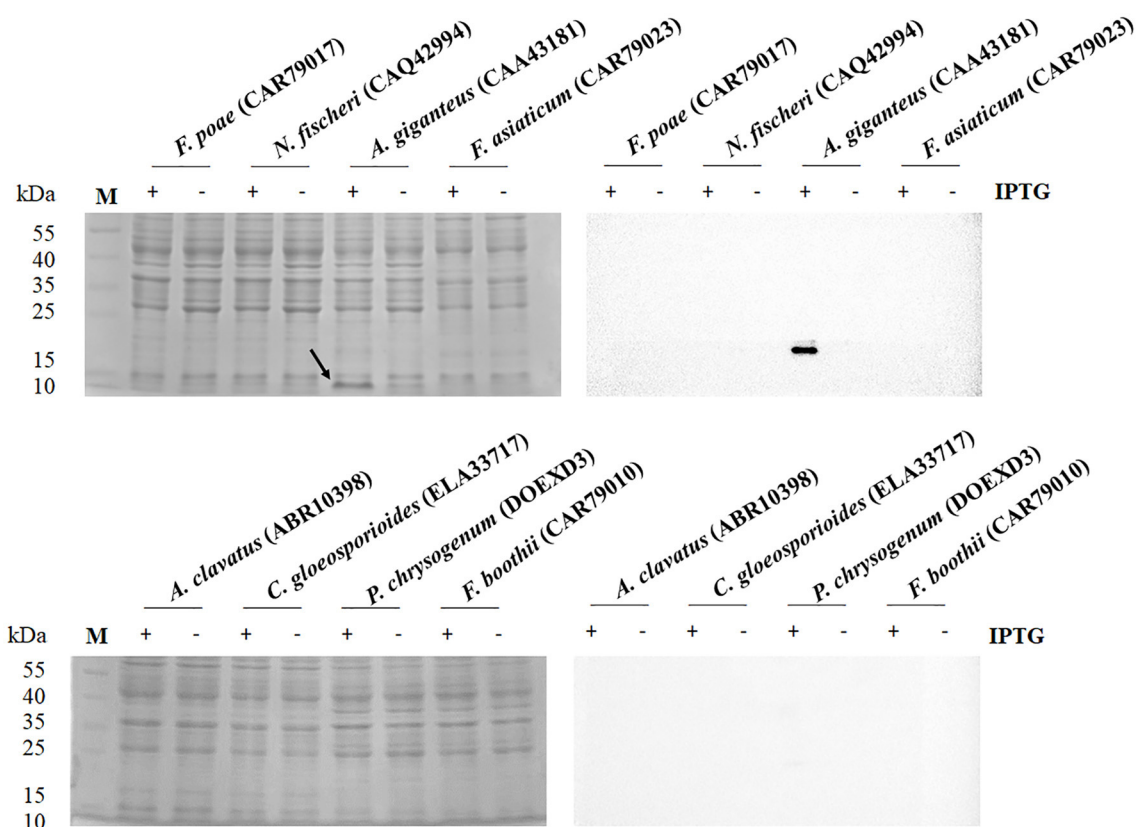


FIGURE 1

SDS-PAGE (left) and Western blot (right) analysis of antifungal protein from the protein accession numbers of CAR79017, CAQ42994, CAA43181, CAR79023, ABR10398, ELA33717, DOEXD3, and CAR79010. The antifungal proteins were carried out in the presence (+) and absence (–) of IPTG at 0.5 mM. The arrow indicates the expressed protein with an expected molecular mass of 9.2 kDa. The M indicates the protein marker.

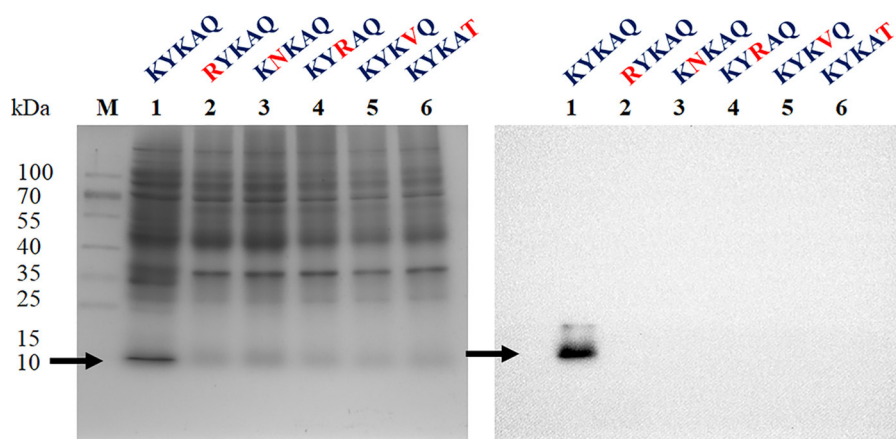


FIGURE 2

SDS-PAGE (left) and Western blot (right) analysis of rAFP with five-point mutations of the chitin-binding motif (KYKAQ). The red letter indicates the point mutations of the chitin-binding motif. The arrow indicates the expressed protein with the expected molecular mass of 9.2 kDa. The M indicates the protein marker.

as a medical treatment. Given that 100 µg/ml of rAFP can achieve a good fungal inhibition rate, the effect of different doses of rAFP from 0 to 100 µg/ml on RAW264.7 cells

was analyzed. No cytotoxicity was observed, and the survival rate of the RAW264.7 cells was maintained at almost 100% (Figure 5).

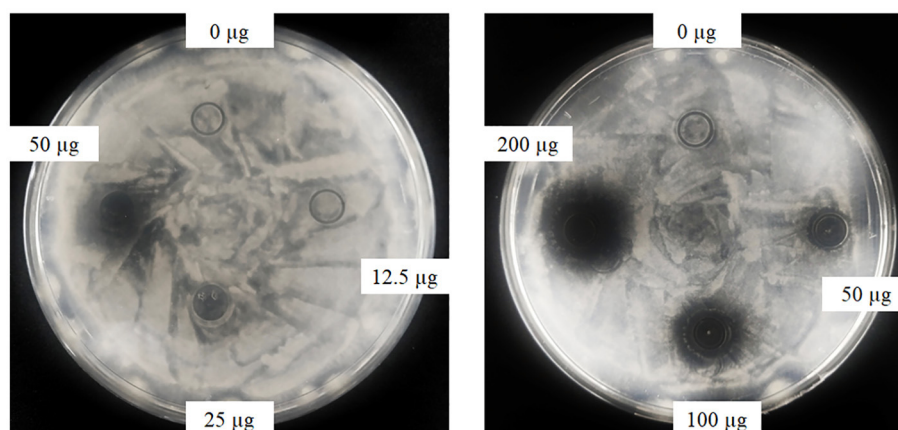


FIGURE 3

Antifungal activity of the rAFP with different concentrations (0, 12.5, 25, 50, 100, and 200 μg) against *P. variotii* CICC40716 using the Oxford plate assay. The plates were cultured at 30°C for 24 h, while the growth inhibitions of *P. variotii* CICC40716 were observed.

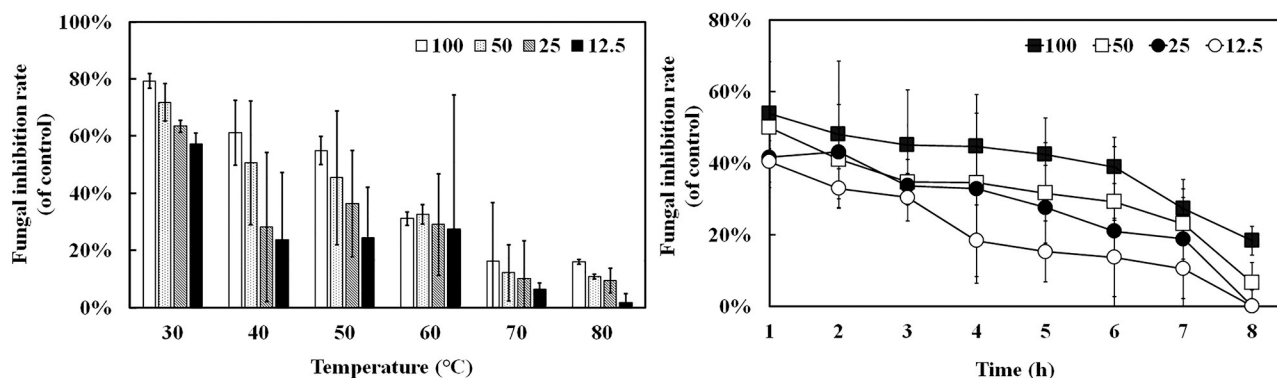


FIGURE 4

Antifungal activity of the rAFP pre-heated from 30 to 80°C for 1 h with different concentrations (12.5, 25, 50, and 100 $\mu\text{g/mL}$) against *P. variotii* CICC40716. The thermostability assay of the rAFP pre-heated at 50°C from 1 to 8 h. The fungal inhibition rate was calculated as follows: $[(\text{OD}_{600} \text{ of control} - \text{OD}_{600} \text{ of rAFP treatment}) / \text{OD}_{600} \text{ of control}] \times 100$.

3.5. Effect of temperature on the rAFP protein structure by fluorescence and circular dichroism spectroscopy

Given that the intrinsic fluorophores of tyrosine and phenylalanine occupying 10% of the rAFP with six Tyr and one Phe were distributed around the cysteine disulfide bonds, the effect of temperature on the antifungal protein structure was investigated using the fluorescence spectroscopy. The rAFP had a strong emission at 343 nm under an excitation of 280 nm. The change in fluorescence emission intensity was observed in the rAFP pre-heated at 50°C from 0 to 8 h (Figure 6). The fluorescence emission intensity of the rAFP decreased and shifted to 335 nm with an increase in thermal pretreatment. After the thermal pretreatment for 2, 4, 6, and 8 h, the fluorescence emission intensity of the rAFP was reduced by 12.0, 19.4, 37.2, and 43.2%, respectively, based on the strong emission at 343 nm.

Thus, CD spectroscopy in the wavelength range of 180–260 nm was performed to further study the change in the protein structure of rAFP by thermostability (Table 1). The results indicated that the amount of helix and β -turn in the rAFP decreased with the increase in thermal pretreatment. After pre-heating for 8 h at 50°C, the helix and β -turn of the rAFP were reduced by 47 and 33.9%, respectively.

3.6. Effect of the rAFP on the cell membrane integrity of *P. variotii* CICC40716

To confirm whether the rAFP will affect the integrity of the cell membrane, PI, a fluorescent dye, was utilized. PI dye can enter the damaged cell membrane and react with DNA and RNA to emit red fluorescence. Fluorescence microscope observations were made in the presence and absence of the rAFP for the *P.*

variotii CICC40716. However, no red fluorescence was observed in the control, thereby indicating the intact cell membrane of *P. variotii* CICC40716 (Figure 7). The red fluorescence in *P. variotii* CICC40716 was significantly perceived in the presence of 50 and 100 $\mu\text{g/ml}$ of rAFP. Thus, the cell membranes of the *P. variotii* CICC40716 were damaged, and their permeability was improved.

3.7. RNA-seq analysis of *P. variotii* CICC40716 with the rAFP treatment

For the RNA-seq analysis, *P. variotii* CICC40716 was treated with and without rAFP (50 $\mu\text{g/ml}$). An average of 21,982,300 clean reads was obtained from each treatment in triplicate (Supplementary Table 2). The clean reads of each sample were

mapped back to the assembled transcripts. The assembled transcripts accounted for an average of 92.46% of clean reads. Pearson's correlation was carried out to examine the gene expression correlation of the triplicates. The results showed that the triplicate of each treatment with and without the rAFP had a high correlation with an average of 0.99 and 0.93, respectively.

The RNA sequencing results suggested that a total of 10,177 unigenes with a threshold of BLAST E-value not larger than $1e-5$ and HMMER E-value larger than $1e-10$ were detected in these samples. A total of 5,164, 7,744, and 5,983 unigenes were annotated based on the COG, GO, and KEGG databases, respectively. After rAFP treatment, 531 DEGs with more than a 2-fold change in *P. variotii* CICC40716 were identified by the volcano plot (Figure 8). The numbers of upregulated and downregulated genes were 280 and 251 genes, respectively. COG, GO classification, and KEGG pathway of DEGs are shown in Figure 9. The 15 most upregulated and downregulated genes with the rAFP treatment are shown in Supplementary Tables 3, 4. The multidrug transporter genes corresponding to the resistance of antifungal agents can be influenced by antifungal drugs (Wu et al., 2016; Samaras et al., 2020). Table 2 shows the effect of the rAFP on the genes involved in the multidrug transporter. In the COG database, general function prediction only (R), lipid transport and metabolism (I), secondary metabolites biosynthesis, transport and catabolism (Q), amino acid transport and metabolism (E), carbohydrate transport and metabolism (G), and inorganic ion transport and metabolism can be perceived in the most upregulated and downregulated function classes (Figure 10). In the KEGG pathway, the rich factor indicated the ratio of the DEGs (sample) enriched in the pathway to the amounts of annotated genes (background) (Figure 11). Moreover, the closer the q -value is to 0, the more significant the enrichment is. Biotin and tyrosine metabolism were observed in the high rich factor and low q -value in the upregulation of the KEGG pathway, respectively, whereas synthesis and degradation of ketone bodies and amino sugar and nucleotide

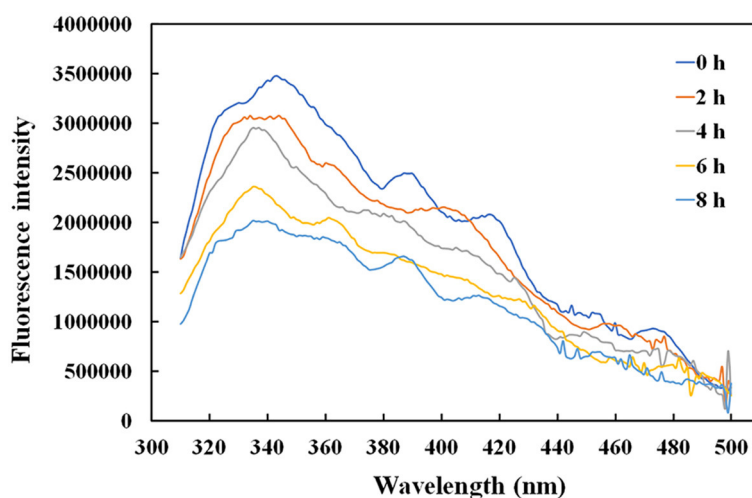
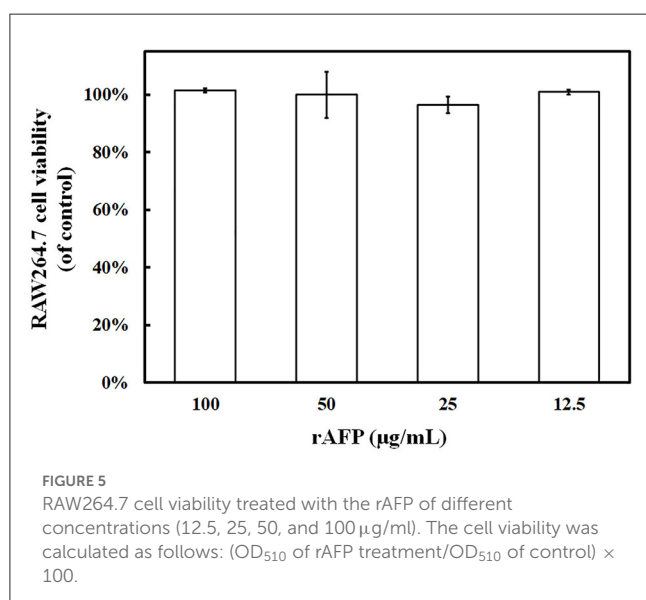
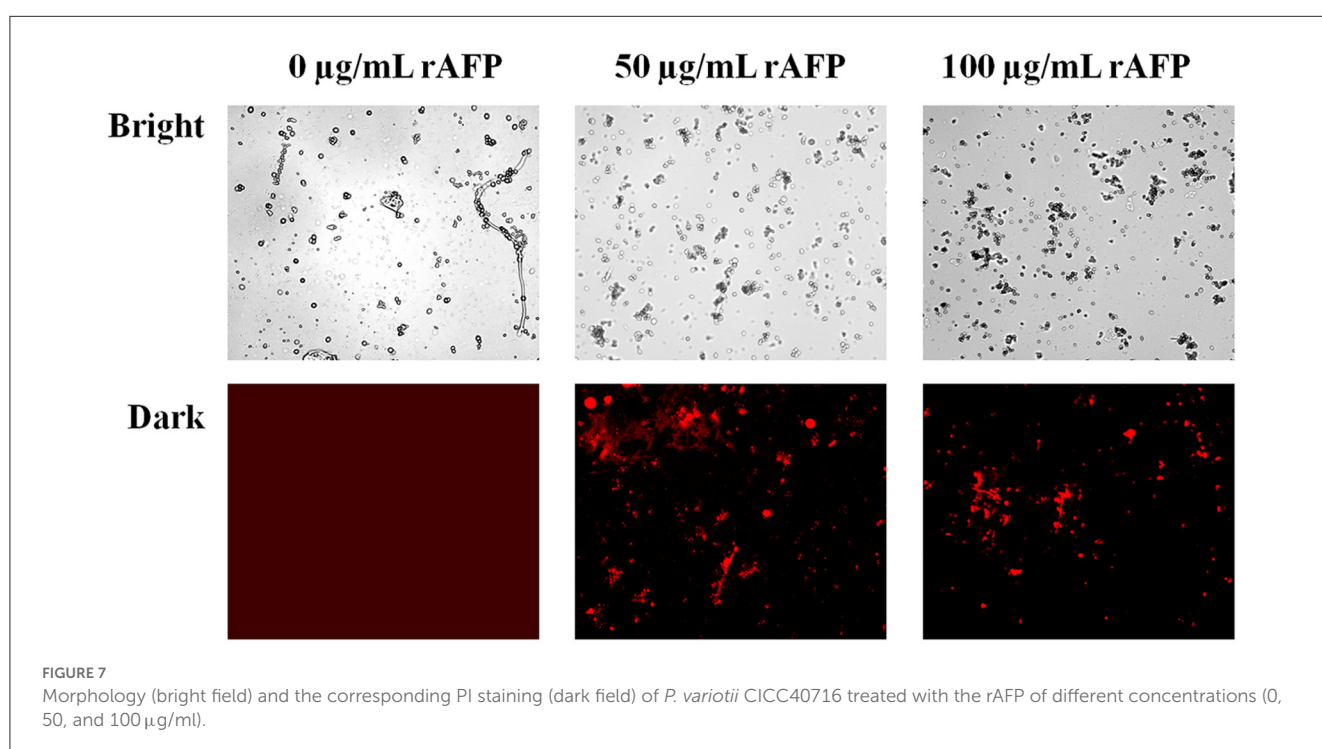


FIGURE 6
Fluorescence spectra of rAFP pre-heated at 50°C from 0 to 8 h using an ELISA reader.

TABLE 1 CD spectra of rAFP pre-heated at 50°C from 0 to 8 h.

Time	Helix	Antiparallel	Parallel	β -Turn	Random coil
0 h	21 \pm 0.4%	70.7 \pm 2.2%	13.8 \pm 1.7%	24.7 \pm 0.6%	38.1 \pm 1.1%
1 h	20.77 \pm 0.61%	41.77 \pm 3.21%	16.3 \pm 0.3%	21.13 \pm 0.57%	46.07 \pm 0.32%
2 h	18.57 \pm 0.85%	28.17 \pm 2.25%	14.17 \pm 0.59%	19.8 \pm 0.2%	45.47 \pm 0.35%
3 h	15.87 \pm 0.9%	26.4 \pm 3.46%	14.37 \pm 0.9%	18.67 \pm 0.4%	43.8 \pm 0.35%
4 h	14.83 \pm 0.35%	40.67 \pm 0.58%	14.23 \pm 1.32%	18.4 \pm 0.26%	42.73 \pm 0.78%
5 h	13.6 \pm 0.35%	40.27 \pm 0.58%	18.13 \pm 1.01%	17 \pm 0.62%	59.23 \pm 1.18%
6 h	12.8 \pm 0.3%	42.8 \pm 0.46%	15.27 \pm 1.04%	17.43 \pm 0.45%	41.03 \pm 0.51%
7 h	12.1 \pm 0.3%	38.93 \pm 0.64%	21.17 \pm 0.75%	16.73 \pm 0.4%	57.37 \pm 0.67%
8 h	11.13 \pm 0.68%	41.73 \pm 2.35%	16.8 \pm 0.61%	16.33 \pm 0.55%	44.8 \pm 0.85%

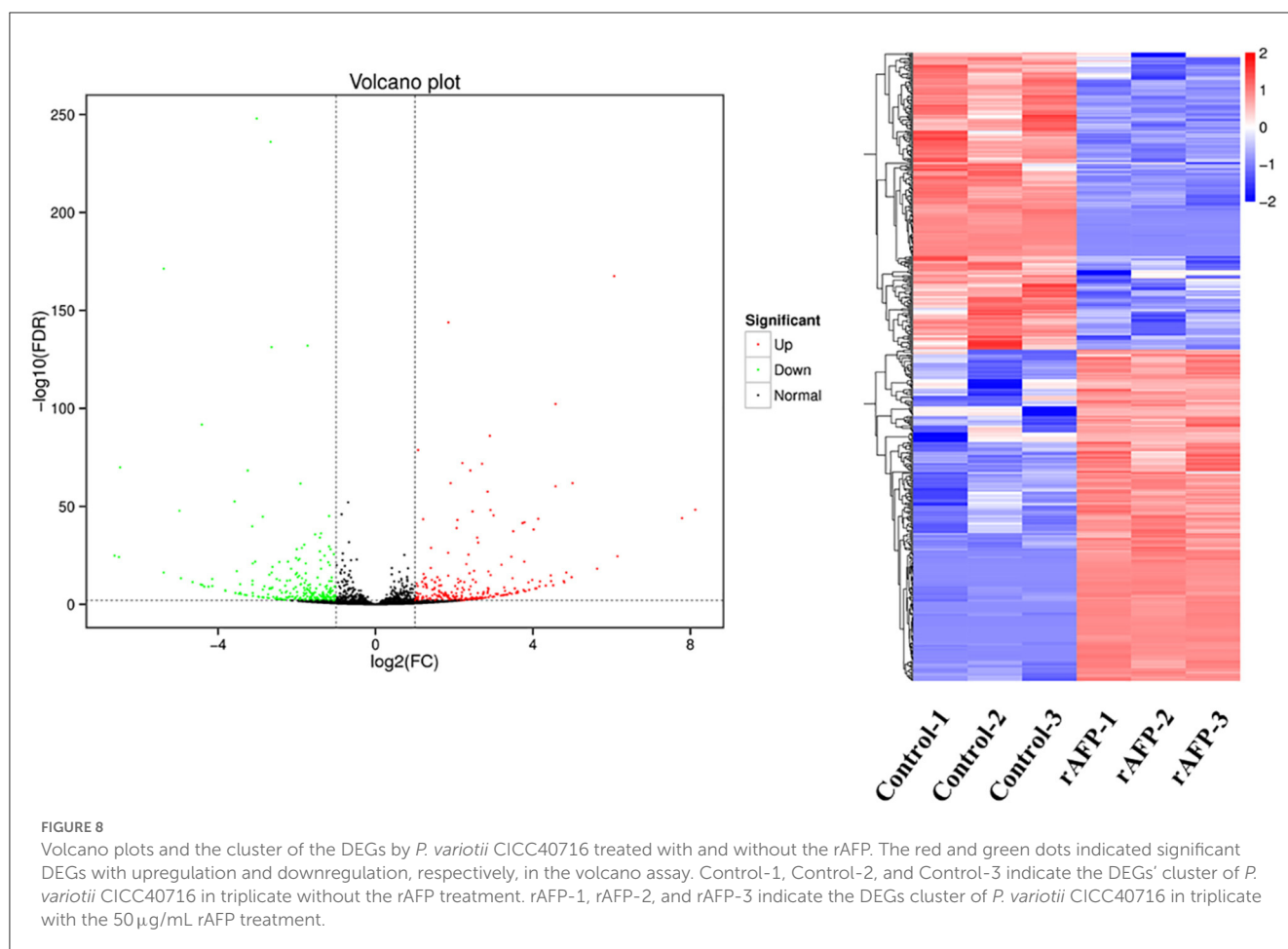


sugar metabolism were found in that of the downregulation of the KEGG pathway. On the one hand, in the GO database, the most upregulated genes involved in response to oxidative stress, integral component membrane, and oxidoreductase activity were shown in biological processes, cellular components, and molecular functions, respectively (Figure 12). On the other hand, the most downregulated genes involved in methylation, integral component membrane, and 6-phosphofructo-2-kinase activity were identified in biological processes, cellular components, and molecular functions, respectively.

Eight genes containing four upregulated genes and four downregulated genes were randomly selected for real-time RT-PCR to verify the findings of RNA-seq analysis. The results revealed that the gene regulation using real-time RT-PCR was consistent with the change in RNA-seq with and without the rAFP treatment (Supplementary Table 5).

4. Discussion

Some studies have been conducted on the heterologous expression of antifungal proteins. Recombinant mature AFP from *A. giganteus* expressed in the yeast *Pichia pastoris* is indistinguishable from the natural AFP (Lopez-Garcia et al., 2010). However, Glu-Ala-Glu-Ala-Glu repeats at the N-terminal of the AFP inactivated its antifungal activity. Moreover, the AFP was transferred into *A. niger* and had a very low expression level with a maximal concentration of 350 μ g/L (Wnendt et al., 1994). Meanwhile, MAFP1 derived from *Monascus pilosus* can be expressed and obtained from *E. coli* with approximately 1 mg/L of culture (Tu et al., 2016). Nevertheless, the recombinant MAFP1 has lower antifungal activity than that of the native protein. Therefore, the heterologous expression of fungal defensin is difficult. Thus, in the present study, the codon optimization of fungal defensin was carried out to avoid the incompatibility of codon usage bias,



resulting in low expression or protein misfolding. Unfortunately, only the AFP derived from *A. giganteus* was expressed in *E. coli* (Figure 1). Even if the antifungal protein between *A. giganteus* (CAA43181) and *A. clavatus* (ABR10398) had only two amino acid differences, the usage of synonymous codons for gene expression may be the factor that caused the defensin derived from *A. clavatus* to fail to express in *E. coli*. Furthermore, the His-tag fused on the N-terminus or C-terminus of AFP may result in different expression levels. The C-terminal His-tag may interrupt the protein folding process of the other antifungal proteins (Li et al., 2009). Thus, the recombinant AFP of *A. giganteus* (CAA43181) was used to study its characterization and antifungal mechanism.

A conserved chitin-binding domain, CKYKAQ, involved in the inhibition of chitin synthesis of sensitive fungi existed in AFP of *A. giganteus* (Hagen et al., 2007). K15R, Y16N, K17R, A18V, and Q19T were the five-point mutations designed for heterologous expression in *E. coli* to characterize the chitin-binding domain. Unexpectedly, no protein in these mutations was produced (Figure 2). Cys14 was considered a disulfide bond pairing to Cys40, and Cys14 to Tyr16 was located in one of the five antiparallel β -strands based on the protein structure of AFP in the PDB (Campos-Olivas et al., 1995). In addition, Lys15, Tyr16, and Ala18 had polar contacts with the adjacent amino acids such as Lys6, Tyr8, Thr23, and Gly21, respectively, based on a PyMOL analysis (Supplementary Figure 2) (Janson et al., 2017). Although no polar contact was found in Lys17

and Gln19, Gly21 and Tyr3 were close to the two amino acids with short distances of 2.21 and 2.37 Å, respectively, thereby suggesting the existence of van der Waals interactions to maintain the protein conformation. In contrast, no polar contact was identified in the mutation of Y16N, K17R, and A18V, whereas K15R and Q19T had polar contacts with Lys6, Tyr3, and Ser20. The change in interactions from charge matching of certain side groups and van der Waals coordination between these mutation regions may result in the inability to produce antifungal proteins in *E. coli* (Liu et al., 2020). Although the ability of this conserved chitin-binding domain to inhibit fungi cannot be demonstrated, the motif would affect whether or not the rAFP can be expressed and folded.

The rAFP had an antifungal effect on *P. variotii* CICC40716. Meanwhile, no cytotoxicity was observed in the RAW264.7 cell. The selective advantage suggested that the rAFP had the potential as a fungicide for medicine. Little attention has been devoted to the thermostability of AFP from *A. giganteus*. However, a volume of research has been published on thermostable plant defensins from cowpea seeds and *Phaseolus vulgaris* L. (Chan and Ng, 2013; Thery and Arendt, 2018). In the present study, 100 μ g/ml of rAFP still retained over 40% antifungal activity after 50°C pretreatment for 5 h, thereby suggesting the certain thermal stability of the rAFP (Figure 4). Furthermore, its thermostability may be due to high β -sheet contents, and salt-bridge interactions of Lys, Asp, Arg, and Glu account for 28.8% of

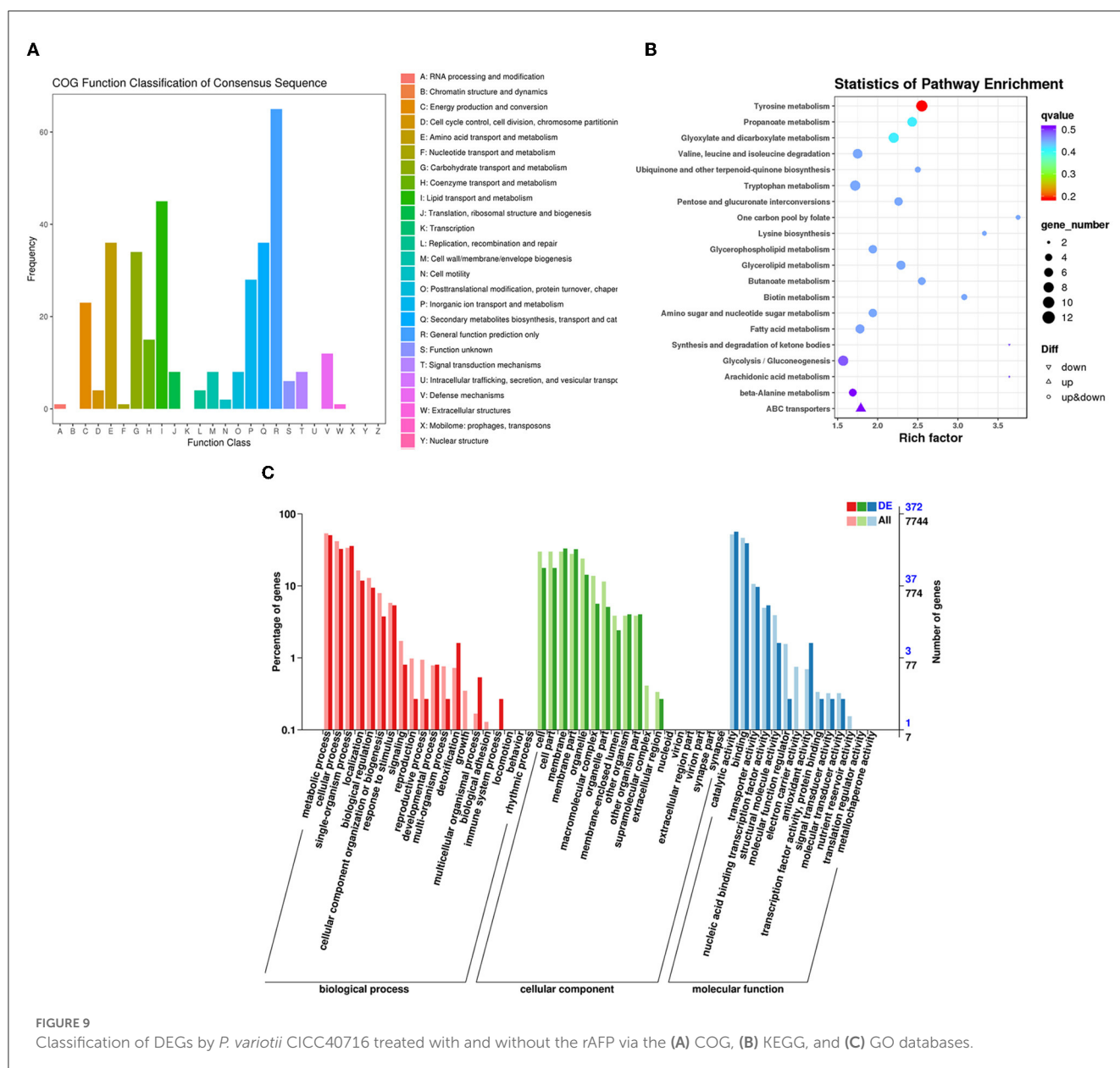


FIGURE 9

Classification of DEGs by *P. variotii* CICC40716 treated with and without the rAFP via the (A) COG, (B) KEGG, and (C) GO databases.

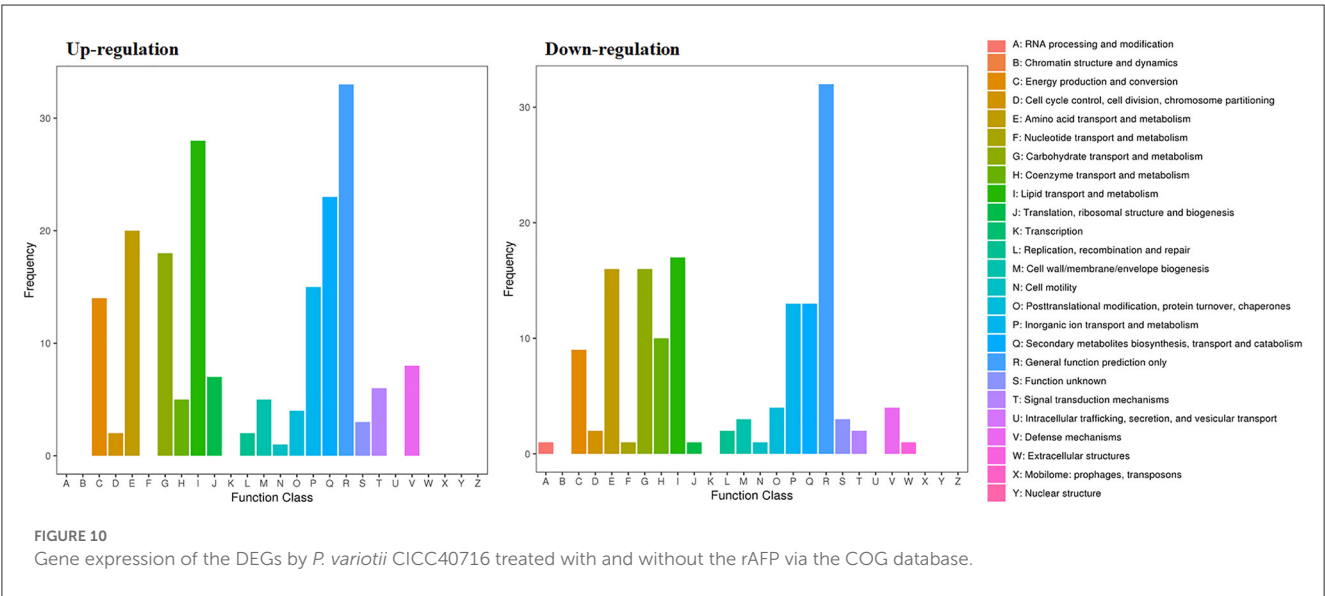
the rAFP (Zhou et al., 2008; Niu et al., 2015). Although tryptophan was responsible as a good fluorescent indicator in the change in the molecular structure because of its high sensitivity to photophysical parameters (Zhdanova et al., 2015), tyrosine could be used to monitor the conformational change in tryptophan-lacking protein (Zhdanova et al., 2017). In this study, the intrinsic fluorophores of tyrosine and phenylalanine of the rAFP distributed around the cysteine disulfide bonds were observed under a maximal emission peak at 343 nm (Figure 6). As the heat treatment time of the rAFP increased, the fluorescence emission intensity declined and shifted from 343 to 335 nm, thereby indicating the conformational change in the protein structure. This result was similar to the tryptophan as the fluorescent probe to measure protein unfolding, ranging from 330 nm (hydrophobic environment) to 350 nm (hydrophilic environment) of the fluorescence peak (Kotov et al., 2021). Therefore, CD spectroscopy was used to further investigate the

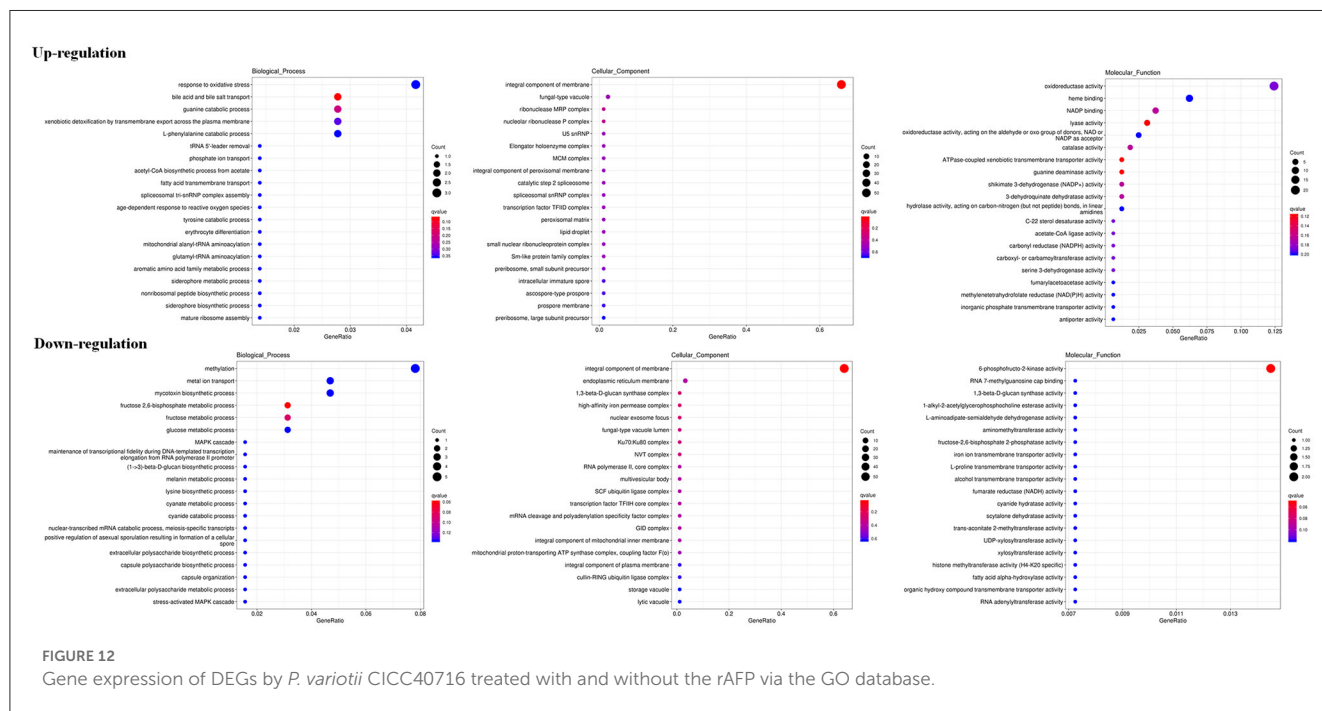
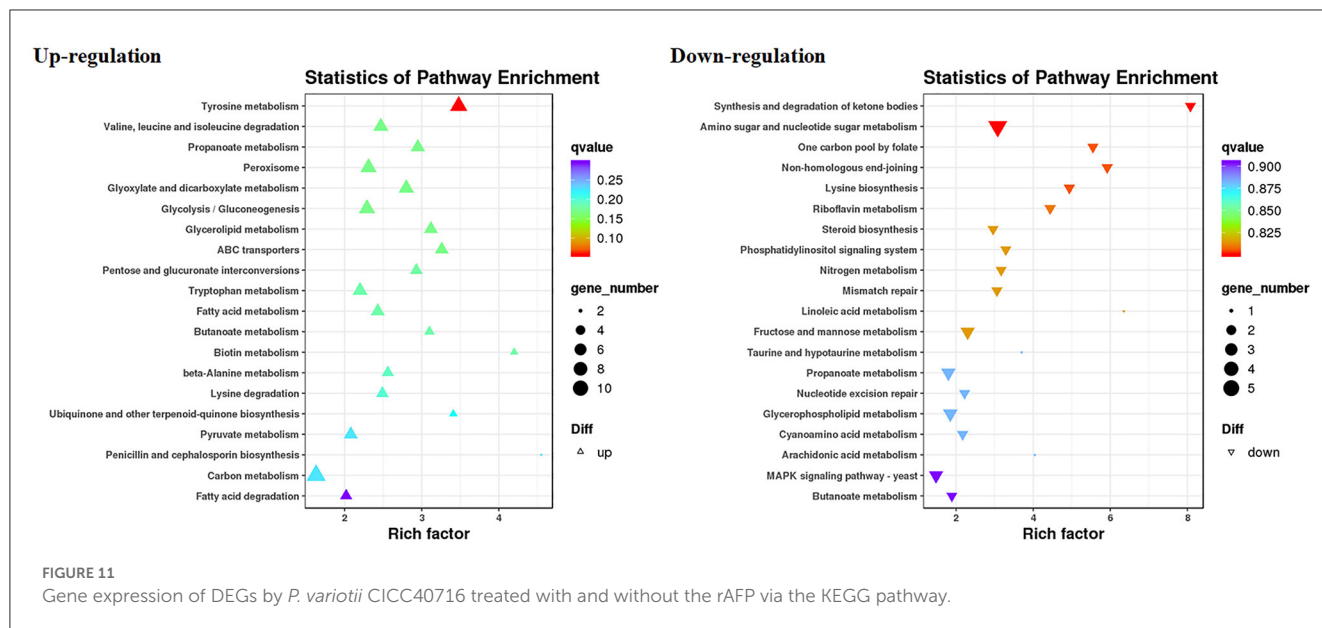
effect of thermal unfolding on the secondary structure of the rAFP. The main secondary structure of the antiparallel arrangement in the rAFP was consistent with the protein structure of the previous report (Table 1) (Campos-Olivas et al., 1995). Different protein structures, such as the increased helix and β -sheet contents, additional salt bridges, decreased cavities, and chain flexibility, could be responsible for the contribution of thermostability (Zhou et al., 2008). CD spectroscopy revealed that the helical and β -turn structures of the rAFP attributed to thermal stability collapsed as the heating time increased. This result was consistent with the findings of antifungal activity and fluorescence.

Several efflux transporters in fungi including ATP binding cassette (ABC) superfamily transporters, major facilitator superfamily (MFS) transporters, multidrug and toxic compound extrusion (MATE), small multidrug resistance (SMR), and resistance-nodulation-cell division (RND) are correlated with

TABLE 2 Multidrug resistance transporter genes responding to the ratio of the rAFP treatment to control *P. variotii* CICC40716.

Regulation	ID	DNA size (bp)	NR annotation	Swiss-prot annotation	log ₂ ratio
Upregulation	c13492.graph_c0	3,198	MFS transporter, putative	Major facilitator superfamily multidrug transporter mfsB	5.633
	c20529.graph_c0	2,162	Lactose permease	MFS-type transporter oryC	3.981
	c22476.graph_c0	2,493	Hypothetical protein	Probable glucose transporter HXT5	3.501
	c22033.graph_c0	1,097	Hypothetical protein	MFS-type transporter oryC	2.846
	c20536.graph_c0	5,933	ABC drug exporter AtrF	ABC multidrug transporter atrF	2.751
	c17990.graph_c1	2,262	ABC multidrug transporter Mdr1	ABC multidrug transporter mdr1	2.102
	c16566.graph_c0	2,157	Putative siderophore iron transporter	Major facilitator copper-regulated transporter crmC	2.027
	c17990.graph_c0	3,108	ABC multidrug transporter Mdr1	ABC multidrug transporter mdr1	1.908
	c21886.graph_c0	2,626	Putative MFS drug efflux pump	MFS-type transporter VdtG	1.477
	c13207.graph_c0	2,707	MATE efflux family protein subfamily	Uncharacterized transporter	1.185
	c19500.graph_c0	1,105	MFS transporter	–	1.017
Downregulation	c22950.graph_c0	1,538	MFS general substrate transporter	MFS transporter PfmaC	–3.419
	c19986.graph_c0	2,067	Hypothetical protein PVAR5_0967	Transporter mfs1	–2.820
	c23933.graph_c2	1,908	MFS monosaccharide transporter	Low-affinity glucose transporter HXT3	–2.694
	c22200.graph_c0	9,011	Hypothetical protein	Uncharacterized MFS-type transporter	–1.578
	c23297.graph_c1	1,181	MFS transporter	MFS transporter M2	–1.552
	c18577.graph_c0	2,637	MFS transporter	Uncharacterized membrane protein	–1.178
	c22560.graph_c1	9,533	Major facilitator superfamily domain-containing protein	Multidrug resistance protein fnx1	–1.015
	c22719.graph_c0	1,864	MFS monocarboxylate transporter	MFS-type transporter	–1.010





resistance to fungicides (Kuroda and Tsuchiya, 2009; Rahman et al., 2017; Samaras et al., 2020). In general, these efflux transporters associated with multidrug resistance (MDR) are expressed against fungicides such as *Penicillium digitatum* and *Zymoseptoria tritici* (Omran et al., 2015; Wu et al., 2016). A total of 19 efflux transporters were identified in this study in the DEGs of *P. variotii* CICC40716 corresponding to 11 and eight upregulated and downregulated genes by RNA-seq analysis, respectively (Table 2). A limited number of ABC transporters and MATE that contributed to upregulation was perceived. In contrast, the gene expression levels of MFS transporters were upregulated and downregulated. Thus, the ABC

transporters and MATE served as the sensitive gene induced by the rAFP.

The cell wall protects the cell from osmotic change and shapes the cell form, and several carbohydrate metabolic activities are necessary for cell wall biosynthesis (Song et al., 2022). Mitogen-activated protein kinase (MAPK) is necessary for cell wall integrity pathway (CWIP) activation (Rocha et al., 2015; Gurgel et al., 2019). In this study, the changes in the metabolic pathways of downregulation such as amino sugar and nucleotide sugar metabolism, as well as the MAPK signaling pathway involved in the cell wall integrity, can be found after mapping the DEGs to the KEGG database (Figure 11). The result corresponded to

the PI assay, thereby suggesting the collapse of the cell wall and damage to the cell membrane (Figure 7). In contrast, tyrosine metabolism in the upregulation pathway was greatly affected, which may be responsible for drug resistance (Zhang et al., 2021). This was also observed in the extract of *Amaranthus tricolor* leaf as a bacteriostatic agent against *Acidovorax avenae* subsp. *citrulli* (Zhang et al., 2021).

ROS increase induced by antifungal protein is one of the factors that can inhibit fungal growth (Oshiro et al., 2019). Thus, the antioxidant defense system was triggered to eliminate ROS by activating antioxidant enzymes such as catalase, peroxidase, and superoxide dismutase (Glorieux and Calderon, 2017). In the present study, the corresponding upregulated DEGs were enriched in response to the oxidative stress of biological processes based on the GO database (Figure 12). Catalase and cytochrome c peroxidase were identified and upregulated in response to oxidative stress after the rAFP treatment of *P. variotii* CICC40716 (Glorieux and Calderon, 2017; Shin et al., 2017). Moreover, the corresponding upregulated DEGs were enriched in the oxidoreductase activity of molecular function. The encoding proteins of laccase, multicopper oxidase, and nitroreductase contributing to ROS scavenging could be found (Pompeu et al., 2019; Zhou et al., 2021; Monteiro et al., 2022). These results suggested that the ROS increase in the *P. variotii* CICC40716 treated by the rAFP induced the activation of antioxidant defense enzymes.

5. Conclusion

IFIs with drug resistance are an issue of global public health. Thus, new antifungal drugs are necessary to be developed. Herein, the rAFP derived from the optimal sequence of *A. giganteus* (CAA43181) was expressed in *E. coli*, and it was capable of antifungal effects against the *P. variotii* CICC40716. After pre-heating for 8 h at 50°C, the great fluorescence emission of the rAFP was shifted from 343 to 335 nm. Moreover, the helix and β -turn of the rAFP decreased with the increase in thermal pretreatment, indicating the destruction of the protein secondary structure. However, the rAFP was not cytotoxic to RAW264.7 cells and may influence the integrity of the cell wall and cell membrane of the *P. variotii* CICC40716. Furthermore, the upregulation of the antioxidant defense system indicated the increase in ROS, thereby resulting in fungal death. Consequently, the rAFP can be a fungal inhibitor for medical treatment.

References

- Apweiler, R., Bairoch, A., Wu, C. H., Barker, W. C., Boeckmann, B., Ferro, S., et al. (2004). UniProt: the universal protein knowledgebase. *Nucleic Acids Res.* 32, D115–119. doi: 10.1093/nar/gkh131
- Ashburner, M., Ball, C. A., Blake, J. A., Botstein, D., Butler, H., Cherry, J. M., et al. (2000). Gene ontology: tool for the unification of biology. The Gene Ontology Consortium. *Nat. Genet.* 25, 25–29. doi: 10.1038/75556
- Asif, A. A., Roy, M., and Ahmad, S. (2021). *Paecilomyces* pneumonia despite voriconazole prophylaxis: a case report and literature review. *Eur. J. Case Rep. Intern. Med.* 8, 002651. doi: 10.12890/2021_002651
- Ben-Ami, R. (2023). Systemic antifungal therapy for invasive pulmonary infections. *J. Fungi* 9, 144. doi: 10.3390/jof9020144
- Buchfink, B., Xie, C., and Huson, D. H. (2015). Fast and sensitive protein alignment using DIAMOND. *Nat. Methods* 12, 59–60. doi: 10.1038/nmeth.3176
- Campos-Olivas, R., Bruix, M., Santoro, J., Lacadena, J., Martinez del Pozo, A., Gavilanes, J. G., et al. (1995). NMR solution structure of the antifungal protein from *Aspergillus giganteus*: evidence for cysteine pairing isomerism. *Biochemistry* 34, 3009–3021. doi: 10.1021/bi00009a032
- Chan, Y. S., and Ng, T. B. (2013). Northeast red beans produce a thermostable and pH-stable defensin-like peptide with potent antifungal activity. *Cell Biochem. Biophys.* 66, 637–648. doi: 10.1007/s12013-012-9508-1
- Criado, P. R., Junior, W. B., and Matta, V. (2021). First report of cutaneous mycetoma by *Paecilomyces variotii* and the successful treatment with combined

Data availability statement

The datasets presented in this study can be found in online repositories. The names of the repository/repositories and accession number(s) can be found in the article/Supplementary material.

Author contributions

Y-PC contributed to conceptualization, writing original draft preparation, writing review and editing, project administration, and funding acquisition. YL, FC, and HW contributed to data curation. SZ contributed to the software. All authors contributed to the manuscript and approved the submitted version.

Funding

This study was supported by the Natural Science Foundation of Fujian Province, China, grant number 2022J011402.

Conflict of interest

The authors declare that the research was conducted in the absence of any commercial or financial relationships that could be construed as a potential conflict of interest.

Publisher's note

All claims expressed in this article are solely those of the authors and do not necessarily represent those of their affiliated organizations, or those of the publisher, the editors and the reviewers. Any product that may be evaluated in this article, or claim that may be made by its manufacturer, is not guaranteed or endorsed by the publisher.

Supplementary material

The Supplementary Material for this article can be found online at: <https://www.frontiersin.org/articles/10.3389/fmicb.2023.1172257/full#supplementary-material>

- itraconazole and terbinafine along with resection surgeries. *Aust. J. Dermatol.* 62, e397–e399. doi: 10.1111/ajd.13592
- Deng, Y. Y., Li, J. Q., Wu, S. F., Zhu, Y. P., Chen, Y. W., and He, F. C. (2006). Integrated NR database in protein annotation system and its localization. *Comp. Eng.* 32, 71–76. doi: 10.1109/INFOCOM.2006.241
- Fizil, A., Gaspari, Z., Barna, T., Marx, F., and Batta, G. (2015). “Invisible” conformers of an antifungal disulfide protein revealed by constrained cold and heat unfolding, CEST-NMR experiments, and molecular dynamics calculations. *Chemistry* 21, 5136–5144. doi: 10.1002/chem.201404879
- Glorieux, C., and Calderon, P. B. (2017). Catalase, a remarkable enzyme: targeting the oldest antioxidant enzyme to find a new cancer treatment approach. *Biol. Chem.* 398, 1095–1108. doi: 10.1515/hsz-2017-0131
- Grabherr, M. G., Haas, B. J., Yassour, M., Levin, J. Z., Thompson, D. A., Amit, I., et al. (2011). Full-length transcriptome assembly from RNA-Seq data without a reference genome. *Nat. Biotechnol.* 29, 644–652. doi: 10.1038/nbt.1883
- Gurgel, I., Jorge, K., Malacco, N., Souza, J. A. M., Rocha, M. C., Fernandes, M. F., et al. (2019). The *Aspergillus fumigatus* mucin MsbA regulates the cell wall integrity pathway and controls recognition of the fungus by the immune system. *mSphere* 4, e00350–e00319. doi: 10.1128/mSphere.00350-19
- Hagen, S., Marx, F., Ram, A. F., and Meyer, V. (2007). The antifungal protein AFP from *Aspergillus giganteus* inhibits chitin synthesis in sensitive fungi. *Appl. Environ. Microbiol.* 73, 2128–2134. doi: 10.1128/AEM.02497-06
- Huber, A., Hajdu, D., Bratschun-Khan, D., Gaspari, Z., Varbanov, M., Philippot, S., et al. (2018). New antimicrobial potential and structural properties of PAFB: a cationic, cysteine-rich protein from *Penicillium chrysogenum* Q176. *Sci. Rep.* 8, 1751. doi: 10.1038/s41598-018-20002-2
- Jacobs, S. E., Wengenack, N. L., and Walsh, T. J. (2020). Non-*Aspergillus* hyaline molds: emerging causes of sino-pulmonary fungal infections and other invasive mycoses. *Semin. Respir. Crit. Care Med.* 41, 115–130. doi: 10.1055/s-0039-3401989
- Janson, G., Zhang, C., Prado, M. G., and Paiardini, A. (2017). PyMod 2.0: improvements in protein sequence-structure analysis and homology modeling within PyMOL. *Bioinformatics* 33, 444–446. doi: 10.1093/bioinformatics/btw638
- Jones, P., Binns, D., Chang, H. Y., Fraser, M., Li, W., McAnulla, C., et al. (2014). InterProScan 5: genome-scale protein function classification. *Bioinformatics* 30, 1236–1240. doi: 10.1093/bioinformatics/btu031
- Koonin, E. V., Fedorova, N. D., Jackson, J. D., Jacobs, A. R., Krylov, D. M., Makarova, K. S., et al. (2004). A comprehensive evolutionary classification of proteins encoded in complete eukaryotic genomes. *Genome Biol.* 5, R7. doi: 10.1186/gb-2004-5-2-r7
- Kotov, V., Mlynek, G., Vesper, O., Pletzer, M., Wald, J., Teixeira-Duarte, C. M., et al. (2021). In-depth interrogation of protein thermal unfolding data with MoltenProt. *Protein Sci.* 30, 201–217. doi: 10.1002/pro.3986
- Kovacs, B., Hegedus, N., Balint, M., Szabo, Z., Emri, T., Kiss, G., et al. (2014). *Penicillium* antifungal protein (PAF) is involved in the apoptotic and autophagic processes of the producer *Penicillium chrysogenum*. *Acta Microbiol. Immunol. Hung.* 61, 379–388. doi: 10.1556/amicro.61.2014.3.10
- Kuroda, T., and Tsuchiya, T. (2009). Multidrug efflux transporters in the MATE family. *Biochim. Biophys. Acta* 1794, 763–768. doi: 10.1016/j.bbapap.2008.11.012
- Langmead, B., Trapnell, C., Pop, M., and Salzberg, S. L. (2009). Ultrafast and memory-efficient alignment of short DNA sequences to the human genome. *Genome Biol.* 10, R25. doi: 10.1186/gb-2009-10-3-r25
- Lazarus, J. E., Branda, J. A., Gandhi, R. G., Barshak, M. B., Zachary, K. C., and Barczak, A. K. (2020). Disseminated intravascular infection caused by *Paecilomyces variotii*: case report and review of the literature. *Open Forum Infect. Dis.* 7, ofaa166. doi: 10.1093/ofid/ofaa166
- Li, Y., Yang, G., Huang, X., Ye, B., Liu, M., Lin, Z., et al. (2009). Recombinant glutamine synthetase (GS) from *C. glutamicum* existed as both hexamers & decamers and C-terminal His-tag enhanced inclusion bodies formation in *E. coli*. *Appl. Biochem. Biotechnol.* 159, 614–622. doi: 10.1007/s12010-008-8493-8
- Lionakis, M. S., Lewis, R. E., and Kontoyiannis, D. P. (2018). Breakthrough invasive mold infections in the hematologic patient: current concepts and future directions. *Clin. Infect. Dis.* 67, 1621–1630. doi: 10.1093/cid/ciy473
- Liu, J., Zeng, J., Zhu, C., Miao, J., Huang, Y., and Heinz, H. (2020). Interpretable molecular models for molybdenum disulfide and insight into selective peptide recognition. *Chem. Sci.* 11, 8708–8722. doi: 10.1039/D0SC01443E
- Lopez-Garcia, B., Moreno, A. B., San Segundo, B., De los Rios, V., Manning, J. M., Gavilanes, J. G., et al. (2010). Production of the biotechnologically relevant AFP from *Aspergillus giganteus* in the yeast *Pichia pastoris*. *Protein Expr. Purif.* 70, 206–210. doi: 10.1016/j.pep.2009.11.002
- Love, M. I., Huber, W., and Anders, S. (2014). Moderated estimation of fold change and dispersion for RNA-seq data with DESeq2. *Genome Biol.* 15, 550. doi: 10.1186/s13059-014-0550-8
- Monteiro, T., Moreira, M., Gaspar, S. B. R., and Almeida, M. G. (2022). Bilirubin oxidase as a single enzymatic oxygen scavenger for the development of reductase-based biosensors in the open air and its application on a nitrite biosensor. *Biosens. Bioelectron.* 217, 114720. doi: 10.1016/j.bios.2022.114720
- Niu, C., Zhu, L., Zhu, P., and Li, Q. (2015). Lysine-based site-directed mutagenesis increased rigid β -sheet structure and thermostability of mesophilic 1,3-1,4- β -glucanase. *J. Agric. Food Chem.* 63, 5249–5256. doi: 10.1021/acs.jafc.5b00480
- Omrane, S., Sghyer, H., Audeon, C., Lanen, C., Duplaix, C., Walker, A. S., et al. (2015). Fungicide efflux and the MgMFS1 transporter contribute to the multidrug resistance phenotype in *Zymoseptoria tritici* field isolates. *Environ. Microbiol.* 17, 2805–2823. doi: 10.1111/1462-2920.12781
- Oshiro, K. G. N., Rodrigues, G., Monges, B. E. D., Cardoso, M. H., and Franco, O. L. (2019). Bioactive peptides against fungal biofilms. *Front. Microbiol.* 10, 2169. doi: 10.3389/fmicb.2019.02169
- Paege, N., Jung, S., Schape, P., Muller-Hagen, D., Ouedraogo, J. P., Heiderich, C., et al. (2016). A transcriptome meta-analysis proposes novel biological roles for the antifungal protein AnAFP in *Aspergillus niger*. *PLoS ONE* 11, e0165755. doi: 10.1371/journal.pone.0165755
- Paixão Marques, D., Carvalho, J., Rocha, S., and Domingos, R. (2019). A case of pulmonary mycetoma caused by *Paecilomyces variotii*. *Eur. J. Case Rep. Intern. Med.* 6, 001040. doi: 10.12890/2019_001040
- Patino, B., Vazquez, C., Manning, J. M., Roncero, M. I. G., Cordoba-Canero, D., Di Pietro, A., et al. (2018). Characterization of a novel cysteine-rich antifungal protein from *Fusarium graminearum* with activity against maize fungal pathogens. *Int. J. Food Microbiol.* 283, 45–51. doi: 10.1016/j.jfoodmicro.2018.06.017
- Pompeu, G. B., Pietrobbon, V. C., Andreote, C. C. F., Ferreira, L. F. R., Aguiar, M., Sartori, S. B., et al. (2019). Role of the antioxidant defense system during the production of lignocellulolytic enzymes by fungi. *Int. Microbiol.* 22, 255–264. doi: 10.1007/s10123-018-00045-1
- Rahman, T., Yarnall, B., and Doyle, D. A. (2017). Efflux drug transporters at the forefront of antimicrobial resistance. *Eur. Biophys. J.* 46, 647–653. doi: 10.1007/s00249-017-1238-2
- Rocha, M. C., Godoy, K. F., de Castro, P. A., Hori, J. I., Bom, V. L., Brown, N. A., et al. (2015). The *Aspergillus fumigatus* *pkcA* G579R mutant is defective in the activation of the cell wall integrity pathway but is dispensable for virulence in a neutropenic mouse infection model. *PLoS ONE* 10, e0135195. doi: 10.1371/journal.pone.0135195
- Samaras, A., Ntasiou, P., Myresiotis, C., and Karaoglaidis, G. (2020). Multidrug resistance of *Penicillium expansum* to fungicides: whole transcriptome analysis of MDR strains reveals overexpression of efflux transporter genes. *Int. J. Food Microbiol.* 335, 108896. doi: 10.1016/j.jfoodmicro.2020.108896
- Sambrook, J., and Russell, D. W. (2001). *Molecular Cloning: A Laboratory Manual*. 3rd Edn. Cold Spring Harbor, NY: Cold Spring Harbor Laboratory Press.
- Sanguinetti, M., Posteraro, B., Beigelman-Aubry, C., Lamothe, F., Dunet, V., Slavin, M., et al. (2019). Diagnosis and treatment of invasive fungal infections: looking ahead. *J. Antimicrob. Chemother.* 74, ii27–ii37. doi: 10.1093/jac/dkz041
- Shin, Y., Lee, S., Ku, M., Kwak, M. K., and Kang, S. O. (2017). Cytochrome c peroxidase regulates intracellular reactive oxygen species and methylglyoxal via enzyme activities of erythroascorbate peroxidase and glutathione-related enzymes in *Candida albicans*. *Int. J. Biochem. Cell Biol.* 92, 183–201. doi: 10.1016/j.biocel.2017.10.004
- Song, G., Du, S., Sun, H., Liang, Q., Wang, H., Yan, M., et al. (2022). Antifungal mechanism of (E)-2-hexenal against *Botrytis cinerea* growth revealed by transcriptome analysis. *Front. Microbiol.* 13, 951751. doi: 10.3389/fmicb.2022.951751
- Sprute, R., Salmanton-Garcia, J., Sal, E., Malaj, X., Falces-Romero, I., Hatvani, L., et al. (2021). Characterization and outcome of invasive infections due to *Paecilomyces variotii*: analysis of patients from the FungiScope(R) registry and literature reports. *J. Antimicrob. Chemother.* 76, 765–774. doi: 10.1093/jac/dkaa481
- Tatusov, R. L., Galperin, M. Y., Natale, D. A., and Koonin, E. V. (2000). The COG database: a tool for genome-scale analysis of protein functions and evolution. *Nucleic Acids Res.* 28, 33–36. doi: 10.1093/nar/28.1.33
- Thery, T., and Arendt, E. K. (2018). Antifungal activity of synthetic cowpea defensin Cp-thionin II and its application in dough. *Food Microbiol.* 73, 111–121. doi: 10.1016/j.fm.2018.01.006
- Tu, C. Y., Chen, Y. P., Yu, M. C., Hwang, I. E., Wu, D. Y., and Liaw, L. L. (2016). Characterization and expression of the antifungal protein from *Monascus pilosus* and its distribution among various *Monascus* species. *J. Biosci. Bioeng.* 122, 27–33. doi: 10.1016/j.jbiosc.2015.12.009
- Utesch, T., de Miguel Catalina, A., Schattenberg, C., Paege, N., Schmieder, P., Krause, E., et al. (2018). A computational modeling approach predicts interaction of the antifungal protein AFP from *Aspergillus giganteus* with fungal membranes via its γ -core motif. *mSphere* 3, e00377–e00318. doi: 10.1128/mSphere.00377-18
- Varadi, G., Toth, G. K., and Batta, G. (2018). Structure and synthesis of antifungal disulfide β -strand proteins from filamentous fungi. *Microorganisms* 7, 5. doi: 10.3390/microorganisms7010005
- Wendt, S., Ulbrich, N., and Stahl, U. (1994). Molecular cloning, sequence analysis and expression of the gene encoding an antifungal-protein from *Aspergillus giganteus*. *Curr. Genet.* 25, 519–523. doi: 10.1007/BF00351672

- Wu, Z., Wang, S., Yuan, Y., Zhang, T., Liu, J., and Liu, D. (2016). A novel major facilitator superfamily transporter in *Penicillium digitatum* (PdMFS2) is required for prochloraz resistance, conidiation and full virulence. *Biotechnol. Lett.* 38, 1349–1357. doi: 10.1007/s10529-016-2113-4
- Zhang, Y., Gao, K., Wang, C., and Liu, S. (2021). A novel antibacterial component and the mechanisms of an *Amaranthus tricolor* leaf ethyl acetate extract against *Acidovorax avenae* subsp. *citriculi*. *Int. J. Mol. Sci.* 23, 312. doi: 10.3390/ijms23010312
- Zhdanova, N. G., Maksimov, E. G., Arutyunyan, A. M., Fadeev, V. V., and Shirshin, E. A. (2017). Tyrosine fluorescence probing of conformational changes in tryptophan-lacking domain of albumins. *Spectrochim. Acta A Mol. Biomol. Spectrosc.* 174, 223–229. doi: 10.1016/j.saa.2016.11.038
- Zhdanova, N. G., Shirshin, E. A., Maksimov, E. G., Panchishin, I. M., Saletsky, A. M., and Fadeev, V. V. (2015). Tyrosine fluorescence probing of the surfactant-induced conformational changes of albumin. *Photochem. Photobiol. Sci.* 14, 897–908. doi: 10.1039/c4pp00432a
- Zhou, X. X., Wang, Y. B., Pan, Y. J., and Li, W. F. (2008). Differences in amino acids composition and coupling patterns between mesophilic and thermophilic proteins. *Amino Acids* 34, 25–33. doi: 10.1007/s00726-007-0589-x
- Zhou, Y., Lv, H., Li, H., Li, J., Yan, Y., Liu, F., et al. (2021). Nitroreductase increases menadione-mediated oxidative stress in *Aspergillus nidulans*. *Appl. Environ. Microbiol.* 87, e0175821. doi: 10.1128/AEM.01758-21



OPEN ACCESS

EDITED BY

Guangshun Wang,
University of Nebraska Medical Center,
United States

REVIEWED BY

Carlos Minahk,
CCT CONICET Tucuman, Argentina
Jianhua Wang,
Chinese Academy of Agricultural Sciences
(CAAS), China
Takeshi Zendo,
Kyushu University, Japan

*CORRESPONDENCE

Arnoldas Kaunietis
✉ arnoldas.kaunietis@gmc.vu.lt

RECEIVED 17 April 2023

ACCEPTED 24 May 2023

PUBLISHED 15 June 2023

CITATION

Koniuchovaitė A, Petkevičiūtė A, Bernotaitė E,
Gricajeva A, Gegeckas A, Kalėdienė L and
Kaunietis A (2023) Novel leaderless bacteriocin
geobacillin 6 from thermophilic bacterium
Parageobacillus thermoglucosidasius.
Front. Microbiol. 14:1207367.
doi: 10.3389/fmicb.2023.1207367

COPYRIGHT

© 2023 Koniuchovaitė, Petkevičiūtė,
Bernotaitė, Gricajeva, Gegeckas, Kalėdienė and
Kaunietis. This is an open-access article
distributed under the terms of the [Creative Commons Attribution License \(CC BY\)](https://creativecommons.org/licenses/by/4.0/). The
use, distribution or reproduction in other
forums is permitted, provided the original
author(s) and the copyright owner(s) are
credited and that the original publication in this
journal is cited, in accordance with accepted
academic practice. No use, distribution or
reproduction is permitted which does not
comply with these terms.

Novel leaderless bacteriocin geobacillin 6 from thermophilic bacterium *Parageobacillus thermoglucosidasius*

Ana Koniuchovaitė, Akvilė Petkevičiūtė, Emilija Bernotaitė,
Alisa Gricajeva, Audrius Gegeckas, Lilija Kalėdienė and
Arnoldas Kaunietis*

Department of Microbiology and Biotechnology, Institute of Biosciences, Life Sciences Center, Vilnius
University, Vilnius, Lithuania

Bacterial resistance to conventional antibiotics has urged us to develop alternative strategies against bacterial pathogens. Moreover, a demand for food products containing no chemical preservatives has led us to search for new alternative technologies for food preservation. Bacteriocins – ribosomally synthesized antimicrobial peptides – have been proposed as a new alternative to conventional antibiotics or chemicals for food preservation. This study describes biosynthesis and characterization of a novel leaderless bacteriocin, geobacillin 6, which was identified in the thermophilic bacterium *Parageobacillus thermoglucosidasius*. Its amino acid sequence shows low similarity to other bacteriocins and it is the first leaderless-type bacteriocin identified in thermophilic bacteria. Based on structure assessment, the bacteriocin forms a multi-helix bundle. Geobacillin 6 exhibits a relatively narrow antimicrobial spectrum, it is active in the μM range and against Gram-positive bacteria, mostly thermophilic species closely related to the producer strain. Bacteriocin demonstrates stability over pH 3–11 and is highly thermostable, retaining 100% of its activity after incubation at 95°C for 6h. Geobacillin 6 has potential in the food industry and biotechnological processes where contamination with thermophilic bacteria is undesirable.

KEYWORDS

leaderless bacteriocin, thermophilic bacteria, geobacillin, *Parageobacillus*, heterologous expression

1. Introduction

Bacterial resistance to conventional antibiotics has dramatically increased. Multidrug-resistant opportunistic microorganisms are spreading and today it is a major threat to public health. New antibacterial drugs against global priority pathogens have been developed, but they are derived from already established antibiotic classes. Unfortunately, only a few antibacterial agents of novel classes have been discovered to date. For this reason, scientists are urged to develop and propose new alternative strategies against bacterial pathogens. Moreover, the increasing demand for chemical-free food products and the potential health hazards of artificial additives used in food preservation have led to a search for alternative technologies for the preservation of food products (Cotter et al., 2005, 2013; [Global Action Plan on Antimicrobial Resistance](#), 2015).

Bacteriocins are ribosomally synthesized antimicrobial peptides or small proteins produced by bacteria. These antimicrobials have an antagonistic activity against other bacteria meanwhile the producer has immunity to the produced bacteriocin. Bacteriocins are very diverse in their size, structure, mode of action, or immunity mechanisms. These peptides can target different receptors and have broad or narrow antimicrobial spectrum (Soltani et al., 2021).

Bacteriocins can have antimicrobial activity against multi-drug resistant pathogens and biopreservation using these antimicrobial peptides as an alternative to conventional antibiotics is a promising area. Because they are thermostable, retains stability in a wide pH range, have no color and odor, and can be inactivated by proteolytic enzymes, bacteriocins can be used as a biotechnological tool in the food and pharmaceutical industries (Bhattacharya et al., 2022). To date, only one of bacteriocin, nisin synthesized by *Lactococcus lactis*, is licensed as a biopreservative and is exploited in the food industry (Subramanian and Smith, 2015). Recently, in the United States through the GRAS regulatory procedure, some recombinant bacteriocins produced in plants have received promising regulatory reviews for application as food antibacterials (Hahn-Löbmann et al., 2019). In addition to their potential use in the medicine and food industries, these antimicrobials have perspectives for use in food animals and aquaculture, as therapeutics against bacterial infections. Thus, bacteriocins represent feasible alternatives to antibiotics (Pereira et al., 2022).

Studies on bacteriocins produced by extremophiles, like thermophilic bacteria, are very limited. Most of these antimicrobials are described very obscurely and most importantly, the amino acid sequences have not been revealed and provided. Usually, they are described as bacteriocin-like substances. To date, only four bacteriocins from thermophilic bacteria have been identified and well-characterized (Garg et al., 2012; Egan et al., 2018; Kaunietis et al., 2019; Vaičiškaitė et al., 2019). Thus, the group of bacteria is an unexplored and rich source of novel bacteriocins. Thermophiles can reveal new and promising antibacterial agents with useful properties such as high thermostability.

In canned food and dairy industries contamination with thermophilic spore-forming microorganisms is responsible for a 'flat' sour spoilage of canned foods and products like evaporated milk. If the temperature is suitable, thermophilic bacteria can grow and form biofilms in dairy manufacturing plants, potentially causing contamination. This can lead to product spoilage due to the production of acids and enzymes (Kalogridou-Vassiliadou, 1992; Watterson et al., 2014; Burgess et al., 2015; Seale et al., 2015; Berendsen et al., 2016). Thermophilic microorganisms are utilized in industrial-level bioethanol or lactate production. However, contamination with other thermophiles during these processes is also possible (Cripps et al., 2009; Bacon et al., 2017). Bacteriocins active against thermophiles could be used to avoid contamination of thermophilic spore-forming bacteria in these industry processes.

This study reveals novel antimicrobial peptide geobacillin 6 encoded in thermophilic bacteria *Parageobacillus thermoglucosidasius* DSM 2542. This peptide represents a small subclass of leaderless bacteriocins, which compared to other bacteriocins do not have leader sequences and require no post-translational modifications to obtain antimicrobial activity (Masuda et al., 2012).

2. Methods

2.1. Bioinformatics analysis

The genome sequences of *P. thermoglucosidasius* DSM 2542 (GenBank: LAKX00000000) were derived from the NCBI database at.¹ Bacteriocin gene mining in the genome of *P. thermoglucosidasius* DSM 2542 was performed by BAGEL4 web-server at.² Prediction of signal sequence in bacteriocin was performed by SignalP 5.0 Server at.³ BLAST protein sequence analysis was performed using the NCBI database at.⁴ and the UniProt database at.⁵ Protein sequence alignment was performed using the UniProt database at.⁶ Protein structure prediction was performed by the I-TASSER web server at.⁷ To evaluate the secondary structure of the peptide a DichroWeb online analysis was performed on a web-server at.⁸

2.2. Growth media and cultivation conditions

For routine cultivation of thermophilic bacteria CASO broth (Roth) or NB medium was used and supplemented with 15 g/L agar (Oxoid) when needed. For NB medium preparation 10 g/L of tryptone from casein (Roth), 5 g/L of meat extract, and 5 g/L of NaCl (Roth) were used. For mesophilic bacteria cultivation LB or LB-agar (Biolab) media were used. Yeasts were grown in YPD medium, which contained 2% peptone from casein (Roth), 1% yeast extract (Roth), and 2% glucose (Roth) and supplemented with 15 g/L agar (Fisher Scientific) when needed. Medium selection for each strain in experiments is listed in [Supplementary File 1](#).

Growth media supplemented with glycerol [20% (w/w)] were used as stock culture stored at -75°C temperature. Mesophilic bacteria strains were cultivated in a thermostat or thermoshaker with aeration at 37°C , thermophilic bacteria at -55°C , and yeasts at -30°C .

2.3. Antimicrobial activity assays

For the spot on a lawn assay using mesophiles, an overnight culture of the indicator strain was prepared by cultivating it at $30/37^{\circ}\text{C}$. Then, 1% of the culture was inoculated into melted agar medium and poured into Petri plates. Once the medium solidified, 10 μL of the bacteriocin sample was spotted on the plate. The plate was then incubated overnight in a thermostat at $30/37^{\circ}\text{C}$. The next day, the growth inhibition zone of the indicator strain was evaluated on the plate.

For the antimicrobial activity assay using thermophiles, a fresh colony of the indicator strain was inoculated into a liquid medium and cultivated

1 <https://www.ncbi.nlm.nih.gov/genome>

2 <http://bagel4.molgenrug.nl>

3 <https://services.healthtech.dtu.dk/service.php?SignalP-5.0>

4 <https://blast.ncbi.nlm.nih.gov/Blast.cgi>

5 <https://www.uniprot.org/blast>

6 <https://www.uniprot.org/align>

7 <https://zhanggroup.org/I-TASSER>

8 <http://dichroweb.cryst.bbk.ac.uk/html/home.shtml>

overnight at 55°C in a thermoshaker. The following morning, the culture was inoculated (2–3%) into fresh medium and cultivated until the optical density (OD) reached 1–1.5. Then, the culture was mixed with melted agar medium at a ratio of 1:10 and poured into Petri plates.

For the spot on a lawn assay, 10 µl of the sample was spotted on the plate. To compare the activity between different samples, serial two-fold dilutions of the samples were made and dispersed on the plate. The arbitrary unit of antibacterial activity per milliliter (AU/ml) was defined using a formula $2^n \times 1 \text{ ml/V}$, where V represents the sample volume (ml) and n represents the titer of the reciprocal highest dilution that results in growth inhibition of the indicator strain (Daba et al., 1991). Next, the plate was incubated overnight at 55°C in a thermostat. The following day, the growth inhibition zone of the indicator strain was evaluated on the plate. A list of bacteria and yeast strains with their respective cultivation conditions can be found in [Supplementary File 1](#).

2.4. Reagents for DNA extraction and cloning

DNA amplification was conducted using Phusion HF DNA polymerase, while genomic DNA extraction was performed using the GeneJET Genomic DNA Purification Kit. For plasmidic DNA extraction, the GeneJET Plasmid Miniprep Kit was used. Amplified or digested DNA were cleaned with the GeneJET PCR Purification Kit. For DNA cloning T4 DNA Ligase enzyme was used. For DNA digestion restriction endonucleases FastDigest NcoI and FastDigest BamHI were used. DNA extraction or amplification was confirmed by 1% agarose gel electrophoretic analyses. All reagents and kits mentioned in this section were purchased from Thermo Fisher Scientific and used according to manufacturers' recommendations.

2.5. Cloning of DNA coding *His-TEV-geo6A* gene into a vector

A synthetic DNA coding Geo6A precursor peptide with optimized codon sequences for *E. coli* was ordered using GeneArt Strings DNA Fragments (Thermo Fisher Scientific) biosynthesis service. The DNA sequence was designed ([Supplementary File 2](#)) to code His6-tag and TEV peptidase recognition sites at the N-terminus of the peptide. DNA fragment *His-TEV-geo6A* was ligated into vector pET15b between NcoI and BamHI restriction sites using T4 DNA ligase and restriction endonucleases. The ligated DNA was transformed into *E. coli* DH5α by electroporation. Positive transformants were selected on LB-agar plates containing 50 µg/mL ampicillin and by colony PCR using Duet-up1 (5'-GGATCTCGACGCTCTCCCT-3') and T7 Terminator (5'-GCTAGTTATTGCTCAGCGG-3') primers. The constructed vector containing cloned gene (pET-His-TEV-geo6A) was extracted from bacteria culture and the DNA sequence of the insert was confirmed by Sanger sequencing.

2.6. Heterologous expression of *His-TEV-geo6A* gene

E. coli BL21 (DE3) cells were transformed with pET-His-TEV-geo6A vector and inoculated to liquid LB medium containing 50 µg/

ml ampicillin and cultivated in a thermoshaker. The overnight culture was inoculated (1%) to fresh medium with antibiotics and grown until OD reached 0.9–1.2. Then gene expression was induced using IPTG 1 mM end concentration. After 4 h of cultivation in thermoshaker bacterial culture was collected by centrifugation at 5,000 ×g for 20 min at 4°C. Harvested cells were resuspended in buffer A (25 mM sodium phosphate, 500 mM NaCl, pH 7.4) and kept at –75°C temperature until further use.

2.7. Purification of bacteriocin

After induction harvested cells were sonicated on ice for 20 min using ultrasound sonicator VCX 130 (Sonics and Materials) with cycle 5 s ON and 10 s OFF and using 35% amplitude. Cell debris was separated by centrifugation at 15,000 ×g for 20 min at 4°C. The supernatant containing soluble fraction was diluted with binding buffer A up to 100 ml and filtered using a 0.45 µm filter. Further protein purification was performed using the BioLogic DuoFlow chromatography system (Bio-Rad) and the sample was loaded on Ni²⁺ affinity chromatography column HisTrap HP 1 ml (GE) previously equilibrated in the buffer A (section 2.6). After sample application, the column was washed with buffer B (25 mM sodium phosphate, 500 mM NaCl, 20 mM imidazole, pH 7.4). Protein was eluted using a step gradient with buffer C (25 mM sodium phosphate, 500 mM NaCl, 500 mM imidazole, pH 7.4). Elution fractions containing peptides were collected and further loaded on HiTrap HP 5 ml (GE) desalting column using buffer D (50 mM sodium phosphate, 100 mM NaCl, pH 7.4). Next, elution fractions of desalted protein were mixed with TEV protease, which was made in our laboratory according to [Kapust et al. \(2001\)](#). The reaction was performed in buffer D containing 5 mM DTT and incubated in a water bath for 4 h at 37°C temperature. After treatment with protease sample was diluted in buffer E (20 mM sodium phosphate, pH 7.4) and loaded on cation exchange column UNO S-1 (Bio-Rad) previously equilibrated in the same buffer D. Further, the column was washed with buffer D and protein was eluted using linear grading with buffer E (20 mM sodium phosphate, 1 M NaCl, pH 7.4). Elution fractions were collected and analyzed using tricine-SDS-PAGE (section 2.8).

2.8. Tricine-SDS-PAGE analysis

Cell samples or elution samples were analyzed by tricine-SDS-PAGE ([Schägger, 2006](#)). The electrophoresis was carried out using 4% stacking and 16% separating polyacrylamide gels. Following protein electrophoresis, the gel was stained using PageBlue Protein Staining Solution (Thermo Fisher Scientific) as per the manufacturer's instructions.

2.9. Bacteriocin thermostability and stability in different pH ranges

For thermostability assay purified recombinant Geo6 was incubated at different temperatures: 60°C, 80°C and 100°C for 2 h and at 95°C up to 6 h. After incubation, serial two-fold dilutions of samples

were made using medium, and further antibacterial activity of bacteriocin was assessed by spot on a lawn assay.

For evaluation of stability at different pH ranges, purified recombinant Geo6 was mixed with 25 mM Britton-Robinson buffer solutions (Ebihara et al., 2016) with different pH values in a ratio of 1:20. After incubation at room temperature for 2 h samples were neutralized with NaOH or HCl solutions to pH 7. Further, samples were diluted two-fold using a medium and assessed for antibacterial activity using spot on a lawn assay.

2.10. Minimum inhibitory concentration assay

MICs of Geo6 were determined according to the method of Wiegand et al. (2008) with some modifications. An indicator strain sensitive to bacteriocin was grown overnight at 55°C in a thermoshaker. The next day it was inoculated (2–3%) into fresh medium and cultivated until OD reached 1–1.5. The culture was further diluted and adjusted to 1×10^6 CFU/ml. A 95 µl of the medium was mixed with 5 µl of Geo6 and serial two-fold dilutions of suspension were made with the medium. Next, diluted mixtures were dispersed (100 µl) in a 96-well plate. A volume of 100 µl of previously prepared cell suspension was dispersed and mixed with the diluted bacteriocin in every well on the plate. As a result, the final volume of suspension in the well containing diluted bacteriocin and bacteria cells was 200 µl and the final concentration of the bacteria culture in the well was 5×10^5 CFU/ml. For each experiment, three replicates were made in the plate. Wells with positive controls contained a mixture of medium (95 µl) and Geo6 (5 µl), and negative controls contained bacteria suspension (5×10^5 CFU/ml) in the medium (100 µl). The plate was placed into a bag to prevent medium evaporation and put into a box, which was incubated overnight at 55°C in a thermoshaker. The next day, the growth inhibition was evaluated in the wells of the plate.

2.11. Live/dead assay

An indicator strain *G. kaustophilus* HTA 426^T sensitive to bacteriocin was grown in BHI medium at 55°C till OD 0.5 was reached. Next, the bacteria culture was treated with 600 nM of Geo6 and further cultivated for 30 min. Then, the cell culture was centrifuged at 3000 ×g for 5 min and further washed two times with 0.9% NaCl solution (centrifuged at 3000 ×g for 5 min). After the last wash, cells were suspended in 0.9% NaCl solution and stained using LIVE/DEAD BacLight Bacterial Viability Kit (Invitrogen) containing SYTO9 and fluorescent dyes according to manufacturers' recommendations. Cells were incubated in the dark at room temperature for 15 min. Next, cells were centrifuged at 3000 ×g for 5 min and washed two times with 0.9% NaCl solution (centrifuged at 3000 ×g for 5 min). Further, 10 µl of Geo6 treated cells and nontreated control cells suspensions were spotted onto objective slides and examined using a fluorescence microscope using filters FITC (480/500 nm) and Texas Red (490/635 nm).

2.12. Circular dichroism spectroscopy

Peptide solution was prepared in 10 mM sodium phosphate buffer (pH 7.4) and at a final concentration of 10 µM. The circular dichroism (CD) data was collected using a J-810 CD Spectrophotometer (JASCO) in a Cuvette of 0.125 cm path length and in a range of 190–280 nm at 0.5 nm intervals. The spectrum of the scan was recorded with a 2 nm optical bandwidth and presented as the average of 4 scans. Baseline measurements were recorded using a buffer solution and then subtracted from the sample scan.

2.13. Geo6 thermal shift assay

As an indicator of thermal denaturation in varying pH or other conditions a fluorescent SYPRO Orange dye (Invitrogen) that binds to hydrophobic parts of protein during its unfolding was used in this work. SYPRO Orange 50× stock solution was prepared by diluting 2.5 µl of 5,000× concentrate into 250 µl of deionized (DI) water. A volume of 2.5 µl of 50× SYPRO Orange was aliquoted into a white HardShell 96-well PCR plate (Bio-Rad). Different pH buffer solutions (25 mM Britton-Robinson, pH 3–11; Bendikienė et al., 2004) were added to aliquoted SYPRO Orange followed by adding an appropriately diluted solution of purified Geo6 into the wells at a final concentration of 0.25 nmol/ml (1.3 µg/ml). The final volume of the mixture was 25 µl. The negative control was 25 mM of Britton-Robinson buffer solutions in a range of pH 3 to 11, with 2.5 µl of SYPRO Orange. Lysozyme (final concentration of 100 µg/ml) diluted in 25 mM Britton-Robinson buffer (pH 5 and 6) and mixed with 2.5 µl of SYPRO Orange was used as a positive control. A curve experiment for DNA with the elimination of the initial denaturation step at 95°C was used. The melt curve temperature range was set from 20°C to 95°C in increments of 0.5°C for 5 s. Each experimental condition was prepared in triplicate. Thermal shift analysis or differential scanning fluorimetry (DSF) of Geo6 was performed in CFX Touch Real TIME PCR System (Bio-Rad) using CFX Manager (Bio-Rad) software.

3. Results and discussion

3.1. Identification of biosynthetic gene cluster of geobacillin 6

To reveal new antimicrobial peptides encoded in thermophilic bacteria, we screened a series of NCBI-available genomes from various *Geobacillus* and *Parageobacillus* spp. bacteria stored in the microorganism collection of the Department of Microbiology and Biotechnology at Vilnius University's Life Sciences Center. Genome analysis using the BAGEL4 web tool revealed that the genomic DNA of the thermophilic bacteria *P. thermoglucosidasius* DSM 2542 encoded a gene cluster of 5,709 bp in length (Figure 1) and presumably is responsible for the biosynthesis of a novel bacteriocin. This strain was confirmed to produce antimicrobial substances using a spot on a lawn assay (Figure 2). The gene cluster contained 6 genes, which were named here *geo6ABCDEF*, could be related to the biosynthesis of the novel bacteriocin, that we have named geobacillin 6 (Geo6).

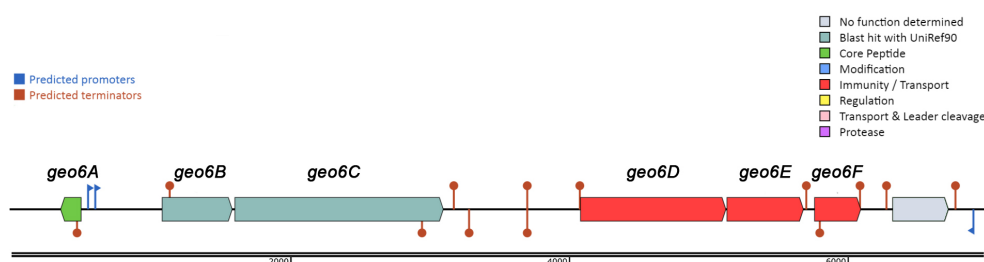


FIGURE 1

Biosynthetic gene cluster of bacteriocin Geo6 identified using BAGEL4 web tool. Represented genes *geo6ABCDEF* in DNA contig (GenBank: LAKX01000053.1) were identified in the genome of *P. thermoglucosidarius* DSM 2542 (GenBank: LAKX00000000).

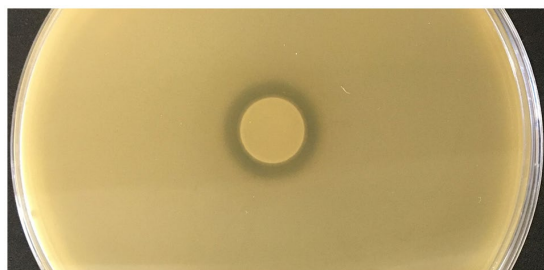


FIGURE 2

Assessment of antimicrobial activity of *P. thermoglucosidarius* DSM 2542. Indicator strain inoculated into the agar plate - *Geobacillus kaustophilus* HTA 426, bacterial suspension spotted into the center of the plate - *P. thermoglucosidarius* DSM 2542.

BLAST analysis and alignment of the *geo6A* gene product (Figures 3, 4) revealed that the encoded 48 amino acid length peptide, Geo6, shares sequence similarity with a group of leaderless bacteriocins: lacticins Q and Z, aureocin A54, epidermicin NI01, and BhtB (Perez et al., 2018). The highest sequence similarity was observed with lacticin Q (52%) and lacticin Z (54%).

Further analysis of the gene cluster observed that the *geo6D*, *geo6E*, and *geo6F* genes encode proteins with 78, 78, and 84% sequence similarity, respectively, to proteins annotated as ABC transporters. While the *geo6B* and *geo6C* genes encode proteins with 51 and 34% sequence similarity, respectively, to proteins annotated as Pleckstrin homology (PH) domain-containing proteins. Additionally, they exhibit 46 and 29% similarity, respectively, to proteins annotated as transmembrane YdbS and YdbT proteins, respectively.

The PH domains are small modular domains, which occur in a large variety of signaling proteins and serve as simple targeting domains that bind lipids in eukaryotic cells. However, these proteins are also present in bacteria (Cozier et al., 2004; Xu et al., 2010). Based on Butcher and Helmann (2006) research, the YdbST proteins can be responsible for resistance to antimicrobial compound(s) produced by *Bacillus amyloliquefaciens*. A recent study suggests that proteins containing PH domains and proteins similar to YdbST constitute transporters dedicated to leaderless bacteriocins (Pérez-Ramos et al., 2021). In addition, studies of gene clusters coding for bacteriocin lacticin Q (Iwatani et al., 2013) and aureocin A54 (Nascimento et al., 2012) showed that their biosynthetic loci encode proteins similar to

ABC transporters. The secretion of the lacticin Q in *L. lactis* QU5 is strictly controlled by the presence of LnqBCDEF, which confers the secretion and self-immunity of lacticin Q. It was revealed that the LnqEF proteins are the minimal unit required for sufficient immunity. Whereas LnqBCD, showing sequence similarity to ABC transporters, are considered accessory proteins, which support the activity of the LnqEF (Iwatani et al., 2012, 2013).

However, studies have demonstrated that the production of leaderless bacteriocins can occur independently of the biosynthesis machinery. It has been shown that the synthesis of active bacteriocin is possible with the production of only the precursor peptide (Netz et al., 2002b).

Based on previous studies and analysis of the *geo6ABCDEF* genes, it can be suggested that these genes are responsible for the biosynthesis of Geo6 (Table 1). The *geo6A* gene encodes the bacteriocin precursor peptide Geo6, while the *geo6BCDEF* genes are dedicated to transport and immunity, as observed in other biosynthetic gene clusters of leaderless bacteriocins. Some gene clusters of leaderless bacteriocins also contain genes responsible for biosynthesis regulation (Perez et al., 2018). However, in the identified gene cluster, which was encoded in a relatively short DNA contig (6,966 bp, GenBank: LAKX01000053.1), only one gene outside of *geo6ABCDEF* was found. No other genes associated with bacteriocin biosynthesis or regulation were identified.

3.2. Biosynthesis and purification of Geo6

Further, gene *geo6A* was heterologously expressed in *E. coli* for biosynthesis and purification of recombinant bacteriocin. For this purpose, we used a synthetic gene with optimized codons for *E. coli* bacteria. In addition, the gene was designed to encode His6-tag and TEV peptidase recognition site in the N-terminus of the peptide (Figure 5). The new gene of bacteriocin precursor, His-TEV-*geo6A*, was cloned into pET-15b vector downstream T7 promoter and induced for expression in *E. coli* BL21 (DE3) cells. The synthesized peptide His-TEV-Geo6 was purified from soluble cell lysate fraction using Ni²⁺ affinity chromatography, desalted by gel chromatography, then treated with TEV protease to cleave His-tag sequence and finally purified to homogeneity by cation exchange chromatography (Figure 6A). The recombinant bacteriocin Geo6 had additional Gly upstream of the Met at the N-terminus of the peptide.

```

BhtB 1 - - M W G R I L A F V A K Y G T K A V Q W A W K N K W F L L S L G - - - - E A V F D Y I R S I W G - 44
AucA 1 - M S W L N F L K Y I A K Y G K K A V S A A W K Y K G K V L E W L N V G P T L E W V W Q K L K K I A G L - 51
Geo6 1 M A T F L R I V - - A Q L S S K A A K W A L D N K D K V L K W I R D G M A I D W I I D K I N D I V G - - 48
NI01 1 M A A F M K L I Q F L A T K G Q K Y V S L A W K H K G T I L K W I N A G Q S F E W I Y K Q I K K L W A - - 51
LnqQ 1 M A G F L K V V Q L L A K Y G S K A V Q W A W A N K G K I L D W L N A G Q A I D W V V S K I K Q I L G I K 53
LnqZ 1 M A G F L K V V Q I L A K Y G S K A V Q W A W A N K G K I L D W I N A G Q A I D W V V E K I K Q I L G I K 53

```

FIGURE 3

Sequence alignment of leaderless bacteriocins. Alignment of peptides: BhtB (UniProt: Q3YB73), AucA (UniProt: Q8GPI4), NI01 (UniProt: H9BG66), LnqQ (UniProt: A4UVR2), LnqZ (UniProt: A7M6Q0), Geo6 (GeneBank: KJX67188.1), were performed using the UniProt database.

BhtB	100.00%	40.91%	35.00%	30.23%	40.91%	40.91%
AucA	40.91%	100.00%	31.91%	36.00%	47.06%	45.10%
Geo6	35.00%	31.91%	100.00%	31.25%	52.08%	54.17%
NI01	30.23%	36.00%	31.25%	100.00%	47.06%	49.02%
LnqQ	40.91%	47.06%	52.08%	47.06%	100.00%	94.34%
LnqZ	40.91%	45.10%	54.17%	49.02%	94.34%	100.00%

FIGURE 4

Percent identity matrix of leaderless bacteriocins. Alignment of peptides: BhtB (UniProt: Q3YB73), AucA (UniProt: Q8GPI4), NI01 (UniProt: H9BG66), LnqQ (UniProt: A4UVR2), LnqZ (UniProt: A7M6Q0), Geo6 (GeneBank: KJX67188.1), were performed using UniProt database.

3.3. Determination of antibacterial activity spectrum and minimal inhibitory concentration of recombinant geobacillin 6

Purified Geo6 peptide was evaluated for the antibacterial activity using spot on a lawn assay against 36 bacteria and 4 yeast strains, including Gram-positive, Gram-negative, and pathogenic strains (Table 2). Results demonstrated that bacteriocin was active against 12 out of 19 thermophilic bacteria strains tested, including *Aeribacillus pallidus* DSM 3670^T, *Anoxybacillus tepidamans* DSM 16325^T, *Parageobacillus toebii* DSM 14590^T, and various *Geobacillus* spp. bacteria strains (Figure 6B). Additionally, we observed small antibacterial activity against one mesophilic bacterium, *Bacillus zanthoxyli* CH07. However, the yeasts *Saccharomyces cerevisiae* or *Candida* spp., as well as the mesophilic bacteria *Bacillus* spp., *Staphylococcus* spp., *Pseudomonas aeruginosa*, *Enterococcus faecalis*, *Salmonella enterica*, *Escherichia coli*, *Acinetobacter baumannii*, and *Stenotrophomonas maltophilia* strains used in the assay were not susceptible to the bacteriocin.

In addition, the MIC values of Geo6 were evaluated against some susceptible thermophilic bacteria strains (Table 2). It was demonstrated that the MIC value for *G. thermodenitrificans* DSM 465^T was 2.34 μM, for *G. lituanicus* DSM 15325^T – 585 nM, for *G. thermoleovorans* DSM 5366^T – 585 nM, for *G. kaustophilus* HTA 426–293 nM, and for *P. toebii* DSM 14590^T it was 4.45 μM.

For comparison, previous studies have shown that pallidocin, a glycosin-type bacteriocin produced by thermophilic bacteria *A. pallidus* strain 8, was active in the pM range against other thermophiles, and a 2.4 pM concentration of pallidocin inhibited the growth of thermophilic bacterium *P. genomospecies* 1 strain NUB36187 (Kaunietis et al., 2019). Other leaderless bacteriocins are active in the μM and nM ranges (Fujita et al., 2007; Iwatani et al., 2007) and have a broad spectrum of activity. Studies showed that lactacin Q was active against a variety of tested Gram-positive bacteria strains, including *Bacillus* spp., *Lactobacillus* spp., *Enterococcus* spp., *Pediococcus* spp., *Lactococcus* spp., *Streptococcus* spp., and some other species. The highest activity was detected against *B. coagulans* JCM 2257^T (MIC – 1.6 nM), *L. sakei* subsp. *sakei* JCM 1157^T (MIC – 3.2 nM), *P. dextrinicus* JCM 5887^T (MIC – 7.3 nM). No activity was detected against the Gram-positive bacteria *Escherichia coli* JM109 (Iwatani et al., 2007). Bacteriocin aureocin A54 had a narrower antibacterial activity spectrum, it was active against some tested Gram-positive indicator bacteria strains, including *Brochothrix* sp., *Carnobacterium* spp., *Lactococcus* spp., and *Staphylococcus* spp. The lowest MIC values were detected against *B. campestris* ATCC 43754–2 μM, and *L. lactis* ATCC 19257–250 nM (Acedo et al., 2016).

Our results show that Geo6, as well as other leaderless bacteriocins lactacin Q or aureocin A54, are active in nM concentrations, in contrast to the bacteriocin pallidocin from another thermophilic bacterium, which can kill bacteria in pM concentrations. However, Geo6, similar to pallidocin, is active against Gram-positive and mostly against closely related thermophilic bacteria, including *Geobacillus* spp., *Aeribacillus* sp., *Anoxybacillus* sp., and *Parageobacillus* sp. strains. Other leaderless bacteriocins, such as lactacin Q and aureocin A54, inhibit Gram-positive bacteria as well. However, they have a wider antibacterial spectrum and kill more than just closely related bacteria.

3.4. Determination of mode of action

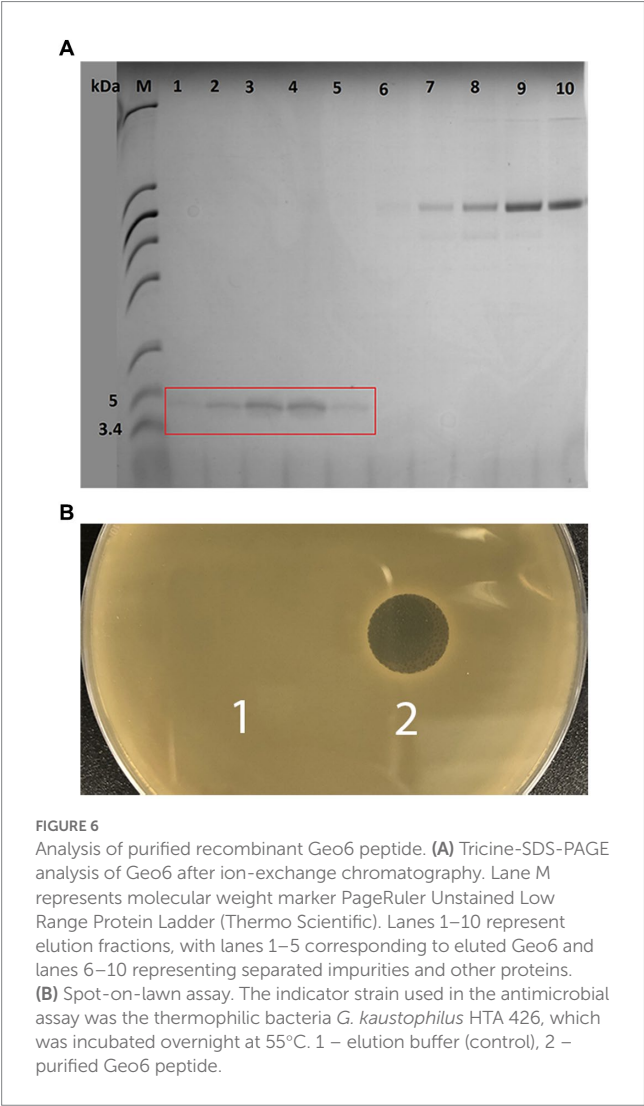
Cells of *G. kaustophilus* HTA 426^T were treated with Geo6, and membrane integrity was assayed using the fluorescent dyes SYTO9 and PI (Figure 7). The experiment showed that bacteria cells treated with the bacteriocin emitted red fluorescence, since propidium iodide can enter only cells with damaged membranes. In contrast, control cells not exposed to Geo6 emitted green fluorescence, indicating an intact membrane. These results suggest that Geo6 destabilizes the membrane of indicator cells. This can be supported by the fact that the peptide has a high charge, its theoretical isoelectric point (pI) value is 9.3. Cationic peptides tend to be attracted to an anionic cell membrane. Moreover, our suggestion that Geo6 targets the cell membrane is in agreement with a recent study on leaderless bacteriocins, epidermicin NI01 (*Staphylococcus epidermidis*) and

TABLE 1 Annotation of identified gene cluster.

Gene name	<i>geo6A</i>	<i>geo6B</i>	<i>geo6C</i>	<i>geo6D</i>	<i>geo6E</i>	<i>geo6F</i>
Annotation	Lacticin Q-like, aureocin A53-like peptide	PH domain-containing protein, transmembrane protein YdbS	PH domain-containing protein, transmembrane protein YdbT	ABC transporter domain-containing protein, bacitracin transporter	ABC transporter, permease YhcI	ABC transporter, permease YhcI
Proposed function	Bacteriocin precursor	Transport/immunity	Transport/immunity	Transport/immunity	Transport/immunity	Transport/immunity



FIGURE 5 His-TEV-Geo6 peptide sequence. Blue depicts His-tag sequence for Ni²⁺ affinity chromatography purification, red depicts the TEV protease recognition site, green depicts Geo6 bacteriocin sequence.



aureocin A53, which revealed the unique mode of action of these peptides. It comprises several distinctive methods of membrane disruption, and it was found that a four-helix bundle structure is necessary to complete the mechanism of membrane disruption (Hammond et al., 2020). Research on aureocin A53 and lacticin Q showed permeabilization of the bacterial cell membrane, followed by membrane potential disruption, efflux of various vital compounds, and termination of macromolecular synthesis (Netz et al., 2002a; Fujita et al., 2007). It was also shown that lacticin Q forms at least 4.6 nm pores (Yoneyama et al., 2009).

3.5. Geo6 stability at different temperatures and pH ranges

The purified recombinant Geo6 was exposed to different temperatures, and the thermal stability of the bacteriocin was evaluated after treatment by using a spot-on-lawn assay. The results showed that after treatment at 60°C, 70°C, and even 100°C for 2 h, the peptide retained 100% of its antibacterial activity. Furthermore, incubation of the peptide for up to 6 h at 95°C did not abolish its activity, and after incubation at room temperature for 24 h, the peptide remained 100% active. Additionally, Geo6 stability was evaluated in different pH ranges. Incubation in the pH range of 3–11 showed that Geo6 retained 100% of its activity in acidic and alkaline environments. These results are consistent with observations from experiments with other leaderless bacteriocins, such as lacticin Q or Bht-B, which remained active after treatment at high temperatures and in a wide pH range (Fujita et al., 2007).

3.6. Geo6 structure prediction

Analysis of the Geo6 peptide sequence using the SignalP bioinformatics tool confirmed that it has no signal or leader peptide,

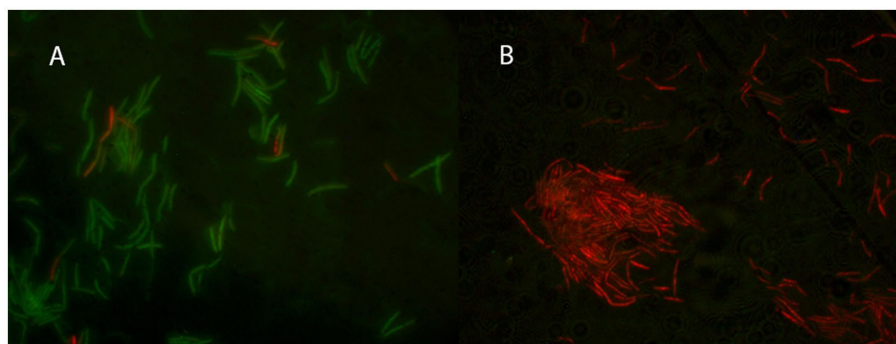


FIGURE 7

Fluorescent microscopy of thermophilic bacteria *G. kaustophilus* HTA 426^T cells. In (A) the control cells not treated with Geo6, while in (B) bacteria cells were treated with Geo6 for 30 min. The cells were stained using fluorescent dyes SYTO9 and PI. SYTO9 is capable of permeating the cell membranes and binding to the DNA of both live and dead cells. PI can only enter cells with damaged membranes and binds to the DNA. In (A) most of the cells exhibited green fluorescence, indicating that they were alive and healthy, with only a few cells showing red fluorescence due to membrane damage. In (B) all the cells exhibited red fluorescence, indicating that they were dead, as their membranes were no longer intact and the PI dye was able to bind to the DNA.

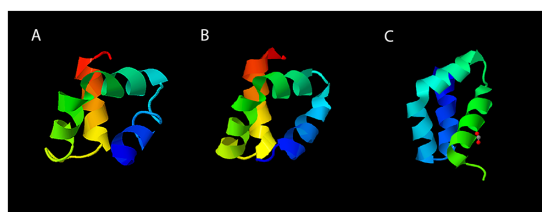


FIGURE 8

Three-dimensional structures of leaderless bacteriocins. The structure of Geo6 (A) was predicted using I-TASSER web tool. Experimentally determined 3D structures of AucA (B) and LnkQ (C) were derived from the RCSB PDB archive. The PDB numbers for AucA and LnkQ are 2N8O and 7P5R, respectively. In the visualizations, different colors are assigned to the different chains within the peptide structure. This color scheme distinguishes and visualizes the individual components of the peptide. The N-terminus is represented in blue, followed by green, yellow, orange, and finally red for the C-terminus.

consistent with other leaderless bacteriocins. Three-dimensional structure prediction using I-TASSER suggested that Geo6 is predominantly formed from α -helices. Furthermore, structure assembly simulation showed that Geo6 forms four distinct helices, which fold into a compact, globular assembly (Figure 8), similar to other leaderless bacteriocins such as epidermicin NI01 (PDB: 6SIF), aureocin A54 (PDB: 2N8O) and lactacin Q (PDB: 2N8P). Previous studies using structure prediction tools suggested a similar assembly for other leaderless bacteriocins such as lactacin Z, weissellicins Y and M, and enterocins L50A and L50B (Acedo et al., 2016). The secondary structure of Geo6 was evaluated using circular dichroism (CD) spectroscopy (Figure 9). The CD spectra revealed the presence of α -helical structure of the peptide in an aqueous solution. These findings are consistent with the predictions made by I-TASSER and are in agreement with previous studies on epidermicin NI01 and aureocin A54 (Hammond et al., 2020). Computational analysis of the spectra further estimated that α -helices may make up 75% of the peptide. It is well-known that the presence of α -helices and their

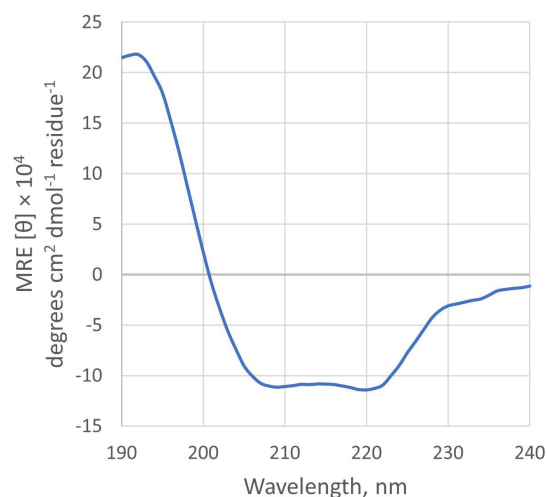


FIGURE 9

CD spectra of Geo6. Conditions: 10 μ M of peptide in 10 mM sodium phosphate buffer (pH 7.4), 25°C.

enhanced conformational stability contribute significantly to the thermal stability of proteins (Yakimov et al., 2016). This observation provides a plausible explanation for the remarkable stability of Geo6 at high temperatures.

3.7. Geo6 analysis using thermal shift assay

A recent study using the CD spectroscopy method confirmed the formation of helical structures in epidermicin NI01 and aureocin A53 in aqueous buffers. It also revealed that epidermicin NI01 undergoes denaturation at 60°C and exhibits a reversible two-state conversion between helical and unfolded forms (Hammond et al., 2020). Due to these interesting findings, we decided to employ a thermal shift assay, also known as differential scanning fluorimetry

TABLE 2 Antibacterial activity spectrum and MIC values of Geo6.

Microorganism name	Strain name	Growth temperature	Growth inhibition	MIC
<i>Aeribacillus pallidus</i>	DSM 3670 ^T	55°C	+++	NA
<i>Anoxybacillus tepidamans</i>	DSM 16315 ^T	55°C	–	NA
<i>Anoxybacillus tepidamans</i>	DSM 16325 ^T	55°C	+	NA
<i>Geobacillus stearothermophilus</i>	DSM 22 ^T	55°C	+	NA
<i>Geobacillus stearothermophilus</i>	DSM 13240	55°C	+	NA
<i>Geobacillus lituanicus</i>	DSM 15325 ^T	55°C	+++	585 nM
<i>Geobacillus gargensis</i>	DSM 15378 ^T	55°C	+	NA
<i>Geobacillus caldoxylosilyticus</i>	DSMZ 12833	55°C	–	NA
<i>Geobacillus debilis</i>	DSM 16016 ^T	55°C	++	NA
<i>Geobacillus jurassicus</i>	DSM 15726 ^T	55°C	+	NA
<i>Geobacillus kaustophilus</i>	HTA 426	55°C	+++	293 nM
<i>Geobacillus subterraneus</i>	DSM 13552 ^T	55°C	–	NA
<i>Geobacillus thermocatenulatus</i>	DSM 730	55°C	–	NA
<i>Geobacillus thermodenitrificans</i>	DSM 465 ^T	55°C	++	2.34 µM
<i>Geobacillus thermoleovorans</i>	DSM 5366 ^T	55°C	+++	585 nM
<i>Geobacillus uzenensis</i>	DSM 13551 ^T	55°C	–	NA
<i>Parageobacillus genomospecies 1</i>	NUB 36187	55°C	–	NA
<i>Parageobacillus thermoglucosidasius</i>	DSM 2542 ^T	55°C	–	NA
<i>Parageobacillus toebii</i>	DSM 14590 ^T	55°C	+	4.45 µM
<i>Bacillus spizizenii</i>	ATCC 6633	37°C	–	NA
<i>Bacillus subtilis</i>	168	37°C	–	NA
<i>Bacillus velezensis</i>	CH02	37°C	–	NA
<i>Bacillus zanthoxyli</i>	CH07	37°C	+	NA
<i>Pseudomonas aeruginosa</i>	ATCC 27853 (P)	37°C	–	NA
<i>Staphylococcus epidermidis</i>	ATCC 12228 (P)	37°C	–	NA
<i>Staphylococcus aureus subsp. aureus</i>	ATCC 25923 (P)	37°C	–	NA
<i>Staphylococcus saprophyticus</i>	AG1	37°C	–	NA
<i>Enterococcus faecalis</i>	DSMZ 2570 (P)	30°C	–	NA
<i>Salmonella enterica serovar Typhimurium</i>	LK (P)	30°C	–	NA
<i>Saccharomyces cerevisiae</i>	α'1	30°C	–	NA
<i>Candida lusitanae</i>	CL18 (P)	30°C	–	NA
<i>Candida guilliermondii</i>	EL (P)	30°C	–	NA
<i>Candida albicans</i>	ATCC 14053 (P)	30°C	–	NA
<i>Acinetobacter baumannii</i>	Ab171 (P)	37°C	–	NA
<i>Acinetobacter baumannii</i>	Ab169 (P)	37°C	–	NA
<i>Acinetobacter baumannii</i>	Ab141 (P)	37°C	–	NA
<i>Stenotrophomonas maltophilia</i>	SM21 (P)	37°C	–	NA
<i>Stenotrophomonas maltophilia</i>	SM3 (P)	37°C	–	NA
<i>Stenotrophomonas maltophilia</i>	D53 (P)	37°C	–	NA
<i>Escherichia coli</i>	BL21 (DE3)	37°C	–	NA

P refers to pathogenic strain.

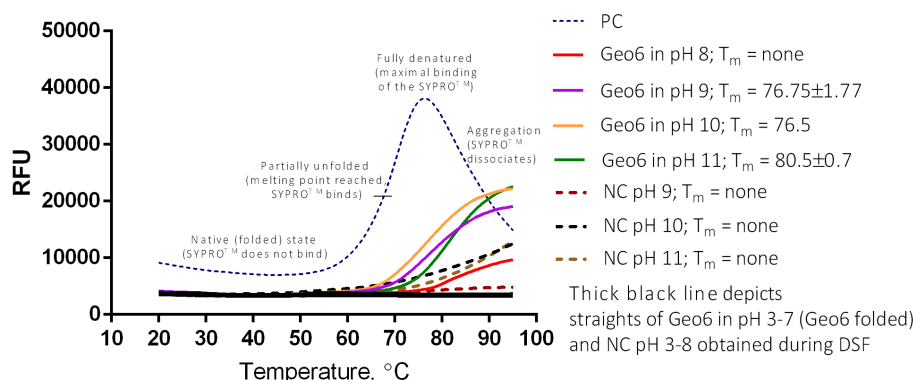


FIGURE 10

DSF or thermal shift of Geo6 bacteriocin. All Geo6 samples were suspended in 25mM Briton-Robinson buffer with different pH values (pH 3–11) and with SYPRO Orange dye. PC – positive control of 100µg/ml lysozyme solution in 25mM Briton-Robinson buffer, pH 6, and with SYPRO Orange dye. NC – negative controls in 25mM Briton-Robinson buffer solutions (pH 3–11) with SYPRO Orange dye. Samples with Geo6 (pH 3–7) and NCs (pH 3–8) depicted in black straight lines indicate no fluorescence change. NCs in pH 9–11 depicted in colored dotted lines indicate slight fluorescence change. Samples with Geo6 in pH 8–11 depicted in colored straight lines indicate moderate fluorescence change. PC displays a typical sigmoidal line of unfolded protein, demonstrating significant fluorescence change. RFU – relative fluorescence units.

(DSF), to analyze the thermal denaturation of Geo6 under different pH ranges and temperatures. Additionally, to the best of our knowledge, this method has never been employed to study the stability and structural changes of bacteriocins.

The fluorescent dye (SYPRO Orange) used in this assay is highly fluorescent in non-polar environments, such as hydrophobic sites on unfolded proteins, compared to an aqueous solution where the fluorescence is quenched. By monitoring the increase in fluorescence, we can observe the binding of the dye to the hydrophobic amino acids of the unfolded peptide, which are normally hidden within the helical structure. Additionally, the DSF method enables the use of small sample volumes and low concentrations (Niesen et al., 2007).

The analysis showed that Geo6 remained in its unfolded state over a range of pH 3–7 during the increase of temperatures from 20°C to 95°C, and the formation of typical melt curves did not occur during the DSF assay (Figure 10). Such results imply that Geo6 remained extremely stable under the DSF conditions and stand in line with the results obtained in the spot on a lawn assay. Partial unfolding or thermal denaturation of Geo6 was detected in the range of pH 9–11, implying that in these conditions the peptide starts to denature (melting temperatures (T_m) of 76.5–80.5°C were determined). However, the observed melting curves did not indicate full denaturation or aggregation. A slight increase in relative fluorescence units (RFU) was also detected at pH 8, and the appropriate negative controls within the pH range of 9–11 also exhibited increased RFU. As a result, the findings of the DSF assay for Geo6 within the pH range of 8–11 are inconclusive and represent a major limitation of this study in accurately determining the stability of Geo6 within this pH range. Given that Geo6 has a pI value of 9.3, it can become negatively charged at pH levels higher than its pI, potentially leading to the destabilization of the bacteriocin. Despite the inconclusive results at pH 8–11, the denaturation or unfolding of Geo6 within the pH range 3–7 was not observed, which contradicts the findings of the previous study on epidermicin NI01 and aureocin A53 using CD spectroscopy analysis (Hammond et al., 2020).

4. Conclusion

To date, at least 33 antimicrobial peptides falling into the leaderless bacteriocin subclass have been identified and characterized. Their molecular weight varies between 2.8–6.0kDa and they are produced mainly by mesophilic *Enterococcus*, *Weissella*, *Staphylococcus*, *Lactococcus*, *Bacillus*, and *Streptococcus* spp. bacteria (Perez et al., 2018). This study demonstrates that thermophilic strain *P. thermoglucosidarius* DSM 2542 encodes a novel cationic leaderless bacteriocin, Geo6, with a molecular weight of 5.5kDa. Three-dimensional structure prediction and CD spectroscopy determined that it resembles structures of other leaderless bacteriocins, comprising the helical structure. The bacteriocin was heterologously synthesized in *E. coli* and purified using chromatographic methods.

Our findings demonstrated that Geo6 has extreme stability in high temperatures and a wide pH range. Geo6 is active in µM and nM concentrations, as other leaderless bacteriocins as lacticins Q/Z work in the nM range too (Fujita et al., 2007; Iwatani et al., 2007). Moreover, only one *Bacillus* sp. strain and some thermophilic *Geobacillus* spp., *Parageobacillus* sp. or *Aeribacillus* sp. strains demonstrated susceptibility to Geo6 which shows bacteriocin has a narrow antibacterial activity spectrum and is active mostly against thermophilic bacteria. The determined mode of action showed that Geo6 works through cytoplasmic membrane permeabilization, in a similar way to other leaderless bacteriocins (Hammond et al., 2020).

Considering Geo6 stability in harsh environments and its activity against thermophilic bacteria, it could be applied in the food industry and in biotechnological processes where contamination with thermophilic bacteria is undesirable. Furthermore, the identification and characterization of novel bacteriocins like Geo6 contribute to our understanding of the diversity of bacteriocins and expand our knowledge about antimicrobial peptides. This knowledge, in turn, can facilitate the adoption of antimicrobial peptides in diverse biotechnological sectors.

Leaderless bacteriocins, such as Geo6, possess significant potential in various applications due to their simple structure compared to other bacteriocins. They can be fused with signal peptides of other proteins, in this way production at high yields and secretion in other microorganisms or eukaryotic cells could be easily achieved. In addition, the determination of bacteriocin structure in genes allows their easy modifications and improvements.

Data availability statement

The original contributions presented in the study are included in the article/[Supplementary material](#), further inquiries can be directed to the corresponding author.

Author contributions

AKa: conceptualization, methodology, investigation, supervision, funding acquisition, and writing – original draft. AKo, AP, EB, and AGE: investigation. AGR: investigation, and writing – review and editing. LK: funding acquisition. All authors contributed to the article and approved the submitted version.

Funding

This project has received funding from European Social Fund (project no 09.3.3-LMT-K-712-22-0095) under a grant agreement with the Research Council of Lithuania (LMTLT).

References

- Acedo, J. Z., van Belkum, M. J., Lohans, C. T., Towle, K. M., Miskolzie, M., and Vederas, J. C. (2016). Nuclear magnetic resonance solution structures of lactacin Q and aureocin A53 reveal a structural motif conserved among leaderless bacteriocins with broad-spectrum activity. *Biochemistry* 55, 733–742. doi: 10.1021/acs.biochem.5b01306
- Bacon, L. F., Hamley-Bennett, C., Danson, M. J., and Leak, D. J. (2017). Development of an efficient technique for gene deletion and allelic exchange in *Geobacillus* spp. *Microb. Cell Factories* 16:58. doi: 10.1186/s12934-017-0670-4
- Bendikienė, V., Surinienaitė, B., Juodka, B., and Safarikova, M. (2004). Insights into catalytic action mechanism of *Pseudomonas mendocina* 3121-1 lipase. *Enzym. Microb. Technol.* 34, 572–577. doi: 10.1016/j.enzmictec.2004.01.006
- Berendsen, E. M., Wells-Bennik, M. H. J., Krawczyk, A. O., de Jong, A., van Heel, A., Holsappel, S., et al. (2016). Draft genome sequences of seven thermophilic spore-forming bacteria isolated from foods that produce highly heat-resistant spores, comprising *Geobacillus* spp., *Caldibacillus debilis*, and *Anoxybacillus flavithermus*. *Genome Announc.* 4:e00105-16. doi: 10.1128/genomeA.00105-16
- Bhattacharya, D., Nanda, P. K., Pateiro, M., Lorenzo, J. M., Dhar, P., and Das, A. K. (2022). Lactic acid bacteria and bacteriocins: novel biotechnological approach for biopreservation of meat and meat products. *Microorganisms* 10:2058. doi: 10.3390/microorganisms10102058
- Burgess, S. A., Cox, M. P., Flint, S. H., Lindsay, D., and Biggs, P. J. (2015). Draft genome sequences of three strains of *Geobacillus stearothermophilus* isolated from a milk powder manufacturing plant. *Genome Announc.* 3:e00939-15. doi: 10.1128/genomeA.00939-15
- Butcher, B. G., and Helmann, J. D. (2006). Identification of *Bacillus subtilis* sigmaW-dependent genes that provide intrinsic resistance to antimicrobial compounds produced by *Bacilli*. *Mol. Microbiol.* 60, 765–782. doi: 10.1111/j.1365-2958.2006.05131.x
- Cotter, P. D., Hill, C., and Ross, R. P. (2005). Bacteriocins: developing innate immunity for food. *Nat. Rev. Microbiol.* 3, 777–788. doi: 10.1038/nrmicro1273
- Cotter, P. D., Ross, R. P., and Hill, C. (2013). Bacteriocins - a viable alternative to antibiotics? *Nat. Rev. Microbiol.* 11, 95–105. doi: 10.1038/nrmicro2937
- Cozier, G. E., Carlton, J., Bouyoucef, D., and Cullen, P. J. (2004). Membrane targeting by pleckstrin homology domains. *Curr. Top. Microbiol. Immunol.* 282, 49–88. doi: 10.1007/978-3-642-18805-3_3
- Cripps, R. E., Eley, K., Leak, D. J., Rudd, B., Taylor, M., Todd, M., et al. (2009). Metabolic engineering of *Geobacillus thermoglucosidarius* for high yield ethanol production. *Metab. Eng.* 11, 398–408. doi: 10.1016/j.ymben.2009.08.005
- Daba, H., Pandian, S., Gosselin, J. F., Simard, R. E., Huang, J., and Lacroix, C. (1991). Detection and activity of a bacteriocin produced by *Leuconostoc mesenteroides*. *Appl. Environ. Microbiol.* 57, 3450–3455. doi: 10.1128/aem.57.12.3450-3455.1991
- Ebihara, A., Kawamoto, S., Shibata, N., Yamaguchi, T., Suzuki, F., and Nakagawa, T. (2016). Development of a modified Britton-Robinson buffer with improved linearity in the alkaline pH region. *Biojournal Sci. Technol.* 3:m150006.
- Egan, K., Field, D., Ross, R. P., Cotter, P. D., and Hill, C. (2018). *In silico* prediction and exploration of potential bacteriocin gene clusters within the bacterial genus *geobacillus*. *Front. Microbiol.* 9:2116. doi: 10.3389/fmicb.2018.02116
- Fujita, K., Ichimasa, S., Zendo, T., Koga, S., Yoneyama, F., Nakayama, J., et al. (2007). Structural analysis and characterization of lactacin Q, a novel bacteriocin belonging to a new family of unmodified bacteriocins of Gram-positive bacteria. *Appl. Environ. Microbiol.* 73, 2871–2877. doi: 10.1128/AEM.02286-06
- Garg, N., Tang, W., Goto, Y., Nair, S. K., and van der Donk, W. A. (2012). Lantibiotics from *Geobacillus thermodenitrificans*. *Proc. Natl. Acad. Sci.* 109, 5241–5246. doi: 10.1073/pnas.1116815109
- Global Action Plan on Antimicrobial Resistance (2015). Available at: <https://www.who.int/publications/i/item/9789241509763>
- Hahn-Löbmann, S., Stephan, A., Schulz, S., Schneider, T., Shaverskyi, A., Tüsel, D., et al. (2019). Colicins and salmocins – new classes of plant-made non-antibiotic food antibacterials. *Front. Plant Sci.* 10:437. doi: 10.3389/fpls.2019.00437

Acknowledgments

We are grateful to colleagues from the Department of Biochemistry and Molecular Biology, Julija Armalytė and Laurita Klimkaitė, for sharing *Acinetobacter* and *Stenotrophomonas* spp. strains to test the antibacterial activity of Geo6. We are thankful to colleague Giedrius Sasnauskas from the Department of Protein - DNA Interactions for the opportunity to measure spectra of the peptide using the CD spectrophotometer.

Conflict of interest

The authors declare that the research was conducted in the absence of any commercial or financial relationships that could be construed as a potential conflict of interest.

Publisher's note

All claims expressed in this article are solely those of the authors and do not necessarily represent those of their affiliated organizations, or those of the publisher, the editors and the reviewers. Any product that may be evaluated in this article, or claim that may be made by its manufacturer, is not guaranteed or endorsed by the publisher.

Supplementary material

The Supplementary material for this article can be found online at: <https://www.frontiersin.org/articles/10.3389/fmicb.2023.1207367/full#supplementary-material>

- Hammond, K., Lewis, H., Halliwell, S., Desriac, F., Nardone, B., Ravi, J., et al. (2020). Flowering poration – a synergistic multi-mode antibacterial mechanism by a bacteriocin fold. *iScience* 23:101423. doi: 10.1016/j.isci.2020.101423
- Iwatani, S., Horikiri, Y., Zendo, T., Nakayama, J., and Sonomoto, K. (2013). Bifunctional gene cluster lncBCDEF mediates bacteriocin production and immunity with differential genetic requirements. *Appl. Environ. Microbiol.* 79, 2446–2449. doi: 10.1128/AEM.03783-12
- Iwatani, S., Yoneyama, F., Miyashita, S., Zendo, T., Nakayama, J., and Sonomoto, K. (2012). Identification of the genes involved in the secretion and self-immunity of lactacin Q, an unmodified leaderless bacteriocin from *Lactococcus lactis* QU 5. *Microbiology (N Y)* 158, 2927–2935. doi: 10.1099/mic.0.062943-0
- Iwatani, S., Zendo, T., Yoneyama, F., Nakayama, J., and Sonomoto, K. (2007). Characterization and structure analysis of a novel bacteriocin, lactacin Z, produced by *Lactococcus lactis* QU 14. *Biosci. Biotechnol. Biochem.* 71, 1984–1992. doi: 10.1271/bbb.70169
- Kalogridou-Vassiliadou, D. (1992). Biochemical activities of *Bacillus* species isolated from flat sour evaporated milk. *J. Dairy Sci.* 75, 2681–2686. doi: 10.3168/jds.S0022-0302(92)78030-8
- Kapust, R. B., Tözsér, J., Fox, J. D., Anderson, D. E., Cherry, S., Copeland, T. D., et al. (2001). Tobacco etch virus protease: mechanism of autolysis and rational design of stable mutants with wild-type catalytic proficiency. *Protein Eng. Des. Sel.* 14, 993–1000. doi: 10.1093/protein/14.12.993
- Kaunietis, A., Buivydas, A., Čitavičius, D. J., and Kuipers, O. P. (2019). Heterologous biosynthesis and characterization of a glycocin from a thermophilic bacterium. *Nat. Commun.* 10:1115. doi: 10.1038/s41467-019-09065-5
- Masuda, Y., Zendo, T., and Sonomoto, K. (2012). New type non-lantibiotic bacteriocins: circular and leaderless bacteriocins. *Benef. Microbes* 3, 3–12. doi: 10.3920/BM2011.0047
- Nascimento, J. D. S., Coelho, M. L. V., Ceotto, H., Potter, A., Fleming, L. R., Salehian, Z., et al. (2012). Genes involved in immunity to and secretion of aureocin A53, an atypical class II bacteriocin produced by *Staphylococcus aureus* A53. *J. Bacteriol.* 194, 875–883. doi: 10.1128/JB.06203-11
- Netz, D. J. A., Bastos, M., and Sahl, H. G. (2002a). Mode of action of the antimicrobial peptide aureocin A53 from *Staphylococcus aureus*. *Appl. Environ. Microbiol.* 68, 5274–5280. doi: 10.1128/AEM.68.11.5274-5280.2002
- Netz, D. J. A., Pohl, R., Beck-Sickinger, A. G., Selmer, T., Pierik, A. J., Bastos, M., et al. (2002b). Biochemical characterisation and genetic analysis of aureocin A53, a new, atypical bacteriocin from *Staphylococcus aureus*. *J. Mol. Biol.* 319, 745–756. doi: 10.1016/S0022-2836(02)00368-6
- Niesen, F. H., Berglund, H., and Vedadi, M. (2007). The use of differential scanning fluorimetry to detect ligand interactions that promote protein stability. *Nat. Protoc.* 2, 2212–2221. doi: 10.1038/nprot.2007.321
- Pereira, W. A., Mendonça, C. M. N., Urquiza, A. V., Marteinsson, V. Þ., LeBlanc, J. G., Cotter, P. D., et al. (2022). Use of probiotic bacteria and bacteriocins as an alternative to antibiotics in aquaculture. *Microorganisms* 10:1705. doi: 10.3390/microorganisms10091705
- Perez, R. H., Zendo, T., and Sonomoto, K. (2018). Circular and leaderless bacteriocins: biosynthesis, mode of action, applications, and prospects. *Front. Microbiol.* 9:2085. doi: 10.3389/fmicb.2018.02085
- Pérez-Ramos, A., Ladjouzi, R., Benachour, A., and Drider, D. (2021). Evidence for the involvement of pleckstrin homology domain-containing proteins in the transport of enterocin DD14 (EntDD14); a leaderless two-peptide bacteriocin. *Int. J. Mol. Sci.* 22:12877. doi: 10.3390/ijms222312877
- Schägger, H. (2006). Tricine-SDS-PAGE. *Nat. Protoc.* 1, 16–22. doi: 10.1038/nprot.2006.4
- Seale, B., Burgess, S., Flint, S., Brooks, J., Bremer, P., and Parkar, S. (2015). “Thermophilic spore-forming bacilli in the dairy industry” in *Biofilms in the Dairy Industry*, eds K. H. Teh, S. Flint, J. Brooks, and G. Knight (Chichester, UK: John Wiley & Sons, Ltd), 112–137.
- Soltani, S., Hammami, R., Cotter, P. D., Rebuffat, S., Said, L. B., Gaudreau, H., et al. (2021). Bacteriocins as a new generation of antimicrobials: toxicity aspects and regulations. *FEMS Microbiol. Rev.* 45:fuaa039. doi: 10.1093/femsre/fuua039
- Subramanian, S., and Smith, D. L. (2015). Bacteriocins from the rhizosphere microbiome – from an agriculture perspective. *Front. Plant Sci.* 6:909. doi: 10.3389/fpls.2015.00909
- Vaičiukauskaitė, M., Ger, M., Valius, M., Maneikis, A., Lastauskienė, E., Kalėdienė, L., et al. (2019). Geobacillin 26 - high molecular weight bacteriocin from a thermophilic bacterium. *Int. J. Biol. Macromol.* 141, 333–344. doi: 10.1016/j.ijbiomac.2019.09.047
- Watterson, M. J., Kent, D. J., Boor, K. J., Wiedmann, M., and Martin, N. H. (2014). Evaluation of dairy powder products implicates thermophilic sporeformers as the primary organisms of interest. *J. Dairy Sci.* 97, 2487–2497. doi: 10.3168/jds.2013-7363
- Wiegand, I., Hilpert, K., and Hancock, R. E. W. (2008). Agar and broth dilution methods to determine the minimal inhibitory concentration (MIC) of antimicrobial substances. *Nat. Protoc.* 3, 163–175. doi: 10.1038/nprot.2007.521
- Xu, Q., Bateman, A., Finn, R. D., Abdubek, P., Astakhova, T., Axelrod, H. L., et al. (2010). Bacterial pleckstrin homology domains: a prokaryotic origin for the PH domain. *J. Mol. Biol.* 396, 31–46. doi: 10.1016/j.jmb.2009.11.006
- Yakimov, A. P., Afanaseva, A. S., Khodorkovskiy, M. A., and Petukhov, M. G. (2016). Design of stable α -helical peptides and thermostable proteins in biotechnology and biomedicine. *Acta Nat.* 8, 70–81. doi: 10.32607/20758251-2016-8-4-70-81
- Yoneyama, F., Imura, Y., Ohno, K., Zendo, T., Nakayama, J., Matsuzaki, K., et al. (2009). Peptide-lipid huge toroidal pore, a new antimicrobial mechanism mediated by a lactococcal bacteriocin, lactacin Q. *Antimicrob. Agents Chemother.* 53, 3211–3217. doi: 10.1128/AAC.00209-09



OPEN ACCESS

EDITED BY

Rustam Aminov,
University of Aberdeen, United Kingdom

REVIEWED BY

Jianhua Wang,
Chinese Academy of Agricultural Sciences
(CAAS), China
Eugene A. Rogozhin,
Institute of Bioorganic Chemistry (RAS), Russia

*CORRESPONDENCE

Lihong Liu
✉ hongllh@126.com

RECEIVED 13 June 2023

ACCEPTED 22 August 2023

PUBLISHED 05 September 2023

CITATION

Chen X, Su S, Yan Y, Yin L and Liu L (2023) Anti-*Pseudomonas aeruginosa* activity of natural antimicrobial peptides when used alone or in combination with antibiotics.
Front. Microbiol. 14:1239540.
doi: 10.3389/fmicb.2023.1239540

COPYRIGHT

© 2023 Chen, Su, Yan, Yin and Liu. This is an open-access article distributed under the terms of the [Creative Commons Attribution License \(CC BY\)](https://creativecommons.org/licenses/by/4.0/). The use, distribution or reproduction in other forums is permitted, provided the original author(s) and the copyright owner(s) are credited and that the original publication in this journal is cited, in accordance with accepted academic practice. No use, distribution or reproduction is permitted which does not comply with these terms.

Anti-*Pseudomonas aeruginosa* activity of natural antimicrobial peptides when used alone or in combination with antibiotics

Xueqi Chen¹, Shan Su², Yan Yan¹, Limei Yin¹ and Lihong Liu^{1*}

¹Department of Pharmacy, China-Japan Friendship Hospital, Beijing, China, ²Department of Pharmacy, The Affiliated Taian City Central Hospital of Qingdao University, Taian, China

The World Health Organization has recently published a list of 12 drug-resistant bacteria that posed a significant threat to human health, and *Pseudomonas aeruginosa* (*P. aeruginosa*) was among them. In China, *P. aeruginosa* is a common pathogen in hospital acquired pneumonia, accounting for 16.9–22.0%. It is a ubiquitous opportunistic pathogen that can infect individuals with weakened immune systems, leading to hospital-acquired acute and systemic infections. The excessive use of antibiotics has led to the development of various mechanisms in *P. aeruginosa* to resist conventional drugs. Thus, there is an emergence of multidrug-resistant strains, posing a major challenge to conventional antibiotics and therapeutic approaches. Antimicrobial peptides are an integral component of host defense and have been found in many living organisms. Most antimicrobial peptides are characterized by negligible host toxicity and low resistance rates, making them become promising for use as antimicrobial products. This review particularly focuses on summarizing the inhibitory activity of natural antimicrobial peptides against *P. aeruginosa* planktonic cells and biofilms, as well as the drug interactions when these peptides used in combination with conventional antibiotics. Moreover, the underlying mechanism of these antimicrobial peptides against *P. aeruginosa* strains was mainly related to destroy the membrane structure through interacting with LPS or increasing ROS levels, or targeting cellular components, led to cell lysis. Hopefully, this analysis will provide valuable experimental data on developing novel compounds to combat *P. aeruginosa*.

KEYWORDS

antimicrobial peptides, *Pseudomonas aeruginosa*, *Escherichia coli*, drug resistance, biofilms, interaction

1. Background

As a common opportunistic gram-negative pathogen, *Pseudomonas aeruginosa* (*P. aeruginosa*) is a significant cause of nosocomial infection, leading to a variety of infections such as pneumonia, bacteremia, and urinary tract infections (Terzi et al., 2014; Yaeger et al., 2021). Individuals with weakened immune systems, such as those with metabolic diseases, hematological diseases, and malignant tumors, are more susceptible to *P. aeruginosa* infection (Burrows, 2018; Yaeger et al., 2021). The drugs commonly used for treating *P. aeruginosa* infection in clinical settings include penicillin, cephalosporins, aztreonam, aminoglycosides, fluoroquinolones and carbapenems (Moore and Flaws, 2011; Jangra et al., 2022). However, due to the inappropriate use of antibiotics, the resistance of *P. aeruginosa* to carbapenems and many

other antibacterial drugs has increased rapidly, making the number of drug-resistant strains continue to arise and bringing challenges to clinical treatment (Hancock and Speert, 2000; Jangra et al., 2022). Therefore, there is an urgent need to develop new strategies to combat resistant *P. aeruginosa* infections.

The natural immune system serves as a functional and physiological barrier against microbial infections. Within this system, there are important effectors called antimicrobial peptides (AMPs) or host defense peptides (HDPs). Studies have shown that AMPs not only play a role in the regulation of inflammatory response, immune system, and apoptosis pathway, but they also exhibit a broad spectrum of antimicrobial activities (Su et al., 2010; Cho et al., 2012; Hancock et al., 2012; Buda De Cesare et al., 2020). Currently, more than 3,000 natural AMPs derived from microorganisms, plants, mammals, amphibians, and insects have been registered in the Antimicrobial Peptide Database (unmc.edu) (Bin Hafeez et al., 2021).

Most AMPs are composed of 10–100 amino acids and have an amphiphilic conformation, which can bind to the negatively charged components of bacterial cell surface, and integrate with the lipid bilayer, or enter the cytoplasm through the cell membrane, thus exhibit great antimicrobial activity against pathogens (Huan et al., 2020; Lachowicz et al., 2020). Multiple studies have demonstrated that many AMPs possess good antibacterial properties on their own. For example, BCp12 had been found to possess obvious antimicrobial activity against *Staphylococcus aureus*, *Listeria monocytogenes*, *Escherichia coli* (*E. coli*) and *Salmonella typhimurium* strains, with minimum inhibitory concentrations (MICs) of 0.4–1.6 mg/mL. Moreover, BCp12 induced low hemolytic activity and cytotoxicity on mammalian cells (Zhao et al., 2020). Furthermore, the combination of AMPs and traditional antibiotics demonstrated synergistic antimicrobial effects, and the combination not only enhanced the effectiveness of the two, but also expanded the antimicrobial spectrum of antibiotics. Notably, L₁G, L₇A and L₁GA₃K possessed good bioactivity, mild cytotoxicity, and high stability, and could rapidly kill bacteria by membrane rupture and intracellular materials release, with a MIC of 4–32 µM. Moreover, when combined with rifampicin, polymyxin B, and gentamicin, they exhibited either synergistic or additive effects against gram-negative bacteria (Zhu et al., 2021). AMPs may exert their antibacterial effects through different mechanisms, either by directly interacting with the bacterial membrane or by targeting other cellular components. The membrane-mediated mechanisms of action can be described by models: (1) the toroidal pore model, AMPs can enter the membrane vertically, the lipids would be dragged and bended by AMPs when they form the toroidal pore; (2) the barrel-stave model, AMPs can insert into the membrane, forming barrels and opening stable and transmembrane pores, thereby destabilizing the membrane potential and promoting leakage of ions and biomolecules; (3) the carpet-stave model, AMPs can act as detergents by localizing on the horizontal plane of the plasma membrane, then causing alterations and destruction; (4) the aggregate channel model, AMPs can competitively displace lipopolysaccharides (LPS)-associated divalent cations, leading to nonstructural aggregation of AMPs and lipids that disrupts the outer and inner membranes (Lee et al., 2011; Huan et al., 2020; Roque-Borda et al., 2021). In the non-membrane-targeted mechanism of action of AMPs, they can enter cells by direct penetration or endocytosis, and achieve antimicrobial activity through several mechanisms: (1) affecting nucleic acid and protein synthesis; (2)

inhibiting enzyme activity and energy metabolism; (3) destroying cellular organelles; (4) producing oxidative stress response (Nguyen et al., 2011; Lei et al., 2019; Saeed et al., 2022).

In this review, we have presented a comprehensive summary of the inhibitory effects of natural AMPs used alone, and in combination with other drugs against *P. aeruginosa* planktonic cells and biofilms in Tables 1, 2. Moreover, we also summarized the relevant antibacterial mechanisms of AMPs, although they still needed to be further investigated. We believe this review will provide valuable experimental data for developing novel anti-*P. aeruginosa* agents.

2. Anti-*Pseudomonas aeruginosa* activity of AMPs

The AMP database has documented many AMPs that have been derived from various lives, including 335 bacteriocins from bacteria, 4 AMPs from archaea, 8 AMPs from protozoa, 13 AMPs from fungi, 342 AMPs from plants, 2,200 AMPs from animals, and some synthetic peptides (Zhu et al., 2017; Boparai and Sharma, 2020a; Perez-Rodriguez et al., 2022a). In this review, our focus is on AMPs that have anti-*P. aeruginosa* effects, and we have categorized them into six different groups according to their origins: *microorganisms*, *plants*, *mammals*, *insects*, *amphibians*, and a varied group of *others*. In Table 1, we summarized the inhibitory activity of natural AMPs against *P. aeruginosa* according to different sources, and ranked the antibacterial activity from strongest to weakest.

2.1. AMPs from *microorganisms*

Numerous researchers have found and isolated a variety of AMPs from *bacteria* and *fungi*, which have significant antibacterial activity against different types of pathogens (Andrá et al., 2001; Szekeres et al., 2005; Buda De Cesare et al., 2020; Boparai and Sharma, 2020b).

The rumen is a complex microbiome consisting of various microorganisms, including fungi, bacteria, and viruses (Morgavi et al., 2013; McCann et al., 2014; Oyama et al., 2017). Many researchers have regarded it as a potential resource for discovering new AMPs. For example, Oyama et al. and Mulkern et al. reported that Lynronne-1, 2, 3, and P15s (with 2.83–3.08 kDa in size) were identified from *bovine rumen microbiome* all possessed good antibacterial activity (Privé et al., 2015; Oyama et al., 2017; Mulkern et al., 2022). In these two studies, researchers found that the four peptides possessed significant *in vitro* activity against *P. aeruginosa* and *E. coli*, with MICs of 4–512 and 32–64 µg/mL, respectively. *In vivo* experiments, local administration of Lynronne-1 (10% w/v) significantly reduced the number of bacteria infected by methicillin-resistant *Staphylococcus aureus* (MRSA) in mice (Oyama et al., 2017). In addition, in *Galleria mellonella* (*G. mellonella*) infection model, treatment with Lynronne 1 and Lynronne 2 at 32 and 128 mg/kg resulted in a 100% survival rate of the larvae (Mulkern et al., 2022). Among them, Lynronne-2 had the highest safety, as it did not exhibit any cytotoxicity toward HUVEC and HepG2 cells at a concentration of 128 µg/mL. However, Lynronne-1 and Lynronne-3 showed some degree of toxicity, with their 50% lethal concentration (LC₅₀) values of 98.1 and 128 µg/mL (Oyama et al., 2017). In addition to their ability to bind to bacterial membrane lipids and enhance membrane permeability, Lynronne-1

TABLE 1 Antimicrobial peptides (AMPs) with activity against *Pseudomonas aeruginosa*.

Classification	Source	Code (ID)	AMPs	Molecular weight (kDa)	Strains	Inhibitory activities	Proposed Mechanism of Action	References
Microorganisms	Bacteria	AP02929	Lynronne-1	2.83	<i>P. aeruginosa</i> (n = 10)	MIC = 16–64 µg/mL	Reduces <i>arcA</i> , <i>arcB</i> and <i>arcC</i> expression	Oyama et al. (2017)
	Bacteria	AP02930	Lynronne-2	2.86		MIC = 32–256 µg/mL		
	Bacteria	AP02931	Lynronne-3	3.08		MIC = 64–512 µg/mL		
	Bacteria	AP02939	P15s	2.86	<i>P. aeruginosa</i> (n = 8)	MIC = 64–512 µg/mL	Reduces <i>arcD</i> expression	Mulkern et al. (2022)
	<i>Lactobacillus acidophilus</i> ATCC 4356	–	Acidocin 4,356	8.5	<i>P. aeruginosa</i> ATCC 27853	MIC ₉₀ = 128.22 µg/mL ACD (128.22 µg/mL) → killed >90% biofilm; ACD (256.44 µg/mL) → eradicated large parts of biofilm	Enhances bacterial membrane perturbation, inhibits virulence factors	Modiri et al. (2020)
	<i>Actinomyces ruminicola</i>	AP03310	Actifensin	4.1	<i>P. aeruginosa</i> ATCC 27853	MIC/MBC = 1,448 µg/mL Actifensin (724 µg/mL) → reduced >70% biofilm	Increases ROS production, disrupts cell membrane	Gbala et al. (2022)
Plants	Spinach	–	Defensin-d2	5.8	<i>P. aeruginosa</i> ATCC 27853	MIC = 7.5 µg/mL MBC = 123 µg/mL Defensin-d2 (3.75 µg/mL) → reduced >70% biofilm	Increases ROS production, disrupts cell membrane	Gbala et al. (2022)
	<i>Medicago Truncatula</i>	AP02428	Core MtDef4	1.98	<i>P. aeruginosa</i>	IC ₅₀ = 1.7–4.2 µM	Damages bacterial outer membranes	Sathoff et al. (2020), Velivelli et al. (2018)
	<i>Medicago Truncatula</i>	–	Core MtDef5	2.04	<i>P. aeruginosa</i>	IC ₅₀ = 8.5–14.6 µM	Interferes with DNA synthesis and transcription	

(Continued)

TABLE 1 (Continued)

Classification	Source	Code (ID)	AMPs	Molecular weight (kDa)	Strains	Inhibitory activities	Proposed Mechanism of Action	References
Mammals	Porcine	AP00195	Porcine protegrin-1	2.59	<i>P. aeruginosa</i> (n = 5)	MIC = 0.3–0.8 µg/mL	Disrupts cell membrane	Turner et al. (1998)
	Human	–	FLG2-4	70–140	<i>P. aeruginosa</i> ATCC33354	MEC = 0.4 µM	Induces membrane blebbing, impairs DNA polymerases processivity, thereby stops bacterial replication	Hansmann et al. (2015)
	Human	–	LL-37	4.493	<i>P. aeruginosa</i> (n = 6)	MIC = 8–32 µg/mL LL-37 (16 µg/mL) → inhibited 80% biofilm formation; LL-37 (4 µg/mL) → made pre-formed biofilm thinner	Reduces bacterial cells attachment, stimulates motility twitch, suppresses the expression of key QS signaling molecules, downregulates biofilm formation-related genes expression	Turner et al. (1998) , Overhage et al. (2008)
	Cattle	AP00366	BMAP-27	3.47	<i>P. aeruginosa</i> strains (n = 25)	MIC ₉₀ /MBC ₉₀ = 16 µg/mL BMAP-27 (8 µg/mL) → reduced biofilm formation; BMAP-27 (80 µg/mL) → against pre-formed biofilms	Induces of membrane permeabilization	Skerlavaj et al. (1996) , Pompilio et al. (2012)
	Cattle	AP00367	BMAP-28	3.32		MIC ₉₀ /MBC ₉₀ = 32 µg/mL BMAP-28 (16 µg/mL) → reduced biofilm formation; BMAP-28 (160 µg/mL) → against pre-formed biofilms	Induces of membrane permeabilization	
	Human	–	Human β-defensin 2	4–5	<i>P. aeruginosa</i>	LD ₉₀ = 10 µg/mL HBD2 (0.25–0.5 µM) → reduced 75% biofilm	Induces the change of the biofilm surface topology	Schröder and Harder (1999) , Parduchio et al. (2020)

(Continued)

TABLE 1 (Continued)

Classification	Source	Code (ID)	AMPs	Molecular weight (kDa)	Strains	Inhibitory activities	Proposed Mechanism of Action	References
Insects	<i>Apis mellifera</i>	–	Jelleines I	0.95	<i>P. aeruginosa</i> ATCC 27853	MIC = 10 µg/mL	Disrupts cell membrane	Fontana et al. (2004)
	<i>Apis mellifera</i>	–	Jelleines II	1.05		MIC = 15 µg/mL	–	
	<i>Apis mellifera</i>	–	Jelleines III	1.08		MIC = 30 µg/mL	–	
	<i>Hermetia Illucens</i>	–	Hill-Cec 1	4.79	<i>P. aeruginosa</i> (n = 4)	MIC = 1 µM IC ₅₀ (1.3 ± 0.57 µM) → reduced 50% biofilm mass; IC ₅₀ (2.1 ± 0.52 µM) → reduced 50% biofilm visibility	Causes membrane depolarization and membrane damage	Van Moll et al. (2022)
	<i>Hermetia Illucens</i>	–	Hill-Cec 10	5.28		MIC = 1 µM IC ₅₀ (7.5 ± 3.5 µM) → reduced 50% biofilm mass; IC ₅₀ (11 ± 1.7 µM) → reduced 50% biofilm visibility	Causes membrane depolarization and membrane damage	
Amphibians	<i>Phyllomedusa hypochondrialis</i> frogs	–	Dermaseptin K ₄ K ₂₀ S ₄	2.88	<i>P. aeruginosa</i> PA01	MIC = 0.39 µg/mL	Breaks down membrane lipids and disperses bacteria	Zairi et al. (2014)
	<i>Phyllomedusa hypochondrialis</i> frogs	–	Dermaseptin K ₄ S ₄	2.86		MIC = 12.5 µg/mL	Breaks down membrane lipids and disperses bacteria	
	<i>Limnonectes kuhlii</i> Frog	AP02106	Temporin-LK1	1.95	<i>P. aeruginosa</i> (n = 2)	MIC = 2.5 µg/mL	–	Wang et al. (2013)
	<i>Limnonectes kuhlii</i> Frog	AP02110	Rugosin-LK2	3.46		MIC = 2.5 µg/mL	–	
	<i>Limnonectes kuhlii</i> Frog	AP02109	Rugosin-LK1	3.52		MIC = 5 µg/mL	–	
	<i>Limnonectes kuhlii</i> Frog	AP02107	Gaegurin-LK1	2.57		MIC = 5–10 µg/mL	–	
	<i>Limnonectes kuhlii</i> Frog	AP02108	Gaegurin-LK2	2.52		MIC = 5–10 µg/mL	–	
	<i>Green edible frog Pelophylax lessonae</i>	–	Esculentin (1–21)	2.61	<i>P. aeruginosa</i> (n = 9)	MIC = 4 µM MBEC = 6 µM MBCb = 12 µM	Penetrates biofilm plasma membrane, and causes β-galactosidase release	Luca et al. (2013)
	<i>Hylarana latouchii</i>	–	Brevinin-1HL	2.5	<i>P. aeruginosa</i> ATCC27853	MIC = 256 µg/mL MBIC = 256 µg/mL	Destroys cell membranes and binds to bacterial DNA	Lin et al. (2021)
	<i>Hylarana latouchii</i>	–	Temporin-HLa	1.88		MIC >512 µg/mL	Destroys cell membranes and binds to bacterial DNA	
	<i>Hylarana latouchii</i>	–	Temporin-HLb	1.5		MIC >512 µg/mL	Destroys cell membranes and binds to bacterial DNA	

(Continued)

TABLE 1 (Continued)

Classification	Source	Code (ID)	AMPs	Molecular weight (kDa)	Strains	Inhibitory activities	Proposed Mechanism of Action	References
Others	Fish	–	Gaduscidin-1	2.49	<i>P. aeruginosa</i> PAO1	MIC = 2 μ M Gad-1 (64 μ M) \rightarrow cleared 60–72% biofilm; Gad-1 (32–64 μ M) \rightarrow inhibited biofilm formation completely	Reduces <i>P. aeruginosa</i> viability in biofilms, cleaves eDNA	Portelinha and Angeles-Boza (2021)
	<i>Morone saxatilis</i>	AP00473	Piscidin 1	3	<i>P. aeruginosa</i> PAO1	MIC = 16 μ M	Disrupts cell membranes	Salger et al. (2016)
	<i>Morone saxatilis</i>	AP00474	Piscidin 3	2.92		MIC = 32 μ M	Possesses nuclease activity and destroys eDNA	
	<i>Alligator mississippiensis</i>	DRAMP20805	Apo5	3.13	<i>P. aeruginosa</i> (<i>n</i> = 2)	EC ₅₀ = 0.0878–0.467 μ g/mL	Disrupts cell membranes	Barksdale et al. (2016)
	<i>Alligator mississippiensis</i>	DRAMP20806	Apo6	2.79		EC ₅₀ = 0.13–1.17 μ g/mL	Disrupts cell membranes	
	<i>Alligator mississippiensis</i>	AP02517	A1P	4.13	<i>P. aeruginosa</i> PAO1	EC ₅₀ = 38.6 μ g/mL	–	
	<i>Alligator mississippiensis</i>	–	APOC1 _{64–88}	3.1	<i>P. aeruginosa</i>	EC ₅₀ = 0.948–11.1 μ M	–	Bishop et al. (2015)
			APOC1 _{67–88}	2.77				
			A1P _{394–428}	4.11				
			FGG _{398–413}	3.93				
			FGG _{401–413}	1.56				
	<i>Silkworm Bombyx mori</i>	AP01259	ABP-CM4	3.79	<i>P. aeruginosa</i> ATCC 27853	MIC = 16 μ M	Destroys cell membrane and interacts with DNA	Li et al. (2020)
	<i>Brown garden snail</i>	–	<i>Helix aspersa</i> mucus	30–100	<i>P. aeruginosa</i> (<i>n</i> = 2)	Measurable zones of inhibition (11.12 mm and 11.63 mm) were observed	–	Pitt et al. (2015)
	<i>Brown garden snail</i>	–	<i>Cornu aspersum</i> mucus	17.5–37.4	<i>P. aeruginosa</i> (<i>n</i> = 7)	Mean zones of inhibition recorded were all between 9 and 13 mm	–	Pitt et al. (2019)

MIC, minimum inhibitory concentration; MBC, minimum bactericidal concentration; MEC, minimal effective concentration; EC₅₀, half-maximal effective concentrations; IC₅₀, half maximal inhibitory concentration; LD₅₀, 90% lethal dose; MBEC, minimum concentration preventing re-growth of bacteria from the treated biofilm, within 4 h; MBCb, minimum concentration required to reduce the number of viable biofilm cells of $\geq 3 \log_{10}$ (99.9% killing) after 2 h; MBIC, minimum biofilm inhibitory concentration; Ref, reference; –, unknown.

and 2 downregulated genes expression of *arcA*, *arcB*, and *arcC*, while P15s decreased *arcD* expression and indirectly affected arginine metabolism.

In addition to *rumen microbiome*, bacteriocins produced by *Lactic acid bacteria* (LAB) had been extensively studied due to their safety and utility. Acidocin 4356 (ACD) is a novel bacteriocin with a size of 8.3 kDa, which was isolated from *Lactobacillus acidophilus* ATCC 4356 (Modiri et al., 2020). ACD had antimicrobial activity against both *E. coli* and *P. aeruginosa*, causing 35 and 80% inhibition of their growth at the same concentration. As shown in Table 1, ACD had inhibitory effects against *P. aeruginosa* planktonic cells, with an MIC₉₀ of 128.22 µg/mL. Additionally, ACD showed potent anti-*P. aeruginosa* biofilm activity, killing over 90% of biofilms at a concentration of 128.22 µg/mL and significantly reducing the pre-formed biofilms at a concentration of 256.44 µg/mL. In *in vivo* experiments, ACD was found to effectively suppress infection caused by *P. aeruginosa* in mice. Compared with the control group, the peptide-treated mouse lung slices exhibited the decreased recruitment of macrophages and lung cells, as well as a reduction in epithelial hyperplasia and structural degeneration. Mechanism of action experiments revealed that ACD not only enhanced bacterial membrane perturbation, but also reduced the production of *P. aeruginosa* virulence factors, such as pyoverdine siderophore, pyocyanin toxin, secretory protease, and elastase enzyme (Modiri et al., 2020). Moreover, it had a low hemolytic activity of less than 20% on human erythrocytes at a concentration of 400 µg/mL, indicating its potential as a promising therapeutic compound. Actifensin, a bacteriocin produced by *Actinomyces ruminicola* with a molecular weight of 4.1 kDa. It exhibited weak antibacterial activity against *P. aeruginosa* strains with MIC of 1448 µg/mL, whereas predominantly inhibited methicillin-resistant *S. aureus* and *Candida albicans* with MIC values of 23 µg/mL and 45 µg/mL. Its mechanism of anti-*P. aeruginosa* may be related to induce reactive oxygen species (ROS) generation, thereby destroyed cellular membrane permeability, but further molecular mechanisms were unclear (Sugrue et al., 2020; Gbala et al., 2022). More importantly, it has been found to have a high biosafety, and it causes less than 1.5% hemolysis on mouse erythrocytes in all tested concentrations.

2.2. AMPs from plants

Plant defensins are small cationic peptides with 5–7 kDa in size that contain multiple cysteine groups to safeguard plants against microbial invasion (Gbala et al., 2022). These peptides have a wide-ranging ability to inhibit the growth of various pathogens including filamentous fungi and bacteria (Perez-Rodriguez et al., 2022b), we summarized the data on the inhibitory activity of several plant-derived AMPs against *P. aeruginosa* in Table 1.

Many peptides found in *spinach leaves* exhibited antimicrobial activities. One such peptide is So-D1-7, which was effective to against gram-positive and gram-negative bacterial pathogens as well as fungi at concentrations below 20 µM (Segura et al., 1998). Another antibacterial component identified in *spinach leaves* was Defensin-d2, which had a molecular weight of 5.8 kDa. It had been found to be more active against *P. aeruginosa* than *E. coli* *in vitro*, with the MIC values of 7.5 and 30 µg/mL, respectively (Gbala et al., 2022). Defensin-d2 also had the ability to inhibit biofilm formation of *P. aeruginosa* in a concentration dependent manner. When treated

with 3.75 µg/mL of defensin-d2 for 24 h, the mass percentage of biofilm was reduced by more than 70% (Gbala et al., 2022). The related mechanism was similar to that of actifensin, involving increased production of ROS production and disruption of cell membrane. The highest hemolysis rate of 2.89% was observed at the concentration of 985 µg/mL.

Medicago truncatula, a type of plant, contained various peptides that exhibited antimicrobial activities against human pathogens. These peptides interacted with the phospholipids of fungal cell membranes, causing an increase in membrane permeability and ultimately leading to fungi cell death (Sathoff et al., 2019). In a study conducted by Sathoff et al. it was found that core MtDef4 and MtDef5 (with the molecular weights of 1.98–2.04 kDa) derived from *Medicago truncatula*, were able to inhibit the growth of *P. aeruginosa* with IC₅₀ = 1.7–4.2 and 8.5–14.6 µM, respectively (Sathoff et al., 2019, 2020). Moreover, Core MtDef4 could induce gene expression of the amino arabinose modification of LPS and surface polycation spermidine production operons, and it could damage outer membranes of *P. aeruginosa*, while MtDef5 appeared to interfere with DNA synthesis and transcription (Velivelli et al., 2018; Sathoff et al., 2020).

2.3. AMPs from mammals

AMPs derived from *human* play a crucial role in the human immune system, which can protect the body from pathogen invasion by reducing their virulence factors (Bosso et al., 2018). Therefore, the exploration of *human* peptides may be significant for developing antimicrobial drugs. As illustrated in Table 1, specific description of several AMPs derived from *mammals* with significant anti-*P. aeruginosa* activity are shown below.

Protegrins and their derivatives are a new class of AMP antibiotics derived from mammals, which have been proved to have a wide range of antimicrobial activities, including gram-positive and gram-negative bacteria as well as fungi (Bellm et al., 2000). Porcine protegrin-1 (PG-1), an AMP with a molecular weight of 2.59 kDa, had *in vitro* antimicrobial activities against gram-negative bacteria. It effectively inhibited the growth of *E. coli* and *P. aeruginosa* planktonic cells, with MICs of 0.2–0.5 and 0.3–0.8 µg/mL, respectively (Turner et al., 1998). The mechanistic studies revealed that PG-1 was capable of binding to the membrane, forming voltage-gated channels within the lipid bilayer and dissolving liposomes, ultimately leading to the disruption of the cell membrane and cell death (Bellm et al., 2000). The results of the cell cytotoxicity experiment showed that PG-1 had limited effects on mammalian cells, only reducing cell number at concentrations over 50 µg/mL (Morrone et al., 2019).

Apart from the physical skin barrier-stratum corneum, *human skin* also has an innate defense barrier. This barrier consists of AMPs and proteins, which help to control the growth of microorganisms on the body surface and reduce the risk of infection (Elias, 2005; Gallo and Hooper, 2012; Harder et al., 2013). Filaggrin-2 (FLG2), also known as ifapsoriasin, is expressed in *human skin* and serves to protect the skin from environmental damage (Wu et al., 2009). The radial diffusion assays provided evidence that FLG2-4, with a molecular mass ranging from 70 to 140 kDa, had powerful antimicrobial activities against *P. aeruginosa* and *E. coli* planktonic cells with MEC of 0.4 µM and 2.4 µM, respectively (Hansmann et al., 2015). Besides, the underlying anti-*P. aeruginosa* mechanism of

TABLE 2 The anti-*Pseudomonas aeruginosa* activity of antimicrobial peptides (AMPs) when used in combination with drugs.

Source	AMPs	Code (ID)	Molecular weight (kDa)	Agents	Strains	Cell types	Antimicrobial effects		References
							FICI	Interpretation	
Microorganism	Nisin	–	3.35	Colistin	<i>P. aeruginosa</i> (n = 6)	Planktonic cells	0.375–0.625	SYN (4), ADD (2)	Jahangiri et al. (2021)
Human	P10	–	3.11	Ceftazidime	<i>P. aeruginosa</i> (n = 6)	Planktonic cells	0.375–0.75	SYN (4), ADD (2)	Jahangiri et al. (2021)
				Doripenem			0.5–0.625	SYN (5), ADD (1)	
	LL-37	–	4.49	Colistin	<i>P. aeruginosa</i> (n = 2)	Planktonic cells	0.38- >0.5	SYN (1), ADD (1)	Han et al. (2022)
				Vancomycin			≥0.5	SYN (1), ADD (1)	
				Polymyxin B			0.38- >0.5	SYN (1), ADD (1)	
				Ciprofloxacin	<i>P. aeruginosa</i> (n = 4)	Biofilms	–	SYN (4), ADD (1)	Dosler and Karaaslan (2014)
				Tobramycin			–	SYN (2), ADD (3)	
				Colistin			-	SYN (2), ADD (3)	
Frog	Magainin II	AP00144	2.48	Rifampicin	<i>P. aeruginosa</i> (n = 2)	Planktonic cells	0.312	SYN	Cirioni et al. (2008)
	Lys-[Trp6] hy-a1	–	1.87	Ciprofloxacin	<i>P. aeruginosa</i> ATCC 9027	Planktonic cells	0.37	SYN	Carneiro et al. (2020)
						Biofilms	0.5625	ADD	
	Ocellatins-PT3	–	2.53	Ciprofloxacin	<i>P. aeruginosa</i> (n = 2)	Planktonic cells	0.25–0.38	SYN	Bessa et al. (2018)
				Ceftazidime			0.38–0.5	SYN	
	Citropin 1.1	AP00351	1.62	Colistin	<i>P. aeruginosa</i> (n = 3)	Planktonic cells	0.26–0.75	SYN (2), ADD (1)	Jorge et al. (2017)
						Biofilms	–	SYN (2), IDD (1)	
	Temporin A	AP00094	1.4			Planktonic cells	0.27–0.75	SYN (2), ADD (1)	
						Biofilms	–	SYN (2), ADD (1)	
Cationic AMP	Colistin	AP02204	1.22	NCL195	<i>P. aeruginosa</i> (n = 25)	Planktonic cells	0.12–0.5	SYN	Nguyen et al. (2021)
				Ciprofloxacin	<i>P. aeruginosa</i>	Biofilms	–	SYN	Pamp et al. (2008)
				Tetracycline		Biofilms	–	SYN	
Crab	Tachyplesin I	AP00214	2.27	Colistin	<i>P. aeruginosa</i> (n = 3)	Planktonic cells	0.38–0.63	SYN (2), ADD (1)	Jorge et al. (2017)
						Biofilms	–	SYN (1), ADD (2)	
	Sphistin	AP02814	3.96	Azithromycin	<i>P. aeruginosa</i> ATCC 9027	Planktonic cells	0.35	SYN	Liu et al. (2020)
				Rifampicin			0.3125	SYN	
Bee	Melittin	AP00146	2.87	Doripenem	<i>P. aeruginosa</i> (n = 5)	Planktonic cells	0.01–0.06	SYN	Akbari et al. (2019)
				Ceftazidime			0.02–0.5	SYN	
Bovine	LfcinB (20–25) ₄	–	4.84	Ciprofloxacin	<i>P. aeruginosa</i> ATCC 27853	Planktonic cells	0.09	SYN	Vargas-Casanova et al. (2019)

(Continued)

TABLE 2 (Continued)

Source	AMPs	Code (ID)	Molecular weight (kDa)	Agents	Strains	Cell types	Antimicrobial effects		References
							FICI	Interpretation	
<i>King Cobra</i>	OH-CATH30	AP00923	3.61	Ciprofloxacin	<i>P. aeruginosa</i> (n = 4)	Planktonic cells	0.375–0.5	SYN	Li et al. (2014)
				Levofloxacin			0.375–0.5	SYN	
<i>Aedes aegypti</i>	Cecropin A2	–	3.6	Tetracycline	<i>P. aeruginosa</i> (n = 18)	Planktonic cells	0.25	SYN	Zheng et al. (2017)
<i>Giant silk moth</i>	Cecropin A	AP03235	3.88	Rifampicin	<i>P. aeruginosa</i> (n = 2)	Planktonic cells	0.312	SYN	Cirioni et al. (2008)
<i>Amide</i>	CAMA	–	1.77	Ciprofloxacin	<i>P. aeruginosa</i> (n = 4)	Biofilms	-	SYN	Dosler and Karaaslan (2014)
<i>Synthetic</i>	AMP38	–	1.25	Imipenem	<i>P. aeruginosa</i> (n = 4)	Planktonic cells	0.07–0.18	SYN	Rudilla et al. (2016)
						Biofilms	0.25	SYN	
<i>Synthetic</i>	OW peptide	–	0.99	Ampicillin	<i>P. aeruginosa</i> ATCC 2114	Planktonic cells	0.38	SYN	Al Tall et al. (2019)
				Chloramphenicol			0.41	SYN	
<i>Synthetic</i>	Lin-SB056-1	–	1.26	EDTA	<i>P. aeruginosa</i> (n = 2)	Biofilms	-	SYN	Maisetta et al. (2017)
<i>Synthetic</i>	P5	–	2.36	Meropenem	<i>P. aeruginosa</i> M13513	Planktonic cells	–	SYN	Martinez et al. (1861)
<i>Synthetic</i>	Melimine	AP02709	3.8	Ciprofloxacin	<i>P. aeruginosa</i> ATCC 27853	Biofilms	–	SYN	Yasir et al., 2020

FICI, fractional inhibitory concentration index; SYN, synergy; ADD: addition; Ref, reference; –, unknown.

FLG2-4 appears to involve inducing membrane blebbing, disrupting DNA polymerases activity, ultimately halting bacterial replication.

Cathelicidin LL-37 is a cationic AMP that is produced by *humans*, and has a molecular weight of 4.493 kDa. It is a broad-spectrum cathelicidin known for its strong chemotaxis and immunomodulatory properties. Besides, it plays a role in regulating the systems of immune, respiratory, gastrointestinal, and skin by participating in molecular pathways (Sørensen et al., 2001; Zanetti, 2005; Burton and Steel, 2009; Fabisiak et al., 2016).

LL-37 exhibited strong efficacy against most detected gram-negative bacteria. In broth microdilution assay, LL-37 demonstrated moderate antimicrobial activity against *E. coli* and *P. aeruginosa* with MIC values of 6–32 and 8–32 µg/mL, respectively (Turner et al., 1998). In addition, LL-37 displayed potent anti-biofilm activities, inhibiting 80% biofilm formation of *P. aeruginosa* at 16 µg/mL and reducing the thickness of pre-formed biofilm at 4 µg/mL (Overhage et al., 2008). The quorum sensing (QS) system was closely related to bacterial biofilms formation, the expression of virulence factors, and multiple drug resistance pathways (Al Akeel et al., 2019). There are two characteristic QS systems in *P. aeruginosa*: the Las system and the RhI system (Yu and Ma, 2017). LL-37 was found to inhibit *P. aeruginosa* biofilm formation through various mechanisms, including reducing bacterial cells attachment, stimulating motility twitch, suppressing the expression of key QS signaling molecules and significantly downregulating the expression of more than 50 biofilm formation-related genes, including *lasI* and *rhlR* genes (Overhage et al., 2008). However, it is important to note that LL-37 has high toxicity to mammalian cells. Therefore, further application of LL-37 may require structural modifications or combination with other drugs to mitigate this toxicity.

In a recent study, researchers identified two cathelicidins called BMAP-27 and 28 from *bovine*, they had the molecular masses of about 3.5 kDa. Both BMAP-27 and BMAP-28 had significant antibacterial properties against *P. aeruginosa* and *E. coli*, with MIC values of 1 µM and 0.25–2 µM (Skerlavaj et al., 1996). Another study found that these two AMPs have MIC₉₀ values 16 and 32 µg/mL for 25 other strains of *P. aeruginosa* (Pompilio et al., 2012). Besides, BMAP-27 and 28 were not only effective in reducing the formation of *P. aeruginosa* biofilms, but also showed efficacy against biofilms that had already formed, with the concentration of 8–16 and 80–160 µg/mL, respectively (Pompilio et al., 2012). The antibacterial mechanism was related to the rapid induction of membrane permeabilization (Xie et al., 2020). However, these two cathelicidins have certain cytotoxicity to human red blood cells and neutrophils. One way to address this issue is by shortening the C-terminal of the cathelicidins, which greatly reduces their cytotoxicity without compromising their antibacterial activity.

Human beta-defensin 2 (HBD2) was one of the *human* β-defensins with a molecular mass of 4–5 kDa, it has been found to have multiple physiological functions (Yang et al., 1999). HBD2 showed significant antimicrobial activity against *E. coli* and *P. aeruginosa* with LD₅₀ of 10 µg/mL (Schröder and Harder, 1999). At the concentration of 0.25–0.5 µM, HBD2 exhibited inhibitory effect against *P. aeruginosa* biofilm formation, although it did not inhibit metabolic activity (Pardue et al., 2020). The results also indicated that HBD2 could induce the change of the biofilm surface topology, then interfering with the transport of biofilm precursors into the extracellular space. Furthermore, HBD2 has been found to be biocompatible and safe,

with no toxicity observed in hMSCs, osteoblasts, keratinocytes or HeLa cells at any concentration tested (Warnke et al., 2013).

2.4. AMPs from insects

Many AMPs were isolated from the plasma and leukocyte extracts of *insects*, and these have been shown to possess strong antibacterial effects (Van Moll et al., 2022). In recent years, many studies investigating the anti-*P. aeruginosa* activity of insect AMPs had been carried out, and we summarized some of the findings below.

Royal jelly (RJ) is a substance secreted by the hypopharyngeal and mandibular glands of *worker bees*, and it is enriched with protein, carbohydrates, vitamins, and minerals (Fujiwara et al., 1990; Fontana et al., 2004). A study has discovered novel AMPs (Jelleines) in RJ that have broad-spectrum antimicrobial activities, including gram-positive and gram-negative bacteria (Fontana et al., 2004). The molecular mass of Jelleines I-III is approximately 1 kDa. They displayed good *in vitro* antibacterial activity against *E. coli* and *P. aeruginosa*, with MIC values of 2.5–15 and 10–30 µg/mL, respectively (Fontana et al., 2004). Further investigations indicate that Jelleine-I could form aggregates that accumulated in the head group region of the membrane, leading to cell membrane disruption and leakage (Cabrera et al., 2014). Jelleine-I has been reported to have a hemolytic effect of 5–11.3% on rat erythrocytes and mouse erythrocytes, which possesses the potential for further study.

Two cecropins (Hill-Cec1 and Hill-Cec10) that were discovered in *black soldier fly* and are 4.79 and 5.28 kDa in size, had been found to effectively inhibit the growth of *P. aeruginosa* and *E. coli* planktonic cells, with the MIC values of 0.25 and 1 µM, respectively (Van Moll et al., 2022). The biofilm mass could be reduced by 50% when the concentration of Hill-Cec1 and Hill-Cec10 were 1.3 ± 0.57 µM and 7.5 ± 3.5 µM, respectively. However, they had no scavenging effect on the pre-formed biofilm. Furthermore, they exerted their antimicrobial effects by disrupting the cell membrane of *P. aeruginosa* and causing its depolarization. In addition, both cecropins showed a low hemolysis rate of less than 10% at a concentration of 64 µM, indicating a higher level of safety.

2.5. AMPs from amphibians

Previous studies had identified a variety of AMPs from *amphibian skin* and their antimicrobial activities had been demonstrated (Simmaco et al., 1994; Ponti et al., 1999; Luca et al., 2013). Here, we summarized the anti-*P. aeruginosa* activity of several AMPs.

Dermaseptins are a family of linear polycationic peptide consisting of 28 to 34 amino acids, which were originally isolated from the skin of *Phyllomedusa sauvagei*, a tree-dwelling *South American frog* (Mor et al., 1991). Numerous studies have confirmed that dermaseptins exhibited significant and extensive antimicrobial activities against various microorganisms, including gram-positive and gram-negative bacteria (Marynka et al., 2007; Zairi et al., 2007; Zairi et al., 2013), fungi (Morton et al., 2007), viruses (Bergaoui et al., 2013), and protozoa (Dagan et al., 2002; Efron et al., 2002). A study demonstrated that dermaseptin K₄S₄ and K₄K₂₀S₄, which have a molecular mass of about 2.8 kDa, displayed antibacterial effects

against *P. aeruginosa* PA01 and *E. coli* MG1655, with MIC of 0.39–12.5 µg/mL and 0.19–0.39 µg/mL, respectively (Zāiri et al., 2014). In addition, when the concentration of dermaseptin derivatives were 2-fold of MIC, the pre-formed biofilm of *P. aeruginosa* wasn't dissolved or disrupted, but the survival rate of biofilm cells was significantly reduced. The mechanisms of anti-*P. aeruginosa* biofilm may be similar to another dermaseptin derivative, S4(1–16) M4Ka, which inhibited biofilm formation by breaking down membrane lipids and dispersing bacteria (Quilès et al., 1858). Moreover, their CC₅₀ (50% cytotoxic concentration) value was around 28 µg/mL. Although their toxicity is much lower than that of dermaseptin S4, further structural optimization is still urgent for their future study.

Wang G et al. had identified five AMPs (Temporin-LK1, gaegurin-LK1, gaegurin-LK2, rugosin-LK1, and rugosin-LK2) with molecular masses ranging from 1.95 to 3.52 kDa from skin secretions of *Limnonectes kuhlii* frogs (Wang et al., 2013). Experimental results demonstrated that they all possessed very effective antibacterial activities against *P. aeruginosa* and *E. coli* ML-35P strains, with MIC of 2.5–10 µg/mL and 10–50 µg/mL, respectively, indicating the potential to treat bacterial infections. These five AMPs also have slight hemolytic activities, causing the lysis of rabbit red blood cells in varying percentages. Temporin-LK1, gaegurin-LK1, gaegurin-LK2, rugosin-LK1, and rugosin-LK2 can induce the hemolysis of 10.2, 5.6, 6.2, 3.8, and 6.1%, respectively.

Esculentin (1–21), which was isolated from amphibian skin and had a size of 2.61 kDa, demonstrated efficacy on planktonic cells of gram-negative bacterial pathogen *P. aeruginosa* and *E. coli*, with MIC of 3.2 µM and 0.65 µM (Islas-Rodríguez et al., 2009). Another study found that Esc (1–21) also exhibited antibacterial effects against MDR clinical isolates of *P. aeruginosa*, with the MICs of 4–8 µM (Luca et al., 2013). Esc (1–21) also had potent anti-*P. aeruginosa* biofilm effects, the minimum biofilm eradication concentration (MBEC) and minimum bactericidal concentration (MBCb) were 6 µM and 12 µM, respectively. Furthermore, in *in vivo* experiments, it was observed that Esc (1–21) significantly increased the survival rate of mice with *P. aeruginosa* sepsis or pulmonary infection (Luca et al., 2013). The mechanism of action showed that it can anti-*P. aeruginosa* PAO1 biofilm by penetrating biofilm plasma membrane and causing the release of β-galactosidase (Luca et al., 2013). Esc (1–21) did not show any toxicity to human erythrocytes, lung epithelial cells or mouse macrophages *in vitro* at the concentration of MIC.

Lin et al. discovered three AMPs (brevin-1HL, temporin-HLa, and temperin-HLb) from the skin secretion of *Hylarana latouchii*, and they had a molecular weight of 1.5–2.5 kDa (Lin et al., 2021). Brevin-1HL exhibited a moderate effect against *P. aeruginosa* planktonic cells and biofilm, with MIC and MBIC of 256 and 512 µg/mL, respectively. Temporin-HLa and temperin-HLb only showed a weak inhibitory effect on *P. aeruginosa*, with MIC over 512 µg/mL. The study also revealed that these three peptides induced bacterial death by destroying cell membranes and binding to bacterial DNA. Among them, only Brevinin-1HL possesses the bactericidal effects against *E. coli*, with an MBC of 128 µg/mL. However, it should be noted that Brevinin-1HL exhibits strong hemolytic activity on horse red blood cells, causing 86.8% of hemolysis at 256 µg/mL (Lin et al., 2021).

2.6. AMPs from other groups

In addition to the AMPs mentioned above, we have also compiled a list of AMPs with great antimicrobial activities identified from other groups in Table 1, such as *fishes*, *alligators*, *silkworm*, and *snails*. One of these AMPs, called Gaduscidin-1 (Gad-1), was originated from *Atlantic cod*, and has been shown to have antibacterial effect against *P. aeruginosa* (Portelinha and Angeles-Boza, 2021). Gad-1 exhibited inhibitory effect against *P. aeruginosa* planktonic cells, with the MIC of 2 µg/mL and 16 µg/mL at PH 6.4 and 7.4, respectively. Furthermore, Gad-1 was also effective in removing 60–72% of the pre-formed biofilm at a concentration of 64 µM. It also could completely inhibit biofilm formation when the concentration exceeding 32 µM (Portelinha and Angeles-Boza, 2021). Moreover, biofilms contain extracellular DNA (eDNA), which not only helps in stabilizing the structure of biofilms but also promotes horizontal gene transfer, ultimately leading to increased biofilm resistance to antibiotics (Whitchurch et al., 2002; Wilton et al., 2016; Nolan et al., 2020). In addition to reducing the viability of *P. aeruginosa* in biofilms, Gad-1 can cleave eDNA, making it be a possible compound for the treatment of bacterial biofilms.

Piscidins were isolated from *fishes* and could kill a variety of microorganisms, including methicillin-resistant *Staphylococcus aureus* (Salger et al., 2016). Libardo et al. had tested the antimicrobial activities of piscidin 1 and piscidin 3 with the molecular mass of approximately 3 kDa, which showed excellent activity against *E. coli* and moderate anti-*P. aeruginosa* activities, with MICs of 2–8 µM and 16–32 µM, respectively (Salger et al., 2016). It is interesting to note that although these two AMPs are similar, they possess distinct antibacterial mechanisms of action. Piscidin 1 disrupts cell membrane, while piscidin-3 forms covalent bonds with Cu²⁺ through its N-terminal amino acid and exerts nuclease activity, leading to the disruption of *P. aeruginosa* eDNA and displaying anti-biofilm activity (Libardo et al., 2017). However, both piscidins have high hemolytic activity at a concentration of 25 µg/mL.

Crocodilian animals, which are a group of ancient creatures, have also been studied for their antimicrobial properties (Merchant et al., 2006; Darville et al., 2010). Researchers had discovered three AMPs derived from *Alligator mississippiensis* that have varying degrees of anti-*P. aeruginosa* activity and different mechanisms of action. Apo5 and Apo6, which have molecular masses of 3.13 and 2.79 kDa, respectively, displayed moderate anti-*E. coli* effects and stronger anti-*P. aeruginosa* activities, with EC₅₀ of 3.85–19.7 and 0.0878–1.17 µg/mL. The underlying mechanism may be related to disrupt membrane (Barksdale et al., 2016). While A1P, with a molecular weight of 4.13 kDa, showed weaker inhibition against *P. aeruginosa* PAO1 with an EC₅₀ of 38.6 µg/mL, and stronger inhibition against *E. coli* strains with an EC₅₀ of 2.51–9.2 µg/mL. The main mechanism of action was not related to the disruption of cell membranes or DNA binding (Barksdale et al., 2016). These three AMPs have high safety profiles, with minimal hemolytic effects on erythrocytes at 300 µg/mL, and no significant cytotoxic to A549 cells at the concentration of 100 µg/mL. Bishop et al. discovered eight AMPs from *Alligator mississippiensis* plasma, and had evaluated their antimicrobial effects (Bishop et al., 2015). The data showed that five AMPs (APOC1₆₄₋₈₈, APOC1₆₇₋₈₈, FGG₃₉₈₋₄₁₃, FGG₄₀₁₋₄₁₃, A1P₃₉₄₋₄₂₈), which have molecular masses ranging from 1.56 to 4.11 kDa, possessed antibacterial

activities against *E. coli* and *P. aeruginosa* *in vitro*, with EC₅₀ of 0.099–0.332 μ M and 0.948–11.1 μ M, respectively.

ABP-CM4, a peptide with a size of 3.79 kDa, was isolated from the hemolymph of the silkworm, *Bombyx mori* (Li et al., 2020). It showed promising activity against several microorganisms, in particular *P. aeruginosa* ATCC 27853 and *E. coli* K₁₂D₃₁, with MIC of 16 μ M and 12 μ M *in vitro*. The main mechanism of action of ABP-CM4 was the disruption of cell membrane and interaction with DNA. Importantly, ABP-CM4 was not cytotoxic to HEK-293 cells even at a concentration of 80 μ M.

The mucus secreted by snails also exhibits antibacterial properties. For instance, Pitt et al. demonstrated that antimicrobial substance with 30–100 kDa in size in *Helix aspersa* mucus displayed inhibitory effects against two *P. aeruginosa* strains collected by laboratory. The antimicrobial disc diffusion assay showed obvious measurable zones of inhibition, with values of 11.12 mm and 11.63 mm (Pitt et al., 2015). Furthermore, researchers discovered that AMPs with molecular masses of 17.5–37.4 kDa, identified in *Cornu aspersum* mucus, could inhibited *P. aeruginosa* strains obtained from patients with cystic fibrosis. The mean zones of inhibition recorded were all between 9 and 13 mm (Pitt et al., 2019).

After summarizing the above antibacterial effects of AMPs, we found many AMPs from different sources exhibit activity against both *P. aeruginosa* and anti-*E. coli*. In general, higher concentrations of AMPs are required to kill *P. aeruginosa* compared to *E. coli*. The MIC values of AMPs were typically smaller than those of conventional antibiotics, indicating that the antibacterial potency of AMPs was generally stronger than conventional antibiotics. Notably, PG-1, FLG2-4, Jelleines and five AMPs derived from *Limnonectes kuhlii* skin secretions all possessed significant anti-planktonic cells effects *in vitro*, with MIC values ranged from 0.3 to 10 μ g/mL. Furthermore, AMPs have a distinct antibacterial mechanism compared to traditional antibiotics, which makes it difficult for pathogenic bacteria to develop resistance to AMPs. The mechanism of action of AMPs involving disrupting cell membrane structure, as seen in protegrin-1, BMAP-27 and 28, Jelleines, Hill-Cec 1, and Dermaseptin K₄S₄. In addition, some AMPs exerted antibacterial effects by interacting with DNA of *P. aeruginosa* and impeding the substance metabolism, such as MtDef5, FLG2-4, Brevinin-1HL, Temporin-Hla, and ABP-CM4. Additionally, the hemolytic activity of these natural AMPs is quite low, except for LL-37 and piscidins. Thus, these results of these studies have shown that AMPs had the potential to be used as antibacterial candidate. However, further research is needed to determine their effectiveness in biofilm prevention, as well as their applicability *in vivo* and in clinical settings.

3. Interactions of AMPs with antibiotics

The above studies showed that AMPs primarily worked by damaging bacterial membrane. This was achieved by forming pores, which disrupted the osmotic pressure balance and finally led to cell lysis (Zhang et al., 2001; Hollmann et al., 2018; Luo and Song, 2021). The antibacterial mechanism of conventional antibiotics involves inhibiting of DNA replication, DNA transcription, cell wall synthesis, or targeting of topoisomerases and penicillin-binding proteins (PBPs) (Abushaheen et al., 2020). Unfortunately, MDR bacteria strains can

prevent the entry of conventional antibiotics into bacterial cells, resulting in antimicrobial treatment failure (Abushaheen et al., 2020).

In theory, AMPs can increase the permeability of the cytoplasmic membrane, allowing antibiotics to enter the bacterial body and exert their antibacterial effects. Some studies have demonstrated that certain AMPs, when combined with conventional antibiotics, have a synergistic inhibitory effect against human pathogens. One example is the use of colistin in combination with azithromycin, erythromycin, and clarithromycin to treat MDR *Klebsiella pneumoniae*, *P. aeruginosa* and *Acinetobacter baumannii*. This combination increased membrane permeation and helped antibiotics enter the cells, thereby inhibiting the synthesis of ribosomal proteins (Ramchuran et al., 2018). Similarly, the combination of HBD3 and LL-37 with tigecycline, moxifloxacin, piperacillin / tazobactam and meropenem has been found to have synergistic effects against *Clostridium difficile* infections (Di Luca et al., 2014). However, not every combination of AMPs and conventional antibiotics have a synergistic antibacterial effect. Some combinations may exhibit indifference or even antagonistic effects. For instance, MDL-3 derived from housefly larvae demonstrated an antagonistic effect against *Salmonella Typhimurium* 50,013 when combined with penicillin or streptomycin. Consequently, more research is needed to understand the mechanisms of action for each AMP and antibiotic are different, as well as the complex relationship between the drug combination and bacteria.

One of the promising approaches for treating *P. aeruginosa* resistant infections is the combination therapy with two antibacterial drugs that have a synergistic effect (Giacometti et al., 1999; Mataraci Kara et al., 2020). Previous studies have shown that a considerable number of AMPs not only show anti-*P. aeruginosa* activities alone, but also display synergistic or additive effects in combination with drugs or compounds (Giacometti et al., 1999; Cirioni et al., 2006; Hollmann et al., 2018; Lei et al., 2019; Mataraci Kara et al., 2020). We have summarized these interactions of AMP-antibiotics combinations against *P. aeruginosa* in Table 2.

3.1. Microorganism-derived AMPs

Jahangiri et al. had evaluated the effects of nisin (with 3.35 kDa in size) in combination with colistin against six *P. aeruginosa* strains. They found that the MIC of nisin was reduced from 128 to 256 μ g/mL to 16–32 μ g/mL, the MIC of colistin was reduced from 0.5–8 μ g/mL to 0.125–4 μ g/mL, and the FICI was 0.375–0.625, displaying a synergistic antibacterial effect against four *P. aeruginosa* strains (Jahangiri et al., 2021). In a previous study, it was observed that nisin Z combined with antibiotics had synergistic effects on *P. fluorescens* isolates ($n=5$). No obvious antibacterial effect was observed when nisin Z used alone, while the MIC was decreased to 0.125–25 μ g/mL when combined with antibiotics. Also, the MIC of antibiotics was reduced to 0.015–125 μ g/mL, and FICI values were 0.01–0.5 (Naghmouchi et al., 2012).

3.2. Human-derived AMPs

P10, a molecule with a size of 3.11 kDa, displayed antimicrobial activity against both *Acinetobacter baumannii* and *P. aeruginosa* strains with MICs of 8–32 and 8–16 μ g/mL, respectively. When P10

was combined with antibiotics (ceftazidime and doripenem), it was found to have synergistic ($n=4-5$) or additive ($n=1-2$) activities against *P. aeruginosa* isolates. The MIC of P10 was reduced from 8 to 16 $\mu\text{g/mL}$ to 2–8 $\mu\text{g/mL}$, the MIC of ceftazidime was reduced from 4 to 64 $\mu\text{g/mL}$ to 1–32 $\mu\text{g/mL}$, the MIC of doripenem was reduced from 2 to 16 $\mu\text{g/mL}$ to 0.5–4 $\mu\text{g/mL}$, respectively (Jahangiri et al., 2021). LL-37 also displayed synergistic or additive bactericidal effects on *P. aeruginosa* planktonic cells when used in combination with colistin, vancomycin, and polymyxin B, with FICI of ≥ 0.38 (Han et al., 2022). The research further explained that the LL-37-antibiotic combination worked synergistically by increasing permeability of bacterial cell membranes, allowing antibiotics to enter *P. aeruginosa* more easily and exerted the antibacterial effects. Another study demonstrated that LL-37-antibiotics combination also displayed synergism or addition against *P. aeruginosa* biofilms. The MBEC values for antibiotics and LL-37 were 80–5,120 and ≥ 640 mg/L, respectively. When combined with LL-37 at the concentration of 64 mg/L, the MBEC value of antibiotics could be significantly reduced by 8 times (Dosler and Karaaslan, 2014).

3.3. Frog and crab-derived AMPs

Magainins are a kind of AMPs that originate from the skin of African clawed frog *Xenopus laevis* (Zasloff, 1987; Chopra, 1993). Numerous studies have demonstrated that magainin II has inhibitory activities on gram-negative and gram-positive bacteria, fungi, and protozoa (Jacob and Zasloff, 1994; Zairi et al., 2009). Magainin II has a molecular mass of 2.48 kDa and exhibits antimicrobial activity when used alone. Results of microbroth dilution assay showed that the MIC of magainin II against *E. coli* D31 and *P. aeruginosa* was 5 and 4 $\mu\text{g/mL}$, while rifampicin had no significant antibacterial effect when used alone. Furthermore, Cirioni and his colleagues demonstrated that magainin II in combination with rifampicin exhibited synergistic effects against *P. aeruginosa* strains both *in vitro* and *in vivo*, with a FICI of 0.312 (Cirioni et al., 2008). It is worth mentioning that *in vivo* experiments showed that the combination intervention resulted in good outcomes, including reduced mortality rates, cytokines levels, and improved treatment of bacteremia.

Lys-[Trp6]hy-a1 (lys-al) was an AMP isolated from the skin secretion of the frog *Hypsiboas albopunctatus*, with a molecular weight of 1.87 kDa (Castro et al., 2009; da Silva et al., 2013). Lys-al had the ability to inhibit *P. aeruginosa* ATCC 9027 planktonic strains, with the MIC and MBC of 125 $\mu\text{g/mL}$ (Carneiro et al., 2020). Moreover, when Lys-al was used in combination with ciprofloxacin, it showed synergistic effects against *P. aeruginosa* isolates with a FICI of 0.37, the MIC of ciprofloxacin and lys-a1 was reduced by 4–8 times. Besides, the combination of ciprofloxacin/lys-a1 also displayed an additive inhibitory effect on pre-formed biofilm of *P. aeruginosa*. Furthermore, it was observed that the shape of the cells had changed and the surface had become uneven after treatment with ciprofloxacin/lys-a1. Researchers speculated that cell membrane damage could lead to cytoplasm leakage or increase the possibility of antibiotic entry, ultimately resulting in synergistic antimicrobial effects.

Bessa et al. demonstrated that ocellatinPT3 (with a molecular weight of 2.53 kDa), an AMP isolated from the skin secretion of the frog *Leptodactylus pustulatus*, possessed inhibitory activities against planktonic cells and biofilms of *P. aeruginosa* (Oliveira et al., 2016;

Bessa et al., 2018). When ocellatin-PT3 combined with ciprofloxacin and ceftazidime, it showed synergistic effects on MDR strains, the MIC of them could be reduced 4–8 times, and the FICI was between 0.25 and 0.5. Furthermore, ocellatin PT3 with a concentration over 256 $\mu\text{g/mL}$ could inhibit the biofilm formation of *P. aeruginosa*. Ocellatin-PT3 exerted its antimicrobial effects primarily by acting on the LPS of *P. aeruginosa*.

Colistin is the last line of AMP antibiotic in clinical practice, and it is generally used in combination with other antibiotics to treat MDR bacterial infection (Petrosillo et al., 2008; Park et al., 2016; Almutairi, 2022; Xie et al., 2022). AMPs called Citropin 1.1 and temporin A with molecular weights of 1.62 and 1.4 kDa were secreted by the dorsal gland and submental gland of *Litoria citropa* and the skin of European red frog *Rana temporaria*, respectively (Simonetti et al., 2008; Ghiselli et al., 2011). Previous research by Jorge et al. demonstrated that colistin-citropin 1.1 combination and colistin-temporin A combination both had synergistic and additive inhibitory effects against *P. aeruginosa* planktonic cells, with the FICI range from 0.26 to 0.75 (Jorge et al., 2017). Similar synergistic and additive effects were also observed against *P. aeruginosa* biofilms. In addition, Pamp SJ et al. found that colistin was effective in killing cells with low metabolic activity in *P. aeruginosa* biofilms (Pamp et al., 2008). Ciprofloxacin and tetracycline could kill metabolically active biofilm cells, therefore, when colistin combined with these two antibiotics, a significant synergistic effect was observed, resulting in the complete eradication of almost all biofilm cells of *P. aeruginosa* (Pamp et al., 2008). NCL195 is a new antibiotic with little cytotoxicity, which belongs to the analog of robenidine (Ogunniyi et al., 2017). It exerted obvious antibacterial activity against *Streptococcus pneumoniae*, *Staphylococcus aureus*, *A. baumannii*, and *K. pneumoniae* strains by disturbing their cell membrane potential, with the MIC ranged from 0.25 to 8 $\mu\text{g/mL}$ (Ogunniyi et al., 2017). Recently, Nguyen and his colleagues found that the combination of NCL195 and colistin exhibited significant synergism against *P. aeruginosa* ($n=18$) planktonic cells with a time- and concentration-dependent manner, the MIC of NCL195 was reduced from >256 to 0.5–4 $\mu\text{g/mL}$, the MIC of colistin was reduced from 0.25–2 to 0.03–1 $\mu\text{g/mL}$, and the FICI index was 0.12–0.5 (Nguyen et al., 2021). In addition, the researchers also observed that the combination of NCL195-colistin caused more cell membrane damage to the cell membrane compared to colistin alone, which was considered as the synergistic antibacterial mechanism.

Tachyplesin I was originated from the blood cells of *Tachyplesus tridentatus*, it had a molecular weight of 2.27 kDa and possessed extensive bactericidal abilities (Xie et al., 2016). It is found that tachyplesin I in combination with colistin had the synergistic and additive inhibitory activities against *P. aeruginosa* planktonic cells, the MICs of them were reduced by 4–8 times and 2–8 times, respectively. Similarly, they also exhibited synergism and addition against biofilms (Jorge et al., 2017). Another AMP called sphistin, with the molecular mass of 3.96 kDa, was derived from the mud crab *Scylla paramamosain*. It showed potent synergistic activity when used in combination with azithromycin and rifampicin against *P. aeruginosa* planktonic cells, the MICs of antibiotics were reduced from 180 to 18 and 2.5 to 0.625 $\mu\text{g/mL}$, respectively (Chen et al., 2015; Liu et al., 2020). The MIC of AMP was decreased from 24 to 1.5–6 $\mu\text{mol/L}$, and the FICI was below 0.35 (Liu et al., 2020). When sphistin combined with the two antibiotics, the cell membrane permeability of *P. aeruginosa* was increased, which

facilitated the uptake of antibiotics and allowed them to display antibacterial effects.

3.4. Others

AMP melittin (with 2.87 kDa in size) is the main constituent of bee (*Apis mellifera*) venom and has broad-spectrum antibacterial activities (Li et al., 2017). The MIC values of melittin against *P. aeruginosa* were ranged from 1 to 8 µg/mL, while the MIC values against *Acinetobacter baumannii* were even lower at 0.25–0.5 µg/mL. Many reports demonstrated that it also possessed synergistic effect in combination with some conventional antibiotics (such as vancomycin, oxacillin, and amikacin) against MDR strains (Al-Ani et al., 2015). Akbari et al. reported that melittin exerted synergism against MDR *P. aeruginosa* strains when combined with doripenem and ceftazidime with the FICI of 0.01–0.5 (Akbari et al., 2019). The MIC of antibiotics was reduced from 8 to 64 µg/mL to 0.12–1 µg/mL and 4–64 µg/mL to 0.5–8 µg/mL, the MIC of AMP was reduced from 1 to 8 µg/mL to 0.03–0.5 µg/mL, as well as cytotoxicity was reduced by 100-fold.

LfcinB is a 25-amino acid peptide derived from bovine lactoferricin, which possessed a broad spectrum of phycolgical activity (Román et al., 2019). The AMP LfcinB (20–25)₄ was a short peptide with 4.84 kDa in size derived from LfcinB, which has been demonstrated to have antibacterial activity against *P. aeruginosa* and *E. coli*, with MICs of 11 µM and 5–22 µM, respectively. When the concentration of LfcinB (20–25)₄ was 11 µM, it exhibited a 14% hemolytic activity. When LfcinB (20–25)₄ combined with ciprofloxacin, it showed synergistic effects against *P. aeruginosa* (Vargas-Casanova et al., 2019). The MIC of AMP was decreased from 100 to 3.1 µg/mL, the MICs of ciprofloxacin were reduced from 0.4 to 0.02 µg/mL, and FICI was 0.09.

OH-CATH30, a peptide isolated from the king cobra with a size of 3.61 kDa, exhibited antibacterial activity with MIC values of 3.125–25 µg/mL against *P. aeruginosa* and MIC values of 1.56–12.5 µg/mL against *E. coli* (Zhao et al., 2008; Li et al., 2012). OH-CATH30 had a low hemolytic activity against human red blood cells, even at a high concentration of 400 µg/mL. It also exhibited low cytotoxicity against HaCaT cell lines, with an LD₅₀ (half-lethal dose) above 200 µg/mL (Li et al., 2012). Moreover, studies of the interaction between the peptide and ciprofloxacin/levofloxacin demonstrated synergistic effects against four *P. aeruginosa* isolates, with the FICI value of 0.375–0.5 (Li et al., 2014).

Cecropin A2 is a 36-residue α-helical cationic AMP with 3.6 kDa in size derived from mosquito *Aedes aegypti*, and it possessed antibacterial activities (Zheng et al., 2017). The AMP exhibited little hemolytic activity and toxicity toward mammalian cells. The MICs against clinical *P. aeruginosa* isolates were found to be 32–64 µg/mL, while the MICs against other gram-negative bacteria ranged from 2 to 32 µg/mL. The combination of cecropin A2 and tetracycline exerted synergistic activities against the planktonic cells of eighteen *P. aeruginosa* strains, and the MIC of AMP and antibiotic was reduced by 8-fold, with a FICI value of 0.25. Furthermore, the intervention of Cecropin A2-tetracycline combination also showed synergistic protection in *G. mellonella* models *in vivo* experiments. The researchers found that Cecropin A2 could bind to the LPS of *P. aeruginosa*, causing membrane permeation and interacting with

bacterial DNA, thereby facilitating the transfer of tetracycline to the cytoplasm. In addition, an earlier study proved that the combination of cecropin A (with the molecular mass of 3.88 kDa) and rifampicin also had synergistic inhibitory activity against *P. aeruginosa* strains, with the FICI index of 0.312 < 0.5 (Cirioni et al., 2008).

A study found that CAMA, a cecropin (1–7)-melittin A (2–9) amide with the molecular weight of 1.77 kDa, exerted a strong synergism when used in combination with ciprofloxacin against preformed biofilms of *P. aeruginosa* (*n* = 4) (Dosler and Karaaslan, 2014). After treatment with this combination, MBEC values of antibiotic and CAMA were reduced 8 times and 10 times, respectively.

The existing AMPs can be designed in a more thoughtful way to enhance chemical and physical properties, leading to improved effectiveness. Studies have shown that certain *synthetic* or *semi-synthetic* AMPs exhibited more significant synergistic activities against *P. aeruginosa* planktonic cells and biofilms when used in combination with traditional antibiotics (Martinez et al., 1861; Rudilla et al., 2016; Maisetta et al., 2017; Al Tall et al., 2019; Yasir et al., 2020). For example, the combination of AMP 38 (a novel *synthetic* cyclodipeptide analog of polymyxin) with imipenem had synergistic activities against imipenem-resistant *P. aeruginosa in vitro*, with a FICI of 0.07–0.18 (Rudilla et al., 2016). The AMP-antibiotic combination also exhibited a synergistic effect against biofilms, the MBEC of them were reduced from ≥500 to 62.5 µg/mL, and the FICI was 0.25. Cytotoxicity tests showed that mice administered 100 and 200 mg/kg AMP 38 survived without signs of toxicity, and it had an LD₅₀ value of 283 mg/kg. The synergistic antibacterial mechanism was similar to the above-mentioned mechanisms, AMP 38 destroyed cell membrane, and facilitated the entry of imipenem, which subsequently exerted its antibacterial effect at low concentrations. The synthesis of AMPs provides new insights for fighting against MDR strains, since an unlimited number of new compounds with antibacterial effects can be designed.

Based on the above studies, we found that most of the AMPs showed significant synergistic anti-*P. aeruginosa* effects *in vitro* when used in combination with antibacterial drugs. The combination therapy reduced the effective concentration of antibiotics, expanded the range of action of antibiotics, and improved the efficacy of antibiotics, suggesting the feasibility of drug combination strategy. Studies have shown that the synergistic antimicrobial mechanisms of AMP in combination with conventional antibiotics mainly include the following four mechanisms: (1) AMP could inhibit membrane ion channels, prevented the pumping out of antibiotics, or inhibited antibiotic-degrading enzymes' activities (Dey et al., 2021); (2) AMP could load antibiotics and promote the uptake of antibiotics by bacteria to broaden the antibiotic's antimicrobial spectrum; (3) AMP could interact with microbial membranes to increase the permeability, which in turn allowed more antibiotics access to the interior of the bacteria; (4) AMP could enhance the anti-biofilm activity of antibiotics by interfering with signaling pathways involved in biofilm formation and maintenance (de la Fuente-Núñez et al., 2014, 2015). In this article, we have summarized the synergistic anti-*P. aeruginosa* mechanisms of LL-37, lys-al, Ocellatin-PT3, NCL195, sphistin, Cecropin A2 and AMP 38, they could increase the cell membrane permeability by disrupting the cell membrane or binding to LPS, which increased the opportunity of antibiotics into bacterial interior. However, most of the current studies on AMPs-antibiotic synergistic antimicrobials did not have enough sufficient clinical data, therefore,

in-depth studies on AMPs combined with antimicrobials against *P. aeruginosa* need to be carried out in the future.

4. Clinical studies on some AMPs

With the increase in research, some AMPs had entered clinical trials, while most required more detailed and validated studies to learn about their antimicrobial activity and mechanism of action. To date, at least 20 AMPs had entered clinical trials (Mercer and O'Neil, 2013).

For example, Pexiganan, which possessed potent antibacterial activities *in vitro*, has passed two phase III clinical trials, demonstrated its efficacy, safety, and effectiveness against infected diabetic foot ulcers (Lipsky et al., 2008). In addition, Omiganan exhibited rapid and potent antibacterial activity by disrupting the bacterial plasma membrane. Currently, a 1% gel product of Omiganan (Omigard) was in a phase III trial to demonstrate its efficacy in the prevention of catheter-related infections. Besides, Omiganan had also been used in the treatment of rosacea and has successfully completed a phase II trial (Fritsche et al., 2008; Kang et al., 2014). Brilacidin had potent bactericidal activity against both resistant gram-positive and gram-negative bacteria. In 2014, a phase II trial enrolled 215 patients with acute bacterial skin and skin structure infections caused by MRSA and found that the therapeutic efficacy of Brilacidin administered intravenously was comparable to daptomycin (Méndez-Samperio, 2014). POL7080, a mimic of the antimicrobial peptide Protegrin-1, had anti-MDR *P. aeruginosa* effects both *in vitro* and *in vivo*. Currently, POL7080 had successfully completed Phase I clinical trial for the treatment of *P. aeruginosa* infections, demonstrating the safety and good tolerability (Tillotson and Theriault, 2013; Romano et al., 2019). There are also many AMPs that have passed Phase I/II clinical trials, but failed to obtain satisfactory results in Phase III trials, such as Isegran (Giles et al., 2004; Trotti et al., 2004; Kollef et al., 2006; Elad et al., 2012; Mercer and O'Neil, 2013). Moreover, several AMPs, such as Plectasin NZ2114 and MU1140, had exhibited remarkable therapeutic efficacy in preclinical researches, and they held great promise for further clinical development (Marr et al., 2006; Ghobrial et al., 2009; Breidenstein et al., 2015).

5. Discussion

In this review, we summarized the anti-*P. aeruginosa* activities of AMPs used alone and interactions with some conventional antibiotics. *In vitro* studies have shown that certain AMPs display obvious inhibitory effects against *P. aeruginosa* planktonic cells with MICs $\leq 10 \mu\text{g/mL}$, AMPs exerted their antimicrobial effects mainly by disrupting bacterial cell membranes or interacting with DNA. Moreover, a considerable number of AMPs-antibiotics combination have significant synergistic inhibitory effects against *P. aeruginosa* planktonic cells, as well as the biofilm formation. *In vivo* studies, some combinations have also increased the survival rate and reduced the extent of infection among infected animal models. The AMPs-antibiotics synergistic combination not only helped to reduce the individual concentration and broaden the antibacterial spectrum, but also decreased drug resistance, toxicity, and other side effects. Most of the synergistic mechanisms of action were that AMPs could increase cell membrane permeability, making it easier for antibiotics

to enter bacterial interior, and then exerted their antimicrobial effects. Although the synergistic antibacterial effects of AMP in combination with antibiotics had been demonstrated *in vitro*, the validation of their clinical synergistic activity has been rarely studied due to its limitations and different pharmacological properties from antibiotics. In addition, it is worth noting that some AMPs have been found to exert their antimicrobial effects through a combination of membrane-targeted and non-membrane-targeted modalities. For instance, arenicin-3 is a novel AMP that not only binds to the outer and cellular membranes of bacteria and disrupts their integrity, but also transfers to the cytoplasm to inhibit protein synthesis, ultimately exerting significant anti-gram-negative effects (Ciurac et al., 2019). Therefore, the cell membrane is no longer the only target of AMPs against pathogens. AMPs can act on the cell wall or intracellular nucleic acids, proteins, enzymes, or organelles to inhibit crucial intracellular processes, then leading to metabolic inhibition of the pathogens and causing bacterial death. Further research on the intracellular target of AMPs is of great significance in preventing the development of resistance in pathogens.

Although AMPs have potential therapeutic benefits compared with traditional antibiotics, they also have certain limitations, which hinder the clinical development and application. AMPs extracted naturally have low purity and quantity, as well as poor absorption, distribution, metabolism, excretion characteristics, low permeability and solubility (Di, 2015). A great number of researchers found that some properties of AMPs can be improved by changing peptide composition, making post-translational modification, recombining AMPs, and using computer-assisted discovery and design, which were meaningful to translate AMPs into useful clinical candidates for development (Irazazabal et al., 1858; Matsuzaki, 2009; Deo et al., 2022). Researchers usually use a variety of methods to design efficient, low-toxicity, and stable AMPs. These methods include: (1) replacement of amino acids in the peptide sequence with non-natural α -amino acid derivatives, such as D-amino acids, hexafluoroleucine, and α -amino-guanidinopropionic acid; (2) N-terminal acetylation or C-terminal amidation; (3) dimerization and disulfide bond cyclization; (4) optimization of physicochemical properties. Focusing on these studies will provide valuable insights into the application of AMPs in complex disease and lay a solid foundation for innovative drug development.

6. Conclusion

Natural AMPs have anti-*P. aeruginosa* and *E. coli* activity with low MIC values when used alone, and they act primarily by interacting with cell membranes or targeting organelles within the cell. Membrane-targeted antimicrobial mechanisms include four models. In this review, the antimicrobial mechanisms of Ocellatin-PT3 and Cecropin A2 are associated with LPS binding; the antimicrobial mechanisms of ACD and defensin-d2 are associated with an increase in the level of ROS. And the profound antimicrobial mechanisms of many other AMPs still need to be further discussed. In addition, based on the study of the antibacterial effect of natural AMPs alone or in combination with antibiotics against *P. aeruginosa in vitro*, it is still necessary to explore the synergistic antibacterial mechanism further or continue to develop AMPs structural analogs. Besides, it is imperative to further ensure the efficacy and safety of combined treatment *in vivo* animal models, which will be of great significance against clinical *P. aeruginosa* infection.

Author contributions

XC collected and analyzed the data of the review, and wrote the whole review and created Tables 1, 2. SS, YY, and LY helped with it. LH contributed to the writing to this article. All authors have reviewed and approved the manuscript. All authors contributed to the article and approved the submitted version.

Acknowledgments

Thanks for the department of pharmacy, China Japan Friendship Hospital.

References

- Abushaheen, M. A., Muzahed, A. J., Fatani, M., Alosaimi, W., Mansy, M., George, S., et al. (2020). Antimicrobial resistance, mechanisms and its clinical significance. *Disease-A-Month* 66:100971. doi: 10.1016/j.disamonth.2020.100971.
- Akbari, R., Hakemi-Vala, M., Pashaie, F., Bevalian, P., Hashemi, A., and Pooshang Bagheri, K. (2019). Highly synergistic effects of melittin with conventional antibiotics against multidrug-resistant isolates of *Acinetobacter baumannii* and *Pseudomonas aeruginosa*. *Microb. Drug Resist.* 25, 193–202. doi: 10.1089/mdr.2018.0016
- Al Akeel, R., Mateen, A., and Syed, R. (2019). An alanine-rich peptide attenuates quorum sensing-regulated virulence and biofilm formation in *Staphylococcus aureus*. *J. AOAC Int.* 102, 1228–1234. doi: 10.5740/jaoacint.18-0251
- Al Tall, Y., Abualhaijaa, A., Qaoud, M. T., Alsaggar, M., Masadeh, M., and Alzoubi, K. H. (2019). The ultrashort peptide OW: a new antibiotic adjuvant. *Curr. Pharm. Biotechnol.* 20, 745–754. doi: 10.2174/1389201020666190618111252
- Al-Ani, I., Zimmermann, S., Reichling, J., and Wink, M. (2015). Pharmacological synergism of bee venom and melittin with antibiotics and plant secondary metabolites against multi-drug resistant microbial pathogens. *Phytomed. Int. J. Phytother. Phytopharmacol.* 22, 245–255. doi: 10.1016/j.phymed.2014.11.019
- Almutairi, M. M. (2022). Synergistic activities of colistin combined with other antimicrobial agents against colistin-resistant *Acinetobacter baumannii* clinical isolates. *PLoS One* 17:e0270908. doi: 10.1371/journal.pone.0270908
- Andr , J., Berninghausen, O., and Leippe, M. (2001). Cecropins, antibacterial peptides from insects and mammals, are potentially fungicidal against *Candida albicans*. *Med. Microbiol. Immunol.* 189, 169–173. doi: 10.1007/s430-001-8025-x
- Barksdale, S. M., Hrifko, E. J., Chung, E. M., and van Hoek, M. L. (2016). Peptides from American alligator plasma are antimicrobial against multi-drug resistant bacterial pathogens including *Acinetobacter baumannii*. *BMC Microbiol.* 16:189.
- Bellm, L., Lehrer, R. I., and Ganz, T. (2000). Protegrins: new antibiotics of mammalian origin. *Expert Opin. Investig. Drugs* 9, 1731–1742.
- Bergaoui, I., Zairi, A., Tangy, F., Aouni, M., Selmi, B., and Hani, K. (2013). *In vitro* antiviral activity of dermaseptin S(4) and derivatives from amphibian skin against herpes simplex virus type 2. *J. Med. Virol.* 85, 272–281. doi: 10.1002/jmv.23450
- Bessa, L. J., Eaton, P., Dematei, A., Pl cido, A., Vale, N., Gomes, P., et al. (2018). Synergistic and antibiofilm properties of ocellatin peptides against multidrug-resistant *Pseudomonas aeruginosa*. *Future Microbiol.* 13, 151–163. doi: 10.2217/fmb-2017-0175
- Bin Hafeez, A., Jiang, X., Bergen, P. J., and Zhu, Y. (2021). Antimicrobial peptides: an update on classifications and databases. *Int. J. Mol. Sci.* 22. doi: 10.3390/ijms222111691
- Bishop, B. M., Juba, M. L., Devine, M. C., Barksdale, S. M., Rodriguez, C. A., Chung, M. C., et al. (2015). Bioprospecting the American alligator (*Alligator mississippiensis*) host defense peptidome. *PLoS One* 10:e0117394. doi: 10.1371/journal.pone.0117394
- Boparai, J. K., and Sharma, P. K. (2020a). Mini review on antimicrobial peptides, sources, mechanism and recent applications. *Protein Pept. Lett.* 27, 4–16. doi: 10.2174/18755305MTAWE80
- Boparai, J. K., and Sharma, P. K. (2020b). Mini review on antimicrobial peptides, sources, mechanism and recent applications. *Protein Pept. Lett.* 27, 4–16. doi: 10.2174/18755305MTAWE80
- Bosso, M., St ndker, L., Kirchhoff, F., and M nch, J. (2018). Exploiting the human peptidome for novel antimicrobial and anticancer agents. *Bioorg. Med. Chem.* 26, 2719–2726. doi: 10.1016/j.bmc.2017.10.038
- Breidenstein, E. B., Courvalin, P., and Meziane-Cherif, D. (2015). Antimicrobial activity of Plectasin NZ2114 in combination with Cell Wall targeting antibiotics against VanA-type *Enterococcus faecalis*. *Microb. Drug Resist.* 21, 373–379. doi: 10.1089/mdr.2014.0221
- Buda De Cesare, G., Cristy, S. A., Garsin, D. A., and Lorenz, M. C. (2020). Antimicrobial peptides: a new frontier in antifungal therapy. *MBio* 11. doi: 10.1128/mBio.02123-20
- Burrows, L. L. (2018). The therapeutic pipeline for *Pseudomonas aeruginosa* infections. *ACS Infect. Dis.* 4, 1041–1047. doi: 10.1021/acscinfecdis.8b00112
- Burton, M. F., and Steel, P. G. (2009). The chemistry and biology of LL-37. *Nat. Prod. Rep.* 26, 1572–1584. doi: 10.1039/b912533g
- Cabrera, M. P., Baldissera, G., Silva-Gon alves Lda, C., Souza, B. M., Riske, K. A., Palma, M. S., et al. (2014). Combining experimental evidence and molecular dynamic simulations to understand the mechanism of action of the antimicrobial octapeptide jelleine-I. *Biochemistry* 53, 4857–4868. doi: 10.1021/bi5003585
- Carneiro, V. A., de Oliveira, S. T., Silva, R. L., de Sousa Duarte, H., Silva, M. L., Matos, M. N. C., et al. (2020). Antimicrobial and antibiofilm activity of Lys-[Trp6]hy-a1 combined with ciprofloxacin against gram-negative Bacteria. *Protein Pept. Lett.* 27, 1124–1131. doi: 10.2174/0929866527666200416145549
- Castro, M. S., Ferreira, T. C., Cilli, E. M., Crusca, E., Mendes-Giannini, M. J., Sebben, A., et al. (2009). Hylin a1, the first cytolytic peptide isolated from the arboreal south American frog *Hypsiboas albopunctatus* ("spotted treefrog"). *Peptides* 30, 291–296. doi: 10.1016/j.peptides.2008.11.003
- Chen, B., Fan, D. Q., Zhu, K. X., Shan, Z. G., Chen, F. Y., Hou, L., et al. (2015). Mechanism study on a new antimicrobial peptide Sphistin derived from the N-terminus of crab histone H2A identified in haemolymphs of *Scylla paramamosain*. *Fish Shellfish Immunol.* 47, 833–846. doi: 10.1016/j.fsi.2015.10.010
- Cho, J., Hwang, I. S., Choi, H., Hwang, J. H., Hwang, J. S., and Lee, D. G. (2012). The novel biological action of antimicrobial peptides via apoptosis induction. *J. Microbiol. Biotechnol.* 22, 1457–1466. doi: 10.4014/jmb.1205.05041
- Chopra, I. (1993). The magainins: antimicrobial peptides with potential for topical application. *J. Antimicrob. Chemother.* 32, 351–353. doi: 10.1093/jac/32.3.351
- Cirioni, O., Giacometti, A., Ghiselli, R., Kamysz, W., Orlando, F., Mocchegiani, F., et al. (2006). Citropin 1.1-treated central venous catheters improve the efficacy of hydrophobic antibiotics in the treatment of experimental staphylococcal catheter-related infection. *Peptides* 27, 1210–1216. doi: 10.1016/j.peptides.2005.10.007
- Cirioni, O., Silvestri, C., Ghiselli, R., Orlando, F., Riva, A., Mocchegiani, F., et al. (2008). Protective effects of the combination of alpha-helical antimicrobial peptides and rifampicin in three rat models of *Pseudomonas aeruginosa* infection. *J. Antimicrob. Chemother.* 62, 1332–1338. doi: 10.1093/jac/dkn393
- Ciumac, D., Gong, H., Hu, X., and Lu, J. R. (2019). Membrane targeting cationic antimicrobial peptides. *J. Colloid Interface Sci.* 537, 163–185. doi: 10.1016/j.jcis.2018.10.103
- da Silva, B. R., de Freitas, V. A., Carneiro, V. A., Arruda, F. V., Lorenz n, E. N., de Aguiar, A. S., et al. (2013). Antimicrobial activity of the synthetic peptide Lys-a1 against oral streptococci. *Peptides* 42, 78–83. doi: 10.1016/j.peptides.2012.12.001
- Dagan, A., Efron, L., Gaidukov, L., Mor, A., and Ginsburg, H. (2002). *In vitro* antiparasitoid effects of dermaseptin S4 derivatives. *Antimicrob. Agents Chemother.* 46, 1059–1066. doi: 10.1128/AAC.46.4.1059-1066.2002
- Darville, L. N., Merchant, M. E., Hasan, A., and Murray, K. K. (2010). Proteome analysis of the leukocytes from the American alligator (*Alligator mississippiensis*) using mass spectrometry. *Comp. Biochem. Physiol. Part D Genomics Proteomics* 5, 308–316. doi: 10.1016/j.cbd.2010.09.001
- de la Fuente-N  ez, C., Ref uveille, F., Haney, E. F., Straus, S. K., and Hancock, R. E. (2014). Broad-spectrum anti-biofilm peptide that targets a cellular stress response. *PLoS Pathog.* 10:e1004152. doi: 10.1371/journal.ppat.1004152

- de La Fuente-Núñez, C., Refeuille, F., Mansour, S. C., Reckseidler-Zenteno, S. L., Hernández, D., Brackman, G., et al. (2015). D-enantiomeric peptides that eradicate wild-type and multidrug-resistant biofilms and protect against lethal *Pseudomonas aeruginosa* infections. *Chem. Biol.* 22, 196–205. doi: 10.1016/j.chembiol.2015.01.002
- Deo, S., Turton, K. L., Kainth, T., Kumar, A., and Wieden, H. J. (2022). Strategies for improving antimicrobial peptide production. *Biotechnol. Adv.* 59:107968. doi: 10.1016/j.biotechadv.2022.107968
- Dey, R., Mukherjee, S., Barman, S., and Haldar, J. (2021). Macromolecular nanotherapeutics and antibiotic adjuvants to tackle bacterial and fungal infections. *Macromol. Biosci.* 21:e2100182. doi: 10.1002/mabi.202100182
- Di, L. (2015). Strategic approaches to optimizing peptide ADME properties. *AAPS J.* 17, 134–143. doi: 10.1208/s12248-014-9687-3
- Di Luca, M., Maccari, G., and Nifosi, R. (2014). Treatment of microbial biofilms in the post-antibiotic era: prophylactic and therapeutic use of antimicrobial peptides and their design by bioinformatics tools. *Pathog. Dis.* 70, 257–270. doi: 10.1111/2049-632X.12151
- Dosler, S., and Karaaslan, E. (2014). Inhibition and destruction of *Pseudomonas aeruginosa* biofilms by antibiotics and antimicrobial peptides. *Peptides* 62, 32–37. doi: 10.1016/j.peptides.2014.09.021
- Efron, L., Dagan, A., Gaidukov, L., Ginsburg, H., and Mor, A. (2002). Direct interaction of dermaseptin S4 aminoheptanoyl derivative with intraerythrocytic malaria parasite leading to increased specific antiparasitic activity in culture. *J. Biol. Chem.* 277, 24067–24072. doi: 10.1074/jbc.M202089200
- Elad, S., Epstein, J. B., Raber-Durlacher, J., Donnelly, P., and Strahilevitz, J. (2012). The antimicrobial effect of Isegran HCl oral solution in patients receiving stomatotoxic chemotherapy: analysis from a multicenter, double-blind, placebo-controlled, randomized, phase III clinical trial. *J. Oral Pathol. Med.* 41, 229–234. doi: 10.1111/j.1600-0714.2011.01094.x
- Elias, P. M. (2005). Stratum corneum defensive functions: an integrated view. *J. Invest. Dermatol.* 125, 183–200. doi: 10.1111/j.0022-202X.2005.23668.x
- Fabisiak, A., Murawska, N., and Fichna, J. (2016). LL-37: cathelicidin-related antimicrobial peptide with pleiotropic activity. *Pharmacol. Rep.* 68, 802–808. doi: 10.1016/j.pharep.2016.03.015
- Fontana, R., Mendes, M. A., de Souza, B. M., Konno, K., César, L. M., Malaspina, O., et al. (2004). Jelleines: a family of antimicrobial peptides from the Royal Jelly of honeybees (*Apis mellifera*). *Peptides* 25, 919–928. doi: 10.1016/j.peptides.2004.03.016
- Fritsche, T. R., Rhomberg, P. R., Sader, H. S., and Jones, R. N. (2008). Antimicrobial activity of omiganan pentahydrochloride tested against contemporary bacterial pathogens commonly responsible for catheter-associated infections. *J. Antimicrob. Chemother.* 61, 1092–1098. doi: 10.1093/jac/dkn074
- Fujiwara, S., Imai, J., Fujiwara, M., Yaeshima, T., Kawashima, T., and Kobayashi, K. (1990). A potent antibacterial protein in royal jelly. Purification and determination of the primary structure of royalisin. *J. Biol. Chem.* 265, 11333–11337. doi: 10.1016/S0021-9258(19)38596-5
- Gallo, R. L., and Hooper, L. V. (2012). Epithelial antimicrobial defence of the skin and intestine. *Nat. Rev. Immunol.* 12, 503–516. doi: 10.1038/nri3228
- Gbala, I. D., Macharia, R. W., Bargul, J. L., and Magoma, G. (2022). Membrane permeabilization and antimicrobial activity of recombinant defensin-d2 and Actifensin against multidrug-resistant *Pseudomonas aeruginosa* and *Candida albicans*. *Molecules* 27:4325. doi: 10.3390/molecules27144325
- Ghiselli, R., Silvestri, C., Cirioni, O., Kamysz, W., Orlando, F., Calcinari, A., et al. (2011). Protective effect of citropin 1.1 and tazobactam-piperacillin against oxidative damage and lethality in mice models of gram-negative sepsis. *J. Surg. Res.* 171, 726–733. doi: 10.1016/j.jss.2010.03.055
- Ghobrial, O. G., Derendorf, H., and Hillman, J. D. (2009). Pharmacodynamic activity of the lantibiotic MU1140. *Int. J. Antimicrob. Agents* 33, 70–74. doi: 10.1016/j.ijantimicag.2008.07.028
- Giacometti, A., Cirioni, O., Barchiesi, F., Fortuna, M., and Scalise, G. (1999). *In-vitro* activity of cationic peptides alone and in combination with clinically used antimicrobial agents against *Pseudomonas aeruginosa*. *J. Antimicrob. Chemother.* 44, 641–645. doi: 10.1093/jac/44.5.641
- Giles, F. J., Rodriguez, R., Weisdorf, D., Wingard, J. R., Martin, P. J., Fleming, T. R., et al. (2004). A phase III, randomized, double-blind, placebo-controlled, study of isegranan for the reduction of stomatitis in patients receiving stomatotoxic chemotherapy. *Leuk. Res.* 28, 559–565. doi: 10.1016/j.leukres.2003.10.021
- Han, W., Wei, Z., and Camesano, T. A. (2022). New antimicrobial peptide-antibiotic combination strategy for *Pseudomonas aeruginosa* inactivation. *Biointerphases* 17:041002. doi: 10.1116/6.0001981
- Hancock, R. E., Nijnik, A., and Philpott, D. J. (2012). Modulating immunity as a therapy for bacterial infections. *Nat. Rev. Microbiol.* 10, 243–254. doi: 10.1038/nrmicro2745
- Hancock, R. E., and Speert, D. P. (2000). Antibiotic resistance in *Pseudomonas aeruginosa*: mechanisms and impact on treatment. *Drug Resist. Updat.* 3, 247–255. doi: 10.1054/drup.2000.0152
- Hansmann, B., Schröder, J. M., and Gerstel, U. (2015). Skin-derived C-terminal Filaggrin-2 fragments are *Pseudomonas aeruginosa*-directed antimicrobials targeting bacterial replication. *PLoS Pathog.* 11:e1005159. doi: 10.1371/journal.ppat.1005159
- Harder, J., Schröder, J. M., and Gläser, R. (2013). The skin surface as antimicrobial barrier: present concepts and future outlooks. *Exp. Dermatol.* 22, 1–5. doi: 10.1111/exd.12046
- Hollmann, A., Martinez, M., Maturana, P., Semorile, L. C., and Maffia, P. C. (2018). Antimicrobial peptides: interaction with model and biological membranes and synergism with chemical antibiotics. *Front. Chem.* 6:204.
- Huan, Y., Kong, Q., Mou, H., and Yi, H. (2020). Antimicrobial peptides: classification, design, application and research Progress in multiple fields. *Front. Microbiol.* 11:582779. doi: 10.3389/fmicb.2020.582779
- Irazabal, L. N., Porto, W. F., Ribeiro, S. M., Casale, S., Humblot, V., Ladram, A., et al. (1958). Selective amino acid substitution reduces cytotoxicity of the antimicrobial peptide mastoparan. *Biochim. Biophys. Acta* 2016, 2699–2708.
- Islas-Rodriguez, A. E., Marcellini, L., Orioni, B., Barra, D., Stella, L., and Mangoni, M. L. (2009). Esculentin 1-21: a linear antimicrobial peptide from frog skin with inhibitory effect on bovine mastitis-causing bacteria. *J. Pept. Sci. Off. Publ. Euro. Pept. Soc.* 15, 607–614. doi: 10.1002/psc.1148
- Jacob, L., and Zasloff, M. (1994). Potential therapeutic applications of magainins and other antimicrobial agents of animal origin. *Ciba Found. Symp.* 186, 197–216.
- Jahangiri, A., Neshani, A., Mirhosseini, S. A., Ghazvini, K., Zare, H., and Sedighian, H. (2021). Synergistic effect of two antimicrobial peptides, nisin and P10 with conventional antibiotics against extensively drug-resistant *Acinetobacter baumannii* and colistin-resistant *Pseudomonas aeruginosa* isolates. *Microb. Pathog.* 150:104700. doi: 10.1016/j.micpath.2020.104700
- Jangra, V., Sharma, N., and Chhillar, A. K. (2022). Therapeutic approaches for combating *Pseudomonas aeruginosa* infections. *Microbes Infect.* 24:104950. doi: 10.1016/j.micinf.2022.104950
- Jorge, P., Grzywacz, D., Kamysz, W., Lourenço, A., and Pereira, M. O. (2017). Searching for new strategies against biofilm infections: colistin-AMP combinations against *Pseudomonas aeruginosa* and *Staphylococcus aureus* single- and double-species biofilms. *PLoS One* 12:e0174654. doi: 10.1371/journal.pone.0174654
- Kang, S. J., Park, S. J., Mishig-Ochir, T., and Lee, B. J. (2014). Antimicrobial peptides: therapeutic potentials. *Expert Rev. Anti-Infect. Ther.* 12, 1477–1486. doi: 10.1586/14787210.2014.976613
- Kollef, M., Pittet, D., Sánchez García, M., Chastre, J., Fagon, J. Y., Bonten, M., et al. (2006). A randomized double-blind trial of isegranan in prevention of ventilator-associated pneumonia. *Am. J. Respir. Crit. Care Med.* 173, 91–97. doi: 10.1164/rccm.200504-656OC
- Lachowicz, J. I., Szczepski, K., Scano, A., Casu, C., Fais, S., Orrù, G., et al. (2020). The best peptidomimetic strategies to undercover antibacterial peptides. *Int. J. Mol. Sci.* 21. doi: 10.3390/ijms21197349
- Lee, C. C., Sun, Y., Qian, S., and Huang, H. W. (2011). Transmembrane pores formed by human antimicrobial peptide LL-37. *Biophys. J.* 100, 1688–1696. doi: 10.1016/j.bpj.2011.02.018
- Lei, J., Sun, L., Huang, S., Zhu, C., Li, P., He, J., et al. (2019). The antimicrobial peptides and their potential clinical applications. *Am. J. Transl. Res.* 11, 3919–3931.
- Li, J., Koh, J. J., Liu, S., Lakshminarayanan, R., Verma, C. S., and Beuerman, R. W. (2017). Membrane active antimicrobial peptides: translating mechanistic insights to design. *Front. Neurosci.* 11:73. doi: 10.3389/fnins.2017.00073
- Li, S. A., Lee, W. H., and Zhang, Y. (2012). Efficacy of OH-CATH30 and its analogs against drug-resistant bacteria in vitro and in mouse models. *Antimicrob. Agents Chemother.* 56, 3309–3317. doi: 10.1128/AAC.06304-11
- Li, S. A., Liu, J., Xiang, Y., Wang, Y. J., Lee, W. H., and Zhang, Y. (2014). Therapeutic potential of the antimicrobial peptide OH-CATH30 for antibiotic-resistant *Pseudomonas aeruginosa* keratitis. *Antimicrob. Agents Chemother.* 58, 3144–3150. doi: 10.1128/AAC.00095-14
- Li, J. F., Zhang, J. X., Li, G., Xu, Y. Y., Lu, K., Wang, Z. G., et al. (2020). Antimicrobial activity and mechanism of peptide CM4 against *Pseudomonas aeruginosa*. *Food Funct.* 11, 7245–7254. doi: 10.1039/D0FO01031F
- Libardo, M. D. J., Bahar, A. A., Ma, B., Fu, R., McCormick, L. E., Zhao, J., et al. (2017). Nuclease activity gives an edge to host-defense peptide piscidin 3 over piscidin 1, rendering it more effective against persisters and biofilms. *FEBS J.* 284, 3662–3683. doi: 10.1111/febs.14263
- Lin, Y., Lin, T., Cheng, N., Wu, S., Huang, J., Chen, X., et al. (2021). Evaluation of antimicrobial and anticancer activities of three peptides identified from the skin secretion of *Hylarana latouchii*. *Acta Biochim. Biophys. Sin.* 53, 1469–1483. doi: 10.1093/abbs/gmab126
- Lipsky, B. A., Holroyd, K. J., and Zasloff, M. (2008). Topical versus systemic antimicrobial therapy for treating mildly infected diabetic foot ulcers: a randomized, controlled, double-blinded, multicenter trial of pexiganan cream. *Clin. Infect. Dis.* 47, 1537–1545. doi: 10.1086/593185
- Liu, J., Chen, F., Wang, X., Peng, H., Zhang, H., and Wang, K. J. (2020). The synergistic effect of *Mud crab* antimicrobial peptides Sphistatin and Sph(12-38) with antibiotics azithromycin and rifampicin enhances bactericidal activity against *Pseudomonas aeruginosa*. *Front. Cell. Infect. Microbiol.* 10:572849. doi: 10.3389/fcimb.2020.572849
- Luca, V., Stringaro, A., Colone, M., Pini, A., and Mangoni, M. L. (2013). Esculentin(1-21), an amphibian skin membrane-active peptide with potent activity on

both planktonic and biofilm cells of the bacterial pathogen *Pseudomonas aeruginosa*. *Cell. Mol. Life Sci.* 70, 2773–2786. doi: 10.1007/s00018-013-1291-7

Luo, Y., and Song, Y. (2021). Mechanism of antimicrobial peptides: antimicrobial, anti-inflammatory and antibiofilm activities. *Int. J. Mol. Sci.* 22. doi: 10.3390/ijms222111401

Maisetta, G., Grassi, L., Esin, S., Serra, I., Scorciapino, M. A., Rinaldi, A. C., et al. (2017). The semi-synthetic peptide Lin-SB056-1 in combination with EDTA exerts strong antimicrobial and antibiofilm activity against *Pseudomonas aeruginosa* in conditions mimicking cystic fibrosis sputum. *Int. J. Mol. Sci.* 18. doi: 10.3390/ijms18091994

Marr, A. K., Gooderham, W. J., and Hancock, R. E. (2006). Antibacterial peptides for therapeutic use: obstacles and realistic outlook. *Curr. Opin. Pharmacol.* 6, 468–472. doi: 10.1016/j.coph.2006.04.006

Martinez, M., Gonçalves, S., Felício, M. R., Maturana, P., Santos, N. C., Semorile, L., et al. (1861). Synergistic and antibiofilm activity of the antimicrobial peptide P5 against carbapenem-resistant *Pseudomonas aeruginosa*. *Biochim. Biophys. Acta Biomembr.* 2019, 1329–1337.

Marynka, K., Rotem, S., Portnaya, I., Cogan, U., and Mor, A. (2007). *In vitro* discriminative antipseudomonal properties resulting from acyl substitution of N-terminal sequence of dermaseptin s4 derivatives. *Chem. Biol.* 14, 75–85. doi: 10.1016/j.chembiol.2006.11.009

Mataraci Kara, E., Yilmaz, M., İstanbullu Tosun, A., and Özbek Çelik, B. (2020). Synergistic activities of ceftazidime-avibactam in combination with different antibiotics against colistin-nonsusceptible clinical strains of *Pseudomonas aeruginosa*. *Infect. Dis.* 52, 616–624.

Matsuzaki, K. (2009). Control of cell selectivity of antimicrobial peptides. *Biochim. Biophys. Acta* 1788, 1687–1692. doi: 10.1016/j.bbame.2008.09.013

McCann, J. C., Wickersham, T. A., and Loor, J. J. (2014). High-throughput methods redefine the rumen microbiome and its relationship with nutrition and metabolism. *Bioinform. Biol. Insig.* 8, 109–125. doi: 10.4137/BBI.S15389

Méndez-Samperio, P. (2014). Peptidomimetics as a new generation of antimicrobial agents: current progress. *Infect. Drug Resist.* 7, 229–237. doi: 10.2147/IDR.S49229

Mercer, D. K., and O'Neil, D. A. (2013). Peptides as the next generation of anti-infectives. *Future Med. Chem.* 5, 315–337. doi: 10.4155/fmc.12.213

Merchant, M. E., Leger, N., Jerkins, E., Mills, K., Pallansch, M. B., Paulman, R. L., et al. (2006). Broad spectrum antimicrobial activity of leukocyte extracts from the American alligator (*Alligator mississippiensis*). *Vet. Immunol. Immunopathol.* 110, 221–228. doi: 10.1016/j.vetimm.2005.10.001

Modiri, S., Kasra Kermanshahi, R., Soudi, M. R., Arab, S. S., Khammari, A., Cousineau, B., et al. (2020). Multifunctional Acidocin 4356 combats *Pseudomonas aeruginosa* through membrane perturbation and virulence attenuation: experimental results confirm molecular dynamics simulation. *Appl. Environ. Microbiol.* 86. doi: 10.1128/AEM.00367-20

Moore, N. M., and Flaws, M. L. (2011). Treatment strategies and recommendations for *Pseudomonas aeruginosa* infections. *Clin. Lab. Sci. J. Am. Soc. Med. Technol.* 24, 52–56. doi: 10.29074/ascls.24.1.52

Mor, A., Nguyen, V. H., Delfour, A., Migliore-Samour, D., and Nicolas, P. (1991). Isolation, amino acid sequence, and synthesis of dermaseptin, a novel antimicrobial peptide of amphibian skin. *Biochemistry* 30, 8824–8830. doi: 10.1021/bi00100a014

Morgavi, D. P., Kelly, W. J., Janssen, P. H., and Attwood, G. T. (2013). Rumen microbial (meta)genomics and its application to ruminant production. *Anim. Int. J. Anim. Biosci.* 7, 184–201.

Morrone, G., Simonetti, O., Brenciani, A., Brescini, L., Kamysz, W., Kamysz, E., et al. (2019). *In vitro* activity of Protegrin-1, alone and in combination with clinically useful antibiotics, against *Acinetobacter baumannii* strains isolated from surgical wounds. *Med. Microbiol. Immunol.* 208, 877–883. doi: 10.1007/s00430-019-00624-7

Morton, C. O., Dos Santos, S. C., and Coote, P. (2007). An amphibian-derived, cationic, alpha-helical antimicrobial peptide kills yeast by caspase-independent but AIF-dependent programmed cell death. *Mol. Microbiol.* 65, 494–507. doi: 10.1111/j.1365-2958.2007.05801.x

Mulkern, A. J., Oyama, L. B., Cookson, A. R., Creevey, C. J., Wilkinson, T. J., Olleik, H., et al. (2022). Microbiome-derived antimicrobial peptides offer therapeutic solutions for the treatment of *Pseudomonas aeruginosa* infections. *NPJ Biofil. Microb.* 8:70. doi: 10.1038/s41522-022-00332-w

Naghmouchi, K., Le Lay, C., Baah, J., and Drider, D. (2012). Antibiotic and antimicrobial peptide combinations: synergistic inhibition of *Pseudomonas fluorescens* and antibiotic-resistant variants. *Res. Microbiol.* 163, 101–108. doi: 10.1016/j.resmic.2011.11.002

Nguyen, L. T., Haney, E. F., and Vogel, H. J. (2011). The expanding scope of antimicrobial peptide structures and their modes of action. *Trends Biotechnol.* 29, 464–472. doi: 10.1016/j.tibtech.2011.05.001

Nguyen, H. T., Venter, H., Veltman, T., Williams, R., O'Donovan, L. A., Russell, C. C., et al. (2021). *In vitro* synergistic activity of NCL195 in combination with colistin against gram-negative bacterial pathogens. *Int. J. Antimicrob. Agents* 57:106323. doi: 10.1016/j.ijantimicag.2021.106323

Nolan, L. M., Turnbull, L., Katrib, M., Osvath, S. R., Losa, D., Lazenby, J. J., et al. (2020). *Pseudomonas aeruginosa* is capable of natural transformation in biofilms. *Microbiology* 166, 995–1003. doi: 10.1099/mic.0.000956

Ogunniyi, A. D., Khazandi, M., Stevens, A. J., Sims, S. K., Page, S. W., Garg, S., et al. (2017). Evaluation of robenidine analog NCL195 as a novel broad-spectrum antibacterial agent. *PLoS One* 12:e0183457. doi: 10.1371/journal.pone.0183457

Oliveira, M., Gomes-Alves, A. G., Sousa, C., Mirta Marani, M., Plácido, A., Vale, N., et al. (2016). Ocellatin-PT antimicrobial peptides: high-resolution microscopy studies in antileishmania models and interactions with mimetic membrane systems. *Biopolymers* 105, 873–886. doi: 10.1002/bip.22925

Overhage, J., Campisano, A., Bains, M., Torfs, E. C., Rehm, B. H., and Hancock, R. E. (2008). Human host defense peptide LL-37 prevents bacterial biofilm formation. *Infect. Immun.* 76, 4176–4182. doi: 10.1128/IAI.00318-08

Oyama, L. B., Girdwood, S. E., Cookson, A. R., Fernandez-Fuentes, N., Privé, F., Vallin, H. E., et al. (2017). The rumen microbiome: an underexplored resource for novel antimicrobial discovery. *NPJ Biofil. Microb.* 3:33.

Pamp, S. J., Gjermansen, M., Johansen, H. K., and Tolker-Nielsen, T. (2008). Tolerance to the antimicrobial peptide colistin in *Pseudomonas aeruginosa* biofilms is linked to metabolically active cells, and depends on the pmr and mexAB-oprM genes. *Mol. Microbiol.* 68, 223–240. doi: 10.1111/j.1365-2958.2008.06152.x

Parduchio, K. R., Beadell, B., Ybarra, T. K., Bush, M., Escalera, E., Trejos, A. T., et al. (2020). The antimicrobial peptide human Beta-defensin 2 inhibits biofilm production of *Pseudomonas aeruginosa* without compromising metabolic activity. *Front. Immunol.* 11:805. doi: 10.3389/fimmu.2020.00805

Park, G. C., Choi, J. A., Jang, S. J., Jeong, S. H., Kim, C. M., Choi, I. S., et al. (2016). *In vitro* interactions of antibiotic combinations of colistin, tigecycline, and Doripenem against extensively drug-resistant and multidrug-resistant *Acinetobacter baumannii*. *Ann. Lab. Med.* 36, 124–130. doi: 10.3343/alm.2016.36.2.124

Perez-Rodriguez, A., Eraso, E., Quindós, G., and Mateo, E. (2022a). Antimicrobial peptides with anti-Candida activity. *Int. J. Mol. Sci.* 23:9264. doi: 10.3390/ijms23169264

Perez-Rodriguez, A., Eraso, E., Quindós, G., and Mateo, E. (2022b). Antimicrobial peptides with anti-Candida activity. *Int. J. Mol. Sci.* 23. doi: 10.3390/ijms23169264

Petrosillo, N., Ioannidou, E., and Falagas, M. E. (2008). Colistin monotherapy vs. combination therapy: evidence from microbiological, animal and clinical studies. *Clin. Microbiol. Infect.* 14, 816–827. doi: 10.1111/j.1469-0691.2008.02061.x

Pitt, S. J., Graham, M. A., Dedi, C. G., Taylor-Harris, P. M., and Gunn, A. (2015). Antimicrobial properties of mucus from the brown garden snail *Helix aspersa*. *Br. J. Biomed. Sci.* 72, 174–181; quiz 208. doi: 10.1080/09674845.2015.11665749

Pitt, S. J., Hawthorne, J. A., Garcia-Maya, M., Alexandrovich, A., Symonds, R. C., and Gunn, A. (2019). Identification and characterisation of anti-*Pseudomonas aeruginosa* proteins in mucus of the brown garden snail, *Cornu aspersum*. *Br. J. Biomed. Sci.* 76, 129–136. doi: 10.1080/09674845.2019.1603794

Pompilio, A., Crocetta, V., Scocchi, M., Pomponio, S., Di Vincenzo, V., Mardirossian, M., et al. (2012). Potential novel therapeutic strategies in cystic fibrosis: antimicrobial and anti-biofilm activity of natural and designed α -helical peptides against *Staphylococcus aureus*, *Pseudomonas aeruginosa*, and *Stenotrophomonas maltophilia*. *BMC Microbiol.* 12:145. doi: 10.1186/1471-2180-12-145

Ponti, D., Mignogna, G., Mangoni, M. L., De Biase, D., Simmaco, M., and Barra, D. (1999). Expression and activity of cyclic and linear analogues of esculetin-1, an antimicrobial peptide from amphibian skin. *Eur. J. Biochem.* 263, 921–927. doi: 10.1046/j.1432-1327.1999.00597.x

Portelinha, J., and Angeles-Boza, A. M. (2021). The antimicrobial peptide Gad-1 clears *Pseudomonas aeruginosa* biofilms under cystic fibrosis conditions. *Chembiochem* 22, 1646–1655. doi: 10.1002/cbic.202000816

Privé, F., Newbold, C. J., Kaderbhai, N. N., Girdwood, S. G., Golyshina, O. V., Golyshin, P. N., et al. (2015). Isolation and characterization of novel lipases/esterases from a bovine rumen metagenome. *Appl. Microbiol. Biotechnol.* 99, 5475–5485. doi: 10.1007/s00253-014-6355-6

Quilès, F., Saadi, S., Francius, G., Bacharouche, J., and Humbert, F. (1858). *In situ* and real time investigation of the evolution of a *Pseudomonas fluorescens* nascent biofilm in the presence of an antimicrobial peptide. *Biochim. Biophys. Acta* 2016, 75–84.

Ramchuran, E. J., Somboro, A. M., Abdel Monaim, S. A. H., Amoako, D. G., Parboosing, R., Kumalo, H. M., et al. *In Vitro antibacterial activity of Teixobactin derivatives on clinically relevant bacterial isolates* *Front Microbiol.* 9 (2018) 1535.

Román, J. T., Fuenmayor, C. A., Zuluaga Dominguez, C. M., Clavijo-Grimaldo, D., Acosta, M., García-Castañeda, J. E., et al. (2019). Pullulan nanofibers containing the antimicrobial palindromic peptide LfcinB (21–25)(pal) obtained via electrospinning. *RSC Adv.* 9, 20432–20438. doi: 10.1039/C9RA03643A

Romano, K. P., Warrier, T., Poulsen, B. E., Nguyen, P. H., Loftis, A. R., Saebi, A., et al. (2019). Mutations in pmrB confer cross-resistance between the LptD inhibitor POL7080 and colistin in *Pseudomonas aeruginosa*. *Antimicrob. Agents Chemother.* 63. doi: 10.1128/AAC.00511-19

Roque-Borda, C. A., da Silva, P. B., Rodrigues, M. C., Azevedo, R. B., Di Filippo, L., Duarte, J. L., et al. (2021). Challenge in the discovery of new drugs: antimicrobial peptides against WHO-list of critical and high-priority Bacteria. *Pharmaceutics* 13. doi: 10.3390/pharmaceutics13060773

Rudilla, H., Fusté, E., Cajal, Y., Rabanal, F., Vinuesa, T., and Viñas, M., Synergistic antipseudomonal effects of synthetic peptide AMP38 and carbapenems. *Molecules* (Basel, Switzerland) 21 (2016). doi: 10.3390/molecules21091223

- Saeed, S. I., Mergani, A., Akilu, E., and Kamaruzzman, N. F. (2022). Antimicrobial peptides: bringing solution to the rising threats of antimicrobial resistance in livestock. *Front. Vet. Sci.* 9:851052. doi: 10.3389/fvets.2022.851052
- Salger, S. A., Cassidy, K. R., Reading, B. J., and Noga, E. J. (2016). A diverse family of host-Defense peptides (Piscidins) exhibit specialized anti-bacterial and anti-protozoal activities in fishes. *PLoS One* 11:e0159423. doi: 10.1371/journal.pone.0159423
- Sathoff, A. E., Lewenza, S., and Samac, D. A. (2020). Plant defensin antibacterial mode of action against *Pseudomonas* species. *BMC Microbiol.* 20:173.
- Sathoff, A. E., Velivelli, S., Shah, D. M., and Samac, D. A. (2019). Plant defensin peptides have antifungal and antibacterial activity against human and plant pathogens. *Phytopathology* 109, 402–408. doi: 10.1094/PHYTO-09-18-0331-R
- Schröder, J.-M., and Harder, J. (1999). Human beta-defensin-2. *Int. J. Biochem. Cell Biol.* 31, 645–651. doi: 10.1016/S1357-2725(99)00013-8
- Segura, A., Moreno, M., Molina, A., and García-Olmedo, F. (1998). Novel defensin subfamily from spinach (*Spinacia oleracea*). *FEBS Lett.* 435, 159–162. doi: 10.1016/S0014-5793(98)01060-6
- Simmaco, M., Mignogna, G., Barra, D., and Bossa, F. (1994). Antimicrobial peptides from skin secretions of *Rana esculenta*. Molecular cloning of cDNAs encoding esculentin and brevinins and isolation of new active peptides. *J. Biol. Chem.* 269, 11956–11961. doi: 10.1016/S0021-9258(17)32666-2
- Simonetti, O., Cirioni, O., Goteri, G., Ghiselli, R., Kamysz, W., Kamysz, E., et al. (2008). Temporin a is effective in MRSA-infected wounds through bactericidal activity and acceleration of wound repair in a murine model. *Peptides* 29, 520–528. doi: 10.1016/j.peptides.2007.12.011
- Skerlavaj, B., Gennaro, R., Bagella, L., Merluzzi, L., Risso, A., and Zanetti, M. (1996). Biological characterization of two novel cathelicidin-derived peptides and identification of structural requirements for their antimicrobial and cell lytic activities. *J. Biol. Chem.* 271, 28375–28381. doi: 10.1074/jbc.271.45.28375
- Sørensen, O. E., Follin, P., Johnsen, A. H., Calafat, J., Tjabringa, G. S., Hiemstra, P. S., et al. (2001). Human cathelicidin, hCAP-18, is processed to the antimicrobial peptide LL-37 by extracellular cleavage with proteinase 3. *Blood* 97, 3951–3959. doi: 10.1182/blood.V97.12.3951
- Su, Y., Zhang, K., and Schluesener, H. J. (2010). Antimicrobial peptides in the brain. *Arch. Immunol. Ther. Exp.* 58, 365–377. doi: 10.1007/s00005-010-0089-7
- Sugrue, I., O'Connor, P. M., Hill, C., Stanton, C., and Ross, R. P. (2020). Actinomyces produces defensin-like bacteriocins (Actifensins) with a highly degenerate structure and broad antimicrobial activity. *J. Bacteriol.* 202. doi: 10.1128/JB.00529-19
- Szekeres, A., Leitgeb, B., Kredics, L., Antal, Z., Hatvani, L., Manczinger, L., et al. (2005). Peptaibols and related peptaibiotics of Trichoderma. A review. *Acta Microbiol. Immunol. Hung.* 52, 137–168. doi: 10.1556/AMicr.52.2005.2.2
- Terzi, H. A., Kulah, C., and Ciftci, I. H. (2014). The effects of active efflux pumps on antibiotic resistance in *Pseudomonas aeruginosa*. *World J. Microbiol. Biotechnol.* 30, 2681–2687. doi: 10.1007/s11274-014-1692-2
- Tillotson, G. S., and Theriault, N. (2013). New and alternative approaches to tackling antibiotic resistance. *F1000prime Rep.* 5:51. doi: 10.12703/P5-51
- Trotti, A., Garden, A., Warde, P., Symonds, P., Langer, C., Redman, R., et al. (2004). A multinational, randomized phase III trial of isegagan HCl oral solution for reducing the severity of oral mucositis in patients receiving radiotherapy for head-and-neck malignancy. *Int. J. Radiat. Oncol. Biol. Phys.* 58, 674–681. doi: 10.1016/S0360-3016(03)01627-4
- Turner, J., Cho, Y., Dinh, N. N., Waring, A. J., and Lehrer, R. I. (1998). Activities of LL-37, a cathelin-associated antimicrobial peptide of human neutrophils. *Antimicrob. Agents Chemother.* 42, 2206–2214. doi: 10.1128/AAC.42.9.2206
- Van Moll, L., De Smet, J., Paas, A., Tegtmeyer, D., Vilcinskas, A., Cos, P., et al. (2022). In vitro evaluation of antimicrobial peptides from the black soldier fly (*Hermetia Illucens*) against a selection of human pathogens. *Microbiol. Spectr.* 10:e0166421. doi: 10.1128/spectrum.01664-21
- Vargas-Casanova, Y., Rodríguez-Mayor, A. V., Cardenas, K. J., Leal-Castro, A. L., Muñoz-Molina, L. C., Fierro-Molina, R., et al. (2019). Synergistic bactericide and antibiotic effects of dimeric, tetrameric, or palindromic peptides containing the RWQWR motif against gram-positive and gram-negative strains. *RSC Adv.* 9, 7239–7245. doi: 10.1039/C9RA00708C
- Velivelli, S. L. S., Islam, K. T., Hobson, E., and Shah, D. M. (2018). Modes of action of a bi-domain plant defensin MtDef5 against a bacterial pathogen *Xanthomonas campestris*. *Front. Microbiol.* 9:934. doi: 10.3389/fmicb.2018.00934
- Wang, G., Wang, Y., Ma, D., Liu, H., Li, J., Zhang, K., et al. (2013). Five novel antimicrobial peptides from the Kuhl's wart frog skin secretions, *Limnodynastes kuhlii*. *Mol. Biol. Rep.* 40, 1097–1102. doi: 10.1007/s11033-012-2152-4
- Warnke, P. H., Voss, E., Russo, P. A., Stephens, S., Kleine, M., Terheyden, H., et al. (2013). Antimicrobial peptide coating of dental implants: biocompatibility assessment of recombinant human beta defensin-2 for human cells. *Int. J. Oral Max. Impl.* 28. doi: 10.11607/jomi.2594
- Whitchurch, C. B., Tolker-Nielsen, T., Ragas, P. C., and Mattick, J. S. (2002). Extracellular DNA required for bacterial biofilm formation. *Science* 295:1487. doi: 10.1126/science.295.5559.1487
- Wilton, M., Charron-Mazenod, L., Moore, R., and Lewenza, S. (2016). Extracellular DNA acidifies biofilms and induces aminoglycoside resistance in *Pseudomonas aeruginosa*. *Antimicrob. Agents Chemother.* 60, 544–553. doi: 10.1128/AAC.01650-15
- Wu, Z., Hansmann, B., Meyer-Hoffert, U., Gläser, R., and Schröder, J. M. (2009). Molecular identification and expression analysis of flaggrin-2, a member of the S100 fused-type protein family. *PLoS One* 4:e5227. doi: 10.1371/journal.pone.0005227
- Xie, M., Chen, K., Chan, E. W., and Chen, S. (2022). Synergistic antimicrobial effect of colistin in combination with econazole against multidrug-resistant *Acinetobacter baumannii* and its Persisters. *Microbiology Spectrum* 10:e0093722. doi: 10.1128/spectrum.00937-22
- Xie, H., Wei, J., and Qin, Q. (2016). Antiviral function of Tachyplesin I against iridovirus and nodavirus. *Fish Shellfish Immunol.* 58, 96–102. doi: 10.1016/j.fsi.2016.09.015
- Xie, F., Zan, Y., Zhang, X., Zhang, H., Jin, M., Zhang, W., et al. (2020). Differential abilities of mammalian Cathelicidins to inhibit bacterial biofilm formation and promote multifaceted immune functions of neutrophils. *Int. J. Mol. Sci.* 21. doi: 10.3390/ijms21051871
- Yaeger, L. N., Coles, V. E., Chan, D. C. K., and Burrows, L. L. (2021). How to kill *Pseudomonas*-emerging therapies for a challenging pathogen. *Ann. N. Y. Acad. Sci.* 1496, 59–81. doi: 10.1111/nyas.14596
- Yang, D., Chertov, O., Bykovskaia, S. N., Chen, Q., Buffo, M. J., Shogan, J., et al. (1999). Beta-defensins: linking innate and adaptive immunity through dendritic and T cell CCR6. *Science* 286, 525–528. doi: 10.1126/science.286.5439.52
- Yasir, M., Dutta, D., and Willcox, M. D. P. (2020). Activity of antimicrobial peptides and ciprofloxacin against *Pseudomonas aeruginosa* biofilms. *Molecules* 25. doi: 10.3390/molecules25173843
- Yu, S., and Ma, L. (2017). [Iron uptake and biofilm formation in *Pseudomonas aeruginosa*]. *Sheng wu gong cheng xue bao = Chin. J. Biotechnol.* 33, 1489–1512. doi: 10.13345/j.cjb.170140
- Zaïri, A., Ferrières, L., Latour-Lambert, P., Beloin, C., Tangy, F., Ghigo, J. M., et al. (2014). In vitro activities of dermaseptins K4S4 and K4K20S4 against *Escherichia coli*, *Staphylococcus aureus*, and *Pseudomonas aeruginosa* planktonic growth and biofilm formation. *Antimicrob. Agents Chemother.* 58, 2221–2228. doi: 10.1128/AAC.02142-13
- Zairi, A., Tangy, F., Bouassida, K., and Hani, K. (2009). Dermaseptins and magainins: antimicrobial peptides from frogs' skin-new sources for a promising spermicides microbicides-a mini review. *J. Biomed. Biotechnol.* 2009:452567. doi: 10.1155/2009/452567
- Zairi, A., Tangy, F., Ducos-Galand, M., Alonso, J. M., and Hani, K. (2007). Susceptibility of *Neisseria gonorrhoeae* to antimicrobial peptides from amphibian skin, dermaseptin, and derivatives. *Diagn. Microbiol. Infect. Dis.* 57, 319–324. doi: 10.1016/j.diagmicrobio.2006.11.006
- Zaïri, A., Tangy, F., and Hani, K. (2013). Dermaseptin S4 derivative K4K20S4: a potential candidate for development of a new microbicide contraceptive agent-an in vitro study. *Euro. J. Contracept. Reprod. Health Care* 18, 79–87. doi: 10.3109/13625187.2013.769950
- Zanetti, M. (2005). The role of cathelicidins in the innate host defenses of mammals. *Curr. Issues Mol. Biol.* 7, 179–196.
- Zasloff, M. (1987). Magainins, a class of antimicrobial peptides from *Xenopus* skin: isolation, characterization of two active forms, and partial cDNA sequence of a precursor. *Proc. Natl. Acad. Sci. U. S. A.* 84, 5449–5453. doi: 10.1073/pnas.84.15.5449
- Zhang, L., Rozek, A., and Hancock, R. E. (2001). Interaction of cationic antimicrobial peptides with model membranes. *J. Biol. Chem.* 276, 35714–35722. doi: 10.1074/jbc.M104925200
- Zhao, H., Gan, T. X., Liu, X. D., Jin, Y., Lee, W. H., Shen, J. H., et al. (2008). Identification and characterization of novel reptile cathelicidins from elapid snakes. *Peptides* 29, 1685–1691. doi: 10.1016/j.peptides.2008.06.008
- Zhao, Q., Shi, Y., Wang, X., and Huang, A. (2020). Characterization of a novel antimicrobial peptide from buffalo casein hydrolysate based on live bacteria adsorption. *J. Dairy Sci.* 103, 11116–11128. doi: 10.3168/jds.2020-18577
- Zheng, Z., Tharmalingam, N., Liu, Q., Jayamani, E., Kim, W., Fuchs, B. B., et al. (2017). Synergistic efficacy of *Aedes aegypti* antimicrobial peptide cecropin A2 and tetracycline against *Pseudomonas aeruginosa*. *Antimicrob. Agents Chemother.* 61. doi: 10.1128/AAC.00686-17
- Zhu, M., Liu, P., and Niu, Z.-W. (2017). A perspective on general direction and challenges facing antimicrobial peptides. *Chin. Chem. Lett.* 28, 703–708. doi: 10.1016/j.ccl.2016.10.001
- Zhu, N., Zhong, C., Liu, T., Zhu, Y., Gou, S., Bao, H., et al. (2021). Newly designed antimicrobial peptides with potent bioactivity and enhanced cell selectivity prevent and reverse rifampin resistance in gram-negative bacteria. *Euro. J. Pharm. Sci.* 158:105665. doi: 10.1016/j.ejps.2020.105665



OPEN ACCESS

EDITED BY

Octavio Luiz Franco,
Catholic University of Brasília (UCB), Brazil

REVIEWED BY

Carla Cugini,
The State University of New Jersey,
United States
Lucia Lombardi,
Imperial College London, United Kingdom

*CORRESPONDENCE

Yingxia Zhang
✉ zhangyingxia@hainanu.edu.cn

RECEIVED 26 July 2023

ACCEPTED 12 September 2023

PUBLISHED 26 September 2023

CITATION

Jiang S, Zha Y, Zhao T, Jin X, Zhu R, Wei S,
Wang R, Song Y, Li L, Lyu J, Hu W, Zhang D,
Wang M and Zhang Y (2023) Antimicrobial
peptide temporin derivatives inhibit biofilm
formation and virulence factor expression
of *Streptococcus mutans*.
Front. Microbiol. 14:1267389.
doi: 10.3389/fmicb.2023.1267389

COPYRIGHT

© 2023 Jiang, Zha, Zhao, Jin, Zhu, Wei, Wang,
Song, Li, Lyu, Hu, Zhang, Wang and Zhang. This
is an open-access article distributed under the
terms of the [Creative Commons Attribution
License \(CC BY\)](https://creativecommons.org/licenses/by/4.0/). The use, distribution or
reproduction in other forums is permitted,
provided the original author(s) and the
copyright owner(s) are credited and that the
original publication in this journal is cited, in
accordance with accepted academic practice.
No use, distribution or reproduction is
permitted which does not comply with
these terms.

Antimicrobial peptide temporin derivatives inhibit biofilm formation and virulence factor expression of *Streptococcus mutans*

Shangjun Jiang¹, Yanmei Zha², Ting Zhao¹, Xiao Jin¹,
Ruiying Zhu¹, Shuangshuang Wei², Rong Wang¹, Yanting Song¹,
Lushuang Li¹, Junchen Lyu³, Wenting Hu¹, Daqi Zhang⁴,
Manchuriga Wang⁵ and Yingxia Zhang^{1*}

¹Key Laboratory of Tropical Biological Resources of Ministry of Education, School of Pharmaceutical Sciences, Collaborative Innovation Center of One Health, Hainan University, Haikou, China, ²College of Life Sciences, Hainan University, Haikou, China, ³School of Science, Hainan University, Haikou, China, ⁴Department of Neurology, The First Affiliated Hospital of Hainan Medical University, Haikou, China, ⁵School of Animal Science and Technology, Hainan University, Haikou, China

Introduction: Temporin-GHa obtained from the frog *Hylarana guentheri* showed bactericidal efficacy against *Streptococcus mutans*. To enhance its antibacterial activity, the derived peptides GHaR and GHa11R were designed, and their antibacterial performance, antibiofilm efficacy and potential in the inhibition of dental caries were evaluated.

Methods: Bacterial survival assay, fluorescent staining assay and transmission electron microscopy observation were applied to explore how the peptides inhibited and killed *S. mutans*. The antibiofilm efficacy was assayed by examining exopolysaccharide (EPS) and lactic acid production, bacterial adhesion and cell surface hydrophobicity. The gene expression level of virulence factors of *S. mutans* was detected by qRT-PCR. Finally, the impact of the peptides on the caries induced ability of *S. mutans* was measured using a rat caries model.

Results: It has been shown that the peptides inhibited biofilm rapid accumulation by weakening the initial adhesion of *S. mutans* and reducing the production of EPS. Meanwhile, they also decreased bacterial acidogenicity and aciduricity, and ultimately prevented caries development in vivo.

Conclusion: GHaR and GHa11R might be promising candidates for controlling *S. mutans* infections.

KEYWORDS

antimicrobial peptides, temporin, *Streptococcus mutans*, antibiofilm, anti-caries

Introduction

Dental caries adversely affects more than 60% of school-aged children and most adults worldwide and has been identified as the third major disease endangering human health by the World Health Organization (WHO) after cardiovascular diseases and malignant tumors (Peres et al., 2019). When oral microorganisms attach to tooth surfaces, an acquired biofilm is formed, mainly composed of salivary glycoproteins. Subsequently, the initially established weak interaction between bacterial adhesins and cell membrane glycoprotein receptors

became stronger, followed by more bacteria aggregating to the attached bacteria, forming multispecies communities, known as dental plaque biofilms. Biofilms are constructed by highly organized oral microorganisms and are rich in proteins, extracellular polysaccharides (EPSs), carbohydrates, and nucleic acids, providing a perfect extracellular polymer matrix for the subsequent adhesion of oral cariogenic bacteria, in some cases leading to the progression of oral biofilms into cariogenic biofilms (Mosaddad et al., 2019). Among the oral bacteria, *Streptococcus*, *Actinomyces*, and *Lactobacilli* contribute more to secreting glucan to cell surfaces, thereby strengthening the adhesion of cariogenic microorganisms to teeth. At the same time, they ferment carbohydrates into lactic acid, which continuously demineralizes teeth and leads to the tooth decay (Ma et al., 2015; Lemos et al., 2019).

Streptococcus mutans is considered to be the dominant etiologic bacteria in dental caries (Lemos et al., 2019) and a potential risk factor in cardiovascular diseases, as it has been detected on cardiac valves and atherosclerotic plaques in patients (Nakano et al., 2006). *Streptococcus mutans* secretes a large amount of lactic acid synthesized by lactate dehydrogenase (LDH) in the presence of dietary sugars in oral cavity, causing serious damage to dental hard tissues (Ma et al., 2022). Most bacteria have difficulty growing in a low pH environment created by lactic acid, but *S. mutans* actively pumps protons out of the cells by consuming ATP to maintain intracellular pH and ensure growth, which leads to remarkable aciduricity (Harper and Loesche, 1983). In addition, *S. mutans* can synthesize extracellular polysaccharides (EPS) using dietary sucrose by its glucosyltransferases (GTFs) and fructosyltransferases (FTFs) (Zhang et al., 2021) and secrete them onto cell surfaces, enhancing the adhesion ability of *S. mutans*; meanwhile, they also provide a matrix for colonization of other cariogenic bacteria, leading the dental plaque biofilm formation (Klein et al., 2015). The microorganisms embedded in biofilms exhibit low metabolic activities and strong tolerance to antimicrobial reagents (Yue et al., 2018). Therefore, targeting *S. mutans* has become an effective way to prevent the onset of dental caries or treat early caries.

Antimicrobial peptides (AMPs) with broad-spectrum activities against pathogenic microorganisms have widely found in natural organisms, which are important components in the body's innate immune system and produced by almost all tissues and cells that are regularly exposed to microorganisms (Wiesner and Vilcinskas, 2010). The oral cavity is an open environment, in which the microbiome is acquired in childhood and will fluctuate in the proportion of species by such as diet and age. Once the homeostasis is broken, the pathogenic microorganisms might be predominant and cause oral diseases (Diamond et al., 2008). Several antimicrobial peptides, including statin, defensin, and LL-37, were founded in the oral epithelium and saliva and were considered to be the core defense system in the oral cavity (Guncu et al., 2015). Additionally, known as host defense peptides, these naturally occurring AMPs in the oral cavity are involved in regulating the innate immune response of host cells and exhibit resistance to oral pathogenic microorganisms (Griffith et al., 2022).

Temporin peptides, first found in amphibians, are one of the shortest naturally occurring peptide families, consisting of 10–14 amino acid residues. Because of their low manufacturing cost and diverse activities, these peptides are ideal candidates for therapeutic drug development (Wang et al., 2016). Through previous studies,

we cloned natural antimicrobial peptide temporin-GHa (GHa) (FLQHIIGALGHLF-NH₂) (Dong et al., 2017). In this article, we designed temporin-GHa11R (GHa11R) (FLQHIIGALGRFLF-NH₂) and temporin-GHaR (GHaR) (FLQRIIGALGRFLF-NH₂) to improve the antimicrobial and antibiofilm activities under physiological conditions by enhancing the net positive charges of GHa. The bacteriostatic effects and mechanism of action of the derived peptides were measured *in vitro*. The anti-carries properties of GHaR and GHa11R were studied in the caries rat model induced by *S. mutans*.

Materials and methods

Peptides, bacterial strains, and growth conditions

The peptides were synthesized by Ji'er Biochemical (Shanghai, China) with a purity greater than 95%. Before use, the peptides were dissolved in sterile deionized water at the concentration of 2 mM as stock solution, and diluted with phosphate buffered saline (PBS) to work concentration. *Streptococcus mutans* UA159 was purchased from Guangdong Microbial Culture Collection Center (Guangzhou, China) and cultured anaerobically in brain heart infusion broth (BHI; Thermo Fisher, CN) at 37°C under mixed gas conditions of 5% CO₂, 10% H₂, and 85% N₂ to logarithmic growth phase before experiments. The colony forming units (CFUs) and the optical density at 600 nm (OD₆₀₀) of the bacteria were plotted. OD₆₀₀ = 0.1 is equal to the density of *S. mutans* at 2×10^6 CFU/mL in BHI.

Streptococcus sanguis ATCC 10556 and *Porphyromonas gingivalis* ATCC 33277 were cultured anaerobically in BHI. *Bifidobacterium adolescentis* ATCC 15703 and *B. breve* ATCC 15700 were cultured anaerobically in MRS broth (MRS; Thermo Fisher, CN) containing 0.05% L-cysteine hydrochloride. *Lactobacillus acidophilus* ATCC 4356 was cultured anaerobically in MRS broth.

Peptide structure determination by circular dichroism (CD) spectroscopy

The peptides (1 mM) were dissolved in 10 mM PBS, 30 mM sodium dodecyl sulfate (SDS) and 50% (v/v) trifluoroethanol (TFE), respectively. The peptide spectrum was scanned by a CD spectrometer (Brighttime Chirscan, Applied Photophysics Limited, UK) at wavelengths of 190 nm to 260 nm with a speed of 10 nm/min.

Antibacterial activity assay

Equal volumes (50 μ L) of bacterial suspension (2×10^6 CFU/mL) and the peptide solution were mixed in wells on polystyrene plates (Corning, USA). After the plates were incubated anaerobically for 24 h, the OD₆₀₀ was measured. In negative control group, the peptides were replaced with PBS

only, and chlorhexidine (CHX) was used as a positive control. The minimum inhibitory concentration (MIC) is defined as the minimum concentration that inhibits the visible growth of bacteria within 24 h. The minimum bactericidal concentration (MBC) is the minimum concentration that kills 99% of bacterial cells determined by colony counting (Cao et al., 2020).

Time killing assay

The bacterial suspension (2×10^6 CFU/mL, 100 μ L) in BHI was mixed with the same volume of the peptide solution (3.1–12.5 μ M). The peptides were replaced with PBS only in the negative control. Aliquots of the mixtures were pipetted at 0, 15, 30, 45, 60, 90, 120, and 180 min, and plated on BHI agar after proper dilution. The plates were incubated anaerobically for 48 h, followed by colony counting.

Observation of bacteria by transmission electron microscopy (TEM)

After exposing to the peptides ($4 \times \text{MIC}$) for 1 h, the bacteria (1×10^9 CFU/mL) were collected, fixed with 2.5% glutaraldehyde and dehydrated in serially diluted ethanol solutions at room temperature. The peptides were replaced with PBS only in the negative control. After embedding in resin for 48 h at 60°C, the bacteria were sliced into 60–80 nm sections and loaded on 150 mesh copper mesh. After staining with 2% uranium acetate, the sections were washed with 70% ethanol solution and ultra-pure water, respectively, then re-stained with 2.6% lead citrate solution. After washing and drying overnight, the sections were observed by TEM (HT7800, Hitachi, Japan) (Zhang et al., 2022).

Cell membrane integrity assay

The cell membrane integrity was studied by fluorescent staining (Zhang et al., 2020). *Streptococcus mutans* (1×10^9 CFU/mL) pre-treated with the peptides ($1 \times \text{MIC}$) for 1 h was centrifuged and collected to remove the peptides. The bacteria were fixed with 4% paraformaldehyde for 1 h, followed by staining with PI solution (10 μ g/mL) for 15 min in the dark. Then the bacteria were collected by centrifugation and stained with DAPI solution (10 μ g/mL) for 15 min. The bacteria were washed, collected, and observed under an inverted fluorescence microscope with *S. mutans* treated with PBS as a negative control.

To confirm the impact of the peptides on *S. mutans* cell membranes, *S. mutans* treated with the peptides and stained with PI as described above were detected by flow cytometry (BF32366, Beckman Coulter, Brea, CA, USA).

Glycolytic pH drops and acid tolerance assay

Influence of the peptides on acid-producing capacity of *S. mutans* has been assessed (Wang et al., 2018). The bacterial

suspension was adjusted to 1×10^8 CFU/mL in BHI broth (the initial pH was 7.2) containing the peptides ($1/2 \times \text{MIC}$, at which the bacterial growth was not affected), and 1% (w/v) glucose was added to trigger glycolysis. In negative control, the peptides were replaced with PBS only. After incubating for 180 min, an aliquot of the suspension was sampled every 30 min for detecting the pH value using a glass electrode pH meter.

Acid tolerance of *S. mutans* was assessed (Svensater et al., 1997). Bacteria (1×10^6 CFU/mL) grown in tryptone-yeast extract medium (TYEM) broth (pH 7.5, containing 20 mM glucose) were transferred to BHI culture medium (pH 5.5) with or without the peptides ($1/2 \times \text{MIC}$). The same volume of suspension was diluted and applied to BHI agar for determining the number of viable bacteria. After the remaining suspension was incubated for 2 h, the pH was immediately reduced to the killing pH (3.0) for *S. mutans* by adding 20% hydrochloric acid and further incubated for 3 h. The suspensions were also plated. After incubating all plates anaerobically for 48 h, the total CFUs were calculated.

Lactic acid production assay

The bacterial suspensions (1×10^6 CFU/mL, 2 mL) were added to each well containing a coverslip on a 24-well microtiter plate, and incubated anaerobically for 24 h. After discarding planktonic bacteria, the coverslips covered by biofilms were removed to a new 24-well plate, and treated by the peptides ($1/2 \times \text{MIC}$, containing 2% sucrose) in buffered peptone water (BPW). In negative control, the peptides were replaced with PBS only. After incubating anaerobically for 180 min, the supernatant was collected, and the production of lactic acid was measured by lactic acid measurement kit (Solarbio, China). OD₅₇₀ was recorded and the concentration of lactic acid was calculated (Chen et al., 2020).

Cell membrane permeabilization and F₁F₀-ATPase assay

The permeabilized cells were prepared and the activity of F₁-F₀ ATPase was determined (Xu et al., 2011). In general, *S. mutans* was collected and dispersed in Tris-HCl buffer (pH 7.0) containing 10 mM MgSO₄ and 10% (v/v) toluene. After swirling for 1 min, the bacterial suspension was incubated for 5 min at 37°C and rapidly frozen in liquid nitrogen. The frozen cells were quickly thawed and re-frozen twice. After collecting and exposing to the peptides ($1/2 \times \text{MIC}$) for 120 min, the bacteria were collected by centrifugation and resuscitated in Tris-maleate buffer (pH 7.0, containing 10 mM MgCl₂). Finally, 5 mM ATP was added to trigger F₁-F₀ ATPase activity. In negative control, the peptides were replaced with PBS only. The released phosphate was identified (Bencini et al., 1983).

The assay of inhibition biofilm formation

The effect of the derived peptides on the biofilm formation of *S. mutans* was evaluated (de Breij et al., 2018). Briefly, an equal volume of bacterial suspension (2×10^6 CFU/mL) in BHI broth

containing 1% sucrose (BHIs) was mixed with the peptide solution (0.8 to 25 μ M) on a 96-well polystyrene plate (Corning, USA), and incubated anaerobically for 24 h. In negative control, the peptides were replaced with PBS only. After discarding the supernatant, the remaining biofilm was rinsed twice with PBS, fixed by methanol solution and thoroughly dried. CV solution (0.1%) was added to stain the biofilm for 15 min. After the excess dye was thoroughly washed with PBS, 200 μ L of ethanol was added and OD₅₉₅ was determined.

Bacterial adhesion assay

The activity of the derived peptides on the bacterial adhesion ability was evaluated both on 96-well polystyrene plate surfaces and saliva-coated surfaces (Zhang et al., 2020). Bacterial suspension (1×10^9 CFU/mL) was treated with the peptides ($4 \times$ MIC) for 15 min and the unbound peptides were removed by centrifugation ($3,000 \times g$, 3 min). In negative control, the peptides were replaced with PBS only. After resuspending in BHI broth, an aliquot of the suspension was pipetted, plated on BHI agar, and cultured anaerobically for 48 h. The CFUs were calculated to determine the number of viable bacteria. A 96-well polystyrene plate was precoated with 100 μ L of artificial saliva at 37°C for 15 min. After the saliva was removed, the saliva-coated plate was prepared. The remaining suspension (100 μ L) was added to a polystyrene plate or a saliva-coated plate and incubated for 1 h under static conditions. After discarding the supernatant, the plates were gently washed twice with PBS to remove unadhered bacteria. After adding 200 μ L of PBS to each well, all the plates were sonicated three times at a power of 120 W and a frequency of 40 kHz on ice for 90 s with an interval of 30 s. The sonication fluid was plated and the CFUs were numbered. The bacterial adhesion rate was expressed as the CFUs of adhesive bacteria divided by the CFUs of the viable bacteria.

Cell surface hydrophobicity assay

The bacterial suspension (1×10^9 CFU/mL) was incubated with the derived peptides (0.8–25 μ M) in Phosphate urea magnesium (PUM) buffer for 20 min, and the OD₅₅₀ of the bacterial suspension was measured. Cetane (200 μ L) was added to the remaining bacterial suspension, vortexed, and settled for 30 min. In negative control, the peptides were replaced with PUM only. The supernatant was pipetted to determine the OD₅₅₀. The degree of changes in surface hydrophobicity of *S. mutans* was shown as a percentage decrease of the OD₅₅₀ (Kim et al., 2019).

Water-insoluble EPS measurement

The production of water-insoluble EPS in biofilms was evaluated by phenol-sulfuric acid method (Abdel-Aziz et al., 2020). Briefly, equal volumes of bacterial suspension (1×10^6 CFU/mL) and the peptides ($1 \times$ MIC) were mixed in a 24-well polystyrene plate and incubated anaerobically for 24 h to generate biofilms. In

negative control, the peptides were replaced with PBS only. After discarding planktonic bacteria, the biofilms were collected and washed twice to clean out water-soluble EPS. After centrifugation, the pellet was re-suspended in 1 M NaOH solution (200 μ L) for 2 h to extract water-insoluble EPS. Finally, 5% frozen phenol and sulfuric acid were added to the mixture at 1:1:5 (volume ratio), incubated for 1 h, followed by measuring OD₆₂₅.

Confocal laser scanning microscope (CLSM) observation

The EPS distribution in biofilms was observed by CLSM (Deng et al., 2021). Equal volumes (1 mL) of the bacterial suspension (2×10^6 CFU/mL) in BHIs broth and the peptides solution ($1 \times$ MIC) were mixed in each well containing a coverslip on a 24-well polystyrene plate. In negative control, the peptides were replaced with PBS only. Alexa Fluor 647 glucan (1 μ mol/L) was used to label the dextran conjugate for 24 h. After that, *S. mutans* nucleic acids were labeled with SYTO 9 (2.5 μ mol/L). CLSM (TCS SP8, LEICA, Germany) was used to observe.

The expression of virulence genes by quantitative real-time reverse transcription PCR (qRT-PCR)

The expression levels of virulence genes in *S. mutans* were measured by qRT-PCR with 16S rRNA serving as a quantified internal control (Xiong et al., 2020; Aqawi et al., 2021). *Streptococcus mutans* in the logarithmic growth phase was diluted to 1×10^6 CFU/mL in BHIs broth, pretreated with the peptides ($1/2 \times$ MIC, diluted with BHIs) for 8 h and total RNA was purified. In negative control, the peptides were replaced with PBS only. The first-strand cDNA was synthesized using RT kit (TES201, Tsingke, China). The tested genes and primers are listed (Table 1). The reaction was performed on a CFX96 real-time system (CFX Connect, Bio-Rad, USA). Gene expression was presented by using the $2^{-\Delta \Delta C_t}$ method and normalized to the 16S rRNA level.

Cytotoxicity assay on human oral keratinocytes (HOK)

The cytotoxicity of the peptides was measured by the Cell Counting Kit-8 (CCK-8) (Utheim et al., 2016). Briefly, HOK cells (5,000 cells/well) were inoculated in a 96-well plate. After reaching 80% confluence, the cells were exposed to the peptides (3.1, 6.2, 12.5, 25, 50, and 100 μ M) for 2 h. In negative control, the peptides were replaced with PBS only. Then CCK-8 solution (10 μ L) was added and incubated for 2 h. OD₄₅₀ was measured.

Anti-caries assay on a caries rat model

The anti-caries effect of GHaR and GHa11R was detected in a caries rat model infected by *S. mutans* (Wang et al., 2018;

TABLE 1 The primers used for quantitative real-time reverse transcription PCR.

Gene	Forward primer	Reverse primer
16S RNA	AGCGTTGTCCGATTATTTG	CTACGCATTTCACCGCTACA
gtfB	CACTATCGGCGGTTACGAAT	CAATTGGAGCAAGTCAGCA
gtfC	GATGCTGCAAACTTCGAACA	TATTGACGCTGCGTTTCTTG
gtfD	TTGACGGTGTTCGTGTTGAT	AAAGCGATAGGCGCAGTTTA
ldh	AAAAACCAGGCGAACTCGC	CTGAACGCGCATCAACATCA
atpD	TGTTGATGGTCTGGGTGAAA	TTTGACGGTCTCCGATAACC

Tian et al., 2022). Twenty-seven *Sprague Dawley* (SD) male rats aged 18 days (Slyke Jingda Experimental Animal Co., Ltd., China) were fed food (supplemented with 0.1% ampicillin) and water (containing 4,000 U/mL penicillin) for 3 days to sterilize the oral endogenous microorganisms. At the age of 22–24 days, 24 rats were anesthetized by isoflurane and infected orally with 200 μ L of *S. mutant* (1×10^9 CFU/mL) once daily. Twenty-four hours after the last infection, a sterile cotton swab was used to scratch the oral cavity of the rats, which was then rinsed with PBS. The solution was plated on Mitis Salivarius agar (MSA) containing 20 U/mL bacitracin to confirm colonization. The infected rats were randomly divided into 4 groups with 6 rats in each, including the negative control group (UA159 + PBS), the positive control group (UA159 + CHX), and two peptide-treated groups (UA159 + GHaR and UA159 + GHa11R). Uninfected rats served as the blank group. The rat teeth were evenly brushed with a sterilized cotton swab soaked with 200 μ L of PBS, CHX, GHaR or GHa11R three times a week for 8 weeks. All rats were fed Keyes 2,000 # cariogenic diet and purified water containing 5% sucrose. The health status of the rats was recorded. At the age of 81 days, after suffocation by CO₂, the left and right mandibles were removed. After autoclaving at 121°C for 10 min, the mandibles were cleaned by peeling off the remaining tissue, washed with PBS, and stained overnight with 0.4% murexide. The main groove of the tooth was exposed by a proximal sagittal semi-section and observed under a stereo microscope (M205 FA, LEICA, Germany) to assess the caries level according to a modified Keyes score. An “E” score of 1 indicates that the caries involved only the enamel. A “D” score of 2 indicates that the caries did not exceed 1/4 of the dentin thickness. A “Dm” score of 3 indicates that the range of caries was 1/4–3/4 of the dentin thickness. A “Dx” score of 4 indicates that the caries was more than 3/4 of the dentin thickness. The score for each mandible was the sum of the scores for the first and second molars.

Statistical analysis

The experiments were performed independently three times in triplicates. The data in the tables and graphs was a representation of one biological replicate and presented as the mean \pm standard deviation (SD). The data were analyzed statistically using *t*-test with the GraphPad Prism, with a *P*-value of less than 0.05 considered

statistically significant when comparing the treated groups to the control groups.

Results

The characteristics and structures of GHa and its derived peptides

In our previous study, we performed sequence alignment on different AMPs and found that the positively charged amino acid lysine (Lys, K) in temporin peptides occurs more frequently than arginine (Arg, R) and histidine (His, H), while in the antibiofilm peptides, R and K are similarly chosen over H (Xie et al., 2019). In order to obtain derived peptides with antibiofilm efficacy, we used R to replace the H at GHa to design GHaR and GHa11R. Compared with GHa, the charge, amphiphilic index (AI) and Boman index (BI) of GHaR and GHa11R increased, and the grand average of hydropathy value (GRAVY) decreased (Table 2). Generally, α -helical AMPs with high amphiphilicity show strong activity; meanwhile their GRAVY is positive, and BI is negative or close to 0 (Saporito et al., 2018). The changes in the physiochemical characteristics of the derived peptides may enhance their antibacterial activities.

The structures of the peptides are shown in Figure 1. The spiral wheel of the peptides presented that on the one side the hydrophilic amino acid residues were located, while the hydrophobic residues were arranged on the opposite side, forming the hydrophilic and hydrophobic surfaces, respectively. The CD spectrum revealed that the peptides showed a random-coiled structure in aqueous conditions, while dissolved in a solvent of SDS (30 mM) or TFE (50%), they shown typical α -helical structures, indicating that GHa and the derived peptides had an amphiphile α -helical structure in simulated bacterial membranes. The predicted 3D structure of the peptides is also an α -helix structure. Meanwhile, the increased amphiphilicity of the derived peptides indicated that they have a more stable amphipathic α -helix structure than that of the parent peptide (Abbassi et al., 2013).

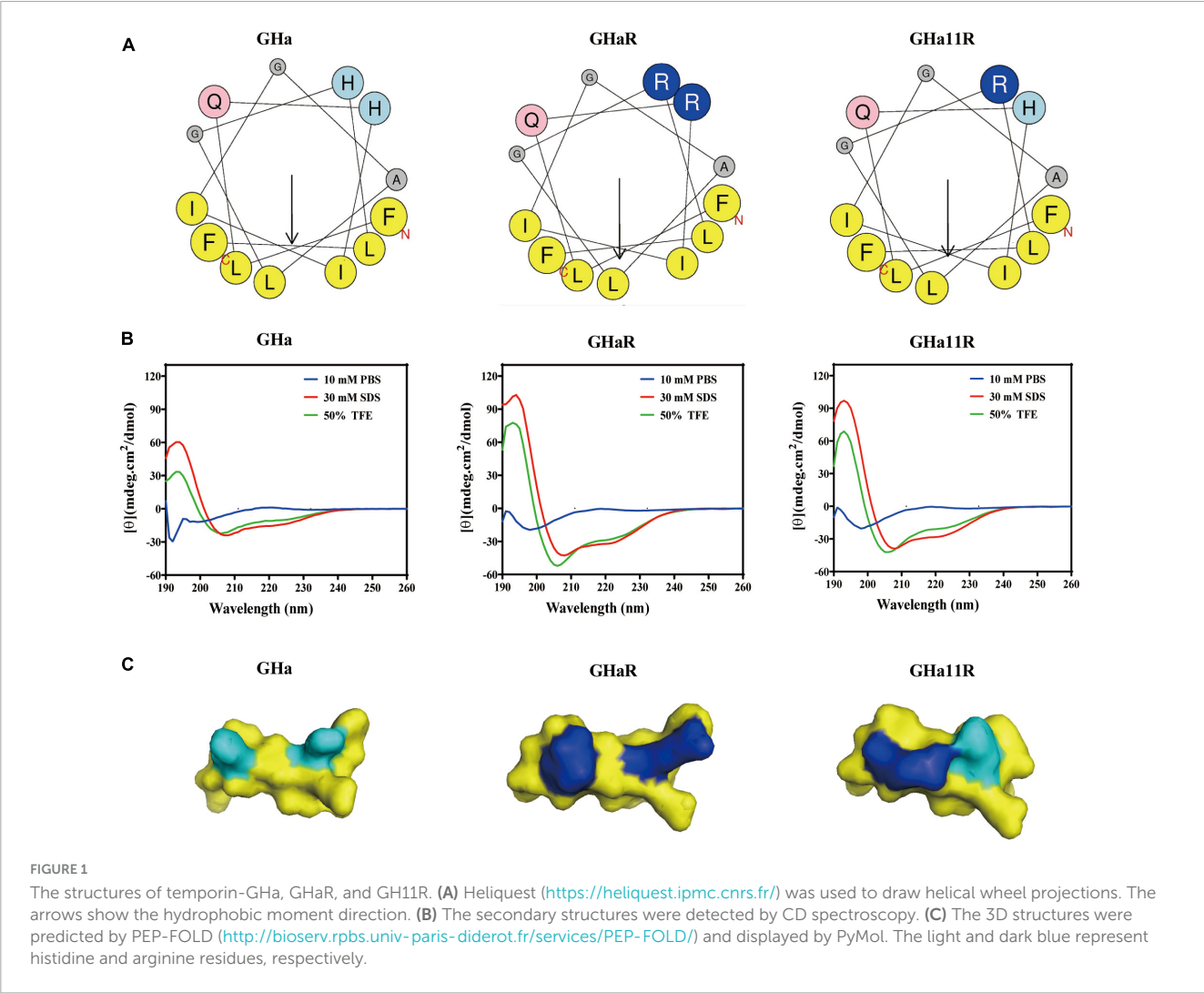
The peptides show stronger antibacterial activity against *S. mutans* than against the tested probiotics

GHa has mild antibacterial activity against *S. mutans* with MIC of 12.5 μ M and MBC of 25 μ M. By mutating the amino acid residues of GHa, the ability of the derived peptides GHa11R and GHaR to inhibit *S. mutans* growth was improved, with the MIC decreased by 4 times and 8 times, respectively. The antibacterial efficacy of the peptides against several oral etiologic bacteria and probiotics was detected. As shown in Table 3, the peptides also showed good inhibitory activity against the oral pathogenic bacteria *S. sanguinis* and *P. gingivalis*, which are associated with oral infections and cardiovascular diseases. Comparatively, GHa and its derived peptides against pathogenic bacteria had lower MIC/MBC values; however, they showed higher antibacterial concentrations against the tested probiotics. CHX exhibits strong antibacterial efficacy against both pathogenic bacteria and probiotics.

TABLE 2 The characteristics of temporin-GHa, GHaR, and GHa11R.

Peptides	Amin acid sequence	MW	Charge ^a	pI ^a	AI ^a	BI ^b	GRAVY ^b
GHa	FLQHIIGALGHLF	1464.76	1	7.67	0.32	−1.49	1.315
GHaR	FLQRIIGALGRLF	1502.86	2	12.1	0.47	0.08	1.115
GHa11R	FLQHIIGALGRLF	1483.87	1.5	10.5	0.4	−0.7	1.215

^aCalculated by Database of Antimicrobial Activity and Structure of Peptides (DBAASP) <https://www.dbaasp.org/home>. isoelectric point (pI), amphiphilicity index (AI).
^bPredicted by Antimicrobial Peptide Database (APD3) <https://aps.unmc.edu/AP/>. Boman index (BI, kcal/mol).



The peptides exerted antibacterial activity by damaging cell membrane integrity

The bacteriostatic activity of GHa, GHaR, and GHa11R against planktonic *S. mutans* was investigated (Figure 2A). GHaR inhibited *S. mutans* growth at 3.1 μ M and GHa11R at 6.2 μ M, similar to CHX. The time-killing kinetics demonstrated that the killing effect of these peptides on *S. mutans* was concentration- and time-dependent. After treatment with 6.2 μ M GHaR and GHa11R, all bacteria were killed within 90 ~ 120 min (Figure 2B). The microscopic morphology of *S. mutans* was observed under TEM.

As shown in Figure 2C, the bacterial cell membrane was destroyed, resulting in leakage of cellular contents.

Fluorescence staining revealed the membrane destruction mechanism of the peptides

As shown in Figure 2D, after the bacteria were treated with the peptides (1 \times MIC), PI penetrated cell membranes, showing red fluorescence, which indicated that the structure of *S. mutans* cell membranes was destroyed. Flow cytometry was used to further

TABLE 3 The MIC/MBC of the derived peptides against pathogenic bacteria and probiotics.

Stains	MIC/MBC (μ M)			
	GHa	GHaR	GHa11R	CHX
<i>Streptococcus mutans</i> UA159	12.5/25	1.6/3.1	3.1/6.2	0.8/1.6
<i>Streptococcus sanguis</i> ATCC 10556	1.6/3.1	12.5/12.5	6.2/12.5	0.8/1.6
<i>Porphyromonas gingivalis</i> ATCC 33277	12.5/25	3.1/6.2	6.2/12.5	0.8/1.6
<i>Bifidobacterium adolescentis</i> ATCC 15703	50/50	6.2/12.5	25/25	3.1/12.5
<i>Bifidobacterium breve</i> ATCC 15700	100/200	50/50	100/100	25/25
<i>Lactobacillus acidophilus</i> ATCC 4356	25/50	50/100	50/100	25/50

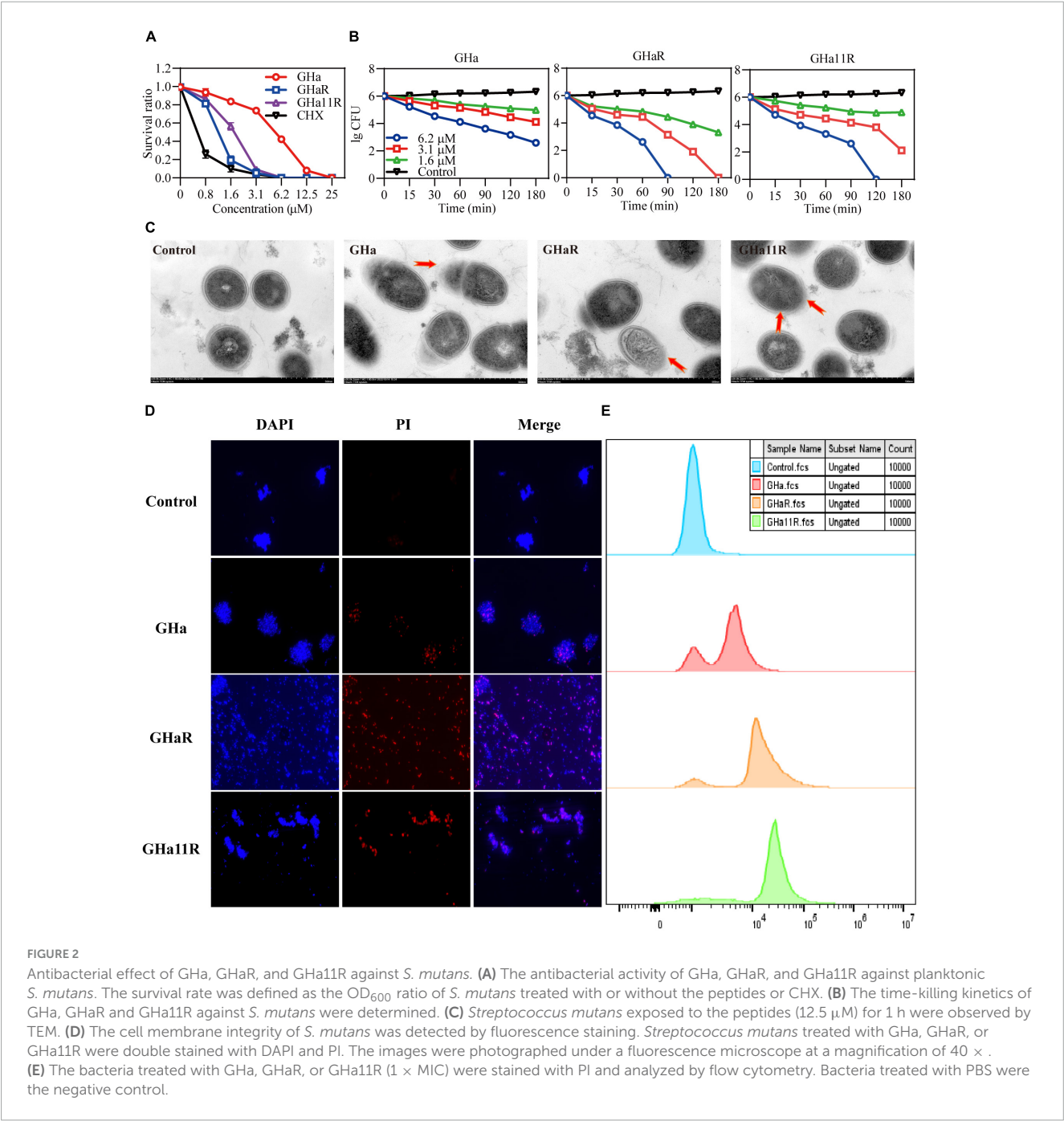


FIGURE 2 Antibacterial effect of GHa, GHaR, and GHa11R against *S. mutans*. (A) The antibacterial activity of GHa, GHaR, and GHa11R against planktonic *S. mutans*. The survival rate was defined as the OD₆₀₀ ratio of *S. mutans* treated with or without the peptides or CHX. (B) The time-killing kinetics of GHa, GHaR and GHa11R against *S. mutans* were determined. (C) *Streptococcus mutans* exposed to the peptides (12.5 μM) for 1 h were observed by TEM. (D) The cell membrane integrity of *S. mutans* was detected by fluorescence staining. *Streptococcus mutans* treated with GHa, GHaR, or GHa11R were double stained with DAPI and PI. The images were photographed under a fluorescence microscope at a magnification of 40 × . (E) The bacteria treated with GHa, GHaR, or GHa11R (1 × MIC) were stained with PI and analyzed by flow cytometry. Bacteria treated with PBS were the negative control.

detect the membrane destruction efficiency of the peptides on *S. mutans*. In comparison with the untreated bacteria, after 1 h of treatment with the peptides ($1 \times \text{MIC}$), a large number of *S. mutans* stained by PI was detected (Figure 2E).

The peptides decreased the acidogenicity and aciduricity of *S. mutans*

As shown in Figure 3A, the pH value of the suspension in the control group declined sharply from 7.4 to 4.5 within 180 min. After exposure to the peptides, the drop in pH was alleviated and decreased to 5.4, indicating that the peptides inhibited the acidogenicity of *S. mutans*, especially GHaR and GHa11R. The effect of the peptides on the acid production of *S. mutans* was further determined (Figure 3B). In comparison with GHa, GHaR and GHa11R reduced lactic acid production by 50% within 180 min. After 3 h incubation under killing pH conditions, 10% of the *S. mutans* bacteria without the peptide treatment still survived, while the treated bacteria decreased to less than 1% of their original population (Figure 3C). Meanwhile, the activity of $F_1\text{-}F_0\text{-ATPase}$ related to acid tolerance of *S. mutans* decreased by 50–70% after being treated with $1/2 \times \text{MIC}$ of the peptides for 120 min (Figure 3D).

The peptides inhibited the attachment of *S. mutans* biofilms

As shown in Figure 4A, when *S. mutans* was incubated with sub-MICs of GHaR and GHa11R for 24 h, more than 25–30% of the bacterial biomass in the *S. mutans* biofilms has been inhibited. Furthermore, we explored the attachment ability of the bacteria to polystyrene plates and saliva-coated polystyrene plates (Figure 4B). After treatment with GHaR and GHa11R, more than 60% of the *S. mutans* attached to polystyrene plates was reduced, indicating that the peptides disturbed the initial adhesion of *S. mutans*, thus inhibiting biofilm formation. Applying saliva to the surface of the polystyrene plate significantly enhanced bacterial attachment, with doubling biofilm formation in the negative control. However, both GHaR and GHa11R still showed effective efficacy in preventing the initial attachment of biofilms.

To explain how the peptides impact the adhesion ability of *S. mutans*, the hydrophobicity of bacterial surfaces exposed to the peptides was investigated. Nearly 40% of *S. mutans* in the negative control was transferred from the aqueous phase to the organic phase. After treatment, approximately 20% of *S. mutans* was transferred, and the percentage decreased dose-dependently (Figure 4C), confirming that the peptides decreased the hydrophobicity of *S. mutans*.

The peptides reduced the EPS production in biofilms

The glucan labeled by Alexa Fluor 647 can be embedded into EPS during the synthesis of the *S. mutans* biofilm matrix, showing

red fluorescence under CLSM. The biofilms in the blank control were tightly packed, and EPS was highly expressed (Figure 4D). Although GHa ($1/2 \times \text{MIC}$) showed no significant efficacy on the *S. mutans* biofilms, GHaR and GHa11R destroyed the confluent, tightly packed layers of the biofilms, resulting in scattered clusters of bacteria in the biofilms. As shown in Figure 4E, the EPS in biofilms decreased significantly after exposure to the derived peptides. The inhibitory activity of the peptides on EPS production has been explored (Figure 4F). The water-insoluble EPS production had been decreased by 40–50% after the bacteria were exposed to GHaR and GHa11R.

The peptides downregulated virulence gene expression in *S. mutans*

As shown in Figure 5A, the tested genes were downregulated after treatment with sub-MICs of the peptides, especially the *gtfB* and *gtfC*, which encode water-insoluble EPS, and the *ldh*. GHaR and GHa11R reduced the expression of the *gtfB* and *gtfC* genes by 70 to 80%. GHa11R reduced the expression of the *gtfD* gene by more than 99%. For the *ldh* gene, both GHaR and GHa11R reduced the expression of the *gtfD* gene by more than 95%.

The peptides showed less cytotoxicity

After HOK cells were cocultured with GHa and its derived peptides, cell viability was detected. The results showed that GHa and GHa11R had no toxic effect on HOK cells at a concentration of 100 μM (Figure 5B). GHaR showed a weak inhibitory effect on cell viability at concentrations greater than 12.5 μM . However, the cytotoxicity was not dose dependent, and at least 80% of HOK cells treated with 100 μM GHaR were still alive.

The peptides showed anti-carries activity in rats

The derived peptides exhibited better antibacterial efficacy than that of GHa, so we investigated whether GHaR and GHa11R reduce the incidence and severity of tooth decay in a rat caries model (Figure 6A). As shown in Figure 6B, all molars of the rats inoculated with *S. mutans* showed progressive development of dental caries. As indicated by the arrows, the lesions on the sulci surface were significantly more extensive in the control group. The total Keyes scores in mandibular first molar and second molar of the rats were evaluated. The severity of dental caries was decreased by treated with 25 μM GHaR and GHa11R (Figure 6C). GHaR showed effective anti-carries activity as good as CHX.

Discussion

The oral microbiome consisting of bacteria, fungi, and viruses, is a complicated microbial ecosystem in living organisms (Jiang et al., 2021). The balance of the microbiome is crucial for

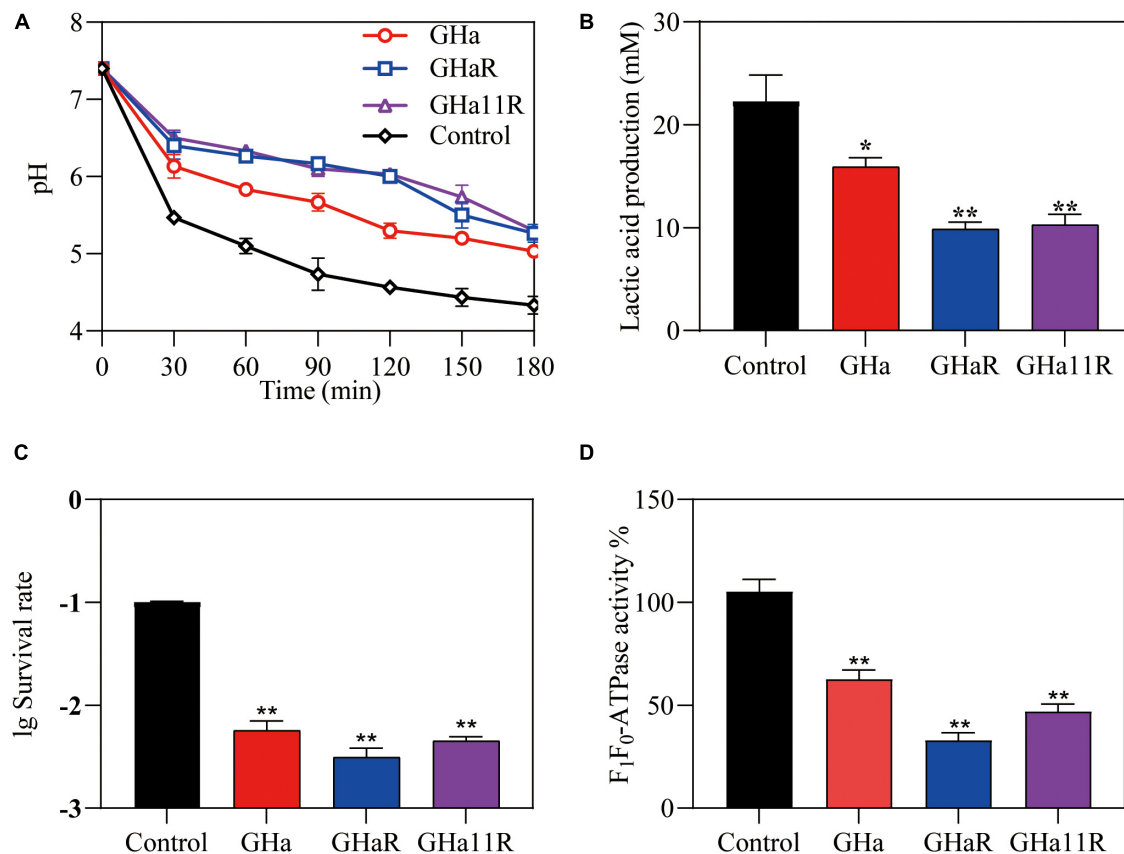


FIGURE 3

Effects of GHa and its derived peptides on the acidogenicity and aciduricity of *S. mutans*. (A) Effects of the peptides on glycolytic pH, (B) lactic acid production, and (C) aciduricity of *S. mutans* were assayed. (D) The F₁-F₀ ATPase activity of *S. mutans* after 120 min of treatment with GHa, GHaR and GHa11R was determined. The final concentration of the peptides was 1/2 × MIC. *Represents comparison with the control. **P* < 0.05 and ***P* < 0.01.

maintaining oral health; if lost, predominant pathogens may cause oral diseases, such as dental caries, periodontitis and oral mucositis (Lamont et al., 2018). AMPs, the important molecules in the innate immune system, participate in defending oral microbial infection and controlling resident microbial populations with other innate defense molecules in the oral cavity (Devine, 2003). The cell walls of bacteria, both Gram-positive and Gram-negative, are rich in teichoic acid and lipopolysaccharide, respectively, resulting in negatively charged surfaces, whereas most AMPs have net positive charges due to the basic amino acid residues in their amino acid sequences (Savini et al., 2020). When bacteria are exposed to AMPs, the positive charges of AMPs interact with the negative charges on the bacterial cell surfaces through electrostatic forces, which results in AMPs penetrating the bacterial cells or damaging the cell membranes to exert bactericidal efficacy (Ho et al., 2013).

Histatins are the main AMPs in saliva and are rich in histidine (Griffith et al., 2022), aggregating and integrating into the lipid bilayer of cell membranes and ultimately causing microbial cell death (Lynge Pedersen and Belstrom, 2019). Inspired by the role of histatins in oral defense, we applied the same histidine-rich cationic AMP temporin-GHa to *S. mutans*, and it showed antibacterial activity. It was calculated that the average frequency of occurrence of the positively charged amino acid residues H, R, and K are 2.14%, 5.97%, and 9.72% in 3,569 AMPs in APD3 (Wang et al., 2016), indicating that K and R are the most abundant positively

charged amino acids in AMPs. Comparatively, H (pKa 6.5) carries no charge at physiological pH and only a positive charge at low pH (Kacprzyk et al., 2007). The amino acid sequence was changed by substituting R for H, at position 11 to produce the derived peptide GHa11R, which improved the interaction of GHa with the anionic membranes of *S. mutans*. The antibacterial activity of GHa11R (MIC of 3.1 μM) was 4 times higher than that of GHa, and the efficacy of inhibiting biofilm formation was also significantly improved, while the cytotoxicity was similar to that of GHa, without showing a toxic effect on HOK cells at a concentration of 100 μM. To further explore the contribution of the positive charges on the antimicrobial activity and cytotoxicity of GHa, two H amino acid residues on GHa were substituted by R, leading to GHaR, whose antibacterial performance was also enhanced with an MIC of 1.6 μM, and the bactericidal efficacy on *S. mutans* was faster than that of GHa11R. Although the cytotoxicity of GHaR to HOK cells was increased, at least 80% of HOK cells survived at a concentration of 100 μM. We confirmed that the increase of the net positive charges in peptides improves the activity of AMPs and correspondingly enhances their toxicity to cells (Ramezanzadeh et al., 2021).

The mechanism of action of the peptides on *S. mutans* was determined. Both DAPI and PI can bind to DNA, while DAPI passes through intact cell membranes and PI penetrates damaged cell membranes. *S. mutans* treated with GHa and its derived

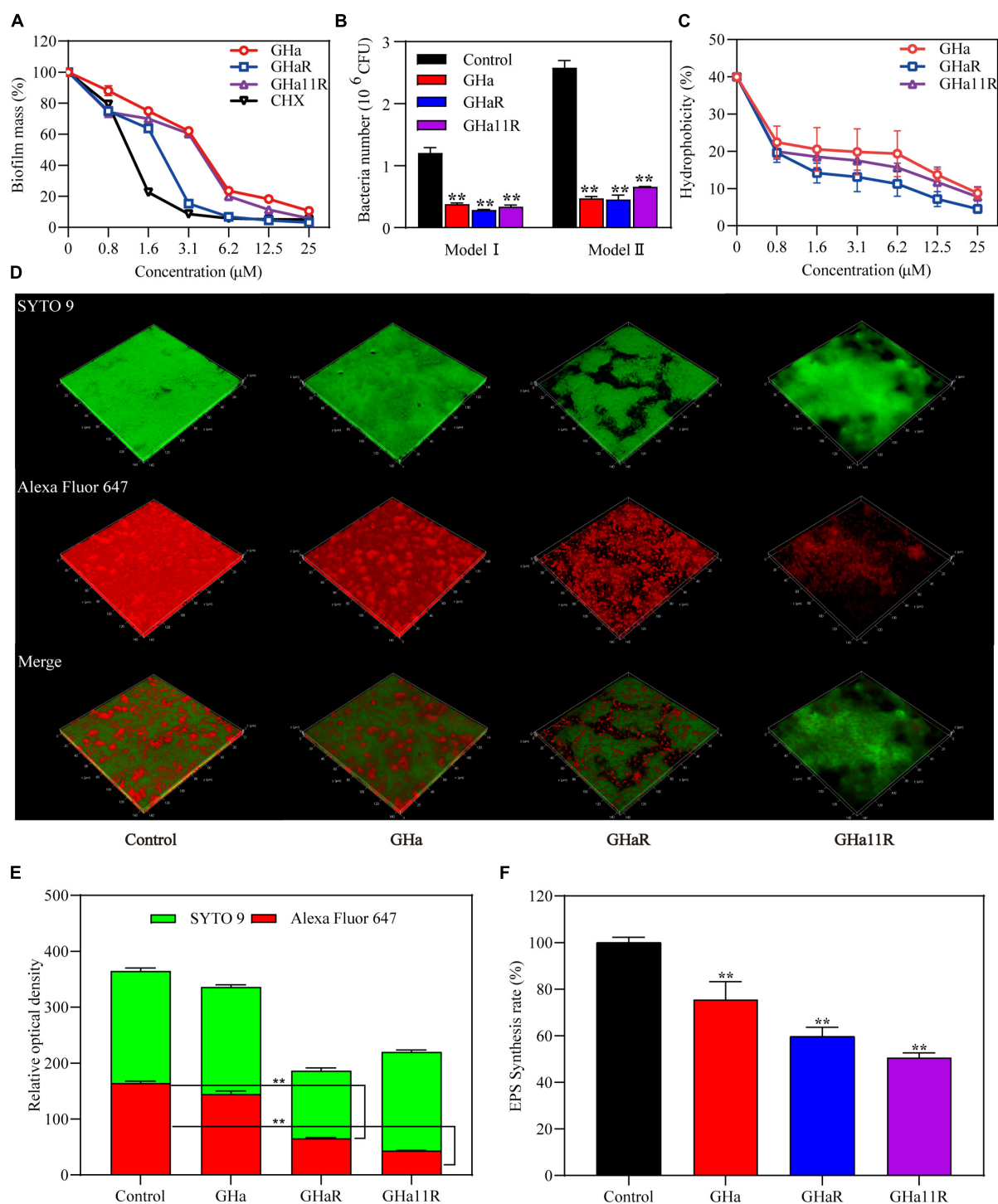


FIGURE 4

The peptides inhibited *S. mutans* biofilm formation. (A) The peptides inhibited the formation of biofilms. After incubation with the peptides for 24 h, the biomass in the biofilms was measured. (B) The peptides inhibited the initial bacterial adhesion. Model I represents *S. mutans* adhesion on polyethylene plates, and Model II represents *S. mutans* adhesion on polyethylene plates precoated with artificial saliva. (C) The peptides reduced the hydrophobicity of *S. mutans*. (D) Observation of *S. mutans* biofilms by CLSM. Representative images of glucan distribution and biofilms are presented. EPS marked with Alexa Fluor 647 are in red; the bacteria labeled with SYTO 9 are in green. Images were taken at 64 × magnification. (E) Quantitative data of bacteria and EPS biomass. (F) The peptides reduced EPS production in biofilms of *S. mutans*. *Represents comparison with the control. ** $P < 0.01$.

peptides showed bright red fluorescence after double staining with PI and DAPI, indicating that the membrane permeability was increased and the membrane integrity was damaged. The

results were further confirmed by flow cytometry assay. The clear and smooth cell surface edge of the peptide-treated bacteria was lost; the large-scale damage of the membranes and the rupture

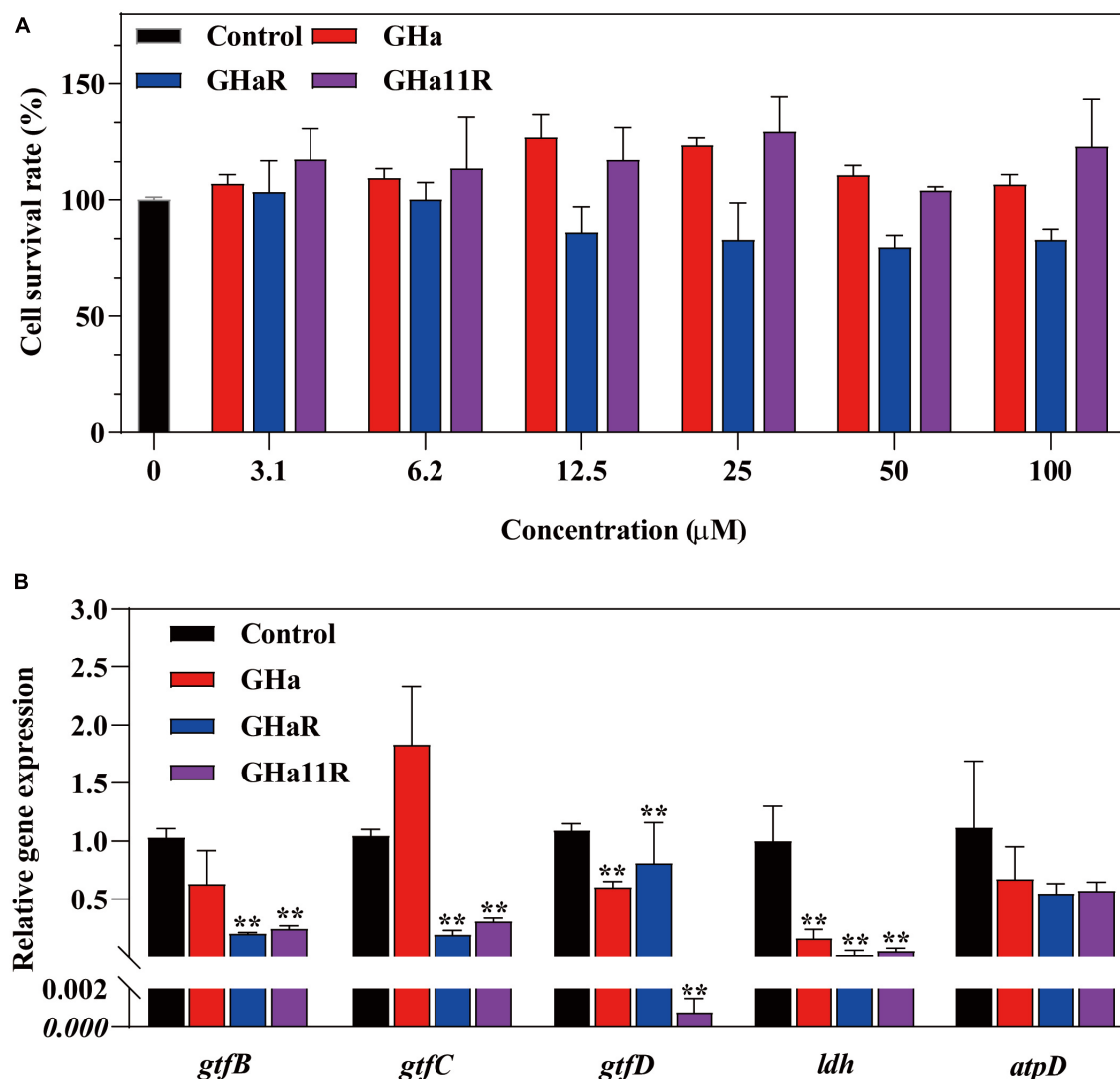


FIGURE 5

(A) The cytotoxicity of GHa, GHaR and GHa11R was tested by CCK-8 assay on human oral keratinocytes. *Represents comparison with the control. (B) The effect of GHa, GHaR, and GHa11R on virulence gene expression in *S. mutans* biofilms was tested by qRT-PCR. Gene expression in the peptide-treated *S. mutans* in comparison with the untreated control was quantified. ** $P < 0.01$.

of the membrane surfaces were clearly observed through SEM. Therefore, GHa and its derived peptides exerted their killing effect on *S. mutans* by increasing the cell membrane permeability, leading to the destruction of their integrity and leakage of intracellular components.

The cariogenic potential of *S. mutans* is regulated mainly by its virulence factor related genes (Shanmugam et al., 2020). Through our research, *S. mutans* carotenoid virulence factors were blocked by GHa and its derived peptides, which reduced the bacteria's capacity for acidogenicity and aciduricity, decreased the production of EPS, and prevented the growth of biofilms. One of the main pathogenic features of *S. mutans* is lactic acid production, in which LDH encoded by the *ldh* gene, plays a key role (Allen et al., 2021). GHa, GHaR, and GHa11R significantly inhibited the expression of the *ldh* gene, thereby reducing lactic acid production and alleviating the pH drop in *S. mutans*. Acid resistance and production of *S. mutans* are highly correlated, which determines

whether *S. mutans* can survive in the acidic environment created by itself. F₁-F₀ ATPase regulates and maintains the acid-base characteristics by participating in proton transport, which reflects the acid resistance level of *S. mutans* (Sekiya et al., 2019). The expression of the *atpD* gene encoding the α subunit of the F₁-F₀ ATPase was downregulated by the peptides, resulting in a reduction in the aciduricity of *S. mutans*. In general, GHa and its derived peptides showed the ability to reduce cariogenic virulence of *S. mutans* by inhibiting the expression of acidogenicity genes and aciduricity genes of *S. mutans*.

During biofilm formation, *S. mutans* initially attaches to tooth surfaces, followed by the production of EPS, which can be utilized as a matrix to encourage the aggregation of additional pathogen, ultimately leading to the creation of multispecies biofilms (Zhang et al., 2021). We found that the adhesion ability of *S. mutans* exposed to the peptides was weakened, which reduced the initial bacterial attachment and blocked or

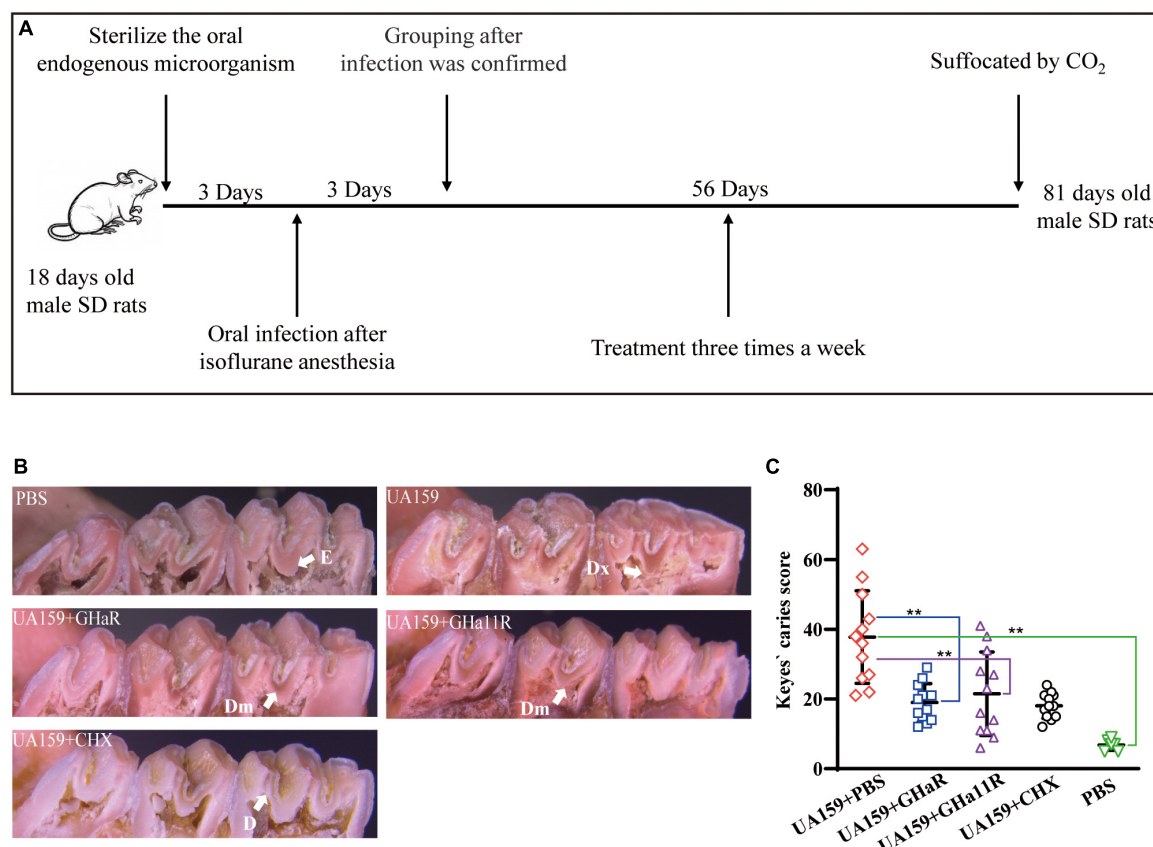


FIGURE 6

Anti-carries efficacy of the peptides. **(A)** Schematic diagram of the experimental scheme for establishment of the rat caries model. **(B)** Pit and fissure caries lesions on the mandibular molars were observed by stereoscopic microscopy. The arrows indicate the lesions on the sulci surface. E indicates that the caries involved only the enamel. D indicates that the caries did not exceed 1/4 of the dentin thickness. Dm indicates that the range of caries was 1/4–3/4 of the dentin thickness. Dx indicates that the caries was more than 3/4 of the dentin thickness. **(C)** Total Keyes scores of the caries on the first and second mandibular molars were evaluated. *Represents comparison with the control. *P < 0.05 and **P < 0.01.

delayed the biofilm formation at the initial stage. *S. mutans* synthesizes EPS by Gtfs converting sucrose into sticky gelatinous extracellular glucan, providing a perfect matrix for other oral microorganisms to attach (Ma et al., 2015). There are three Gtfs in *S. mutans*, namely, GtfB, GtfC, and GtfD (Bowen and Koo, 2011). Water-insoluble glucans are produced by GtfB, and soluble glucans synthesized by GtfD mainly; while GtfC catalyzes both soluble and insoluble glucans (Ma et al., 2021). Therefore, downregulating the expression of Gtfs is a significant way to inhibit the initial biofilm formation. The expression of the *gtfB*, *gtfC* and *gtfD* genes in *S. mutans* was downregulated significantly by GHa, GHaR, and GHa11R, especially that of *gtfB* and *gtfC*, which decreased by nearly 80%. GHa and its derived peptides reduced EPS production by 20–40% at sub-MICs. Downregulation of Gtfs expression by the peptides reduced the production of EPS and impaired subsequent adhesion and biofilm formation. We further observed EPS in the biofilms using CLSM and found that in the blank control, *S. mutans* formed dense and thick biofilms, and many bacteria clustered together in it; EPS expression was highly coincident with the biofilms by labeling with Alexa Fluor 647 glucan *in situ*. In comparison with GHa, the derived peptides GHaR and GHa11R showed better inhibitory efficacy of EPS synthesis, especially GHaR, which

significantly reduced the accumulation of *S. mutans* biofilms and decreased EPS production; although GHa11R showed mild inhibitory activity on *S. mutans* aggregation, the production of EPS was reduced significantly. In conclusion, GHaR and GHa11R exhibited different performances in inhibiting biofilm formation. GHaR showed a stronger effect in reducing the initial adhesion and hydrophobicity of *S. mutans* and subsequently inhibited the accumulation of biofilms. GHa11R reduced the expression of EPS-related genes, showing a stronger effect in reducing the EPS synthesis.

The safety of AMPs has been a concern in their application. GHa and GHa11R were not toxic to HOK cells at a concentration of 100 μ M; although GHaR showed slight cytotoxicity, the IC₅₀ was more than 100 μ M, indicating that GHa and its derived peptides have excellent biocompatibility. We tested the effect of the peptides on other oral pathogenic bacteria and found that they showed strong antibacterial activity against *S. sanguinis*, which plays an important role in the formation of upper and subgingival plaques, and *P. gingivalis*, the main pathogenic bacteria of periodontal disease. In addition, we tested the inhibitory ability of GHa and its derived peptides against several common probiotic bacteria, such as *Bifidobacterium* and *Lactobacillus*, and the results demonstrated that the peptides showed much

higher inhibitory concentrations for probiotic bacteria than oral pathogenic bacteria. These results indicated that the peptides at the therapeutic concentration selectively exerted bactericidal efficacy on oral pathogenic bacteria, which has positive significance for the application of GHa and its derivatives to oral diseases. We evaluated the *in vivo* effects of GHaR and GHa11R in a rat caries model. The results of Keyes scores showed that compared with the model group, caries development significantly slowed in the GHaR and GHa11R groups, and the severity of caries was controlled. The results demonstrated that GHaR and GHa11R had the potential to relieve caries related to *S. mutans* in the oral cavity of rats.

Here, we designed temporin-GHa-derived peptides GHaR and GHa11R, which showed selectively strong antibacterial activity against oral etiologic bacteria, including *S. mutans*, *S. sanguinis*, and *P. gingivalis*. The derived peptides exerted bactericidal efficacy on *S. mutans* plankton by interrupting the integrity and permeability of cell membranes, resulting in intracellular component leakage. They also showed antibiofilm activity against *S. mutans* by reducing surface hydrophobicity, disturbing the initial adhesion, and inhibiting virulence factor production, including lactic acid and EPS. GHaR and GHa11R delay the development of dental caries associated with *S. mutans* in the oral cavity of rats, showing promising application in the treatment of *S. mutans* infections.

Data availability statement

The original contributions presented in this study are included in the article/supplementary material, further inquiries can be directed to the corresponding author.

Ethics statement

The animal study was approved by the Animal Ethics Committee of Hainan University. The study was conducted in accordance with the local legislation and institutional requirements.

References

- Abbassi, F., Raja, Z., Oury, B., Gazanion, E., Piesse, C., Sereno, D., et al. (2013). Antibacterial and leishmanicidal activities of temporin-SHd, a 17-residue long membrane-damaging peptide. *Biochimie* 95, 388–399. doi: 10.1016/j.biochi.2012.10.015
- Abdel-Aziz, M. M., Emam, T. M., and Raafat, M. M. (2020). Hindering of cariogenic *Streptococcus mutans* biofilm by fatty acid array derived from an endophytic *Arthrographis kalrae* strain. *Biomolecules* 10:811. doi: 10.3390/biom10050811
- Allen, L. L., Heng, N. C. K., and Tompkins, G. R. (2021). *Streptococcus salivarius* isolates of varying acid tolerance exhibit F₁F₀-ATPase conservation. *Caries Res.* 55, 288–291. doi: 10.1159/000516175
- Aqawi, M., Sionov, R. V., Gallily, R., Friedman, M., and Steinberg, D. (2021). Antibiofilm activity of cannabigerol against *Streptococcus mutans*. *Microorganisms* 9:10. doi: 10.3390/microorganisms9102031
- Bencini, D. A., Shanley, M. S., Wild, J. R., and O'Donovan, G. A. (1983). New assay for enzymatic phosphate release: Application to aspartate transcarbamylase and other enzymes. *Anal. Biochem.* 132, 259–264. doi: 10.1016/0003-2697(83)90005-2
- Bowen, W. H., and Koo, H. (2011). Biology of *Streptococcus mutans*-derived glucosyltransferases: Role in extracellular matrix formation of cariogenic biofilms. *Caries Res.* 45, 69–86. doi: 10.1159/000324598
- Cao, Y., Yin, H., Wang, W., Pei, P., Wang, Y., Wang, X., et al. (2020). Killing *Streptococcus mutans* in mature biofilm with a combination of antimicrobial and antibiofilm peptides. *Amino Acids* 52, 1–14. doi: 10.1007/s00726-019-02804-4
- Chen, H., Tang, Y., Weir, M. D., Gao, J., Imazato, S., Oates, T. W., et al. (2020). Effects of *S. mutans* gene-modification and antibacterial monomer dimethylaminohexadecyl methacrylate on biofilm growth and acid production. *Dent. Mater.* 36, 296–309. doi: 10.1016/j.dental.2019.12.001

Author contributions

SJ: Writing–original draft, Writing–review and editing, Conceptualization. YZ: Methodology, Writing–review and editing. TZ: Methodology, Writing–review and editing. XJ: Methodology, Writing–review and editing. RZ: Methodology, Writing–review and editing. SW: Writing–review and editing. RW: Writing–review and editing. YS: Writing–review and editing. LL: Writing–review and editing. JL: Writing–review and editing. WH: Writing–review and editing. DZ: Writing–review and editing. MW: Writing–review and editing. YZ: Writing–original draft, Writing–review and editing.

Funding

The author(s) declare financial support was received for the research, authorship, and/or publication of this article. This work was supported by the Hainan Science and Technology Project under Grant ZDYF2021SHFZ042, the National Natural Science Foundation of China under Grants 32060130 and 82104129, the Natural Science Foundation of Hainan Province under Grant 820MS140, and the Foundation of Collaborative Innovation Center of One Health of Hainan University under Grant XTCX2022JKB05.

Conflict of interest

The authors declare that the research was conducted in the absence of any commercial or financial relationships that could be construed as a potential conflict of interest.

Publisher's note

All claims expressed in this article are solely those of the authors and do not necessarily represent those of their affiliated organizations, or those of the publisher, the editors and the reviewers. Any product that may be evaluated in this article, or claim that may be made by its manufacturer, is not guaranteed or endorsed by the publisher.

- de Breij, A., Riool, M., Cordfunke, R. A., Malanovic, N., de Boer, L., Koning, R. I., et al. (2018). The antimicrobial peptide SAAP-148 combats drug-resistant bacteria and biofilms. *Sci. Transl. Med.* 10:eaa4044. doi: 10.1126/scitranslmed.aan4044
- Deng, Y., Yang, Y., Zhang, B., Chen, H., Lu, Y., Ren, S., et al. (2021). The vicK gene of *Streptococcus mutans* mediates its cariogenicity via exopolysaccharides metabolism. *Int. J. Oral Sci.* 13:45. doi: 10.1038/s41368-021-00149-x
- Devine, D. A. (2003). Antimicrobial peptides in defence of the oral and respiratory tracts. *Mol. Immunol.* 40, 431–443. doi: 10.1016/s0161-5890(03)00162-7
- Diamond, G., Beckloff, N., and Ryan, L. K. (2008). Host defense peptides in the oral cavity and the lung: Similarities and differences. *J. Dent. Res.* 87, 915–927. doi: 10.1177/154405910808701011
- Dong, Z., Luo, W., Zhong, H., Wang, M., Song, Y., Deng, S., et al. (2017). Molecular cloning and characterization of antimicrobial peptides from skin of *Hyalarana guentheri*. *Acta Biochim. Biophys. Sin.* 49, 450–457. doi: 10.1093/abbs/gmx023
- Griffith, A., Mateen, A., Markowitz, K., Singer, S. R., Cugini, C., Shimizu, E., et al. (2022). Alternative antibiotics in dentistry: Antimicrobial peptides. *Pharmaceutics* 14:1679. doi: 10.3390/pharmaceutics14081679
- Guncu, G. N., Yilmaz, D., Kononen, E., and Gursay, U. K. (2015). Salivary antimicrobial peptides in early detection of periodontitis. *Front. Cell. Infect. Microbiol.* 5:99. doi: 10.3389/fcimb.2015.00099
- Harper, D. S., and Loesche, W. J. (1983). Effect of pH upon sucrose and glucose catabolism by the various genogroups of *Streptococcus mutans*. *J. Dent. Res.* 62, 526–531. doi: 10.1177/00220345830620050101
- Ho, S., Pothoulakis, C., and Koon, H. W. (2013). Antimicrobial peptides and colitis. *Curr. Pharm. Des.* 19, 40–47. doi: 10.2174/13816128130108
- Jiang, W., Deng, Z., Dai, X., and Zhao, W. (2021). PANoptosis: A new insight into oral infectious diseases. *Front. Immunol.* 12:789610. doi: 10.3389/fimmu.2021.789610
- Kacprzyk, L., Rydengard, V., Morgelin, M., Davoudi, M., Pasupuleti, M., Malmsten, M., et al. (2007). Antimicrobial activity of histidine-rich peptides is dependent on acidic conditions. *Biochim. Biophys. Acta* 1768, 2667–2680. doi: 10.1016/j.bbame.2007.06.020
- Kim, K., An, J. S., Lim, B. S., and Ahn, S. J. (2019). Effect of bisphenol A glycol methacrylate on virulent properties of *Streptococcus mutans* UA159. *Caries Res.* 53, 84–95. doi: 10.1159/000490197
- Klein, M. I., Hwang, G., Santos, P. H., Campanella, O. H., and Koo, H. (2015). *Streptococcus mutans*-derived extracellular matrix in cariogenic oral biofilms. *Front. Cell. Infect. Microbiol.* 5:10. doi: 10.3389/fcimb.2015.00010
- Lamont, R. J., Koo, H., and Hajishengallis, G. (2018). The oral microbiota: Dynamic communities and host interactions. *Nat. Rev. Microbiol.* 16, 745–759. doi: 10.1038/s41579-018-0089-x
- Lemos, J. A., Palmer, S. R., Zeng, L., Wen, Z. T., Kajfasz, J. K., Freires, I. A., et al. (2019). The biology of *Streptococcus mutans*. *Microbiol. Spectr.* 7:1. doi: 10.1128/microbiolspec.GPP3-0051-2018
- Lyne Pedersen, A. M., and Belstrom, D. (2019). The role of natural salivary defences in maintaining a healthy oral microbiota. *J. Dent.* 80(Suppl. 1), S3–S12. doi: 10.1016/j.jdent.2018.08.010
- Ma, C., Chen, F., Zhang, Y., Sun, X., Tong, P., Si, Y., et al. (2015). Comparison of oral microbial profiles between children with severe early childhood caries and caries-free children using the human oral microbe identification microarray. *PLoS One* 10:e0122075. doi: 10.1371/journal.pone.0122075
- Ma, Q., Pan, Y., Chen, Y., Yu, S., Huang, J., Liu, Y., et al. (2022). Acetylation of lactate dehydrogenase negatively regulates the acidogenicity of *Streptococcus mutans*. *mBio* 13:e021322. doi: 10.1128/mbio.02013-22
- Ma, Q., Pan, Y., Chen, Y., Yu, S., Huang, J., Liu, Y., et al. (2021). Acetylation of glucosyltransferases regulates *Streptococcus mutans* biofilm formation and virulence. *PLoS Pathog.* 17:e1010134. doi: 10.1371/journal.ppat.1010134
- Mosaddad, S. A., Tahmasebi, E., Yazdani, A., Rezvani, M. B., Seifalian, A., Yazdani, M., et al. (2019). Oral microbial biofilms: An update. *Eur. J. Clin. Microbiol. Infect. Dis.* 38, 2005–2019. doi: 10.1007/s10096-019-03641-9
- Nakano, K., Inaba, H., Nomura, R., Nemoto, H., Takeda, M., Yoshioka, H., et al. (2006). Detection of cariogenic *Streptococcus mutans* in extirpated heart valve and atheromatous plaque specimens. *J. Clin. Microbiol.* 44, 3313–3317. doi: 10.1128/JCM.00377-06
- Peres, M. A., Macpherson, L. M. D., Weyant, R. J., Daly, B., Venturelli, R., Mathur, M. R., et al. (2019). Oral diseases: A global public health challenge. *Lancet* 394, 249–260. doi: 10.1016/S0140-6736(19)31146-8
- Ramezanzadeh, M., Saeedi, N., Mesbahfar, E., Farrokh, P., Salimi, F., and Rezaei, A. (2021). Design and characterization of new antimicrobial peptides derived from aurein 1.2 with enhanced antibacterial activity. *Biochimie* 181, 42–51. doi: 10.1016/j.biochi.2020.11.020
- Saporito, P., Vang Mouritzen, M., Lobner-Olesen, A., Jenssen, H. (2018). LL-37 fragments have antimicrobial activity against *Staphylococcus epidermidis* biofilms and wound healing potential in HaCaT cell line. *J. Pept. Sci.* 24:e3080. doi: 10.1002/psc.3080
- Savini, F., Loffredo, M. R., Troiano, C., Bobone, S., Malanovic, N., Eichmann, T. O., et al. (2020). Binding of an antimicrobial peptide to bacterial cells: Interaction with different species, strains and cellular components. *Biochim. Biophys. Acta Biomembr.* 1862:183291. doi: 10.1016/j.bbame.2020.183291
- Sekiya, M., Izumisawa, S., Iwamoto-Kihara, A., Fan, Y., Shimoyama, Y., Sasaki, M., et al. (2019). Proton-pumping F-ATPase plays an important role in *Streptococcus mutans* under acidic conditions. *Arch. Biochem. Biophys.* 666, 46–51. doi: 10.1016/j.abb.2019.03.014
- Shanmugam, K., Sarveswari, H. B., Udayashankar, A., Swamy, S. S., Pudipeddi, A., Shanmugam, T., et al. (2020). Guardian genes ensuring subsistence of oral *Streptococcus mutans*. *Crit. Rev. Microbiol.* 46, 475–491. doi: 10.1080/1040841X.2020.1796579
- Svensater, G., Larsson, U. B., Greif, E. C., Cvitkovitch, D. G., and Hamilton, I. R. (1997). Acid tolerance response and survival by oral bacteria. *Oral Microbiol. Immunol.* 12, 266–273. doi: 10.1111/j.1399-302x.1997.tb00390.x
- Tian, Y., Zhang, Y., Zhang, M., Chen, X., Lei, L., and Hu, T. (2022). Antisense vicR-loaded dendritic mesoporous silica nanoparticles regulate the biofilm organization and cariogenicity of *Streptococcus mutans*. *Int. J. Nanomedicine* 17, 1255–1272. doi: 10.2147/IJN.S334785
- Utheim, T. P., Islam, R., Fostad, I. G., Eidet, J. R., Sehic, A., Olstad, O. K., et al. (2016). Storage temperature alters the expression of differentiation-related genes in cultured oral keratinocytes. *PLoS One* 11:e0152526. doi: 10.1371/journal.pone.0152526
- Wang, G., Li, X., and Wang, Z. (2016). APD3: The antimicrobial peptide database as a tool for research and education. *Nucleic Acids Res.* 44, D1087–D1093. doi: 10.1093/nar/gkv1278
- Wang, Y., Wang, X., Jiang, W., Wang, K., Luo, J., Li, W., et al. (2018). Antimicrobial peptide GH12 suppresses cariogenic virulence factors of *Streptococcus mutans*. *J. Oral Microbiol.* 10:1442089. doi: 10.1080/20002297.2018.1442089
- Wiesner, J., and Vilcinskis, A. (2010). Antimicrobial peptides: The ancient arm of the human immune system. *Virulence* 1, 440–464. doi: 10.4161/viru.1.5.12983
- Xie, Z., Wei, H., Meng, J., Cheng, T., Song, Y., Wang, M., et al. (2019). The analogs of Temporin-GHa exhibit a broader spectrum of antimicrobial activity and a stronger antibiofilm potential against *Staphylococcus aureus*. *Molecules* 24:4173. doi: 10.3390/molecules24224173
- Xiong, K., Chen, X., Hu, H., Hou, H., Gao, P., and Zou, L. (2020). Antimicrobial effect of a peptide containing novel oral spray on *Streptococcus mutans*. *Biomed. Res. Int.* 2020:6853652. doi: 10.1155/2020/6853652
- Xu, X., Zhou, X. D., and Wu, C. D. (2011). The tea catechin epigallocatechin gallate suppresses cariogenic virulence factors of *Streptococcus mutans*. *Antimicrob. Agents Chemother.* 55, 1229–1236. doi: 10.1128/AAC.01016-10
- Yue, J., Yang, H., Liu, S., Song, F., Guo, J., and Huang, C. (2018). Influence of naringenin on the biofilm formation of *Streptococcus mutans*. *J. Dent.* 76, 24–31. doi: 10.1016/j.jdent.2018.04.013
- Zhang, J., Chen, C., Chen, J., Zhou, S., Zhao, Y., Xu, M., et al. (2020). Dual mode of anti-biofilm action of G3 against *Streptococcus mutans*. *ACS Appl. Mater. Interfaces* 12, 27866–27875. doi: 10.1021/acsami.0c00771
- Zhang, Q., Ma, Q., Wang, Y., Wu, H., and Zou, J. (2021). Molecular mechanisms of inhibiting glucosyltransferases for biofilm formation in *Streptococcus mutans*. *Int. J. Oral Sci.* 13:30. doi: 10.1038/s41368-021-00137-1
- Zhang, Z., Yang, Y., Sun, Q., Zeng, W., and Li, Y. (2022). Inhibition of biofilm formation and virulence factors of cariogenic oral pathogen *Streptococcus mutans* by shikimic acid. *Microbiol. Spectr.* 10:e0119922. doi: 10.1128/spectrum.01199-22



OPEN ACCESS

EDITED BY

Jianhua Wang,
Chinese Academy of Agricultural Sciences
(CAAS), China

REVIEWED BY

Attilio Fabbretti,
University of Camerino, Italy
Sonia Ilaria Maffioli,
Naicons Srl, Italy

*CORRESPONDENCE

Yunlong Li
✉ liyunlong@cdxzy.cn
Sanfeng Chen
✉ chensf@cau.edu.cn

RECEIVED 14 June 2023

ACCEPTED 04 September 2023

PUBLISHED 26 September 2023

CITATION

Li Y and Chen S (2023) Structure modification
of an antibiotic: by engineering the fusaricidin
bio-synthetase A in *Paenibacillus polymyxa*.
Front. Microbiol. 14:1239958.
doi: 10.3389/fmicb.2023.1239958

COPYRIGHT

© 2023 Li and Chen. This is an open-access
article distributed under the terms of the
[Creative Commons Attribution License \(CC BY\)](https://creativecommons.org/licenses/by/4.0/).
The use, distribution or reproduction in other
forums is permitted, provided the original
author(s) and the copyright owner(s) are
credited and that the original publication in this
journal is cited, in accordance with accepted
academic practice. No use, distribution or
reproduction is permitted which does not
comply with these terms.

Structure modification of an antibiotic: by engineering the fusaricidin bio-synthetase A in *Paenibacillus polymyxa*

Yunlong Li^{1*} and Sanfeng Chen^{2*}

¹Chengdu NewSun Crop Science Co. Ltd., Chengdu, China, ²State Key Laboratory of Agrobiotechnology, College of Biological Sciences, China Agricultural University, Beijing, China

Fusaricidin, a lipopeptide antibiotic, is specifically produced by *Paenibacillus polymyxa* strains, which could strongly inhibit *Fusarium* species fungi. Fusaricidin bio-synthetase A (FusA) is composed of six modules and is essential for synthesizing the peptide moiety of fusaricidin. In this study, we confirmed the FusA of *Paenibacillus polymyxa* strain WLY78 involved in producing Fusaricidin LI-F07a. We constructed six engineered strains by deletion of each module within FusA from the genome of strain WLY78. One of the engineered strains is able to produce a novel compound that exhibits better antifungal activity than that of fusaricidin LI-F07a. This new compound, known as fusaricidin [Δ Ala⁶] LI-F07a, has a molecular weight of 858. Our findings reveal that it exhibits a remarkable 1-fold increase in antifungal activity compared to previous fusaricidin, and the fermentation yield reaches ~55 mg/L. This research holds promising implications for plant protection against infections caused by *Fusarium* and *Botrytis* pathogen infection.

KEYWORDS

gene engineering, [Δ Ala⁶] fusaricidin LI-F07a, structure modification, homologous recombination, biocontrol agent

1. Introduction

Non-ribosomal peptide synthetase (NRPS) is a microbial systemic enzyme that produces secondary metabolites such as lipopeptide antibiotics (Shokrollahi et al., 2021). In general, NRPS enzymes consist of multiple modules, with each module capable of accommodating several domains, including the condensation domain, adenylation (A) domain, thiolation (T) domain, epimerization (E) domain, and thioester (TE) domain (Marahiel, 2016; Izoré et al., 2021). In certain literature, the T domain is alternatively referred to as the peptidyl carrier protein (PCP) domain (Rüschbaum et al., 2022). Additionally, it has been demonstrated that the C domains contain two catalytic tunnels that connect the donor-PCP and acceptor-PCP domain-binding sites to the active site. These tunnels serve as the pathway for the donor and acceptor substrates to access the active site (Samel et al., 2007).

The structure of a three-module NRPS contains an initiation module (core A-T domain), an elongation module (core C-A-T domain) that can be followed by an E domain, and a termination module (core C-A-T-TE domain) (Calcott and Ackerley, 2015; Izoré et al., 2021). The bio-synthesis process of peptide moiety can be divided by these domains into several steps, beginning with post-translational modification of each T domain by attachment of a 4'-phosphopantetheine (4'-pp) cofactor. The 4'-pp group serves as a flexible arm that facilitates

the coordination of substrate movement between catalytic sites (Kittilä et al., 2016; Zhang et al., 2022). Within each module, the A domain plays a crucial role in recognizing a specific monomer and activating it as an aminoacyl adenylate. Subsequently, it attaches the activated monomer to the 4'-pp group located on the adjacent T domain (Schwarzer et al., 2002; Zhu et al., 2019). In a sequential fashion, beginning with the first module, each C domain facilitates the formation of peptide bonds by linking the donor substrate, which is attached to the upstream T domain, with the acceptor substrate, which is attached to the downstream T domain (Wheadon and Townsend, 2021). Before the condensation reaction takes place, it is possible that each T domain may require interaction with additional tailoring domains, such as the E domain. The E domain plays a role in modifying the substrate carried by each module, including the ability to catalyze racemization (Kim et al., 2022). Once the peptide chain reaches the termination module, the product is released by a thioesterase (TE) domain through hydrolysis or intramolecular cyclization. Following this, the synthesis cycle can be repeated to generate multiple copies of the same peptide (Marahiel, 2016; Hühner et al., 2019).

Fusaricidin is an important antibiotic family produced by *Paenibacillus polymyxa* with great potential use in medical and agricultural applications (Kajimura and Kaneda, 1996; Lee et al., 2012; Haron et al., 2019; Jeong et al., 2019). So far, 14 fusaricidin members have been reported, consisting of an invariable 15-guanidino-3-hydroxypentadecanoic acid and a variable cyclic hexapeptide (Deng et al., 2011; Vater et al., 2015; Reimann et al., 2017). The variable cyclic hexadepsipeptide moiety of fusaricidin usually contains six amino acid residues: L-Thr¹, X², X³, D-allo-Thr⁴, X⁵, and D-Ala⁶ (Han et al., 2012). Among the family, fusaricidin LI-F07a has better antimicrobial activity than other fusaricidin analogs. Based on the current knowledge, L-Thr¹, D-Val², L-Phe³, D-allo-Thr⁴, D-Asn⁵, and D-Ala⁶ constitute the cyclic hexadepsipeptide moiety within LI-F07a (Reimann et al., 2017).

The discovery of penicillin in 1928 started the golden age of natural product antibiotic discovery that peaked in the mid-1950s (Hutchings et al., 2019). Since then, a gradual decline in antibiotic discovery and development and the evolution of antibiotic resistance in many human pathogens has led to the current antimicrobial resistance crisis (Larsson and Flach, 2022). We believe that the future of antibiotic findings looks bright as new technologies such as genome mining and editing are deployed to discover new antibiotics with diverse bioactivities (Albarano et al., 2020).

In our previous studies, we reported the strain WLY78 produces fusaricidin, and the fermented strain could be used for bio-controlling the *Fusarium* head blight in wheat (Li and Chen, 2019; Li et al., 2021). While acknowledging the effectiveness of this biocontrol strain, we are not content with maintaining the present status. Our primary motivation is to proactively prevent the potential emergence of microbial resistance issues, which serves as a driving force for our continuous advancements. Our objective is to optimize the NRPS enzymes involved in the synthesis of existing antibiotics strategically. This optimization aims to enhance the effectiveness of antibiotics. In our current study, we have created a new fusaricidin antibiotic by modifying the FusA. Briefly, we analyzed the function of FusA and confirmed it could biosynthesize fusaricidin LI-F07a. Then, each module within FusA was reorganized by gene modification. Moreover, we found that one of the engineered strains produced a novel

fusaricidin derivative. The structure of this novel compound was identified as [Δ Ala⁶] fusaricidin LI-F07a. Meaningfully, this new compound exhibits stronger activity than fusaricidin LI-F07a in inhibiting the pathogen fungi *F. asiaticum*. Finally, this novel substance was successfully applied to prevent plants from being infected by pathogens: *Fusarium oxysporum* and *Botrytis cinerea*.

2. Materials and methods

2.1. Microorganisms, plasmids, and culture conditions

The source of strains and plasmids is summarized in [Supplementary Table S1](#). *Escherichia coli* DH5 α was cultivated at 37°C in Luria–Bertani (LB) broth for cloning plasmids. *P. polymyxa* strain was cultivated at 30°C in Katznelson–Lochhead (KL) broth for the production of fusaricidin and its derivatives (Paulus and Gray, 1964). The pathogens *Fusarium asiaticum*, *Fusarium oxysporum*, and *Botrytis cinerea* were cultivated at 28°C in a potato dextrose agar (PDA) medium. A temperature-sensitive shuttle vector, pRN5101, containing the ori(Ts) and erm^R of pE194ts and the oriEc, amp^R, and multicloning region of pBR322, was used for gene deletion in *P. polymyxa* (Villafane et al., 1987; Lereclus et al., 1992). If necessary, LB broth was solidified using 1.5% agar, and the antibiotics were added at the following concentrations: 100 μ g/mL ampicillin (95% purity, for selecting *E. coli* transformants) and 5 μ g/mL erythromycin (95% purity, for selecting *P. polymyxa* transformants).

2.2. Bioinformatics analysis of FusA for its substrate prediction

The genome of our strain WLY78 is genome sequenced (please refer to GenBank: ALJV000000000). The *fusA* gene and the *fus* gene cluster sequence have been deposited to GenBank (AYC81015.1 and MH368541.1). For the A domains alignment, the amino acid sequence of each A domain was extracted from FusA via the antiSMASH bacterial version program (Blin et al., 2023). The GenBank numbers of these A domains from different NRPSs are listed in [Supplementary Table S2](#). The “ten code residues” were acquired from a previous study (Stachelhaus et al., 1999). Ten code residues located at positions 235, 236, 239, 278, 299, 301, 322, 330, 331, and 517 within each A domains were extracted and subsequently combined to form a new amino acid sequence for the purpose of sequence alignment. The phylogenetic tree was constructed to predict the substrate specificity by using the software MEGA 5.0.

2.3. Modification of FusA

The cyclic peptide moiety of fusaricidin is composed of six amino acids that were assembled by six modules. To produce a novel fusaricidin derivative, each of the six modules (M1, M2, M3, M4, M5, and M6) within FusA was deleted *via* homologous recombination ([Supplementary Figure S1](#)).

The method of assembling fragments and plasmids was carried out according to the manufacturer's instruction (Gibson Assembly Kit,

ThermoFisher). Briefly, two homologous arms (each with 1 kb in length) flanking the deleting module were PCR amplified from the genomic DNA of *P. polymyxa*. The two homologous arms were assembled into the suicide plasmid pRN5101 digested by *Bam*HI (0.75 U/ μ L, TaKaRa), yielding six recombinant plasmids: pRN-M1, pRN-M2, pRN-M3, pRN-M4, pRN-M5, and pRN-M6. Each of these recombinant plasmids was transformed in *P. polymyxa*, and the single-crossover transformants were selected for erythromycin resistance as previously described (Zhang et al., 2013). Subsequently, the double-crossover (marker-free deletion) mutants were selected from the initial erythromycin resistance transformants after several rounds of non-selective growth at 39°C and confirmed by PCR amplification. Finally, we acquired six mutant strains that carry the engineered *FusA*: Δ M1, Δ M2, Δ M3, Δ M4, Δ M5, and Δ M6. The primers for the PCR are listed in [Supplementary Table S3](#).

2.4. Antifungal activity assays

To assess the antifungal activity of wild-type strain and its genetically engineered strains, the inhibition zone against the fungus *F. asiaticum* was measured as previously described (Li and Chen, 2019). In brief, *F. asiaticum* was inoculated at the center of the PDA medium. Next, 1 μ L of strain cell suspensions (10^7 CFU/mL) was inoculated around the fungus, maintaining a constant distance of 2 cm. All the plates were then incubated at 28°C for 4 days, and the inhibition effect on fungi hyphae growth was recorded.

To test the antifungal activity of purified component, including LI-F07a and [Δ Ala⁶] fusaricidin LI-F07a, the *F. asiaticum* and *B. cinerea* spores were collected. The spore concentration of each pathogen was adjusted to 10^8 CFU/mL. A total of 1 mL of each spore suspension was added to 20 mL of warm and melted PDA medium. Three aseptic rings made of stainless steel were placed onto the solidified medium plate, and 100 μ L of LI-F07a (20 mg/L) and 100 μ L of [Δ Ala⁶] fusaricidin LI-F07a (20 mg/L) were injected into two separate rings. Then, 100 μ L of methanol, which dissolved the above two substances, was injected into the ring of the medium plate as a control. After 4 days of culture at 28°C, the diameter of the inhibition zone could be observed and recorded.

2.5. Control effect assays

To test the control effect of fusaricidin LI-F07 and its novel derivative against plant pathogen *in vivo*, we used two pathogen fungi to infect the cucumber seedlings as the model according to a previous method (Li et al., 2015). Initially, the cucumber seedlings (*Cucumis sativus* Linn.) were planted in the mixture containing 150 g peat soil and 50 g vermiculite in 10-cm pots. When the seedlings reached the three-leaves period, 10 mL of fusaricidin LI-F07a (20 mg/L) and its novel derivative (20 mg/L) was sprayed onto the seedling leaves, with 10 mL of water being used as the control. At 12 h after spray, 5 mL of spore suspensions (10^8 cfu/mL) collected from two pathogen fungi (*F. oxysporum* and *B. cinerea*) was inoculated by foliar spray. Each group contained eight seedlings. At 21 days post-inoculation, we investigated the disease severity by the following grades: 0, number of leaves with no symptoms; 1, number of leaves with <25% area with disease spots; 2, number of leaves with 25–50% area with disease

spots; 3, number of leaves with 50–75% area with disease spots; 4, number of leaves with 75–100% area with disease spots; 5, number of leaves with 100% area with disease spots. The disease index (DI) was determined by the formula below (Yan et al., 2006):

$$DI = \frac{\sum (g \times N_g)}{h \times N_t}$$

Where g is the grade value, N_g is the number of leaves of the corresponding grade, h is the highest-grade value, and N_t is the total number of leaves in each group.

The control effect (CE) was calculated as follows (Yan et al., 2006):

$$CE(\%) = \left[1 - \frac{DI_{treatment}}{DI_{control}} \right] \times 100\%$$

2.6. Extraction, purification, and identification of antifungal component

To extract the purified fusaricidin or its potential derivative, the wild-type strain or Δ M6-engineered strain was cultivated in 100 mL of KL broth at 37°C for 3 days at 220 rpm. The fermentation was extracted by 10 mL of ethyl acetate for 5 h at 4°C. Then, the ethyl acetate phase was dried. The strain pellets were extracted in methanol by vigorously shaking for 1 h. The weight of methanol was twice the weight of the strain. The methanol supernatant collected by centrifugation was then dried. The two dried components could be dissolved in 1 mL of methanol.

To analyze the difference of the crude extractions between the wild-type strain and Δ M6 mutant, we compared their chromatography peaks via analytical HPLC (Shimadzu LC-20AT) at UV 210 nm with a C18 reversed-phase column (150 \times 4.6 mm). The condition for detecting fusaricidin has been described previously with some modifications (Li et al., 2007). It is listed as follows: injection volume 10 μ L, flow rate 0.8 mL/min, and solvent gradient ranging from 40% B (acetonitrile) with 60% D (0.1% formic acid in water) to 90% B (acetonitrile) with 10% D (0.1% formic acid in water) in 30 min.

To acquire the antifungal substances, we purified the crude extractions using preparative HPLC (Shimadzu LC-16P) at UV 210 nm by the following method: 1 mL of crude extract was injected into a C18 reversed-phase column (250 \times 10 mm) with 0.1% trifluoroacetic acid in 90% acetonitrile solution at 20 mL/min. Each peak was collected specifically for antifungal activity assays, and only the peaks showing activity were selected for subsequent LC–MS analysis.

The conditions for LC–MS (Agilent 1,290-6470A) were conducted under positive mode as described previously, with minor modifications (Vater et al., 2015). The conditions for LC isolation were as follows: 30% A (0.1% formic acid in water) with 70% B (0.1% formic acid in methanol) and flow rate 0.45 mL/min. The conditions for MS were as follows: gas temperature 300°C, drying gas flow 5 L/min, nebulizer 30 psi, capillary voltage 3.5 kV, sheath gas heater 350°C, sheath gas flow 11 L/min, and fragmentation voltage 140 V. When performing MS–MS, an additional parameter was collision voltage (10 V), while all other conditions remained as described above.

2.7. Statistical analysis

All the experiments were repeated three times with a similar result. The significant difference ($P < 0.01$) of data was analyzed by one-way ANOVA with Duncan's multiple-range test using SPSS version 22 statistical software (Chicago, United States).

3. Results

3.1. *Paenibacillus polymyxa* possesses FusA coding gene and produces fusaricidin LI-F07a

To predict whether our wild-type strain could produce fusaricidin LI-F07a, we analyzed its genome sequence and found the FusA coding gene. FusA harbors six highly similar modules consisting of at least three domains: an adenylation (A), a thiolation (T), and a condensation (C) domain. In addition, there is an epimerization (E) domain in the second, fourth, and fifth modules and a termination (TE) domain in the sixth module (Figure 1A).

To determine the substrate of each A domain within FusA, we compared each of the A domains within FusA with those known substrate-activating A domains and aligned them. As shown in Figure 1B, phylogenetic analysis revealed the potential substrate specificity of these A domains within each module: the first A domain of FusA (FusA-A1) could recognize threonine (Thr), the second A domain of FusA (FusA-A2) could recognize valine (Val), the third A domain of FusA (FusA-A3) could recognize phenylalanine (Phe), the fourth A domain of FusA (FusA-A4) could recognize threonine (Thr), the fifth A domain of FusA (FusA-A5) could recognize asparagine (Asn), and the sixth A domain of FusA (FusA-A6) could recognize alanine (Ala). A similar sequence alignment based on the "ten code residues" also demonstrated that the six A domains within FusA in strain WLY78 could, respectively, recognize Thr, Val, Phe, Thr, Asn, and Ala (Figure 1C). Therefore, FusA is supposed to biosynthesize hexadepsipeptide in the following order: Thr¹-Val²-Phe³-Thr⁴-Asn⁵-Ala⁶, which is a part of fusaricidin LI-F07a (Figure 1D).

To verify our prediction, we prepared *P. polymyxa* strain fermentation and crude extractions. Then, we analyzed the extractions and collected a component peak that showed strong antifungal activity by HPLC at 18.7 min (Figure 2A). This active component was identified by LC-MS and yielded an ion peak at $m/z = 931.81$, which represents the ratio of the mass of the protonated fusaricidin LI-F07a to its charge (Figure 2B). Subsequently, the ion of m/z of 931.81 was used as precursor for MS-MS fragmentation. As shown in Figure 2C, the ion of m/z 256.07 represents the 15-guanidino-3-hydroxypentadecanoic acid side chain, and the ion of m/z 676.54 represents the cyclic hexadepsipeptide fragment. The N-terminal stepwise cleavage of cyclic hexadepsipeptide was Thr (551.41), Val (452.19), Phe (305.11), and Thr (473.44), while the C-terminal stepwise cleavage of cyclic hexadepsipeptide was Ala (587.65) and Asn (473.44). In all, these fragment ions are completely consistent with the molecular structure of fusaricidin LI-F07a, demonstrating that fusaricidin LI-F07a could be synthesized by *P. polymyxa*.

3.2. Modifying the 6th FusA module enhances the antifungal activity of bacterium

To design a new and more efficient antibiotic fusaricidin against *Fusarium* fungi, we inactivated each of the six modules within FusA, yielding six engineered strains that, respectively, contain different types of FusAs: $\Delta M1$, $\Delta M2$, $\Delta M3$, $\Delta M4$, $\Delta M5$, and $\Delta M6$ (Figure 3A). Each engineered strain was confirmed by PCR analysis (Supplementary Figure S2). As a consequence, the inhibiting effect against *F. asiaticum* of two engineered strains with $\Delta M1$ and $\Delta M5$ decreased slightly. Those engineered strains carrying $\Delta M2$, $\Delta M3$, and $\Delta M4$ completely lost their antifungal activities. Meanwhile, the strain with $\Delta M6$ showed a larger inhibition zone than the wild-type strain, suggesting that $\Delta M6$ might produce a more efficient compound rather than fusaricidin LI-F07a (Figure 3B).

3.3. The new compound is characterized as [ΔAla^6] fusaricidin LI-F07a

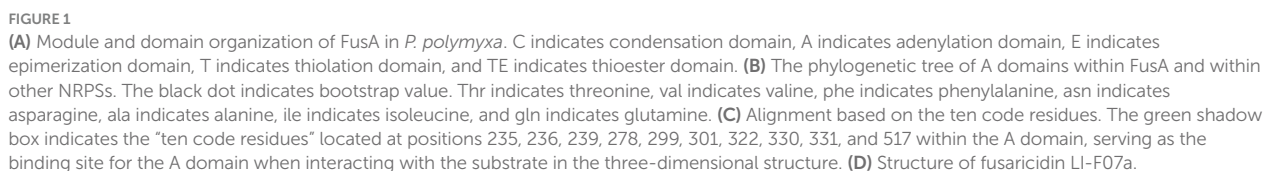
To identify the structure of this compound, we isolated and detected this active component from the fermentation broth of the $\Delta M6$ -engineered strain by HPLC at 22.8 min (Figure 4A). Then, we analyzed this fraction by LC-MS and observed an ion peak at 859.60 Da (Figure 4B), which was ~ 72 Da (the mass of Ala) smaller than fusaricidin LI-F07 (931.81 Da), suggesting this compound lacks the sixth amino acid (Ala) from fusaricidin LI-F07a. To further confirm its structure, we used the ion 859.60 Da as a precursor for MS-MS fragment ion analysis. As shown in Figure 4C, the fragment ion 256.21 Da represents the 15-guanidino-3-hydroxypentadecanoic acid side chain, and the ion 604.54 Da represents the cyclic hexadepsipeptide of this new substance. The N-terminal stepwise cleavage of cyclic hexadepsipeptide was Thr (479.36 Da) and Val (380.25 Da), while the C-terminal stepwise cleavage of cyclic hexadepsipeptide was Asn (472.08 Da) and Thr (371.09 Da). Therefore, we believe that the fracture fragments from ion 859.71 Da roughly match the molecular fragmentation pattern of [ΔAla^6] fusaricidin LI-F07a, which was identified as a novel fusaricidin derivative.

3.4. [ΔAla^6] Fusaricidin LI-F07a exhibits great antimicrobial ability both *in vitro* and *in vivo*

With the same concentration at 20 mg/L, [ΔAla^6] fusaricidin LI-F07a shows 1-fold higher antifungal activities against *F. oxysporum* and *B. cinerea* than that of fusaricidin LI-F07a (Figure 5A). Meanwhile, the CE values of [ΔAla^6] fusaricidin LI-F07a against cucumber *fusarium* wilt and cucumber gray mold reach 95 and 98.1%, while those of fusaricidin LI-F07a only reach 84 and 76.2%, respectively (Figure 5B).

4. Discussion

The *Paenibacillus* species is a powerful bio-fungicide and has many potential applications. So far, 14 fusaricidin analog members



identification. Now, the genome mining method has rapidly paved the way for predicting secondary metabolites within microorganisms. Similarly, we used the genome mining strategy to predict the genome and found the FusA coding gene, suggesting that FusA producing fusaricidin LI-F07a is a great possibility (Figure 1A). The A domain within NRPS is reported to be essential in recognizing the substrate that consists of lipopeptide in a 1:1 manner (Marahiel et al., 1997; Stachelhaus et al., 1999). According to the principle above, a lot of

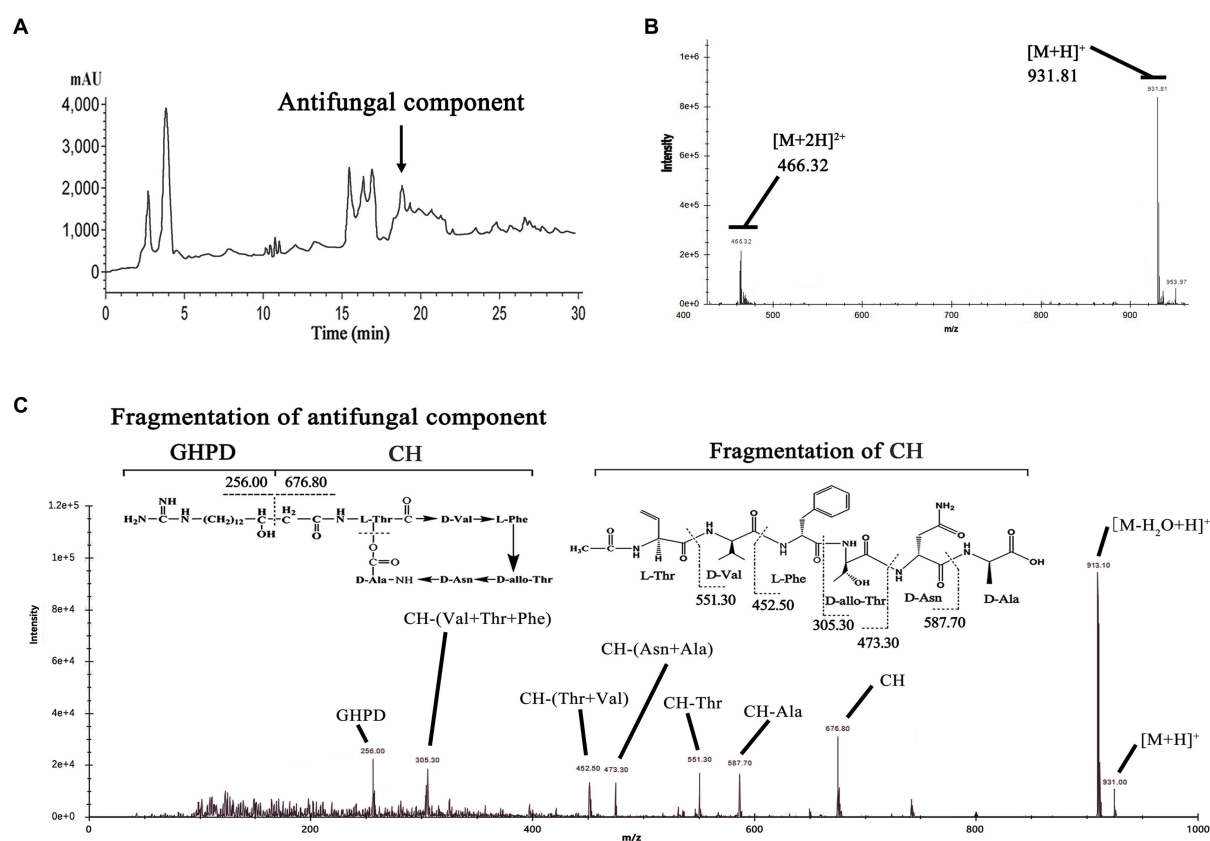


FIGURE 2

(A) Analytical HPLC profile at UV 210 nm of crude extracts from wild-type strain carrying *FusA*. The active ingredient indicated by the arrow is fusaricidin LI-F07a, which was later detected by activity tests and mass spectrometry. (B) Mass spectrum analysis of antifungal component peak. The number 931.81 indicates the mass of fusaricidin LI-F07a. (C) MS-MS analysis of peaks at m/z 931.81 as a precursor. CH indicates cyclic hexapeptide. GHPD indicates 15-guanidino-3-hydroxypentadecanoic acid.

known A domains were aligned with our A domains within *FusA*, and then, we acquired the substrate of our A domains, which matches the structure of peptide moiety within fusaricidin LI-F07a (Figure 1B). Furthermore, we also noticed the “ten code residues” located at positions 235, 236, 239, 278, 299, 301, 322, 330, 331, and 517 within the A domain. It has been previously reported that these residues serve as the binding site for the A domain when interacting with the substrate in the three-dimensional structure (Conti et al., 1997; Stachelhaus et al., 1999). Since the “ten code residues” are extracted from the A domains, the alignment of either the “A domain” or the “ten code residues” supports the same conclusion (Figure 1C).

Mass spectrometry fragment ion analysis is a reliable detection method and particularly powerful for the structural characterization of analogous compounds (Kurusu et al., 1987; Han et al., 2012). This method has successfully characterized more than 10 fusaricidin members (Vater et al., 2015). With a similar method, we demonstrated that our strain could produce fusaricidin LI-F07a by LC-MS-MS fragment ion analysis (Figure 2). All of the fusaricidin members are lipid-modified non-ribosomal cyclic hexadepsipeptides containing four D-amino acids and two L-amino acids. This particular ω -functionalized lipid side chain is of key importance for the antibiotic activity of the fusaricidins and their selective inhibition of fungal cells

due to the interaction with phospholipid cell membranes (Bionda et al., 2012). However, these fusaricidin members with different activity share the same lipid side chain except the cyclic hexadepsipeptide (Kurusu et al., 1987). How much the cyclic hexadepsipeptide of fusaricidin contributes to its antifungal activity still needs to be explored. Therefore, we intend to modify the cyclic hexadepsipeptide of fusaricidin LI-F07a to see whether its antifungal activity is affected.

In past decades, a rational design of novel peptide antibiotics method has been developed by modifying one domain and domain fusion within NRPS in *Bacillus* sp. and *Paenibacillus* sp. (Stachelhaus et al., 1995; Mootz et al., 2000; Yakimov et al., 2000; Han et al., 2012). However, only modifying one domain may cause a decrease in substrate-recognition ability due to the incompatibility of other domains in the same module. This is because, in addition to the A domain in NRPS, other domains such as C, T, and E also exhibit specific substrate recognition. If we could knock out an entire module from the NRPS without causing frameshift mutations, some instances might result in the production of a peptide that is missing a corresponding amino acid.

Therefore, we did not replace any A domains but directly deleted each of modules that consist of the A domain and its neighboring domains (Figure 3A). Excluding the pleiotropic

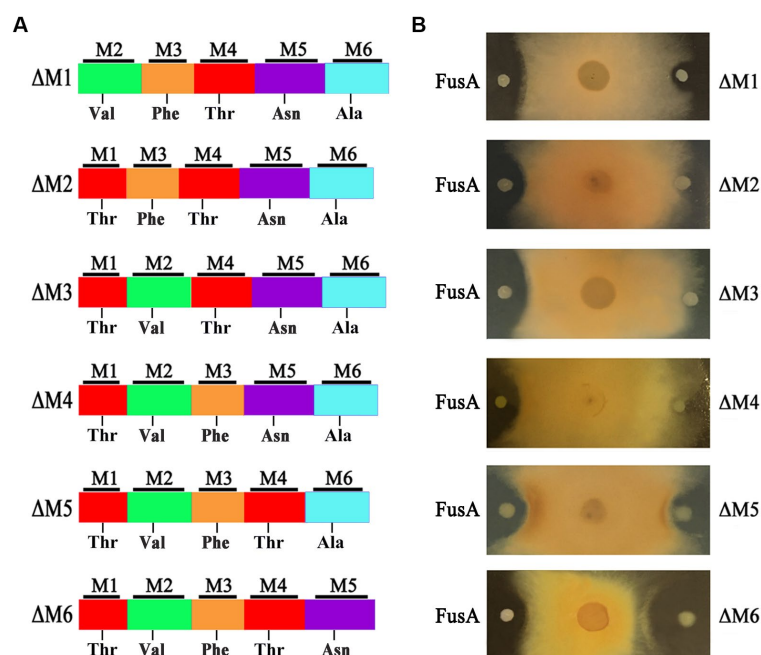


FIGURE 3

(A) Module organization of modified FusA and its substrate. (B) The inhibition effect of wild-type strain containing FusA and engineered strain carrying modified FusA against *F. asiaticum*.

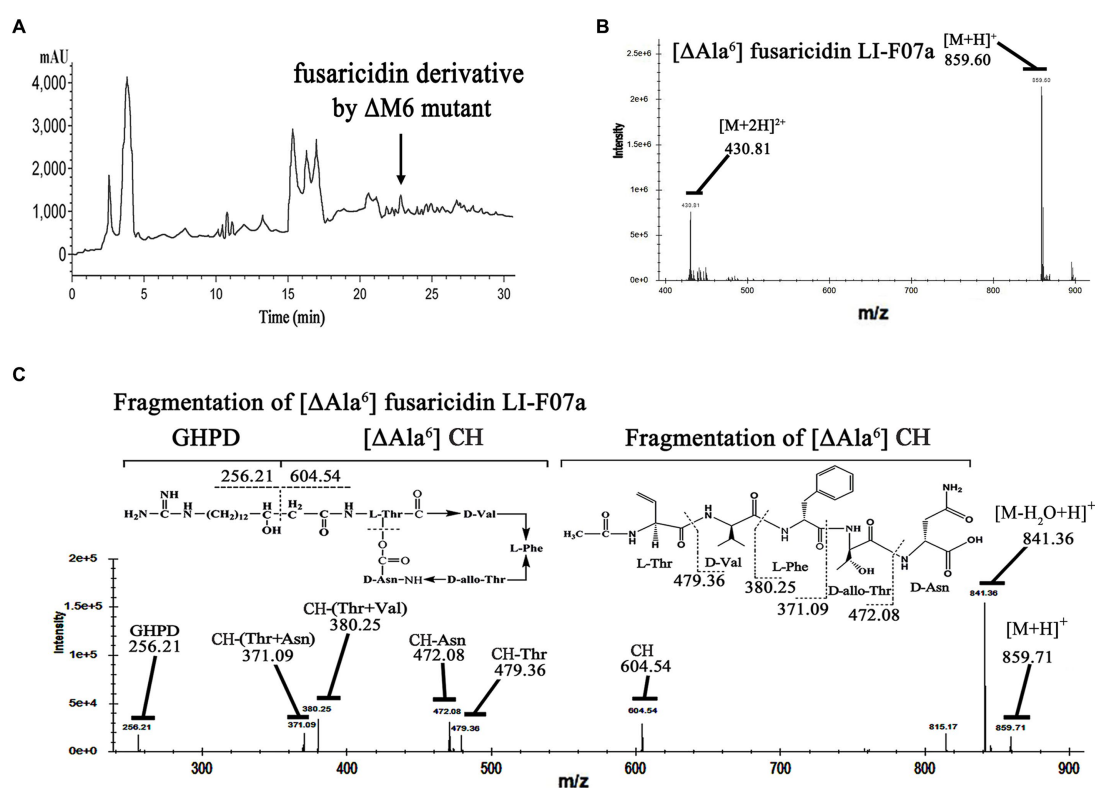


FIGURE 4

(A) Analytical HPLC profile at UV 210 nm of crude extracts from engineered strain carrying ΔM6. The active ingredient indicated by the arrow is [ΔAla⁶] fusaricidin LI-F07a, which was later detected by activity tests and mass spectrometry. (B) Mass spectrum analysis of antifungal component peak. The number 859.60 indicates the mass of [ΔAla⁶] fusaricidin LI-F07a. (C) MS-MS analysis of peaks at m/z 856 as a precursor. CH indicates cyclic hexapeptide. GHPD indicates 15-guanidino-3-hydroxypentadecanoic acid.

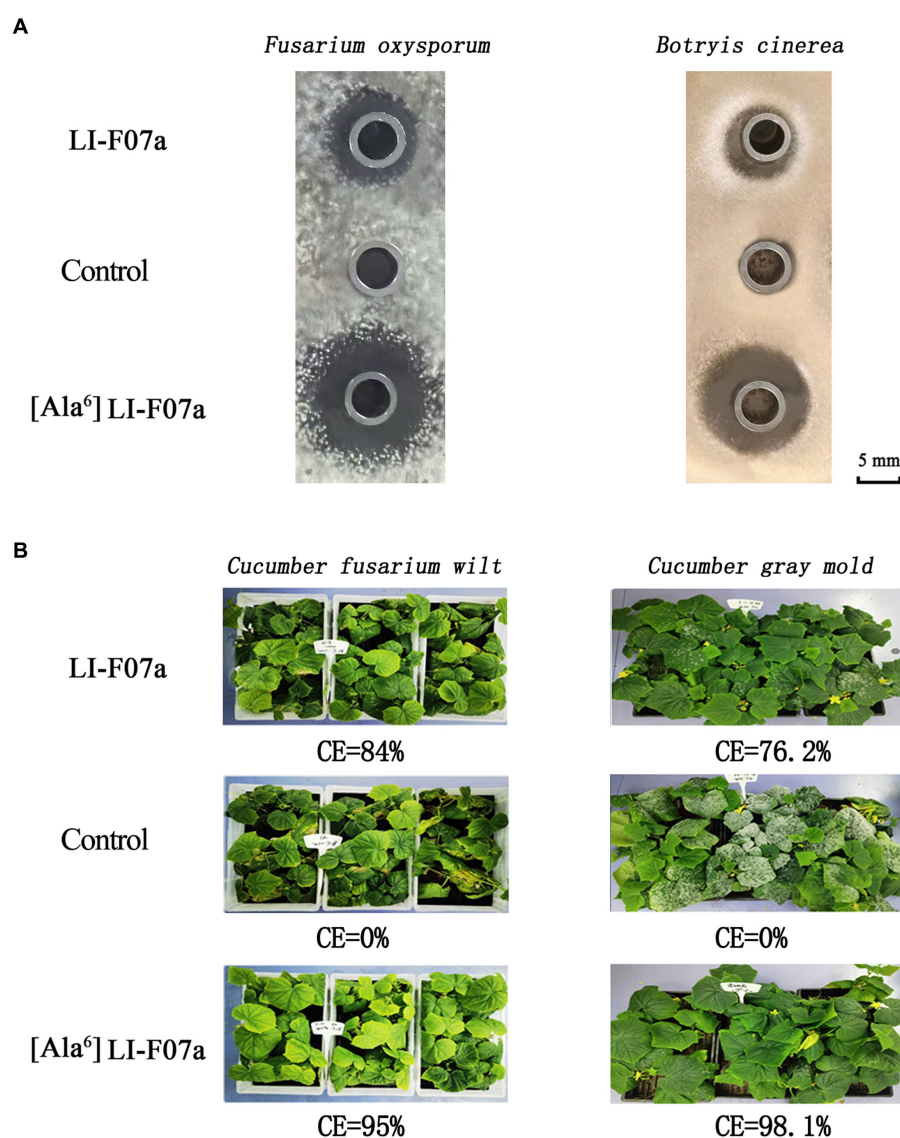


FIGURE 5

(A) Antifungal activity of fusaricidin LI-F07a and [Ala⁶] fusaricidin LI-F07a against *F. oxysporum* and *B. cinerea*. (B) Control effect of fusaricidin LI-F07a and [Ala⁶] fusaricidin LI-F07a against cucumber fusarium wilt and cucumber gray mold.

effect of a mutation in prokaryotes is generally considered easier compared to eukaryotic cells. In prokaryotes, such as our strain, the genome is typically continuous without introns. Introns are non-coding regions in the genome of eukaryotes that can contribute to the pleiotropic effects observed during gene knockout by introducing complexity in gene expression regulation and splicing. However, in prokaryotes, the absence of introns means that gene knockout does not involve the splicing or regulatory complexities associated with introns (Setubal et al., 2018). Moreover, frameshift mutations are one of the main factors that can contribute to the pleiotropic effects of gene knockout. When designing primers for homologous recombination double exchange, we have meticulously considered and designed the primers to effectively prevent any subsequent frameshift mutations resulting from the knockout. Even if the subsequent primary amino acid sequence changes due to a frameshift

mutation, a frameshift protein may still retain its structure and functionality. In fact, deleterious frameshift mutations have been proposed to be potential drivers for molecular evolution. Based on this shiftability, many genes and certain genomes are naturally optimized for frameshift tolerance (Wang et al., 2022). Importantly, we ensured the absence of frameshift mutations by conducting thorough sequencing analysis. We successfully acquired a strain with engineered $\Delta M6$ that showed a more enhanced antifungal activity than the wild-type strain with FusaA (Figure 3B). However, a former study had created a mutant with inactivated 4'-phosphopantetheinyl transferase, which could disrupt the production of NRPS/NPKS-dependent metabolites such as fusaricidins and still kept its antagonistic activity against *Fusarium culmorum*. They emphasized that the biofilm matrix formation may be of major importance in its antagonism (Timmusk et al., 2019). There could potentially exist an

antagonistic relationship between fusaricidins and exopolysaccharides production. It has been demonstrated that fusaricidin inhibits *Bacillus subtilis* by specifically targeting the mechanism of exopolysaccharide production (Yu et al., 2012). Additionally, we observed a similar phenomenon where the capacity for biofilm synthesis was enhanced in $\Delta M2$, $\Delta M5$, and $\Delta M6$ mutants. This enhancement may be associated with increased polysaccharides production. However, except for $\Delta M6$, none of these strains produced antibacterial effects in our study. Therefore, we suppose that the enhanced effect of this engineered strain should be attributed to the new compound [ΔAla^6] fusaricidin LI-F07a (Figure 4C). Indeed, both *in vitro* and *in vivo*, [ΔAla^6] fusaricidin LI-F07a did show stronger ability against *F. oxysporum* and *B. cinerea* than fusaricidin LI-F07a (Figure 5).

Until the completion of our study, it remained inconclusive whether the fungicidal activity of our mutants was affected by small peptides or the failure of peptide chains to cyclize due to the early peptide chain breakage caused by knocking out. Usually, the production of fusaricidin LI-F07a ranges from 12 mg/L to 76 mg/L (Raza et al., 2010; Han et al., 2012). In our wild-type strain, the maximum yield of fusaricidin LI-F07a is ~60 mg/L. In the engineered strain M6, the production of [ΔAla^6] fusaricidin LI-F07a is ~55 mg/L. Based on the comparison of the yield data before and after the genetic modification, it can be observed that the synthesis efficiency of the derivative is reduced by approximately 10 percent. The engineered $\Delta M6$ shows promising potential as a sustainable choice that can meet diverse industrial and agricultural demands. [ΔAla^6] fusaricidin LI-F07a can be applied effectively to prevent plants from being infected by *Fusarium* species pathogens.

Data availability statement

The original contributions presented in the study are included in the article/Supplementary material, further inquiries can be directed to the corresponding authors.

References

- Albarano, L., Esposito, R., Ruocco, N., and Costantini, M. (2020). Genome mining as new challenge in natural products discovery. *Mar. Drugs* 18:199. doi: 10.3390/md18040199
- Bionda, N., Stawikowski, M., Stawikowska, R., Cudic, M., López-Vallejo, F., Treitl, D., et al. (2012). Effects of cyclic lipopeptide structural modulation on stability, antibacterial activity, and human cell toxicity. *ChemMedChem* 7, 871–882. doi: 10.1002/cmdc.201200016
- Blin, K., Shaw, S., Augustijn, H. E., Reitz, Z. L., Biermann, F., Alanjary, M., et al. (2023). antiSMASH 7.0: new and improved predictions for detection, regulation, chemical structures and visualisation. *Nucleic Acids Res.* 51, W46–W50. doi: 10.1093/nar/gkad344
- Calcott, M. J., and Ackerley, D. F. (2015). Portability of the thiolation domain in recombinant pyoverdine non-ribosomal peptide synthetases. *BMC Microbiol.* 15:162. doi: 10.1186/s12866-015-0496-3
- Choi, S. K., Park, S. Y., Kim, R., Lee, C. H., Kim, J. F., and Park, S. H. (2008). Identification and functional analysis of the fusaricidin biosynthetic gene of *Paenibacillus polymyxa* E681. *Biochem. Biophys. Res. Commun.* 365, 89–95. doi: 10.1016/j.bbrc.2007.10.147
- Conti, E., Stachelhaus, T., Marahiel, M. A., and Brick, P. (1997). Structural basis for the activation of phenylalanine in the non-ribosomal biosynthesis of gramicidin S. *EMBO J.* 16, 4174–4183. doi: 10.1093/emboj/16.14.4174
- Deng, Y., Lu, Z., Lu, F., Zhang, C., Wang, Y., Zhao, H., et al. (2011). Identification of LI-F type antibiotics and di-n-butyl phthalate produced by *Paenibacillus polymyxa*. *J. Microbiol. Methods* 85, 175–182. doi: 10.1016/j.mimet.2011.02.013
- Han, J. W., Kim, E. Y., Lee, M. J., Kim, S. Y., Bang, E., and Kim, B. S. (2012). Site-directed modification of the adenylation domain of the fusaricidin nonribosomal peptide synthetase for enhanced production of fusaricidin analog. *Biotechnol. Lett.* 34, 1327–1334. doi: 10.1007/s10529-012-0913-8
- Haron, M. H., Avula, B., Shi, Q., Li, X. C., Ashfaq, M. K., Bae, J. Y., et al. (2019). Quantitative determination and pharmacokinetic study of fusaricidin a in mice plasma and tissues using ultra-high performance liquid chromatography-tandem mass spectrometry. *J. Pharm. Biomed. Anal.* 170, 187–192. doi: 10.1016/j.jpba.2019.03.042
- Hühner, E., Öqvist, K., and Li, S. M. (2019). Design of α -keto carboxylic acid dimers by domain recombination of nonribosomal peptide synthetase (NRPS)-like enzymes. *Org. Lett.* 21, 498–502. doi: 10.1021/acs.orglett.8b03793
- Hutchings, M. I., Truman, A. W., and Wilkinson, B. (2019). Antibiotics: past, present and future. *Curr. Opin. Microbiol.* 51, 72–80. doi: 10.1016/j.mib.2019.10.008
- Izoré, T., Candace Ho, Y. T., Kaczmarek, J. A., Gavrilidou, A., Chow, K. H., Steer, D. L., et al. (2021). Structures of a non-ribosomal peptide synthetase condensation domain suggest the basis of substrate selectivity. *Nat. Commun.* 12:2511. doi: 10.1038/s41467-021-22623-0
- Jeong, H., Choi, S. K., Ryu, C. M., and Park, S. H. (2019). Chronicle of a soil bacterium: *Paenibacillus polymyxa* E681 as a tiny guardian of plant and human health. *Front. Microbiol.* 10:467. doi: 10.3389/fmicb.2019.00467
- Kajimura, Y., and Kaneda, M. (1996). Fusaricidin a, a new depsipeptide antibiotic produced by *Bacillus polymyxa* KT-8 taxonomy, fermentation, isolation, structure

Author contributions

YL performed the research and drafted the manuscript. SC made crucial revisions of the manuscript. All authors contributed to the article and approved the submitted version.

Funding

The funders of this work are Chengdu NewSun Crop Science Company Limited (No. SWHCRR001) and the National Key Research and Development Program of China Award (No. 2017YFD0200807).

Conflict of interest

YL was employed by Chengdu NewSun Crop Science Co. Ltd.

The authors declare that this study received funding from Chengdu NewSun Crop Science Co. Ltd. This funder was engaged in the purifications, the greenhouse trails and the writing of this article.

Publisher's note

All claims expressed in this article are solely those of the authors and do not necessarily represent those of their affiliated organizations, or those of the publisher, the editors and the reviewers. Any product that may be evaluated in this article, or claim that may be made by its manufacturer, is not guaranteed or endorsed by the publisher.

Supplementary material

The Supplementary material for this article can be found online at: <https://www.frontiersin.org/articles/10.3389/fmicb.2023.1239958/full#supplementary-material>

- elucidation and biological activity. *J. Antibiot.* 49, 129–135. doi: 10.7164/antibiotics.49.129
- Kim, W. E., Ishikawa, F., Re, R. N., Suzuki, T., Dohmae, N., Kakeya, H., et al. (2022). Developing crosslinkers specific for epimerization domain in NRPS initiation modules to evaluate mechanism. *RSC Chem. Biol.* 3, 312–319. doi: 10.1039/D2CB00005A
- Kittilä, T., Mollo, A., Charkoudian, L. K., and Cryle, M. J. (2016). New structural data reveal the motion of carrier proteins in nonribosomal peptide synthesis. *Angew. Chem. Int. Ed. Engl.* 55, 9834–9840. doi: 10.1002/anie.201602614
- Kuroda, J., Fukai, T., and Nomura, T. (2001). Collision-induced dissociation of ring-opened cyclic depsipeptides with a guanidino group by electrospray ionization/ion trap mass spectrometry. *J. Mass Spectrom.* 36, 30–37. doi: 10.1002/jms.101
- Kurusu, K., Ohba, K., Arai, T., and Fukushima, K. (1987). New peptide antibiotics LI-F03, F04, F05, F07, and F08, produced by *Bacillus polymyxa*. I. Isolation and characterization. *J. Antibiot.* 40, 1506–1514. doi: 10.7164/antibiotics.40.1506
- Larsson, D. G. J., and Flach, C. F. (2022). Antibiotic resistance in the environment. *Nat. Rev. Microbiol.* 20, 257–269. doi: 10.1038/s41579-021-00649-x
- Lee, S. H., Cho, Y. E., Park, S.-H., Balaraju, K., Park, J. W., Lee, S. W., et al. (2012). An antibiotic fusaricidin: a cyclic depsipeptide from *Paenibacillus polymyxa* E681 induces systemic resistance against *Phytophthora* blight of red-pepper. *Phytoparasitica* 41, 49–58. doi: 10.1007/s12600-012-0263-z
- Lereclus, D., Vallade, M., Chaufaux, J., Arantes, O., and Rambaud, S. (1992). Expansion of insecticidal host range of *Bacillus thuringiensis* by in vivo genetic recombination. *Biotechnology* 10, 418–421. doi: 10.1038/nbt0492-418
- Li, J., Beatty, P., Shah, S., and Jensen, S. (2007). Use of PCR-targeted mutagenesis to disrupt production of fusaricidin-type antifungal antibiotics in *Paenibacillus polymyxa*. *Appl. Environ. Microbiol.* 73, 3480–3489. doi: 10.1128/AEM.02662-06
- Li, Y., and Chen, S. (2019). Fusaricidin produced by *Paenibacillus polymyxa* WLY78 induces systemic resistance against *fusarium* wilt of cucumber. *Int. J. Mol. Sci.* 20:E5240. doi: 10.3390/ijms20205240
- Li, Y., Gu, Y., Li, J., Xu, M., Wei, Q., and Wang, Y. (2015). Biocontrol agent *Bacillus amyloliquefaciens* LJ02 induces systemic resistance against cucurbits powdery mildew. *Front. Microbiol.* 6:883. doi: 10.3389/fmicb.2015.00883
- Li, Y., Zhang, H., Li, Y., and Chen, S. (2021). Fusaricidin biosynthesis is controlled via a KinB-Spo0A-AbrB signal pathway in *Paenibacillus polymyxa* WLY78. *Mol. Plant-Microbe Interact.* 34, 1378–1389. doi: 10.1094/MPMI-05-21-0117-R
- Marahiel, M. A. (2016). A structural model for multimodular NRPS assembly lines. *Nat. Prod. Rep.* 33, 136–140. doi: 10.1039/C5NP00082C
- Marahiel, M. A., Stachelhaus, T., and Mootz, H. D. (1997). Modular peptide synthetases involved in nonribosomal peptide synthesis. *Chem. Rev.* 97, 2651–2674. doi: 10.1021/cr960029e
- Mootz, H. D., Schwarzer, D., and Marahiel, M. A. (2000). Construction of hybrid peptide synthetases by module and domain fusions. *Proc. Natl. Acad. Sci. U. S. A.* 97, 5848–5853. doi: 10.1073/pnas.100075897
- Paulus, H., and Gray, E. (1964). The biosynthesis of polymyxin B by growing cultures of *Bacillus polymyxa*. *J. Biol. Chem.* 239, 865–871. doi: 10.1016/S0021-9258(18)51670-7
- Raza, W., Yang, X., Wu, H., Huang, Q., Xu, Y., and Shen, Q. (2010). Evaluation of metal ions (Zn^{2+} , Fe^{3+} and Mg^{2+}) effect on the production of fusaricidin-type antifungal compounds by *Paenibacillus polymyxa* SQR-21. *Bioresour. Technol.* 101, 9264–9271. doi: 10.1016/j.biortech.2010.07.052
- Reimann, M., Sandjo, L. P., Antelo, L., Thines, E., Siepe, I., and Opatz, T. (2017). A new member of the fusaricidin family-structure elucidation and synthesis of fusaricidin E. *Beilstein J. Org. Chem.* 13, 1430–1438. doi: 10.3762/bjoc.13.140
- Rüschbaum, J., Steinchen, W., Mayerthaler, F., Feldberg, A. L., and Mootz, H. D. (2022). FRET monitoring of a nonribosomal peptide synthetase elongation module reveals carrier protein shuttling between catalytic domains. *Angew. Chem.* 61:e202212994. doi: 10.1002/anie.202212994
- Samel, S. A., Schoenafinger, G., Knappe, T. A., Marahiel, M. A., and Essen, L. O. (2007). Structural and functional insights into a peptide bond-forming bidomain from a nonribosomal peptide synthetase. *Structure* 15, 781–792. doi: 10.1016/j.str.2007.05.008
- Schwarzer, D., Mootz, H. D., Linne, U., and Marahiel, M. A. (2002). Regeneration of misprimed nonribosomal peptide synthetases by type II thioesterases. *Proc. Natl. Acad. Sci. U. S. A.* 99, 14083–14088. doi: 10.1073/pnas.212382199
- Setubal, J. C., Almeida, N. F., and Wattam, A. R. (2018). Comparative genomics for prokaryotes. *Methods Mol. Biol.* 1704, 55–78. doi: 10.1007/978-1-4939-7463-4_3
- Shokrollahi, N., Ho, C.-L., Zainudin, N. A. I. M., Wahab, M. A. W. B. A., and Wong, M.-Y. (2021). Identification of non-ribosomal peptide synthetase in *Ganoderma boninense* pat. That was expressed during the interaction with oil palm. *Sci. Rep.* 11:16330. doi: 10.1038/s41598-021-95549-8
- Stachelhaus, T., Mootz, H. D., and Marahiel, M. A. (1999). The specificity-conferring code of adenylation domains in nonribosomal peptide synthetases. *Chem. Biol.* 6, 493–505. doi: 10.1016/S1074-5521(99)80082-9
- Stachelhaus, T., Schneider, A., and Marahiel, M. A. (1995). Rational design of peptide antibiotics by targeted replacement of bacterial and fungal domains. *Sci.* 269, 69–72. doi: 10.1126/science.7604280
- Timms, S., Copolovici, D., Copolovici, L., Teder, T., Nevo, E., and Behers, L. (2019). *Paenibacillus polymyxa* biofilm polysaccharides antagonise *fusarium graminearum*. *Sci. Rep.* 9:662. doi: 10.1038/s41598-018-37718-w
- Vater, J., Niu, B., Dietel, K., and Borris, R. (2015). Characterization of novel fusaricidins produced by *Paenibacillus polymyxa*-M1 using MALDI-TOF mass spectrometry. *J. Am. Soc. Mass Spectrom.* 26, 1548–1558. doi: 10.1007/s13361-015-1130-1
- Villafane, R., Bechhofer, D. H., Narayanan, C. S., and Dubnau, D. (1987). Replication control genes of plasmid pE194. *J. Bacteriol.* 169, 4822–4829. doi: 10.1128/jb.169.10.4822-4829.1987
- Wang, X., Dong, Q., Chen, G., Zhang, J., Liu, Y., and Cai, Y. (2022). Frameshift and wild-type proteins are often highly similar because the genetic code and genomes were optimized for frameshift tolerance. *BMC Genomics* 23:416. doi: 10.1186/s12864-022-08435-6
- Wheaton, M. J., and Townsend, C. A. (2021). Evolutionary and functional analysis of an NRPS condensation domain integrates β -lactam, D-amino acid, and dehydroamino acid synthesis. *Proc. Natl. Acad. Sci. U. S. A.* 118:e2026017118. doi: 10.1073/pnas.2026017118
- Yakimov, M. M., Giuliano, L., Timmis, K. N., and Golyshin, P. N. (2000). Recombinant acylheptapeptide lichenysin: high level of production by *Bacillus subtilis* cells. *J. Mol. Microbiol. Biotechnol.* 2, 217–224.
- Yan, Z., Dolstra, O., Prins, T., Stam, P., and Visser, P. (2006). Assessment of partial resistance to powdery mildew (*Podosphaera pannosa*) in a tetraploid rose population using a spore-suspension inoculation method. *Eur. J. Plant Pathol.* 114, 301–308. doi: 10.1007/s10658-005-5995-x
- Yu, W. B., Yin, C. Y., Zhou, Y., and Ye, B. C. (2012). Prediction of the mechanism of action of fusaricidin on *Bacillus subtilis*. *PLoS One* 7:e50003. doi: 10.1371/journal.pone.0050003
- Zhang, W., Ding, Y., Yao, L., Liu, K., and Du, B. (2013). Construction of gene knock-out system for *Paenibacillus polymyxa* SC2. *Acta Microbiol. Sin.* 53, 1258–1266.
- Zhang, S., Fan, S., Zhu, J., Zhou, L., Yan, X., Yang, Z., et al. (2022). Enhanced rishirilide biosynthesis by a rare in-cluster phosphopantetheinyl transferase in *Streptomyces xanthophaeus*. *Microbiol. Spectr.* 10:e0324722. doi: 10.1128/spectrum.03247-22
- Zhu, M., Wang, L., and He, J. (2019). Chemical diversification based on substrate promiscuity of a standalone adenylation domain in a reconstituted NRPS system. *ACS Chem. Bio.* 14, 256–265. doi: 10.1021/acschembio.8b00938



OPEN ACCESS

EDITED BY

Guangshun Wang,
University of Nebraska Medical Center,
United States

REVIEWED BY

Fengyu Du,
Qingdao Agricultural University, China
Shivankar Agrawal,
Indian Council of Medical Research, India

*CORRESPONDENCE

Chang Li
✉ lichang661@126.com
Tian-Yi Yu
✉ tianoo3000@163.com
Yue-Hu Pei
✉ peiyueh@vip.163.com

RECEIVED 13 August 2023

ACCEPTED 12 September 2023

PUBLISHED 02 October 2023

CITATION

Liu S-X, Ou-Yang S-Y, Lu Y-F, Guo C-L, Dai S-Y,
Li C, Yu T-Y and Pei Y-H (2023) Recent
advances on cyclodepsipeptides: biologically
active compounds for drug research.
Front. Microbiol. 14:1276928.
doi: 10.3389/fmicb.2023.1276928

COPYRIGHT

© 2023 Liu, Ou-Yang, Lu, Guo, Dai, Li, Yu and
Pei. This is an open-access article distributed
under the terms of the [Creative Commons
Attribution License \(CC BY\)](#). The use,
distribution or reproduction in other forums is
permitted, provided the original author(s) and
the copyright owner(s) are credited and that
the original publication in this journal is cited,
in accordance with accepted academic
practice. No use, distribution or reproduction is
permitted which does not comply with these
terms.

Recent advances on cyclodepsipeptides: biologically active compounds for drug research

Si-Xuan Liu¹, Si-Yi Ou-Yang¹, Yong-Fu Lu¹, Chun-Lin Guo¹,
Si-Yang Dai¹, Chang Li^{1,2*}, Tian-Yi Yu^{3*} and Yue-Hu Pei^{1*}

¹Department of Medicinal Chemistry and Natural Medicine Chemistry, College of Pharmacy, Harbin Medical University, Harbin, China, ²Key Laboratory of Gut Microbiota and Pharmacogenomics of Heilongjiang Province, College of Pharmacy, Harbin Medical University, Harbin, China, ³The Third Affiliated Hospital of Heilongjiang University of Traditional Chinese Medicine, Harbin, China

Cyclodepsipeptides are a large family of peptide-related natural products consisting of hydroxy and amino acids linked by amide and ester bonds. A number of cyclodepsipeptides have been isolated and characterized from fungi and bacteria. Most of them showed antitumor, antifungal, antiviral, antimalarial, and antitrypanosomal properties. Herein, this review summarizes the recent literatures (2010–2022) on the progress of cyclodepsipeptides from fungi and bacteria except for those of marine origin, in order to enrich our knowledge about their structural features and biological sources.

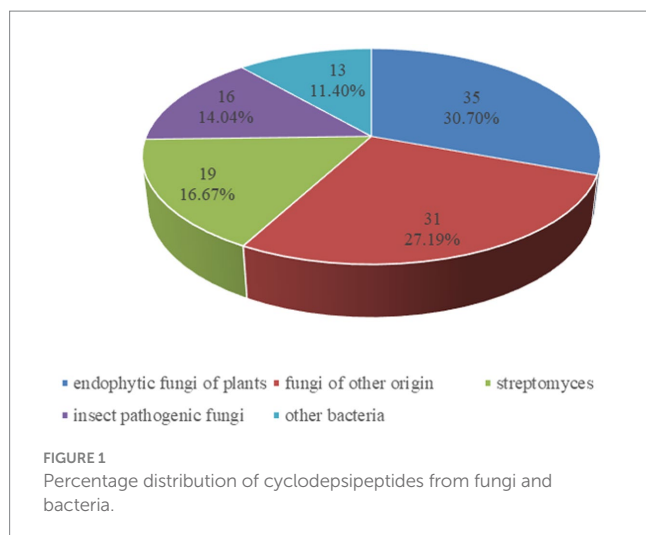
KEYWORDS

cyclodepsipeptide, fungi, bacteria, antimicrobial, biological activity

Introduction

Cyclodepsipeptides are an important group of polypeptides, which contain one or more amino acids replaced by a hydroxy acid, resulting in at least one ester bond in the core ring structure (Lemmens-Gruber et al., 2009; Buckton et al., 2021). Cyclodepsipeptides exhibit a broad spectrum of biological activities including antitumor, antifungal, antiviral, antimalarial, and antitrypanosomal activities (Moore, 1996; Nihei et al., 1998; Du et al., 2014). Due to their unique structural and biological properties, cyclodepsipeptides have emerged as promising lead structures for crop protection and human and veterinary medicine (Sivanathan and Scherkenbeck, 2014).

The dominant sources of cyclodepsipeptides are fermentations of various fungi and bacteria. In addition, abundant cyclodepsipeptides have been isolated from algae, plants and marine organism (Sivanathan and Scherkenbeck, 2014; Negi et al., 2017). Because several reports have summarized the progress of the marine cyclodepsipeptides (Zeng et al., 2023), our review focused on the recent advances of cyclodepsipeptides from bacteria and fungi from plants, insects or soil except for marine organism. As a result, from 2010 to the present, 114 cyclodepsipeptides have been isolated and identified through an extensive literature search, including Web of Science, SciFinder, and PubChem tools. Included in the list of search terms were “cyclodepsipeptides,” “endophytic fungi,” and “insect pathogenic fungi” as well as “streptomyces,” “fungi,” “bacteria.” As shown in Figure 1, the major producers of cyclodepsipeptides are endophytic fungi of plants, which made up 30.70%, followed by fungi of other origin (27.19%), streptomyces (16.67%), insect pathogenic fungi (14.04%), and other bacteria (11.40%).



Biologically active cyclodepsipeptides

Cyclodepsipeptides from endophytic fungi of plants

The endophytic fungi from *Fusarium* and *Trichoderma* genus were the main producers of cyclodepsipeptides. Chemical investigation on the fungus *Sarocladium kiliense* HDN11-112 from mangroves, led to the characterization of saroclide A (1) and saroclide B (2), two cyclic depsipeptides with 7-hydroxy-4-methyl-3-oxodec-4-enoic acid (HMODA) unit. They were a couple of epimerides with different L- and D-Pro configurations of the proline units. Saroclide A (1) exhibited a lowering blood lipid effect, while saroclide A (1) and B (2) were invalid for four pathogenic microorganisms and five cancer cell lines (Guo et al., 2018). Using a genome-wide *Candida albicans* fitness test, a new cyclodepsipeptide, phaeofungin (3), containing a β , γ -dihydroxy- γ -methylhexadecanoic acid (DHMHDA) unit and seven amino acids, was isolated from *Phaeosphaeria* sp. Using the same method, another structurally different cyclodepsipeptide, phomafungin (4), was isolated from *Phoma* sp. 3 showed good antifungal activity to *Aspergillus fumigatus* with the MIC value at 8–16 μ g/mL and *Trichophyton mentagrophytes* with the MIC value at 4 μ g/mL (Singh et al., 2013). Isaridins A (5) and B (6) were isolated from *Beauveria* sp. Lr89, which was isolated from the roots of *Maytenus hookeri* Loes (Li et al., 2011). Fusaripeptide A (7), a novel cyclodepsipeptide, obtained from the culture of the plant endophytic fungus *Fusarium* sp. 7 showed significant antifungal activity against *A. fumigatus*, *Candida glabrata*, *Candida albicans* and *Candida krusei* (IC₅₀ 0.11–0.24 μ M). In addition, it exhibited potent anti-malarial activity against *Plasmodium falciparum* (IC₅₀ 0.34 μ M) (Ibrahim et al., 2018). W493 C (8) and W493 D (9), two novel cyclic depsipeptides, as well as two known cyclic depsipeptides, W493 A (10) and W493 B (11), were isolated from the mangrove plant *Ceriops tagal* endophytic fungus *Fusarium* sp. 8 and 9 showed antifungal activity toward *Cladosporium cladosporioides* (Lv et al., 2015). Bioassay-guided isolation and purification yielded four new cyclodepsipeptides, trichodestruxins A (12), B (13), C (14) and D (15), as well as two known cyclodepsipeptides, destruxin E2 chlorohydrin (16) and destruxin A2 (17), isolated from the fungus *Trichoderma harzianum*. 14 and 16 were evaluated for their cytotoxicity against HT-29, A549, and P388 cell lines

with IC₅₀ values at 0.7–10.3 μ M (Liu et al., 2020; Table 1). Chaetomiamide A (18), a rare cyclodepsipeptide, was isolated from the fungus *Chaetomium* sp. from the root of *Cymbidium goeringii*, it also exhibited weak cytotoxicity toward HL-60 cell line with IC₅₀ values of 35.2 μ M (Wang et al., 2017; Figure 2).

A *Celtis sinensis*-derived *Fusarium* sp. HU0174, produced acuminatums A–D (19–22), as well as beauvericin (23). Acuminatum D (22) was a novel cyclic depsipeptide. 19–22 exhibited potent inhibitory activity against *Penicillium digitatum* and *Curvularia lunata* using the AGAR disc diffusion methods (Li et al., 2021). Cultivation of the plant endophytic fungus *Fusarium* sp. led to the isolation of four novel compounds, fusarihexasins C (24), D (25), E (26), and enniatin Q (27), together with the known beauvericin (23), MK1688 (28), enniatin I (29), viscumamide (30). The cytotoxic activities of these compounds were tested using MRMT-1, HepG-2, and Huh-7 cell lines, respectively (Table 1). 27–29, and 23 exhibited strong cytotoxic activities (Wang et al., 2022; Figure 3). Two depsipeptides named xylariaceins A–B (31–32) were isolated and identified from endophytes *Xylariaceae* BSNB-0294. Both xylariaceins A (31) and B (32) inhibited the growth of *Fusarium oxysporum* (Barthélemy et al., 2021). In addition, three cyclohexadepsipeptides, destruxin A4 (33), trichomide B (34) and homodestcardin (35), isolated from the endophytic fungus *Fusarium chlamydosporum*, were found to be lethal to brine shrimp, 33 showed significant activity with LD₅₀ at 2.78 μ g/mL. It was even better than the positive control (7.75 μ g/mL) (Wang et al., 2020).

In conclusion, the genus *Fusarium* and *Trichoderma* were the main producers of cyclodepsipeptides in endophytic fungi. In addition, the genus *Beauveria*, *Sarocladium*, *Muscodora*, *Chaetomium*, *Phoma*, *Phaeosphaeria* could produce diverse cyclodepsipeptides as well (Figure 4).

Cyclodepsipeptides from insect pathogenic fungi

Cordyceps cardinalis NBRC 103832, the insect pathogenic fungus, yielded a class of new depsipeptides, cardinalisamides A (36), B (37), C (38). The bioactivity results indicated that 36–38 exhibited *in vitro* antitrypanosomal activity against *Trypanosoma brucei brucei* with IC₅₀ values of 8.56, 8.65 and 8.63 μ g/mL, respectively (Umeyama et al., 2014). Cordycecin A (39), a new cyclodepsipeptide, together with beauvericin E (40), beauvericin J (41), beauvericin (23) and beauvericin A (42), were isolated from the fungus *Cordyceps cicadae*, which was a fungus parasitic on the larvae of *Cicada flammata* as the host insect (Wang et al., 2014). Compounds 23, 40–42 exhibited cytotoxicity toward HepG2 and HepG2/ADM cells with IC₅₀ values at 2.40–14.48 μ M. The insect pathogenic fungus *Beauveria felina* yielded iso-isariin B (43) and isaridin E (44) (Langenfeld et al., 2011; Figure 5).

Verlamelins A (45) and B (46) were isolated from insect pathogenic fungus *Lecanicillium* sp. HF627. 45 showed broad antifungal activity against plant pathogenic fungi (Ishidoh et al., 2014). Conoideocrellide A (47) was a new cyclodepsipeptide isolated from the entomopathogenic fungus *Conoideocrella tenuis* BCC 18627. Unfortunately, tests showed that 47 had no biological activity in protocols for antiplasmodial and antiviral properties as well as cytotoxicity against a number of cancer cell lines (Isaka et al., 2011). The isolation of entomopathogenic fungus

TABLE 1 The inhibitory effects of CDPs on different cancer cell lines.

Compound	Cells	IC ₅₀ (μM)	References	Compound	Cells	IC ₅₀ (μM)	References
12	HT-29	7.8 ± 0.1	Liu et al. (2020)	27	Huh-7	3.3 ± 0.3	Wang et al. (2022)
	A549	15.6 ± 0.1			MRMT-1	2.8 ± 0.2	
	P388	17.0 ± 0.3			HepG-2	1.4 ± 0.3	
13	HT-29	16.7 ± 0.2	Liu et al. (2020)	28	Huh-7	9.1 ± 1.0	Wang et al. (2022)
	A549	8.8 ± 0.1			MRMT-1	6.8 ± 0.5	
	P388	19.1 ± 0.2			HepG-2	3.3 ± 0.4	
14	HT-29	3.4 ± 0.1	Liu et al. (2020)	29	Huh-7	6.2 ± 0.5	Wang et al. (2022)
	A549	10.3 ± 0.3			MRMT-1	2.7 ± 0.2	
	P388	8.4 ± 0.1			HepG-2	2.8 ± 0.2	
15	A549	17.5 ± 0.1	Liu et al. (2020)	30	Huh-7	>50	Wang et al. (2022)
16	HT-29	0.7 ± 0.1	Liu et al. (2020)		MRMT-1	>50	
	A549	4.9 ± 0.2			HepG-2	14.1 ± 3.4	
	P388	3.7 ± 0.1		39	HepG-2	>50	Wang et al. (2014)
17	HT-29	9.3 ± 0.2	Liu et al. (2020)		HepG-2/ADM	>50	
	A549	13.1 ± 0.1		40	HepG-2	13.67 ± 2.59	Wang et al. (2014)
	P388	12.5 ± 0.2			HepG-2/ADM	14.48 ± 1.68	
18	HL-60	35.2	Wang et al. (2017)	41	HepG-2	5.04 ± 0.20	Wang et al. (2014)
23	Huh-7	4.3 ± 1.2	Wang et al. (2022)		HepG-2/ADM	2.67 ± 0.09	
	MRMT-1	8.7 ± 0.2		42	HepG-2	2.81 ± 0.86	Wang et al. (2014)
	HepG-2	1.0 ± 0.1			HepG-2/ADM	2.93 ± 0.15	
24	Huh-7	>50	Wang et al. (2022)	61	HeLa KB3.1	28	Helaly et al. (2018)
	MRMT-1	>50		82	BT-549	2.5	Luo et al. (2022)
	HepG-2	20.1 ± 11.4		104	HCT-116	0.11	Plaza et al. (2012)
25	Huh-7	30.3 ± 7.2	Wang et al. (2022)				
	MRMT-1	17.3 ± 1.1					
	HepG-2	15.4 ± 4.2					
26	Huh-7	46.2 ± 2.5	Wang et al. (2022)				
	MRMT-1	>50					
	HepG-2	10.7 ± 7.7					

IC₅₀, concentration required for 50% inhibition.

Ophiocordyceps coccidiicola NBRC 100683 mutant strain IU-3 provided three cyclodepsipeptides, destruxins A (48), B (49), and destruxin E chlorohydrin (50). The *in vitro* antitrypanosomal activity exhibited that the IC₅₀ values for 48–50 against *T. b. brucei* GUTat3.1 were 0.33, 0.16 and 0.061 μg/mL (Ganaha et al., 2016). The entomopathogenic fungus *Ophiocordyceps communis* BCC 16475 yielded a new cyclodepsipeptide, cordycommunin (51). 51 was demonstrated to have growth inhibitory effect on *Mycobacterium tuberculosis* H37Ra (MIC 15 μM) (Haritakun et al., 2010; Figures 6, 7; Table 2).

Cyclodepsipeptides from fungi of other origin

Desmethyloisarinidin E (52), desmethyloisarinidin C2 (53), isarinidin F (54) and isarinidin E (44), isarinidin C2 (55), destruxin A (48), resetoxin B (56), and roseocardin (57) were collected from hefilamentous fungus *Beauveria felina*. On the elastase release in

neutrophils and the FMLP-induced superoxide anion generation, 52 and 53 showed specific inhibitory action. Compound 52 demonstrated particular inhibition on superoxide anion generation with an IC₅₀ at 10.0 μM, while 53 exhibited specific activity on elastase release with an IC₅₀ at 10.01 μM (Chung et al., 2013). A fungus linked with nematodes that shared affinities with the genus *Ophiosphaerella*, produced ophiotine (58), along with two new derivatives arthrichitin (59) and arthrichitin B (60) as well as one known compound arthrichitin C (61). Only 61 exhibited a low level of cytotoxicity, with an IC₅₀ value of 28 μM against HeLa cells KB3.1 (Helaly et al., 2018; Figure 8).

A new cyclodepsipeptide isarinidin H (62), as well as known compounds isariin A (63), isariin E (64), nodupetide (65), iso-isariin D (66) and iso-isariin B (43) isarinidin E (44), desmethyloisarinidin E (52) were identified from *Amphichorda guana*. Based on the bioassay, the novel cyclodepsipeptide isarinidin H (62) exhibited suppression of *Bacillus subtilis* at 12.5 μM and displayed potent antifungal activities toward *Alternaria solan* (IC₅₀ 15.6 μM) (Liang et al., 2021). A new

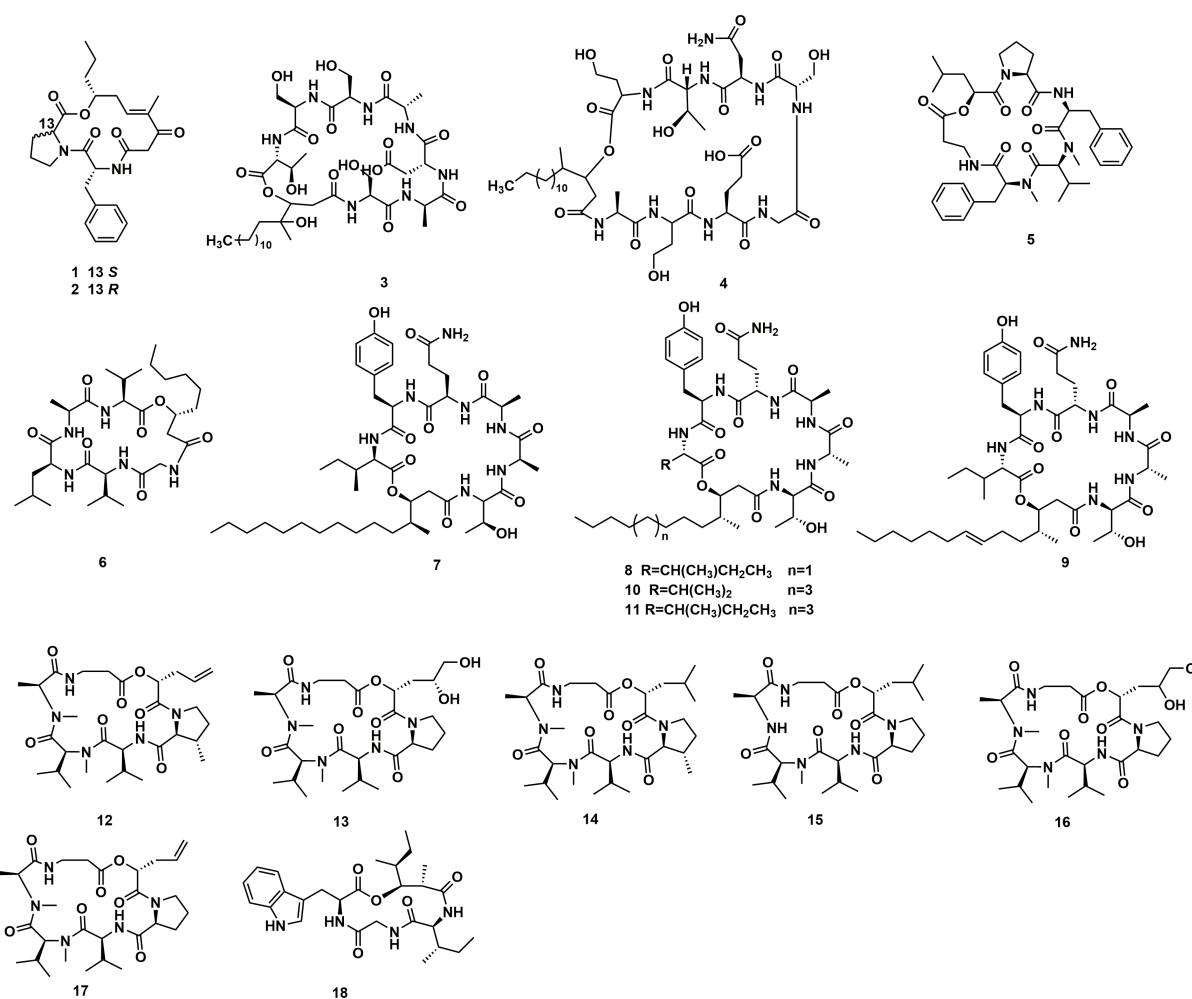


FIGURE 2
Chemical structures of CDPs 1–18.

class of cyclodepsipeptides SCH 217048 (**67**), SCH 218157 (**68**), together with pleosporin A (**69**) were collected from an elephant dung fungus BCC 7069. With IC₅₀ values of 1.6, 6.4, and 1.6 µg/mL, respectively, all three compounds demonstrated antimalarial efficacy against *P. falciparum* K1 (Isaka et al., 2014). Artrichitin (**70**) and lipopeptide 15G256e (**71**) were isolated from freshwater ascomycetes (*Delitschia* sp.). Under hypoxic conditions, the African American prostate cancer cell line (E006AA-hT) was resistant to the antiproliferative effects of both **70** and **71** (Rivera-Chávez et al., 2019). Two known cyclodepsipeptides named SCH 378161 (**72**) and SCH 217048 (**67**) were isolated from organic extracts of axenic *Clohesyomyces aquaticus* (Dothideomycetes) (El-Elm et al., 2017; Figure 9).

The cyclic depsipeptides clavariopsins A–I (**73–81**) were found through fractions of the extract of the aquatic hyphomycete *Clavariopsis aquatica*. They provided significant or moderate antifungal activity toward primarily multihost plant pathogens (Soe et al., 2019). Xylaroamide A (**82**), a cyclic depsipeptide, was isolated from an endolichenic *Xylaria* sp. Following a series of biological tests, it was discovered that **82** had an IC₅₀ value of 2.5 µM and had the most powerful impact on the human triple-negative epithelial breast cancer

cell line, BT-549. In addition, **82** strongly induced cell cycle arrest in G0/G1 phase in BT-549 cells by using cycle distribution analysis (Luo et al., 2022; Figures 10, 11).

Cyclodepsipeptides from streptomyces

Ulleungamides A (**83**) and B (**84**), two new cyclic depsipeptides, were found in terrestrial cultured strains *Streptomyces* sp. Only *Staphylococcus aureus* and *Salmonella typhimurium* showed growth inhibition by ulleungamide A (**83**) without cytotoxicity. Besides, Comparing **83** to **84**, the selective antibacterial activity showed that the hydroxy group at position C-4 significantly lowered the activity (Son et al., 2015). Atrovimycin (**85**), featuring a novel vicinal-hydroxylated cinnamic acylchain, was a cyclodepsipeptide separated from *Streptomyces atrovirens* LQ13. A series of biological assays revealed that **85** showed a significant activity toward *F. oxysporum* and antitubercular activity against *Mycobacterium tuberculosis* H37Rv both *in vitro* (with MIC of 2.5 µg/mL) and *in vivo* (Liu et al., 2019; Figure 12).

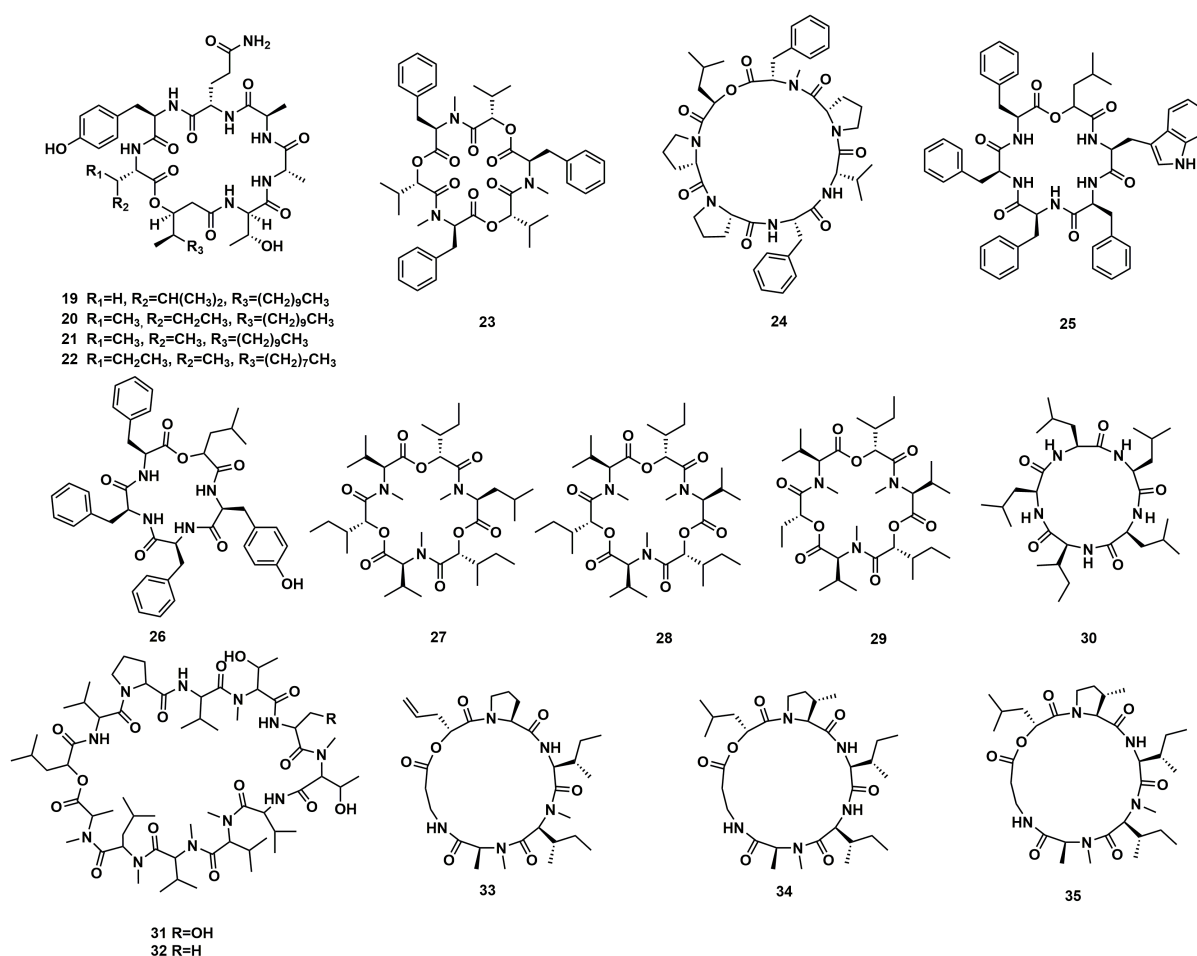


FIGURE 3
Chemical structures of CDPs 19–35.

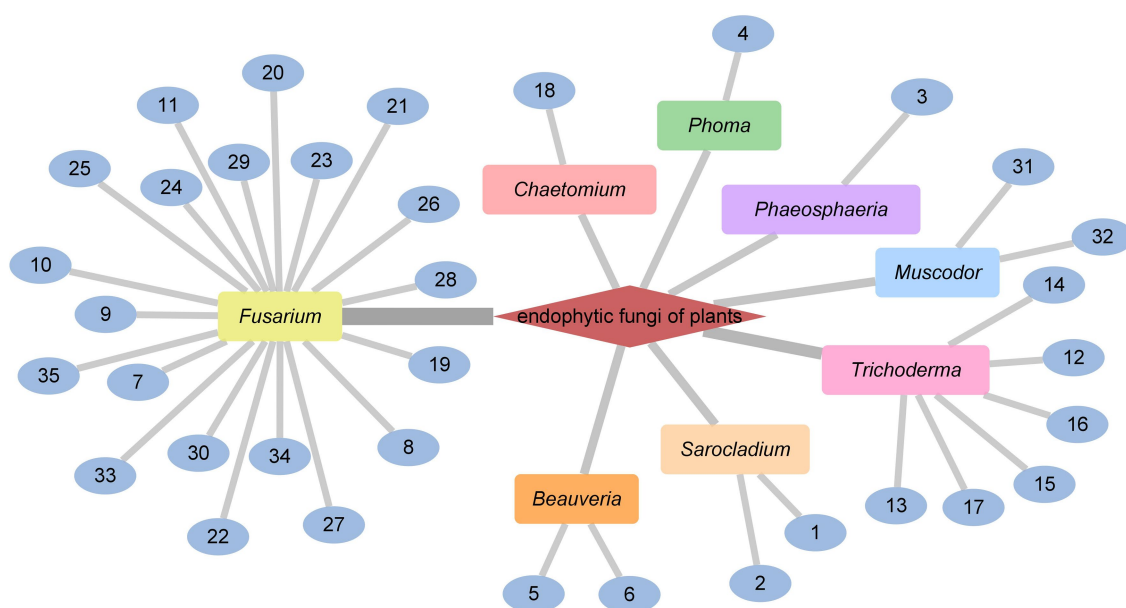


FIGURE 4
CDPs from endophytic fungi of plants.

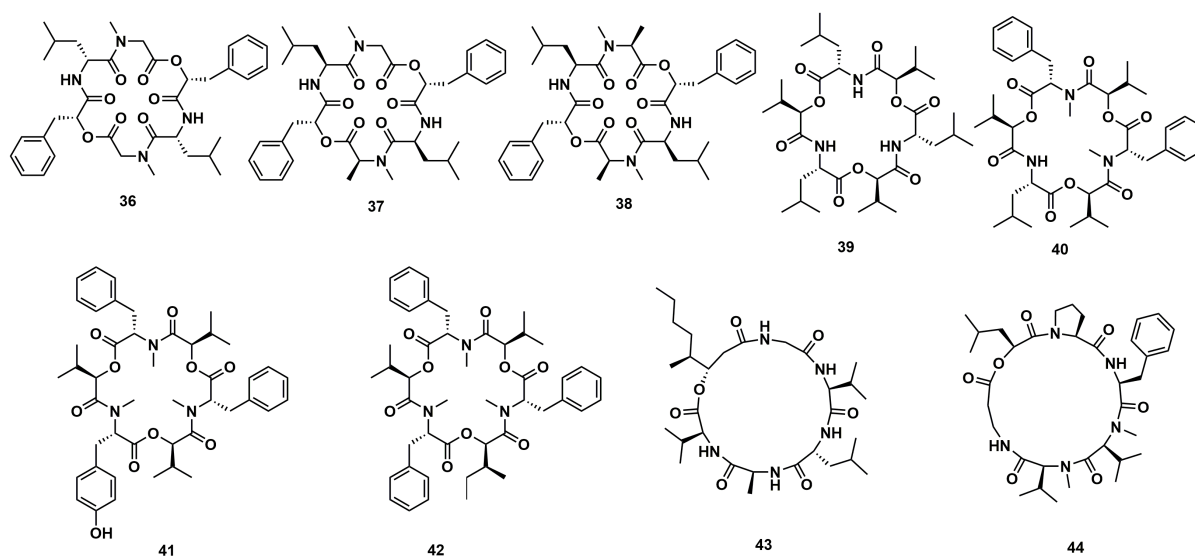


FIGURE 5
Chemical structures of CDPs 36–44.

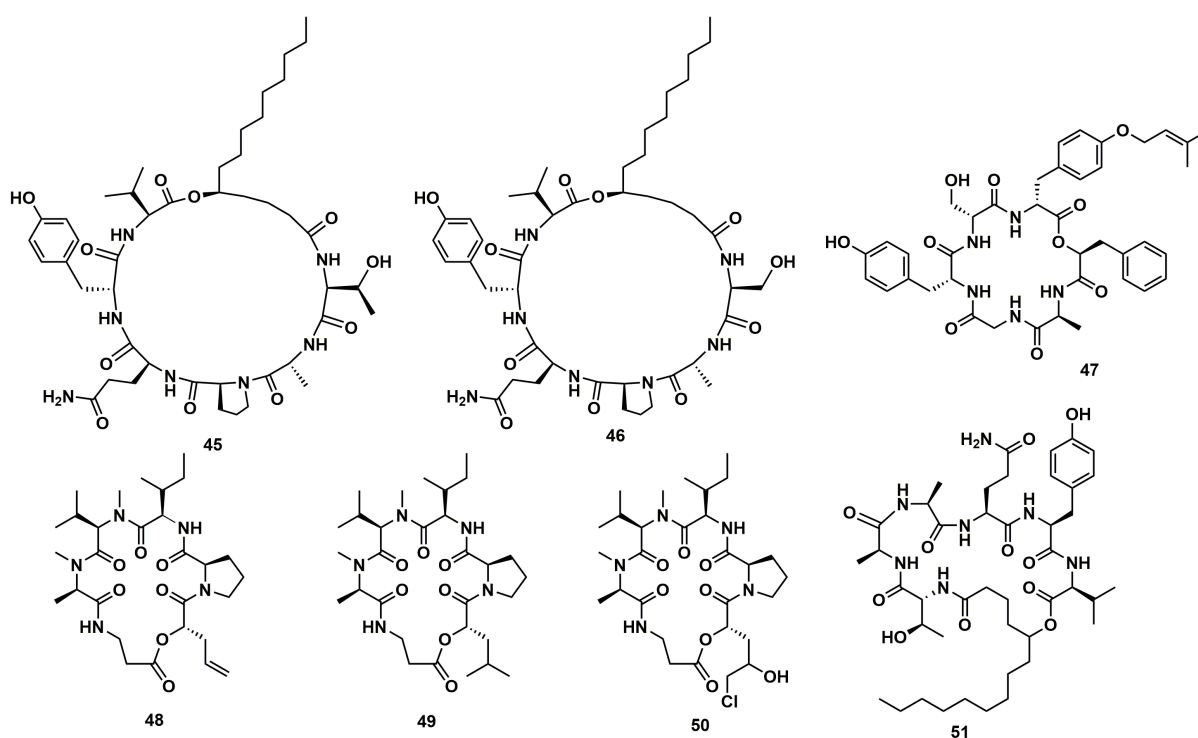


FIGURE 6
Chemical structures of CDPs 45–51.

From cultures of the soil-derived *Streptomyces* sp., dinghupeptins A–D (**86–89**) were isolated. The 3-amino-6-hydroxypiperidone unit-containing compounds **86** and **87** demonstrated selective chymotrypsin inhibitory action, with IC_{50} values of 2.1 and 1.1 μ M, respectively (Yang et al., 2018). Skyllamycins D (**90**) and E (**91**) were isolated from Lichen-sourced *Streptomyces* sp. KY11784, as well as three known

ones skyllamycins A – C (**92–94**). Antibacterial tests showed that (Table 2), in comparison to previously reported congeners, skyllamycin D (**90**) had better activity against *Bacillus subtilis* E168 (Bracegirdle et al., 2021). NC-1 (**95**), a cyclodepsipeptide containing a cinnamoyl side chain, was discovered in *Streptomyces* sp. FXJ1.172 that originated in red soil. **95** was evaluated to show moderate antimicrobial activity against

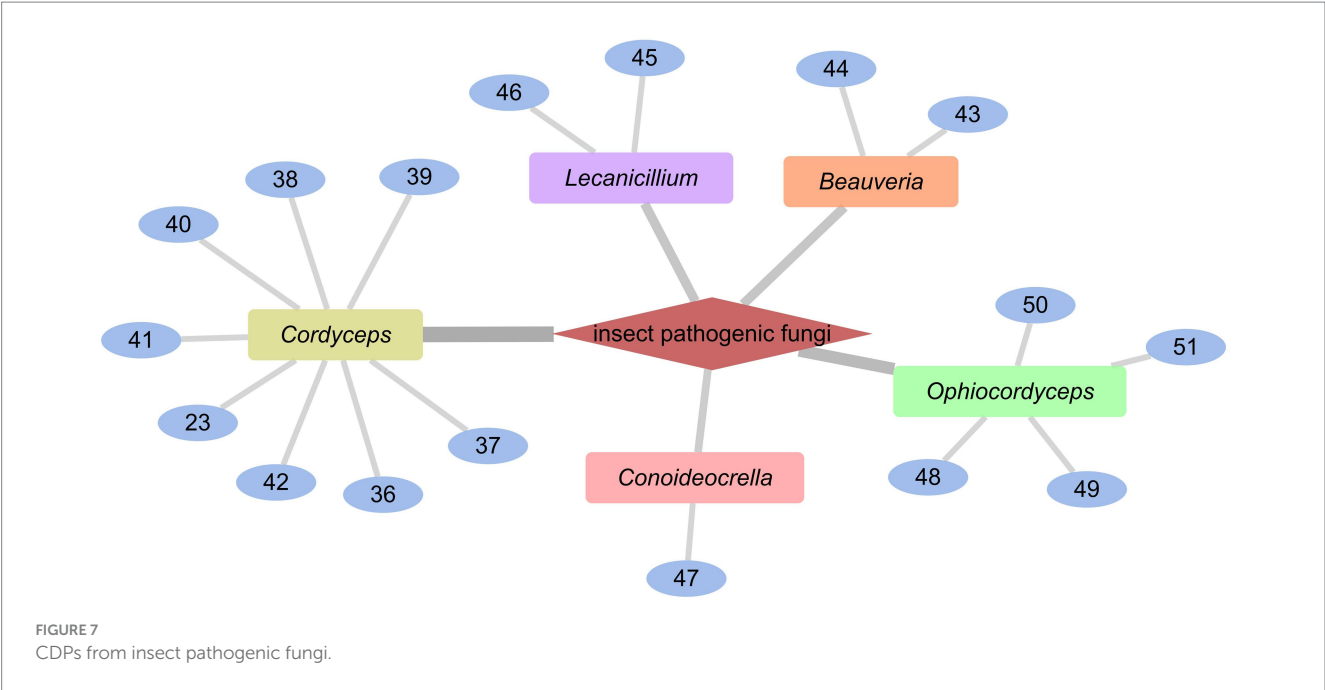


TABLE 2 The anti-fungal or anti-bacteria effects of CDPs.

Compound	Strains	MIC/ IC ₅₀	References
3	<i>Candida albicans</i>	^a 16–32 µg/mL	Singh et al. (2013)
	<i>Aspergillus fumigatus</i>	^a 8–16 µg/mL	
	<i>Trichophyton mentagrophytes</i>	^a 4 µg/mL	
7	<i>Candida albicans</i>	^b 0.11 µM	Ibrahim et al. (2018)
	<i>Candida glabrata</i>	^b 0.24 µM	
	<i>Candida krusei</i>	^b 0.19 µM	
	<i>Aspergillus fumigates</i>	^b 0.14 µM	
51	<i>Mycobacterium tuberculosis</i> H37Ra	^b 15 µM	Haritakun et al. (2010)
62	<i>Bacillus subtilis</i>	^b 12.5 µM	Liang et al. (2021)
	<i>Alternaria solan</i>	^b 15.6 µM	
85	<i>Mycobacterium tuberculosis</i> H37Rv	^a 2.5 µg/mL	Liu et al. (2019)
90	<i>Bacillus subtilis</i> E168	^a 8 µg/mL	Bracegirdle et al. (2021)
91	<i>Bacillus subtilis</i> E168	^a 16 µg/mL	Bracegirdle et al. (2021)
92	<i>Bacillus subtilis</i> E168	^a 32 µg/mL	Bracegirdle et al. (2021)
95	<i>Mycobacterium bovis</i> bacille Calmette–Guérin (BCG)	^a 44.4 µM	Liu et al. (2016)
101	<i>Mycobacterium smegmatis</i>	^c 2 µg/mL	Dardić et al. (2017)
102	<i>Mycobacterium tuberculosis</i> mc ² 6,230 strains	^a 82.8 µg/mL	Shin et al. (2021)
106	<i>Candida albicans</i>	^b 73 nM	Hoffmann et al. (2015)

^aMIC, minimal inhibitory concentration; ^bIC₅₀, concentration required for 50% inhibition; ^cIC₈₀, concentration required for 80% inhibition.

Mycobacterium bovis bacille Calmette–Guérin (BCG) (Liu et al., 2016; Figure 13).

A group of cyclodepsipeptides that included piperazic acid, svetamycins A (96), B (97), C (98), D (99), F (100) and G (101), were separated from *Streptomyces* sp. DSM14386. With an IC₈₀ value of 2 µg/mL, 101, the strongest antibacterial compound in this group of substances, prevented the development of *Mycobacterium smegmatis* (Dardić et al., 2017; Figure 14).

Cyclodepsipeptides from other bacteria

Spectroscopic analysis elucidated structures of two new compounds, coprisamides C and D (102 and 103), discovered from a dung beetle gut bacterium, *Micromonospora* sp. UTJ3. 102 exhibited a moderate inhibitory effect on the *Mycobacterium tuberculosis* mc² 6,230 strain (Shin et al., 2021). Aetheramides A (104), and B (105), which had IC₅₀ values of 0.015 and 0.018 µM,

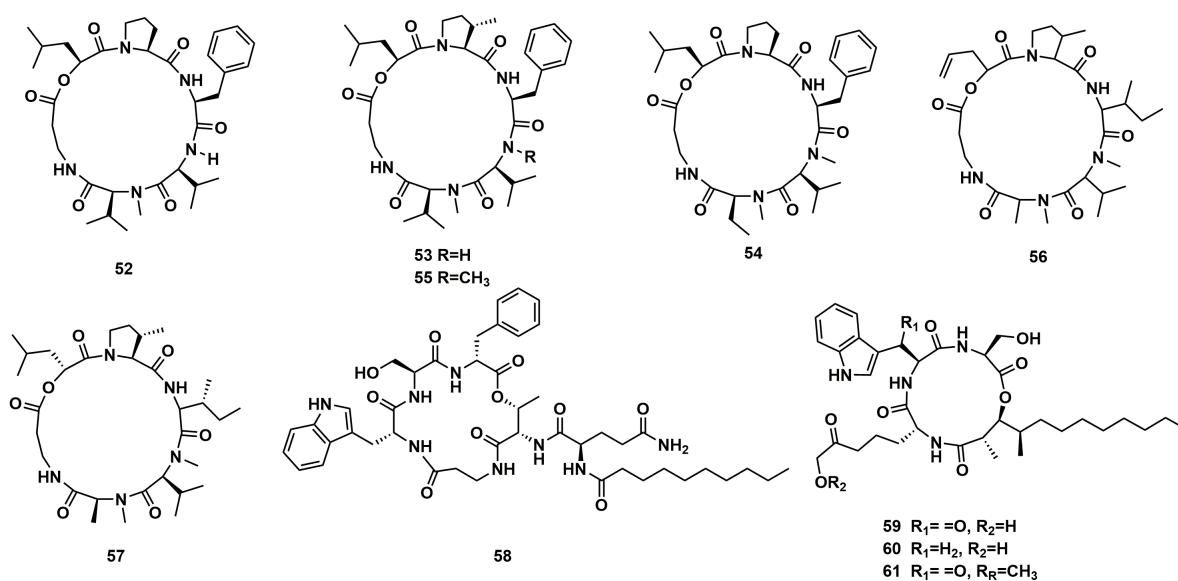


FIGURE 8
Chemical structures of CDPs 52–61.

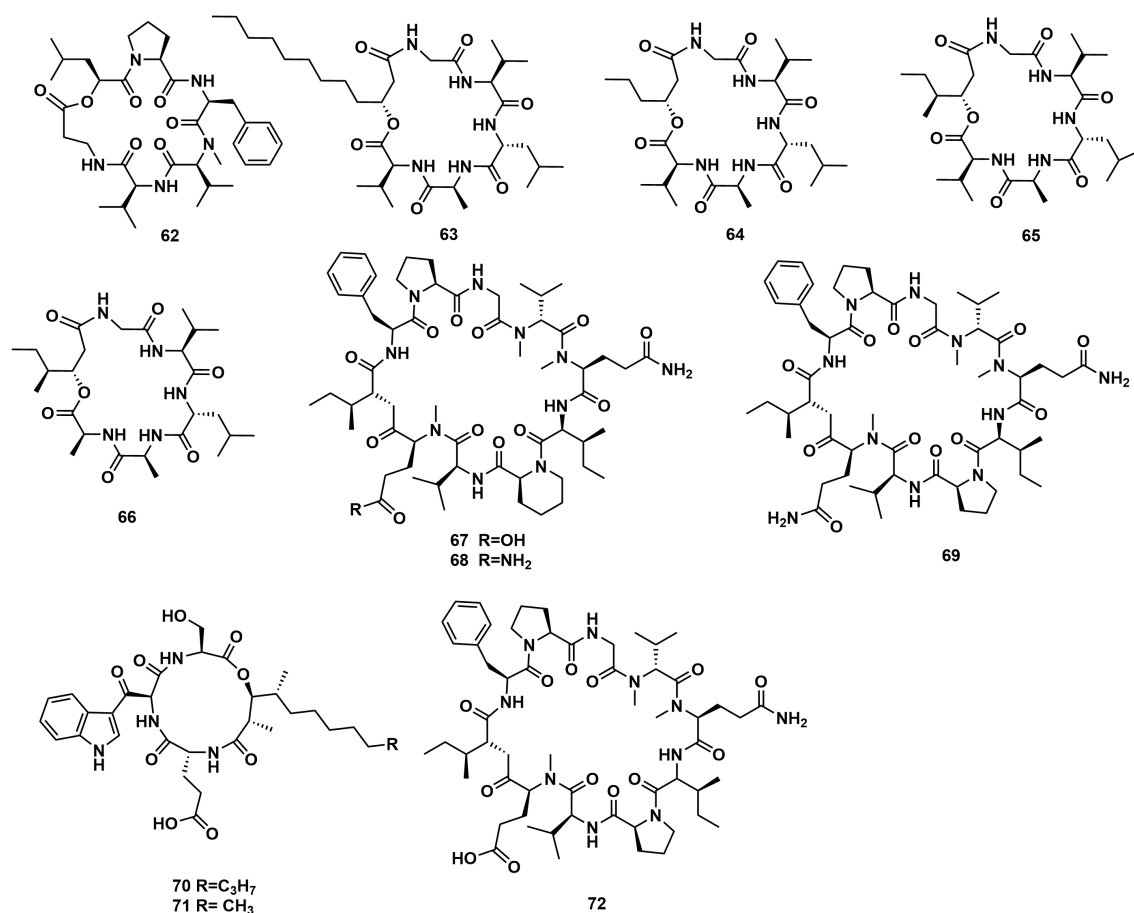


FIGURE 9
Chemical structures of CDPs 62–72.

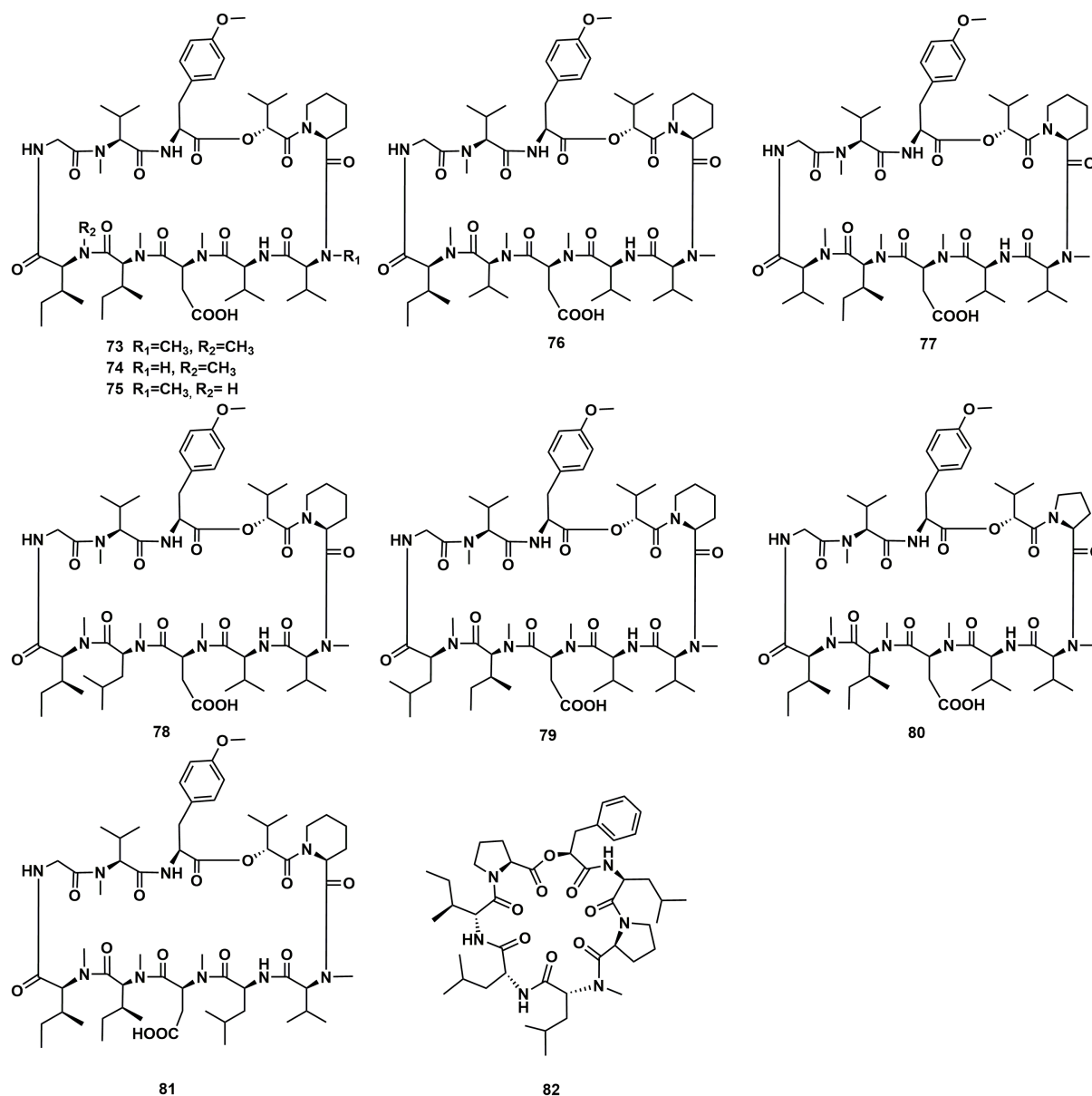


FIGURE 10
Chemical structures of CDPs 73–82.

respectively, showed strong inhibitory effects against HIV-1 (Table 3). Furthermore, **104** displayed cytotoxic activity with an IC_{50} value of 0.11 μM against the human HCT-116 (Plaza et al., 2012; Figure 15). Nannocystin A (**106**) was discovered from a myxobacterial genus, *Nannocystis* sp. The IC_{50} value for compound **106**, which inhibited the growth of *C. albicans*, was 73 nM, indicating a strong antifungal activity. Besides **106**, *Nannocystis* sp. also yielded nannocystin A1 (**107**), nannocystin A0 (**108**), nannocystin B (**109**), nannocystin B1 (**110**) and nannocystin Ax (**111**) (Hoffmann et al., 2015; Krastel et al., 2015). Alveolaride A (**112**), alveolaride B (**113**) and alveolaride C (**114**) were isolated from *Microascus alveolaris* strain PF1466. Alveolaride A (**112**) exhibited a potent inhibitory effect on the plant pathogens *Zymoseptoria tritici*, *Ustilago maydis*, and *Pyricularia oryzae*. Alveolaride C (**114**) was solely effective toward *U. maydis*, but

alveolaride B (**113**) was effective toward both *U. maydis* and *Z. tritici* under *in vitro* conditions (Fotso et al., 2018; Figure 15).

Discussions

The chemical structures of cyclodepsipeptides, especially the absolute configurations, were complicated and difficult to determine, different methods were needed. Among them, Marfey's method, modified Mosher's method, and X-Ray diffraction analysis besides 1D-NMR and 2D-NMR (Wang et al., 2014; Liu et al., 2020; Wang et al., 2022) were the best choices for determination of the configurations for those compounds. Moreover, the MS–MS fragment analysis was also of great use for judging its sequence of the amino acids (Chung et al., 2013; Liu et al., 2020).

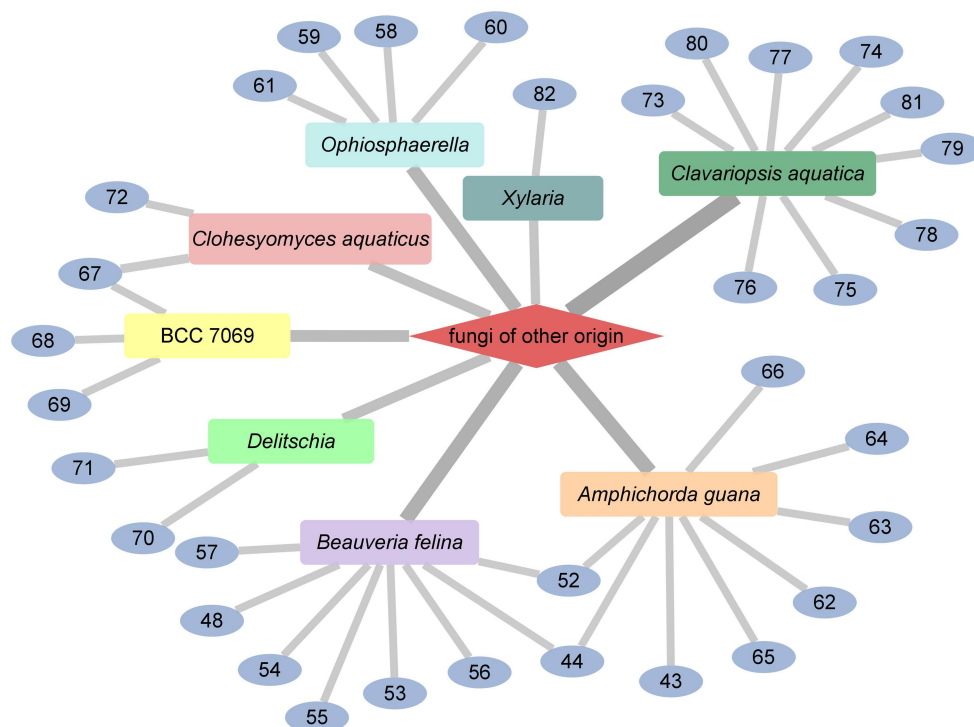


FIGURE 11
CDPs from fungi of other origin.

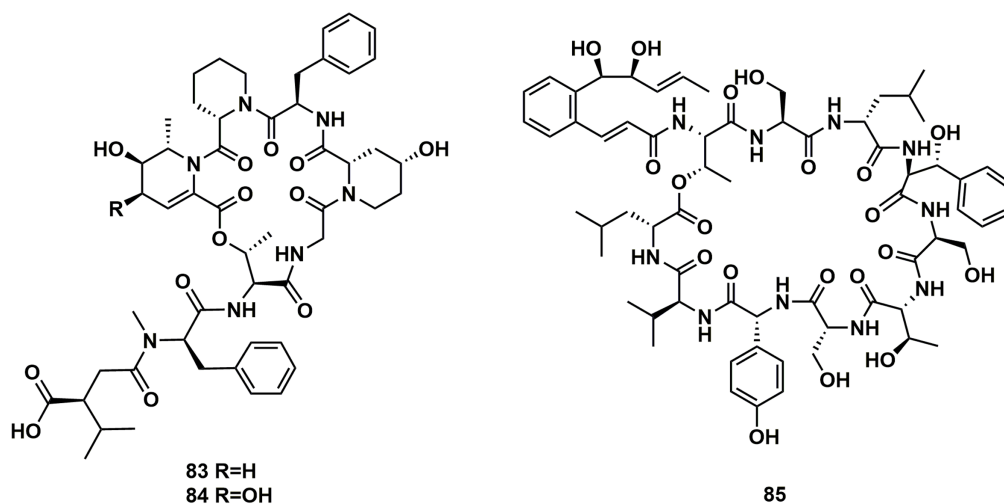


FIGURE 12
Chemical structures of CDPs 83–85.

As expected, an abundance of fungi and bacteria-derived cyclodepsipeptides were isolated, and most of them showed significant cytotoxic activities. It was suggested that the cyclic depsipeptide structure was of great importance for the biological activity, because in cytotoxicity assay, the linear homologs of the cyclohexadepsipeptide paecilodepsipeptide A were inactive (Hamann et al., 1996). In addition, the scope of bioactivity of cyclodepsipeptides spanned a range from cytotoxicity, and anti-bacterial to anti-malarial activity. Thus, it was suggested that cyclodepsipeptides were desirable chemical species, and could be further applied as leading compounds in drug research.

Although most of the fungi and bacteria have been shown to be a rich source for discovering cyclodepsipeptides, the number of new cyclodepsipeptides was still limited. Conventional isolation method was time-consuming and inefficient, it was necessary to develop a more effective method to explore cyclodepsipeptide candidates. Fortunately, some studies have illustrated that the biosynthesis of cyclodepsipeptides were accomplished nonribosomally by cyclodepsipeptide synthetases (Bills et al., 2014; Du et al., 2014; Aleti et al., 2015; Liu et al., 2015), thus, targeted discovery of cyclodepsipeptides by genomic analysis became possible. By use of

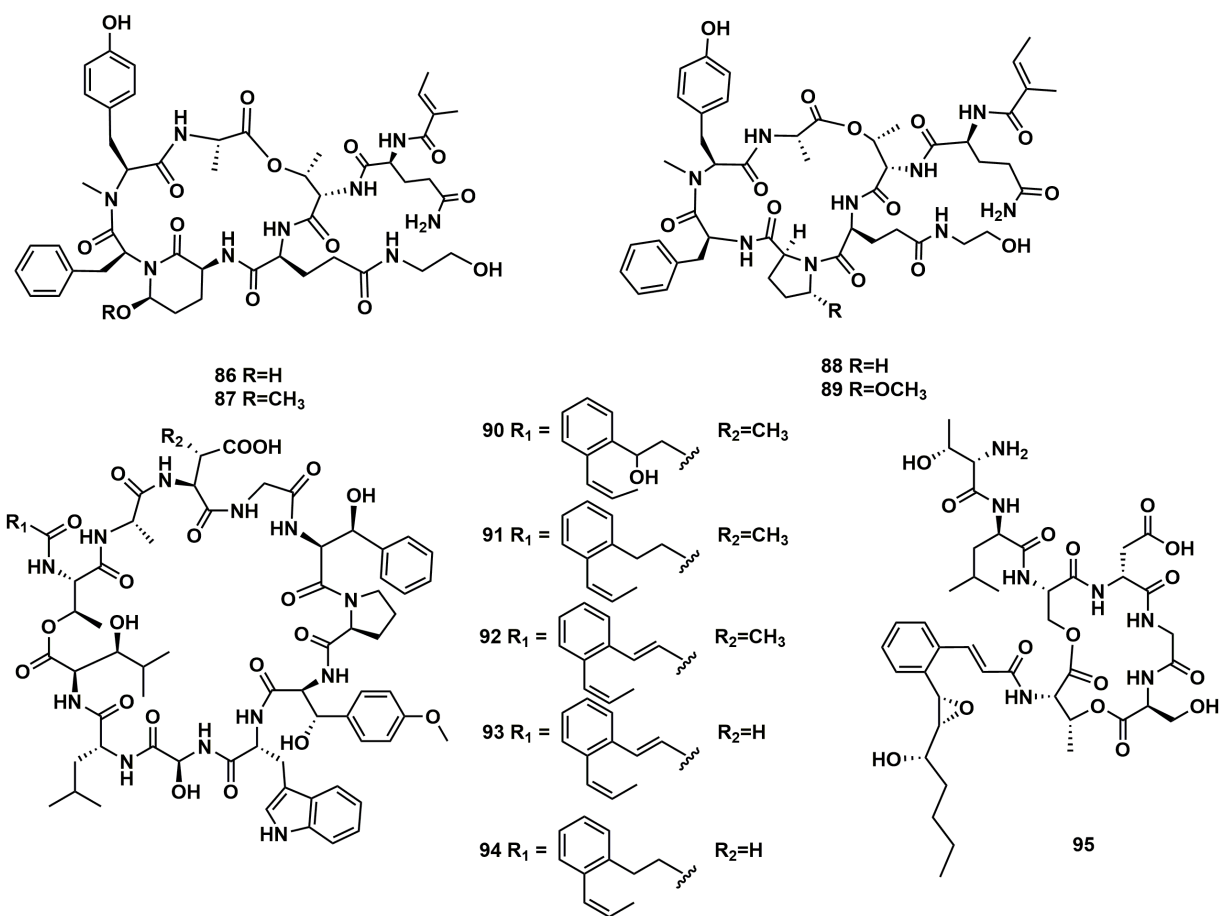


FIGURE 13
Chemical structures of CDPs 86–95.

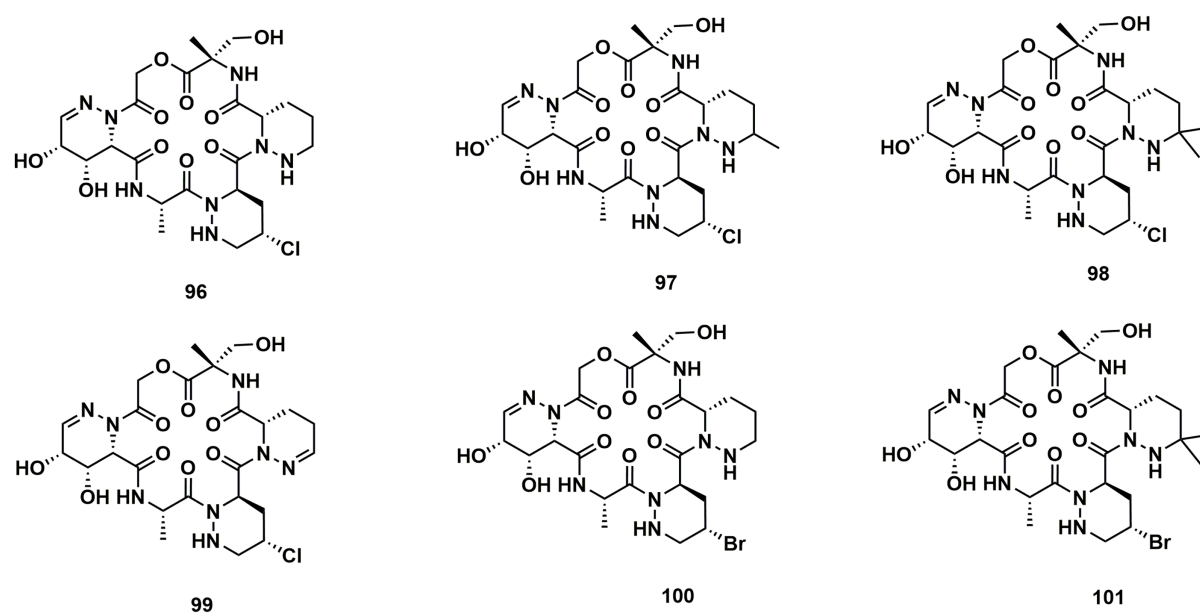


FIGURE 14
Chemical structures of CDPs 96–101.

TABLE 3 Other biological activities of CDPs.

Compound	Biological activity	Materials	LD ₅₀ , IC ₅₀	References
33	Brine shrimp lethal	Brine shrimp	^a 2.78 µg/mL	Wang et al. (2020)
36	Antitrypanosomal activity	<i>Trypanosoma brucei brucei</i>	^b 8.56 µg/mL	Umeyama et al. (2014)
37	Antitrypanosomal activity	<i>Trypanosoma brucei brucei</i>	^b 8.65 µg/mL	Umeyama et al. (2014)
38	Antitrypanosomal activity	<i>Trypanosoma brucei brucei</i>	^b 8.63 µg/mL	Umeyama et al. (2014)
48	Antitrypanosomal activity	<i>Trypanosoma brucei brucei</i> GUTat3.1	^b 0.33 µg/mL	Ganaha et al. (2016)
49	Antitrypanosomal activity	<i>Trypanosoma brucei brucei</i> GUTat3.1	^b 0.16 µg/mL	Ganaha et al. (2016)
50	Antitrypanosomal activity	<i>Trypanosoma brucei brucei</i> GUTat3.1	^b 0.061 µg/mL	Ganaha et al. (2016)
52	Superoxide anion production inhibition	Human neutrophils	^b 10.00 ± 0.80 µM	Chung et al. (2013)
53	Superoxide anion production inhibition	Human neutrophils	^b 10.90 ± 0.59 µM	Chung et al. (2013)
	Elastase release inhibition	Human neutrophils	^b 10.01 ± 0.46 µM	
44	Superoxide anion production inhibition	Human neutrophils	^b 12.21 ± 0.98 µM	Chung et al. (2013)
	Elastase release inhibition	Human neutrophils	^b 12.76 ± 1.00 µM	
55	Superoxide anion production inhibition	Human neutrophils	^b 10.09 ± 0.83 µM	Chung et al. (2013)
	Elastase release inhibition	Human neutrophils	^b 12.12 ± 0.72 µM	
57	Elastase release inhibition	Human neutrophils	^b 15.09 ± 0.28 µM	Chung et al. (2013)
67	Antimalarial activity	<i>Plasmodium falciparum</i> K1	^b 1.6 µg/mL	Isaka et al. (2014)
68	Antimalarial activity	<i>Plasmodium falciparum</i> K1	^b 6.4 µg/mL	Isaka et al. (2014)
69	Antimalarial activity	<i>Plasmodium falciparum</i> K1	^b 1.6 µg/mL	Isaka et al. (2014)
86	Selective chymotrypsin inhibition	Chymotrypsin	^b 2.1 µM	Yang et al. (2018)
87	Selective chymotrypsin inhibition	Chymotrypsin	^b 1.1 µM	Yang et al. (2018)
104	Antiviral activity	HIV-1	^b 0.015 µM	Plaza et al. (2012)
105	Antiviral activity	HIV-1	^b 0.018 µM	Plaza et al. (2012)

^aLD₅₀, concentration required for 50% lethality; ^bIC₅₀, concentration required for 50% inhibition.

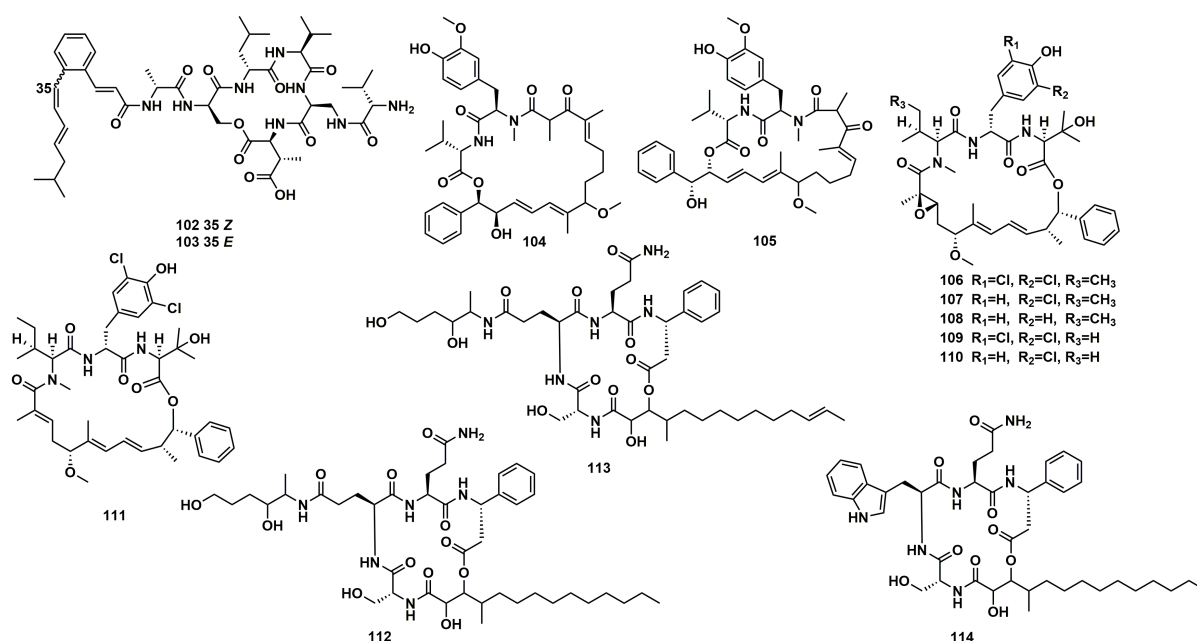


FIGURE 15
Chemical structures of CDPs 102–114.

targeted isolation methods, such as genome mining as well as molecular networking method (Duncan et al., 2015; Paulo et al., 2019; Wei et al., 2021; Clements-Decker et al., 2022), should be paid more attention in the future in order to obtain those bioactive compounds more efficiently.

In addition, due to the small amount of cyclodepsipeptides from natural products, investigations on *in vivo* effects and on the detailed mechanism of the bioactivities were limited. To solve this problem, sufficient compound material was however required. Facing the problem, total synthesis and heterologous expression of genes or gene clusters in microbial hosts were two better ways, which were keys to access industrially and pharmaceutically relevant compounds in an economically affordable and sustainable manner (Stolze and Kaiser, 2013; Doi, 2014; Roderich et al., 2015).

Conclusion

In conclusion, this review gave an overview of as many as 114 natural cyclodepsipeptides isolated and identified from fungi and bacteria since 2010, among them, endophytic fungi of plant were the largest group of producers. The review enriched our knowledge about structural features of cyclodepsipeptides and their biological sources.

Author contributions

S-XL: Data curation, Investigation, Writing – original draft. S-YO-Y: Data curation, Investigation, Writing – original draft. Y-FL:

Data curation, Investigation, Writing – original draft. C-LG: Data curation, Investigation, Writing – original draft. S-YD: Data curation, Investigation, Writing – original draft. CL: Investigation, Project administration, Writing – review & editing. T-YY: Investigation, Project administration, Writing – review & editing. Y-HP: Investigation, Project administration, Supervision, Writing – review & editing.

Funding

The author(s) declare that no financial support was received for the research, authorship, and/or publication of this article.

Conflict of interest

The authors declare that the research was conducted in the absence of any commercial or financial relationships that could be construed as a potential conflict of interest.

Publisher's note

All claims expressed in this article are solely those of the authors and do not necessarily represent those of their affiliated organizations, or those of the publisher, the editors and the reviewers. Any product that may be evaluated in this article, or claim that may be made by its manufacturer, is not guaranteed or endorsed by the publisher.

References

- Aleti, G., Sessitsch, A., and Brader, G. (2015). Genome mining: prediction of lipopeptides and polyketides from *Bacillus* and related firmicutes. *Comput. Struct. Biotech.* 13, 192–203. doi: 10.1016/j.csbj.2015.03.003
- Barthélemy, M., Elie, N., Genta-Jouve, G., Stien, D., Touboul, D., and Eparvier, V. (2021). Identification of antagonistic compounds between the palm tree *Xylariale* endophytic fungi and the phytopathogen *Fusarium oxysporum*. *J. Agric. Food Chem.* 69, 10893–10906. doi: 10.1021/acs.jafc.1c03141
- Bills, G., Li, Y., Chen, L., Yue, Q., Niu, X. M., and An, Z. Q. (2014). New insights into the echinocandins and other fungal non-ribosomal peptides and peptaibiotics. *Nat. Prod. Rep.* 31, 1348–1375. doi: 10.1039/C4NP00046C
- Bracegirdle, J., Hou, P., Nowak, V. V., Ackerley, D. F., Keyzers, R. A., and Owen, J. G. (2021). Skyllamycins D and E, non-ribosomal cyclic depsipeptides from lichen-sourced *Streptomyces anulatus*. *J. Nat. Prod.* 84, 2536–2543. doi: 10.1021/acs.jnatprod.1c00547
- Buckton, L. K., Rahimi, M. N., and McAlpine, S. R. (2021). Cyclic peptides as drugs for intracellular targets: the next frontier in peptide therapeutic development. *Chemistry* 27, 1487–1513. doi: 10.1002/chem.201905385
- Chung, Y. M., El-Shazly, M., Chuang, D. W., Hwang, T. L., Asai, T., Oshima, Y., et al. (2013). Suberoylanilide hydroxamic acid, a histone deacetylase inhibitor, induces the production of anti-inflammatory cyclodepsipeptides from *Beauveria felina*. *J. Nat. Prod.* 76, 1260–1266. doi: 10.1021/np400143j
- Clements-Decker, T., Rautenbach, M., Khan, S., and Khan, W. (2022). Metabolomics and genomics approach for the discovery of serrawettin W2 lipopeptides from *Serratia marcescens* NP2. *J. Nat. Prod.* 85, 1256–1266. doi: 10.1021/acs.jnatprod.1c01186
- Dardić, D., Lauro, G., Bifulco, G., Laboudie, P., Sakhaei, P., Bauer, A., et al. (2017). Svetamycins A–G, unusual Piperazic acid-containing peptides from *Streptomyces* sp. *J. Org. Chem.* 82, 6032–6043. doi: 10.1021/acs.joc.7b00228
- Doi, T. (2014). Synthesis of the biologically active natural product cyclodepsipeptides apratoxin A and its analogues. *Chem. Pharm. Bull.* 62, 735–743. doi: 10.1248/cpb.14-00268
- Du, Y. H., Wang, Y. M., Huang, T. T., Tao, M. F., Deng, Z. X., and Lin, S. J. (2014). Identification and characterization of the biosynthetic gene cluster of polyoxypeptin A, a potent apoptosis inducer. *BMC Microbiol.* 14, 1–12. doi: 10.1186/1471-2180-14-30
- Duncan, K. R., Crüsemann, M., Lechner, A., Sarkar, A., Li, J., Ziemert, N., et al. (2015). Molecular networking and pattern-based genome mining improves discovery of biosynthetic gene clusters and their products from *Salinispora* species. *Chem. Biol.* 22, 460–471. doi: 10.1016/j.chembiol.2015.03.010
- El-Elmat, T., Raja, H. A., Day, C. S., McFeeters, H., McFeeters, R. L., and Oberlies, N. H. (2017). α -Pyrone derivatives, tetra/hexahydroxanthones, and cyclodepsipeptides from two freshwater fungi. *Bioorg. Med. Chem.* 25, 795–804. doi: 10.1016/j.bmc.2016.11.059
- Fotso, S., Graupner, P., Xiong, Q., Gilbert, J. R., Hahn, D., Avila-Adame, C., et al. (2018). Alveolarides: antifungal peptides from *microascus alveolaris* active against phytopathogenic fungi. *J. Nat. Prod.* 81, 10–15. doi: 10.1021/acs.jnatprod.7b00337
- Ganaha, M., Yoshii, K., Ōtsuki, Y., Iguchi, M., Okamoto, Y., Iseki, K., et al. (2016). *In vitro* antitrypanosomal activity of the secondary metabolites from the mutant strain IU-3 of the insect pathogenic fungus *Ophiocordyceps coccidiicola* NBRC 100683. *Chem. Pharm. Bull.* 64, 988–990. doi: 10.1248/cpb.c16-00220
- Guo, W. Q., Wang, S., Li, N., Li, F., Zhu, T. J., Gu, Q. Q., et al. (2018). Saroclides A and B, cyclic depsipeptides from the mangrove-derived fungus *Sarocladium kiliense* HDN11-112. *J. Nat. Prod.* 81, 1050–1054. doi: 10.1021/acs.jnatprod.7b00644
- Hamann, M. T., Otto, C. S., Scheuer, P. J., and Dunbar, D. C. (1996). Kahalalides: bioactive peptides from a marine mollusk *Elysia rufescens* and its algal diet *Bryopsis* sp. *J. Org. Chem.* 61, 6594–6600. doi: 10.1021/jo960877+
- Haritakun, R., Sappan, M., Suvannakad, R., Tasanathai, K., and Isaka, M. (2010). An antimycobacterial cyclodepsipeptide from the entomopathogenic fungus *Ophiocordyceps communis* BCC 16475. *J. Nat. Prod.* 73, 75–78. doi: 10.1021/np900520b
- Helaly, S. E., Ashrafi, S., Teponno, R. B., Bernecker, S., Dababat, A. A., Maier, W., et al. (2018). Nematicidal cyclic lipodepsipeptides and a xanthocillin derivative from a phaeosphaeriaceous fungus parasitizing eggs of the plant parasitic nematode *Heterodera filipjevi*. *J. Nat. Prod.* 81, 2228–2234. doi: 10.1021/acs.jnatprod.8b00486
- Hoffmann, H., Kogler, H., Heyse, W., Matter, H., Caspers, M., Schummer, D., et al. (2015). Discovery, structure elucidation, and biological characterization of nannocystin

- a, a macrocyclic myxobacterial metabolite with potent antiproliferative properties. *Angew. Chem. Int. Ed.* 54, 10145–10148. doi: 10.1002/anie.201411377
- Ibrahim, S. R., Abdallah, H. M., Elkhayat, E. S., Al Musayeb, N. M., Asfour, H. Z., Zayed, M. F., et al. (2018). Fusaripeptide a: new antifungal and anti-malarial cyclodepsipeptide from the endophytic fungus *Fusarium* sp. *J. Asian Nat. Prod. Res.* 20, 75–85. doi: 10.1080/10286020.2017.1320989
- Isaka, M., Palasarn, S., Komwijit, S., Somrithipol, S., and Sommai, S. (2014). Pleosporin a, an antimalarial cyclodepsipeptide from an elephant dung fungus (BCC 7069). *Tetrahedron Lett.* 55, 469–471. doi: 10.1016/j.tetlet.2013.11.063
- Isaka, M., Palasarn, S., Supothina, S., Komwijit, S., and Luangsard, J. J. (2011). Bioactive compounds from the scale insect pathogenic fungus *Conoideocrella tenuis* BCC 18627. *J. Nat. Prod.* 74, 782–789. doi: 10.1021/np100849x
- Ishidoh, K., Kinoshita, H., Igarashi, Y., Ihara, F., and Nihira, T. (2014). Cyclic lipodepsipeptides verlamelin A and B, isolated from entomopathogenic fungus *Lecanicillium* sp. *J. Antibiot.* 67, 459–463. doi: 10.1038/ja.2014.22
- Krastel, P., Roggo, S., Schirle, M., Ross, N. T., Perruccio, F., Aspesi, P. Jr., et al. (2015). Nannocystin A: an elongation factor 1 inhibitor from myxobacteria with differential anticancer properties. *Angew. Chem. Int. Ed.* 54, 10149–10154. doi: 10.1002/anie.201505069
- Langenfeld, A., Blond, A., Gueye, S., Herson, P., Nay, B., Dupont, J., et al. (2011). Insecticidal cyclodepsipeptides from *Beauveria felina*. *J. Nat. Prod.* 74, 825–830. doi: 10.1021/np100890n
- Lemmens-Gruber, R., Kamyar, M., and Dornetshuber, R. (2009). Cyclodepsipeptides-potential drugs and lead compounds in the drug development process. *Curr. Med. Chem.* 16, 1122–1137. doi: 10.2174/092986709787581761
- Li, J. T., Fu, X. L., Zeng, Y., Wang, Q., and Zhao, P. J. (2011). Two cyclopeptides from endophytic fungus *Beauveria* sp. Lr89 isolated from *Maytenus hookeri*. *Nat. Prod. Res. Dev.* 23, 667–669.
- Li, X. J., Li, F. M., Xu, L. X., Li, L., and Peng, Y. H. (2021). Antifungal secondary metabolites of endophytic *Fusarium* sp. HU0174 from *Celtis sinensis*. *Nat. Prod. Res. Dev.* 33, 943–950.
- Liang, M., Lyu, H. N., Ma, Z. Y., Li, E. W., Cai, L., and Yin, W. B. (2021). Genomics-driven discovery of a new cyclodepsipeptide from the guanophilic fungus *Amphichorda guana*. *Org. Biomol. Chem.* 19, 1960–1964. doi: 10.1039/D1OB00100K
- Liu, M. H., Liu, N., Shang, F., and Huang, Y. (2016). Activation and identification of NC-1: a cryptic cyclodepsipeptide from red soil-derived *Streptomyces* sp. FXJ1. 172. *Eur. J. Org. Chem.* 2016, 3943–3948. doi: 10.1002/ejoc.201600297
- Liu, Q., Liu, Z. Y., Sun, C. L., Shao, M. W., Ma, J. Y., Wei, X. Y., et al. (2019). Discovery and biosynthesis of atrovimycin, an antitubercular and antifungal cyclodepsipeptide featuring vicinal-dihydroxylated cinnamic acyl chain. *Org. Lett.* 21, 2634–2638. doi: 10.1021/acs.orglett.9b00618
- Liu, Z. G., Sun, Y., Tang, M. Y., Sun, P., Wang, A. Q., Hao, Y. Q., et al. (2020). Trichodestruxins A–D: cytotoxic Cyclodepsipeptides from the endophytic Fungus *Trichoderma harzianum*. *J. Nat. Prod.* 83, 3635–3641. doi: 10.1021/acs.jnatprod.0c00808
- Liu, J., Wang, B., Li, H. Z., Xie, Y. C., Li, Q. L., Qin, X. J., et al. (2015). Biosynthesis of the anti-infective marformycins featuring pre-NRPS assembly line N-formylation and O-methylation and post-assembly line C-hydroxylation chemistries. *Org. Lett.* 17, 1509–1512. doi: 10.1021/acs.orglett.5b00389
- Luo, M. N., Chang, S. S., Li, Y. H., Xi, X. M., Chen, M. H., He, N., et al. (2022). Molecular networking-based screening led to the discovery of a cyclic heptadepsipeptide from an endolichenic *Xylaria* sp. *J. Nat. Prod.* 85, 972–979. doi: 10.1021/acs.jnatprod.1c01108
- Lv, F., Daletos, G., Lin, W., and Proksch, P. (2015). Two new cyclic depsipeptides from the endophytic fungus *Fusarium* sp. *Nat. Prod. Commun.* 10, 1667–1670. doi: 10.3390/molecules23010169
- Moore, R. (1996). Cyclic peptides and depsipeptides from cyanobacteria: a review. *J. Ind. Microbiol.* 16, 134–143. doi: 10.1007/BF01570074
- Negi, B., Kumar, D., and Rawat, D. S. (2017). Marine peptides as anticancer agents: a remedy to mankind by nature. *Curr. Protein. Pept. Sc.* 18, 885–904. doi: 10.2174/1389203717666160724200849
- Nihei, K., Itoh, H., Hashimoto, K., Miyairi, K., and Okuno, T. (1998). Antifungal cyclodepsipeptides, W493 A and B, from *Fusarium* sp.: isolation and structural determination. *Biosci. Biotechnol. Biochem.* 62, 858–863. doi: 10.1271/bbb.62.858
- Paulo, B. S., Sigrist, R., Angolini, C. F., and De Oliveira, L. G. (2019). New cyclodepsipeptide derivatives revealed by genome mining and molecular networking. *ChemistrySelect* 4, 7785–7790. doi: 10.1002/slct.201900922
- Plaza, A., Garcia, R., Bifulco, G., Martinez, J. P., Hüttel, S., Sasse, F., et al. (2012). Aetheramides A and B, potent HIV-inhibitory depsipeptides from a myxobacterium of the new genus “*Aetherobacter*”. *Org. Lett.* 14, 2854–2857. doi: 10.1021/ol3011002
- Rivera-Chávez, J., El-Elmat, T., Gallagher, J. M., Graf, T. N., Fournier, J., Panigrahi, G. K., et al. (2019). Delitypyrones: α -Pyrone derivatives from a freshwater *Delitschia* sp. *Planta Med.* 85, 62–71. doi: 10.1055/a-0654-5850
- Roderich, D. S., Thomas Schweder, S., Sophia, Z., and Jana, K. (2015). *Bacillus subtilis* as heterologous host for the secretory production of the non-ribosomal cyclodepsipeptide enniatin. *Appl. Microbiol. Biotechnol.* 99, 681–691. doi: 10.1007/s00253-014-6199-0
- Shin, Y. H., Ban, Y. H., Kim, T. H., Bae, E. S., Shin, J., Lee, S. K., et al. (2021). Structures and biosynthetic pathway of coprisamides C and D, 2-alkenylcinnamic acid-containing peptides from the gut bacterium of the carrion beetle *Silpha perforata*. *J. Nat. Prod.* 84, 239–246. doi: 10.1021/acs.jnatprod.0c00864
- Singh, S. B., Ondeyka, J., Harris, G., Herath, K., Zink, D., Vicente, F., et al. (2013). Isolation, structure, and biological activity of phaeofungin, a cyclic lipodepsipeptide from a *Phaeosphaeria* sp. using the genome-wide *Candida albicans* fitness test. *J. Nat. Prod.* 76, 334–345. doi: 10.1021/np300704s
- Sivanathan, S., and Scherkenbeck, J. (2014). Cyclodepsipeptides: a rich source of biologically active compounds for drug research. *Molecules* 19, 12368–12420. doi: 10.3390/molecules190812368
- Soe, T. W., Han, C., Fudou, R., Kaida, K., Sawaki, Y., Tomura, T., et al. (2019). Clavariopsins C–I, antifungal cyclic depsipeptides from the aquatic hyphomycete *Clavariopsis aquatica*. *J. Nat. Prod.* 82, 1971–1978. doi: 10.1021/acs.jnatprod.9b00366
- Son, S., Ko, S. K., Jang, M., Lee, J. K., Ryoo, I. J., Lee, J. S., et al. (2015). Ulleungamides A and B, modified α , β -dehydropepicolic acid containing cyclic depsipeptides from *Streptomyces* sp. KCB13F003. *Org. Lett.* 17, 4046–4049. doi: 10.1021/acs.orglett.5b01969
- Stolze, S. C., and Kaiser, M. (2013). Case studies of the synthesis of bioactive cyclodepsipeptide natural products. *Molecules* 18, 1337–1367. doi: 10.3390/molecules18021337
- Umeyama, A., Takahashi, K., Grudniewska, A., Shimizu, M., Hayashi, S., Kato, M., et al. (2014). *In vitro* antitrypanosomal activity of the cyclodepsipeptides, cardinalisamides A–C, from the insect pathogenic fungus *Cordyceps cardinalis* NBRC 103832. *J. Antibiot.* 67, 163–166. doi: 10.1038/ja.2013.93
- Wang, F. Q., Jiang, J., Hu, S., Ma, H. R., Zhu, H. C., Tong, Q. Y., et al. (2017). Secondary metabolites from endophytic fungus *Chaetomium* sp. induce colon cancer cell apoptotic death. *Fitoterapia* 121, 86–93. doi: 10.1016/j.fitote.2017.06.021
- Wang, Y. J., Liu, C. Y., Wang, Y. L., Zhang, F. X., Lu, Y. F., Dai, S. Y., et al. (2022). Cytotoxic cyclodepsipeptides and cyclopentane derivatives from a plant-associated fungus *Fusarium* sp. *J. Nat. Prod.* 85, 2592–2602. doi: 10.1021/acs.jnatprod.2c00555
- Wang, J., Zhang, D. M., Jia, J. F., Peng, Q. L., Tian, H. Y., Wang, L., et al. (2014). Cyclodepsipeptides from the ascocarps and insect-body portions of fungus *Cordyceps cicadae*. *Fitoterapia* 97, 23–27. doi: 10.1016/j.fitote.2014.05.010
- Wang, Z. F., Zhang, W., Xiao, L., Zhou, Y. M., and Du, F. Y. (2020). Characterization and bioactive potentials of secondary metabolites from *Fusarium chlamydosporum*. *Nat. Prod. Res.* 34, 889–892. doi: 10.1080/14786419.2018.1508142
- Wei, Q., Bai, J., Yan, D. J., Bao, X. Q., Li, W. T., Liu, B. Y., et al. (2021). Genome mining combined metabolic shunting and OSMAC strategy of an endophytic fungus leads to the production of diverse natural products. *Acta Pharm. Sin.* B 11, 572–587. doi: 10.1016/j.apsb.2020.07.020
- Yang, L., Li, H. X., Wu, P., Mahal, A., Xue, J. H., Xu, L. X., et al. (2018). Dinghupeptins A–D, chymotrypsin inhibitory cyclodepsipeptides produced by a soil-derived *Streptomyces*. *J. Nat. Prod.* 81, 1928–1936. doi: 10.1021/acs.jnatprod.7b01009
- Zeng, M. Y., Tao, J. Y., Xu, S., Bai, X. L., and Zhang, H. W. (2023). Marine organisms as a prolific source of bioactive depsipeptides. *Mar. Drugs* 21:120. doi: 10.3390/md21020120



OPEN ACCESS

EDITED BY

Fohad Mabood Husain,
King Saud University, Saudi Arabia

REVIEWED BY

Jianhua Wang,
Chinese Academy of Agricultural Sciences
(CAAS), China
Ammar Almaaytah,
Jordan University of Science and Technology,
Jordan
Axel Hollmann,
National Scientific and Technical Research
Council (CONICET), Argentina

*CORRESPONDENCE

Gianna Palmieri
✉ gianna.palmieri@ibbr.cnr.it

[†]These authors have contributed equally to this work and share first authorship

[†]These authors have contributed equally to this work and share last authorship

RECEIVED 22 June 2023

ACCEPTED 18 September 2023

PUBLISHED 05 October 2023

CITATION

Agrillo B, Porritiello A, Gratino L, Balestrieri M, Proroga YT, Mancusi A, Cozzi L, Vicenza T, Dardano P, Miranda B, Escrivá PV, Gogliettino M and Palmieri G (2023) Antimicrobial activity, membrane interaction and structural features of short arginine-rich antimicrobial peptides.
Front. Microbiol. 14:1244325.
doi: 10.3389/fmicb.2023.1244325

COPYRIGHT

© 2023 Agrillo, Porritiello, Gratino, Balestrieri, Proroga, Mancusi, Cozzi, Vicenza, Dardano, Miranda, Escrivá, Gogliettino and Palmieri. This is an open-access article distributed under the terms of the [Creative Commons Attribution License \(CC BY\)](https://creativecommons.org/licenses/by/4.0/). The use, distribution or reproduction in other forums is permitted, provided the original author(s) and the copyright owner(s) are credited and that the original publication in this journal is cited, in accordance with accepted academic practice. No use, distribution or reproduction is permitted which does not comply with these terms.

Antimicrobial activity, membrane interaction and structural features of short arginine-rich antimicrobial peptides

Bruna Agrillo^{1†}, Alessandra Porritiello^{2†}, Lorena Gratino², Marco Balestrieri², Yolande Therese Proroga³, Andrea Mancusi³, Loredana Cozzi⁴, Teresa Vicenza⁴, Principia Dardano⁵, Bruno Miranda⁵, Pablo V. Escrivá^{6,7}, Marta Gogliettino^{2†} and Gianna Palmieri^{2,8*}

¹Ampure S.R.L., Napoli, Italy, ²National Research Council (IBBR-CNR), Institute of Biosciences and Bioresources, Napoli, Italy, ³Department of Food Microbiology, Istituto Zooprofilattico Sperimentale del Mezzogiorno, Portici, Italy, ⁴Department of Food Safety, Nutrition and Veterinary Public Health, Istituto Superiore di Sanità, Rome, Italy, ⁵National Research Council (ISASI-CNR), Institute of Applied Sciences and Intelligent Systems, Napoli, Italy, ⁶Laboratory of Molecular Cell Biomedicine, University of the Balearic Islands, Palma, Spain, ⁷Laminar Pharmaceuticals, Palma, Spain, ⁸Materias S.R.L., Naples, Italy

Antimicrobial activity of many AMPs can be improved by lysine-to-arginine substitution due to a more favourable interaction of arginine guanidinium moiety with bacterial membranes. In a previous work, the structural and functional characterization of an amphipathic antimicrobial peptide named RiLK1, including lysine and arginine as the positively charged amino acids in its sequence, was reported. Specifically, RiLK1 retained its β -sheet structure under a wide range of environmental conditions (temperature, pH, and ionic strength), and exhibited bactericidal activity against Gram-positive and Gram-negative bacteria and fungal pathogens with no evidence of toxicity on mammalian cells. To further elucidate the influence of a lysine-to-arginine replacement on RiLK1 conformational properties, antimicrobial activity and peptide-liposome interaction, a new RiLK1-derivative, named RiLK3, in which the lysine is replaced with an arginine residue, was projected and characterised in comparison with its parental compound. The results evidenced that lysine-to-arginine mutation not only did not assure an improvement in the antimicrobial potency of RiLK1 in terms of bactericidal, virucidal and fungicidal activities, but rather it was completely abolished against the hepatitis A virus. Therefore, RiLK1 exhibited a wide range of antimicrobial activity like other cationic peptides, although the exact mechanisms of action are not completely understood. Moreover, tryptophan fluorescence measurements confirmed that RiLK3 bound to negatively charged lipid vesicles with an affinity lower than that of RiLK1, although no substantial differences from the structural and self-assembled point of view were evidenced. Therefore, our findings imply that antimicrobial efficacy and selectivity are affected by several complex and interrelated factors related to substitution of lysine with arginine, such as their relative proportion and position. In this context, this study could provide a better rationalisation for the optimization of antimicrobial peptide sequences, paving the way for the development of novel AMPs with broad applications.

KEYWORDS

antimicrobial compound, cationic arginine-rich peptide, arginine, membrane interaction, spectroscopy

1. Introduction

Antimicrobial peptides (AMPs), also defined as small molecular-mass proteins, are short amino acid sequences, able to efficiently kill or prevent the growth of microorganisms through various and broad mechanisms of action. These compounds have been found in different forms of life from microorganisms to humans including fish, plants, amphibians, invertebrates, birds, and mammals. Moreover, AMPs are evolutionarily conserved in the genome and in the higher organisms they are essential components of the innate and adaptive immune systems, playing an essential role in defending against microbial infections (Giuliani et al., 2008; Peters et al., 2010; Wang S. et al., 2016; Huan et al., 2020; Erdem Büyükkiraz and Kesmen, 2022).

In 1939, the microbiologist René Dubos isolated from a soil *Bacillus* strain the first antimicrobial compound, named gramicidin, which was able to protect mice from pneumococcal infection (Van Epps, 2006). Next, several AMPs have been identified and characterised from both the prokaryotic (bacteriocins) and eukaryotic (cathelicidins, defensins) organisms, allowing to collect several information on their most basic chemical-physical parameters (Zasloff, 2002; Phoenix et al., 2013; Yazici et al., 2018). These studies provided important indications for a further development of these compounds, leading to *in silico* design of new antimicrobial compounds on the basis of natural or non-natural peptide sequences. In general, AMPs share several key properties, including amphipathicity, mean hydrophobicity, and net cationic charge owed to the presence of lysine and arginine as basic residues. Moreover, these compounds can adopt a variety of conformational structures, such as β -sheet and random-coil structures, although most of them exhibit α -helical structures (Ebenhan et al., 2014; Wang et al., 2019; Pirtskhalava et al., 2021).

AMPs explicate their antimicrobial activity through many different mechanisms. The most studied AMPs initially interact with common targets on surface of cells without the need for specific receptors. The amphipathicity and the net cationic nature of these membrane-active AMPs are believed to be the main driving force for their cell selectivity and interaction resulting in membrane integrity disruption (Pirtskhalava et al., 2021). Indeed, cationic AMPs can strongly bind the negatively charged bacterial membranes, due to the presence of a large proportion of phospholipids (such as phosphatidylglycerol and cardiolipin) and peptidoglycans (such as lipoteichoic acids) in the Gram-positive bacteria, and lipopolysaccharides (LPS) in the outer membrane for Gram-negative bacteria (Andersson et al., 2016; Omardien et al., 2016). On the other hand, the architecture of bacterial membranes markedly differs from that of the mammalian cell envelope which includes mostly zwitterionic phospholipids (such as sphingomyelin and phosphatidylcholine), providing a reasonable means for positively charged AMPs to target bacteria in a selective manner. In this context, drugs and biological agents targeting membrane lipid bilayers has received great attention during the latest years (Escribá et al., 2015). Thus, “membrane lipid therapy” (or melitherapy) arises as a new approach to developed therapeutic agents to treat different conditions, including infectious diseases.

Therefore, the strategy for the development of an efficient AMP includes a good balance among charge, hydrophobicity, amphipathicity, secondary and tertiary structure, and mode of action which are all important variables to identify candidates of success

However, the discovery in the last decade of a lot of AMPs with great diversity in the distribution of amino acids along their sequence, made the study of these peptides more complex. In contrast to the difficulty intrinsic to this variety, short amphipathic peptides can represent simpler models of AMPs to investigate the role of hydrophobic and electrostatic interactions in peptide structure-activity correlations (Torres et al., 2019; Pirtskhalava et al., 2021; Chakraborty et al., 2022).

Recently, a new 10-amino acid peptide, namely RiLK1 (Agrillo et al., 2020; Falcigno et al., 2021), was designed based on the dodecapeptide 1018-K6 (Palmieri et al., 2018; Colagiorgi et al., 2020; Festa et al., 2021; Ambrosio et al., 2022), a compound derived from a bovine HDP (host defence peptide) bacterenecin, belonging to the cathelicidins family. Structural and functional analysis, revealed that RiLK1 is extremely active toward fungi, viruses, Gram-positive and-negative bacteria at low micromolar concentrations, showing no effects on human cell lines investigated in terms of viability and morphology. Moreover, results evidenced a conformational propensity of RiLK1 to self-assembling in regular structures in a more efficient way than the parent peptide 1018-K6, providing a possible explanation for the potent bactericidal, antifungal and anti-biofilm activities exhibited by RiLK1 in comparison to 1018-K6.

Herein, with the aim to investigate the effects of an increased arginine (R) composition in the sequence of RiLK1 (mixed R/K), a single amino acid substitution of the basic lysine (K) residue with arginine was projected. Indeed, despite the identical charge of R and K, the former residues are more prevalent in naturally occurring AMPs than latter, suggesting that the guanidinium group may be preferable for antimicrobial activity than the amine group, as confirmed in many studies (Yeaman and Yount, 2003; Hristova and Wimley, 2011).

Therefore, the new peptide, named RiLK3 (all R), was projected and characterised in comparison with its parental compound RiLK1 in terms of structural, functional and self-assembly properties as well as peptide-membrane interaction. The changes in the conformational propensity of peptides were measured by CD and fluorescence spectroscopy while their tendency for self-assembling was analysed by Fourier transform infrared spectroscopy (FT-IR) and cross-linking experiments. Then, the antimicrobial activity against the pathogen's bacteria, fungi and viruses was evaluated together with peptide-lipid membrane interactions.

2. Materials and methods

2.1. Synthesis and *in silico* design of RiLK3

The peptides RiLK1 and RiLK3 used in this work were purchased from GenScript Biotech (Leiden, Netherlands) and obtained at >95% purity. The peptides were stored as a lyophilized powder at -20°C . Before experimental analyses, fresh solutions in 100% dimethyl sulfoxide (DMSO, Sigma Aldrich, Milan, Italy) were prepared, briefly vortexed, and sonicated, and these samples were used as stock solutions. The following web server and software were utilized to determine all the relevant physicochemical properties of RiLK1 and RiLK3: PlifPred (PPred) (Mathur et al., 2018), PEPLife (Mathur et al., 2016), Antimicrobial Peptide Database3 (APD3) (Wang G. et al., 2016), and collection of antimicrobial peptides (CAMP) (Waghu et al., 2016).

2.2. Antibacterial assay

The minimum bactericidal concentration (MBC) was determined by the standard broth micro-dilution method in accordance with the [Clinical and Laboratory Standards Institute \(2015\)](#). For micro-broth dilution assay, *Listeria monocytogenes* (isolated from food products), *Escherichia coli* (strain ATCC 25922), *Staphylococcus aureus* (strain ATCC 25923), *Salmonella Typhimurium* isolated from food and *Pseudomonas aeruginosa* (strain ATCC 27853) were grown in BPW (Thermo Fisher, Milan, Italy). Bacterial cells were cultured at 37°C in the culture media until collection and then diluted in fresh broth to a final concentration of 1.5×10^3 CFU/mL (CFU, colony forming units). Next, serial dilutions of RiLK3 and RiLK1 in BPW (ranging from 1 to 75 µM), prepared starting from stock solutions in DMSO, were added to each bacterial suspension and incubated at 37°C for 6 h. Control samples containing only cell suspension and DMSO were also used. The MBCs were determined by transferring 50 µL of each bacterial cell suspensions onto selective agar plates (*L. monocytogenes*, Agar Listeria acc. to Ottaviani & Agosti (ALOA)—Microbiol, Macchiareddu (CA)—Italy; *S. typhimurium*, *Salmonella* Chromogenic agar—Oxoid, Madrid, Spain; *S. aureus*, Baird Parker agar base—Oxoid, Madrid, Spain; β -glucuronidase-positive *E. coli*, Triptone Bile X-glucuronide Agar (TBX)—Oxoid, Madrid, Spain; *P. aeruginosa*, *pseudomonas* agar base with CFC supplement—Oxoid, Madrid, Spain) incubated 24/48 h at 37°C for *L. monocytogenes* (ISO 11290-1:2017), *S. typhimurium* (ISO 6579-1:2020), and *S. aureus* (ISO 6888-1:1999) while *E. coli* (ISO 16649-1:2018) was incubated 24 h at 44°C and *P. aeruginosa* at 25°C for 48 h (ISO 13720:2010). MBC is defined as the lowest concentration of peptide at which more than 99.9% of the bacterial cells are killed. All values were obtained as the mean of three independent experiments conducted in triplicate.

2.3. Antifungal assays

Fungal strains were purchased from the American Type Culture Collection (ATCC, Manassas, VA, United States) as follows: *Aspergillus brasiliensis* ATCC 9341 and *Candida albicans* ATCC 14053 strains. Briefly, the cell suspension of both fungal species was adjusted to 1.0×10^5 CFU/mL in buffered peptone water (BPW) (bioMerieux, Florence, Italy). Peptide stock solutions in DMSO were added to the cell suspension at a final concentration of 25 µM and 50 µM and incubated for 6 h at 37°C. The minimum fungicidal concentration (MFC) was determined by plating 100 µL cultures on DG18 plates (Dichloran 18% Glycerol Agar—ISO 21527-2) for CFU counting. After 7 days at 25°C, the MFC was defined as the lowest peptide concentration that resulted in 99.9% killing compared with the drug-free group. The analyses were performed in triplicate on three different experiments.

2.4. Antiviral assay

The hepatitis A virus (HAV) HM 175 strain was replicated in Frp3 cells cultured in minimum essential medium with Earle's salts (MEM), supplemented with 1% glutamine, 2% non-essential amino acids and 2% fetal bovine serum (FBS), at 37°C in 5% CO₂. EuroClone, (Milan, Italy) provided all cell culture media. The viral suspension was

prepared by 3 cycles freeze and thaw lysis of infected monolayer, clarified using low-speed centrifugation (800 × g) to remove residual debris, then the sample was aliquoted and stored at −80°C until use. The obtained HAV stock suspension revealed a final concentration of 4.6×10^6 TCID₅₀/mL, calculated by determining the 50% tissue culture infectious dose by the [Reed and Muench \(1938\)](#) method using tenfold serial dilutions in 24-well plates. Preliminary tests were performed on the Frp3 cell lines (non-human primate cell line derived from Fetal kidney) to determine the peptide concentration that did not produce any cytotoxic effects. Cell viability was evaluated by 3-(4,5 dimethylthiazol-2-yl)-2,5-diphenyltetrazolium bromide (MTT) assay ([Manger et al., 1993](#)). Peptide solutions were prepared in serum-free MEM at several concentrations in the range from 100 to 10 µM, treated overnight at 4°C with antibiotic/anti-mycotic solution (EuroClone) and assayed on 24–48 h cell monolayers in a 24-well plate. The monolayers were incubated for 1 h at 37°C in 5% CO₂. Thereafter, cells were washed twice with Dulbecco's Phosphate Buffer Solution (DPBS, EuroClone) and maintained with MEM supplemented with 2% of FBS for 48 h in 5% CO₂ at 37°C. After that, the medium was removed and 300 µL of MTT (Sigma Aldrich, Milan, Italy) solution (5 mg/mL) was added. The monolayers were incubated for 15–30 min at 37°C in 5% CO₂. Therefore, the MTT was removed and 500 µL DMSO was added to each well to dissolve the purple formazan. The absorbance was measured at 570 nm. DMSO and culture medium were used as controls. Therefore, solutions of 40 µM and 80 µM concentration for each peptide were chosen to treat HAV at a concentration of 4.6×10^4 TCID₅₀/mL. The suspensions containing the peptides and virus were incubated for 1 h at room temperature (RT). Then the viral infectivity was investigated on Frp3 cells. Untreated HAV suspension and 40 µM and 80 µM peptide solutions, incubated at the same conditions, were used as controls. Each treatment was assayed in triplicate. Viral titrations were performed by determining the TCID₅₀/mL. Briefly, 100 µL of serial tenfold dilutions of each sample were assayed in 24-well tissue culture plates containing 24–48 h monolayers of Frp3 cells, and incubated for 1 h in 5% CO₂ at 37°C. After that, the wells were washed twice with 200 µL of PBS, and 500 µL of MEM supplemented with 2% of FBS were added to each well. The infections were carried out for up to 14 days in 5% CO₂ at 37°C with a daily visual inspection. After 7 days the culture medium was changed. The virucidal efficacy of peptides was estimated by comparing the titres of the viral suspension treated with the titre of the untreated virus. The reduction in viral infectivity was evaluated as log reduction value (LRV) by calculating the log₁₀ N₀/N₁, where N₀ is the titre for untreated viral suspension and N₁ is the titre for treated viral suspension.

2.5. Circular dichroism spectroscopy

Circular dichroism (CD) analysis was performed by Jasco J-810 spectropolarimeter. The samples were loaded into a quartz cuvette of 0.1 cm path length (Hellma Analytics) and the spectra were recorded in the 195 nm–250 nm range at a scan speed of 20 nm/min, by averaging 5 scans and in the presence or absence of SDS. The effect of pH on the secondary structure of RiLK1 and RiLK3 was analysed by dissolving the samples at a concentration of 80 µM in different buffer solutions at 10 mM concentration: glycine-HCl, pH 2.0; Tris-HCl, pH 7.0; glycine-NaOH, pH 11.0. Next, SDS (50 mM final concentration)

was added to each sample, which was incubated up to 48 h at 25°C and analysed by CD spectroscopy. The folding kinetic measurements of the peptides were performed after the addition of SDS (50 mM) to each sample (80 µM in 10 mM Tris-HCl, pH 7.0) up to 24 h incubation. CD experiments were also carried out in 10 mM Tris-HCl buffer pH 7.0 as function of SDS concentration at a peptide concentration of 80 µM. For thermal stability analyses, the peptides were prepared to a final concentration of 80 µM in 10 mM Tris-HCl, pH 7.0 in the presence of 50 mM SDS and then they were incubated at 4, 37 and 90°C up to 48 h before acquired the CD spectra. A blank spectrum of a sample containing all components except the peptide was acquired for the baseline-correction of the CD spectra of the peptide. The mean residue ellipticity ($[\theta]$, deg. cm² dmol⁻¹) was obtained by the equation $[\theta] = 100 \theta / cnl$, where θ is the ellipticity (mdeg), c is the peptide concentration (mM), n is the number of residues, and l is the path length (cm). The percentage of secondary structure was estimated by the DICHROWEB site (Whitmore and Wallace, 2004, 2008), using the K2D algorithm (Perez-Iratxeta and Andrade-Navarro, 2008).

2.6. Fluorescence spectroscopy

Trp fluorescence emission spectra were recorded at 25°C on a Shimadzu RF-6000 spectrofluorometer (Kyoto, Japan) with both excitation and emission slit widths set at 5 nm. The intrinsic tryptophan was excited at a wavelength of 280 nm and the emission was monitored between 300 and 400 nm. The folding kinetic experiments of RiLK1 and RiLK3 were performed after the addition of SDS (50 mM) to each sample (80 µM concentration in 10 mM Tris-HCl buffer pH 7.0) up to 24 h incubation. Fluorescence measurements were also carried out in 10 mM Tris-HCl buffer pH 7.0 as a function of SDS concentration at a peptide concentration of 80 µM. The effect of pH on peptide folding was analysed by dissolving the peptides at a final concentration of 50 µM in different buffer solutions at 10 mM concentration: glycine-HCl, pH 2.0; Tris-HCl, pH 7.0; glycine-NaOH, pH 11.0. Then, SDS (50 mM) was added to each sample, which was incubated up to 48 h at 25°C and monitored by fluorescence spectroscopy. For thermal stability, the peptides were prepared to a final concentration of 80 µM in 10 mM Tris-HCl buffer pH 7.0 in the presence of 50 mM SDS and then they were incubated at 4, 37 and 90°C up to 48 h.

2.7. Peptide cross-linking

Either RiLK3 or RiLK1 at 240 µM concentration in the presence of SDS micelles (150 mM) in 10 mM sodium phosphate buffer pH 7.0 was cross-linked with or without glutaraldehyde at 4% (v/v) in the dark at 37°C for 24 h. The samples (10 µL) were analysed by tris-tricine SDS-PAGE (17%). The electrophoresis was conducted at 30 mA for 1 h at room temperature. Gel filtration chromatography was performed on Superdex 30 Increase (10/300 GL, Pharmacia Biotech, Milan, Italy) column connected to an AKTA FPLC system (GE Healthcare, Italy), pre-equilibrated with 50 mM Tris-HCl buffer (pH 7.5) containing 150 mM NaCl and 20% Acetonitrile. Standard protein markers (BioRad code 151-1901) were utilized to calibrate the gel filtration column. The fractions eluted by the column were collected and analysed by fluorescence spectroscopy.

2.8. Fourier transform infrared spectroscopy analysis

A Nicolet iS50 Fourier transform infrared (FT-IR) spectrometer (Thermo Scientific) equipped with macro-diamond based attenuated total reflection (ATR) module (smart iTX-diamond by Thermo Scientific) and DTGS KBr detector was utilized to collect FT-IR spectra of sample powders. Powders were in direct contact with the diamond plate of the ATR module using a pressuring tip. The background was acquired from the diamond plate in the air without samples. All spectra were recorded using 16 scans in the range from 4000 to 525 cm⁻¹ with a 0.482 cm⁻¹ spectral resolution. Each sample was analysed in triplicate and averaged. Moreover, to determine any secondary structure of samples, according to Wi et al. (1998), Rea et al. (2014) and Portaccio et al. (2015), the amide I band was analysed. In particular, the deconvolution of FT-IR spectra in the range 1700–1600 cm⁻¹ was released by fitting data with multi-Lorentzian peaks corresponding to the minima of second derivative spectra. Second derivative spectra were obtained with Savitsky–Golay derivative function algorithm on 7 data points by in-home software.

2.9. Preparation of model membranes: multilamellar vesicles

Model membranes (liposomes) were prepared using lipid stock solutions (10 mM) in chloroform:methanol (2:1, v/v) of 1-palmitoyl-2-oleoyl-sn-glycero-3-phosphoethanolamine (POPE) (Avanti Polar Lipids, Alabaster, United States), 1,2-dioleoyl-sn-glycero-3-phosphoethanolamine (DOPE) (Avanti Polar Lipids, Alabaster, United States), L- α -lysophosphatidylcholine (Egg Lecithin, PC) (Avanti Polar Lipids, Alabaster, United States), N-Acyl-D-sphingosine-1-phosphocholine (chicken egg yolk, SM) (Sigma-Aldrich, St. Louis, MO, United States), phosphatidyl serine (PS) (Avanti Polar Lipids, Alabaster, United States), 1',3'-bis [1,2-dioleoyl-sn-glycero-3-phospho]-glycerol (Cardiolipin 18:1, CL) (Avanti Polar Lipids, Alabaster, United States) and 1-palmitoyl-2-oleoyl-sn-glycero-3-phosphatidylglycerol (POPG) (Larodan AB, Sweden). Lipid films were made in glass vials by mixing a volume of phospholipid stock solutions to achieve the desired molar ratio as reported below. Next, the solutions (2 mL) were dried under argon flow and then subjected to a vacuum for at least 3 h to remove traces of the solvent. A sufficient volume of binding buffer composed of 4-(2-hydroxyethyl) piperazine-1-ethanesulfonic acid 10 mM (HEPES, Sigma-Aldrich) and NaCl 100 mM (Sigma-Aldrich), pH 7.2 was used to resuspend the lipidic film, yielding 2 mM lipid phosphorus. Lipid suspensions were freshly prepared before each experiment. The membrane lipid composition for eukaryotic and prokaryotic cells (% mol) was reported in Table 1.

2.10. Lipid binding assay

Reaction mixtures were prepared in Eppendorf tubes combining each lipid solution (at the fixed lipid phosphorus molar concentration of 1800 µM) with pre-formed liposomes containing different amounts of peptide, ranging from 20 to 100 µM (when saturation did not occur, higher peptide concentrations were tested). The samples were vigorously vortexed and incubated at room temperature for 30 min to allow

TABLE 1 Lipid composition of eukaryotic and prokaryotic membranes.

Membrane	PC	SM	PS	DOPE	POPE	POPG	CL
Eukaryotic membrane ^a	40	15	5		40		
Zwitterionic membrane	100						
<i>Salmonella Typhimurium</i> ^{b,GN}				78		18	4
<i>Staphylococcus aureus</i> ^{c,GP}						58	42

PC, phosphatidylcholine; SM, sphingomyelin; PS, phosphatidylserine; DOPE, dioleoyl-phosphatidylethanolamine; POPE, palmito-yl-oleoyl-phosphatidylethanolamine; POPG, palmitoyl-oleoyl-phosphatidylglycerol; CL, cardiolipin. GN, Gram-negative bacteria; GP, Gram-positive bacteria.

^aCasares et al. (2019).

^bBarbosa et al. (2019).

^cEpand and Epand (2011).

binding. Analogous samples, made with the buffer solution vehicle rather than the stock peptide solution, were used as negative controls. At the end of the incubation period, the solutions were transferred carefully to polycarbonate centrifuge tubes (1 mL, 8 × 51 mm: Beckman Coulter, United States) and centrifuged at 60,000 × g (20,000 rpm, outer row) for 1 h at 20°C (Beckman LE-80 Ultracentrifuge; rotor type 25). Therefore, the supernatant was removed and the pellet was washed (two-three times) with the binding buffer to eliminate the aggregated peptide eventually precipitated and resuspended with the same buffer containing sodium dodecyl sulfate (SDS, Thermo Fisher, Germany) at a final concentration of 1%. The binding of the peptide to the model membranes was assessed by quantifying the amount of RiLK1 or RiLK3 in the pellet and supernatant using calibration curves generated by adding known amounts of the peptide to control supernatants or pellets of vesicles prepared in the absence of the peptide (see above). Peptide binding to multilamellar vesicles (MLVs) was monitored by fluorescence spectroscopy taking advantage of the presence of the tryptophan residues in RiLK1 or RiLK3.

2.11. Steady-state tryptophan fluorescence

Tryptophan (Trp) fluorescence spectra were recorded for each supernatant and pellet sample after 30 min of stirring at 900 rpm in a Thermo-Shaker (TS-100: Biosan) at room temperature (Ambrosio et al., 2022). The variation in Trp emission was monitored between 300 and 450 nm excitation, at λ_{ex} = 280 nm, by a Shimadzu RF-6000 spectrofluorometer (Kyoto, Japan). Slit widths were 2.5 nm for excitation and 5 nm for emission, and each spectrum was corrected by subtracting the liposome background.

2.12. Morphological characterization and surface charge measurements

The hydrodynamic size and ζ -potential of *Salmonella*- and *Staphylococcus*-like liposomes were measured by Zetasizer Nano-ZS instrument (Malvern Instrument Ltd., Cambridge, United Kingdom) equipped with a He-Ne laser (633 nm, fixed scattering angle of 173°, 25°C). The size (d) and the polydispersity index (PDI) of the obtained liposomes (at an initial concentration of 2 mM) were measured by diluting them down to 0.2 mM in MilliQ water. The liposome suspensions (1 mL for each type) were inserted in a standard disposable cuvette and three measurements ($n = 3$) of their size and PDI were performed. The ζ -potential of the bacterial-mimic liposomes and the

peptides (before and after their interaction with them) were measured in triplicate ($n = 3$) by using disposable zeta-potential cuvettes (1 mL). ζ -potential measurements were performed for peptides (RiLK 1 and RiLK 3) at a concentration of 0.01 mM, and after liposome:peptide interaction at two different ratios (20:1 and 2:1). The interactions between bacterial-like liposomes and peptides were performed as reported in Section 2.10. To achieve the suitable concentrations for ζ -potential measurements, the incubations were performed at 10 times higher concentrations and underwent a 1:10 dilution in MilliQ water before ζ -potential measurements. The two different liposome:peptide ratios were obtained by fixing the peptide concentration at 0.1 mM and changing the liposome concentration, accordingly.

2.13. Statistical analyses

Lipid binding and antimicrobial assays were performed by GraphPad Prism® (version 9.5.0, software San Diego, CA, United States). All experiments were carried out at least three times and the data were reported as the mean (M) ± standard deviation (s.d.). The statistical significance of differences between samples in the presence or absence of peptides was calculated through one-way analysis of variance (ANOVA) with Bonferroni *post hoc* comparisons, with a significance level of $p < 0.05$.

3. Results and discussion

3.1. Rational design of RiLK3

The rational design of AMPs represents a practical strategy to obtain a peptide with improved antibacterial properties. Therefore, a study for analysing the structural elements which govern the antimicrobial action of the already characterised peptide RiLK1 was performed with the aim to provide important information for further modifications of key residues and the generation of new RiLK1-based antimicrobial agents.

It is widely reported that cationic residues are fundamental for the antimicrobial activity of amphipathic AMPs as they attract the peptide to the negatively charged bacterial membranes via electrostatic interaction (Yeaman and Yount, 2003). In this context, arginine is reported to be more efficacious in mediating peptide-membrane interactions as its guanidinium moiety displays a stronger H-bonding capability with the phospho-rich membrane surface of the bacteria compared to the primary amine moiety of lysine (Yeaman and Yount, 2003; Hristova and Wimley, 2011). Moreover, the arginine

TABLE 2 Physicochemical properties of the mutated peptide RiLK3 in comparison with those of the parent RiLK1.

Parameters	RiLK1 ^a	RiLK3
Sequence	NH ₂ -RLKWVRIWRR-CONH ₂	NH ₂ -RLR ^W VRIWRR-CONH ₂
Molecular weight (Da)	1468.96	1495.83
Bomax index (kcal/mol)	4.70	5.6
Net charge	+5	+5
Half-life (sec)	855.71	852.61
Hydrophobicity	−0.56	−0.63
Hydropathicity	−1.12	−1.18
Amphipathicity	1.35	1.23
Hydrophilicity	0.31	0.31

The mutated amino acid residue of the parental peptide RiLK1 is highlighted in red.

^aAgrillo et al. (2020).

TABLE 3 Antimicrobial properties of the mutated peptide RiLK3 in comparison with those of the parent RiLK1.

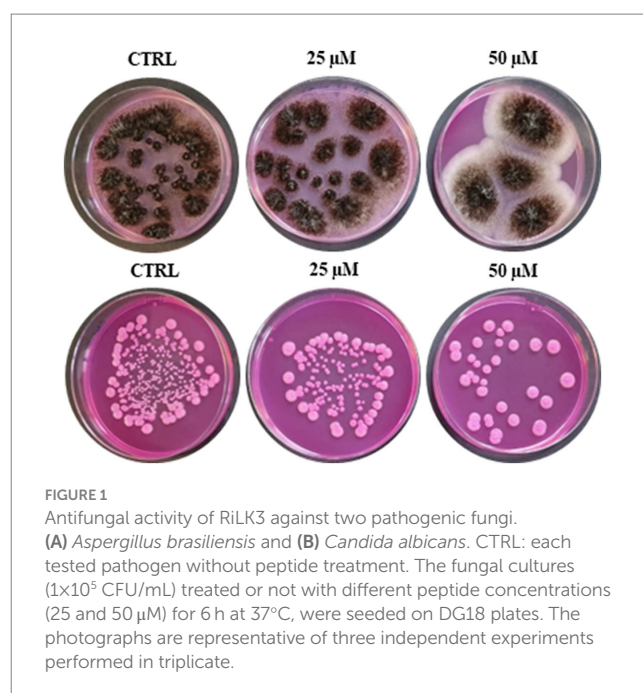
Strain	RiLK1	RiLK3
	MBC (μM)	MBC (μM)
<i>P. aeruginosa</i> (ATCC 27853)	50.0	50.0
<i>S. typhimurium</i> (wild strain)	2.5 ^a	5.0
<i>E. coli</i> (ATCC 25922)	2.0 ^a	2.0
<i>S. aureus</i> (ATCC 25923)	16.0 ^a	75.0
<i>L. monocytogenes</i> (wild strain)	2.0 ^a	18.0

^aAgrillo et al. (2020).

side-chains can form bidentate interactions with lipids leading to enhance the membrane curvature and then the activity, while lysine residues do not induce this curvature on their own, producing only monodentate interactions (Schmidt et al., 2012; Cutrona et al., 2015). Afterwards, increased arginine/guanidinium vs. lysine/amine composition appears to improve the antimicrobial potency of peptides, although this trend is not universally observed (Cutrona et al., 2015). Therefore, to investigate on the structure and function of RiLK1, a 10-mer analogue, named RiLK3 was projected by replacing the lysine residue at position 3 with arginine (Hristova and Wimley, 2011). Following this *in silico* site-directed mutagenesis approach, the designed AMP was characterised using four online software packages to predict the relevant physicochemical parameters, which are recognized to be necessary to perform the biological function. This investigation was carried out to make sure that RiLK3 retained similar or better features as the parental ones. According to the data reported in Table 2, the RiLK1-derivative peptide displayed improved performances compared to the RiLK1 in terms of Boman index, hydropathicity and hydrophobicity, which are properties considered important for peptide-membrane interactions (Torres et al., 2017).

3.2. Antibacterial, antifungal and antiviral activity of RiLK3

To assess the impact of the performed substitution on the antibacterial activity of the mutant RiLK3, the minimal bactericidal

**FIGURE 1**

Antifungal activity of RiLK3 against two pathogenic fungi.

(A) *Aspergillus brasiliensis* and (B) *Candida albicans*. CTRL: each tested pathogen without peptide treatment. The fungal cultures (1×10⁵ CFU/mL) treated or not with different peptide concentrations (25 and 50 μM) for 6 h at 37°C, were seeded on DG18 plates. The photographs are representative of three independent experiments performed in triplicate.

concentrations (MBCs) of the peptide were measured against some of the most representative Gram-negative (*S. typhimurium*, *E. coli* and *P. aeruginosa*) and Gram-positive foodborne pathogens (*S. aureus* and *L. monocytogenes*), and compared with those of the parental RiLK1. As reported in Table 3, the RiLK1-analog peptide RiLK3 showed a bactericidal activity equal to that of RiLK1 against *E. coli* (MBC = 2.0 μM) and *P. aeruginosa* (MBC = 50 μM) strains. In contrast, RiLK3 showed a lesser bactericidal activity than its parental RiLK1 against *L. monocytogenes*, *S. typhimurium* and *S. aureus*, with MBC values 9-, 2- and 4.5-times higher than those of RiLK1, respectively.

Due to the increasing incidence of drug-resistant fungi and the limitations of existing treatment strategies for infections caused by fungi, the fungicidal activity of RiLK3 (Figure 1) was also evaluated *in vitro* against two of the most common fungal pathogens such as *A. brasiliensis* and *C. albicans* and compared with that previously determined for RiLK1 (Agrillo et al., 2020). The antifungal susceptibility testing clearly revealed that RiLK3 was less active than its parent, inhibiting only ~87% growth of *A. brasiliensis* and ~90% growth of *C. albicans* even at the highest concentration tested (50 μM), whereas RiLK1 at 25 μM concentration had a total inhibitory effect on the growth of both fungi (MFC) (Agrillo et al., 2020).

Finally, the antiviral effects of RiLK1 and RiLK3 were investigated *in vitro* for the first time against the hepatitis A virus (HAV) to assess whether the lysine to arginine substitution affected the virucidal activity. Indeed, HAV is a non-enveloped single-stranded RNA virus provoking acute hepatitis in humans, a worldwide infectious disease. For this reason, the development of new antivirals against HAV may be important for the control of viral infections. Firstly, the cytotoxicity of the two peptides on the Frp3 cell lines was assessed at different concentrations, revealing that both molecules did not have any effect on the viability of Frp3 cell line at all the doses tested (data not shown). Therefore, the antiviral assays were performed and the results of the virucidal effects are summarised in Table 4. Interestingly, HAV treated with RiLK1 showed a decrease in viral infectivity greater than 1 log in comparison with the untreated virus at both 80 μM (1.4 log) and 40 μM

(1.1 log) concentrations, corresponding to a reduction in the infectious potency of 96.6% and 93.3%, respectively. Conversely, RiLK3 was unable to inhibit HAV infection at the same concentrations tested.

Therefore, these findings are interesting in light of other works in which it is reported that increased arginine content not necessarily determine an improvement of the AMP activity, providing further indications for the design of new antimicrobial peptides (Hristova and Wimley, 2011; Cutrona et al., 2015).

3.3. Structural characterization of RiLK3

Studies of peptide-detergent interaction are very important for AMP research taking into consideration the peculiarity of their mechanism of action activity, which is usually via bacterial membrane disturbance (Hancock and Rozek, 2002; Benfield and Henriques, 2020). Commonly, this interaction induces conformational changes to the peptides themselves, which are mainly unstructured in solution. In this context, CD spectroscopy was performed to understand the role of secondary structural features on the antimicrobial potency of RiLK3 peptide in comparison with its parental RiLK1, using the negatively charged SDS as a prokaryotic membrane-mimetic model.

TABLE 4 *In vitro* effect of RiLK1 and RiLK3 peptides on HAV infectivity by calculating log reduction value (LRV).

	Viral titre after treatment	Log reduction value
	(logTCID ₅₀ /mL ± SD)	(logTCID ₅₀ /mL ± SD)
Untreated HAV	4.7 ± 0.2	
RiLK1 (80 µM)	3.3 ± 0.2	1.4 ± 0.4
RiLK1 (40 µM)	3.6 ± 0.1	1.1 ± 0.3
RiLK3 (80 µM)	4.4 ± 0.1	0.3 ± 0.3
RiLK3 (40 µM)	4.4 ± 0.1	0.3 ± 0.3

For this analysis, CD spectra of both peptides were recorded at a constant concentration (80 µM) in 10 mM Tris-HCl buffer (pH 7.0) and in the absence or presence of SDS solutions, below and above the critical micelle concentration (cmc). As shown in Figure 2, the CD spectra of RiLK3 (Figure 2A) and RiLK1 (Figure 2B) showed a pronounced negative band below 200 nm in a water solution, indicating a predominantly random coil secondary structure, typical of an unstructured peptide. After adding increasing concentrations of SDS (3–150 mM), both peptides exhibited CD spectra very similar in shape when in contact with the oppositely charged amphiphile. Specifically, in solutions at the SDS concentration below cmc (3 mM), RiLK3 and RiLK1 adopted mainly α/β -mixed conformations, which underwent a dramatic shape change when the detergent was present in micellar concentration (50 and 150 mM). As depicted in Figure 2, both peptides showed a more complex folded conformation, that was not correlated with the common secondary structure elements (α -helix, β -strand, or random coil), and that could be due to the co-existence of multiple α/β -like subpopulations and/or the propensity to form higher-ordered self-aggregates, which assemble into bigger oligomeric species in equilibrium with partially structured monomers. Subsequently, the folding kinetics of RiLK3 and RiLK1 were monitored in the presence of 50 mM SDS during 24 h incubation. The CD spectra (Figures 3A,B) evidenced that each peptide retained its own complex conformational distribution during the time, as confirmed by the assessment of the secondary structure elements performed by the K2D software (Supplementary Table S1). Therefore, from the structural point of view, the modification of the identity of the basic residues did not induce appreciable changes in the secondary structure of the mutant in comparison to the wild-type peptide.

To corroborate the CD data, the same analyses were carried out by fluorescence, taking advantage of the occurrence of two tryptophan residues in both sequences. In aqueous solution, the maximal fluorescence emission (λ_{max}) for the two peptides was observed at ~350 nm, a value that is typical for the Trp indole group

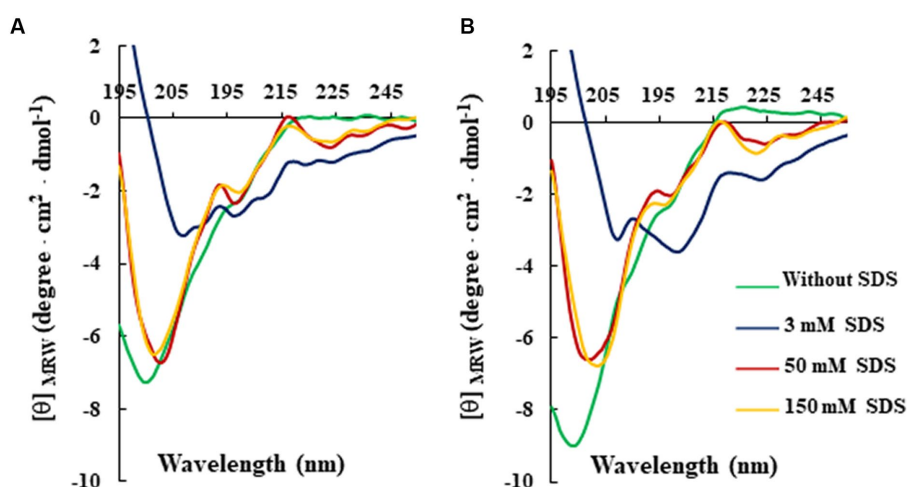


FIGURE 2 Effect of SDS concentration on the secondary structure of RiLK3 and RiLK1 monitored by circular dichroism. Far-UV CD spectra of (A) RiLK3 and (B) RiLK1. All spectra were recorded at a peptide concentration of 80 µM in 10 mM Tris-HCl, pH 7.0 and at 25°C in the absence (green lines) or presence of SDS at different concentrations.

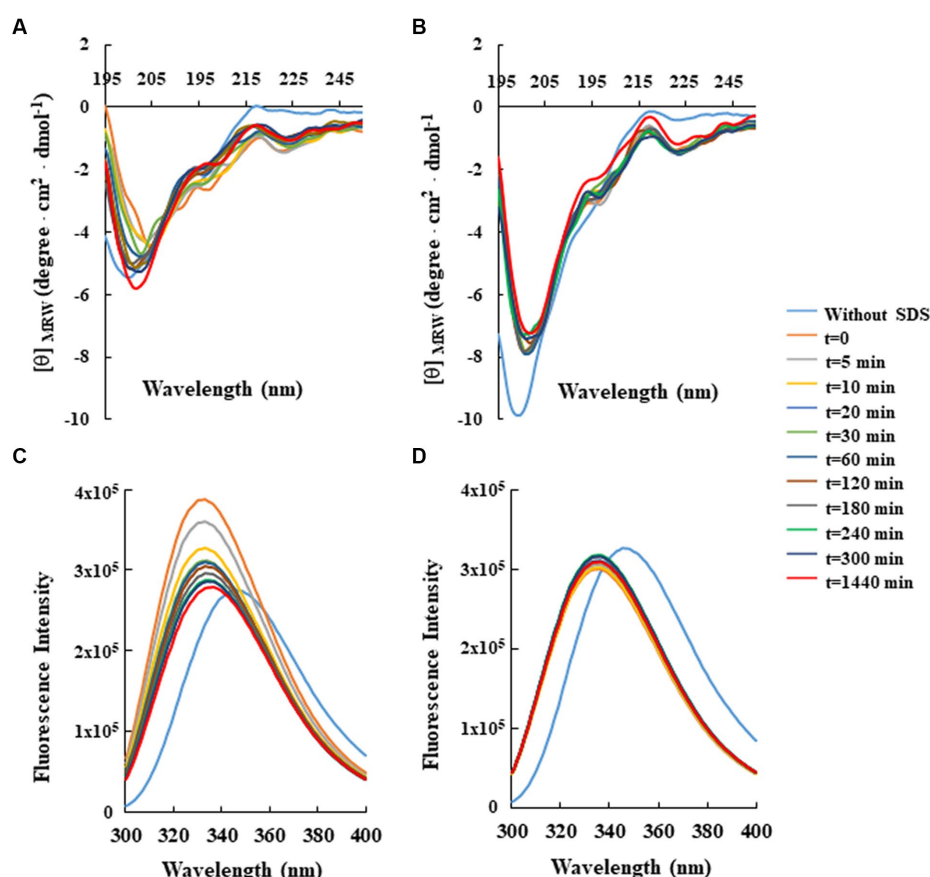


FIGURE 3

Time-dependent effect of SDS on the secondary and tertiary structure of RiLK3 and RiLK1 monitored by spectroscopic techniques. Far-UV circular dichroism spectra of (A) RiLK3 and (B) RiLK1. Intrinsic fluorescence emission spectra of (C) RiLK3 and (D) RiLK1. All spectra were recorded at a peptide concentration of 80 μ M in 10 mM Tris-HCl, pH 7.0 in the presence or absence (blue lines) of SDS (50 mM) during 24 h incubation at 25°C.

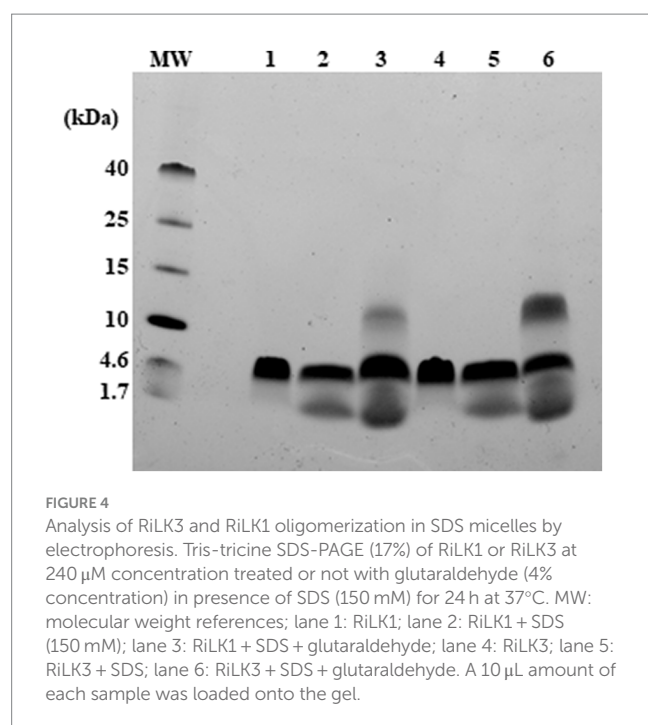
fully exposed to hydrophilic environments and that is consistent with the disordered secondary structure observed at this condition by CD (Figures 3C,D). Immediately after SDS addition at 50 mM concentration ($t=0$), an increase in the quantum yield of fluorescence accompanied by a concomitant blue shift of λ_{\max} from 350 to 335 nm, was observed for RiLK3, indicative of a reduction in the polarity around the Trp residues and an ordered structural reorganisation. As the incubation time increased, the fluorescence intensity gradually decreased, suggesting a strong involvement of one or both Trp residues in hydrophobic interactions with the detergent micelles, resulting in their shielding (Figure 3C). Another source of quenching might be the interaction between tryptophan and the tryptophan-flanking lysine in the peptide under investigation (Zhao and Kinnunen, 2002), like. Moreover, the tryptophan residues could suffer from fluorescence self-quenching if peptide oligomerization takes place upon binding, as also evidenced by CD spectra.

Concerning RiLK1, the addition of SDS shifted λ_{\max} to lower wavelengths without affecting the fluorescence intensity, which remained constant for the whole incubation period (24h). This behaviour could be due to a fast saturation of Trp fluorescence, indicative of reaching a stationary phase in which the peptide does not remain really “stationary” but it continuously modifies its highly dynamic supramolecular conformations with time.

Next, the effect of pH and temperature-effects on peptide-SDS complexes were investigated, being both physicochemical parameters that strongly influence the AMP efficacy. As shown in Supplementary Figures S1, S2, the changes in pH or temperature monitored up to 48 h did not markedly affect the structural and folding stability of RiLK3 when in complex with SDS micellar solutions in the experimental range analysed. The same behaviour was also observed with RiLK1 (Supplementary Figures S3, S4), confirming the ability of both molecules to adapt to different environmental conditions and therefore to retain their antimicrobial activity at different temperatures and pH values. Remarkably, a structural-functional correlation does not emerge in this study as the weakened activity of the arginine mutant is not accompanied by distinctly different structures than those observed for the lysine mutant, as evidenced by our spectroscopic data.

3.4. Oligomerization of RiLK3 or RiLK1 in SDS micelles

The tendency of RiLK1 and RiLK3 to oligomerize in the presence of SDS micelles was also assessed by performing glutaraldehyde-mediated cross-linking experiments. At high concentrations of glutaraldehyde, both peptides demonstrated to form predominantly

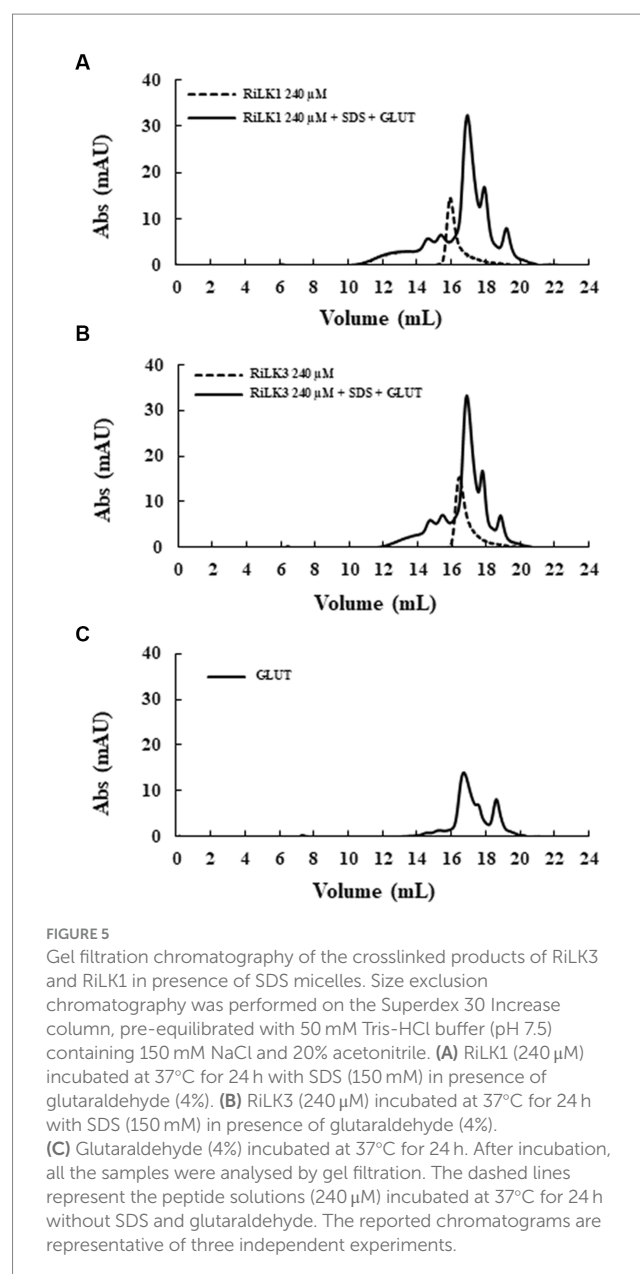


trimeric states as evidenced by the presence of a prominent SDS-PAGE band corresponding to molecular mass of ~5 kDa upon incubation of peptide/SDS with the cross-linker (Figure 4). Moreover, cross-linked species belonging to larger (about 12 kDa) or lesser (about 1.7 kDa) molecular masses corresponding to monomeric state, were also seen, albeit with minor populations. However, upon treatment with SDS micelles in the absence of glutaraldehyde a detectable oligomerization corresponding to the trimeric state of RiLK3 and RiLK1 was observed. This behaviour could indicate a covalent association among the peptide molecules as it was not disrupted by SDS detergent unlike the high-mass oligomers, which may be non-covalent nature. It is worth noting that both peptides, RiLK3 and RiLK1, appeared to migrate on the SDS-PAGE as trimeric species in the absence of cross-linker and SDS micelles, thus suggesting a propensity of peptides to self-assemble.

To gain insights into the oligomerization propensity of the two peptides in the presence of membrane mimics, size exclusion chromatography was performed on the same samples analysed by SDS-PAGE. As depicted in Figure 5, in the absence of detergent and glutaraldehyde, monomers of RiLK1 and RiLK3 were observed. After adding the cross-linker, a homogeneous population containing peptide species with high molecular weights was present in the cross-linked samples, as demonstrated also by the fluorescence assays performed on the fractions eluted and collected from the size-exclusion column (data not shown). The obtained results confirmed the oligomerization behaviour of both AMPs when in contact with membrane-like environments.

3.5. FT-IR analysis of RiLK1 and RiLK3

To obtain further information on the possible self-assembly propensity of RiLK1 and RiLK3, the Fourier transform infrared spectroscopy (FT-IR) was applied in the range from 4000 to 525 cm^{-1}



(Wi et al., 1998). Usually, polypeptides show nine characteristic IR absorption bands: amide A and B around 3300 and 3100 cm^{-1} , respectively, attributed to NH stretching; amide I in the range of 1600–1700 cm^{-1} responsible for C=O stretching; amide II and III in the range 1480–1575 cm^{-1} and 1229–1301 cm^{-1} , respectively, attributed to CN stretching and NH bending; amide IV in the range 625–767 cm^{-1} , attributed to OCN bending; amide V in the range 640–800 cm^{-1} , attributed to out of plane NH bending; amide VI in the range 537–606 cm^{-1} , attributed to out of plane C=O bending; amide VII around 200 cm^{-1} , attributed to skeletal torsion (Wi et al., 1998; Rea et al., 2014; Portaccio et al., 2015). Specifically, the universally available amide I band (1600–1700 cm^{-1}) is the most utilised probe for the estimation of the secondary structural composition and conformational changes of peptides, due to the high sensitivity of the C=O stretching frequency to small changes in molecular geometry and hydrogen bonding pattern, i.e., to each secondary structure (Rea et al., 2014; Portaccio et al., 2015). In this context, RiLK1 and RiLK3

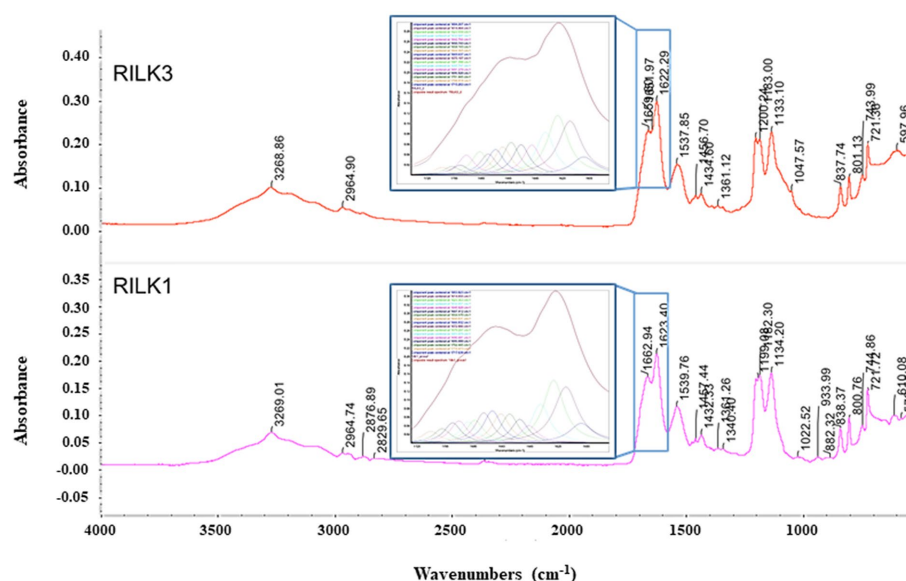


FIGURE 6

FTIR absorption spectra of RILK1 and RILK3 in powder form. Main peaks are underlined. Into the boxes, the amide I bands of RILK1 and RILK3, respectively with their deconvolution data analysis, were reported.

present the typical peptide spectrum with almost all amide bands previously described. Specifically, the absorption spectra of RILK1 and RILK3 analysed in powder form are reported in Figure 6 while the assignment of the peaks is presented in Supplementary Table S2. Moreover, a more detailed analysis on the structure was provided by the second derivative and decomposition of the amide I band into sub-bands. The deconvolved spectra were fitted with Lorentzian bands, whose results are resumed into the boxes of Figure 6 and in Supplementary Tables S3, S4. Any peaks correspond to a C=O stretching frequency that can be linked to a specific secondary structure. As shown in Figure 6, the absorption spectrum of RILK1 in powder form presents a large double peak in the range 1600–1700 cm^{-1} , with a relative maximum at 1622 cm^{-1} , usually attributed to β -sheet, and at 1663 cm^{-1} , usually attribute to 310-Helix. The deconvolved spectra allowed us to carry out a quantitative analysis of the content of the secondary elements present in the RILK1 structure. Specifically, it was found that structures of type β are responsible for 74.3% of the vibrational modes into the peptide (Supplementary Table S3). Similarly, also absorption spectrum of RILK3 in powder form presents a large peak in the range 1600–1700 cm^{-1} , with relative maxima at 1622 cm^{-1} , usually attributed to β -sheet, at 1652 cm^{-1} , usually attribute to α Helix, and at 1660 cm^{-1} , usually attribute to 310-Helix. The deconvolved spectra revealed that structures of type β are responsible for 69.3% of the vibrational modes into RILK3, while α type components are only 11.9% (Supplementary Table S4).

3.6. Binding assays

In general, the primary target of most natural AMPs (Huang et al., 2004; Lohner and Blondelle, 2005) is recognised to be the bacterial membranes that typically contain negatively charged phospholipids, which promote the binding of the cationic peptides (Zasloff, 2002;

Jenssen et al., 2006; Lohner et al., 2008; Lohner, 2009). This could be the reason of the highly selectivity of AMPs towards microorganisms, in view of the differences between the lipid composition of mammalian and bacterial membranes. Therefore, membrane interaction emerged as a key factor to consider the mode of action of these peptides (Matos et al., 2010). In this context, in order to investigate the effects that RiLK1 and RiLK3 exerted at the level of the cell membrane, a study of the interaction between the two peptides and biomimetic model systems of variable lipid compositions was performed by monitoring changes in the intrinsic fluorescence of Trp. These studies also provide valuable information about the molecular basis of the membrane lipid-peptide interaction, as the electrostatic binding may cause shallow surface peptide depots (plaque formation) or intercalation into (pore formation) the lipid bilayer. Upon binding to negatively charged MLVs resembling the membranes of the Gram-negative *Salmonella* and the Gram-positive *Staphylococcus*, a blue shift of the maximum wavelength in the peptide Trp emission spectra was observed in both the lipid environments, indicating the transfer of Trp residues in peptides from the aqueous phase to a more hydrophobic environment in lipid membranes. On the contrary, there was small or no blue shift when the peptides were added to zwitterionic or neutral MLVs, indicative of a negligible partitioning of the peptides into these membranes. From the binding isotherms of RiLK1 (Figure 7) and RiLK3 (Figure 8) upon binding to negatively charged lipid vesicles as a function of lipid-to-peptide molar ratio and the linear regression to the one-site binding model (Figures 7, 8), the dissociation constant K_d and the maximal binding capacity B_{max} were obtained. It is worth noting that RiLK1 displayed a much higher affinity to the bacterial membranes than RiLK3, thus suggesting differences in the membrane mode interaction of the two peptides, although RiLK1 bound about 8-fold more tightly to anionic *Salmonella* than to anionic *Staphylococcus* bilayers, probably due to their distinct lipid compositions and to the surface charge of the membranes. Therefore, this result shows a higher affinity in the binding of RiLK1 to Gram-negative bacterial membranes compared to Gram-positive lipid bilayers. This would

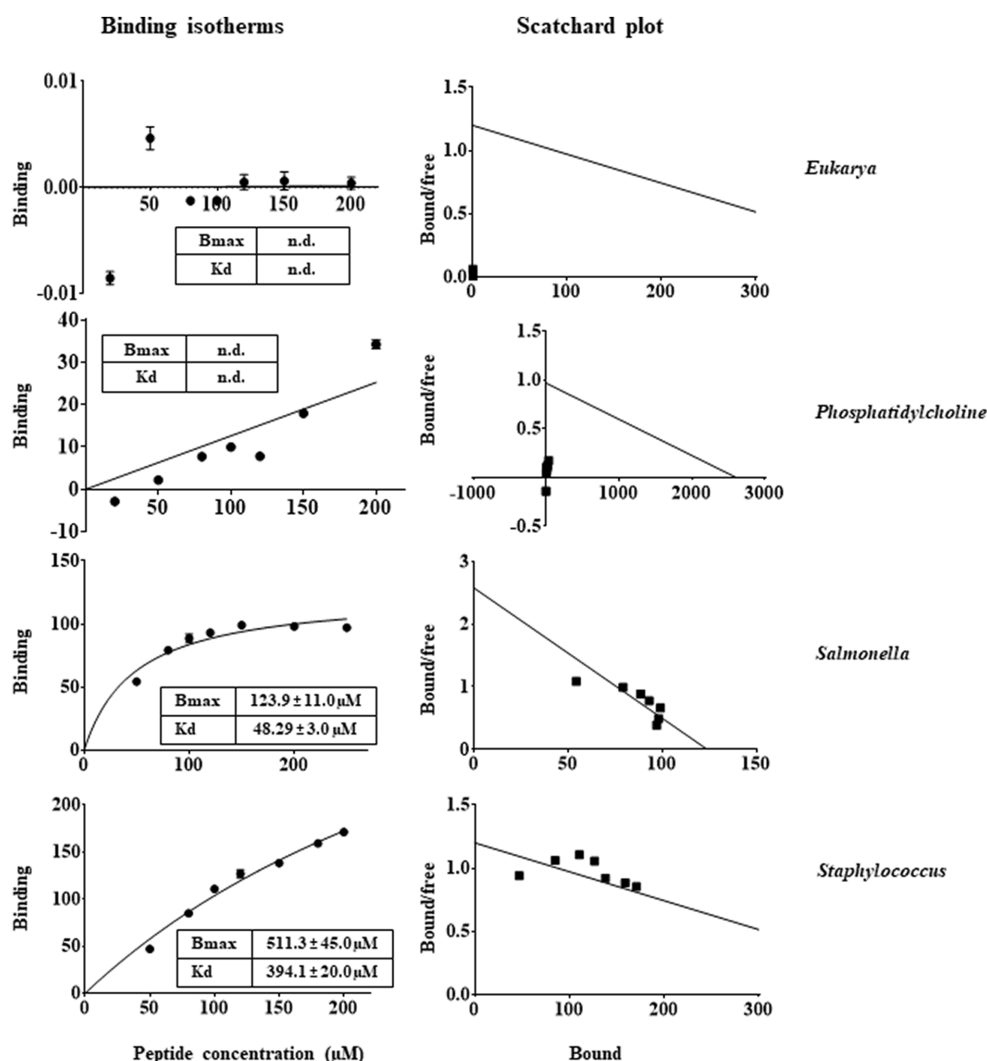


FIGURE 7

Trp fluorescence analysis of binding of RiLK1 to MLVs. Binding isotherms calculated from Trp fluorescence intensity at 335 nm of RiLK1 (1 μM) with model membrane vesicles (30 μM) in HEPES buffer with NaCl 150 mM. Scatchard plot analysis for the binding data of RiLK1. Data are presented as means \pm s.d. of different samples analysed in quadruplicate. n.d. the equation could not fit the data, not possible to determine.

be consistent with the hypothesis that the Gram-negative bacteria are more easily killed by RiLK1 because their membranes have a high concentration of zwitterionic lipids together with anionic lipids. This result is supported by *in vitro* antimicrobial assays previously described, where the Gram-negative bacterial species *S. typhimurium* that has a high content of the zwitterionic lipid DOPE, also has MBC value that is substantially lower than that determined for the Gram-positive *S. aureus*, whose membrane lipids are largely anionic (POPG and CL) and are devoid of uncharged lipids.

In line with the K_d values of RiLK1 binding to these membranes, B_{\max} values were smaller than those of RiLK3, demonstrating the higher affinity of RiLK1 with respect to RiLK3 for bacterial membranes. However, saturation upon binding of both peptides to the *Staphylococcus*-like membranes was not achieved under the experimental conditions used, thus indicating that a higher ligand concentration was required and suggesting that RiLK1 and RiLK3 bound less specifically to this type of membrane. Conversely, no changes in the binding curves were observed in the presence of MLVs of PC or PC:POPE 40:40 mimicking

zwitterionic and eukaryal membranes (Figures 7, 8), demonstrating that RiLK1 and RiLK3 had essentially no affinity for these uncharged membranes and suggesting that the electrostatic forces play a crucial role in the membrane-peptide interaction, thus driving the preference of the two AMPs for the bacterial cells over eukaryotic ones.

In conclusion, it is clear that increasing the arginine content as in RiLK3 (5 arginine residues compared to 4 in RiLK1) did not enhance its interaction with prokaryotic membranes and its antimicrobial activity. Therefore, it is likely that an optimal number of arginine residues at the specific positions along the peptide sequence can represent the driving force for an efficient cell-penetrating ability of arginine-rich peptides.

3.7. Dynamic light scattering and ζ -potential analysis

To further assess the effects of RiLK1 and RiLK3 on the overall structure of bacterial membranes, a preliminary physical-chemical

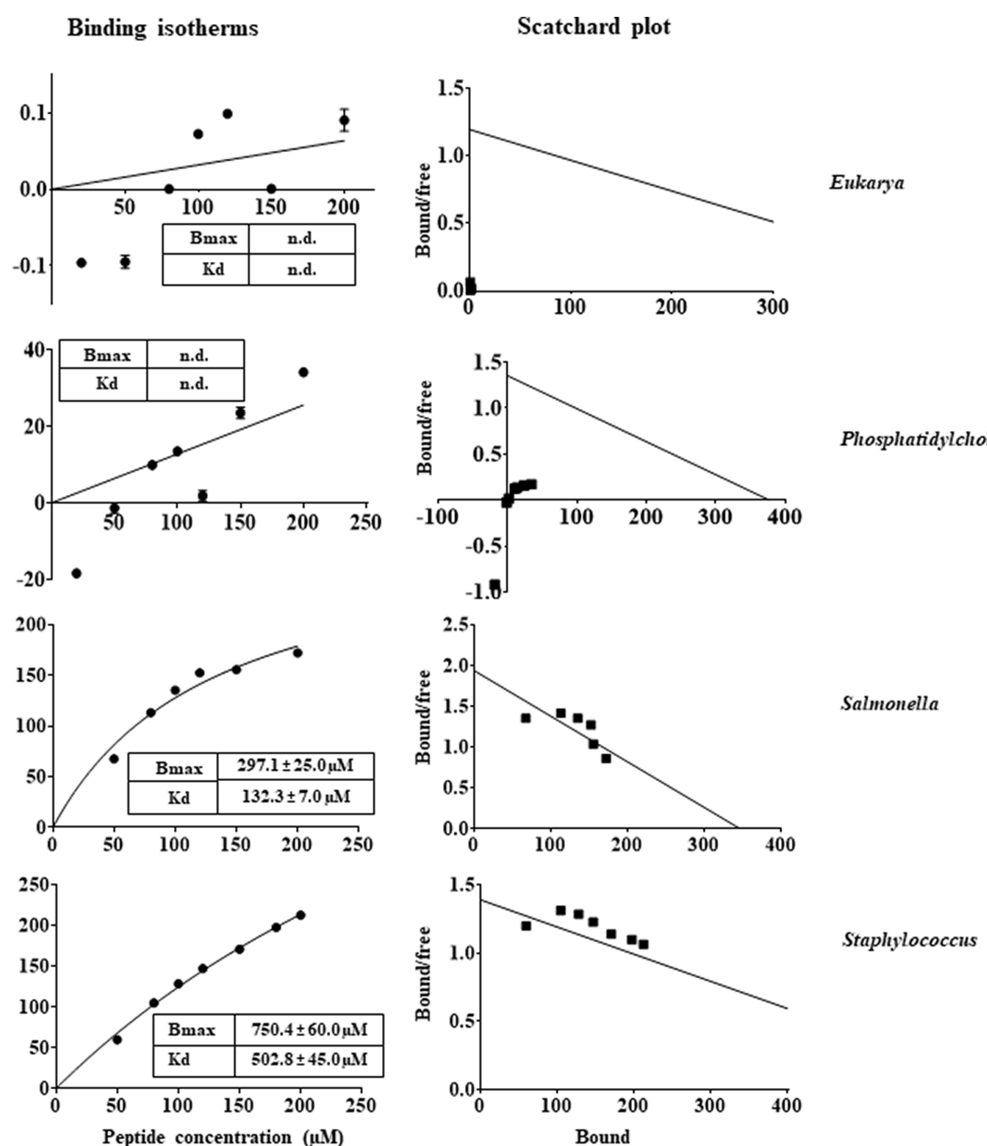


FIGURE 8

Trp fluorescence analysis of binding of RiLK3 to MLVs. Binding isotherms calculated from Trp fluorescence intensity at 335 nm of RiLK3 ($1 \mu\text{M}$) with model membrane vesicles ($30 \mu\text{M}$) in HEPES buffer with NaCl 150 mM . Scatchard plot analysis for the binding data of RiLK3. Data are presented as means \pm s.d. of different samples analysed in quadruplicate. n.d. the equation could not fit the data, not possible to determine.

characterization of our liposomal model systems, with or without AMPs, was carried out by performing dynamic light scattering (DLS) and ζ -potential measurements. DLS measurements of the *Salmonella*-like liposome at a concentration of 0.2 mM showed a monodisperse distribution with mean size (d) of $600 \pm 300 \text{ nm}$ and a polydispersity index (PDI) of 0.21 (Figure 9A). In the same way, DLS measurements were performed on *Staphylococcus*-like liposomes, revealing the presence of two main populations: the first population exhibited a mean size (d_1) of $200 \pm 60 \text{ nm}$, while the second one exhibited a mean size (d_2) of $1500 \pm 600 \text{ nm}$ (Figure 9B). Due to the presence of the two populations, the measured PDI value increased to 0.47 , as compared to the one obtained for *Salmonella*-like liposomes. Then, ζ -potential measurements were carried out to highlight the interactions between the peptides (RiLK1 and RiLK3) with both bacterial-mimic liposome types (Figure 9C). First, the ζ -potential of *Salmonella*-mimic liposome

and both peptides, before and after the interaction in two different ratios (liposome:peptide $20:1$ and $2:1$, respectively), was measured. *Salmonella*-like liposomes exhibited a highly negative surface charge ($-73 \pm 6 \text{ mV}$), guaranteeing sufficiently high electrostatic repulsion among the liposomes and avoiding the formation of clusters and/or precipitates (Figure 9D—blue bars). Therefore, the suspension resulted to be highly stable. RiLK1 and RiLK3 peptides exhibited, instead, a positive surface charge ($28 \pm 6 \text{ mV}$ and $30 \pm 8 \text{ mV}$, respectively) and resulted to be stable in solution (Figure 9D—yellow bars). The interaction of *Salmonella*-like liposomes with RiLK1 and RiLK3 peptides in a ratio of $20:1$ (Figure 9D—red bars) and $2:1$ (Figure 9D—green bars) was assessed by the net surface charge variation. More precisely, the interaction of *Salmonella*-mimic liposomes with RiLK1 caused a high change in the net charge measurement for both interaction ratios. Differently, RiLK3 needed a ratio of $2:1$ to

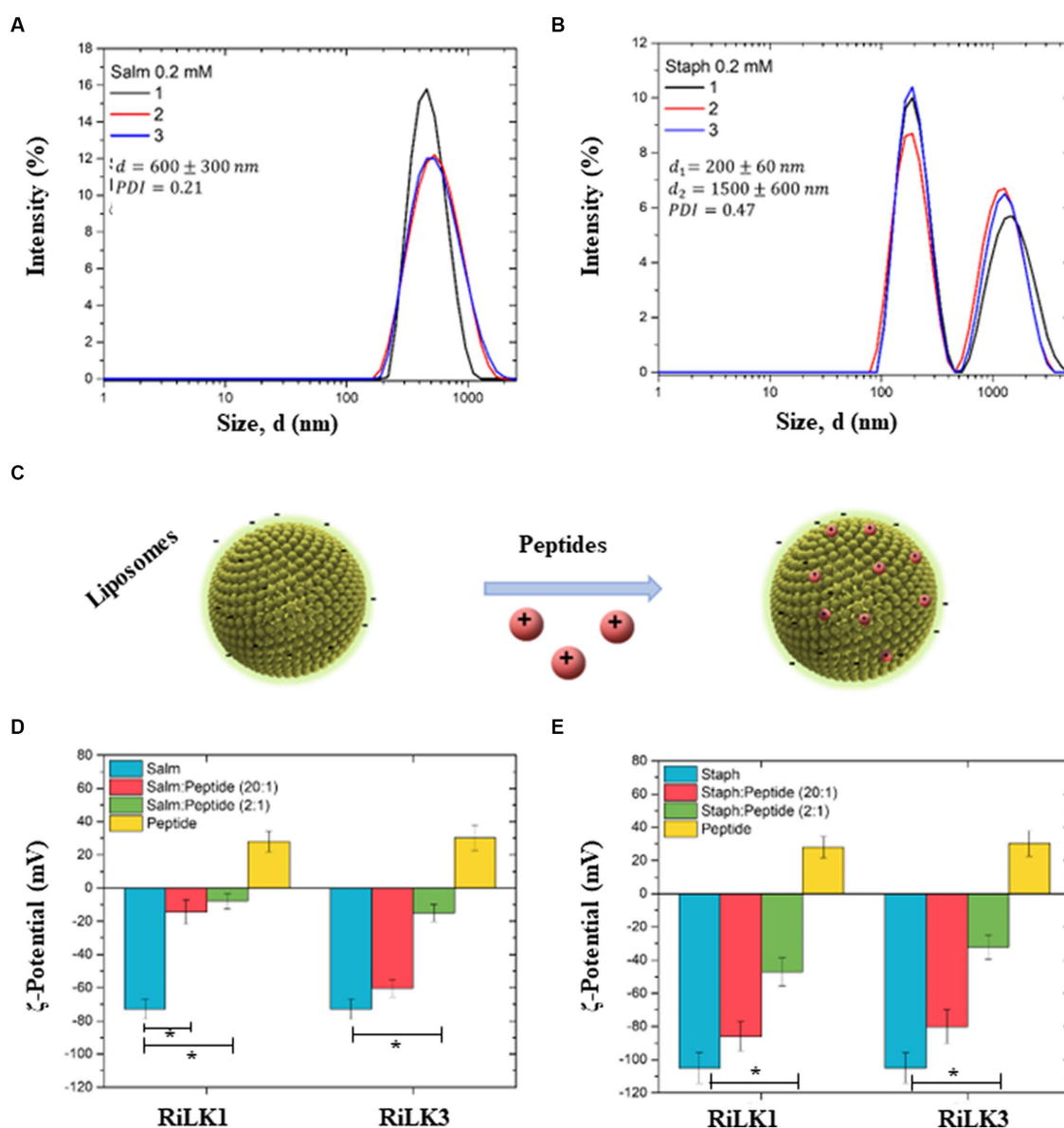


FIGURE 9

Dynamic light scattering and ζ -potential analysis of bacterial membrane liposomes. (A) Hydrodynamic size distribution (d) of *Salmonella*-like liposomes (0.2 mM). The mean d value, and the PDI are reported ($n = 3$). (B) Hydrodynamic size distribution of *Staphylococcus*-like liposomes (0.2 mM). Two main populations, whose mean sizes are denoted as d_1 and d_2 , are identified as well as the PDI is reported ($n = 3$). (C) Schematic representation of the interaction between liposomes (*Salmonella* and *Staphylococcus*) and peptides (RiLK1 and RiLK3). (D) ζ -potential histograms of *Salmonella* liposomes (blue), interacting with RiLK1 and RiLK3 peptides in liposome:peptide ratio of 20:1 (red) and 2:1 (green). ζ -potential of the peptides alone are also reported (yellow). (E) ζ -potential histograms of *Staphylococcus* liposomes (blue), interacting with RiLK1 and RiLK3 peptides in liposome:peptide ratio of 20:1 (red) and 2:1 (green). ζ -potential of the peptides alone are also reported (yellow). *Significant differences ($p < 0.05$) between the bacterial-like liposomes alone (light blue) and the bacterial-like liposomes in the presence of the peptides (red or green).

significantly affect the surface charge of *Salmonella*-like liposomes. This corresponds to a higher peptide concentration needed to be effectively available on the liposome surface.

Analogously, the ζ -potential of *Staphylococcus*-mimic liposomes standing alone and after the interaction with the two peptides in the same ratios chosen for *Salmonella*-mimic liposomes (20:1 and 2:1, respectively), was measured. *Staphylococcus*-like liposomes exhibited a higher negative surface charge (-105 ± 9 mV) than those of *Salmonella*, (Figure 9E—blue bars). Therefore, the suspension resulted to be highly stable. RiLK1 and RiLK3 positive surface charges are

reported in Figure 9E (yellow bars) for comparison. Also, in this case, the interaction of *Staphylococcus*-like liposomes with RiLK1 and RiLK3 peptides in a ratio of 20:1 (Figure 9E—red bars) and 2:1 (Figure 9E—green bars) was assessed by the net surface charge variation. Differently from the results obtained from the interaction of *Salmonella*-mimic liposomes with RiLK1 or RiLK3, a lower change in the net charge measurements was observed for both peptides at a liposome:peptide ratio of 20:1 (Figure 9E—red bars). A higher variation was observed for both peptides at higher peptide concentrations (ratio 2:1), as reported in Figure 9E (green bars).

4. Conclusion

In this study, the already characterised decapeptide RiLK1 was modified through the substitution of the positively charged residue Lysine into Arginine, obtaining the mutant peptide RiLK3. The antimicrobial analysis demonstrated that the derivative RiLK3 displayed lower or in some cases negligible antibacterial, antifungal, or antiviral activity compared to its parent, despite they did not exhibit any evident differences from the structural point of view. Moreover, as the first proof of evidence, experimental analyses with model lipid vesicles highlighted that increasing the composition of arginine versus lysine residue did not improve membrane interaction of RiLK3 mutant towards bacterial-like anionic membranes.

This work demonstrates that *de novo* generation of AMPs is still not a trivial endeavour and the prediction of peptide characteristics needs to be made on a case-by-case. Moreover, the results evidence that just one peptide (RiLK1) is able to be active against three different types of pathogens, thus suggesting diverse modes of action, as reported also for the human cathelicidin LL-37 (Barlow et al., 2011; Wong et al., 2011). Indeed, while antibacterial activity could be deduced by the liposome binding assays, the action against viruses and fungi is much less comprehensible. It is likely that RiLK1 is targeted against highly preserved structures, e.g., the phospholipid membrane or other constitutive components like peptidoglycans in Gram-negative and Gram-positive bacteria, or glucan in the fungal cell wall. Concerning the antiviral activity, some preliminary indications lead us to speculate that the peptide may act directly on the hepatitis virion rather than on the host cell. However, further investigations are in progress to better elucidate the mechanisms of action of RiLK1 as antiviral and antifungal agent.

Data availability statement

The raw data supporting the conclusions of this article will be made available by the authors, without undue reservation.

Author contributions

AP, LG, TV, AM, BM, and BA performed the experiments. YP, GP, and LC: funding acquisition. GP, MG, PD, and LC: data curation, formal analysis, and writing original draft. PE and MB: software,

designed the tables and figures and review. All authors contributed to the article and approved the submitted version.

Funding

This work was supported by the project IZSME 06/20 RC-“Dalle superfici agli alimenti: nuove soluzioni per alimenti più sicuri (NewSan)”.

Acknowledgments

The authors would like to thank project POR FESR CAMPANIA 2014-2020-Dispositivi medici funzionalizzati con peptidi antimicrobici per contrastare le co-infezioni batteriche in pazienti affetti da COVID-19 and project PNRR—PE000000003, PE10—Modelli per un'alimentazione sostenibile, “ON Foods”—Research and Innovation Network on Food and Nutrition Sustainability, Safety and Security—Working ON Foods.

Conflict of interest

BA was employed by Ampure S.R.L. PE is a founder of Laminar Pharmaceuticals. GP is a scientific consultant of Materias S.R.L.

The remaining authors declare that the research was conducted in the absence of any commercial or financial relationships that could be construed as a potential conflict of interest.

Publisher's note

All claims expressed in this article are solely those of the authors and do not necessarily represent those of their affiliated organizations, or those of the publisher, the editors and the reviewers. Any product that may be evaluated in this article, or claim that may be made by its manufacturer, is not guaranteed or endorsed by the publisher.

Supplementary material

The Supplementary material for this article can be found online at: <https://www.frontiersin.org/articles/10.3389/fmicb.2023.1244325/full#supplementary-material>

References

- Agrillo, B., Proroga, Y. T. R., Gogliettino, M., Balestrieri, M., Tatè, R., Nicolais, L., et al. (2020). A safe and multitasking antimicrobial decapeptide: the road from *de novo* design to structural and functional characterization. *Int. J. Mol. Sci.* 21:6952. doi: 10.3390/ijms21186952
- Ambrosio, R. L., Rosselló, C. A., Casares, D., Palmieri, G., Anastasio, A., and Escribá, P. V. (2022). The antimicrobial peptide 1018-K6 interacts distinctly with eukaryotic and bacterial membranes, the basis of its specificity and bactericidal activity. *Int. J. Mol. Sci.* 23:12392. doi: 10.3390/ijms232012392
- Andersson, D. I., Hughes, D., and Kubicek-Sutherland, J. Z. (2016). Mechanisms and consequences of bacterial resistance to antimicrobial peptides. *Drug Resist. Updat.* 26, 43–57. doi: 10.1016/j.drug.2016.04.002
- Barbosa, S. C., Nobre, T. M., Volpati, D., Cilli, E. M., Correa, D. S., and Oliveira, O. N. (2019). The cyclic peptide labaditin does not Alter the outer membrane integrity of *Salmonella enterica* serovar typhimurium. *Sci. Rep.* 9:1993. doi: 10.1038/s41598-019-38551-5
- Barlow, P. G., Svoboda, P., Mackellar, A., Nash, A. A., York, I. A., Pohl, J., et al. (2011). Antiviral activity and increased host defense against influenza infection elicited by the human cathelicidin LL-37. *PLoS One* 6:e25333. doi: 10.1371/journal.pone.0025333
- Benfield, A. H., and Henriques, S. T. (2020). Mode-of-action of antimicrobial peptides: membrane disruption vs. intracellular mechanisms. *Front. Med. Technol.* 2:610997. doi: 10.3389/fmedt.2020.610997
- Casares, D., Escribá, P. V., and Rosselló, C. A. (2019). Membrane lipid composition: effect on membrane and organelle structure, function and compartmentalization and therapeutic avenues. *Int. J. Mol. Sci.* 20:2167. doi: 10.3390/ijms20092167

- Chakraborty, S., Chatterjee, R., and Chakravorty, D. (2022). Evolving and assembling to pierce through: evolutionary and structural aspects of antimicrobial peptides. *Comput. Struct. Biotechnol. J.* 20, 2247–2258. doi: 10.1016/j.csbj.2022.05.002
- Clinical and Laboratory Standards Institute (2015). Methods for dilution of antimicrobial susceptibility tests for bacteria that grow aerobically; approved standard—10th edn. CLSI document M07-A10, Wayne, PA: Clinical and Laboratory Standards Institute.
- Colagiorgi, A., Festa, R., Di Ciccio, P. A., Gogliettino, M., Balestrieri, M., Palmieri, G., et al. (2020). Rapid biofilm eradication of the antimicrobial peptide 1018-K6 against *Staphylococcus aureus*: a new potential tool to fight bacterial biofilms. *Food Control* 107:106815. doi: 10.1016/j.foodcont.2019.106815
- Cutrona, K. J., Kaufman, B. A., Figueroa, D. M., and Elmore, D. E. (2015). Role of arginine and lysine in the antimicrobial mechanism of histone-derived antimicrobial peptides. *FEBS Lett.* 589, 3915–3920. doi: 10.1016/j.febslet.2015.11.002
- Ebenhan, T., Gheysens, O., Kruger, H. G., Zeevaert, J. R., and Sathekge, M. M. (2014). Antimicrobial peptides: their role as infection-selective tracers for molecular imaging. *Biomed. Res. Int.* 2014:867381. doi: 10.1155/2014/867381
- Epand, R. M., and Epand, R. F. (2011). Bacterial membrane lipids in the action of antimicrobial agents. *J. Pept. Sci.* 17, 298–305. doi: 10.1002/psc.1319
- Erdem Büyükkiraz, M., and Kesmen, Z. (2022). Antimicrobial peptides (AMPs): a promising class of antimicrobial compounds. *J. Appl. Microbiol.* 132, 1573–1596. doi: 10.1111/jam.15314
- Escribá, P. V., Busquets, X., Inokuchi, J., Balogh, G., Török, Z., Horváth, I., et al. (2015). Membrane lipid therapy: modulation of the cell membrane composition and structure as a molecular base for drug discovery and new disease treatment. *Prog. Lipid Res.* 59, 38–53. doi: 10.1016/j.plipres.2015.04.003
- Falcigno, L., D'Auria, G., Palmieri, G., Gogliettino, M., Aggrillo, B., Tatè, R., et al. (2021). Key physicochemical determinants in the antimicrobial peptide RiLK1 promote amphipathic structures. *Int. J. Mol. Sci.* 22:10011. doi: 10.3390/ijms221810011
- Festa, R., Ambrosio, R. L., Lamas, A., Gratinio, L., Palmieri, G., Franco, C. M., et al. (2021). A study on the antimicrobial and antibiofilm peptide 1018-k6 as potential alternative to antibiotics against food-pathogen *Salmonella enterica*. *Foods* 10:1372. doi: 10.3390/foods10061372
- Giuliani, A., Pirri, G., Bozzi, A., Di Giulio, A., Aschi, M., and Rinaldi, A. C. (2008). Antimicrobial peptides: natural templates for synthetic membrane-active compounds. *Cell. Mol. Life Sci.* 65, 2450–2460. doi: 10.1007/s00018-008-8188-x
- Hancock, R. E., and Rozek, A. (2002). Role of membranes in the activities of antimicrobial cationic peptides. *FEMS Microbiol. Lett.* 206, 143–149. doi: 10.1111/j.1574-6968.2002.tb11000.x
- Hristova, K., and Wimley, W. C. (2011). A look at arginine in membranes. *J. Membr. Biol.* 239, 49–56. doi: 10.1007/s00232-010-9323-9
- Huan, Y., Kong, Q., Mou, H., and Yi, H. (2020). Antimicrobial peptides: classification, design, application and research progress in multiple fields. *Front. Microbiol.* 11:582779. doi: 10.3389/fmicb.2020.582779
- Huang, H. W., Chen, F.-Y., and Lee, M.-T. (2004). Molecular mechanism of peptide-induced pores in membranes. *Phys. Rev. Lett.* 92:198304. doi: 10.1103/PhysRevLett.92.198304
- Jenssen, H., Hamill, P., and Hancock, R. E. (2006). Peptide antimicrobial agents. *Clin. Microbiol. Rev.* 19, 491–511. doi: 10.1128/CMR.00056-05
- Lohner, K. (2009). New strategies for novel antibiotics: peptides targeting bacterial cell membranes. *Gen. Physiol. Biophys.* 28, 105–116. doi: 10.4149/gpb_2009_02_105
- Lohner, K., and Blondelle, S. E. (2005). Molecular mechanisms of membrane perturbation by antimicrobial peptides and the use of biophysical studies in the design of novel peptide antibiotics. *Comb. Chem. High Throughput Screen.* 8, 241–256. doi: 10.2174/1386207053764576
- Lohner, K., Sevcik, E., and Pabst, G. (2008). Chapter five liposome-based biomembrane mimetic systems: implications for lipid–peptide interactions. *Adv. Planar Lipid Bilayers Liposomes* 6, 103–137. doi: 10.1016/S1554-4516(07)06005-X
- Manger, R. L., Leja, L. S., Lee, S. Y., Hungerford, J. M., and Wekell, M. M. (1993). Tetrazolium-based cell bioassay for neurotoxins active on voltage-sensitive sodium channels: semiautomated assay for saxitoxins, brevetoxins and ciguatoxins. *Anal. Biochem.* 214, 190–194. doi: 10.1006/abio.1993.1476
- Mathur, D., Prakash, S., Anand, P., Kaur, H., Agrawal, P., Mehta, A., et al. (2016). PEPLife: a repository of the half-life of peptides. *Sci. Rep.* 6:36617. doi: 10.1038/srep36617
- Mathur, D., Singh, S., Mehta, A., Agrawal, P., and Raghava, G. P. S. (2018). *In silico* approaches for predicting the half-life of natural and modified peptides in blood. *PLoS One* 13:e0196829. doi: 10.1371/journal.pone.0196829
- Matos, P. M., Franquelim, H. G., Castanho, M. A. R. B., and Santos, N. C. (2010). Quantitative assessment of peptide-lipid interactions. Ubiquitous fluorescence methodologies. *Biochim. Biophys. Acta* 1798, 1999–2012. doi: 10.1016/j.bbame.2010.07.012
- Omardien, S., Brul, S., and Zaat, S. A. (2016). Antimicrobial activity of cationic antimicrobial peptides against Gram-positives: current progress made in understanding the mode of action and the response of bacteria. *Front. Cell Dev. Biol.* 4:111. doi: 10.3389/fcell.2016.00111
- Palmieri, G., Balestrieri, M., Capuano, F., Proroga, Y. T. R., Pomilio, F., Centorame, P., et al. (2018). Bactericidal and antibiofilm activity of batenecin-derivative peptides against the food-pathogen *Listeria monocytogenes*: new perspectives for food processing industry. *Int. J. Food Microbiol.* 279, 33–42. doi: 10.1016/j.jfoodmicro.2018.04.039
- Perez-Iratxeta, C., and Andrade-Navarro, M. A. (2008). K2d2: estimation of protein secondary structure from circular dichroism spectra. *BMC Struct. Biol.* 8, 25–29. doi: 10.1186/1472-6807-8-25
- Peters, B. M., Shirliff, M. E., and Jabra-Rizk, M. A. (2010). Antimicrobial peptides: primeval molecules or future drugs? *PLoS Pathog.* 6:e1001067. doi: 10.1371/journal.ppat.1001067
- Phoenix, D. A., Dennison, S. R., and Harris, F. (2013). Antimicrobial peptides: their history, evolution, and functional promiscuity. *Antimicrob. Pept.* 8, 1–37. doi: 10.1002/9783527652853.CH1
- Pirtskhalava, M., Vishnepolsky, B., and Grigolava, M. (2021). Physicochemical features and peculiarities of interaction of antimicrobial peptides with the membrane. *Pharmaceuticals* 14:471. doi: 10.3390/ph14050471
- Portaccio, M., Gravagnuolo, A. M., Longobardi, S., Giardina, P., Rea, I., De Stefano, L., et al. (2015). ATR FT-IR spectroscopy on Vmh2 hydrophobin self-assembled layers for Teflon membrane bio-functionalization. *Appl. Surf. Sci.* 351, 673–680. doi: 10.1016/j.apsusc.2015.05.182
- Rea, I., Sansone, L., Terracciano, M., De Stefano, L., Dardano, P., Giordano, M., et al. (2014). Photoluminescence of graphene oxide infiltrated into mesoporous silicon. *J. Phys. Chem. C* 118, 27301–27307. doi: 10.1021/jp506539n
- Reed, L. J., and Muench, H. (1938). A simple method of estimating fifty per cent endpoint. *Am. J. Hyg.* 27, 493–497. doi: 10.1093/OXFORDJOURNALS.AJEA.A118408
- Schmidt, N. W., Tai, K. P., Kamdar, K., Mishra, A., Lai, G. H., Zhao, K., et al. (2012). Arginine in α -defensins: differential effects on bactericidal activity correspond to geometry of membrane curvature generation and peptide-lipid phase behaviour. *J. Biol. Chem.* 287, 21866–21872. doi: 10.1074/jbc.M112.358721
- Torres, M. D. T., Pedron, C. N., Araújo, I., Silva, P. I. Jr., Silva, F. D., and Oliveira, V. X. (2017). Decoralin analogs with increased resistance to degradation and lower hemolytic activity. *ChemistrySelect* 2, 18–23. doi: 10.1002/slct.201601590
- Torres, M. D. T., Sothiselvam, S., Lu, T. K., and de la Fuente-Nunez, C. (2019). Peptide design principles for antimicrobial applications. *J. Mol. Biol.* 431, 3547–3567. doi: 10.1016/j.jmb.2018.12.015
- Van Epps, H. L. (2006). Rene dubos: unearthing antibiotics. *J. Exp. Med.* 203:259. doi: 10.1084/jem.2032fta
- Waghu, F. H., Barai, R. S., Gurung, P., and Idicula-Thomas, S. (2016). CAMPR3: a database on sequences, structures and signatures of antimicrobial peptides. *Nucleic Acids Res.* 44, D1094–D1097. doi: 10.1093/nar/gkv1051
- Wang, J., Dou, X., Song, J., Lyu, Y., Zhu, X., Xu, L., et al. (2019). Antimicrobial peptides: promising alternatives in the post feeding antibiotic era. *Med. Res. Rev.* 39, 831–859. doi: 10.1002/med.21542
- Wang, G., Li, X., and Wang, Z. (2016). APD3: the antimicrobial peptide database as a tool for research and education. *Nucleic Acids Res.* 44, D1087–D1093. doi: 10.1093/nar/gkv1278
- Wang, S., Zeng, X., Yang, Q., and Qiao, S. (2016). Antimicrobial peptides as potential alternatives to antibiotics in food animal industry. *Int. J. Mol. Sci.* 17:603. doi: 10.3390/ijms17050603
- Whitmore, L., and Wallace, B. A. (2004). DICHROWEB, an online server for protein secondary structure analyses from circular dichroism spectroscopic data. *Nucleic Acids Res.* 32, W668–W673. doi: 10.1093/nar/gkh371
- Whitmore, L., and Wallace, B. A. (2008). Protein secondary structure analyses from circular dichroism spectroscopy: methods and reference databases. *Biopolymers* 89, 392–400. doi: 10.1002/bip.20853
- Wi, S., Pancoska, P., and Keiderling, T. A. (1998). Predictions of protein secondary structures using factor analysis on Fourier transform infrared spectra: effect of Fourier self-deconvolution of the amide I and amide II bands. *Biospectroscopy* 4, 93–106. doi: 10.1002/(SICI)1520-6343(1998)4:2<93::AID-BSPY2>3.0.CO;2-T
- Wong, J. H., Ng, T. B., Legowska, A., Rolka, K., Hui, M., and Cho, C. H. (2011). Antifungal action of human cathelicidin fragment (LL13–37) on *Candida albicans*. *Peptides* 32, 1996–2002. doi: 10.1016/j.peptides.2011.08.018
- Yazici, A., Ortucu, S., Taskin, M., and Marinelli, L. (2018). Natural-based antibiofilm and antimicrobial peptides from microorganisms. *Curr. Top. Med. Chem.* 18, 2102–2107. doi: 10.2174/1568026618666181112143351
- Yeaman, M. R., and Yount, N. Y. (2003). Mechanisms of antimicrobial peptide action and resistance. *Pharmacol. Rev.* 55, 27–55. doi: 10.1124/pr.55.1.2
- Zaslloff, M. (2002). Antimicrobial peptides of multicellular organisms. *Nature* 415, 389–395. doi: 10.1038/415389a
- Zhao, H., and Kinnunen, P. K. J. (2002). Binding of the antimicrobial peptide temporin L to liposomes assessed by Trp fluorescence. *J. Biol. Chem.* 277, 25170–25177. doi: 10.1074/jbc.M203186200



OPEN ACCESS

EDITED BY

Cesar de la Fuente-Nunez,
University of Pennsylvania, United States

REVIEWED BY

Paramita Sarkar,
Julius Maximilian University of Würzburg,
Germany

Jih-Hang Jiang,
Monash University, Australia

*CORRESPONDENCE

Dejing Shang
✉ djs Shang@lnu.edu.cn

RECEIVED 31 July 2023

ACCEPTED 09 October 2023

PUBLISHED 24 October 2023

CITATION

Ji F, Tian G, Shang D and Jiang F (2023)
Antimicrobial peptide 2K4L disrupts
the membrane of multidrug-resistant
Acinetobacter baumannii and protects mice
against sepsis.
Front. Microbiol. 14:1258469.
doi: 10.3389/fmicb.2023.1258469

COPYRIGHT

© 2023 Ji, Tian, Shang and Jiang. This is an
open-access article distributed under the terms
of the [Creative Commons Attribution License](https://creativecommons.org/licenses/by/4.0/)
(CC BY). The use, distribution or reproduction
in other forums is permitted, provided the
original author(s) and the copyright owner(s)
are credited and that the original publication in
this journal is cited, in accordance with
accepted academic practice. No use,
distribution or reproduction is permitted which
does not comply with these terms.

Antimicrobial peptide 2K4L disrupts the membrane of multidrug-resistant *Acinetobacter baumannii* and protects mice against sepsis

Fangyu Ji¹, Guoxu Tian¹, Dejing Shang^{1,2*} and Fengquan Jiang³

¹School of Life Science, Liaoning Normal University, Dalian, China, ²Liaoning Provincial Key Laboratory of Biotechnology and Drug Discovery, Liaoning Normal University, Dalian, China, ³Department of Clinical Laboratory, The First Affiliated Hospital of Dalian Medical University, Dalian, China

Antimicrobial peptides represent a promising therapeutic alternative for the treatment of antibiotic-resistant bacterial infections. 2K4L is a rationally-designed analog of a short peptide temporin-1CEc, a natural peptide isolated and purified from the skin secretions of the Chinese brown frog *Rana chensinensis* by substituting amino acid residues. 2K4L adopt an α -helical conformation in a membrane-mimetic environment and displayed an improved and broad-spectrum antibacterial activity against sensitive and multidrug-resistant Gram-negative and Gram-positive bacterial strains. Here, the action mechanism of 2K4L on multidrug-resistant *Acinetobacter baumannii* (MRAB) and protection on MRAB-infected mice was investigated. The results demonstrated high bactericidal activity of 2K4L against both a multidrug-resistant *A. baumannii* 0227 strain (MRAB 0227) and a sensitive *A. baumannii* strain (AB 22934), indicating a potential therapeutic advantage of this peptide. Strong positively-charged residues significantly promoted the electrostatic interaction on 2K4L with lipopolysaccharides (LPS) of the bacterial outer membrane. High hydrophobicity and an α -helical conformation endowed 2K4L to remarkably increase the permeability of *A. baumannii* cytoplasmic membrane by depolarization of membrane potential and disruption of membrane integration, as well as leakage of fluorescein from the liposomes. Additionally, 2K4L at low concentrations inhibited biofilm formation and degraded mature 1-day-old MRAB 0227 biofilms by reducing the expression of biofilm-related genes. In an invasive *A. baumannii* infection model, 2K4L enhanced the survival of sepsis mice and decreased the production of the proinflammatory cytokines downregulating the phosphorylation level of signaling protein in MAPK and NF- κ B signaling pathways, indicating that 2K4L represents a novel therapeutic antibiotic candidate against invasive multidrug-resistant bacterial strain infections.

KEYWORDS

antimicrobial peptide, multidrug resistance, *Acinetobacter baumannii*, membrane, biofilm, sepsis, inflammation

1. Introduction

Microbial resistance to antibiotics has proven to be a serious public health problem that urgently needs to be addressed. The emergence and prevalence of multidrug resistant (MDR) pathogenic bacteria poses a serious threat to human health worldwide (Krishnamurthy et al., 2016). Antibiotic-resistant infections kill approximately 5.3 million people each year globally. If effective strategies do not counteract these hospital-acquired infections, an estimated 10 million deaths annually will be caused by the infections by 2050 (Avershina et al., 2021). *Acinetobacter baumannii* is one of the most multidrug-resistant pathogens of the ESKAPE group that causes hospital-acquired infections (*Enterococcus faecium*, *Staphylococcus aureus*, *Klebsiella pneumoniae*, *A. baumannii*, *Pseudomonas aeruginosa*, and *Enterobacter* spp.) (Kumar et al., 2021; Dehbanipour and Ghalavand, 2022). *A. baumannii* can escape the attack of antibiotics and survive in a hospital environment for prolonged time periods because of its remarkable ability to take up genetic material encoding drug resistance from the environment, resulting in the emergence of multidrug resistance (Ayoub Moubareck and Hammoudi Halat, 2020). In addition, biofilms of *A. baumannii* act as a barrier for bacteria to resist external attacks, thus increasing bacterial resistance (Mea et al., 2021). Numerous clinical studies have shown that multidrug resistance of *A. baumannii* to the class antibiotics carbapenems, tigecycline, and colistin is now widespread, and carbapenem-resistant *A. baumannii* is ranked 1st in the list.

A. baumannii infections trigger excessive inflammatory reactions, leading to endotoxic shock, sepsis, and even death (Routsis et al., 2010; Muzahed et al., 2017). Sepsis, is a systemic inflammatory response syndrome (SIRS) caused by infections of pathogenic microorganisms, especially gram-negative bacteria (Carcillo and Fields, 2002; Uhle et al., 2015; Sehgal et al., 2020). Throughout the course of sepsis, the massive release of proinflammatory factors caused by an excessive inflammatory response plays the most important role. Therefore, inhibition of an excessive inflammatory response is particularly important in the treatment of sepsis (Jacobi, 2002). Sepsis requires immediate treatment with intravenous fluids and antibiotics, and broad-spectrum antibiotics are recommended for severe sepsis (Dellinger et al., 2013; Rhee et al., 2020; Im et al., 2022). However, multidrug resistance among various bacterial strains is currently leading to worldwide resistance to a wide range of antibiotics. The overuse and misuse of antibiotics has led to the emergence of extensively multidrug-resistant bacterial strains resulting in increased mortality in patients with bacteremia or sepsis (Magrone et al., 2018; Luna-Reyes et al., 2021). Therefore, the development of new therapeutic antibiotics is urgently needed to combat *A. baumannii* infections and the side effects caused by *A. baumannii*. Among the various antimicrobial options, antimicrobial peptides (AMPs) have been widely regarded as a promising solution to combat MDR bacteria (Moravej et al., 2018). Unlike the bactericidal effects of traditional antibiotics, AMPs interact with bacterial membranes through electrostatic charges or hydrophobic groups and physically disrupt bacterial morphology (Mookherjee et al., 2020). This antimicrobial mechanism of membrane destabilization might be the most promising way to

solve the multi-drug resistance problem because a fundamental changes in membrane composition be a very slow process (Moravej et al., 2018). In addition, it has been reported that AMPs not only have antimicrobial activity but also have antibiofilm, anti-inflammatory, and antitumor activity and could be potential therapeutic candidates for sepsis due to their multiple properties (Kumagai et al., 2020; Nagaoka et al., 2020).

The AMP 2K4L and 2K2L used in this study was designed and synthesized based on the amino acid sequence and structure of temporin-1CEc, a natural peptide from the skin secretion of *Rana chensinensis*, by substituting amino acid residues (Ji et al., 2022). Both peptides with 13 amino residues and amidation of carboxyl terminals adopt an α -helical secondary structure in a membrane-like environment. 2K4L and 2K2L showed broad-spectrum antibacterial activity against the sensitive and multidrug resistant bacteria. While 2K4L with the high hydrophobic value exhibited fourfold higher antibacterial activity than 2K2L although both peptides composed of the same net positive charges (+5). In the present study, the antibacterial activity and action mechanism of 2K4L against clinically isolated multidrug-resistant *A. baumannii* *in vivo* and *in vitro* were investigated. We aimed to elucidate the protective action of 2K4L on *A. baumannii*-induced sepsis mice and provide a potential therapeutic option for antibiotic-resistant pathogens.

2. Materials and methods

2.1. Peptides

The peptides (purity $\geq 95\%$) 2K2L (IIPPLKKFLKKL-NH₂) and 2K4L (IILLLKKFLKKL-NH₂) used in this study were synthesized by GL Biochemistry Inc (Shanghai, China). The results of reversed-phase high performance liquid chromatography (RP-HPLC) and MALDI-TOF mass spectrometry were shown in [Supplementary Figure 1](#). Both 2K2L and 2K4L have net charges of +5, and the mean hydrophobicity is 14.94 and 17.14, respectively. Mean hydrophobicity values (H) for peptides were calculated according to Mant et al. (2009).

2.2. Bacteria

The multidrug-resistant *Acinetobacter baumannii* (MRAB 0227) strain was obtained from The First Affiliated Hospital of Dalian Medical University, and identification and antimicrobial susceptibility testing of the multidrug-resistant bacteria was performed by an automated MicroScan® WalkAway 96 Plus system (Siemens Ltd., Germany). Standard strain *A. baumannii* CICC 22933 (AB 22933) was acquired from the China Centre for Industrial Culture Collection. Bacteria were grown in Luria Bertani (LB) medium at 37°C overnight.

2.3. Animals and ethical statement

SPF C57BL/6 male mice (6–8 weeks, 18–22 g) were purchased from Liaoning Changsheng Biotechnology Co., Ltd., and housed

under standard conditions of light and temperature in the Laboratory Animal Center at Liaoning Normal University. Mice had free access to standard laboratory chow and water. All animal experiments in this study were approved by the Animal Use and Care Committee of Liaoning Normal University (the ethical approval number: LL2023062).

2.4. Minimum inhibitory concentration (MIC) assay

The minimum inhibitory concentration (MIC) of the peptides was determined using a standard microdilution method in 96-well microtiter plates. Briefly, bacterial cells were grown in LB medium at 37°C overnight. Then, 100 µL of diluted bacterial cultures (diluted to 2×10^5 CFU/mL with LB medium) was mixed with 100 µL of serially diluted peptide solutions (concentration ranging from 3.13 to 200 µM) in a 96-well plate and incubated at 37°C for 16–18 h. The absorbance (OD_{600}) of each sample was measured using a microtiter plate reader (Varioskan Flash Microplate Reader, Thermo Scientific Co., Beijing, China). The MIC was defined as the lowest peptide concentration that inhibited bacterial growth by 95%. Three duplicates were performed for each condition.

2.5. Time-kill kinetics assay

The bactericidal kinetics of peptides against *A. baumannii* were determined by time-kill curves. Briefly, log-phase cultures of AB 22933 and MRAB 0227 (1×10^5 CFU/mL) were mixed with 10 µL of peptides at final concentrations of $0.5 \times$ MIC, $2 \times$ MIC and $8 \times$ MIC and incubated with shaking at 37°C for 0–180 min. An incubation in the absence of peptide was used as a control. At 0, 15, 30, 60, 90, 120 and 180 min of incubation, the peptides were removed by centrifugation at 4,000 rpm for 10 min, and the serially diluted bacterial suspension was spread on agar plates and cultured at 37°C overnight. The number of bacterial colonies was calculated by linear regression analysis of a plot of \log_{10} CFU versus time. There was no bacterial colony on the agar plates coated with the original bacterial solution, and the number of bacterial colonies was calculated as 0. Three duplicates were performed for each condition.

2.6. Scanning electron microscopy

The cell morphology of MRAB 0227 was observed by using scanning electron microscopy (SEM). Mid-log phase bacterial cultures (1×10^5 CFU/mL) were treated with $1 \times$ MIC and $2 \times$ MIC of peptides at 37°C for 1 h. After washing 3 times with distilled water, bacterial cells were fixed with 2.5% glutaraldehyde (pH 7.2–7.4) for 2 h and then dehydrated by using a stepwise gradient of ethanol. The bacterial samples were smeared and spread on a glass slide, dried at room temperature and coated with approximately 5 ng of gold/palladium. The images were observed with a scanning electron microscopy (Hitachi SU8010, Hitachi, Japan).

2.7. Atomic force microscopy

The cell morphology of MRAB 0227 was further observed by using atomic force microscopy (AFM). Briefly, mid-log phase bacterial cultures (1×10^5 CFU/mL) were treated with $0.5 \times$ MIC and $2 \times$ MIC of peptides at 37°C for 1 h. After washing 3 times with distilled water, bacterial cells were fixed with 2.5% glutaraldehyde (pH 7.2–7.4) for 2 h. Subsequently, 20 µL bacterial suspension was incubated on the mica for 30 min at room temperature. The alterations in the bacterial cell surface were imaged by MFP-3D Origin™ Atomic Force Microscope (Oxford Instruments, USA) in the contact operation mode with a spring constant of 0.08 N/m. Images of the topography and 3D-image were acquired simultaneously. The roughness values were measured over the entire bacterial cell surface on 200 nm \times 200 nm areas. The average surface root-mean-square (RMS) roughness was calculated from ten fields of three cells estimated during two independent experiments. The data were analyzed with Asylum Research AFM (Santa Barbara, CA, USA).

2.8. Bactericidal activity assay

The bactericidal activity of peptides was examined using a LIVE/DEAD BacLight™ Bacterial Viability kit L7012 (Molecular Probes Inc., Eugene, OR, USA) according to the manufacturers' instructions by using confocal laser scanning microscopy (LSM-710, Carl Zeiss Microimaging, Germany). Briefly, mid-log phase AB 22933 and MRAB 0227 (1×10^5 CFU/mL) were treated with peptides at a final concentration of $0.5 \times$ MIC and $2 \times$ MIC at 37°C for 1 h. Polymyxin B (PMB) was used as a positive control. After washing three times with PBS, the bacterial cells were stained with the fluorescent dyes SYTO-9 and propidium iodide (PI) for 30 min at 4°C in the dark according to the kit instructions. The cells were washed three times with PBS, coated on a glass slide and fixed. The images were observed by confocal laser scanning microscopy, and SYTO-9 (green) and PI (red) fluorescence intensities were measured at wavelengths of 485 nm/530 nm and 485 nm/630 nm (excitation/emission), respectively. The bacterial live percentage was calculated by dividing the green fluorescence intensity by the red fluorescence intensity.

2.9. Fluorescein release assay

Large unilamellar vesicles (LUVs) composed of POPE/POPG/cholesterol were obtained to mimic the cell membranes of gram-negative bacteria as previously described (Konate et al., 2020). Briefly, POPE, POPG and cholesterol were dissolved in chloroform according to mass ratios of 1.85:0.15:1, 1:1:1 and 0.15:1.85:1, respectively, mixed and sonicated in an ultrasonic washer and then dried via vacuum evaporation to obtain a thin film on the wall of a round-bottomed flask. After the lipid film was hydrated with 5 mM TES buffer (pH 7.4), a calcein solution (dissolved in 50 mM TES, 100 mM NaCl, pH 7.4) was added to the sample. The calcein-loaded LUVs were prepared by ultrasonication over ten freeze-thaw cycles in liquid nitrogen until homogeneous and then extruded through 0.22-µm polycarbonate

membranes. Free calcein was removed by gel filtration through a Sephadex G-50 column and eluted using TES buffer, and the LUVs encapsulating calcein were eluted with the void volume. Different concentrations of peptides (final concentration of 3.13–100 μM) were added to the calcein-loaded LUVs and incubated at 25°C for 30 min in the dark. PMB and piperacillin were used as positive and negative controls, respectively. The calcein fluorescence intensity was recorded at excitation/emission wavelengths of 480 nm/530 nm, and the calcein release rate was calculated by the following formula: calcein release rate (%) = $100 \times (F - F_0) / (F_t - F_0)$, where F and F_t are the fluorescence intensity measured after adding peptides or Triton X-100, respectively, and F_0 is the fluorescence intensity of PBS.

The preparation of CF and FITC-dextran type dye-loaded LUVs was identical to that of calcein-loaded LUVs. A mass ratio of POPE, POPG and cardiolipin was 18:4:3, which mimic the cell membranes of *A. baumannii* (Jiang et al., 2020). Three duplicates were performed for each condition.

2.10. Inner membrane depolarization

Bacterial membrane depolarization was measured using the membrane potential-sensitive fluorescent dye DiSC3-5 (Sigma Aldrich, Shanghai, China). Mid-log phase bacterial cultures were collected by centrifugation at 4,000 rpm for 10 min washed twice with 5 mM HEPES (pH 7.2), and resuspended in HEPES to 1×10^5 CFU/mL. After the addition of 0.5 μM EDTA, the bacterial suspension was incubated with DiSC3-5 at a final concentration of 4 μM in a black NBS microplate until DiSC3-5 dye was taken up at a maximum amount by bacterial cells. Peptides at final concentrations of 1, 2 and 4 \times MIC were added to the bacterial samples. Triton X-100 (0.1%) was used as a positive control. DiSC3-5 fluorescence was monitored at an excitation wavelength of 622 nm and an emission wavelength of 670 nm at intervals of 1 min. Membrane depolarization ability was examined by the dye fluorescence intensity change as recorded on a microtiter plate reader. For each dye concentration, at least three measurements were repeated. Three duplicates were performed for each condition.

2.11. NBD fluorescence measurements

NBD [N-(7-Nitrobenz-2-Oxa-1,3-Diazol-4-yl)-1,2-Dihexadecanoyl, MedChemExpress, USA]-labeled peptides (final concentration of 3.13–100 μM) were added to a black NBS microplate (Sun et al., 2015). LUVs (PE, PG and CL at a mass ratio of 18:4:3) were added to the microplate and the molar ratio of lipid to peptide was 1, 5, 10, 20, 40 and 60. After 65 min, proteinase K (10 $\mu\text{g}/\text{mL}$) was added. The fluorescence intensity was recorded every 5 min before and after the addition of proteinase K at the excitation and emission wavelengths of 470 nm and 530 nm, respectively. Three duplicates were performed for each condition.

2.12. Super-resolution fluorescence microscopy

Bacterial membrane images were observed by super-resolution fluorescence microscopy. Mid-log phase MRAB

0227 (1×10^5 CFU/mL) was treated with the AF488 (Alexa Fluor 488, Invitrogen, Shanghai, China)-labeled peptide at a final concentration of 0.5 \times MIC and 2 \times MIC at 37°C for 1 h. After centrifugation at 4,000 rpm/min for 10 min, the bacterial cells were incubated with 20 μL FMTM 4-64FX dye (fixable analog of FMTM 4-64 membrane stain) at a concentration of 5 $\mu\text{g}/\text{mL}$ on ice for 10 min with regular mixing. The cells were collected by centrifugation, washed with HBSS, and then fixed in 2% paraformaldehyde for 10 min at room temperature. Then, 3D-SIM was performed using a microscope system (DeltaVision OMX version; GE Healthcare, UK).

2.13. Outer membrane permeability

Outer membrane permeability was analyzed by using 1-N-phenylmethylamine (NPN, Solarbio, Beijing, China) dye (Sun et al., 2015). Ninety microliters of mid-log phase bacteria (1×10^5 CFU/mL) was plated in a 96-well plate and mixed with 20 μL of 10 μM NPN solution and 10 μL of peptides at a concentration range from 3.13 to 200 μM . After incubating for 1 h, the fluorescence intensities of the samples were measured with an LB970 fluorescence microplate reader. The excitation and emission wavelengths were 350 nm and 420 nm, respectively. Gentamicin was used as a positive control. The untreated group was used as a negative control. The fluorescent intensity was calculated by the following formula: fluorescent intensity = $F_p - F_0$, where F_p and F_0 are the fluorescence intensity measured after adding peptides or the negative control, respectively. Three duplicates were performed for each condition.

2.14. Zeta potential measurement

The zeta potentials of the bacterial outer membrane were measured on a Zetasizer Nano ZS (Malvern Instruments, UK). Mid-log phase bacteria (1×10^5 CFU/mL) in disposable zeta cells were titrated with the peptides (concentration range from 1.56 to 50 μM). The determination of zeta potential was performed by a total of 5 measurements of 100 runs for all concentrations of the peptides. Three duplicates were performed for each condition.

2.15. LPS neutralization

Neutralization of lipopolysaccharides (LPS) was measured by using a pierceTM chromogenic endotoxin quant kit (Thermo Scientific, USA) according to the manufacturers' instructions. The peptides were mixed with 1 EU/mL LPS working solution in pyrotube depyrogenated test tubes and incubated at 37 °C for 1 h. Then 100 μL of the mixture was added to an equal volume of limulus amoebocyte lysate (LAL) reagent and was incubated at 37°C for 15 min. A total of 100 μL of the chromogenic substrate was added and incubated for 10 min, followed by the addition of 500 μL of azo reagent 1, 2, and 3 in sequence. After mixing, the mixture was added into a non-pyrogenic 96-well tissue culture plate and the yellow color that developed due to cleavage of the substrate was then measured at 545 nm. The neutralization proportional was calculated according to the standard curve, and the light absorption

value of LPS working fluid of 1 EU/mL was set as a negative control. Three duplicates were performed for each condition.

2.16. Disassociation of LPS

FITC- LPS (SigmaAldrich, Shanghai, China) was vortexed in 10 mM SP buffer (pH = 6.8) to a final concentration of 1 mg/mL. FITC- LPS aggregates were treated with peptides and the molar ratio of peptides to LPS was 0, 1, 2, 5, 10, 15 and 20. The fluorescence intensity was monitored with an emission wavelength at 515 nm and an excitation wavelength at 488 nm by using Varioskan Flash Microplate Reader (Thermo Scientific Co., Beijing). The molar ratio of peptides to LPS was 0 as a negative control. The fluorescent intensity was calculated by the following formula: fluorescent intensity = $F_p - F_0$, where F_p and F_0 are the fluorescence intensity measured after adding peptides or the negative control, respectively. Three duplicates were performed for each condition.

Dynamic light-scattering (DLS) was used to measure the particle size distributions of LPS with and without peptides by Malvern Zetasizer Nano 2S90 (Malvern Instruments, UK). LPS solution in SP buffer (1 mg/mL) was heated to 60 °C and cooled to 20 °C repeatedly three times and then placed in 4 °C overnight to form LPS aggregates. The peptides were dissolved in SP buffer at a concentration of 1 mg/mL. Measurements were performed of LPS aggregates, the peptides and LPS with peptides after incubation for 30 min. The standard CONTIN method was used to analyze the data. Three duplicates were performed for each condition.

2.17. Preparation of bacterial protoplasts

Protoplasts were prepared according to previously described procedures (Figuerola et al., 2018). Briefly, mid-log phase bacteria were collected by centrifugation, washed twice with 10 mM phosphate buffer (pH 7.0), and then resuspended in 0.5 M sucrose solution in phosphate buffer at a final concentration of 1×10^7 CFU/mL. Lysozyme (final concentration 80 µg/mL) and 0.5 µM EDTA were added to the bacterial suspension and incubated for 2 h at 37°C in a shaker. The sphere-shaped bacteria observed by an optical microscope showed the successful preparation of protoplasts. The solutions were washed twice with 0.25 M sucrose solution before resuspension in buffer containing 5 mM HEPES, 20 mM glucose and 100 mM KCl, pH 7.0. The MIC value of peptides against bacterial protoplast was determined according to the experimental method of MIC assay. Three duplicates were performed for each condition.

2.18. Biofilm formation assay

Biofilm formation of the MRAB 0227 and AB 22933 strains was examined according to our previous work (Shang et al., 2017). Briefly, 100 µL of mid-log phase bacterial cells (1×10^5 CFU/mL) and 100 µL $1/8 \times$ MIC, $1/4 \times$ MIC, and $1 \times$ MIC peptide were placed into a 96-well polystyrene microtiter plate and incubated at 37°C for 24 h. The suspended bacteria were carefully removed by

centrifugation, and the adherent bacteria with biofilms were fixed with methanol for 15 min. The adherent bacteria with biofilms were resuspended and the viability of biofilm-associated cells was evaluated by CFU counting. Then the bacteria were stained with 0.1% (w/v) crystal violet dye for 5 min, resuspended with PBS and quantified by measurement at 590 nm in a microtiter plate reader (Varioskan Flash Microplate Reader, Thermo Scientific Co., Beijing, China). PMB and piperacillin (PIP) were used as positive and negative controls, respectively. The inhibition percentage of biofilm formation was calculated using the following formula: $(OD_{\text{nontreated}} - OD_{\text{peptide}}) / OD_{\text{nontreated}} \times 100\%$. The lowest concentration of peptide required to inhibit biofilm formation by $\geq 50\%$ was defined as the minimum biofilm inhibitory concentration (MBIC₅₀). Three duplicates were performed for each condition.

2.19. One-day-old biofilm disaggregation assay

Disaggregation of 1-day-old biofilms was determined as described by Shang et al. (2014). The formed 1-day-old biofilms were washed with PBS and then incubated with the peptides at concentrations of $1 \times$ MIC, $2 \times$ MIC, and $4 \times$ MIC for 24 h. The biofilm was then fixed, stained, resuspended and quantified as described above. The minimum biofilm reduction concentration (MBRC₅₀) was defined as the lowest peptide concentration that reduced the biofilm by $\geq 50\%$. Three duplicates were performed for each condition.

2.20. Quantitative real-time PCR

Mid-log phase MRAB 0227 cultures (final concentration of 1×10^5 CFU/mL) were incubated with the peptides at concentrations of $1/4 \times$ MIC, $1/2 \times$ MIC, and $1 \times$ MIC at 37°C for 1 h. After centrifugation and collection, RNA was extracted when the bacterial count reached 10^8 CFU. The bacterial cultures were washed with PBS and digested with 20 µL lysozyme (3 mg/mL) after centrifugation at 10,000 rpm for 5 min. Then, preparation and reverse transcription of total RNA was carried out as described previously (Licht et al., 2005). cDNA was amplified with a HiScript® II Q RT SuperMix for qPCR (+gDNA wiper) kit (Vazyme, Nanjing, China). Real-time quantitative PCR was performed with TB Green® Premix Ex Taq™ II (Tli RNaseH Plus) (TaKaRa, Dalian, China) on an ABI-Prism 7500 Fast sequence detection system (Applied Biosystems). Gene expression levels were calculated according to the comparative cycle threshold (Ct) method after normalization with an internal control 16S rRNA. All primer sequences are shown in Table 1. The sequences were synthesized by Sangon Biotech (Shanghai, China). Three duplicates were performed for each condition.

2.21. Cytotoxicity assay

The cytotoxicity of 2K4L was tested via the CCK-8 assay (Beyotime, Shanghai, China). Briefly, PMA-induced adherent

TABLE 1 Genes and primer sequences.

Gene	Forward	Reverse	Gene ID
<i>bmfR</i>	CTGGTAGGTAATGCAGTTCG	GAGAGACCCAAACCATAACC	66398311
<i>ompA</i>	CTCTTGCTGGCTTAAACGTA	GCAATTTCTGGCTTGATTG	66397663
<i>csuA/B</i>	ATGCGGTAAATACTCAAGCA	TCACAGAAATATTGCCACCT	43164957
<i>csuE</i>	ATGCATGTTCTCTGGACTGATGTTGAC	CGACTTGTACCGTGACCGTATCTTGATAAG	66396671

THP-1 cells (5×10^5 /mL) were incubated with 2K4L (1.56 to 100 μ M) in 96-well plates for 24 h. Under a dark condition, CCK8 solution was added to each well and cultured for 3 h. The optical density (OD) of each well at 450 nm was measured using a microtiter plate reader (Varioskan Flash Microplate Reader, Thermo Scientific Co., Beijing, China). Two duplicates were performed for each condition.

2.22. Mouse infection model

One hundred twenty wild-type male C57BL/6 mice (6–8 weeks old, weighing 18–20 g) were randomly divided into eight groups ($n = 15$ /group): (1) 0.9% NaCl group (blank control); (2) MRAB 0227-infected group (control); (3) MRAB 0227 + dexamethasone (DXM, positive control); (4)–(5): MRAB 0227 + 2K4L (1 and 2 mg/kg weight, respectively); (6) AB 22933-infected group (control); (7) AB 22933 + DXM (positive control); and (8) AB 22933 + 2K4L (2 mg/kg weight). The mouse infection models were established as follows: briefly, mid-log phase of either MRAB 0227 (8×10^6 CFU/mouse) or AB 22933 (1×10^8 CFU/mouse) was injected i.p., into mice. After 24 h of infection, the animals received a daily treatment with 2K4L at different doses or 0.9% NaCl or DXM (2 mg/kg weight) for 7 days. Mouse stimulation reactions, the strength of activity, mental state, and body weight were recorded every day. Successful establishment of the model was marked by gradual development of some symptoms of sepsis in mice (no appetite, slow activity, erect body hair, unresponsive stimulation, sticky eye secretions, sticky stools, etc.). On Days 2 and 7 of peptide administration, the mice were sacrificed, the serum was collected for later analysis of liver functions and proinflammatory factors, and lung and liver tissues were collected for histochemical observation and Western blotting. Additionally, the liver, lung, kidney and blood on days 7 of peptide administration were collected for determination of bacterial density.

2.23. Liver function assay

The activities of alanine transaminase (ALT) and aspartate aminotransferase (AST) in mouse serum were determined to examine the magnitude of hepatic injury by using a VITROS 5600 automatic biochemical immunoassay analyzer (Ortho-Clinical Diagnostics, Inc.).

2.24. Histochemistry observation by H&E

At Days 2 and 7 of drug treatment, mouse livers, lungs and kidneys were collected and rinsed three times with normal

saline and then immediately fixed in 4% formaldehyde before embedding in paraffin. Paraffin sections were sliced and stained with hematoxylin and eosin (H&E). The pathological changes in mouse tissue sections were observed under a microscope and photographed.

2.25. Bacterial colony counting in mouse organs

At Days 7 of peptide treatment, the mouse organs of livers, lungs, and kidneys with the mass of 1 g were collected and homogenized under sterile conditions. Homogenate was serially diluted in sterile saline, and spread on nutrient agar plates. The agar plates were incubated at 37°C overnight, and the bacterial colony in livers, lungs and kidneys (\log_{10} CFU/g organ) of each mouse was counted. A similar method was performed to determine the CFU per mL of blood and the bacterial colony of blood (\log_{10} CFU/mL blood) in each mouse was calculated. Two duplicates were performed for each condition.

2.26. Measurement of proinflammatory cytokines

The serum was collected from mouse blood on Days 2 and 7 of peptide administration to measure the proinflammatory factors TNF- α and IL-6. Proinflammatory cytokines were measured by using enzyme-linked immunosorbent assay (ELISA) kits (Neobioscience Technology, Shanghai, China) according to the manufacturer's instructions. Three duplicates were performed for each condition.

2.27. Western blot

Proteins were extracted from mouse liver tissue using RIPA lysis buffer that was suitably combined with a mixture of protease inhibitors and phosphatase inhibitors. Protein concentrations in the supernatant were quantified by using a BCA Protein Assay Kit (Beyotime, Shanghai, China). Proteins were separated by 10% sodium dodecyl sulfate-polyacrylamide gel electrophoresis (SDS-PAGE) and then wet electrotransferred to polyvinylidene fluoride (PVDF) transfer membranes for 90 min. Then, 5% skim milk in TBST (20 mM Tris pH 7.5, 150 mM NaCl, and 0.1% Tween 20) was used to block the PVDF membranes at room temperature for 2 h. Subsequently, the membranes were incubated with primary antibodies against ERK, JNK, p38, I- κ B and NF- κ B and phosphorylated ERK, JNK, p38, I- κ B and NF- κ B overnight at

4°C. After washing with TBST, the membranes were incubated with horseradish peroxidase-conjugated secondary antibodies (1:5,000) for 2 h at room temperature. Finally, an ECL chemiluminescence substrate (Thermo Scientific, USA) was used to develop the immunoreactivity of the membranes. Protein-antibody complexes were detected using an Azure c500 imaging system (Azure Biosystems, USA) and normalized using GAPDH as an internal control. Two duplicates were performed for each condition.

2.28. Statistical analysis

All experiments were performed in triplicate. The results are generally expressed as the means and standard errors. Statistical analyses were performed by GraphPad Prism 6.0 software. A two-tailed unpaired Student's *t*-test was used to test for statistical significance. Significance is indicated as * for $p < 0.05$ and ** for $p < 0.01$.

3. Results

3.1. Antimicrobial activities of 2K4L against *A. baumannii*

2K4L displayed strong antibacterial activity against *A. baumannii* with MIC values of 6.25 μM for MRAB 0227 and 3.13 μM for AB 22933. 2K2L had lower antibacterial activity than 2K4L, with MIC values of 25 μM for MRAB 0227 and 12.5 μM for AB 22933 (Ji et al., 2022). Compared to 2K2L, 2K4L has the same net positive charges (+5) but a high mean hydrophobic value (14.94 and 17.14, respectively), suggesting that the hydrophobicity of the peptide plays an important role in antibacterial activity against both multidrug-resistant and sensitive *A. baumannii*. The positive control Polymyxin B (PMB) and Gentamycin (GEN) displayed high antibacterial activity against MRAB 0227 and AB 22933. MIC values of PMB were 1.56 μM against MRAB 0227 and AB 22933, and GEN were 3.13 and 1.56 μM against MRAB 0227 and AB 22933, respectively. Piperacillin (PIP), a negative control had no antibacterial activity against MRAB 0227 and AB 22933 (MIC > 100 μM). The killing kinetics of the peptides against *A. baumannii* were shown in Figure 1A. The bactericidal activities of the peptides were time- and concentration dependent. The 2K4L at a concentration of 8 \times MIC completely killed MRAB 0227 within 90 min but completely killed AB 22933 within only 30 min. The 2K2L at a concentration of 8 \times MIC required 90 min and 60 min to completely kill MRAB 0227 and AB 22933.

The bactericidal function of the peptides on MRAB 0227 could be observed by SEM through the morphological changes of bacterial cells treated with the peptide for 1 h (Figure 1B). In the control group, untreated bacterial cells exhibited smooth and bright membrane surfaces. Treatment with 2K4L at concentrations of 1 \times MIC and 2 \times MIC led to rupture and collapse of bacterial cells and leakage of the intracellular contents. 2K2L at concentrations of 1 \times MIC and 2 \times MIC showed similar results to 2K4L.

The morphological changes of MRAB 0227 cells were further observed by using AFM (Figure 1C). The untreated MRAB 0227 cells were smooth surfaced and short rod shaped with a height of

approximate 280 nm. After exposure to the peptides, the bacterial surface was highly granular with irregular grooves, and the bacterial collapse to a height of less than 100 nm, suggesting the release of bacterial intracellular contents. The irregularities were well reflected by the profiles presented in Figures C-1, C-2. The bacterial cells treated with 0.5 \times MIC 2K4L exhibited deep grooves (20 nm deep and about 150 nm in diameter) in the central part of the cell, and the deep grooves were 80 nm as 2K4L concentration increased by 2 \times MIC. While the bacterial cells treated with 2K2L at a concentration of 0.5 \times MIC and 2 \times MIC were observed deep grooves with 20 nm deep and about 100 nm in diameter. The analysis of cell surface roughness also confirmed the above results. The root-mean-square (RMS) roughness values of the control group were estimated as 14.63, and the RMS roughness values increased by 27.04 and 32.31 after the treatment of 0.5 \times MIC and 2 \times MIC of 2K4L, respectively. These results indicated that 2K4L and 2K2L damaged the integrity of MRAB 0227 cells, cause leakage of the intracellular contents, leading to a bacterial death. 2K4L showed stronger antibacterial activity than 2K2L against *A. baumannii* in a concentration-dependent manner ($p < 0.01$).

3.2. Membrane-activity mechanism of 2K4L against *A. baumannii*

3.2.1. 2K4L damages membrane integrity and leads to the forming of membrane pore in *A. baumannii*

First, cell membrane damage to *A. baumannii* was observed by confocal laser scanning microscopy using a Live/Dead BacLight™ kit. SYTO-9 dye can penetrate intact cell membranes to show green fluorescence, and PI shows red fluorescence after entering bacterial cells through damaged cell membranes. Figure 2A illustrated an image of 100% green fluorescence (live bacteria) in the untreated MRAB 0227 (Figure 2A1) and AB 22933 (Figure 2A6) groups, while green fluorescence decreased, and red fluorescence occurred after treatment with 2K4L and 2K2L (Figures 2A2–A5, A6–A10). Treatment with 2K4L at concentrations of 0.5 \times MIC and 2 \times MIC decreased the percentages of live MRAB 0227 bacteria by 97.6 and 99.3%, respectively (Figure 2B), and killed AB 22933 cells by 81.9 and 93.0%, respectively (Figure 2C). 2K2L at a concentration of 2 \times MIC decreased the percentages of live MRAB 0227 and AB 22933 bacteria by 96.0 and 92.2%, respectively (Figures 2B, C). The results suggested that 2K4L had a strong ability to disrupt the bacterial membrane system.

The membrane-disrupting activity of 2K4L as a cationic AMP on neutral and negatively charged membranes was investigated in three calcein-encapsulating large unilamellar vesicles (LUVs). The results showed that the peptides could rapidly disrupt the mimic membrane, resulting in leakage calceins in a concentration-dependent manner. As shown in Figures 2D–F, a treatment of 12.5 μM 2K4L caused 65.2, 82.3 and 100% calceins leakage from the LUVs at ratios of POPE/POPG/Chol = 1.85/0.15/1, 1/1/1 and 0.15/1.85/1, respectively, suggesting that 2K4L as a cationic AMP showed a strong ability to damage the negatively charged membrane. Similarly, 12.5 μM 2K2L caused 32.1, 52.2 and 62.3% calceins leakage from the LUVs at ratios of POPE/POPG/Chol = 1.85/0.15/1, 1/1/1 and 0.15/1.85/1,

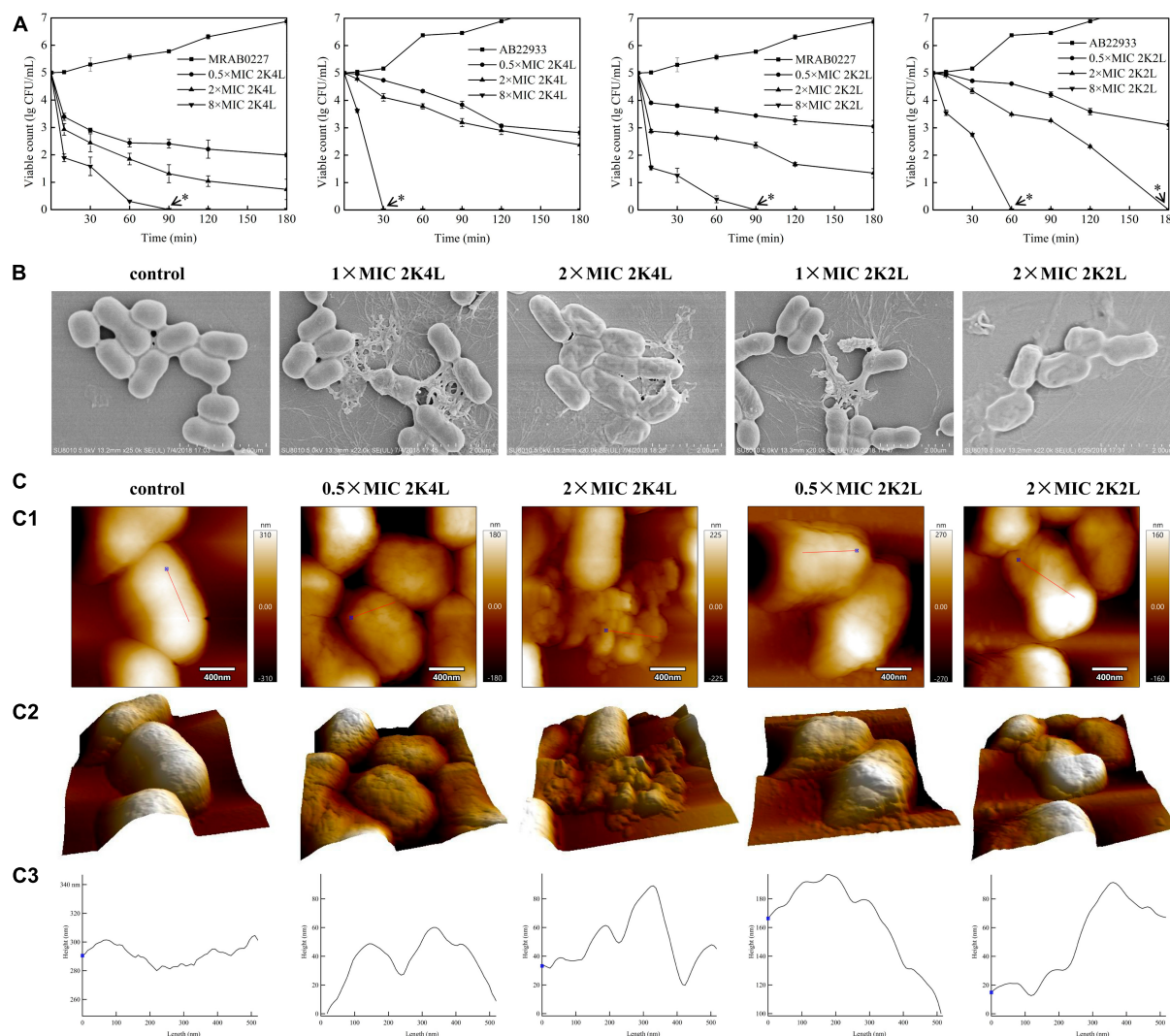


FIGURE 1

Bactericidal activity of the peptides against *A. baumannii*. (A) Killing kinetics of the peptides for the MRAB 0227 and AB 22933 strain. Co-incubation *A. baumannii* (1×10^5 CFU/mL) with the different concentrations of peptides (0.5 \times MIC, 2 \times MIC and 8 \times MIC) for 0–180 min. Aliquots were collected at 0, 15, 30, 60, 90, 120 and 180 min to count the bacteria. The data are presented as the mean \pm SEM ($n = 3$). * in the figure suggested that no bacteria was detected at this concentration and time; (B) scanning electron micrograph of MRAB 0227 cells (B1) and MRAB 0227 (1×10^5 CFU/mL) treated with 1 \times MIC (B2) and 2 \times MIC (B3) of 2K4L, 1 \times MIC (B4) and 2 \times MIC (B5) of 2K2L for 1 h (scale bar = 2 μ m, $n = 3$); (C) atomic force microscope of MRAB 0227 cells (1×10^5 CFU/mL) treated without (control) or in the presence of peptide for 1 h. An analysis of contact mode images was presented. (C-1) topography and (C-2) 3D images; (C-3) section profiles corresponding to red lines in (C-1) (scale bar = 400 nm, $n = 3$).

respectively. The 2K4L induced the release of calceins from LUVs with different compositions better than 2K2L ($P < 0.05$). The results suggested that 2K4L disrupted the LUVs membrane, resulting in leakage of the intracellular content (calceins), and the higher the negatively charged POPG proportion in the liposome membrane was, the greater the calcein release induced by the peptides.

Subsequently, the degree damage of bacterial membrane was determined by measuring the pore sizes of membrane using fluorescent dyes of various molecular weights and sizes in LUVs mimicking the cell membrane of *A. baumannii*. The diameter of the carboxyfluorescein (CF) was less than 1 nm and FITC-dextran 4 (FD 4), FITC-dextran 10 (FD 10) and FITC-dextran 20 (FD 20) was 2.8 nm, 4.6 nm and 6.6 nm, respectively. As shown

in Figure 2G, FD 10 and FD 20 with diameters of 4.6 nm and 6.6 nm almost had not been released after a treatment of 2K4L for 15 min. While 2K4L at a concentration of 50 μ M induced 90 and 80% leakage of CF and FD 4 with diameters of less than 2.8 nm, respectively, and the leakage of CF and FD 4 was more than 95% when 2K4L concentration increased 100 μ M. 2K2L at a concentration of 50 μ M induced 85 and 60% leakage of CF and FD 4, respectively, and 100 μ M 2K2L lead to the leakage of CF and FD 4 was approximately 93 and 80%, respectively (Figure 2H). However, FD 10 and FD 20 almost had not been released after a treatment of 2K4L at a concentration of 100 μ M for 15 min, suggesting that the pore size of LUVs mimicking the cell membranes of *A. baumannii* induced by 2K4L and 2K2L was less than 4.6 nm.

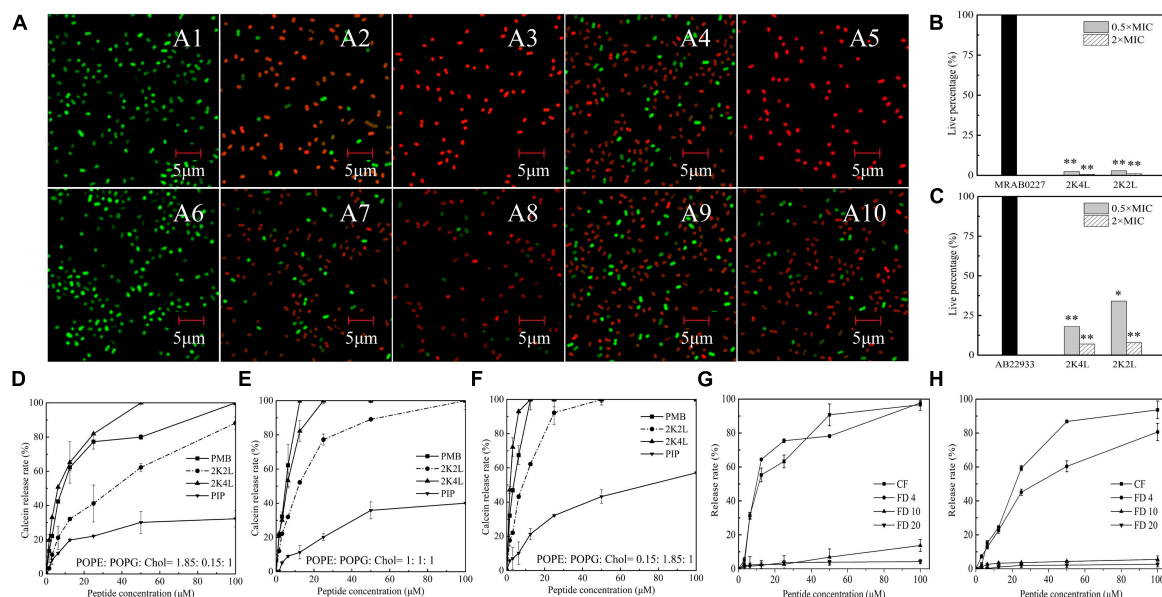


FIGURE 2

The effect of the peptides on bacterial inner membrane integrity and the leakage of fluorescein. (A–C) Laser scanning confocal microscopy images against *A. baumannii*. Mid-log phase AB 22933 and MRAB 0227 (1×10^5 CFU/mL) were treated with peptides at a final concentration of $0.5 \times \text{MIC}$ and $2 \times \text{MIC}$ at 37°C for 1 h. The bacterial cells were washed, fixed, and stained with SYTO-9 (green) and PI (red). (A1) MRAB 0227 cells; (A2,A3) MRAB 0227 cells treated with $0.5 \times \text{MIC}$ and $2 \times \text{MIC}$ of 2K4L; (A4,A5) MRAB 0227 cells treated with $0.5 \times \text{MIC}$ and $2 \times \text{MIC}$ of 2K2L; (A6) AB 22933 cells; (A7,A8) AB 22933 cells treated with $0.5 \times \text{MIC}$ and $2 \times \text{MIC}$ of 2K4L; (A9,A10) AB 22933 cells treated with $0.5 \times \text{MIC}$ and $2 \times \text{MIC}$ of 2K2L (scale bar = $5 \mu\text{m}$, $n = 3$); (B,C) live percentage of MRAB 0227 (B) and AB 22933 (C) cells treated with the peptide for 1 h. * ($P < 0.05$) and ** ($P < 0.01$) indicate statistically significant differences between peptide and the MRAB 0227/AB 22933 group; (D–F) calceins release from LUVs liposomes composed of POPE: POPG: Chol = 1.85: 0.15: 1 (D), POPE: POPG: Chol = 1: 1: 1 (E) and POPE: POPG: Chol = 0.15: 1.85: 1 (F); (G,H) fluorescein release encapsulated in liposomes composed of PE: PG: CL = 18: 4: 3 by peptides [(G) 2K4L; (H) 2K2L].

3.2.2. 2K4L depolarizes the inner membrane and inserts into the membrane of *A. baumannii*

The inner membrane potential of *A. baumannii* was detected by using the membrane potential-sensitive dye DiSC3-5 to understand the depolarization ability of 2K4L on the *A. baumannii* inner membrane. As shown in Figures 3A, B, the fluorescence intensity of DiSC3-5 decreased as the dye concentrated in the cytoplasmic membrane from 0 to 11 min, resulting in a self-quenched fluorescence after the dye was added to the MRAB 0227 (Figure 3A) and AB 22933 (Figure 3B) cells. 2K4L was added to the bacterial samples until DiSC3-5 dye was taken up at a maximum amount at 11 min. 2K4L disrupted the membrane potential and caused cytoplasmic membrane depolarization of *A. baumannii* in a concentration-dependent manner, and complete membrane depolarization induced by the peptide occurred in 7–10 min. 2K4L at a concentration of $4 \times \text{MIC}$ rapidly increased the fluorescence intensity of MRAB 0227 and AB 22933 cells by 68.0 and 68.1%, respectively, compared to the positive control Triton X-100 (defined as 100% cytoplasmic membrane depolarization).

The interaction mode between 2K4L and the membrane was investigated by measuring the fluorescence intensity of NBD-labeled 2K4L in the presence of liposomes. NBD fluorescence of NBD-labeled peptide on membrane surface can be degraded by protease K, leading to decrease of fluorescence intensity (Sun et al., 2015). The peptides could be hydrolyzed by proteases resulting in a decrease of fluorescence intensity. When peptides inserted into the membrane, NBD will not be hydrolyzed by proteinase K, and their fluorescence intensity will be sustained.

As shown in Figure 3C, the fluorescence intensity of NBD-labeled 2K4L at $6.25\text{--}100 \mu\text{M}$ remained essentially unchanged after an addition of proteinase K, suggesting that the peptide was able to insert into the membrane. Figure 3D showed that the fluorescence intensity of NBD-labeled 2K2L at low concentration ($3.13\text{--}12.5 \mu\text{M}$) gradually reduced following the adding of protease K, but the fluorescence intensity was unchanged at $25\text{--}100 \mu\text{M}$ 2K2L. It was indicated that at low concentrations 2K2L remained on the bacterial membrane surface and susceptible to proteolytic attack by proteinase K, and high concentrations of 2K2L could be inserted into the membrane.

The effect of 2K4L on the bacterial membrane was observed by using super-resolution fluorescence microscopy imaging using 3D structured illumination microscopy (3D-SIM). FM4-64 is a membrane-selective red fluorescent dye used to label bacterial cell membranes and AF488 is a green fluorescence dye with amino-reactive activity to be used to label the peptide. Figure 3E showed the images of FM4-64FX-labeled lipid membranes of MRAB 0227 cells incubated with AF488-labeled 2K4L at a concentration of $0.5 \times \text{MIC}$ and $2 \times \text{MIC}$ for 1 h. After treatment with AF488-labeled 2K4L at a concentration of $0.5 \times \text{MIC}$ for 1 h, 2K4L (green fluorescence) was localized uniformly around the MRAB 0227 cell membrane and observed on the membrane surface of the bacterial cells, but the membrane integrity was not damaged. However, when the concentration of 2K4L increased to $2 \times \text{MIC}$, MRAB 0227 cells were observed an incomplete membrane compared to the control group, suggesting that the high concentration of peptide disrupted the membrane integrity of MRAB 0227 cells. 2K2L exhibited similar

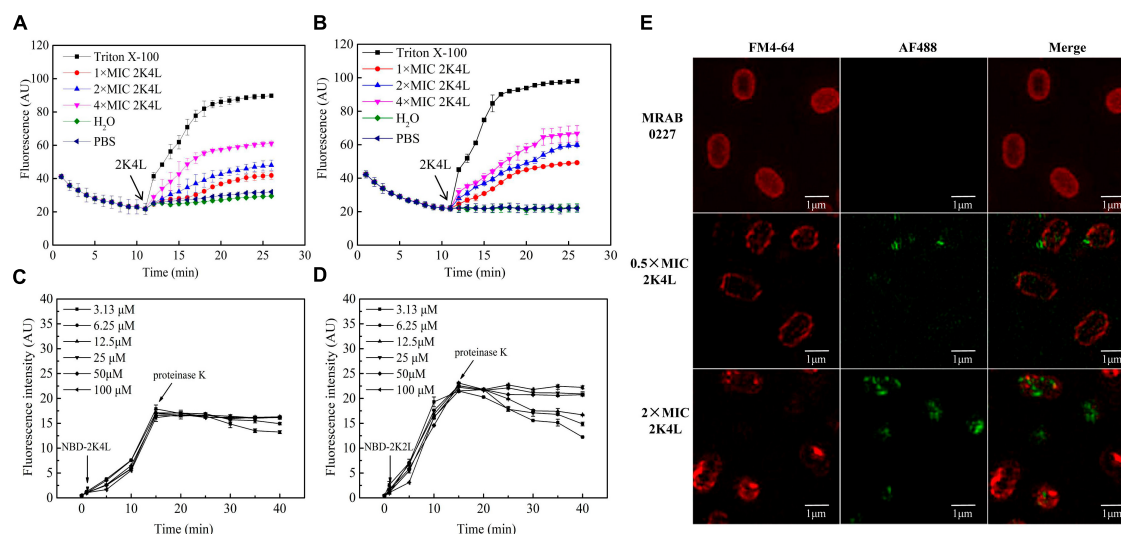


FIGURE 3

The inner membrane permeability of *A. baumannii* and accessibility of 2K4L to *A. baumannii*. (A,B) Depolarization of the inner membrane permeability of MRAB 0227 (A) and AB 22933 strain (B). The bacterial suspension (1×10^5 CFU/mL) was incubated with DiSC3-5 for 11 min, then peptides at final concentrations of 1, 2 and 4 \times MIC were added to the bacterial samples. The data are presented as the mean \pm SEM ($n = 3$); (C,D) protection of NBD-labeled 2K4L (3.13–100 μ M) at various concentrations against proteolytic digestion in the presence of MRAB 0227 (C) and AB 22933 (D). The data are presented as the mean \pm SEM ($n = 3$); (E) super-resolution fluorescence microscopy images of the membrane of MRAB 0227 treated with 2K4L. The MRAB 0227 cell membrane was stained with FM4-64FX (red) and 2K4L with AF488 (green) in all images (scale bar = 1 μ m, $n = 3$).

damaging effects on the membrane structure integrity of MRAB 0227 cells (Supplementary Figure 2).

3.2.3. Effect of 2K4L on the outer membrane of *A. baumannii*

The permeability of the bacterial outer membrane was assessed by using the hydrophobic fluorescent probe 1-N-phenylnaphthylamine (NPN). NPN fluorescence is quenched in aqueous solution, whereas a strong fluorescence intensity is exhibited when NPN is exposed to a hydrophobic environment. Once the bacterial outer membrane is damaged, NPN enters the membrane, resulting in an increase in fluorescence intensity. The 2K4L induced a significant increase in the fluorescence intensity of NPN in MRAB 0227 (Figure 4A) and AB 22933 (Figure 4B) cells in a concentration-dependent manner. Compared with gentamicin (positive control), 12.5 μ M 2K4L increased the fluorescence intensity by 70.7 and 94.4% in MRAB 0227 and AB 22933, respectively, and 12.5 μ M 2K2L caused an increase in the fluorescence intensity by 53.7 and 72.4%, respectively. Both 2K4L and 2K2L were able to permeate into the hydrophobic outer membrane of *A. baumannii*, and 2K4L with high hydrophobicity exhibited a higher permeability ability than 2K2L ($P < 0.05$).

The zeta potential results indicated the interaction of the positively charged 2K4L and the negatively charged outer membrane surface of *A. baumannii*. After titration with 2K4L at concentrations ranging from 1.56 to 50 μ M, the net charges on the outer membrane surface changed from -21.4 to $+7.9$ mV for MRAB 0227 cells (Figure 4C) and from -14.8 to $+12.8$ mV for AB 22933 cells (Figure 4D), indicated that the negative charges on the outer membrane surface of *A. baumannii* cells were neutralized by the positive charges of the peptide. The results suggested that 2K4L

could bind to the surface of *A. baumannii* cells through electrostatic interactions.

LPS is a major component of the outer membrane of Gram-negative bacteria, which serve as barrier for bacteria. Firstly, the interaction of the peptides and LPS was measured through the ability to neutralize LPS using a Pierce's Endotoxin Quantitative Kit. As shown in Figure 4E, the peptides inhibited the LPS-mediated activation of the LAL enzyme. 2K4L inhibited more than 80% of the endotoxin at a concentration of 50 μ M, while 2K2L did at a concentration of 100 μ M. The result suggested that 2K4L and 2K2L could neutralize LPS.

LPS aggregates play a key role in protecting bacteria from invasion exogenous chemicals (Bello et al., 2015). Here, FITC-labeled LPS polymer depolymerization experiment was used to investigate the effect of 2K4L on the structure of LPS aggregates. Monomer-LPS molecules tend to aggregate with each other to form macromolecular aggregates with molecular weight of more than 1,000 kDa, but the fluorescence quenching occurred when FITC-labeled LPS formed soluble aggregates (Bhunia et al., 2009). As shown in Figure 4F, the fluorescence intensity gradually increased after the addition of the peptides. When the molar ratio of 2K4L/LPS increased to 10, the fluorescence intensity remained constant at 2.9 AU. The fluorescence intensity was stable at the molar ratio of 2K2L/LPS = 15. The results suggests that 2K4L and 2K2L can dissociate the aggregated state of LPS oligomers.

As shown in Figure 4G, LPS aggregates into two different sized polymers in its natural state, including a mean diameter of 100 nm (small, 48%) and 6,000 nm (large, 52%), respectively. However, in the presence of 2K4L, large LPS aggregates (a mean diameters of 6,000 nm) was totally disappeared indicating that 2K4L had a strong depolymerization on LPS aggregates. Similarly, 2K2L could disaggregate LPS aggregates.

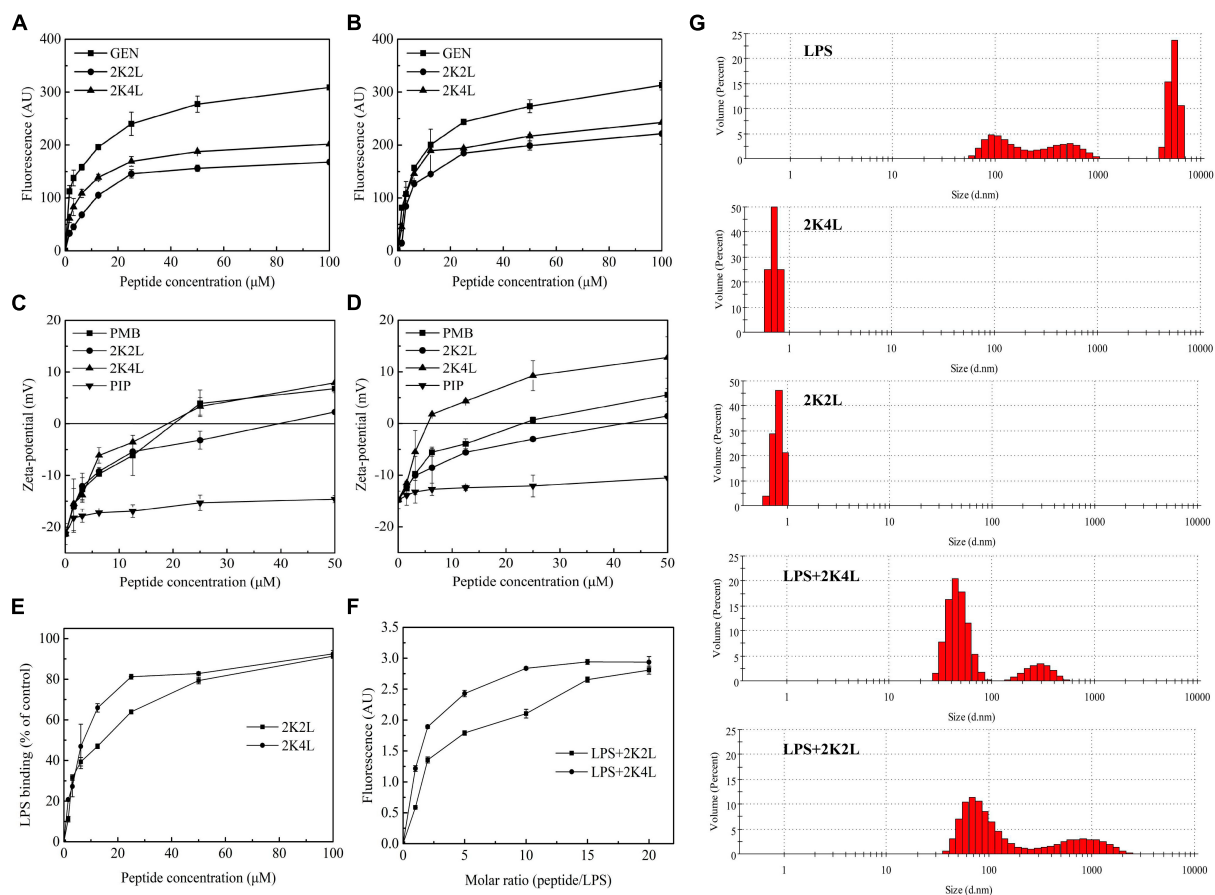


FIGURE 4

The outer membrane permeability of *A. baumannii* and interaction/disaggregation of LPS by the peptides. (A,B) The outer membrane permeability by NPN fluorescence detection of MRAB 0227 (A) and AB 22933 (B) after a treatment of the peptides. The data are presented as the mean \pm SEM ($n = 3$); (C,D) zeta potential changes of MRAB 0227 (C) and AB 22933 (D) treated with the peptides. The data are presented as the mean \pm SEM ($n = 3$); (E) the ability of the peptides to bind LPS using pierceTM chromogenic endotoxin quant kit. The data are presented as the mean \pm SEM ($n = 3$); (F) fluorescence intensity changes of FITC-labeled LPS in the presence of the peptides; (G) size distribution of LPS, the peptides and LPS in the presence of the peptides by measure the particle size using DLS. The data are presented as the mean \pm SEM ($n = 3$).

By testing the antibacterial activity of 2K4L on protoplasts, it was demonstrated that the protection of the outer cell membrane against bacteria was the key to the activity of the antimicrobial peptide. The protoplast of *A. baumannii* was prepared by removing the bacterial cell wall with lysozyme. Compared with intact bacteria, 2K4L showed significantly increased antimicrobial activity against *A. baumannii* protoplasts. The MIC value of 2K4L against MRAB 0227 decreased fourfold from 6.25 to 1.56 μM , while the value against AB 22933 decreased fourfold from 3.13 to 0.78 μM . This result indicated that the outer membrane acted as a barrier to protect bacterial cells and affected the antibacterial activity of 2K4L against *A. baumannii*.

3.3. 2K4L inhibited the biofilm formation of *A. baumannii*

A. baumannii is prone to form biofilms on solid surfaces and cause infection in clinical settings (Sivaranjani et al., 2018). Here, we found that 2K4L exhibited not only membrane disruption activity against *A. baumannii* but also antibiofilm effects. The

peptides inhibited biofilm formation in a concentration-dependent manner. Compared to the control (no peptide treatment), the biofilm formation was inhibited by 2K4L at concentrations of 1/8, 1/4 and 1 \times MIC for 46, 48 and 53% in MRAB 0227 cells (Figure 5A), respectively. While the inhibition rate of 2K4L on the biofilm formation was for 14, 27 and 49% in AB 22933 cells (Figure 5B), respectively. The MBIC₅₀ values of 2K4L on the MRAB 0227 and AB 22933 strains were approximately equal to the respective 1 \times MIC value. The 2K2L and polymyxin B (PMB, a positive control) showed antibiofilm-forming effects similar to the antibiofilm-forming effects of 2K4L, but piperacillin (PIP, a negative control) did not show antibiofilm activity.

It was found that AMPs was less sensitive to the mature biofilms (Otto, 2006). Cationic peptides could be rejected or sequestered by the extracellular polymeric molecules of biofilms, significantly hindering the interaction with bacterial cells (Grassi et al., 2017). The result indicated that the 2K4L also had a disaggregation effect on the biofilm that had been formed for one day. The 2K4L at a concentration of 1 \times MIC reduced the attached biofilm biomass by 29% for MRAB 0227 (Figure 5C) and by only 36%

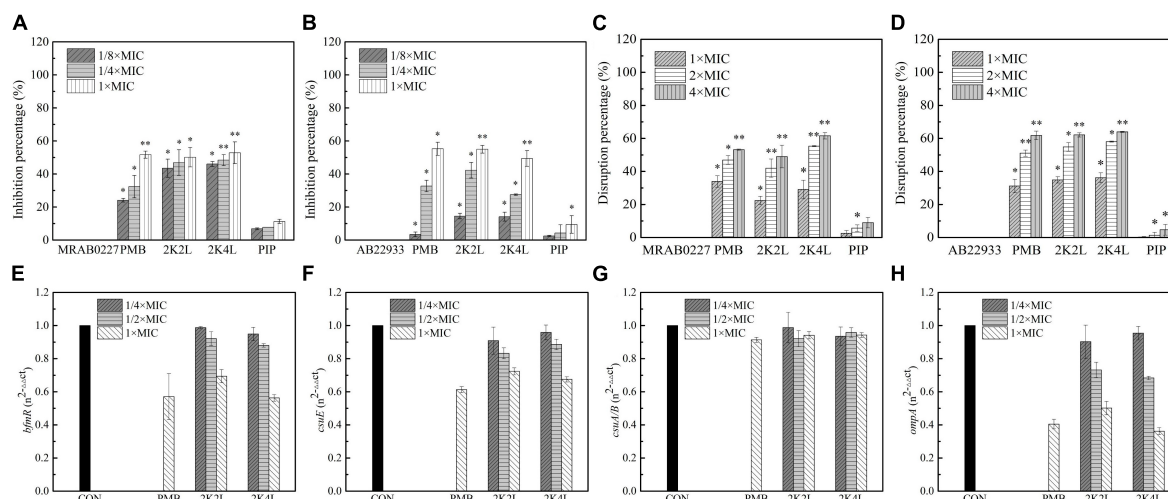


FIGURE 5

Effects of the peptides on *A. baumannii* biofilm. (A,B) Inhibitory percentage of the peptides (1/8 × , 1/4 × and 1 × MIC) on biofilm forming of MRAB 0227 and AB 22933 (1×10^5 CFU/mL); (C,D) disaggregation of 1-day mature biofilm by the peptides (1 × MIC, 2 × MIC, and 4 × MIC); * ($P < 0.05$) and ** ($P < 0.01$) indicate statistically significant differences between peptide and the MRAB 0227/AB 22933 group; (E–H) expression of biofilm associated genes *bmfR* (E), *csuE* (F), *csuA/B* (G) and *ompA* (H) of MRAB 0227 by RT-qPCR. The data are presented as the mean ± SEM ($n = 3$).

for AB 22933 (Figure 5D). The 2K2L at a concentration of 1 × MIC reduced the attached biofilm biomass by 22% for MRAB 0227 and by 35% for AB 22933. The results indicated that the peptides at a low concentration exhibited a low disaggregation effect on the 1-day mature biofilms of *A. baumannii*. As the peptide concentration increased to two to fourfold of the MIC, the attached 1-day mature biofilm biomass significantly decreased, but the survival rates of bacteria were found to be significantly decreased (Supplementary Figure 3), suggesting that 2K4L and 2K2L at a concentration greater than 2 × MIC might reduce the biomass of an attached 1-day mature biofilm by killing bacteria within it. The MBRC₅₀ values of 2K4L and 2K2L on MRAB 0227 biofilm were approximately twofold and fourfold of the MIC and approximately twofold of the MIC for 2K2L and 2K4L on AB 22933.

Biofilm formation of *A. baumannii* is affected by many factors (Sivaranjani et al., 2018). Among these factors, there are some genes related to the adhesion and formation of biofilms on abiotic and biotic surfaces. Here, the *bmfR*, *ompA*, *csuA/B*, and *csuE* genes associated with the formation of biofilms were investigated to understand the effects of 2K4L on biofilm formation of MRAB 0227 by quantitative RT-qPCR. The results showed that 2K4L and 2K2L at a sub-MIC concentration (1/4 × MIC and 1/2 × MIC) could not decrease the expression of the genes *bmfR* (Figure 5E) and *csuE* (Figure 5F), and the gene expression was slightly decreased after treatment with 1 × MIC of peptide. The 2K4L showed no effect on the expression of the *csuA/B* gene (Figure 5G) but significantly decreased the expression of the *ompA* gene (Figure 5H). *OmpA* protein is one of the major outer membrane proteins of gram-negative bacteria related to maintaining the structural integrity and stability of the outer membrane and plays an important role in bacterial adherence and biofilm formation. The 2K4L reduced RNA levels of *bmfR*, *csuE*, and *OmpA*, which is likely to reduce the formation of biofilms.

3.4. Protective action of 2K4L on sepsis mice infected with *A. baumannii*

2K4L had strong antibacterial activity against bacteria, but low toxicity in THP-1 cells. As shown in Supplementary Figure 4A, the survival rate of THP-1 cells gradually decreased with increasing concentration after co-incubation of 2K4L for 24 h. The concentration of 2K4L was less than 6.25 μM with a survival rate of more than 60%. As shown in Supplementary Figure 4B, the survival rate of 2K4L in mice (from 1 to 10 mg/kg body weight) was 100%. It was suggested that 2K4L exhibited non-toxic *in vivo*. To investigate the protective effects of 2K4L, mice were infected with *A. baumannii* and treated with the peptide after infection. After 2 days of injection of MRAB 0227 at a dose of 8×10^6 CFU/mouse, the survival rate was only 33% of the 0.9% NaCl group (Figure 6A). The administration of 1 mg/kg and 2 mg/kg 2K4L increased the mouse survival rate to 53 and 60% of the 0.9% NaCl group, respectively. At 2 and 7 days after the administration of 2 mg/kg 2K4L, the mouse body weight significantly increased compared to the body weight of the MRAB 0227 infected mice (Figure 6B) ($p < 0.001$). The positive control DXM group had a 67% increased survival rate compared with the infected group. The infectious mouse model was also successfully established by injecting the sensitive *A. baumannii* AB 22933 strain. Treatment with 2 mg/kg 2K4L increased the mouse survival rate from 27% of the infected group to 60% (Supplementary Figure 3A). The body weight changes within 7 days of the administration of 2 mg/kg 2K4L were similar to the body weight changes of the MRAB 0227-infected group (Supplementary Figure 5B).

The liver function data showed that the ALT and AST levels of the MRAB 0227-infected model mice were significantly increased, and both were more than sixfold the levels of the control group, while the administration of 2K4L significantly decreased ALT and AST levels in a concentration-dependent manner (Figures 6C, D). At 7 days of administration of 2 mg/kg 2K4L, ALT and AST

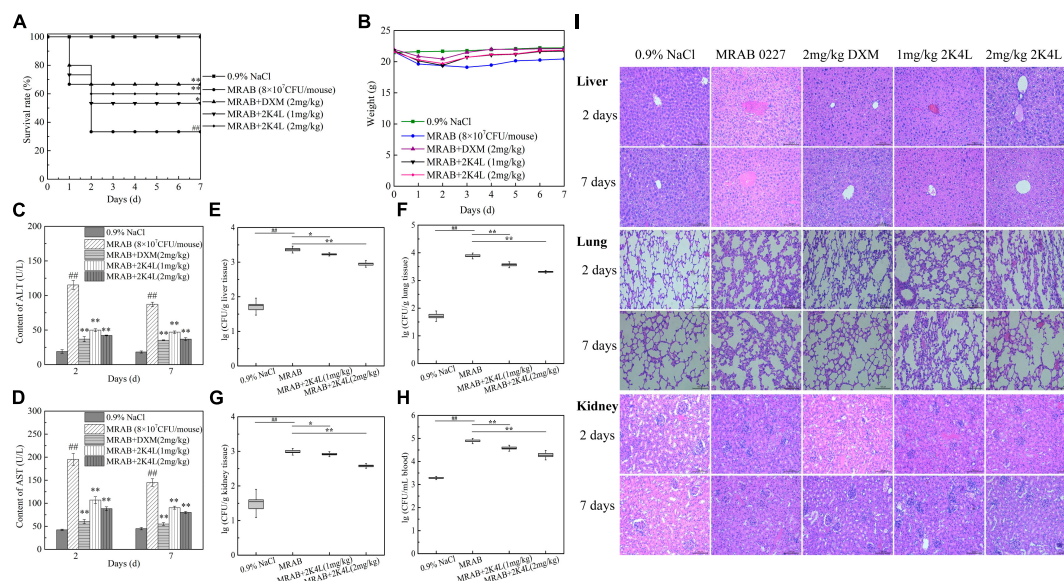


FIGURE 6

Protection of 2K4L against sepsis mice caused by the MRAB 0227 infection. A total of 6–8 weeks male C57BL/6 mice were injected with MRAB 0227 (8×10^6 CFU/mouse) or AB 22933 (1×10^8 CFU/mouse) and treated with 2K4L (1 and 2 mg/kg weight) or 0.9% NaCl or DXM (2 mg/kg weight) for 7 days ($n = 15$ /group). On Days 2 and 7 of peptide administration, the serum was collected for liver functions and proinflammatory factors, and lung and liver tissues were collected for histochemical observation and Western blotting. The data are presented as the mean \pm SEM ($n = 3$). (A) Survival rate of mice; (B) body weight of mice; (C,D) liver function (ALT; AST) analysis; (E–H) bacterial density in infected mouse organs. At Day 7 of peptide treatment, the liver (F), lung (G), kidney (H) and blood (I) of each mouse were collected and the bacterial density determined ($n = 3$). ## $P < 0.01$ indicates statistically significant differences between the MRAB 0227 group and 0.9% NaCl. * $P < 0.05$ and ** $P < 0.01$ indicate statistically significant differences between peptide and the MRAB 0227 group; (I) pathological observation of liver, lung and kidney by H&E staining (scale bar = 200 μ m, $n = 3$).

levels decreased by 57.6 and 44.6% compared to the MRAB 0227-infected model mice, respectively. In AB 22933-infected model mice, 2 mg/kg 2K4L decreased ALT and AST levels by 57.8 and 47.2%, respectively (Supplementary Figures 5C, D).

The antibacterial efficacy *in vivo* was examined in sepsis mice induced by *A. baumannii*. As shown in Figures 6E–H, MRAB 0227 infection significantly increased the bacterial density in the mouse organs compared with 0.9% NaCl group. On 7 days, the treatment of 2 mg/kg 2K4L significantly reduced the MRAB 0227 density in the liver (Figure 6E), lung (Figure 6F), kidney (Figure 6G) and blood (Figure 6H) by 61.4, 73.3, 61.1, and 75.3%, respectively. At 7 days of administration of 2 mg/kg 2K4L, the AB 22933 density in the liver (Supplementary Figure 5E), lung (Supplementary Figure 5F), kidney (Supplementary Figure 5G) and blood (Supplementary Figure 5H) by 88.7, 76.7, 61.1 and 56.1%, respectively.

The mouse liver, lung and kidney were collected and examined by histopathology. As shown in Figure 6I, the liver tissues were severely damaged, manifested as swollen, necrotic and irregular distribution of liver cells in MRAB 0227-infected model mice. The lung tissues showed alveolar defects or swelling, as alveolar septa were significantly thickened and inflammatory cells were increased in the alveoli, and some degree of tissue deformation was displayed in MRAB 0227-infected model mice. MRAB 0227 infection damaged mouse kidneys. The glomeruli showed morphological changes, and the capillaries in the glomeruli were dilated. The glomerular sacs shrank in space and even adhered to the glomeruli. At 2 days and 7 days after 2K4L administration, the damaged liver, lung and kidney were significantly improved. These results

indicated that 2K4L could protect mouse organs from damage caused by *A. baumannii*.

The anti-inflammatory effects of 2K4L were investigated in sepsis mice induced by *A. baumannii*. First, the levels of TNF- α and IL-6 in mice were detected. As shown in Figures 7A, B, the levels of TNF- α and IL-6 were significantly increased in MRAB 0227-treated sepsis mice. The treatment of 2 mg/kg 2K4L inhibited the production of TNF- α in mice infected with MRAB 0227 by 45.7 and 75.3% on days 2 and 7, respectively. Consistently, 2K4L 2 mg/kg treatment reduced IL-6 in mice infected with MRAB 0227 by 39.4 and 65.5% on days 2 and 7. In line with the above data, the release of TNF- α and IL-6 was reduced by 2K4L in AB 22933-treated sepsis mice (Figures 7C, D).

The NF- κ B signaling pathway is a classic pathway that regulates inflammation (Lawrence, 2009). As shown in Figures 7E, F, the expression of phosphorylated I κ B (p -I κ B) and NF- κ B p65 (p -p65) significantly increased in MRAB 0227- and AB 22933-induced sepsis mouse livers compared with the control group. After 2 days of 2K4L administration, the expression levels of p -I κ B and p -p65 were downregulated by 29.8 and 28.8%, respectively. And the expression levels of p -I κ B and p -p65 were downregulated by 42.4 and 38.9%, respectively, at 7 days compared to the MRAB 0227-treated sepsis mice. However, the expression levels of non-phosphorylated I κ B and NF- κ B p65 were different in the liver tissue of each administration group (Supplementary Figures 6A, B), suggesting that 2K4L reduced the inflammatory response by downregulating the phosphorylation levels of the signaling proteins I κ B and NF- κ B in *A. baumannii*-treated sepsis mice.

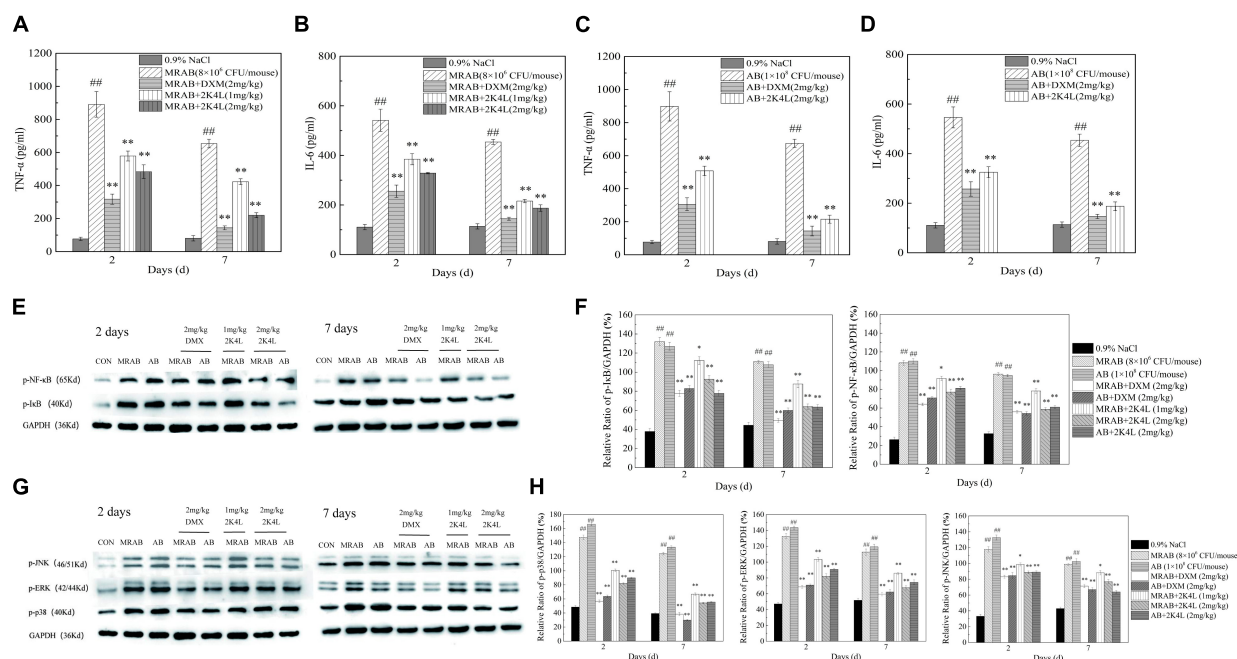


FIGURE 7

2K4L inhibited inflammatory response induced by *A. baumannii* in sepsis mice. (A–D) Effects of 2K4L on the production of TNF-α and IL-6 in the sepsis mice serum induced by MRAB 0227 and AB 22933; (E,F) proteins were extracted from mouse liver tissue at Days 2 and 7 of peptide treatment. Western blotting analysis of the effects of 2K4L on the expression of p-NF-κB and p-IκB; (G,H) western blotting analysis of the effects of 2K4L on the expression of p-JNK, p-ERK and p-p38. ## ($P < 0.01$) indicates statistically significant differences between the MRAB 0227/AB 22933 group and control (0.9% NaCl). * ($P < 0.05$) and ** ($P < 0.01$) indicate statistically significant differences between peptide and the MRAB 0227/AB 22933 group. The data are presented as the mean ± SEM ($n = 3$).

The mitogen activated protein kinase (MAPK) signaling pathway is another of the typical inflammatory response pathway (Leifer and Medvedev, 2016). Here, the phosphorylation of the signaling proteins in MAPK pathway were determined to further understand the anti-inflammatory effects of 2K4L. In addition, the effects of 2K4L on the MAPK signaling pathway were examined. As shown in Figures 7G, H, MRAB 0227 infection significantly increased the phosphorylated levels of p38 (p -p38), ERK (p -ERK) and JNK (p -JNK) in mouse livers. A total of 1 mg/kg 2K4L at 2 days downregulated the expression of p -p38 by 31.9%, p -ERK by 22.1% and p -JNK by 16.2% compared to the group of MRAB 0227-induced shock mice, respectively. While 2K4L at 7 days downregulated the expression of p -p38 by 54.7%, p -ERK by 35.1% and p -JNK by 25.1%, respectively. When the dose of 2K4L increased to 2 mg/kg, the expression levels of p -p38 were downregulated by 63.2%, p -ERK by 48.9% and p -JNK by 34.6% at 7 days of 2K4L treatment. The expression levels of non-phosphorylated p38, ERK and JNK were different in the liver tissue of each administration group (Supplementary Figures 6C, D). The results suggested that 2K4L downregulated the phosphorylation level of MAPK signaling proteins in *A. baumannii*-induced sepsis mice.

4. Discussion

Acinetobacter baumannii is one of the most troublesome pathogens causing various pathogenic infections in the modern healthcare system, since it is able to escape from available

antibiotics resulting in multidrug-resistant strains (Peleg et al., 2008). The increasing antibiotic resistance of *A. baumannii* is related to its multiple drug resistance mechanisms, including enzymatic modification of antibiotic molecules, modification of antibiotic target sites, expression of efflux pumps, and downregulation of cell membrane porin channel expression (Anaya-López et al., 2013). The development and research of antimicrobial agents against multidrug-resistant *A. baumannii* is urgent, while antimicrobial peptides are a potentially effective option. In particular, the killing effect of cationic antimicrobial peptides on bacteria is rapid and efficient, directly acting on the bacterial cell membrane, so resistance is less likely to develop (He et al., 2021). The 2K4L is composed of 4 positively charged lysine residues and amidation of carboxyl terminals, which endows it with broad-spectrum antibacterial activity against gram-negative and gram-positive bacteria (Ji et al., 2022). In the present study, 2K4L, as a cationic peptide, displayed high antibacterial activity against multidrug-resistant *A. baumannii* (MRAB0227 strain) and sensitive *A. baumannii* (AB22394 strain), with MIC values of 6.25 and 3.13 μM, respectively. In addition, high hydrophobicity (17.14) and amphipathic α-helical confirmation in a membrane-mimetic environment enhanced the antibacterial potency of 2K4L against the *A. baumannii* strain. The 2K2L is an analog of 2K4L and is composed of the same net positive charge of 5 but low hydrophobicity (14.94) compared to 2K4L. Consequently, 2K4L showed a fourfold higher antibacterial potency against MRAB 0227 and AB 22394 than 2K2L. The present results further confirmed that hydrophobicity promoted the interaction of cationic AMPs

with the more negatively charged bacterial cell membrane and increased antimicrobial potency (Hong et al., 2021). The 2K4L at high concentrations ($8 \times \text{MIC}$) rapidly killed AB 22933 and MRAB 0227 only within 30 min and 90 min, suggesting that the peptide was clearly bactericidal against *A. baumannii* and similar to other frog skin peptides (das Neves et al., 2019; Sharma et al., 2019; Luo and Song, 2021). Scanning electron microscopy and atomic force microscope images confirmed that 2K4L resulted in bacterial cell rupture and collapse, leading to bacterial death.

AMPs, especially cationic AMPs, are universally accepted to act as completely different action mechanisms from traditional antibiotics (Ciurac et al., 2019; Tornesello et al., 2020; Juhl et al., 2021). According to previous literature, a two-step mechanism of AMPs is adopted: (i) they selectively bind to negatively charged bacterial surfaces by electrostatic interaction, causing the outer membrane permeability to change; and (ii) unstructured linear peptides in solution fold into an amphipathic α -helical conformation in the membrane environment, which is easy to insert into the cytoplasmic membrane, leading to leakage of cell contents because of transmembrane potential changes, finally resulting in cell death (Sinha et al., 2017; Bechinger et al., 2020). Similar to other cationic AMPs, 2K4L exhibited strong electrostatic interactions with the negatively charged outer membranes of *A. baumannii* and increased outer membrane permeability. Five net positive charges of 2K4L have been confirmed to facilitate interaction with MRAB 0227, and AB 22933 cell walls contain negatively charged lipopolysaccharides (zeta potential). The 2K2L with the same net positive charges (+5) showed similar effects on the outer membranes of MRAB 0227 and AB 22933 cells, suggesting that positive charges in AMPs play an important role in interacting with the bacterial outer membrane. While LPS exists as aggregates in the outer membrane of cells, FITC-labeled 2K4L fluorescence and DLS measurement also clearly demonstrated that 2K4L could dissociate the aggregated state of lipopolysaccharides. These results indicated that 2K4L interacted with the lipopolysaccharides head group through electrostatic interaction, which caused 2K4L to insert into the acyl-chain of lipopolysaccharides through hydrophobic interaction leading a significant perturbation of the lipopolysaccharides packing organization.

Although there is no universal agreement regarding the precise mechanism of AMPs to the cytoplasmic membrane, the carpet model is broadly accepted (Fernandez et al., 2012; Bechinger, 2015). In this model, AMP first deposits on the cell membrane surface like a carpet by binding its positive charges to the negatively charged phospholipid head groups and then inserts into the hydrophobic core of the lipid bilayer as the AMP concentration increases, destabilizing the cell membrane and eventually forming holes or pores to kill bacterial cells (Wang et al., 2016; Usmani et al., 2021). Our data showed that 2K4L could rapidly depolarize the cytoplasmic membrane of MRAB 0227 and AB 22933 in a concentration-dependent manner, leading to large-scale permeabilization of the membrane and eventually killing bacterial cells. In this process, the hydrophobicity of AMP is a main influential factor in the interaction with the bacterial cell membrane. NBD- labeled peptides fluorescence experiment suggested that 2K4L could insert into PE/PG/CL LUVs membrane. Due to the fluorescence intensity showing practically no change when proteinase K was added, it indicated that the NBD-terminal of 2K4L totally penetrated into the LUVs membrane within

3.13–100 μM . Value compared with 2K4L, 2K2L with a low hydrophobic which may be related to its limited ability inserted into the membrane at high concentration. Then 2K4L damaged the integrity of the bacterial cell membrane, resulting in the inflow of SYTO-9 and even PI dyes. Similar results were also observed in mimic membranes, and 2K4L led to the formation of a pore between 2.6 nm and 4.6 nm in mimic membranes of MRAB 0227.

Many reports have shown that biofilm formation is one of the major causes of the rapid development of *A. baumannii* resistance to antimicrobials (Irani et al., 2018; Shahed-Al-Mahmud et al., 2021). *A. baumannii* biofilms colonize a variety of surfaces, including healthcare-associated medical devices (Pompilio et al., 2021), hospital furniture (Orsinger-Jacobsen et al., 2013), and even most abiotic surfaces (Gaddy et al., 2009; Paricio et al., 2019), leading to an increase in the long-term survival of *A. baumannii* in the hospital environment and causing medical device-associated infections (Choi et al., 2009). The 2K4L at subinhibitory concentrations ($1/8$ and $1/4 \times \text{MIC}$) inhibited the biofilm formation of multidrug-resistant *A. baumannii* by approximately 50%, suggesting that 2K4L could interfere with the normal formation of biofilms at a concentration not enough to fully inhibit bacterial growth. The antibiofilm activity of 2K4L was also assessed in another stage: in 24 h mature biofilms. However, 2K4L at $1 \times \text{MIC}$ concentrations only reduced the attached biofilm biomass by 30%, and the 24 h mature biofilms significantly reduced when the peptide concentration increased to two to fourfold of the MIC, but bacterial survival rates were found to be significantly decreased. The results suggested that the peptides at a concentration greater than $2 \times \text{MIC}$ might decompose the formed biofilm by killing bacteria since bacterial biofilms are more difficult to eradicate than their planktonic counterparts.

Biofilm formation/maintenance of *A. baumannii* can be influenced by many factors, including nutrient availability (Flannery et al., 2020; Nie et al., 2020), macromolecular secretions (Luo et al., 2015; Moon et al., 2017) and complex regulatory networks, such as the chaperone-usher (Csu) pili system (Kim et al., 2019) and two-component system (*BfmS/BfmR*) (Kim et al., 2019). The production of pili and the formation of biofilms on abiotic surfaces depend on *csuE* gene expression of the *csuA/BABCD* locus regulated by *bfmS* and *bfmR* genes in *A. baumannii*. However, our present study showed that 2K4L slightly decreased the gene expression of *bmfR* and *csuE* and had no effect on the expression of the *csuA/B* gene. Interestingly, 2K4L significantly decreased the expression of the *ompA* gene encoding *OmpA* protein (outer membrane protein A), a macromolecular secretion that plays an important role in *A. baumannii* pathogenesis, such as cell adherence, biofilm formation, antimicrobial resistance, serum resistance, apoptosis and immunomodulation (An et al., 2019; Tiku et al., 2021). *OmpA* from *A. baumannii* is believed to make up a potential virulence factor with multiple important effects in pathogenesis and signal processing (Kwon et al., 2017; Shirazi et al., 2019). The 2K4L has been proven to be able to reduce the expression of some biofilm-related genes, thereby inhibiting the adhesion and formation of biofilms.

Clinical application of AMPs is often limited by severe instability and toxicity *in vivo*. 2K4L was non-toxic to mice. To investigate the protective effects of 2K4L *in vivo*, we examined the function of 2K4L in a sepsis mouse model with *A. baumannii* infection. Indeed, direct evidence has shown that 2K4L significantly

increased the survival rate of infected mice and decreased ALT and AST levels in serum compared to MRAB 0227-infected model mice. Additionally, 2K4L exhibited strong efficacy by reducing bacterial organ density in the mouse sepsis model causing that severe damage of mouse liver, lung and kidney tissues caused by MRAB 0227 infection was improved. It indicated that the low toxicity of 2K4L was *in vivo* and had the protection of sepsis mice by reducing bacterial burden. The present study also demonstrated that 2K4L could reduce the release of TNF- α and IL-6 showing significant anti-inflammatory activity *in vivo*, and downregulate the phosphorylation levels of MAPK and NF- κ B signaling proteins in the proinflammatory pathway activated by *A. baumannii* infection. The results suggested that 2K4L not only exerted antibacterial activity against multidrug-resistant *A. baumannii* and multidrug-sensitive *A. baumannii* *in vitro* but also protected sepsis mice *in vivo*.

In conclusion, 2K4L presented high antibacterial potential against *A. baumannii* *in vivo* and *in vitro*, especially killing a clinically isolated multidrug-resistant strain by targeting the non-receptor-mediated membrane system and biofilm formation. Most importantly, 2K4L showed remarkable protection in *A. baumannii*-infected sepsis mice by downregulating the expression of proinflammatory signaling pathway proteins, leading to a decrease in the production of the proinflammatory factors TNF- α and IL-6. Therefore, 2K4L can be expected to be a potential candidate to fight increasing bacterial resistance and can be developed as a new therapeutic agent for *A. baumannii*-induced sepsis.

Data availability statement

The original contributions presented in this study are included in this article/[Supplementary material](#), further inquiries can be directed to the corresponding author.

Ethics statement

The animal study was approved by the Liaoning Normal University. The study was conducted in accordance with the local legislation and institutional requirements.

References

- An, Z., Huang, X., Zheng, C., and Ding, W. (2019). *Acinetobacter baumannii* outer membrane protein A induces HeLa cell autophagy via MAPK/JNK signaling pathway. *Int. J. Med. Microbiol.* 309, 97–107. doi: 10.1016/j.ijmm.2018.12.004
- Anaya-López, J., López-Meza, J., and Ochoa-Zarzosa, A. (2013). Bacterial resistance to cationic antimicrobial peptides. *Crit. Rev. Microbiol.* 39, 180–195. doi: 10.3109/1040841X.2012.699025
- Avershina, E., Shapovalova, V., and Shipulin, G. (2021). Fighting antibiotic resistance in hospital-acquired infections: Current state and emerging technologies in disease prevention, diagnostics and therapy. *Front. Microbiol.* 12:707330. doi: 10.3389/fmicb.2021.707330
- Ayoub Moubareck, C., and Hammoudi Halat, D. (2020). Insights into *Acinetobacter baumannii*: A review of microbiological, virulence, and resistance traits in a threatening nosocomial pathogen. *Antibiotics* 9:119. doi: 10.3390/antibiotics9030119
- Bechinger, B. (2015). The SMART model: Soft membranes adapt and respond, also transiently, in the presence of antimicrobial peptides. *J. Pept. Sci.* 21, 346–355. doi: 10.1002/psc.2729
- Bechinger, B., Juhl, D., Glattard, E., and Aisenbrey, C. (2020). Revealing the mechanisms of synergistic action of two magainin antimicrobial peptides. *Front. Med. Technol.* 2:615494. doi: 10.3389/fmedt.2020.615494
- Bello, G., Eriksson, J., Terry, A., Edwards, K., Lawrence, M., Barlow, D., et al. (2015). Characterization of the aggregates formed by various bacterial lipopolysaccharides in solution and upon interaction with antimicrobial peptides. *Langmuir* 31, 741–751. doi: 10.1021/la503267k
- Bhunia, A., Mohanram, H., Domadia, P., Torres, J., and Bhattacharjya, S. (2009). Designed beta-boomerang antiendotoxic and antimicrobial peptides: structures and activities in lipopolysaccharide. *J. Biol. Chem.* 284, 21991–22004. doi: 10.1074/jbc.M109.013573

Author contributions

FaJ: Data curation, Formal analysis, Methodology, Writing – original draft, Writing – review and editing. GT: Data curation, Writing – review and editing. DS: Data curation, Funding acquisition, Methodology, Writing – original draft, Writing – review and editing. FeJ: Writing – review and editing.

Funding

The authors declare financial support was received for the research, authorship, and/or publication of this article. This work was supported by grants from the National Natural Science Foundation of China (32070440).

Conflict of interest

The authors declare that the research was conducted in the absence of any commercial or financial relationships that could be construed as a potential conflict of interest.

Publisher's note

All claims expressed in this article are solely those of the authors and do not necessarily represent those of their affiliated organizations, or those of the publisher, the editors and the reviewers. Any product that may be evaluated in this article, or claim that may be made by its manufacturer, is not guaranteed or endorsed by the publisher.

Supplementary material

The Supplementary Material for this article can be found online at: <https://www.frontiersin.org/articles/10.3389/fmicb.2023.1258469/full#supplementary-material>

- Carcillo, J., and Fields, A. (2002). American college of critical care medicine task force committee members. Clinical practice parameters for hemodynamic support of pediatric and neonatal patients in septic shock. *Crit. Care Med.* 30, 1365–1378. doi: 10.1097/00003246-200206000-00040
- Choi, A., Slamti, L., Avci, F., Pier, G., and Maira-Litrán, T. (2009). The pgaABCD locus of *Acinetobacter baumannii* encodes the production of poly-beta-1-6-N-acetylglucosamine, which is critical for biofilm formation. *J. Bacteriol.* 191, 5953–5963. doi: 10.1128/JB.00647-09
- Ciumac, D., Gong, H., Hu, X., and Lu, J. (2019). Membrane targeting cationic antimicrobial peptides. *J. Colloid Interface Sci.* 537, 163–185. doi: 10.1016/j.jcis.2018.10.103
- das Neves, R., Mortari, M., Schwartz, E., Kipnis, A., and Junqueira-Kipnis, A. (2019). Antimicrobial and antibiofilm effects of peptides from venom of social wasp and scorpion on multidrug-resistant *Acinetobacter baumannii*. *Toxins* 11:216. doi: 10.3390/toxins11040216
- Dehbanipour, R., and Ghalavand, Z. (2022). *Acinetobacter baumannii*: Pathogenesis, virulence factors, novel therapeutic options and mechanisms of resistance to antimicrobial agents with emphasis on tigecycline. *J. Clin. Pharm. Ther.* 47, 1875–1884. doi: 10.1111/jcpt.13787
- Dellinger, R., Levy, M., Rhodes, A., Annane, D., Gerlach, H., Opal, S., et al. (2013). Surviving sepsis campaign: international guidelines for management of severe sepsis and septic shock: 2012. *Crit. Care Med.* 41, 580–637. doi: 10.1097/CCM.0b013e31827e83af
- Fernandez, D., Le Brun, A., Whitwell, T., Sani, M., James, M., and Separovic, F. (2012). The antimicrobial peptide aurein 1.2 disrupts model membranes via the carpet mechanism. *Phys. Chem. Chem. Phys.* 14, 15739–15751. doi: 10.1039/c2cp43099a
- Figueroa, D., Wade, H., Montales, K., Elmore, D., and Darling, L. (2018). Production and visualization of bacterial spheroplasts and protoplasts to characterize antimicrobial peptide localization. *J. Vis. Exp.* 138:57904. doi: 10.3791/57904
- Flannery, A., Le Berre, M., Pier, G., O’Gara, J., and Kilcoyne, M. (2020). Glycomics microarrays reveal differential in situ presentation of the biofilm polysaccharide poly-N-acetylglucosamine on *Acinetobacter baumannii* and *Staphylococcus aureus* cell surfaces. *Int. J. Mol. Sci.* 21:2465. doi: 10.3390/ijms21072465
- Gaddy, J., Tomaras, A., and Actis, L. (2009). The *Acinetobacter baumannii* 19606 OmpA protein plays a role in biofilm formation on abiotic surfaces and in the interaction of this pathogen with eukaryotic cells. *Infect. Immun.* 77, 3150–3160. doi: 10.1128/IAI.00096-09
- Grassi, L., Maisetta, G., Maccari, G., Esin, S., and Batoni, G. (2017). Analogs of the frog-skin antimicrobial peptide Temporin 1TB exhibit a wider spectrum of activity and a stronger antibiofilm potential as compared to the parental peptide. *Front. Chem.* 5:24. doi: 10.3389/fchem.2017.00024
- He, S., Stone, T., and Deber, C. (2021). Uncoupling amphipathicity and hydrophobicity: Role of charge clustering in membrane interactions of cationic antimicrobial peptides. *Biochemistry* 60, 2586–2592. doi: 10.1021/acs.biochem.1c00367
- Hong, M., Kim, M., and Park, Y. (2021). Comparative antimicrobial activity of Hp404 peptide and its analogs against *Acinetobacter baumannii*. *Int. J. Mol. Sci.* 22:5540. doi: 10.3390/ijms22115540
- Im, Y., Kang, D., Ko, R., Lee, Y., Lim, S., Park, S., et al. (2022). Time-to-antibiotics and clinical outcomes in patients with sepsis and septic shock: a prospective nationwide multicenter cohort study. *Crit. Care* 26:19. doi: 10.1186/s13054-021-03883-0
- Irani, N., Basarideh, E., Samiee, F., Fateh, A., Shooraj, F., Rahimi, A., et al. (2018). The inhibitory effect of the combination of two new peptides on biofilm formation by *Acinetobacter baumannii*. *Microb. Pathog.* 121, 310–317. doi: 10.1016/j.micpath.2018.05.051
- Jacobi, J. (2002). Pathophysiology of sepsis. *Am. J. Health Syst. Pharm.* 59, S3–S8. doi: 10.1093/ajhp/59.suppl_1.S3
- Ji, F., Zhao, Y., Jiang, F., and Shang, D. (2022). Membrane mechanism of temporin-1CEC, an antimicrobial peptide isolated from the skin secretions of *Rana chensinensis*, and its systemic analogs. *Bioorg. Chem.* 119:105544. doi: 10.1016/j.bioorg.2021.105544
- Jiang, X., Yang, K., Yuan, B., Han, M., Zhu, Y., Roberts, K., et al. (2020). Molecular dynamics simulations informed by membrane lipidomics reveal the structure-interaction relationship of polymyxins with the lipid A-based outer membrane of *Acinetobacter baumannii*. *J. Antimicrob. Chemother.* 75, 3534–3543. doi: 10.1093/jac/dkaa376
- Juhl, D., Glattard, E., Aisenbrey, C., and Bechinger, B. (2021). Antimicrobial peptides: mechanism of action and lipid-mediated synergistic interactions within membranes. *Faraday Discuss.* 232, 419–434. doi: 10.1039/d0fd00041h
- Kim, S., Kim, M., Kim, S., Son, J., Kim, S., Lee, Y., et al. (2019). The sensor kinase BfmS controls production of outer membrane vesicles in *Acinetobacter baumannii*. *BMC Microbiol.* 19:301. doi: 10.1186/s12866-019-1679-0
- Konate, K., Seisel, Q., Vivès, E., Boisguérin, P., and Deshayes, S. (2020). Fluorescent leakage assay to investigate membrane destabilization by cell-penetrating peptide. *J. Vis. Exp.* 166:62028. doi: 10.3791/62028
- Krishnamurthy, M., Moore, R., Rajamani, S., and Panchal, R. (2016). Bacterial genome engineering and synthetic biology: combating pathogens. *BMC Microbiol.* 16:258. doi: 10.1186/s12866-016-0876-3
- Kumagai, Y., Murakami, T., Kuwahara-Arai, Iba, T., Reich, J., and Nagaoka, I. (2020). Antimicrobial peptide LL-37 ameliorates a murine sepsis model via the induction of microvesicle release from neutrophils. *Innate Immun.* 26, 565–579. doi: 10.1177/1753425920936754
- Kumar, S., Anwer, R., and Azzi, A. (2021). Virulence potential and treatment options of multidrug-resistant (MDR) *Acinetobacter baumannii*. *Microorganisms* 9:2104. doi: 10.3390/microorganisms9102104
- Kwon, H., Kim, S., Oh, M., Na, S., Kim, Y., Jeon, Y., et al. (2017). Outer membrane protein A contributes to antimicrobial resistance of *Acinetobacter baumannii* through the OmpA-like domain. *J. Antimicrob. Chemother.* 72, 3012–3015. doi: 10.1093/jac/dkx257
- Lawrence, T. (2009). The nuclear factor NF-kappaB pathway in inflammation. *Cold Spring Harb. Perspect. Biol.* 1:a001651. doi: 10.1101/cshperspect.a001651
- Leifer, C., and Medvedev, A. (2016). Molecular mechanisms of regulation of Toll-like receptor signaling. *J. Leukoc. Biol.* 100, 927–941. doi: 10.1189/jlb.2MR0316-117RR
- Licht, A., Preis, S., and Brantl, S. (2005). Implication of CcpN in the regulation of a novel untranslated RNA (SR1) in *Bacillus subtilis*. *Mol. Microbiol.* 58, 189–206. doi: 10.1111/j.1365-2958.2005.04810.x
- Luna-Reyes, I., Pérez-Hernández, E., Delgado-Coello, B., and Mas-Oliva, J. (2021). Peptides as therapeutic molecules to neutralize gram-negative bacterial lipopolysaccharides in sepsis and septic shock. *Arch. Med. Res.* 52, 798–807. doi: 10.1016/j.arcmed.2021.08.001
- Luo, T., Rickard, A., Srinivasan, U., Kaye, K., and Foxman, B. (2015). Association of blaOXA-23 and bap with the persistence of *Acinetobacter baumannii* within a major healthcare system. *Front. Microbiol.* 6:182. doi: 10.3389/fmicb.2015.00182
- Luo, Y., and Song, Y. (2021). Mechanism of antimicrobial peptides: antimicrobial, anti-inflammatory and antibiofilm activities. *Int. J. Mol. Sci.* 22:11401. doi: 10.3390/ijms22111401
- Magrone, T., Russo, M., and Jirillo, E. (2018). Antimicrobial peptides in human disease: therapeutic approaches. Second of two parts. *Curr. Pharm. Des.* 24, 1148–1156. doi: 10.2174/1381612824666180327155230
- Mant, C., Kovacs, J., Kim, H., Pollock, D., and Hodges, R. (2009). Intrinsic amino acid side-chain hydrophilicity/hydrophobicity coefficients determined by reversed-phase high-performance liquid chromatography of model peptides: comparison with other hydrophilicity/hydrophobicity scales. *Biopolymers* 92, 573–595. doi: 10.1002/bip.21316
- Mea, H., Yong, P., and Wong, E. (2021). An overview of *Acinetobacter baumannii* pathogenesis: Motility, adherence and biofilm formation. *Microbiol. Res.* 247:126722. doi: 10.1016/j.micres.2021.126722
- Mookherjee, N., Anderson, M., Haagsman, H., and Davidson, D. (2020). Antimicrobial host defence peptides: Functions and clinical potential. *Nat. Rev. Drug Discov.* 19, 311–332. doi: 10.1038/s41573-019-0058-8
- Moon, K., Weber, B., and Feldman, M. (2017). Subinhibitory concentrations of trimethoprim and sulfamethoxazole prevent biofilm formation by *Acinetobacter baumannii* through inhibition of Csu Pilus Expression. *Antimicrob. Agents Chemother.* 61:e00778–17. doi: 10.1128/AAC.00778-17
- Moravej, H., Moravej, Z., Yazdanparast, M., Heiat, M., Mirhosseini, A., Moosazadeh Moghaddam, M., et al. (2018). Antimicrobial Peptides: Features, Action, and Their Resistance Mechanisms in Bacteria. *Microb. Drug Resist.* 24, 747–767. doi: 10.1089/mdr.2017.0392
- Muzaheed, Alzahrani, F., and Sattar Shaikh, S. (2017). *Acinetobacter baumannii* infection in transfusion dependent thalassemia patients with sepsis. *Biomed. Res. Int.* 2017:2351037. doi: 10.1155/2017/2351037
- Nagaoka, I., Tamura, H., and Reich, J. (2020). Therapeutic potential of cathelicidin peptide LL-37, an antimicrobial agent, in a murine sepsis model. *Int. J. Mol. Sci.* 21:5973. doi: 10.3390/ijms21175973
- Nie, D., Hu, Y., Chen, Z., Li, M., Hou, Z., Luo, X., et al. (2020). Outer membrane protein A (OmpA) as a potential therapeutic target for *Acinetobacter baumannii* infection. *J. Biomed. Sci.* 27:26. doi: 10.1186/s12929-020-0617-7
- Orsinger-Jacobsen, S., Patel, S., Vellozzi, E., Gialanella, P., Nimrichter, L., Miranda, K., et al. (2013). Use of a stainless steel washer platform to study *Acinetobacter baumannii* adhesion and biofilm formation on abiotic surfaces. *Microbiology* 159, 2594–2604. doi: 10.1099/mic.0.068825-0
- Otto, M. (2006). Bacterial evasion of antimicrobial peptides by biofilm formation. *Curr. Top. Microbiol. Immunol.* 306, 251–258. doi: 10.1007/3-540-29916-5_10
- Paricio, L., Neufeld, B., and Reynolds, M. (2019). Combined influence of nitric oxide and surface roughness in biofilm reduction across bacteria strains. *Biointerphases* 14:021004. doi: 10.1116/1.5089246
- Peleg, A., Seifert, H., and Paterson, D. (2008). *Acinetobacter baumannii*: Emergence of a successful pathogen. *Clin. Microbiol. Rev.* 21, 538–582. doi: 10.1128/CMR.00058-07

- Pompilio, A., Scribano, D., Sarshar, M., Di Bonaventura, G., Palamara, A., and Ambrosi, C. (2021). Gram-negative bacteria holding together in a biofilm: The *Acinetobacter baumannii* way. *Microorganisms* 9:1353. doi: 10.3390/microorganisms9071353
- Rhee, C., Kadri, S., Dekker, J., Danner, R., Chen, H., Fram, D., et al. (2020). Prevalence of antibiotic-resistant pathogens in culture-proven sepsis and outcomes associated with inadequate and broad-spectrum empiric antibiotic use. *JAMA Netw. Open*. 3:e202899. doi: 10.1001/jamanetworkopen.2020.2899
- Routs, C., Pratikaki, M., Platsouka, E., Sotiropoulou, C., Nanas, S., Markaki, V., et al. (2010). Carbapenem-resistant versus carbapenem-susceptible *Acinetobacter baumannii* bacteremia in a Greek intensive care unit: Risk factors, clinical features and outcomes. *Infection* 38, 173–180. doi: 10.1007/s15010-010-0008-1
- Sehgal, M., Ladd, H., and Totapally, B. (2020). Trends in epidemiology and microbiology of severe sepsis and septic shock in children. *Hosp. Pediatr.* 10, 1021–1030. doi: 10.1542/hpeds.2020-0174
- Shahed-Al-Mahmud, M., Roy, R., Sugiokto, F., Islam, M., Lin, M., Lin, L., et al. (2021). Phage ϕ AB6-borne depolymerase Combats *Acinetobacter baumannii* biofilm formation and infection. *Antibiotics* 10:279. doi: 10.3390/antibiotics10030279
- Shang, D., Liang, H., Wei, S., Yan, X., Yang, Q., and Sun, Y. (2014). Effects of antimicrobial peptide L-K6, a temporin-1CEb analog on oral pathogen growth, *Streptococcus mutans* biofilm formation, and anti-inflammatory activity. *Appl. Microbiol. Biotechnol.* 98, 8685–8695. doi: 10.1007/s00253-014-5927-9
- Shang, D., Meng, X., Zhang, D., and Kou, Z. (2017). Antibacterial activity of chensinin-1b, a peptide with a random coil conformation, against multiple-drug-resistant *Pseudomonas aeruginosa*. *Biochem. Pharmacol.* 143, 65–78. doi: 10.1016/j.bcp.2017.07.017
- Sharma, D., Choudhary, M., Vashist, J., Shrivastava, R., and Bisht, G. (2019). Cationic antimicrobial peptide and its poly-N-substituted glycine congener: Antibacterial and antibiofilm potential against *A. baumannii*. *Biochem. Biophys. Res. Commun.* 518, 472–478. doi: 10.1016/j.bbrc.2019.08.062
- Shirazi, A., Shafiei, M., Solgi, H., Aslani, M., Azizi, O., and Badmasti, F. (2019). Different virulence capabilities and *ompA* Expressions in ST2 and ST513 of multidrug-resistant *Acinetobacter baumannii*. *Curr. Microbiol.* 76, 723–731. doi: 10.1007/s00284-019-01686-9
- Sinha, S., Zheng, L., Mu, Y., Ng, W., and Bhattacharjya, S. (2017). Structure and interactions of a host defense antimicrobial peptide thanatin in lipopolysaccharide micelles reveal mechanism of bacterial cell agglutination. *Sci. Rep.* 7:17795. doi: 10.1038/s41598-017-18102-6
- Sivaranjani, M., Srinivasan, R., Aravindraja, C., Karutha Pandian, S., and Veera Ravi, A. (2018). Inhibitory effect of α -mangostin on *Acinetobacter baumannii* biofilms - an *in vitro* study. *Biofouling* 34, 579–593. doi: 10.1080/08927014.2018.1473387
- Sun, Y., Dong, W., Sun, L., Ma, L., and Shang, D. (2015). Insights into the membrane interaction mechanism and antibacterial properties of chensinin-1b. *Biomaterials* 37, 299–311. doi: 10.1016/j.biomaterials.2014.10.041
- Tiku, V., Kofoed, E., Yan, D., Kang, J., Xu, M., Reichelt, M., et al. (2021). Outer membrane vesicles containing *OmpA* induce mitochondrial fragmentation to promote pathogenesis of *Acinetobacter baumannii*. *Sci. Rep.* 11:618. doi: 10.1038/s41598-020-79966-9
- Tornesello, A., Borrelli, A., Buonaguro, L., Buonaguro, F., and Tornesello, M. (2020). Antimicrobial peptides as anticancer agents: Functional properties and biological activities. *Molecules* 25:2850. doi: 10.3390/molecules25122850
- Uhle, F., Lichtenstern, C., Brenner, T., and Weigand, M. (2015). Sepsis und Multiorganversagen - Pathophysiologie der Sepsis [Pathophysiology of sepsis]. *Anesthesiol. Intens. Notfallmed Schmerzther.* 50, 114–122. doi: 10.1055/s-0041-100391
- Usmani, Y., Ahmed, A., Faizi, S., Versiani, M., Shamshad, S., Khan, S., et al. (2021). Antimicrobial and biofilm inhibiting potential of an amide derivative [N-(2', 4'-dinitrophenyl)-3 β -hydroxyurs-12-en-28-carbonamide] of ursolic acid by modulating membrane potential and quorum sensing against colistin resistant *Acinetobacter baumannii*. *Microb. Pathog.* 157:104997. doi: 10.1016/j.micpath.2021.104997
- Wang, C., Zolotar'skaya, O., Nair, S., Ehrhardt, C., Ohman, D., Wynne, K., et al. (2016). Real-Time observation of antimicrobial polycation effects on *Escherichia coli*: Adapting the carpet model for membrane disruption to quaternary copolyoxetanes. *Langmuir* 12, 2975–2984. doi: 10.1021/acs.langmuir.5b04247



OPEN ACCESS

EDITED BY

Octavio Luiz Franco,
Catholic University of Brasilia (UCB), Brazil

REVIEWED BY

Giovanna Batoni,
University of Pisa, Italy
Lucia Lombardi,
Imperial College London, United Kingdom

*CORRESPONDENCE

Robert Bucki
✉ buckirobert@gmail.com

RECEIVED 08 September 2023

ACCEPTED 02 November 2023

PUBLISHED 17 November 2023

CITATION

Skłodowski K, Suprewicz Ł, Chmielewska-Deptuła SJ, Kaliniak S, Okła S, Zakrzewska M, Minarowski Ł, Mróz R, Daniluk T, Savage PB, Fiedoruk K and Bucki R (2023) Ceragenins exhibit bactericidal properties that are independent of the ionic strength in the environment mimicking cystic fibrosis sputum. *Front. Microbiol.* 14:1290952. doi: 10.3389/fmicb.2023.1290952

COPYRIGHT

© 2023 Skłodowski, Suprewicz, Chmielewska-Deptuła, Kaliniak, Okła, Zakrzewska, Minarowski, Mróz, Daniluk, Savage, Fiedoruk and Bucki. This is an open-access article distributed under the terms of the [Creative Commons Attribution License \(CC BY\)](https://creativecommons.org/licenses/by/4.0/). The use, distribution or reproduction in other forums is permitted, provided the original author(s) and the copyright owner(s) are credited and that the original publication in this journal is cited, in accordance with accepted academic practice. No use, distribution or reproduction is permitted which does not comply with these terms.

Ceragenins exhibit bactericidal properties that are independent of the ionic strength in the environment mimicking cystic fibrosis sputum

Karol Skłodowski¹, Łukasz Suprewicz¹,
Sylvia Joanna Chmielewska-Deptuła¹, Szczepan Kaliniak²,
Sławomir Okła^{2,3}, Magdalena Zakrzewska¹, Łukasz Minarowski⁴,
Robert Mróz⁴, Tamara Daniluk¹, Paul B. Savage⁵,
Krzysztof Fiedoruk¹ and Robert Bucki^{1*}

¹Department of Medical Microbiology and Nanobiomedical Engineering, Medical University of Białystok, Białystok, Poland, ²Holy Cross Cancer Center, Kielce, Poland, ³Institute of Health Science, Collegium Medicum, Jan Kochanowski University of Kielce, Kielce, Poland, ⁴2nd Department of Lung Diseases and Tuberculosis, Medical University of Białystok, Białystok, Poland, ⁵Department of Chemistry and Biochemistry, Brigham Young University, Provo, UT, United States

The purpose of the work was to investigate the impact of sodium chloride (NaCl) on the antimicrobial efficacy of ceragenins (CSAs) and antimicrobial peptides (AMPs) against bacterial and fungal pathogens associated with cystic fibrosis (CF) lung infections. CF-associated bacterial (*Pseudomonas aeruginosa*, *Ochrobactrum* spp., and *Staphylococcus aureus*), and fungal pathogens (*Candida albicans*, and *Candida tropicalis*) were used as target organisms for ceragenins (CSA-13 and CSA-131) and AMPs (LL-37 and omiganan). Susceptibility to the tested compounds was assessed using minimal inhibitory concentrations (MICs) and bactericidal concentrations (MBCs), as well as by colony counting assays in CF sputum samples supplemented with various concentrations of NaCl. Our results demonstrated that ceragenins exhibit potent antimicrobial activity in CF sputum regardless of the NaCl concentration when compared to LL-37 and omiganan. Given the broad-spectrum antimicrobial activity of ceragenins in the microenvironments mimicking the airways of CF patients, ceragenins might be promising agents in managing CF disease.

KEYWORDS

ceragenins, antimicrobial peptides, cystic fibrosis, sodium chloride, sputum scope statement

1 Introduction

Cystic fibrosis (CF) is an inherited disorder characterized by the malfunction of the CF transmembrane conductance regulator (CFTR) protein, which plays an essential role in maintaining the balance of salt and water in airway epithelial cells (Saint-Criq and Gray, 2017). Due to the loss or impairment of this function in CF, the passage of chloride and sodium ions across the cell membrane is impaired, producing thick, sticky mucus (Boucher, 2004). Compared to healthy individuals, CF sputum contains about 5% less water, as well as a higher concentration

of several mucins, anionic polyelectrolytes such as DNA, actin, and increased concentrations of proteases, resulting in the presence of very viscous mucus in the airways (Bhat et al., 1996; Lapierre et al., 2017; McKelvey et al., 2020; Akkerman-Nijland et al., 2021). The accumulation of mucus and impaired mucosal clearance create a favorable environment for bacterial and fungal colonization, causing chronic and recurrent infections that significantly affect the quality of life and survival of CF patients (Bhagirath et al., 2016; Turcios, 2020).

Furthermore, *Pseudomonas aeruginosa* and other CF pathogens produce highly antibiotic-tolerant biofilms that significantly impair the treatment of CF patients (Pragman et al., 2016; Simonin et al., 2019). Up to 95% of CF individuals not treated with CFTR potentiators and modulators, struggle with respiratory failure due to chronic bacterial infections accompanied by airway inflammation (Lyczak et al., 2002; Schaupp et al., 2023).

Cationic antimicrobial peptides (AMPs) are components of the innate immune response and serve as the first line of defense against pathogens. Broad-spectrum antimicrobial activity and immunomodulatory properties make AMPs promising candidates for antimicrobial agents (Rossi et al., 2008; Mansour et al., 2014; Lei et al., 2019). For instance, cathelicidin LL-37 is an endogenous AMP released from hCAP-18 protein that is synthesized by a variety of cell types, including mucosal epithelial cells, and immune cells, (Majewski et al., 2018) while omiganan is a new synthetic cationic peptide, consisting of 12 amino acids (Javia et al., 2022).

However, AMPs have certain limitations, such as susceptibility to protease or a high salt concentration, and a high propensity to interact with various extracellular matrix components (ECM), compromising their antimicrobial activity and widespread use as antimicrobial agents (Ng et al., 2017; McKelvey et al., 2020). For example, the high ionic strength and decreased pH of the surface liquid in CF lungs, via disruption of hydrogen bonding patterns, are potent AMPs inhibitors (Anderson and Yu, 2005; Kandasamy and Larson, 2006). Likewise, their direct interactions with highly abundant CF sputum and negatively charged biopolymers, including DNA, F-actin (Tang et al., 2005), and mucins (Felgentreff et al., 2006), lead to the formation of large and elongated aggregates.

Synthetic ceragenins (CSAs) are non-peptide analogs of natural AMPs that retain their antimicrobial properties while addressing some drawbacks, leading to an extended half-life in body fluids and tissues (Leszczyńska et al., 2011; Pollard et al., 2012; Sinclair et al., 2012; Durnaś et al., 2017). In addition, ceragenins show reduced potential for resistance induction, likely due to multiple mechanisms of action, including permeabilization of the microbial cell membranes and induction of reactive oxygen species. Therefore, ceragenins possess a broad spectrum of microorganisms, including multidrug-resistant (MDR) strains growing in planktonic and biofilm forms (Chmielewska et al., 2020; Paprocka et al., 2022; Tokajuk et al., 2022). Ceragenins have also demonstrated immunomodulatory and antiviral effects, making them promising candidates for versatile therapeutic applications (Howell et al., 2009; Bucki et al., 2015; Suprewicz et al., 2023).

The introduction of CFTR modulators has undoubtedly been a groundbreaking achievement in the management of CF, alleviating the underlying defect and substantially improving clinical outcomes, including reductions in infectious complications (Haq et al., 2022). However, continued research into new antimicrobial strategies is essential, as not all CF patients respond equally to CFTR modulators,

and some continue to face persistent and difficult infections (McGarry et al., 2022). For instance, individuals with CFTR mutations, such as Phe508del, may not experience significant improvements in lung function or other symptoms, and infectious complications in the airways continue to pose a substantial challenge (Habib et al., 2019). Preventing the latter requires the prolonged use of antibiotics, which has led to the emergence of drug-resistant strains, underscoring the urgency for novel antimicrobial strategies. In addition, CFTR modulators may cause side effects, such as gastrointestinal and respiratory issues or headaches, impairing patients' quality of life (Dagenais et al., 2020). Moreover, the cost of CFTR modulators may be a barrier to access for some patients or healthcare systems, thereby limiting this treatment to the world's wealthiest nations (Zampoli et al., 2023). Finally, although short-term studies indicate that CFTR modulators improve lung function and quality of life, their long-term effects are still under investigation (Taylor-Cousar et al., 2023). Therefore, research and development of innovative antimicrobial strategies to ensure the health of individuals with CF is far from complete. This study evaluated the antimicrobial efficacy of ceragenins and AMPs against CF-associated pathogens in CF sputum samples alone and supplemented with NaCl excess.

2 Materials and methods

2.1 Bacterial strains

The following reference bacterial and fungal strains were tested in the study: *Staphylococcus aureus* Xen29, (Caliper Life Science Inc., Hopkinton, MA, USA), *Pseudomonas aeruginosa* ATCC 27853 (non-mucoid strain) (ATCC, Manassas, VA, USA), and *Candida albicans* ATCC 10231 (ATCC, Manassas, VA, USA). In addition, in experiments with artificially contaminated sputum, *P. aeruginosa* PAO1 DSM 19880 strain (mucoid strain) (DSMZ, DSMZ, Germany) with inserted pMF230 plasmid encoding a beta-lactamase gene ensuring resistance to carbenicillin (Nivens et al., 2001) was used to differentiate it from *P. aeruginosa* (susceptible to carbenicillin) present in sputum sample collected from CF patient (see below). The pMF230 plasmid (Addgene, Watertown, MA, USA) was electroporated into *P. aeruginosa* PAO1 DSM 19880 using MicroPulser Electroporator (BioRad, Hercules, CA, USA) according to the procedure described by Choi et al. (2006), and transformants were further selected and maintained on LB agar plates with carbenicillin (400 µg/mL).

In addition, single clinical isolates of *P. aeruginosa* 4B (mucoid strain), *Ochrobactrum* spp. 10B, *C. albicans* 12B, and *C. tropicalis* 178 collected at the Department of Medical Microbiology and Nanobiomedical Engineering in Białystok, Poland, were included in the study. *S. aureus*, *P. aeruginosa*, *Ochrobactrum* spp., and *Candida* strains were cultured and maintained on the recommended selective media purchased from Biomaxima (Lublin, Poland), i.e., Chapman, Cetrimide, and Sabouraud dextrose agar with chloramphenicol, respectively.

2.2 Compounds and experimental settings

Ceragenins were synthesized as described previously (Ding et al., 2002), whereas LL-37 and omiganan were commercially purchased

from Lipopharm company (Gdańsk, Poland). The ceragenins and AMPs were dissolved in deionized water to ensure the absence of NaCl in the solution. The impact of NaCl concentrations on the antimicrobial activity of ceragenins and AMPs against the bacteria and fungi was analyzed using Mueller–Hinton (MH) broth, RPMI medium supplemented with D-(+)-glucose, and MOPS and deionized water. To that end, NaCl (Chempur, Piekary Śląskie, Poland) was suspended in these media to the final concentrations of 20 mM, 60 mM, 100 mM, 150 mM, and 300 mM. In addition, sputum samples from four cystic fibrosis patients, one positive for *P. aeruginosa*, one positive for *S. aureus*, the third positive for *P. aeruginosa*, *Aspergillus* and methicillin-resistant *Staphylococcus aureus* (MRSA) and the fourth positive for *C. albicans*, were included in the respective experiments in conditions mimicking CF lungs. For this purpose, sputum samples were diluted with deionized water to obtain 10 and 20% sputum solutions and used alone or supplemented with 150 mM or 300 mM NaCl.

2.3 Susceptibility testing

Microbial susceptibility testing was carried out using the serial microdilution method by current EUCAST (European Committee on Antimicrobial Susceptibility Testing) recommendations on 96-well microtiter plates with final volumes of 200 μ L. For bacteria, minimum inhibitory concentrations (MICs) were determined in Mueller-Hinton broth (Sigma-Aldrich, Burlington, MA, USA), and minimum bactericidal concentrations (MBCs) were determined by placing 10 μ L dilutions with no visible growth in the MIC test on the appropriate selective agar medium. For fungi, MIC was determined in 2xRPMI medium (Sigma-Aldrich, Burlington, MA, USA) supplemented with D-(+)-glucose (Sigma-Aldrich, Burlington, MA, USA) and MOPS (Sigma-Aldrich, Burlington, MA, USA) diluted twice with deionized water, while minimum fungicidal concentration (MFC) was determined by plating each sample (10 μ L) on Sabouraud dextrose agar with the chloramphenicol. The final microbial concentration in the well was approximately 5×10^5 CFU (colony-forming units)/mL. MIC, MBC, and MFC values were determined after 24 h incubation.

2.4 Killing assay

A killing assay (colony counting assay) was performed to determine the bactericidal and fungicidal activity of LL-37, omiganan, CSA-13, and CSA-131 against selected clinical strains of *P. aeruginosa* and *C. tropicalis*. Briefly, individual colonies of bacteria and fungi were resuspended at $\sim 10^8$ CFU/mL and diluted to 10^5 CFU/mL in sterile deionized water. Tests were performed using the AMPs and ceragenins in the 1–100 μ g/mL concentration range. After 60 min of incubation at 37°C, the plates were transferred to ice, and samples were serially diluted from 10 to 1,000 times. Then 10 μ L aliquots of each dilution were placed on Luria-Bertani (LB) low-salt agar containing 400 μ g/mL carbenicillin (Sigma-Aldrich, Burlington, MA, USA) or on Sabouraud dextrose agar with chloramphenicol and incubated overnight at 37°C to determine the number of visible colonies. The addition of carbenicillin to LB agar selected *P. aeruginosa* PAO1 (resistant to

carbenicillin) and inhibited the growth of carbenicillin-susceptible to *P. aeruginosa* present in the sputum. The colony-forming units (CFU/mL) of each sample were determined by the dilution factor.

Furthermore, the above procedure was repeated using sterile deionized water with 150 mM and 300 mM NaCl as well as 10 and 20% sputum collected from CF patients alone and supplemented with 150 mM and 300 mM NaCl. Due to higher bacterial survival in the presence of 20% compared to 10% sputum, the 20% sputum was selected for further experiments. After incubating the sputum samples 2 μ L of Sputasol (Oxoid, Basingstoke, Hampshire, UK) was added to liquefy them, followed by the pathogens counting on the selective agars.

2.5 Optical microscopy and DNA measurement

DNA concentration was quantified by absorbance at 260 nm using a NanoDrop One spectrophotometer (Thermo Fisher Scientific, Waltham, MA, USA). In our study of sputum samples from cystic fibrosis patients, YOYO-1 staining (Invitrogen, Carlsbad, CA) was used to visualize DNA at a final concentration of 1 μ M. Additionally, F-actin was visualized using Rhodamine Phalloidin (Thermo Fisher Scientific, Waltham, MA, USA) at a final concentration of 0.15 μ M. Fluorescence images were recorded using a Leica DMi8 microscope (Wetzlar, Germany).

2.6 Statistical analysis

All statistical analyses were conducted using Graph Pad Prism, version 8 (GraphPad Software, Inc., San Diego, CA). The data collected were reported as the mean \pm standard deviation (SD) of three experiments. The significance of differences was determined using the two-tailed Student's test and a p -value ≤ 0.05 was considered to be statistically significant. All results were compared to the control, which were samples treated only with CSAs: CSA-13 and CSA-131, and AMPs: LL-37 and omiganan for each inducible concentration.

3 Results

3.1 The antimicrobial activity of ceragenins is not affected by high NaCl concentration

The antimicrobial activity of CSA-13 and CSA-131 against all tested bacterial and fungal strains was not affected by increasing NaCl concentration (Table 1 and Table 2), since variation in the MIC and MBC values was limited to only one dilution. On the contrary, NaCl at a concentration of 300 mM elevated 8-fold MIC and ≥ 8 -fold MBC values for LL-37 and *P. aeruginosa* PAO1 as well as 8-fold MIC and ≥ 16 -fold MBC values for *Ochrobactrum* spp. 10B (Table 1). A similar increase in MIC/MBC values was also noted for omiganan and *C. tropicalis* 178 (Table 2), where the MIC value increased from 16 μ g/mL in the absence of salt concentration to 64 μ g/mL at 300 mM NaCl, and the MFC increased from 32 μ g/mL to 128 μ g/mL, respectively.

TABLE 1 Minimum inhibitory concentration (MIC) and minimum bactericidal concentration (MBC) values of CSA-13, CSA-131, and LL-37 against *Staphylococcus aureus* Xen29, and *Pseudomonas aeruginosa* ATCC 27853 and DSM 19880, and two clinical isolates – *P. aeruginosa* 4B and *Ochrobactrum* spp. 10B in the presence of NaCl concentration (0–300 mM).

Compound	NaCl [mM]	MIC/MBC [μg/mL]				
		<i>Staphylococcus aureus</i> Xen29	<i>Pseudomonas aeruginosa</i> ATCC 27853	<i>Pseudomonas aeruginosa</i> PAO1 DSM 19880	<i>Pseudomonas aeruginosa</i> 4B	<i>Ochrobactrum</i> spp. 10B
CSA-13	0	0.5/0.5	2/4	2/2	1/2	1/2
	20	0.5/0.5	2/4	2/2	1/2	1/2
	60	0.5/0.5	2/4	2/4	1/2	1/2
	100	0.5/0.5	2/4	2/4	1/2	1/2
	150	0.5/0.5	2/4	2/4	1/2	1/2
	300	0.5/0.5	2/4	2/4	1/4	1/4
CSA-131	0	0.5/1	2/4	1/1	2/2	0.5/1
	20	0.5/1	2/4	1/1	2/4	0.5/1
	60	0.5/1	2/4	1/1	2/2	0.5/1
	100	0.5/0.5	2/4	1/2	2/2	0.5/1
	150	0.5/0.5	2/4	1/1	2/4	0.5/0.5
	300	0.5/0.5	2/4	1/1	2/4	0.5/1
LL-37	0	>256/>256	128/128	16/32	128/128	8/16
	20	-*	-	16/64	-	8/32
	60	-	-	16/64	-	8/32
	100	-	-	32/64	-	16/32
	150	-	-	64/128	-	16/64
	300	-	-	128/>256	-	64/>256

* - not determined.

3.2 Ceragenins retain antimicrobial activity in CF sputum and NaCl excess

A killing assay was performed to evaluate the potential inhibitory effect on ceragenins and AMPs of CF sputum (diluted to 10 and 20%) alone and supplemented with 150 mM and 300 mM NaCl.

The highest NaCl concentration was obtained by combining 20% sputum (containing on average 65 mM NaCl; data not shown) and 300 mM NaCl, yielding an approximate concentration of 340 mM NaCl. As shown in Figure 1, 20% sputum from Patient A decreased the antimicrobial activity of CSA-131 against all *P. aeruginosa*. In contrast, in the presence of 10% sputum, the antibacterial activity of CSA-131 against *P. aeruginosa* 1,414 remained unchanged but decreased four-fold for both *P. aeruginosa* ATCC 27853 and *P. aeruginosa* 4B. Moreover, in 20% of sputum, the antibacterial activity of CSA-131 decreased four-fold across all strains (Figure 1). Nevertheless, this inhibitory effect was not augmented by 150 mM and 300 mM NaCl (Figures 2A,B). Similar results were obtained for CSA-13, CSA-131, and *Candida tropicalis* 178 (Figures 3A,B). On the contrary, the antimicrobial activity of LL-37 and omiganan was significantly attenuated in the presence of both sputum and NaCl (Figures 2F, 3F, 4C, 4F, 5C, 5F). Briefly, NaCl alone resulted in ≥ 2.5 -fold increase of the killing dose (concentrations at which all pathogens are effectively eradicated) for LL-37, i.e., from 40 μg/mL to over 100 μg/mL, against *P. aeruginosa* PAO1 DSM19880 strain (Figure 2C), and ≥ 5 -fold

increase of the killing dose for omiganan, i.e., from 20 μg/mL to over 100 μg/mL, against *C. tropicalis* 178 (Figure 3C). Furthermore, in 20% sputum from Patient B, the killing doses against *P. aeruginosa* increased from 10 to 40 μg/mL for CSA-13, and from 5 to 20 μg/mL for CSA-131 (Figures 2D,E). Similarly, the killing doses against *C. tropicalis* increased from 20 to 100 μg/mL for CSA-13 and CSA-131 (Figures 3D,E). In Patient D's 20% sputum solution, the killing doses of both *P. aeruginosa* and *C. tropicalis* were unchanged for CSA-13 and CSA-131 (5 μg/mL) (Figures 4A,B, 5A,B), while in 20% of the sputum of Patient C, the killing doses against the test strains increased (Figures 4D,E, 5D,E). In addition, the presence of 20% solutions of sputum samples from each patient increased the lethal doses from 40 to 100 μg/mL for LL-37 and from 20 to 100 μg/mL for omiganan for the tested strains (Figures 2F, 3F, 4C, 4F, 5C, 5F). It should be noted that omiganan was ineffective against *C. tropicalis* in the presence of 20% sputum (regardless of the patient sample) and 300 mM (Figures 3F, 5C, 5F), while the log (CFU) for LL-37 increase from ~ 4.8 to ~ 5.05 (Figures 2F, 4C, 4F).

3.3 CF sputum contains high concentrations of DNA

Among the sputum samples analyzed, the one containing *P. aeruginosa*, MRSA, and *Aspergillus* exhibited the highest DNA

TABLE 2 Minimum inhibitory concentration (MIC) and minimum fungicidal concentration (MFC) values of CSA-13, CSA-131, and omiganan against *Candida albicans* ATCC 10231, and two clinical isolates – *C. albicans* 12B and *C. tropicalis* 178 in the presence of NaCl concentration (0–300 mM).

Compound	NaCl [mM]	MIC/MFC [μ g/mL]		
		<i>Candida albicans</i> ATCC 10231	<i>Candida albicans</i> 12B	<i>Candida tropicalis</i> 178
CSA-13	0	4/4	4/4	0.25/0.5
	20	4/4	4/4	0.25/0.25
	60	4/4	4/4	0.5/0.5
	100	4/4	4/4	0.5/0.5
	150	4/8	4/4	0.5/0.5
	300	4/8	4/4	0.5/0.5
CSA-131	0	1/1	2/2	0.5/0.5
	20	1/1	2/2	0.5/0.5
	60	1/2	2/2	0.5/0.5
	100	1/1	2/2	0.5/0.5
	150	1/2	2/2	0.5/0.5
	300	1/1	2/2	0.5/0.5
Omiganan	0	>256/>256	>256/>256	16/32
	20	.*	-	16/32
	60	-	-	16/32
	100	-	-	16/32
	150	-	-	32/64
	300	-	-	64/128

* - not determined.

concentration, with a value of 6.66 ± 0.38 mg/mL. In contrast, lower DNA concentrations were observed in sputum samples containing only *P. aeruginosa* (3.86 ± 0.43 mg/mL), and the lowest DNA concentrations were found in samples with *C. albicans* (1 ± 0.01 mg/mL) and *S. aureus* (0.75 ± 0.21 mg/mL) (Figure 6B). The representative images show highly condensed bundles containing DNA and F-actin, which is characteristic of the sputum of CF patients (Figure 6A) (Sheils et al., 1996; Tomkiewicz et al., 1998; Tang et al., 2005).

4 Discussion

This study presents a comparative analysis of the antimicrobial efficacy of ceragenins and AMPs in the context of CF sputum and varying NaCl levels. The investigation aimed to reveal the potential of these agents as alternative therapeutic options for managing CF-associated infections, where conventional antibiotics frequently face limitations due to microbial resistance and the challenging CF microenvironment (López-Causapé et al., 2015).

Respiratory colonization and infection by *P. aeruginosa* are the leading causes of morbidity and mortality in CF patients. It is noteworthy that around 80% of patients are chronically colonized with

P. aeruginosa by the age of 20 (Koch, 2002). Additionally, CF patients are commonly colonized by other bacterial and fungal pathogens, including methicillin-resistant *Staphylococcus aureus*, *Mycobacterium abscessus* complex, *Burkholderia cepacia* complex, *Aspergillus fumigatus*, and *Candida* species (Chotirmall et al., 2010; Bhagirath et al., 2016). Although *Ochrobactrum* infections are relatively uncommon in CF patients, this pathogen deserves attention due to its inherent resistance to antibiotics, the potential to cause chronic infections with clinical implications, and problems with identification (Carvalho Filho et al., 2018). *Ochrobactrum* spp. isolates have been found to exhibit high resistance to beta-lactam antibiotics, except carbapenems, due to the presence of an AmpC-like β -lactamase. Additionally, resistance to aminoglycosides and fluoroquinolones is an emerging issue that further complicates treatment efforts (Alonso et al., 2017; Yagel et al., 2020).

CF sputum is a complex milieu consisting of DNA, mucins, inflammatory cells, and various proteins (Morrison et al., 2019). It also contains varying levels of sodium chloride, a critical electrolyte. Studies have reported that CF sputum shows elevated levels of sodium chloride compared to this healthy individuals. In detail, the concentration of NaCl in the sputum of CF patients and healthy individuals is approximately 179.66 mM (10.5 g/L) and 126.62 mM (7.4 g/L), respectively. It is consistent with *in vivo* measurements in animal models of CFs in mice and *in vitro* in human bronchial epithelial models (Zabner et al., 1998; Jayaraman et al., 2001; Lapierre et al., 2017). Similarly, according to Joris et al., NaCl concentration in the airway surface fluid (ASF) of CF patients was 120–170 mM compared to 80 mM in subjects without cystic fibrosis (Joris et al., 1993). On the other hand, the average DNA concentration in CF sputum was found to be within the range of 0.2–20 mg/mL (White et al., 1985; Brandt et al., 1995; Lewenza, 2013; Sarkar, 2020), consistent with our findings.

The decreased antimicrobial activity of ceragenins against *P. aeruginosa* strains in the sputum may result from the presence of *S. aureus*, which was isolated from the sputum used in the study. Indeed, in the case of chronic CF infection, the number of microorganisms in the sputum of the respiratory tract reaches 10^7 – 10^9 CFU/mL, resulting from the inoculum effect, which substantially affects antimicrobial susceptibility testing results (Turner et al., 2015). Furthermore, while charge-based interactions can influence the antimicrobial activity of ceragenins in the presence of abundant in sputum linear polyelectrolytes, like actin or DNA, they are notably weaker compared to their impact on cationic AMPs, such as LL37, HB71, and WLBU2 (Bucki et al., 2007).

A widespread application of AMPs as antimicrobial agents is hindered by their sensitivity to several physicochemical factors frequently present in infected sites, such as a high salt concentration in the CF airway surface fluid (Goldman et al., 1997). For instance, in patients with cystic fibrosis, the activity of AMPs is significantly lower in the ASL than in normal ASL (Smith et al., 1996; Hiemstra, 2007).

Indeed, our results show that the antimicrobial activity of both LL-37 and omiganan against CF-associated pathogens is NaCl concentration-dependent. Similarly, Bals et al. and Tanaka et al. demonstrated that the antimicrobial activity of LL-37 diminishes with rising NaCl concentrations (Bals et al., 1998; Tanaka et al., 2000). Several studies have highlighted the limitations of AMPs in their antimicrobial activity. A high-salt environment has been found to

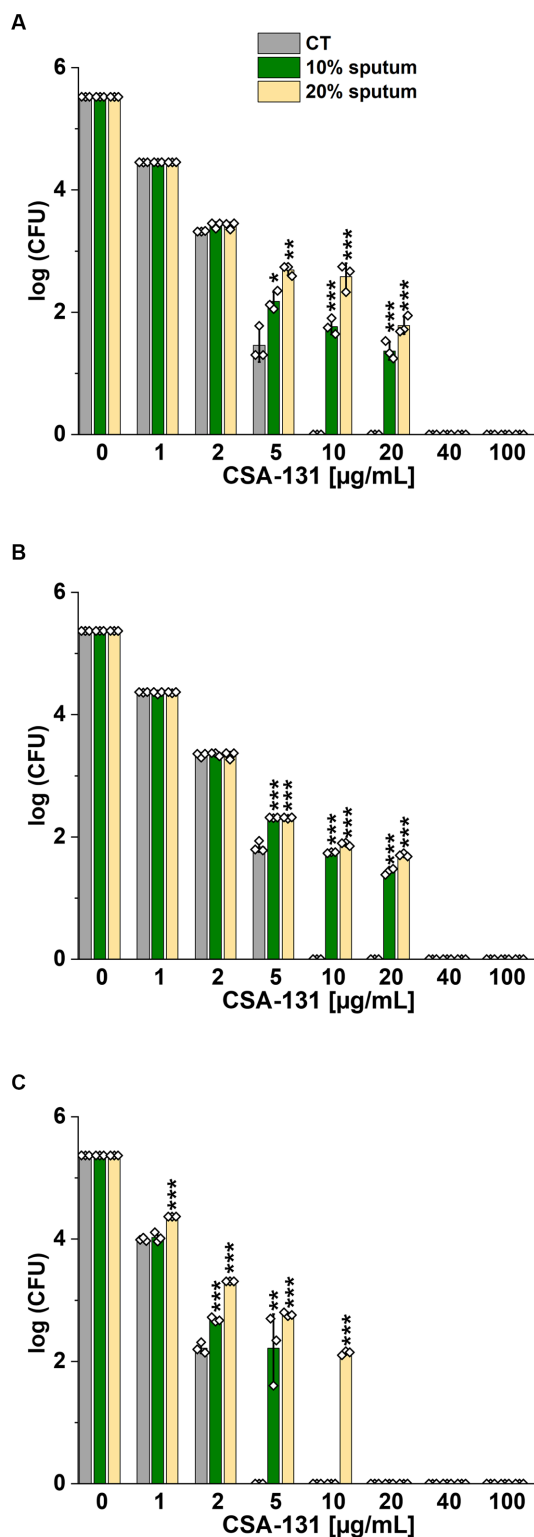


FIGURE 1
Bactericidal activity of CSA-131 against *Pseudomonas aeruginosa* ATCC 27853 (A) and *P. aeruginosa* PAO1 DSM 19880 (B) and clinical isolate *P. aeruginosa* 4B (C) in 10 and 20% solution of CF sputum collected from Patient A. Results show the mean \pm SD, $n = 3$; * indicates statistical significance at $p \leq 0.05$, ** $p \leq 0.01$, and *** $p \leq 0.001$ by Student's t -test.

impair the effectiveness of AMPs, as observed in the case of peptides like indolicidin, human beta-defensin-1, histidine-rich peptide P-113, gramicidins, magainins, and bactenecins (Goldman et al., 1997; Lee et al., 1997; Wu et al., 1999; Rothstein et al., 2001). In CF sputum, the presence of bacterial endotoxin lipopolysaccharide (LPS) is one of the factors leading to the inhibition of LL-37 antimicrobial activity (Bucki et al., 2007). Additionally, the secretion of two zinc-dependent metalloproteases, ZmpA and ZmpB, by *Burkholderia cepacia* can lead to the inactivation of AMPs, such as human beta-defensin-1 and LL-37 (Kooi and Sokol, 2009). These findings shed light on the challenges in utilizing AMPs as effective therapeutic agents in CF patients.

The structure of an AMP plays a vital role in determining its antimicrobial activity. It is believed that the helical, oligomeric conformation of LL-37 is crucial to the protein's antimicrobial activity. Hence, the highest LL-37 antimicrobial activity is observed with maximum helix content, while intermediate and low activity corresponds to lower helix content and a disordered secondary structure. These findings suggest that the optimal antimicrobial activity of LL-37 necessitates an oligomeric α -helical structure before its interaction with the bacterial membrane (Johansson et al., 1998). Studies have demonstrated that increased NaCl concentration can induce conformational changes in LL-37. Specifically, at higher NaCl concentrations, LL-37 may undergo structural alterations and adopt a more random or disordered conformation resulting in decreased antimicrobial activity (Park et al., 2004; Huang et al., 2014).

In contrast, omiganan does not display a helical structure. However, the presence of positively charged sodium ions affects electrostatic interactions of this cationic AMP with microbial cell membranes (Mojsoska and Jenssen, 2015; Ghosh et al., 2021). Hence, in high-salt environments, the antimicrobial activity of omiganan may decrease, rendering it less effective against certain microorganisms. This dependence on salt concentration can affect its efficacy in physiological conditions where salt levels fluctuate, such as respiratory tract or skin infections (Brown, 2021).

On the other hand, the antimicrobial activity of ceragenins is independent of the concentration of NaCl, likely due to their unique structural properties. The smaller size of CSA-13 and CSA-131 than LL-37 and omiganan, along with distinct charge densities and lower positive charges, ensure their stability and resistance to changes in the ionic environment, including fluctuations in NaCl concentration and anionic polyelectrolytes, such as extracellular DNA (eDNA), F-actin, and mucin (Hashemi et al., 2018). In addition, the direct targeting of membrane lipids by ceragenins makes them less vulnerable to salt concentration compared to the highly charge-based AMPs mechanism of action (Epand et al., 2007).

Mucoid strains of *P. aeruginosa* that produce a thick alginate biofilm are typically more resistant to antimicrobials than non-mucoid strains due to the protective nature of the biofilm, which limits their penetration and, consequently, their efficacy (Nichols et al., 1989; Meluleni et al., 1995; Stewart, 1996; Hentzer et al., 2001). *P. aeruginosa* is well-known for its ability to develop antibiotic resistance, for example, through upregulation of genes encoding efflux pumps, which effectively remove antibiotics from the cell (Tomás et al., 2010). The favorable biocompatibility of CSA has been reported in previous work (Piktel et al., 2020; Paprocka et al., 2021; Suprewicz et al., 2023). For

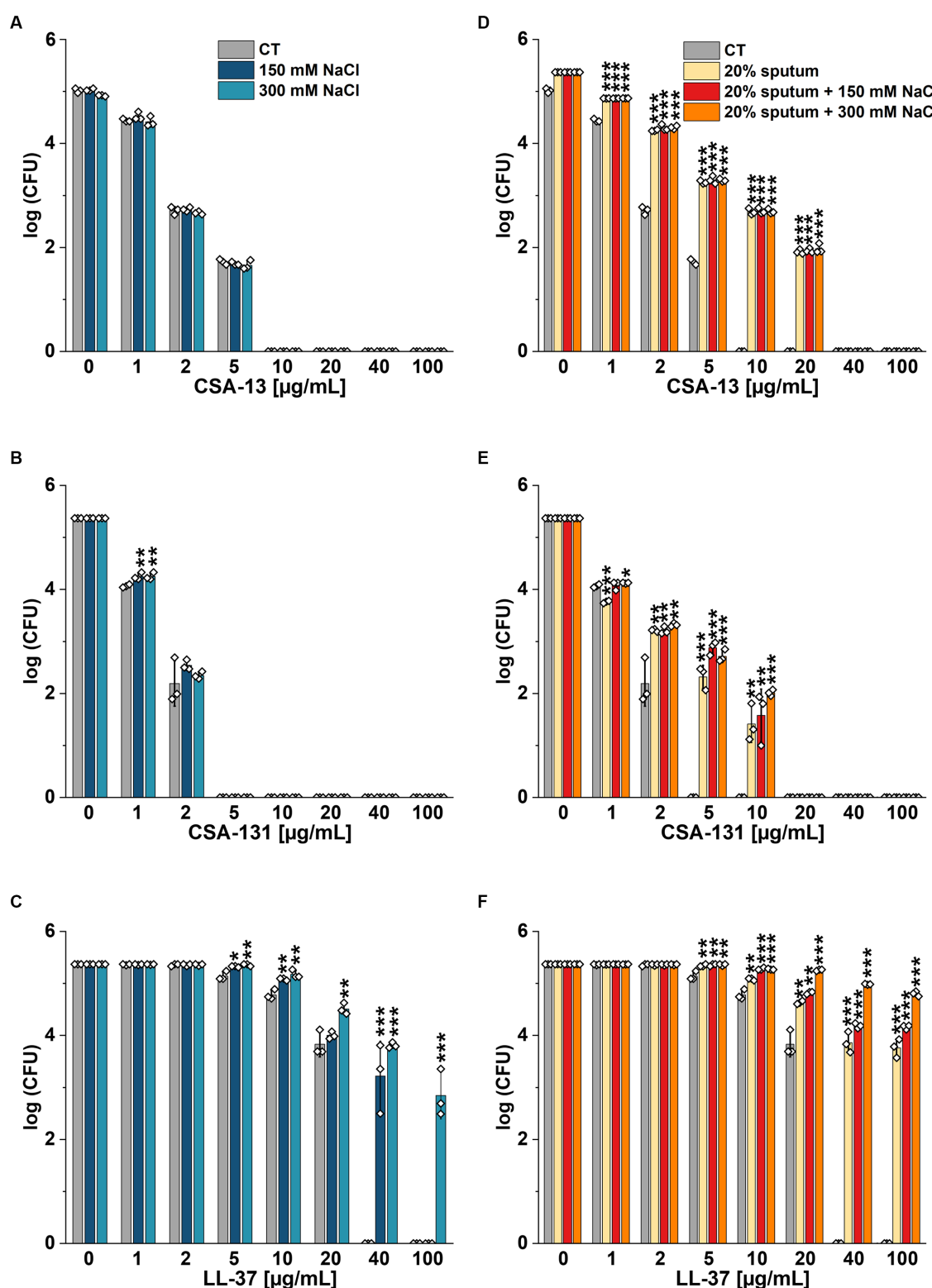


FIGURE 2

Bactericidal activity of CSA-13 (A,D), CSA-131 (B,E), and LL-37 (C,F) against *Pseudomonas aeruginosa* PAO1 DSM 19880 strain. Bacterial survival was evaluated in sterile deionized water (CT) (A–C), and in 20% solution of CF sputum collected from Patient B (D–F), without NaCl and with NaCl at a concentration of 150 mM and 300 mM. Results show the mean \pm SD ($n = 3$). * indicates statistical significance at $p \leq 0.05$, ** ≤ 0.01 , and *** ≤ 0.001 by Student's t -test.

CSA-13 and CSA-131, the viability of human basal alveolar epithelial adenocarcinoma cells (A549) at a concentration of 10 µg/mL CSA-13 and CSA-131 was maintained at approximately 60 and 80%,

respectively (Piktel et al., 2020; Paprocka et al., 2021; Suprewicz et al., 2023). Additionally, the problem of cytotoxicity can be effectively solved by the incorporation of Pluronic, a compound that increases

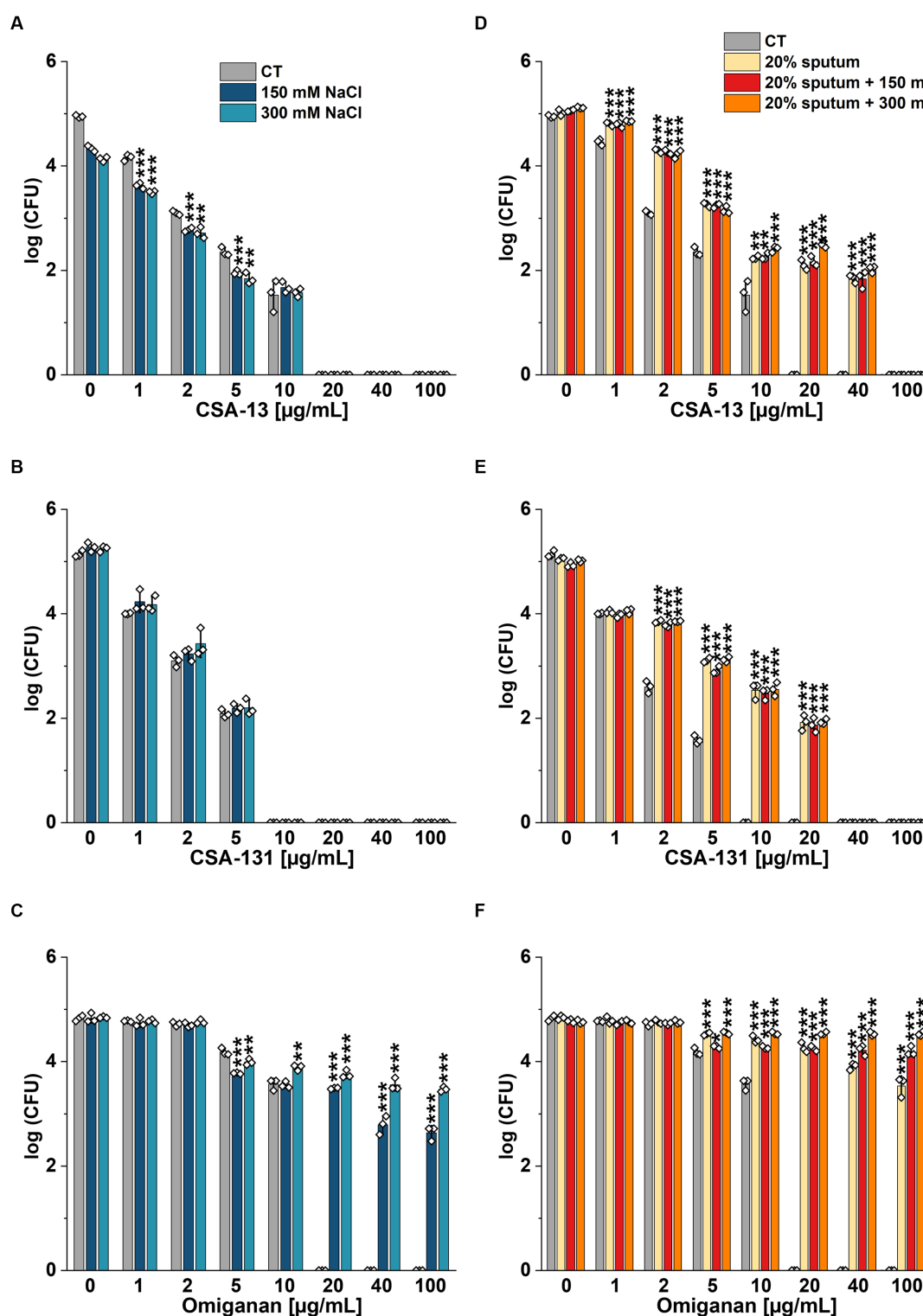


FIGURE 3

Fungicidal activity of CSA-13 (A,D), CSA-131 (B,E), and omiganan (C,F) against the clinical strain of *Candida tropicalis* 178. Fungal survival was evaluated in distilled water supplemented with NaCl (A–C), and in 20% solution of *CF* sputum collected from Patient B (D–F) alone and supplemented with NaCl at a concentration of 150 mM and 300 mM. Results show the mean \pm SD ($n = 3$). * indicates statistical significance at $p \leq 0.05$, ** ≤ 0.01 , and *** ≤ 0.001 by Student's *t*-test.

cell viability and alleviates the hemolytic effects of CSAs while maintaining their antimicrobial activity (Leszczyńska et al., 2011; Paprocka et al., 2021).

Understanding the disparate modes of action and resistance to changes in salt concentration provides valuable insights into the therapeutic potential of ceragenins as effective antimicrobial agents,

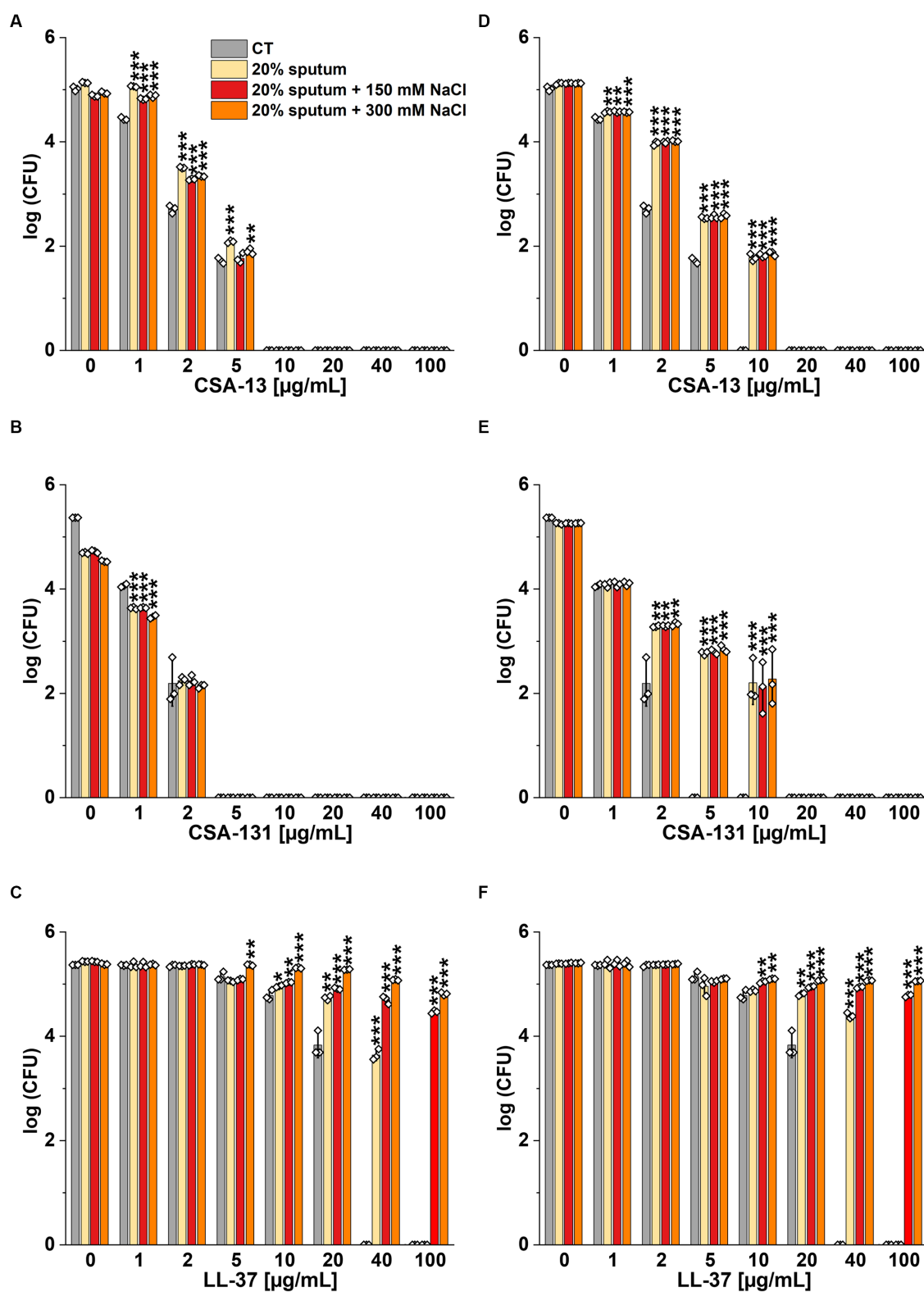


FIGURE 4

Bactericidal activity of CSA-13 (A,D), CSA-131 (B,E), and LL-37 (C,F) against *Pseudomonas aeruginosa* PAO1 DSM 19880 strain. Bacterial survival was evaluated in 20% solution of CF sputum collected from patient D (A-C), and from Patient C (D-F), without NaCl and with NaCl at a concentration of 150 mM and 300 mM. Results show the mean \pm SD ($n = 3$). * indicates statistical significance at $p \leq 0.05$, ** ≤ 0.01 , and *** ≤ 0.001 by Student's t -test.

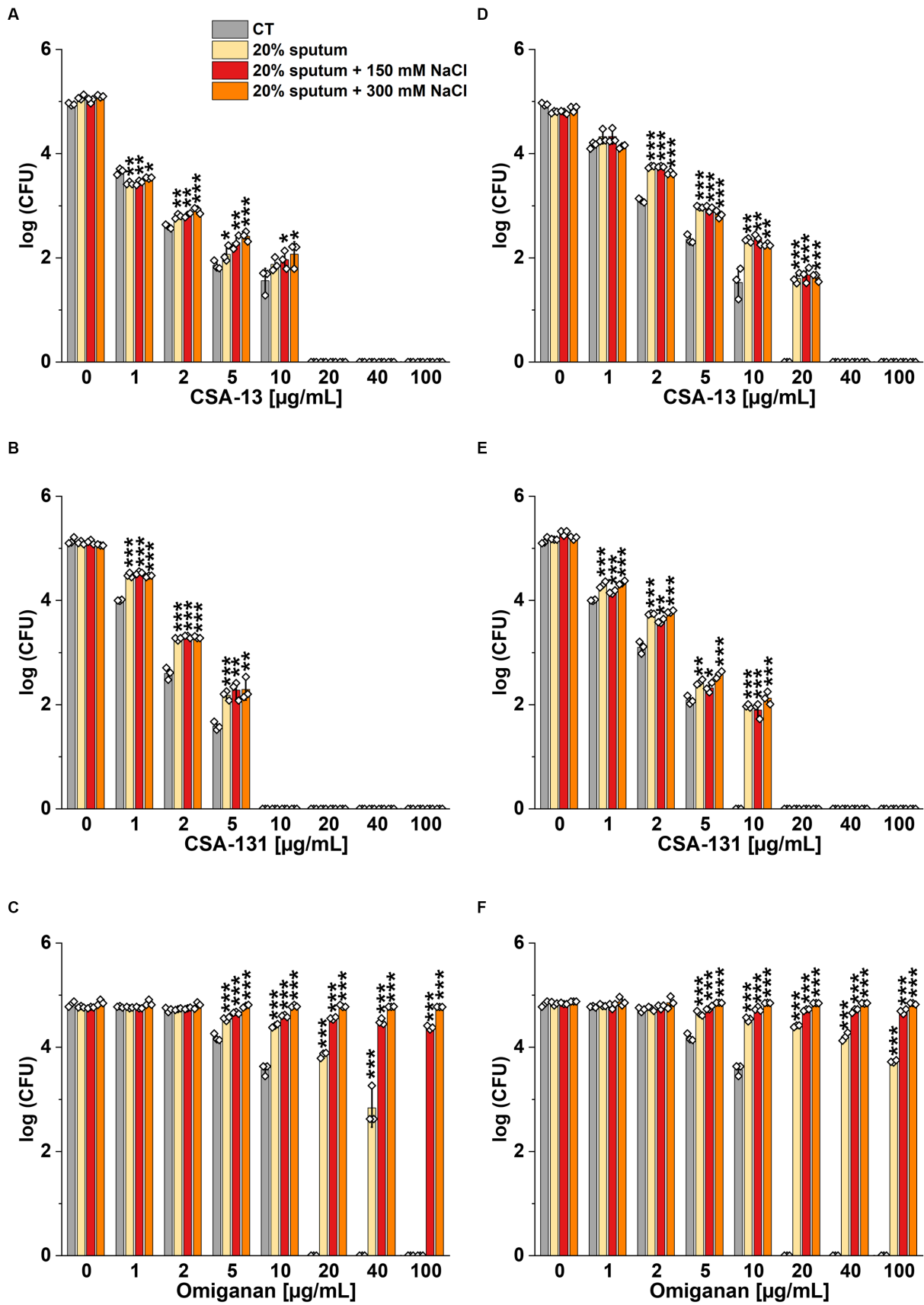


FIGURE 5 Fungicidal activity of CSA-13 (A,D), CSA-131 (B,E), and omiganan (C,F) against the clinical strain of *Candida tropicalis* 178. Fungal survival was evaluated in 20% solution of CF sputum from Patient D (A-C), and from Patient C (D-F), alone and supplemented with NaCl at a concentration of 150 mM and 300 mM. Results show the mean \pm SD ($n = 3$). * indicates statistical significance at $p \leq 0.05$, ** ≤ 0.01 , and *** ≤ 0.001 by Student's t -test.

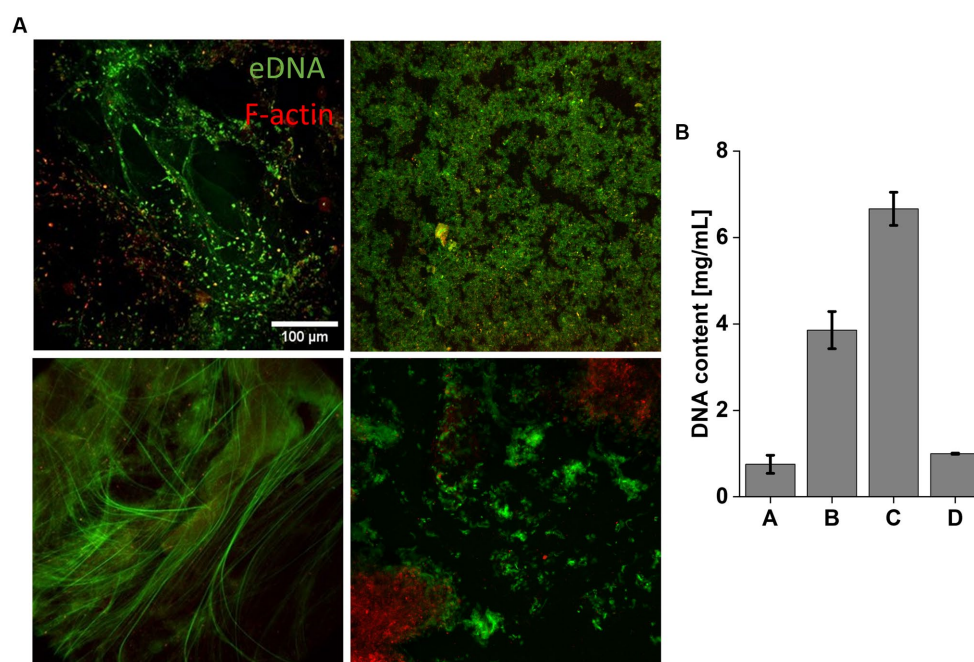


FIGURE 6

Representative microscopic images of sputum collected from CF patients. Top left image shows sputum from Patient A, top right image – Patient B, bottom left image – Patient C, bottom right image – Patient D. The DNA are shown green and F-actin in red. Scale bar 100 μm (A). (B) Mean DNA concentration in CF sputum. Results show the mean \pm SD ($n = 3$).

particularly in managing infections in complex biological environments, such as CF lungs. Further research in this area is critical to elucidate the intricacies of ceragenin activity and its implications for clinical applications. The intrinsic stability and resistance to changes in NaCl concentration make ceragenins promising candidates for combating infections in complex environments like the CF sputum (Bucki et al., 2007; Leszczyńska et al., 2011).

5 Conclusion

Our study provides a comprehensive comparative analysis of the efficacy of ceragenins and AMPs in the context of CF sputum and varying NaCl concentrations. We investigated the antimicrobial activity of CSA-13, CSA-131, LL-37, and omiganan against CF-associated pathogens, evaluating their performance under different conditions. Our findings revealed that ceragenins, specifically CSA-13 and CSA-131, exhibited remarkable antimicrobial efficacy, surpassing natural (LL-37) and synthetic (omiganan) AMPs. Notably, the antimicrobial activity of ceragenins remained consistent across a wide range of NaCl concentrations, underscoring their resistance to changes in ionic environments. In contrast, the antimicrobial activity of LL-37 and omiganan was reduced in high-salt environments, potentially compromising their performance in CF sputum, a condition where NaCl levels can vary. The structural properties of ceragenins and their lipid-based mode of action likely contribute to their stability and sustained antimicrobial activity, even under salt excess condition. These properties highlight the potential of ceragenins as promising candidates for combating CF-associated infections and overcoming limitations observed in natural and synthetic AMPs.

Scope statement

The study investigated the effect of sodium chloride (NaCl) on the antimicrobial efficacy of the cathelicidin LL-37, and their synthetic mimetic ceragenins (Ceragenins), which are considered as potential therapeutic agents in cystic fibrosis (CF) lung infections. The susceptibility of cystic fibrosis-associated bacterial pathogens (*Pseudomonas aeruginosa*, *Ochrobactrum* spp. and *Staphylococcus aureus*) and fungal pathogens (*Candida albicans* and *C. tropicalis*) to these compounds was determined using Minimum Inhibitory Concentrations (MIC) and Bactericidal Concentrations (MBC) tests in sputum samples collected from patients diagnosed with CF. Furthermore, a colony-counting assay was used to assess the effect of varying NaCl concentrations on tested agents' antimicrobial activity. The findings reveal that ceragenins exhibit potent antimicrobial activity in CF sputum, regardless of the NaCl concentration when compared to LL-37 and omiganan. Given the broad-spectrum antimicrobial activity of ceragenins in microenvironments resembling the airways of CF patients, they represent promising agents for managing CF disease. This manuscript aligns with the journal's scope as it contributes to the field of microbiology and infectious diseases. The investigation provides valuable insights into the development of effective antimicrobial strategies to combat CF-associated infections.

Data availability statement

The raw data supporting the conclusions of this article will be made available by the authors, without undue reservation.

Ethics statement

The studies involving humans were approved by Bioethics Committee of Medical University of Białystok. The studies were conducted in accordance with the local legislation and institutional requirements. The participants provided their written informed consent to participate in this study.

Author contributions

KS: Conceptualization, Formal analysis, Writing – original draft, Data curation, Investigation, Methodology, Software, Writing – review & editing. ŁS: Formal analysis, Investigation, Methodology, Software, Writing – review & editing, Visualization. SC-D: Methodology, Software, Visualization, Writing – review & editing. SK: Methodology, Writing – review & editing, Investigation, Resources. SO: Methodology, Writing – review & editing, Software, Visualization. MZ: Software, Formal analysis, Investigation, Writing – original draft. ŁM: Formal analysis, Investigation, Data curation, Resources, Writing – review & editing. RM: Formal analysis, Investigation, Resources, Writing – review & editing, Supervision. TD: Formal analysis, Investigation, Writing – review & editing, Methodology, Validation. PS: Formal analysis, Investigation, Validation, Writing – review & editing, Supervision. KF: Formal analysis, Supervision, Validation, Writing – review & editing, Project administration, Visualization, Writing – original draft. RB: Formal analysis, Validation, Writing – original draft, Conceptualization, Resources.

References

- Akkerman-Nijland, A. M., Akkerman, O. W., Grasmeyer, F., Hagedoorn, P., Frijlink, H. W., Rottier, B. L., et al. (2021). The pharmacokinetics of antibiotics in cystic fibrosis. *Expert Opin. Drug Metab. Toxicol.* 17, 53–68. doi: 10.1080/17425255.2021.1836157
- Alonso, C. A., Kwabugbe, Y. A., Anyanwu, M. U., Torres, C., and Chah, K. F. (2017). Diversity of *Ochrobactrum* species in food animals, antibiotic resistance phenotypes and polymorphisms in the bla OCH gene. *FEMS Microbiol. Lett.* 364:178. doi: 10.1093/femsle/fnx178
- Anderson, R. C., and Yu, P.-L. (2005). Factors affecting the antimicrobial activity of ovine-derived cathelicidins against *E. Coli* 0157: H7. *Int. J. Antimicrob. Agents* 25, 205–210. doi: 10.1016/j.ijantimicag.2004.10.010
- Bals, R., Wang, X., Zasloff, M., and Wilson, J. M. (1998). The peptide antibiotic LL-37/hCAP-18 is expressed in epithelia of the human lung where it has broad antimicrobial activity at the airway surface. *Proc. Natl. Acad. Sci.* 95, 9541–9546. doi: 10.1073/pnas.95.16.9541
- Bhagirath, A. Y., Li, Y., Somayajula, D., Dadashi, M., Badr, S., and Duan, K. (2016). Cystic fibrosis lung environment and *Pseudomonas aeruginosa* infection. *BMC Pulm. Med.* 16:174. doi: 10.1186/s12890-016-0339-5
- Bhat, P. G., Flanagan, D. R., and Donovan, M. D. (1996). Drug diffusion through cystic fibrotic mucus: steady-state permeation, rheologic properties, and glycoprotein morphology. *J. Pharm. Sci.* 85, 624–630. doi: 10.1021/js950381s
- Boucher, R. (2004). New concepts of the pathogenesis of cystic fibrosis lung disease. *Eur. Respir. J.* 23, 146–158. doi: 10.1183/09031936.03.00057003
- Brandt, T., Breitenstein, S., von der Hardt, H., and Tümmler, B. (1995). DNA concentration and length in sputum of patients with cystic fibrosis during inhalation with recombinant human DNase. *Thorax* 50, 880–882. doi: 10.1136/thx.50.8.880
- Brown, R. B. (2021). Sodium toxicity in the nutritional epidemiology and nutritional immunology of COVID-19. *Medicina* 57:739. doi: 10.3390/medicina57080739
- Bucki, R., Byfield, F. J., and Janmey, P. A. (2007). Release of the antimicrobial peptide LL-37 from DNA/F-actin bundles in cystic fibrosis sputum. *Eur. Respir. J.* 29, 624–632. doi: 10.1183/09031936.00080806
- Bucki, R., Niemirówicz, K., Wnorowska, U., Byfield, F. J., Piktel, E., Wątek, M., et al. (2015). Bactericidal activity of ceragenin CSA-13 in cell culture and in an animal model of peritoneal infection. *Antimicrob. Agents Chemother.* 59, 6274–6282. doi: 10.1128/AAC.00653-15
- Bucki, R., Sostarecz, A. G., Byfield, F. J., Savage, P. B., and Janmey, P. A. (2007). Resistance of the antibacterial agent ceragenin CSA-13 to inactivation by DNA or F-actin and its activity in cystic fibrosis sputum. *J. Antimicrob. Chemother.* 60, 535–545. doi: 10.1093/jac/dkm218
- Carvalho Filho, É. B., Marson, F. A. L., and Levy, C. E. (2018). Challenges in the identification of *Ochrobactrum anthropi* in blood and sputum cultures of patients with cystic fibrosis. *Rev. Epidemiol. E Controle Infecção*. 8, 189–191. doi: 10.17058/reci.v1i2.9967
- Chmielewska, S. J., Skłodowski, K., Piktel, E., Suprewicz, Ł., Fiedoruk, K., Daniluk, T., et al. (2020). NDM-1 Carbapenemase-producing Enterobacteriaceae are highly susceptible to Ceragenins CSA-13, CSA-44, and CSA-131. *Infect. Drug Resist.* 13, 3277–3294. doi: 10.2147/IDR.S261579
- Choi, K.-H., Kumar, A., and Schweizer, H. P. (2006). A 10-min method for preparation of highly electrocompetent *Pseudomonas aeruginosa* cells: application for DNA fragment transfer between chromosomes and plasmid transformation. *J. Microbiol. Methods* 64, 391–397. doi: 10.1016/j.mimet.2005.06.001
- Chotirmall, S. H., Greene, C. M., and McElvaney, N. G. (2010). Candida species in cystic fibrosis: a road less travelled. *Med. Mycol.* 48, S114–S124. doi: 10.3109/13693786.2010.503320
- Dagenais, R. V., Su, V. C., and Quon, B. S. (2020). Real-world safety of CFTR modulators in the treatment of cystic fibrosis: a systematic review. *J. Clin. Med.* 10:23. doi: 10.3390/jcm10010023
- Ding, B., Guan, Q., Walsh, J. P., Boswell, J. S., Winter, T. W., Winter, E. S., et al. (2002). Correlation of the antibacterial activities of cationic peptide antibiotics and cationic steroid antibiotics. *J. Med. Chem.* 45, 663–669. doi: 10.1021/jm0105070
- Durnaś, B., Piktel, E., Wątek, M., Wollny, T., Gózdź, S., Smok-Kalwat, J., et al. (2017). Anaerobic bacteria growth in the presence of cathelicidin LL-37 and selected ceragenins delivered as magnetic nanoparticles cargo. *BMC Microbiol.* 17:167. doi: 10.1186/s12866-017-1075-6
- Eband, R. F., Savage, P. B., and Eband, R. M. (2007). Bacterial lipid composition and the antimicrobial efficacy of cationic steroid compounds (Ceragenins). *Biochim. Biophys. Acta* 1768, 2500–2509. doi: 10.1016/j.bbame.2007.05.023
- Felgentreff, K., Beisswenger, C., Griese, M., Gulder, T., Bringmann, G., and Bals, R. (2006). The antimicrobial peptide cathelicidin interacts with airway mucus. *Peptides* 27, 3100–3106. doi: 10.1016/j.peptides.2006.07.018

Funding

The author(s) declare financial support was received for the research, authorship, and/or publication of this article. This work was supported by the National Science Center, Poland, under grant: UMO-2018/30/M/NZ6/00502 and the Medical University of Białystok (SUB/1/DN/22/001/1122), Poland.

Conflict of interest

PS and RB are the consultants for N8 Medical, Inc. and report personal fees from N8.

The remaining authors declare that the research was conducted in the absence of any commercial or financial relationships that could be construed as a potential conflict of interest.

The author(s) declared that they were an editorial board member of Frontiers, at the time of submission. This had no impact on the peer review process and the final decision.

Publisher's note

All claims expressed in this article are solely those of the authors and do not necessarily represent those of their affiliated organizations, or those of the publisher, the editors and the reviewers. Any product that may be evaluated in this article, or claim that may be made by its manufacturer, is not guaranteed or endorsed by the publisher.

- Ghosh, S., Pandit, G., Debnath, S., Chatterjee, S., and Satpati, P. (2021). Effect of monovalent salt concentration and peptide secondary structure in peptide-micelle binding. *RSC Adv.* 11, 36836–36849. doi: 10.1039/D1RA06772A
- Goldman, M. J., Anderson, G. M., Stolzenberg, E. D., Kari, U. P., Zasloff, M., and Wilson, J. M. (1997). Human β -defensin-1 is a salt-sensitive antibiotic in lung that is inactivated in cystic fibrosis. *Cells* 88, 553–560. doi: 10.1016/S0092-8674(00)81895-4
- Habib, A.-R. R., Kajbafzadeh, M., Desai, S., Yang, C. L., Skolnik, K., and Quon, B. S. (2019). A systematic review of the clinical efficacy and safety of CFTR modulators in cystic fibrosis. *Sci. Rep.* 9:7234. doi: 10.1038/s41598-019-43652-2
- Haq, I., Almulhem, M., Soars, S., Poulton, D., and Brodrie, M. (2022). Precision medicine based on CFTR genotype for people with cystic fibrosis. *Pharmgenomics Pers. Med.* 15, 91–104. doi: 10.2147/PGPM.S245603
- Hashemi, M. M., Holden, B. S., and Savage, P. B. (2018). “Ceragenins as non-peptide mimics of endogenous antimicrobial peptides” in *Fighting Antimicrobial Resistance*. ed. A. Budimir (Zagreb, Croatia: IAPC Publishing), 139–169.
- Hentzer, M., Teitzel, G. M., Balzer, G. J., Heydorn, A., Molin, S., Givskov, M., et al. (2001). Alginate overproduction affects *Pseudomonas aeruginosa* biofilm structure and function. *J. Bacteriol.* 183, 5395–5401. doi: 10.1128/JB.183.18.5395-5401.2001
- Hiemstra, P. (2007). Antimicrobial peptides in the real world: implications for cystic fibrosis. *Eur. Respir. J.* 29, 617–618. doi: 10.1183/09031936.00017007
- Howell, M. D., Streib, J. E., Kim, B. E., Lesley, L. J., Dunlap, A. P., Geng, D., et al. (2009). Ceragenins: a class of antiviral compounds to treat orthopox infections. *J. Invest. Dermatol.* 129, 2668–2675. doi: 10.1038/jid.2009.120
- Huang, Y., He, L., Li, G., Zhai, N., Jiang, H., and Chen, Y. (2014). Role of helicity of α -helical antimicrobial peptides to improve specificity. *Protein Cell* 5, 631–642. doi: 10.1007/s12338-014-0061-0
- Javia, A., Misra, A., and Thakkar, H. (2022). Liposomes encapsulating novel antimicrobial peptide Omiganan: characterization and its pharmacodynamic evaluation in atopic dermatitis and psoriasis mice model. *Int. J. Pharm.* 624:122045. doi: 10.1016/j.ijpharm.2022.122045
- Jayaraman, S., Song, Y., Vetrivel, L., Shankar, L., and Verkman, A. (2001). Noninvasive in vivo fluorescence measurement of airway-surface liquid depth, salt concentration, and pH. *J. Clin. Invest.* 107, 317–324. doi: 10.1172/JCI11154
- Johansson, J., Gudmundsson, G. H., MnE, R., Berndt, K. D., and Agerberth, B. (1998). Conformation-dependent antibacterial activity of the naturally occurring human peptide LL-37. *J. Biol. Chem.* 273, 3718–3724. doi: 10.1074/jbc.273.6.3718
- Joris, L., Dab, I., and Quinton, P. M. (1993). Elemental composition of human airway surface fluid in healthy and diseased airways. *Am. J. Respir. Crit. Care Med.* 148, 1633–1637. doi: 10.1164/ajrccm/148.6_pt_1.1633
- Kandasamy, S. K., and Larson, R. G. (2006). Effect of salt on the interactions of antimicrobial peptides with zwitterionic lipid bilayers. *Biochim. Biophys. Acta* 1758, 1274–1284. doi: 10.1016/j.bbame.2006.02.030
- Koch, C. (2002). Early infection and progression of cystic fibrosis lung disease. *Pediatr. Pulmonol.* 34, 232–236. doi: 10.1002/ppul.10135
- Kooi, C., and Sokol, P. A. (2009). *Burkholderia cenocepacia* zinc metalloproteases influence resistance to antimicrobial peptides. *Microbiology* 155, 2818–2825. doi: 10.1099/mic.0.028969-0
- Lapierre, S. G., Phelippeau, M., Hakimi, C., Didier, Q., Reynaud-Gaubert, M., and Dubus, J.-C. (2017). Cystic fibrosis respiratory tract salt concentration: an exploratory cohort study. *Medicine* 96:e8423. doi: 10.1097/MD.00000000000008423
- Lee, I. H., Cho, Y., and Lehrer, R. I. (1997). Effects of pH and salinity on the antimicrobial properties of clavanins. *Infect. Immun.* 65, 2898–2903. doi: 10.1128/iai.65.7.2898-2903.1997
- Lei, J., Sun, L., Huang, S., Zhu, C., Li, P., He, J., et al. (2019). The antimicrobial peptides and their potential clinical applications. *Am. J. Transl. Res.* 11, 3919–3931.
- Leszczyńska, K., Namiot, A., Cruz, K., Byfield, F., Won, E., and Mendez, G. (2011). Potential of ceragenin CSA-13 and its mixture with pluronic F-127 as treatment of topical bacterial infections. *J. Appl. Microbiol.* 110, 229–238. doi: 10.1111/j.1365-2672.2010.04874.x
- Lewenza, S. (2013). Extracellular DNA-induced antimicrobial peptide resistance mechanisms in *Pseudomonas aeruginosa*. *Front. Microbiol.* 4:21. doi: 10.3389/fmicb.2013.00021
- López-Causapé, C., Rojo-Molinero, E., Macia, M. D., and Oliver, A. (2015). The problems of antibiotic resistance in cystic fibrosis and solutions. *Expert Rev. Respir. Med.* 9, 73–88. doi: 10.1586/17476348.2015.995640
- Lyczak, J. B., Cannon, C. L., and Pier, G. B. (2002). Lung infections associated with cystic fibrosis. *Clin. Microbiol. Rev.* 15, 194–222. doi: 10.1128/CMR.15.2.194-222.2002
- Majewski, K., Kozłowska, E., Żelechowska, P., and Brzezińska-Błaszczak, E. (2018). Serum concentrations of antimicrobial peptide cathelicidin LL-37 in patients with bacterial lung infections. *Cent. Eur. J. Immunol.* 43, 453–457. doi: 10.5114/ceji.2018.81355
- Mansour, S. C., Pena, O. M., and Hancock, R. E. (2014). Host defense peptides: front-line immunomodulators. *Trends Immunol.* 35, 443–450. doi: 10.1016/j.it.2014.07.004
- McGarry, M. E., Gibb, E. R., Oates, G. R., and Schechter, M. S. (2022). Left behind: the potential impact of CFTR modulators on racial and ethnic disparities in cystic fibrosis. *Paediatr. Respir. Rev.* 42, 35–42. doi: 10.1016/j.prrv.2021.12.001
- McKelvey, M. C., Weldon, S., McAuley, D. F., Mall, M. A., and Taggart, C. C. (2020). Targeting proteases in cystic fibrosis lung disease. Paradigms, progress, and potential. *Am. J. Respir. Crit. Care Med.* 201, 141–147. doi: 10.1164/rccm.201906.1190PP
- Meluleni, G. J., Grout, M., Evans, D. J., and Pier, G. B. (1995). Mucoid *Pseudomonas aeruginosa* growing in a biofilm in vitro are killed by opsonic antibodies to the mucoid exopolysaccharide capsule but not by antibodies produced during chronic lung infection in cystic fibrosis patients. *J. Immunol.* 155, 2029–2038. doi: 10.4049/jimmunol.155.4.2029
- Mojsoska, B., and Jenssen, H. (2015). Peptides and peptidomimetics for antimicrobial drug design. *Pharmaceuticals* 8, 366–415. doi: 10.3390/ph8030366
- Morrison, C. B., Markovetz, M. R., and Ehre, C. (2019). Mucus, mucins, and cystic fibrosis. *Pediatr. Pulmonol.* 54, S84–S96. doi: 10.1002/ppul.24530
- Ng, S. M. S., Teo, S. W., Yong, Y. E., Ng, F. M., Lau, Q. Y., Jureen, R., et al. (2017). Preliminary investigations into developing all-D Omiganan for treating mupirocin-resistant MRSA skin infections. *Chem. Biol. Drug Des.* 90, 1155–1160. doi: 10.1111/cbdd.13035
- Nichols, W. W., Evans, M. J., Slack, M. P., and Walmsley, H. L. (1989). The penetration of antibiotics into aggregates of mucoid and non-mucoid *Pseudomonas aeruginosa*. *Microbiology* 135, 1291–1303. doi: 10.1099/00221287-135-5-1291
- Nivens, D. E., Ohman, D. E., Williams, J., and Franklin, M. J. (2001). Role of alginate and its O acetylation in formation of *Pseudomonas aeruginosa* microcolonies and biofilms. *J. Bacteriol.* 183, 1047–1057. doi: 10.1128/JB.183.3.1047-1057.2001
- Paprocka, P., Durnas, B., Mańkowska, A., Skłodowski, K., Król, G., Zakrzewska, M., et al. (2021). New β -lactam antibiotics and ceragenins—a study to assess their potential in treatment of infections caused by multidrug-resistant strains of *Pseudomonas aeruginosa*. *Infect. Drug Resist.* 14, 5681–5698. doi: 10.2147/IDR.S338827
- Paprocka, P., Mańkowska, A., Skłodowski, K., Król, G., Wollny, T., Lesiak, A., et al. (2022). Bactericidal activity of Ceragenin in combination with ceftazidime, levofloxacin, co-Trimoxazole, and Colistin against the opportunistic pathogen *Stenotrophomonas maltophilia*. *Pathogens* 11:621. doi: 10.3390/pathogens11060621
- Park, I. Y., Cho, J. H., Kim, K. S., Kim, Y.-B., Kim, M. S., and Kim, S. C. (2004). Helix stability confers salt resistance upon helical antimicrobial peptides. *J. Biol. Chem.* 279, 13896–13901. doi: 10.1074/jbc.M311418200
- Piktel, E., Markiewicz, K. H., Wilczewska, A. Z., Daniluk, T., Chmielewska, S., Niemirówicz-Laskowska, K., et al. (2020). Quantification of synergistic effects of Ceragenin CSA-131 combined with iron oxide magnetic nanoparticles against cancer cells. *Int. J. Nanomedicine* 15, 4573–4589. doi: 10.2147/IJN.S255170
- Pollard, J. E., Snarr, J., Chaudhary, V., Jennings, J. D., Shaw, H., Christiansen, B., et al. (2012). In vitro evaluation of the potential for resistance development to ceragenin CSA-13. *J. Antimicrob. Chemother.* 67, 2665–2672. doi: 10.1093/jac/dks276
- Pragman, A. A., Berger, J. P., and Williams, B. J. (2016). Understanding persistent bacterial lung infections: clinical implications informed by the biology of the microbiota and biofilms. *Clin. Pulm. Med.* 23, 57–66. doi: 10.1097/CPM.0000000000000108
- Rossi, L. M., Ranganamy, P., Zhang, J., Qiu, X. Q., and Wu, G. Y. (2008). Research advances in the development of peptide antibiotics. *J. Pharm. Sci.* 97, 1060–1070. doi: 10.1002/jps.21053
- Rothstein, D. M., Spacciopoli, P., Tran, L. T., Xu, T., Roberts, F. D., Dalla Serra, M., et al. (2001). Anticandida activity is retained in P-113, a 12-amino-acid fragment of histatin 5. *Antimicrob. Agents Chemother.* 45, 1367–1373. doi: 10.1128/AAC.45.5.1367-1373.2001
- Saint-Criq, V., and Gray, M. A. (2017). Role of CFTR in epithelial physiology. *Cell. Mol. Life Sci.* 74, 93–115. doi: 10.1007/s00108-016-2391-y
- Sarkar, S. (2020). Release mechanisms and molecular interactions of *Pseudomonas aeruginosa* extracellular DNA. *Appl. Microbiol. Biotechnol.* 104, 6549–6564. doi: 10.1007/s00253-020-10687-9
- Schaupp, L., Addante, A., Völler, M., Fentker, K., Kuppe, A., Bardua, M., et al. (2023). Longitudinal effects of elxacaftor/tezacaftor/ivacaftor on sputum viscoelastic properties, airway infection and inflammation in patients with cystic fibrosis. *Eur. Respir. J.* 62:2202153. doi: 10.1183/13993003.02153-2022
- Sheils, C. A., Käs, J., Travassos, W., Allen, P. G., Janmey, P. A., Wohl, M. E., et al. (1996). Actin filaments mediate DNA fiber formation in chronic inflammatory airway disease. *Am. J. Pathol.* 148, 919–927.
- Simonin, J., Bille, E., Crambert, G., Noel, S., Dreano, E., Edwards, A., et al. (2019). Author correction: airway surface liquid acidification initiates host defense abnormalities in cystic fibrosis. *Sci. Rep.* 9:17535. doi: 10.1038/s41598-019-54253-4
- Sinclair, K., Pham, T., Farnsworth, R., Williams, D., Loc-Carrillo, C., Horne, L., et al. (2012). Development of a broad spectrum polymer-released antimicrobial coating for the prevention of resistant strain bacterial infections. *J. Biomed. Mater. Res. A* 100, 2732–2738. doi: 10.1002/jbm.a.34209
- Smith, J. J., Travis, S. M., Greenberg, E. P., and Welsh, M. J. (1996). Cystic fibrosis airway epithelia fail to kill bacteria because of abnormal airway surface fluid. *Cells* 85, 229–236. doi: 10.1016/S0092-8674(00)81099-5
- Stewart, P. S. (1996). Theoretical aspects of antibiotic diffusion into microbial biofilms. *Antimicrob. Agents Chemother.* 40, 2517–2522. doi: 10.1128/AAC.40.11.2517
- Suprewicz, Ł., Szczepański, A., Lenart, M., Piktel, E., Fiedoruk, K., Barreto-Duran, E., et al. (2023). Ceragenins exhibit antiviral activity against SARS-CoV-2 by increasing the expression and release of type I interferons upon activation of the host's immune response. *Antivir. Res.* 217:105676. doi: 10.1016/j.antiviral.2023.105676

- Tanaka, D., Miyasaki, K., and Lehrer, R. (2000). Sensitivity of *Actinobacillus actinomycetemcomitans* and *Capnocytophaga* spp. to the bactericidal action of LL-37: a cathelicidin found in human leukocytes and epithelium. *Oral Microbiol. Immunol.* 15, 226–231. doi: 10.1034/j.1399-302x.2000.150403.x
- Tang, J. X., Wen, Q., Bennett, A., Kim, B., Sheils, C. A., Bucki, R., et al. (2005). Anionic poly (amino acid)s dissolve F-actin and DNA bundles, enhance DNase activity, and reduce the viscosity of cystic fibrosis sputum. *Am. J. Phys. Lung Cell. Mol. Phys.* 289, L599–L605. doi: 10.1152/ajplung.00061.2005
- Taylor-Cousar, J. L., Robinson, P. D., Shteinberg, M., and Downey, D. G. (2023). CFTR modulator therapy: transforming the landscape of clinical care in cystic fibrosis. *Lancet* 402, 1171–1184. doi: 10.1016/S0140-6736(23)01609-4
- Tokajuk, J., Deptuła, P., Chmielewska, S. J., Skłodowski, K., Mierzejewska, Ż. A., Grądzka-Dahlke, M., et al. (2022). Ceragenin CSA-44 as a means to control the formation of the biofilm on the surface of tooth and composite fillings. *Pathogens* 11:491. doi: 10.3390/pathogens11050491
- Tomás, M., Doumith, M., Warner, M., Turton, J. F., Beceiro, A., and Bou, G. (2010). Efflux pumps, Opr D porin, amp C β -lactamase, and multiresistance in *Pseudomonas aeruginosa* isolates from cystic fibrosis patients. *Antimicrob. Agents Chemother.* 54, 2219–2224. doi: 10.1128/AAC.00816-09
- Tomkiewicz, RP, Kishioka, C., Freeman, J., and Rubin, BK. *DNA and actin filament ultrastructure in cystic fibrosis sputum. Cilia, mucus, and mucociliary interactions* New York: Dekker. (1998): 333–341.
- Turcios, N. L. (2020). Cystic fibrosis lung disease: an overview. *Respir. Care* 65, 233–251. doi: 10.4187/respcare.06697
- Turner, K. H., Wessel, A. K., Palmer, G. C., Murray, J. L., and Whiteley, M. (2015). Essential genome of *Pseudomonas aeruginosa* in cystic fibrosis sputum. *Proc. Natl. Acad. Sci.* 112, 4110–4115. doi: 10.1073/pnas.1419677112
- White, R., Woodward, S., Leppert, M., O'Connell, P., Hoff, M., Herbst, J., et al. (1985). A closely linked genetic marker for cystic fibrosis. *Nature* 318, 382–384. doi: 10.1038/318382a0
- Wu, M., Maier, E., Benz, R., and Hancock, R. E. (1999). Mechanism of interaction of different classes of cationic antimicrobial peptides with planar bilayers and with the cytoplasmic membrane of *Escherichia coli*. *Biochemistry* 38, 7235–7242. doi: 10.1021/bi9826299
- Yagel, Y., Sestito, S., Motro, Y., Shnaiderman-Torban, A., Khalfin, B., Sagi, O., et al. (2020). Genomic characterization of antimicrobial resistance, virulence, and phylogeny of the genus *Ochrobactrum*. *Antibiotics* 9:177. doi: 10.3390/antibiotics9040177
- Zabner, J., Smith, J. J., Karp, P. H., Widdicombe, J. H., and Welsh, M. J. (1998). Loss of CFTR chloride channels alters salt absorption by cystic fibrosis airway epithelia in vitro. *Mol. Cell* 2, 397–403. doi: 10.1016/S1097-2765(00)80284-1
- Zampoli, M., Morrow, B., and Paul, G. (2023). Real-world disparities and ethical considerations with access to CFTR modulator drugs: mind the gap! *Front. Pharmacol.* 14:1163391. doi: 10.3389/fphar.2023.1163391



OPEN ACCESS

EDITED BY

Octavio Luiz Franco,
Catholic University of Brasilia (UCB), Brazil

REVIEWED BY

Shabir A. Bhat,
University of California, Los Angeles,
United States
Axel Hollmann,
National Scientific and Technical Research
Council (CONICET), Argentina

*CORRESPONDENCE

Ricardo Pinheiro de Souza Oliveira
✉ rpsolive@usp.br

[†]These authors have contributed equally to this work

RECEIVED 11 October 2023

ACCEPTED 17 November 2023

PUBLISHED 14 December 2023

CITATION

Bermúdez-Puga S, Dias M, Freire de Oliveira T, Mendonça CMN, Yokomizo de Almeida SR, Rozas EE, do Nascimento CAO, Mendes MA, Oliveira De Souza de Azevedo P, Almeida JR, Proaño-Bolaños C and Oliveira RPDs (2023) Dual antibacterial mechanism of [K4K15]CZS-1 against *Salmonella* Typhimurium: a membrane active and intracellular-targeting antimicrobial peptide. *Front. Microbiol.* 14:1320154. doi: 10.3389/fmicb.2023.1320154

COPYRIGHT

© 2023 Bermúdez-Puga, Dias, Freire de Oliveira, Mendonça, Yokomizo de Almeida, Rozas, do Nascimento, Mendes, Oliveira De Souza de Azevedo, Almeida, Proaño-Bolaños and Oliveira. This is an open-access article distributed under the terms of the [Creative Commons Attribution License \(CC BY\)](https://creativecommons.org/licenses/by/4.0/). The use, distribution or reproduction in other forums is permitted, provided the original author(s) and the copyright owner(s) are credited and that the original publication in this journal is cited, in accordance with accepted academic practice. No use, distribution or reproduction is permitted which does not comply with these terms.

Dual antibacterial mechanism of [K4K15]CZS-1 against *Salmonella* Typhimurium: a membrane active and intracellular-targeting antimicrobial peptide

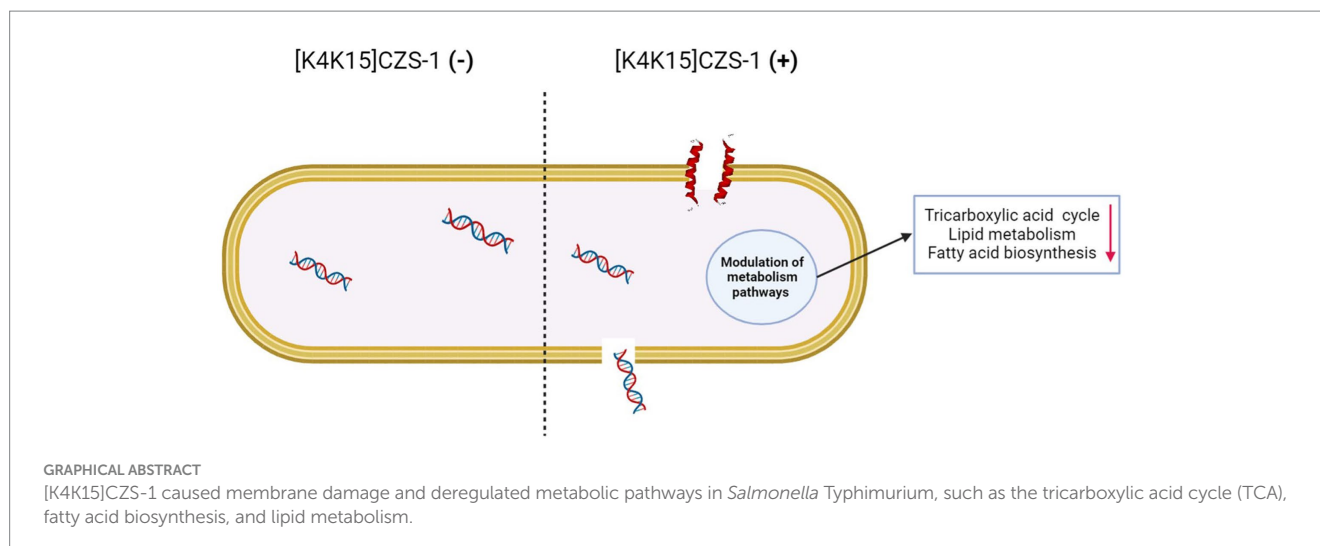
Sebastián Bermúdez-Puga^{1†}, Meriellen Dias^{1†}, Taciana Freire de Oliveira¹, Carlos Miguel Nóbrega Mendonça¹, Sonia Regina Yokomizo de Almeida², Enrique Eduardo Rozas³, Claudio Augusto Oller do Nascimento³, Maria Anita Mendes³, Pamela Oliveira De Souza de Azevedo¹, José R. Almeida^{4,5}, Carolina Proaño-Bolaños⁴ and Ricardo Pinheiro de Souza Oliveira^{1*}

¹Microbial Biomolecules Laboratory, Faculty of Pharmaceutical Sciences, University of São Paulo, São Paulo, Brazil, ²Department of Anatomy, Biomedical Sciences Institute, University of São Paulo, São Paulo, Brazil, ³Dempster MS Lab, Chemical Engineering Department of Polytechnic School of University of São Paulo, São Paulo, Brazil, ⁴Biomolecules Discovery Group, Universidad Regional Amazónica Ikiam, Tena, Napo, Ecuador, ⁵School of Pharmacy, University of Reading, Reading, United Kingdom

Salmonella genus is a leading cause of food-borne infections with strong public health impact and economic ramifications. The development of antimicrobial resistance added complexity to this scenario and turned the antibiotic drug discovery into a highly important challenge. The screening of peptides has served as a successful discovery platform to design new antibiotic candidates. Motivated by this, the antimicrobial and cytotoxic properties of three cruzioseptins against *Salmonella* Typhimurium and RAW 264.7 murine macrophage cells, respectively, were investigated. [K4K15]CZS-1 was the most potent antimicrobial peptide identified in the screening step with a minimum inhibitory concentration (MIC) of 16 µg/mL (7.26 µM) and moderate cytotoxicity. From a structural point of view, *in vitro* and *in silico* techniques evidenced that [K4K15]CZS-1 is a α -helical cationic antimicrobial peptide. In order to capture mechanistic details and fully decipher their antibacterial action, we adopted a multidimensional approach, including spectroscopy, electron microscopy and omics analysis. In general lines, [K4K15]CZS-1 caused membrane damage, intracellular alterations in *Salmonella* and modulated metabolic pathways, such as the tricarboxylic acid (TCA) cycle, fatty acid biosynthesis, and lipid metabolism. Overall, these findings provide deeper insights into the antibacterial properties and multidimensional mode of action of [K4K15]CZS-1 against *Salmonella* Typhimurium. In summary, this study represents a first step toward the screening of membrane-acting and intracellular-targeting peptides as potential bio-preservatives to prevent foodborne outbreaks caused by *Salmonella*.

KEYWORDS

antimicrobial peptides, cruzioseptin, mechanism of action, metabolomics, membranolytic effect



1 Introduction

Foodborne diseases constitute a major problem due to the millions of infections and thousands of deaths generated every year. *Salmonella* spp., *Campylobacter* spp., and *Listeria* spp. are some of the bacterial pathogens involved in this global threat to food safety and human health (Gutiérrez-Del-Río et al., 2018). Several studies have pointed out that *Salmonella enterica* subsp. *enterica* serovar Typhimurium (*S. Typhimurium*) is the most common etiological agent of food-poisoning outbreaks caused by this genus (Gordon et al., 2008; Xia et al., 2015). *Salmonella* contamination can drastically affect the production chain and survive for extended periods in low-moisture conditions due to simple nutritional requirements (Sánchez-Maldonado et al., 2018; Finger et al., 2019; Ehuwa et al., 2021).

To date, traditional antibiotics and antibacterial physical treatments have been widely used to inhibit microbial growth and increase the shelf-life of food (Rai et al., 2016; Adaro et al., 2023). However, the prolonged use of antibiotics have been associated with the emergence of multi-resistant microorganisms, representing a serious public and life-threatening health problem (Ehuwa et al., 2021; Moretta et al., 2021). As a result, a roadmap to tackle this challenge must include the discovery of antimicrobial chemical scaffolds that are less susceptible to bacterial resistance and compatible with safety and quality of food.

Antimicrobial peptides (AMPs) have been becoming attractive lead compounds in ambitious programs to produce the next-generation of antibiotics for application in the food industry (Lima et al., 2021). AMPs combine several better properties compared to conventional chemical preservatives, such as high antimicrobial potency, low propensity to develop bacterial resistance, low toxicity, broad-spectrum of antimicrobial activity, and multiple mode of action (Benfield and Henriques, 2020; Li et al., 2021). An example of peptides candidates are cruzioseptins, a frog AMP family isolated from *Cruziophyla calcarifer* (Proaño-Bolaños et al., 2016). These multifunctional short molecules have shown antibacterial, antifungal, and antiprotozoal properties (Proaño-Bolaños et al., 2016; Mendes et al., 2020; Cuesta et al., 2021). Their sequences have been employed as a template to generate more active and selective cruzioseptin analogs. Fine-tuning cruzioseptins led to the identification of a potent

antibacterial peptide named [K4K15]CZS-1 with reduced toxicity (Bermúdez-Puga et al., 2023). The antimicrobial mechanism of natural and engineered cruzioseptins on *Staphylococcus aureus*, *Escherichia coli*, and *Leishmania* spp. seems to involve the electrostatic interaction and consequently disrupting of cell membrane (Mendes et al., 2020; Valdivieso-Rivera et al., 2022; Bermúdez-Puga et al., 2023).

Many studies have focused on the membranolytic action of peptides on pathogens associated nosocomial hospital-acquired infections. A limited number of studies have explored the effect of peptide candidates on bacteria causing food poisoning and their mode of action from a multidimensional perspective. It is crucial to clarify in depth how AMPs works to avoid the resistance in microbial pathogens and bring them from screening step to the point of therapeutic use (Benfield and Henriques, 2020; Li et al., 2021). Traditionally, electron microscopy have been widely employed to visualize the membrane-damaging activities of peptides. In line with this, modern technologies, such as the metabolomics constitute valuable analytical tools to build a comprehensive understanding of biochemical alterations in pathogens after AMP exposure. However, there are few examples of integrative efforts combining different strategies to explore this mechanistic scenario (Bo et al., 2014; Sun et al., 2023). Based on this, the aim of this work was to expand the current understanding of the potential applications of CZS-9, CZS12, [K4K15]CZS-1, by examining the activities against *S. Typhimurium* and RAW 264.7 murine macrophage cells. In addition, the mechanisms underlying the antimicrobial properties were investigated integrating electron microscopy and metabolomics approaches.

2 Materials and methods

2.1 Solid-phase peptide synthesis

Three peptides CZS-9: GFLDVITHVGVKAVGKAALNAV N EMVNQ-NH₂, CZS-12: GFLDVVKHVGKAVGKAALNAVNDLV N Q-NH₂, and [K4K15]CZS-1: GFLKIVKGVGVKALKAVSKLF-NH₂ were synthesized by solid-phase peptide synthesis using the Fmoc chemistry in a Liberty Blue automated microwave peptide synthesizer (CEM Corporation). Fmoc Rink Amide (LL) (CEM Corporation,

USA) was used as the solid resin support, N, N'-dimethylformamide was utilized as the main solvent for the synthesis, and diisopropylcarbodiimide/Oxyma base was employed as an activator of amino acids during the coupling process. Fmoc protector groups were removed with piperidine 20%. While an acidic cocktail containing trifluoroacetic acid (TFA) 92.5%, triisopropyl silane 2.5%, 3,6-dioxa-1,8-octanedithiol 2.5%, and water 2.5%, was used to cleave the peptide product from the resin and to remove the protector groups from the side chains of amino acids. Crude peptides were washed and precipitated with cold diethyl ether. Finally, the synthesized peptides were freeze-dried in vacuum conditions at -80°C at a pressure of 0.09 mT and stored at -20°C .

2.2 Characterization and purification of synthetic peptides

The purity of crude peptides was assessed by reverse-phase high performance liquid chromatography (RP-HPLC) equipped with a two-pump chromatograph (Agilent Technologies) coupled to a C18 analytical column ($250 \times 4.6 \text{ mm}$, $5 \mu\text{m}$) and a UV-VIS detector at 220 nm. In brief, 1 mg of peptide was dissolved in 200 μL of water/TFA solution (99.9/0.1 v/v). Peptides were eluted by applying a gradient linear system from 99% mobile phase A (99.9% water/0.1% TFA) to 99% mobile phase B (99.9% acetonitrile/0.1% TFA) at a flow rate of 1 mL/min for 55 min. Additionally, the molecular mass of peptides was corroborated by matrix-assisted laser ionization/desorption time-of-flight mass spectrometry (MALDI-TOF MS) (Bruker Daltonics).

Crude peptides that did not present a purity $>80\%$ were purified by RP-HPLC using a two-pump chromatograph (Agilent technologies) coupled to a C18 analytical column ($50 \times 21.2 \text{ mm}$, $5 \mu\text{m}$) and a UV-VIS detector at 220 nm. In summary, 15 mg of peptides were dissolved in 800 μL water/TFA solution (99.9/0.1 v/v) and filtered through a $0.22 \mu\text{m}$ membrane filter. The sample was injected at a flow rate of 2.5 mL/min for 10 min with a linear gradient from 53% mobile phase A to 53% mobile phase B. The purified peptide was lyophilized, and the analysis of purity was evaluated using the methodology mentioned above.

2.3 Determination of secondary structures of AMPs by circular dichroism (CD)

The secondary structure of AMPs in different environments was determined on a Jasco J-720 spectropolarimeter (Jasco, Tokyo, Japan) at 25°C using a 2 mm path-length rectangular quartz cell and baseline corrected using proper control. For this assay, peptides, with a purity of $>90\%$, were dissolved in deionized water at pH 7 (mimicking the aqueous environment) or 30 mM SDS micelles (mimicking a prokaryotic cell membrane with a negative charge) at final concentration of 0.1 mg/mL (CZS-9: 0.42 mM, CZS-12: 0.38 mM, [K4K15]CZS-1: 0.45 mM). The spectra were recorded between 190 and 260 nm using the following parameters: 20 nm/min scan speed, 0.2 nm data pitch, 1 s response time, 1 nm band width, and 3 accumulations. The acquired circular dichroism (CD) signal spectra were then converted to mean residue ellipticity with the following equation:

$$\theta_M = \frac{\theta_{abs}}{c * l * n}$$

where θ_M is the mean residue ellipticity ($\text{deg} \cdot \text{cm}^2 \cdot \text{dmol}^{-1}$), θ_{abs} is the observed ellipticity corrected for the buffer at a given wavelength (mdeg), c is the peptide concentration (mM), l is the path length (mm), and n is the number of amino acids.

2.4 Prediction of physicochemical properties and three-dimensional structures of peptides

The HELIQUEST server was used to predict the physicochemical properties and the helical wheel diagram of peptides (Gautier et al., 2008). The theoretical mass was calculated by the Bachem Peptide Calculator.¹ In addition, the three-dimensional structure of peptides was obtained using the I-TASSER server (Roy et al., 2010) and the models were visualized with BIOVIA Discovery Studio v.4.5 (BIOVIA, San Diego, CA, USA).

2.5 Minimum inhibitory concentration (MIC) and minimum bactericidal concentration (MBC) assays

The MIC and MBC of AMPs was determined against *Salmonella enterica* subsp. *enterica* serovar Typhimurium, following the protocol by Proaño-Bolaños et al. (2016) with minor modifications. In summary, different peptide concentrations (1–512 $\mu\text{g/mL}$) were prepared by serial dilution with dimethyl sulfoxide (DMSO). Pathogenic bacterium was grown in Brain Heart Infusion (BHI) medium at 37°C until to reach the concentration of 1×10^6 UFC/mL. Subsequently, the bacterial suspension was mixed with the peptide dilutions and were transferred to a 96 well sterile microplate. A DMSO solution instead of peptide and BHI medium without bacteria were included as controls. The microplates were incubated at 37°C for 18 h. After the incubation time, the absorbance was measured at 600 nm using a microplate reader (Synergy HTX, Biotek). The MIC value was determined as the minimal concentration that did not show bacterial growth in the measurement by optical density. Finally, 10 μL of each concentration without bacterial growth was subcultured on BHI agar (1% v/v) plates and incubated at 37°C overnight. MBC value was defined as the lowest peptide concentration without any bacterial growth occurrence.

2.6 Cell-based assay for assessing the peptide toxicity

RAW-264.7 macrophage cell line was grown in Dulbecco's Modified Eagle Medium – high glucose (DMEM) (Thermo Fisher Scientific) supplemented with 10% fetal bovine serum (FBS) (Thermo

¹ Retrieved from: <https://www.bachem.com/knowledge-center/peptide-calculator/>, 5 July 2023.

Fischer Scientific) and 1% antibiotic-antimycotic solution (Thermo Fisher Scientific) and then incubated at 37°C under humidified conditions in a 5% CO₂ atmosphere after cells reached 70–80% confluency. The growth medium was refreshed every 2–3 days. The cells were washed twice with phosphate buffer saline (PBS) and harvested using 0.25% trypsin–EDTA (Sigma-Aldrich Corporation, St. Louis, MO, USA).

For cytotoxicity evaluation, cells were plated in 96-well plates (100 µL/well) at a density of 2×10⁴ cells/mL and incubated for 24 h at 37°C in 5% CO₂. Subsequently, the medium was removed from the plate, and the adherent cells were incubated with 90 µL of cell culture media and 10 µL of pure peptide (1 µg/mL to 512 µg/mL). The plates were incubated for 24 h at 37°C in 5% CO₂, and after incubation, 100 µL of 3-(4,5-dimethylthiazol-2-yl)-2,5-diphenyl tetrazolium bromide (MTT) solution (5 mg/mL) (Sigma-Aldrich Corporation, St. Louis, MO, USA) were added to each well. The plates were further incubated at 37°C in 5% CO₂ for 3 h. Afterwards, the medium was removed and formazan crystals were dissolved with 100 µL of DMSO. The absorbance was measured at 540 nm and the percentages of viable cells were calculated:

$$\%Cell\ viability = \frac{Mean\ Optical\ density\ treated}{Mean\ Optical\ density\ untreated} \times 100$$

Cells treated with Triton x-100 (0.1% v/v) and DMEM medium with 1% DMSO (v/v) were used as positive and negative controls, respectively. Five replicates were made for each AMPs sample.

2.7 Measurement of release nucleic acids

To evaluate if the bacterial membrane is compromised by the [K4K15]CZS-1 effect, a nucleic acid release assay was employed according to Tang et al. (2008) with minor modifications. Briefly, *Salmonella* Typhimurium was growing exponentially on BHI at 37°C until reaching an optical density (OD) of 0.4. The bacterial suspension (1×10⁸ UFC/mL) was washed twice and resuspended with PBS. The pathogenic bacteria were incubated at 37°C for 2 h with the peptide at a final concentration of 1 xMIC, 2 xMIC, and 4 xMIC. As a negative control, bacteria were incubated with PBS 1X. Subsequently, samples were filtered using 0.22 µm syringe filters to remove the bacterial cells. Finally, the supernatant was measured at 260 nm using a microplate reader (Synergy HTX, Biotek).

2.8 Scanning electron microscopy

The morphological changes of the bacterial membrane after treatment with [K4K15]CZS-1 were observed under scanning electron microscopy (SEM). *Salmonella* Typhimurium was grown in BHI at 37°C to mid-logarithmic phase. Later, the bacterial pellet was harvested by centrifugation at 4000 rpm for 10 min, washed with PBS 1X for two times, and resuspended in PBS 1X. Bacterial cells were incubated at 37°C for 2 h with 4 xMIC of [K4K15]CZS-1. Subsequently, cells were fixed with 2.5% (v/v) glutaraldehyde at 4°C overnight. The bacteria cells were washed twice with PBS to remove the glutaraldehyde and dehydrated with a graded ethanol series (50, 70, 90, and 100% ethanol) at each dilution for 10 min. The same procedure was repeated for the control, however, bacterial cells were not

incubated with the peptide. Finally, all the samples were transferred to a coverslip, left to dry at room temperature for 1 h, and coated 10 s with gold. It was visualized under a scanning electron microscope with 15 kV resolution (LEO 435VP).

2.9 Transmission electron microscopy

The intracellular alterations and changes in structural integrity of *S. Typhimurium* were investigated under transmission electron microscopy (TEM). In summary, the pretreatment of bacterial cells was under the same conditions described for the SEM assay. After pre-fixation with 2.5% glutaraldehyde, the bacterial pellet was washed twice with PBS and subsequently post-fixed with 2% osmium tetroxide in PBS for 2 h. The bacterial cells were washed twice with PBS and dehydrated in a graded ethanol series (50, 70, 90, and 100% for 8 min in each step) and incubated in 100% ethanol (10 min), a 1:1 mixture of 100% ethanol and acetone (10 min), and pure acetone (10 min). The samples were immersed in a mixture of absolute acetone and epoxy resin (1:1) for 30 min and pure epoxy resin overnight. Finally, an ultramicrotome was used to cut ultrathin slices, which were then stained with uranyl acetate and lead citrate. Samples were examined using a transmission electron microscope (Morgagni 268D).

2.10 Metabolomics analysis of *Salmonella* Typhimurium treated with [K4K15]CZS-1

Perturbations in the intracellular metabolite profiling of bacterial cells induced by [K4K15]CZS-1 was analyzed by gas chromatography coupled with a mass spectrometer (GC–MS). To this end, *S. Typhimurium* cells were grown in the presence (0.5 and 1 xMIC) or absence of the peptide [K4K15]CZS-1 for 18 h. After the incubation period, the bacterial pellet was harvested by centrifugation at 4000 rpm for 10 min and then washed twice with PBS 1X. Later, the bacterial pellet was dried in a vacuum concentrator. The intracellular metabolites were extracted using 1 mL of methanol, followed by a shake for 30 s, a sonication process for 15 min, and finally drying in a vacuum centrifuge. Three biological replicates were performed for each sample.

The derivatization process was carried out by adding 100 µL of a solution with proportions of N-methyl-N-(trimethylsilyl) trifluoroacetamide (50%) and a solvent mixture: acetonitrile/dichloromethane/cyclohexane (5:4:1) and 5% trimethylamine (50%). The samples were agitated for 30 s and were placed in a 60°C thermal bath for 1 h. Following that, the samples were centrifuged for 2 min at 12,000 g. GC–MS was used to analyze the supernatant.

2.11 Secretome analysis of *Salmonella* Typhimurium treated with [K4K15]CZS-1

Alterations in the extracellular metabolite profiling of *S. Typhimurium* incubated with or without [K4K15]CZS-1 were studied by GC–MS. In this assay, the cell-free supernatant (CFS) of *S. Typhimurium* incubated with (0.5 and 1 xMIC of [K4K15]CZS-1 for 18 h) or without peptides was dried in a vacuum concentrator. Later, extracellular metabolites present in the CFS were obtained by

adding 300 μ L of methanol and agitating it for 2 min. The sample was then dried in the vacuum centrifuge. Three biological replicates were performed for each sample. Finally, the derivatization was performed according to the methodology described previously, and the metabolites were analyzed using GC–MS.

2.12 Identification of metabolites by GC–MS

Analysis was performed by a GS-MS system (Shimadzu TQ-8050). Two μ L of sample was injected with a split ratio of 1:10. Helium was used as a carrier gas at a constant flow rate of 1 mL/min. The GCMSsolution Smart MRM version 4.2. GC–MS analysis was utilized, and the running time of each sample was 67 min. The injection, interface, and ionization source temperatures were 280°C, 280°C, and 250°C, respectively. The initial temperature was set to 100°C, then raised to 320°C in a linear ramp of 4°C/min, and finally maintained at 320°C for 8 min. The mass fingerprints of 568 compounds are included in the Shimadzu Smart Metabolites Database: metabolites identified if their scanned ion pairs are 80% compatible with the database.

2.13 Data analysis

2.13.1 Omics analysis

The GC–MS/MS data were analyzed using Web-based MetaboAnalyst 5.0 free software (updated and maintained by the Xia Lab at McGill University). The metabolite relative abundances were submitted to multivariate statistical analyses, such as principal component analysis (PCA) and partial least squares discriminant analysis (PLS-DA), which were performed with MetaboAnalyst 5.0 free software. Additionally, differentially expressed metabolites were detected by a student's *t*-test with a *p* value of less than 0.05 and the main metabolites were shown using a hierarchical cluster graph. The determination of stress indicators (Biomarker meta-analysis) was carried out using the meta-analysis approach based on the combination of the *p*-values. The identified metabolites, with mean local confidence scores $\geq 80\%$, were compared in the KEGG PATHWAY database.

2.13.2 Statistical analysis

GraphPad Prism 8.0 software (GraphPad Software Inc., San Diego, CA, USA) was used for statistical analysis. The acquired data were reported as mean \pm standard deviation and evaluated using

analysis of variance (ANOVA), followed by post-hoc Tukey multiple comparison. *p* < 0.05 was considered as significant.

3 Results

3.1 Sequence analysis and physicochemical properties of AMPs

Two cruzioseptins, CZS-9 and CZS-12, isolated from the skin secretion of *Cruziophylla calcarifer*, and a cruzioseptin analog, [K4K15] CZS-1, were selected for this study (Table 1). Natural cruzioseptins present a high degree of identity in the primary structure, and both peptides have a length of 27 amino acids. However, the net charge varies on CZS-9 and CZS-12, with values of +1 and +2, respectively. On the other hand, [K4K15]CZS-1 has a net charge of +6, a length of 21 amino acids, and higher hydrophobicity than other cruzioseptins.

3.2 Synthesis, characterization, and purification of AMPs

The synthetic AMPs presented a purity of 82.37% for CZS-9, 89.92% for CZS-12, and 64.48% for [K4K15]CZS-1 (Supplementary Figure S1). Subsequently, a purification step of [K4K15]CZS-1 was performed and its analysis by RP-HPLC indicated a 94.48% purity. Additionally, the expected molecular weight of these three peptides is in accordance with the theoretical mass, confirming their chemical identities (Supplementary Figure S1; Table 1).

3.3 Secondary structures and *in silico* three dimensional structures

In silico tools were used to obtain the helical wheel projection and the three-dimensional structures of all AMPs (Figure 1). According to HELIQUEST and I-TASSER analysis, all three peptides tended to form an α -helix with an amphipathic structure. In addition, the secondary structure of AMPs in the presence of aqueous solution or 30 mM SDS micelles was investigated by CD spectroscopy (Figure 1). All peptides display a random coil structure in aqueous solution, as indicated by the appearance of a negative peak near at 200 nm. On the other hand, all peptides form an α -helix in the SDS micelles, which is determined by the two negative bands at 208 and 222 nm and one positive band at 192 nm.

TABLE 1 Primary sequences of cruzioseptins and their predicted physicochemical properties.

AMPs	Sequence	Theoretical mass (Da)	Hydrofobicity	Net charge	Length (aa)	Reference
CZS-9	GFLDVITHVGKAVGKAALNAVNMVNQ-NH ₂	2795.26	0.393	1	27	Proaño-Bolaños et al. (2016)
CZS-12	GFLDVVKHVKGKAVGKAALNAVNDLVNQ-NH ₂	2776.22	0.335	2	27	Proaño-Bolaños et al. (2016)
[K4K15] CZS-1	GFLKIVKGVGKVALKAVSKLF-NH ₂	2201.8	0.523	6	21	Bermúdez-Puga et al. (2023)

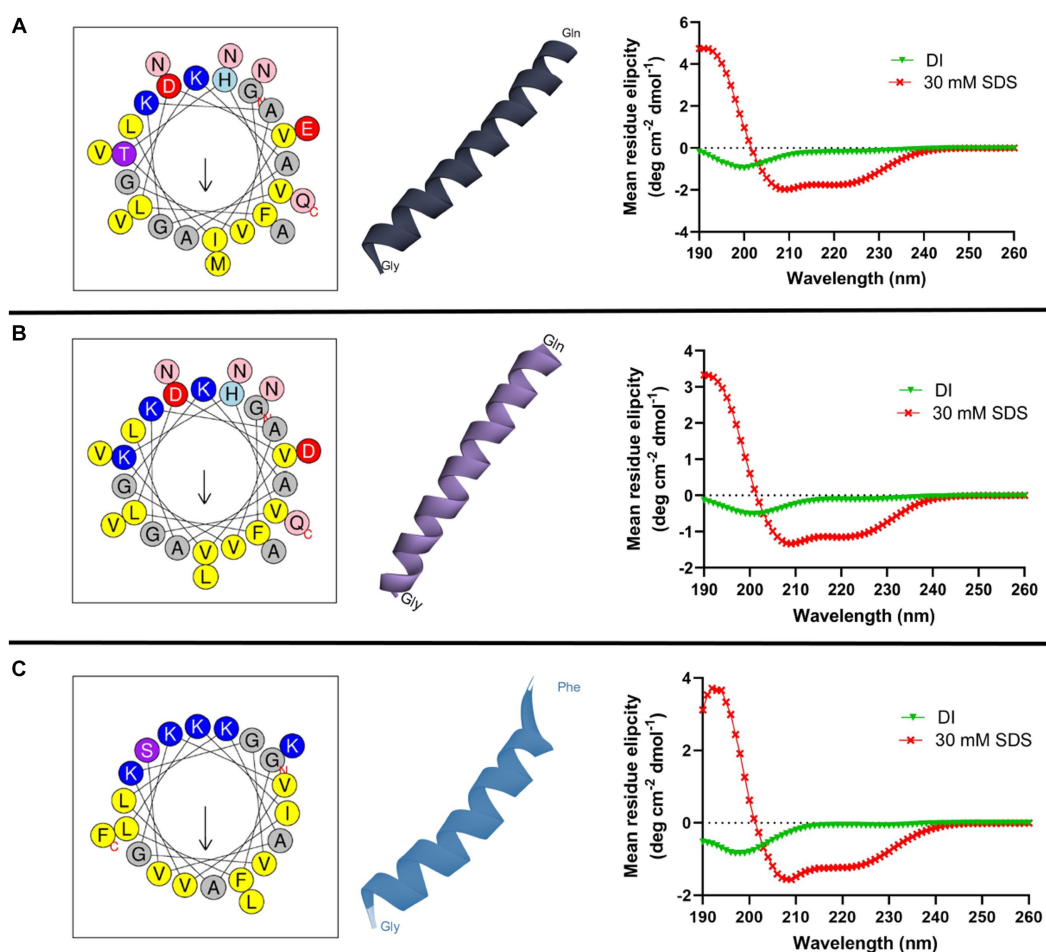


FIGURE 1

Helical wheel diagram, three-dimensional structure, and circular dichroism spectra of cruzioseptins: (A) CZS-9, (B) CZS-12, and (C) [K4K15]CZS-1. In the helical wheel plot, non-polar residues are shown in yellow, polar residues in purple, basic residues in blue/blue light, and acid residues in red. Uncharged residues such as alanine and glycine are in gray, while asparagine and glutamine are in pink. The secondary structure of peptides was investigated in deionized water (DI) and 30 mM SDS micelles. All peptides showed a random coil structure and a α -helix structure in an aqueous solution and an SDS solution, respectively.

3.4 Antibacterial and cytotoxic activity of cruzioseptins

The antibacterial effect of the three peptides against *S. Typhimurium* was evaluated and summarized in Table 2. CZS-9 has no antibacterial activity against *S. Typhimurium*. CZS-12 was only active at the highest concentration tested. Whereas, the engineered peptide, [K4K15]CZS-1, was highly active with a MIC value of 7.26 μ M. On the other hand, the MBC value of [K4K15]CZS-1 showed a 2 fold increase in comparison with the MIC values.

The cytotoxicity profiles of these peptides against RAW 264.7 murine macrophage cells were also evaluated after 24 h of incubation using the same concentrations used for MIC assays. The most promising peptide of this study, [K4K15]CZS-1, showed a cytotoxic effect at the MIC concentration (16 μ g/mL), with a cell viability percentage of 57.8% (Figure 2). On the other hand, CZS-9 displayed higher toxicity at the highest peptide concentrations (256–512 μ g/mL) compared to CZS-12. Given the high antimicrobial activity and moderate toxicity of [K4K15]CZS-1 compared to the other

cruzioseptins, this peptide was chosen to perform electron microscopy assays and metabolomics studies to elucidate its full ranges of action against *S. Typhimurium*.

3.5 Membranolytic effect of [K4K15]CZS-1

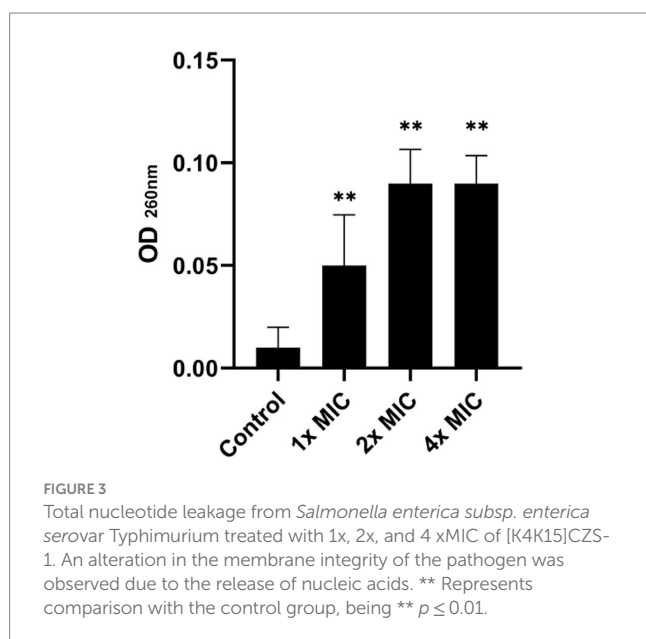
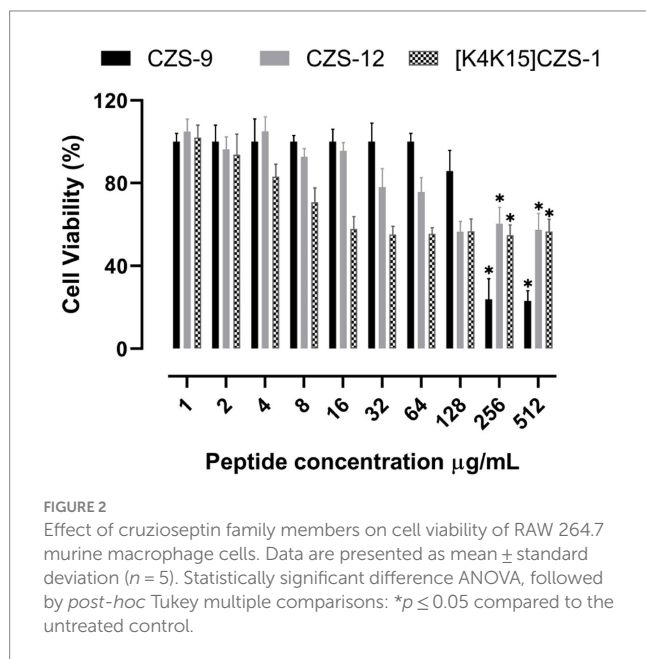
The bacterial membrane is the primary target in the mechanism of action of most antimicrobial peptides. In this sense, the release of nucleic acids is considered a good biomarker to evaluate the integrity of the cell membrane, which can be easily monitored through absorbance at 260 nm. As depicted in Figure 3, the nucleic acid leakage assay showed a release of DNA/RNA in a dose-dependent manner. This indicates that the cell membrane of *S. Typhimurium* was compromised by exposure to the [K4K15]CZS-1 treatment.

To corroborate the result above, SEM was performed to visualize the effect of the peptide [K4K15]CZS-1 (4 xMIC) on bacterial membranes. As shown in Figures 4B,C, the morphology of peptide-treated *S. Typhimurium* cells resulted in membrane roughening,

TABLE 2 Minimum inhibitory concentration (MIC) and minimum bactericidal concentration (MBC) of cruzioseptin family members.

Strain	MIC $\mu\text{g/mL}$ (μM)		
	CZS-9	CZS-12	[K4K15]CZS-1
<i>Salmonella enterica subsp. enterica</i> serovar Typhimurium	>512 (>183.17)	512 (184.42)	16 (7.26)

Strain	MBC $\mu\text{g/mL}$ (μM)		
	CZS-9	CZS-12	[K4K15]CZS-1
<i>Salmonella enterica subsp. enterica</i> serovar Typhimurium	>512 (>183.17)	>512 (>184.42)	64 (29.04)



corrugation, and cell lysis. On the contrary, a normal shape and smooth surface were observed on the bacterial cells without peptide treatment (Figure 4A).

Likewise, the membrane integrity and alterations in the intracellular content of *Salmonella* before and after peptide treatment were observed using TEM. In Figure 4D, the intact membrane structure and uniform intracellular contents of untreated bacteria are displayed. While *S. Typhimurium* cells after peptide treatment showed a condensed cytoplasmic content and significant changes in the membrane morphology of the bacteria (Figures 4E,F). For instance, TEM images indicated deterioration of cell membranes, cell swelling, and vacuoles composition.

3.6 Effect of [K4K15]CZS-1 treatment on intracellular and extracellular metabolite profiles of *Salmonella Typhimurium*

3.6.1 Metabolome analysis

The GC-MS results revealed that the quantities of metabolites were higher in *S. Typhimurium* treated with 1.0 xMIC of [K4K15]CZS-1 (Figure 5A). However, when treated with 0.5 xMIC, *S. Typhimurium* showed no differences compared to the control group. The treated group exhibited a remarkable 74.7% difference in metabolites compared to the control group, with metabolite quantities being three times higher than those detected in the untreated *S. Typhimurium* cells. On the other hand, only 20 metabolites were shared between the control and the highest concentration (1 xMIC) of the treatment. The relationship between the control and 1.0 xMIC of [K4K15]CZS-1 treated samples can be observed in the PCA plot depicting PC1/PC2 scores (Figure 5B).

For the hierarchical cluster analysis (HCA), a multivariate data analysis was also done through an ANOVA. Based on this, the HCA result is consistent with the PCA analysis, corroborating a similar pattern clustering. In addition, the 25 most significant metabolites were categorized based on their compound type and their position in the metabolic pathway. These categories include amino acids, membrane structure-related compounds, carbohydrates, and alcohols (Figure 6). Among 25 differential metabolites, 6 of them were up-regulated, such as 1,6-Anhydroglucose, 3-Hydroxybutyric acid, 2-Hydroxyisovaleric, norvaline, putrescine, and trehalose, in the treatment with 1 xMIC [K4K15]CZS-1.

The other 19 metabolites were down-regulated, which include several organic acids, fatty acids, carbohydrates, and amino acids. On the other hand, the KEGG enrichment analysis was made to get more information about the metabolic pathway for each differential metabolite (Figure 6). For instance, the up-regulated 1,6-Anhydroglucose and trehalose are related to carbohydrate metabolism. Succinic acid and fumaric acid, two down-regulated

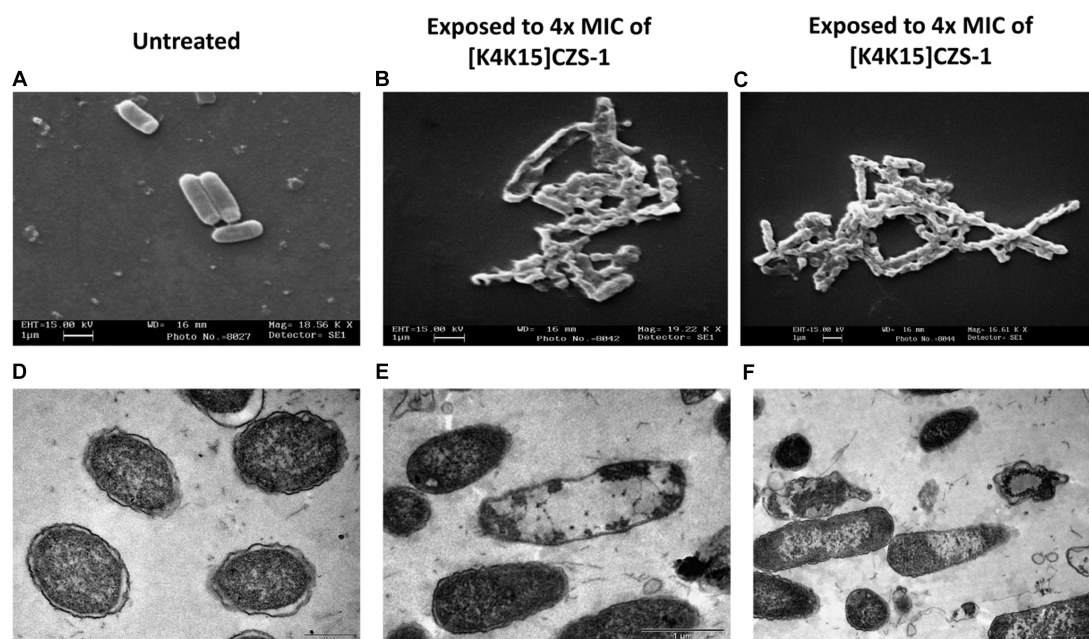


FIGURE 4

Morphological changes and intracellular alterations in *Salmonella enterica subsp. enterica serovar Typhimurium* exposed to 4 xMIC of [K4K15]CZS-1 was observed by scanning electron microscopy (SEM) and transmission electron microscopy (TEM). SEM micrographs of *S. Typhimurium*: (A) no peptide treatment (control) and (B,C) [K4K15]CZS-1-treated cells. TEM images of *S. Typhimurium*: (D) untreated cells (control), (E,F) [K4K15]CZS-1-treated bacterial cells. The scale bar value for (A–E) is 1 µm, while for (D) it is 0.5 µm.

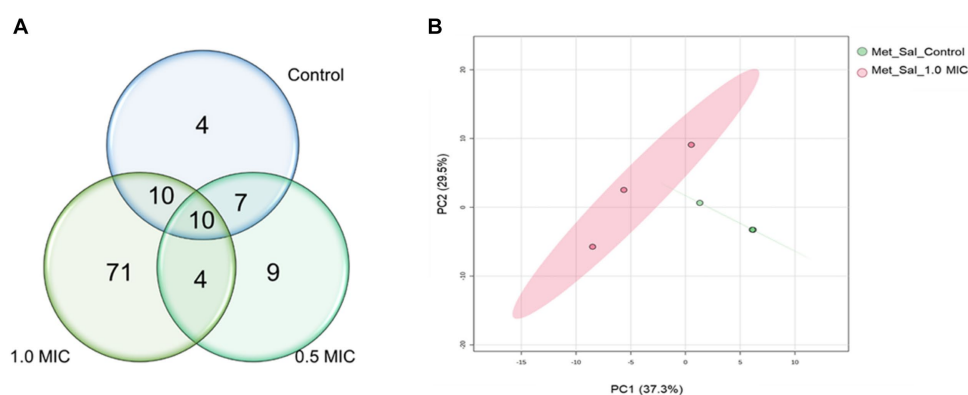


FIGURE 5

Venn diagram and PCA analysis of intracellular metabolites identified in the samples of *Salmonella enterica subsp. enterica serovar Typhimurium* incubated with [K4K15]CZS-1: (A) Venn diagram shows the total of intracellular metabolites of control and [K4K15]CZS-1-treated bacterial cells; and (B) the metabolome PCA analysis of *S. Typhimurium* between the control group and treated group with 1.0 xMIC of [K4K15]CZS-1.

metabolites, are intermediates of the tricarboxylic acid (TCA) cycle. While trehalose and lactic acid are associated with cellular stress. The obtained results from the metabolic profiling, which include the identification of significant metabolites with their corresponding fold change trends, were further correlated with the heat map distribution.

3.6.2 Secretome analysis

The effect of [K4K15]CZS-1 on the secretome of *S. Typhimurium* was also evaluated through a metabolomic study by GC-MS. Therefore, the metabolites excreted into the extracellular space

were analyzed. A total of 88, 74, and 40 metabolites were identified in the control group and in the both peptide treatments (0.5 xMIC and 1 xMIC), respectively (Figure 7A). In this sense, bacteria incubated with AMP suffered a 54.5% reduction in the production of extracellular metabolites.

A multivariate data analysis was performed to visualize the group separation and identify the changes in the extracellular metabolite profile. In fact, there is no significant variation in the metabolite profile induced by 0.5x MIC treatment. Therefore, this data was removed for the subsequent analysis. A PCA analysis of the extracellular metabolites was performed with *S. Typhimurium*

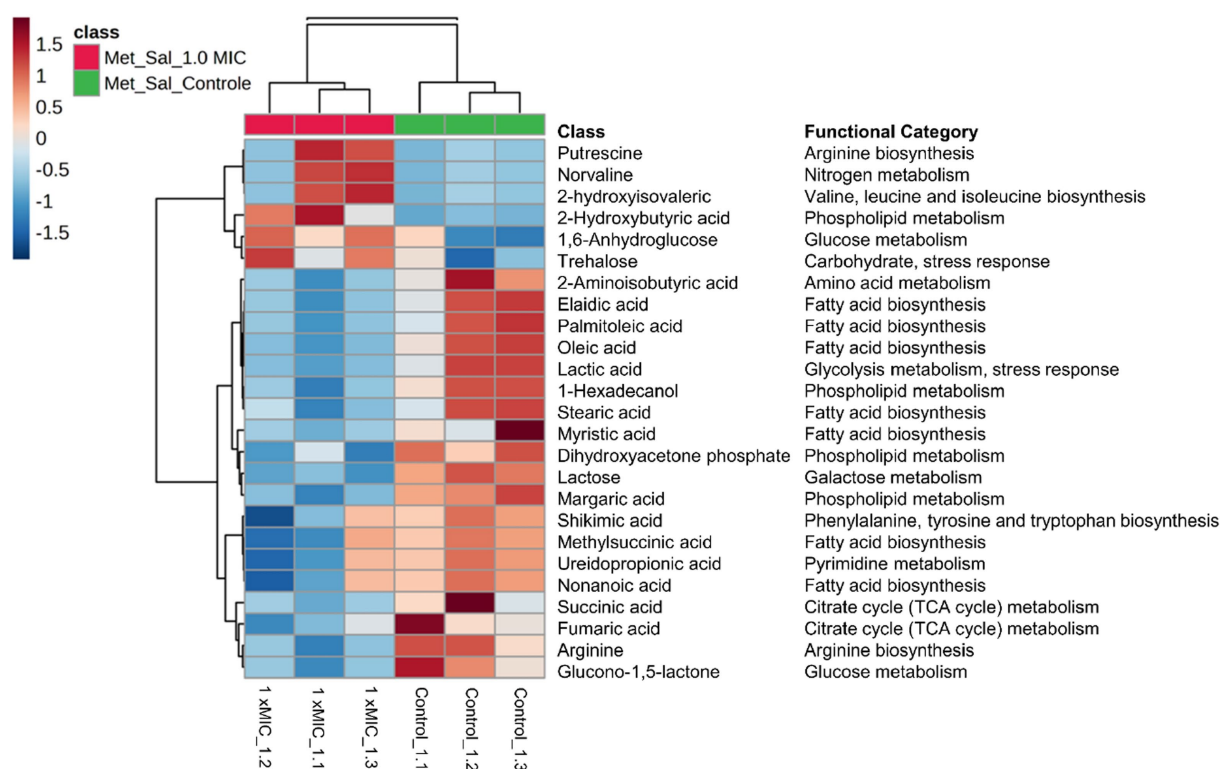


FIGURE 6

Hierarchical cluster analysis of the 25 most differential metabolites with their respective functional categories. Intracellular metabolites identified in *Salmonella enterica* subsp. *enterica* serovar Typhimurium treated without or with [K4K15] CZS-1. Red or blue indicate higher or lower relative metabolite abundance, respectively.

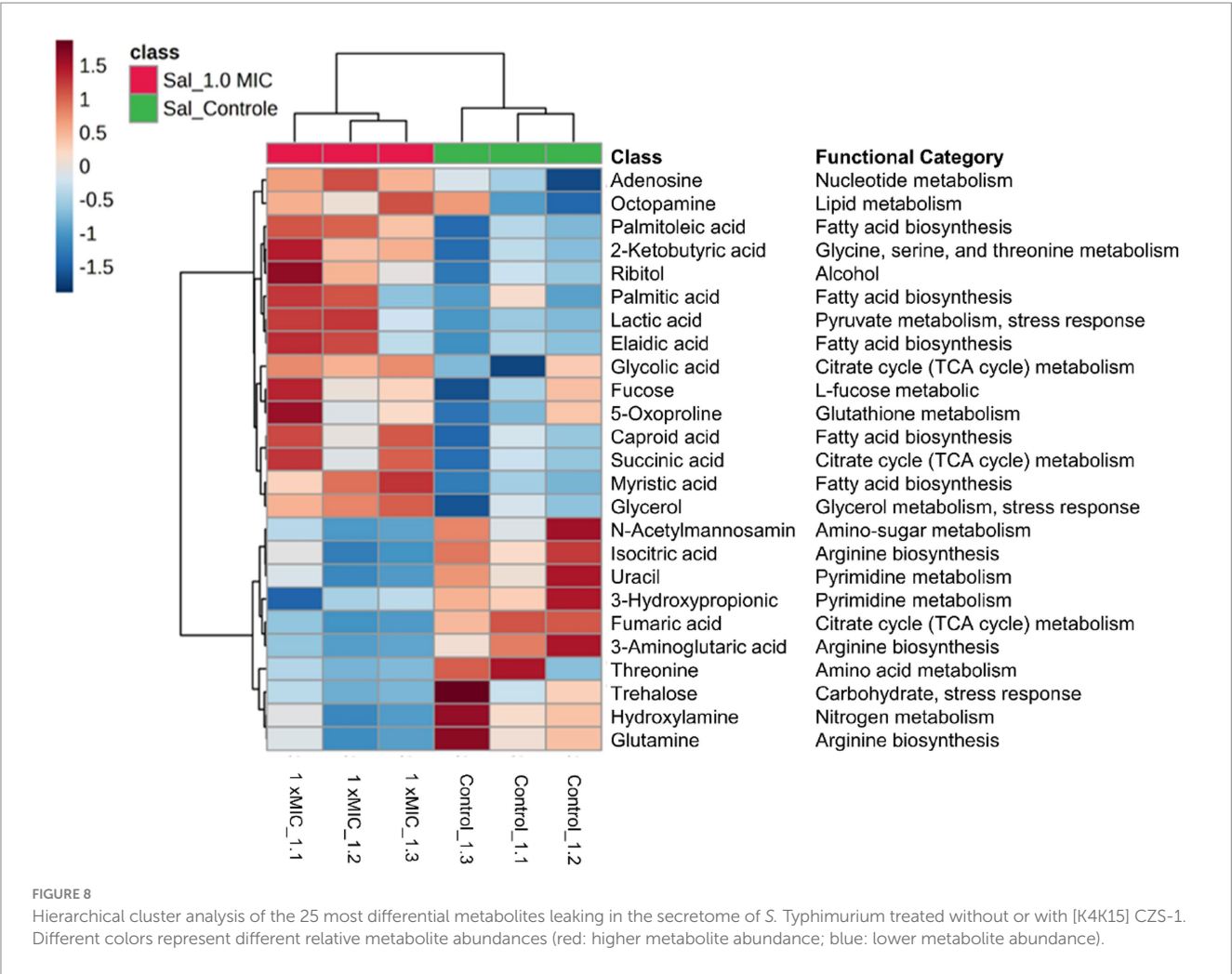
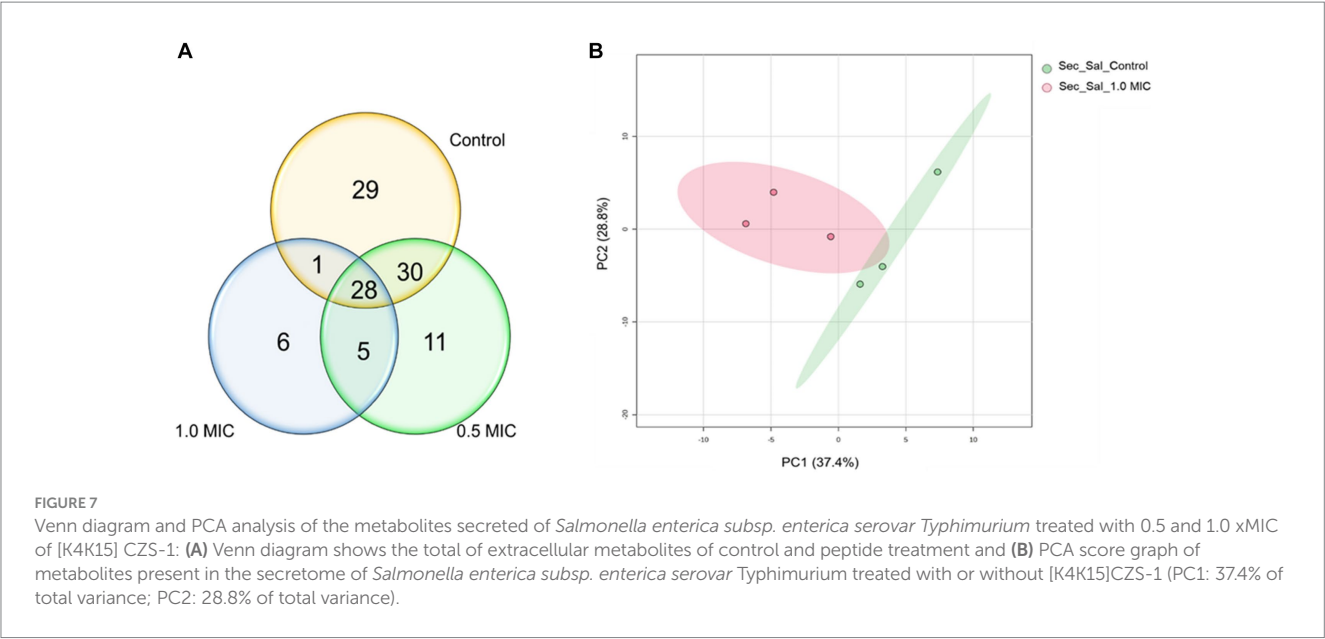
in the presence or absence of peptide. The PCA graph demonstrated the clustering of each treatment and clearly shows the separation between them (Figure 7B). In addition, it is possible to observe that the grouping of control samples were the ones that presented a greater influence in PC1, while the samples treated with 1.0 xMIC [K4K15] CZS-1 were the most representative in PC2, since these metabolites were in lower concentrations.

The HCA showed that there was a significant difference between each group, clustering by treatment, which is a result similar to the PCA analysis. Likewise, the heatmap showed the 25 most significant and different metabolites of the untreated control group and the peptide-treated group (Figure 8). A total of 15 metabolites were more abundant after treatment with 1 xMIC [K4K15]CZS-1, with an increase in the expression of succinic acid, ribitol, palmitoleic acid, palmitic acid, octopamine, N-acetylmannosamine, lactic acid, glycolic acid, glycerol, fucose, elaidic acid, caproic acid, adenosine, 5-oxoproline, and 2-ketobutyric acid. The other 10 metabolites were down-regulated, which include amino acids, carbohydrates, fatty acids, and nitrogenous bases. Subsequently, a KEGG enrichment analysis was conducted to understand the biological pathways involved in the perturbation with the peptide treatment. As shown in Figure 8, several metabolic routes are being up-regulated, such as fatty acid biosynthesis, and lipid metabolism. On the other hand, pyrimidine metabolism and nitrogen metabolism are some pathways that are down-regulated.

4 Discussion

In the current study, the anti-Salmonella activity of three cruzioseptins was evaluated. [K4K15]CZS-1 and CZS-12 inhibited the bacterial growth of this pathogen. These findings are consistent with other AMPs (Gong et al., 2010; Festa et al., 2021). For instance, 1,018-K6 inhibited four isolates of *S. Typhimurium* at the same concentration range (16 µg/mL) as [K4K15]CZS-1 (Festa et al., 2021). Intriguingly, CZS-9, did not show antibacterial activity, even at the highest concentration tested (512 µg/mL). Possibly, the difference in the antimicrobial potential between cruzioseptins relies on the positive net charge. CZS-9, CZS-12, and [K4K15]CZS-1 present a net charge of +1, +2, and +6, respectively. In fact, basic amino acids (arginine or lysine) are the main characters involved in the first step of the mechanism of action through an interaction with the negatively charged bacterial membrane (van der Weide et al., 2019; Wang H. et al., 2020). Several authors reported the close relationship between increased cationicity of AMPs and improved antimicrobial activity (Gao et al., 2016; Wang H. et al., 2020; Bermúdez-Puga et al., 2023).

In a translational-biology plan, the assessment of cytotoxicity of peptides in early stages anticipates possible issues in the drug development (Shi et al., 2022). In this context, the toxicity of three cruzioseptins was screened against RAW 264.7 murine macrophage cells using colorimetric cell-based assays. CZS-9 showed reduced cell viability at the two highest tested concentrations compared to CZS-12.



Based on the physicochemical parameters of both peptides, CZS-9 is more hydrophobic compared to CZS-12. According to previous studies (Chen et al., 2007; Yang et al., 2013), AMPs with a higher hydrophobicity induced higher toxicity activity against mammalian cells. On the other hand, the cytolytic effect of [K4K15]CZS-1 on RAW 264.7 murine macrophage cells was moderate at the MIC concentration. Several

strategies for peptide engineering could be explored to overcome this drawback of [K4K15]CZS-1 (Torres et al., 2018; Kang et al., 2022).

Taking into account the higher antibacterial property of [K4K15]CZS-1, this peptide was chosen to gain insights into the full range of mechanism of action against *S. Typhimurium*. Recently, we demonstrated that [K4K15]CZS-1 acts on the bacterial membrane of Gram-negative *Escherichia coli* (Bermúdez-Puga et al., 2023). Therefore, we initially hypothesized that this molecule also induces membrane damage in *Salmonella*. To corroborate this premise, we combined different experimental strategies, such as a nucleic acid leakage assay and electron microscopy (SEM and TEM). In fact, the results demonstrated that there was a release of DNA and RNA into the extracellular environment, supporting the permeability of the bacterial cell membrane after incubation with this peptide. Likewise, SEM and TEM micrographs exhibited remarkable changes on the bacterial surface compared to untreated cells. This membranolytic effect is in line with the findings of other studies, where permeabilization of the membrane of *Salmonella* spp. is observed after AMP treatment (Lappe et al., 2009; Gong et al., 2010).

TEM observations also revealed that [K4K15]CZS-1 generated intracellular changes in *S. Typhimurium* cells. To create a more comprehensive picture, the metabolic changes were investigated through the analysis of intracellular and extracellular metabolites using an untargeted metabolomic approach by GS-MS combined with multivariate statistical analysis (Supplementary Table S1). The results showed significant differences in the intracellular metabolite profile among the untreated and peptide-treated groups. Bacterial cells incubated with this peptide exhibited a notable reduction in the expression of compounds associated with fatty acid biosynthesis, phospholipid metabolism, and the TCA cycle.

Fatty acids and phospholipids are the major constituents of the bacterial cell wall (Beld et al., 2015; Marquardt et al., 2015), which form a mechanical defense barrier against environmental stress, including antimicrobial compounds (Mueller and Levin, 2020). Here, we observed nine intracellular compounds involved in fatty acid biosynthesis and phospholipid metabolism being down-regulated. This finding shows that [K4K15]CZS-1 might inhibit two important metabolic pathways of the biochemical machinery required to maintain the cell membrane structure. Therefore, this likely impairs the repair of membrane damage induced by synthetic cruzioseptin. In fact, other researchers have also shown that cationic peptides induce variations in the expression of intracellular molecules involved in membrane structure (Bo et al., 2014; Sun et al., 2023). On the other hand, the TCA cycle is a central metabolic pathway which functions as a point of convergence in the catabolism of sugar, lipids, or amino acids in all aerobic microorganisms (Li et al., 2017). [K4K15]CZS-1 negatively affected the TCA cycle, as observed by the low concentration of succinic and fumaric acids. Our findings about the disruption of the energy metabolism are consistent with other studies (Bo et al., 2014; Wang R. et al., 2020).

On the basis of our results, the proposed antibacterial mechanism of [K4K15]CZS-1 against *Salmonella enterica* subsp. *enterica* serovar Typhimurium integrates a series of modulations leading to cell death and minimizing the possibility of resistance. These mechanistic details are schematized in Figure 9. [K4K15]CZS-1 present a random coil conformation in a hydrophilic environment and adopts an α -helix structure after the interaction with membranes (hydrophobic medium). This bacterial membrane-[K4K15]CZS-1 interaction likely occurs through electrostatic attraction between basic amino acids and anionic components of the bacterial membrane. Subsequently, the

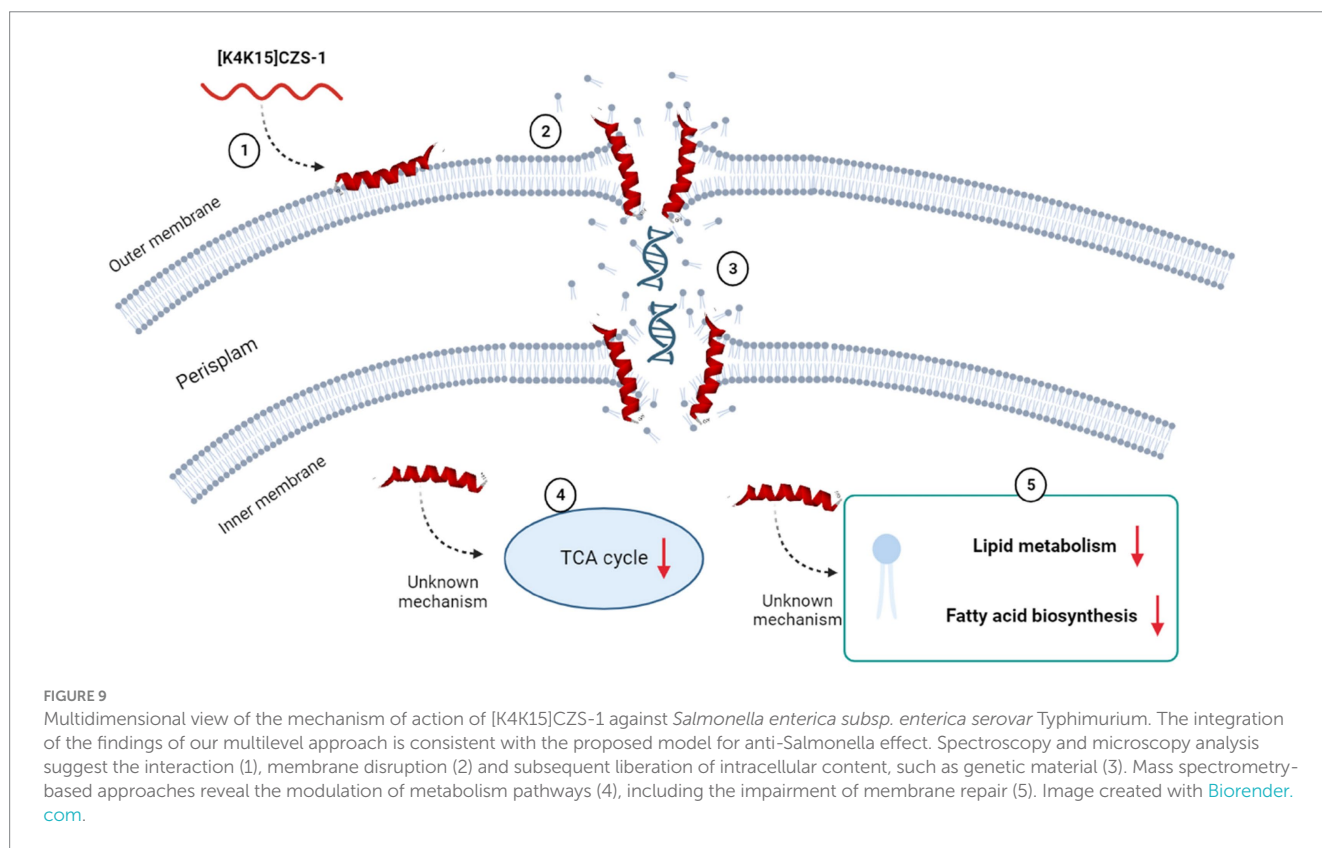
AMP causes changes in the permeability of the cell membrane and releases the intracellular content, including genetic material. Additionally, [K4K15]CZS-1 acts on intracellular targets, inhibiting the TCA cycle, fatty acid biosynthesis, and phospholipid metabolism. These findings have also been described in earlier investigations. Some AMPs inhibit the bacterial growth through a dual antibacterial mechanism characterized by membrane-active and intracellular-active interactions (Hsu et al., 2005; Shi et al., 2016).

The study of metabolites presents in the secretome of *S. Typhimurium* also focused on understanding the variations induced by AMP (Supplementary Table S2). This result could help us in exploring the possible mechanism of action and the response generated by the bacteria in the presence of AMP. The extracellular metabolites present in *S. Typhimurium* cells incubated with AMP were significantly different compared to the control group. Metabolic changes, including carbohydrate, alcohol, lipid metabolism, fatty acid biosynthesis, amino acid metabolism, and the TCA cycle, were observed. However, we think that some modifications observed in the composition of the extracellular metabolite profile could be due to bacterial membrane damage and subsequently the release of intracellular content. For instance, a high expression of several molecules that are synthesized inside the cell was visualized, such as adenosine, glycolic and succinic acids.

Metabolomics analysis also revealed the presence of various protective compounds (Supplementary Table S2). For instance, trehalose is a non-glucose reducing disaccharide, generally considered a protective substance of the cell membrane. It can also function as an antioxidant, an osmoregulatory solute, or a carbohydrate reserve that can be mobilized during times of stress (Hounsa et al., 1998; Benaroudj et al., 2001; Ye et al., 2012). Glycerol is another compound with a protective function. Glycerol acts as a modulator, which can help to transfer compounds across the cell wall. On the other hand, studies have shown that several microorganisms cope with the toxic effects of reactive oxygen species (ROS) by accumulating non-reducing disaccharides such as trehalose in the intracellular medium as well as polyalcohols such as glycerol and arabitol (Sánchez-Fresneda et al., 2013; Galdiero et al., 2021). It is known that in organisms grown in an aerobic environment, the formation of ROS is a consequence of an active oxidative metabolism or the presence of external hazardous agents (Cabiscot et al., 2000). Therefore, the presence of both compounds in the peptide-treated group may indicate a metabolic response generated due to the stress.

5 Conclusion

[K4K15]CZS-1 exhibited promising antibacterial properties, which can benefit the development of innovative strategies to prevent *Salmonella*-induced food poisoning. A multidimensional view of the mechanism of action of bioactive cruzioseptin through complementary approaches evidenced a broad effect integrating membranolysis, modulation of metabolic pathways, and intracellular targeting activities. This expands the current landscape of mechanism of action of antimicrobial cruzioseptins and reinforces the multiple strategies used by AMPs to avoid bacteria resistance. Taking these findings together, they motivate further investigations focused on the stability and structure-function-guided optimizations of cruzioseptins to enrich the probability of success through the biotechnological application of peptide-based agents on food industry.



Data availability statement

The original contributions presented in the study are included in the article/[Supplementary files](#), further inquiries can be directed to the corresponding author.

Author contributions

SB-P: Conceptualization, Formal analysis, Investigation, Methodology, Visualization, Writing – original draft. MD: Investigation, Methodology, Writing – original draft. TF: Investigation, Methodology, Writing – original draft. CM: Investigation, Writing – original draft. SY: Investigation, Writing – original draft. ER: Investigation, Writing – review & editing. CN: Investigation, Methodology, Writing – review & editing. MM: Investigation, Methodology, Writing – review & editing. PO: Writing – review & editing. JA: Formal analysis, Writing – review & editing. CP-B: Formal analysis, Investigation, Writing – review & editing. RO: Conceptualization, Formal analysis, Funding acquisition, Investigation, Project administration, Supervision, Writing – review & editing.

Funding

The author(s) declare financial support was received for the research, authorship, and/or publication of this article. This study was funded by São Paulo Research Foundation (FAPESP) (grants

2018/25511-1, 2022/04841-9, 2022/02936-2, 2022/07556-3 and 2020/15599-9). Additionally, the authors acknowledge the financial support by National Council for Scientific and Technological Development (CNPq) (grants 312923/2020-1 and 408783/2021-4), and by Coordination for the Improvement of Higher Education Personnel (CAPES), Finance Code 001.

Conflict of interest

The authors declare that the research was conducted in the absence of any commercial or financial relationships that could be construed as a potential conflict of interest.

Publisher's note

All claims expressed in this article are solely those of the authors and do not necessarily represent those of their affiliated organizations, or those of the publisher, the editors and the reviewers. Any product that may be evaluated in this article, or claim that may be made by its manufacturer, is not guaranteed or endorsed by the publisher.

Supplementary material

The Supplementary material for this article can be found online at: <https://www.frontiersin.org/articles/10.3389/fmicb.2023.1320154/full#supplementary-material>

References

- Adaro, M., Ibáñez, Á. G. S., Origone, A. L., Vallés, D., Guzmán, F., Vega, A., et al. (2023). Enzymatic synthesis of new antimicrobial peptides for food purposes. *Front. Microbiol.* 14:1153135. doi: 10.3389/fmicb.2023.1153135
- Beld, J., Lee, D. J., and Burkart, M. D. (2015). Fatty acid biosynthesis revisited: structure elucidation and metabolic engineering. *Mol. Biosyst.* 11, 38–59. doi: 10.1039/c4mb00443d
- Benaroudj, N., Lee, D. H., and Goldberg, A. L. (2001). Trehalose accumulation during cellular stress protects cells and cellular proteins from damage by oxygen radicals. *J. Biol. Chem.* 276, 24261–24267. doi: 10.1074/jbc.M101487200
- Benfield, A. H., and Henriques, S. T. (2020). Mode-of-action of antimicrobial peptides: membrane disruption vs. intracellular mechanisms. *Front. Med. Technol.* 2:610997. doi: 10.3389/fmedt.2020.610997
- Bermúdez-Puga, S., Morán-Marcillo, G., Espinosa De los Monteros-Silva, N., Naranjo, R. E., Toscano, F., Vizuete, K., et al. (2023). Inspiration from cruzioseptin-1: membranolytic analogue with improved antibacterial properties. *Amino Acids* 55, 113–124. doi: 10.1007/s00726-022-03209-6
- Bo, T., Liu, M., Zhong, C., Zhang, Q., Su, Q.-Z., Tan, Z.-L., et al. (2014). Metabolomic analysis of antimicrobial mechanisms of e-poly-L-lysine on *Saccharomyces cerevisiae*. *J. Agric. Food Chem.* 62, 4454–4465. doi: 10.1021/jf500505n
- Cabiscol, E., Tamarit, J., and Ros, J. (2000). Oxidative stress in bacteria and protein damage by reactive oxygen species. *Int. Microbiol.* 3, 3–8.
- Chen, Y., Guarnieri, M. T., Vasil, A. I., Vasil, M. L., Mant, C. T., and Hodges, R. S. (2007). Role of peptide hydrophobicity in the mechanism of action of alpha-helical antimicrobial peptides. *Antimicrob. Agents Chemother.* 51, 1398–1406. doi: 10.1128/AAC.00925-06
- Cuesta, S. A., Reinoso, C., Morales, F., Pilaquinga, F., Morán-Marcillo, G., Proaño-Bolaños, C., et al. (2021). Novel antimicrobial cruzioseptin peptides extracted from the splendid leaf frog, *Cruziohylla calcarifer*. *Amino Acids* 53, 853–868. doi: 10.1007/s00726-021-02986-w
- Ehuwa, O., Jaiswal, A. K., and Jaiswal, S. (2021). Salmonella, food safety and food handling practices. *Foods* 10:907. doi: 10.3390/foods10050907
- Festa, R., Ambrosio, R. L., Lamas, A., Grattino, L., Palmieri, G., Franco, C. M., et al. (2021). A study on the antimicrobial and Antibiofilm peptide 1018-K6 as potential alternative to antibiotics against food-pathogen *Salmonella enterica*. *Foods* 10:1372. doi: 10.3390/foods10061372
- Finger, J. A. F. F., Baroni, W. S. G. V., Maffei, D. F., Bastos, D. H. M., and Pinto, U. M. (2019). Overview of foodborne disease outbreaks in Brazil from 2000 to 2018. *Foods* 8:434. doi: 10.3390/foods8100434
- Galdiero, E., Salvatore, M. M., Maione, A., Carraturo, F., Galdiero, S., Falanga, A., et al. (2021). Impact of the peptide WMR-K on dual-species biofilm *Candida albicans*/Klebsiella pneumoniae and on the untargeted Metabolomic profile. *Pathogens* 10:214. doi: 10.3390/pathogens10020214
- Gao, Y., Wu, D., Xi, X., Wu, Y., Ma, C., Zhou, M., et al. (2016). Identification and characterisation of the antimicrobial peptide, Phylloseptin-PT, from the skin secretion of *Phyllomedusa tarsius*, and comparison of activity with designed, cationicity-enhanced analogues and diastereomers. *Molecules* 21:1667. doi: 10.3390/molecules21121667
- Gautier, R., Douguet, D., Antonny, B., and Drin, G. (2008). HELIQUEST: a web server to screen sequences with specific alpha-helical properties. *Bioinformatics* 24, 2101–2102. doi: 10.1093/bioinformatics/btn392
- Gong, H.-S., Meng, X.-C., and Wang, H. (2010). Mode of action of plantaricin MG, a bacteriocin active against *Salmonella typhimurium*. *J. Basic Microbiol.* 50, S37–S45. doi: 10.1002/jobm.201000130
- Gordon, M. A., Graham, S. M., Walsh, A. L., Wilson, L., Phiri, A., Molyneux, E., et al. (2008). Epidemics of invasive *Salmonella enterica* serovar enteritidis and *S. enterica* Serovar typhimurium infection associated with multidrug resistance among adults and children in Malawi. *Clin. Infect. Dis.* 46, 963–969. doi: 10.1086/529146
- Gutiérrez-Del-Río, I., Fernández, J., and Lombó, F. (2018). Plant nutraceuticals as antimicrobial agents in food preservation: terpenoids, polyphenols and thiols. *Int. J. Antimicrob. Agents* 52, 309–315. doi: 10.1016/j.ijantimicag.2018.04.024
- Houns, C.-G., Brandt, E. V., Thevelein, J., Hohmann, S., and Prior, B. A. (1998). Role of trehalose in survival of *Saccharomyces cerevisiae* under osmotic stress. *Microbiology (Reading, Engl)* 144, 671–680. doi: 10.1099/00221287-144-3-671
- Hsu, C.-H., Chen, C., Jou, M.-L., Lee, A. Y.-L., Lin, Y.-C., Yu, Y.-P., et al. (2005). Structural and DNA-binding studies on the bovine antimicrobial peptide, indolicidin: evidence for multiple conformations involved in binding to membranes and DNA. *Nucleic Acids Res.* 33, 4053–4064. doi: 10.1093/nar/gki725
- Kang, S.-J., Nam, S. H., and Lee, B.-J. (2022). Engineering approaches for the development of antimicrobial peptide-based antibiotics. *Antibiotics (Basel)* 11:1338. doi: 10.3390/antibiotics11101338
- Lappe, R., Motta, A. S., Sant'Anna, V., and Brandelli, A. (2009). Inhibition of *Salmonella Enteritidis* by cerein 8A, EDTA and sodium lactate. *Int. J. Food Microbiol.* 135, 312–316. doi: 10.1016/j.jfoodmicro.2009.09.003
- Li, Y., Shao, X., Xu, J., Wei, Y., Xu, F., and Wang, H. (2017). Tea tree oil exhibits antifungal activity against *Botrytis cinerea* by affecting mitochondria. *Food Chem.* 234, 62–67. doi: 10.1016/j.foodchem.2017.04.172
- Li, S., Wang, Y., Xue, Z., Jia, Y., Li, R., He, C., et al. (2021). The structure-mechanism relationship and mode of actions of antimicrobial peptides: a review. *Trends Food Sci. Technol.* 109, 103–115. doi: 10.1016/j.tifs.2021.01.005
- Lima, P. G., Oliveira, J. T. A., Amaral, J. L., Freitas, C. D. T., and Souza, P. F. N. (2021). Synthetic antimicrobial peptides: characteristics, design, and potential as alternative molecules to overcome microbial resistance. *Life Sci.* 278:119647. doi: 10.1016/j.lfs.2021.119647
- Marquardt, D., Geier, B., and Pabst, G. (2015). Asymmetric lipid membranes: towards more realistic model systems. *Membranes (Basel)* 5, 180–196. doi: 10.3390/membranes5020180
- Mendes, B., Proaño-Bolaños, C., Gadelha, F. R., Almeida, J. R., and Miguel, D. C. (2020). Cruzioseptins, antibacterial peptides from *Cruziohylla calcarifer* skin, as promising leishmanicidal agents. *Pathog. Dis.* 78:53. doi: 10.1093/femspd/ftaa053
- Moretta, A., Scieuzo, C., Petrone, A. M., Salvia, R., Manniello, M. D., Franco, A., et al. (2021). Antimicrobial peptides: a new hope in biomedical and pharmaceutical fields. *Front. Cell. Infect. Microbiol.* 11:668632. doi: 10.3389/fcimb.2021.668632
- Mueller, E. A., and Levin, P. A. (2020). Bacterial Cell Wall quality control during environmental stress. *MBio* 11:20. doi: 10.1128/mBio.02456-20
- Proaño-Bolaños, C., Zhou, M., Wang, L., Coloma, L. A., Chen, T., and Shaw, C. (2016). Peptidomic approach identifies cruzioseptins, a new family of potent antimicrobial peptides in the splendid leaf frog, *Cruziohylla calcarifer*. *J. Proteome* 146, 1–13. doi: 10.1016/j.jpro.2016.06.017
- Rai, M., Pandit, R., Gaikwad, S., and Kövics, G. (2016). Antimicrobial peptides as natural bio-preservative to enhance the shelf-life of food. *J. Food Sci. Technol.* 53, 3381–3394. doi: 10.1007/s13197-016-2318-5
- Roy, A., Kucukural, A., and Zhang, Y. (2010). I-TASSER: a unified platform for automated protein structure and function prediction. *Nat. Protoc.* 5, 725–738. doi: 10.1038/nprot.2010.5
- Sánchez-Fresneda, R., Guirao-Abad, J. P., Argüelles, A., González-Párraga, P., Valentin, E., and Argüelles, J.-C. (2013). Specific stress-induced storage of trehalose, glycerol and D-arabitol in response to oxidative and osmotic stress in *Candida albicans*. *Biochem. Biophys. Res. Commun.* 430, 1334–1339. doi: 10.1016/j.bbrc.2012.10.118
- Sánchez-Maldonado, A. F., Lee, A., and Farber, J. M. (2018). Methods for the control of foodborne pathogens in low-moisture foods. *Annu. Rev. Food Sci. Technol.* 9, 177–208. doi: 10.1146/annurev-food-030117-012304
- Shi, J., Chen, C., Wang, D., Wang, Z., and Liu, Y. (2022). The antimicrobial peptide L114 combats multidrug-resistant bacterial infections. *Commun. Biol.* 5:926. doi: 10.1038/s42003-022-03899-4
- Shi, W., Li, C., Li, M., Zong, X., Han, D., and Chen, Y. (2016). Antimicrobial peptide melittin against *Xanthomonas oryzae* pv. *Oryzae*, the bacterial leaf blight pathogen in rice. *Appl. Microbiol. Biotechnol.* 100, 5059–5067. doi: 10.1007/s00253-016-7400-4
- Sun, A., Huang, Z., He, L., Dong, W., Tian, Y., Huang, A., et al. (2023). Metabolomic analyses reveal the antibacterial properties of a novel antimicrobial peptide MOp3 from *Moringa oleifera* seeds against *Staphylococcus aureus* and its application in the infecting pasteurized milk. *Food Control* 150:109779. doi: 10.1016/j.foodcont.2023.109779
- Tang, Y.-L., Shi, Y.-H., Zhao, W., Hao, G., and Le, G.-W. (2008). Insertion mode of a novel anionic antimicrobial peptide MDpep5 (Val-Glu-Ser-Trp-Val) from Chinese traditional edible larvae of housefly and its effect on surface potential of bacterial membrane. *J. Pharm. Biomed. Anal.* 48, 1187–1194. doi: 10.1016/j.jpba.2008.09.006
- Torres, M. D. T., Pedron, C. N., Higashikuni, Y., Kramer, R. M., Cardoso, M. H., Oshiro, K. G. N., et al. (2018). Structure-function-guided exploration of the antimicrobial peptide polybia-CP identifies activity determinants and generates synthetic therapeutic candidates. *Commun. Biol.* 1:221. doi: 10.1038/s42003-018-0224-2
- Valdivieso-Rivera, F., Bermúdez-Puga, S., Proaño-Bolaños, C., and Almeida, J. R. (2022). Deciphering the limitations and antibacterial mechanism of cruzioseptins. *Int. J. Pept. Res. Ther.* 28:73. doi: 10.1007/s10989-022-10383-4
- van der Weide, H., Vermeulen-de Jongh, D. M. C., van der Meijden, A., Boers, S. A., Kreft, D., Ten Kate, M. T., et al. (2019). Antimicrobial activity of two novel antimicrobial peptides AA139 and SET-M33 against clinically and genotypically diverse *Klebsiella pneumoniae* isolates with differing antibiotic resistance profiles. *Int. J. Antimicrob. Agents* 54, 159–166. doi: 10.1016/j.ijantimicag.2019.05.019
- Wang, H., He, H., Chen, X., Zhou, M., Wei, M., Xi, X., et al. (2020). A novel antimicrobial peptide (Kassinaturin-3) isolated from the skin secretion of the African frog, *Kassina senegalensis*. *Biology (Basel)* 9:148. doi: 10.3390/biology9070148
- Wang, R., Zhai, S., Liang, Y., Teng, L., Wang, D., and Zhang, G. (2020). Antibacterial effects of a polypeptide-enriched extract of *Rana chensinensis* via the regulation of energy metabolism. *Mol. Biol. Rep.* 47, 4477–4483. doi: 10.1007/s11033-020-05508-1
- Xia, X., Zhang, L., and Wang, Y. (2015). The antimicrobial peptide cathelicidin-BF could be a potential therapeutic for *Salmonella typhimurium* infection. *Microbiol. Res.* 171, 45–51. doi: 10.1016/j.micres.2014.12.009

Yang, Q.-Z., Wang, C., Lang, L., Zhou, Y., Wang, H., and Shang, D.-J. (2013). Design of potent, non-toxic anticancer peptides based on the structure of the antimicrobial peptide, temporin-1CEa. *Arch. Pharm. Res.* 36, 1302–1310. doi: 10.1007/s12272-013-0112-8

Ye, Y., Wang, X., Zhang, L., Lu, Z., and Yan, X. (2012). Unraveling the concentration-dependent metabolic response of *Pseudomonas* sp. HF-1 to nicotine stress by ¹H NMR-based metabolomics. *Ecotoxicology* 21, 1314–1324. doi: 10.1007/s10646-012-0885-4



OPEN ACCESS

EDITED BY

Shangshang Qin,
Zhengzhou University, China

REVIEWED BY

Yuan Liu,
Yangzhou University, China
En Zhang,
Zhengzhou University, China
Yong Zhang,
Hainan Medical University, China

*CORRESPONDENCE

Ya Hao

✉ haoya@caas.cn;
✉ 474894066@qq.com
Jianhua Wang
✉ wangjianhua@caas.cn;
✉ wangjianhua.peking@qq.com

RECEIVED 01 November 2023

ACCEPTED 04 December 2023

PUBLISHED 21 December 2023

CITATION

Li X, Hao Y, Yang N, Mao R, Teng D and Wang J (2023) Plectasin: from evolution to truncation, expression, and better druggability. *Front. Microbiol.* 14:1304825. doi: 10.3389/fmicb.2023.1304825

COPYRIGHT

© 2023 Li, Hao, Yang, Mao, Teng and Wang. This is an open-access article distributed under the terms of the [Creative Commons Attribution License \(CC BY\)](https://creativecommons.org/licenses/by/4.0/). The use, distribution or reproduction in other forums is permitted, provided the original author(s) and the copyright owner(s) are credited and that the original publication in this journal is cited, in accordance with accepted academic practice. No use, distribution or reproduction is permitted which does not comply with these terms.

Plectasin: from evolution to truncation, expression, and better druggability

Xuan Li^{1,2,3}, Ya Hao^{1,2,3*}, Na Yang^{1,2,3}, Ruoyu Mao^{1,2,3}, Da Teng^{1,2,3} and Jianhua Wang^{1,2,3*}

¹Gene Engineering Laboratory, Feed Research Institute, Chinese Academy of Agricultural Sciences, Beijing, China, ²Innovative Team of Antimicrobial Peptides and Alternatives to Antibiotics, Feed Research Institute, Chinese Academy of Agricultural Sciences, Beijing, China, ³Key Laboratory of Feed Biotechnology, Chinese Academy of Agricultural Sciences, Department of Agriculture and Rural Affairs, Beijing, China

Non-computational classical evolution analysis of plectasin and its functional relatives can especially contribute tool value during access to meet requirements for their better druggability in clinical use. *Staphylococcus aureus* is a zoonotic pathogen that can infect the skin, blood, and other tissues of humans and animals. The impact of pathogens on humans is exacerbated by the crisis of drug resistance caused by the misuse of antibiotics. In this study, we analyzed the evolution of anti-*Staphylococcus* target functional sequences, designed a series of plectasin derivatives by truncation, and recombinantly expressed them in *Pichia pastoris* X-33, from which the best recombinant Ple-AB was selected for the druggability study. The amount of total protein reached 2.9 g/L following 120 h of high-density expression in a 5-L fermenter. Ple-AB was found to have good bactericidal activity against gram-positive bacteria, with minimum inhibitory concentration (MIC) values ranging between 2 and 16 µg/mL. It showed good stability and maintained its bactericidal activity during high temperatures, strong acid and alkali environments. Notably, Ple-AB exhibited better druggability, including excellent trypsin resistance, and still possessed approximately 50% of its initial activity following exposure to simulated intestinal fluids for 1 h. *In vitro* safety testing of Ple-AB revealed low hemolytic activity against mouse erythrocytes and cytotoxicity against murine-derived macrophages. This study successfully realized the high expression of a new antimicrobial peptide (AMP), Ple-AB, in *P. pastoris* and the establishment of its oral administration as an additive form with high trypsin resistance; the study also revealed its antibacterial properties, indicating that truncation design is a valuable tool for improving druggability and that the candidate Ple-AB may be a novel promising antimicrobial agent.

KEYWORDS

plectasin, evolution, truncation, expression, druggability

Introduction

Staphylococcus aureus (*S. aureus*) is a gram-positive bacterium that frequently attacks the skin, soft tissues, and bloodstream of humans, colonizing many parts of the body and causing host infections (Pollitt et al., 2018; Pidwill et al., 2020; Mohammad et al., 2021). Atopic dermatitis caused by *S. aureus* is one of the most common skin diseases in children, affecting up to a quarter of children in the UK and Ireland (Harkins et al., 2018). Meanwhile, *S. aureus* bloodstream infections are one of the most common and severe bacterial infections worldwide;

they caused a high risk of metastatic complications of up to 20–30% and many in-hospital mortalities (Kim et al., 2004; Jung and Rieg, 2018). The fundamental reason for the prevalence of *S. aureus* is that it has developed resistance to almost all the classes of antibiotics, and infections caused by drug-resistant strains of *S. aureus* have reached global epidemic proportions. The overall burden of staphylococcal diseases, particularly those caused by methicillin-resistant strains of *S. aureus* (MRSA), is increasing in healthcare and community settings in many countries (Assis et al., 2017). The discovery of penicillin ushered in the ‘age of antibiotics,’ but it took less than a decade for penicillin resistance to emerge (Chambers and DeLeo, 2009). The use of antibiotics such as streptogramin, virginiamycin, florfenicol, and rifampicin over the last few decades has not solved the problem of antibiotic resistance but has rather exacerbated this crisis (Foster, 2017). More worryingly, resistance to cell membrane-targeting daptomycin and cell wall-targeting vancomycin, the last line of antibiotics against *S. aureus*, has successively emerged (Jahan et al., 2022; Yang et al., 2023). The first case of vancomycin-resistant *Staphylococcus aureus* was reported in Japan in 1997, followed by sporadic reports of daptomycin- and vancomycin-resistant strains (Humphries et al., 2013; Miller et al., 2016). Although these resistant strains have not spread frequently on a large scale, they are still a strong warning that the search for new antibacterial drugs is imperative.

As important components of the host innate defense system, antimicrobial peptides (AMPs) have a narrower window of mutation-selection and a more diverse mechanism of action than other classic antimicrobial drugs, thereby reducing the risk of bacterial resistance development (Chen et al., 2018; Jiang et al., 2021; Li et al., 2021). Simultaneously, the high intracellular activity of AMPs and their good synergy with other antibiotics results in a low residual level, low dosage, and longer administration interval of the drug in organisms (Yang et al., 2021, 2023). In another aspect, AMPs are from innate defending system with natural compatibility in body playing as a role of peace keeper during daily health maintenance unlike the traditional antibiotics and chemical drugs specially for overcoming intensive pathogens and severe infections usually with the obvious side effects as residual, cytotoxic, resistance and others via role of heavy weapons or killers; In fact, the former is usually more important than the latter as a whole on purpose of green health, and they are connected each other closely via a balance keeping attributing into the same goal, it is of unique great importance especially under the almost dry or empty pipeline of new drug R & D for years; Corresponding, the iron triangle theory of the health protection built by AMPs, vaccines, and antibiotics is conducive to maintaining a reasonable balance among pathogens, antimicrobial agents, and drug-resistance (Hao et al., 2022). However, AMPs also have some drawbacks, such as low stability due to enzyme sensitivity, high toxicity, and low bioavailability (Wang et al., 2021; Aminov, 2022). The instability of AMPs is a major impediment to their entry into clinical studies, especially the enzymatic sensitivity of peptides that are extremely susceptible to degradation by proteases in the gastrointestinal (GI) tract and tissue proteolysis when injected, which limits their oral and intravenous availability. To date, only one peptide drug has been approved for clinical use as a GLP-1 receptor antagonist and is permitted for oral use, semaglutide (Wang et al., 2022). Therefore, it is essential to obtain a peptide drug that is highly stable and resistant to protease hydrolysis in the blood, tissue, brain and GI environments. Numerous studies

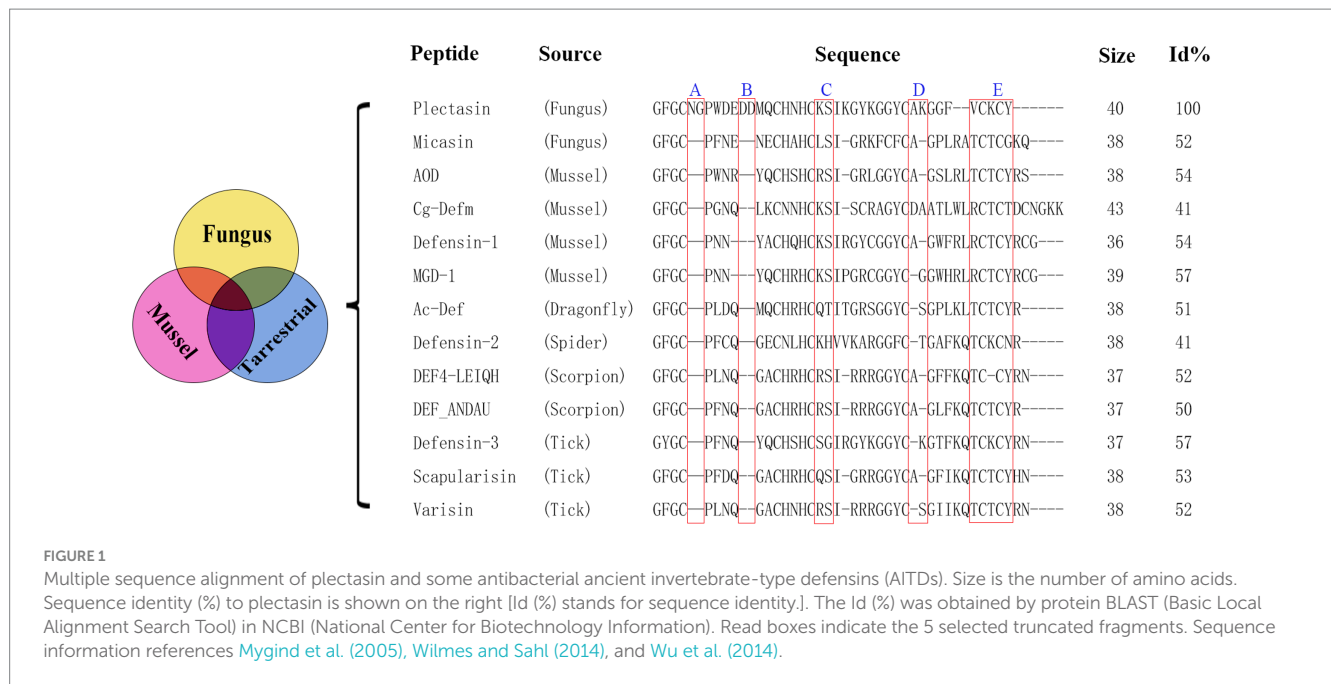
have shown that the biological characteristics of AMPs are closely related to their physicochemical properties such as their positive charge, amphiphilicity, and secondary structure (Yang et al., 2017; Bonnel et al., 2020). The advantages of derivative peptides, such as arenicin-3, 17KKV, and others demonstrate the feasibility of the molecular design of a peptide by deleting or replacing some amino acid residues to change its physicochemical properties and obtain a more efficient and stable antimicrobial peptide (Elliott et al., 2020; Takada et al., 2022). However, the question of how to delete or substitute has been suspended without a clear answer; currently, the only feasible way is to randomly try in different laboratories, which requires a huge industrial labor input.

Plectasin was the first fungal defensin isolated from *Pseudoplectania nigrella* (Mygind et al., 2005) and has been taken as a typical model of similar fungal metabolites for nearly 20 years since its discovery in 2005. It borrows the interaction with the peptidoglycan precursor, Lipid II, to inhibit the synthesis of the cell wall for bactericidal purposes (Schneider et al., 2010; Liu et al., 2020; Pohl et al., 2022). Plectasin has antibacterial activity against gram-positive bacteria, especially *Streptococcus* and *Staphylococcus* (Brinch et al., 2009), however, it is trypsin-sensitive and highly cytotoxic at high concentrations (Zhang et al., 2011; Yang et al., 2019). Although the derivative peptides of plectasin, NZ2114 and MP1106, show stronger antimicrobial activity to some extent due to their high CPP (cell-penetrating peptide) activity as an additional source force, the shortcomings of trypsin sensitivity and higher cytotoxicity have not been well addressed (Wang et al., 2018). Here, using a non-computer-aided classical experiential BI (bioinformatics) tool, we performed multiple sequence alignment analyses between plectasin and 12 other antibacterial ancient invertebrate-type defensins (AITDs) with a similar conserved cysteine-stabilized α -helix and β -sheet structural (CS $\alpha\beta$) motif and similar antimicrobial activity based on previous reports (Figure 1; Mygind et al., 2005; Mandal et al., 2009; Wilmes and Sahl, 2014; Wu et al., 2014) to find an operation entrance for further improvement. In this study, we compared the effect of five different oligopeptide fragments (three types of oligopeptide regions, including redundant, easy mutation/indetermination, and C-terminal) with plectasin via DNA truncating. These five fragments were named as followed: A: Asn5-Gly6, B: Asp11-Asp12, C: Lys20-Ser21, D: Ala30-Lys31, and E: Val36-Cys37-Lys38-Cys39-Tyr40. Ple-AB lacking four amino acids (Asn5, Gly6, Asp11, and Asp12) was selected as the only candidate with bioactivity, and this was confirmed by yeast expression and activity screening. We achieved efficient expression of the antimicrobial peptide Ple-AB in *P. pastoris* X-33, deduced its structure–function relationship, characterized its druggability and evaluated its ability to combat *S. aureus* *in vitro*.

Materials and methods

Peptide design

Since plectasin was discovered in 2005 (Mygind et al., 2005), other fungal defensin-like peptides (fDLPs) have been also identified from a diverse species by a comparative genomics approach. On the basis of sequence, structural, and functional similarity, these defensins can be divided into some major types (Wu et al., 2014), plectasin is classified as antibacterial ancient invertebrate-type defensins (AITDs).



We selected sequences that share the conserved sequence of plectasin which is antibacterial activity specially and among different species that lived in different environments, and delete possible redundant fragments (A and B) at the same time. By comparison, we find their similarities and differences, meanwhile, we hope to design antimicrobial fragments that can be used in a wide range of environments, including forests, oceans and others. At present, synthetic biology, chemical biosynthesis, and artificial intelligence still are difficult to accurately reconstruct the original appearance and details of biological evolution over hundreds of millions of years, and our experiential molecular design is therefore worthy of expenditure, experimentation and expectation.

A series of plectasin derivatives were designed based on multiple sequence alignments. The ExPASy server was used to analyze differences in the physicochemical properties between the derived and parent peptides.

Expression and purification

The recombinant expression vector was constructed by ligating the designed and optimized sequence to the pPICZαA inducible expression vector, relying on the preference of the codon of *P. pastoris*. The linearized plasmid was transferred into *P. pastoris* X-33 for expression and the resulting product was verified for activity using an inhibition zone assay (against *S. aureus* ATCC 43300) before the active peptide was expressed at a high density in a 5-L fermenter ([Mao et al., 2015](#)). The supernatant was purified using the AKTA Express system. The fermentation supernatant was collected by centrifugation (5,000 rpm, 30 min), filtered with micro-filtration membranes (0.45 μm). According to the isoelectric point of the target product, the corresponding A (50 mM sodium phosphate buffer, pH 6.7) and B (50 mM sodium phosphate buffer, 600 mM NaCl, pH 6.7) buffers were configured and purified by HiPrep SP FF cation exchange column (GE Healthcare). The protein samples were eluted by increasing the NaCl

concentration in a stepwise manner, and the corresponding elution peak was collected. The purified product was verified using tricine-sodium dodecyl sulfate-polyacrylamide gel electrophoresis (Tricine-SDS-PAGE) and matrix-assisted laser desorption/ionization-time-of-flight mass spectrometry (MALDI-TOF MS) ([Zhang et al., 2014](#)).

Structure analysis

The secondary structure of the AMPs was analyzed by circular dichroism (CD). The Ple-AB was quantified to 70 μg/mL using ddH₂O, 20 mM sodium dodecyl sulfate (SDS), and 50% trifluoroethanol (TFE), to simulate hydrophobic environments and microbial membranes ([Liu et al., 2020](#)). The detailed operation is outlined in a previous experiment ([Yang et al., 2019](#)).

Antibacterial activity of Ple-AB

Minimum inhibitory concentration

The minimum inhibitory concentration (MIC) of the peptides was assayed using the micro broth dilution method, which is an important indicator of the antibacterial activity of the AMPs ([Liu et al., 2021](#)). MIC plates were prepared by adding 10 μL of peptide solution (different concentrations of 10–1,280 μg/mL at a 2-fold ratio) and 90 μL of bacterial suspension (1 × 10⁵ CFU/mL, logarithmic growth stage) to a 96-well microtiter plate; and the same amount (10 μL) of sterile saline was used as a negative control. The MIC was defined as the lowest concentration of ones at which no visible bacterial growth was observed. All the assays were repeated thrice.

Bacterial kinetics assay *in vitro*

The bactericidal efficiency of Ple-AB was evaluated by plotting a time-kill curve ([Zheng et al., 2021](#)). Single colonies of the *S. aureus* ATCC43300 were picked for overnight activation, and 1% were

transferred and incubated at 37°C until the logarithmic growth phase. The bacterial broth (1×10^5 CFU/mL) was incubated at 37°C and 250 rpm with final concentrations of 1×, 2×, and 4× MIC of AMPs and antibiotics. Samples of 100 µL of bacteria were taken at 0, 0.5, 1, 2, 4, 6, 8, 10, 12, and 24 h, diluted, and coated to count the number of single colonies and plot the time-killing curve.

Post-antibiotic effect

Staphylococcus aureus ATCC43300 in the logarithmic growth phase was diluted to 1×10^8 CFU/mL with fresh culture medium, incubated with 1×, 2×, and 4× MIC Ple-AB at 37°C for 2 h, and then diluted 1,000 times with MHB to terminate the bactericidal effect of the AMPs or antibiotics. They were incubated at 37°C and 250 rpm, sampled, and coated on MHA plates for colony counting every hour. Phosphate-buffered saline (PBS) was used as a negative control, and vancomycin was used as a positive control. The calculation formula for the Post-antibiotic effect (PAE) was based on previous study (Wu et al., 2022).

Biosafety and stability of Ple-AB

Hemolysis

The hemolytic properties of the peptides were evaluated by measuring the amount of hemoglobin released from fresh mouse erythrocytes (Yang et al., 2019). Blood was collected from mice in sodium heparin anticoagulation tubes, and the erythrocytes were washed three or more times with 0.9% saline to obtain an 8% erythrocyte suspension. The erythrocyte suspension was mixed with an equal volume of Ple-AB at concentrations of 0.5–256 µg/mL, incubated at 37°C, and the absorbance values were measured at 540 nm. PBS and 0.1% Triton X-100 were used as the blank (A_0) and positive controls (A_{100}), respectively. Hemolysis (%) = $[(A - A_0)/(A_{100} - A_0)] \times 100$, and three replicates were conducted for each case.

Cytotoxicity

The cytotoxicity of Ple-AB toward the murine macrophage RAW 264.7 (Peking Union Medical College) was tested using the MTT assay (Wang et al., 2018). Cells (2.5×10^4 CFU/mL) were incubated at 37°C for 24 h, and thereafter Ple-AB at a concentration of 2–256 µg/mL was added for 24 h. The supernatant was washed twice, 5 µg/mL 3-(4,5-dimethylthiazol-2-yl)-2,5-diphenyltetrazolium bromide (MTT) solution was added, and the mixture was incubated for 4 h. The absorbance of each well was measured at 570 nm using a microplate reader. PBS (A_{control}) was used as the control. Survival rate (%) = $(A/A_{\text{control}}) \times 100$ was calculated.

In vivo safety

Eight 6-week-old ICR mice were randomly divided into two groups and injected intraperitoneally with Ple-AB (10 mg/kg, body weight) and saline for six consecutive days. The mice were observed for mobility, feeding, and other behaviors. They were weighed daily, and blood was collected on the 7th day for hematological and biochemical analyses. Simultaneously, the heart, liver, spleen, lungs, and kidneys were collected for tissue fixation and hematoxylin–eosin (HE) staining to observe any pathological changes (Shishkina et al., 2023).

Thermal, pH, salts, serum, and protease stability

The stability of Ple-AB was assessed based on its antibacterial activity against *S. aureus* ATCC43300. Temperature stability was determined by incubation at 20, 40, 60, 80, and 100°C for 1 h (Li et al., 2020). The pH stability was determined by incubation in buffers with a pH of 2, 4, 6, 8, and 10 for 4 h (Yang et al., 2017). The peptides were incubated with different concentrations of metal ions, serum, artificial gastric fluid, and simulated intestinal fluid to assess their stability in the blood and intestines (Lyu et al., 2019). All the treatments were performed in triplicates.

Results

Peptide design based on a classical non-computational bioinformatic tool

Based on plectasin and its special antibacterial activity, the sequences and their alignment analysis of 13 similar defensins from publications are shown in Figure 1; these were derived from six different species (fungus, mussel, dragonfly, spider, scorpion, and tick). Plectasin shares 41–57% sequence similarity with 12 other similar defensins from fungi and invertebrates. In comparison with other AITDs, plectasin had additional Asn5, Gly6 (fragment A), and anionic amino acids (Asp11–Asp12, fragment B) in its N-loop region, suggesting that A and B do not contribute into antimicrobial activity. Their original role in native living source is unknown, and a similar situation existed in fragments C and D (Figure 1; Wilmes and Sahl, 2014; Wu et al., 2014, 2022). In this work, we tried the classical non-computational DNA editing technique instead of modern CRISPR editing for the macro-genome, focusing on the improvement/reconstruction of the complex metabolism and non-synthetic biology using a modern computer-aided design that focuses on the fine *de novo* design for core drug candidates. Firstly, five key conserved residues were kept unchangeable except for special purposes (Mygind et al., 2005). Next, 15 new peptides were designed by simple DNA truncating to obtain three types of oligopeptide regions, including redundancy (A, B), easy mutation/indetermination (C, D) and the C-terminal region (E) of plectasin. Except for region E, we analyzed and considered the former four fragments as useless for antibacterial activities due to their weak or unclear bioinformation regarding antibacterial activity contribution and support. Because 12 other peptides from different species were completely lacking regions A and B (Figure 1), these two were selected first for truncation. Similarly, C and D were regarded as easy mutation or non-constituent regions for special antibacterial functions. Finally, the last fragment E, which contains two key residues Cys-37 and Cys-39, was deleted to check whether it is necessary for structure and function as a whole. Therefore, in this experiment, we selected the five target oligopeptide fragments and sequentially truncated them individually or in combination to construct 15 new peptide derivatives of plectasin, hoping to achieve better derivatives that merge the merits of druggability. The five new peptides Ple-A, Ple-B, Ple-C, Ple-D and Ple-E were constructed by individually truncating A, B, C, D, and E, respectively. Moreover, another six new peptides, Ple-AB, Ple-AC, Ple-AD, Ple-BC, Ple-BD, and Ple-CD were constructed by truncating six two-combination fragments, respectively; and more four new peptides Ple-ABC, Ple-ABD, Ple-ACD and Ple-BCD were constructed

by truncating four three-combination fragments, respectively, as a scaffolding and free climbing tool (Table 1).

Bioinformatics analysis of the derived peptides from truncation design

The sequences of the 15 novel peptides from plectasin truncation were analyzed for their physicochemical properties using biological software. These new derived peptides were constructed by composing of 34–38 amino acids lacking five different fragments, with an isoelectric point range of 6.00–8.62, a positive charge number of $-1 \sim +3$, and increased hydrophobicity compared to plectasin (Table 1), from our experiences of the recombination expression of many defensin AMPs (Zhang et al., 2011, 2014; Li et al., 2017; Yang et al., 2019; Liu et al., 2020; Hao et al., 2023; Jin et al., 2023). We cannot exactly estimate and know their possible expression results but only try them one by one, even though they have shown good feasibility of recombination expression based on their net charge number, pI, instability index, and other parameters, and also we cannot know whether they have normal biological activities expect testing.

Construction of recombinant plasmids and screening for positive transformants

A total of 15 recombinant plasmids were constructed. As shown in Figure 2A (using Ple-AB as an example), following double digestion by *XhoI* and *NotI*, the codon-optimized sequences of the Ple-A–Ple-BCD gene were inserted into the pPICZαA plasmid. The 15 types of recombinant plasmids pPIC-Ple-A, ..., pPIC-Ple-BCD were linearized using *PmeI* and transferred into *P. pastoris* X-33 receptor cells. The positive transformants (96 for each sequence) were selected

and cultured in 48-well plates for 120 h. The induced supernatant of the transformants was analyzed by inhibition circle screening and Tricine-SDS-PAGE, and the results indicated that Ple-AB exhibited better antibacterial activity. Four Ple-AB-positive transformants with good inhibitory effects were selected for expression in 1-L shake flasks using the same method. The expression levels were 203, 176, 174, and 137 mg/L, and the transformants with the highest expression were selected for the high-density induced expression in a 5-L fermenter.

Expression and purification

Transformants of Ple-AB with the correct sequence and high expression were selected for the high-density expression in 5-L fermenters. After 120 h of induced expression, the total secreted protein and total biomass of Ple-AB were 2.90 g/L and 332.5 g/L, respectively, and the target band of Ple-AB (4 kDa) was clearly observed in the gel. It is clear from the inhibition circle diagram that antibacterial activity increased with fermentation time (Figures 2B–D). Subsequently, purification was performed using cation-exchange chromatography, and the corresponding elution peak of Ple-AB was observed and collected. As shown in Figure 2E, a single target band was obtained by Tricine-SDS-PAGE, and the relative molecular weight of the purified protein was verified to be 4002.43 Da using MALDI-TOF MS, which is consistent with the theoretical relative molecular mass of Ple-AB (4006.66 Da).

Structure analysis

The secondary structure of Ple-AB was analyzed using CD. The results showed that Ple-AB had positive peaks at 186 nm and 211 nm and a negative peak at 197 nm. In addition, the α -helices of

TABLE 1 Physicochemical properties of peptides derived from plectasin.

No.	Name	Sequence	Length	M.W.	PI	Charge	GRAVY	II
0	Plectasin	GFGCNGPWDEDDMQCHNHCKSIKGYKGGYCAKGGFVCKCY	40	4407.99	7.77	+1	−0.695	13.82
1	Ple-A	GFGCPWDEDDMQCHNHCKSIKGYKGGYCAKGGFVCKCY	38	4236.83	7.77	+1	−0.629	23.05
2	Ple-B	GFGCNGPWDEMQCHNHCKSIKGYKGGYCAKGGFVCKCY	38	4177.81	8.62	+3	−0.547	8.96
3	Ple-C	GFGCNGPWDEDDMQCHNHCKIKGYKGGYCAKGGFVCKCY	38	4192.74	6.87	0	−0.608	14.02
4	Ple-D	GFGCNGPWDEDDMQCHNHCKSIKGYKGGYCGGFVCKCY	38	4208.74	6.87	0	−0.676	17.89
5	Ple-E	GFGCNGPWDEDDMQCHNHCKSIKGYKGGYCAKGGF	35	3811.23	6.88	0	−0.909	14.37
6	Ple-AB	GFGCPWDEMQCHNHCKSIKGYKGGYCAKGGFVCKCY	36	4006.66	8.62	+3	−0.469	18.42
7	Ple-AC	GFGCPWDEDDMQCHNHCKIKGYKGGYCAKGGFVCKCY	36	4021.58	6.87	0	−0.533	23.77
8	Ple-AD	GFGCPWDEDDMQCHNHCKSIKGYKGGYCGGFVCKCY	36	4027.58	6.87	0	−0.606	26.13
9	Ple-BC	GFGCNGPWDEMQCHNHCKIKGYKGGYCAKGGFVCKCY	36	3962.56	8.30	+2	−0.447	8.90
10	Ple-BD	GFGCNGPWDEMQCHNHCKSIKGYKGGYCGGFVCKCY	36	3978.56	8.30	+2	−0.519	11.26
11	Ple-CD	GFGCNGPWDEDDMQCHNHCKIKGYKGGYCGGFVCKCY	36	3993.48	6.00	−1	−0.583	16.61
12	Ple-ABC	GFGCPWDEMQCHNHCKIKGYKGGYCAKGGFVCKCY	34	3791.40	8.30	+2	−0.359	18.92
13	Ple-ABD	GFGCPWDEMQCHNHCKSIKGYKGGYCGGFVCKCY	34	3807.40	8.30	+2	−0.435	21.41
14	Ple-ACD	GFGCPWDEDDMQCHNHCKIKGYKGGYCGGFVCKCY	34	3822.33	6.00	−1	−0.503	27.08
15	Ple-BCD	GFGCNGPWDEMQCHNHCKIKGYKGGYCGGFVCKCY	34	3763.31	7.78	+1	−0.412	11.33

Length: amino acid number; MW, molecular weight (Da); PI, isoelectric point; GRAVY, grand average of hydropathicity; II, instability index; <http://web.expasy.org/protparam/>.

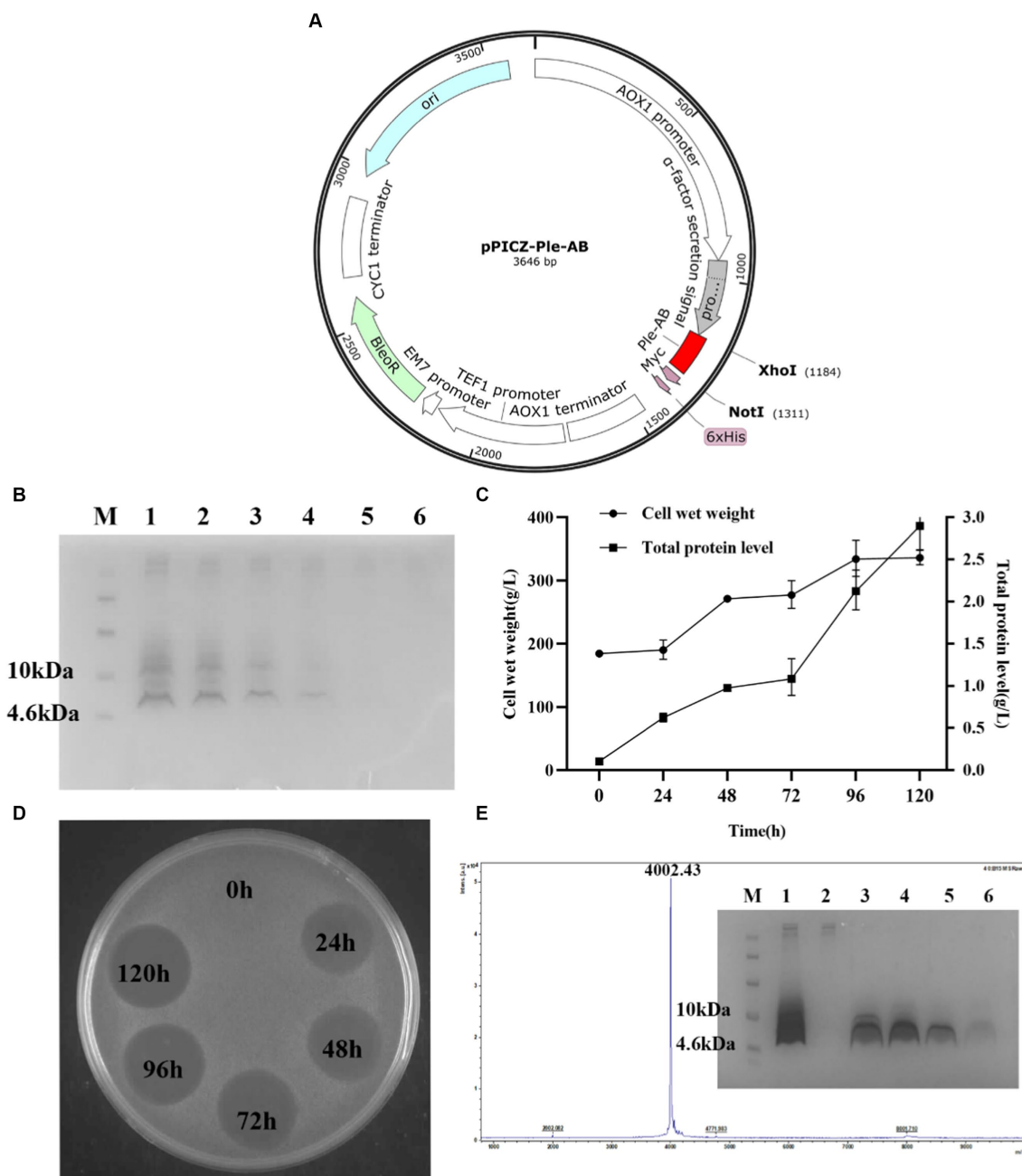


FIGURE 2

Expression and purification of Ple-AB in *P. pastoris* X-33 at 5 L fermentor. **(A)** Schematic representation of the recombinant expression plasmid pPICZ-Ple-AB. **(B)** Tricine-SDS PAGE gel electrophoresis for Ple-AB expression. Lane M indicated the protein molecular weight marker (6 μ L). Lane 1–6 indicated fermentation supernatants of Ple-AB (10 μ L) taken at 120, 96, 72, 48, 24, 0h of induction, respectively. **(C)** Time curves of Ple-AB total secreted protein levels and cell wet weight during high density fermentation. **(D)** Inhibition of *S. aureus* ATCC43300 by Ple-AB fermentation supernatant with different induction times. **(E)** MALDI-TOF MS analysis of purified Ple-AB and Tricine-SDS-PAGE analysis of Ple-AB purified by cation exchange chromatography. Lane 1: 120h fermentation supernatant; Lane 2: penetration peak; Lanes 3–4: 22.5% B-eluting peak; Lane 5–6: 60% B-eluting target peak.

Ple-AB increased in SDS; this alteration may facilitate the entry of Ple-AB into the microbial cell membrane. Meanwhile, it was found that the random coil of Ple-AB increased in the TFE solution, inferring that Ple-AB may not easily cause damage to the mammalian cell membrane (Figure 3A and Table 2). The amphipathy of plectasin and Ple-AB is observed in the helical wheel diagram in Figure 3B; compared to plectasin, Ple-AB has

two additional positive charges and increased hydrophobicity. The results of the 3D structural simulations predicted that Ple-AB is structurally similar to plectasin with a typical CS α β conformation (Mandal et al., 2009), including an α -helix (residues 8–16), an antiparallel β -sheet layer (residues 23–27 and 32–36) and three disulfide bonds (Cys4-Cys26, Cys11-Cys33 and Cys15-Cys35) (Figures 3C,D).

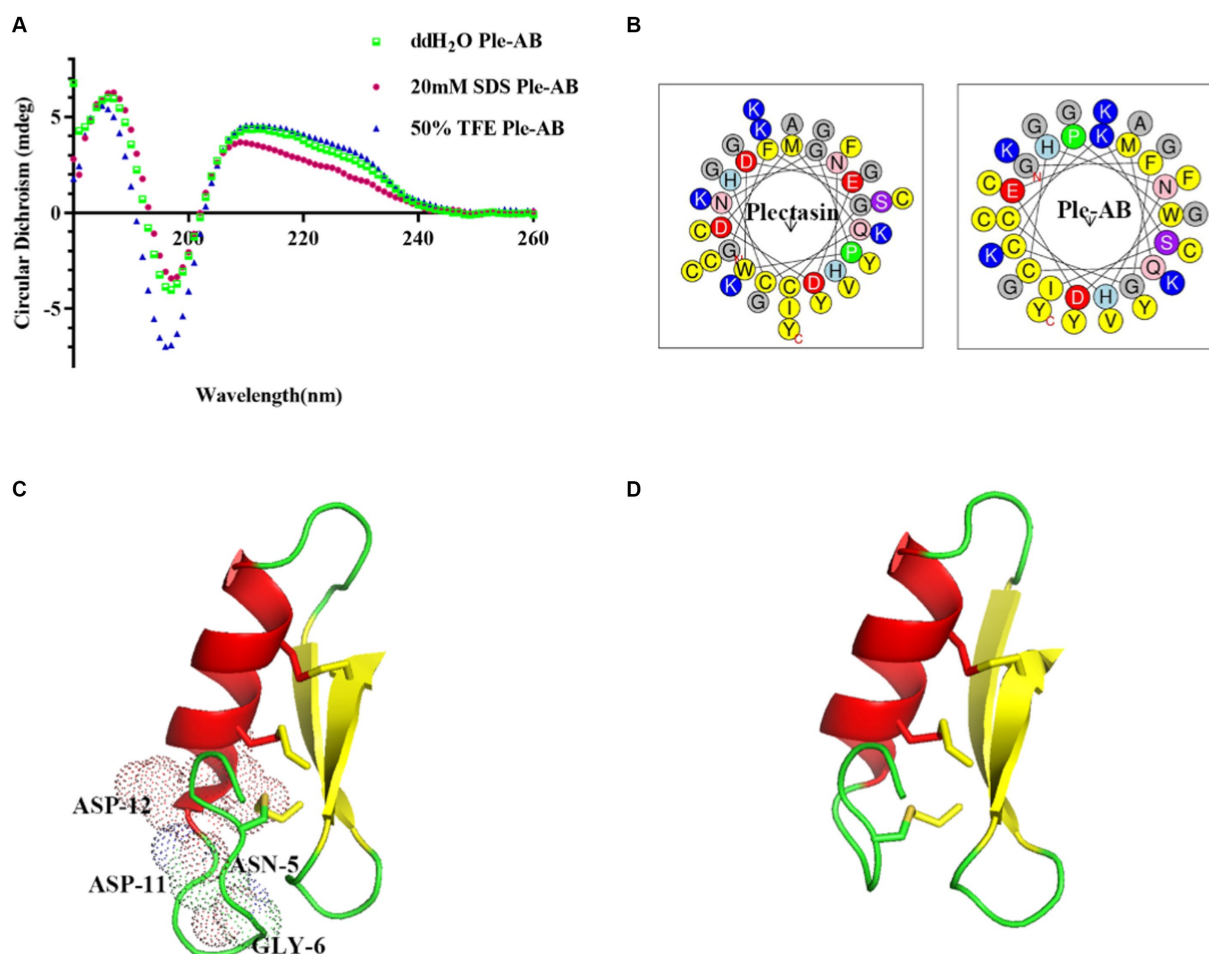


FIGURE 3

The structure analysis of plectasin and Ple-AB. (A) CD spectra of Ple-AB in ddH₂O, 20 mM SDS, and 50% TFE. (B) Observations on the amphipathy of plectasin and Ple-AB in the spiral wheel model (yellow represents hydrophobic amino acids, red is negatively charged acidic amino acids, blue is positively charged basic amino acids and purple is hydrophilic amino acids). (C) Molecular mimicry of plectasin. Light dots represent truncated residues. (D) Molecular mimicry of Ple-AB. Molecular model was generated with PyMOL 1.8.

TABLE 2 Ratio of secondary structure of Ple-AB in different solutions.

Indices (%)	ddH ₂ O	20 mM SDS	50% TFE
Helix	3.08	3.57	2.53
Antiparallel	55.60	56.45	43.58
Parallel	3.17	3.29	2.73
Beta-turn	13.25	13.08	15.98
Random coil	25.09	23.60	35.09

Antimicrobial activity of Ple-AB

Minimum inhibitory concentration determination

The antibacterial spectrum of Ple-AB is shown in Table 3. The results showed that Ple-AB exhibited good antibacterial activity against Gram-positive bacteria, especially against *Streptococcus* including *S. agalactiae* ATCC13813, *S. dysgalactiae* CVCC3938, and *S. agalactiae* CAU-FRI-2022-02, with MICs in the range of 2–4 µg/mL. Ple-AB was also found to be inactive against gram-negative

bacteria. Meanwhile, the MIC of Ple-AB against *Candida albicans* CICC 98001 was determined, as shown in Table 3, which was greater than 128 µg/mL.

In vitro bacterial kinetics assay

Staphylococcus aureus ATCC43300 was used as the test strain and the bactericidal ability of Ple-AB was examined based on the kinetics of bactericidal time (Figure 4A). The 1× and 2× MIC Ple-AB were able to kill all the strains within 4 h, and the 4× MIC Ple-AB achieved 99% bactericidal activity within 2 h. However, the 2× MIC vancomycin (the MIC value of vancomycin for *S. aureus* ATCC43300 was 1 µg/mL) required 6 h to kill all the strains, which was weaker than that of Ple-AB.

Post-antibiotic effect

The post-antibiotic effect is an important parameter in evaluating the pharmacokinetics of new drugs. The PAE was determined by treating *S. aureus* ATCC43300 with 1×, 2×, and 4× MIC antimicrobial agents for 2 h (Figure 4B). The PAE values of Ple-AB for *S. aureus* ATCC43300 were dose-dependent and exhibited better inhibition

TABLE 3 The MIC values of Ple-AB.

Strains	MIC (μg/mL)	MIC (μg/mL)	MBC (μg/mL)	Source
	Plectasin	Ple-AB		
Gram-positive bacteria				
<i>S. aureus</i> ATCC43300	4 ^a	16	32	ATCC
<i>S. aureus</i> ATCC25923	NT	16	64	ATCC
<i>S. aureus</i> CVCC546	16 ^a	8	16	CVCC
<i>S. aureus</i> E48	4 ^a	4	16	NWAFU
<i>S. epidermidis</i> ATCC35984	16	4	8	ATCC
<i>S. epidermidis</i> ATCC12228	8	2	8	ATCC
<i>S. dysgalactiae</i> CVCC3938	NT	4	4	CVCC
<i>S. agalactiae</i> ATCC13813	2	4	4	ATCC
<i>S. agalactiae</i> CAU-FRI-2022-01	NT	4	32	CAU
<i>S. agalactiae</i> CAU-FRI-2022-02	NT	2	4	CAU
Gram-negative bacteria				
<i>E. coli</i> ATCC25922	>128	>128	NT	ATCC
<i>E. coli</i> O157	>128 ^a	>128	NT	CVCC
<i>Shigella</i> CMCC3926	>128	>128	NT	CGCC
<i>S. enteriditis</i> CVCC3377	>128	>128	NT	CVCC
<i>P. aeruginsoa</i> CICC21630	>128 ^a	>128	NT	CICC
Fungus				
<i>Candida albicans</i> CICC 98001	>128	>128	NT	CICC

ATCC, American Typical Culture Collection; CVCC, China Veterinary Microbial Strain Collection Management Centre; CICC, China Center of Industrial Culture Collection; CMCC, National Center for Medical Culture Collection. The bovine clinical *S. aureus* E48 strain was donated by Prof. Zhao Xin (Northwest A&F University). *S. agalactiae* CAU-FRI-2022-01 and CAU-FRI-2022-02 isolated from bovine mastitis tissue were obtained from China Agricultural University (CAU). NT, no test. ^aData were cited from previous results (Yang et al., 2019).

than vancomycin at 1 \times , 2 \times , and 4 \times MIC concentrations for the 1.15, 1.18, and 2.25 h time points, respectively.

Ple-AB had low toxicity, and high stability

Low toxicity

To evaluate safety, the hemolytic activity and cytotoxicity of Ple-AB were determined. The hemolysis of mouse erythrocytes treated with different concentrations (0.5–256 $\mu\text{g/mL}$) of Ple-AB was first analyzed, and the results showed that the hemolytic rates were all less than 2%, even at the highest concentration, the hemolytic rate was only 1.07% (Figure 5A). The cytotoxicity of Ple-AB was then measured using a MTT assay, and the results showed that there was no significant cytotoxicity to the mouse peritoneal macrophages RAW264.7 at concentrations of 2–256 $\mu\text{g/mL}$, and the cell survival rate was above 80% (Figure 5B). This indicated that Ple-AB has a good *in vitro* safety profile.

In vivo safety

During the safety test cycle in mice, it was observed that the mice had a slight tendency to lose weight on the second day after the injection; however, on the third day, the weight of the mice returned to normal (Figure 5C). One week after the intraperitoneal injection, HE staining of the heart, liver, spleen, lungs, and kidneys showed no differences in histological morphology (Figure 5D). The whole blood

cell profiles and serum biochemical indices were not significantly different between the test and control group (Tables 4–6).

High stability

Staphylococcus aureus ATCC43300 was used as the test strain to analyze the *in vitro* stability of Ple-AB (Table 7). Ple-AB was incubated at different temperature and pH values ranging from 20 to 100°C and 2–10, respectively; the MIC values increased twofold only at 100°C and pH 10, but were not affected under the other conditions. After incubating Ple-AB with different concentrations of serum and ions, the antibacterial activity remained unchanged, indicating that Ple-AB is highly stable (Table 7).

Ple-AB was incubated with artificial gastric juice for 2 h, and the MIC value remained at 16 $\mu\text{g/mL}$, indicating that it is tolerant to pepsin. It is worth noting that Ple-AB still possessed approximately 50% of its initial activity following incubation in the simulated intestinal fluids for 1 h and lasted for 2 h of incubation, indicating that Ple-AB is tolerant to trypsin (Table 7). Therefore, Ple-AB exhibited desirable stability; this is vital for GI administration and has the importance of applications, as only one case different from other fungi defensins and the derivatives has been reported so far.

Discussion

Staphylococcus aureus is the most common pathogen in septic infections, causing localized septicemia, pneumonia, pericarditis,

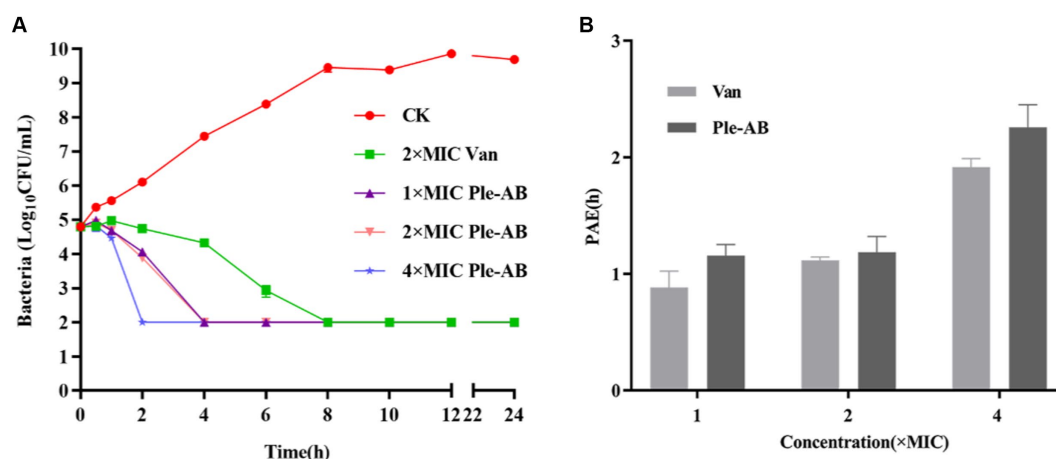


FIGURE 4

Bactericidal profile and post-antibiotic effect of Ple-AB. (A) Time killing curves of 1x, 2x, and 4x MICs of Ple-AB against *S. aureus* ATCC43300. (B) Post-antibiotic effect of 1x, 2x, and 4x MIC of Ple-AB against *S. aureus* ATCC43300. Van stands for the vancomycin.

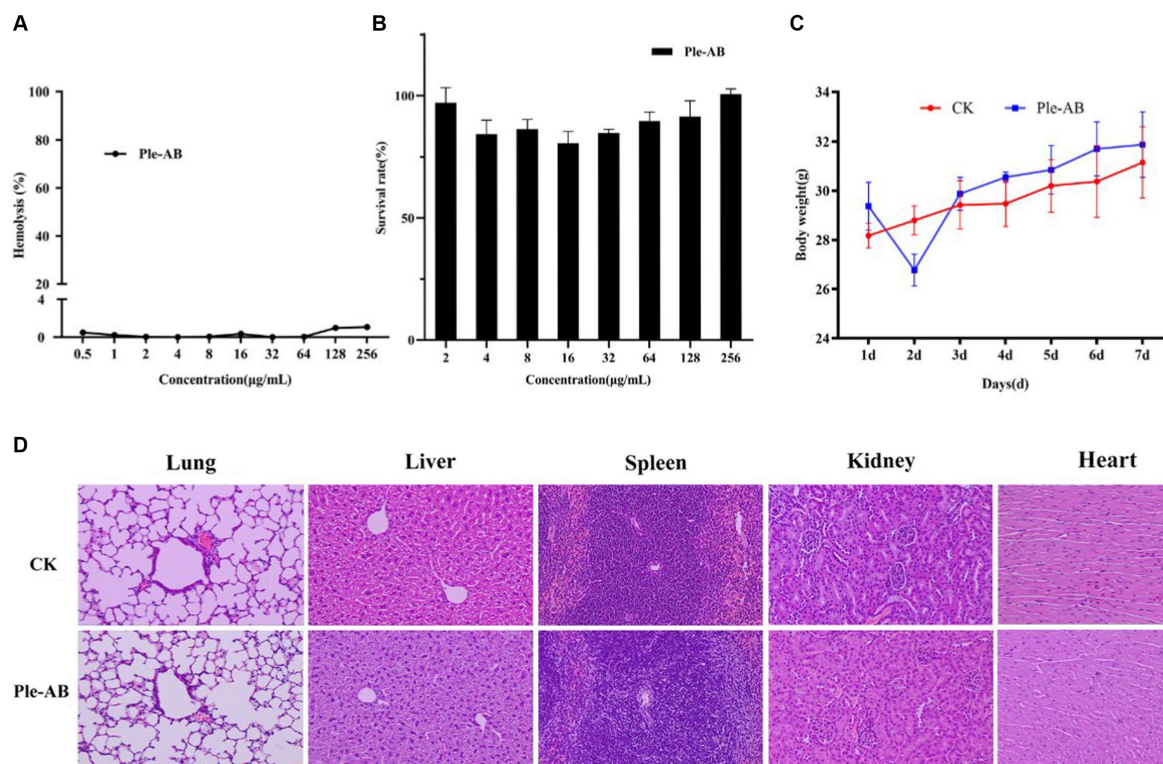


FIGURE 5

Safety of Ple-AB. (A) Hemolytic activity of Ple-AB at different concentrations (0.5–256 µg/mL) against mouse erythrocytes. (B) Cytotoxic effects of Ple-AB at different concentrations (2–256 µg/mL) on mouse macrophages RAW264.7. (C) Body weight changes and (D) tissue sections by HE (magnification 200x) of mice after injection of Ple-AB 1 week.

pseudomembranous enteritis and, in severe cases, systemic infections such as septicemia and sepsis (Paling et al., 2017; Lei et al., 2018; Pollitt et al., 2018). *S. aureus* can cause persistent and recurrent infections and lead to the constant emergence of drug-resistant strains, posing a serious threat to human, animal, and public health safety (Guo et al., 2020). In this study, truncation, a simple DNA editing operation, was used as a powerful tool to improve the

druggability of the fungal defensin plectasin; moreover, Ple-AB showed the strong antimicrobial activity against *Staphylococcus* at low MIC values of 4–16 µg/mL (Table 3).

Many efforts have been made by researchers to bring plectasin, an extremely promising fungal defensin, to the early stages of clinical application (Brinch et al., 2009). In 2011, our group expressed and purified recombinant plectasin in *P. pastoris* with a total secretion of

TABLE 4 Hematological indices in mice.

Parameters	WBC (10 ⁹ /L)	NEUT (10 ⁹ /L)	LYM (10 ⁹ /L)	MONO (10 ⁹ /L)	EO (10 ⁹ /L)	BASO (10 ⁹ /L)	NEUT %	LYM %	MONO %	EO %	BASO %
CK	7.30 ± 1.72	1.28 ± 0.392	5.50 ± 1.161	0.20 ± 0.045	0.23 ± 0.113	0.08 ± 0.026	17.42 ± 1.85	75.56 ± 3.15	2.72 ± 0.57	3.19 ± 0.85	1.12 ± 0.21
Ple-AB	7.89 ± 0.94	1.49 ± 0.354	5.89 ± 0.585	0.24 ± 0.066	0.19 ± 0.106	0.09 ± 0.027	18.78 ± 1.66	74.8 ± 3.02	3 ± 0.49	2.33 ± 1.24	1.09 ± 0.34

TABLE 5 Hematological indices in mice.

Parameters	RBC (10 ¹² /L)	HBG (g/L)	HCT %	MCV (fL)	MCH (pg)	MCHC (g/L)	PLT (10 ⁹ /L)	MPV (fL)	PDW %	PLCR %	RDW-CV (10 ⁹ /L)	RDW-SD %	PCT %
CK	9.75 ± 0.5	129.25 ± 9.25	40.63 ± 2.17	40.08 ± 1.52	12.88 ± 0.57	32.81 ± 1.03	775.5 ± 53.5	6.53 ± 0.67	15.4 ± 1.1	13.95 ± 1.25	19.38 ± 0.72	42.95 ± 3.35	0.02 ± 0.006
Ple-AB	9.44 ± 0.82	128 ± 12	41.3 ± 2.4	41.73 ± 1.17	13.48 ± 0.67	32.86 ± 1.73	782.3 ± 48.25	6.63 ± 0.57	15.85 ± 0.75	15.35 ± 3.65	18.58 ± 1.97	44.55 ± 3.65	0.02 ± 0.01

TABLE 6 Serum biochemical indices in mice.

Parameters	Glucose (mmol/L)	Ca ²⁺ (mmol/L)	Phosphorous (mmol/L)	Urea Nitrogen (mmol/L)	Creatinine (μmol/L)	Total protein (g/L)	Albumin (g/L)	Globulin (g/L)	ALB/ GLO	AST (IU/L)	ALT (IU/L)	AST/ALT
CK	1.60 ± 0.14	1.39 ± 0.05	3.24 ± 0.29	9.4 ± 0.58	85.57 ± 6.03	53.81 ± 3.54	34.98 ± 2.53	18.83 ± 0.50	1.86 ± 0.12	25.72 ± 1.56	47.15 ± 4.82	0.55 ± 0.06
Ple-AB	1.59 ± 0.15	1.38 ± 0.06	3.33 ± 0.20	11.6 ± 0.8	83.13 ± 4.57	54.41 ± 4.56	35.59 ± 4.58	18.82 ± 0.25	1.90 ± 0.25	25.85 ± 2.33	49.07 ± 6.21	0.53 ± 1.11

0.748 g/L following 120 h of induction in recombinant yeast (Zhang et al., 2011). Various peptide derivatives have been designed to increase expression; most of these derivative peptides were designed and constructed based on the mutation or substitution of single or multiple amino acids, which is the most common and efficient method (e.g., NZ2114, MP1102) (Andes et al., 2009; Zhang et al., 2015; Koseki et al., 2023). These mutants showed significantly increased expression of *P. pastoris* and exhibited high antibacterial activity.

However, their poor druggability remains a challenge. AMPs are derived from a wide variety of plants, animals, and microorganisms, and vary highly with environmental factors such as temperature, humidity, and other factors; they live in different locations, resulting in their sequence diversity across species. Based on previous reports, we selected 12 defensins from six species with sequences, structures and functions similar to that of plectasin for the multi-sequence alignment (Mygind et al., 2005; Wilmes and Sahl, 2014; Wu et al., 2014). It is known that the antimicrobial action of plectasin depends on the five key amino acids Phe2, Gly3, Cys4, His18, and Cys37, in which, the Phe2, Gly3, Cys4, and Cys37 interact with the pyrophosphate group of the bacterial cell-wall precursor Lipid II via hydrogen bonding, in addition, and a salt bridge is formed between the side chain of His18 and the D-γ-glutamic acid of Lipid II, thus inhibiting cell-wall biosynthesis (Mandal et al., 2009; Schneider et al., 2010). Other peptides also contain the five key amino acids involved in the plectasin-Lipid II interaction, signifying a conserved lipid II-binding motif (Figure 1). A truncation instead of a substitution approach was used to improve the properties of plectasin for the first time in this study. Five fragments, A–E (Figure 1) were selected for truncation. In comparison with the other 12 defensins, only plectasin has two spare redundant fragments, A and B, in its N-loop region (Figure 1). We examined whether the deletion of fragments A and B affect the activity of the Plectasin. The C-segment is a mutation-prone region at the end of the α-helical structure. The D-fragment is an indetermination region in the β-sheet parallel structure, and the E-fragment function as a control and is relatively conserved in a sheet at the C-terminal. Simultaneously, these three fragments were selected for deletion to study their effect. Therefore, the above core residues, groups, and domains remained unchanged, except for the E-terminus, during our truncation operation. Screening revealed that none of the truncated segments individually showed activity. Interestingly, only Ple-AB, following the simultaneous truncation of fragments A and B, showed normal or higher activity; the other combined truncated derived peptides showed no activity. This means that A and B have an equal role as structural or functional supports; this is reported for the first time in our study. Of greater importance is that fragments A and B seem no contribution to the apparent antibacterial function, but are essential as the plectasin source living, i.e., in *Pseudoplectania nigrella* (Mygind et al., 2005) as a whole in their environment. Moreover, the fact that double truncation of AB improved its expression and druggability especially in antitrypsin proteolysis reminds that not only fragment AB might play roles as the balancing of symmetrical structure in peptide, co-handshaking and co-locking during targeting toward pathogens, but also as the possible special trypsin sensitive region, they both are probably key sites that host trypsin access, recognize and bind specifically with plectasin. However, to reveal further details about how important fragments A and B from *Pseudoplectania nigrella* (Mygind et al., 2005) are to other fungi and invertebrates would be very interesting but is beyond the aim or scope

TABLE 7 Thermal, pH, salts, and protease stability of Ple-AB against *S. aureus* ATCC 43300.

Treatment		MIC ($\mu\text{g/mL}$)
		Ple-AB
Control		16
Temperature		
	20°C	16
	40°C	16
	60°C	16
	80°C	16
	100°C	32
pH		
	2	16
	4	16
	6	16
	8	16
	10	32
Salts		
	Na ⁺ (150 mM)	16
	K ⁺ (4.5 mM)	16
	NH ₄ ⁺ (6 μM)	16
	Zn ²⁺ (8 μM)	16
	Mg ²⁺ (1 mM)	16
	Ca ²⁺ (2.5 mM)	16
	Fe ³⁺ (4 μM)	16
Simulated Gastric Fluid (1–2 h)		16
Artificial Intestinal Fluid (1 h)		32
Serum (25%) (1–8 h)		16
Serum (50%) (1–8 h)		16

of our study. Similar details regarding fragments C and D are worth studying in subsequent steps.

The length, positive charge number, and amphiphilicity of the derived peptide Ple-AB were altered, reducing the peptide chain length from 40 to 36 amino acids, reducing the molecular weight from 4407.99 to 4006.66 Da, increasing the charge number from +1 to +3, and increasing the hydrophobicity from -0.695 to -0.469 (Table 1). The high-density expression of Ple-AB also increased, with a total secretion of 2.9 g/L following 120 h of induction in recombinant yeast (Figure 2C), while the expression level of plectasin was relatively low 748.63 mg/L (Zhang et al., 2011); the cytotoxicity (<1%) and hemolytic (1.07%) activity were also significantly reduced (Figure 5B) compared to plectasin (<5.31 and 68%, respectively) at the concentration of 256 $\mu\text{g/mL}$ (Zhang et al., 2011; Yang et al., 2019). Ple-AB also exhibited superior antibacterial effects against vancomycin in terms of its bactericidal kinetics and PAE *in vitro* (Figures 4A,B). Notably, its stability *in vitro* was the above characteristics of Ple-AB were significantly better than that of the other peptide derivatives, with better druggability contributing directly into its application steps and progress.

It is worth noting that plectasin and its series of derivative peptides lost activity after 15–30 min of co-incubation with the simulated intestinal fluid (Lei et al., 2018), but the tolerance or resistance of Ple-AB to trypsin was highly ameliorated, still possessing approximately 50% of its initial activity after incubation with the simulated intestinal fluids for 1 h (Table 7). In the same simulated *in vitro* environment, the trypsin tolerance time of Ple-AB was three times greater than that of plectasin and its series of derivative peptides. Clinical applications require drugs that exhibit high structural stability in complex and variable *in vivo* environments. During oral administration, many factors, including solubility, absorption, and stability, affect the oral bioavailability of a drug. The most challenging factor for the gastrointestinal transport of therapeutic proteins is proteolysis, (Loussouarn et al., 2020) which restricts golden time and stability ensuring its feasibility during application. Protein hydrolases are classified into two main groups, exopeptidases and endopeptidases. To resist the exopeptidases, they can often be blocked by “end-capping.” This is a chemical modification of the N-terminal and C-terminal amino or carboxylic acid functional groups (Brinckerhoff et al., 1999). For trypsin as an endopeptidase, common resistance improvements include sequence modification, cyclization, incorporation of unnatural amino acids, introduction of peptidomimetic elements, and nanoengineering of antimicrobial peptide polymers (Choi et al., 2013; Koopmans et al., 2015; Zhao et al., 2016). These strategies attempt to modify or mask the potential peptide cleavage sites as much as possible to reduce protease recognition and proteolysis, with the side effect of increasing uncertainty in the prediction of biological activity (Zhu et al., 2020). In general, the shorter the peptide, the stronger the proteolysis resistance. This is because shorter molecular lengths may result in fewer total cleavage sites and greater access difficulty for various enzymes, including tryptic degradation. Thus, reducing the size of the peptide is also a viable strategy to resist trypsin (Zou et al., 2022). The deletion of four amino acids in Ple-AB compared to plectasin not only resulted in a reduction in the overall length, but the truncated amino acids also likely changed the amphiphilicity of the whole peptide structure (Figure 3B), thus contributing to better druggability. The optimization of amphiphilicity can improve protein stability (Stone et al., 2019); the stability results of Ple-AB confirm the possibility of this deduction, provides a new idea and tool for improving trypsin resistance, and is an important step toward the early availability of cationic antimicrobial peptides as orally active drugs.

As we know, both CRISPR/Cas and computer-aided design are powerful intelligent tools, particularly for the complex macro-biomolecular characteristics in higher living organisms and drug candidates from synthetic chemicals. However, they are not suitable for the design, modification, and preparation of *de novo* defensins and other AMPs with strong cationic polarity and low stability. Surprisingly, simple DNA truncation guided by evolution analysis proved to be a powerful free climbing and scaffolding tool to successfully try and improve druggability in this work. Its importance of methodology could be highly expected from plectasin as the first defensin and model AMP in fungi with better feasibilities and possibilities during screening for new antibacterial agents from fungi source.

Overall, this work reminds us that truncation is an effective and powerful tool to carry out simple DNA editing for the purpose of improving defensin druggability, and its feasibility has been confirmed in this study. The successful high-density expression of Ple-AB in *P. Pastoris* contributes to a reduction in the cost of peptide drugs, and the better antibacterial characteristics specifically for

druggability and safety shown by Ple-AB *in vivo* and *in vitro* also prove it to be a better drug candidate. The reason that Ple-AB increases tolerance to trypsin and its antimicrobial mechanism still need to be explored and disclosed.

Data availability statement

The datasets presented in this study can be found in online repositories. The names of the repository/repository and accession number(s) can be found in the article/supplementary material.

Ethics statement

The animal study was approved by the Animal Care and Use Committee of the Feed Research Institute of Chinese Academy of Agricultural Sciences. The study was conducted in accordance with the local legislation and institutional requirements.

Author contributions

XL: Data curation, Formal analysis, Investigation, Writing – original draft, Methodology. YH: Funding acquisition, Methodology, Validation, Writing – review & editing, Resources, Conceptualization, Supervision. NY: Methodology, Validation, Writing – review & editing. RM: Methodology, Resources, Writing – review & editing. DT: Methodology, Resources, Writing – review & editing, Project administration. JW: Conceptualization, Funding acquisition, Project

administration, Resources, Validation, Writing – review & editing, Supervision, Methodology.

Funding

The author(s) declare financial support was received for the research, authorship, and/or publication of this article. This research was funded by the National Natural Science Foundation of China (Grant Nos. 31702146 and 31872393), the AMP Direction of the National Innovation Program of Agricultural Science and Technology in CAAS (Grant CAAS-ASTIP-2013-FRI-02), and the Key Project of Alternatives to Antibiotics for Feed (Grant CAAS-ZDXT2018008) and Animal (Grant CAAS-ZDRW202111) Usages—the National Agricultural Science and Technology Innovation Program.

Conflict of interest

The authors declare that the research was conducted in the absence of any commercial or financial relationships that could be construed as a potential conflict of interest.

Publisher's note

All claims expressed in this article are solely those of the authors and do not necessarily represent those of their affiliated organizations, or those of the publisher, the editors and the reviewers. Any product that may be evaluated in this article, or claim that may be made by its manufacturer, is not guaranteed or endorsed by the publisher.

References

- Aminov, R. (2022). Editorial: insights in antimicrobials, resistance, and chemotherapy: 2021. *Front. Microbiol.* 13:1037326. doi: 10.3389/fmicb.2022.1037326
- Andes, D., Craig, W., Nielsen, L. A., and Kristensen, H. H. (2009). In vivo pharmacodynamic characterization of a novel plectasin antibiotic, NZ2114, in a murine infection model. *Antimicrob. Agents Chemother.* 53, 3003–3009. doi: 10.1128/AAC.01584-08
- Assis, L. M., Nedeljković, M., and Dessen, A. (2017). New strategies for targeting and treatment of multi-drug resistant *Staphylococcus aureus*. *Drug Resist. Updat.* 31, 1–14. doi: 10.1016/j.drug.2017.03.001
- Bonnel, C., Legrand, B., Simon, M., Clavie, M., Masnou, A., Jumas-Bilak, E., et al. (2020). Tailoring the physicochemical properties of antimicrobial peptides onto a thiazole-based gamma-peptide foldamer. *J. Med. Chem.* 63, 9168–9180. doi: 10.1021/acs.jmedchem.0c00077
- Brinch, K. S., Sandberg, A., Baudoux, P., Van Bambeke, F., Tulkens, P. M., Fridtjof-Møller, N., et al. (2009). Plectasin shows intracellular activity against *Staphylococcus aureus* in human THP-1 monocytes and in a mouse peritonitis model. *Antimicrob. Agents Chemother.* 53, 4801–4808. doi: 10.1128/AAC.00685-09
- Brinkerhoff, L. H., Kalashnikov, V. V., Thompson, L. W., Yamshchikov, G. V., Pierce, R. A., Galavotti, H. S., et al. (1999). Terminal modifications inhibit proteolytic degradation of an immunogenic mart-127-35 peptide: implications for peptide vaccines. *Int. J. Cancer* 83, 326–334. doi: 10.1002/(SICI)1097-0215(19991029)83:3<326::AID-IJC7>3.0.CO;2-X
- Chambers, H. F., and DeLeo, F. R. (2009). Waves of resistance: *Staphylococcus aureus* in the antibiotic era. *Nat. Rev. Microbiol.* 7, 629–641. doi: 10.1038/nrmicro2200
- Chen, J., Gao, M., Wang, L., Li, S., He, J., Qin, A., et al. (2018). Aggregation-induced emission probe for study of the bactericidal mechanism of antimicrobial peptides. *ACS Appl. Mater. Interfaces* 10, 11436–11442. doi: 10.1021/acsami.7b18221
- Choi, H., Hwang, J. S., Kim, H., and Lee, D. G. (2013). Antifungal effect of CopA3 monomer peptide via membrane-active mechanism and stability to proteolysis of enantiomeric D-CopA3. *Biochem. Biophys. Res. Commun.* 440, 94–98. doi: 10.1016/j.bbrc.2013.09.021
- Elliott, A. G., Huang, J. X., Neve, S., Zuegg, J., Edwards, I. A., Cain, A. K., et al. (2020). An amphipathic peptide with antibiotic activity against multidrug-resistant gram-negative bacteria. *Nat. Commun.* 11:3184. doi: 10.1038/s41467-020-16950-x
- Foster, T. J. (2017). Antibiotic resistance in *Staphylococcus aureus*. Current status and future prospects. *FEMS Microbiol. Rev.* 41, 430–449. doi: 10.1093/femsre/fux007
- Guo, Y., Song, G., Sun, M., Wang, J., and Wang, Y. (2020). Prevalence and therapies of antibiotic-resistance in *Staphylococcus aureus*. *Front. Cell. Infect. Microbiol.* 10:107. doi: 10.3389/fcimb.2020.00107
- Hao, Y., Teng, D., Mao, R., Yang, N., and Wang, J. (2023). Site mutation improves the expression and antimicrobial properties of fungal Defense. *Antibiotics (Basel)*. 12:1283. doi: 10.3390/antibiotics12081283
- Hao, Y., Wang, J., de la Fuente-Nunez, C., and Franco, O. L. (2022). Editorial: antimicrobial peptides: molecular design, structure-function relationship, and biosynthesis optimization. *Front. Microbiol.* 13:888540. doi: 10.3389/fmicb.2022.888540
- Harkins, C. P., McAleer, M. A., Bennett, D., McHugh, M., Fleury, O. M., Pettigrew, K. A., et al. (2018). The widespread use of topical antimicrobials enriches for resistance in *Staphylococcus aureus* isolated from patients with atopic dermatitis. *Br. J. Dermatol.* 179, 951–958. doi: 10.1111/bjd.16722
- Humphries, R. M., Pollett, S., and Sakoulas, G. (2013). A current perspective on daptomycin for the clinical microbiologist. *Clin. Microbiol. Rev.* 26, 759–780. doi: 10.1128/CMR.00030-13
- Jahan, N., Patton, T., and O'Keefe, M. (2022). The influence of antibiotic resistance on innate immune responses to *Staphylococcus aureus* infection. *Antibiotics (Basel)* 11:542. doi: 10.3390/antibiotics11050542
- Jiang, Y., Chen, Y., Song, Z., Tan, Z., and Cheng, J. (2021). Recent advances in design of antimicrobial peptides and polypeptides toward clinical translation. *Adv. Drug Deliv. Rev.* 170, 261–280. doi: 10.1016/j.addr.2020.12.016

- Jin, Y., Yang, N., Teng, D., Mao, R., Hao, Y., and Wang, J. (2023). Molecular modification of Kex2 P1' site enhances expression and druggability of fungal defensin. *Antibiotics (Basel)*. 12:786. doi: 10.3390/antibiotics12040786
- Jung, N., and Rieg, S. (2018). Essentials in the management of *S. aureus* bloodstream infection. *Infection* 46, 441–442. doi: 10.1007/s15010-018-1130-8
- Kim, S. H., Park, W. B., Lee, K. D., Kang, C. I., Bang, J. W., Kim, H. B., et al. (2004). Outcome of inappropriate initial antimicrobial treatment in patients with methicillin-resistant *Staphylococcus aureus* bacteraemia. *J. Antimicrob. Chemother.* 54, 489–497. doi: 10.1093/jac/dkh366
- Koopmans, T., Wood, T. M., Hart, P., Kleijn, L. H. J., Hendrickx, A. P. A., Willems, R. J. L., et al. (2015). Semisynthetic lipopeptides derived from nisin display antibacterial activity and lipid II binding on par with that of the parent compound. *J. Am. Chem. Soc.* 137, 9382–9389. doi: 10.1021/jacs.5b04501
- Koseki, J., Hayashi, S., Kojima, Y., Hirose, H., and Shimamura, T. (2023). Topological data analysis of protein structure and inter/intra-molecular interaction changes attributable to amino acid mutations. *Comput. Struct. Biotechnol. J.* 21, 2950–2959. doi: 10.1016/j.csbj.2023.05.009
- Lei, Z., Zhang, D., Lu, B., Zhou, W., and Wang, D. (2018). Activation of mast cells in skin abscess induced by *Staphylococcus aureus* (*S. aureus*) infection in mice. *Res. Vet. Sci.* 118, 66–71. doi: 10.1016/j.rvsc.2018.01.016
- Li, T., Wang, Z., Han, H., Teng, D., Mao, R., Hao, Y., et al. (2020). Dual antibacterial activities and biofilm eradication of a marine peptide-N6NH₂ and its Analogs against multidrug-resistant *Aeromonas veronii*. *Int. J. Mol. Sci.* 21:9637. doi: 10.3390/ijms21249637
- Li, Z., Wang, X., Wang, X., Teng, D., Mao, R., Hao, Y., et al. (2017). Improved antibacterial activity of the marine peptide N6 against intracellular *Salmonella Typhimurium* by conjugating with the cell-penetrating peptide Tat11 via a cleavable linker. *J. Med. Chem.* 61, 7991–8000. doi: 10.1021/acs.jmedchem.8b01079
- Li, S., Wang, Y., Xue, Z., Jia, Y., Li, R., He, C., et al. (2021). The structure-mechanism relationship and mode of actions of antimicrobial peptides: a review. *Trends Food Sci. Technol.* 109, 103–115. doi: 10.1016/j.tifs.2021.01.005
- Liu, H., Yang, N., Mao, R., Teng, D., Hao, Y., Wang, X., et al. (2020). A new high-yielding antimicrobial peptide NZX and its antibacterial activity against *Staphylococcus hyicus* in vitro/vivo. *Appl. Microbiol. Biotechnol.* 104, 1555–1568. doi: 10.1007/s00253-019-10313-3
- Liu, H., Yang, N., Teng, D., Mao, R., Hao, Y., Ma, X., et al. (2021). Fatty acid modified-antimicrobial peptide analogues with potent antimicrobial activity and topical therapeutic efficacy against *Staphylococcus hyicus*. *Appl. Microbiol. Biotechnol.* 105, 5845–5859. doi: 10.1007/s00253-021-11454-0
- Loussouarn, A., Behar, G., Pecorari, F., Croyal, M., and Renodon-Corniere, A. (2020). Characterization of Affitin proteolytic digestion in biorelevant media and improvement of their stabilities via protein engineering. *Sci. Rep.* 10:19703. doi: 10.1038/s41598-020-76855-z
- Lyu, Y., Chen, T., Shang, L., Yang, Y., Li, Z., Zhu, J., et al. (2019). Design of Trp-Rich Dodecapeptides with broad-Spectrum antimicrobial potency and membrane-disruptive mechanism. *J. Med. Chem.* 62, 6941–6957. doi: 10.1021/acs.jmedchem.9b00288
- Mandal, K., Pentelute, B. L., Tereshko, V., Thammavongsa, V., Schneewind, O., Kossiakoff, A. A., et al. (2009). Racemic crystallography of synthetic protein enantiomers used to determine the X-ray structure of plectasin by direct methods. *Protein Sci.* 18, 1146–1154. doi: 10.1002/pro.127
- Mao, R., Teng, D., Wang, X., Zhang, Y., Jiao, J., Cao, X., et al. (2015). Optimization of expression conditions for a novel NZ2114-derived antimicrobial peptide-MP1102 under the control of the GAP promoter in *Pichia pastoris* X-33. *BMC Microbiol.* 15:57. doi: 10.1186/s12866-015-0389-5
- Miller, W. R., Bayer, A. S., and Arias, C. A. (2016). Mechanism of action and resistance to daptomycin in *Staphylococcus aureus* and *enterococci*. *Cold Spring Harb. Perspect. Med.* 6:a026997. doi: 10.1101/cshperspect.a026997
- Mohammad, M., Na, M., Hu, Z., Nguyen, M. T., Kopparapu, P. K., Jarneborn, A., et al. (2021). *Staphylococcus aureus* lipoproteins promote abscess formation in mice, shielding bacteria from immune killing. *Commun. Biol.* 4:432. doi: 10.1038/s42003-021-01947-z
- Mygind, P. H., Fischer, R. H., Schnorr, K. M., Hansen, M. T., Sonksen, C. P., Ludvigsen, S., et al. (2005). Plectasin is a peptide antibiotic with therapeutic potential from a saprophytic fungus. *Nature* 437, 975–980. doi: 10.1038/nature04051
- Paling, F. P., Wolkewitz, M., Bode, L. G. M., Klein Klouwenberg, P. M. C., Ong, D. S. Y., Depuydt, P., et al. (2017). *Staphylococcus aureus* colonization at ICU admission as a risk factor for developing *S. aureus* ICU pneumonia. *Clin. Microbiol. Infect.* 23, 49.e9–49.e14. doi: 10.1016/j.cmi.2016.09.022
- Pidwill, G. R., Gibson, J. F., Cole, J., Renshaw, S. A., and Foster, S. J. (2020). The role of macrophages in *Staphylococcus aureus* infection. *Front. Immunol.* 11:620339. doi: 10.3389/fimmu.2020.620339
- Pohl, C., Effantin, G., Kandiah, E., Meier, S., Zeng, G., Streicher, W., et al. (2022). pH- and concentration-dependent supramolecular assembly of a fungal defensin plectasin variant into helical non-amyloid fibrils. *Nat. Commun.* 13:3162. doi: 10.1038/s41467-022-30462-w
- Politti, E. J. G., Szkuta, P. T., Burns, N., and Foster, S. J. (2018). *Staphylococcus aureus* infection dynamics. *PLoS Pathog.* 14:e1007112. doi: 10.1371/journal.ppat.1007112
- Schneider, T., Kruse, T., Wimmer, R., Wiedemann, I., Sass, V., Pag, U., et al. (2010). Plectasin, a fungal defensin, targets the bacterial cell wall precursor lipid II. *Science* 328, 1168–1172. doi: 10.1126/science.1185723
- Shishkina, L. N., Mazurkov, O. Y., Bormotov, N. I., Skarnovich, M. O., Serova, O. A., Mazurkova, N. A., et al. (2023). Safety and pharmacokinetics of the substance of the anti-smallpox drug NIOCH-14 after Oral administration to laboratory animals. *Viruses* 15:205. doi: 10.3390/v15010205
- Stone, T. A., Cole, G. B., Ravamehr-Lake, D., Nguyen, H. Q., Khan, F., Sharpe, S., et al. (2019). Positive charge patterning and hydrophobicity of membrane-active antimicrobial peptides as determinants of activity, toxicity, and pharmacokinetic stability. *J. Med. Chem.* 62, 6276–6286. doi: 10.1021/acs.jmedchem.9b00657
- Takada, M., Ito, T., Kurashima, M., Matsunaga, N., Demizu, Y., and Misawa, T. (2022). Structure-activity relationship studies of substitutions of cationic amino acid residues on antimicrobial peptides. *Antibiotics (Basel)* 12:19. doi: 10.3390/antibiotics12010019
- Wang, C., Hong, T., Cui, P., Wang, J., and Xia, J. (2021). Antimicrobial peptides towards clinical application: delivery and formulation. *Adv. Drug Deliv. Rev.* 175:113818. doi: 10.1016/j.addr.2021.05.028
- Wang, D., Shi, J., Chen, C., Wang, Z., and Liu, Y. (2022). Truncated Pleurocidin derivative with high pepsin hydrolysis resistance to combat multidrug-resistant pathogens. *Pharmaceutics* 14:2025. doi: 10.3390/pharmaceutics14102025
- Wang, X., Wang, X., Teng, D., Mao, R., Hao, Y., Yang, N., et al. (2018). Increased intracellular activity of MP1102 and NZ2114 against *Staphylococcus aureus* in vitro and in vivo. *Sci. Rep.* 8:4204. doi: 10.1038/s41598-018-22245-5
- Wilmes, M., and Sahl, H. G. (2014). Defensin-based anti-infective strategies. *Int. J. Med. Microbiol.* 304, 93–99. doi: 10.1016/j.ijmm.2013.08.007
- Wu, Y., Gao, B., and Zhu, S. (2014). Fungal defensins, an emerging source of anti-infective drugs. *Chin. Sci. Bull.* 59, 931–935. doi: 10.1007/s11434-014-0165-1
- Wu, Y., Yang, N., Mao, R., Hao, Y., Teng, D., and Wang, J. (2022). In vitro pharmacodynamics and bactericidal mechanism of fungal defensin-derived peptides NZX and P2 against *Streptococcus agalactiae*. *Microorganisms* 10:881. doi: 10.3390/microorganisms10050881
- Yang, N., Aminov, R., Franco, O. L., de la Fuente-Nunez, C., and Wang, J. (2023). Editorial: community series in antimicrobial peptides: molecular design, structure function relationship and biosynthesis optimization. *Front. Microbiol.* 14:1125426. doi: 10.3389/fmicb.2023.1125426
- Yang, Z., He, S., Wu, H., Yin, T., Wang, L., and Shan, A. (2021). Nanostructured antimicrobial peptides: crucial steps of overcoming the bottleneck for clinics. *Front. Microbiol.* 12:710199. doi: 10.3389/fmicb.2021.710199
- Yang, N., Liu, X., Teng, D., Li, Z., Wang, X., Mao, R., et al. (2017). Antibacterial and detoxifying activity of NZ17074 analogues with multi-layers of selective antimicrobial actions against *Escherichia coli* and *Salmonella enteritidis*. *Sci. Rep.* 7:3392. doi: 10.1038/s41598-017-03664-2
- Yang, N., Teng, D., Mao, R., Hao, Y., Wang, X., Wang, Z., et al. (2019). A recombinant fungal defensin-like peptide-P2 combats multidrug-resistant *Staphylococcus aureus* and biofilms. *Appl. Microbiol. Biotechnol.* 103, 5193–5213. doi: 10.1007/s00253-019-09785-0
- Zhang, Y., Teng, D., Mao, R., Wang, X., Xi, D., Hu, X., et al. (2014). High expression of a plectasin-derived peptide NZ2114 in *Pichia pastoris* and its pharmacodynamics, postantibiotic and synergy against *Staphylococcus aureus*. *Appl. Microbiol. Biotechnol.* 98, 681–694. doi: 10.1007/s00253-013-4881-2
- Zhang, Y., Teng, D., Wang, X., Mao, R., Cao, X., Wang, J., et al. (2015). In vitro and in vivo characterization of a new recombinant antimicrobial peptide, MP1102, against methicillin-resistant *Staphylococcus aureus*. *Appl. Microbiol. Biotechnol.* 99, 6255–6266. doi: 10.1007/s00253-015-6394-7
- Zhang, J., Yang, Y., Teng, D., Tian, Z., Wang, S., and Wang, J. (2011). Expression of plectasin in *Pichia pastoris* and its characterization as a new antimicrobial peptide against *Staphylococcus* and *Streptococcus*. *Protein Expr. Purif.* 78, 189–196. doi: 10.1016/j.pep.2011.04.014
- Zhao, Y., Zhang, M., Qiu, S., Wang, J., Peng, J., Zhao, P., et al. (2016). Antimicrobial activity and stability of the D-amino acid substituted derivatives of antimicrobial peptide polybia-MPI. *AMB Express* 6:122. doi: 10.1186/s13568-016-0295-8
- Zheng, X., Teng, D., Mao, R., Hao, Y., Yang, N., Hu, F., et al. (2021). A study on fungal defensin against multidrug-resistant *Clostridium perfringens* and its treatment on infected poultry. *Appl. Microbiol. Biotechnol.* 105, 7265–7282. doi: 10.1007/s00253-021-11500-x
- Zhu, Y., Shao, C., Li, G., Lai, Z., Tan, P., Jian, Q., et al. (2020). Rational avoidance of protease cleavage sites and symmetrical end-tagging significantly enhances the stability and therapeutic potential of antimicrobial peptides. *J. Med. Chem.* 63, 9421–9435. doi: 10.1021/acs.jmedchem.0c00583
- Zou, W., Zhang, Y., Zhou, M., Chen, X., Ma, C., Wang, T., et al. (2022). Exploring the active core of a novel antimicrobial peptide, palustrin-2LTb, from the Kuatun frog, *Hylarana latouchii*, using a bioinformatics-directed approach. *Comput. Struct. Biotechnol. J.* 20, 6192–6205. doi: 10.1016/j.csbj.2022.11.016



OPEN ACCESS

EDITED BY

Guangshun Wang,
University of Nebraska Medical Center,
United States

REVIEWED BY

Ruifang Li,
Henan University of Technology, China
Santi M. Mandal,
Indian Institute of Technology Kharagpur, India
Jayaram L. N.,
Dayananda Sagar College of Engineering, India

*CORRESPONDENCE

Uwe Müller
✉ u.mueller@vetmed.uni-leipzig.de
Alexandra Brakel
✉ alexandra.brakel@uni-leipzig.de

RECEIVED 27 October 2023

ACCEPTED 18 December 2023

PUBLISHED 08 January 2024

CITATION

Brakel A, Grochow T, Fritsche S, Knappe D,
Krizsan A, Fietz SA, Alber G, Hoffmann R and
Müller U (2024) Evaluation of proline-rich
antimicrobial peptides as potential lead
structures for novel antimycotics against
Cryptococcus neoformans.
Front. Microbiol. 14:1328890.
doi: 10.3389/fmicb.2023.1328890

COPYRIGHT

© 2024 Brakel, Grochow, Fritsche, Knappe,
Krizsan, Fietz, Alber, Hoffmann and Müller. This
is an open-access article distributed under the
terms of the [Creative Commons Attribution
License \(CC BY\)](https://creativecommons.org/licenses/by/4.0/). The use, distribution or
reproduction in other forums is permitted,
provided the original author(s) and the
copyright owner(s) are credited and that the
original publication in this journal is cited, in
accordance with accepted academic practice.
No use, distribution or reproduction is
permitted which does not comply with these
terms.

Evaluation of proline-rich antimicrobial peptides as potential lead structures for novel antimycotics against *Cryptococcus neoformans*

Alexandra Brakel^{1,2*}, Thomas Grochow³, Stefanie Fritsche^{2,4},
Daniel Knappe^{1,2}, Andor Krizsan^{1,2}, Simone A. Fietz³,
Gottfried Alber^{2,4}, Ralf Hoffmann^{1,2} and Uwe Müller^{2,4*}

¹Institute of Bioanalytical Chemistry, Faculty of Chemistry and Mineralogy, Bioanalytical Chemistry, Leipzig University, Leipzig, Germany, ²Center for Biotechnology and Biomedicine, Leipzig University, Leipzig, Germany, ³Institute of Veterinary Anatomy, Histology and Embryology, Faculty of Veterinary Medicine, Leipzig University, Leipzig, Germany, ⁴Institute of Immunology/Molecular Pathogenesis, Faculty of Veterinary Medicine, Leipzig University, Leipzig, Germany

Background: Cryptococcosis and cryptococcal meningitis, caused by *Cryptococcus neoformans* infections, lead to approximately 180,000 deaths per year, primarily in developing countries. Individuals with compromised immune systems, e.g., due to HIV infection (AIDS) or chemotherapy, are particularly vulnerable. Conventional treatment options are often limited and can cause severe side effects. Therefore, this study aimed to investigate the antifungal effect of insect-derived proline-rich antimicrobial peptides (PrAMPs) against *C. neoformans*. These peptides are known for their low toxicity and their high efficacy in murine infection models, making them a promising alternative for treatment.

Results: A preliminary screening of the minimal inhibitory concentrations (MICs) of 20 AMPs, including the well-known PrAMPs Onc112, Api137, and Chex1Arg20 as well as the cathelicidin CRAMP against the *C. neoformans* strains 1841, H99, and KN99 α revealed promising results, with MICs as low as 1.6 μ mol/L. Subsequent investigations of selected peptides, determining their influence on fungal colony-forming units, confirmed their strong activity. The antifungal activity was affected by factors such as peptide net charge and sequence, with stronger effects at higher net charges probably due to better intracellular uptake confirmed by confocal laser scanning microscopy. Inactive scrambled peptides suggest a specific intracellular target, although scanning electron microscopy showed that PrAMPs also damaged the cell exterior for a low proportion of the cells. Possible pore formation could facilitate entry into the cytosol.

KEYWORDS

antifungal peptide, fungal pathogen, intracellular mode-of-action, proline-rich antimicrobial peptide (PrAMP), scanning electron microscopy

1 Introduction

Fungal infections are widespread in populations of both developing and developed countries. Most people suffer from superficial fungal infections, usually of the skin, hair, or nails, during their lifetime that are not a major health concern (Bongomin et al., 2017; Fisher et al., 2020). Although the number of invasive fungal infections is significantly lower, it is of greater concern due to its high mortality rate, accounting for 1.5 million deaths per year. Species of *Candida*, *Pneumocystis*, *Aspergillus*, or *Cryptococcus* are responsible for approximately 90% of the deaths, primarily affecting individuals with compromised immune systems (Brown et al., 2012; Schmiedel and Zimmerli, 2016; Fisher et al., 2020). The prevalence of fungal infections, such as cryptococcosis or cryptococcal meningitis caused by *Cryptococcus neoformans*, has been steadily increasing since the 1950s, particularly in developing countries, due to HIV infection (AIDS) and modern immunosuppressive and invasive medical interventions, including chemotherapy (Hazen, 1995). Exposure to *C. neoformans* occurs primarily through inhalation of airborne organisms into the lungs, often transmitted by feces of various avian species (Cafarchia et al., 2006). The fungus primarily targets the central nervous system, causing inflammation of the brain and meninges (Park et al., 2009).

C. neoformans can be divided into three serotypes, i.e., serotype A (*C. n. var. grubii*), serotype D (*C. n. var. neoformans*), and a hybrid form (serotype AD). Differences in the capsular composition, melanin production, or maximum growth temperature, pose severe challenges in the development of antifungal drugs, as they must be effective against all strains and ideally should not induce resistance (Samarasinghe et al., 2018; Casadevall et al., 2019). It is also important that the antifungals are effective against all variants so that they can be used consistently regardless of the geographical occurrence of the serotypes, e.g., serotype A is predominant worldwide and serotype D is predominant in Europe (Martinez et al., 2001; Montoya et al., 2021).

The main drugs used for treatment are amphotericin B, fluconazole, and flucytosine in various combinations (Ngan et al., 2022). The administration of these antifungals is problematic due to their nephro- and neurotoxicity, as well as various gastrointestinal side effects (Muhaj et al., 2022). In addition, the rapid emergence of drug resistance is a growing challenge, underscoring the urgent need for the development of new classes of antifungal agents (Denning and Hope, 2010; Fisher et al., 2022).

In the quest for novel anti-infectives, antimicrobial peptides have attracted considerable attention in recent decades. Most of the antifungal peptides studied rely primarily on membrane disruption owing to their structural characteristics, such as positive charge and hydrophobicity (Sharma et al., 2017; Li et al., 2021; Sharma et al., 2022). However, a lytic mode of action always carries the risk of adverse effects, which is why intracellular mechanisms are preferred (Struyfs et al., 2021). Proline-rich AMPs (PrAMPs), which have been extensively studied *in vitro* and *in vivo* primarily for their activity against Gram-negative and Gram-positive bacteria over the past two decades, target the bacterial ribosome (Krizsan et al., 2014; Kolano et al., 2021). Short PrAMPs were originally isolated from insects, such as the milkweed bug (*Oncopeltus fasciatus*) or the honeybee (*Apis mellifera*), and further optimized for therapeutic applications by improving their activity against various bacteria and their protease (serum) stability (Knappe et al., 2010; Berthold et al., 2013; Knappe et al., 2016). Synthetic derivatives such as Api137, Onc112, or Chex1Arg20 bind to the

chaperone DnaK and the 70S ribosome after active transport into the cell, thereby inhibiting protein folding, and translation during protein biosynthesis (Krizsan et al., 2014, 2015a,b; Brakel et al., 2022a,b). PrAMPs have proven to be valid lead compounds due to their high efficacy in murine infection models and their low adverse effects in animals, all of which can be attributed to their bacteria-specific uptake and targeting of the bacterial ribosome (Holfeld et al., 2015; Schmidt et al., 2017; Brakel et al., 2019). Little is known about the activity of PrAMPs against eukaryotic pathogens, e.g., fungi or protozoan parasites. In this context, we have devoted ourselves to the aforementioned fungus, *C. neoformans*, which is one of the main causes of death caused by invasive fungi. The mammalian PrAMPs SP-E (from porcine saliva) and Bac7 (from bovine neutrophils) are active against *C. neoformans* in the low micromolar range (Benincasa et al., 2004; Conti et al., 2013). Initial investigations have suggested the possibility of an intracellular mode of action against fungi, but to our knowledge, this has not been pursued further. Given the promising properties of insect-derived PrAMPs, this study aimed to investigate their activity against *C. neoformans* for the first time. While native apidaecin 1b, drosocin, and pyrrhocoricin were inactive against *C. neoformans*, a few optimized analogs of apidaecin and the designer peptide Chex1Arg20, also called ARV-1502, were highly active against three clinically relevant pathogenic *C. neoformans* strains with minimum inhibitory concentrations (MICs) of 4 mg/L (1.6 to 3 μ mol/L). Fluorescence microscopy confirmed that these peptides enter the fungal cells, suggesting an intracellular mechanism. Interestingly, reverse sequences showed similar activities, challenging the ribosome as the primary target.

2 Materials and methods

2.1 Materials

Reagents were obtained from the following manufacturers: Carl Roth GmbH & Co. KG (Karlsruhe, Germany): Agar-Agar (Kobe I), ethanol (HPLC grade), D (+)-glucose monohydrate (> 99.5%), glutaraldehyde (25%, for electron microscopy) 1,1,1,3,3,3-hexamethyldisilazane (HMDS, \geq 98%), paraformaldehyde, sodium dodecyl sulfate (SDS, >99.5%), and sodium hydroxide (> 98%); Degussa AG (Hanau, Germany): Osmium tetroxide (75%); Sigma Aldrich Chemie GmbH (Taufkirchen, Germany): Amphotericin B, 5(6)-carboxyfluorescein (for fluorescence), dimethyl sulfoxide (DMSO, \geq 99.9%), disodium hydrogen phosphate (> 98%), fluconazole, flucytosine, glycerol-gelatin mounting medium (GG1), poly-L-lysine solution (0.01%), sodium dihydrogen phosphate (>99%), thiazolyl blue tetrazolium bromide (MTT; \geq 97.5%), and Triton X-100; Thermo Fisher Scientific Inc. (Darmstadt, Germany): Gibco® DMEM/F-12 medium, Gibco® PBS, Gibco® Penicillin–Streptomycin (10,000 U/mL), and Gibco® Trypsin–EDTA (0.5%); VWR International GmbH (Darmstadt, Germany): peptone (from casein).

Porcine blood (fattening hybrid pig, German Landrace x Pietrain) for the determination of hemolytic activity was obtained from the Veterinary Faculty of the Leipzig University. The blood collection was performed in accordance with the German Animal Welfare legislation and approved by the Landesdirektion Sachsen (reference number 25–5131/556/16).

2.2 Peptide synthesis

Peptides were synthesized in-house using Fmoc/Bu-chemistry on Rink amide or Wang resin and purified by RP-HPLC using a linear acetonitrile gradient in the presence of 0.1% TFA as previously reported (Knappe et al., 2010; Berthold et al., 2013). Masses were confirmed by ESI-MS and the purities (> 90%) were determined by RP-HPLC recording the absorbance at 214 nm. To obtain fluorophore-labeled peptides, 5(6)-carboxyfluorescein was coupled to the N-terminus of Onc112, Chex1Arg20, Chex1Arg20 D4K and Apidaecin 1b or at the δ -amino group of ornithine of Api88, Api137 and Api795 upon completion of the peptide synthesis.

2.3 Microorganisms, media, and growth conditions

The encapsulated strain *C. neoformans* 1841 (serotype D), which was originally isolated from the cerebrospinal fluid (CSF) of an AIDS patient was obtained from F. Hoffmann-La Roche Ltd., Basel (Decken et al., 1998). H99 and KN99 α (both serotype A) were kindly provided by K.J. Kwon-Chung (NIH, Bethesda, MD, USA) and G. Jarbon (Institute Pasteur, Paris, France), respectively.

The strains were grown in Sabouraud medium (SAB, 2% glucose, 1% peptone) overnight at 30°C on an orbital shaker (80 rpm). The cells were centrifuged (10 min, 4°C, 400 \times g, Allegra X-22R, Rotor SX4250, Beckmann Coulter, Krefeld, Germany) and the cell pellet was washed with phosphate buffer (10 mmol/L Na₂HPO₄/NaH₂PO₄, pH 7.5). After a second centrifugation step, the cells were re-suspended and cell counts (mentioned in the respective method section) were adjusted with 50% SAB in phosphate buffer. Colony-forming units (CFU) were determined on SAB agar plates (2% glucose, 1% peptone, 2% agar).

2.4 Broth microdilution assay

MIC values were determined using a liquid broth microdilution assay in sterile 96-well plates (polystyrene F-bottom, Greiner Bio-One GmbH) with a total volume of 100 μ L per well. Aqueous peptide solutions (3 g/L) were serially diluted twofold with 50% SAB in phosphate buffer starting at a peptide concentration of 128 mg/L (50 μ L/well). Overnight cultures were performed as described above. The cell count was adjusted to 1×10^5 CFU/mL to achieve a final concentration of 5×10^4 CFU/mL per well (50 μ L/well). Plates were incubated at 30°C and the optical density was measured at 595 nm (OD₅₉₅) after 24 h and 48 h, respectively, using a microplate reader (Victor³, Perkin Elmer, Waltham, USA). The MIC was defined as the lowest peptide concentration preventing visible fungal growth. Experiments were performed as triplicates and repeated at least once on another day.

2.5 Antifungal activity assay

To determine antifungal activity by plating out on agar plates, overnight cultures were diluted to 5×10^4 CFU/mL with 50% SAB in phosphate buffer. Aqueous peptide solutions were added at various concentrations (20 μ L) to the cell suspension (80 μ L). Samples were incubated at 30°C on an orbital shaker (750 rpm, Titramax 1,000,

Heidolph Instruments GmbH & Co. KG, Schwabach, Germany) for 3 h. After incubation, samples were stored on ice and diluted 30-fold with phosphate buffer. Aliquots of the diluted cell suspensions (100 μ L) were plated onto SAB agar plates. Plates were incubated at 30°C and colonies were counted after 24 h and 48 h, respectively.

2.6 Time-kill assay

The kinetic effects of the antifungal activity were determined by diluting overnight cultures to 5×10^4 CFU/mL with 50% SAB in phosphate buffer. Aqueous peptide solutions (20 μ L) were added to the cell suspension (80 μ L) to give a final peptide concentration of 2.5 μ mol/L. Samples were incubated at 30°C on an orbital shaker (750 rpm, Titramax 1,000, Heidolph Instruments GmbH & Co. KG) for 24 h. Before incubation (0 min) and after 45 min, 90 min, 3 h, 6 h, and 24 h incubation, aliquots (10 μ L) of samples were taken and diluted with phosphate buffer (10 mmol/L, pH 7.5) to observe countable cell colonies. Aliquots (100 μ L) of the diluted cell suspensions were plated on SAB agar plates. Plates were incubated at 30°C and colonies were counted after 24 h.

2.7 Confocal laser scanning microscopy (CLSM) and deconvolution

Overnight cultures of *C. neoformans* 1841 were prepared as described above and adjusted with 50% SAB in phosphate buffer to reach 5×10^6 CFU/mL. Aqueous peptide solutions (20 μ L) were added to the cell suspension (80 μ L) to give a final peptide concentration of 25 μ mol/L in each well. Samples were incubated at 30°C on an orbital shaker (750 rpm, Titramax 1,000, Heidolph Instruments GmbH & Co. KG) for 3 h. Afterwards, samples were centrifuged (2,000 \times g, 10 min, 4°C, Microfuge 22R, Beckmann Coulter), cell pellets were washed with ice-cold phosphate-buffered saline (PBS, 100 μ L) and centrifuged again. The supernatant was discarded and the cells were fixed with 4% paraformaldehyde in PBS (25 μ L, 30 min, RT). After centrifugation, the cell pellets were re-suspended in 2.5 μ L PBS. For immobilization, glycerol-gelatin mounting medium was heated to 60°C in a water bath. A small drop was placed on a microscope slide, the re-suspended cell suspension was pipetted into the drop and covered with a coverslip. Samples were analyzed with a Leica TCS SP8 DMI8 confocal laser-scanning microscope (Leica Microsystems, Mannheim, Germany) using the objective HC PL APO CS2 63 \times /1.30 GLYC and the software Leica Application Suite X (LAS-X 3.5.7). 5(6)-carboxyfluorescein labeled peptides were excited at 496 nm (HyD detection range 503–600 nm). Measurements across z-axis with 50 to 90 layers (12 to 15 μ m) were taken.

CLSM images were deconvoluted using the software Huygens Professional 20.10 (SVI, Hilversum, The Netherlands) with following deconvolution parameters: Classic Maximum Likelihood Estimation (CMLE) algorithm, maximum iterations = 30, quality change threshold = 0.01, signal-to-noise-ratio = 13, background = 0. Imaris 9.9 (Oxford Instruments, Abingdon, UK) was used for 3D visualization.

2.8 Scanning electron microscopy (SEM)

Overnight cultures of *C. neoformans* 1841 were prepared as described and adjusted with 50% SAB in phosphate buffer to reach

1×10^8 CFU/mL. Aqueous peptide solutions (20 μ L) were added to the cell suspension (80 μ L) to give a final peptide concentration of 200 μ mol/L. Samples were incubated at 30°C on an orbital shaker (750 rpm) for 3 h. Samples were centrifuged (2,000 \times g, 10 min, 4°C, Microfuge 22R, Beckmann Coulter), cell pellets were washed with ice-cold phosphate-buffered saline (PBS, 100 μ L) and centrifuged again. Cell pellets were re-suspended in PBS (25 μ L) and adhered overnight in humid atmosphere to glass coverslips (Borosilicate Glass, VWR International GmbH) previously coated with 0.001% poly-L-lysine (in case of Critical-Point Drying). Cells were fixed (2% glutaraldehyde, 2% paraformaldehyde, in PBS) for 60 min and afterwards stained with 1% OsO₄ in PBS for 60 min. The cells were gradually dehydrated in ethanol series (30, 50, 70, 85, 90, 96% (once), and 100% (thrice) for 10 min. The coverslips were critical-point-dried (Baltec CPD 030, BAL-TEC GmbH, Schalksmühle, Germany) or air-dried after incubation with HMDS (3 min, RT) and sputter coated with 20 nm gold/palladium (Baltec MED 020, BAL-TEC GmbH). Cells were visualized using the SEM secondary electron detector (Zeiss EVO LS 15 LaB₆, Carl Zeiss Microscopy Deutschland GmbH).

GraphPad Prism 10.0.3 software was used for statistical analysis of the recorded data. A Dunnett's multiple comparisons test (Ordinary-one-way ANOVA) was performed.

2.9 Cytotoxicity

Human embryonic kidney (HEK293) and human hepatoma (HepG2) cells were cultured in Dulbecco's modified Eagle's/Ham's F-12 medium (DMEM/F-12) containing 10% (v/v) fetal bovine serum and 1% (v/v) penicillin/streptomycin. Cells (20,000 in 200 μ L per well) were seeded into a 96-well plate (polystyrene F-bottom, Greiner Bio-One GmbH) and incubated for 24 h (37°C, 5% CO₂). Cells were washed with PBS (100 μ L) and peptide solutions (0.6 g/L in DMEM/F-12) were added. The positive control was a dilution series from 12 to 1.5% (v/v) DMSO and the negative control was 12% (v/v) PBS. After incubation (37°C, 24 h, 5% CO₂), the supernatant was discarded, fresh medium (90 μ L/well) and MTT (10 μ L/well, 5 g/L in PBS) were added, and the plate was incubated for 4 h (37°C, 5% CO₂). A solution (100 μ L) of sodium dodecyl sulfate (10% (v/v)) in hydrochloric acid (10 mmol/L) was added and the plate was incubated again for 24 h (37°C, 5% CO₂). Absorbance was recorded at 570 nm relative to the reference at 650 nm (PARADIGM™ microplate reader). All samples were corrected for the background absorbance of the medium. Relative cell viability was calculated as the ratio of absorbances recorded for treated and untreated cells (Kolano et al., 2021; Brakel et al., 2022a,b).

2.10 Hemolytic activity

Porcine blood was collected in EDTA tubes, stored at room temperature (RT) for 60 min, centrifuged (5 min, 1,000 \times g, 4°C), and the plasma supernatant removed. Concentrated porcine erythrocytes were diluted in PBS (2%) and 50 μ L/well were added to a serial peptide dilution series from 600 to 5 mg/L in PBS (50 μ L/well) in 96-well polypropylene plates (V-bottom, Greiner Bio-One GmbH) and incubated (37°C, 1 h). The plates were centrifuged (5 min, 1,000 \times g, 4°C), the supernatants (100 μ L) were transferred to flat-bottom 96-well plates, and the absorbance was recorded at 405 nm on a

microplate reader (PARADIGM™, Molecular Devices). PBS was used as negative control, and a serial dilution of triton X-100 from 0.1 to 0.00078% was used as a positive control (Czihal et al., 2012; Mohammed et al., 2023).

3 Results

3.1 Antifungal activity

Since *C. neoformans* infections can be caused by different serotypes (A and D) and mating types (α and α), three strains were included in this study. To investigate the influence of serotype on AMPs activity on fungi, strain *C. neoformans* H99 was chosen as an example for serotype A and *C. neoformans* 1841 for serotype D. The sexual morph KN99 α , which is closely related to strain H99, was included because the mating type α (MAT α) form is the more virulent form (Lin and Heitman, 2006). Thus, possible influences of the differences in the strains on the activity can be detected. The activity of 20 AMPs from four different PrAMP families, CRAMP, reverse CRAMP (sequences listed in Table 1), and the antifungals amphotericin B, fluconazole, and flucytosine were tested against *C. neoformans* strains 1841 (serotype D), H99 (serotype A), and KN99 α (serotype A, mating type MAT α) using a microdilution assay in 96-well-plates (Table 2). Although clear and reproducible MICs were already obtained after 24 h of incubation, the plates were further incubated and second MICs were determined after a total incubation time of 48 h. Interestingly, significant differences were observed among the PrAMPs, despite similar sequence motifs consisting of proline and the basic amino acids arginine, lysine, and ornithine. Natural insect-derived PrAMPs, i.e., apidaecin 1b, drosocin, and pyrrhocoricin, were inactive against *C. neoformans*, i.e., MICs of > 61, 58, and 55 μ mol/L (always > 128 mg/L), respectively, whereas analogs optimized for enhanced antibacterial activities, such as Api795, Api813, Api822, Onc112, and Chex1Arg20, showed moderate to good activities with MICs ranging from ~1.6 to 6.7 μ mol/L (i.e., 4 to 16 mg/L). Interestingly, all three *C. neoformans* strains tested were equally susceptible to each peptide, e.g., the MIC of the most active peptide Chex1Arg20 D4K was always 1.6 μ mol/L (4 mg/L). Amphotericin B was highly active (< 0.22 μ mol/L; < 0.2 mg/L), fluconazole was moderately active with strain-dependent MICs ranging from 13 to 105 μ mol/L (4 to 32 mg/L), and flucytosine was virtually inactive with MICs of at least 496 μ mol/L (64 mg/L) under the conditions tested. In addition, the CFU counts were determined after incubating *C. neoformans* strains with selected peptides or antifungal agents for three hours before plating the cell suspensions on agar (Figure 1). The lowest concentration of PrAMPs tested (0.25 μ mol/L) reduced the CFU by ~24% (\pm 15%) on average after 48 h. At 10-fold higher concentrations (2.5 μ mol/L), the CFU varied much more for the different peptides. For example, Api88 did not significantly reduce the CFU of *C. neoformans* strains H99 and KN99 α , whereas CRAMP and Chex1Arg20 D4K strongly reduced the CFU with only a few colonies observed. With the exception of apidaecin 1b, fungal cell viability was reduced by an average of 81% by all peptides at the highest peptide concentration tested (25 μ mol/L). Chex1Arg20 D4K and CRAMP completely suppressed the fungi at peptide concentrations \geq 2.5 μ mol/L, with no colonies visible even after 48 h. Interestingly, delayed colony formation was observed for Chex1Arg20, Onc112, and Api795, with only small colonies appearing after more than 24 h.

TABLE 1 List of peptides used, including their sequence, number of amino acids (aa), molecular weight (MW), and net charge.

Peptide	Sequence	Length (aa)	MW (g/mol)	Net charge
Api88	gu-ONNRPVYIPRPRPPHRL-NH ₂	18	2,289	+6
Api88 rev	gu-LRPHPPRPRPIYVPRNNO-NH ₂	18	2,289	+6
Api88 rev*	gu-LRPHPPRPRPIYVPRNNO-NH ₂	20	2,542	+7
Api88 scr	gu-OPNRYIRPRLPPHPNRPV-NH ₂	18	2,289	+6
Api137	gu-ONNRPVYIPRPRPPHRL-OH	18	2,290	+5
Api795	gu-OIOIORPVYOPRPRPPHRL-OH	20	2,517	+7
Api813	gu-OIOIORPVYOPRPRPPHRR-OH	20	2,560	+9
Api822	OIOIORPVYOPRPRPPHRR-OH	20	2,463	+9
Apidaecin 1b	GNNRPVYIPQPRPPHRL-OH	18	2,107	+3
Apidaecin 1b scr	GPLRIYVPHPPRPNQNR-OH	18	2,107	+3
Onc72	VDKPPYLPRPRPPROIYNO-NH ₂	19	2,304	+6
Onc72 rev	ONYIORPPRPRPLYPPKDV-NH ₂	19	2,304	+6
Onc112	VDKPPYLPRPRPPRIYNR-NH ₂	19	2,388	+6
Chex1Arg20	ChexRPDKPRPYLPRPRPPVR-NH ₂	20	2,475	+7
Chex1Arg20 rev	RVPRPPRPRPLYPRPKDPRChex-NH ₂	20	2,475	+7
Chex1Arg20 scr	DRVPRPKPRChexRPPYRPLP-NH ₂	20	2,475	+7
Chex1Arg20 D4K	ChexRPKKPRPYLPRPRPPVR-NH ₂	20	2,488	+9
Drosocin	GKPRPYSRPTSHRPIRV-OH	19	2,199	+5
Pyrrhocoricin	VDKGSYLPRPTPRPIYNRN-OH	20	2,340	+3
Bac7 1–60	RRIRPRPRLPRPRPLPFPRGPRPIRPLPFPRGPRPIP RPLPFPRGPRPIPRP-OH	60	7,023	+17
CRAMP	GLLRKGGEKIGELKKIGQKIKNFFQKLVPQPEQ-OH	34	3,876	+6
CRAMP rev	QEPQPVLKQFFNKIKQGIKKLEGIKEGGKRLG-OH	34	3,876	+6

rev-reversed sequence; scr – scrambled sequence; gu – 1,1,3,3 tetramethyl guanidine; NH₂ – C-terminal amidation; Chex – 1-amino cyclohexyl carboxylic acid; O – 1-ornithine; r – d-arginine.

Both the MICs and the CFUs indicated that the peptide charge might influence their antifungal activity. Apidaecin 1b, with its moderate positive net charge of +3, was inactive against *C. neoformans* (MIC > 61 µmol/L; > 128 mg/L), whereas the related peptides Api137 and Api88, with higher net charges of +5 and +6, respectively, showed enhanced activity. Api137 showed a moderate improvement of antifungal activity with MICs of 14 to 28 µmol/L (i.e., 32 to 64 mg/L). Amidation at the C-terminus (Api88) further improved the MIC to as low as 3.5 µmol/L (8 mg/L). Similarly, substitution of Asp4Lys in Chex1Arg20 improved antifungal properties of Chex1Arg20 D4K. Although the MIC decreased by only one dilution step from 3.2 to 1.6 µmol/L (8 to 4 mg/L), this substitution prevented the “re-growth” effect on agar plates observed for Chex1Arg20. Unexpectedly, substitution of D-Arg in Onc112 to Orn (Onc72) increased the MIC by up to three dilution steps, despite similar net charges at neutral pH.

The trend of a more pronounced effect with higher peptide concentrations was particularly evident in the determination of CFU after plating cell suspensions incubated with 25 µmol/L peptide (Figure 2A). In this case, increased net charges correlated well with decreased cell viability ($R^2 = 0.8830$). This trend was also observed at 10- and 100-fold lower peptide concentrations, although it was not significant ($R^2 = 0.4034$ and $R^2 = 0.5784$, Figures 2B,C).

A time-kill assay showed that in addition to different dose-dependent activities, the peptides also had time-dependent effects. Therefore, the fungal cells were incubated with peptides at concentrations close to the MIC values of the active peptides (2.5 µmol/L) and aliquots were plated after defined time points to

determine the CFUs. No viable cells were detected after 45 min of incubation with Chex1Arg20 D4K (Figure 3), which was only slightly slower than amphotericin B. The PrAMPs Api88, Onc112, and Api795 showed a delayed antifungal effect, but showed a clear effect after 3 h. Apidaecin 1b had only a weak effect in the first 3 h before the CFU increased again to the CFU of the control.

To gain insight into the mechanism, reverse sequences of selected peptides were tested. For this purpose, one active peptide from the apidaecin (Api88) and oncocin groups (Onc72), Chex1Arg20, and CRAMP were selected and synthesized with a reverse sequence. Unexpectedly, all reverse peptides were as active as the corresponding forward sequences. Therefore, the highly active peptides Api88 and Chex1Arg20, which have been extensively studied in our group, and apidaecin 1b (control) were selected to synthesize peptides with the scrambled sequences. All three scrambled peptides were basically inactive, especially considering the MICs at 48 h, which increased from 3.6 to 52 µmol/L (8 to 64 or 128 mg/L) for Chex1Arg20 and from 7.0 to 28 or 56 µmol/L (16 to 64–128 mg/L) for Api88 (Table 2). The scrambled sequence of apidaecin 1b remained inactive. This clearly showed that the activity was sequence-dependent, with forward and reverse sequences showing equal activity.

3.2 Confocal laser scanning microscopy (CLSM)

CLSM was used to investigate whether the PrAMPs studied enter fungal cells in a manner similar to bacterial cells (Mattiuazzo et al.,

TABLE 2 Minimum inhibitory concentrations (MICs) of tested peptides are sequence-dependent. MICs were determined for various peptides and antimycotics against the *C. neoformans* strains 1841, H99, and KN99 α .

Peptide	MIC (μ mol/L)					
	1841		H99		KN99 α	
	24 h	48 h	24 h	48 h	24 h	48 h
Api88	3.5	7.0	7.0	3.5	3.5	7.0
Api88 rev	7.0	7.0	7.0	14	7.0	14
Api88 rev*	3.1	3.1	3.1	3.1	3.1	3.1
Api88 scr	7.0	14–28	28	56	28	56
Api137	14	28	14	28	14–28	28–56
Api795	1.6	3.2	3.2	3.2	1.6–3.2	3.2
Api813	3.1	3.1	1.6	1.6–3.2	1.6–3.2	1.6–3.2
Api822	3.2	3.2	3.2	3.2	3.2	3.2
Apidaecin 1b	> 61	> 61	> 61	> 61	> 61	> 61
Apidaecin 1b scr	> 61	> 61	> 61	> 61	> 61	> 61
Onc72	28	56	14	28–56	14–28	56
Onc72 rev	28	56	28	56	28	56
Onc112	3.3	6.7	3.3–6.7	6.7	3.3–6.7	6.7–13
Chex1Arg20	1.6	3.2	1.6	1.6–3.2	1.6	3.2
Chex1Arg20 rev	3.2	3.2	3.2	3.2–6.5	3.2	6.5
Chex1Arg20 scr	13–26	26–52	26	52	26	52
Chex1Arg20 D4K	1.6	1.6	1.6	1.6	1.6	1.6
Drosocin	29	58	58	>58	>58	>58
Pyrrhocoricin	>55	>55	>55	>55	>55	>55
Bac7 1–60	1.1	1.1	1.1	1.1	1.1	1.1–2.2
CRAMP	2.1	2.1	2.1	2.1	2.1	2.1
CRAMP rev	1.0	2.1	1.0	2.1	1.0–2.1	2.1
Amphotericin B	0.06–0.23	0.13	<0.02	0.04–0.09	0.09	0.17
Fluconazole	105	105	53	53–105	13	26
Flucytosine	496	992	496	>992	992	>992

The MIC values were determined twice at 24 h and 48 h. Shown is the mean of six replicates ($n=6$) performed as triplicates on two separate days. MICs are expressed in μ mol/L. MICs expressed in mg/L are listed additionally in [Supplementary Table S1](#). * at Api88 rev* indicates an extended version with a sequence listed in [Table 1](#).

2007; Krizsan et al., 2015a), as opposed to mammalian cells (Hansen et al., 2012; Bluhm et al., 2016). This technique allows investigating whether the peptides are mainly present in the capsule and membrane region, or whether they are able to penetrate the capsule and cell membrane and reach the cytoplasm. Thus, N-terminally 5(6)-carboxyfluorescein (Cf)-labeled peptides Onc112, Chex1Arg20 (and D4K), and apidaecin 1b as well as Api88, Api137 and Api795 carrying Cf at the δ -amino group of Orn-1 due to guanidation of the N-terminus were synthesized. Cf-Api795, Cf-Onc112, and Cf-Chex1Arg20 were slightly more active against *C. neoformans* 1841, while Cf-Chex1Arg20 D4K, Cf-Api88, and Cf-Api137 were slightly less active than the corresponding unlabeled peptides

([Supplementary Table S3](#)). Since all Cf-labeled peptides were similarly active as the unlabeled analogs on *C. neoformans* 1841, we assumed that their cellular distribution is also very similar. Thus, fungal cultures were incubated with no peptide (control) or one of the Cf-labeled peptides, which were selected from different peptide families with different antifungal activity, at 30°C for 3 h. The cells were prepared for CLSM, immobilized on glass slides, and studied under the microscope using light imaging and fluorescence.

As expected, the control sample showed no fluorescence, whereas cells incubated with Cf-labeled sequences of Onc112, Chex1Arg20, Chex1Arg20 D4K, Api795, and Api88 showed intense, non-uniformly distributed fluorescence, mainly in the cytoplasmic region. Whole-cell scans clearly demonstrated the fluorescence inside the cells, although some cells showed more intense spots for Cf-Api88 or less fluorescent areas for Cf-Api795, Cf-Chex1Arg20 D4K, and Cf-Onc112 ([Figure 4](#); [Supplementary Figure S3](#)). These observations could not be attributed to distinct cellular compartments. To gain a more comprehensive understanding of the peptide distribution within the cells, a 3D visualization was conducted. This analysis unveiled certain regions within the cells where no fluorescence signal was detected, indicating the absence of the peptide in these areas. However, it remained open, whether this lack of fluorescence is due to a dented or damaged membrane.

In some cells near the daughter cell encapsulation, the Cf-labeled peptide appeared to be transferred from the mother cell to the daughter cell. Interestingly, mother and daughter cells often showed similar fluorescence intensities ([Figure 4](#), Cf-Chex1Arg20, Cf-Api795), but sometimes one of the cells was less fluorescent ([Figure 4](#) Cf-Api137, [Supplementary Figure S2](#) Cf-Api88, Cf-Onc112). In some images, two cells appeared to “exchange” the fluorescence ([Supplementary Figure S2](#) Cf-Onc112, Cf-Api795, [Figure 4](#) Cf-Chex1Arg20, Cf-Api795). Whether the cells were already within the budding process at the time of peptide addition and the peptides were taken up simultaneously by mother and daughter cell or whether the cell only transferred the peptide from mother to daughter cell during early budding after peptide uptake is not evident from this experiment.

Fungi incubated with Cf-Api137 showed much weaker or no fluorescence, requiring much higher laser power to excite the fluorophore, most likely indicating a much lower concentration than observed for Cf-Api88. This was even more evident with the inactive sequence Cf-apidaecin 1b, where no fluorescence could be detected in the majority of cells. However, a few cells displayed a fluorescence in the cytosol ([Figure 4](#); [Supplementary Figure S3](#)). In general, the antimicrobial activity correlated with the fluorescence intensity and thus with the presence of the peptide in the cytoplasm.

3.3 Scanning electron microscopy

To test possible lytic effects of the peptides on the fungi, the fungi were treated with PrAMPs and examined by SEM ([Figure 5](#)). The cell number and corresponding peptide concentration had to be increased due to the more complex sample preparation compared to the antifungal activity assay and CLSM. A control sample treated in the same manner but without the addition of peptide predominantly showed intact, round cells with only ~1 to 3% of the cells damaged. When incubated with PrAMPs Chex1Arg20, Api88, and Onc112 the

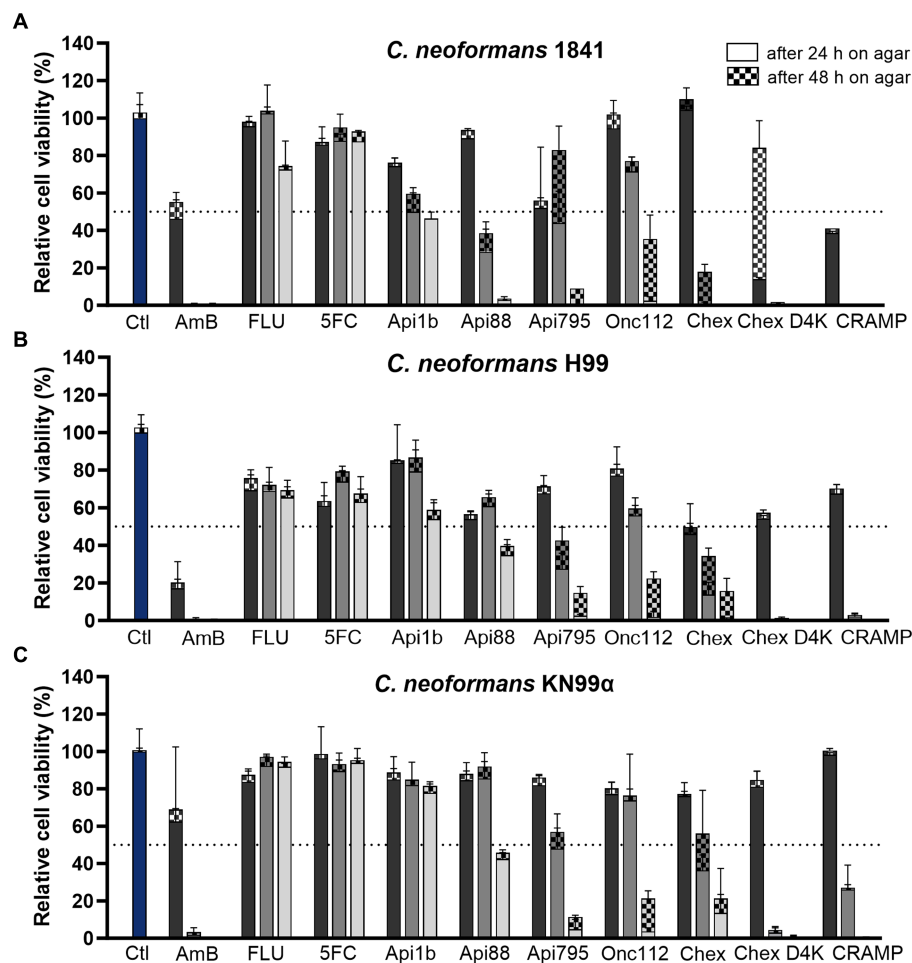


FIGURE 1
PrAMPs and the cathelicidin CRAMP have a concentration-dependent effect on cell viability and are able to reduce colony-forming units. Relative cell viability of *C. neoformans* strains (A) 1841, (B) H99, and (C) KN99α was assessed after incubation (3 h, 30°C) with AMPs and antifungals at concentrations of 0.25 μmol/L (darker gray), 2.5 μmol/L (gray), and 25 μmol/L (lighter gray). Divided bars show colony-forming units (CFU) counted after 24 h (no pattern) and 48 h (checked) incubation at 30°C. Samples were normalized to the control sample (no peptide or antifungal, blue). Dotted line indicates 50% inhibition. Shown is the mean of four replicates ($n = 4$) performed as duplicates on two separate days and the associated standard deviation. Absolute CFU counts are shown in [Supplementary Figure S1](#) and [Supplementary Table S2](#). Ctl – control; AmB – Amphotericin B; FLU – fluconazole; 5FC – flucytosine; Chex – Chex1Arg20; Chex D4K – Chex1Arg20 D4K.

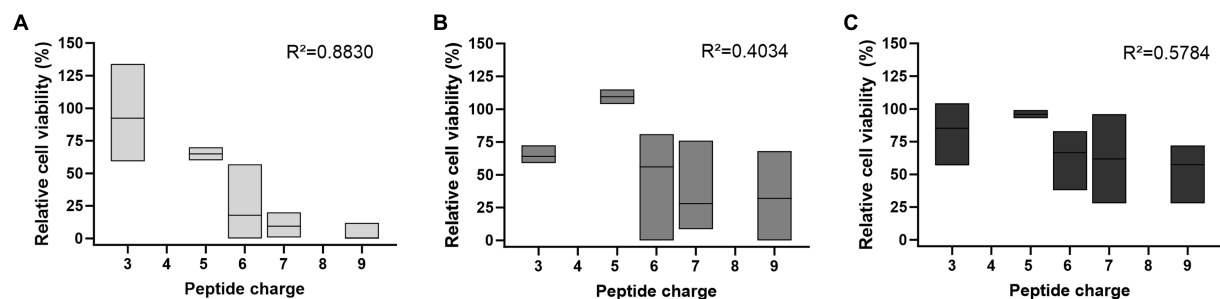


FIGURE 2
The peptide net charge influences the antifungal activity against *C. neoformans* 1841, which depends on the peptide concentration used. Antifungal activity was determined by the number of CFU on SAB agar after incubation with (A) 25 μmol/L, (B) 2.5 μmol/L, or (C) 0.25 μmol/L peptide, shown as floating bar graph. Results were normalized to the control sample (no peptide). CFU counts were determined after 48 h. Data rely on all peptides listed in [Supplementary Table S1](#), except Bac7 1–60 as well as the reverse and scrambled sequences. The mean between peptides is indicated with a solid line. Simple linear regression tests (Pearson correlation) were performed using GraphPad Prism 10.0.3.

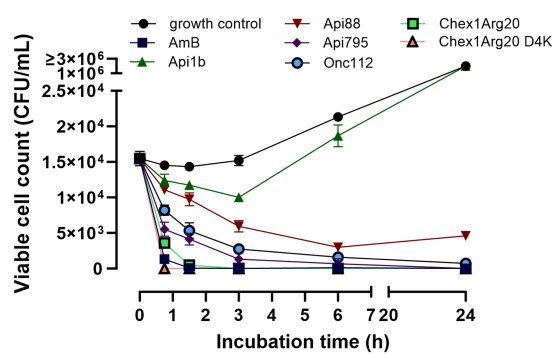


FIGURE 3

PrAMPs show a time-dependent effect on *C. neoformans* 1841. Fungal cells were incubated with peptides or Amphotericin B (2.5 μ mol/L) and aliquots were plated after defined time point for determination of the CFU. An untreated sample is used as a growth control. The mean value from triplicates with the corresponding standard deviation is shown.

majority of cells appeared intact, only a small portion showed deep indentations (Figures 5, 6). No significant differences were observed between the three peptides. Although very low, the proportion of damaged cells within the peptide-treated cells was significantly higher than in the untreated control cells. In order to confirm these observations and to analyze whether other PrAMPs, including the inactive peptide apidaecin 1b, induce a similar effect on the fungi, cells were treated with seven different PrAMPs in a second batch (Supplementary Figure S4). Cells with comparable damage were observed for all peptides with the proportion of damaged cells being significantly higher in all peptide-treated cells than in the control (Supplementary Figure S4). The lowest percentage of damaged cells was observed for apidaecin 1b. Similarly, treatment with the less active peptide Chex1Arg20 scrambled resulted in a slightly lower percentage of damaged cells than Chex1Arg20, although no significant difference was observed between the two peptides. Similarly, there were no significant differences between cells treated with Chex1Arg20 and the reverse sequence or the derivative with the D4K substitution. Overall, round shaped cells were observed in the treated samples, with the exception of indentations, while no other damage to the cell capsule was observed in contrast to cells incubated with DMSO (data not shown). Additionally, cells in various stages of budding were observed. Thus, the antifungal activity of the tested peptides did not correlate with the observed rather low damage to the cell capsule, indicating a minor side effect.

3.4 Cytotoxicity and hemolytic activity

Having observed the high activity and partially rapid kill kinetics on eukaryotic fungal cells, the active peptides including the reverse and scrambled peptides were studied for possible toxic effects on eukaryotic mammalian cells, i.e., human liver (HepG2) and kidney cell lines (HEK293) (Figure 7). In agreement with previous studies (Czihal et al., 2012; Fritsche et al., 2012; Kolano et al., 2021; Brakel et al., 2022a,b), the cell viability of both cell lines was only slightly reduced by the most active peptides at peptide concentrations of 600 mg/L (between 234 and 285 μ mol/L). The peptide concentration

used was 150-fold above the MIC for the most active peptide (Chex1Arg20 D4K), which demonstrates a high safety margin. Reverse and scrambled sequences also had no cytotoxic effect. In contrast, amphotericin B (125 mg/L) showed strong cytotoxicity, as already described in the literature (Gurudevan et al., 2018).

All PrAMPs tested, including the reverse and scrambled peptides, showed no significant hemolytic activity compared to the untreated control (addition of PBS) up to concentrations of 600 mg/L (234 to 285 μ mol/L), as previously reported for some PrAMPs (Czihal et al., 2012; Krieger et al., 2021; Mohammed et al., 2023), in contrast to a strong hemolytic effect observed for amphotericin B already at the lowest concentration tested (125 mg/L; 135 μ mol/L) (Supplementary Figure S5).

4 Discussion

Cryptococcal meningitis and cryptococcosis caused by *C. neoformans* infections are typically treated with a combination of high-dose liposomal amphotericin B, flucytosine, and fluconazole, followed by a prolonged low-dose fluconazole therapy for at least 8 weeks (Ngan et al., 2022). However, access to liposomal amphotericin B and flucytosine and safe administration are severely limited, especially in developing countries, leading to the use of less effective regimens. Moreover, these drugs have tremendous side effects due to their high toxicity, particularly kidney damage. In general, the development of antifungal drugs is more challenging compared to drugs targeting bacteria, because the membranes and targets of eukaryotic fungal cells are more similar to those of mammalian cells (Denning and Bromley, 2015; Chen et al., 2021). For instance, the peptide indolicidin acts intracellularly against bacteria by inhibiting DNA, RNA, and protein synthesis, but has a membrane-disrupting effect on fungal cells (Subbalakshmi and Sitaram, 1998; Lee et al., 2003). AMPs could be a valid alternative therapeutic strategy, but positively charged AMPs often utilize a membrane-disrupting effect and a lytic mode of action, resulting in an increased risk of cytotoxicity to mammalian cells (Brakel et al., 2022a,b). Research on PrAMPs has mainly focused on their activity against Gram-negative and Gram-positive bacteria and has linked their activity to intracellular targets, i.e., the bacterial 70S ribosome and DnaK, mostly based on research in *Escherichia coli*. PrAMPs are highly efficient in murine models of bacterial infection and show only mild side effects (Knappe et al., 2012). Low cytotoxicity against various mammalian cells, e.g., HEK, Hep and HeLa, and hemolytic activity has already been shown for a variety of PrAMPs (Lai et al., 2019; Kolano et al., 2021; Brakel et al., 2022a,b). This was confirmed in this publication, including reversed and scrambled sequences. In addition, confocal laser scanning microscopy experiments showed that Api137, among others, is not taken up into HeLa cells (Hansen et al., 2012; Bluhm et al., 2016). Similarly, PrAMPs do not have any immunomodulatory effects and do not affect dendritic cells or macrophages (Fritsche et al., 2012). Therefore, they appear to be promising candidates for the treatment of fungal infections. However, the antifungal activity, especially against *C. neoformans*, and the underlying mechanisms are poorly understood. Only two mammalian PrAMPs, Bac7 (1-35) and SP-E, have been shown to be effective against *C. neoformans*, with MIC values as low as 4 μ mol/L (Benincasa et al., 2004; Conti et al., 2013). Although intact cell membranes suggested a non-lytic mechanism, the mode of action

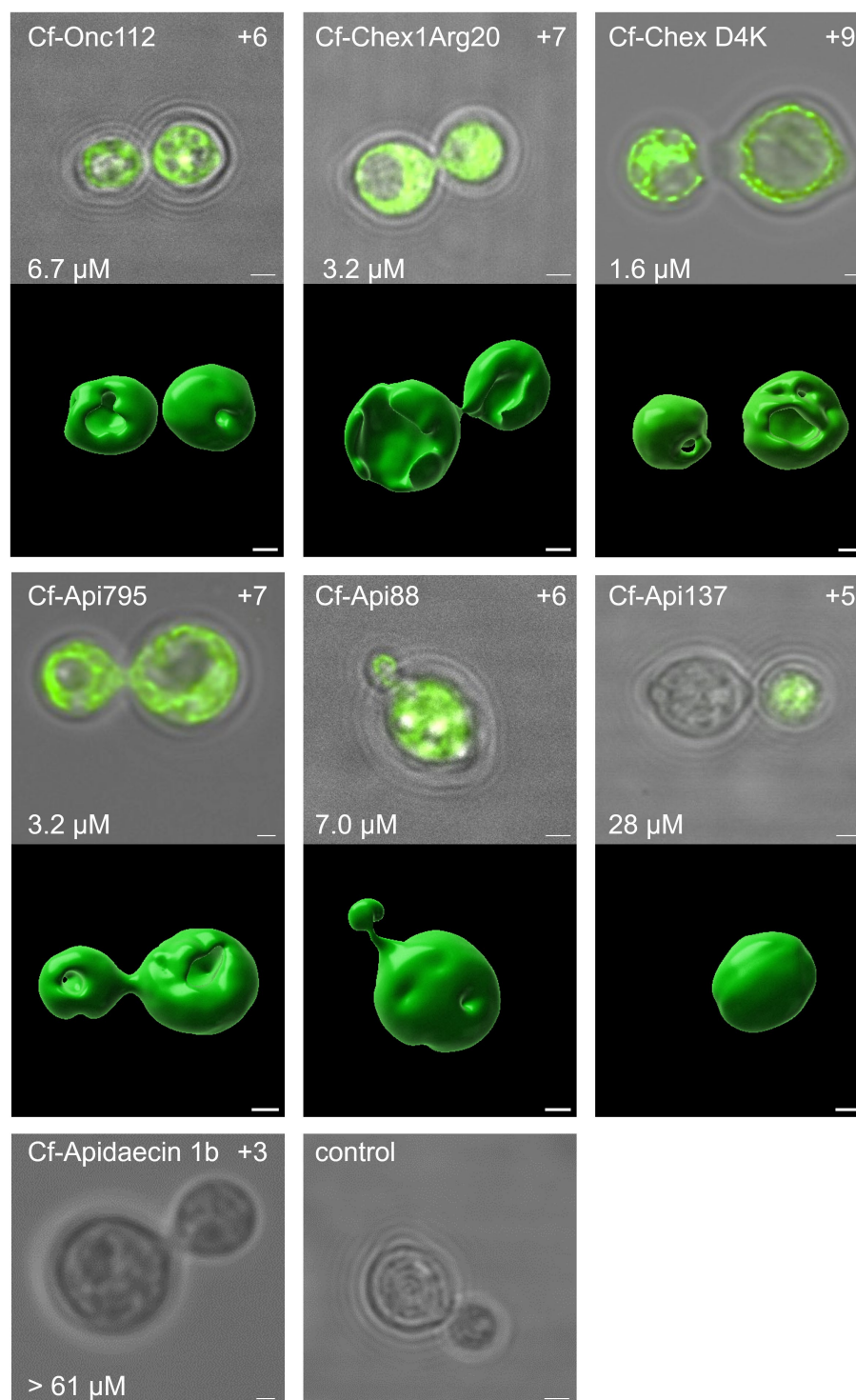


FIGURE 4

The antifungal activity as well as the net charge of the peptides was found to correlate with the intracellular uptake. Confocal laser scanning images of *C. neoformans* 1841 cells incubated with Cf-labeled peptides (25 $\mu\text{mol/L}$, 30°C, 3 h). Cells were immobilized on glass slides and the fluorescence was measured for the entire cell ($\lambda_{\text{ex}} = 496 \text{ nm}$, $\lambda_{\text{em}} = 503\text{--}600 \text{ nm}$). For each peptide, the central z-stack was shown as an overlay of the white light image and fluorescence channel after deconvolution. The MIC (after 48 h, lower left corner) and net charge (upper right corner) are provided for each peptide as well. Additionally, for peptides with detectable fluorescence, a 3D visualization was prepared using Imaris. Scale bar, 1 μm .

was not further investigated. Compared to these peptides, the insect-derived PrAMPs studied here are much shorter and have different motifs. Nevertheless, they showed comparable or even superior non-lytic antifungal activity against *C. neoformans*. The most active

peptide, Chex1Arg20 D4K, reached an MIC of 1.6 $\mu\text{mol/L}$ (4 mg/L), which is similar to the widely investigated AMPs, such as the cathelicidin CRAMP (2.1 $\mu\text{mol/L}$, this study), the defensin mimetic brilacidin (2.5 $\mu\text{mol/L}$, (Dos Reis et al., 2023)), the artificial

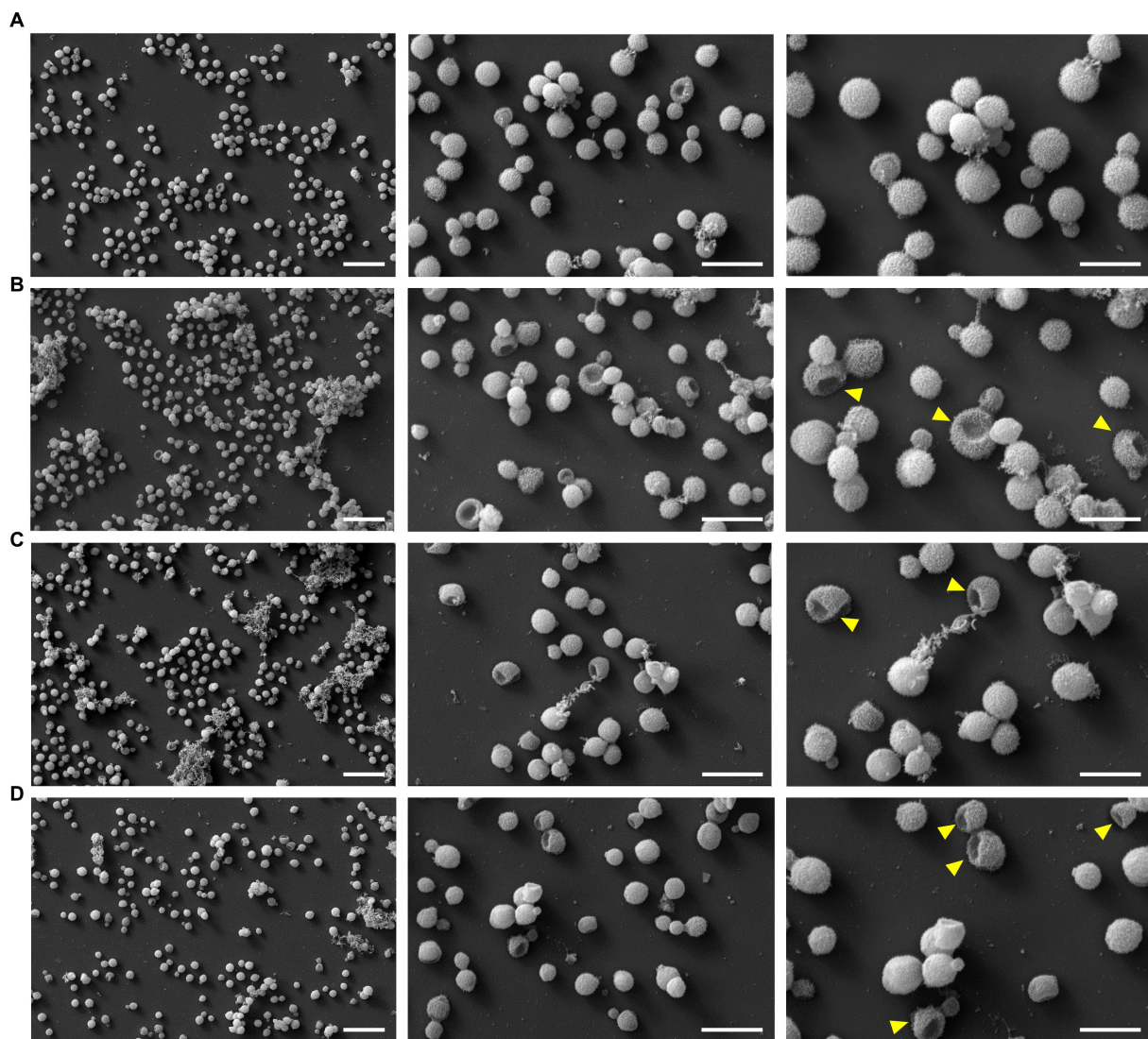


FIGURE 5

Images of scanning electron microscopy showed damaging effect on fungal cell exterior. Cells were incubated (A) without peptide (control) or with (B) Chex1Arg20, (C) Api88 or (D) Onc112 and visualized using three different magnifications [5 k (left, scale bar 20 μ m), 15 k (middle, scale bar 10 μ m), and 25 k (right, scale bar 6 μ m)]. Examples of damaged fungal cells are marked with a yellow arrow in the 25 k figures.

VG16KRKP (10 μ mol/L, (Datta et al., 2016)) or Bac7 1–60 (1.1 μ mol/L, this study). Importantly, Chex1Arg20, Api88, and Onc112 showed similar good activities against all three *C. neoformans* strains tested. It is very encouraging that the peptides were equally active against the tested serotype A strains H99 and KN99 α (*C. neoformans* var. *grubii*) and serotype D strain 1841 (*C. neoformans* var. *neoformans*). As mentioned above, the more virulent serotype A is globally dominant, while serotype D prevails in Europe. Therefore, it is crucial for antifungal agents to exhibit activity against both serotypes. Differences between the strains, e.g., capsule composition or melanin production, which may occur, did not appear to affect the antifungal activity (Samarasinghe et al., 2018; Casadevall et al., 2019).

Even though fungal cells and bacterial cells differ in their composition and structure, an overlap in the activity against *C. neoformans* and Gram-negative bacteria was observed for some of the PrAMPs tested. This has the potential advantage of translating previous findings and observations to fungi. The finding that

peptides that are active against bacteria *in vitro* are also effective *in vivo*, as has already been shown in various infection models, provides hope for the potential efficacy of PrAMPs *in vivo* against *C. neoformans* (Ostorhazi et al., 2014; Schmidt et al., 2016, 2017). Importantly, these PrAMPs were as efficient as standard antibiotics in these mouse infection models, despite much higher MICs, suggesting that the MICs for bacteria must be evaluated differently than for small molecules. If this is also true for fungi, it would indicate high efficacy against *C. neoformans* infections (Knappe et al., 2015). However, further investigation and confirmation are still required. So far, only *in vitro* data have been considered in this study, which may not accurately reflect the conditions *in vivo*. This has been observed with antifungal agents such as fluconazole and flucytosine, which are effective in treating *C. neoformans* infections but show lower activity under the *in vitro* conditions used. Interestingly, even small structural changes in the apidaecin sequences, i.e., apidaecin 1b, Api88, and Api137, had a strong effect

on the antifungal activity, suggesting a sequence-specific target interaction with forward and reversed sequences showing similar activities.

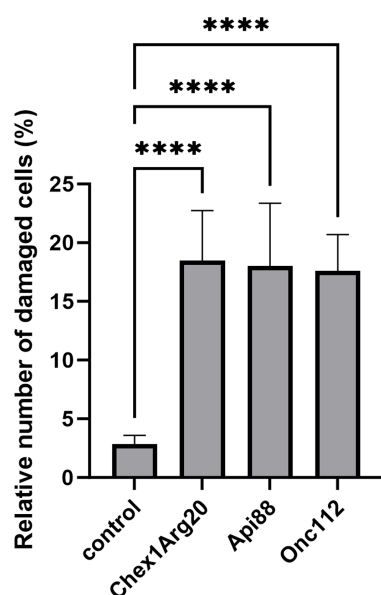


FIGURE 6

Fungal cells treated with the PrAMPs Chex1Arg20, Api88, and Onc112 showed partially indentation. Cells were incubated without peptide (control) or with Chex1Arg20, Api88 or Onc112. All samples shown were treated under the same conditions. Damaged and intact cells from five SEM images were counted per peptide, and the relative proportion of damaged cells was calculated. Data represent the mean including the standard deviation ($n = 5$). Data were analyzed using Dunnett's multiple comparisons test (GraphPad Prism 10.0.3, **** $p < 0.0001$).

The putative intracellular mode of action is a very significant finding, supported by CLSM images showing fluorescence in the cytoplasmic region after incubation of *C. neoformans* with Cf-labeled PrAMPs (Figure 4; Supplementary Figure S3). At this point, we can only speculate about potential targets, such as the ribosomes at the endoplasmic reticulum, which is the primary target of PrAMPs in bacteria, i.e., the 70S ribosome (Krizsan et al., 2014, 2015a,b; Seefeldt et al., 2015; Graf et al., 2017). Binding of PrAMPs to the eukaryotic 80S ribosome has not yet been demonstrated. However, studies have shown that the PrAMP Bac7 (1-35) can inhibit *in vitro* translation in a eukaryotic system, albeit with a 2.5-fold higher IC_{50} compared to the *E. coli* system (Seefeldt et al., 2016). Given the activity of Bac7 (1-35) against *C. neoformans*, one could speculate that the 80S ribosome might be a possible target (Benincasa et al., 2004). Interestingly, the reverse sequences did not seem to have a decisive influence, as similar MIC values were measured for Api88, Onc72, and Chex1Arg20 and the corresponding reverse sequences. In contrast, the sequence was important for the activity of Api88 and Chex1Arg20, as indicated by the high MICs for scrambled sequences, presumably due to poorer target binding (Table 2). Initial investigations using SEM showed that the PrAMPs, may also have a slight membrane-damaging effect on the fungi (Figure 5), as some cells showed a dented shape. Similar membrane damage was already observed by (Sharma et al. (2017, 2022)). However, based on the results shown here, it is unlikely that damage to the cell exterior is the major mechanism of PrAMPs, as it was observed also for inactive sequences, such as Chex1Arg20 scrambled. There was no clear trend between membrane damage and MIC values for the peptides tested, suggesting that the observed cell damage is a minor side effect caused by the sample preparation conditions, probably occurring in cells already killed by the peptides. In addition, peptide concentrations well above the MIC were used due to the relatively high cell number (10^8 CFU/mL) required for sample preparation. In addition, no nucleotide release from the cytosol could

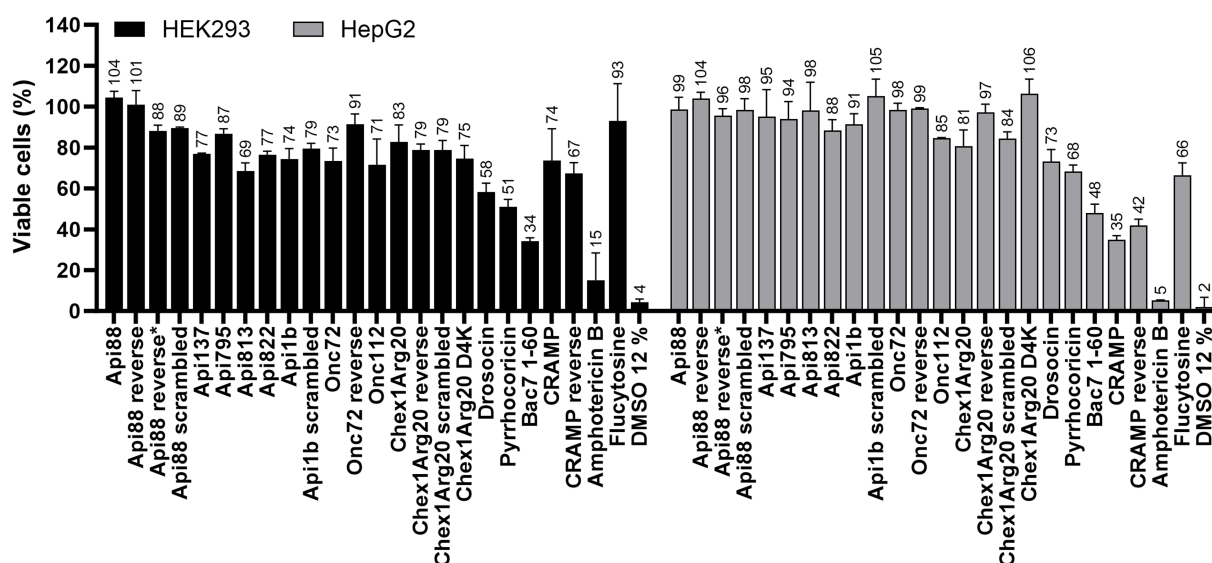


FIGURE 7

Effect of AMPs and antifungal agents on the cell viability of eukaryotic cell lines HEK293 (black) and HepG2 (grey). Cells were incubated with peptides (0.6 g/L), flucytosine (0.6 g/L) or amphotericin B (0.125 g/L) for 24 h. Samples were normalized to a sample incubated with PBS (12%). A sample incubated with DMSO (12%) served as a positive control. Each bar represents the mean of triplicates with the corresponding standard deviation.

be detected after incubation with the PrAMPs, which makes membrane leakage unlikely. Interestingly, incubation with CRAMP resulted in a slight increase in nucleic acid release ([Supplementary Figure S6; Method M1](#)).

Interestingly, the fungi could be observed in different budding states after peptide incubation with CLSM, ranging from cells with early budding to those with almost completed budding ([Figure 4](#)). However, since these observations are only snapshots, it remains open whether the fungi were still capable to complete the budding process despite the peptide treatment or whether budding was halted at this stage. Nevertheless, the peptide was distributed in the mother and daughter cells, although partially different fluorescence intensities were observed in each cell. Assuming that the budding process is not stalled by the peptide uptake, the peptide would be distributed to the nascent cells, resulting in a lower (diluted) peptide concentration in each cell. This could explain the observed regrowth effects on agar plates.

The CLSM data also suggest that cellular uptake of *Cf*-Api137 and *Cf*-Apidaecin 1b is less efficient than for *Cf*-labeled Chex1Arg20, Api88, and Onc112, which may potentially explain the lower activity of Api137 and the inactivity of apidaecin 1b. The only difference between Api137 and Api88 is the C-terminus, i.e., a carboxyl group instead of an amide, respectively, which decreases the peptide net charge by one. The importance of the peptide charge has been reported for the uptake of PrAMPs in *E. coli* ([Futaki et al., 2013](#); [Kolano et al., 2021](#)), where higher positive charges improve the uptake, probably due to their enhanced interaction with the negatively charged bacterial membrane composed of lipopolysaccharides. The ionic interactions allow better accumulation of the peptides on the bacterial surface and facilitate passive diffusion into the periplasm prior to transporter-mediated uptake ([Lohner and Blondelle, 2005](#)). However, the cell wall and capsule of *C. neoformans* differ significantly from those of bacteria. Nonetheless, a common feature is the negative charge of the outermost layer, the capsule, which is not composed of LPS in *C. neoformans*, but of complex polysaccharides, such as glucuronoxylomannan (GXM) and glucuronoxylomannogalactan (GXMGal) ([O'Meara and Alspaugh, 2012](#); [Casadevall et al., 2019](#)). Thus, cationic AMPs with a higher net charge can interact more strongly with the capsule, resulting in increased peptide accumulation on the surface that may improve penetration into the cell. Another significant difference is the composition of the cell wall, which includes various glucans, chitin, chitosan, mannoproteins, and most importantly, the characteristic melanin layer ([Garcia-Rubio et al., 2019](#)). Melanin is a hydrophobic, negatively charged polymer of phenolic and/or indolic compounds, also known as the “antifungal resistance factor” because it reduces susceptibility to antifungal drugs ([Ikeda et al., 2003](#); [Nosanchuk and Casadevall, 2006](#)). Incubation of melanin with amphotericin B significantly reduced its activity against *C. neoformans*, while the small molecules fluconazole and flucytosine remained unaffected ([Casadevall et al., 2000](#)). Our studies showed that Api88, Api795, Onc112, and Chex1Arg20 were able to enter the fungal cytoplasm after passing the fungal cell wall and capsule including the melanin layer. It can be speculated that both the positive charge of the peptides and a certain degree of hydrophobicity are advantageous, which may be caused by repeated Pro-Arg-Pro motifs, which are characteristic

of insect-derived PrAMPs. The observed differences in activity among the PrAMPs tested are most likely due to differences in charge and basicity rather than hydrophobicity, as they differ only slightly in this respect. The natural PrAMPs apidaecin 1b, drosocin, and pyrrhocoricin were inactive against *C. neoformans*, possibly due to their lower net charge compared to the optimized derivatives, which likely results in poorer uptake. However, it should be noted that charge alone does not explain the differences in activity, as seen for Onc112 and Onc72 and especially for the scrambled peptides. There must be further structural features important for the antifungal activity in order to obtain an ideal interplay between uptake, target binding, and target inhibition.

5 Conclusion

Bovine and especially short insect-derived PrAMPs have been extensively studied and rationally optimized for potential systemic therapeutic antibacterial treatments over the last decades due to their high protease stability and low intrinsic toxicity, such as the development of the designer peptides Api88, Api137, Onc72, Onc112, and Chex1Arg20 with proven efficacy in various murine bacterial infection models. Here, we showed for the first time that these peptides are also highly active against several clinically relevant *C. neoformans* strains that are difficult to treat with current antifungal agents. The observed MICs were as low as previously reported for the most susceptible Gram-negative bacteria, i.e., *E. coli* and *K. pneumoniae*. Interestingly, reverse sequences were similarly active, while scrambled sequences were essentially inactive. Fluorescence microscopy revealed that the peptides enter the cytoplasm of apparently intact cells in larger quantities, most likely ruling out a membranolytic mechanism, and suggesting an intracellular target, possibly the fungal ribosome in analogy to the established mode of action in Gram-negative bacteria. However, the different composition and structure of the bacterial and fungal ribosomes requires confirmation of the proposed target, as the active peptides could by chance hit another target resulting in a different mechanism. However, scanning electron microscopy showed that PrAMPs also have a slight damaging effect on the cell exterior, which could facilitate entry into the cell interior.

Data availability statement

The original contributions presented in the study are included in the article/[Supplementary material](#), further inquiries can be directed to the corresponding author.

Author contributions

AB: Conceptualization, Formal analysis, Investigation, Methodology, Visualization, Writing – original draft. TG: Formal analysis, Investigation, Methodology, Visualization, Writing – review & editing. SF: Investigation, Writing – review & editing, Methodology. DK: Investigation, Writing – review & editing. AK: Methodology, Writing – review & editing. SAF: Methodology, Resources, Writing – review & editing. GA: Resources, Writing – review & editing. RH:

Conceptualization, Methodology, Resources, Writing – review & editing. UM: Conceptualization, Investigation, Methodology, Writing – review & editing.

Funding

The author(s) declare financial support was received for the research, authorship, and/or publication of this article. The publication was funded by the Open Access Publishing Fund of Leipzig University, which is supported by the German Research Foundation within the program Open Access Publication Funding.

Acknowledgments

We thank Johannes Kacza for technical support at the confocal laser scanning microscope and Gregor Pfeifer for SEM preparation. We gratefully acknowledge the support of the BioImaging Core Facility and the Electron Microscopy Laboratory of the Veterinary Anatomical Institute of the Leipzig University for image acquisition. We would like to thank Annika Breitsfelder for collecting and providing the porcine blood.

References

- Benincasa, M., Scocchi, M., Podda, E., Skerlavaj, B., Dolzani, L., and Gennaro, R. (2004). Antimicrobial activity of Bac7 fragments against drug-resistant clinical isolates. *Peptides* 25, 2055–2061. doi: 10.1016/j.peptides.2004.08.004
- Berthold, N., Czihal, P., Fritsche, S., Sauer, U., Schiffer, G., Knappe, D., et al. (2013). Novel apidaecin 1b analogs with superior serum stabilities for treatment of infections by gram-negative pathogens. *Antimicrob. Agents Chemother.* 57, 402–409. doi: 10.1128/AAC.01923-12
- Bluhm, M. E., Schneider, V. A., Schäfer, I., Piantavigna, S., Goldbach, T., Knappe, D., et al. (2016). N-terminal Ile-Orn- and Trp-Orn-motif repeats enhance membrane interaction and increase the antimicrobial activity of Apidaecins against *Pseudomonas aeruginosa*. *Front. Cell Dev. Biol.* 4:39. doi: 10.3389/fcell.2016.00039
- Bongomin, F., Gago, S., Oladele, R. O., and Denning, D. W. (2017). Global and multi-National Prevalence of fungal diseases-estimate precision. *J. Fungi (Basel)* 3:3. doi: 10.3390/jof3040057
- Brakel, A., Kolano, L., Kraus, C. N., Otvos, L., and Hoffmann, R. (2022a). Functional effects of ARV-1502 analogs against bacterial Hsp70 and implications for antimicrobial activity. *Front. Chem.* 10:798006. doi: 10.3389/fchem.2022.798006
- Brakel, A., Krizsan, A., Itzenga, R., Kraus, C. N., Otvos, L., and Hoffmann, R. (2022b). Influence of substitutions in the binding motif of proline-rich antimicrobial peptide ARV-1502 on 70S ribosome binding and antimicrobial activity. *Int. J. Mol. Sci.* 23:23. doi: 10.3390/ijms23063150
- Brakel, A., Volke, D., Kraus, C. N., Otvos, L., and Hoffmann, R. (2019). Quantitation of a novel engineered anti-infective host defense peptide, ARV-1502: pharmacokinetic study of different doses in rats and dogs. *Front. Chem.* 7:753. doi: 10.3389/fchem.2019.00753
- Brown, G. D., Denning, D. W., Gow, N. A., Levitz, S. M., Netea, M. G., and White, T. C. (2012). Hidden killers: human fungal infections. *Sci. Transl. Med.* 4:165rv13. doi: 10.1126/scitranslmed.3004404
- Cafarchia, C., Romito, D., Iatta, R., Camarda, A., Montagna, M. T., and Otranto, D. (2006). Role of birds of prey as carriers and spreaders of *Cryptococcus neoformans* and other zoonotic yeasts. *Med. Mycol.* 44, 485–492. doi: 10.1080/13693780600735452
- Casadevall, A., Coelho, C., Cordero, R. J., Dragotakes, Q., Jung, E., Vij, R., et al. (2019). The capsule of *Cryptococcus neoformans*. *Virulence* 10, 822–831. doi: 10.1080/21505594.2018.1431087
- Casadevall, A., Rosas, A. L., and Nosanchuk, J. D. (2000). Melanin and virulence in *Cryptococcus neoformans*. *Curr. Opin. Microbiol.* 3, 354–358. doi: 10.1016/S1369-5274(00)00103-X
- Chen, Y.-C., Yang, Y., Zhang, C., Chen, H.-Y., Chen, F., and Wang, K.-J. (2021). A novel antimicrobial peptide Sparamosin26-54 from the mud crab *Scylla paramamosain* showing potent antifungal activity against *Cryptococcus neoformans*. *Front. Microbiol.* 12:746006. doi: 10.3389/fmicb.2021.746006
- Conti, S., Radicioni, G., Ciociola, T., Longhi, R., Polonelli, L., Gatti, R., et al. (2013). Structural and functional studies on a proline-rich peptide isolated from swine saliva endowed with antifungal activity towards *Cryptococcus neoformans*. *Biochim. Biophys. Acta* 1828, 1066–1074. doi: 10.1016/j.bbame.2012.12.013
- Czihal, P., Knappe, D., Fritsche, S., Zahn, M., Berthold, N., Piantavigna, S., et al. (2012). Api88 is a novel antibacterial designer peptide to treat systemic infections with multidrug-resistant gram-negative pathogens. *ACS Chem. Biol.* 7, 1281–1291. doi: 10.1021/cb300063v
- Datta, A., Yadav, V., Ghosh, A., Choi, J., Bhattacharyya, D., Kar, R. K., et al. (2016). Mode of action of a designed antimicrobial peptide: high potency against *Cryptococcus neoformans*. *Biophys. J.* 111, 1724–1737. doi: 10.1016/j.bpj.2016.08.032
- Decken, K., Köhler, G., Palmer, K.-L., Wunderlin, A., Mattner, F., Magram, J., et al. (1998). Interleukin-12 is essential for a protective Th1 response in mice infected with *Cryptococcus neoformans*. *Infect. Immun.* 66, 4994–5000. doi: 10.1128/IAI.66.10.4994-5000.1998
- Denning, D. W., and Bromley, M. J. (2015). Infectious disease. How to bolster the antifungal pipeline. *Science* 347, 1414–1416. doi: 10.1126/science.aaa6097
- Denning, D. W., and Hope, W. W. (2010). Therapy for fungal diseases: opportunities and priorities. *Trends Microbiol.* 18, 195–204. doi: 10.1016/j.tim.2010.02.004
- Dos Reis, T. F., De, C. P. A., Bastos, R. W., Pinzan, C. F., Souza, P. F., Ackloo, S., et al. (2023). A host defense peptide mimetic, brilacidin, potentiates caspofungin antifungal activity against human pathogenic fungi. *Nat. Commun.* 14:2052. doi: 10.1038/s41467-023-37573-y
- Fisher, M. C., Alastruey-Izquierdo, A., Berman, J., Bicanic, T., Bignell, E. M., Bowyer, P., et al. (2022). Tackling the emerging threat of antifungal resistance to human health. *Nat. Rev. Microbiol.* 20, 557–571. doi: 10.1038/s41579-022-00720-1
- Fisher, M. C., Gurr, S. J., Cuomo, C. A., Bleher, D. S., Jin, H., Stukenbrock, E. H., et al. (2020). Threats posed by the fungal kingdom to humans, wildlife, and agriculture. *MBio* 11:11. doi: 10.1128/mBio.00449-20
- Fritsche, S., Knappe, D., and Berthold, N., Buttler H von, Hoffmann, R., and Alber, G. Absence of in vitro innate immunomodulation by insect-derived short proline-rich antimicrobial peptides points to direct antibacterial action in vivo. *J. Pept. Sci.* (2012) 18:599–608. doi: 10.1002/psc.2440
- Futaki, S., Hirose, H., and Nakase, I. (2013). Arginine-rich peptides: methods of translocation through biological membranes. *Curr. Pharm. Des.* 19, 2863–2868. doi: 10.2174/1381612811319160003
- Garcia-Rubio, R., De, O. H. C., Rivera, J., and Trevijano-Contador, N. (2019). The fungal Cell Wall: Candida, Cryptococcus, and aspergillus species. *Front. Microbiol.* 10:2993. doi: 10.3389/fmicb.2019.02993

Conflict of interest

RH was a member of the scientific advisory board of EnBiotix, Inc. DK was a coworker of EnBiotix GmbH.

The remaining authors declare that the research was conducted in the absence of any commercial or financial relationships that could be construed as a potential conflict of interest.

Publisher's note

All claims expressed in this article are solely those of the authors and do not necessarily represent those of their affiliated organizations, or those of the publisher, the editors and the reviewers. Any product that may be evaluated in this article, or claim that may be made by its manufacturer, is not guaranteed or endorsed by the publisher.

Supplementary material

The Supplementary material for this article can be found online at: <https://www.frontiersin.org/articles/10.3389/fmicb.2023.1328890/full#supplementary-material>

- Graf, M., Mardirossian, M., Nguyen, F., Seefeldt, A. C., Guichard, G., Scocchi, M., et al. (2017). Proline-rich antimicrobial peptides targeting protein synthesis. *Nat. Prod. Rep.* 34, 702–711. doi: 10.1039/c7np00020k
- Gurudev, S., Francis, A. P., and Jayakrishnan, A. (2018). Amphotericin B-albumin conjugates: synthesis, toxicity and anti-fungal activity. *Eur. J. Pharm. Sci.* 115, 167–174. doi: 10.1016/j.ejps.2018.01.017
- Hansen, A., Schäfer, I., Knappe, D., Seibel, P., and Hoffmann, R. (2012). Intracellular toxicity of proline-rich antimicrobial peptides shuttled into mammalian cells by the cell-penetrating peptide penetratin. *Antimicrob. Agents Chemother.* 56, 5194–5201. doi: 10.1128/AAC.00585-12
- Hazen, K. C. (1995). New and emerging yeast pathogens. *Clin. Microbiol. Rev.* 8, 462–478. doi: 10.1128/CMR.8.4.462
- Holfeld, L., Herth, N., Singer, D., Hoffmann, R., and Knappe, D. (2015). Immunogenicity and pharmacokinetics of short, proline-rich antimicrobial peptides. *Future Med. Chem.* 7, 1581–1596. doi: 10.4155/fmc.15.91
- Ikedo, R., Sugita, T., Jacobson, E. S., and Shinoda, T. (2003). Effects of melanin upon susceptibility of *Cryptococcus* to antifungals. *Microbiol. Immunol.* 47, 271–277. doi: 10.1111/j.1348-0421.2003.tb03395.x
- Knappe, D., Adermann, K., and Hoffmann, R. (2015). Oncocin Onc72 is efficacious against antibiotic-susceptible *Klebsiella pneumoniae* ATCC 43816 in a murine thigh infection model. *Biopolymers* 104, 707–711. doi: 10.1002/bip.22668
- Knappe, D., Fritsche, S., Alber, G., Köhler, G., Hoffmann, R., and Müller, U. (2012). Oncocin derivative Onc72 is highly active against *Escherichia coli* in a systemic septicemia infection mouse model. *J. Antimicrob. Chemother.* 67, 2445–2451. doi: 10.1093/jac/dks241
- Knappe, D., Goldbach, T., Hatfield, M. P., Palermo, N. Y., Weinert, S., Sträter, N., et al. (2016). Proline-rich antimicrobial peptides optimized for binding to *Escherichia coli* chaperone DnaK. *Protein Pept. Lett.* 23, 1061–1071. doi: 10.2174/0929866523666160719124712
- Knappe, D., Piantavigna, S., Hansen, A., Mechler, A., Binas, A., Nolte, O., et al. (2010). Oncocin (VDKPPYLPRPRPPRRYNNR-NH₂): a novel antibacterial peptide optimized against gram-negative human pathogens. *J. Med. Chem.* 53, 5240–5247. doi: 10.1021/jm100378b
- Kolano, L., Knappe, D., Berg, A., Berg, T., and Hoffmann, R. (2021). Effect of amino acid substitutions on 70S ribosomal binding, cellular uptake, and antimicrobial activity of Oncocin Onc112. *ChemBiochem* 23:e202100609. doi: 10.1002/cbic.202100609
- Krieger, A.-K., Knappe, D., Öhlmann, S., Mayer, L., Eder, I. B., Köller, G., et al. (2021). Proline-rich antimicrobial peptide Api137 is bactericidal in porcine blood infected ex vivo with a porcine or human *Klebsiella pneumoniae* strain. *J. Glob. Antimicrob. Resist.* 24, 127–135. doi: 10.1016/j.jgar.2020.12.012
- Krizsan, A., Knappe, D., and Hoffmann, R. (2015a). Influence of the yjiL-mdtM gene cluster on the antibacterial activity of proline-rich antimicrobial peptides overcoming *Escherichia coli* resistance induced by the missing SbmA transporter system. *Antimicrob. Agents Chemother.* 59, 5992–5998. doi: 10.1128/AAC.01307-15
- Krizsan, A., Prah, C., Goldbach, T., Knappe, D., and Hoffmann, R. (2015b). Short proline-rich antimicrobial peptides inhibit either the bacterial 70S ribosome or the assembly of its large 50S subunit. *ChemBiochem* 16, 2304–2308. doi: 10.1002/cbic.201500375
- Krizsan, A., Volke, D., Weinert, S., Sträter, N., Knappe, D., and Hoffmann, R. (2014). Insect-derived proline-rich antimicrobial peptides kill bacteria by inhibiting bacterial protein translation at the 70S ribosome. *Angew. Chem.* 53, 12236–12239. doi: 10.1002/anie.201407145
- Lai, P.-K., Tresnak, D. T., and Hackel, B. J. (2019). Identification and elucidation of proline-rich antimicrobial peptides with enhanced potency and delivery. *Biotechnol. Bioeng.* 116, 2439–2450. doi: 10.1002/bit.27092
- Lee, D. G., Kim, H. K., and Kim, S. M., Park, Y., Park, S.-C., Jang, S.-H., et al. (2003). Fungicidal effect of indolicidin and its interaction with phospholipid membranes. *Biochem. Biophys. Res. Commun.* (2003) 305: doi: 10.1016/s0006-291x(03)00755-1, 305–310
- Li, T., Li, L., Du, F., Sun, L., Shi, J., Long, M., et al. (2021). Activity and mechanism of action of antifungal peptides from microorganisms: a review. *Molecules* 26:26. doi: 10.3390/molecules26113438
- Lin, X., and Heitman, J. (2006). The biology of the *Cryptococcus neoformans* species complex. *Annu. Rev. Microbiol.* 60, 69–105. doi: 10.1146/annurev.micro.60.080805.142102
- Lohner, K., and Blondelle, S. E. (2005). Molecular mechanisms of membrane perturbation by antimicrobial peptides and the use of biophysical studies in the design of novel peptide antibiotics. *Comb. Chem. High Throughput Screen.* 8, 241–256. doi: 10.2174/1386207053764576
- Martinez, L. R., Garcia-Rivera, J., and Casadevall, A. (2001). *Cryptococcus neoformans* var. *neoformans* (serotype D) strains are more susceptible to heat than *C. neoformans* var. *grubii* (serotype a) strains. *J. Clin. Microbiol.* 39, 3365–3367. doi: 10.1128/JCM.39.9.3365-3367.2001
- Mattiuzzo, M., Bandiera, A., Gennaro, R., Benincasa, M., Pacor, S., Antcheva, N., et al. (2007). Role of the *Escherichia coli* SbmA in the antimicrobial activity of proline-rich peptides. *Mol. Microbiol.* 66, 151–163. doi: 10.1111/j.1365-2958.2007.05903.x
- Mohammed, G. K., Böttger, R., Krizsan, A., Volke, D., Mötzing, M., Li, S.-D., et al. (2023). In vitro properties and pharmacokinetics of temporarily PEGylated Onc72 prodrugs. *Adv. Healthc. Mater.* 12:e2202368. doi: 10.1002/adhm.202202368
- Montoya, M. C., Magwene, P. M., and Perfect, J. R. (2021). Associations between *Cryptococcus* genotypes, phenotypes, and clinical parameters of human disease: a review. *J. Fungi (Basel)* 7:7. doi: 10.3390/jof7040260
- Muhaj, F. F., George, S. J., Nguyen, C. D., and Tying, S. K. (2022). Antimicrobials and resistance part II: antifungals, antivirals, and antiparasitics. *J. Am. Acad. Dermatol.* 86, 1207–1226. doi: 10.1016/j.jaad.2021.11.065
- Ngan, N. T., Flower, B., and Day, J. N. (2022). Treatment of Cryptococcal meningitis: how have we got here and where are we going? *Drugs* 82, 1237–1249. doi: 10.1007/s40265-022-01757-5
- Nosanchuk, J. D., and Casadevall, A. (2006). Impact of melanin on microbial virulence and clinical resistance to antimicrobial compounds. *Antimicrob. Agents Chemother.* 50, 3519–3528. doi: 10.1128/AAC.00545-06
- O'Meara, T. R., and Alspaugh, J. A. (2012). The *Cryptococcus neoformans* capsule: a sword and a shield. *Clin. Microbiol. Rev.* 25, 387–408. doi: 10.1128/CMR.00001-12
- Osthorazi, E., Nemes-Nikodem, É., Knappe, D., and Hoffmann, R. (2014). In vivo activity of optimized apidaecin and oncocin peptides against a multiresistant, KPC-producing *Klebsiella pneumoniae* strain. *Protein Pept. Lett.* 21, 368–373. doi: 10.2174/09298665113206660107
- Park, B. J., Wannemuehler, K. A., Marston, B. J., Govender, N., Pappas, P. G., and Chiller, T. M. (2009). Estimation of the current global burden of cryptococcal meningitis among persons living with HIV/AIDS. *AIDS* 23, 525–530. doi: 10.1097/QAD.0b013e3283222fac
- Samarasinghe, H., Aceituno-Caicedo, D., Cogliati, M., Kwon-Chung, K. J., Rickerts, V., Velegaki, A., et al. (2018). Genetic factors and genotype-environment interactions contribute to variation in melanin production in the fungal pathogen *Cryptococcus neoformans*. *Sci. Rep.* 8:9824. doi: 10.1038/s41598-018-27813-3
- Schmidt, R., Knappe, D., Wende, E., Osthorazi, E., and Hoffmann, R. (2017). In vivo efficacy and pharmacokinetics of optimized Apidaecin analogs. *Front. Chem.* 5:15. doi: 10.3389/fchem.2017.00015
- Schmidt, R., Osthorazi, E., Wende, E., Knappe, D., and Hoffmann, R. (2016). Pharmacokinetics and in vivo efficacy of optimized oncocin derivatives. *J. Antimicrob. Chemother.* 71, 1003–1011. doi: 10.1093/jac/dkv454
- Schmiedel, Y., and Zimmerli, S. (2016). Common invasive fungal diseases: an overview of invasive candidiasis, aspergillosis, cryptococcosis, and pneumocystis pneumonia. *Swiss Med. Wkly.* 146:w14281. doi: 10.4414/smw.2016.14281
- Seefeldt, A. C., Graf, M., Pérébasque, N., Nguyen, F., Arenz, S., Mardirossian, M., et al. (2016). Structure of the mammalian antimicrobial peptide Bac7(1-16) bound within the exit tunnel of a bacterial ribosome. *Nucleic Acids Res.* 44, 2429–2438. doi: 10.1093/nar/gkv1545
- Seefeldt, A. C., Nguyen, F., Antunes, S., Pérébasque, N., Graf, M., Arenz, S., et al. (2015). The proline-rich antimicrobial peptide Onc112 inhibits translation by blocking and destabilizing the initiation complex. *Nat. Struct. Mol. Biol.* 22, 470–475. doi: 10.1038/nsmb.3034
- Sharma, K., Aaghaz, S., Maurya, I. K., Singh, S., Rudramurthy, S. M., Kumar, V., et al. (2022). Ring-modified histidine-containing cationic short peptides exhibit Anticryptococcal activity by cellular disruption. *Molecules* 28:28. doi: 10.3390/molecules28010087
- Sharma, K. K., Maurya, I. K., Khan, S. I., Jacob, M. R., Kumar, V., Tikoo, K., et al. (2017). Discovery of a membrane-active, ring-modified histidine containing ultrashort amphiphilic peptide that exhibits potent inhibition of *Cryptococcus neoformans*. *J. Med. Chem.* 60, 6607–6621. doi: 10.1021/acs.jmedchem.7b00481
- Struyfs, C., Cammue, B. P., and Thevissen, K. (2021). Membrane-interacting antifungal peptides. *Front. Cell Dev. Biol.* 9:649875. doi: 10.3389/fcell.2021.649875
- Subbalakshmi, C., and Sitaram, N. (1998). Mechanism of antimicrobial action of indolicidin. *FEMS Microbiol. Lett.* 160, 91–96. doi: 10.1111/j.1574-6968.1998.tb12896.x



OPEN ACCESS

EDITED BY

Jianhua Wang,
Chinese Academy of Agricultural Sciences
(CAAS), China

REVIEWED BY

Ali Zarezadeh Mehrabadi,
Iran University of Medical Sciences, Iran
Heng Zheng,
China Pharmaceutical University, China
Carolina Muñoz-Camargo,
University of Los Andes, Colombia

*CORRESPONDENCE

Linlin Lu
✉ lulinlin2007@hotmail.com
Xuezhen Ma
✉ 18660229289@126.com
Shicui Zhang
✉ sczhang@ouc.edu.cn

†These authors have contributed equally to
this work

RECEIVED 14 October 2023

ACCEPTED 27 December 2023

PUBLISHED 17 January 2024

CITATION

Qu B, Yuan J, Liu X, Zhang S, Ma X and Lu L
(2024) Anticancer activities of natural
antimicrobial peptides from animals.
Front. Microbiol. 14:1321386.
doi: 10.3389/fmicb.2023.1321386

COPYRIGHT

© 2024 Qu, Yuan, Liu, Zhang, Ma and Lu. This
is an open-access article distributed under
the terms of the [Creative Commons
Attribution License \(CC BY\)](https://creativecommons.org/licenses/by/4.0/). The use,
distribution or reproduction in other forums
is permitted, provided the original author(s)
and the copyright owner(s) are credited and
that the original publication in this journal is
cited, in accordance with accepted academic
practice. No use, distribution or reproduction
is permitted which does not comply with
these terms.

Anticancer activities of natural antimicrobial peptides from animals

Baozhen Qu^{1†}, Jiangshui Yuan^{2†}, Xueli Liu^{1,3}, Shicui Zhang^{4,5*},
Xuezhen Ma^{6*} and Linlin Lu^{1*}

¹Qingdao Cancer Prevention and Treatment Research Institute, Qingdao Central Hospital, University of Health and Rehabilitation Sciences (Qingdao Central Medical Group), Qingdao, China, ²Department of Clinical Laboratory, Qingdao Hospital, University of Health and Rehabilitation Sciences (Qingdao Municipal Hospital), Qingdao, China, ³Medical Ethics Committee Office, Qingdao Central Hospital, University of Health and Rehabilitation Sciences (Qingdao Central Medical Group), Qingdao, China, ⁴College of Life and Geographic Sciences, Key Laboratory of Biological Resources and Ecology of Pamirs Plateau in Xinjiang Uygur Autonomous Region, Kashi University, Kashi, China, ⁵Institute of Evolution & Marine Biodiversity, Ocean University of China, Qingdao, China, ⁶Department of Oncology, Qingdao Central Hospital, University of Health and Rehabilitation Sciences (Qingdao Central Medical Group), Qingdao, China

Cancer is the most common cause of human death worldwide, posing a serious threat to human health and having a negative impact on the economy. In the past few decades, significant progress has been made in anticancer therapies, but traditional anticancer therapies, including radiation therapy, surgery, chemotherapy, molecular targeted therapy, immunotherapy and antibody-drug conjugates (ADCs), have serious side effects, low specificity, and the emergence of drug resistance. Therefore, there is an urgent need to develop new treatment methods to improve efficacy and reduce side effects. Antimicrobial peptides (AMPs) exist in the innate immune system of various organisms. As the most promising alternatives to traditional drugs for treating cancers, some AMPs also have been proven to possess anticancer activities, which are defined as anticancer peptides (ACPs). These peptides have the advantages of being able to specifically target cancer cells and have less toxicity to normal tissues. More and more studies have found that marine and terrestrial animals contain a large amount of ACPs. In this article, we introduced the animal derived AMPs with anti-cancer activity, and summarized the types of tumor cells inhibited by ACPs, the mechanisms by which they exert anti-tumor effects and clinical applications of ACPs.

KEYWORDS

antimicrobial peptides, anticancer peptides, animals, marine, terrestrial, mechanisms, clinical applications

1 Introduction

Cancer has emerged as a major cause of human death worldwide, which poses a serious threat to public health and have a negative impact on the economy (Deo et al., 2022). In the past few decades, our understanding of the origin of cancer has developed to a widespread acceptance that cancer is the result of an evolutionary process driven by natural

selection of mutations, subsequent genetic and carcinogenic mutations (Somarelli et al., 2020). Based on statistics from the World Health Organization (WHO) in 2019, cancer is the first or second major cause of death before the age of 70 in 112 out of 183 countries, and ranks third or fourth out of 23 other countries (Sung et al., 2021). According to GLOBOCAN 2020 published by the International Agency for Research on Cancer (IARC), in 2020, there were 19.3 million new cancer cases and 9.9 million new cancer deaths worldwide (Ferlay et al., 2020). The number of cancer deaths will keep growing, with an estimated 13 million deaths by 2030 (Asasira et al., 2022). Among all the cancers, female breast cancer is the most commonly diagnosed cancer, closely followed by lung, colorectal, prostate, and gastric cancers. Lung cancer is the leading cause of cancer death, followed by colorectal, liver, gastric and female breast cancers (Ferlay et al., 2020). The characteristics of all types of neoplastic cells are unregulated cell growth caused by genetic mutations in a small amount of inherited or environmental stimuli, which can achieve replication immortality, avoid cell death, escape from the host immune system, and so on (Schiliro and Firestein, 2021). Well-known signaling pathways, such as the mitogen-activated protein kinase (MAPK), nuclear factor kappa-B (NF- κ B), Wnt, transforming growth factor- β (TGF- β), Notch, Hippo, Janus kinase (JAK)/signal transducer and activator of transcription (STAT), Hedgehog (Hh), and phosphoinositide 3-kinase (PI3K)/AKT pathways, as well as transcription factors, including heat shock transcription factor 1 (HSF1), hypoxia-inducible factor (HIF), Snail, P53, and Twist, constitute complex regulatory networks to modulate the formation, activation, heterogeneity, metabolic characteristics and malignant phenotype of cancers (Fang et al., 2023).

The current therapeutic strategies for treating cancer, include radiation therapy, surgery, chemotherapy, molecular targeted therapy, immunotherapy and antibody-drug conjugate (ADC). For example, conventional chemotherapy, one of the most widely used cancer treatment methods, kills cancer cells by inhibiting cell growth or division. Chemotherapeutics (i.e., alkylating agents, antimetabolic agents, antineoplastic antibiotics, platinating agents, and plant-derived alkaloids) exert anti-tumor effects through direct cytotoxic effects or indirectly by affecting the cell cycle (Okunaka et al., 2021). Progress in molecular targeted drugs has prolonged survival (Li et al., 2023), particularly in patients with lung cancer harboring epidermal growth factor receptor (EGFR) mutations (i.e., erlotinib, gefitinib, afatinib, dacomitinib, and osimertinib) or anaplastic lymphoma kinase (ALK) rearrangement (i.e., ceritinib, alectinib, brigatinib, ensartinib, lorlatinib), and in patients with breast cancer harboring human epidermal growth factor receptor 2 (HER2) amplification (i.e., trastuzumab). Furthermore, cancer immunotherapies targeting the interaction of programmed cell death 1 (PD-1) with its major ligands, PD-L1 and PD-L2 are considered to usher in the era of modern oncology. Drugs that block PD-1 (pembrolizumab, nivolumab, and cemiplimab) or PD-L1 (atezolizumab, durvalumab, and avelumab) promote endogenous anti-tumor immunity and have been considered effective strategies for cancer treatment due to their broad activity spectrum (Topalian et al., 2020). It is worth noting that in recent years, ADC has become a promising cancer treatment method for solid and hematological malignancies. ADC assembles cytotoxic drugs (payloads) by covalently linking them

to monoclonal antibodies (mAbs) and delivering them to tumor tissues expressing their specific antigens, with the advantage of low toxicity and improved treatment rates (Fuentes-Antrás et al., 2023). Currently, the US Food and Drug Administration (USFDA) has approved 13 types of ADCs for the treatment of various types of solid tumors and hematological malignancies (Maiti et al., 2023). However, there are still several obstacles that will affect and limit their curative effect. These treatment modalities have been found to have no specificity for cancer cells resulting in affecting the cell division of normal cells, thereby damaging the repair of healthy tissues (Ziaja et al., 2020). Besides, cancer patients often develop multi-drug resistance (MDR) to chemotherapeutics acquired by tumors (Ziaja et al., 2020). Thus, the development of novel tumor-targeted therapies that could effectively target tumor cells with lower/minor toxicity to normal cells and battle drug resistance is a top priority for treating cancer. In recent decades, researchers have focused on finding new anticancer strategies and have shifted their attention to antimicrobial peptides (AMPs).

AMPs are natural bioactive peptides with diverse structural properties that are produced by bacteria, fungi, plants and animals, and act as the first line of defense against invading pathogens (Wang G. et al., 2022). In 1981, the first important animal derived AMP named cecropins was identified from the Cecropia silk moth, followed by magainin from *Xenopus laevis* in 1987 (Steiner et al., 1981; Zasloff, 1987). After that, numerous other natural AMPs were discovered in almost all organisms (Han et al., 2021; Ma et al., 2021). Since then, more than 3000 AMPs have been deposited in the Antimicrobial Peptide Database.¹ In addition to having broad-spectrum antibacterial effects, an increasing number of AMPs have been proven to have other physiological functions including antifungal, antiviral, antioxidative, antithrombotic, antihypertensive and immunomodulatory (Macedo et al., 2021; Quah et al., 2023). Importantly, many AMPs also demonstrated possess antitumor activity. Most AMPs rely on destructing cell membranes or changing cell membrane permeability to kill bacteria or cancer cells (Lyu et al., 2019), but some AMPs can also via non-membranes disruptive mechanisms exert anti-cancer effects. For instance, cecropins and LL-37 could induce apoptosis and necrosis of tumor cells (Qin et al., 2019; Yang et al., 2021), melittin could suppress tumor angiogenesis and reactivate immune cells (Zhang and Chen, 2017; Duffy et al., 2020).

Anticancer peptides (ACPs) have many unique advantages compared to chemotherapy drugs, such as biocompatibility, efficient therapeutic efficacy, low risk of drug resistance appearing in tumor cells, and limited or no toxicity against mammalian cells (Karami Fath et al., 2022; Lath et al., 2023). In addition, ACPs have immunogenicity and low difficulty in synthesis and modification, with a short half-life *in vivo*, making it possible for them to be put into clinical anti-cancer drug candidates (Karami Fath et al., 2022). In this review, we summarize and describe the anticancer effects and the mode of action of AMPs derived from marine and terrestrial animal sources based on their order of evolution, and we further discuss the clinical applications of ACPs.

¹ <https://aps.unmc.edu/>

2 The structural classifications and selective recognition to tumor cells of AMPs

Generally, the naturally produced AMPs are cationic and amphipathic, with the net charge at neutral pH ranging from +2 to +9 (Costa et al., 2011). Most AMPs are short in length, usually containing 10–50 L-amino acids, which are rich in lysine, arginine and large amounts of other hydrophobic residues (>30%) (Maroti et al., 2011). So why can AMPs inhibit or kill bacteria? Notably, the surfaces of Gram-positive and Gram-negative bacteria are rich in lipopolysaccharides and teichoic acid, which result in a net negative charge generated on the cell membrane surface. Therefore, the cationic and amphipathic nature of AMPs can generate electrostatic interactions with negative charges on the surface of bacteria and interact with various hydrophilic and hydrophobic components (Luo and Song, 2021). At present, the AMPs can be classified as α -helical, β -sheet, mixed α -helical/ β -sheet, as well as cyclic and unstructured (neither α -helix nor β -sheet) AMPs according to the secondary structure (Liang et al., 2020). Among them, the α -helix peptides are the most studied type of AMPs. In aqueous solution, α -helical AMPs possess a linear structure, but when come in contact with bacterial membranes or organic solvents these adopt an amphipathic helical structure, which contributes to insert into the cell membrane (Mahlapuu et al., 2016). Specifically, α -helical AMPs adhere to negatively charged bacterial membranes through electrostatic interactions, inserting their hydrophobic domains into the bacterial membrane, resulting in membrane deformation (Liang et al., 2020). The two most studied and representative peptides in this group are human LL-37 and magainin 2 (MG2) (see sections “3.2.2 ACPs derived from amphibians and 3.2.4 ACPs derived from mammals” for details). β -sheet AMPs are typically molecules composed of at least two antiparallel β -sheet, which contain 6 to 8 cysteine residues and are further stabilized by forming two or more disulfide bonds (Lewies et al., 2015). At present, defensins are the most widely studied family of β -sheet AMPs (see section “3.2.4 ACPs derived from mammals” for details). Tachyplesin I is another β -sheet AMPs which forms a uniquely rigid and stable β -hairpin with three tandem tetrapeptide repeats (Luan et al., 2021). The third type, α -helix/ β -sheet mixed structure, stabilized three to four disulfide bond bridges, is another major structural motif of some AMPs. For instance, cysteine-stabilized $\alpha\beta$ (CS $\alpha\beta$) defensins consist of a single α -helix and β -sheets with two or three antiparallel chains, with the length varying from 34 to 54 amino acid residues (Dias Rde and Franco, 2015). Insect heliomicin and fungi defensin eurocin are two typical representatives of CS $\alpha\beta$ defensins. The fourth type of cyclic peptides contains one or two disulfide bonds to form this conformation. The typical representative is bacteriocins, which normally come from bacteria rather than animals. For example, plantacyclin B21AG and bacteriocins enterocin 7A are two circular bacteriocins, which display antimicrobial activity. Finally, the unstructured (neither α -helix nor β -sheet) AMPs rich in specific amino acids such as tryptophan, proline, and arginine, and typically around 15 amino acids, exhibit a linear structure (Schibli et al., 2002). This unstructured type of AMPs usually presents a disordered or loose curly structure before interaction with the lipid bilayer, and will quickly fold into active conformation once

contact with the membrane (Johansson et al., 1998). Indolicidin, from cytoplasmic granules of bovine neutrophils, is a typical linear AMP rich in tryptophan and proline (Smirnova et al., 2020). LF11 is another short linear AMP based on the human lactoferrin (Zhang et al., 2022).

In the manner of cell membrane destruction modes, ACPs and AMPs have similar mechanisms leading to thinning, forming pores, changing the degree of curvature of the cell membrane, etc. These actions can lead to changes in the overall membrane potential of the cell membrane, and loss of membrane potential gradient, thus stopping the synthesis of ATP and the termination of cell metabolism, and ultimately leading to the death of cells (Chiangjong et al., 2020; Luan et al., 2021). There are three commonly recognized types of cell membrane destruction modes, i.e., the barrel-stave model, the toroidal model, and the carpet model (Li et al., 2021; Erdem Büyükkiraz and Kesmen, 2022). The barrel-stave model has the most extensively study. In this model, after binding to the cell membrane, ACPs/AMPs are arranged vertically with the cell membrane and aggregate with each other to form a cylindrical insertion into the cell membrane, thereby forming pores on the cell membrane. In the toroidal model, after the ACPs/AMPs combine with the cell membrane, the cell membrane bends inward to form a hole, which is composed of the hydrophilic head of the lipid bilayer and ACPs/AMPs. The carpet model has a strong destructive effect on cell membranes. In the model, ACPs/AMPs bind to the cell membrane and are parallel to the surface of the cell membrane. After reaching a certain concentration of ACPs/AMPs, the cell membrane is broken down into small particles one by one.

In the manner of non-membrane destruction modes, ACPs could display anti-tumor activity by mediating the necrosis or apoptosis of cancer cells, inhibiting angiogenesis, immune cell recruitment and activating certain regulatory functional proteins (Huan et al., 2020; Jafari et al., 2022).

Why do ACPs recognize tumor cells specifically? In this respect, the abundant presence of anions on the surface of tumor cells significantly increases the electrostatic interaction between ACPs and the surface of cancer cells. However, compared with tumor cells, healthy cell membranes have zwitterion phosphatidylcholine and sphingomyelin in an outer leaflet and anionic phosphatidylserine (PS) and the phosphatidylethanolamine in the inner leaflet with the asymmetric distribution (Chiangjong et al., 2020). The outer leaflet of the plasma membrane of tumor cells usually contains a large amount of negatively charged PS, which is 3–7 times more than normal cells (Haider and Soni, 2022). In addition, anionic molecules such as O-glycosylated mucins, sialylated gangliosides and heparin sulfate, which are overexpressed in tumor tissue and closely related to the occurrence and progression of tumors, also greatly increase the number of negative charges on the surface of tumor cells (Luong et al., 2020). Moreover, the differences in membrane fluidity and cell surface area between tumor cells and normal cells are also considered important reasons for the preferential action of ACPs on tumor cells. Cholesterol accumulates in a larger amount on the cell membrane of normal cells than in cancer cells, which could effectively reduce the membrane fluidity to prevent cationic peptides from inserting into the cell membrane (Norouzi et al., 2022). On the contrary, most cancer cells have lower cholesterol content on their membranes, making them more fluid than normal

cells (Luan et al., 2021), leading to ACP being more prone to disrupting membrane stability. Another interesting characteristic of cancer cells is the expression of a large number of microvilli in their plasma membrane, which increases the surface area of the membrane and thus increases the affinity of ACPs to tumor cells (Luan et al., 2021).

3 Animal sources of AMPs with anticancer activity

The natural environment is considered a vital source of novel therapeutic drugs. The ocean, accounting for approximately 71% of the earth's surface area, represents more than half of the biodiversity worldwide. Marine animals are important providers of natural active peptides (Chakniramol et al., 2022). At present, many bioactive peptides with anticancer potential have been identified from various marine animals (Figure 1), mainly concentrated in sponges, mollusks, marine arthropods, ascidians and fish (Zhang et al., 2021; Chakniramol et al., 2022; Wong et al., 2023). Some known ACPs from terrestrial animals (Figure 1), including terrestrial arthropods, amphibians, reptiles and mammals, have also been proven to have broad application prospects, serving as novel anti-tumor drugs or auxiliary therapeutic measures for cancer treatment (Pan et al., 2020; Tornesello et al., 2020). In Tables 1, 2, we comprehensively classified the natural ACPs of marine and terrestrial animals based on their order of evolution to the greatest extent possible, and provided a detailed introduction to the representative ACPs among them in the following section.

3.1 ACPs isolated from marine animals

3.1.1 ACPs derived from sponges

Sponges are filter-feeding animals that cope with hazardous particles by producing neutralizing bioactive compounds such as peptides. In the past 20 years, researchers have focused on sponges-isolated peptides such as jaspamide, koshikamides, and theonellamide G, which exhibited extensive cytotoxicity to various cancer cells. These peptides with unusual amino acids or non-amino acid parts compared to other animal derived ACPs. Jaspamide and koshikamides were the special structured cyclic depsipeptides found in the genus *Jaspis johnstoni* and the *Theonella* sp. respectively, exhibiting cytotoxicity to various cancer cells, like prostate, breast carcinomas, acute myeloid leukemia and colon cancer cells (Schweikart et al., 2013; Kang et al., 2018). Whereas, theonellamide G is a glycopeptide, obtained from the *Theonella swinhoei*, exhibiting cytotoxic effects against HCT-16 human colon adenocarcinoma cell line (Macedo et al., 2021).

3.1.2 ACPs derived from marine mollusks

Marine mollusks rely on their physical barriers and innate immune systems to resist the most diverse pathogens, due to the adaptive immunity has not yet evolved. Since the 1990s, a few marine mollusks ACPs have been identified. Dolastatin 10 was the first marine mollusk ACP identified from the Indian Ocean sea hare *Dolabella Auricularia* (Bai et al., 1990), and is still considered one of the most powerful anti-cancer peptides found so far. It could inhibit the proliferation of human lymphoma, lung cancer,

ovarian carcinoma, prostate cancer, soft tissue sarcoma, breast cancer and pancreatic cancer by inhibiting microtubule assembly and tubulin polymerization, and inducing apoptosis and Bcl-2 phosphorylation (Gao et al., 2021). Adcetris® is an ADC drug modified from dolastatin 10, containing a CD30-specific mAb conjugated to monomethyl auristatin E (MMAE). It was approved by FDA in 2011 and became the second ADC drug to enter the oncology market (Tong et al., 2021).

3.1.3 ACPs derived from marine arthropods

Arthropods are one of the most successful animals in adapting and surviving in the marine environment, not only due to their solid shells but also because of their complete inner immunity compared to other marine animals. AMPs play a vital in the immune system. Currently, various AMPs that have been proven as ACPs in marine arthropods are mainly concentrated in shrimps and crabs. For example, shrimp anti-lipopolysaccharide factor (SALF) displayed antitumor activity against Hela cells by apoptosis related death receptor/NF- κ B signaling pathway. When combined with cisplatin, the inhibitory effect on Hela cells is more pronounced (Lin et al., 2010). The novel ACPs polyphemusins from the horseshoe crab *Limulus polyphemus* were discovered to against human cancer cells. In an anti-tumor research, polyphemusin II was examined to destroy the cell membranes of the human erythroleukemia K562 cell line by inducing necrotic cell death (Paredes-Gamero et al., 2012). Another study indicated that polyphemusin III could lead to rapid permeabilization of the cytoplasmic membrane of human leukemia cells HL-60 (Marggraf et al., 2018).

3.1.4 ACPs derived from marine ascidians

Ascidians belong to the phylum of Chordata and are the most evolved group of marine organisms. Unique cyclic and linear peptides containing unusual amino acids derived from ascidians have increased our knowledge regarding novel ACPs. Styelin D, an ACP with 32 residues containing two specific amino acids (dihydroxyarginine and dihydroxylysine) from blood cells of the ascidian *Styela clava*, showed significant cytotoxic and hemolytic to human cervical cancer epithelial cell line ME-180 (Taylor et al., 2000). Moreover, turgencin A and turgencin B with six cysteine residues are two novel linear ACPs, derived from the ascidian *Synoicum turgens*, which showed obvious anticancer activities to suppress the proliferation of melanoma cancer cell line A2058 and the human fibroblast cell line MRC-5 (Hansen et al., 2020).

3.1.5 ACPs derived from fish

Bioactive peptides are indispensable components of fish innate immune system, to prevent the invasion of pathogens from the aquatic microorganisms ecosystems. Fish ACPs mainly identified from the fish mucus, among them, pardaxin, piscidin, and epinecidin-1 are the representative beings. Pardaxin is the most widely studied ACP present in the Red Sea Moses sole (*Pardachirus marmoratus*). It is composed of α -helix with 33 amino acid residues and has been experimentally confirmed in several studies on different cancer cell lines to show anticancer potential through multiple mechanisms of action. For example, pardaxin could arrest the cell cycle of cancer cells in the G2/M phase, thereby interfering with the cell proliferation process (Eghtedari et al., 2021). Moreover, pardaxin has been researched for its

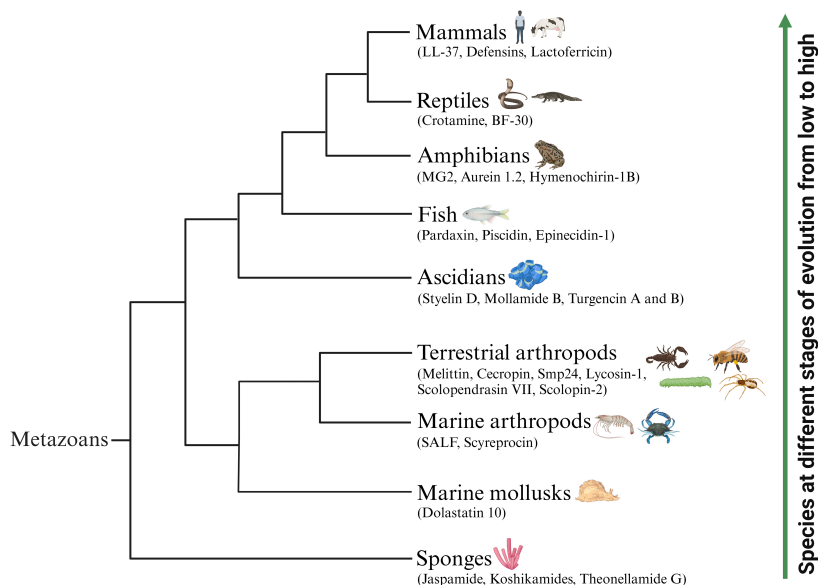


FIGURE 1

Schematic representation of representative animal-origin ACPs according to the animal's evolution order. Some known ACPs which have been identified from various marine animals mainly concentrated in sponges, mollusks, marine arthropods, ascidians and fish. Several representative ACPs also isolated from terrestrial animals including terrestrial arthropods, amphibians, reptiles and mammals.

antitumor properties via inducing apoptotic cell death in various cancer cell lines such as fibrosarcoma (Wu et al., 2012), oral squamous carcinoma (Han et al., 2015), ovarian cancer cells (Chen et al., 2021) and cervical carcinoma (Huang and Chen, 2013). Besides that, pardaxin was also demonstrated to cause cell necrosis in fibrosarcoma (Lin et al., 2013) and autophagy in ovarian cancer cells (Chen et al., 2021). Furthermore, it is particularly noteworthy that the endoplasmic reticulum (ER)-targeting ability of pardaxin in cancer cells (Qin et al., 2020). The piscidin family is an important component of the innate immunity of teleost, and recent studies have shown that they have extensive antibacterial and anticancer activities. A study reported that piscidin-1 could inhibit the motility and proliferation of HT1080 (human fibrosarcoma cell line) via inducing apoptotic and necrotic activity (Lin et al., 2012). Another study observed that piscidin-4 displayed significant cytotoxicity toward non-small cell lung cancer (NSCLC) cell lines such as A549, NCI-H661, NCI-H1975 and HCC827 (Ting and Chen, 2018). In this research, piscidin-4 caused NSCLC cell death through the necrotic pathway rather than the apoptotic pathway. Another common peptide was epinecidin-1, a naturally occurring peptide isolated from orange-spotted grouper (*Epinephelus coioides*), which exhibited inhibitory activity on human lung cancer and glioblastoma by regulating the process of cell apoptosis and necrosis (Su et al., 2020; Yu et al., 2023).

3.2 ACPs isolated from terrestrial animals

3.2.1 ACPs derived from terrestrial arthropods

Terrestrial arthropods are rich sources of novel bioactive compounds, including ACPs, which are mainly derived from three main classes: Insecta, Arachnida, and Chilopoda.

Insect AMPs are critical factors of the insect immune system, and also show toxic effects on many cancer cells (Table 2). Bee venom is a kind of important insect-derived AMPs with anti-tumor effects. Melittin is an amphiphilic bioactive peptide derived from the honey bee *Apis mellifera* and is the most researched and representative bee venom-derived AMP. Melittin induced a variety of cell death mechanisms, such as apoptosis, cell cycle arrest, and angiogenesis (Soliman et al., 2019). Experimental studies have proven that melittin exhibited anticancer activity in prostate cancer, ovarian carcinoma, glioma, astrocytoma, hepatocellular carcinoma, leukemic, lung tumor, squamous carcinoma, osteosarcoma and renal cancer cells (Xu et al., 2017; Soliman et al., 2019; Yu et al., 2020). However, the use and application of melittin in clinical experiments was limited because of its widespread cytotoxicity against both tumor cells and normal cells. Therefore, the recent research hotspots of melittin mainly focused on developing safe and stable melittin delivery systems (Wang A. et al., 2022). In addition, A classic AMP from silkworms is cecropin, which was considered as a necrosis-inducing peptide and exhibited anti-proliferation activity to leukemia cells, gastric carcinoma, bladder cancer, fibrosarcoma and HCC (Qin et al., 2019).

The ACPs in Arachnida are mainly concentrated in the venom of scorpions and spiders (Table 2). Smp24, a cationic AMP isolated from the venom gland of the Egyptian scorpion *Scorpio maurus palmatus*, has been proven to show potent suppressing effects on leukemic tumor cell lines (KG1-a and CCRF-CEM) and human lung cancer cell lines (A549, H3122, PC-9, and H460). Furthermore, its inhibition of the A549 cell migration ability is through the mediation of filamentous actin (F-actin) and the changes of MMP-2/9 and TIMP-1/2 protein expressions (Guo et al., 2022). Spider AMPs with anti-cancer activities have also been reviewed. Spider venom-derived peptide lycosin-1 was proven to inhibit seven cancer cell lines proliferation *in vitro* and effectively

TABLE 1 Antimicrobial peptides (AMPs) with potential anticancer activity derived from marine animals, their application and mechanisms of action.

Peptides	Source	Group	Structure	Application	Mechanism of action	References
Jaspamide	<i>Jaspis johnstoni</i>	Sponges	Cyclic	Human prostate cancer, breast carcinomas, acute myeloid leukemia	Regulate caspase-3 protein, regulate the reduction of Bcl-2	Schweikart et al., 2013
Koshikamide H	<i>Theonella</i> sp.	Sponges	Cyclic	Human colon cancer	NR	Kang et al., 2018
Theonellamide G	<i>Theonella swinhoei</i>	Sponges	Cyclic	Human colon cancer	NR	Macedo et al., 2021
Callyaerins A–F and H	<i>Callyspongia aerizusa</i>	Sponges	Cyclic	Mouse lymphoma, human cervix carcinoma, rat brain tumor	NR	Ibrahim et al., 2010
Dolastatin 10	<i>Dolabella Auricularia</i>	Mollusks	Cyclic	Human lymphoma, lung cancer, ovarian carcinoma, prostate cancer, soft tissue sarcoma, breast cancer and pancreatic cancer	Inhibit microtubule assembly and tubulin polymerization, induce apoptosis and Bcl-2 phosphorylation	Gao et al., 2021
Kahalalide F	<i>Elysia rufescens</i>	Mollusks	Cyclic	Ovaries, breast, prostate, colon, liver tumor cells	Disturbance of lysosomal membrane, mediation of oncosis, alteration of cell membrane permeability and regulation of apoptosis	Wyer et al., 2022
KLH	<i>Megathura crenulata</i>	Mollusks	α -helical/ β -sheet mixed	Breast, pancreatic, prostate cancer, esophageal adenocarcinoma	Regulation of apoptosis	Petrova et al., 2023
SALF	<i>Penaeus monodon</i>	Arthropods	Cyclic	Human cervical cancer	Regulate apoptosis related death receptor/NF- κ B signaling pathway	Lin et al., 2010
Scyreprocin	<i>Scylla paramamosain</i>	Arthropods	α -helical	Human lung cancer	Accumulation of ROS and the release of Ca ²⁺ , dysfunction of mitochondrial function, activation of caspase-3	Yang et al., 2022
Ss-arasin	<i>Scylla serrata</i>	Arthropods	Random coil	Human cervical cancer, human colon carcinoma	NR	Anju et al., 2019
Penaeidin	<i>P. vannamei</i>	Arthropods	α -helical and random coil	Human kidney cancer	Induction of apoptosis	Meng et al., 2014
Tachyplesin I	<i>Tachypleus tridentatus</i>	Arthropods	β -sheet	Liver cancer, leukemia, gastric adenocarcinoma	Mediate the classic complement pathway	Li et al., 2003 ; Chen et al., 2005
Polyphemusin II	<i>Limulus polyphemus</i>	Arthropods	β -sheet	Human erythroleukemia	Induce necrotic cell death	Paredes-Gamero et al., 2012
Polyphemusin III	<i>Limulus polyphemus</i>	Arthropods	β -sheet	Human leukemia	Induce permeabilization of the cytoplasmic membrane	Marggraf et al., 2018
Styelin D	<i>Styela clava</i>	Ascidians	α -helical	Human cervical cancer	NR	Taylor et al., 2000
Turgencin A, B	<i>Synoicum turgens</i>	Ascidians	α -helical and random coil	Human melanoma cancer	NR	Hansen et al., 2020
Pardaxin	<i>Pardachirus marmoratus</i>	Fish	α -helical	Fibrosarcoma, oral squamous carcinoma, ovarian cancer, cervical carcinoma	Cell cycle arrest, induction of apoptosis, necrosis and autophagy	Wu et al., 2012 ; Huang and Chen, 2013 ; Lin et al., 2013 ; Han et al., 2015 ; Chen et al., 2021 ; Eghtedari et al., 2021

(Continued)

TABLE 1 (Continued)

Peptides	Source	Group	Structure	Application	Mechanism of action	References
Piscidin-1	<i>Morone saxatilis</i> x <i>M. chrysops</i>	Fish	α -helical	Human fibrosarcoma	Induce apoptotic and necrotic activity	Lin et al., 2012
Piscidin-4	<i>Oreochromis niloticus</i>	Fish	α -helical	NSCLC	Regulate necrotic pathway	Ting and Chen, 2018
Epinecidin-1	<i>Epinephelus coioides</i>	Fish	α -helical	Human lung cancer and glioblastoma	Regulate cell apoptosis and necrosis	Su et al., 2020; Yu et al., 2023
MSP-4	<i>Oreochromis niloticus</i>	Fish	α -helical	Liver cancer, cervical cancer, fibrosarcoma, osteosarcoma	Induce the apoptosis	Kuo et al., 2018
TH1-5, TH2-3	<i>Oreochromis mossambicus</i>	Fish	α -helical/ β -sheet mixed	Human fibrosarcoma, human cervical cancer, human breast cancer	Induce cell lysis, down-regulate the c-Jun gene, induce an inflammatory response, induce the apoptosis	Eghtedari et al., 2021
TFD-100	<i>Gadus macrocephalus</i>	Fish	Unknown	Human prostate cancer	Inhibit adhesion of PC3 to endothelial cells through binding to galactin-3	Guha et al., 2013
Chrysophsin-1	<i>Chrysophrys major</i>	Fish	α -helical	Human fibrosarcoma, histiocytic lymphoma, cervical carcinoma	Membrane depolarizing lytic mechanism	Hsu et al., 2011
NRC-03, NRC-07	<i>Pseudopleuronectes americanus</i>	Fish	α -helical	Multiple myeloma, breast carcinoma	DNA breakage, the accumulation of ROS	Hilchie et al., 2011, 2013
YALRAH	<i>Setipinna taty</i>	Fish	Linear	Prostate cancer	Induction of apoptosis	Song et al., 2014

NR, not reported.

suppressed tumor growth *in vivo*. Mechanistically, it mediated the mitochondrial death pathway, making cancer cells sensitive to apoptosis, and inactivated the STAT3 pathway (Shen et al., 2018).

Centipedes are typical venomous arthropods. Lee et al. (2015) reported an ACP isolated from the Centipede, *Scolopendra subspinipes mutilans* called scolopendrasin VII. The results showed that scolopendrasin VII reduced the viability of the leukemia cells by inducing necrosis. Scolopin-2, a cationic AMP from centipede venoms, displayed anti-proliferation activities to tumor cell lines such as HeLa, HepG2 and K562 and did not show toxic side effects on normal cells (Yan et al., 2018).

3.2.2 ACPs derived from amphibians

The skin secretions of amphibians are composed of various bioactive peptides, and hundreds of skin AMPs have been isolated from frogs and toads (Oelkrug et al., 2015), some of which also exhibited selective cytotoxicity against cancer cells (Conlon et al., 2014). For example, MG2, isolated from *Xenopus laevis* skin, has demonstrated antitumor activity against human lung cancer and bladder cancer via forming pores on the cell membrane (Ghaly et al., 2023). Aurein 1.2 is a peptide found in the frog *Litoria aurea*, which was reported to exhibit high activity against 55 different cancer cell lines *in vitro* (Rozek et al., 2000; Dennison et al., 2007). Furthermore, hymenochirin-1B is a cationic α -helix peptide belonging to the hymenochirin family from the frog *Hymenochirus boettgeri*, and has been reported to exert antineoplastic activities against lung cancer cells NCI-H1299 and A549 by inducing apoptosis and cell cycle arrest through the mitochondrial pathway (Zhang et al., 2019). Additionally, many other ACPs from amphibians and their mechanisms of action are summarized in Table 2.

3.2.3 ACPs derived from reptiles

Reptile-derived ACPs mainly from the venom of snakes. Crota mine is one of the main peptides of the venom of the South American rattlesnake *Crotalus durissus terrificus*. It acted on the permeabilization of lysosomes, the release of Ca^{2+} from the endoplasmic reticulum and the destruction of mitochondrial membrane potential (Urta and Araya-Maturana, 2022), then showed cytotoxicity toward various cancer cells, such as human pancreatic carcinoma cells Mia PaCa-2, human melanoma cells SK-Mel-28 and murine melanoma cells B16-F10. Another remarkable ACP containing 30 amino acids named cathelicidin-BF (BF-30) was found in the snake *Bungarus fasciatus*. In a study, BF-30 suppressed the growth of mouse melanoma cell B16F10 in a dose and time-dependent manner. *In vivo* experiments, BF-30 obviously inhibited melanoma development in B16F10 tumor-bearing mice without adverse reactions occurring (Wang et al., 2013). In addition, Qi et al. (2020) designed a BF-30 derivative, LBF-14, which exhibited significant anti-melanoma action through disrupting the cell membrane, and then binding to the genomic DNA to suppress the migration and angiogenesis of melanoma cells.

3.2.4 ACPs derived from mammals

Several representative ACPs in mammals have been extensively studied (Table 2). Among them, three of the peptides that have been extensively studied are LL-37, defensins, and lactoferricin. The human cathelicidin, LL-37, participated in the killing process

TABLE 2 Antimicrobial peptides (AMPs) with potential anticancer activity derived from terrestrial animals, their application and mechanisms of action.

Peptides	Source	Group	Structure	Application	Mechanism of action	References
Melittin	<i>Apis mellifera</i>	Arthropods	α -helical	Human prostate cancer, ovarian carcinoma, glioma, astrocytoma, hepatocellular carcinoma, leukemic, lung tumor, squamous carcinoma, osteosarcoma and renal cancer	Induce apoptosis, cell cycle arrest and angiogenesis	Xu et al., 2017 ; Soliman et al., 2019 ; Yu et al., 2020
Mastoparan	<i>Polybia paulista</i>	Arthropods	α -helical	Human glioma, human bladder cancer, human lung cancer	Induction of apoptosis, alteration of mitochondrial permeability	Alhakamy et al., 2021
Decoralin	<i>Oreumenes decorates</i>	Arthropods	α -helical	Human breast cancer	Mediate the necrosis	Torres et al., 2018
Cecropins	<i>Hyalophora cecropia</i>	Arthropods	α -helical	Human leukemia, gastric carcinoma, bladder, kidney cancer, fibrosarcoma	Induction of necrosis	Qin et al., 2019
Harmoniasin	<i>Harmonia axyridis</i>	Arthropods	Unknown	Human leukemia	Induce apoptotic and necrotic cell deaths	Kim et al., 2013
Alloferon-1	<i>Calliphora vicina</i>	Arthropods	Unknown	Murine leukemia	Induce the cytotoxicity of natural killer cell	Chernysh et al., 2012
Smp24	<i>Scorpio maurus palmatus</i>	Arthropods	α -helical	Human leukemia, human lung cancer	Mediation of F-actin, regulation of MMP-2/9 and TIMP-1/2	Guo et al., 2022
AaeAP1a, AaeAP2a	<i>Androctonus aeneas</i>	Arthropods	α -helical, β -sheet and random coil	Human lung cancer, human prostate cancer, human breast cancer	NR	Du et al., 2015
Gomesin	<i>Acanthoscurria gomesiana</i>	Arthropods	β -sheet	Human melanoma and chronic myeloid leukemia	Target and destroy tumor cell membranes	Troeira Henriques et al., 2017
Lycosin-1	<i>Lycosa singoriensis</i>	Arthropods	α -helical	Human cervical, lung, prostate, colon and liver cancer, human fibrosarcoma	Inactivate STAT3 pathway, induce apoptosis	Shen et al., 2018
Ltc2a	<i>Lachesana tarabaei</i>	Arthropods	α -helical	Human erythroleukemia	Target cancer cell membranes and form pores	Vorontsova et al., 2011
Scolopendrasin VII	<i>Scolopendra subspinipes mutilans</i>	Arthropods	Unknown	Human leukemia	Induction of necrosis	Lee et al., 2015
Scolopin-2	<i>Scolopendra subspinipes mutilans</i>	Arthropods	α -helical	Human cervical cancer, human liver cancer, human leukemia	Regulate caspase-related apoptosis pathways	Yan et al., 2018
MG2	<i>Xenopus laevis</i>	Amphibians	α -helical	Human lung cancer, human bladder cancer	Form pores on the cell membrane	Ghaly et al., 2023
Aurein 1.2	<i>Litoria aurea</i>	Amphibians	α -helical	Leukemia, melanoma, Lung, colon, ovarian, renal, prostate and breast cancer	Interact with cancer cell membranes	Rozek et al., 2000 ; Dennison et al., 2007
Hymenochirin-1B	<i>Hymenochirus boettgeri</i>	Amphibians	α -helical	Human lung cancer	Induce apoptosis and cell cycle arrest	Zhang et al., 2019

(Continued)

TABLE 2 (Continued)

Peptides	Source	Group	Structure	Application	Mechanism of action	References
Dermaseptins	<i>Phyllomedusa bicolor</i>	Amphibians	α -helical	Human prostate cancer, breast cancer, B-lymphoma, glioblastoma, pancreatic cancer, melanoma	Interact with the lipids of the plasma membrane	Dos Santos et al., 2017
Alyteserin-2a	<i>Alytes obstetricans</i>	Amphibians	α -helical	Human breast, colon, lung and liver cancer	Inhibit the release of IL-10 and TGF- β	Conlon et al., 2013
BR-2R	<i>Rana ridibunda</i>	Amphibians	α -helical	Human breast cancer, human lung cancer	Induce apoptosis and cell cycle arrest	Hassanvand Jamadi et al., 2017
Kassinatuerin-3	<i>Kassina senegalensis</i>	Amphibians	α -helical	Human lung, prostate cancer and glioblastoma	NR	Wang et al., 2020
Crotamine	<i>Crotalus durissus terrificus</i>	Reptiles	α -helical/ β -sheet mixed	Human pancreatic carcinoma, human melanoma, murine melanoma	Permeabilization of lysosomes, release of Ca^{2+} from endoplasmic reticulum, destruction of mitochondrial membrane potential	Urrea and Araya-Maturana, 2022
BF-30	<i>Bungarus fasciatus</i>	Reptiles	α -helical	Mouse melanoma	Cytoplasmic membrane permeabilization and DNA-binding	Wang et al., 2013 ; Qi et al., 2020
KT2, RT2	<i>Crocodylus siamensis</i>	Reptiles	α -helical	Human colon cancer, human cervical cancer	Induction of apoptosis	Maijaroen et al., 2018
LL-37	<i>Homo sapiens</i>	Mammals	α -helical	Gastric cancer, human T leukemia, human oral squamous cell carcinoma, human colon cancer, human lung cancer	Activate tumor-suppressing bone morphogenetic protein, regulate caspase-independent apoptosis	Okumura et al., 2004 ; Mader et al., 2009 ; Wu et al., 2010 ; Ren et al., 2013 ; Yang et al., 2021
Defensins	<i>Homo sapiens</i>	Mammals	β -sheet	Human myeloid leukemia, lymphoblastoid B cells, cervical neoplasia	Membrane lysis, regulation of apoptosis, inhibition of neovascularization	Tornesello et al., 2020
Lactoferrin	<i>Bos taurus</i>	Mammals	β -sheet	Human leukemia, human neuroblastoma, human breast, colon, gastric and ovary cancer	Cell cycle arrest, induce cell apoptosis and necrosis, inhibit cell metastasis and angiogenesis, immune regulation	Rahman et al., 2021
ChMAP-28	<i>Capra hircus</i>	Mammals	α -helical	Human leukemia, human bosom adenocarcinoma, human epidermoid carcinoma, murine melanoma	Cause cell membrane permeability, induce necrotic death	Emelianova et al., 2018

NR, not reported.

of various tumor cells. For example, [Wu et al. \(2010\)](#) indicated that LL-37 showed cytotoxicity to gastric cancer cells by activating tumor-suppressing bone morphogenetic protein signaling via suppression of proteasome. LL-37 could also inhibit the growth of Jurkat human T leukemia cells, human oral squamous cell carcinoma (OSCC) cells SAS-H1 and colon cancer cells via caspase-independent apoptosis ([Okumura et al., 2004](#); [Mader et al., 2009](#); [Ren et al., 2013](#)). Importantly, LL-37 has been modified to many shorter sequences to exhibit lower toxicity and higher efficiency. 17BIPHE2, the shortest modified LL-37, could induce apoptosis of human lung cancer better than LL-37 ([Yang et al., 2021](#)). Defensins, an important group of cysteine-rich and β -sheet AMPs widely presented in various mammals, have been discovered to display cytolytic activity against several cancer cell lines, such as human myeloid leukemia cell line U937, K562, lymphoblastoid B cells IM-9 and WIL-2 and cervical neoplasia. Furthermore, the anti-cancer activities of α -defensins, including the human neutrophil peptides (HNP) 1–3, have been proven through the manner of membrane lysis and apoptosis as well as inhibition of neovascularization in tumor cells ([Tornesello et al., 2020](#)). Lactoferricin is a cationic peptide identified from the acid-pepsin hydrolysis of lactoferrin in mammalian milk and exhibited cytotoxic activity against a panel of microorganisms and cancer cells. Lactoferricin mainly exerted anti-tumor effects through cell cycle arrest, inducing cell apoptosis and necrosis, inhibiting cancer cell metastasis and angiogenesis, and immune regulation ([Rahman et al., 2021](#)).

4 Mechanisms of AMPs underlying their anti-cancer effects

Due to the non-specific destruction of the plasma membrane by ACPs, they exhibit therapeutic potential for tumors that are ineffective in traditional drug therapy. Although some of the main mechanisms of action have been reported, the exact mechanisms of the toxic effect of ACPs on cancer cells remain controversial. Generally speaking, the anti-cancer effect of bioactive peptides can be achieved by regulating membrane or non-membrane mechanisms ([Harris et al., 2013](#)).

4.1 Membranes disruptive mechanisms

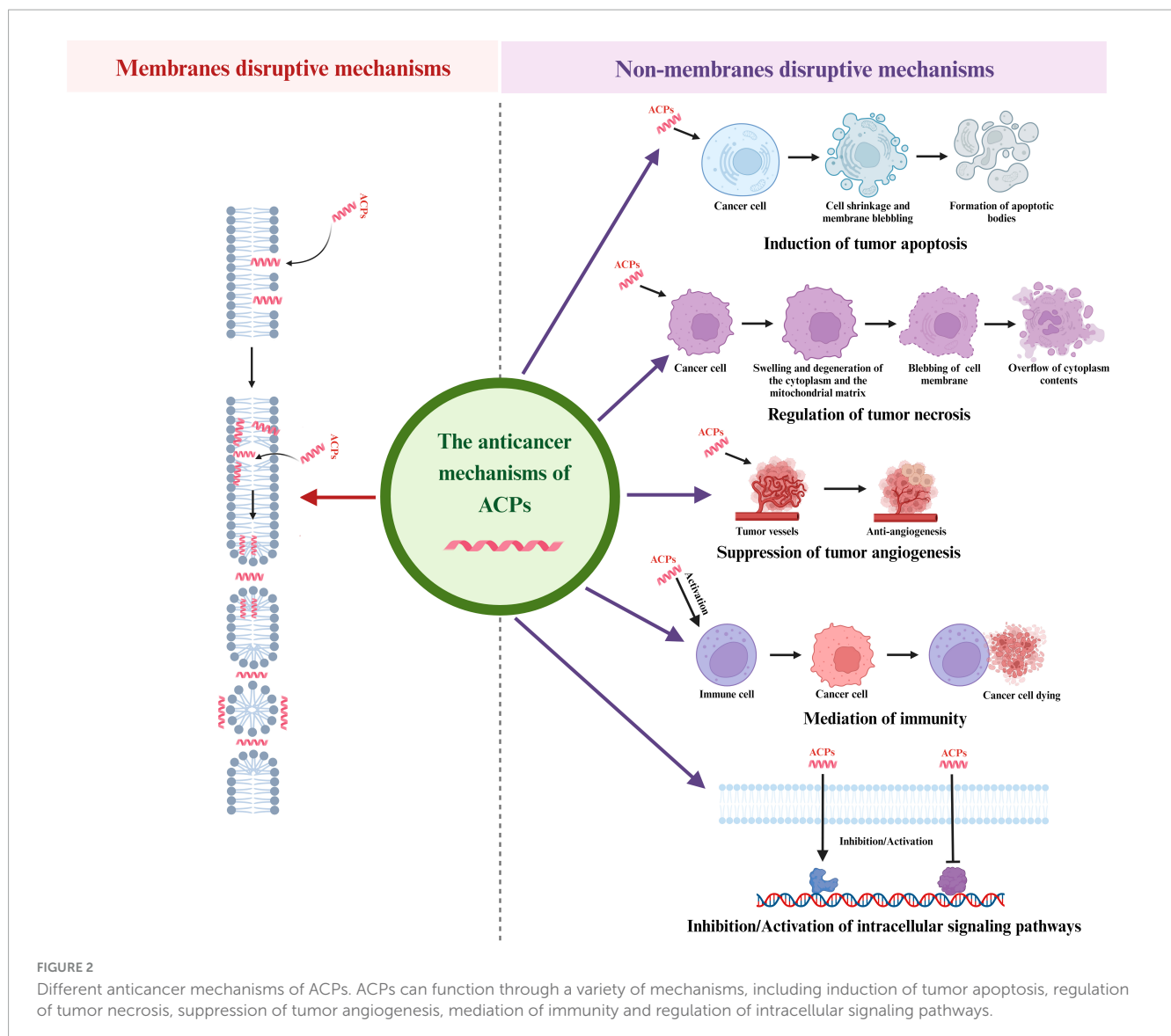
As mentioned in the section “2 The structural classifications and selective recognition to tumor cells of AMPs” of this article, the destruction modes of ACPs on tumor cell membranes is similar to that of AMPs induced bacterial membrane damage ([Figure 2](#)). For example, a study reported by [Papo et al. \(2006\)](#) indicated that a short host defense-like peptide could selectively recognize cancer cells mainly via binding with negatively charged PS on the cell surface, leading to depolarization of cell plasma membrane and cell death. Therefore, peptide-lipid interaction is the committed step to effectively destroy tumor cell membranes. Another research also demonstrated that the spider venom Ltc2a could induce tumor cell membrane blebbing, swelling, and ultimately cell death. Interestingly, this peptide interacted with the outer membrane leaflet of tumor cells, thereby inducing PS externalization. Due to the formation of membrane pores in tumor cells, their permeability

to anionic molecules is stronger than that of cationic molecules, and the redistribution of PS toward the outer leaflet of the membrane was discovered in the tumor cells ([Vorontsova et al., 2011](#)). Moreover, several ACPs such as cecropins, pardaxin, magainins and melittin were proven that they induce the formation of pores in tumor cell membranes through the barrel-stave model, toroidal model and carpet model, and lead to tumor lysis and death ([Ryan et al., 2013](#); [Han et al., 2015](#); [Kashiwada et al., 2016](#); [Pino-Angeles et al., 2016](#); [Zhang S. K. et al., 2016](#)).

4.2 Non-membranes disruptive mechanisms

4.2.1 Induction of tumor apoptosis

Apoptosis is a gene-directed program developed by multicellular organisms to control cell proliferation to cope with DNA damage during development or after cell stress. The characteristics of the apoptosis process are cell shrinkage, membrane blebbing, chromatin condensation and nuclear fragmentation and then small membrane-bound apoptotic bodies are released and swallowed by macrophages or adjacent cells. There are two major pathways of apoptosis in mammalian cells: mitochondrial-mediated endogenous pathways and death receptor-mediated exogenous pathways. In the mitochondrial-mediated endogenous pathways of apoptosis, cell apoptosis is caused by mitochondrial dysfunction and membrane damage, resulting the release of the Cyt c. The Cyt c-induced apoptosis is mainly initiated by the apoptotic protease (Caspase) pathway ([Dave et al., 2011](#)). The early opening of the mitochondrial permeability transition pore (mPTP) in the inner mitochondrial membrane (IMM) is a key reason in primary necrosis. These changes lead to extreme swelling of mitochondrial permeability, ultimately resulting in necrotic cell death ([Mulder et al., 2013](#)). In the death receptor pathway, various external factors act as promoters of cell apoptosis, and then transmit apoptotic signals through different signal transduction systems, inducing cell apoptosis. Fas and Fas ligand (FasL/CD95L) are the two most important apoptosis-inducing molecules in cancer cells ([Shimoyama et al., 2015](#)). Cell apoptosis plays a vital role in eliminating cancer cells without causing damage to normal cells or surrounding tissues. Regulating the apoptosis pathway in tumor cells will be an effective method for cancer prevention and treatment, and peptides that can induce tumor cell apoptosis ([Figure 2](#)) are gradually becoming significant candidates for the development of novel anticancer medicines. [Ceremuga et al. \(2020\)](#) found a dose dependent decrease of mitochondrial membrane potential in human leukemia cells treated with melittin, which confirmed the process of cell apoptosis and suggested a potential pathway related to the intrinsic mechanism that depended on mitochondria. A study in 2022 demonstrated that NRC-03 could induce apoptosis in OSCC cells through the cyclophilin D (CypD)-mPTP axis mediated mitochondrial oxidative stress ([Hou et al., 2022](#)). In terms of exogenous pathways mediated by death receptors, SALF is a typical peptide that exerted anti-tumor effects through the apoptosis-related death receptor/NF- κ B signaling pathway ([Lin et al., 2010](#)). Moreover, in recent years, researchers have also found that both endogenous and exogenous apoptosis pathways were



involved in ACPs induced cancer cell apoptosis. For example, MSP-4 could induce apoptosis via activation of extrinsic Fas/FasL- and intrinsic mitochondria-mediated pathways in the osteosarcoma cell line (Kuo et al., 2018). In another study, the expression of the cell apoptosis key proteins, such as CytC, caspase-9, and caspase-3 in the endogenous mitochondrial pathway, and Fas, FasL in the exogenous death receptor pathway were significantly up-regulated after treating lung cancer cells with dermaseptin (Dong et al., 2020). In addition, Ju and co-workers found that both the caspases mediating extrinsic and mitochondria intrinsic pathways were activated in Brevinin-1RL1 induced apoptosis (Ju et al., 2021).

4.2.2 Regulation of tumor necrosis

Necrosis is defined as an unexpected, uncontrolled, and non-programmed form of cell death. Accidental necrosis is usually caused by chemical or physical damage, ultimately leading to chromatin flocculation, swelling and degeneration of the cytoplasm and the mitochondrial matrix, blebbing of the cellular membrane, and overflow of cytoplasm contents to the outside of cells (Padanilam, 2003). Necrosis inducing peptides

are a group of lytic peptides that destroy cell membranes (Figure 2). Compared with traditional chemotherapy drugs, they have higher selectivity toward cancer cells and do not induce multidrug resistance, making them a promising new class of anticancer drugs (Bhutia and Maiti, 2008). For instance, Su et al. (2019) found that piscidin 4 displayed anti-tumor activity on glioblastoma cell lines via inducing mitochondrial hyperpolarization and mitochondrial dysfunction, followed by DNA damage and necrosis. A study in 2019 revealed that melittin induced cell death mostly occurred by necrosis in MCF-7 and MDA-MB-231 cells (Daniluk et al., 2019). Moreover, it was reported that decoralin could induce necrosis in cancer cells by enhancing the stiffness of the cell membrane (Mirzaei et al., 2021). It was also pointed out that cathelicidin reduced the tumor growth and regulated necrosis of cancer cells by releasing tumor necrosis factor- α (TNF- α) and granules enzymes (Mahmoud et al., 2022). Furthermore, Smp24 could induce necrosis of A549 cells through damaging the integrity of the cell membrane, mitochondrial and nuclear membranes (Guo et al., 2022).

4.2.3 Suppression of tumor angiogenesis

Angiogenesis is the process through which novel blood vessels are formed from pre-existing ones and it is a multi-step process involving endothelial cell (EC) proliferation and migration (Starzec et al., 2006). Angiogenesis plays an important role in the growth, invasion, and metastasis of tumors. Specifically, nutrition, oxygen supply, and metabolic waste excretion in tumors are regulated through a complex network of tumor microvessels (De Palma et al., 2017). Tumor angiogenesis is completed via a range of sequential steps, which further result in the development of cancer. The process of angiogenesis is mainly triggered by the tumor itself, and as malignant tumors continue to grow, tumor cells become hypoxic (Marme, 2018). Hypoxia is the basic initiating factor for tumor angiogenesis (De Palma et al., 2017). Moreover, there are many growth factors involved in tumor angiogenesis, such as vascular endothelial growth factor (VEGF), epidermal growth factor (EGF), angiogenin (Ang), fibroblast growth factor (FGF), platelet-derived growth factor (PDGF), TNF- α and placental growth factor (PLGF) (Al-Ostoot et al., 2021). Therefore, inhibiting angiogenesis is an effective way to hinder tumor development. Many bioactive peptides exert effective anti-angiogenic and anti-cancer effects mainly by blocking the interaction between growth factors and their receptors (Figure 2). For example, Zhang Z. et al. (2016) pointed out that melittin was capable of suppressing cathepsin S-induced angiogenesis by blocking of the VEGF-A/VEGFR-2/mitogen-activated protein kinase 1 (MEK1)/extracellular signal-regulated kinase 1/2 (Erk1/2) signaling pathway. Moreover, it has been proved that lactoferrin could reduce the growth of blood vessels in colon cancer cells and the mechanism was validated to be associated with the inhibition of angiogenesis related pathways, including VEGFR2, vascular endothelial growth factor A (VEGFA), PI3K, Akt, and Erk1/2 (Li et al., 2017). Another study indicated that the downregulation of FGFR1 was an indication of the novel anti-angiogenic activity of dermaseptins in rhabdomyosarcoma cells (Abdille et al., 2021).

4.2.4 Mediation of immunity

Malignant tumor cells recruit multiple cell types through generating cytokines and growth factors, such as endothelial cells, inflammatory immune cells, and fibroblasts (Liotta and Kohn, 2001). These different types of cells and extracellular matrix molecules constitute the tumor microenvironment (Devaud et al., 2013). Inflammatory reactions are involved in various biological processes (Medzhitov, 2008; Wang P. et al., 2022). In the tumor microenvironment, there is a delicate balance between anti-tumor immunity and tumor-derived proinflammatory activity, which limits the progress of anti-tumor immunity (Murugaiyan and Saha, 2013). Many peptides display cytotoxicity against tumor cells by activating the human immune system, thereby achieving the goal of curing cancer (Figure 2). Research has shown that both alloferon-1 and alloferon-2 could induce the cytotoxicity of natural killer cells in mammals, such as mice and humans. In a mouse tumor transplantation model, alloferon-1 monotherapy showed moderate tumor suppression comparable to low-dose chemotherapy (Chernysh et al., 2012). Another study indicated that lactoferrin could up-regulate the components of non-specific immunity against cancer, including interferon- γ (IFN- γ), caspase-1 and interleukin-18 (IL-18). When interacting with

danger associated molecules (DAMPs) derived from cancer cells, membrane components of innate immunity, such as pattern recognition receptor (PRR), trigger a response of inflammasomes, resulting in activation of caspase-1, which cleaves pro-IL18 and produces IL-18. IL-18 is a potent pro-inflammatory cytokine that acts as an IFN- γ -inducer factor in NK and T cells with effector cell lysis activity on cancer cells (Cui et al., 2014). Additionally, Tang et al. (2022) designed a tumor microenvironment (TME) responsive MnO₂-melittin nanoparticles (M-M NPs). The M-M NPs could activate cGAS-STING pathway and promote the maturation of antigen-presenting cells to initiate systemic anti-tumor immune response such as increasing the production of tumor-specific T cells and more pro-inflammatory cytokines and chemokines.

4.2.5 Regulation of other intracellular signaling pathways

A more possible mechanism of cancer cell growth inhibitory activity of AMPs is associated with modulating various cell regulatory/signaling pathways intracellularly (Figure 2). Janmaat and others have demonstrated that kahalalide F exerted cytotoxic activity on cancer cells by regulating ErbB3 and the downstream PI3K-Akt signaling pathway (Janmaat et al., 2005). Another study mentioned that melittin suppressed the PI3K/Akt/mTOR signaling pathway, leading to an inhibition of EGF-induced breast cancer cell migration and invasion (Jeong et al., 2014). A report of Uen et al. (2019) found that pardaxin exhibited anti-cancer activity to leukemic cells via regulating toll-like receptor (TLR2)/MyD88 signaling pathway. Specifically, pardaxin induced leukemia cells to differentiate into macrophages like cells with immunostimulatory functions, including phagocytic ability and production of superoxide anions, by activating MyD88 protein. Furthermore, cecropin A has been shown to down-regulate MEK/ERK phosphorylation. The MAPK/ERK signaling pathway is responsible for the regulation of cell division, cell cycle or transcription regulation in cancer cells (Zhai et al., 2019). A recent study in 2022 confirmed that melittin could inhibit the growth of osteosarcoma 143B cells, which was associated with the suppression of Wnt/ β -catenin signaling pathway activity and cause apoptosis through up-regulating the ratio of Bax/Bcl-2 (Xie et al., 2022).

5 Clinical applications of ACPs

Although significant progress has been made in the treatment and prevention of various cancers, one of the main issues with cancer therapies is heavy side effects. In contrast, the ACP agents exhibit cytotoxicity against cancer cells at low concentrations without toxicity to normal tissues and therefore provide new strategies for cancer treatment. In addition, the peptides also have characteristics such as small size, simple synthesis, ability to enter the cell layer, high specificity and affinity, and lower immunogenicity than chemotherapy drugs (Eghtedari et al., 2021). At last, another advantage of using peptides as therapy is that they do not accumulate in the kidney or liver, which greatly limits their toxic reactions (Marqus et al., 2017).

Several peptide anti-tumor drugs have been completed or are currently undergoing clinical trials. For instance, balixafortide is

based on polyphemusin, a natural peptide from the crab. The completed results of phase I and II trials have shown that the combination of balixafortide and ibuprofen enhanced the anti-tumor effect of HER2 negative metastatic breast cancer patients and improved tolerance compared to ibuprofen alone, without producing dose limiting toxicities (Pernas et al., 2018). The blockade of the C-X-C chemokine receptor type 4 (CXCR4) pathway by balixafortide played a crucial role in inhibiting metastasis and diffusion, making tumor cells sensitive to chemotherapy, and activating the immune system in the TME. Therefore, balixafortide may show great potential for its forthcoming phase III trial (NCT03786094). LL-37 is the most studied human ACP and the completed clinical trial (NCT02225366) in 2021 evaluated the appropriate dose of LL-37 for intratumoral administration in melanoma patients (Jafari et al., 2022). Another ACP called LTX-315, a lactoferrin-derived lytic peptide, is currently undergoing a phase I multicenter study (NCT01058616) to evaluate its therapeutic efficacy against various types of transdermal accessible tumors.

In the past few decades, the USFDA has approved several ACP drugs. For example, gonadotropin-releasing hormone (GnRH) analog leuprolide acetate (Lupron®) was used to treat prostate cancer in 1990. It possessed immunomodulatory effects including reduction of the production of TNF- α , IL-1 β and other inflammatory cytokines to exert anti-cancer function (Guzmán-Soto et al., 2016). Adcetris® is an ADC drug developed based on dolastatin 10 for the treatment of lymphoma, which was launched in 2011 and successfully overcame obstacles in the clinical application of dolastatin 10 as a single drug. Before Adcetris® was developed, dolastatin 10 failed in phase II clinical trial owing to adverse reactions such as hematological and vascular toxicities (von Mehren et al., 2004). Subsequently, researchers used ADC technology to couple monoclonal antibodies with dolastatin 10 derivatives and utilized the specificity of antibodies to transport drugs to target tissues for their anti-cancer functions. At last, Adcetris® effectively reduced the systemic toxicity and side effects.

6 Conclusion

Terrestrial and marine animals contain abundant bioactive peptides that have been successfully developed and have achieved good therapeutic effects, such as antioxidant, antibacterial, anticancer, immune regulation, etc. In this review, we summarized the main animal-origin ACPs according to the animal's evolution order and their anti-tumor mechanisms that have been reported in the past decades. Comprehensively, ACPs exert anti-cancer activity

through membrane disruptive and non-membrane disruptive mechanisms including mediation of the necrosis or apoptosis of cancer cells, inhibition of angiogenesis, recruitment of immune cells and activation of certain regulatory functional proteins. Then we reviewed the clinical applications of ACPs. Encouragingly, an increasing number of peptide anti-tumor drugs have been approved for commercialization by the USFDA or undergoing clinical trials. In all, we expect that, with the accumulation of ACPs conducted in clinical trials in the future, ACPs could become one of the novel choices for the clinical treatment of cancers.

Author contributions

BQ: Conceptualization, Writing – original draft. JY: Conceptualization, Writing – original draft. XL: Methodology, Writing – original draft. SZ: Supervision, Visualization, Writing – review and editing. XM: Writing – review and editing. LL: Project administration, Writing – review and editing.

Funding

The author(s) declare financial support was received for the research, authorship, and/or publication of this article. This work was supported by Shandong Province Medical and Health Technology Development Plan Project (202203100062) and Qingdao Medical and Health Research Guidance Project (2022-WJZD100).

Conflict of interest

The authors declare that the research was conducted in the absence of any commercial or financial relationships that could be construed as a potential conflict of interest.

Publisher's note

All claims expressed in this article are solely those of the authors and do not necessarily represent those of their affiliated organizations, or those of the publisher, the editors and the reviewers. Any product that may be evaluated in this article, or claim that may be made by its manufacturer, is not guaranteed or endorsed by the publisher.

References

- Abdille, A. A., Kimani, J., Wamunyokoli, F., Bulimo, W., Gavamukulya, Y., and Maina, E. N. (2021). Dermaseptin B2's anti-proliferative activity and down regulation of anti-proliferative, angiogenic and metastatic genes in rhabdomyosarcoma RD cells *in vitro*. *Adv. Biosci. Biotechnol.* 12, 337–359. doi: 10.4236/abb.2021.1210022
- Alhakamy, N. A., Ahmed, O. A. A., Md, S., and Fahmy, U. A. (2021). Mastoparan, a peptide toxin from wasp venom conjugated fluvastatin nanocomplex for suppression of lung cancer cell growth. *Polymers (Basel)* 13:4225. doi: 10.3390/polym13234225
- Al-Ostoot, F. H., Salah, S., Khamees, H. A., and Khanum, S. A. (2021). Tumor angiogenesis: current challenges and therapeutic opportunities. *Cancer Treat. Res. Commun.* 28:100422. doi: 10.1016/j.ctarc.2021.100422
- Anju, A., Smitha, C. K., Preetha, K., Boobal, R., and Rosamma, P. (2019). Molecular characterization, recombinant expression and bioactivity profile of an antimicrobial peptide, Ss-arasin from the Indian mud crab, *Scylla serrata*. *Fish Shellfish Immunol.* 88, 352–358. doi: 10.1016/j.fsi.2019.03.007

- Asasira, J., Lee, S., Tran, T. X. M., Mpamani, C., Wabinga, H., Jung, S. Y., et al. (2022). Infection-related and lifestyle-related cancer burden in Kampala, Uganda: projection of the future cancer incidence up to 2030. *BMJ Open* 12:e056722. doi: 10.1136/bmjopen-2021-056722
- Bai, R., Pettit, G. R., and Hamel, E. (1990). Dolastatin 10, a powerful cytostatic peptide derived from a marine animal. inhibition of tubulin polymerization mediated through the vinca alkaloid binding domain. *Biochem. Pharmacol.* 39, 1941–1949. doi: 10.1016/0006-2952(90)90613-p
- Bhutia, S. K., and Maiti, T. K. (2008). Targeting tumors with peptides from natural sources. *Trends Biotechnol.* 26, 210–217. doi: 10.1016/j.tibtech.2008.01.002
- Ceremuga, M., Stela, M., Janik, E., Gorniak, L., Synowiec, E., Sliwinski, T., et al. (2020). Melittin-A natural peptide from bee venom which induces apoptosis in human leukaemia cells. *Biomolecules* 10:247. doi: 10.3390/biom10020247
- Chakniramol, S., Wierschem, A., Cho, M. G., and Bashir, K. M. I. (2022). Physiological and clinical aspects of bioactive peptides from marine animals. *Antioxidants (Basel)* 11:1021. doi: 10.3390/antiox11051021
- Chen, J., Xu, X. M., Underhill, C. B., Yang, S., Wang, L., Chen, Y., et al. (2005). Tachyplesin activates the classic complement pathway to kill tumor cells. *Cancer Res.* 65, 4614–4622. doi: 10.1158/0008-5472.CAN-04-2253
- Chen, Y. P., Shih, P. C., Feng, C. W., Wu, C. C., Tsui, K. H., Lin, Y. H., et al. (2021). Pardaxin activates excessive mitophagy and mitochondria-mediated apoptosis in human ovarian cancer by inducing reactive oxygen species. *Antioxidants (Basel)* 10:1883. doi: 10.3390/antiox10121883
- Chernysh, S., Irina, K., and Irina, A. (2012). Anti-tumor activity of immunomodulatory peptide alloferon-1 in mouse tumor transplantation model. *Int. Immunopharmacol.* 12, 312–314. doi: 10.1016/j.intimp.2011.10.016
- Chiangjong, W., Chutipongtanate, S., and Hongeng, S. (2020). Anticancer peptide: physicochemical property, functional aspect and trend in clinical application (Review). *Int. J. Oncol.* 57, 678–696. doi: 10.3892/ijo.2020.5099
- Conlon, J. M., Mechkaraska, M., Lukic, M. L., and Flatt, P. R. (2014). Potential therapeutic applications of multifunctional host-defense peptides from frog skin as anti-cancer, anti-viral, immunomodulatory, and anti-diabetic agents. *Peptides* 57, 67–77. doi: 10.1016/j.peptides.2014.04.019
- Conlon, J. M., Mechkaraska, M., Prajeep, M., Arafat, K., Zaric, M., Lukic, M. L., et al. (2013). Transformation of the naturally occurring frog skin peptide, alyteserin-2a into a potent, non-toxic anti-cancer agent. *Amino Acids* 44, 715–723. doi: 10.1007/s00726-012-1395-7
- Costa, F., Carvalho, I. F., Montelaro, R. C., Gomes, P., and Martins, M. C. (2011). Covalent immobilization of antimicrobial peptides (AMPs) onto biomaterial surfaces. *Acta Biomater.* 7, 1431–1440. doi: 10.1016/j.actbio.2010.11.005
- Cui, J., Chen, Y., Wang, H. Y., and Wang, R. F. (2014). Mechanisms and pathways of innate immune activation and regulation in health and cancer. *Hum. Vaccin. Immunother.* 10, 3270–3285. doi: 10.4161/21645515.2014.979640
- Daniluk, K., Kutwin, M., Grodzik, M., Wierzbicki, M., Strojny, B., Szczepaniak, J., et al. (2019). Use of selected carbon nanoparticles as melittin carriers for MCF-7 and MDA-MB-231 human breast cancer cells. *Materials (Basel)* 13:90. doi: 10.3390/ma13010090
- Dave, K. R., Bhattacharya, S. K., Isabel, S. R., Anthony, D., Cameron, D., Lin, H. W., et al. (2011). Activation of protein kinase C delta following cerebral ischemia leads to release of cytochrome C from the mitochondria via bad pathway. *PLoS One* 6:e22057. doi: 10.1371/journal.pone.0022057
- De Palma, M., Bizziato, D., and Petrova, T. V. (2017). Microenvironmental regulation of tumour angiogenesis. *Nat. Rev. Cancer* 17, 457–474. doi: 10.1038/nrc.2017.51
- Dennison, S. R., Harris, F., and Phoenix, D. A. (2007). The interactions of aurein 1.2 with cancer cell membranes. *Biophys. Chem.* 127, 78–83. doi: 10.1016/j.bpc.2006.12.009
- Deo, S. V. S., Sharma, J., and Kumar, S. (2022). GLOBOCAN 2020 report on global cancer burden: challenges and opportunities for surgical oncologists. *Ann. Surg. Oncol.* 29, 6497–6500. doi: 10.1245/s10434-022-12151-6
- Devaud, C., John, L. B., Westwood, J. A., Darcy, P. K., and Kershaw, M. H. (2013). Immune modulation of the tumor microenvironment for enhancing cancer immunotherapy. *Oncoimmunology* 2:e25961. doi: 10.4161/onci.25961
- Dias Rde, O., and Franco, O. L. (2015). Cysteine-stabilized alphabeta defensins: from a common fold to antibacterial activity. *Peptides* 72, 64–72. doi: 10.1016/j.peptides.2015.04.017
- Dong, Z., Hu, H., Yu, X., Tan, L., Ma, C., Xi, X., et al. (2020). Novel frog skin-derived peptide dermaseptin-PP for lung cancer treatment: *in vitro/vivo* evaluation and anti-tumor mechanisms study. *Front. Chem.* 8:476. doi: 10.3389/fchem.2020.00476
- Dos Santos, C., Hamadat, S., Le Saux, K., Newton, C., Mazouni, M., Zargarian, L., et al. (2017). Studies of the antitumor mechanism of action of dermaseptin B2, a multifunctional cationic antimicrobial peptide, reveal a partial implication of cell surface glycosaminoglycans. *PLoS One* 12:e0182926. doi: 10.1371/journal.pone.0182926
- Du, Q., Hou, X., Wang, L., Zhang, Y., Xi, X., Wang, H., et al. (2015). AaeAP1 and AaeAP2: novel antimicrobial peptides from the venom of the scorpion, *Androctonus aeneas*: structural characterisation, molecular cloning of biosynthetic precursor-encoding cDNAs and engineering of analogues with enhanced antimicrobial and anticancer activities. *Toxins (Basel)* 7, 219–237. doi: 10.3390/toxins7020219
- Duffy, C., Sorolla, A., Wang, E., Golden, E., Woodward, E., Davern, K., et al. (2020). Honeybee venom and melittin suppress growth factor receptor activation in HER2-enriched and triple-negative breast cancer. *NPJ Precis. Oncol.* 4:24. doi: 10.1038/s41698-020-00129-0
- Eghtedari, M., Jafari Porzani, S., and Nowruzi, B. (2021). Anticancer potential of natural peptides from terrestrial and marine environments: a review. *Phytochem. Lett.* 42, 87–103. doi: 10.1016/j.phytol.2021.02.008
- Emelianova, A. A., Kuzmin, D. V., Pantelev, P. V., Sorokin, M., Buzdin, A. A., and Ovchinnikova, T. V. (2018). Anticancer activity of the goat antimicrobial peptide ChMAP-28. *Front. Pharmacol.* 9:1501. doi: 10.3389/fphar.2018.01501
- Erdem Büyükkiraz, M., and Kesmen, Z. (2022). Antimicrobial peptides (AMPs): a promising class of antimicrobial compounds. *J. Appl. Microbiol.* 132, 1573–1596. doi: 10.1111/jam.15314
- Fang, Z., Meng, Q., Xu, J., Wang, W., Zhang, B., Liu, J., et al. (2023). Signaling pathways in cancer-associated fibroblasts: recent advances and future perspectives. *Cancer Commun. (Lond.)* 43, 3–41. doi: 10.1002/cac2.12392
- Ferlay, J., Ervik, M., Lam, F., Colombet, M., Mery, L., Piñeros, M., et al. (2020). *Global cancer observatory: cancer today*. Lyon: International Agency for Research on Cancer.
- Fuentes-Antrás, J., Genta, S., Vijenthira, A., and Siu, L. L. (2023). Antibody-drug conjugates: in search of partners of choice. *Trends Cancer* 9, 339–354. doi: 10.1016/j.trecan.2023.01.003
- Gao, G., Wang, Y., Hua, H., Li, D., and Tang, C. (2021). Marine antitumor peptide dolastatin 10: biological activity, structural modification and synthetic chemistry. *Mar. Drugs* 19:363. doi: 10.3390/md19070363
- Ghaly, G., Tallima, H., Dabbish, E., Badr ElDin, N., Abd El-Rahman, M. K., Ibrahim, M. A. A., et al. (2023). Anti-cancer peptides: status and future prospects. *Molecules* 28:1148. doi: 10.3390/molecules28031148
- Guha, P., Kaptan, E., Bandyopadhyaya, G., Kaczanowska, S., Davila, E., Thompson, K., et al. (2013). Cod glycopeptide with picomolar affinity to galectin-3 suppresses T-cell apoptosis and prostate cancer metastasis. *Proc. Natl. Acad. Sci. U.S.A.* 110, 5052–5057. doi: 10.1073/pnas.1202653110
- Guo, R., Liu, J., Chai, J., Gao, Y., Abdel-Rahman, M. A., and Xu, X. (2022). Scorpion peptide Smp24 exhibits a potent antitumor effect on human lung cancer cells by damaging the membrane and cytoskeleton *in vivo* and *in vitro*. *Toxins (Basel)* 14:438. doi: 10.3390/toxins14070438
- Guzmán-Soto, I., Salinas, E., and Quintanar, J. L. (2016). Leuprolide acetate inhibits spinal cord inflammatory response in experimental autoimmune encephalomyelitis by suppressing NF- κ B activation. *Neuroimmunomodulation* 23, 33–40. doi: 10.1159/000438927
- Haider, T., and Soni, V. (2022). Response surface methodology and artificial neural network-based modeling and optimization of phosphatidylserine targeted nanocarriers for effective treatment of cancer: *in vitro* and *in silico* studies. *J. Drug Deliv. Sci. Technol.* 75:103663. doi: 10.1016/j.jddst.2022.103663
- Han, H. H., Teng, D., Mao, R. Y., Hao, Y., Yang, N., Wang, Z. L., et al. (2021). Marine peptide-N6NH₂ and its derivative-GUON6NH₂ have potent antimicrobial activity against intracellular *Edwardsiella tarda* *in vitro* and *in vivo*. *Front. Microbiol.* 12:637427. doi: 10.3389/fmicb.2021.637427
- Han, Y., Cui, Z., Li, Y. H., Hsu, W. H., and Lee, B. H. (2015). *In vitro* and *in vivo* anticancer activity of pardaxin against proliferation and growth of oral squamous cell carcinoma. *Mar. Drugs* 14:2. doi: 10.3390/md14010002
- Hansen, I. K. O., Isaksson, J., Poth, A. G., Hansen, K. O., Andersen, A. J. C., Richard, C. S. M., et al. (2020). Isolation and characterization of antimicrobial peptides with unusual disulfide connectivity from the colonial ascidian *Syncoicum turgens*. *Mar. Drugs* 18:51. doi: 10.3390/md18010051
- Harris, F., Dennison, S. R., Singh, J., and Phoenix, D. A. (2013). On the selectivity and efficacy of defense peptides with respect to cancer cells. *Med. Res. Rev.* 33, 190–234. doi: 10.1002/med.20252
- Hassanvand Jamadi, R., Yaghoubi, H., and Sadeghizadeh, M. (2017). Brevinin-2R and derivatives as potential anticancer peptides: synthesis, purification, characterization and biological activities. *Int. J. Peptide Res. Ther.* 25, 151–160. doi: 10.1007/s10989-017-9656-7
- Hilchie, A. L., Conrad, D. M., Coombs, M. R., Zemlak, T., Doucette, C. D., Liwski, R. S., et al. (2013). Pleurocidin-family cationic antimicrobial peptides mediate lysis of multiple myeloma cells and impair the growth of multiple myeloma xenografts. *Leuk. Lymphoma* 54, 2255–2262. doi: 10.3109/10428194.2013.770847
- Hilchie, A. L., Doucette, C. D., Pinto, D. M., Patrzykat, A., Douglas, S., and Hoskin, D. W. (2011). Pleurocidin-family cationic antimicrobial peptides are cytolytic for breast carcinoma cells and prevent growth of tumor xenografts. *Breast Cancer Res.* 13:R102. doi: 10.1186/bcr3043
- Hou, D., Hu, F., Mao, Y., Yan, L., Zhang, Y., Zheng, Z., et al. (2022). Cationic antimicrobial peptide NRC-03 induces oral squamous cell carcinoma cell apoptosis

- via CypD-mPTP axis-mediated mitochondrial oxidative stress. *Redox Biol.* 54:102355. doi: 10.1016/j.redox.2022.102355
- Hsu, J. C., Lin, L. C., Tzen, J. T., and Chen, J. Y. (2011). Characteristics of the antitumor activities in tumor cells and modulation of the inflammatory response in RAW264.7 cells of a novel antimicrobial peptide, chrysopsin-1, from the red sea bream (*Chrysophrys major*). *Peptides* 32, 900–910. doi: 10.1016/j.peptides.2011.02.013
- Huan, Y., Kong, Q., Mou, H., and Yi, H. (2020). Antimicrobial peptides: classification, design, application and research progress in multiple fields. *Front. Microbiol.* 11:582779. doi: 10.3389/fmicb.2020.582779
- Huang, T. C., and Chen, J. Y. (2013). Proteomic analysis reveals that pardaxin triggers apoptotic signaling pathways in human cervical carcinoma HeLa cells: cross talk among the UPR, c-Jun and ROS. *Carcinogenesis* 34, 1833–1842.
- Ibrahim, S. R., Min, C. C., Teuscher, F., Ebel, R., Kakoschke, C., Lin, W., et al. (2010). Callaerins A-F and H, new cytotoxic cyclic peptides from the Indonesian marine sponge *Callispongia aerizusa*. *Bioorg. Med. Chem.* 18, 4947–4956. doi: 10.1016/j.bmc.2010.06.012
- Jafari, A., Babajani, A., Sarraimi Forooshani, R., Yazdani, M., and Rezaei-Tavirani, M. (2022). Clinical applications and anticancer effects of antimicrobial peptides: from bench to bedside. *Front. Oncol.* 12:819563. doi: 10.3389/fonc.2022.819563
- Janmaat, M. L., Rodriguez, J. A., Jimeno, J., Kruij, F. A., and Giaccone, G. (2005). Kahalalide F induces necrosis-like cell death that involves depletion of ErbB3 and inhibition of Akt signaling. *Mol. Pharmacol.* 68, 502–510. doi: 10.1124/mol.105.011361
- Jeong, Y. J., Choi, Y., Shin, J. M., Cho, H. J., Kang, J. H., Park, K. K., et al. (2014). Melittin suppresses EGF-induced cell motility and invasion by inhibiting PI3K/Akt/mTOR signaling pathway in breast cancer cells. *Food Chem. Toxicol.* 68, 218–225. doi: 10.1016/j.fct.2014.03.022
- Johansson, J., Gudmundsson, G. H., Rottenberg, M. E., Berndt, K. D., and Agerberth, B. (1998). Conformation-dependent antibacterial activity of the naturally occurring human peptide LL-37. *J. Biol. Chem.* 273, 3718–3724. doi: 10.1074/jbc.273.6.3718
- Ju, X., Fan, D., Kong, L., Yang, Q., Zhu, Y., Zhang, S., et al. (2021). Antimicrobial peptide brevinin-1RL1 from frog skin secretion induces apoptosis and necrosis of tumor cells. *Molecules* 26:2059. doi: 10.3390/molecules26072059
- Kang, H. K., Choi, M. C., Seo, C. H., and Park, Y. (2018). Therapeutic properties and biological benefits of marine-derived anticancer peptides. *Int. J. Mol. Sci.* 19:919. doi: 10.3390/ijms19030919
- Karami Fath, M., Babakhaniyan, K., Zokaie, M., Yaghoubian, A., Akbari, S., Khorsandi, M., et al. (2022). Anti-cancer peptide-based therapeutic strategies in solid tumors. *Cell. Mol. Biol. Lett.* 27:33. doi: 10.1186/s11658-022-00332-w
- Kashiwada, A., Mizuno, M., and Hashimoto, J. (2016). pH-dependent membrane lysis by using melittin-inspired designed peptides. *Org. Biomol. Chem.* 14, 6281–6288. doi: 10.1039/c6ob01002d
- Kim, I. W., Lee, J. H., Kwon, Y. N., Yun, E. Y., Nam, S. H., Ahn, M. Y., et al. (2013). Anticancer activity of a synthetic peptide derived from harmoniasin, an antibacterial peptide from the ladybug *Harmonia axyridis*. *Int. J. Oncol.* 43, 622–628. doi: 10.3892/ijo.2013.1973
- Kuo, H. M., Tseng, C. C., Chen, N. F., Tai, M. H., Hung, H. C., Feng, C. W., et al. (2018). MSP-4, an antimicrobial peptide, induces apoptosis via activation of extrinsic Fas/FasL- and intrinsic mitochondria-mediated pathways in one osteosarcoma cell line. *Mar. Drugs* 16:8. doi: 10.3390/md16010008
- Lath, A., Santal, A. R., Kaur, N., Kumari, P., and Singh, N. P. (2023). Anti-cancer peptides: their current trends in the development of peptide-based therapy and anti-tumor drugs. *Biotechnol. Genet. Eng. Rev.* 39, 45–84. doi: 10.1080/02648725.2022.2082157
- Lee, J. H., Kim, I. W., Kim, S. H., Kim, M. A., Yun, E. Y., Nam, S. H., et al. (2015). Anticancer activity of the antimicrobial peptide scolopendrasin VII derived from the centipede, *Scolopendra subspinipes mutilans*. *J. Microbiol. Biotechnol.* 25, 1275–1280. doi: 10.4014/jmb.1503.03091
- Lewies, A., Wentzel, J. F., Jacobs, G., and Du Plessis, L. H. (2015). The potential use of natural and structural analogues of antimicrobial peptides in the fight against neglected tropical diseases. *Molecules* 20, 15392–15433. doi: 10.3390/molecules200815392
- Li, H. Y., Li, M., Luo, C. C., Wang, J. Q., and Zheng, N. (2017). Lactoferrin exerts antitumor effects by inhibiting angiogenesis in a HT29 human colon tumor model. *J. Agric. Food Chem.* 65, 10464–10472. doi: 10.1021/acs.jafc.7b03390
- Li, M. S. C., Mok, K. K. S., and Mok, T. S. K. (2023). Developments in targeted therapy & immunotherapy-how non-small cell lung cancer management will change in the next decade: a narrative review. *Ann. Transl. Med.* 11:358. doi: 10.21037/atm-22-4444
- Li, Q. F., Ou-Yang, G. L., Peng, X. X., and Hong, S. G. (2003). Effects of tachyplesin on the regulation of cell cycle in human hepatocarcinoma SMMC-7721 cells. *World J. Gastroenterol.* 9, 454–458. doi: 10.3748/wjg.v9.i3.454
- Li, S., Wang, Y., Xue, Z., Jia, Y., Li, R., He, C., et al. (2021). The structure-mechanism relationship and mode of actions of antimicrobial peptides: a review. *Trends Food Sci. Technol.* 109, 103–115. doi: 10.1016/j.tifs.2021.01.005
- Liang, Y., Zhang, X., Yuan, Y., Bao, Y., and Xiong, M. (2020). Role and modulation of the secondary structure of antimicrobial peptides to improve selectivity. *Biomater. Sci.* 8, 6858–6866. doi: 10.1039/d0bm00801j
- Lin, H. J., Huang, T. C., Muthusamy, S., Lee, J. F., Duann, Y. F., and Lin, C. H. (2012). Piscidin-1, an antimicrobial peptide from fish (hybrid striped bass *morone saxatilis* x *M. chrysops*), induces apoptotic and necrotic activity in HT1080 cells. *Zoolog. Sci.* 29, 327–332. doi: 10.2108/zsj.29.327
- Lin, M. C., Hui, C. F., Chen, J. Y., and Wu, J. L. (2013). Truncated antimicrobial peptides from marine organisms retain anticancer activity and antibacterial activity against multidrug-resistant *Staphylococcus aureus*. *Peptides* 44, 139–148. doi: 10.1016/j.peptides.2013.04.004
- Lin, M. C., Lin, S. B., Chen, J. C., Hui, C. F., and Chen, J. Y. (2010). Shrimp anti-lipopolysaccharide factor peptide enhances the antitumor activity of cisplatin in vitro and inhibits HeLa cells growth in nude mice. *Peptides* 31, 1019–1025. doi: 10.1016/j.peptides.2010.02.023
- Liotta, L. A., and Kohn, E. C. (2001). The microenvironment of the tumour-host interface. *Nature* 411, 375–379. doi: 10.1038/35077241
- Luan, X., Wu, Y., Shen, Y., Zhang, H., Zhou, Y., Chen, H., et al. (2021). Cytotoxic and antitumor peptides as novel chemotherapeutics. *Nat. Prod. Rep.* 38, 7–17. doi: 10.1039/D0NP00019A
- Luo, Y., and Song, Y. (2021). Mechanism of antimicrobial peptides: antimicrobial, anti-inflammatory and antibiofilm activities. *Int. J. Mol. Sci.* 22:11401. doi: 10.3390/ijms222111401
- Luong, H. X., Thanh, T. T., and Tran, T. H. (2020). Antimicrobial peptides-Advances in development of therapeutic applications. *Life Sci.* 260:118407. doi: 10.1016/j.lfs.2020
- Lyu, C., Fang, F., and Li, B. (2019). Anti-tumor effects of melittin and its potential applications in clinic. *Curr. Protein Pept. Sci.* 20, 240–250. doi: 10.2174/1389203719666180612084615
- Ma, X. X., Yang, N., Mao, R. Y., Hao, Y., Yan, X., Teng, D., et al. (2021). The pharmacodynamics study of insect defensin DLP4 against toxigenic *Staphylococcus hyicus* ACCC 61734 in vitro and vivo. *Front. Cell. Infect. Microbiol.* 11:638598. doi: 10.3389/fcimb.2021.638598
- Macedo, M. W. F. S., Cunha, N. B. d., Carneiro, J. A., Costa, R. A. d., Alencar, S. A. d., Cardoso, M. H., et al. (2021). Marine organisms as a rich source of biologically active peptides. *Front. Mar. Sci.* 8:667764. doi: 10.3389/fmars.2021.667764
- Mader, J. S., Mookherjee, N., Hancock, R. E., and Bleackley, R. C. (2009). The human host defense peptide LL-37 induces apoptosis in a calpain- and apoptosis-inducing factor-dependent manner involving Bax activity. *Mol. Cancer Res.* 7, 689–702. doi: 10.1158/1541-7786.MCR-08-0274
- Mahlapuu, M., Hakansson, J., Ringstad, L., and Bjorn, C. (2016). Antimicrobial peptides: an emerging category of therapeutic agents. *Front. Cell. Infect. Microbiol.* 6:194. doi: 10.3389/fcimb.2016.00194
- Mahmoud, M. M., Alenezi, M., Al-Hejin, A. M., Abujamel, T. S., Aljoud, F., Noorwali, A., et al. (2022). Anticancer activity of chicken cathelicidin peptides against different types of cancer. *Mol. Biol. Rep.* 49, 4321–4339. doi: 10.1007/s11033-022-07267-7
- Maijaroen, S., Jangpromma, N., Daduang, J., and Klaynongsruang, S. (2018). KT2 and RT2 modified antimicrobial peptides derived from *Crocodylus siamensis* Leucrocin I show activity against human colon cancer HCT-116 cells. *Environ. Toxicol. Pharmacol.* 62, 164–176. doi: 10.1016/j.etap.2018.07.007
- Maiti, R., Patel, B., Patel, N., Patel, A., and Dhanesha, N. (2023). Antibody drug conjugates as targeted cancer therapy: past development, present challenges and future opportunities. *Arch. Pharm. Res.* 46, 361–388. doi: 10.1007/s12272-023-01447-0
- Marggraf, M. B., Pantelev, P. V., Emelianova, A. A., Sorokin, M. I., Bolosov, I. A., Buzdin, A. A., et al. (2018). Cytotoxic potential of the novel horseshoe crab peptide polyphemusin III. *Mar. Drugs* 16:466. doi: 10.3390/md16120466
- Marme, D. (2018). Tumor angiogenesis: a key target for cancer therapy. *Oncol. Res. Treat.* 41:164. doi: 10.1159/000488340
- Maroti, G., Kereszt, A., Kondorosi, E., and Mergaert, P. (2011). Natural roles of antimicrobial peptides in microbes, plants and animals. *Res. Microbiol.* 162, 363–374. doi: 10.1016/j.resmic.2011.02.005
- Marques, S., Pirogova, E., and Piva, T. J. (2017). Evaluation of the use of therapeutic peptides for cancer treatment. *J. Biomed. Sci.* 24:21. doi: 10.1186/s12929-017-0328-x
- Medzhitov, R. (2008). Origin and physiological roles of inflammation. *Nature* 454, 428–435. doi: 10.1038/nature07201
- Meng, M. X., Ning, J. F., Yu, J. Y., Chen, D. D., Meng, X. L., Xu, J. P., et al. (2014). Antitumor activity of recombinant antimicrobial peptide penaeidin-2 against kidney cancer cells. *J. Huazhong Univ. Sci. Technol. Med. Sci.* 34, 529–534. doi: 10.1007/s11596-014-1310-4
- Mirzaei, S., Fekri, H. S., Hashemi, F., Hushmandi, K., Mohammadinejad, R., Ashrafzadeh, M., et al. (2021). Venom peptides in cancer therapy: an updated review on cellular and molecular aspects. *Pharmacol. Res.* 164:105327. doi: 10.1016/j.phrs.2020.105327

- Mulder, K. C., Lima, L. A., Miranda, V. J., Dias, S. C., and Franco, O. L. (2013). Current scenario of peptide-based drugs: the key roles of cationic antitumor and antiviral peptides. *Front. Microbiol.* 4:321. doi: 10.3389/fmicb.2013.00321
- Murugaiyan, G., and Saha, B. (2013). IL-27 in tumor immunity and immunotherapy. *Trends Mol. Med.* 19, 108–116. doi: 10.1016/j.molmed.2012.12.002
- Norouzi, P., Mirmohammadi, M., and Houshdar Tehrani, M. H. (2022). Anticancer peptides mechanisms, simple and complex. *Chem. Biol. Interact.* 368:110194. doi: 10.1016/j.cbi.2022.110194
- Oelkrug, C., Hartke, M., and Schubert, A. (2015). Mode of action of anticancer peptides (ACPs) from amphibian origin. *Anticancer Res.* 35, 635–643.
- Okumura, K., Itoh, A., Isogai, E., Hirose, K., Hosokawa, Y., Abiko, Y., et al. (2004). C-terminal domain of human CAP18 antimicrobial peptide induces apoptosis in oral squamous cell carcinoma SAS-H1 cells. *Cancer Lett.* 212, 185–194. doi: 10.1016/j.canlet.2004.04.006
- Okunaka, M., Kano, D., Matsui, R., Kawasaki, T., and Uesawa, Y. (2021). Comprehensive analysis of chemotherapeutic agents that induce infectious neutropenia. *Pharmaceuticals* 14:681. doi: 10.3390/ph14070681
- Padanilam, B. J. (2003). Cell death induced by acute renal injury: a perspective on the contributions of apoptosis and necrosis. *Am. J. Physiol. Renal Physiol.* 284, F608–F627. doi: 10.1152/ajprenal.00284.2002
- Pan, X., Xu, J., and Jia, X. (2020). Research progress evaluating the function and mechanism of anti-tumor peptides. *Cancer Manag. Res.* 12, 397–409. doi: 10.2147/cmar.S232708
- Papo, N., Seger, D., Makovitzki, A., Kalchenko, V., Eshhar, Z., Degani, H., et al. (2006). Inhibition of tumor growth and elimination of multiple metastases in human prostate and breast xenografts by systemic inoculation of a host defense-like lytic peptide. *Cancer Res.* 66, 5371–5378. doi: 10.1158/0008-5472.CAN-05-4569
- Paredes-Gamero, E. J., Martins, M. N., Cappabianco, F. A., Ide, J. S., and Miranda, A. (2012). Characterization of dual effects induced by antimicrobial peptides: regulated cell death or membrane disruption. *Biochim. Biophys. Acta* 1820, 1062–1072. doi: 10.1016/j.bbagen.2012.02.015
- Pernas, S., Martin, M., Kaufman, P. A., Gil-Martin, M., Gomez Pardo, P., and Lopez-Tarruella, S. (2018). Balixafortide plus eribulin in HER2-negative metastatic breast cancer: a phase 1, single-arm, dose-escalation trial. *Lancet Oncol.* 19, 812–824. doi: 10.1016/S1470-2045(18)30147-5
- Petrova, M., Vlahova, Z., Schröder, M., Todorova, J., Tzintzarov, A., and Gospodinov, A. (2023). Antitumor activity of bioactive compounds from *Rapana venosa* against human breast cell lines. *Pharmaceuticals (Basel)* 16:181. doi: 10.3390/ph16020181
- Pino-Angeles, A., Leveritt, J. M., and Lazaridis, T. (2016). Pore structure and synergy in antimicrobial peptides of the Magainin family. *PLoS Comput. Biol.* 12:e1004570. doi: 10.1371/journal.pcbi.1004570
- Qi, J., Wang, W., Lu, W., Chen, W., Sun, H., and Shang, A. (2020). Design and biological evaluation of dual novel BF-30 analogs for the treatment of malignant melanoma. *J. Cancer* 11, 7184–7195. doi: 10.7150/jca.47549
- Qin, B., Yuan, X., Jiang, M., Yin, H., Luo, Z., Zhang, J., et al. (2020). Targeting DNA to the endoplasmic reticulum efficiently enhances gene delivery and therapy. *Nanoscale* 12, 18249–18262. doi: 10.1039/d0nr03156a
- Qin, Y., Qin, Z. D., Chen, J., Cai, C. G., Li, L., Feng, L. Y., et al. (2019). From antimicrobial to anticancer peptides: the transformation of peptides. *Recent Pat. Anticancer Drug Discov.* 14, 70–84. doi: 10.2174/1574892814666190119165157
- Quah, Y., Tong, S. R., Bojarska, J., Giller, K., Tan, S. A., Ziara, Z. M., et al. (2023). Bioactive peptide discovery from edible insects for potential applications in human health and agriculture. *Molecules* 28:1233. doi: 10.3390/molecules28031233
- Rahman, R., Fonseka, A. D., Sua, S. C., Ahmad, M., Rajendran, R., Ambu, S., et al. (2021). Inhibition of breast cancer xenografts in a mouse model and the induction of apoptosis in multiple breast cancer cell lines by lactoferricin B peptide. *J. Cell. Mol. Med.* 25, 7181–7189. doi: 10.1111/jcmm.16748
- Ren, S. X., Shen, J., Cheng, A. S., Lu, L., Chan, R. L., Li, Z. J., et al. (2013). FK-16 derived from the anticancer peptide LL-37 induces caspase-independent apoptosis and autophagic cell death in colon cancer cells. *PLoS One* 8:e63641. doi: 10.1371/journal.pone.0063641
- Rozek, T., Wegener, K. L., Bowie, J. H., Olver, I. N., Carver, J. A., Wallace, J. C., et al. (2000). The antibiotic and anticancer active aurein peptides from the Australian Bell Frogs *Litoria aurea* and *Litoria raniformis* the solution structure of aurein 1.2. *Eur. J. Biochem.* 267, 5330–5341. doi: 10.1046/j.1432-1327.2000.01536.x
- Ryan, L., Lamarre, B., Diu, T., Ravi, J., Judge, P. J., Temple, A., et al. (2013). Anti-antimicrobial peptides: folding-mediated host defense antagonists. *J. Biol. Chem.* 288, 20162–20172. doi: 10.1074/jbc.M113.459560
- Schibli, D. J., Epand, R. F., Vogel, H. J., and Epand, R. M. (2002). Tryptophan-rich antimicrobial peptides: comparative properties and membrane interactions. *Biochem. Cell Biol.* 80, 667–677. doi: 10.1139/o02-147
- Schilero, C., and Firestein, B. L. (2021). Mechanisms of metabolic reprogramming in cancer cells supporting enhanced growth and proliferation. *Cells* 10:1056. doi: 10.3390/cells10051056
- Schweikart, K., Guo, L., Shuler, Z., Abrams, R., Chiao, E. T., Kolaja, K. L., et al. (2013). The effects of jaspamide on human cardiomyocyte function and cardiac ion channel activity. *Toxicol. In Vitro* 27, 745–751. doi: 10.1016/j.tiv.2012.12.005
- Shen, H., Xie, Y., Ye, S., He, K., Yi, L., and Cui, R. (2018). Spider peptide toxin lycosin-I induces apoptosis and inhibits migration of prostate cancer cells. *Exp. Biol. Med. (Maywood)* 243, 725–735. doi: 10.1177/1535370218772802
- Shimoyama, M., Kanda, T. L., Koyama, Y., Suda, T., Sakai, Y., Hatakeyama, K., et al. (2015). Expression of fas ligand is an early event in colorectal carcinogenesis. *J. Surg. Oncol.* 76, 63–68. doi: 10.1002/1096-9098(200101)76:1
- Smirnova, M. P., Kolodkin, N. I., Kolobov, A. A., Afonin, V. G., Afonina, I. V., Stefanenko, L. I., et al. (2020). Indolicidin analogs with broad-spectrum antimicrobial activity and low hemolytic activity. *Peptides* 132:170356. doi: 10.1016/j.peptides.2020.170356
- Soliman, C., Eastwood, S., Truong, V. K., Ramsland, P. A., and Elbourne, A. (2019). The membrane effects of melittin on gastric and colorectal cancer. *PLoS One* 14:e0224028. doi: 10.1371/journal.pone.0224028
- Somarelli, J. A., Gardner, H., Cannataro, V. L., Gunady, E. F., Boddy, A. M., Johnson, N. A., et al. (2020). Molecular biology and evolution of cancer: from discovery to action. *Mol. Biol. Evol.* 37, 320–326. doi: 10.1093/molbev/msz242
- Song, R., Wei, R., Luo, H., and Yang, Z. (2014). Isolation and identification of an antiproliferative peptide derived from heated products of peptic hydrolysates of half-fin anchovy (*Setipinna taty*). *J. Funct. Foods* 10, 104–111. doi: 10.1016/j.jff.2014.06.010
- Starzec, A., Vassy, R., Martin, A., Lecouvey, M., Di Benedetto, M., Crepin, M., et al. (2006). Antiangiogenic and antitumor activities of peptide inhibiting the vascular endothelial growth factor binding to neuropilin-1. *Life Sci.* 79, 2370–2381. doi: 10.1016/j.lfs.2006.08.005
- Steiner, H., Hultmark, D., Engström, Å., Bennich, H., and Boman, H. G. (1981). Sequence and specificity of two antibacterial proteins involved in insect immunity. *Nature* 292, 246–248. doi: 10.1038/292246a0
- Su, B. C., Pan, C. Y., and Chen, J. Y. (2019). Antimicrobial peptide TP4 induces ROS-mediated necrosis by triggering mitochondrial dysfunction in wild-type and mutant p53 glioblastoma cells. *Cancers (Basel)* 11:171. doi: 10.3390/cancers11020171
- Su, B. C., Wu, T. H., Hsu, C. H., and Chen, J. Y. (2020). Distribution of positively charged amino acid residues in antimicrobial peptide epinecidin-1 is crucial for in vitro glioblastoma cytotoxicity and its underlying mechanisms. *Chem. Biol. Interact.* 315:108904. doi: 10.1016/j.cbi.2019.108904
- Sung, H., Ferlay, J., Siegel, R. L., Laversanne, M., Soerjomataram, I., Jemal, A., et al. (2021). Global cancer statistics 2020: GLOBOCAN estimates of incidence and mortality worldwide for 36 cancers in 185 countries. *CA Cancer J. Clin.* 71, 209–249. doi: 10.3322/caac.21660
- Tang, S., Zhou, L., He, H., Cui, L., Ren, Z., and Tai, Y. (2022). MnO₂-melittin nanoparticles serve as an effective anti-tumor immunotherapy by enhancing systemic immune response. *Biomaterial* 288:121706. doi: 10.1016/j.biomaterials.2022.121706
- Taylor, S. W., Craig, A. G., Fischer, W. H., Park, M., and Lehrer, R. I. (2000). Styelin D, an extensively modified antimicrobial peptide from ascidian hemocytes. *J. Biol. Chem.* 275, 38417–38426. doi: 10.1074/jbc.M006762200
- Ting, C. H., and Chen, J. Y. (2018). Nile tilapia derived TP4 shows broad cytotoxicity toward to non-small-cell lung cancer cells. *Mar. Drugs* 16:506. doi: 10.3390/md16120506
- Tong, J. T. W., Harris, P. W. R., Brimble, M. A., and Kavianinia, I. (2021). An insight into FDA approved antibody-drug conjugates for cancer therapy. *Molecules* 26:5847. doi: 10.3390/molecules26195847
- Topalian, S. L., Taube, J. M., and Pardoll, D. M. (2020). Neoadjuvant checkpoint blockade for cancer immunotherapy. *Science* 367:eaax0182. doi: 10.1126/science.aax0182
- Tornesello, A. L., Borrelli, A., Buonaguro, L., Buonaguro, F. M., and Tornesello, M. L. (2020). Antimicrobial peptides as anticancer agents: functional properties and biological activities. *Molecules* 25:2850. doi: 10.3390/molecules25122850
- Torres, M. D. T., Andrade, G. P., Sato, R. H., Pedron, C. N., Manieri, T. M., Cerchiaro, G., et al. (2018). Natural and redesigned wasp venom peptides with selective antitumoral activity. *Beilstein J. Org. Chem.* 14, 1693–1703. doi: 10.3762/bjoc.14.144
- Troeira Henriques, S., Lawrence, N., Chaoasis, S., Ravipati, A. S., Cheneval, O., Benfield, A. H., et al. (2017). Redesign spider peptide with improved antimicrobial and anticancer properties. *ACS Chem. Biol.* 12, 2324–2334. doi: 10.1021/acscchembio.7b00459
- Uen, W. C., Choong, C. Y., Tai, C. J., and Tai, C. J. (2019). Pardaxin promoted differentiation and maturation of leukemic cells via regulating TLR2/MyD88 signal against cell proliferation. *Evid. Based Complement. Alternat. Med.* 2019:7035087. doi: 10.1155/2019/7035087
- Urrea, F. A., and Araya-Maturana, R. (2022). Putting the brakes on tumorigenesis with snake venom toxins: new molecular insights for cancer drug discovery. *Semin. Cancer Biol.* 80, 195–204. doi: 10.1016/j.semcancer.2020.05.006
- von Mehren, M., Balcerzak, S. P., Kraft, A. S., Edmonson, J. H., Okuno, S. H., Davey, M., et al. (2004). Phase II trial of dolastatin-10, a novel anti-tubulin agent, in metastatic soft tissue sarcomas. *Sarcoma* 8, 107–111. doi: 10.1080/13577140400009163

- Vorontsova, O. V., Egorova, N. S., Arseniev, A. S., and Feofanov, A. V. (2011). Haemolytic and cytotoxic action of laticin Ltc2a. *Biochimie* 93, 227–241. doi: 10.1016/j.biochi.2010.09.016
- Wang, A., Zheng, Y., Zhu, W., Yang, L., Yang, Y., and Peng, J. (2022). Melittin-based nano-delivery systems for cancer therapy. *Biomolecules* 12:118. doi: 10.3390/biom12010118
- Wang, G., Zietz, C. M., Mudgapalli, A., Wang, S., and Wang, Z. (2022). The evolution of the antimicrobial peptide database over 18 years: milestones and new features. *Protein Sci.* 31, 92–106. doi: 10.1002/pro.4185
- Wang, H., He, H., Chen, X., Zhou, M., Wei, M., Xi, X., et al. (2020). A novel antimicrobial peptide (Kassinatuerin-3) isolated from the skin secretion of the African frog, *Kassina senegalensis*. *Biology (Basel)* 9:148. doi: 10.3390/biology9070148
- Wang, H., Ke, M., Tian, Y., Wang, J., Li, B., Wang, Y., et al. (2013). BF-30 selectively inhibits melanoma cell proliferation via cytoplasmic membrane permeabilization and DNA-binding *in vitro* and in B16F10-bearing mice. *Eur. J. Pharmacol.* 707, 1–10. doi: 10.1016/j.ejphar.2013.03.028
- Wang, P., Zhang, X., Zheng, X., Gao, J., Shang, M., Xu, J., et al. (2022). Folic acid protects against hyperuricemia in C57BL/6J mice via ameliorating gut-kidney axis dysfunction. *J. Agric. Food Chem.* 70, 15787–15803. doi: 10.1021/acs.jafc.2c06297
- Wong, Y. H., Wong, S. R., and Lee, S. H. (2023). The therapeutic anticancer potential of marine-derived bioactive peptides: a highlight on pardaxin. *Int. J. Pept. Res. Ther.* 29:90. doi: 10.1007/s10989-023-10562-x
- Wu, S. P., Huang, T. C., Lin, C. C., Hui, C. F., Lin, C. H., and Chen, J. Y. (2012). Pardaxin, a fish antimicrobial peptide, exhibits antitumor activity toward murine fibrosarcoma *in vitro* and *in vivo*. *Mar. Drugs* 10, 1852–1872.
- Wu, W. K., Sung, J. J., To, K. F., Yu, L., Li, H. T., Li, Z. J., et al. (2010). The host defense peptide LL-37 activates the tumor-suppressing bone morphogenetic protein signaling via inhibition of proteasome in gastric cancer cells. *J. Cell. Physiol.* 223, 178–186. doi: 10.1002/jcp.22026
- Wyer, S., Townsend, D. M., Ye, Z., Kourtidis, A., Choo, Y. M., and de Barros, A. L. B. (2022). Recent advances and limitations in the application of kahalalides for the control of cancer. *Biomed. Pharmacother.* 148:112676. doi: 10.1016/j.biopha.2022
- Xie, X., Li, Y., Zhu, H., Chen, L., Chen, D., Lin, S., et al. (2022). Melittin inhibits growth of human osteosarcoma 143B cells through induction of apoptosis via suppressing the Wnt/ β -catenin signaling pathway. *Anticancer Agents Med. Chem.* 22, 3172–3181. doi: 10.2174/1871520622666220509121627
- Xu, T., Cui, T., Peng, L., Kong, S., Zou, J., and Tian, X. (2017). The anti-hepatocellular carcinoma activity of Mel-P15 is mediated by natural killer cells. *Oncol. Lett.* 14, 6901–6906. doi: 10.3892/ol.2017.7018
- Yan, W., Lu, J., Li, G., Wei, H., and Ren, W. H. (2018). Amidated Scolopin-2 inhibits proliferation and induces apoptosis of HeLa cells *in vitro* and *in vivo*. *Biotechnol. Appl. Biochem.* 65, 672–679. doi: 10.1002/bab.1661
- Yang, T., Li, J., Jia, Q., Zhan, S., Zhang, Q., Wang, Y., et al. (2021). Antimicrobial peptide 17BIPHE2 inhibits the proliferation of lung cancer cells *in vitro* and *in vivo* by regulating the ERK signaling pathway. *Oncol. Lett.* 22:501. doi: 10.3892/ol.2021.12762
- Yang, Y., Chen, H. Y., Hao, H., and Wang, K. J. (2022). The anticancer activity conferred by the mud crab antimicrobial peptide scyrepocin through apoptosis and membrane disruption. *Int. J. Mol. Sci.* 23:5500. doi: 10.3390/ijms23105500
- Yu, H. H., Wu, L. Y., Hsu, P. L., Lee, C. W., and Su, B. C. (2023). Marine antimicrobial peptide epinecidin-1 inhibits proliferation induced by lipoteichoic acid and causes cell death in non-small cell lung cancer cells via mitochondria damage. *Probiotics Antimicrob. Proteins* doi: 10.1007/s12602-023-10130-1 [Epub ahead of print].
- Yu, R., Wang, M., Wang, M., and Han, L. (2020). Melittin suppresses growth and induces apoptosis of non-small-cell lung cancer cells via down-regulation of TGF- β -mediated ERK signal pathway. *Braz. J. Med. Biol. Res.* 54, e9017–e9025. doi: 10.1590/1414-431X20209017
- Zaslloff, M. (1987). Magainins, a class of antimicrobial peptides from *Xenopus* skin: isolation, characterization of two active forms, and partial cDNA sequence of a precursor. *Proc. Natl. Acad. Sci. U.S.A.* 84, 5449–5453. doi: 10.1073/pnas.84.15.5449
- Zhai, Z., Zhang, F., Cao, R., Ni, X., Xin, Z., Deng, J., et al. (2019). Cecropin A alleviates inflammation through modulating the gut microbiota of C57BL/6 mice with DSS-induced IBD. *Front. Microbiol.* 10:1595. doi: 10.3389/fmicb.2019.01595
- Zhang, Q. T., Liu, Z. D., Wang, Z., Wang, T., Wang, N., Wang, N., et al. (2021). Recent advances in small peptides of marine origin in cancer therapy. *Mar. Drugs* 19:115. doi: 10.3390/md19020115
- Zhang, R., Li, Z., Gu, X., Zhao, J., Guo, T., and Kong, J. (2022). Probiotic *Bacillus subtilis* LF11 protects intestinal epithelium against *Salmonella* infection. *Front. Cell. Infect. Microbiol.* 12:837886. doi: 10.3389/fcimb.2022.837886
- Zhang, S. F., and Chen, Z. (2017). Melittin exerts an antitumor effect on non-small cell lung cancer cells. *Mol. Med. Rep.* 16, 3581–3586. doi: 10.3892/mmr.2017.6970
- Zhang, S. K., Song, J. W., Gong, F., Li, S. B., Chang, H. Y., Xie, H. M., et al. (2016). Design of an alpha-helical antimicrobial peptide with improved cell-selective and potent anti-biofilm activity. *Sci. Rep.* 6:27394. doi: 10.1038/srep27394
- Zhang, Y., Sun, C., Xiao, G., and Gu, Y. (2019). Host defense peptide Hymenochirin-1B induces lung cancer cell apoptosis and cell cycle arrest through the mitochondrial pathway. *Biochem. Biophys. Res. Commun.* 512, 269–275. doi: 10.1016/j.bbrc.2019.03.029
- Zhang, Z., Zhang, H., Peng, T., Li, D., and Xu, J. (2016). Melittin suppresses cathepsin S-induced invasion and angiogenesis via blocking of the VEGF-A/VEGFR-2/MEK1/ERK1/2 pathway in human hepatocellular carcinoma. *Oncol. Lett.* 11, 610–618. doi: 10.3892/ol.2015.3957
- Ziaja, M., Dziedzic, A., Szafraniec, K., and Piastowska-Ciesielska, A. (2020). Cecropins in cancer therapies-where we have been? *Eur. J. Pharmacol.* 882:173317. doi: 10.1016/j.ejphar.2020.173317



OPEN ACCESS

EDITED BY

Rustam Aminov,
University of Aberdeen, United Kingdom

REVIEWED BY

Bindu Subhadra,
Long Island University, United States
Paramita Sarkar,
Julius Maximilian University of Würzburg,
Germany

*CORRESPONDENCE

Zhenlin Ouyang
✉ Zhenlin.ouyang@xjtu.edu.cn
Yurong Wen
✉ Yurong.Wen@xjtu.edu.cn

RECEIVED 14 September 2023

ACCEPTED 05 February 2024

PUBLISHED 27 February 2024

CITATION

Ouyang Z, He W, Jiao M, Yu Q, Guo Y,
Refat M, Qin Q, Zhang J, Shi Q, Zheng F and
Wen Y (2024) Mechanistic and biophysical
characterization of polymyxin resistance
response regulator PmrA in *Acinetobacter
baumannii*.
Front. Microbiol. 15:1293990.
doi: 10.3389/fmicb.2024.1293990

COPYRIGHT

© 2024 Ouyang, He, Jiao, Yu, Guo, Refat,
Qin, Zhang, Shi, Zheng and Wen. This is an
open-access article distributed under the
terms of the [Creative Commons Attribution
License \(CC BY\)](https://creativecommons.org/licenses/by/4.0/). The use, distribution or
reproduction in other forums is permitted,
provided the original author(s) and the
copyright owner(s) are credited and that the
original publication in this journal is cited, in
accordance with accepted academic
practice. No use, distribution or reproduction
is permitted which does not comply with
these terms.

Mechanistic and biophysical characterization of polymyxin resistance response regulator PmrA in *Acinetobacter baumannii*

Zhenlin Ouyang^{1*}, Wenbo He¹, Min Jiao¹, Qinyue Yu¹,
Yucheng Guo¹, Moath Refat², Qian Qin¹, Jiaxin Zhang¹,
Qindong Shi¹, Fang Zheng² and Yurong Wen^{1*}

¹Shaanxi Provincial Key Laboratory of Sepsis in Critical Care Medicine, Department of Critical Care Medicine, Center for Microbiome Research of Med-X Institute, The First Affiliated Hospital, Xi'an Jiaotong University, Xi'an, China, ²The Key Laboratory of Environment and Genes Related to Disease of Ministry of Education Health Science Center, Xi'an Jiaotong University, Xi'an, China

Introduction: *Acinetobacter baumannii* PmrAB is a crucial two-component regulatory system (TCS) that plays a vital role in conferring resistance to polymyxin. PmrA, a response regulator belonging to the OmpR/PhoB family, is composed of a C-terminal DNA-binding effector domain and an N-terminal receiver domain. The receiver domain can be phosphorylated by PmrB, a transmembrane sensor histidine kinase that interacts with PmrA. Once phosphorylated, PmrA undergoes a conformational change, resulting in the formation of a symmetric dimer in the receiver domain. This conformational change facilitates the recognition of promoter DNA by the DNA-binding domain of PmrA, leading to the activation of adaptive responses.

Methods: X-ray crystallography was carried out to solve the structure of PmrA receiver domain. Electrophoretic mobility shift assay and Isothermal titration calorimetry were recruited to validate the interaction between the recombinant PmrA protein and target DNA. Field-emission scanning electron microscopy (FE-SEM) was employed to characterize the surface morphology of *A. baumannii* in both the PmrA knockout and mutation strains.

Results: The receiver domain of PmrA follows the canonical $\alpha 5\beta 5$ response regulator assembly, which undergoes dimerization upon phosphorylation and activation. Beryllium trifluoride is utilized as an aspartate phosphorylation mimic in this process. Mutations involved in phosphorylation and dimerization significantly affected the expression of downstream *pmrC* and *naxD* genes. This impact resulted in an enhanced cell surface smoothness with fewer modifications, ultimately contributing to a decrease in colistin (polymyxin E) and polymyxin B resistance. Additionally, a conservative direct-repeat DNA PmrA binding sequence TTAAAGNNNNNTTTAAG was identified at the promoter region of the *pmrC* and *naxD* gene. These findings provide structural insights into the PmrA receiver domain

and reveal the mechanism of polymyxin resistance, suggesting that PmrA could be a potential drug target to reverse polymyxin resistance in *Acinetobacter baumannii*.

KEYWORDS

polymyxin resistance, response regulator, *Acinetobacter baumannii*, PmrA, mechanism

1 Introduction

The emergence of multidrug-resistant *Acinetobacter baumannii* infection poses a significant threat as an opportunistic and medically important pathogen, causing a wide range of nosocomial infections (Almasaudi, 2018). This bacterium exhibits a remarkable ability to acquire resistance to multiple antibiotics, with up to 30% of clinical isolates of *A. baumannii* demonstrating resistance to at least three antibiotics commonly used in intensive care units (Uc-Cachón et al., 2019). Antimicrobial-resistant *A. baumannii* strains, including commonly used clinical antibiotics such as imipenem, sulbactam, rifampin, and tigecycline resistant strains, have been isolated with increasing frequency. The situation has led to a rise in the use of polymyxins as antimicrobial agents, resulting in the emergence of strains resistant to polymyxins (Hamidian and Nigro, 2019; Hashemi et al., 2019). *A. baumannii* strains are resistant to a wide range of currently available antibiotics and are of particular concern, due to their potential for spreading within critical care environments (Büchler et al., 2018; Lee et al., 2020). *A. baumannii* has been ranked as the most critical threat among multidrug-resistant bacteria by the World Health Organization due to its remarkable ability to develop resistance to multiple drugs (Bagińska et al., 2019).

Colistin (Polymyxin E) and polymyxin B are cyclic cationic peptides synthesized by the *Bacillus* species. Polymyxin E exhibits a rapid bactericidal effect against Gram-negative bacteria by interacting with the lipid A moiety of lipopolysaccharide (LPS), which leads to the disorganization of the outer membrane (Vaara, 2009). According to reports, there are three main pathways that contribute to the development of polymyxin resistance: (1) specific modification of the lipid A component of the outer membrane lipopolysaccharide, resulting in a reduction of the net negative charge of the outer membrane. (2) Proteolytic cleavage of the antibiotic molecule. (3) Activation of a broad-spectrum efflux pump, which can expel a wide range of antibiotics from the bacterial cell (Duperthuy, 2020).

Lately, some questions have been raised regarding the underlying causes of polymyxin resistance. To date, the following three mechanisms have been firmly confirmed in *A. baumannii*: (1) The emergence of high levels of polymyxin resistance can occur when there is a complete loss of lipid A, leading to a deficient lipopolysaccharide (LPS) in the outer membrane. This resistance is attributed to spontaneous point mutations in genes involved in lipid A synthesis, namely *lpxA*, *lpxC*, or *lpxD*. (2) Acquired polymyxin resistance is commonly mediated by the replacement of lipid A with phosphoethanolamine (pEtN), a process regulated

by the *pmrCAB* operon (Beceiro et al., 2011). The PmrAB TCS controls the expression of PmrC, which encodes the lipid A phosphoethanolamine transferase enzyme. This enzyme plays a crucial role in facilitating the addition of phosphoethanolamine (pEtN) to lipid A. Eliminating negative charges in this alteration impacts the interaction between polymyxin and the cell membrane (Samantha and Vrielink, 2020). (3) The alteration of galactosamine (GalN) is associated with the emergence of polymyxin resistance (Pelletier et al., 2013). N-acetylhexosamine deacetylase (NaxD) is a key enzyme for the deacetylation of N-acetylgalactosamine via attaching with the lipid carrier undecaprenyl phosphate. This step is essential for the subsequent addition of GalN galactosamine to lipid A (Gerson et al., 2020). Upon sensing of environmental stimuli, the PmrAB TCS subsequently facilitates *naxD* transcription (Chin et al., 2015). Furthermore, the development of polymyxin resistance has been attributed to the activation of a broad-spectrum efflux pump due to a mutation in *emrB* gene or alterations in membrane permeability (Lima et al., 2018; Uppalapati et al., 2020).

The response regulator PmrA (Uniprot No: E2FGC2) consists of two main domains: the N-terminal receiver domain (RD, residues 1–116), which responds to the phosphorylation signal from its cognate histidine kinase PmrB, and the C-terminal OmpR/PhoB type DNA binding domain (DBD, residues 129–223), which modulates the expression of the downstream target gene (Gao et al., 2019).

In this particular study, we focused on investigating the role of the PmrAB TCS in polymyxin resistance of *A. baumannii* and providing a deeper understanding of the field. Biophysical, structural biology, and related mutagenesis approaches were adopted to investigate how PmrAs recognize specific DNA sequences and regulate DNA reorganization through their receiver domain. We determined the crystal structure of the *A. baumannii* PmrA receiver domain at 1.6 Å resolution, significant insights at the molecular level, with details underlying the assembly of PmrA. We confirmed that PmrA activates transcription by binding to a conserved DNA motif within the promoters of two operons, namely *pmrC* and *naxD* genes. Additionally, PmrA activates transcription of the two *lipA* modification enzymes, *pmrC* and *naxD* operons, which play crucial roles in polymyxin resistance. Overall, the present study shed new insight into the regulatory mechanism of polymyxin resistance in *A. baumannii* by utilizing multidisciplinary techniques and providing enhanced comprehension of the field. The study may lead to potential strategies to develop antimicrobial drugs targeting polymyxin resistance pathway and benefit the clinical infection treatment associated with multidrug resistant *A. baumannii*.

2 Experimental methods

2.1 Bacterial strains, plasmids, growth conditions, and antibiotics

The bacterial strains and plasmids utilized in this study are summarized in [Supplementary Table 2](#), while the primers employed for cloning and site mutagenesis are documented in [Supplementary Table 3](#). Unless otherwise specified, all strains were cultivated in lysogeny broth (LB), which consists of 10 g/L tryptone (Oxoid, Waltham, MA, United States), 5 g/L yeast extract (Oxoid, Waltham, MA, United States), and 10 g/L NaCl (Sigma-Aldrich, Burlington, MA, United States). For selection purposes, the antibiotics tetracycline (Sigma-Aldrich, Burlington, MA, United States) (20 or 15 µg/mL) and kanamycin (Sigma-Aldrich, Burlington, MA, United States) (25 µg/mL) were added as required ([Tucker et al., 2014](#)).

2.2 Gene knockout construction uses REC_{AB} system

Chromosomal PmrA deletion was constructed using REC_{AB} system ([Tucker et al., 2014](#)). In brief, we harvested the 500 bp upstream and 500 bp downstream DNA fragments of the PmrA using BIO-RAD C1000 Touch PCR thermal cycler. These fragments were designed to flank the kanamycin resistance cassette, amplified from the pKD4 plasmid. *A. baumannii* ATCC19606 carrying pAT04 vector containing REC_{AB} was cultured in LB media supplemented with tetracycline (20 µg/mL). The bacteria were grown to mid-log phase (OD₆₀₀ = 0.3–0.5) at 37°C supplemented with 2 mM IPTG, next bacteria were washed with ice-cold 10% glycerol three times. Approximately 5 µg PCR-product was electroporated into 100 µL *A. baumannii* ATCC19606, and kanamycin (25 µg/mL) was used to select cultivate mutant strains. The selected colonies were verified by PCR and DNA sequencing and then cure the plasmid pAT04 for further use.

For constructing IPTG-inducible PmrA complementation vectors, the primer sets listed in [Table 1](#) were used to prepare the *pmrA* fragment by PCR. The pAT04-PmrA plasmid was generated through seamless cloning. The PCR based site-directed mutagenesis approach described before ([Zheng et al., 2004](#)) was used to construct point mutation. In summary, our methodology involved utilizing a PCR procedure that involves denaturing the DNA template, followed by annealing and extending mutagenic primers using a proprietary DNA polymerase. One distinctive aspect of this system is the removal of parental DNA using *Dpn*⁺ endonuclease, which specifically digests methylated or hemimethylated sequences in the parental DNA. Next, the plasmids were electroporated into the Δ*pmrA* strains. The PmrA complementation and pointed mutation strains were validated by PCR and DNA sequencing.

2.3 Protein expression and purification

The full-length (PmrA FL, 1–244) and receiver domain (PmrA RD, 1–116) of *A. baumannii* PmrA were obtained through PCR

and inserted into the pET28a vector with a 6× His tag at the N-terminus. The constructed plasmids were then transformed into *E. coli* BL21 (DE3) star host cells. The cells were grown in LB medium supplemented with kanamycin (100 µg/mL) at 37°C and 200 rpm until reaching mid-log phase (OD₆₀₀ = 0.6–0.8). Following induction with 1 mM IPTG, the cultures were incubated for 8 h before harvesting the cells through centrifugation at 7,000 g (Beckman, Brea, CA, United States). The resulting cell pellets were frozen at –80°C for future use. The recombinant proteins were purified using Ni-NTA Superflow Cartridges (5 ml Qiagen) with ÄKTA pure[™] chromatography system. The eluted protein fractions were concentrated and loaded onto a Superdex 75pg 16/60 size exclusion chromatography column (GE Healthcare, Gens, Switzerland). The column was pre-equilibrated with a standardized buffer solution containing 25 mM Tris (pH 8.0), 150 mM NaCl, and 5% glycerol. During the purification process, 5.3 mM BeSO₄, 35 mM NaF, and 7 mM MgCl₂ were added to facilitate the phosphorylation of PmrA in complex with BeF₃[–] and magnesium. The main protein fractions were further concentrated (> 98% purity as determined by mass spectrometry and SDS-PAGE). The protein concentration was measured using a NanoDrop[®] spectrometer (Thermo Fisher, Waltham, MA, United States) with the extinction coefficient

TABLE 1 X-ray data collection and refinement statistics of PmrA RD.

Crystal	PmrA_Receiver domain
Data collection	
Spacegroup	P 1 21 1
a, b, c (Å)	32.1, 39.1, 92.2
α, β, γ (°)	90.0, 95.86, 90.0
Resolution (Å)	31.94–1.6 (1.66–1.6)
R _{meas}	0.036 (0.419)
Multiplicity	3.1 (2.7)
CC (1/2)	0.999 (0.935)
I/σ(I)	18.56/2.56
Completeness (%)	99.18 (98.28)
Wilson B-factor (Å ²)	23.05
Refinement	
Total reflections	95,955 (12,052)
Unique reflections	30,050 (2,921)
R _{work} /R _{free}	0.1890/0.2386
Number of atoms	
Protein	249
Water	161
Average B-factor (Å ²)	32.79
Protein ADP (Å ²)	32.22
Water ADP (Å ²)	39.88
Ramachandran plot	
Favored/allowed (%)	98/2
Root mean square deviation	
Bond lengths (Å)	0.011
Bond angle (°)	1.18
PDB code	8IMW

Statistics for the highest-resolution shell are shown in parentheses.

generated from the ExPASy ProtParam program¹ (Gasteiger et al., 2005).

2.4 Crystallization and data collection

The recombinant protein of the PmrA receiver domain (PmrA RD) was concentrated to a concentration of 25 mg/mL for screening crystallization conditions. Crystallization screening was conducted at 20°C using a 392-well Hampton crystallization plate, employing commercial kits from Molecular Dimensions and Hampton Research. The sitting-drop vapor-diffusion method was employed for crystallization. The PmrA RD crystals were successfully obtained in a crystallization condition consisting of 0.1 M Sodium malonate at pH 6.0 and 12% w/v Polyethylene glycol 3,350. To prepare the crystals for data collection, all obtained crystals were immersed in a cryoprotectant solution composed of the reservoir solution supplemented with 30% glycerol. Subsequently, the crystals were cryo-cooled in liquid nitrogen to maintain their integrity during the data collection process. X-ray diffraction data were collected from a single crystal using a wavelength of 0.98 Å at the Shanghai Synchrotron Radiation Facility (SSRF) BL18U1 beamline. The data collection was performed at a temperature of 100K to minimize crystal movement and enhance data quality (Ouyang et al., 2021).

2.5 Structure determination and refinement

The X-ray diffraction data obtained were processed and scaled using XDS software (Kabsch, 2010). Detailed information and statistics regarding the data collection are summarized in Table 1. The structure of the PmrA RD protein was determined through molecular replacement, utilizing the *Staphylococcus aureus* ArlR receiver domain (PDB: 6IS3) as a search model (Ouyang et al., 2019), which shares a sequence identity of 41% with PmrA RD. Structural alignment and comparison, specifically the root mean square deviation (RMSD) calculation, were performed using PyMOL. The analysis of structure interfaces and assemblies was conducted using the PDBe PISA server (Krissinel and Henrick, 2007). The crystal structure of PmrA RD was ultimately solved at a resolution of 1.6 Å, belonging to space group P1211, with the following cell dimensions: $a = 32.1$ Å, $b = 39.1$ Å, $c = 92.2$ Å, and $\beta = 95.9^\circ$, while α and γ angles were both 90° . COOT and PHENIX4 were used for model building and refinement (Emsley and Cowtan, 2004; Adams et al., 2010). Individual B-factor, non-crystallographic symmetry (NCS) torsion-angle, and translation/libration/screw (TLS) parameters were used in refinement strategies. The final structure was refined to a final Rwork/Rfree of 0.1890/0.2386, indicating the goodness-of-fit between the model and the experimental data.

¹ <https://web.expasy.org/protparam/>

2.6 Electrophoretic mobility shift assay

The electrophoretic mobility shift assay (EMSA) experiments were conducted according to the protocol provided by the LightShift Chemiluminescent EMSA Kit (Thermo Scientific, Waltham, MA, United States). A 200+ bp biotin-labeled DNA fragments from the upstream regions of *pmrC* (232 bp) and *naxD* (251 bp) were obtained by PCR using the 5'-end biotin-labeled primers listed in Supplementary Table 3. The mutated promoter DNA fragments, as control sequences, were obtained by Site directed mutagenesis PCR using primer listed in Supplementary Table 3. These fragments were used to detect interactions between proteins and DNA. The EMSA reaction followed a previously described protocol (Wen et al., 2017b). In brief, the binding reactions were incubated in a 10 µl volume, containing 1 pmol of DNA and various concentrations of PmrA FL protein, in the binding buffer (10 mM Tris, 50 mM KCl, 1 mM DTT, 5% glycerol, pH 7.5) for 30 min. The samples were then loaded directly onto a 5% native polyacrylamide gel and separated in 0.5× TBE buffer at 100 V on ice. Subsequently, the gels were transferred to a nylon membrane through electroblotting in 0.5× TBE buffer at 300 mA for 90 min at 4 °C. After cross-linking the DNA fragments at 120 mJ/cm² using a commercial UV-light crosslinking instrument equipped with 254 nm bulbs, chemiluminescence was performed to detect the biotin-labeled DNA in the membranes.

2.7 Isothermal titration calorimetry

Isothermal titration calorimetry (ITC) experiments were all performed using a Microcal ITC200 calorimeter (GE Healthcare, Grens, Switzerland) at 25 °C. Before conducting the experiments, samples of DNA (Supplementary Table 3) and protein were prepared with the exact batch of buffer solution (25 mM Tris pH 8.0, 150 mM NaCl, 10% glycerol with or without BeF₃[−] and magnesium), using size-exclusion chromatography. During the purification process, 5.3 mM BeSO₄, 35 mM NaF, and 7 mM MgCl₂ were added for the phosphorylation of PmrA FL.

A volume of 60 µL solution containing PmrA FL protein (150 µM) was loaded into 15 µM of the 17 bp direct-repeat DNA to measure the enthalpy of protein to DNA association. The concentration of PmrA FL protein in the injection syringe ranged between 100 and 150 µM. Injections were performed with 0.4 µL for the first injection and 2 µL from the second to the nineteenth injection, with intervals of 120 s. The ITC data were analyzed using the Microcal ITC data analysis package, specifically utilizing the one-binding site mode, as part of the supplementary features (Wen et al., 2017a).

2.8 RNA isolation and real-time PCR

The PmrA knockout and site-directed mutagenesis strains were grown till reaching the mid-logarithmic phase in LB.

The suspensions were then adjusted to an optical density of 0.01 at OD₆₀₀ and grown for 5 h at 37°C and 200 rpm before harvesting. Total RNA isolation and cDNA synthesis were carried out following previously described methods (Ouyang et al., 2019). In brief, total RNA was extracted using a Qiagen RNeasy Mini kit. Subsequently, the High-Capacity cDNA Reverse Transcription Kit (Bio-Rad, Hercules, CA, United States) was used to synthesize first-strand cDNA from the total RNA, following the manufacturer's instructions and employing 300 ng of total RNA as the template. Expression of *pmrC* and *naxD* were determined by two-step real-time PCR System (Bio-Rad, Hercules, CA, United States). Gene-specific primers were designed to generate specific products of 200 to 250 bp in size (Supplementary Table 3) and annealed at 60°C to account for any variations in the initial material amount. The 16S RNA gene was used as a reference gene. Fold changes in various *pmrC* and *naxD* transcripts in PmrA knockout and site-directed mutagenesis in relative to ATCC19606 were calculated using the $2^{-\Delta\Delta Ct}$ formula.

2.9 Minimal inhibitory concentration (MIC) test

Minimal inhibitory concentration (MIC) was performed using colistin sulfate and polymyxin B by employing broth microdilution in Cation-Adjusted Mueller–Hinton Broth (CAMHB), following the guidelines set by the Clinical and Laboratory Standards Institute (CLSI) (Weinstein, 2018). Each *A. baumannii* strain was diluted with LB broth to get 0.1 OD₆₀₀ from an overnight culture, growth to 0.4 OD₆₀₀ at 37 °C, 220 rpm till mid-log phase. The bacterial concentration was adjusted to 1×10^7 CFU/mL with CAMHB. Colistin sulfate (0.5, 1, 2, 4, 6, 8, 10, 12, 16, 32, 64, 128, 256, 512 µg/mL) and polymyxin B (1, 2, 3, 4, 5, 6, 7, 8 µg/mL) was prepared at various concentrations in CAMHB. A mixture of 50 µl of *A. baumannii* and 50 µl of the polymyxin solutions was added to the wells of polystyrene 96-well microtiter plates (Corning, New York, NY, United States). The microtiter plates were then incubated overnight at 37 °C, and the OD₆₀₀ of each well was measured. The MIC for each tested strain was determined as the lowest concentration of colistin sulfate or polymyxin B that completely inhibited the growth of the bacteria.

2.10 Scanning electron microscopy (SEM)

The strains were cultured on glass slides in LB medium with 2 mM IPTG for 48 h at 37°C without shake. Subsequently, they were fixed with 4% paraformaldehyde for 15 min and 2.5% glutaraldehyde overnight. The fixed specimens underwent dehydration using graded ethanol (30%, 50%, 70%, 85%, 90%, 95%, 100%), 10 min for each step, followed by critical point drying with CO₂. Finally, the samples were coated with 15 nm diameter gold-palladium beads and photographed using a Philips XL-30 scanning electron microscope at 20 kV (Wen et al., 2017a).

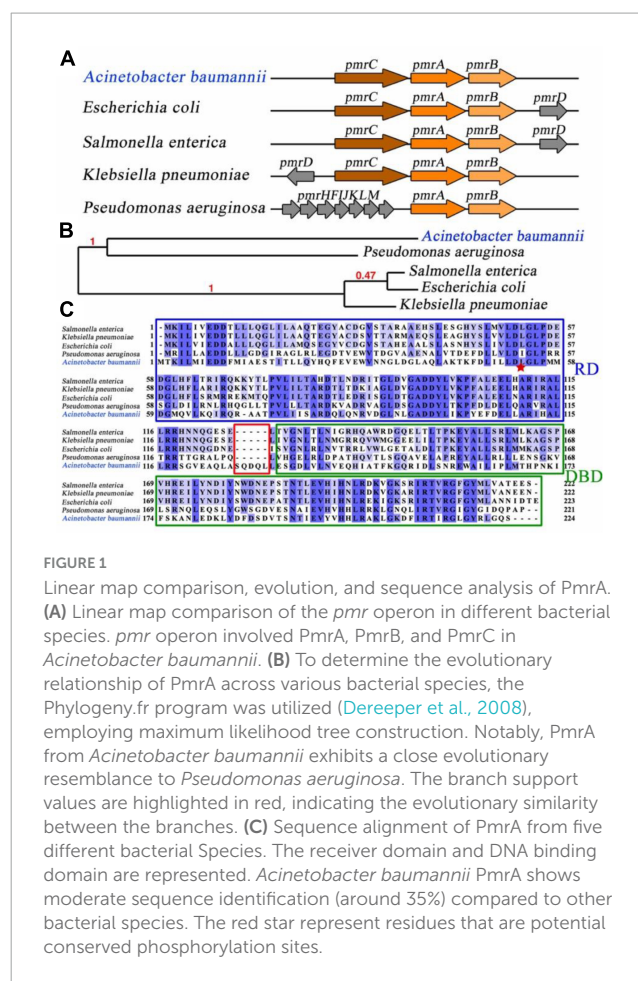


FIGURE 1

Linear map comparison, evolution, and sequence analysis of PmrA. (A) Linear map comparison of the *pmr* operon in different bacterial species. *pmr* operon involved PmrA, PmrB, and PmrC in *Acinetobacter baumannii*. (B) To determine the evolutionary relationship of PmrA across various bacterial species, the Phylogeny.fr program was utilized (Dereeper et al., 2008), employing maximum likelihood tree construction. Notably, PmrA from *Acinetobacter baumannii* exhibits a close evolutionary resemblance to *Pseudomonas aeruginosa*. The branch support values are highlighted in red, indicating the evolutionary similarity between the branches. (C) Sequence alignment of PmrA from five different bacterial species. The receiver domain and DNA binding domain are represented. *Acinetobacter baumannii* PmrA shows moderate sequence identification (around 35%) compared to other bacterial species. The red star represent residues that are potential conserved phosphorylation sites.

3 Results

3.1 Linear map comparison, phylogeny and sequence analysis of PmrA

Pmr operon exhibited identical core components of PmrA, PmrB, and PmrC across various bacterial species. An essential intermediary protein PmrD, can stabilizing the activated form of PmrA, plays a critical role in connecting the two-component systems in *Escherichia coli* (Wang et al., 2021), *Salmonella enterica* (Pescaretti et al., 2011) and *Klebsiella pneumoniae* (Lou et al., 2015). Interestingly, the *pmrD* gene was not appear to be observed in *A. baumannii*, suggesting the existence of alternative mechanisms for coordinated regulation (Figure 1A). Comparative analysis of the *pmrA* gene from 5 distinct bacterial species revealed that *A. baumannii* PmrA has a close evolutionary affinity with *Pseudomonas aeruginosa* PmrA, as indicated by phylogeny analysis (Dereeper et al., 2008; Figure 1B).

Sequence alignment of *A. baumannii* PmrA was conducted by CLUSTALW program (Thompson et al., 1994), showed moderate sequence identity (around 35%) compared to other bacterial species. However, it is worth noting that the linker region between the RD and DBD of *A. baumannii* PmrA contains an extended sequence, namely SQDQL, which provides higher flexibility for

A. baumannii PmrA. Residue D52 is the potential conserved phosphorylation site, which is pointed with a red star (Figure 1C).

3.2 Purification of PmrA and its dimerization in the presence of aspartate phosphorylation analog BeF_3^-

The PmrA full length (FL) protein comprises of a receiver domain (RD) and DNA binding domain (DBD) belonging to the OmpR/PhoB family. To gain insight into the regulatory mechanism of the *A. baumannii* response regulator PmrA, we successfully expressed and purified the recombinant full-length PmrA (PmrA FL), as well as the PmrA receiver domain (PmrA RD) and PmrA DNA binding domain (PmrA DBD), respectively. The size exclusion chromatography (SEC) profiles indicated all constructs behaved as monomers in solution (Figure 2A). SDS-PAGE further analyzed all the purified samples from size-exclusion chromatography, followed by Coomassie Blue Staining

(Figure 2B). Phosphorylation and dimerization are essential for response regulators to effectively identify target DNA and initiate downstream gene activation (Bourret, 2010; Scheller et al., 2020). Beryllium trifluoride has been extensively utilized as an aspartate phosphorylation mimic in the active state (Cho et al., 2001). In this study, full-length PmrA were incubated with BeF_3^- and Mg^{2+} to mimic phosphorylation. Adding BeF_3^- and Mg^{2+} induced PmrA dimerization, as indicated by size exclusion chromatography (Figure 2C).

3.3 Crystal structure of the PmrA receiver domain

The modulation of PmrA-dependent transcriptional regulation is influenced by its N-terminal receiver domain. To gain insight into the regulatory mechanism of PmrA, we conducted crystal structure analysis with a resolution of 1.6 Å. The crystal structure revealed the presence of two PmrA RD molecules in the

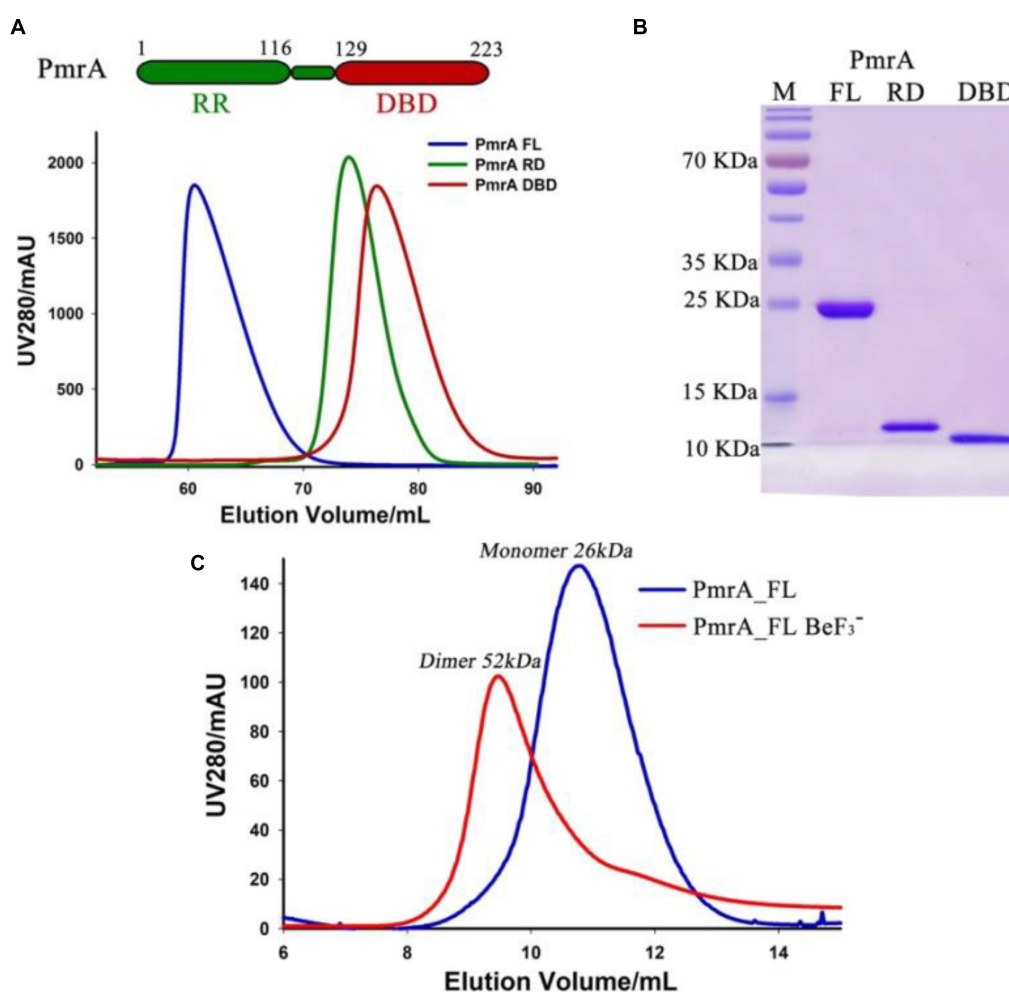


FIGURE 2

Purification of PmrA and its dimerizes in the presence of aspartate phosphorylation analog BeF_3^- . (A) The schematic view illustrates PmrA, while the size exclusion chromatography profile shows PmrA in its full-length (FL, blue), receiver domain (RD, green), and DNA binding domain (DBD, red). (B) Coomassie Blue Staining SDS-PAGE was performed on the SEC purified PmrA samples from panel A. (C) The size exclusion chromatography profile indicates that PmrA exists as a monomer but elutes as a dimer in the presence of the aspartate phosphorylation analog, BeF_3^- , and Mg^{2+} .

asymmetric unit (Table 1). The receiver domain of PmrA adopts a canonical $\alpha 5\beta 5$ topology, forming a central parallel β -sheet flanked by $\alpha 1$, $\alpha 5$ on one side, and $\alpha 2$, $\alpha 3$, $\alpha 4$ on the other side (Figure 3A). Similar to other members of the PhoB family, a significant dimerization interface consisting of $\alpha 4$ - $\beta 5$ - $\alpha 5$ was observed, involving 9 hydrogen bonds and 13 salt bridges. This dimerization interface buries a total surface area of 999 Å², as determined by PDBPISA. Positively charged residues R111, R117, and R118 from $\alpha 5$ interact with negatively charged residues D97, L91, and D96 from $\alpha 4$ across the dimerization interface. Notably, residue R87 from $\alpha 4$ forms a hydrogen bond with E107 from $\alpha 5$ (Figure 3B). Additionally, residue R118 forms hydrogen bonds

across the dimer interface with A72 in the loop between $\alpha 3$ and $\beta 4$. Supplementary Table 1 provides a detailed list of the interactions involved in dimer formation. Structural alignment of the inactivated PmrA receiver domain with the activated and inactivated PhoP (Bachhawat and Stock, 2007) reveals a certain degree of similarity between PmrA and PhoP. The phosphorylation site of PmrA is the highly conserved aspartate residue D52 at the C-terminal end of $\beta 3$. This phosphorylation process is facilitated by residues E8, D9, G54, and L101 (Figure 3C). The PmrA receiver domain shares an overall sequence identity of 26% with the well-characterized OmpR/PhoB family response regulator, PhoP (Figure 3D). Most of the residues involved in dimerization

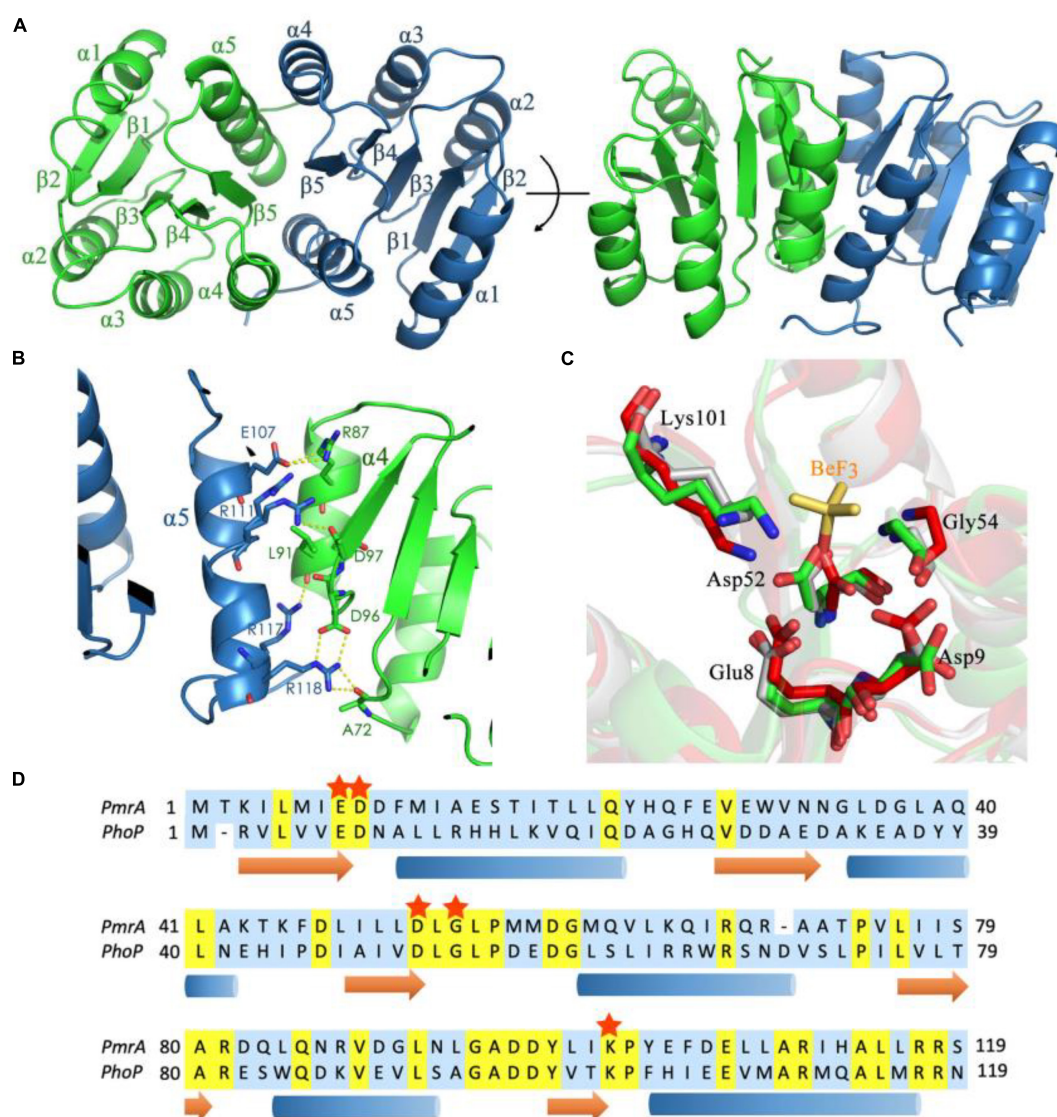


FIGURE 3

Crystal structure of the PmrA receiver domain. (A) The crystal structure of the PmrA receiver domain dimer is depicted in various orientations. The receiver domain of PmrA is composed of five α helices and five β strands, arranged in a parallel β -sheet configuration. The dimerization of the receiver domain occurs through the $\alpha 4$ - $\beta 5$ - $\alpha 5$ motif. (B) The dimerization interface of the PmrA receiver domain is mediated by the $\alpha 4$ - $\beta 5$ - $\alpha 5$ motif. A comprehensive interaction profile can be found in Supplementary Table 1. (C) Alignment of the BeF₃⁻ binding motif of activated PhoP (PDB ID: 2PL1) (red), unactivated PhoP (PDB ID: 2PKX) (gray), and PmrA (green). The BeF₃⁻ (yellow sticks) of PhoP is closer to Lys112 in PmrA. (D) The sequence alignment of the PmrA receiver domain with the extensively studied response regulator PhoP is presented. The conserved aspartate phosphorylation site and the crucial amino acids associated with it are indicated by red stars. Detailed structural statistics can be found in Table 1. The structural coordinates of the receiver domain have been deposited in the Protein Data Bank under the PDB ID: 8IMW.

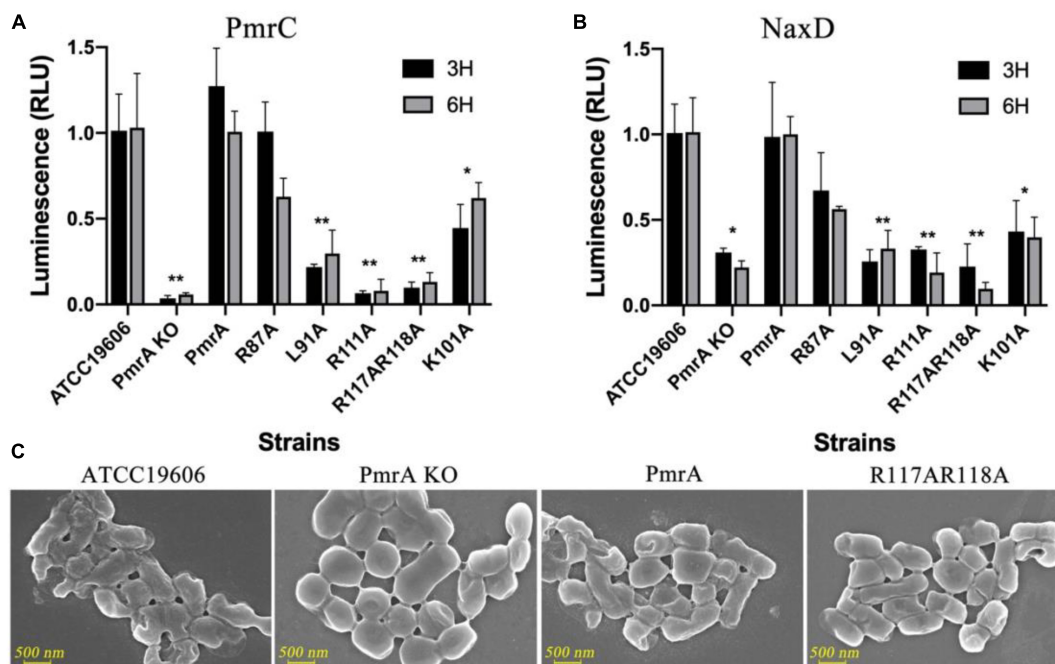


FIGURE 4

PmrA dimerization interface affected *pmrC* and *naxD* gene expression validated using real-time PCR. (A) The expression level of phosphoethanolamine *pmrC* gene was investigated by real-time PCR in ATCC19606, PmrA KO, PmrA, R87A, L91A, R111A, R117AR118A, and K101A strains at 3 and 6 h, respectively. Data are represented as means \pm SD of 4–6 replicates. (B) RT-PCR examined the deacetylase *naxD* gene expression level in all previously mentioned strains at 3 and 6 h. Data are represented as means \pm SD of 4–6 replicates. (C) Field-emission scanning electron microscopy (FE-SEM) experiments of ATCC19606, PmrA KO, PmrA and, R117AR118A. Scale bars represent 500 nm. **, $0.001 < P < 0.01$; *, $0.01 < P < 0.05$.

and phosphorylation, including E8, D9, D52, G54, D96, D97, R101, R111, and R118, exhibit conservation between PmrA and PhoP.

3.4 PmrA controls the expression of the *pmrC* and *naxD* operons

A set of point mutations were introduced to the receiver domain and phosphorylation site to investigate the functional significance of these residues *in vivo*. The impact of these mutations on the transcriptional levels of *pmrC* and *naxD* was monitored, which in turn affects the modification of lipid A in *A. baumannii*. In the PmrA knockout strains, the *pmrC* and *naxD* expression were significantly reduced. The key mutations in conserved residues in PmrA dimerization, including L91, R111, R117, and R118, demonstrated an equivalent reduction to the knockout strain in *pmrC* (Figure 4A) and *naxD* transcription (Figure 4B), thereby confirming the significance of these residues in the regulatory process. Mutations in conserved residues are associated with D52 phosphorylation, including E8, D9, G54 and L101. The L101A mutations were designed to disrupt the phosphorylation of PmrA, resulting in a significant decline in the transcriptional activity of *pmrC* and *naxD*.

To further validate the changes in cell structure and membrane, we examined wildtype, PmrA knockout, PmrA complementation, and R117A R118A mutant strains using field-emission scanning electron microscopy (FE-SEM). LPS

is composed of three structural components: lipid A, core oligosaccharide, and O-specific polysaccharide or O antigen. The unmodified form of lipid A can potentially alter the formation process of LPS. The findings from FE-SEM indicated the observation of rough bacterial cell surfaces in wild-type *A. baumannii* and complement strain. In contrast, the *pmrA* knockout and mutant strains of *A. baumannii* had smooth cell surfaces without lipid A modification over the cell membrane (Figure 4C).

3.5 Antibiotic resistance

The data obtained from minimum inhibitory concentration (MIC) has confirmed the decreased susceptibility of PmrA R87A, L91A, R117AR118A, and L101A strains to polymyxin B and colistin sulfate. The MICs of PmrA knockout strains has noticeably reduced (exceeding four-fold reduction) for polymyxin B and colistin sulfate. Although the R87A strain did not exhibit significantly changed in the expression of genes associated with lipid A modification, it did demonstrate significant alterations in the minimum inhibitory concentration (MIC) of polymyxin B and colistin sulfate. The strain L91A, R111A, and R117AR118A showed a four-fold reduction in MIC of polymyxin B and a 50-fold reduction in MIC for colistin sulfate, respectively. As anticipated, the K101A mutant displayed a potent reduction of MIC for colistin sulfate and polymyxin B, exceeding four-fold (Table 2 and Supplementary Figure 2).

TABLE 2 MIC values of the ATCC19606, PmrA knockout, PmrA WT, PmrA mutant strains of *A. baumannii*.

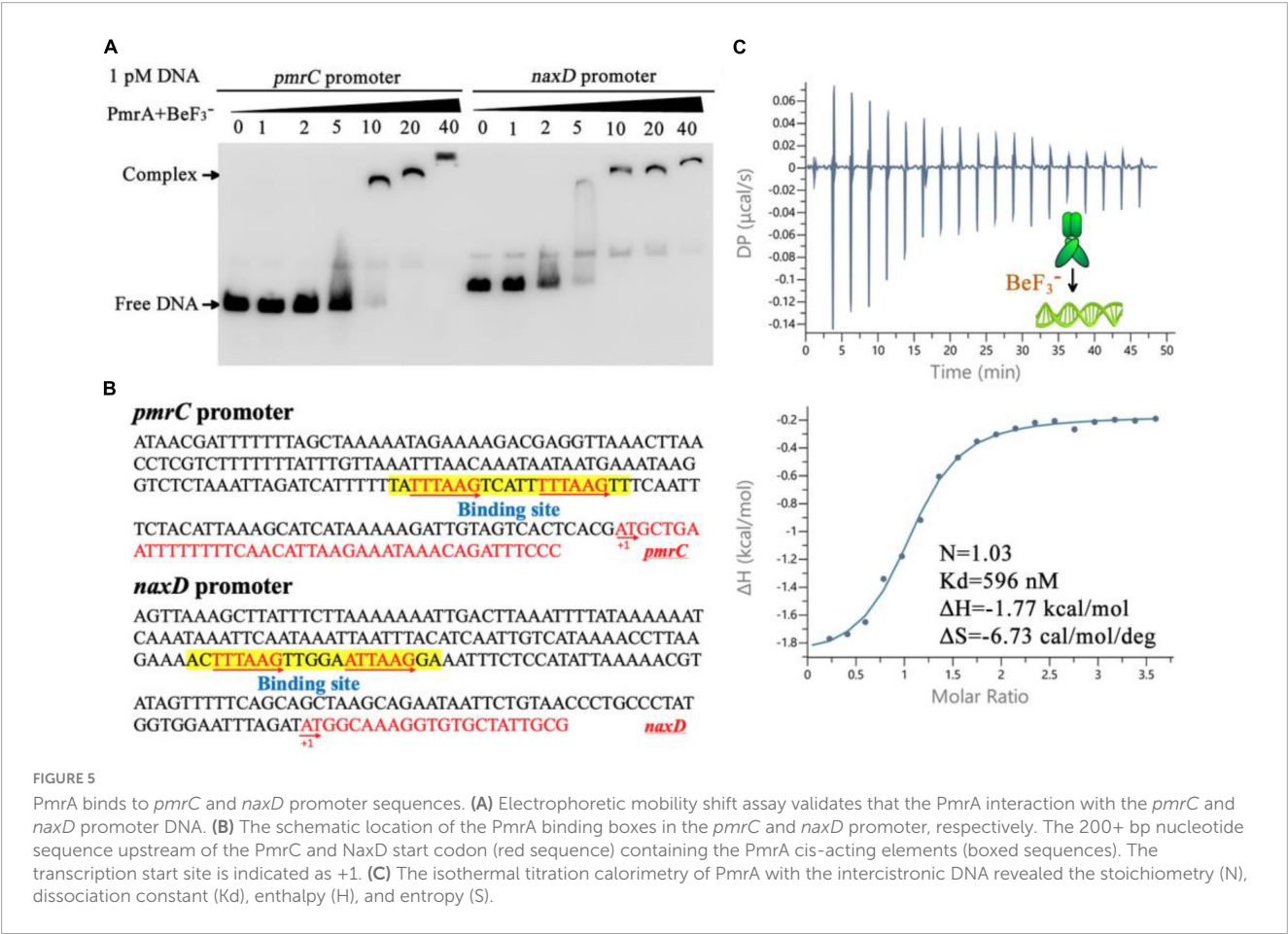
Strain	MIC (μ g/mL)	
	Colistin sulfate	Polymyxin B
ATCC19606	256	8
ΔPmrA	4	2
PmrA_WT	256	7
PmrA_R87A	4	2
PmrA_L91A	8	2
PmrA_R111A	64	6
PmrA_R117AR118A	8	2
PmrA_K101A	2	2

3.6 Identification of a conserved palindromic sequence as the likely PmrA binding site

The modifications of Lipid A was mediated by the *pmrC* and *naxD* genes, specifically through phosphoethanolamine and deacetylase and plays a crucial role in mediating polymyxin resistance in *A. baumannii* (Chin et al., 2015; Seleim et al., 2022). Quantitative real-time PCR results have shown that expression of the *pmrC* and *naxD* operons is controlled by PmrA. To evaluate

the binding ability of PmrA regulator to the *pmrC* and *naxD* promoter, a 200 bp fragment of predicted *pmrC* and *naxD* promoter regions was amplified by PCR and labeled with biotin to facilitate the investigation of its interaction with the PmrA protein by EMSA. The results demonstrated the ability of PmrA protein to bind with the specific sequence, resulting in the inhibition of motility of the *pmrC* and *naxD* promote probe, as seen by EMSA (Figure 5A). The analysis of the promoter sequences in the *pmrC* and *naxD* genes revealed highly conserved PmrA binding sites and TTTAAGNNNNNTTTAAG boxes (Figure 5B). These findings indicate a perfect 6-bp direct-repeat DNA sequence with 5 bp gap located upstream of the *pmrC* and *naxD* gene. Mutations in the TTTAAG region resulted in the absence of any interaction between the PmrA protein and the mutated promoter DNA, as evidenced by the EMSA experiment (Supplementary Figure 1A).

In order to explore the direct interaction between PmrA and the conserved sequence, a 21-base-pair DNA fragment (TATTTAAGTCATTTTAAAGTT) was synthesized, and the binding between PmrA and this DNA sequence was evaluated using isothermal titration calorimetry (ITC) (Figure 5C). The PmrA, when supplemented with BeF₃⁻, showed a significant binding affinity with the direct-repeat DNA. The interaction between these molecules is characterized by an equilibrium dissociation constant (K_d) of 596 nM, a molar reaction enthalpy (H) of -1.77 kcal/mol, and an entropy of -6.73 cal/mol/deg (Figure 5C). Nevertheless, isothermal titration calorimetry experiment cross validated no interaction between PmrA and mutated DNA



(TACCTAGCTCATTCTAGCTT) (Supplementary Figure 1B). Additionally, in the absence of BeF_3^- and magnesium, this experiment did not demonstrate any interaction between PmrA and its target DNA (Supplementary Figure 1C).

4 Discussion

PmrAB TCS is the critical regulator of the phosphoethanolamine transferase PmrC and deacetylase NaxD involved in polymyxin resistance of *A. baumannii*. In addition to its role in polymyxin resistance, PmrAB has been also reported to associate with decrease in biofilm formation capacity, growth rate, fitness, and virulence (Yoon et al., 2013; Farshadzadeh et al., 2018). PmrC played a crucial role in maintaining outer membrane (OM) integrity and has been shown to be linked to bacterial virulence and survival (Sinha et al., 2019). Furthermore, NaxD plays a vital role in resistance to the antimicrobial peptide polymyxin B, as well as in replication within macrophages and *in vivo* virulence (Llewellyn et al., 2012).

Pmr operon of some bacterial strains such as *E. coli*, *S. enterica*, and *K. pneumoniae* encompasses the PmrA, PmrB and PmrC genes and an extra gene encoding a small adapter protein called PmrD. Notably, the activity of the PmrA-PmrB system is regulated by the PmrD protein at a post-transcriptional level (Kox et al., 2000). In *A. baumannii*, the *pmr* operon share the same core components of PmrA, PmrB, and PmrC. The absence of PmrD indicates that the activation of the PmrA-PmrB system could possibly involve other proteins. In the absence of PmrD, it is conceivable that the alternative coordinated mechanisms may regulate this system. However, it is worth noting that although the core components of the *pmr* operon remain consistent across other *Acinetobacter* species, variations in sequence and evolutionary characteristics are evident in the *A. baumannii* compared to the PmrAs that exist across other bacterial species.

Sequence analysis revealed an extended sequence of PmrA in *A. baumannii*, particularly SQDQL, located between the receiver domain (RD) and the C-terminal DNA-binding domain (DBD). Similar to other members of the OmpR/PhoB family, a linker region between these two domains allows the protein to adopt different conformations, such as the “tucked” state (N- and C-terminal domains in proximity) and “extended” state (N- and C-terminal domains distal) (Palethorpe et al., 2022). Extending an additional 5-residues provides the PmrA with remarkable flexibility, which is believed to influence the phosphorylation signaling from the receiver domain (RD) to the C-terminal DNA-binding domain, playing a crucial role in facilitating proper DNA binding.

The phosphorylation simulations results indicated that similar to the classical OmpR/PhoB family response regulator, phosphorylation mediates dimerization and activation (Bachhawat and Stock, 2007). Dimerization of the full-length PmrA will take place in the existence of the aspartate phosphorylation analog BeF_3^- . Furthermore, we provide structural insights into the PmrA receiver domain in this study. PmrA belongs to the bacterial OmpR/PhoB response regulator family and shares secondary structure elements and a two-domain organization with other family members. PmrA features the canonical $(\beta\alpha)_5$ repeat motif. The crystal structure of PmrA reported by Palethorpe et al. (2022),

exhibits the characteristic $\alpha 5/\beta 5$ fold of the receiver domain, where five parallel β -sheets alternate with five amphiphilic α -helices, resulting in the conserved $\beta 1-\alpha 1-\beta 2-\alpha 2-\beta 3-\alpha 3-\beta 4-\alpha 4-\beta 5-\alpha 5$ conformation, which is consistent with our study. Interestingly, the crystal structure of PmrA also reveals the presence of R118 in two alternative conformations, sharing density between the two chains.

Our structure analysis has identified several amino acids playing a crucial role in the dimerization process, including the essential amino acids R118 and A72, L91, D96, D97, R101, R111, and R117. Noteworthy, R111 amino acids have demonstrated also captured in two alternative conformations. More interestingly, our findings underscore the relevance of multiple amino acids in the phosphorylation process, such as E8, D9, D52, G54, and L101. It is necessary to emphasize that most of the residues involved in both dimerization and phosphorylation, specifically E8, D9, D52, G54, D96, D97, R101, R111, and R118, were exceptionally conserved among the OmpR/PhoB family of response regulators.

We further validated the impact of mutations in these pivotal amino acids on the expression of *pmrC* and *naxD* genes, focusing on R111 and R118. We observed an intimate relationship between PmrA mutations and the deformation of bacterial surface morphology. Thoroughly, a knockout of PmrA or a mutation of R118A could result in an abnormal smoothness of the cell surface in *A. baumannii* strains. In parallel, minimum inhibitory concentration (MIC) data revealed that both the gene knockout and the specific mutations of a specific region of the PmrA, including R87A, L91A, R117AR118A, and L101A, resulted in reduced MIC values of *A. baumannii* against colistin sulfate, and polymyxin B.

PmrA has been reported to perform a regulatory role in the expression of PmrC and NaxD gene. It has been suggested that PmrA binds to the promoter regions of these genes and potentially influences their transcription. The predicted binding site sequence is 5'-HTTAAD N5 HTTAAD (Chin et al., 2015; Palethorpe et al., 2022). In line with these studies, our results from the EMSA experiment confirmed the interaction between the PmrA and the promoter region of *pmrC* and *naxD* genes. Sequence analysis reveals a highly conserved and precise DNA binding site (a direct-repeat DNA sequence TTTAAGNNNNNTTTAAG) situated upstream of the *pmrC* and *naxD* gene, which was further validated by the results obtained from an isothermal titration calorimetry experiment. Moreover, the DNA-binding motifs of PmrA appear homologous with other bacterial species. For example, the PmrA recognition sequence of *S. enterica* was found to consist of a direct repeat (YTAAK) (Aguirre et al., 2000), while it consists of two half-sites, 5'-CTTAAT-3', and 5'-CCTAAG-3', in *K. pneumoniae* (Lou et al., 2014).

Beside their crucial contribution to polymyxin tolerance, PmrA, PmrC, and NaxD are also played significant role in biofilm formation, virulence, and bacteria survival in some gram-negative bacteria such as *Escherichia coli*, *Salmonella*, *Klebsiella pneumoniae*, and *Pseudomonas aeruginosa*. Taking *Salmonella* as an example, PmrA can be activated *in vivo* through direct or indirect mechanisms, leading to the regulation of genes involved in lipopolysaccharide modification. This process contributed to the bacterium's survival in both host and non-host environments (Gunn, 2008). In *E. coli*, *pmrAB* has been also reported to influence the cell's resistance to antimicrobial peptides, toxic levels of iron, deoxycholate, and contributes to virulence (Warner et al., 2013).

In conclusion, our findings provide strong evidence that PmrA operates similarly to other two-domain response regulators, employing a distinct activation mechanism where phosphorylation accelerates the dimerization of the effector domain. The physiological relationship between PmrA and polymyxin tolerance was confirmed, highlighting the potential of the PmrAB TCS as a target for developing novel antibiotic agents to combat bacterial polymyxin resistance in *A. baumannii*.

Data availability statement

The datasets presented in this study can be found in online repositories. The names of the repository/repositories and accession number(s) can be found in this article/**Supplementary material**.

Author contributions

ZO: Writing – original draft, Writing – review & editing. WH: Writing – review & editing. MJ: Writing – review & editing. QY: Writing – review & editing. YG: Writing – review & editing. MR: Writing – review & editing. QQ: Writing – review & editing. JZ: Writing – review & editing. QS: Writing – review & editing. FZ: Writing – review & editing. YW: Writing – original draft, Writing – review & editing.

Funding

The authors declare financial support was received for the research, authorship, and/or publication of this article. This work has been funded by the National Natural Science Foundation of China (Nos. 82102402, 82072237, and 32170187), Shaanxi Province Natural Science Funding (Nos. 2023-JC-JQ-63, 2021JQ-381, and

2021JM-007) and China Postdoctoral Science Foundation (Nos. 2020TQ0242 and 2020M683508), and Institutional Foundation of the First Affiliated Hospital of Xi'an Jiaotong University.

Acknowledgments

We thank the staff from the BL18U1/BL19U1 beamline for technical support during data collection at the National Center for Protein Sciences Shanghai (NCPSS) at Shanghai Synchrotron Radiation Facility.

Conflict of interest

The authors declare that the research was conducted in the absence of any commercial or financial relationships that could be construed as a potential conflict of interest.

Publisher's note

All claims expressed in this article are solely those of the authors and do not necessarily represent those of their affiliated organizations, or those of the publisher, the editors and the reviewers. Any product that may be evaluated in this article, or claim that may be made by its manufacturer, is not guaranteed or endorsed by the publisher.

Supplementary material

The Supplementary Material for this article can be found online at: <https://www.frontiersin.org/articles/10.3389/fmicb.2024.1293990/full#supplementary-material>

References

- Adams, P. D., Afonine, P. V., Bunkóczi, G., Chen, V. B., Davis, I. W., Echols, N., et al. (2010). PHENIX: A comprehensive python-based system for macromolecular structure solution. *Acta Crystallogr. D Biol. Crystallogr.* 66, 213–221. doi: 10.1107/S0907444909052925
- Aguirre, A., Lejona, S., Vescovi, E. G., and Soncini, F. C. (2000). Phosphorylated PmrA interacts with the promoter region of *ugd* in *Salmonella enterica* serovar typhimurium. *J. Bacteriol.* 182, 3874–3876. doi: 10.1128/jb.182.13.3874-3876.2000
- Almasaudi, S. B. (2018). *Acinetobacter* spp. as nosocomial pathogens: Epidemiology and resistance features. *Saudi J. Biol. Sci.* 25, 586–596. doi: 10.1016/j.sjbs.2016.02.009
- Bachhaw, P., and Stock, A. M. (2007). Crystal structures of the receiver domain of the response regulator PhoP from *Escherichia coli* in the absence and presence of the phosphoryl analog beryllifluoride. *J. Bacteriol.* 189, 5987–5995. doi: 10.1128/jb.00049-07
- Bagińska, N., Pichlak, A., Górski, A., and Jończyk-Matysiak, E. (2019). Specific and selective bacteriophages in the fight against multidrug-resistant *Acinetobacter baumannii*. *Virol. Sin.* 34, 347–357. doi: 10.1007/s12250-019-00125-0
- Beceiro, A., Llobet, E., Aranda, J., Bengoechea, J. A., Doumith, M., Hornsey, M., et al. (2011). Phosphoethanolamine modification of lipid A in colistin-resistant variants of *Acinetobacter baumannii* mediated by the pmrAB two-component regulatory system. *Antimicrob. Agents Chemother.* 55, 3370–3379. doi: 10.1128/AAC.00079-11
- Bourret, R. B. (2010). Receiver domain structure and function in response regulator proteins. *Curr. Opin. Microbiol.* 13, 142–149.
- Büchler, A. C., Gehring, C., Widmer, A. F., Egli, A., and Tschudin-Sutter, S. (2018). Risk factors for colistin-resistant *Enterobacteriaceae* in a low-endemicity setting for carbapenem resistance—a matched case-control study. *Eurosurveillance* 23:1700777. doi: 10.2807/1560-7917.ES.2018.23.30.1700777
- Chin, C. Y., Gregg, K. A., Napier, B. A., Ernst, R. K., and Weiss, D. S. (2015). A PmrB-regulated deacetylase required for lipid A modification and polymyxin resistance in *Acinetobacter baumannii*. *Antimicrob. Agents Chemother.* 59, 7911–7914. doi: 10.1128/aac.00515-15
- Cho, H., Wang, W., Kim, R., Yokota, H., Damo, S., Kim, S.-H., et al. (2001). BeF acts as a phosphate analog in proteins phosphorylated on aspartate: Structure of a BeF complex with phosphoserine phosphatase. *Proc. Natl. Acad. Sci. U.S.A.* 98, 8525–8530. doi: 10.1073/pnas.131213698
- Dereeper, A., Guignon, V., Blanc, G., Audic, S., Buffet, S., Chevenet, F., et al. (2008). Phylogeny.fr: Robust phylogenetic analysis for the non-specialist. *Nucleic Acids Res.* 36, W465–W469. doi: 10.1093/nar/gkn180
- Duperthuy, M. (2020). Antimicrobial peptides: Virulence and resistance modulation in gram-negative bacteria. *Microorganisms* 8:280.
- Emsley, P., and Cowtan, K. (2004). Coot: Model-building tools for molecular graphics. *Acta Crystallogr. D Biol. Crystallogr.* 60, 2126–2132.

- Farshadzadeh, Z., Taheri, B., Rahimi, S., Shoja, S., Pourhajibagher, M., Haghighi, M. A., et al. (2018). Growth rate and biofilm formation ability of clinical and laboratory-evolved colistin-resistant strains of *Acinetobacter baumannii*. *Front. Microbiol.* 9:153. doi: 10.3389/fmicb.2018.00153
- Gao, R., Bouillet, S., and Stock, A. M. (2019). Structural basis of response regulator function. *Annu. Rev. Microbiol.* 73, 175–197.
- Gasteiger, E., Hoogland, C., Gattiker, A., Duvaud, S. E., Wilkins, M. R., Appel, R. D., et al. (2005). *Protein identification and analysis tools on the ExPASy server*. Berlin: Springer.
- Gerson, S., Lucassen, K., Wille, J., Nodari, C. S., Stefanik, D., Nowak, J., et al. (2020). Diversity of amino acid substitutions in PmrCAB associated with colistin resistance in clinical isolates of *Acinetobacter baumannii*. *Int. J. Antimicrob. Agents* 55:105862. doi: 10.1016/j.ijantimicag.2019.105862
- Gunn, J. S. (2008). The *Salmonella* PmrAB regulon: Lipopolysaccharide modifications, antimicrobial peptide resistance and more. *Trends Microbiol.* 16, 284–290. doi: 10.1016/j.tim.2008.03.007
- Hamidian, M., and Nigro, S. J. (2019). Emergence, molecular mechanisms and global spread of carbapenem-resistant *Acinetobacter baumannii*. *Microb. Genom.* 5:e000306. doi: 10.1099/mgen.0.000306
- Hashemi, M. M., Holden, B. S., Coburn, J., Taylor, M. F., Weber, S., Hilton, B., et al. (2019). Proteomic analysis of resistance of gram-negative bacteria to chlorhexidine and impacts on susceptibility to colistin, antimicrobial peptides, and ceragenins. *Front. Microbiol.* 10:210. doi: 10.3389/fmicb.2019.00210
- Kabsch, W. (2010). XDS. *Acta Crystallogr. D Biol. Crystallogr.* 66(Pt 2), 125–132. doi: 10.1107/s0907444909047337
- Kox, L. F., Wösten, M. M., and Groisman, E. A. (2000). A small protein that mediates the activation of a two-component system by another two-component system. *EMBO J.* 19, 1861–1872. doi: 10.1093/emboj/19.8.1861
- Krissinel, E., and Henrick, K. (2007). Inference of macromolecular assemblies from crystalline state. *J. Mol. Biol.* 372, 774–797. doi: 10.1016/j.jmb.2007.05.022
- Lee, S.-Y., Yun, S. H., Lee, H., Yi, Y.-S., Park, E. C., Kim, W., et al. (2020). Analysis of the extracellular proteome of colistin-resistant Korean *acinetobacter baumannii* strains. *ACS Omega* 5, 5713–5720. doi: 10.1021/acsomega.9b03723
- Lima, W. G., Alves, M. C., Cruz, W. S., and Paiva, M. C. (2018). Chromosomally encoded and plasmid-mediated polymyxins resistance in *Acinetobacter baumannii*: A huge public health threat. *Eur. J. Clin. Microbiol. Infect. Dis.* 37, 1009–1019. doi: 10.1007/s10096-018-3223-9
- Llewellyn, A. C., Zhao, J., Song, F., Parvathareddy, J., Xu, Q., Napier, B. A., et al. (2012). NaxD is a deacetylase required for lipid A modification and F rancisella pathogenesis. *Mol. Microbiol.* 86, 611–627. doi: 10.1111/mtmi.12004
- Lou, Y. C., Wang, I., Rajasekaran, M., Kao, Y. F., Ho, M. R., Hsu, S. T., et al. (2014). Solution structure and tandem DNA recognition of the C-terminal effector domain of PmrA from *Klebsiella pneumoniae*. *Nucleic Acids Res.* 42, 4080–4093. doi: 10.1093/nar/gkt1345
- Lou, Y. C., Weng, T. H., Li, Y. C., Kao, Y. F., Lin, W. F., Peng, H. L., et al. (2015). Structure and dynamics of polymyxin-resistance-associated response regulator PmrA in complex with promoter DNA. *Nat. Commun.* 6:8838. doi: 10.1038/ncomms9838
- Ouyang, Z., Zheng, F., Chew, J. Y., Pei, Y., Zhou, J., Wen, K., et al. (2019). Deciphering the activation and recognition mechanisms of *Staphylococcus aureus* response regulator ArlR. *Nucleic Acids Res.* 47, 11418–11429. doi: 10.1093/nar/gkz891
- Ouyang, Z., Zheng, F., Zhu, L., Felix, J., Wu, D., Wu, K., et al. (2021). Proteolysis and multimerization regulate signaling along the two-component regulatory system AdeRS. *iScience* 24:102476. doi: 10.1016/j.isci.2021.102476
- Palethorpe, S., Milton, M. E., Pesci, E. C., and Cavanagh, J. (2022). Structure of the *Acinetobacter baumannii* PmrA receiver domain and insights into clinical mutants affecting DNA binding and promoting colistin resistance. *J. Biochem.* 170, 787–800. doi: 10.1093/jb/mvab102
- Pelletier, M. R., Casella, L. G., Jones, J. W., Adams, M. D., Zurawski, D. V., Hazlett, K. R., et al. (2013). Unique structural modifications are present in the lipopolysaccharide from colistin-resistant strains of *Acinetobacter baumannii*. *Antimicrob. Agents Chemother.* 57, 4831–4840. doi: 10.1128/AAC.00865-13
- Pescaretti, M. L. M., López, F. E., Morero, R. D., and Delgado, M. A. (2011). The PmrA/PmrB regulatory system controls the expression of the wzzfepE gene involved in the O-antigen synthesis of *Salmonella enterica* serovar typhimurium. *Microbiology* 157(Pt 9), 2515–2521. doi: 10.1099/mic.0.050088-0
- Samantha, A., and Vrielink, A. (2020). Lipid A phosphoethanolamine transferase: Regulation, structure and immune response. *J. Mol. Biol.* 432, 5184–5196.
- Scheller, L., Schmollack, M., Bertschi, A., Mansouri, M., Saxena, P., and Fussenegger, M. (2020). Phosphoregulated orthogonal signal transduction in mammalian cells. *Nat. Commun.* 11, 3085. doi: 10.1038/s41467-020-16895-1
- Seleim, S. M., Mostafa, M. S., Ouda, N. H., and Shash, R. Y. (2022). The role of pmrCAB genes in colistin-resistant *Acinetobacter baumannii*. *Sci. Rep.* 12:20951. doi: 10.1038/s41598-022-25226-x
- Sinha, A., Nyongesa, S., Viau, C., Gruenheid, S., Veyrier, F. J., and Le Moual, H. (2019). PmrC (EptA) and CptA negatively affect outer membrane vesicle production in *Citrobacter rodentium*. *J. Bacteriol.* 201:e00454–18. doi: 10.1128/JB.00454-18
- Thompson, J. D., Higgins, D. G., and Gibson, T. J. (1994). CLUSTAL W: Improving the sensitivity of progressive multiple sequence alignment through sequence weighting, position-specific gap penalties and weight matrix choice. *Nucleic Acids Res.* 22, 4673–4680. doi: 10.1093/nar/22.22.4673
- Tucker, A. T., Nowicki, E. M., Boll, J. M., Knauf, G. A., Burdis, N. C., Trent, M. S., et al. (2014). Defining gene-phenotype relationships in *Acinetobacter baumannii* through one-step chromosomal gene inactivation. *MBio* 5:e01313–14. doi: 10.1128/mBio.01313-14
- Uc-Cachón, A. H., Gracida-Orsorio, C., Luna-Chi, I. G., Jiménez-Guillermo, J. G., and Molina-Salinas, G. M. (2019). High prevalence of antimicrobial resistance among gram-negative isolated bacilli in intensive care units at a tertiary-care hospital in Yucatán Mexico. *Medicina* 55:588. doi: 10.3390/medicina55090588
- Uppalapati, S. R., Sett, A., and Pathania, R. (2020). The outer membrane proteins OmpA, CarO, and OprD of *Acinetobacter baumannii* confer a two-pronged defense in facilitating its success as a potent human pathogen. *Front. Microbiol.* 11:589234. doi: 10.3389/fmicb.2020.589234
- Vaara, M. (2009). New approaches in peptide antibiotics. *Curr. Opin. Pharmacol.* 9, 571–576.
- Wang, C. H., Siu, L. K., Chang, F. Y., Chiu, S. K., and Lin, J. C. (2021). A Resistance Mechanism in Non-mcr Colistin-Resistant *Escherichia coli* in Taiwan: R81H Substitution in PmrA is an independent factor contributing to colistin resistance. *Microbiol. Spectr.* 9:e0002221. doi: 10.1128/Spectrum.00222-21
- Warner, D. M., Duval, V., and Levy, S. B. (2013). The contribution of PmrAB to the virulence of a clinical isolate of *Escherichia coli*. *Virulence* 4, 634–637. doi: 10.4161/viru.25931
- Weinstein, M. P. (2018). *Methods for dilution antimicrobial susceptibility tests for bacteria that grow aerobically*, 11th Edn. Wayne, PA: Clinical and Laboratory Standards Institute.
- Wen, Y., Ouyang, Z., Yu, Y., Zhou, X., Pei, Y., Devreese, B., et al. (2017b). Mechanistic insight into how multidrug resistant *Acinetobacter baumannii* response regulator AdeR recognizes an intercistronic region. *Nucleic Acids Res.* 45, 9773–9787. doi: 10.1093/nar/gkx624
- Wen, Y., Ouyang, Z., Devreese, B., He, W., Shao, Y., Lu, W., et al. (2017a). Crystal structure of master biofilm regulator CsgD regulatory domain reveals an atypical receiver domain. *Protein Sci.* 26, 2073–2082. doi: 10.1002/pro.3245
- Yoon, E., McGann, P., Lesho, E., Waterman, P., Clifford, R., Courvalin, P., et al. (2013). “Biological cost of colistin-resistance in clinical isolates of *Acinetobacter baumannii*,” in *Proceedings of the 23rd European congress of clinical microbiology and infectious diseases*, Berlin.
- Zheng, L., Baumann, U., and Reymond, J.-L. (2004). An efficient one-step site-directed and site-saturation mutagenesis protocol. *Nucleic Acids Res.* 32:e115. doi: 10.1093/nar/gnh110



OPEN ACCESS

EDITED BY

Mona I. Shaaban,
Mansoura University, Egypt

REVIEWED BY

Bijit Bhowmik,
Croda Inc, United States
Leming Sun,
Northwestern Polytechnical University, China
Saurabh Mishra,
Cornell University, United States

*CORRESPONDENCE

Tieli Zhou
✉ wytli@163.com
Mo Shen
✉ shenmo601@163.com

RECEIVED 10 September 2023

ACCEPTED 10 April 2024

PUBLISHED 30 April 2024

CITATION

Han Y, Zhang Y, Zhang X, Huang Z,
Kong J, Wang X, Chen L, Wang Y,
Cao J, Zhou T and Shen M (2024) PAM-1: an
antimicrobial peptide with promise against
ceftazidime-avibactam resistant *Escherichia coli*
infection.
Front. Microbiol. 15:1291876.
doi: 10.3389/fmicb.2024.1291876

COPYRIGHT

© 2024 Han, Zhang, Zhang, Huang, Kong,
Wang, Chen, Wang, Cao, Zhou and Shen. This
is an open-access article distributed under
the terms of the [Creative Commons
Attribution License \(CC BY\)](#). The use,
distribution or reproduction in other forums is
permitted, provided the original author(s) and
the copyright owner(s) are credited and that
the original publication in this journal is cited,
in accordance with accepted academic
practice. No use, distribution or reproduction
is permitted which does not comply with
these terms.

PAM-1: an antimicrobial peptide with promise against ceftazidime-avibactam resistant *Escherichia coli* infection

Yijia Han^{1,2}, Yi Zhang², Xiaodong Zhang¹, Zeyu Huang¹,
Jingchun Kong², Xiuxiu Wang¹, Lijiang Chen¹, Yue Wang¹,
Jianming Cao², Tieli Zhou^{1*} and Mo Shen^{1*}

¹Department of Clinical Laboratory, Key Laboratory of Clinical Laboratory Diagnosis and Translational Research of Zhejiang Province, The First Affiliated Hospital of Wenzhou Medical University, Wenzhou, China, ²School of Laboratory Medicine and Life Science, Wenzhou Medical University, Wenzhou, China

Introduction: Antibiotic misuse and overuse have led to the emergence of carbapenem-resistant bacteria. The global spread of resistance to the novel antibiotic combination ceftazidime-avibactam (CZA) is becoming a severe problem. Antimicrobial peptide PAM-1 offers a novel approach for treating infections caused by antibiotic-resistant bacteria. This study explores its antibacterial and anti-biofilm activities and mechanisms against CZA-resistant *Escherichia coli* (*E. coli*), evaluating its stability and biosafety as well.

Methods: The broth microdilution method, growth curve analysis, crystal violet staining, scanning electron microscopy, and propidium iodide staining/N-phenyl-1-naphthylamine uptake experiments were performed to explore the antibacterial action and potential mechanism of PAM-1 against CZA-resistant *E. coli*. The biosafety in diverse environments of PAM-1 was evaluated by red blood cell hemolysis, and cytotoxicity tests. Its stability was further assessed under different temperatures, serum concentrations, and ionic conditions using the broth microdilution method to determine its minimum inhibitory concentration (MIC). *Galleria mellonella* infection model and RT-qPCR were used to investigate the in vivo antibacterial and anti-inflammatory effects.

Results and discussion: *In vitro* antibacterial experiments demonstrated that the MICs of PAM-1 ranged from 2 to 8 µg/mL, with its effectiveness sustained for a duration of 24 h. PAM-1 exhibited significant antibiofilm activities against CZA-resistant *E. coli* ($p < 0.05$). Furthermore, Membrane permeability test revealed that PAM-1 may exert its antibacterial effect by disrupting membrane integrity by forming transmembrane pores ($p < 0.05$). Red blood cell hemolysis and cytotoxicity tests revealed that PAM-1 exerts no adverse effects at experimental concentrations ($p < 0.05$). Moreover, stability tests revealed its effectiveness in serum and at room temperature. The *Galleria mellonella* infection model revealed that PAM-1 can significantly improve the survival rate of *Galleria mellonella* (>50%) for *in vivo* treatment. Lastly, RT-qPCR revealed that PAM-1 downregulates the expression of inflammatory cytokines ($p < 0.05$). Overall, our study findings highlight the potential of PAM-1 as a therapeutic agent for CZA-resistant *E. coli* infections, offering new avenues for research and alternative antimicrobial therapy strategies.

KEYWORDS

Escherichia coli, biofilm, CZA -resistant, PAM-1, antimicrobial peptide

1 Introduction

Global public health is increasingly threatened by antibiotic resistance, with carbapenem-resistant *Enterobacteriaceae* (CRE) posing a significant challenge by elevating infection rates and mortality (Satlin et al., 2017; van Duin et al., 2020). The limited effectiveness of traditional antibiotics led to the 2015 FDA (Food and Drug Administration) approval of ceftazidime-avibactam (CZA), a novel combination of a cephalosporin and a β -lactamase inhibitor. This innovative combination exhibits *in vitro* activity against *Enterobacterales* harboring β -lactamases of Ambler class A [including extended-spectrum β -lactamases (ESBLs) and *Klebsiella pneumoniae* carbapenemases (KPC)], class C (AmpC cephalosporinases), and some class D enzymes (e.g., OXA-48-type, many of which also possess ESBLs) (Morrill et al., 2015; Falcone et al., 2016; Livermore et al., 2018; Zhang et al., 2018). However, the subsequent global increase in CZA usage has gradually increased CZA resistance, with new cases of CZA-resistant *E. coli* strains being frequently reported (Shields et al., 2016, 2017; Hernández-García et al., 2021). Therefore, developing novel antimicrobial drugs to combat CZA-resistant *E. coli* infections is urgently warranted.

Antimicrobial peptides (AMPs), an intrinsic component of the innate immune system in several animals, confer protection against foreign microorganisms and infectious threats (Pasupuleti et al., 2012). In general, these peptides are short and positively charged and exhibit broad-spectrum antibacterial activity as well as effects on biofilms (Spencer et al., 2018; Luo and Song, 2021). Furthermore, AMPs can regulate inflammatory responses and promote wound healing (Nguyen et al., 2020; Thapa et al., 2020). To enhance the application of antimicrobial peptides (AMPs) in clinical antimicrobial treatments, researchers are actively engaged in identifying and screening AMPs that not only demonstrate potent antimicrobial effects but also exhibit a high level of safety.

PAM-1, an antimicrobial peptide sourced from the cathelicidin gene family in the platypus genome, exhibits significant antibacterial effects against standard strains of *Bacillus subtilis*, *Staphylococcus aureus*, *Streptococcus uberis*, *Streptococcus pyogenes*, *E. coli*, *Salmonella cholerae*, and *Pseudomonas aeruginosa* (Wang et al., 2011). Through bioinformatics analysis, it is predicted that PAM-1 possesses a wide-ranging antibacterial activity against various bacteria. However, regrettably, the antibacterial and antibiofilm activities and the mechanisms of action of PAM-1 against clinical strains remain unelucidated in previous studies.

In the present study, a series of experiments were conducted to investigate the antibacterial, antibiofilm, and anti-inflammatory activities of PAM-1 against CZA-resistant *E. coli* strains. The potential mechanisms by which PAM-1 exerts its antibacterial effects were elucidated, and its stability and safety were thoroughly assessed. Additionally, the *in vivo* efficacy of PAM-1 was evaluated using the *Galleria mellonella* (*G. mellonella*) infection model. The findings of this study suggest that PAM-1 holds promise as a novel antibacterial agent for combating CZA-resistant *E. coli* infections.

2 Methods

2.1 AMP and antibiotics

PAM-1 (95.66%, 100 mg) was synthesized by Nanjing Yuanpeptide Biotechnology Co., Ltd. (Nanjing, China). The amino acid sequence

of PAM-1 is RTKRRIKLIKNGVKKVKDILKNNNIILPGSNEK (Wang et al., 2011). To prepare PAM-1 for the experiments, it was dissolved in double distilled water and stored at -20°C . Ceftazidime ($\geq 99\%$), avibactam ($\geq 99\%$), meropenem (MEM, $\geq 98.0\%$), and imipenem (IPM, $\geq 98.0\%$) used in this study were purchased from Wenzhou Kangtai Biotechnology Co., Ltd. (Zhejiang, China).

2.2 Characterization of PAM-1

PAM-1 was analyzed using a predictive analysis tool in ProtParam of ExPASy (<https://web.expasy.org/protparam/>). The physical and chemical properties of PAM-1, including net charge and relative molecular mass, were determined. The antibacterial activity of PAM-1 was predict using the online software CAMPR3 (<http://www.camp3.bicnirrh.res.in/>).

2.3 Bacteria isolates and growth conditions

Six CZA-susceptible *E. coli* and six CZA-resistant *E. coli* isolates were selected from the First Affiliated Hospital of Wenzhou Medical University. All isolates were identified using MALDI-TOF MS (Quintilla et al., 2018; Ashfaq et al., 2022) (BioMerieux, France). These clinically relevant *E. coli* strains were preserved by freezing them at -80°C in Luria-Bertani (LBT, hermo Fisher Scientific, America) broth containing 30% glycerol. *E. coli* ATCC 25922 was used as the quality control strain.

2.4 Enzyme types of the 12 *Escherichia coli* strains

DNA was extracted from the 12 *E. coli* strains using a bacterial genome extraction kit (Solarbio, Beijing, China) according to the manufacturer's instructions (Zeng et al., 2022). The resistant determinants, including carbapenem genes (*bla*_{KPC}, *bla*_{NDM}, *bla*_{IMP}, *bla*_{VIM}, *bla*_{OXA-23}, and *bla*_{OXA-48}) and ESBL genes (*bla*_{SHV}, *bla*_{TEM}, *bla*_{CTX-M-1}, *bla*_{CTX-M-9}, and *bla*_{CTX-M-14}), were examined via PCR using specific primers (Supplementary Table S1). Subsequently, the positive PCR products were sequenced and aligned using the BLAST tool in NCBI (<https://blast.ncbi.nlm.nih.gov/Blast.cgi>).

2.5 Antimicrobial activity of PAM-1, CZA, and carbapenems against *Escherichia coli*

The broth microdilution method was used to determine the minimum inhibitory concentrations (MICs) of CZA, MEM, IPM, and PAM-1 against the 12 *E. coli* strains (García-Cobos et al., 2008). The 0.5 McFarland bacterial suspension was 1:100 diluted by Mueller Hinton broth (MHB, Thermo Fisher Scientific, America). Then, 100 μL of the bacterial solution was added to a 96-well microplate containing various concentrations of the antibiotics: CZA, MEM, IPM, and PAM-1. The microplates were incubated at 37°C for 16–18 h. The results were interpreted based on the 2020 Clinical and Laboratory Standards Institute guidelines (CLSI). MIC was defined as the lowest concentration of an antibiotic that completely inhibited bacterial growth.

To determine the CRE (MBC), 100 μL of the bacterial suspension from the well corresponding to the MIC and three subsequent wells was

collected and spread onto LB agar plates. Then, the plates were incubated at 37°C for 16–20 h. MBC was determined as the drug concentration that resulted in no bacterial colony formation on the plate.

Each experiment was independently repeated three times to ensure the accuracy and reproducibility of the results.

2.6 Growth curve analysis

The growth curve was determined according to a previously described method, with some modifications (Jayathilaka et al., 2021). The diluted *E. coli* culture was added to a 96-well plate along with PAM-1 at concentrations corresponding to its 1/2 MIC, 1 MIC, 2 MIC, and 4 MIC (ranging from 1–32 µg/mL). The plate was incubated at 37°C for 24 h. Bacterial growth was monitored by measuring the absorbance at 600 nm at different time intervals (0, 2, 4, 6, 8, 10, 12, and 24 h). Each experiment was repeated three times to ensure accuracy and reproducibility.

2.7 Biofilm formation and eradication tests

The effect of PAM-1 on biofilm formation and eradication was determined by performing crystal violet staining (O'Loughlin et al., 2013). The bacterial culture was added to a 96-well plate with the corresponding concentration of PAM-1. After incubation for 24 h at 37°C, the 96-well plate was gently washed with phosphate-buffered saline (PBS, Beijing Solarbio Science & Technology Co., Ltd., Beijing, China) to remove any planktonic bacteria. Then, the plate was allowed to naturally dry at room temperature. Subsequently, a 0.1% crystal violet solution was added to each well, followed by incubation at 37°C for 15 min. After washing the plate with PBS and allowing it to naturally dry, 200 µL of a solution containing 95% ethanol and 5% acetic acid was added to dissolve the crystal violet. Biofilm biomass was calculated by measuring the absorbance at 595 nm. Two separate tests were performed: one to evaluate the effect of PAM-1 on biofilm formation (where the drug was added before biofilm formation) and another to evaluate the eradication of mature biofilms (where the drug was added after biofilm formation). Each test was conducted three times, and each experiment within a test was repeated three times for reliability and consistency.

2.8 Scanning electron microscopy

The SEM was determined according to a previously described method, with some modifications (Zhang et al., 2019). Silicon wafers were placed in the wells and 10 µL of the bacterial suspension was added to 990 µL of MHB containing PAM-1. Then, the plates were incubated for 24 h. Thereafter, the wafers were cleaned three times with PBS, fixed with 2.5% glutaraldehyde, and dehydrated for 5 min using an ethanol concentration gradient (30, 50, 70, 80, 90, 95, and 100%). The final samples were air-dried, gold-sprayed, and observed under a scanning electron microscope (SU8010, Hitachi, Japan).

2.9 Membrane permeability test and ROS detection

To investigate the mechanism of antimicrobial activity of PAM-1, membrane permeability tests were conducted as described previously,

with some modifications (Liu et al., 2017). The bacteria suspension was shaken in the medium to the logarithmic stage and divided into equal parts. Then, different concentrations of PAM-1 were added to the bacterial suspension and was continued to be shaken for 2 h. The sample after centrifugation were resuspended with propidium iodide (PI, Beijing Solarbio Science & Technology Co., Ltd., Beijing, China) and N-phenyl-1-naphthylamine (NPN, Beijing Solarbio Science & Technology Co., Ltd., Beijing, China) solution and incubated in a water bath at 37°C for 30 min. Then, the samples were scanned at excitation wavelengths of 535 nm and 350 nm and emission wavelengths of 615 nm (PI) and 420 nm (NPN), respectively, using a microplate reader (BioTek Synergy NEO2, United States).

To detect reactive oxygen species (ROS), 500 µL of the bacterial suspension containing dichlorodihydrofluorescein diacetate (DCFH-DA, Shanghai Generay Biotech Co., Ltd) was incubated at 37°C for 60 min. After removing excess DCFH-DA probes, the cells were then treated with PAM-1 at 30°C for 2 h. Sterile distilled water was used as the blank control. All samples were scanned at an excitation wavelength of 488 nm and an emission wavelength of 535 nm using a microplate reader (BioTek Synergy NEO2). This assay aimed to investigate the mechanism of action of PAM-1. Each experiment was independently repeated three times.

2.10 Expression of proinflammatory cytokines

To further evaluate the effect of PAM-1 on the expression of proinflammatory factors, reverse transcription quantitative PCR (RT-qPCR) was performed using a previously described method, with slight modifications (de Campos et al., 2020). RAW 264.7 (Procell Life Science and Technology Co., Ltd., China) cells were cultured overnight and Dulbecco's modified Eagle medium (DMEM, Thermo Fisher Scientific, USA) supplemented with 10% fetal bovine serum (FBS, Gibco, USA) was used to culture the cells. The cells were washed three times with PBS, and the culture medium was discarded. Bacteria at a multiplicity of infection (MOI) of 10 were added to infect the cells, followed by treatment with different concentrations of PAM-1 for 2 h. After removing the culture medium and washing with PBS, total RNA was extracted from RAW 264.7 cells using the Trizol total RNA extraction method.

Total RNA was extracted from RAW 264.7 cells using the Trizol total RNA extraction method (Tang et al., 2017; Trendel et al., 2019). After measuring the RNA concentration (DeNovix ultramicro-UV-visible spectrophotometer DS-11, USA), the extracted mRNA was converted into cDNA using the PrimeScript™ RT Reagent Kit according to the manufacturer's instructions. The expression of the inflammatory factors interleukin (IL)-1β and tumor necrosis factor (TNF)-α was assessed using an RT-qPCR system (S100™ Thermal Cycler PCR machine, BIO-RAD, USA). Table S1 lists the specific primers used in this analysis. The 2^{-ΔΔCT} method was used to evaluate the data (Xu et al., 2020), with all values normalized to the expression of the housekeeping gene β-actin. The experiment was conducted three times to ensure reliability and reproducibility.

2.11 Temperature stability

Next, based on a previous study (Dong et al., 2021), we evaluated whether PAM-1 activity is affected by various factors. *E. coli* DC 8873

and DC 8466 were selected as the test strains to explore the effect of temperature. The prepared drug was incubated at different temperatures (−80°C, −20°C, 4°C, 25°C, and 37°C) for 3, 12, and 24 h. The MIC of PAM-1 was determined using the broth microdilution method after the incubation period.

2.12 Serum stability

Next, we evaluated the effect of serum on PAM-1 activity (Zhang et al., 2022). PAM-1 was incubated at 37°C for 24 h with various serum concentrations (0, 5, and 10%). After co-incubating the bacterial culture with serum, the MIC value of PAM-1 was evaluated using the same method mentioned above.

2.13 Ions stability

The effects of the presence of salts on the antimicrobial activity were evaluated as previously described (Kim et al., 2018). PAM-1 was incubated at 37°C with different concentrations of NaCl (0, 50, 100, and 150 mM), CaCl₂ (0, 1.25, 2.5, and 5 mM) or MgCl₂ (0, 0.5, 1, and 2 mM) for 24 h. Subsequently, the MIC of PAM-1 was determined using the broth microdilution method.

2.14 Cytotoxicity of PAM-1

Using RAW 264.7 cells, the safety of PAM-1 was assessed using a previously described method with some modifications (da Luz et al., 2020). The cell suspension (100 µL) containing 1×10^5 cells was inoculated into the wells of a 96-well plate. Then, 10 µL of PAM-1 at various concentrations (1–256 µg/mL) was added to the medium. The plate was incubated at 37°C with 5% CO₂ for 12 h. Thereafter, 10 µL of Cell Counting Kit-8 solution (CCK-8, Beyotime, China) was added to each well, followed by incubation at room temperature in the dark for 1 h. The absorbance of the wells was measured at 450 nm using the SpectraMax iD5 enzyme-labeled meter (BECKMAN, USA). This experiment was repeated three times.

2.15 Hemolysis of red blood cells (RBCs)

The hemolytic activity of PAM-1 was determined as previously described (Dong et al., 2012). Female BALB/c mice were used according to the Chinese National Standards for Laboratory Animals (GB 14925–2010). The Zhejiang Association for Science and Technology SYXK approved these analyses (ID: SYXK [Zhejiang] 2018–0017) and were consistent with the Wenzhou Laboratory Animal Welfare and Ethics standards. Fresh whole blood samples were collected and centrifuged. The RBCs obtained were washed with normal saline and then resuspended with normal saline to form a 5% RBC suspension. PAM-1 at various concentrations (1–80 µg/mL) was added to the 5% RBC suspension in a total volume of 2 mL. After centrifugation, the supernatant was collected and transferred to a 96-well plate. The absorbance of the supernatant was measured at 540 nm to reflect the hemolysis degree. The hemolysis rate was

calculated using the following formula: Hemolysis rate (%) = $(OD_{\text{experimental group}} - OD_{\text{negative control group}}) / (OD_{\text{positive control group}} - OD_{\text{negative control group}})$, where OD represents the absorbance at 540 nm. The negative control group comprised only normal saline, whereas the positive control group comprised 0.1% Triton X-100. This experiment was performed three times.

2.16 In vivo effectiveness of PAM-1 in the *Galleria mellonella* model

The effectiveness of PAM-1 was evaluated *in vivo* by measuring the survival rate of the *G. mellonella* model, which is commonly used as a model organism for studying microbial infections (Tsai et al., 2016; Borjan et al., 2020). The larvae of *G. mellonella* used in this experiment were opalescent and weighed 250–300 mg. Overnight cultures of the bacteria were diluted to a density of 1.5×10^7 CFU/mL. Then, the samples were divided into two groups: control and treatment groups. Furthermore, the treatment group was divided into subgroups, with each subgroup receiving different concentrations of PAM-1 (1/2MIC × 7, 1 MIC × 7, and 2MIC × 7). Using a microinjector, 10 µL of the bacterial suspension (CZA-susceptible *E. coli* DC 8873 and CZA-resistant *E. coli* DC 8466) was injected into the rear left proleg of each *G. mellonella* larva. After 2 h, the control group was administered 10 µL of sterile saline, whereas the treatment group received an appropriate concentration of the PAM-1 injection. To compare the efficacy of PAM-1 with standard agents, CZA was used. The larvae were then incubated at 37°C to measure their survival after 7 days. Larvae were considered dead if they repeatedly failed to respond to physical stimuli. The main experimental outcome was the analysis of the survival rate of *G. mellonella* using Kaplan–Meier analysis and the log-rank test.

2.17 Statistical analysis

All experiments were conducted in triplicate. Data analysis was performed using Prism 8 (GraphPad Software Inc., CA, USA), and the data are presented as mean and standard deviation. Significance was determined by using the two-sample *t*-test and log-rank test and indicated as **p* < 0.05, ***p* < 0.01, and ****p* < 0.001.

3 Results

3.1 Physicochemical properties and determination of the antimicrobial activity of PAM-1

The properties and antibacterial activity of PAM-1 were determined using the Bioanalysis website. Table 1 presents the physical and chemical properties obtained via ProtParam analysis. PAM-1 comprises 34 amino acid residues, carries 9 net charges, and has an isoelectric point of 11.24. The GRAVY index of PAM-1 was −0.774 (negative value represents hydrophilicity), indicating that it exhibits good solubility.

TABLE 1 Analysis of the physicochemical properties of PAM-1.

Peptide	Net charge	Residue	PI	GRAVY	Molecular mass	Aliphatic index	Instability index
PAM-1	9	34	11.24	−0.774	3942.80	120.29	47.46

TABLE 2 Prediction of the antimicrobial activity of PAM-1.

Peptide	Residue	Random forest classifier	Discriminant analysis classifier
PAM-1	34	0.8235	0.991

Next, the antibacterial activity of PAM-1 was predicted via biogenic analysis using CAMPR3. Both algorithms (Random Forest Classifier and Discriminant Analysis classifier) revealed that PAM-1 had better antibacterial activity (Table 2).

3.2 MIC and MBC of PAM-1 against CZA-resistant *Escherichia coli*

Twelve nonrepetitive *E. coli* clinical isolates were selected. PCR was performed to determine the carbapenemase types of the experimental strains. Table 3 summarizes the MICs of PAM-1, CZA, and MEM and the MBC of PAM-1. These results suggest the effective antibacterial activity of PAM-1 against both CZA-resistant and susceptible *E. coli* strains. The MICs ranged from 2 to 8 µg/mL, whereas the MBCs ranged from 2 to 16 µg/mL. This indicates that PAM-1 exerts a bactericidal effect at the MBC.

3.3 PAM-1 inhibits bacterial growth

The effect of PAM-1 on bacterial growth was assessed by measuring OD₆₀₀ changes over 24 h. Figure 1 demonstrates that the growth of the experimental strains was inhibited within 24 h when PAM-1 concentration exceeded or was equal to the 1 MIC. This finding suggests that PAM-1 exhibits a prolonged antibacterial effect on *E. coli* at the 1 MIC, and it even demonstrates a 12 h antibacterial effect on DC 11308 at 1/2 MIC concentration.

3.4 PAM-1 inhibits biofilm growth and eradicates The formed biofilms

Crystal violet staining was used to determine the effect of PAM-1 treatment on inhibiting and eradicating biofilm formation. Figure 2A illustrates a noteworthy reduction in biofilm formation in the PAM-1-treated group compared to the control group. This observation suggests that 1/2 MIC concentration PAM-1 possesses the ability to inhibit the formation of *E. coli* biofilm. Furthermore, it has an analogous efficacy in eradicating the pre-formed biofilms. Additionally, the eradication of established biofilms is achieved in a concentration-dependent manner, as illustrated in Figure 2B.

3.5 PAM-1 destroys bacterial and biofilm structures under SEM

SEM analysis revealed significant morphological changes of *E. coli* biofilm treated with various concentrations of PAM-1 as compared with the untreated control group (Figure 3). In detail, SEM images exhibited a fully formed and dense biofilm in the control group, with no noticeable bacterial destruction. However, a significant decrease in its number and density and changes in its structure were observed after PAM-1 treatment. And some bacteria also showed damage to some extent.

3.6 PAM-1 increases the permeability of bacterial membranes

Figure 4 illustrates that PAM-1 increased bacterial membrane permeability. To investigate the changes in cell membrane permeability induced by PAM-1, two different assays were performed: PI staining and NPN uptake assay. PI is a probe that cannot penetrate the cell membrane and can only bind to the nucleic acid of bacteria with damaged membranes. On the other hand, NPN can help assess the permeability of the outer membrane. Normally, NPN is hindered by the intact outer membrane. However, if the outer membrane structure is compromised and its permeability is altered, NPN can enter the interior of the cell and emit fluorescence. Both PI staining and the NPN uptake assay revealed that the fluorescence intensity of PAM-1 treated group was significantly higher than that of untreated group, indicating that PAM-1 induced a dose-dependent increase in membrane permeability.

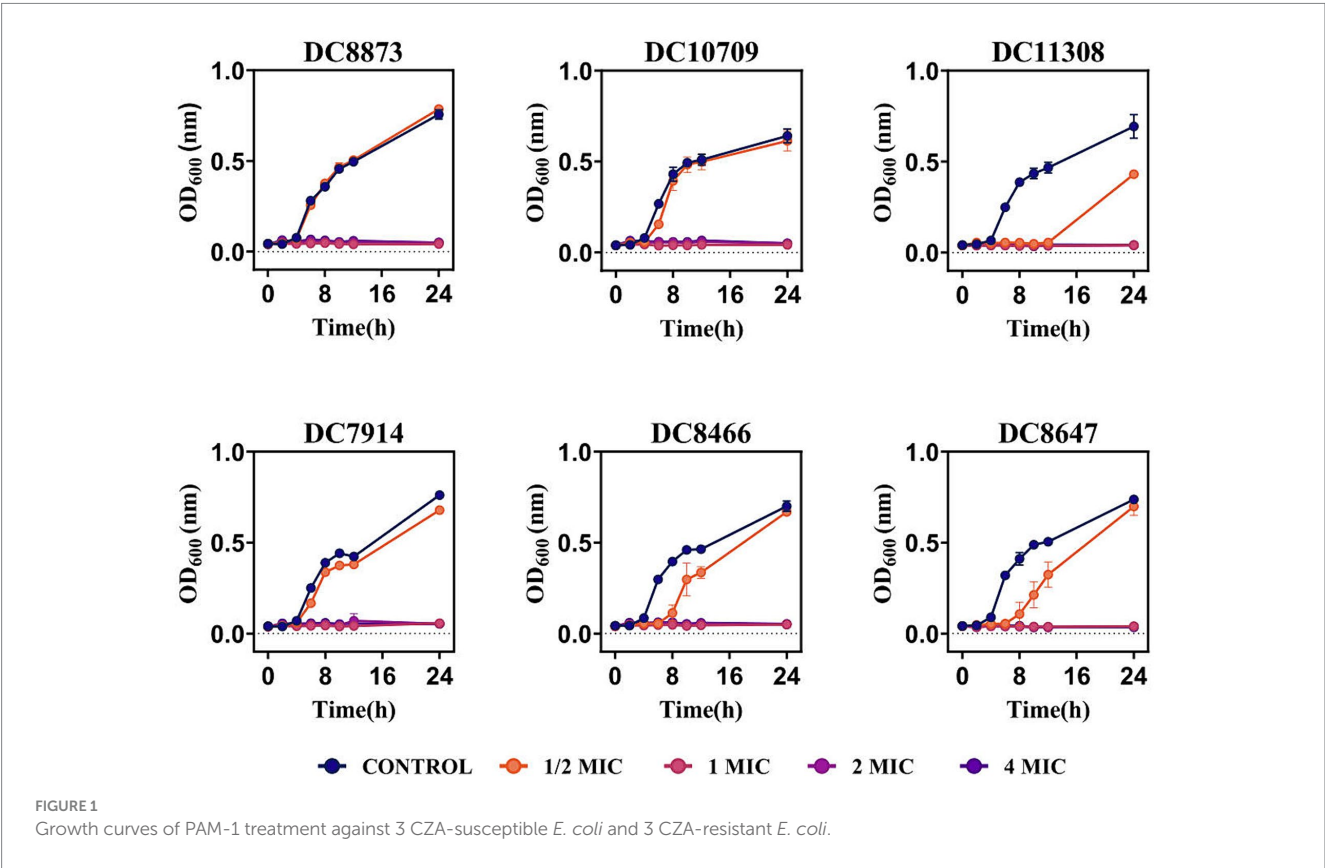
Furthermore, PAM-1 significantly increased ROS levels (Figure 4C); this may have played a role in its antibacterial activity. The level of ROS is closely correlated with the physiological activities of cells. When intracellular ROS production surpasses the cells' natural antioxidant defenses, it induces oxidative stress, resulting in cellular damage and apoptosis (Azad et al., 2009). Collectively, these findings suggest that even at low concentrations, PAM-1 can effectively damage bacterial membranes, increase cell membrane permeability, and ultimately lead to bacterial death.

3.7 PAM-1 decreases the expression of inflammatory cytokines

RT-qPCR was performed to elucidate the anti-inflammatory effects of PAM-1. Initially, using a cytotoxicity assay, we confirmed that an MOI of 10 did not affect cell viability. Therefore, RAW 264.7 cells were infected with bacterial cultures with an MOI of 10; then, the expression of IL-1β and TNF-α was analyzed. Figure 5 demonstrates that DC 8873 and DC 8466

TABLE 3 MICs of ceftazidime/avibactam, carbapenems, and PAM-1 and MBCs of PAM-1 against *Escherichia coli* and the carbapenemase types of strains.

Strains	MIC (μg/mL)					MBC (μg/mL)	Enzyme types
	PAM-1	CZA	MEM	IPM	ETP	PAM-1	
DC7914	4	>64/4 ^R	32 ^R	16 ^R	>64 ^R	4	NDM, TEM, CTX-M-9
DC8439	8	>64/4 ^R	8 ^R	4 ^R	8 ^R	8	NDM
DC8466	8	>64/4 ^R	4 ^R	4 ^R	4 ^R	8	NDM
DC8647	8	>64/4 ^R	8 ^R	8 ^R	8 ^R	16	NDM
DC8823	2	>64/4 ^R	16 ^R	16 ^R	16 ^R	2	NDM
DC10494	8	>64/4 ^R	4 ^R	4 ^R	8 ^R	8	NDM
DC8873	2	1/4 ^S	0.25 ^S	4 ^R	<0.12 ^S	8	TEM, SHV
DC10709	4	0.25/4 ^S	1 ^S	<0.12 ^S	8 ^R	8	CTXM-1, TEM, SHV
DC10740	4	0.5/4 ^S	<0.12 ^S	<0.12 ^S	4 ^R	16	CTX-M-9, SHV
DC11104	4	0.25/4 ^S	2 ^I	<0.12 ^S	1 ^I	16	CTX-M-1, TEM, SHV
DC11305	2	0.5/4 ^S	<0.12 ^S	<0.12 ^S	<0.12 ^S	2	CTX-M-1, TEM, SHV
DC11308	8	0.5/4 ^S	0.5 ^S	0.5 ^S	1 ^I	16	CTX-M-1, TEM, SHV
ATCC25922	4	0.125/4 ^S	0.06	0.25	0.015	4	/



significantly promoted IL-1 β and TNF- α expression compared with the negative control group. However, PAM-1 dose-dependently inhibited IL-1 β and TNF- α expression. The effect was more pronounced in DC 8466, which exhibited more significant inhibition of inflammatory cytokine. This indicates that PAM-1 possesses anti-inflammatory properties.

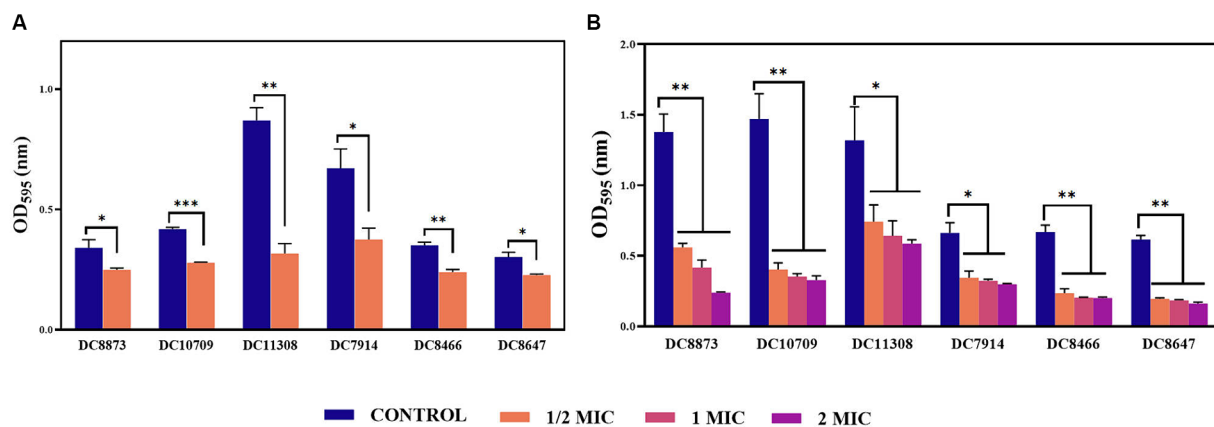


FIGURE 2

The effects of PAM-1 on *E. coli* biofilm. (A) The effect of PAM-1 on biofilm formation. (B) The effect of PAM-1 on the eradication of established biofilms. * $p < 0.05$, ** $p < 0.01$, *** $p < 0.001$ were analyzed by Student's *t*-test. The experiments were conducted thrice.

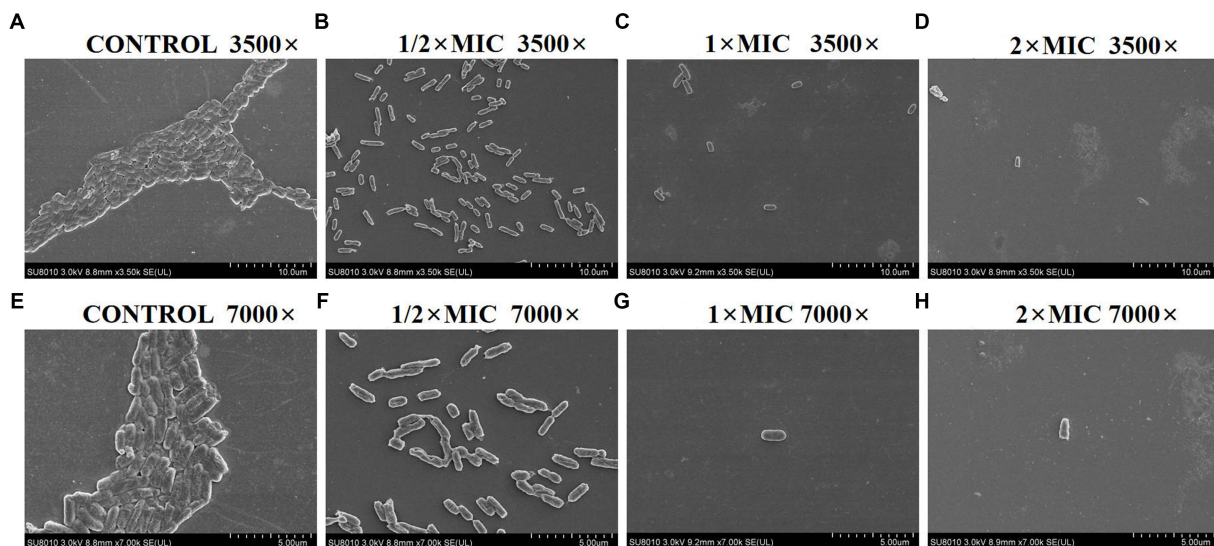


FIGURE 3

SEM images of *E. coli* DC 8466 biofilm and bacterial morphology results among various groups. (A) The broth control group, 3,500 \times , (E) 7,000 \times ; (B) PAM-1 (1/2 MIC), 3,500 \times , (F) 7,000 \times ; (C) PAM-1 (1 MIC), 3,500 \times , (G) 7,000 \times ; (D) PAM-1 (2 MIC), 3,500 \times , (H) 7,000 \times .

3.8 Stability of PAM-1

We investigated the stability of PAM-1 under different conditions, including changes in temperature, serum exposure, and presence of salt ions. Table 4 demonstrates that neither ambient nor low temperatures affected the antibacterial activity of PAM-1. Furthermore, based on the provided instructions, it can be stored at -20°C for extended periods. Moreover, we observed that PAM-1 maintained significant antibacterial activity even in the presence of 10% serum (Table 5). Unfortunately, PAM-1 exhibited poor performance in a saline environment, with the presence of NaCl, CaCl_2 , and MgCl_2 considerably decreasing its antibacterial efficacy (Table 6). This phenomenon could be attributed to the initial

interaction of the positively charged cationic peptide as it interacts with and neutralizes the negatively charged bacterial outer membrane through electrostatic interaction (Bin Hafeez et al., 2021). Moreover, the presence of salt ions not only establishes a salt bridge with lipopolysaccharides to stabilize the outer membrane but also leads to the need for higher concentrations of AMPs to compete with and replace the salt ions on the outer membrane.

3.9 Safety of PAM-1

To further investigate the security of PAM-1, RBC hemolysis and cytotoxicity were assessed (Figure 6). The hemolysis rate was

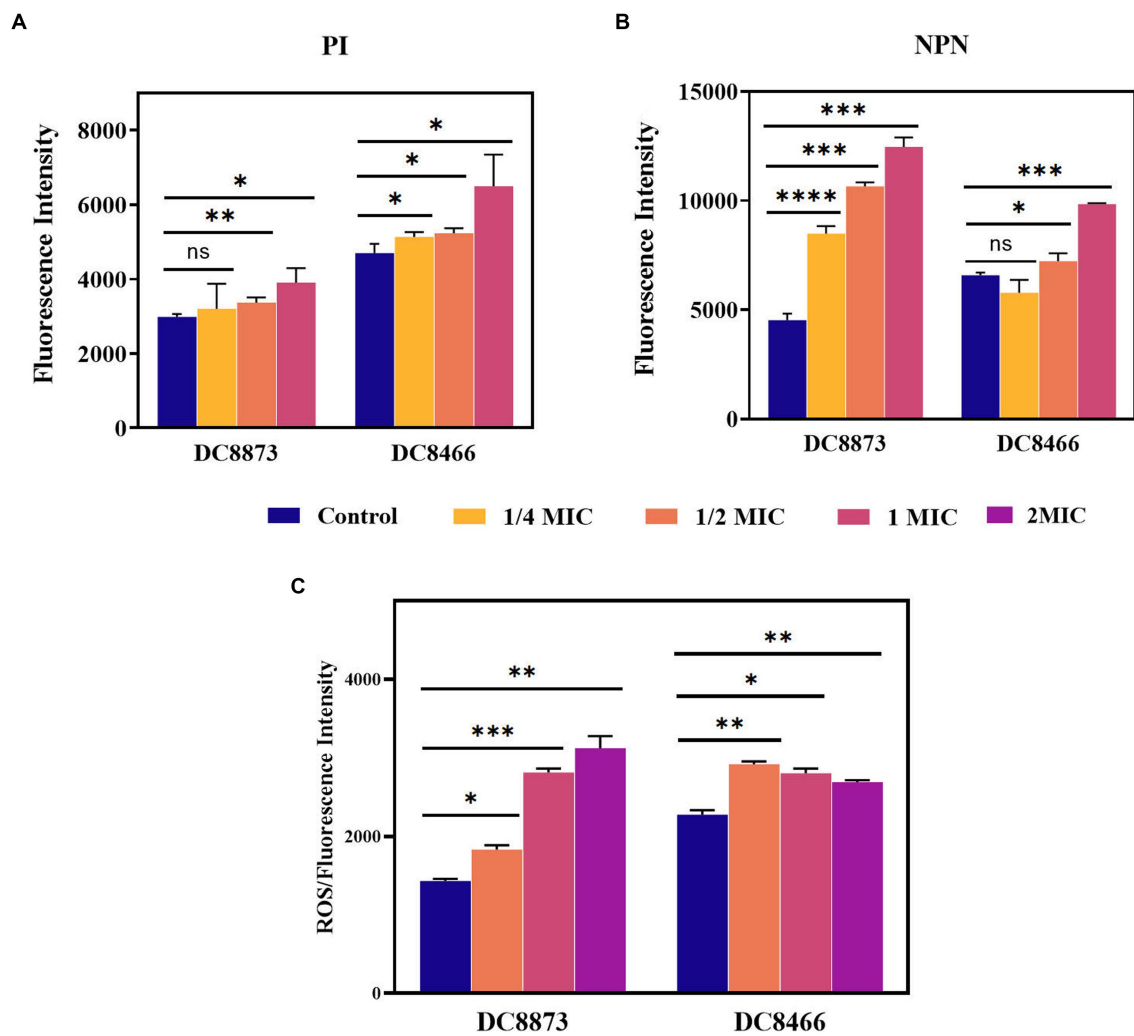


FIGURE 4 The antimicrobial mechanism of PAM-1 was investigated by PI (A), NPN (B), and (C) ROS. The fluorescence intensity of DC 8873 and DC 8466 treated with different concentrations of PAM-1. ns, not statistically significant; * $p < 0.05$, ** $p < 0.01$, *** $p < 0.001$, **** $p < 0.0001$.

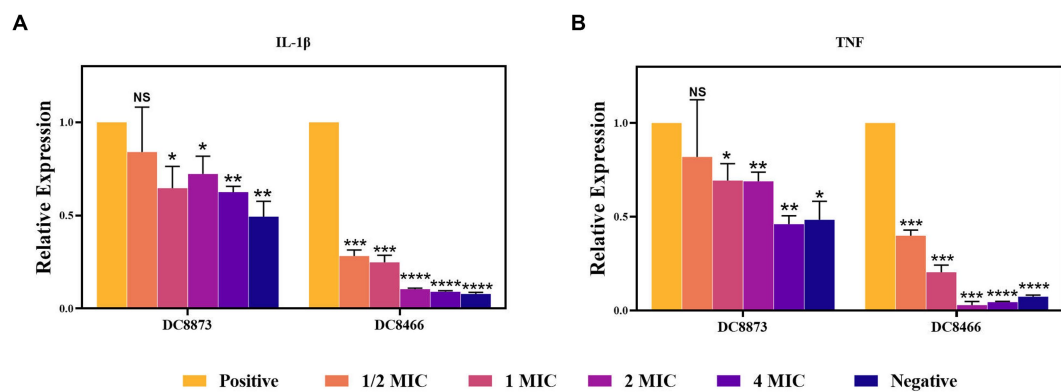


FIGURE 5 The effect of PAM-1 on RAW 264.7 inflammatory factor after *E. coli* infection. Negative, only cells are added; Positive, strain and cell co-infection (without PAM-1); NS, not statistically significant; * $p < 0.05$, ** $p < 0.01$, *** $p < 0.001$, **** $p < 0.0001$.

<3% even when PAM-1 concentration reached 80 $\mu\text{g/mL}$; furthermore, no visible hemolysis was observed (Figure 6A). In addition, PAM-1 exhibited no cytotoxicity in RAW 264.7 cells at a concentration of 256 $\mu\text{g/mL}$ (Figure 6B). Collectively, these findings suggest that PAM-1 holds promising prospects for *in vivo* applications.

TABLE 4 The effect of temperature on the antibacterial activity of PAM-1 [MIC ($\mu\text{g/mL}$)].

Temperature (°C)	Bacterial isolates					
	DC8873			DC8466		
	3 h	12 h	24 h	3 h	12 h	24 h
−80	2	2	2	8	8	8
−20	2	2	2	8	8	8
4	2	2	2	8	8	8
25	2	2	2	8	8	8
37	2	2	2	8	8	8

TABLE 5 The effect of serum on the antibacterial activity of PAM-1 [MIC ($\mu\text{g/mL}$)].

Serum concentration (%)	Bacterial isolates	
	DC8873	DC8466
0	2	8
5	2	8
10	2	8

3.10 PAM-1 can improve the survival rate of *Galleria mellonella*

Considering the findings from *in vitro* antibacterial studies, conducting *in vivo* experiments is vital to confirm the antibacterial activity of PAM-1 in living organisms. To this end, a *G. mellonella* infection model was developed to assess the *in vivo* bactericidal activity of PAM-1 and compare it with that of CZA (Figure 7). Compared with the control group, PAM-1 significantly improved the survival rate of *G. mellonella*. After 7 days of PAM-1 therapy, the survival rates of DC 8873 (CZA-susceptible *E. coli*) and DC 8466 (CZA-resistant *E. coli*) were >60 and >50%, respectively; however, all control subjects died at 7 and 4 days, respectively. Importantly, the survival rate of the PAM-1 treatment groups was either comparable with or higher than that of the CZA treatment groups; this suggests the superior efficacy of PAM-1 over CZA. Collectively, these results suggest the potential efficacy of PAM-1 in treating *E. coli* infections.

4 Discussion

Owing to the worldwide emergence of antibiotic resistance and the declining rate of new antibiotic discovery, exploring novel antimicrobial agents has become an urgent issue. The increase in multidrug-resistant microorganisms poses a challenge for doctors and leads to higher rates of infections and deaths among seriously ill patients (Peleg and Hooper, 2010; Cornejo-Juárez et al., 2015). AMPs have been identified as promising candidates for antimicrobial therapy. They exert broad-spectrum antimicrobial activity and anti-inflammatory effects, have a rapid mode of action, and have minimal drug resistance development in pathogens (Yeaman and Yount, 2003).

AMPs derived from various natural sources, including plants, animals, and humans, provide valuable compositional and structural information. For example, WAM-1 from marsupials exhibits

broad-spectrum antimicrobial activity (Wang et al., 2011); furthermore, AMPs from scorpion venom can kill multidrug-resistant pathogens (Harrison et al., 2014; Hong et al., 2021). However, some AMPs have inherent limitations, including low abundance, cytotoxicity, and instability under some conditions (Mahlapuu et al., 2020).

Although the *in vitro* antibacterial activity of PAM-1, an AMP isolated from the platypus, against standard strains of *B. subtilis*, *S. aureus*, and *E. coli* has been studied (Wang et al., 2011), studies on clinical strains and further assessment of its antibacterial effects and mechanisms in both *in vitro* and *in vivo* settings are lacking. Therefore, in the present study, we elucidated the antibacterial, antibiofilm, and anti-inflammatory activities of PAM-1 and its underlying mechanisms as well as evaluated its safety and efficacy *in vivo*.

First, PAM-1 exhibited significant antibacterial activity against both CZA-sensitive and resistant *E. coli* isolates (Table 3). PI staining and the NPN uptake assay revealed that PAM-1 may kill bacteria by destroying the bacterial membrane (Figure 4). Previous studies have reported that positively charged PAM-1 may disrupt the integrity of the bacterial membrane and exert antibacterial effects by interacting with and neutralizing the negatively charged bacterial outer membrane via electrostatic interactions, thereby forming transmembrane pores via the “barrel-stave” model (Oren and Shai, 1998; Bin Hafeez et al., 2021; Han et al., 2022). Based on this mechanism of action, PAM-1 can sustain antibacterial effects over an extended period, making it a promising therapeutic agent. During aerobic metabolism, cells continuously produce ROS, and protect against ROS overproduction. However, oxidative stress is induced when ROS production overwhelms the natural antioxidant defenses of the cell. PAM-1 may induce bacterial cell damage and apoptosis by significantly increasing ROS levels (Figure 4).

Biofilms are microbial communities attached to solid surfaces; they enhance bacterial adaptability to the environment, impede the penetration of conventional antibiotics, and contribute to recurrent infections (Longo et al., 2014; Flemming et al., 2016). PAM-1 exhibited a notable inhibitory effect on biofilm growth and mature biofilm eradication (Figure 2). SEM analysis revealed that PAM-1 effectively destroys biofilms and inflicts significant damage to the bacteria (Figure 3).

Inflammatory responses play a vital role in defending against pathogens (Kaczyńska et al., 2016). For example, TNF- α actively participates in the pathogenesis of skin infections (Mittal et al., 2010). Bacterial infections often trigger inflammation and associated complications, making it necessary to regulate proinflammatory factor production. RT-qPCR revealed that PAM-1 can effectively alleviate inflammatory responses by decreasing IL-1 β and TNF- α production (Figure 5).

To evaluate the clinical potential of PAM-1, cytotoxicity and RBC hemolysis assays were conducted (Figure 6). Unlike most AMPs, PAM-1 maintained its antibacterial activity at 37°C as well as in the presence of serum (Tables 4, 5). However, Table 6 indicate PAM-1 exhibited instability in the presence of salt ions. This may be because cationic AMPs initially interact with and neutralize the negatively charged bacterial outer membrane via electrostatic interactions (Bin Hafeez et al., 2021). The presence of salt ions not only stabilizes the outer membrane by establishing a salt bridge with lipopolysaccharides but also increases the demand for AMP to replace the salt ions on the outer membrane (Han et al., 2022). Therefore, additional studies are

TABLE 6 The effect of conditions mimicking physiological concentrations of salt on the antibacterial activity of PAM-1 [MIC (μg/mL)].

Salt	Concentration	Bacterial isolates	
		DC8873	DC8466
NaCl	0 mM	2	8
	50 mM	4	32
	100 mM	16	32
	150 mM	16	>128
CaCl ₂	0 mM	2	8
	1.25 mM	4	16
	2.5 mM	4	16
	5 mM	4	16
MgCl ₂	0 mM	2	8
	0.5 mM	>128	>128
	1 mM	>128	>128
	2 mM	>128	>128

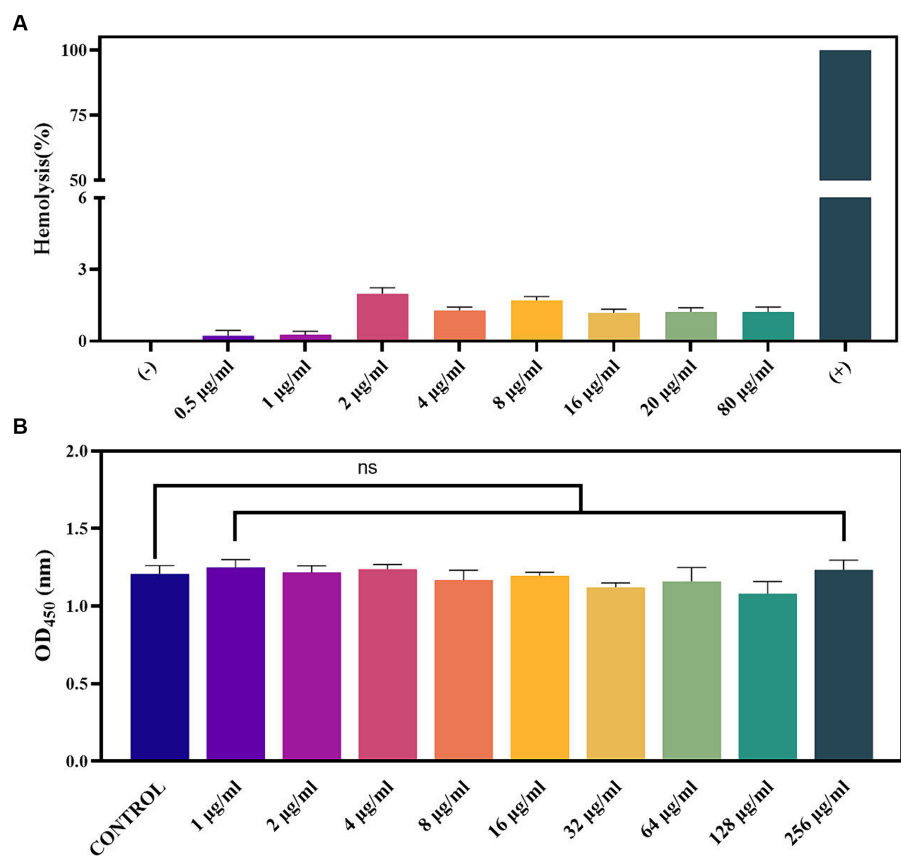


FIGURE 6 Toxicity of PAM-1. (A) The effect of PAM-1 on erythrocytes; (B) cytotoxicity of PAM-1 with different concentrations against RAW 264.7 murine macrophage cell line. ns, not statistically significant.

warranted to explain the competition and stabilization mechanisms between AMP and salt ions and to solve the application of cationic AMPs in high-salt environments.

Based on the findings of the abovementioned experiments, we used the *G. mellonella* larval infection model to further verify the *in vivo* therapeutic effect of PAM-1. Compared with the treatment

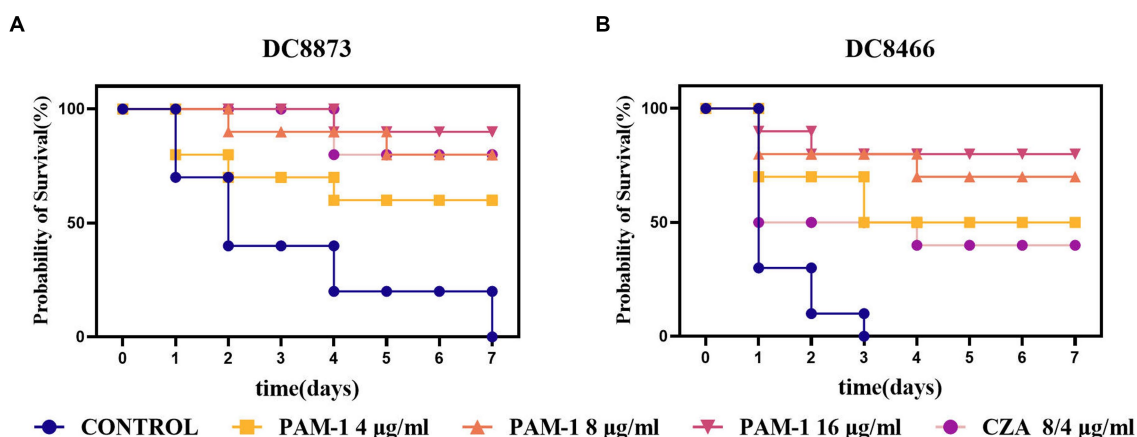


FIGURE 7

The survival rate of *G. mellonella* for different therapies. DC 8873 and DC 8466 as the experimental strains, and the survival rate record of *G. mellonella* in 7 days.

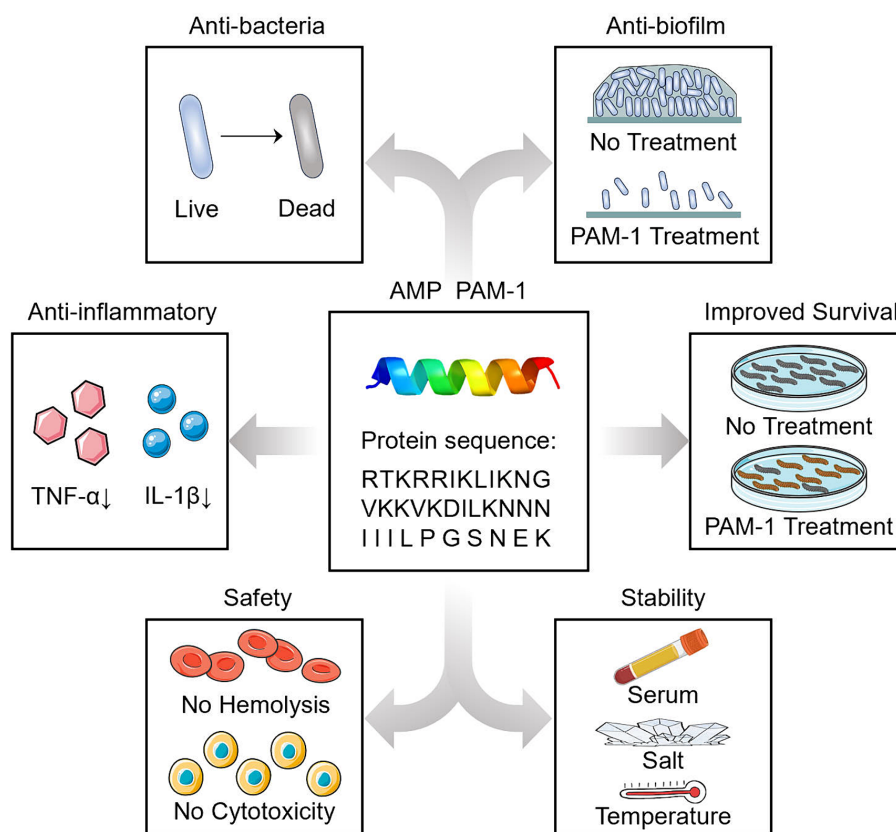


FIGURE 8

Summary diagram.

effect of CZA, the survival rate of *G. mellonella* larvae treated with PAM-1 was similar or better (Figure 7). This suggests that PAM-1 had a good application prospect *in vivo* and can exert a better therapeutic effect than CZA *in vivo*.

This is the first study to demonstrate the antibacterial effect of PAM-1 against CZA-resistant *E. coli* both *in vitro* and *in vivo*. We observed that PAM-1 is a promising agent for treating

CZA-resistant *E. coli* infections. In addition to antibacterial and antibiofilm activities, PAM-1 also exhibits potent anti-inflammatory effects (Figure 8). Although the mechanism underlying the effect of salt ions on its activity deserves further investigation, PAM-1 exhibits good stability and effects in serum, at room temperature, and *in vivo*. Collectively, these findings indicate that PAM-1 is a promising antibacterial agent against drug-resistant *E. coli* infections.

Data availability statement

The original contributions presented in the study are included in the article/[Supplementary material](#), further inquiries can be directed to the corresponding authors.

Ethics statement

The animal study was approved by the Zhejiang Association for Science and Technology SYXK. The study was conducted in accordance with the local legislation and institutional requirements.

Author contributions

YH: Data curation, Formal analysis, Investigation, Methodology, Software, Writing – original draft. YZ: Investigation, Methodology, Validation, Writing – review & editing. XZ: Conceptualization, Supervision, Writing – review & editing. ZH: Investigation, Software, Writing – review & editing. JK: Investigation, Writing – review & editing. XW: Investigation, Project administration, Resources, Writing – review & editing. LC: Investigation, Resources, Writing – review & editing. YW: Methodology, Software, Supervision, Validation, Writing – review & editing. JC: Conceptualization, Data curation, Supervision, Writing – review & editing. TZ: Conceptualization, Funding acquisition, Resources, Supervision, Writing – review & editing. MS: Conceptualization, Resources, Supervision, Writing – review & editing.

References

- Ashfaq, M. Y., da'na, D. A., and al-Ghouti, M. A. (2022). Application of MALDI-TOF MS for identification of environmental bacteria: a review. *J. Environ. Manag.* 305:114359. doi: 10.1016/j.jenvman.2021.114359
- Azad, M. B., Chen, Y., and Gibson, S. B. (2009). Regulation of autophagy by reactive oxygen species (ROS): implications for Cancer progression and treatment. *Antioxid. Redox Signal.* 11, 777–790. doi: 10.1089/ars.2008.2270
- Bin Hafeez, A., Jiang, X., Bergen, P. J., and Zhu, Y. (2021). Antimicrobial peptides: An update on classifications and databases. *Int. J. Mol. Sci.* 22:11691. doi: 10.3390/ijms222111691
- Borjan, J., Meyer, K. A., Shields, R. K., and Wenzler, E. (2020). Activity of ceftazidime-avibactam alone and in combination with polymyxin B against carbapenem-resistant *Klebsiella pneumoniae* in a tandem in vitro time-kill/in vivo *Galleria mellonella* survival model analysis. *Int. J. Antimicrob. Agents* 55:105852. doi: 10.1016/j.ijantimicag.2019.11.009
- Cornejo-Juárez, P., Vilar-Compte, D., Pérez-Jiménez, C., Namendys-Silva, S. A., Sandoval-Hernández, S., and Volkow-Fernández, P. (2015). The impact of hospital-acquired infections with multidrug-resistant bacteria in an oncology intensive care unit. *Int. J. Infect. Dis.* 31, 31–34. doi: 10.1016/j.ijid.2014.12.022
- da Luz, J. Z., Machado, T. N., Bezerra, A. G., de Oliveira Ribeiro, C. A., and Neto, F. F. (2020). Cytotoxicity of bismuth nanoparticles in the murine macrophage cell line RAW 264.7. *J. Mater. Sci. Mater. Med.* 31:95. doi: 10.1007/s10856-020-06427-0
- de Campos, G. Y., Oliveira, R. A., Oliveira-Brito, P. K. M., Roque-Barreira, M. C., and da Silva, T. A. (2020). Pro-inflammatory response ensured by LPS and pam 3CSK4 in RAW 264.7 cells did not improve a fungistatic effect on *Cryptococcus gattii* infection. *PeerJ* 8:e10295. doi: 10.7717/peerj.10295
- Dong, M., Kwok, S. H., Humble, J. L., Liang, Y., Tang, S. W., Tang, K. H., et al. (2021). BING, a novel antimicrobial peptide isolated from Japanese medaka plasma, targets bacterial envelope stress response by suppressing cpx R expression. *Sci. Rep.* 11:12219. doi: 10.1038/s41598-021-91765-4
- Dong, N., Ma, Q., Shan, A., Lv, Y., Hu, W., Gu, Y., et al. (2012). Strand length-dependent antimicrobial activity and membrane-active mechanism of arginine- and valine-rich β -hairpin-like antimicrobial peptides. *Antimicrob. Agents Chemother.* 56, 2994–3003. doi: 10.1128/AAC.06327-11
- Falcone, M., Russo, A., Iacovelli, A., Restuccia, G., Ceccarelli, G., Giordano, A., et al. (2016). Predictors of outcome in ICU patients with septic shock caused by *Klebsiella pneumoniae* carbapenemase-producing *K. pneumoniae*. *Clin. Microbiol. Infect.* 22, 444–450. doi: 10.1016/j.cmi.2016.01.016
- Flemming, H.-C., Wingender, J., Szewzyk, U., Steinberg, P., Rice, S. A., and Kjelleberg, S. (2016). Biofilms: an emergent form of bacterial life. *Nat. Rev. Microbiol.* 14, 563–575. doi: 10.1038/nrmicro.2016.94
- García-Cobos, S., Campos, J., Román, F., Carrera, C., Pérez-Vázquez, M., Aracil, B., et al. (2008). Low β -lactamase-negative ampicillin-resistant *Haemophilus influenzae* strains are best detected by testing amoxicillin susceptibility by the broth microdilution method. *Antimicrob. Agents Chemother.* 52, 2407–2414. doi: 10.1128/AAC.00214-08
- Han, W., Wei, Z., and Camesano, T. A. (2022). New antimicrobial peptide-antibiotic combination strategy for *Pseudomonas aeruginosa* inactivation. *Biointerphases* 17:041002. doi: 10.1116/6.0001981
- Harrison, P. L., Abdel-Rahman, M. A., Miller, K., and Strong, P. N. (2014). Antimicrobial peptides from scorpion venoms. *Toxicon* 88, 115–137. doi: 10.1016/j.toxicon.2014.06.006
- Hernández-García, M., Sánchez-López, J., Martínez-García, L., Becerra-Aparicio, F., Morosini, M. I., Ruiz-Garbajosa, P., et al. (2021). Emergence of the new KPC-49 variant conferring an ESBL phenotype with resistance to ceftazidime-avibactam in the ST131-H30R1 *Escherichia coli* high-risk clone. *Pathogens* 10:67. doi: 10.3390/pathogens10010067
- Hong, M. J., Kim, M. K., and Park, Y. (2021). Comparative antimicrobial activity of Hp404 peptide and its analogs against *Acinetobacter baumannii*. *Int. J. Mol. Sci.* 22:5540. doi: 10.3390/ijms22115540
- Jayatilaka, E. H. T. T., Rajapaksha, D. C., Nikapitiya, C., De Zoysa, M., and Whang, I. (2021). Antimicrobial and anti-biofilm peptide Octominin for controlling multidrug-resistant *Acinetobacter baumannii*. *Int. J. Mol. Sci.* 22:5353. doi: 10.3390/ijms22105353
- Kaczyńska, K., Kogut, E., Zajac, D., Jampolska, M., Andrzejewski, K., Sulejczak, D., et al. (2016). Neurotensin-based hybrid peptide's anti-inflammatory activity in murine model of a contact sensitivity response. *Eur. J. Pharm. Sci.* 93, 84–89. doi: 10.1016/j.ejps.2016.08.012

Funding

The author(s) declare financial support was received for the research, authorship, and/or publication of this article. This work was funded by the Key Laboratory of Clinical Laboratory Diagnosis and Translational Research of Zhejiang Province (2022E10022).

Conflict of interest

The authors declare that the research was conducted in the absence of any commercial or financial relationships that could be construed as a potential conflict of interest.

Publisher's note

All claims expressed in this article are solely those of the authors and do not necessarily represent those of their affiliated organizations, or those of the publisher, the editors and the reviewers. Any product that may be evaluated in this article, or claim that may be made by its manufacturer, is not guaranteed or endorsed by the publisher.

Supplementary material

The Supplementary material for this article can be found online at: <https://www.frontiersin.org/articles/10.3389/fmicb.2024.1291876/full#supplementary-material>

- Kim, M. K., Kang, H. K., Ko, S. J., Hong, M. J., Bang, J. K., Seo, C. H., et al. (2018). Mechanisms driving the antibacterial and antibiofilm properties of Hp1404 and its analogue peptides against multidrug-resistant *Pseudomonas aeruginosa*. *Sci. Rep.* 8:1763. doi: 10.1038/s41598-018-19434-7
- Liu, Y., Ding, S., Dietrich, R., Märklbauer, E., and Zhu, K. (2017). A biosurfactant-inspired Heptapeptide with improved specificity to kill MRSA. *Angew. Chem. Int. Ed. Engl.* 56, 1486–1490. doi: 10.1002/anie.201609277
- Livermore, D. M., Meunier, D., Hopkins, K. L., Doumith, M., Hill, R., Pike, R., et al. (2018). Activity of ceftazidime/avibactam against problem *Enterobacteriaceae* and *Pseudomonas aeruginosa* in the UK, 2015–16. *J. Antimicrob. Chemother.* 73, 648–657. doi: 10.1093/jac/dkx438
- Longo, F., Vuotto, C., and Donelli, G. (2014). Biofilm formation in *Acinetobacter baumannii*. *New Microbiol.* 37, 119–127.
- Luo, Y., and Song, Y. (2021). Mechanism of antimicrobial peptides: antimicrobial, anti-inflammatory and Antibiofilm activities. *Int. J. Mol. Sci.* 22:11401. doi: 10.3390/ijms222111401
- Mahlpuu, M., Björn, C., and Ekblom, J. (2020). Antimicrobial peptides as therapeutic agents: opportunities and challenges. *Crit. Rev. Biotechnol.* 40, 978–992. doi: 10.1080/07388551.2020.1796576
- Mittal, D., Saccheri, F., Vénéreau, E., Pusterla, T., Bianchi, M. E., and Rescigno, M. (2018). TLR4-mediated skin carcinogenesis is dependent on immune and radioresistant cells. *EMBO J.* 29, 2242–2252. doi: 10.1038/emboj.2010.94
- Morrill, H. J., Pogue, J. M., Kaye, K. S., and LaPlante, K. L. (2015). Treatment options for Carbapenem-resistant *Enterobacteriaceae* infections. *Open forum. Infect. Dis.* 2:ofv050. doi: 10.1093/ofid/ofv050
- Nguyen, H. L. T., Trujillo-Paez, J. V., Umehara, Y., Yue, H., Peng, G., Kiatsurayanon, C., et al. (2020). Role of antimicrobial peptides in skin barrier repair in individuals with atopic dermatitis. *Int. J. Mol. Sci.* 21:7607. doi: 10.3390/ijms21207607
- O'Loughlin, C. T., Miller, L. C., Siryaporn, A., Drescher, K., Semmelhack, M. F., and Bassler, B. L. (2013). A quorum-sensing inhibitor blocks *Pseudomonas aeruginosa* virulence and biofilm formation. *Proc. Natl. Acad. Sci. USA* 110, 17981–17986. doi: 10.1073/pnas.1316981110
- Oren, Z., and Shai, Y. (1998). Mode of action of linear amphipathic α -helical antimicrobial peptides. *Biopolymers* 47, 451–463. doi: 10.1002/(SICI)1097-0282(1998)47:6<451::AID-BIP4>3.0.CO;2-F
- Pasupuleti, M., Schmidtchen, A., and Malmsten, M. (2012). Antimicrobial peptides: key components of the innate immune system. *Crit. Rev. Biotechnol.* 32, 143–171. doi: 10.3109/07388551.2011.594423
- Peleg, A. Y., and Hooper, D. C. (2010). Hospital-acquired infections due to gram-negative bacteria. *N. Engl. J. Med.* 362, 1804–1813. doi: 10.1056/NEJMra0904124
- Quintilla, R., Kolecka, A., Casaregola, S., Daniel, H. M., Houbaken, J., Kostrzewa, M., et al. (2018). MALDI-TOF MS as a tool to identify foodborne yeasts and yeast-like fungi. *Int. J. Food Microbiol.* 266, 109–118. doi: 10.1016/j.ijfoodmicro.2017.11.016
- Satlin, M. J., Chen, L., Patel, G., Gomez-Simmonds, A., Weston, G., Kim, A. C., et al. (2017). Multicenter clinical and molecular epidemiological analysis of bacteremia due to Carbapenem-resistant *Enterobacteriaceae* (CRE) in the CRE epicenter of the United States. *Antimicrob. Agents Chemother.* 61, e02349–e02316. doi: 10.1128/AAC.02349-16
- Shields, R. K., Chen, L., Cheng, S., Chavda, K. D., Press, E. G., Snyder, A., et al. (2017). Emergence of ceftazidime-avibactam resistance due to plasmid-borne Bla KPC-3 mutations during treatment of Carbapenem-resistant *Klebsiella pneumoniae* infections. *Antimicrob. Agents Chemother.* 61, e02097–e02016. doi: 10.1128/AAC.02097-16
- Shields, R. K., Potoski, B. A., Haidar, G., Hao, B., Doi, Y., Chen, L., et al. (2016). Clinical outcomes, drug toxicity, and emergence of ceftazidime-avibactam resistance among patients treated for Carbapenem-resistant *Enterobacteriaceae* infections. *Clin. Infect. Dis.* 63, 1615–1618. doi: 10.1093/cid/ciw636
- Spencer, J. J., Pitts, R. E., Pearson, R. A., and King, L. B. (2018). The effects of antimicrobial peptides WAM-1 and LL-37 on multidrug-resistant *Acinetobacter baumannii*. *Pathog Dis* 76. doi: 10.1093/femspd/fty007
- Tang, Y.-T., Huang, Y.-Y., Zheng, L., Qin, S.-H., Xu, X.-P., An, T.-X., et al. (2017). Comparison of isolation methods of exosomes and exosomal RNA from cell culture medium and serum. *Int. J. Mol. Med.* 40, 834–844. doi: 10.3892/ijmm.2017.3080
- Thapa, R. K., Diep, D. B., and Tønnesen, H. H. (2020). Topical antimicrobial peptide formulations for wound healing: current developments and future prospects. *Acta Biomater.* 103, 52–67. doi: 10.1016/j.actbio.2019.12.025
- Trendel, J., Schwarzl, T., Horos, R., Prakash, A., Bateman, A., Hentze, M. W., et al. (2019). The human RNA-binding proteome and its dynamics during translational arrest. *Cell* 176, 391–403.e19. doi: 10.1016/j.cell.2018.11.004
- Tsai, C. J.-Y., Loh, J. M. S., and Proft, T. (2016). *Galleria mellonella* infection models for the study of bacterial diseases and for antimicrobial drug testing. *Virulence* 7, 214–229. doi: 10.1080/21505594.2015.1135289
- van Duin, D., Arias, C. A., Komarow, L., Chen, L., Hanson, B. M., Weston, G., et al. (2020). Molecular and clinical epidemiology of Carbapenem-resistant *Enterobacteriaceae* in the United States: a prospective cohort study. *Lancet Infect. Dis.* 20, 731–741. doi: 10.1016/S1473-3099(19)30755-8
- Wang, J., Wong, E. S. W., Whitley, J. C., Li, J., Stringer, J. M., Short, K. R., et al. (2011). Ancient antimicrobial peptides kill antibiotic-resistant pathogens: Australian mammals provide new options. *PLoS One* 6:e24030. doi: 10.1371/journal.pone.0024030
- Xu, W., Chen, T., Wang, H., Zeng, W., Wu, Q., Yu, K., et al. (2020). Molecular mechanisms and epidemiology of Fosfomycin resistance in *Staphylococcus aureus* isolated from patients at a teaching Hospital in China. *Front. Microbiol.* 11:1290. doi: 10.3389/fmicb.2020.01290
- Yeaman, M. R., and Yount, N. Y. (2003). Mechanisms of antimicrobial peptide action and resistance. *Pharmacol. Rev.* 55, 27–55. doi: 10.1124/pr.55.1.2
- Zeng, W., Liao, W., Zhao, Y., Wang, L., Shu, H., Jia, H., et al. (2022). A selective medium for screening ceftazidime/avibactam resistance in Carbapenem-resistant *Enterobacterales*. *Front. Microbiol.* 13:956044. doi: 10.3389/fmicb.2022.956044
- Zhang, W., Guo, Y., Li, J., Zhang, Y., Yang, Y., Dong, D., et al. (2018). In vitro and in vivo bactericidal activity of ceftazidime-avibactam against Carbapenemase-producing *Klebsiella pneumoniae*. *Antimicrob. Resist. Infect. Control* 7:142. doi: 10.1186/s13756-018-0435-9
- Zhang, X., Shi, S., Yao, Z., Zheng, X., Li, W., Zhang, Y., et al. (2022). Antimicrobial peptide WAM-1: a promising antibacterial and anti-inflammatory drug against carbapenem-resistant *Klebsiella pneumoniae*. *J. Antimicrob. Chemother.* 77, 1903–1911. doi: 10.1093/jac/dkac128
- Zhang, Y., Wang, X., Li, X., Dong, L., Hu, X., Nie, T., et al. (2019). Synergistic effect of Colistin combined with PFK-158 against Colistin-resistant *Enterobacteriaceae*. *Antimicrob. Agents Chemother.* 63, e00271–e00219. doi: 10.1128/AAC.00271-19

Frontiers in Microbiology

Explores the habitable world and the potential of microbial life

The largest and most cited microbiology journal which advances our understanding of the role microbes play in addressing global challenges such as healthcare, food security, and climate change.

Discover the latest Research Topics

[See more →](#)

Frontiers

Avenue du Tribunal-Fédéral 34
1005 Lausanne, Switzerland
frontiersin.org

Contact us

+41 (0)21 510 17 00
frontiersin.org/about/contact

